FACULTY OF MECHANICAL AND CIVIL ENGINEERING
IN KRALJEVO
UNIVERSITY OF KRAGUJEVAC

The Eighth Triennial
International Conference

HEAVY MACHINERY
HM 2014

Proceedings

ZLATIBOR, SERBIA
June 25 - June 28 2014

FACULTY OF MECHANICAL AND CIVIL ENGINEERING KRALJEVO
UNIVERSITY OF KRAGUJEVAC
KRALJEVO – SERBIA

THE EIGHTH INTERNATIONAL TRIENNIAL CONFERENCE

HEAVY MACHINERY
HM 2014

PROCEEDINGS

Zlatibor, June 25 – June 28 2014.

FACULTY OF MECHANICAL AND CIVIL ENGINEERING KRALJEVO
UNIVERSITY OF KRAGUJEVAC
KRALJEVO – SERBIA

THE EIGHTH INTERNATIONAL TRIENNIAL CONFERENCE

HEAVY MACHINERY
HM 2014

PROCEEDINGS

ORGANIZATION SUPPORTED BY:

Ministry of Education and Science, Republic of Serbia

Zlatibor, June 25 – June 28 2014

PUBLISHER:
Faculty of Mechanical and Civil Engineering, Kraljevo

EDITORS:
Prof. dr Milomir Gašić, mech. eng.

PRINTOUT:
SaTCIP d.o.o. Vrnjacka Banja

No. of copies: 200

REVIEWS:
All papers have been reviewed by members of scientific committee

CONFERENCE CHAIRMAN

Prof. dr Milomir Gašić, FMCE Kraljevo

INTERNATIONAL SCIENTIFIC PROGRAM COMMITTEE

CHAIRMAN

Prof. Dr Mile Savković, FMCE Kraljevo

VICE-CHAIRMAN

Prof. Dr Milan Kolarević, FMCE Kraljevo, Serbia

MEMBERS

1. Prof. Dr M. Alamoreanu, TU Bucharest, Romania
2. Prof. Dr S. Arsovski, FME Kragujevac, Serbia
3. Prof. Dr D. Atmadzhova, VTU “Todor Kableshkov”, Sofia, Bulgaria
4. Prof. Dr M. Berg, Royal Institut of Tecnology-KTH, Sweden
5. Prof. Dr H. Bogdevicius, Technical University, Vilnus, Lithuania
6. Prof. Dr S. Bošnjak, FME Belgrade, Serbia
7. Prof. Dr A. Bruja, TU Bucharest, Romanija
8. Prof. Dr Z. Bučevac, FME Belgrade, Serbia
9. Prof. Dr R.Bulatović, FMCE Kraljevo, Serbia
10. Prof. Dr A. Bukvić, FME East Sarajevo, Bosnia and Herzegovina
11. Prof. Dr M. Dedić, FMCE Kraljevo, Serbia
12. Prof. Dr A. I. Dotsenko, MGSU, Moscow, Russia
13. Prof. Dr R. Durković, FME Podgorica, Montenegro
14. Prof. Dr M. Đapić, FMCE Kraljevo, Serbia
15. Prof. Dr Z. Đinović, Integrated MicroSystem, Vienna, Austria
16. Prof. Dr K. Ehmann, Northwestern University, Chicago, USA
17. Prof. Dr A. Emeljanova, HGTUSA Harkov, Ukraine
18. Prof. Dr V. Filipović, FMCE Kraljevo, Serbia
19. Prof. Dr C. Fragassa, University of Bologna, Italy
20. Prof. Dr M. Gagl, Integrated MicroSystem, Vienna, Austria
21. Prof. Dr D. Golubović, FME East Sarajevo, Bosnia and Herzegovina
22. Prof. Dr V. Jovišević, FME Banja Luka, Bosnia and Herzegovina
23. Prof. Dr B. Jerman, FME Ljubljana, Slovenia
24. Prof. Dr Z. Jugović, Tehnical Faculty Čačak, Serbia
25. Prof. Dr V. Karamarković, FMCE Kraljevo, Serbia
26. Prof. Dr M. Karasahin, Demirel Univerity, Istanbul, Turkey
27. Prof. Dr I. Kiričenko, HNADU Kiev, Ukraine
28. Prof. Dr K. Kocman, Tecnical University of Brno, Czech Republic
29. Prof. Dr S. Kolaković, Faculty of Tehnical Sciences, Novi Sad, Serbia
30. Prof. Dr M. Kostic, Northern Illinois University, DeKalb, USA
31. Prof. Dr M. Králik, FME Bratislava, Slovakia
32. Prof. Dr E. Kudrjavcev, MGSU, Moskow, Russia
33. Prof. Dr Đ. Lađinović, Faculty of Tehnical Sciences, Novi Sad, Serbia
34. Prof. Dr LJ. Lukić, FMCE Kraljevo, Serbia
35. Prof. Dr Z. Marinković, FME Niš, Serbia
36. Prof. Dr N. Mešćerin, MGSU, Moskow, Russia
37. Prof. Dr I. I. Nazarenko, KNUBA Kiev, Ukraine

38. Prof. Dr N. Nedić, FMCE Kraljevo, Serbia
39. Prof. Dr N. Nenov, VTU "Todor Kableshkov", Sofia, Bulgaria
40. Prof. Dr V. Nikolić, FME Niš, Serbia
41. Prof. Dr E. Nikolov, Technical University, Sofia, Bulgaria
42. Prof. Dr M. Ognjanović, FME Belgrade, Serbia
43. Prof. Dr J. Peterka, FMS&T, Trnava, Slovakia
44. Prof. Dr D. Petrović, FMCE Kraljevo, Serbia
45. Prof. Dr Z. Petrović, FMCE Kraljevo, Serbia
46. Prof. Dr J. Polajnar, BC University, Prince George, Canada
47. Prof. Dr V. Radonjanin, Faculty of Tehnical Sciences, Novi Sad, Serbia
48. Prof. Dr V. Raičević, FME Kosovska Mitrovica, Serbia
49. Prof. Dr M. Rajović, FMCE Kraljevo, Serbia
50. Prof. Dr M. Stefanovć, FME Kragujevac, Serbia
51. Prof. Dr D. Sever, Maribor, Civil Engineering, Slovenia
52. Prof. Dr M. A. Stepanov, MGSU, Moskow, Russia
53. Prof. Dr I. S. Surovcev, VGSU, Voronezh, Russia
54. Prof. Dr Z. Šoškić, FMCE Kraljevo, Serbia
55. Prof. Dr LJ. Tanović, FME Belgrade, Serbia
56. Prof. Dr S. Trifunović, FMCE Kraljevo, Serbia
57. Prof. Dr J. Vladić, Faculty of Tehnical Sciences, Novi Sad, Serbia
58. Prof. Dr M. Vukićević, FMCE Kraljevo, Serbia
59. Prof. Dr K. Weinert, University of Dortmund, Germany
60. Prof. Dr N. Zrnić, FME Belgrade, Serbia

ORGANIZING COMMITTEE

CHAIRMAN:

Prof. Dr Ljubomir Lukić, FMCE Kraljevo

VICE-CHAIRMAN:

Prof. Dr Zlatan Šoškić, FMCE Kraljevo, Serbia

MEMBERS:

Doc. Dr S. Ćirić-Kostić, FMCE Kraljevo, Serbia
Doc. Dr Lj. Dubonjić, FMCE Kraljevo, Serbia
Doc. Dr O. Erić, FMCE Kraljevo, Serbia
Doc. Dr R. Karamarković, FMCE Kraljevo, Serbia
Doc. Dr M. Maraševič, FMCE Kraljevo, Serbia
Doc. Dr D. Pršić, FMCE Kraljevo, Serbia
Doc. Dr S. Šalinić, FMCE Kraljevo, Serbia
M.Sc. M. Bjelić, FMCE Kraljevo, Serbia
M.Sc. N. Bogojević, FMCE Kraljevo, Serbia
M.Sc. Z. Glavčić, FMCE Kraljevo, Serbia
M.Sc. Lj. Lalović, FMCE Kraljevo, Serbia
M.Sc. G. Marković, FMCE Kraljevo, Serbia
M.A. N. Pavlović, FMCE Kraljevo, Serbia
M.Sc. B. Radičević, FMCE Kraljevo, Serbia
M.Sc. N. Zdravković, FMCE Kraljevo, Serbia

PREFACE

The Faculty of Mechanical Engineering Kraljevo has been traditionally organizing the international scientific conference devoted to heavy machinery every three years. The VIII International Scientific Conference HM 2014 is considering modern methods and new technologies in the fields of transport design in machinery, control energy, production technologies, urban engineering and civili engineering through thematic sessions for the purpose of sustainable competitiveness of economic systems. Modern technologies are exposed to fast changes at the global world level so that their timely application both in large industrial systems and in medium and small enterprises is of considerable importance for the entire development and technological progress of economy as a whole.

The VIII International Scientific Conference Heavy Machinery HM 2014 is a place for exchange of experiences and results accomplished in domestic and foreign science and practice, with the goal to indicate directions of further development of our industry on its way toward integration in european and world economic trends. Exchange of experiences between our and foreign scientific workers should contribute to extension of international scientific-technical collaboration, initiation of new international scientific-research projects and broader international collaboration among universities.

The papers which will be presented at this Conference have been classified into seven thematic fields:

A. EARTH-MOVING AND TRANSPORTATION MACHINERY
B. PRODUCTION TECHNOLOGIES
C. CIVIL ENGINEERING AND MATERIALS
D. AUTOMATIC CONTROL, ROBOTICS AND FLUID TECHNIQUE
E. MACHINE DESIGN AND MECHANICS
F. RAILWAY ENGINEERING
G. URBAN ENGINEERING, THERMAL TECHNIQUE AND ENVIRONMENT PROTECTION

Within this Conference, the First International Students Symposium will be held. The aim is to open a scientific discussion on this actual problem in industry among young students.

The sponsorship by the Ministry of Science of the Republic of Serbia is the proper way to promote science and technology in the area of mechanical engineering in Serbia.

On behalf of the organizer, I would like to express our thanks to all organizations and institutions that have supported this Conference. I would also like to extend our thanks to all authors and participants from abroad and from our country for their contribution to the Conference. And last but not the least, dear guests and participants in the Conference, I wish you a good time in Kraljevo – Vrnjačka Banja and see you again at the Eight Conference, in three years.

Kraljevo – Zlatibor, June 2014

Conference Chairman,

Prof. Dr Milomir Gašić, mech eng.

SESSION B: PRODUCTION TECHNOLOGIES

SESSION C: CIVIL ENGINEERING AND MATERIALS

SESSION D: AUTOMATIC CONTROL, ROBOTICS AND FLUID TECHNIQUE

SESSION E: MECHANICAL DESIGN AND MECHANICS

SESSION F: RAILWAY ENGINEERING

SESSION G: URBAN ENGINEERING, THERMAL TECHNIQUE AND ENVIRONMENT PROTECTION

PLENNARY SESSION

Modelling and Working Simulation of the Mechanism of Axial Piston Hydrostatic Pumps Using Denavit - Hartenberg Method

Adrian Bruja[1], Marian Dima[1]
[1] Technical University of Civil Engineering of Bucharest, Bucharest (Romania)

The Denavit - Hartenberg method is one of the most frequently used methods for studying spatial bar mechanisms. Having in mind that this method can be used for open chain spatial mechanisms, it was used very often for studying the positioning and orientation mechanisms of robots.

In this paper is presented an overview of the method and an application to kinematics study of 2 types of axial piston pumps.

Keywords: Denavit-Hartenberg, mechanisms, spatial bar, open chain, robots, axial piston pumps

1. METHOD OVERVIEW

In this method to every kinematic element is attached a reference frame according to the Denavit - Hartenberg [3] convention. For the open loop kinematic chain composed of consecutive kinematic elements *i-2*, *i-1*, *i* and *i+1* and the kinematic joints linking the elements, Figure 2, the choosing of the reference frames linked to the elements *i-1* and *i* is carried out as follows:

1. Direction of the z_{i-1} axis that links the element *i-1* to i is the joint’s axis;
2. x_{i-1} axis is linked to the element *i-1* and is chosen to the common normal of the z_{i-1} and z_{i-2} axes oriented from O_{i-2} to O_{i-1};
3. Similarly the axis x_i is chosen as common normal of the rotation axes z_{i-1} and z_i oriented from O_{i-1} to O_i;
4. The origins of the reference frames are chosen in the intersection points between the common normal and the axis of the revolute joint, respectively O_{i-2} and O_{i-1};
5. The name of the joint is given by the highest order of the elements that complete the joint.

The *y* axes are chosen so that the reference frame is orthogonal.

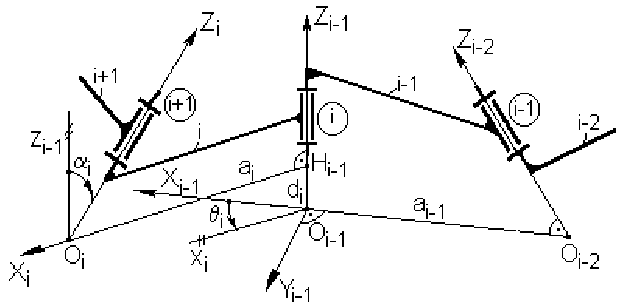

Figure 1.

The geometrical parameters which entirely describe the transition from a reference frame *i-1* to a reference frame i are as follows:

Table 1.

θ_i	Is the joint’s angle from axis x_{i-1} to axis x_i, measured counter clockwise, around axis z_{i-1}
d_i	Is the distance from the origin O_{i-1} to the intersection of the axis z_{i-1} with axis x_i, measured along the axis z_{i-1}
a_i	Is the distance from the intersection of the axis z_{i-1} with x_i to the origin O_i, measured along the axis x_i (or the least distance between z_{i-1} and z_i axes)
α_i	Is the angle between the z_{i-1} axis with the axis z_i, by rotating it around x_i axis counter clockwise.

The transition from reference frame *"i-1"*, attached to the element *i-1*, to the reference frame *"i"*, attached to the element *i*, is carried out as follows:

1. rotation z_{i-1} around axis by angle θ_i, in order to overlap the x_{i-1} axis with x_i;
2. a translation along the axis z_{i-1} with the distance d_i, which brings the origin O_{i-1} in the intermediate position H_{i-1} (Figure 1);
3. a new translation along the axis x_i by the a_i distance, thus overlapping the origin O_{i-1} to O_i;
4. Finally a second rotation around axis x_i by an angle α_i, in order to overlap z_{i-1} axis with z_i.

Each one of these 4 movements can be expressed using an elementary rotation or translation matrix and the resulting movement being the product of the matrices:

$$_{i-1}T^i = Rot(z_{i-1},\theta_i)\cdot Trans(z_{i-1},d_i)\cdot Trans(x_{i-1},a_i)\cdot Rot(x_i,\alpha_i) \quad (1)$$

Doing the multiplication of the elementary matrices

*Corresponding author: Universitatea tehnică de construcţi Bucureşti and bruja@utcb.ro

$$\begin{pmatrix} \cos(\theta_i) & -\sin(\theta_i) & 0 & 0 \\ \sin(\theta_i) & \cos(\theta_i) & 0 & 0 \\ 0 & 0 & 1 & 0 \\ 0 & 0 & 0 & 1 \end{pmatrix} \cdot \begin{pmatrix} 1 & 0 & 0 & 0 \\ 0 & 1 & 0 & 0 \\ 0 & 0 & 1 & d_i \\ 0 & 0 & 0 & 1 \end{pmatrix} \cdot \begin{pmatrix} 1 & 0 & 0 & a_i \\ 0 & 1 & 0 & 0 \\ 0 & 0 & 1 & 0 \\ 0 & 0 & 0 & 1 \end{pmatrix} \cdot \begin{pmatrix} 1 & 0 & 0 & 0 \\ 0 & \cos(\alpha_i) & -\sin(\alpha_i) & 0 \\ 0 & \sin(\alpha_i) & \cos(\alpha_i) & 0 \\ 0 & 0 & 0 & 1 \end{pmatrix} \quad (2)$$

The transition matrix from the reference frame *"i-1"*, attached to the element *i-1*, to the reference frame "*i*", attached to the element *i*, is obtained

$$_{i-1}T^i = \begin{pmatrix} \cos(\theta_i) & -\sin(\theta_i)\cdot\cos(\alpha_i) & \sin(\theta_i)\cdot\sin(\alpha_i) & a_i\cdot\cos(\theta_i) \\ \sin(\theta_i) & \cos(\theta_i)\cdot\cos(\alpha_i) & -\cos(\theta_i)\cdot\sin(\alpha_i) & a_i\cdot\sin(\theta_i) \\ 0 & \sin(\alpha_i) & \cos(\alpha_i) & d_i \\ 0 & 0 & 0 & 1 \end{pmatrix} \quad (3)$$

The said transition matrix (3) sets the position and orientation of the reference frame "*i*", attached to the element i in relation to the reference frame "*i-1*", attached to the element *i-1*.

In this matrix the first 3 columns represent the direction cosines of the reference frame's axes O_i in relation to the reference frame axes O_{i-1}, meaning the orientation of the reference frame O_i in relation to the O_{i-1} reference frame and the 4th column the position of the O_i centre in relation to O_{i-1}.

2. BUILDING THE FORWARD KINEMATIC MODEL FOR THE MECHANISM OF THE AXIAL PISTON HYDROSTATIC PUMPS

In Figure 2a, 2b are presented the working scheme of 2 types of axial piston hydrostatic pumps. In the case presented in Figure 2a the pistons block is rotating along with the disc and the driving shaft, while in the Figure 2b the pistons block and the disc have the rotation about the AC axis blocked and the driving shaft is rotating in relation to these around the C joint. In both cases between the pistons block and the disc, there isn't any relative motion in relation to the AC axis. The equivalent scheme from the pistons kinematics point of view, of the spatial bars mechanism, corresponding to the 2 types of pumps is presented in Figure 2c

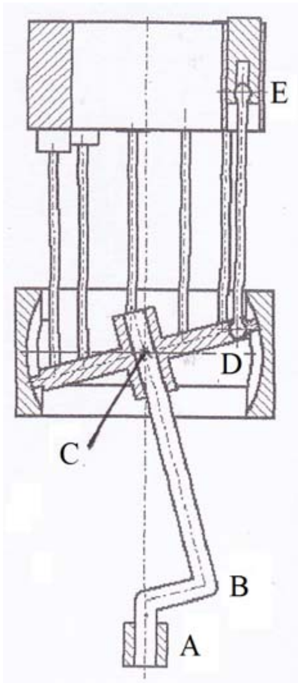

Figure 2b.

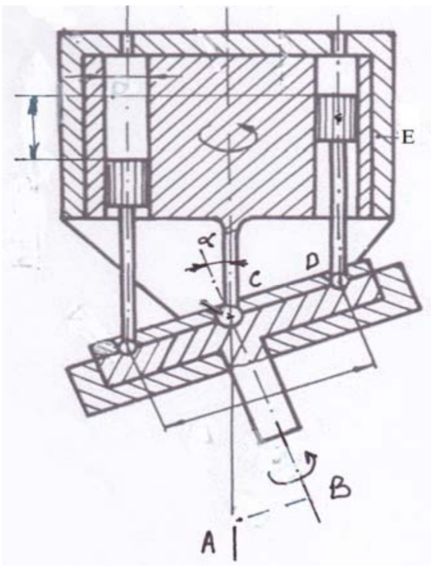

Figure 2a.

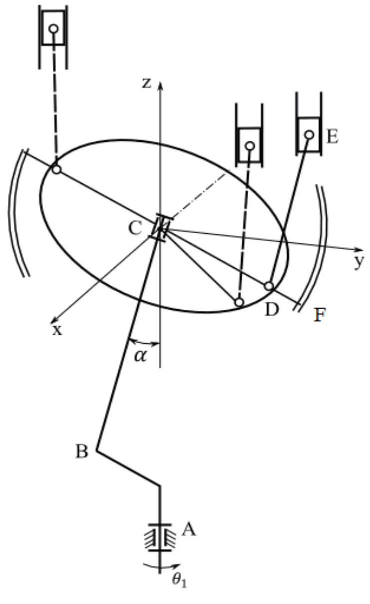

Figure 2c.

2.1. Applying the Method for Kinematics Study of a Point D Over the Discs' Periphery

For the study, is taken into consideration the spatial mechanism ACDF, Figure 2c. The kinematic scheme of this mechanism is equivalent from kinematic point of view to the scheme in Figure 3.

2.1.1. *Attaching the Reference Frames*

According to the §2 the kinematic scheme in Figure 3 is analysed. In this case the z axes of the reference frames will be: z_0 for the element 0, z_1 for the element 1, respectively z_2 for element 2 and z_3 for element 3.

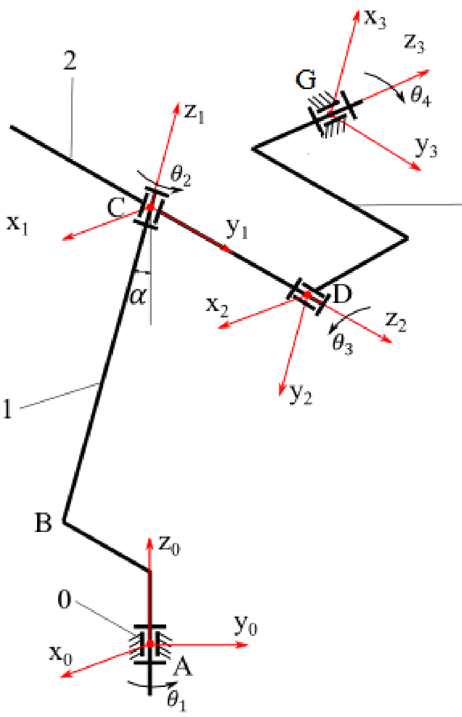

Figure 3.

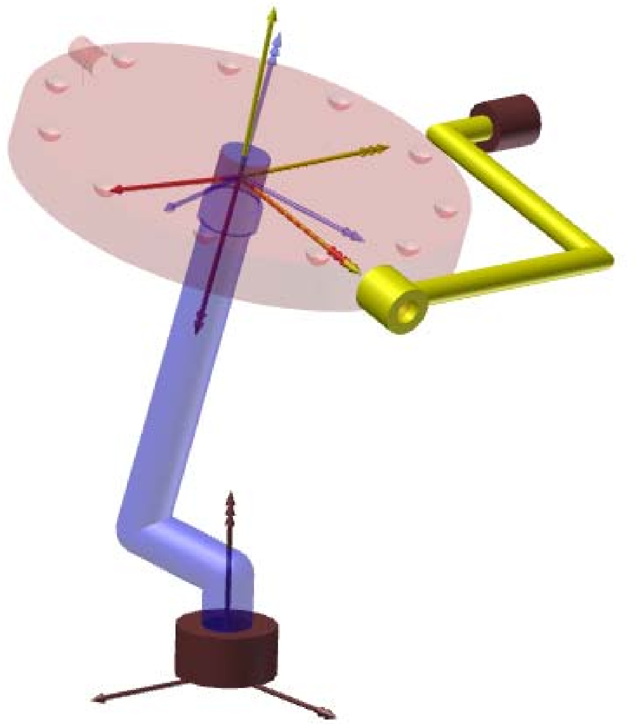

Figure 4.

Axis x_1 is perpendicular on axes z_0 and z_1 and the origin of the reference frame O_1 is at the intersection between the axes x_1 and z_1, point C. The axis x_2 is perpendicular on axes z_1 and z_2 and the origin of the reference frame O_2 is still in point C (intersection between the axes x_2 and z_2). The axis x_3 is perpendicular on axes z_2 and z_3 and the origin of the reference frame O_3 is again in point C (intersection between the axes x_3 and z_3). The reference frames are presented in Figure 4. For easier expressing of the transfer matrixes O_1, O_2, O_3 the origins are considered as in Figure 3 with the condition $\overline{O_1O_2} = 0$ and $\overline{O_2O_3} = 0$.

2.1.2. *Modelling the Displacements of Point D*

As shown in §2, in case of Denavit - Hartenberg method, the transition from one reference frame *i-1* to a reference frame i is done using the transfer matrix ${}_{i-1}T^i$, equations (1,2).

In case of the ACDG mechanism, Figure 3, $i = 1 \ldots 3$ and the transition from a reference frame to another is carried out in the joints A(0→1), C(1→2) and D(2→3).

The matrix ${}_0T^1$

The geometrical parameters that describe the transfer from a reference frame to another, according to.§2, Figure 1, are Θ_i, d_i, a_i, α_i. For the ACDG mechanism these are presented table 1 for every joint.

Table 2.

Joint	θ_i	d_i	a_i	α_i	Variable q_i
A (0-1)	θ_1	d	0	-α	θ_1
C (1-2)	- θ_2	0	0	-π/2	θ_2
D (2-3)	θ_3 -π/2	0	0	π/2	θ_3

Starting from equation (2) based on the parameters in table 1 the transition matrixes are obtained ${}_{i-1}T^i$ for transition from one reference frame to another in case of the studied mechanism.

$$\begin{pmatrix} \cos(\theta_1) & -\sin(\theta_1) & 0 & 0 \\ \sin(\theta_1) & \cos(\theta_1) & 0 & 0 \\ 0 & 0 & 1 & 0 \\ 0 & 0 & 0 & 1 \end{pmatrix} \cdot \begin{pmatrix} 1 & 0 & 0 & 0 \\ 0 & 1 & 0 & 0 \\ 0 & 0 & 1 & d \\ 0 & 0 & 0 & 1 \end{pmatrix} \cdot \begin{pmatrix} 1 & 0 & 0 & 0 \\ 0 & 1 & 0 & 0 \\ 0 & 0 & 1 & 0 \\ 0 & 0 & 0 & 1 \end{pmatrix} \cdot \begin{pmatrix} 1 & 0 & 0 & 0 \\ 0 & \cos(-\alpha) & -\sin(-\alpha) & 0 \\ 0 & \sin(-\alpha) & \cos(-\alpha) & 0 \\ 0 & 0 & 0 & 1 \end{pmatrix} = \begin{pmatrix} \cos(\theta_1) & -\cos(\alpha)\sin(\theta_1) & -\sin(\alpha)\sin(\theta_1) & 0 \\ \sin(\theta_1) & \cos(\alpha)\cos(\theta_1) & \sin(\alpha)\sin(\theta_1) & 0 \\ 0 & -\sin(\alpha) & \cos(\alpha) & d \\ 0 & 0 & 0 & 1 \end{pmatrix} \quad (4)$$

the matrix ${}_1T^2$

$$\begin{pmatrix} \cos(-\theta_2) & -\sin(-\theta_2) & 0 & 0 \\ \sin(-\theta_2) & \cos(-\theta_2) & 0 & 0 \\ 0 & 0 & 1 & 0 \\ 0 & 0 & 0 & 1 \end{pmatrix} \cdot \begin{pmatrix} 1 & 0 & 0 & 0 \\ 0 & 1 & 0 & 0 \\ 0 & 0 & 1 & 0 \\ 0 & 0 & 0 & 1 \end{pmatrix} \cdot \begin{pmatrix} 1 & 0 & 0 & 0 \\ 0 & 1 & 0 & 0 \\ 0 & 0 & 1 & 0 \\ 0 & 0 & 0 & 1 \end{pmatrix} \cdot \begin{pmatrix} 1 & 0 & 0 & 0 \\ 0 & \cos(-\pi/2) & -\sin(-\pi/2) & 0 \\ 0 & \sin(-\pi/2) & \cos(-\pi/2) & 0 \\ 0 & 0 & 0 & 1 \end{pmatrix} = \begin{pmatrix} \cos(\theta_2) & 0 & \sin(\theta_2) & 0 \\ -\sin(\theta_2) & 0 & \cos(\theta_2) & 0 \\ 0 & -1 & 0 & 0 \\ 0 & 0 & 0 & 1 \end{pmatrix} \quad (5)$$

the matrix ${}_2T^3$

$$\begin{pmatrix} \cos(\theta_3-\pi/2) & -\sin(\theta_3-\pi/2) & 0 & 0 \\ \sin(\theta_3-\pi/2) & \cos(\theta_3-\pi/2) & 0 & 0 \\ 0 & 0 & 1 & 0 \\ 0 & 0 & 0 & 1 \end{pmatrix} \cdot \begin{pmatrix} 1 & 0 & 0 & 0 \\ 0 & 1 & 0 & 0 \\ 0 & 0 & 1 & 0 \\ 0 & 0 & 0 & 1 \end{pmatrix} \cdot \begin{pmatrix} 1 & 0 & 0 & 0 \\ 0 & 1 & 0 & 0 \\ 0 & 0 & 1 & 0 \\ 0 & 0 & 0 & 1 \end{pmatrix} \cdot \begin{pmatrix} 1 & 0 & 0 & 0 \\ 0 & \cos(-\pi/2) & -\sin(-\pi/2) & 0 \\ 0 & \sin(-\pi/2) & \cos(-\pi/2) & 0 \\ 0 & 0 & 0 & 1 \end{pmatrix} = \begin{pmatrix} \sin(\theta_3) & 0 & -\cos(\theta_3) & 0 \\ -\cos(\theta_3) & 0 & -\sin(\theta_3) & 0 \\ 0 & 1 & 0 & 0 \\ 0 & 0 & 0 & 1 \end{pmatrix} \quad (6)$$

Forward model ${}_0T^3 = {}_0T^1 \cdot {}_1T^2 \cdot {}_2T^3 \cdot$

$$\begin{pmatrix} \cos(\theta_1) & -\cos(\alpha)\sin(\theta_1) & -\sin(\alpha)\sin(\theta_1) & 0 \\ \sin(\theta_1) & \cos(\alpha)\cos(\theta_1) & \sin(\alpha)\sin(\theta_1) & 0 \\ 0 & -\sin(\alpha) & \cos(\alpha) & d \\ 0 & 0 & 0 & 1 \end{pmatrix} \cdot \begin{pmatrix} \cos(\theta_2) & 0 & \sin(\theta_2) & 0 \\ -\sin(\theta_2) & 0 & \cos(\theta_2) & 0 \\ 0 & -1 & 0 & 0 \\ 0 & 0 & 0 & 1 \end{pmatrix} \cdot \begin{pmatrix} \sin(\theta_3) & 0 & -\cos(\theta_3) & 0 \\ -\cos(\theta_3) & 0 & -\sin(\theta_3) & 0 \\ 0 & 1 & 0 & 0 \\ 0 & 0 & 0 & 1 \end{pmatrix} \quad (7)$$

After calculating the product the transfer matrix ${}_0T^3$ is obtained.

$${}_0T^3 = \begin{pmatrix} n_x & \underline{o_x} & a_x & p_x \\ n_y & o_y & a_y & p_y \\ n_z & o_z & \underline{\underline{a_z}} & p_z \\ 0 & 0 & 0 & 1 \end{pmatrix} = \begin{pmatrix} i_0 \cdot i_3 & \underline{i_0 \cdot j_3} & i_0 \cdot k_3 & p_x \\ j_0 \cdot i_3 & j_0 \cdot j_3 & j_0 \cdot k_3 & p_y \\ k_0 \cdot i_3 & k_0 \cdot j_3 & \underline{\underline{k_0 \cdot k_3}} & p_z \\ 0 & 0 & 0 & 0 \end{pmatrix} \quad (8)$$

where:

$$\begin{aligned} n_x &= \cos(\theta_1)\cdot\cos(\theta_2)\cdot\sin(\theta_3) - \sin(\alpha)\cdot\cos(\theta_3)\cdot\sin(\theta_1) + \cos(\alpha)\cdot\sin(\theta_1)\cdot\sin(\theta_2)\cdot\sin(\theta_3) \\ n_y &= \sin(\alpha)\cdot\cos(\theta_1)\cdot\cos(\theta_3) + \sin(\theta_1)\cdot\cos(\theta_2)\cdot\sin(\theta_3) - \cos(\alpha)\cdot\cos(\theta_1)\cdot\cos(\theta_2)\cdot\sin(\theta_3) \\ n_z &= \cos(\alpha)\cdot\cos(\theta_3) + \sin(\alpha)\cdot\sin(\theta_2)\cdot\sin(\theta_3) \\ o_x &= \cos(\theta_1)\cdot\sin(\theta_2) - \cos(\alpha)\cdot\sin(\theta_1)\cdot\cos(\theta_2) \\ o_y &= \sin(\theta_1)\cdot\sin(\theta_2) + \cos(\alpha)\cdot\cos(\theta_1)\cdot\cos(\theta_2) \\ o_z &= -\sin(\alpha)\cdot\cos(\theta_2) \\ a_x &= -\sin(\alpha)\cdot\sin(\theta_1)\cdot\sin(\theta_3) - \cos(\theta_1)\cdot\cos(\theta_2)\cdot\cos(\theta_3) - \cos(\alpha)\cdot\sin(\theta_1)\cdot\sin(\theta_2)\cdot\cos(\theta_3) \\ a_y &= \sin(\alpha)\cdot\cos(\theta_1)\cdot\sin(\theta_3) - \sin(\theta_1)\cdot\cos(\theta_2)\cdot\cos(\theta_3) + \cos(\alpha)\cdot\cos(\theta_1)\cdot\sin(\theta_2)\cdot\cos(\theta_3) \\ a_z &= \cos(\alpha)\cdot\sin(\theta_3) - \sin(\alpha)\cdot\sin(\theta_2)\cdot\cos(\theta_3) \\ p_x &= 0;\ p_y = 0;\ p_z = d \end{aligned} \quad (9)$$

In these equations, n, o and a are the direction cosines of the reference frame O_3 in relation to the reference frame O_0, p position parameters of the O_3 origin in relation to O_0 and $\overline{i}$, $\overline{j}$ and $\overline{k}$ are the unit vectors of the axes x, y and respectively z.

Taking into account the direction of the reference frames' axes and the direction cosines, and the position parameters an equation system of 12 equations with 12 unknowns is obtained.

In case of ACDG mechanism known variables α and θ_1. For the kinematics study of the point D needs to be determined θ_2 and θ_3.

In order to determine θ_2, knowing that the y_3 is perpendicular on the axis x_0, Figure 3, is considered in (8), direction cosine $o_x = i_0 \cdot j_3 = 0$. Considering the value of θ_2 given by (9) the following equation is obtained

$$\cos(\theta_1)\cdot\sin(\theta_2) - \cos(\alpha)\cdot\sin(\theta_1)\cdot\cos(\theta_2) = 0 \quad (10)$$

Results

$$\theta_2 = f_2(\theta_1, \alpha) \quad (11)$$

For determining θ_3 the axes z_3 and z_0, are considered perpendicular according to Figure 3. As consequence, from equations (8) we obtained $a_z = k_0 \cdot k_3 = 0$.

Taking into account the value of a_z from equations (9) we get the equation of θ_3

$$\cos(\alpha)\cdot\sin(\theta_3) - \sin(\alpha)\cdot\sin(\theta_2)\cdot\cos(\theta_3) = 0 \qquad (12)$$

Taking into consideration the equation (11) we obtain

$$\theta_3 = f_3(\theta_1, \alpha) \qquad (13)$$

Determining the Paths of Points on the Periphery of the Disc

The points D are placed on a circle of radius r, Figure 5, belonging to the disc 2, Figure 3, to which, through the spherical joints, are connected the bars DE, Figure 2, that transmit the movement of the pistons. These points are equally spaced, which depends on the pistons number, over the periphery of the circle of radius r.

By positioning a point D over the periphery of the disc the other positions are determined automatically. Out of these points, from kinematic point of view characteristic are the points D_1 and D, Figure 5.

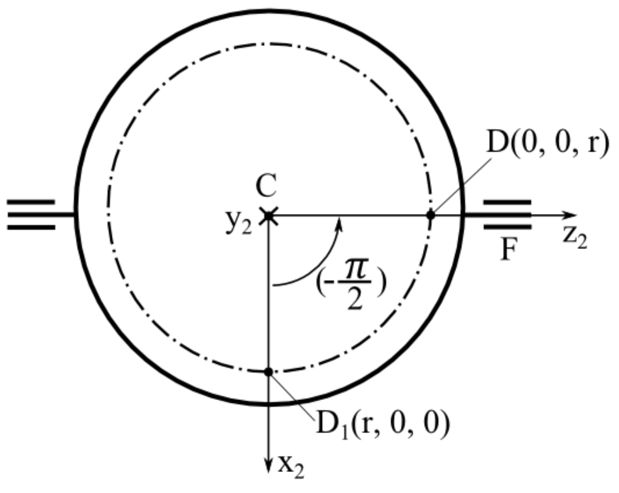

Figure 5.

Trajectory of the Point D_1

The coordinates of point $_{D1}$ related to the origin O_0 are obtained from the equation

$$\begin{pmatrix}(x_D)_0\\(y_D)_0\\(z_D)_0\end{pmatrix} = {}_0T^2\cdot\begin{pmatrix}(x_D)_2\\(y_D)_2\\(z_D)_2\end{pmatrix}$$
$$\begin{pmatrix}x(\theta_1)\\y(\theta_1)\\y(\theta_1)\end{pmatrix} = {}_0T^2\cdot\begin{pmatrix}r\\0\\0\end{pmatrix} \qquad (14)$$

Where the transition matrix ${}_0T^2$ has the form ${}_0T^2 = {}_0T^1 \cdot {}_1T^2$, the product ${}_0T^1 \cdot {}_1T^2$ is in equation (7).

From equation (14) we obtain:

$$\begin{aligned} x(\theta_1) &= f_x(\alpha, r, \theta_1, \theta_2)\\ y(\theta_1) &= f_y(\alpha, r, \theta_1, \theta_2)\\ z(\theta_1) &= f_z(\alpha, r, \theta_1, \theta_2)\end{aligned} \qquad (15)$$

2.1.3. *Motion simulation for points D_1 and D*

The simulation was carried out for the following initial data: d = 160mm, r = 80 mm, α = 15° and α = 30°.
Point D_1

The results are presented in Figure 6a, for $\alpha = 15°$ and in Figure 6b for $\alpha = 30°$.

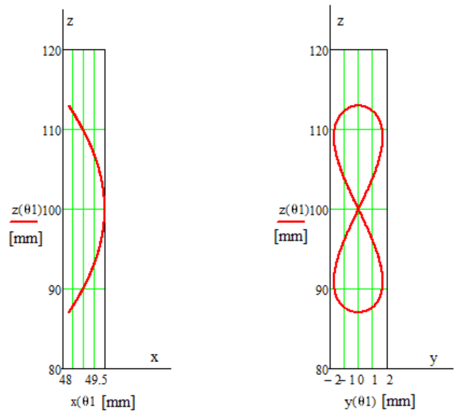

Figure 6a.

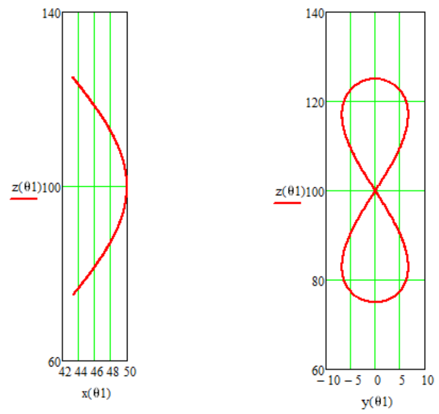

Figure 6b.

Point D

The trajectory of point D is a particular case of point D_1, the motion can be only in plane z_0y_0. The trajectory is a circle of radius r, z and by varying these parameters like in for the point D1 and y will have the values of x from point D1. In plane x_0z_0 the trajectory would be a line contained in plane z_0y_0.

The D_1 trajectories are characteristic to axial piston pumps in Figure 2a , to which all the joints between the disc and the bars have identical trajectories with point D1.

The trajectories of type D are seen in axial piston pumps presented in Figure 2b and are characteristic to the bars on CDF axis, Figure 2c. To these pumps the trajectory is modified from an arc (D) to octoid (D_1) for an apex angle of points D from 0 to π/2, starting from D and from the octoid (D_1) to an arc for an apex angle of π/2 to π (the point on axis CF opposed to D).

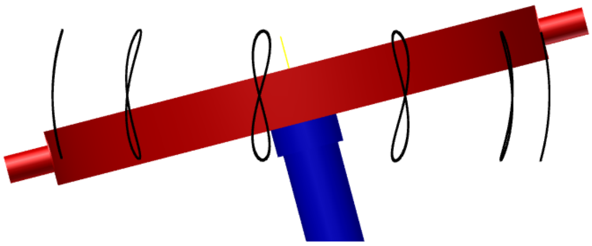

Figure 3.

2.1.4. *The Influence of the Parametres Over the Trajectory*

From equations (15) we can see that the trajectory depens on θ_1, θ_2, α, r, d. Having in mind that θ_1 is the varible and that $\theta_2 = f(\theta_1, \alpha)$ and d doesnţ influence the trajectory, but soleley defines its position in relation to the origin O_0, can be seen that the trajectory is influenced only by α and r. Increasing the angle α leads to the increase of the variation range of z, which in turn leads to the increase of the specific flow of the pump. The increase of angle α leads also to the increase of y which leads to a higher increase of the trajectory length with influence over the velocities of points D.

The increase of radius r has an effect on increasing the variation range of z, with an influence over the specific flow, and an increasing of the variation range of x, having an influence over the velocities of points D.

2.1.5. *Velocities Study for Points D_1, D*

By differentiating over time the equations (10) and (12) the equations of the angular velocities of ω_2 and ω_3 are obtained

$$\omega_2 = f_{2v}(\theta_1, \theta_2, \alpha, \omega_1)\,;\ \omega_3 = f_{3v}(\theta_1, \theta_2, \alpha, \omega_1) \quad (16)$$

By differentiating over time the equations (15) the equations of the velocities components by the x, y, z axes are obtained

$$\begin{aligned} v_x &= f_{xv}(\alpha, r, \theta_1, \theta_2, \omega_1, \omega_2) \\ v_y &= f_{yv}(\alpha, r, \theta_1, \theta_2, \omega_1, \omega_2) \\ v_z &= f_{zv}(\alpha, r, \theta_1, \theta_2, \omega_1, \omega_2) \end{aligned} \quad (17)$$

2.1.6. *Accelerations Study for Points D_1, D*

By differentiating over time the equations (16) and (17) the equations of the angular accelerations of ε_2 and ε_3, and also the equations of the accelerations components by a_x, a_y, a_z axes of points D.

2.2. Kinematics Study of Points E, Pistons' Joints

2.2.1. *Modelling*

The kinematics study of the pistons, points E, Figure 8, is carried out through the closed contours method, which in this case is simpler to apply than other methods, having in mind that the kinematics of point D is already.

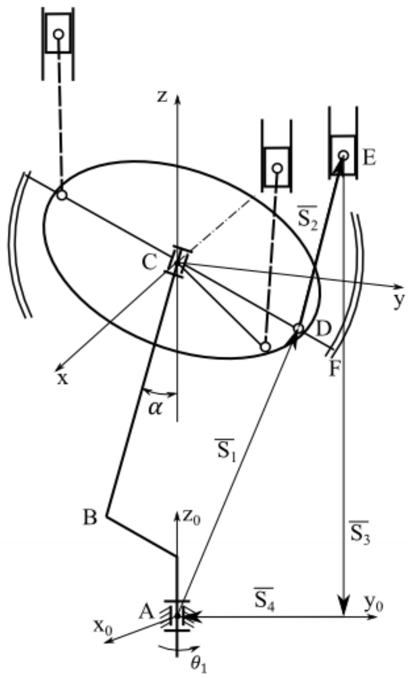

Figure 8.

For the vector $\overline{s}_i$ in Figure 8 we have the condition

$$\sum_{i=1}^{4} \overline{s}_i = 0 \quad (18)$$

In this vector equation there are 2 unknowns, direction of the vector $\overline{s}_2$, and the magnitude of the vector $\overline{s}_3$, so the system is uniquely determined.

By projecting the system (18) on the axes of reference frame $O_0x_0y_0z_0$ and solving the system, the ordinate $z_E = f(\theta_1, \alpha)$, is determined, the position of point E along he axis of the piston.

By successive differentiations over time of the equations zE, the equations of velocities and accelerations of point E, vE and respectively aE are obtained.

2.2.2. *Simulation and kinematic diagrams*

The simulation was carried out using the following parameters: α = 15°, θ_1 = 0 2π; d = 100mm; r = 40mm; DE = 50mm.

The diagram of the **pistons displacements** is presented in Figure 9.

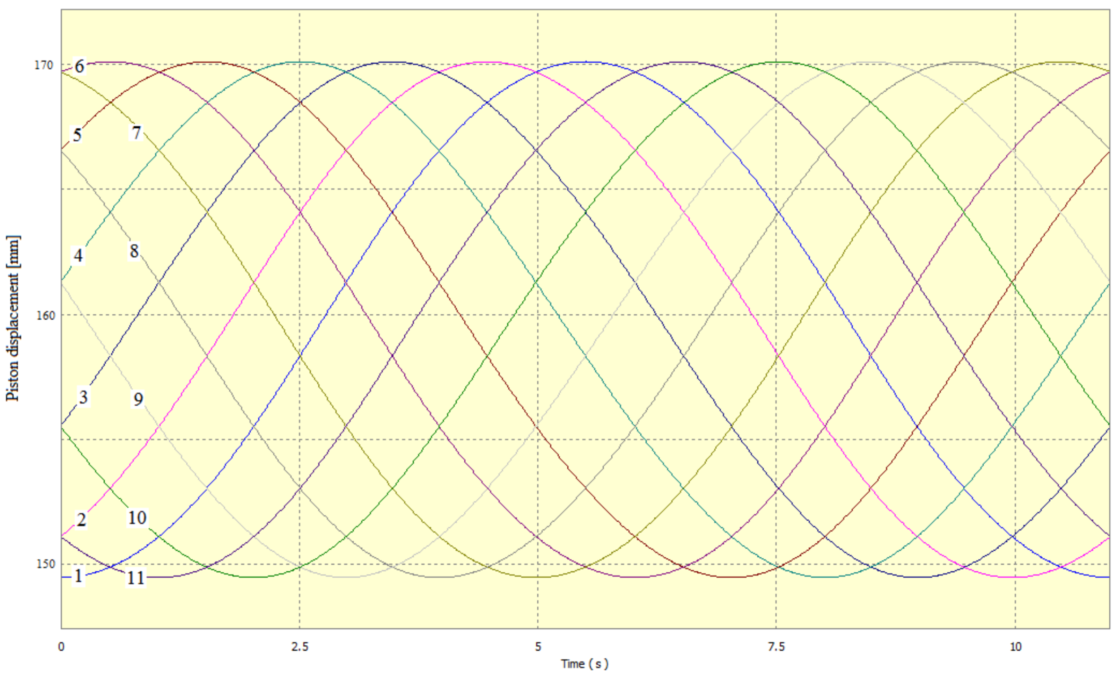

Figure 9.

The diagrams are presented for type tip a) pumps, Figure 2. Variation range of the space is constant for all the pistons, as can be seen in Figure 9 and that, along with the pistons radius give the displacement of the pump. For type b) pumps, Figure 2, the variation range is the same as for type a a), so the displacement is the same. The small differences that appear in the variation of the diagrams is not influencing the pump's working.

In Figure 10 are presented the **velocities** of the 11 pistons in case of type a), Figure 2 for the following kinematic parameters: $\omega_1 = 62{,}8\ rad/s$;($t_{ciclu} = 0{,}1$ s). As it can be seen for all the pistons the maximum value for the top dead position is the same, the resulting velocity being quasi-constant, and so the pumps flow. The unevenness degree is $\delta \approx 4\%$. if the number of pistons is increasing, for the same radius r, δ decreases and vice versa.

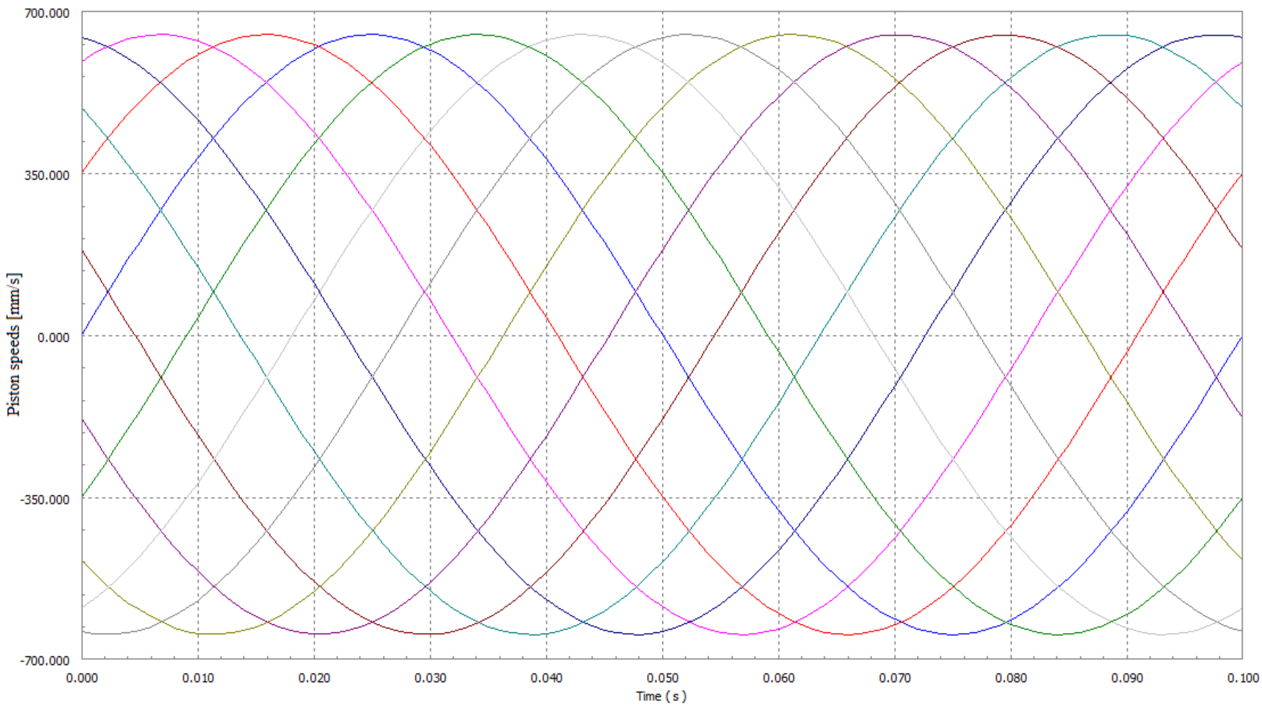

Figure 10.

In Figure 12 the velocities diagrams are presented for the type *b)* pumps, Figure 2. In this case the unevenness is higher than for type a pumps. The unevenness degree is $\delta \approx 10\%$. The velocity difference is due to the differences in pistons' displacements (3.1.3, Figure 7) for the same amount of time.

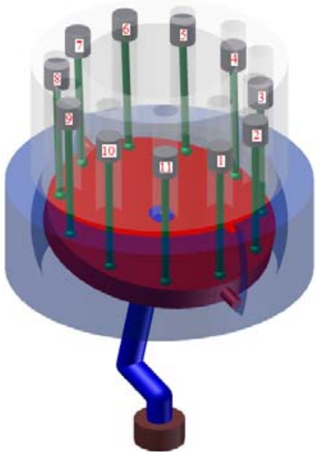

Figure 11.

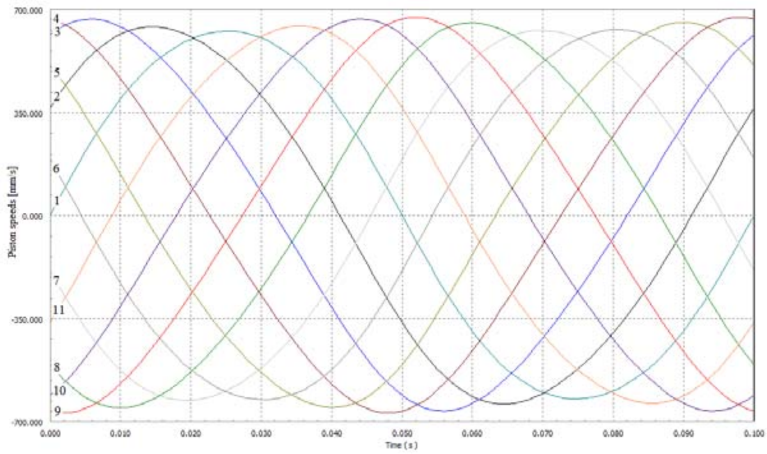

Figure 12.

The acceleration diagrams for type b) piston pumps are presented in Figure 12, ε = 628 rad/s2, tcicly = 0,1s

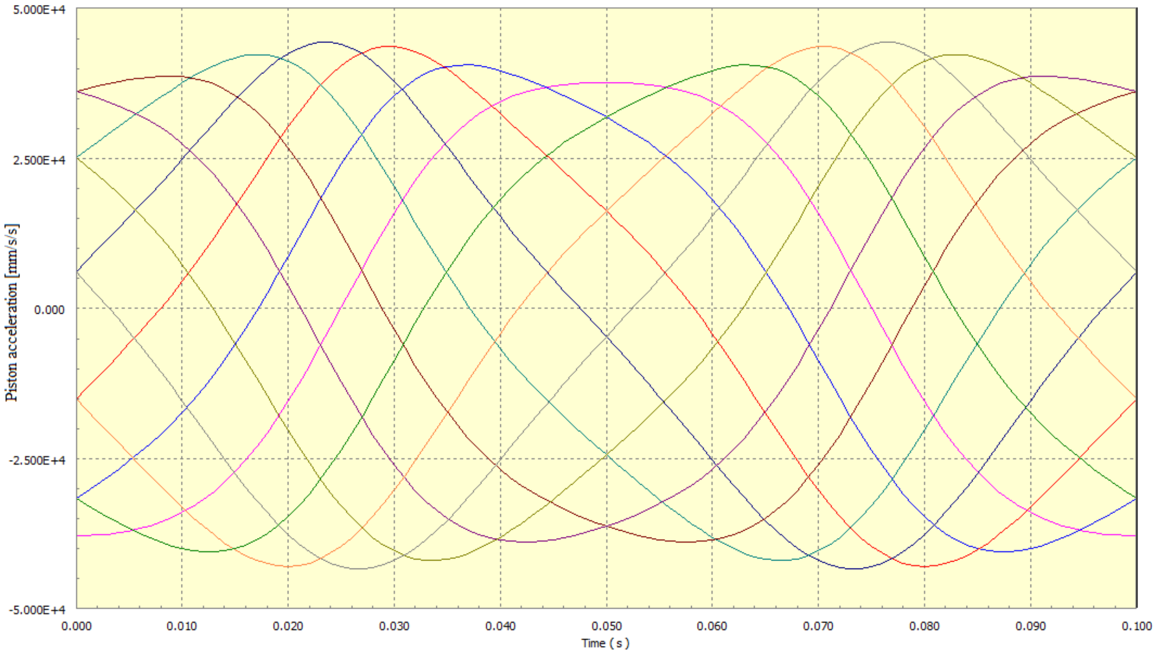

Figure 13.

REFERENCES

[1] Adrian Bruja, Marian Dima Studiul cinematicii mecanismelor convertizoarelor hidrostatice cu ajutorul calculatorului.. Al VI-lea Simpozion Internaţional IFToMM, vol IV, pag. 9-16, 1-5 iunie 1993. Bucureşti.

[2] Michel Casin, Jeanine Metge –Mecanique de la robotique. Dunod,1989

[3] Denavit J. and Hartenberg R. S., 1955, “A Kinematic Notation for Lower-Pair Mechanisms Based on Matrices,” Journal of Applied Mechanics, pp. 215-221.

[4] Fischer, I.S., ‘‘Numerical analysis of displacements in spatial mechanisms with ball joints,’’ Mechanism and Machine Theory, Vol. 35, pp. 1623–1640, 2000.

[5] Richard S. Hartenberg, Jacques Denavit – Kinematic synthesis of linkages. McGraw Hill, 1964

[6] Raghavan M. and Roth B., 1993, "Inverse Kinematics of the General 6R Manipulator and Related Linkages," Journal of Mechanical Design,Transactions of the ASME., Vol. 115, pp. 502-508.

[7] Anghel Raicu, Adrian Bruja. – Mecanisme. UTCB, 1996.

[8] Siciliano, B., s.a. – Robotics. Modelling, Planning and Control, Springer, 2009.

[9] Wolfram Stadler -Analytical robotics and mechatronics.McGraw-Hill 1995.

Definition Rational Gate Frame Size Distribution Unit Double Piston Concrete Pump With Hydraulic Drive

Inga A. Emeliyanova [1*], A. A. Zadorozhny[1], D. V. Legeyda [1], N. A. Melencov [2]
[1] National construction and architectures university of Harkov, Harkov (Ukraine)
[2] *OOO "Stalikonstrukciya" Harkov (Ukraine)*

Analysed the existing design of substations concrete pumps with hydraulic drive. A new design of gate node concrete pump. Models of movement viscoplastic fluids. The conditions for building a model of the motion of the concrete mix in the pipeline. A scheme for calculating the structural and technological parameters of gate distribution unit with a V-shaped channel concrete pump.

Keywords: Viscoplastic environment, Rheology model, Hydraulic concrete pump

1. INTRODUCTION

Transport of concrete mixtures to construction site where work is done, by rule is achieved by double-piston hydraulic concrete pumps and concrete auto-pumps. Depending on maximum size of aggregate grain, concrete pumps performance, cross section of transportation pipeline, the working cylinders will be different and by that also the constructive solution of slide rule splitting frame.

Process of charging the hydraulic concrete pumps while transporting the concrete mixture by pipeline, from the point of saving its original characteristics after the mixing, is always an actual problematics.

Existing constructive solutions of distributional device of modern concrete pumps are especially interesting. Thus, distributional device in the shape of letter S (Figure 1) [1] - is the most common type of working organ of concrete pump.

Pistons of concrete pump cylinders move in opposite phases related to each other. One of them sucks the concrete mixture into the working cylinder from the receiving hopper, and the other pushes it through the distributional device shaped as S, which is in the shape of return pipe for concrete transport.

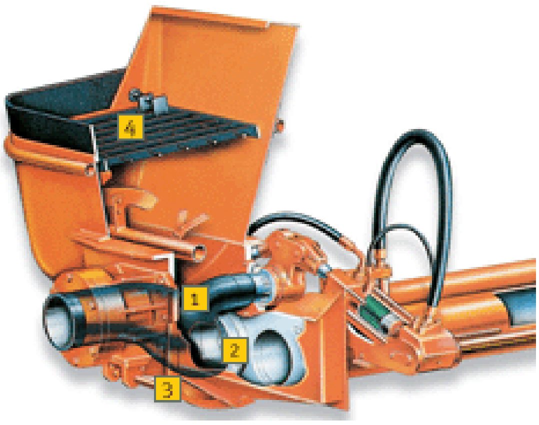

Figure 1: Working organ with distributor in S shape – firm CIFA (Italy)

1 - slide rule in S shape; 2- wear compensation ring; 3- drain hole with limit switch; 4- receiving hopper with mixer

S shaped slide rule is guided by the side-mounted small hydro-cylinders whose one end is connected to the cylinder for transport of mixture, and the other one is articulated with the tube for transport of concrete.

Between the cylinders'ends of concrete pump and distributor with S – nozzle the slide rule rings are set, made of high quality steel, as well as the so called wear compensation rings.

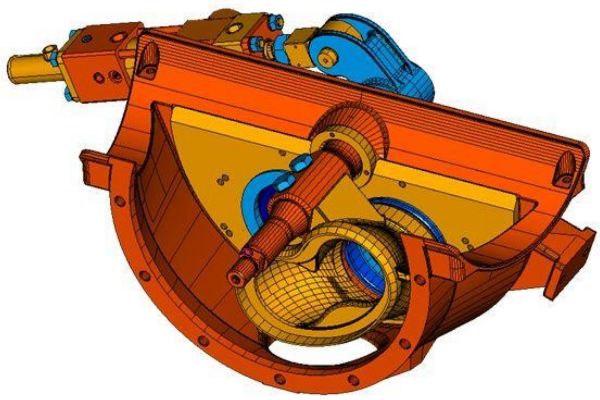

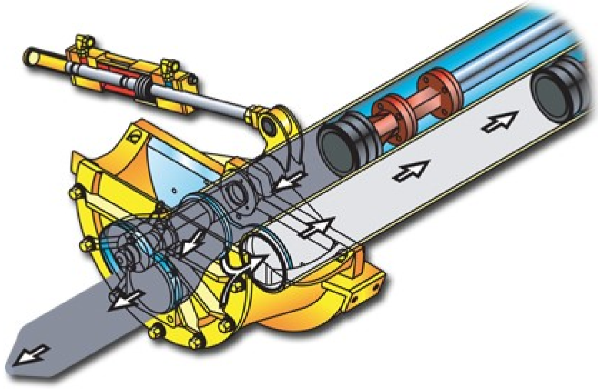

Figure 2: Working organ with rock-slide rule, firm «Schwing» (USA)

*Corresponding author: National construction and architectures university of Harkov and gonch@kstuca.kharkov.ua

Slide rule thickness varies, which contributes its almost complete wear protection. Lower slide rule part is stiffened by ribs that prevent cumulation of material deposit and easy flow of large particles.

Wear compensation ring is set between the slide rule ring and the distribution device that works in authomatic mode. So, the problem of slide rule ring's thickness is eliminated, because after its wear, it is moved forward by compensation ring, in which way the need for constant regulation of this frame is eliminated.

Rock-slide rule (Figure 2), (firm «Schwing», USA) [2] represents a hollow truncated equilateral cup – "smashed" on one side in the middle by horizontal plane.

Undeformed end of rock-slide rule alternately conveys concrete mixture to hydraulic system toward the working cylinders' ends. Each of two „smashed"ends is firmly leaned to the back wall of concrete transport tube that has stiffening-ribs for strong (direct) contact with concrete transport pipeline.

Slide rule that is made in C shape (Figure 3) constructively differs to distribution slide rule shaped in S (Figure 1). It is produced as a separate series of the firm Putzmeister AG (Germany) [3].

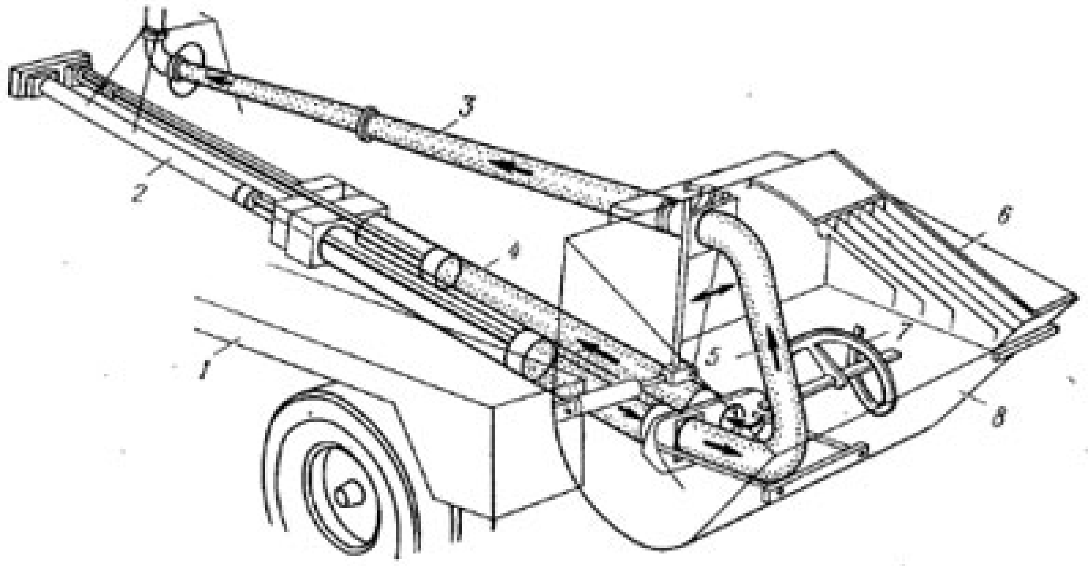

Figure 3: Concrete pump with C slide rule, Firm Putzmeister AG (Germany): 1-vehicle chassis; 2- hydrocylinder; 3- concrete transport tube; 4- working cylinder; 5- C slide rule; 6- grid; 7- smasher; 8- receiving hopper

Articular slide rule (Figure 4) has the shape of a tube whose one end alternately connects to transport cylinders and the other one is articulated with concrete transport tube [4].

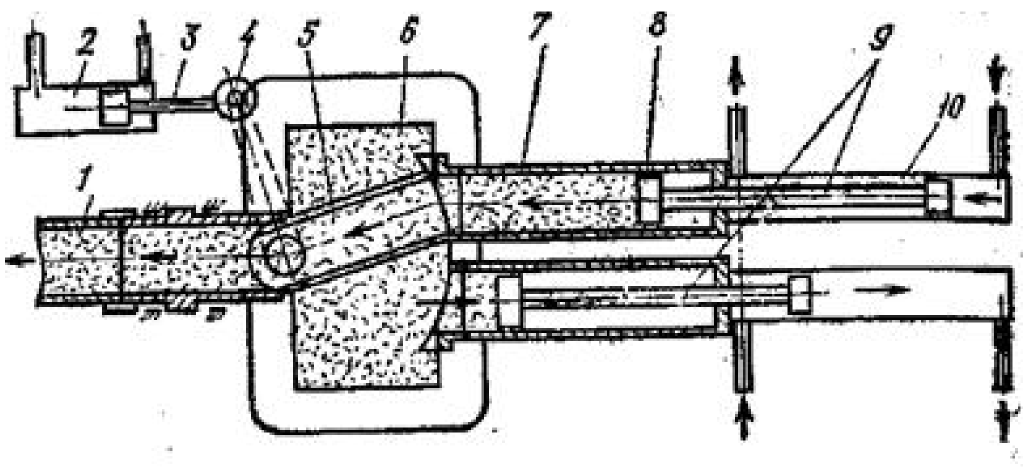

Figure 4: Scheme of concrete pump with articulated slide rule

1- concrete transport tube; 2- hydrocylinder; 3- piston rod; 4- articulated slide rule's swivel arm; 5- articulated slide rule; 6- hopper; 7- working cylinder; 8- working piston; 9- working cylinders' piston rods; 10- hydrocylinder

Dispensing slide rule shaped as a lock that is slanting (Figure 5), is a product of Chinese company Sani. Such slide rule is set on a stationary concrete pump Operation principle of such dispensing slide rule is achieved by additional periodical forced moving of concrete mixture by worm mixer with vanes from receiving hopper into doser for dispensing with a lock.

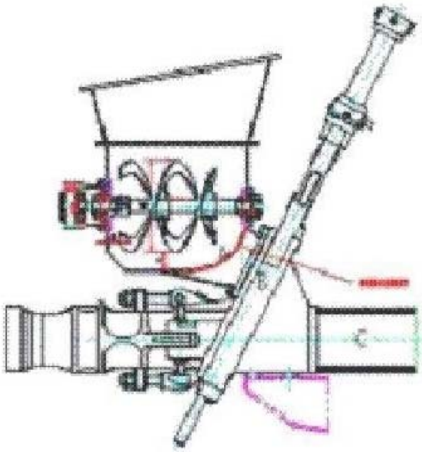

Figure 5: Principle scheme of concrete pump by Chinese company Sani with slanting slide rule for dispensing and with forced charging

On the base of analysis of existing concrete pumps constructions, with the aim of improving the concrete pumps productivity on account of reducing the stoppage during repairs and shortening the time of technical servicing, a new simplified constructive solution of hydraulic slide rule distribution frame has been elaborated, at the Department for Mechanization of Construction Processes on Harkov National University of Construction and Architecture.

Feature of new construction is the position of slide rule distribution frame (Figure 6). Distribution frame is set between the receiving hopper and working cylinders. Such solution has a channel shaped as V and has a possibility of shifting horizontally in relation to central axis of dispensing pipe [6].

Proposed constructive solution of concrete pump is patented and is currently produced in the company OOO" Стальконструкция " Harkov.

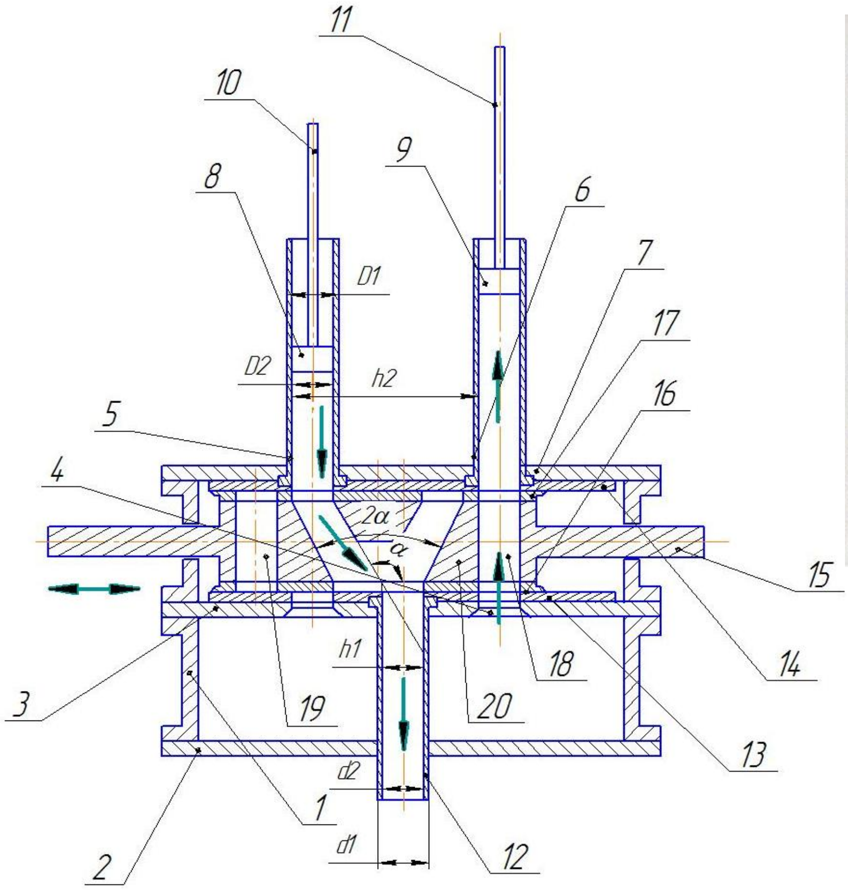

Figure 6: Principle scheme of mixture's moving through channel V, of hydraulic concrete pump's slide rule distribution frame

Concrete pump includes the receiving hopper's body 1 with frontal plate 2 and transient plate of pump's body 3, with holes 4. First working cylinder 5 and second working cylinder 6, are placed on the flange with holes on rear edge of concrete pump's body 7. In first and second working cylinder pistons move 8 and 9 with piston rods 10 i 11. Output flow tube 12 is placed on the flange in the central part of transient plate 3 of pump's body for concrete that comes out of the holes on frontal plate 2 of receiving hopper of pump's body and leans on the frontal part of slide rule plate 13.

Between front and rear slide rule plate 14, along the guide 15 in horizontal direction moves the distribution frame whose channel is in shape V 20 with two holes 18 and 19, which are placed on the rings' ends 16 and 17.

Since the concrete mixture is of medium viscosity, its moving along the pipeline is realised after coping with an initial friction force. Mechanical behaviour of concrete mixture and character of mass conveyance process are characterized by very specific features which have to be taken into consideration while making models of transport working processes.

For model development of mentioned process we should consider the results of researches made by З. П. Шульман [7,8]. In them the proposed model came out from widely applied rheological stiff-plastic viscous models, which has summarized most of the classical equations of rheological fluids:

$$\tau_{ij} = 2 \cdot \left[\frac{\tau_0^{1/n}}{A^{1/m}} + \mu^{1/m} \right] A^{n/m - 1} \cdot \dot{e}_{ij} . \quad (1)$$

here is:

$$A^2 = 2 \cdot \left(\frac{du}{dx}\right)^2 + 2 \cdot \left(\frac{dv}{dy}\right)^2 + 2 \cdot \left(\frac{dw}{dz}\right)^2 + \left(\frac{dv}{dx} + \frac{du}{dy}\right)^2 + \left(\frac{dv}{dz} + \frac{dw}{dy}\right)^2 + \left(\frac{du}{dz} + \frac{dw}{dx}\right)^2 \quad (2)$$

where τ_{ij} – load tensor components due to friction; $\dot{e}_{ij}$ – deformation rate tensor; $u(x,y,z)$, $v(x,y,z)$, $w(x,y,z)$ – concrete mixture particles movement components; (x,y,z) – spatial coordinates; A – deformation rate intensity; τ_0 – obtained mixture's movement tension; n – rheological parameter, m – plasticity parameter. Model (1) flexibly combines plastic and viscous properties of concrete mixture

Taking the concrete mixture's viscous-plastic environment, we should take into account that such mixtures are to be considered as fluids Swed-Bingham. Thereby the dynamic viscosity μ_p for viscous-plastic fluid should be considered as a shift rate function $(\dot{\gamma})$.

If we bring the concrete mixture into the one-dimensional flow, we should pay attention to the following models:

– Swed-Bingham;

$$\tau = \tau_0 + \mu_p \cdot \dot{\gamma}. \quad (3)$$

– Shullman;

$$\tau = [\tau_0^{\frac{1}{n}} + (\mu_p \cdot \dot{\gamma})^{\frac{1}{m}}]^n . \quad (4)$$

Thereby, in calculation-construction and engineering practice there is room for application of empirical curves of flow for cylindrical pipe conductors, related to one another by integral characteristics such as pressure and flow:

– for pipelines of round cross section [9,10];

$$\frac{\Delta P \cdot D}{4 \cdot L} = f\left(\frac{8 \cdot u}{D}\right) = f\left(\frac{4 \cdot Q}{\pi \cdot R^3}\right). \quad (5)$$

where ΔP – pressure (pressure difference); L – pipeline length and diameter ($D = 2R$); i – medium rate per volume loss of mixture flow Q, $u = \left(\frac{4 \cdot Q}{\pi \cdot R^2}\right)$.

Relation $\frac{8 \cdot u}{D}$ for concrete mixture as non-Newton fluid in pipeline of round cross section coincides with movement rate along the pipeline wall.

Finally, for model making for concrete mixture moving along the pipeline, that flows into the two cylinder concrete pump, considering the specific conditions as a base, physical-mechanical properties of mixture, we adopt the generalized model of non-linear viscous-plastic fluid (Z.P. Shullman model), which, after a series of transformations and model simplifications (1), gets the form:

$$\tau^{\frac{1}{n}} = \tau_0^{\frac{1}{n}} + (\mu \cdot \dot{\gamma})^{\frac{1}{n}} . \quad (6)$$

This model generalizes the most used models lately, which take the formerly mentioned values: Newton ($\tau_0 = 0$; $m = 0$), Sen-Venan, Swed-Bingham ($m = n = 1$), Bulkyi-Gershell (n=1), Browne, Ostwald-DeVilly ($\tau_0 = 0$), Keson (m=n=2) and others.

Based on the above mentioned, for determining the wall inclination angle α, for V shape channel (Figure 6) the calculation scheme is shown, which enables to determine the constructive measures of slide rule distribution frame (Figure 7) for the case when concrete mixture from working cylinder of concrete pump is directed to the output port.

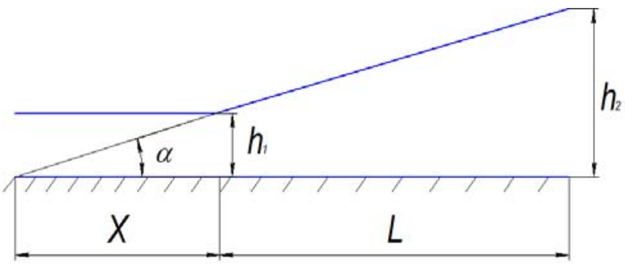

Figure 7: Calculation scheme of concrete mixture movement

h_1 – distance between the inclined walls of V shape channel and direction of conductor for concrete transport, h_2 – distance between the outer walls of working cylinders

For analysis of concrete mixture movement through the V shape slide rule channel we use the equations of motion continuity and motion quantity in cylindric coordinate system (r, θ, z).

$$\frac{1}{r} \cdot \frac{\delta}{\delta r} \cdot (r \cdot \vartheta_r) = 0 \leftrightarrow \vartheta_r = \frac{F_{(\theta)}}{r} . \quad (7)$$

$$\frac{\delta}{\delta r} = \frac{\mu}{r^2} \cdot \frac{\delta^2 \cdot \vartheta_r}{\delta \theta^2}; \ \frac{\delta p}{\delta \theta} = \frac{2\mu}{r} \cdot \frac{\delta \vartheta_r}{\delta \theta} . \quad (8)$$

After the equation differentiation (7) by θ, and the equation (8) by r, the equation system takes the following form:

$$\frac{\delta^2 p}{\delta r \cdot \delta \theta} = \frac{\mu}{r^2} \cdot \frac{\delta}{\delta \theta} \cdot \left(\frac{\delta^2 \cdot \vartheta_r}{\delta \theta^2}\right) = \frac{\mu}{r^2} \cdot \frac{\delta^3 \cdot \vartheta_r}{\delta \theta^3}, \quad (9)$$

$$\frac{\delta^2 p}{\delta \theta \cdot \delta r} = \frac{\delta}{\delta r} \cdot \left\{\frac{2\mu}{r} \cdot \frac{\delta \vartheta_r}{\delta \theta}\right\} = 2\mu \cdot \left\{-\frac{1}{r^2} \cdot \frac{\delta \vartheta_r}{\delta \theta} + \frac{1}{r} \cdot \frac{\delta^2 \vartheta_r}{\delta r \cdot \delta \theta}\right\}, \quad (10)$$

On the base of equalities of the equations' left sides (9) and (10) for concrete mixture's motion rate determination ϑ_r through the right branch of V channel, we can set the following differential equations:

$$\frac{\delta^3 \cdot \vartheta_r}{\delta \theta^3} + 2\frac{\delta \vartheta_r}{\delta \theta} - 2r \cdot \frac{\delta^2 \vartheta_r}{\delta r \cdot \delta \theta} = 0, \quad (11)$$

which we can consider for the following conditions:

$$\vartheta_r(r,\theta=\alpha)=\vartheta_r(r,\theta=-\alpha)=0$$

Volume loss of concrete mixture per channel’s width unit and pressure in V channel are defined as:

$$\tilde{Q}=\int_0^\alpha \vartheta_r\cdot r\cdot d\theta;\ \vartheta_r(r,\theta)= = \frac{\tilde{Q}}{r}\cdot\frac{\{\sin^2\alpha-\sin^2\theta\}}{\{\sin\alpha\cdot\cos\alpha-\alpha+2\alpha\cdot\sin^2\alpha\}} \quad (12)$$

$$p_{(r,\theta)}=p_0+\frac{\mu\cdot\tilde{Q}}{X^2}\cdot\frac{\{\cos^2\theta-\sin^2\theta\}\cdot\left\{\frac{X^2}{r^2}-1\right\}}{\{\sin\alpha\cdot\cos\alpha-\alpha+2\alpha\cdot\sin^2\alpha\}} \quad (13)$$

where p_0- is the pressure on the initial part of V channel (Figures 6, 7); X-even part’s length; θ - current angle in the cylindric coordinate system; 2α - channel’s opening angle.

Side walls’ slope of slide rule’s channel α is determined on the base of constructive parameters h_1, h_2, L (Figure 7).

$$tg\alpha_1=\frac{L+x}{h}. \quad (14)$$

Constructive dimensions of distribution slide rule frame with V channel for various diameters of working cylinders and of the output diameter of concrete transport pipeline are shown in table 1.

Table 1. Constructive dimensions of distribution slide rule frame with V channel for various diameters of working cylinders and of the output diameter of concrete transport pipeline

Working cylinder’s diameter with taking the wall thickness D_1, мм	Internal diameter of working cylinder D_2, мм	Concrete transport pipeline’s diameter with taking the wall thickness d_1, мм	Internal diameter of the concrete transport pipeline d_2, мм	α- saucer-shaped valve’s opening angle grade
120	100	120	100	128-130
144	125	120	100	121-125
180	150	120	100	123-125
210	180	120	100	125
250	220	120	100	123-125
310	250	120	100	124-125

In this way, dependencies (12) and (14) can be used for determining the given constructive dimensions of V shape channel, with taking its throughput capacity at working pressure of concrete pump, and start the designing of distribution slide rule device.

REFERENCES

[1] И. А. Емельянова, А.А. Задорожний, А.С. Непорожнев, Н.А. Меленцов. General classification of hydraulic concrete pumps, Scientific papers collection, Series: Sector engineering, machine construction., Vol. 1 (31) – Полтава: ПолтНТУ, 2012. – pp. 75 – 81, 2012 (in Ukrainian)
[2] Назаренко І. І. Machines for production of construction materials. – К.: КНУБА, – pp. 488, 1999 (in Ukrainian)
[3] Морозов М.К. Mechanical equipment of reinforced concrete factories- Kiev: High School.. pp. 311, 1986 (in Russian)
[4] Хаютин Ю.Г. Monolithic concrete: Technology of production works. –Strojizdat,. pp 447. 1981(in Russian)
[5] http://www.sanychina.ru/betononasos/gidravlika/
[6] Pat. 104755 Ukraine МРК (20.14.01) F04B 15/00 Concrete pump/ Емельянова И.А., Задорожний А.А., Непорожнев А.С., Меленцов Н.А.; Submitter and beneficiary Harkov National University of Construction and Architecture, registration 24 October 2011, publishing 25 April 2013, Бюл.№5.
[7] Емельянова И. А., Zadorožный А.А., Melencov N.A.. Preconditions for study of concrete mixtures transport process by double-piston hydraulic pump, Scientific papers collection, Series: Sector engineering, machine construction., Vol. №2 (30). – Poltava: PNTU, – pp. 23 – 24, 2011 (in Ukrainian).
[8] Емельянова И.А. Задорожный А. А., Меленцов Н.А. Analysis of concrete mixture motion through pipeline when using the double-piston concrete pumps in accordance with the model Swed-Bingham, Corpus of XIV International Scientific and Technical Conference: Applied Hydraulics and Pneumatics – Odessa: Вінниця” Globus-Pres, pp.121 – 122, 2013 (in Ukrainian).
[9] Емельянова И. А., Задорожный А. А., Меленцов Н.А. Defining the concrete pumps productivity, arising from the analysis of concrete mixture motion through pipeline, All Ukrainian scientific and technical magazine Applied Hydraulics and Pneumatics №4 –pp.8-9, 2012 (in Ukrainian) .
[10] И.А. Емельянова, А.А. Задорожный, Ю.В. Човнюк, Н.А. Меленцов Concrete pumps productivity dependence on transported construction mixture propoerties, Magazine Science in Central Russia - ГНУ ВНИИТИН Россельхозакадемия, pp. 9-15, 2013 (in Russian).

Mechanical Behaviour and Friction Evolution on Bolted Connections

Dario Croccolo[1]
[1]DIN Department of Industrial Engineering, Alma Mater Studiorum, Bologna (Italy)

Bolted connections are widely used to join mechanical and civil structures, which, usually, need to be adjusted or changed during their service life. Well-known mechanical applications are, for instance, the connections among the components assembled on front motorbike suspensions as well as the joints between the wheel hub and the wheel rim of vehicles or even bridge structures. Modern engineering materials used as bolts or substrates (for examples aluminium alloys, titanium alloys and composite materials), produce significant modifications to the mechanical behaviour of mated parts since the friction coefficients are subjected to a dramatic evolution both during and after the first tightening operation. This occurrence leads to a wrong estimation of the actual initial load applied to the screws and, as a consequence, to the connected parts. Furthermore an incorrect selection of bolts could be carried out due to the wrong estimation of actual stress field produced on bolt. In this paper the friction coefficient evolution and the mechanical behaviour of bolted joints have been deeply investigated in order to predict the stress field generated on the connected parts.

Keywords: Bolted connections, Friction coefficients, Mechanical behaviour

1. LOADS RELATIONSHIP ON BOLT CONNECTIONS

1.1. ISO geometry and loads equilibrium

In the case of a metric standard (ISO M) profile, the thread longitudinal section is an isosceles triangle with the thread angle β of the screw equal to 60°. According to the scheme of Fig. 1 it is, therefore, possible to relate the axial initial force F_i to the peripheral force F_p by means of the normal force F_N and of the friction force.

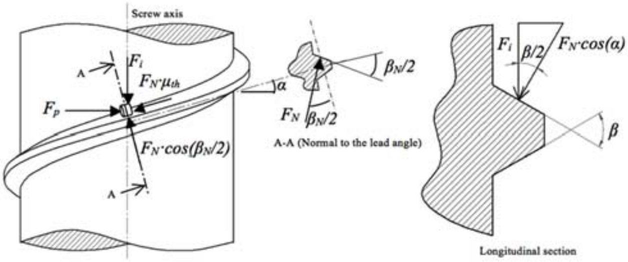

Figure 1: Triangular thread: geometry and equilibrium of forces

The loads equilibrium along the vertical and circumferential directions of screw, produce (1) in which the angle α is the lead angle, the angle β_N is thread angle evaluated on the normal section of the thread (section A-A of Fig. 1) and the T_{th} is the torque moment applied to the thread.

$$T_{th} = F_i \cdot \frac{d_m}{2} \cdot \left[\frac{cos(\frac{\beta_N}{2}) \cdot sin(\alpha) + \mu_{th} \cdot cos(\alpha)}{cos(\frac{\beta_N}{2}) \cdot cos(\alpha) - \mu_{th} \cdot sin(\alpha)} \right] \quad (1)$$

Since $tan(\alpha)=p/(\pi \cdot d_m)$, (1) can be rewritten into (2).

$$T_{th} = F_i \cdot \left[\frac{\frac{p}{2\cdot\pi} + \frac{\mu_{th}\cdot d_m}{2\cdot\cos(\frac{\beta_n}{2})}}{1 - \frac{\mu_{th}\cdot p}{\pi\cdot d_m\cdot\cos(\frac{\beta_n}{2})}} \right] \quad (2)$$

The relationship between β_N and β is expressed by (3) in which $d_m= d_2=d-0.64952p$.

$$\tan(\frac{\beta_n}{2}) = \tan\frac{\beta}{2} \cdot \cos(\alpha) = \tan\beta \cdot \cos\left(\arctan\frac{p}{\pi \cdot d_m}\right) \quad (3)$$

Equation (2) can be confidently approximated with very low errors into (4), which represents the actual relationship between the thread torque moment T_{th} and the initial load F_i for all the ISO screws.

$$T_{th} = F_i \cdot [0.159 \cdot p + 0.577 \cdot \mu_{th} \cdot d_2] \quad (4)$$

1.2. Total torque moment acting on the threaded connections

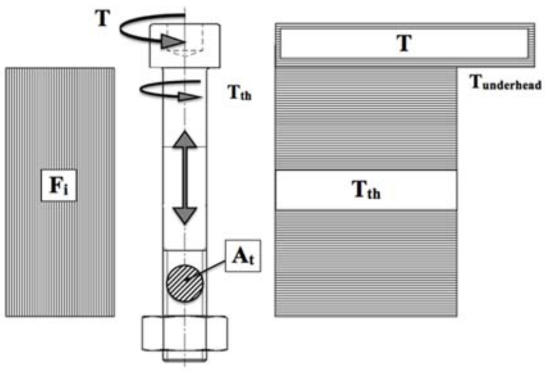

Figure 2: Load scheme (axial and torsional) acting on the screw during the tightening phase

The whole threaded connection and, more precisely, the bolt and the connected substrates, are involved by loads acting under the screw head that must be

*Corresponding author: DIN – Viale Risorgimento, 2 40136 Bologna and dario.croccolo@unibo.it

take into account in order to calculate the total torque moment T to be generated by the torque wrench. As well indicated in the Figure 2, a considerable part of torque ($T_{underhead}=T_u$ and part of T_{th}) is consumed by the friction loads generated between the mating parts (the thread, the screw head and the substrates). The relationship between the total torque moment T and the initial load F_i is expressed by (5) in which μ_u is the under-head friction coefficient and d_A is the average value of the screw head diameter.

Equation (5) represents the basic formula to be used in order to relate the torque moment T to the initial force F_i. The stress field generated on the bolt depend on the initial force F_i and on the thread torque moment T_{th}; both of them are strongly affected by the friction coefficient and by the value of the screw head diameter d_A. Especially in the case of high variation of coefficient of friction value, the (5) leads to high discrepancies in torque moment evaluation, provided that the F_i remains the same.

$$T = T_{th} + T_u = F_i \cdot [0.159 \cdot p + 0.577 \cdot \mu_{th} \cdot d_2 + 0.5 \cdot \mu_u \cdot d_A] \quad (5)$$

2. FRICTION COEFFICIENT EVOLUTION

As well indicated in (5), the tightening torque applied by the torque wrench, is mostly consumed in overcoming two friction components: the underhead component, generated by the sliding of the screw head on the flanges and the thread component generated by the sliding between the male and female threads. The residual torque component produces the fastener tension by generating the initial force. Inaccuracies in determining the friction values may lead to an overestimation or an underestimation of the bolted joint performances. The torque-load relationship is often simplified by using a constant K, known as *torque coefficient* or *nut factor*. The expression for the torque coefficient is reported in (6), where T *Nmm* is the input (total) tightening torque applied to the fastener, F_i *N* is the needed initial load and d *mm* is the nominal screw diameter following the ISO Standard.

$$T = K \cdot F_i \cdot d \quad (6)$$

In the case of screws, nuts and flanges made of steel an effective value of K is *0.20* as suggested in [1, 2]. The present value is proved to remain constant for all the ISO screws if the value of friction coefficient remains equal to *0.14*, but a large variation in K can be found if the friction coefficient changes. For this reason, some recent European Standards prescribe that the appropriate torque coefficient must be provided by the bolt manufacturer [3-5]. Bickford [6] indicates some mean values of the torque coefficient for various combinations of joint materials and surface conditions; however, the scatter is too great to provide a reliable and unique value, especially for critical joints and, furthermore, only steel screws are considered. The precise application of (6) is proposed by Motosh [7] and by VDI 2230 [8], but only in the case of bolt and substrates made of steel and in absence of lubrication between the mating parts the coefficients of friction μ_{th} and μ_u are, usually, considered to be equal to a unique value named μ_{tot}.

The effect of the variation of the coefficient of friction has been deeply investigated in [9-14]. In the case of an M8x1.25 bolt and of a mean value for friction coefficients $\mu_m=\mu_{tot}$ equal to 0.15, it is easy to verify that 88% of the total input torque T is consumed in overcoming the friction loads [11]. Despite the fact that the majority of bolted joints in mechanical and civil systems are still realised with steel screws and steel substrates, many kinds of lightweight materials have been recently adopted for screws and substrates construction [15, 16]. Since the use of threaded fasteners is considered worldwide to be an easy and simple way of joining components, sometimes designers do not take into account the changed boundary conditions, when replacing conventional steel screws and substrates with lightweight ones, or simply when replacing the surface finishing of bolted components. In [11] several failures occurred on clamped joints (Figure 3) due to the wrong estimation of friction coefficients have been examined. Two zinc plated steel screws acting on aluminium alloy have been investigated. The thread and the underhead regions could be anodized or spray-painted: the DOE methodology has been applied to determine reliable values for the friction coefficients (and therefore for initial loads estimation) involved in the joints, in order to avoid any type failures.

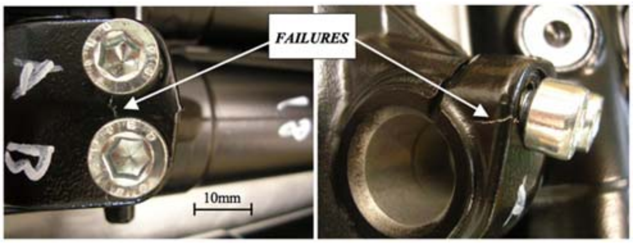

Figure 3: Failures occurred in clamped joints of a front motorbike suspension

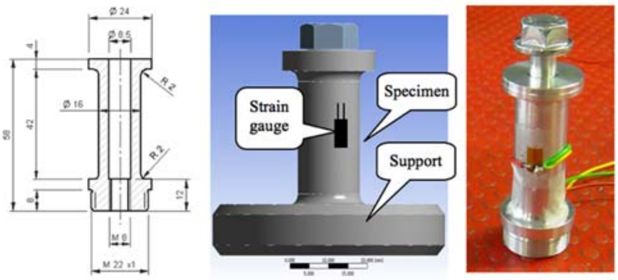

Figure 4: Specific specimens manufactured for retrieving the friction coefficients

Special specimens reported in Figure 4 have been specifically manufactured in order to retrieve the friction coefficients by applying (7). Equation (7) results from (5) adopting the same coefficient of friction for the thread and underhead sliding surfaces.

$$\mu_m = \mu_{tot} = \frac{\frac{T}{F_i} - 0.159 \cdot p}{0.577 \cdot d_2 + 0.5 \cdot d_A} \quad (7)$$

Figure 5: Torque wrench used for the esperimentation

The total torque T was obtained by a calibrated torque wrench illustrated in Figure 5, whereas the initial load F_i=F_V was evaluated by means of a strain gauge, located on the external surface of the specimen reported in Figure 4, which is able to provide the axial compression strain ε_C. The compression force F_C (8) acting on the specimen is equal, in magnitude, to the initial force acting on the screw, since the system works like springs connected in series during the tightening phase. The innovative specimens are cheaper and easier to use than the most common friction machinery, based on displacement transducers, load cells, rotary torque sensors or angle encoders and DC motors [14, 17]. Furthermore, it is possible to avoid the application of strain gauges on the bolt (difficult to perform in the case of nominal diameters lower than 12mm) in order to measure the actual initial force.

$$|F_C| = F_i = |\epsilon_C| \cdot E \cdot A_{eq} \qquad (8)$$

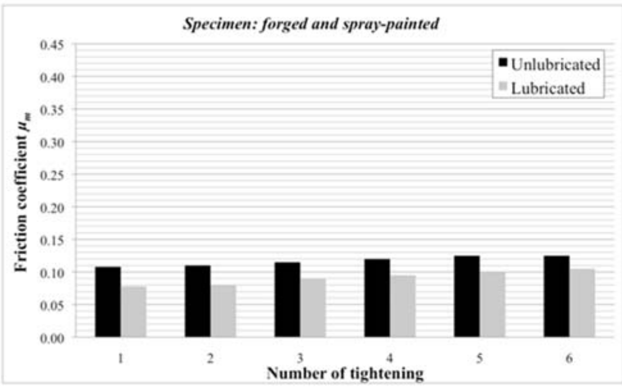

(a)

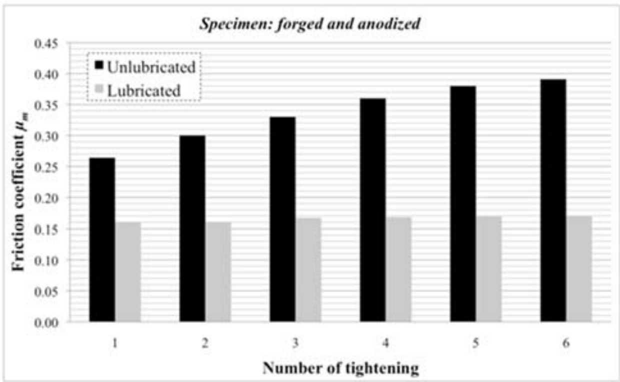

(b)

Figure 6: Bar diagrams of the friction coefficient μ_m for forged specimens ((a): spray-painted (b): anodized) in the case of tightening torque T=15Nm (different series for lubricated and unlubricated specimens)

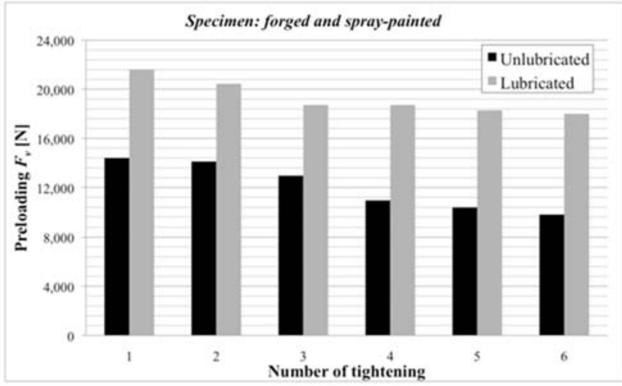

(a)

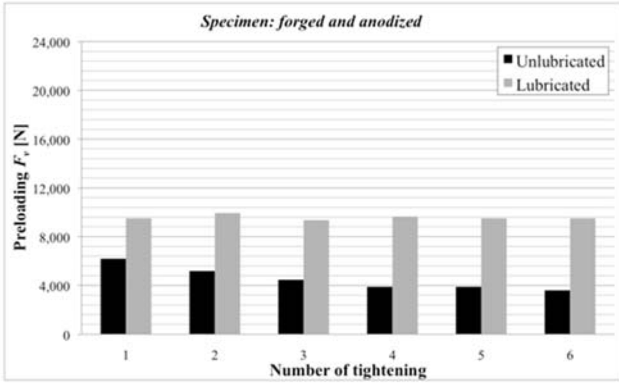

(b)

Figure 7: Bar diagrams of the initial load F_i for forged specimens ((a): spray-painted (b): anodized) in case of tightening torque T=15Nm (different series for lubricated and unlubricated specimens)

The results condensed and collected in the bar diagrams of Figures 6 and 7 have been obtained and analysed by applying the DOE method [18] and the Analysis of Variance (ANOVA) [18, 19].

It is evident that *spray-painted* specimens have the lower value of μ_m=μ_{tot} (the higher initial forces F_i=F_V). In the presence of unspoiled surfaces, the overall friction coefficient decreases from a value of *0.26* in the case of forged, anodized and unlubricated specimens to a value of *0.11* in the case of forged, spray-painted and unlubricated ones, so that the initial force doubles with the same tightening torque *T=15Nm*. Lubrication always increases the initial forces: in the presence of forged and unspoiled surfaces, the overall friction coefficient decreases from a value of *0.11* to *0.08* in the case of spray-painted specimens, and from a value of *0.26* to *0.16* in the case of anodized ones. Finally, considering the effect of the number of tightening and loosening (up to six maintenance operations in a standard lifecycle) the initial force is affected by the tightening replicas mainly in the case of unlubricated and anodized surfaces so that the F_i progressively decreases with the same tightening torque. As a matter of fact surfaces are subjected to wear and spoiling (Fig. 8) by increasing the number of tightening, while lubrication creates a sort of protective film. In the presence of spoiled surfaces, the overall friction coefficient increases from a value of *0.26* to *0.39* in the case of forged, anodized and unlubricated surfaces, whereas a value of *0.16* to *0.17* is observed in the case of forged, anodized and lubricated surfaces.

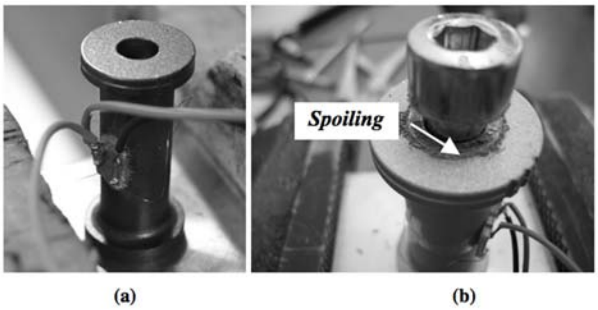

Figure 8: Spray-painted specimens (a): unspoiled surfaces (b): spoiled surfaces

The same outcomes have been observed by changing both bolt and substrate materials. For instance another experimentation has been conducted in the case of titanium screws connected to aluminium substrate in order to replicate the joint between the wheel rim and the wheel hub similar to the sketch reported in Fig. 9, which is a typical connection adopted for wheels of sport cars.

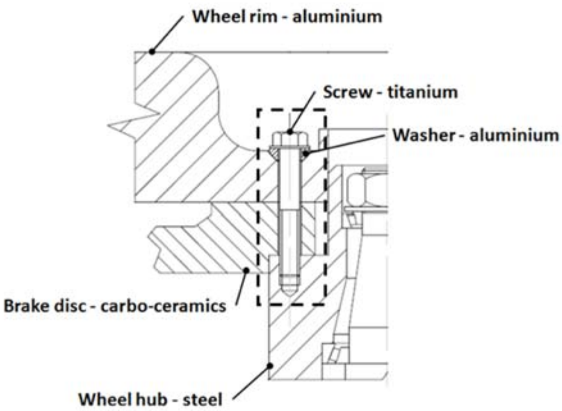

Figure 9: Car wheel assembly with titanium screw

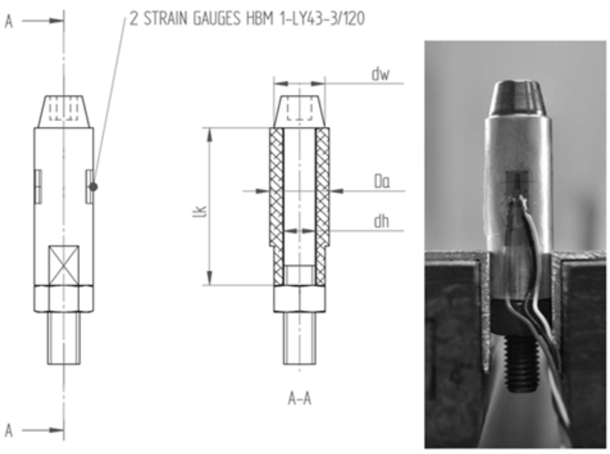

Figure 10: Specific specimens manufactured for retrieving the friction coefficients

In this case, since the investigation has been dedicated to analyse the friction coefficient evolution by changing the number of tightening and the type of lubricant, the specimens were designed and specifically manufactured in order to share the key parameters of the actual components involved in the wheel-rim joint.

The results of the present investigation are collected in the Figures 11, 12 and 13.

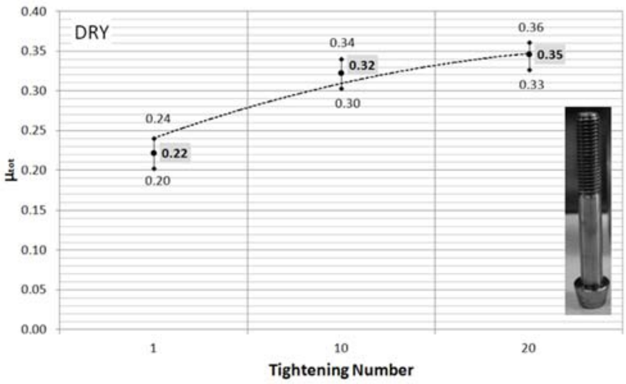

Figure 11: Friction coefficient μ_{tot} (mean, maximum and minimum values) versus tightening number for DRY surfaces

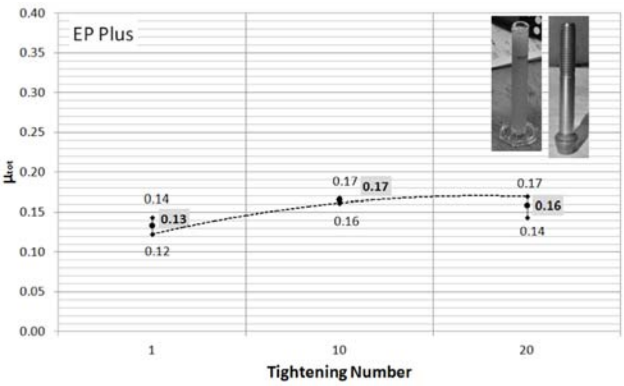

Figure 12: Friction coefficient μ_{tot} (mean, maximum and minimum values) versus tightening number for EP Plus oil lubricated surfaces

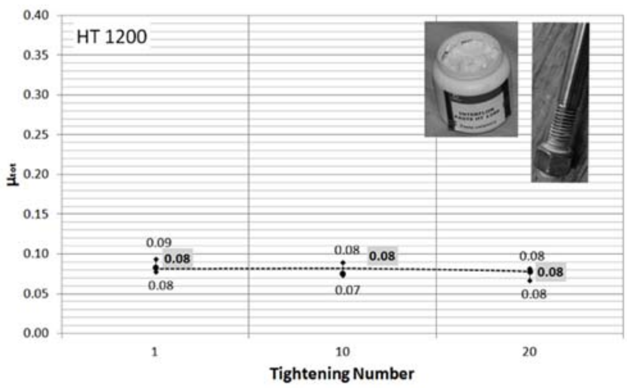

Figure 13: Friction coefficient μ_{tot} (mean, maximum and minimum values) versus tightening number for HT1200 paste lubricated surfaces

The important role played by lubrication in order to reduce and to control the evolution of the coefficients of friction, is extensively evident having a quick look at the results reported into the following diagrams. The lowest and most constant value, has been obtained when the HT1200 paste is applied, whereas in the case of dry surface, the highest value reached by the friction coefficient, produces an initial force notably lower than that predicted for the same torque moment. In some cases the high friction forces produced under the head of screws, lead to undesirable failures, which are well highlighted on the screw head reported in the Fig. 14.

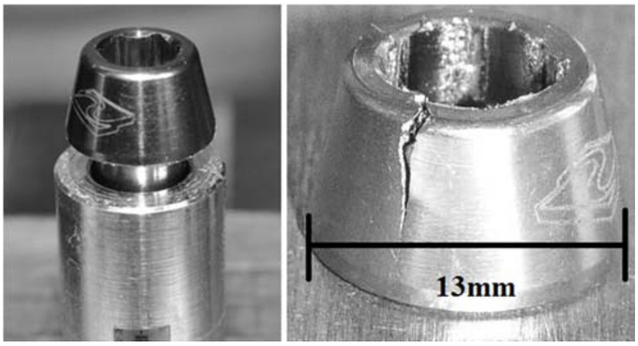

Figure 14: Titanium screw assembled on an aluminium test specimen (left) and failure of the hexagon socket head

The underhead coefficients of friction have been, also, analysed separately respect to the thread ones in order to point out the friction phenomena occurring during the tightening phase [20]. If friction is investigated, the characteristic values of pressure and sliding velocity are fundamental to be analysed. Fig. 15 shows an example of underhead contact parameters useful for the assessment of tribological behaviour. During the assembly phase the sliding velocity, with a linear radius-distribution, is generated by the rotation of the bolt or of the nut, which produce pressure inhomogeneities. Pressure peaks are generated both by detailed support geometry of components in contact and by the local stiffness of parts [21]. A rough approach evaluates the mean values of the present parameters (p_m, v_m and d_m), anyway by doing this some unusual situations can be pointed out especially in the case of different and innovative materials in contact.

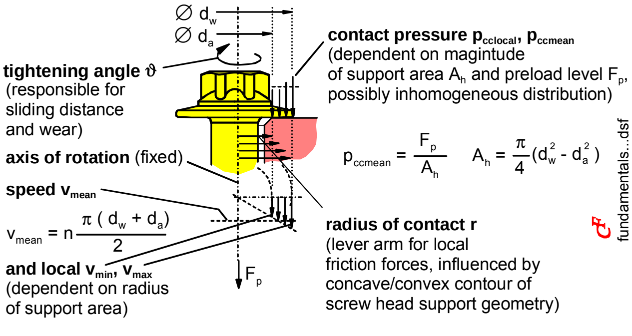

Figure 15: Key parameters for the tribological assessment of bolted joints at head support

For example if different materials for screws ((I) steel, (II) titanium and (III) aluminium) are coupled with different materials for substrates ((i) steel, (ii) aluminium, (iii) magnesium and (iv) CFRP) such as the samples reported in Fig. 16, some unusual outcomes, well highlighted by the diagrams of Fig. 17, can be observed and commented concerning the evolution of the friction coefficients.

The overall (μ_{tot}) friction coefficient trends, reported in Fig. 17, indicate a significant reduction in values when the torque and the initial load increase. The same behaviour has been observed for the underhead friction coefficients that have been separated by mean of the specific torque machine and tools used for the tests and reported in Fig. 18.

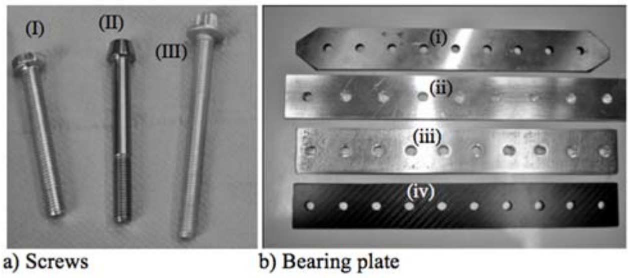

Figure 16: Screws and substrates types

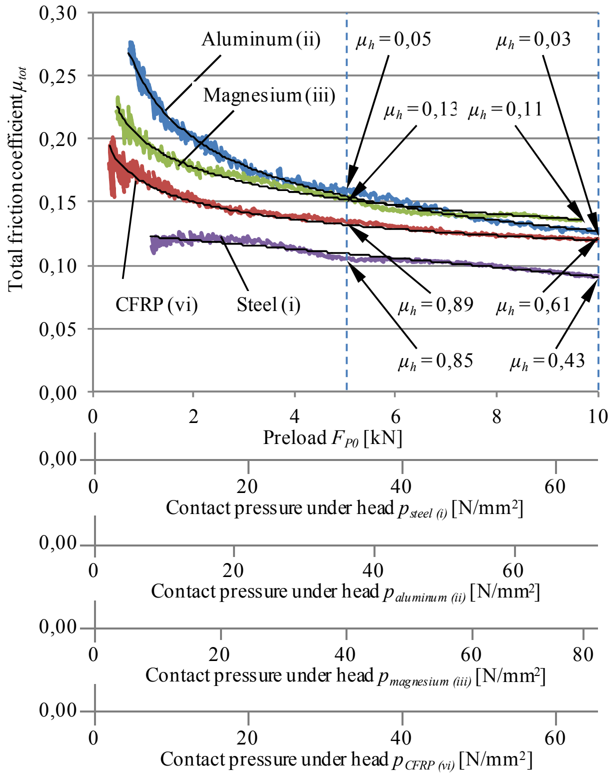

Figure 17: Total friction coefficient diagram for different substrates with aluminum screws unlubricated

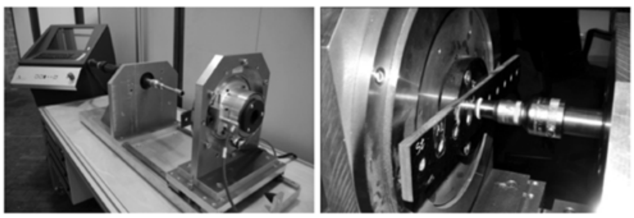

Figure 18: Multi channel testing tools and machine

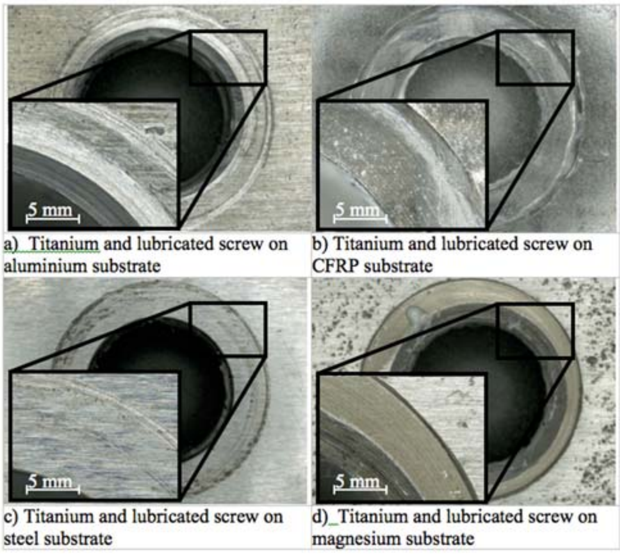

Figure 19: Sliding surface damage after fifth tightening procedures

Doubtless the values of friction coefficient cannot decrease so much and moreover they cannot be so high as those calculated, for instance, in the case of CFRP substrate (μ_h=0.89) with a so large variation during the tightening phase. Since the coefficient of friction values have been calculated by applying (7) and by relating the torque moment to the initial force, their evolution can be influenced by the variation of the pressure distribution and, accordingly, by the variation of the underhead mean diameter. As a matter of fact the sliding surfaces of different substrates assumed different aspects and geometric configurations after the damage due to five tightening operations, as well indicated in the pictures of Fig. 19. Even if it is, actually, important to know the value of friction coefficient corresponding to the torque moment or to initial load applied, the evolution or change of friction forces must be taken into account for the correct selection of bolts and for the stress definition of involved parts.

3. FRICTION COEFFICIENT IMPORTANCE FOR THE BOLT SELECTION AND STRENGTH

The correct definition of friction coefficient values of the actual connections is dramatically important for the bolt selection and strength [22]. Depending on the type of external loads (shear loads, bending moments and torque moments), the forces can be represented by the generic scheme reported in Fig. 20.

For a correct selection, the bolt must be clamped with an initial force F_i (9), which is able to guarantee the transmission of the aforementioned forces (as a general design rule the use of a safety factor is suggested to magnify the external loads). The tension load R_n can be directly equated with a part of F_i, whereas shear load R_t is transmitted via the friction developed among plates by assuming a coefficient of friction equal to μ_p and by applying the Coulomb law in order to relate R_t to F_i.

$$F_i = R_n + \frac{R_t}{\mu_p} \tag{9}$$

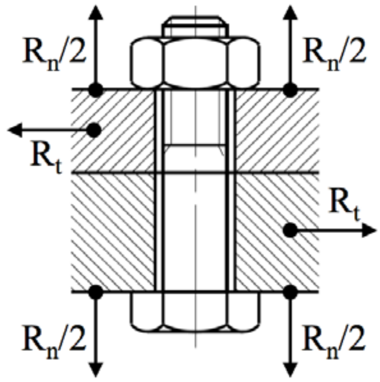

Figure 20: Forces acting on the bolt

The design methodology, which leads to the selection of an appropriate screw, must take into account the elastic behaviour of the bolt-plates system, in particular in presence of external tensile loads. The initial load (F_i) definition is only the first issue for the screw designers that must, then, guarantee the entire life service of joints: therefore the connections must support the initial load as well as the external loads, without producing any kind of failure during all the expected life of the product. For this reason, the attention has to be also dedicated to the study of working loads and failure modes. The well-known force-displacement diagram [6], reported in Fig. 21 is useful to assist this study.

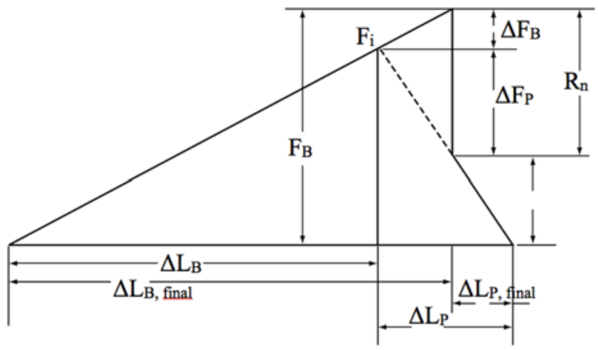

Figure 21: Force-displacement diagram

In brief, during the initial tightening phase the bolt (B) and the plates (P) share the same initial force F_i (the system works as series of springs), to which corresponds different variations in length due to different stiffness. Once the components are clamped, an external load parallel to the bolt axis (R_n), produces an increase of the tension (ΔF_B) acting on the bolt as well as a decrease of the pressure (ΔF_P) acting on the plates: the amounts of ΔF_B and ΔF_P are proportional to the total external load R_n depending on the stiffness of two components (the clamped members work as a parallel of springs because they share the same displacement). The accurate definition (10) of the maximum tensile load F_B acting on the screw is important in order to select the appropriate screw.

$$F_B = F_i + \Delta F_B = F_i + C \cdot R_n \qquad (10)$$

The dimensionless parameter C used in (10) and defined by (11) is called *load factor* and results as a function of bolt (K_B) and plates (K_P) stiffness.

$$C = \frac{K_B}{K_B + K_P} \qquad (11)$$

The calculation of the load factor performed via FEA, is well described in a paper by Cornwell [23] (see also [24-26]) for different materials and geometrical configurations: the main conclusion is that the load factor, for practical applications and in presence of different materials of plates, can be assumed in the range *0.1-0.45* for steel bolts.

The maximum static load acting on the bolt is, therefore, given by the combination of the previous (9) and (10) to obtain the following equation:

$$F_B = F_i + \Delta F_B = \left(R_n + \frac{R_t}{\mu_p}\right) + C \cdot R_n \qquad (12)$$

In addition to the maximum tensile force F_B, the torque moment T_{th} given by (4) acts on the screw body during the tightening phase.

According to the *Von Mises* yield criterion it is possible to calculate the equivalent axial load σ_{EQ} acting on the bolt (13): the axial stress σ_{ax} is equal to F_B/A_t whereas the maximum torsional (shear) stress τ_t is equal to T_{th}/W_t (the stress area A_t and the torsional modulus W_t are calculated using d_t diameter, equal to the average between the minimum d_3 and the mean d_2 diameters of the screw, ($d_t = d - 0.9382 \cdot p$).

$$\sigma_{EQ} = \sqrt{\sigma_{ax}^2 + 3 \cdot \tau_t^2} = \sqrt{\left(\frac{F_B}{A_t}\right)^2 + 3 \cdot \left(\frac{T_{th}}{W_t}\right)^2} = \sqrt{\left(\frac{4 \cdot F_B}{\pi \cdot d_t^2}\right)^2 + 3 \cdot \left(\frac{16 \cdot T_{th}}{\pi \cdot d_t^3}\right)^2} =$$
$$\sqrt{\left[\frac{R_t}{\mu_p} + R_n \cdot (1 + C)\right]^2 + 48 \cdot \left[\left(\frac{R_t}{\mu_p} + R_n\right) \cdot \left(\frac{0.159 \cdot p + 0.577 \cdot \mu_t \cdot d_2}{d_t}\right)\right]^2} \cdot \frac{1}{A_t} = \frac{F_{EQ}}{A_t} \qquad (13)$$

The equivalent axial load depends both on the assembly conditions (initial force and thread coefficient of friction), and on the service conditions (load factor and external loads). In order to select the appropriate screw it is necessary to verify that σ_{EQ} results lower than the Yield point of material $\sigma_{p0.2}$ or lower than the stress under proof load S_p ($S_p \approx 0.9 \cdot \sigma_{p0.2}$ according to ISO898). σ_{EQ} depends on (i) the external loads R_t and R_n, (ii) the thread friction coefficient (μ_t) and the plate friction coefficient (μ_P), (iii) the load factor C, and (iv) the bolt dimensions (p, d_2 and d_t): therefore, in order to select the bolt, it is necessary to know the bolt dimensions as well, so that the right choice needs at least one iteration. For this reason, according to EC3 [27] (13) can be simplified into (14) in the case of steel plates considered much more rigid then the bolt ($C \approx 0$) and assuming a standard value of thread coefficient of friction $\mu_t = 0.15$.

$$\sigma_{EQ} = 1.3 \cdot \frac{F_i}{A_t} = 1.3 \cdot \sigma_i \qquad (14)$$

At this point an interesting issue could be to analyse the trend of the stress ratio $SR = \sigma_{EQ}/\sigma_i$ as a function of the following parameters:

- The bolt nominal diameter (M6…M24);
- The coefficient of friction between plates μ_p (0.1…1);
- The thread coefficient of friction μ_t (0.1…1);
- The load factor C (0, 0.25, 0.5 and 0.75);
- The value of R_t and R_n.

As a matter of fact during the tightening phase C parameter is equal to 0 so that (13) results equal to (15).

$$\sigma_{EQ} = \sqrt{1 + 48 \cdot \left(\frac{0.159 \cdot p + 0.577 \cdot \mu_t \cdot d_2}{d_t}\right)^2} \cdot \frac{\left(\frac{R_t}{\mu_p} + R_n\right)}{A_t}$$
$$\sigma_{EQ} = SR \cdot \frac{\left(\frac{R_t}{\mu_p} + R_n\right)}{A_t} = SR \cdot \frac{F_i}{A_t} = SR \cdot \sigma_i \qquad (15)$$

The trend of SR as a function of the bolt dimension has been analysed, by changing the ratio between R_t and R_n and by fixing the value of the friction coefficients ($\mu_p = 0.2$ and $\mu_t = 0.15$). SR values, reported in Fig. 22, are within 1.32 (M6) and 1.26 (M24) values for all the analysed dimensions, whatever are the values of R_t and R_n: therefore the bolt dimension does not affect the SR value sensibly with discrepancies within 5%.

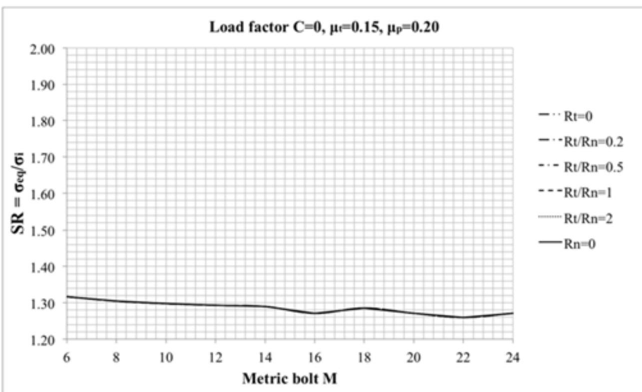

Figure 22: SR as a function of the bolt size for different values of R_t/R_n

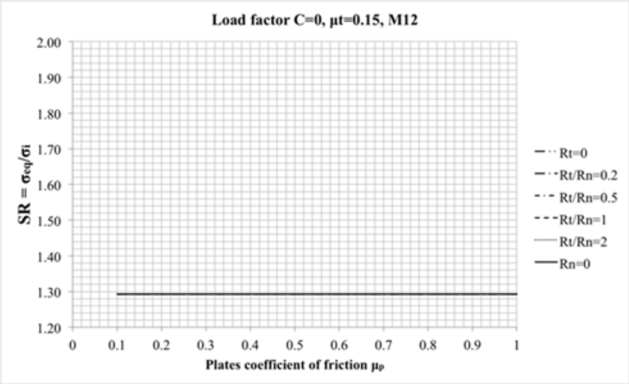

Figure 23: SR as a function of μ_p for different values of R_t/R_n

Since the bolt dimension does not affect significantly the value of the *SR*, it is possible to select a bolt size (for instance M12) and to analyse the variation of *SR* as a function of the coefficient of friction between the plates, by changing the ratio between R_t and R_n, for a fixed value of the thread coefficient of friction ($\mu_t=0.15$). In this case the value of *SR* is constantly equal to 1.3 as well indicated in Fig. 23.

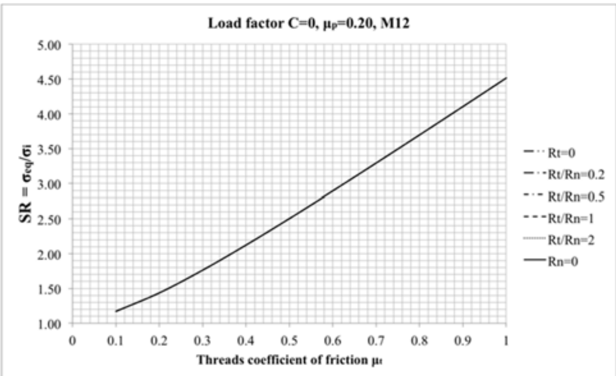

Figure 24: SR as a function of μ_t for different values of R_t/R_n

In the case of variation of μ_t the *SR* value dramatically changes as shown in Fig. 24 so that the value of 1.3 could be no longer valid to assure the right selection of bolts. Whatever are the values of R_t and R_n, *SR* increases almost linearly with the thread coefficient of friction. *SR* always exceeds the value of 2 starting from thread friction coefficients values within 0.3 and 0.4 since the torsional contribution assumes a predominant role. It is important to highlight that the use of lubricated screws produces low values of coefficient of friction almost in every conditions, also in replicated tightening operations as well demonstrated in [11-13]: the values are always lower than 0.17.

4. CONCLUSION

The mechanical behaviour of bolted joints is strongly affected by the friction coefficients evolution. The possibility and capability to control the coefficient of friction values during the tightening operations is strategically important for the right selection of bolts especially in the case of modern connections in which are used innovative materials both for the bolts and for the substrates.

Unfortunately, the evolution of friction coefficient values, is strongly dependent on the lubrication conditions, on the number of tightening and on the initial load values.

The addition of lubricants before the first tightening operation is able to keep constantly low the mean values of coefficient of friction throughout the whole number of tightening.

The simplified formulae proposed by several authors as an effective and easy way of calculating and selecting the bolts, are no longer valid in the case of high values of coefficient of friction.

For the correct definition and calculation of threaded connections it is necessary to apply the whole formulation or equations, painting attention to the evolution of the coefficient of friction during the whole life cycle of bolted connections.

NOMENCLATURE

A_{eq}	Cylindrical equivalent section mm^2
A_t	Screw tensile stress area mm^2
d_2	Pitch (mean) diameter of the thread, d_2=d-0.649·p mm
d_3	Core (minor) diameter of the thread, d_3=d-1.227·p mm
d_t	Stress diameter of the thread, d_t=d-0.938·P mm
p	Thread pitch mm
E	Young's modulus MPa
ν	Poisson's ratio
$\sigma_{p0.2}$	Yield point MPa
S_p	Proof stress MPa
F_i, F_B	Initial load N
K	Torque coefficient
ΔF_B	Increase of tension on the bolt N
ΔF_P	Decrease of tension on the plates N
C	Load factor
R_n	Normal force N
R_t	Shear force N
K_b	Bolt stiffness N/mm
K_p	Plates stiffness N/mm
T	Total torque Nm
T_{th}	Thread torque Nm
ε_C	Axial strain
W_t	Torsion modulus for circular section mm^3
α	Thread lead angle
β	Thread angle on the longitudinal section of the screw
β_N	Thread angle on the section normal to the lead angle
μ_{th}, μ_t	Coefficient of friction between threads
μ_u	Coefficient of friction underhead
μ_{tot}	Global oefficient of friction
σ_{ax}	Axial initial stress related to F_i MPa
σ_{EQ}	Equivalent Von Mises stress acting on the screw shank during the tightening MPa
τ	Shear stress related to T_{th} MPa
SR	Stress ratio

.

REFERENCES

[1] R.C. Juvinall, K.M. Marshek, "Fundamentals of Machine Component Design" 3rd ed., Wiley, New York, (US), (2000)

[2] S.A. Nassar, P.H. Matin, G.C. Barber, "Thread Friction Torque in Bolted Joints" ASME J. of Press. Vess. Tech., Vol. 127, pp. 387–39, (2004)

[3] EN 1993-1-8, "Design of steel structures Part 1-8: Design of joints" (2005)

[4] EN 1090-2, "Execution of steel structures and aluminium structures - Part 2: Technical requirements for steel structures" (2008)

[5] EN 14399-1, "High-strength structural bolting assemblies for preloading - Part 1: General requirements" (2005)

[6] J.H. Bickford, "An Introduction to the Design and Analysis of Bolted Joints" 3rd ed., Marcel Dekker, New York, (US), (1997)

[7] N. Motosh, "Development of Design Charts for Bolts Preload up to the Plastic Range", ASME J. Eng. Ind., Vol. 98, pp 849 – 851, (1976)

[8] VDI 2230, "Systematic calculation of high duty bolted joints – Joints with one cylindrical bolt", (2003)

[9] S.A. Nassar, A.M. Zaki "Effect of coating thickness on the friction coefficients and torque-tension relationship in threaded fasteners" ASME J. of Trib. Vol. 131, (021301) pp. 1-11 (2009)

[10] W. Eccles, I. Sherrington, R.D. Arnell "Frictional changes during repeated tightening of zinc plated threaded fasteners" Trib. Int. Vol. 43 pp. 700–707 (2010)

[11] D. Croccolo, M. De Agostinis, N. Vincenzi "Failure analysis of bolted joints: effect of friction coefficients in torque–preloading relationship" Eng. Fai. Ana. Vol. 18, pp. 364–373, (2011)

[12] Croccolo D., Vincenzi N., "Tightening tests and friction coefficients definition in the steering shaft of front motorbike suspension" Strain – An Int. Jou. for Exp. Mech. Vol. 47, pp. 337-342, (2011)

[13] Croccolo D., De Agostinis M., Vincenzi N., "Influence of tightening procedures and lubrication conditions on titanium screw joints for lightweight applications" Trib. Int. Vol. 55, pp. 68-76, (2012)

[14] S.A. Nassar, H. El-Khiami, G.C. Barber, Q. Zou, T.S. Sun, "An Experimental Study of Bearing and Thread Friction in Fasteners" J. of Trib. Vol. 127, pp. 263-272, (2005)

[15] C. Friedrich, "Reliable light weight fastening of magnesium components in automotive applications". 2004 SAE World Con., Detroit, (Michigan) March 8 - 11, (2004)

[16] C. Friedrich, T. Gerhard, D. Koch., H. Kopfer, "Threaded fastening systems with aluminium components – special characteristics for light weight design". 2009 Eur. Alum. Cong., Düsseldorf, (Germany), November 23 - 24, (2009)

[17] DIN946 "Determination of coefficient of friction of bolt/nut assemblies under specified conditions" (1991)

[18] D.C. Montgomery, "Design and Analysis of Experiment" 5th ed. Wiley, New York, (US), (2001)

[19] R. De Vor, T.H. Chang, J.W. Sutherland, "Statistical Quality Design and Control" Maxwell Mcmillan International Edition, New York, (US), (1992)

[20] Kopfer H., Freidrich C., De Agostinis M., Croccolo D. "Friction characteristics in light weight design focusing bolted joints" - Paper No. IMECE2012-85940, pp. 839-846 ASME Int. Mech. Eng. Con. and Exp. Houston, (US) (2012) http://dx.doi.org/10.1115/IMECE2012-85940

[21] Friedrich, C.; Hubbertz, H.; Dinger, G. "Standardized Calculation of Bolted Joints for Future Requirement" Paper No. IMECE2011-63774, pp. 475-480, 6 pages, Volume 3: Design and Manufacturing Denver, Colorado, November 11–17 (US), (2011) http://dx.doi.org/10.1115/IMECE2011-63774

[22] Croccolo D., De Agostinis M., Vincenzi N. "A contribution to the selection and calculation of screws in high duty bolted joints" Int. J. of Press. Vess. and Pip. Vol. 96-97, pp. 38-48, (2012)

[23] R.E. Cornwell "Computation of load factors in bolted connections" Proc. IMechE Part C: J. Mech. Eng. Sci. Vol. 223, pp.795-808, (2009)

[24] J.G. Williams, R.E. Anley, D.H. Nash, T.G.F. Gray. "Analysis of externally loaded bolted joints: analytical, computational and experimental study" Int. J. of Press. Vess. and Pip. Vol. 86, pp.420–427, (2009)

[25] I.R. Grosse, L.D. Mitchell "Non-linear axial stiffness characteristics of axisymmetric bolted joints" J. of Mech. Des. Vol. 112, pp.442–449, (1990).

[26] J.C. Musto, N.R. Konkle "Computation of member stiffness in design of bolted joints" ASME J. of Mech. Des. Vol. 128, pp.1357–1360, (2006)

[27] Eurocode 3, EN 1993 1-9, (2005).

Dynamic Analysis of Mechanical Systems

E. M. Kudryavtcev, A. A. Ruchkin

The Moscow State Building University (Russia)

It is offered the new approach to complex dynamic analysis of mechanical systems with use of a certain set of modern computer systems. This approach provides high level of dynamic analysis of mechanical systems, including and presentation of received results. It is especially important at the earliest design stages of mechanical systems.

Keywords: Mechanical system, modeling, dynamic analysis

1. INTRODUCTION

There are considered two methodics of the dynamic analysis of mechanical systems on an example of modeling of the mechanism of rotation tower crane. The first methodic is based on a traditional method of the dynamic analysis and the second on the basis of 3D modeling of mechanical systems.

The first methodic includes three stages. At the first stage there is build the marked state graph. Then there is created the system of the differential equations describing functioning of the mechanism of rotation tower crane [1]. Such approach provides presentation of interaction of adjacent bodies of the mechanism and 10 times facilitates construction of corresponding mathematical model for the dynamic analysis of the mechanism.

2. DYNAMIC ANALYSIS IN SYSTEM MATHCAD

The first methodic includes three stages. At the first stage there is build the marked state graph. Then there is created the system of the differential equations describing functioning of the mechanism of rotation tower crane [1]. Such approach provides presentation of interaction of adjacent bodies of the mechanism and 10 times facilitates construction of corresponding mathematical model for the dynamic analysis of the mechanism.

At the second stage there are defined masso-inertial characteristics of the basic rotating elements of the mechanism of rotation. At the third stage there is created the computer model of the mechanism of rotation for performance of numerical experiments in one of mathematical systems. Then there is carried out modeling process.

The first stage. The mechanism of rotation tower crane is represented in the form of consistently connected bodies of rotation. It can be represented in a graphic kind by means of the marked state graph fig. 1.

The rectangle in the marked state graph is a body of the mechanism of rotation tower crane.

The arrows entering or leaving a rectangle, it is the operating moments for rotation bodies. The arrows entering into a rectangle, define reactive and the leaving active moments for rotation bodies.

On each body of rotation the reactive moments of inertia and the moments connected with dissipative and elastic properties of a body can operate.

The sizes connected with dissipative and elastic properties of a body, depend on properties of adjacent bodies with which the given body cooperates.

For drawing up of the differential equations describing work of the mechanism of rotation tower crane it is possible to formulate a following mnemonic rule:

- for each body of system the equation which is represented in the form of the differential equation of the second order;
- the number of members of the equation is equal to number of arrows entering or leaving of a considered body of system;
- each member of the differential equation has the sign. If the arrow is directed to an investigated body of system the member undertakes with a sign plus if from a body with a sign a minus;
- the first member of the sum for each i-th rotating body of the mechanism is equal $I_i \cdot \ddot{\varphi}_i$;
- members for the arrows connecting two adjacent bodies of system, are equal to product of factor of rigidity or диссипации a previous body of system on a difference of required parameters on the given arrow, taking into account transfer numbers between two adjacent bodies of system.

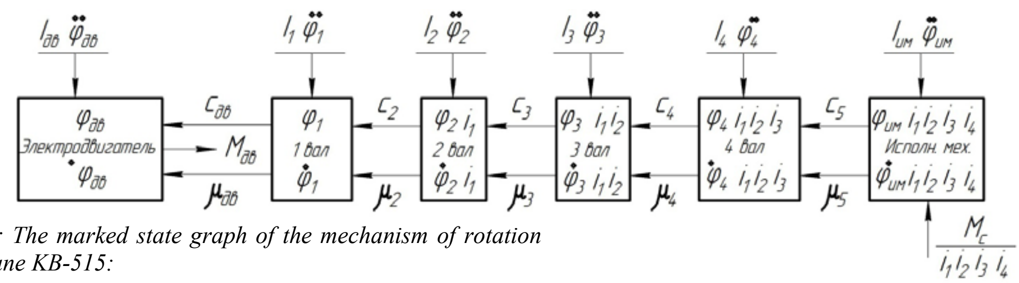

Figure 1: The marked state graph of the mechanism of rotation tower crane KB-515:

*Corresponding author: sdm@mgsu.ru

Using a mnemonic rule, we will write system of the differential equations describing work of the mechanism of rotation crane.

$$I_{\partial в} \cdot \ddot{\varphi}_{\partial в} + \mu_{\partial в} \cdot (\dot{\varphi}_{\partial в} - \dot{\varphi}_1) + c_{\partial в} \cdot (\varphi_{\partial в} - \varphi_1) = M_{\partial в};$$
$$I_1 \cdot \ddot{\varphi}_1 + \mu_2 \cdot (\dot{\varphi}_1 - \dot{\varphi}_2 \cdot i_1) + c_2 \cdot (\varphi_1 - \varphi_2 \cdot i_1) - \mu_{\partial в} \cdot (\dot{\varphi}_{\partial в} - \dot{\varphi}_1) - c_{\partial в} \cdot (\varphi_{\partial в} - \varphi_1) = 0;$$
$$I_2 \cdot \ddot{\varphi}_2 + \mu_3 \cdot (\dot{\varphi}_2 \cdot i_1 - \dot{\varphi}_3 \cdot i_1 \cdot i_2) + c_3 \cdot (\varphi_2 \cdot i_1 - \varphi_3 \cdot i_1 \cdot i_2) - \mu_2 \cdot (\dot{\varphi}_1 - \dot{\varphi}_2 \cdot i_1) - c_2 \cdot \cdot (\varphi_1 - \varphi_2 \cdot i_1) = 0;$$
$$I_3 \cdot \ddot{\varphi}_3 + \mu_4 \cdot (\dot{\varphi}_3 \cdot i_1 \cdot i_2 - \dot{\varphi}_4 \cdot i_1 \cdot i_2 \cdot i_3) + c_4 \cdot (\varphi_3 \cdot i_1 \cdot i_2 - \varphi_4 \cdot i_1 \cdot i_2 \cdot i_3) - \mu_3 \cdot \cdot (\dot{\varphi}_2 \cdot i_1 - \dot{\varphi}_3 \cdot i_1 \cdot i_2) - c_3 \cdot (\varphi_2 \cdot i_1 - \varphi_3 \cdot i_1 \cdot i_2) = 0;$$
$$I_4 \cdot \ddot{\varphi}_4 + \mu_5 \cdot (\dot{\varphi}_4 \cdot i_1 \cdot i_2 i_3 - \dot{\varphi}_{им} \cdot i_1 \cdot i_2 \cdot i_3 \cdot i_4) + c_5 \cdot (\varphi_4 \cdot i_1 \cdot i_2 \cdot i_3 - \varphi_{им} \cdot i_1 \cdot i_2 \cdot i_3 \cdot i_4) - \mu_4 \cdot (\dot{\varphi}_3 \cdot i_1 \cdot i_2 - \dot{\varphi}_4 \cdot i_1 \cdot i_2 \cdot i_3) - c_4 \cdot (\varphi_3 \cdot i_1 \cdot i_2 - \varphi_4 \cdot i_1 \cdot i_2 \cdot i_3) = 0;$$
$$I_{им} \cdot \ddot{\varphi}_{им} - \mu_5 \cdot (\dot{\varphi}_4 \cdot i_1 \cdot i_2 \cdot i_3 - \dot{\varphi}_{им} \cdot i_1 \cdot i_2 \cdot i_3 \cdot i_4) - c_5 \cdot (\varphi_4 \cdot i_1 \cdot i_2 \cdot i_3 - \varphi_{им} \cdot i_1 \cdot i_2 \cdot i_3 \cdot i_4) = -M_c/(i_1 \cdot i_2 \cdot i_3 \cdot i_4).$$

This system completely describes dynamics of work of the mechanism of rotation crane at the appendix to a rotor of the engine of the twisting moment, and to ОПУ the resistance moment.

For simplification of the decision of system of the differential equations of the second order it is expedient to present this system in the form of system of the differential equations of the first order.

$$\frac{d\varphi_{дв}}{dt} = \dot{\varphi}_{дв}; \quad \frac{d\varphi_1}{dt} = \dot{\varphi}_1; \quad \frac{d\varphi_2}{dt} = \dot{\varphi}_2; \quad \frac{d\varphi_3}{dt} = \dot{\varphi}_3; \quad \frac{d\varphi_4}{dt} = \dot{\varphi}_4; \quad \frac{d\varphi_{им}}{dt} = \dot{\varphi}_{им};$$
$$\frac{d\dot{\varphi}_{\partial в}}{dt} = \frac{1}{I_{\partial в}} \cdot \left(M_{\partial в} - \mu_{\partial в} \cdot (\dot{\varphi}_{\partial в} - \dot{\varphi}_1) - c_{\partial в} \cdot (\varphi_{\partial в} - \varphi_1)\right);$$
$$\frac{d\dot{\varphi}_1}{dt} = \frac{1}{I_1} \cdot (-\mu_2 \cdot (\dot{\varphi}_1 - \dot{\varphi}_2 \cdot i_1) - c_2 \cdot (\varphi_1 - \varphi_2 \cdot i_1) + \mu_{\partial в} \cdot (\dot{\varphi}_{\partial в} - \dot{\varphi}_1) + c_{\partial в} \cdot (\varphi_{\partial в} - \varphi_1));$$
$$\frac{d\dot{\varphi}_2}{dt} = \frac{1}{I_2} \cdot (-\mu_3 \cdot (\dot{\varphi}_2 \cdot i_1 - \dot{\varphi}_3 \cdot i_1 \cdot i_2) - c_3 \cdot (\varphi_2 \cdot i_1 - \varphi_3 \cdot i_1 \cdot i_2) + \mu_2 \cdot (\dot{\varphi}_1 - \dot{\varphi}_2 \cdot i_1) + c_2 \cdot \cdot (\varphi_1 - \varphi_2 \cdot i_1));$$
$$\frac{d\dot{\varphi}_3}{dt} = \frac{1}{I_3}(-\mu_4 \cdot (\dot{\varphi}_3 \cdot i_1 \cdot i_2 - \dot{\varphi}_4 \cdot i_1 \cdot i_2 \cdot i_3) - c_4 \cdot (\varphi_3 \cdot i_1 \cdot i_2 - \varphi_4 \cdot i_1 \cdot i_2 \cdot i_3) + \mu_3 \cdot \cdot (\dot{\varphi}_2 \cdot i_1 - \dot{\varphi}_3 \cdot i_1 \cdot i_2) + c_3 \cdot (\varphi_2 \cdot i_1 - \varphi_3 \cdot i_1 \cdot i_2));$$
$$\frac{d\dot{\varphi}_4}{dt} = \frac{1}{I_4}(-\mu_5 \cdot (\dot{\varphi}_4 \cdot i_1 \cdot i_2 \cdot i_3 - \dot{\varphi}_{им} \cdot i_1 \cdot i_2 \cdot i_3 \cdot i_4) - c_5 \cdot (\varphi_4 \cdot i_1 \cdot i_2 \cdot i_3 - \varphi_{им} \cdot i_1 \cdot i_2 \cdot i_3 \cdot i_4) + \mu_4 \cdot (\dot{\varphi}_3 \cdot i_1 \cdot i_2 - \dot{\varphi}_4 \cdot i_1 \cdot i_2 \cdot i_3) + c_4 \cdot (\varphi_3 \cdot i_1 \cdot i_2 - \varphi_4 \cdot i_1 \cdot i_2 \cdot i_3));$$
$$\frac{d\dot{\varphi}_{им}}{dt} = \frac{1}{I_{им}} \cdot (\mu_5 \cdot (\dot{\varphi}_4 \cdot i_1 \cdot i_2 \cdot i_3 - \dot{\varphi}_{им} \cdot i_1 \cdot i_2 \cdot i_3 \cdot i_4) + c_5 \cdot \cdot (\varphi_4 \cdot i_1 \cdot i_2 \cdot i_3 - \varphi_{им} \cdot i_1 \cdot i_2 \cdot i_3 \cdot i_4) - M_c/(i_1 \cdot i_2 \cdot i_3 \cdot i_4));$$

The second stage. Calculation of initial data such as: the moment of inertia of each shaft, factor of rigidity and диссипации each connection etc.

It is possible to present rotating elements of the mechanism of rotation crane in the form of a multistage shaft. Then the moment of inertia for such cylindrical shaft can be calculated under the formula

$$I = \frac{\pi}{32} \cdot \sum_{i=1}^{n} \rho_i \cdot l_i \cdot d_i^4$$

n – number of steps of a shaft;

ρ - material density of which it is made *i*-я a shaft step;

l – length *of i th* step of a shaft, m;

d - diameter *of i th* step of a shaft, m.

The third stage. The computer model of functioning of the mechanism of rotation tower crane is created in one of mathematical systems, for example, Mathcad.

The example of modeling of the mechanism of rotation tower crane in the system Mathcad is more low presented: initial data for calculation, required parameters, computer model and some results of modeling.

Исходные данные для расчета:

Сопротивление повороту, Н*м	Mc := 207000
Момент инерции двигателя, кг*м^2	Idv := 0.065
Момент инерции Вала 1, кг*м^2	I1 := 0.0015
Момент инерции Вала 2, кг*м^2	I2 := 0.0704
Момент инерции Вала 3, кг*м^2	I3 := 1.018
Момент инерции Вала 4, кг*м^2	I4 := 1.3115
Момент инерции Исполнит. механизма, кг*м^2	Im := 10727253
Коэф.жесткости соединения двиг-Вал1, Н*м/рад	cdv := 8443.08
Коэф.жесткости соединения Вал1-Вал2, кН*м/рад	c2 := 342.3
Коэф.жесткости соединения Вал2-Вал3, кН*м/рад	c3 := 643.4
Коэф.жесткости соединения Вал3-Вал4, кН*м/рад	c4 := 2179
Коэф.жесткости соединения Вал4-Исполн.мех, кН*м/рад	c5 := 28071

Коэф. диссипации соединения Двиг.-Вал1, Н*м*с/рад	$\mu dv := 400$
Коэф. диссипации зубчатого зацепления, Н*м*с/рад	$\mu 2 := 1000$
Передаточное число первой ступени	$i1 := 8.059$
Передаточное число второй ступени	$i2 := 6.923$
Передаточное число третьей ступени	$i3 := 4.077$
Передаточное число шестерни и ОПУ	$i4 := 9.722$
Угловая скорость идеального хода ротора двигателя, рад/с	$w0 := 104.67$
Величина критического скольжения	$sk := 0.39$
Максимальный (критический) момент в статическом режиме, Н*м	$Mk := 120.73$

Искомые параметры:

Угол поворота и угловая скорость ротора двигателя	x_0, x_6
Угол поворота и угловая скорость Вала 1 редуктора	x_1, x_7
Угол поворота и угловая скорость Вала 2 редуктора	x_2, x_8
Угол поворота и угловая скорость Вала 3 редуктора	x_3, x_9
Угол поворота и угловая скорость Вала 4 редуктора	x_4, x_{10}
Угол поворота и угловая скорость Исполн. механизма	x_5, x_{11}

Алгоритм расчета:

1. Представление вектора-столбца начальных значений искомых параметров

$$x := (0\ 0\ 0\ 0\ 0\ 0\ 0\ 0\ 0\ 0\ 0\ 0)^T$$

2. Представление вектора-столбца правой части системы дифференциальных уравнений, описывающей работу механизма поворота

$$D(t,x) := \begin{bmatrix} x_6 \\ x_7 \\ x_8 \\ x_9 \\ x_{10} \\ x_{11} \\ \dfrac{1}{Idv}\cdot\left[\dfrac{2\cdot Mk}{\dfrac{1-\dfrac{x_6}{w0}}{sk}+\dfrac{sk}{1-\dfrac{x_6}{w0}}} - \mu dv\cdot(x_6 - x_7) - cdv\cdot(x_0 - x_1)\right] \\ \dfrac{\mu dv\cdot(x_6 - x_7) + cdv\cdot(x_0 - x_1) - \mu 2\cdot(x_7 - x_8\cdot i1) - c2\cdot(x_1 - x_2\cdot i1)}{I1} \\ \dfrac{\mu 2\cdot(x_7 - x_8\cdot i1) + c2\cdot(x_1 - x_2\cdot i1) - \mu 3\cdot(x_8\cdot i1 - x_9\cdot i1\cdot i2) - c3\cdot(x_2\cdot i1 - x_3\cdot i1\cdot i2)}{I2} \\ \dfrac{\mu 3\cdot(x_8\cdot i1 - x_9\cdot i1\cdot i2) + c3\cdot(x_2\cdot i1 - x_3\cdot i1\cdot i2) - \mu 4\cdot(x_9\cdot i1\cdot i2 - x_{10}\cdot i1\cdot i2\cdot i3) - c4\cdot(x_3\cdot i1\cdot i2 - x_4\cdot i1\cdot i2\cdot i3)}{I3} \\ \dfrac{\mu 4\cdot(x_9\cdot i1\cdot i2 - x_{10}\cdot i1\cdot i2\cdot i3) + c4\cdot(x_3\cdot i1\cdot i2 - x_4\cdot i1\cdot i2\cdot i3) - \mu 5\cdot(x_{10}\cdot i1\cdot i2\cdot i3 - x_{11}\cdot i1\cdot i2\cdot i3\cdot i4) - c5\cdot(x_4\cdot i1\cdot i2\cdot i3 - x_5\cdot i1\cdot i2\cdot i3\cdot i4)}{I4} \\ \dfrac{1}{Im}\cdot\left[\mu 5\cdot(x_{10}\cdot i1\cdot i2\cdot i3 - x_{11}\cdot i1\cdot i2\cdot i3\cdot i4) + c5\cdot(x_4\cdot i1\cdot i2\cdot i3 - x_5\cdot i1\cdot i2\cdot i3\cdot i4) - \dfrac{Mc}{i1\cdot i2\cdot i3\cdot i4}\right] \end{bmatrix}$$

3. Представление параметров моделирования.

Начальное время моделирования, с.	$t0 := 0$
Конечное время моделирования, с.	$t1 := 20$
Число шагов интегрирования, шт.	$N := 1000$

4. Решение дифференциальных уравнений методом Рунге-Кутта с адаптивным шагом.

$$Z := Rkadapt(x, t0, t1, N, D)$$

5. Результаты определения искомых параметров.

$$t := Z^{\langle 0\rangle}\quad x_0 := Z^{\langle 1\rangle}\quad x_1 := Z^{\langle 2\rangle}\quad x_2 := Z^{\langle 3\rangle}\quad x_3 := Z^{\langle 4\rangle}\quad x_4 := Z^{\langle 5\rangle}\quad x_5 := Z^{\langle 6\rangle}$$

$$x_6 := Z^{\langle 7\rangle}\quad x_7 := Z^{\langle 8\rangle}\quad x_8 := Z^{\langle 9\rangle}\quad x_9 := Z^{\langle 10\rangle}\quad x_{10} := Z^{\langle 11\rangle}\quad x_{11} := Z^{\langle 12\rangle}$$

6. Представление искомых параметров в графическом виде, в зависимости от времени

There are presented some required parameters depending on time on fig. 2.

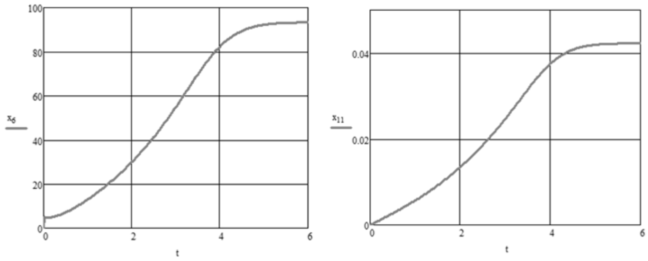

Figure 2: Dependence of angular speed of a rotor of the engine and of rotation tower crane from time

Analyzing the received results of modeling of the mechanism of rotation of tower crane KB-515, it is possible to notice, that dispersal of the engine and an exit of a rotor of the engine on nominal frequency of rotation of a rotary platform occurs approximately in 5 seconds. And fluctuations of elements of a drive practically do not occur.

The presented technique of the analysis of dynamics of work of the mechanism of rotation tower crane can be used at early design stages of such mechanisms. Besides, it can be used and for the analysis of other similar mechanical systems.

3. DYNAMIC ANALYSIS IN SYSTEM UNIVERSAL MECHANISM

The second technique includes the dynamic analysis of the mechanism of rotation tower crane in system **Universal mechanism**. This technique includes some stages. The first stage is directed on creation of three-dimensional model of the mechanism (3D), for example, in system KOMPAS-3D, Solid Works, etc. [1 - 8]. The second stage includes converting of three-dimensional model of the investigated mechanism in dynamic object. This process is carried out automatically. Then completion of dynamic object is spent. The third stage includes installation of a mode of modeling and performance of process of modeling.

At the first stage the three-dimensional model of the mechanism of rotation crane, for example, crane BK 515 in system KOMPAS-3D fig. 3 is created.

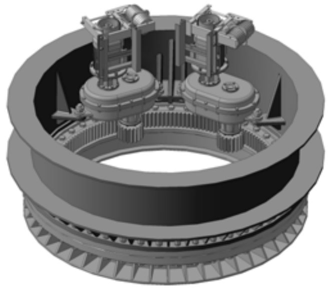

Figure 3: 3D model of the mechanism of rotation of crane KB-515

At the second stage 3D models of the mechanism of rotation tower crane converting is spent to dynamic object of system **Universal mechanism (UM Express)**. Last system is a standard application (library) of system **KOMPAS-3D**.

Completion of dynamic model includes some stages:

- creation of incorporated bodies;
- creation of hinges (for the description position of one body concerning another);
- creation of special forces (in this case special forces are understood as creation of gear gearings between incorporated bodies);
- creation of the scalar moment (simulates the twisting moment of a rotor of the engine);
- creation of forces of resistance (in this case the moment of resistance operating on the oporno-rotary device).

The mechanism of rotation tower crane KB-515 consists of 568 bodies. For modeling of the given object incorporated bodies into which all initial 568 bodies enter are created. The names, for example, **Вал1**, **Вал2**, **Вал3**, **Вал4**, **КОРПУС** and **ОПУ** are given to each of incorporated bodies.

For creation of an incorporated body, it is necessary to open in a window **the List of elements Body** point, Тела there will be a list of bodies of which the given mechanism consists. Further from this list we choose a body, for example, which is a part of the case. Then automatically there is in **the Animation window** this body and a window **the Inspector of object**. In a window **the Inspector of object** is named, for example, **the Case**, Имя: Корпус and then caused вкладка **Details**. Ticks before the name of those bodies which are a part of a body **the Case** are serially put. After end of formation of an incorporated body it is entered commands **to Accept** and Switching **object/element**. There is an incorporated body **the Case** fig. 4.

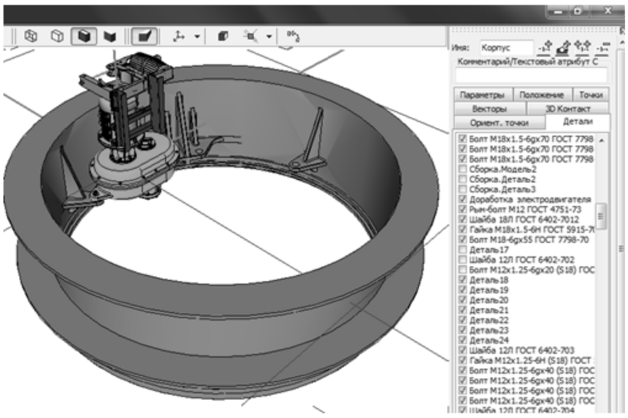

Figure 4: An animation window of system UM with the allocated body ***Kopnyc*** *with opened inset* ***Details*** *in a window* ***Inspector of objects***

Other incorporated bodies are similarly created. Some should be fixed, made of incorporated bodies motionless, namely a body **Case** into which enters: the reducer case, a brake without a brake pulley, статор the engine, a frame connecting the engine with a brake, a rotary platform and elements to which help there is their fastening.

Between other incorporated bodies there should be those or other communications – hinges. For input of the rotary hinge are preliminary created a vector on each body between which should be the hinge. After that in a window **List of elements** we open the list, Шарниры and in it  **Rotary hinge with autopositioning** since initial bodies settle down in the place necessary to us is chosen to a component . There is a corresponding dialogue window and corresponding helps which are necessary for executing. As an example on fig. 5 the result of construction of the rotary hinge between bodies **Корпус** and **Вал2** is shown

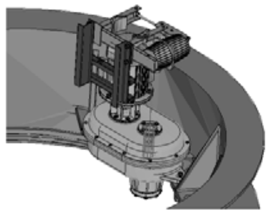

Figure 5: The rotary hinge between bodies ***Корпус-Вал2***

All other rotary hinges are similarly created.

For creation of gear gearings **the List of elements** is used вкладка **Special forces** in a window**.** Here forces for all pairs of the cogwheels transferring rotation in the mechanism are created. For an example we will create special force for bodies **Вал1** and **Вал2. List of elements** is for this purpose clicked by the right button of the mouse on вкладке **Special forces** in a window, and then in the dropping out menu we choose **Cogwheels.** On the right side from **Animation window** there will be a window **Inspector of object.** In it bodies between which gear gearing (**Вал1** and **Вал2**) will be created are specified. For this purpose it is necessary to specify the index points of vectors created earlier for each body, to specify axes of rotation for everyone bodies (axis), to specify transfer number and all other parameters of gear gearing fig. 6.

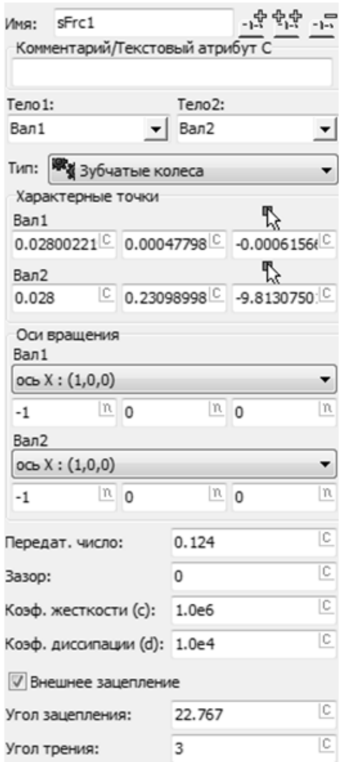

*Figure 6: A window **the Inspector of object** for the special force connecting in gear gearing **Вал1** and **Вал2***

After that automatically there are volume red vectors which specify, that between bodies **Вал1** and **Вал2** gear gearing is created. Special forces for bodies **Вал2-Вал3**, **Вал3-Вал4, Вал4-ОПУ** are similarly created.

Last step of preparation of model to modeling is creation of the scalar moment, the emitting twisting moment of the engine.

For this purpose it is necessary to choose in a window **List of elements** point Скалярные моменты and in the standard image to add a new element in a window **Inspector of object.** We choose in a window **Inspector of object** in entry fields of bodies as the first body **КОРПУС**, and as the second **Вал1** Тело1: Корпус Тело2: Вал1.

Further we pass on вкладку **Position**, and then **the Visual choice** is clicked by the button. We choose the cursor of the mouse **Корпус** vector in **Animation window** which will define local system of co-ordinates at the first body. We will adjust position of the moment concerning axis Y that the moment badge settled down, as is shown in fig. 7. We will put a tick before a word **Auto detection.** The system of co-ordinates of the second body will be automatically combined with system of co-ordinates of the first.

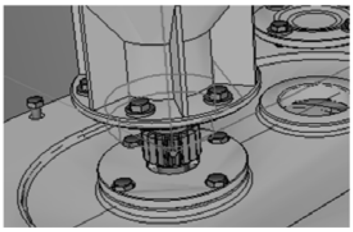

*Figure 7: A moment badge in **Animation window***

We open вкладку **Description** which is in a window **Inspector of object** then in the dropping out menu it is chosen a+b Выражение. In a window **Inspector of object** by means of a window **of Editing of expression** we enter the moment formula in language **Pascal** and it is clicked by the button **Accept** fig. 8.

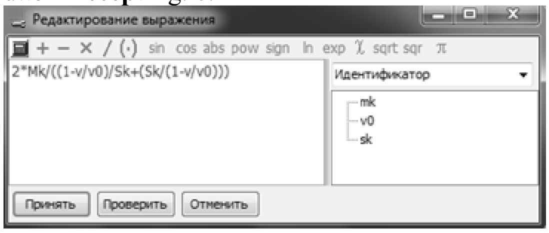

*Figure 8: Mathematical model of the moment of the engine in a window **expression Editing***

Then automatically there are three new identifiers for moment expression (**mk, v0, sk)**. We enter values of these identifiers in the window **Identifiers** located in the left bottom corner of the main window of system **UM** fig. 9.

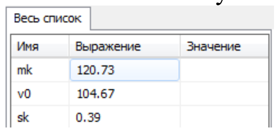

Весь список

Имя	Выражение	Значение
mk	120.73	
v0	104.67	
sk	0.39	

*Figure 9: Result of input of values of identifiers: **mk, v0, sk.***

At the third stage the mode of modeling is established and modeling process is carried out. We click on the panel of tools **Processes** by the button **Pass to the modeling module**. The system will pass in a mode of modeling fig. 10.

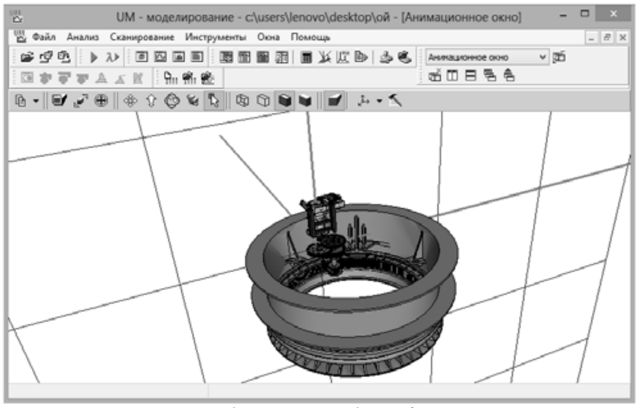

*Figure 10: The main window of system **Universal mechanism** in a modeling mode*

We click by the button **Modeling** and in the appeared window **Inspector of modeling of object** in section a numerical method we choose **Park method,** and also we put ticks opposite to points **Calculation of accelerations and forces of reactions,** and also **Calculation of matrixes Якоби.** We specify modeling time, a step of granting of results and an error fig. 11.

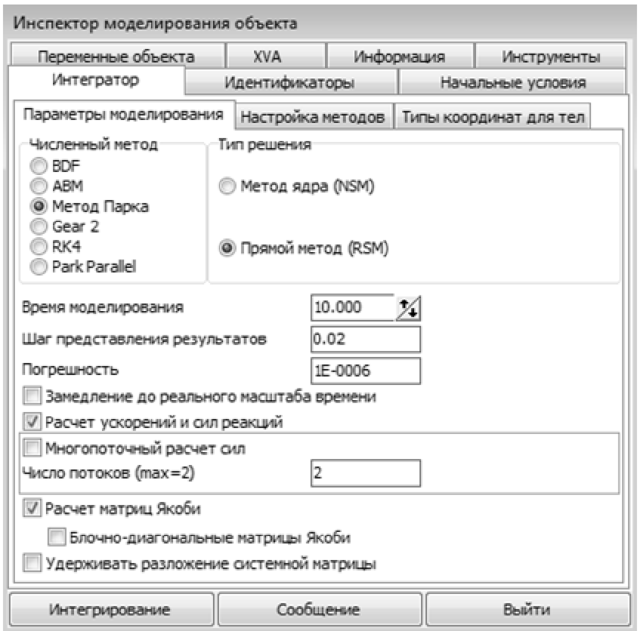

*Figure 11. Options in a window **the Inspector of modeling of object***

We click in a window **Inspector of modeling of object** by the button **Integration** (fig. 11 see). Process of modeling of the mechanism of rotation tower crane with display of rotation of a rotary platform in **Animation window** will begin.

The basic tools for deducing of results are **Animation window, Graphic window** ( ) and window **Master of variables** ( ).

We open a window **Master of variables** and **Container of variables** (button) necessary components of forces and co-ordinates of investigated details or hinges fig. 12 is placed in a window

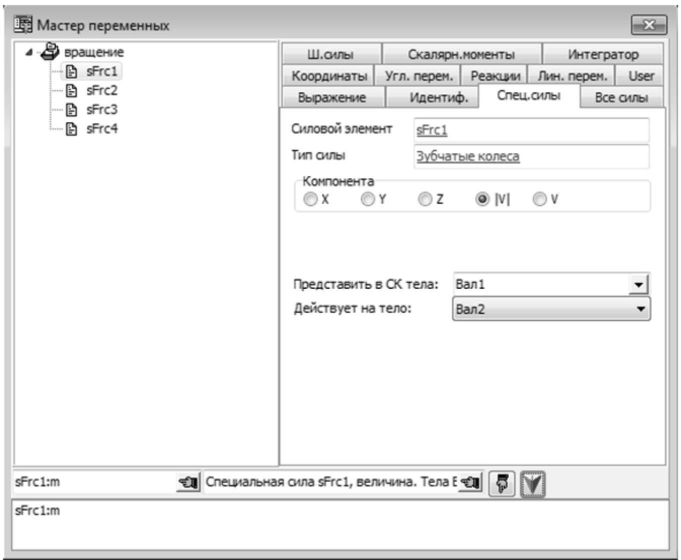

*Figure 12. A window **the Master of variables***

By means of the mouse it is moved variables from the container in graphic or animation windows. Then results of modeling in a graphic kind act in film:

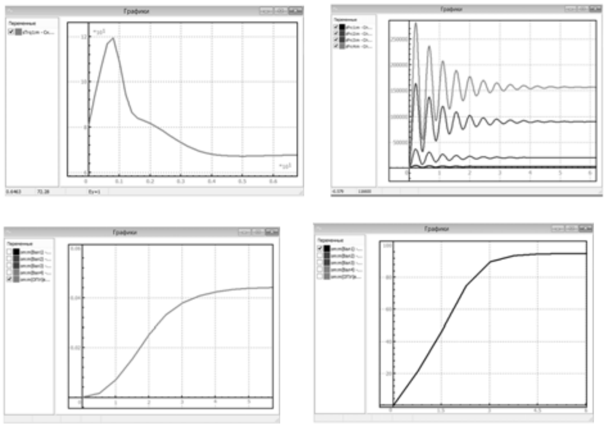

Figure 13. Results of research of the mechanism of turn in a graphic kind from time: the moment on an engine rotor; size of forces in gear gearings; angular speed of a rotor of the engine; angular speed of rotation ОПУ

4. CONCLUSION

Analyzing some results of modeling of the mechanism of rotation tower crane KB-515 in system **Universal mechanism**, it is possible to notice, that dispersal of the engine and an exit of a rotor of the engine on nominal frequency of rotation occurs approximately in 5 seconds. Thus, the results of the dynamic analysis spent by a classical method and by means of given system coincide.

[1]. E.M. Kudryavtcev, “Building cars and the equipment” (with examples of calculations, including and on the computer): The Textbook. – M: Publishing house ASV, p. 328 (2012).
[2]. E.M. Kudryavtcev, V.V.Stepanov,” Execution of final qualifying work on the computer”: the Manual for high schools. - M: the Publishing House “BASTET”,p. 240 (2013).
[3]. E.M. Kudryavtcev, “CAD systems of the machine and the equipment”. The Textbook for high schools. M: Publishing house ASV, p. 382, (2013).
[4]. E.M. Kudryavtcev, “The basis of the automated designing”:The textbook for high schools. M: Publishing centre "Academy", p. 304 (2011).
[5]. E.M. Kudryavtcev,” КОМPAS-3D V10. As much as possible full management”. In 2 volumes. M: DMK Press. p. 1184,(2008).
[6]. E.M. Kudryavtcev, “Modeling, design and calculation of mechanical systems”. M: DMK Press. p. 400, (2008.).
[7]. E.M. Kudryavtcev, “Practical work on КОМPAS-3D V8: Machine-building libraries”. M.: DMK Press, p. 440, (2007).
[8]. E.M. Kudryavtcev, “Machine-building designing Mechanical Desktop”. M.: DMK Press, p. 432 (2006).

SESSION A

EARTH-MOVING AND TRANSPORTATION MACHINERY

General Classification of Small-Sized Technological Sets for Production of Dry Building Mixtures

И. А. Емельянова [1*], В. В. Блажко [1]

[1] Kharkov State Technical University of Civil Engineering and Architecture 61002, Kharkov (Ukraine)

The paper presents general classification of small-sized technological sets for production of dry building mixtures. It also presents the results of experimental testing of a new technological set of equipment for preparation of dry building mixtures.

Keywords: Technological sets, building mixtures, mixer, small-size set

The increased consumption of dry building mixtures makes the manufacturers of equipment, i.e. factories for production of these mixtures to appear in the market with their new accomplishments and solutions that provide a high quality and reliability of their mechanical equipment.

A lot of manufacturing companies have recently been dealing with the problem of utilization of technological sets for the production of dry building mixtures. They use a wide range of technological sets and mini plants.

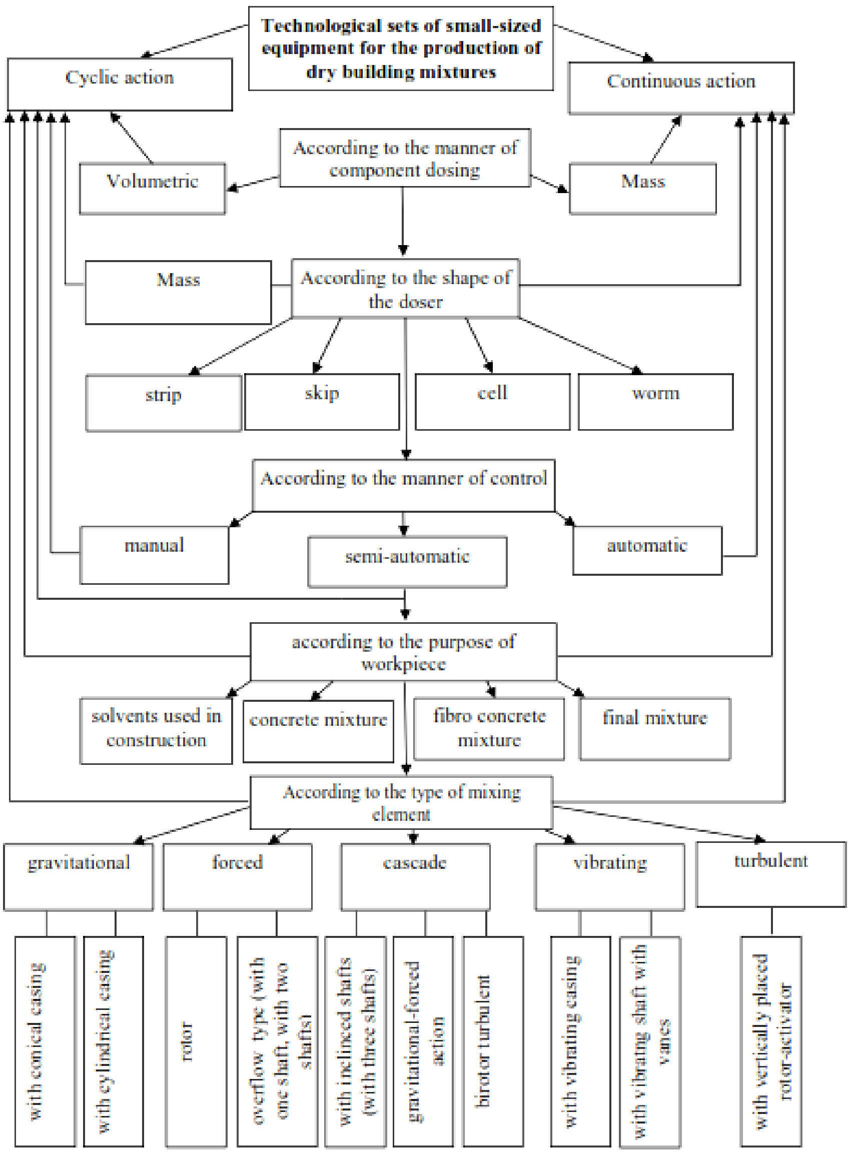

Figure 1. General classification of technological sets of small size equipment for production of dry building mixtures

*Corresponding author: gonch@kstuca.kharkov.ua

Thus, what should be taken into account is the current importance of the mentioned problems as well as the fact that the equipment sets which allow a general classification of such equipment and therefore an illustration of their overview are already used. (Figure 1).

Taking into account the demand for equipment for preparation of dry building mixtures at the Department of Mechanization of the Harkow State Univeristy of Civil Engineering and Architecture, the mini sets shown in Figs. 2, 3 and 4, which cover the mixers mentioned in the previous classification have been designed and implemented in manufacturing .

The main characteristics of operation of the presented sets are their capability to prepare different building mixtures directly on the site. Preparation of a quality (homogeneous) building mixtures is provided by the mixers of new generation. They operate in a cascade regime. Thanks to the simultaneous use of gravitational and forced mixing of components of the mixture, these machines show good results in preparation of building mixture for various purposes (Figs. 2 and 3, position 1).

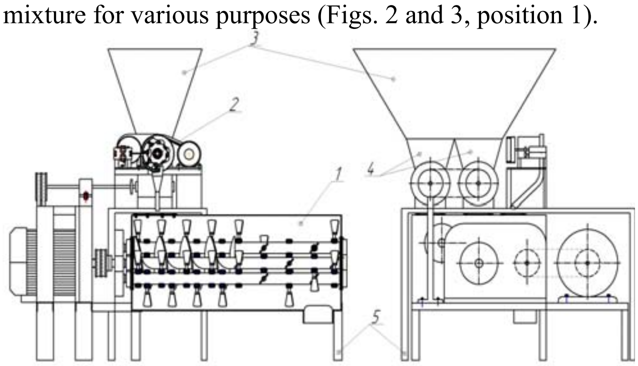

Figure 2. Principle scheme of the technological set of small-sized equipment for preparation of fine grain fibro concrete mixture 1. – mixer with three shafts, 2. – automatic part – asphalt fiber, 3. – bunker components of building mixture, 4. – cell dosers, 5. – mixer frame

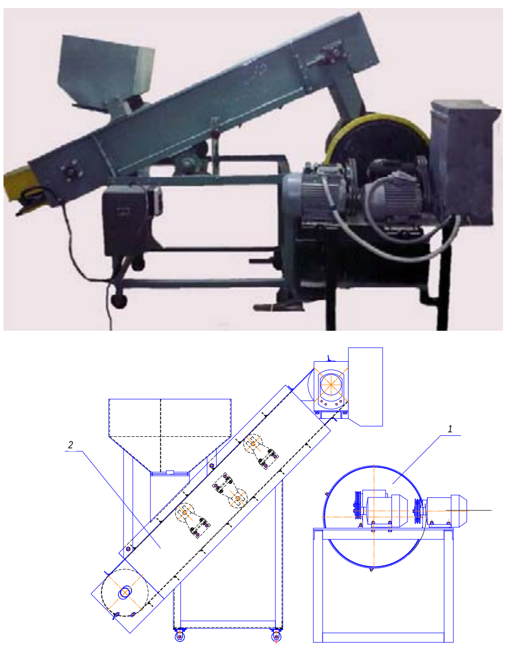

Figure 3. Technological set of the equipment for preparation of building mixture for various purposes, 1. – mixer of a gravitational-forced type 2. – strip-like scraping doser

The cascade principle of mixing means that in rotation of the working bodies the mixture components are raised to the upper part of the working space of the machine, where mixture particles, under the action of gravitational force, fall off them and again onto the rotating vanes of the machine. The process of their motion repeats itself and provides motion of the particles in the working space of the mixer between the left and right sides of the wall along a complex path [1].

A mini set with a new way of mixing patented in Ukraine has recently been developed [2] (Figure 4).

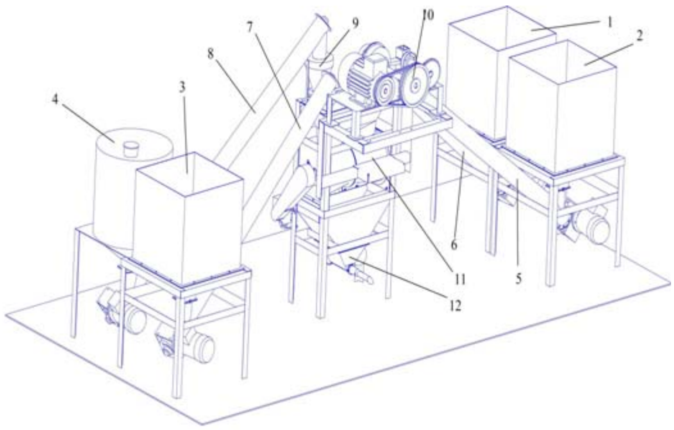

Figure 4. Technological set of the equipment for the production of dry building mixture with the use of a birotor turbulent mixer, 1. – bunker with sand; 2. – bunker with lime; 3. – bunker with dross; 4. – cement silo; 5. – lime doser; 6. – sand doser; 7. – dross doser; 8. – doser for adding cement; 9. – cement doser; 10. – asphalt fibre; 11. – birotor turbulent mixer; 12. – loading machine.

The mixer (Figure 5) operates in the following way. The previously dosed components of the building mixture are put, through the loading pipes 2 and 3, into the casing 1 and fall into the zone of action of the rotor with vanes 13 and 14. Thanks to the rotor rotation in opposite directions with a different number of revolutions n1 = 300 min^{-1}, n2 = 200 min^{-1}, as well as to the angle of vane arrangement $\beta = 55 \ldots 60^{\circ}$, the mixture particles are mixed in a more intense way due to radial and axial velocities.

Radial and axial velocities cause axial pressure, which increases the forces of gravity and friction with the casing walls.

Under the action of the rotary shaft with vanes, the mixture components are transferred to a mixed state and directed to the axial direction toward a narrowed part of the left and right cones. By transferring to the narrow space of the casing, two opposite flows pass by each other and fall into two opposite parts of the casing. Final mixing of the mixture components arise due to the multiple transfer of mixture components to the right and left parts of the casing and vice versa from one flow to the other, which speeds up the mixing process.

The effectiveness of operation of the new set of equipment has been tested experimentally according to the factorial design of the experiment.

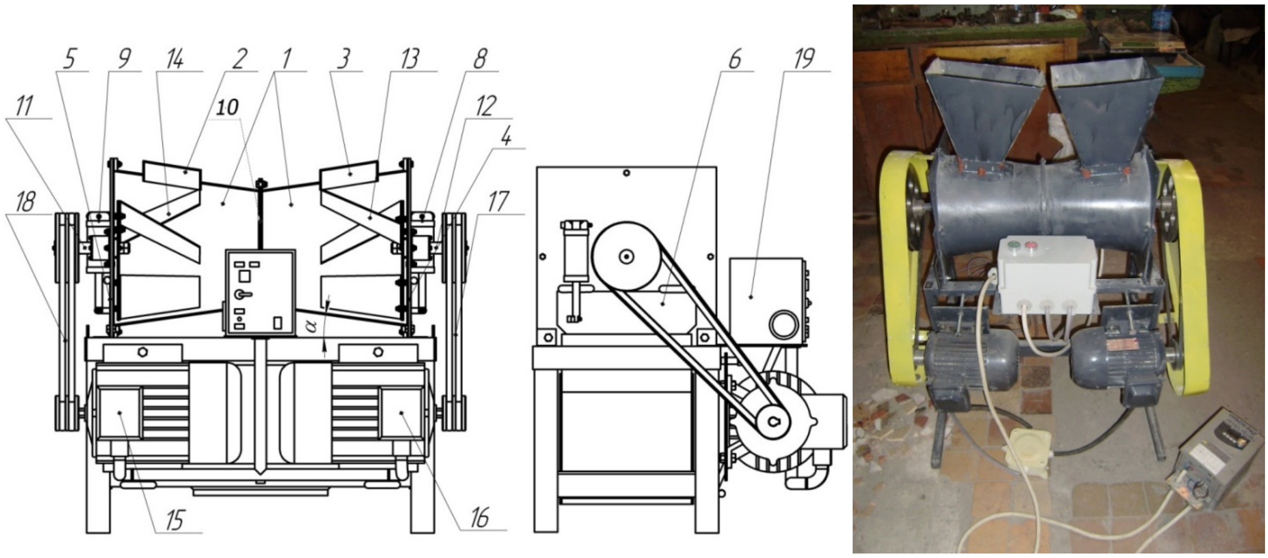

Figure 5. Birotor turbulent mixer, 1. casing; 2, 3. openings for loading; 4, 5 openings for discharging; 6,7. covers; 8, 9. pneumatic cylinders; 10. flanges; 11, 12. shafts; 13,14. rotors with vanes; 15, 16. electromotors; 17, 18. belt drives; 19. control block.

The main function is the homogeneity of the prepared dry building mixture– Y_1. In the process of experimental operation of the mixer, the indicators of homogeneity of mixture and its control mould compressive strength have been evaluated.

The factors influencing the effective operation of the mixer are as follows:

X_1 – the number of revolutions of the working bodies n, revs/min;

X_2 – the time of mixing of components t, sec;

X_3 – the coefficients of filling of the mixer volume K_3, %.

The processed results of exeperimental data and their graphical dependence confirm the efficiency of using the turbulent mixer for preparation of a dry building mixture:

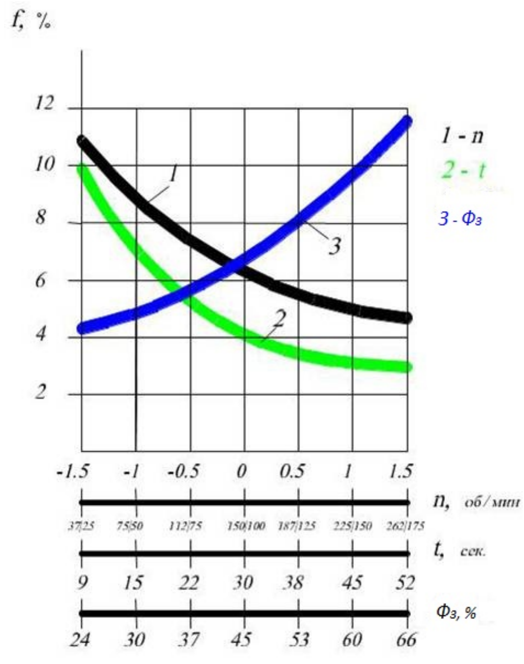

Figure 6. Graphical dependence of the homogeneity of mixture on the influential factors

Graphs 1 and 2 show that the increase in the number of revolutions of the working body and the time for production of the mixture have a positive effect on the mixture homogeneity. The effect of the increased number of revolutions can be explained by the increase in the velocity of circulation of mixture particles and their propagation in the longitudinal direction from one zone of the mixer into the other.

By analyzing the data from graph 2 it can be noticed that the quality of mixture (f -5 ... 7%) can be obtained after 25-30 seconds. The increased coefficient of volume occupancy of the mixer casing negatively influences the degree of mixture homogeneity. For the presented structure of the mixer, the recommended value of the coefficient of casing volume occupancy is within the range K_3 = 37-45%.

The recommended number of revolutions of the shaft is $n_1 = n_2 = 120\text{-}180\ min^{-1}$. The character of the curves presented in Figure 6 shows a significant infleunce of the selected factors on the quality of operation of the mixer.

CONCLUSIONS

The paper presents general classification of small-sized sets of equipment for preparation of dry building mixtures.

The results of preliminary experimental testing of the new model of mixing by forced action confirms the efficiency of utilizing these machines as a part of the technological set for preparation of dry building mixtures.

In accordance with the presented graphs 1-2 (Figure 6), the mixer can be recommended for preparation of quality dry building mixtures in small-sized sets of technological equipment.

REFERENCES

[1] И. А. Емельянова, А. И. Анищенко, С.М. Евель, В. В. Блажко, О. В. Доброходова, Н.А. Меленцов, Mixers

Operating in Cascade Regime, Monograph /– Kharkov: Team Publish Group, 2012 (in Russian)

[2] И. А. Емельянова, А. И. Анищенко, Mixers of Gravitational-Forced Action Operating in Cascade Regime of High Efficiency Machines, Scientific-Production Periodical Journal Science in Central Russia, 2012 – № 1. – pp. 76-81 (in Russian)

[3] И. А. Емельянова, А. И. Анищенко, В. В. Блажко, Determination of the Trajectory of Motion of Concrete Particles after Falling from the Vane of a Rotary Shaft in a Mixer with Forced and Gravitational Action, Scientific Bulletin of Civil Engineering,– Harkow: HDTUBA, HOTV ABU, 2009. – Vol. 51. – pp. 258-262. (in Ukrainian)

Post-Ejection Failure Mode of Post-Driving Machines

William Singhose[1]*, Dooroo Kim[1], Joshua Vaughan[2]
[1]George Woodruff School of Mechanical Engineering
Georgia Institute of Technology, Atlanta, GA (USA)
[2]Department of Mechanical Engineering
University of Louisiana at Lafayette, Lafayette, LA (USA)

Post drivers are useful tools that can drive posts and poles into the ground for various applications. Often, these machines also have the capability to pull posts out of the ground. Post drivers can be hand-held or mechanically driven by an engine, hydraulic power, or pneumatic power. The very large forces needed to drive posts into the ground, or to pull them out, make post drivers inherently dangerous machines. A common method for applying the required driving forces is to drop a heavy weight onto the top of the post. This paper studies the failure mode that occurs when the post being driven into the ground is ejected from the machine. This study includes a review of relevant patents and experiments on a real post driver. The experiments measure the velocity of a post as it is ejected from the machine. These measurements quantify the danger of this failure mode.

Keywords: Post drivers, Failure modes, Hazards, Construction equipment

I. Introduction

Post drivers are machines used, as their name implies, to drive posts and poles into the ground for various applications. These machines also often have the capability to pull posts out of the ground. Post drivers can be hand-held or mechanically driven by an engine, hydraulic power, or pneumatic power. Mechanically-driven post drivers are potentially hazardous and safety standards have been created to regulate such machines [1]. Hazards originate from the large forces that must be applied to drive posts into the ground or to pull them out. Dropping a heavy weight onto the top of the post is one common method for applying the required driving forces. However, this method is subject to misalignment of the drop-weight and post. This misalignment can cause the post to be ejected from the machine as the weight drops. This root cause of failure is consistent with other industrial processes, where misalignment and stuck workpieces have been found to be a leading cause of occupational accidents [2]. The hazardous failure mode examined in this paper is when the post being driven into the ground is ejected from the machine.

A schematic diagram of a typical post driver is shown Figure 1. A post driver typically has a footer that secures the base of the post. This element ensures that the post is driven into the correct location. It also stabilizes the machine during post-driving operations. The top of the post is secured by a cap. The cap can be changed to accommodate different sizes and types of posts. An anvil sits on top of the cap. To drive the post into the ground, the hammer is raised and then dropped onto the anvil.

During operation, the post and/or cap may shift and become misaligned. If the cap does not secure the top of the post, then the post can fall out of the machine. If the anvil or hammer falls while the post is misaligned, then large forces can be applied to the side of the post. These forces can eject the post out of the machine at high speed. This event can damage the machine, nearby property, or injure nearby persons.

Figure 2 illustrates a sequence of machine motions that can lead to a post being ejected from the machine. In

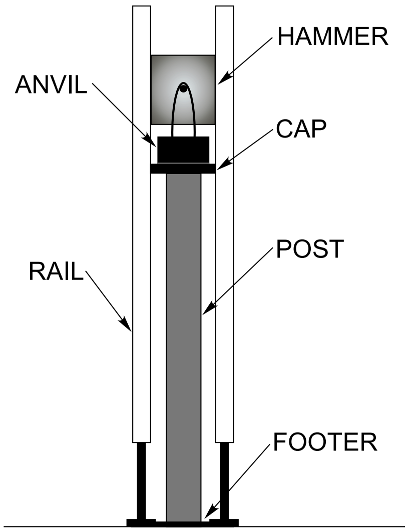

Figure 1: Post Driver.

Figure 2(a), the post is not restrained by the cap, and the hammer is in an elevated position. The second frame, Figure 2(b), shows the hammer dropped onto the anvil. In Figure 2(c), the falling cap/anvil/hammer assembly is sliding down the side of the post and applying lateral forces to the post. Finally, the cap/anvil/hammer assembly has ejected the post in Figure 2(d). Note that this post-ejection event could also occur without the hammer dropping. The cap and anvil are very heavy; their falling weight alone could provide enough force to eject the post.

In order to minimize the occurrence of damage and injuries due to these types of situations, the post needs to be secured within the machine, even when the cap is not properly seated on the top off the post. Without a safety feature in addition to the cap, the machine has a single-point failure mode that can result in catastrophic injuries.

The next section will present a series of relevant patents to illustrate that post ejection is a known safety problem. Then, in Section III, a series of experiments are described that quantifies the dangers of this post-ejection failure mode.

*Corresponding Author: Singhose@gatech.edu

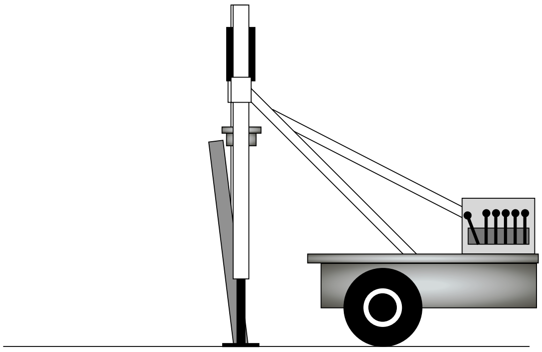

(a) Elevated Hammer and Misaligned Cap

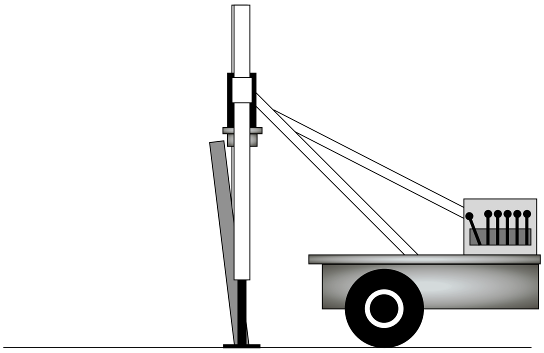

(b) Hammer Contacting the Anvil

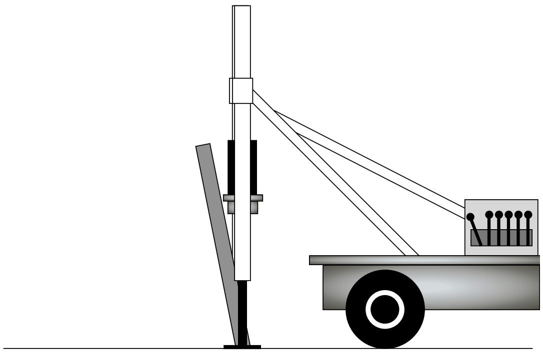

(c) Cap/Anvil/Hammer Ejecting the Post

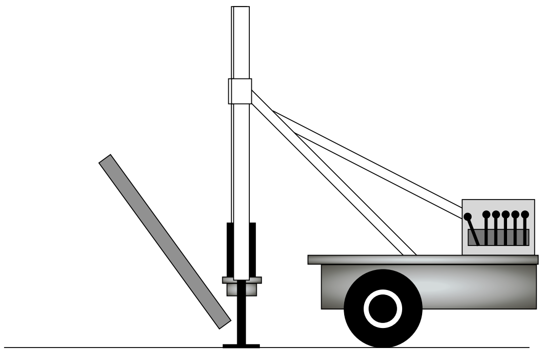

(d) Ejected Post

Figure 2: Post Ejection.

II. Relevant Patents and Products

The post-ejection hazard has driven the creation of several patents on mechanisms and methods that can reduce the risks associated with post ejection. US Patent 4,915,180 from 1990 is an example of one of the earlier solutions to the problem of posts being ejected from the machine [3]. As shown in Figure 3, this patent describes a post sleeve (27) that provides a recessed rectangular guide cavity (35)

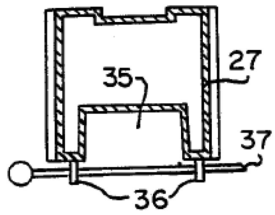

Figure 3: Post-Restraining Mechanism from US Patent 4,915,180.

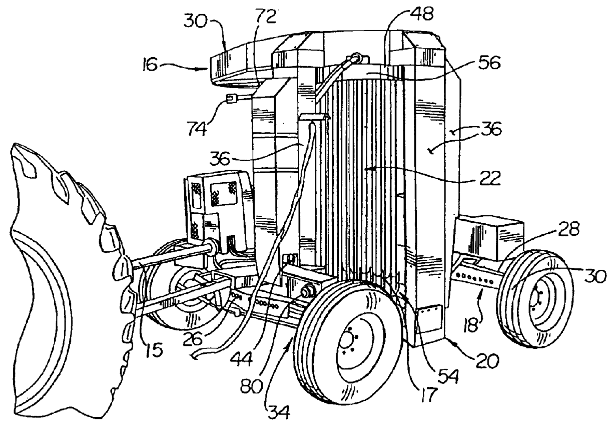

Figure 4: Post-Driving Machine from US Patent 6,938,703.

into which the post is placed in order to drive it into the ground. The post sleeve (27) is provided with a pair of retaining rings (36), welded to opposite sides of its frontal surfaces so that a holding bar (37) may be passed through each ring to bridge the guide cavity (35). This allows the holding bar to restrain a post while the hammer is used to pound the post into the ground.

US Patent 6,938,703 from 2005 describes an apparatus for deploying posts from a magazine supply of fence posts and individually driving them into the ground [4]. Figure 4 shows an overall view of the machine, including the supply of posts in the magazine (22) that are to be driven into the ground. Figure 5 shows a close-up view of the post-driving assembly that generally includes a post driver (66), an adapter to receive and hold a post, a driver housing (68), and a travel carriage. The post driver (66) generally includes a post-holding or retaining mechanism (70, the rotating arms) for holding the post in a position for driven placement by the driver. Without the post-holding mechanism, the post would become misaligned and either enter the ground at the wrong angle or potentially harm the machine operators.

US Patent 7,597,156 from 2009 describes a more elaborate mechanism for retaining the post into position [5]. As seen in Figures 6 and 7, the roller latch assembly (102) provides a force to hold the post within the guide tube. The roller latch assembly is mounted to the circumference of the guide tube (150) in order to apply a lateral force on the post (125) inserted within the guide tube and retained inside. The roller latch assembly consists of a tension adjuster (110), tension plate (112) and a roller latch (120). The roller latch is positioned such that it freely rotates on a pin (114). The tension plate (112) provides the structure against which the tension adjuster (110) supplies the resistive force in order

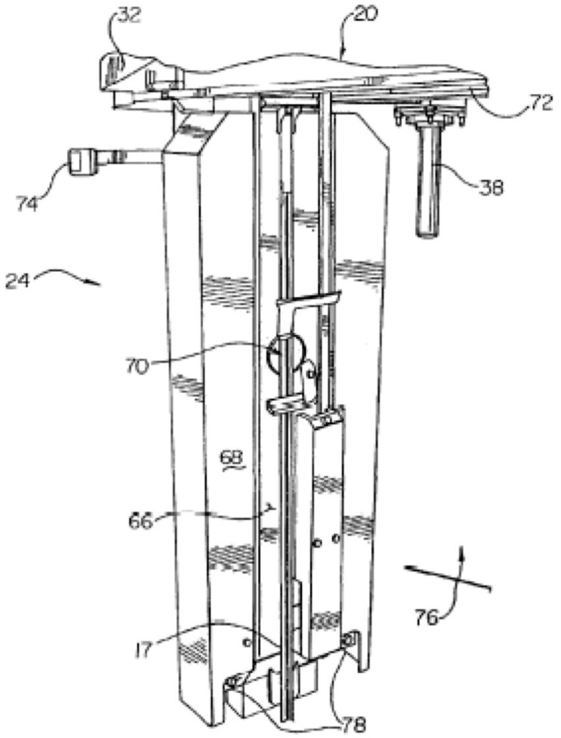

Figure 5: Post-Driving Assembly from US Patent 6,938,703.

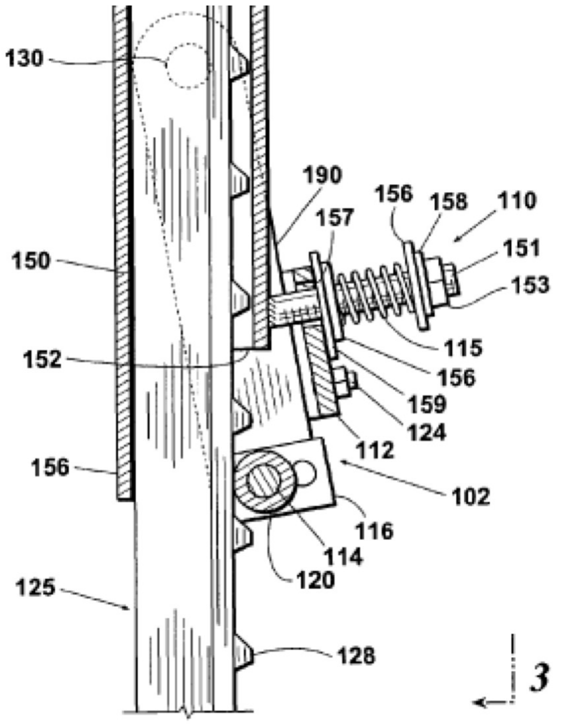

Figure 6: US Patent 7,597,156, Side View.

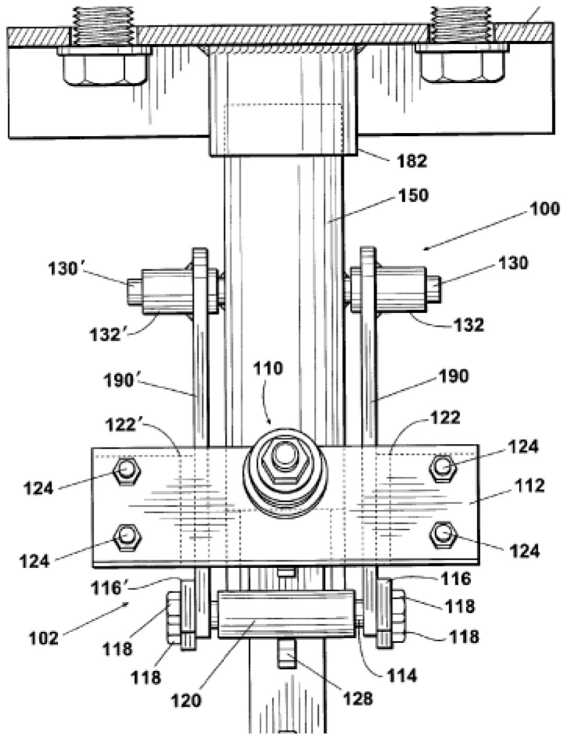

Figure 7: US Patent 7,597,156, Front View.

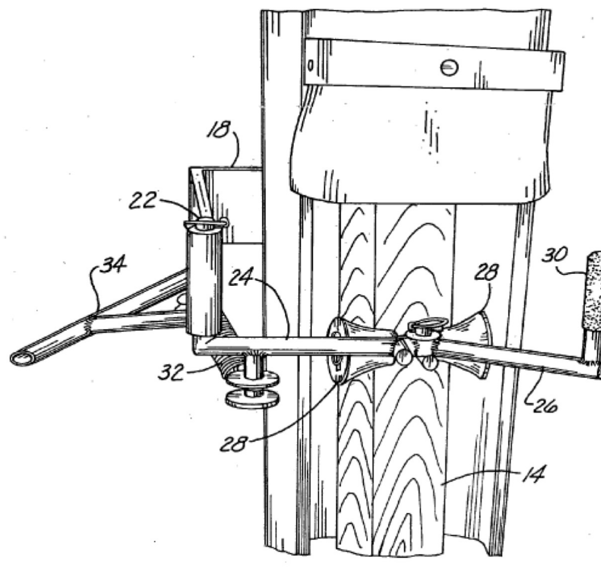

Figure 8: US Patent Application 20060113444.

for the roller latch (120) to retain the tee post (125) within the guide tube (150).

The SM-0011-SAA Safety Arm Attachment manufactured by Shaver Manufacturing Co. LLC is a product currently sold in the commercial market. The spring-loaded safety arm attachment holds the post in the driving ram securely to keep the operator away from the impact area and helps the operator drive the post straight into the ground.

US Patent Application 20060113444 from 2006 describes an invention similar to the Shaver Safety Arm Attachment [6]. As seen in Figure 8, a safety latch is attached to the supporting post of the post driver while the post is being driven into the ground. The lever arm is pivotally attached to the post driver and moveable between the released position and the working position where the roller is supporting the engagement of the post. A spring in the latch maintains the supporting engagement with the post while it is driven.

III. Tests Performed on a Post-Driving Machine

To better understand the post-ejection phenomenon, tests were conducted to measure the velocity of a post

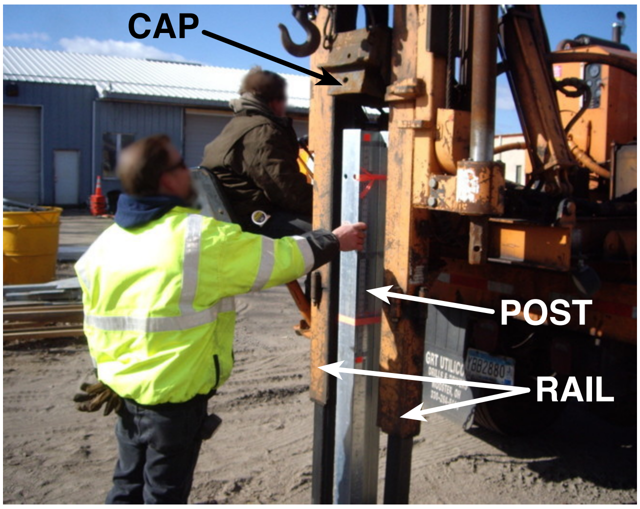

Figure 9: Loading a Post into the Machine.

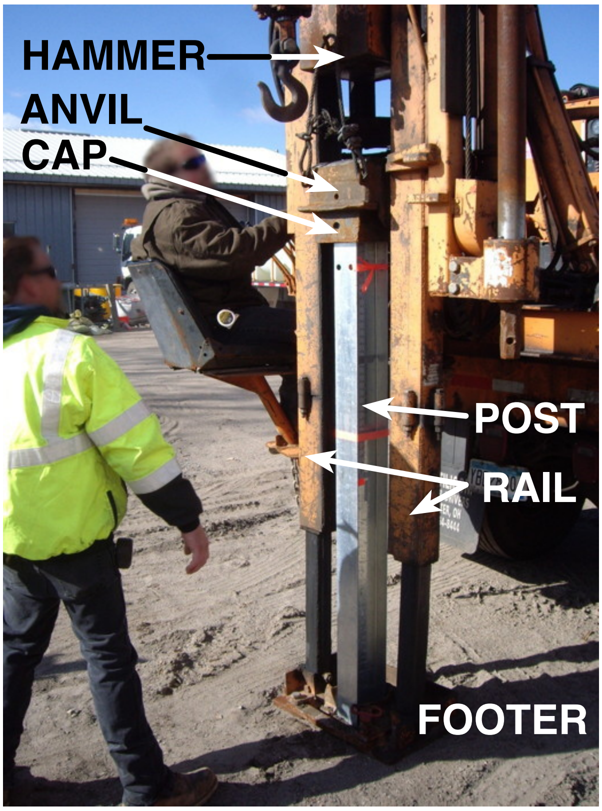

Figure 10: Post Loading and Secured by the Cap.

ejected from a post driver. In order to induce the post-ejection failure mode, tests were performed with the cap shifted to the side of the post, as illustrated previously in Figure 2.

Figure 9 shows a guardrail post being loaded into the machine during the experimental testing. The post secured properly in the machine by the cap is shown in Figure 10. High-contrast tape was attached to the post so that its motions could easily be tracked by machine-vision software. A ruler was also attached to the post so that scaling of the dimensions and speeds could be accurately achieved. A close-up picture of the post is shown in Figure 11.

Figure 11: Post Used in Testing.

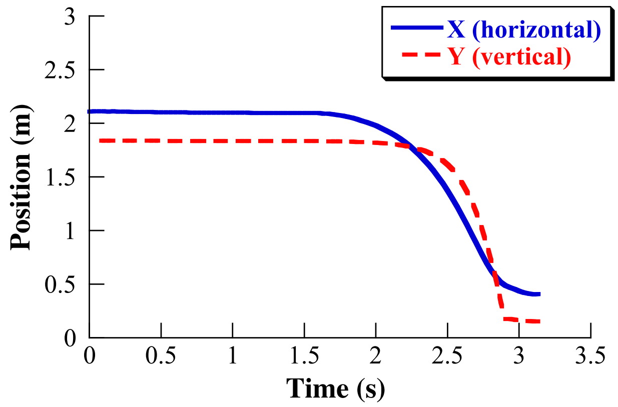

Figure 12: Position of Post Endpoint During Freefall.

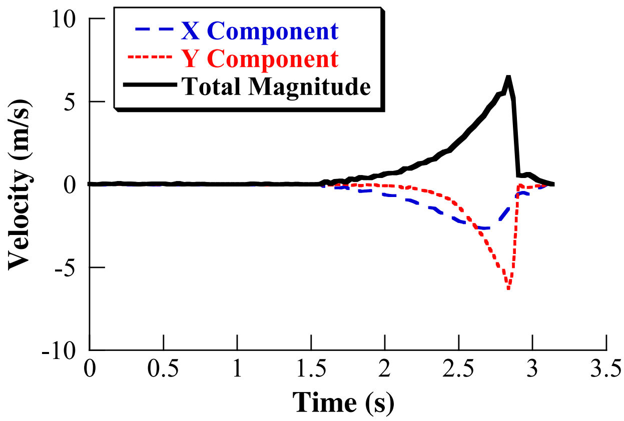

Figure 13: Velocity of Post Endpoint During Freefall.

A. Freefall Motion

An initial test was performed by simply allowing the guardrail post to fall freely under the effects of gravity. This provided a baseline response that can easily be verified by theoretical principles. Furthermore, it provides a check on the calibration of the video-tracking software. Figure 12 shows the position of the post endpoint as it falls during the test. This data was extracted from the video by locating the orange marker near the end of the post at each frame of the video. This pixel location was then converted to meters using the conversion factor provided by the ruler attached to the side of the post.

At the beginning of the fall, the endpoint moves more in the horizontal direction than the vertical direction. As the fall progresses, the endpoint begins to move more in the vertical direction, until it impacts the ground and abruptly comes to a stop. The velocity of the post endpoint is shown in Figure 13. The velocity increases in a parabolic manner until ground impact. Both the position and veloc-

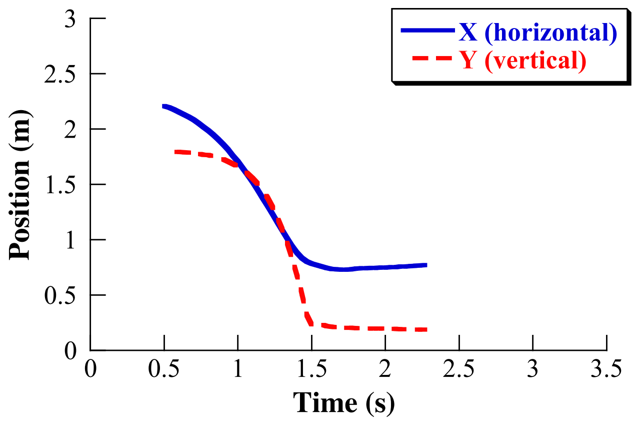

Figure 14: Position of Post Endpoint During Fall From a Released Cap.

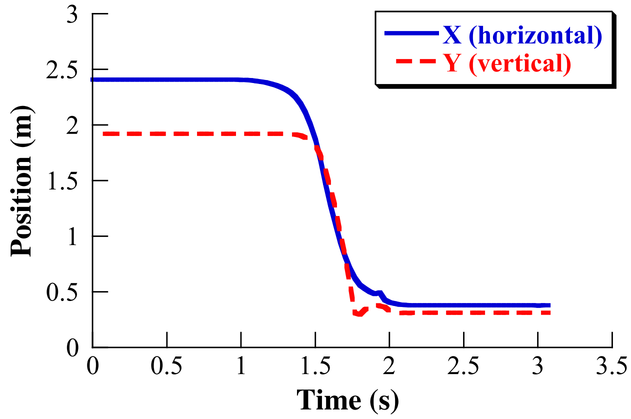

Figure 16: Position of Post Endpoint During Ejection by Falling Cap/Anvil/Hammer.

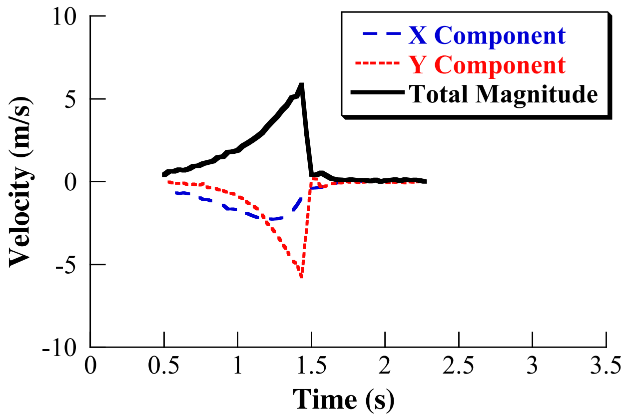

Figure 15: Velocity of Post Endpoint During Fall From a Released Cap.

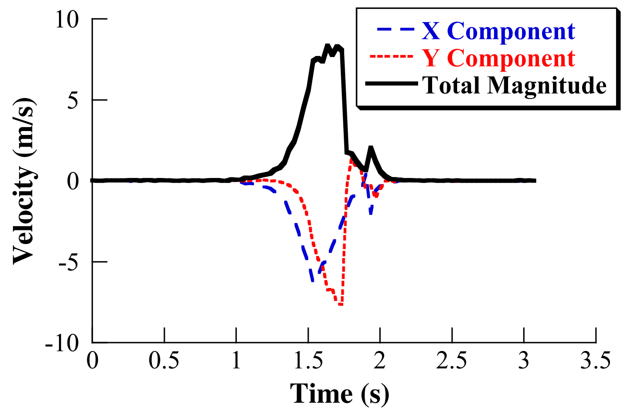

Figure 17: Velocity of Post Endpoint During Ejection by Falling Cap/Anvil/Hammer.

ity responses are what would be expected of an inverted pendulum beam falling over under the effects of gravity [7], [8], [9], [10], [11], [12], [13], [14], [15]. These results demonstrate that the experimental setup and video-tracking algorithm worked well to measure the post motion.

B. Falling From a Released Cap

An additional freefall test was conducted by placing the machine as a slight angle relative to vertical and then using the machine to pull the cap off of the guardrail post. The post then fell out of the machine, much like the initial freefall case. Figure 14 shows the position of the post endpoint as it fell away from the cap under the effect of gravity. The velocity of the post endpoint is shown in Figure 15. Both the position and velocity responses are very similar to the initial freefall test. This is to be expected, as the forces acting on the post in both cases are dominated by the effect of gravity. The cap-release case differs in a small way because the cap imparted some small forces to the post during the releasing process. Furthermore, the post was at a slightly different initial angle when it was released from the cap.

C. Post Ejection Caused by a Falling Cap/Anvil/Hammer

The guardrail post motion occurring during free fall could certainly cause significant injuries to a bystander being hit by the falling post. However, a post being ejected by the falling cap/anvil/hammer assembly, can reach much higher velocities and travel further from the machine.

To measure the post-ejection dynamics caused by a falling cap/anvil/hammer, a guardrail post was placed in the machine at a slight angle without the cap secured. The cap/anvil/hammer assembly was raised above the post and then released in the same manner that occurs during post-driving operations. Figure 16 shows the position of the post endpoint as it was pushed out of the machine by the falling cap/anvil assembly. The endpoint travels much faster from the upright position at the start of the event to the ground impact than it did during the freefall tests. This increased speed is demonstrated clearly by the velocity of the post endpoint shown in Figure 17.

D. Comparison of Post Velocities

In order to better compare the post velocities during freefall and during an ejection event, Figure 18 directly compares the velocities of the three cases described above as a function of the post height as it falls. It is clear that, throughout the fall, the post that was ejected by the falling cap/anvil/hammer travels at a much higher speed. The jagged portion of the curve for the Hammer Ejection

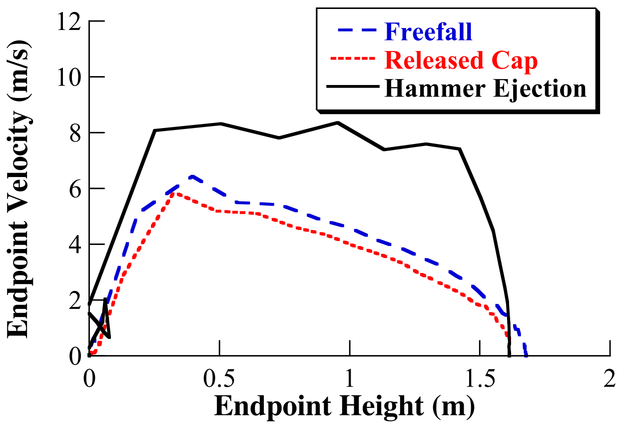

Figure 18: Velocity of Post Endpoint During as a Function of the Height of the Post.

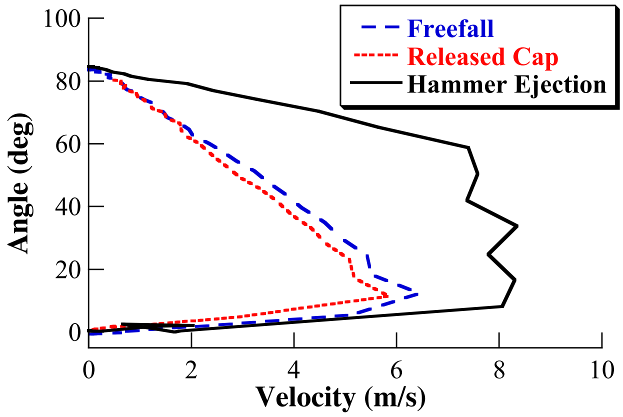

Figure 20: Angle of Post as a Function of Endpoint Velocity.

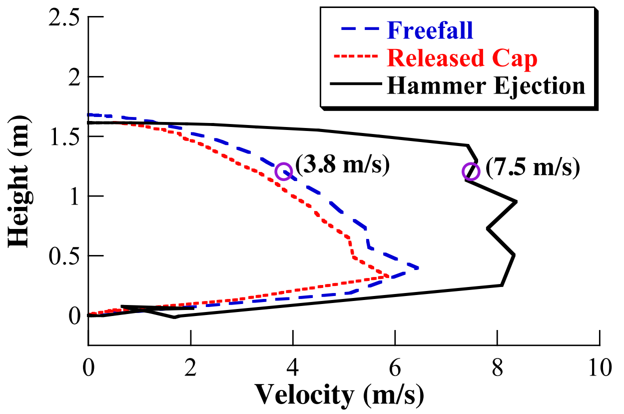

Figure 19: Height of Post as a Function of Endpoint Velocity.

case that occurs near the left side (0 height) is a product of the post bouncing after it hit the ground.

Another way to portray the data is to plot the height of the post endpoint as a function of its velocity. Such a plot is shown in Figure 19. This representation allows us to easily compare the velocity as various heights of the post. For example, if the post experienced freefall and impacted an object when its endpoint was 1.2m (4 feet) above ground, then the endpoint velocity would be 3.8 m/s. On the other hand, if the ejected post hit an object 1.2 m above ground, then its endpoint would be traveling at 7.5 m/s. That is nearly twice as fast as the freefalling post. The data is plotted in a similar manner in Figure 20, which shows the angle of the post as a function of its velocity during the fall.

The results of these tests clearly indicate that a post being ejected from the machine by the falling hammer is much more dangerous than a post that simply falls out under the force of gravity. Therefore, whenever the hammer is in use, the machine should utilize a redundant back-up safety device to restrict this hazardous failure mode. While such a safeguard system does not guarantee safety, proper application has been shown to improve it [16].

IV. CONCLUSIONS

Post drivers have a well-known failure mode wherein the post being driven into the ground can be ejected from the machine when the post is not secured properly. Misalignment of the restraining cap, or accidental use of the wrong cap, is a foreseeable operator error that necessitates the use of a guard against the post-ejection failure mode. Experiments conducted on a post driver indicate that the footer provided virtually no restraint on the post if the cap does not function correctly. Therefore, unless the cap is always secured to the top of the post, there is a significant risk associated with the post being ejected from the machine. Video-tacking measurements during the experiments indicate that the post can be ejected at very high speed and it can travel several meters from the machine.

REFERENCES

[1] R. Poecker and B. Sposito, "Guardrail installation noise level evaluation," Oregon Department of Transportation, Tech. Rep. FHWA-OR-RD-99-23, 1999.
[2] T. Backström and M. Döös, "The technical genesis of machine failures leading to occupational accidents," *International Journal of Industrial Ergonomics*, vol. 19, no. 5, pp. 361 – 376, 1997.
[3] R. T. Schisler, "Post driver," Apr. 10 1990, US Patent 4,915,180.
[4] T. P. Herrmann, "Automated post driver," Sep. 6 2005, US Patent 6,938,703.
[5] J. G. Reid, "Mechanical tee post driver," Oct. 6 2009, US Patent 7,597,156.
[6] E. Parsons, R. Collins, and B. Masters, "Post driver safety latch," Jun. 1 2006, US Patent App. 20060113444.
[7] A. Stephenson, "A new type of dynamic stability," *Proc. of the Manchester Literary and Philosophical Society*, 1908.
[8] E. R. Lowenstern, "Stabilising effect of imposed oscillations on a dynamical system," *Philosophical Magazine*, vol. 13, pp. 458–486, 1932.
[9] F. Phelps and J. H. Jr., "An analytical solution of the inverted pendulum," 1964.
[10] J. L. Bagdanoff and S. J. Citron, "Experiments with an inverted pendulum subject to random parametric excitation," pp. 447–452, 1965.
[11] H. Kalmus, "The inverted pendulum," *American Journal of Physics*, vol. 38, no. 7, p. 874, 1970.
[12] C. W. Anderson, "Learning to control an inverted pendulum with connectionist networks," in *American Control Conference, 1988*, june 1988, pp. 2294 –2298.
[13] T. Yamakawa, "Stabilization of an inverted pendulum by a high-speed fuzzy-logic controller hardware system," *Fuzzy Sets and Systems*, vol. 32, no. 2, pp. 161–180, 1989.

[14] F. Grasser, A. D'Arrigo, S. Colombi, and A. C. Rufer, "Joe: A mobile, inverted pendulum," *IEEE Transactions on Industrial Electronics*, vol. 49, pp. 107–114, February 2002.
[15] J. B. Morrell and D. Field, "Design of a closed loop controller for a two wheeled balancing transporter," in *Proceedings of the 2007 IEEE/RSJ International Conference on Intelligent Robots and Systems*, San Diego, CA, USA, Oct 29 - Nov 2 2007.
[16] T. Backström and M. Döös, "Problems with machine safeguards in automated installations," *International Journal of Industrial Ergonomics*, vol. 25, no. 6, pp. 573 – 585, 2000.

Determining the Inverse Kinematics Model of a Bucket Excavator's Digging Equipment

Marian Dima[1*], Catalin Francu[1*], Radu Ghelmeci[1]
[1]The Faculty of Technological Equipment, Technical University of Civil Engineering, Bucharest (Romania)

This paper presents a method to build the inverse kinematics model of a bucket excavator's digging equipment. The model is determined by using two different methods, the matrix method applied on the decoupled forward kinematics model and respectively the geometric model.

Keywords: Inverse kinematics; Bucket excavator; Matrix method

1. INTRODUCTION

The inverse kinematics model is especially important because it's the base for programming command and control of mechatronic systems. In specialty literature are presented some methods for determining the inverse kinematics model, out of which are used more often: matrix method, geometric method, quaternions method and Jacobi matrix method. In this paper the determination is carried out using the first 2 methods.

The attached problem can be expressed as follows: determine the variables of the driving joints while knowing the position and orientation of the end-effector.

2. INVERSE KINEMATICS MODEL DETERMINED BY USING THE MATRIX METHOD

In this method, the global transformation matrix of the end-effector is known:

$$U = \begin{pmatrix} n_x & o_x & a_x & p_x \\ n_y & o_y & a_y & p_y \\ n_z & o_z & a_z & p_z \\ 0 & 0 & 0 & 1 \end{pmatrix} = \begin{pmatrix} x_0 \cdot x_4 & x_0 \cdot y_4 & x_0 \cdot z_4 & p_x \\ y_0 \cdot x_4 & y_0 \cdot y_4 & y_0 \cdot z_4 & p_y \\ z_0 \cdot x_4 & z_0 \cdot y_4 & y_0 \cdot z_4 & p_z \\ 0 & 0 & 0 & 1 \end{pmatrix} \tag{1}$$

which is the position of the bucket's tooth tip and its orientation related to the fixed reference frame, figure 1.

Applying this method is easier if the entire mechanism is split up in two parts, positioning mechanism having the first 3 degrees of mobility and orientation mechanism having the remaining degrees of mobility.

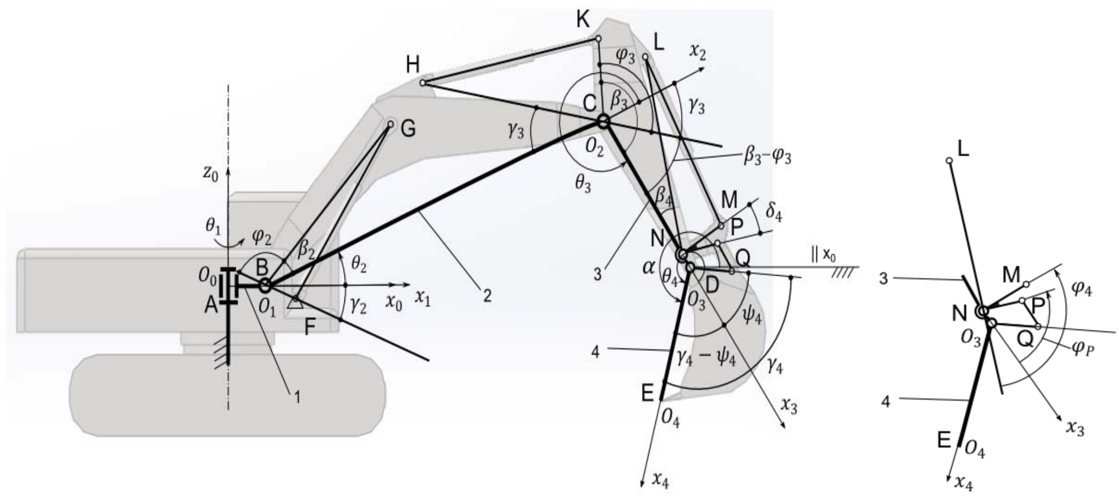

Figure 3: The kinematic scheme of the bucket excavator's digging equipment

According to this division, the forward kinematics model for the excavator's mechanism is expressed as:

$$_0T^4 = {_0T^3} \cdot {_3T^4} \tag{2}$$

First the problem regarding the positioning mechanism is solved for which we have the expression:

$$U_D = {_0T^1} \cdot {_1T^2} \cdot {_2T^3} \tag{3}$$

This relation is multiplied to the right with the inverse matrix of the $_0T^1$, which is $_1T^0$ and is obtained:

$$_1T^0 \cdot U_D = {_1T^2} \cdot {_2T^3} \tag{4}$$

In the right side of the equation is only one unknown, θ_1, and in the left side are the other unknowns.

Doing the calculations:

*Corresponding author: Technical University of Civil Engineering 122-124 Lacul Tei Blv., Bucharest, Romania, francu@mail.utcb.ro

$$\begin{pmatrix} \cos(\theta_1) & \sin(\theta_1) & 0 & -l_1 \\ 0 & 0 & 0 & 0 \\ \sin(\theta_1) & -\cos(\theta_1) & 0 & 0 \\ 0 & 0 & 0 & 1 \end{pmatrix} \cdot \begin{pmatrix} n_x & o_x & a_x & p_{xD} \\ n_y & o_y & a_y & p_{yD} \\ n_z & o_z & a_z & p_{zD} \\ 0 & 0 & 0 & 1 \end{pmatrix} = \begin{pmatrix} \cos(\theta_2) & -\sin(\theta_2) & 0 & l_2 \cdot \cos(\theta_2) \\ \sin(\theta_2) & \cos(\theta_2) & 0 & l_2 \cdot \sin(\theta_2) \\ 0 & 0 & 1 & 0 \\ 0 & 0 & 0 & 1 \end{pmatrix} \cdot \begin{pmatrix} \cos(\theta_3) & -\sin(\theta_3) & 0 & l_3 \cdot \cos(\theta_3) \\ \sin(\theta_3) & \cos(\theta_3) & 0 & l_3 \cdot \sin(\theta_3) \\ 0 & 0 & 1 & 0 \\ 0 & 0 & 0 & 1 \end{pmatrix} \tag{5}$$

or

$$\begin{pmatrix} n_x \cdot \cos(\theta_1) + n_y \cdot \sin(\theta_1) & o_x \cdot \cos(\theta_1) + o_y \cdot \sin(\theta_1) & a_x \cdot \cos(\theta_1) + a_y \cdot \sin(\theta_1) & p_{xD} \cdot \cos(\theta_1) + p_{yD} \cdot \sin(\theta_1) - l_1 \\ n_z & o_z & a_z & p_{zD} \\ n_x \cdot \sin(\theta_1) - n_y \cdot \cos(\theta_1) & o_x \cdot \sin(\theta_1) - o_y \cdot \cos(\theta_1) & a_x \cdot \sin(\theta_1) - a_y \cdot \cos(\theta_1) & p_{xD} \cdot \cos(\theta_1) - p_{yD} \cdot \sin(\theta_1) \\ 0 & 0 & 0 & 1 \end{pmatrix} = \begin{pmatrix} \cos(\theta_2+\theta_3) & -\sin(\theta_2+\theta_3) & 0 & l_2 \cdot \cos(\theta_2) + l_3 \cdot \cos(\theta_2+\theta_3) \\ \sin(\theta_2+\theta_3) & \cos(\theta_2+\theta_3) & 0 & l_2 \cdot \sin(\theta_2) + l_3 \cdot \sin(\theta_2+\theta_3) \\ 0 & 0 & 1 & 0 \\ 0 & 0 & 0 & 1 \end{pmatrix} \tag{6}$$

By comparing the elements from row 3, column 4 of both matrices we obtain:

$$p_{xD} \cdot \cos(\theta_1) - p_{yD} \cdot \sin(\theta_1) = 0 \tag{7}$$

And by solving the equation is obtained:

$$\theta_1 = arctg\left(\frac{p_{yD}}{p_{xD}}\right) \tag{8}$$

By comparing the elements from columns 4, rows 1 and 2 the following system of equations is obtained:

$$\begin{cases} p_{xD} \cdot \cos(\theta_1) + p_{yD} \cdot \sin(\theta_1) - l_1 = l_2 \cdot \cos(\theta_2) + l_3 \cdot \cos(\theta_2+\theta_3) \\ p_{zD} = l_2 \cdot \sin(\theta_2) + l_3 \cdot \sin(\theta_2+\theta_3) \end{cases} \tag{9}$$

by moving to the left side the θ_2 terms, pick up the squared of each equation, adding together the equations and substituting:

$$A = \frac{l_1^2 + l_2^2 - l_3^2 - 2l_1(p_{xD}\cos(\theta_1) - p_{yD}\sin(\theta_1)) + 2p_{xD}p_{yD}\sin(\theta_1)\cos(\theta_1) + (p_{xD}^2 - p_{yD}^2)\cos^2(\theta_1) + p_{yD}^2 + p_{zD}^2}{2l_2 p_{zD}}$$
$$B = \frac{-2l_1l_2 + 2l_2(p_{xD}\cos(\theta_1) + p_{yD}\sin(\theta_1))}{2l_2 p_{zD}} \tag{10}$$

the equation is obtained:

$$A - B\cos(\theta_2) = \sin\theta_2 \tag{11}$$

which can be solved :

$$\theta_2 = \arccos\left(\frac{AB \pm \sqrt{1 + B^2 - A^2}}{1 + B^2}\right) \tag{12}$$

Also from (9), by moving to the left side the θ_2 terms, and dividing the second equation to the first is obtained the θ_3 expression:

$$\theta_3 = arctg\left(\frac{p_{xD} \cdot \cos(\theta_1) + p_{yD} \cdot \sin(\theta_1) - l_1 - l_2 \cdot \cos(\theta_2)}{p_{zD} - l_2 \cdot \sin(\theta_2)}\right) - \theta_2 \tag{13}$$

The angle θ_3 can be determined the same way as θ_2. For that (4) is multiplied to the right with the inverse matrix of ${}_1T^2$ and is obtained:

$${}_2T^1 \cdot {}_1T^0 \cdot U_D = {}_2T^3 \tag{14}$$

which is:

$$\begin{pmatrix} \cos(\theta_2)\cdot(n_x\cos(\theta_1)+n_y\sin(\theta_1))+n_z\sin(\theta_2) & \cos(\theta_2)\cdot(o_x\cos(\theta_1)+o_y\sin(\theta_1))+o_z\sin(\theta_2) & \cos(\theta_2)\cdot(a_x\cos(\theta_1)+a_y\sin(\theta_1)) & \cos(\theta_2)\cdot(p_{xD}\cos(\theta_1)+p_{yD}\sin(\theta_1)-l_1)+p_{zD}\sin(\theta_2)-l_2 \\ -\sin(\theta_2)\cdot(n_x\cos(\theta_1)+n_y\sin(\theta_1))+n_z\cos(\theta_2) & -\sin(\theta_2)\cdot(o_x\cos(\theta_1)+o_y\sin(\theta_1))+o_z\cos(\theta_2) & -\sin(\theta_2)\cdot(a_x\cos(\theta_1)+a_y\sin(\theta_1)) & -\sin(\theta_2)\cdot(p_{xD}\cos(\theta_1)+p_{yD}\sin(\theta_1)-l_1)+p_{zD}\cos(\theta_2) \\ n_x\sin(\theta_1)-n_y\cos(\theta_1) & o_x\sin(\theta_1)-o_y\cos(\theta_1) & a_x\sin(\theta_1)-a_y\cos(\theta_1) & p_{xD}\sin(\theta_1)-p_{yD}\cos(\theta_1) \\ 0 & 0 & 0 & 1 \end{pmatrix} = \begin{pmatrix} \cos(\theta_3) & -\sin(\theta_3) & 0 & l_3\cdot\cos(\theta_3) \\ \sin(\theta_3) & \cos(\theta_3) & 0 & l_3\cdot\sin(\theta_3) \\ 0 & 0 & 1 & 0 \\ 0 & 0 & 0 & 1 \end{pmatrix} \tag{15}$$

Balancing the terms from column 4, rows 1 and 2 and dividing them, we obtain:

$$\theta_3 = arctg\left(\frac{-\sin(\theta_2)\cdot(p_{xD}\cos(\theta_1)+p_{yD}\sin(\theta_1)-l_1)+p_{zD}\cos(\theta_2)}{\cos(\theta_2)\cdot(p_{xD}\cos(\theta_1)+p_{yD}\sin(\theta_1)-l_1)+p_{zD}\sin(\theta_2)-l_2}\right) \tag{16}$$

Now, going to the orientation mechanism, knowing the angle of the bucket in relation to the fixed reference frame naming it α, figure 1, we can write:

$$\theta_2 + \theta_3 + \theta_4 = \alpha \tag{17}$$

$$p_x - p_{xD} = l_4\cos(\alpha)\cos(\theta_1)$$
$$p_y - p_{yD} = l_4\cos(\alpha)\sin(\theta_1) \tag{18}$$
$$p_z - p_{zD} = l_4\sin(\alpha)$$

From equation (17) and (18) follows:

$$\theta_4 = \alpha - \theta_2 - \theta_3 \tag{20}$$

$$p_{xD} = p_x - l_4\cos(\alpha)\cos(\theta_1) \tag{21}$$
$$p_{yD} = p_y - l_4\cos(\alpha)\sin(\theta_1)$$
$$p_{zD} = p_z - l_4\sin(\alpha)$$

Accordingly inverse kinematics model of the backhoe excavator’s digging equipment is:

$$\theta_1 = arctg\left(\frac{p_y}{p_x}\right)$$
$$\theta_2 = \arccos\left(\frac{AB \pm \sqrt{1 + B^2 - A^2}}{1 + B^2}\right)$$
$$\theta_3 = arctg\left(\frac{-\sin(\theta_2)\cdot(p_{xD}\cos(\theta_1)+p_{yD}\sin(\theta_1)-l_1)+p_{zD}\cos(\theta_2)}{\cos(\theta_2)\cdot(p_{xD}\cos(\theta_1)+p_{yD}\sin(\theta_1)-l_1)+p_{zD}\sin(\theta_2)-l_2}\right) \tag{22}$$
$$\theta_4 = \alpha - \theta_2 - \theta_3$$

to which we add the substitutions (10) and (21).

3. INVERSE KINEMATICS MODEL DETERMINED BY USING THE GEOMETRIC METHOD

The kinematic scheme of the open loop kinematic chain of the backhoe excavator’s digging equipment, for a random position is presented figure 2. For this kinematic chain the lengths of the bars are known l_1, l_2, l_3, l_4, position of the bucket’s tooth tip, p_x, p_y, p_z and its orientation α. For these conditions the determination of the angles θ_1, θ_2, θ_3, θ_4 of the joints is required.

$$\theta_1 = arctg\left(\frac{p_y}{p_x}\right) \tag{23}$$

The angle θ_3 is determined from the triangle BCD the cosines law:

$$BD^2 = BC^2 + CD^2 - 2BC \cdot CD \cdot \cos(\pi - \theta_3) \tag{24}$$

Having the substitutions in figure 2,

$$BD = r = \sqrt{r_o^2 + r_v^2}$$
$$r_o = \sqrt{p_x^2 + p_y^2} - l_1 - l_4 \cdot \cos(\alpha) \tag{25}$$
$$r_v = p_z + l_4 \cdot \sin(\alpha)$$

equation (23) becomes:

$$r_o^2 + r_v^2 = l_2^2 + l_3^2 - 2 l_2 l_3 \cos(\pi - \theta_3) \tag{26}$$

and is obtained:

$$\theta_3 = \pi + \arccos\left(\frac{l_2^2 + l_3^2 - r_o^2 - r_v^2}{2 l_2 l_3}\right) \tag{27}$$

if

$$l_2 - l_3 \le r \le l_2 + l_3 \tag{28}$$

Angle θ_2 is determined in 2 steps from the triangles BD_0D and BCD,

$$\theta_2 = \theta_{21} + \theta_{22} \tag{29}$$

From triangle BD_0D is obtained

$$\theta_{21} = arctg\left(\frac{r_v}{r_o}\right) \tag{30}$$

And from triangle BCD by using the sine law is obtained

$$\theta_{22} = \arcsin\left(\frac{l_3 \sin(\theta_3)}{r}\right) \tag{31}$$

and in the end

$$\theta_2 = arctg\left(\frac{r_v}{r_o}\right) + \arcsin\left(\frac{l_3 \sin(\theta_3)}{r}\right) \tag{32}$$

For angle $\theta_4 = \theta_4(\alpha)$ the equation (20) is used.

Accordingly inverse kinematics model of the backhoe excavator’s digging equipment determined by using the geometric method is:

$$\begin{aligned} \theta_1 &= arctg\left(\frac{p_y}{p_x}\right) \\ \theta_2 &= arctg\left(\frac{r_v}{r_o}\right) + \arcsin\left(\frac{l_3 \sin(\theta_3)}{r}\right) \\ \theta_3 &= \pi + \arccos\left(\frac{l_2^2 + l_3^2 - r_o^2 - r_v^2}{2 l_2 l_3}\right) \\ \theta_4 &= \alpha - \theta_2 - \theta_3 \end{aligned} \tag{33}$$

to which we add the substitutions (25).

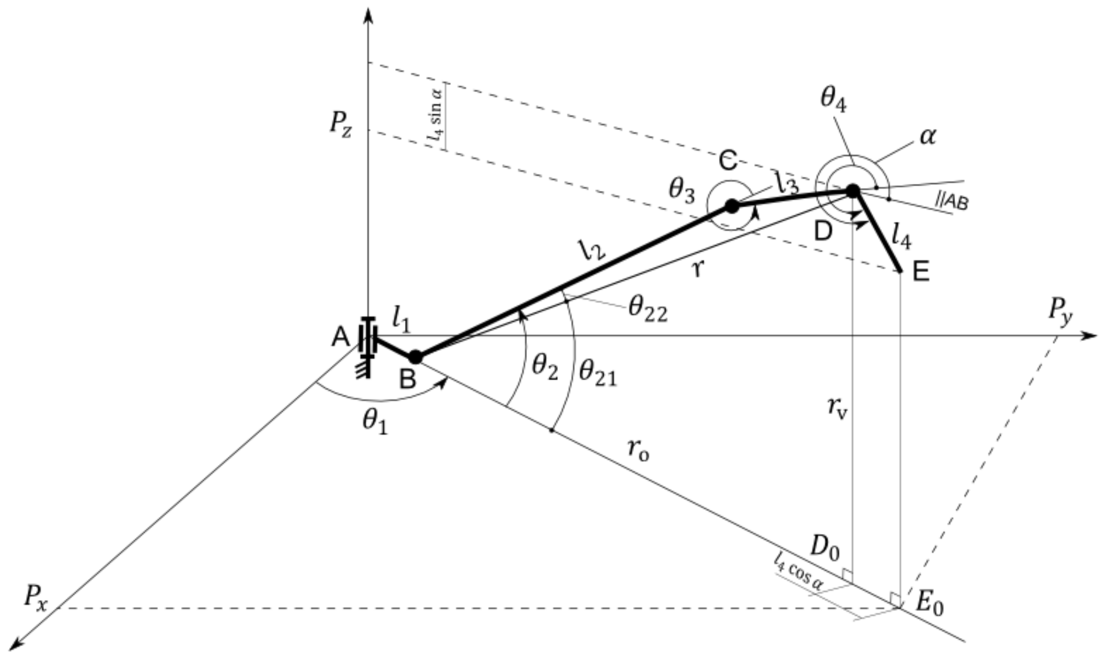

Figure 2: The kinematic scheme of the open loop kinematic chain of the backhoe excavator’s digging equipment

4. THE RELATION BETWEEN THE VARIABLES OF THE DRIVING KINEMATIC JOINTS AND HYDRAULIC CYLINDERS STROKES

Having the substitutions from figure 1, for the hydraulic cylinder FG that is driving the boom we have the equations:

$$\begin{aligned} \varphi_2 &= \pi - \beta_2 - \gamma_2 - \theta_2 \\ s_2 &= \sqrt{BG^2 + BF^2 + 2BG \cdot BF \cdot \cos(\varphi_2)} \end{aligned} \tag{34}$$

Similarly, for the hydraulic cylinder that drives the stick, HK, we have the equations:

$$\varphi_3 = \theta_3 + \beta_3 + \gamma_3 - 2\pi \tag{35}$$

$$s_3 = \sqrt{HC^2 + KC^2 + 2HC \cdot KC \cdot \cos(\varphi_3)}$$

For the hydraulic cylinder of the bucket, the four-bar mechanism DQPN is solved firstly. Beginning with the angle:

$$\psi_4 = \theta_4 + \gamma_4 - 2\pi$$

and substitutions:

$$a = \frac{DQ^2 - PQ^2 + NP^2 + ND^2 - 2 \cdot NP \cdot ND \cdot \cos(\psi_4)}{2 \cdot DQ \cdot NP \cdot \sin(\psi_4)}$$
$$b = \frac{NP \cdot \cos(\psi_4) + ND}{NP \cdot \sin(\psi_4)} \qquad (36)$$

is obtained

$$\varphi_p = \text{acos}\left(\frac{a \cdot b \pm \sqrt{1 + b^2 - a^2}}{1 + b^2}\right) \qquad (37)$$

and finally:

$$\varphi_4 = \beta_4 + \varphi_p + \delta_4$$
$$s_4 = \sqrt{NM^2 + LN^2 + 2NM \cdot LM \cdot \cos(\varphi_4)} \qquad (38)$$

5. ALGORITHM FOR USING THE MATRIX METHOD

a) The desired path of the bucket's tooth tip is bring in parametric form and related to the fixed reference frame $O_0x_0y_0z_0$,

$$x = x(u)$$
$$y = y(u)$$
$$z = z(u)$$

b) The orientation of the bucket is expressed during the movement on the path in relation to the points on the path,

$$\alpha = \alpha(x(u), y(u), z(u))$$

c) Let the values of the path's coordinates be the coordinates of the bucket's tooth tip

$$p_x = x(u)$$
$$p_y = y(u)$$
$$p_z = z(u)$$

d) The angle θ_1 is determined from the first equation (22).

e) The coordinates of the point D are determined from equations (21).

f) The angles θ_2, θ_3, θ_4 are determined with equations (22).

g) The lengths of the hydraulic cylinders are determined with (34), (35) and (38).

6. CONCLUSIONS

- Inverse kinematics model of a bucket excavator's digging equipment can be determined either by using the forward kinematic model or by using the geometric method;
- By comparing the results of the two methods we can observe that 2 of the equations are identical;
- We can also observe that the equations contain inverse trigonometric functions, which means that there are difficulties for the programmer and attention on the numeric results is necessary.

REFERENCES

[1] Siciliano B., Sciavicco L., Villani L., Oriolo G., "*Robotics. Modelling, Planning and Control*", Springer, 2009

[2] Richard S. Hartenberg, Jacques Denavit, "*Kinematic synthesis of linkages*", McGraw Hill, 1964

[3] Raicu, A., Bruja, A., "*Mecanisme*", UTCB, 1996

[4] Brochure "*Volvo Excavators EC140D*"

Adaptation of Earth-Moving Machines to External Loading Conditions

V. Shevchenko[1], Associate Professor, Candidate of Engineering Sciences,
[1]Mechanical Faculty, Department of Road Building Machines, Kharkiv National Automobile and Highway University, Kharkiv (Ukraine)

In the process of field operation earth-moving machines experience combined stresses caused by the work environment. Such impact parameters depend on the excavated soil conditions, kind of work operations performed, type of the implement mounted on the machine. During the machine life-cycle its loading conditions can change many times. The field research revealed that changes in form and type of external loadings do not allow ensuring a high reliability and capacity of an earth-moving machine in any conditions of field operation. To achieve a high level of the mentioned parameters the machine should be equipped with systems enabling adaptation to external loading conditions.

Keywords: Earth-moving Machine, Adaptation, Space of dynamic states

1. INTRODUCTION

Loading conditions for each earth-moving machine (EMM) are variable and individual. Mass-produced machines are designed according to normative techniques and do not always conform to specific conditions of their operation. The latter are determined, first of all, by parameters of the operating environment, type of the most frequently performed working operations, spicifity of performing work by a certain operator. Changing the load conditions often results in decreasing the performance indexes of EMM, such as working capacity, reliability etc. To solve the problem of adaptation of a mass-produced machine to real operation conditions, at the stage of development there required a thorough investigation of all its possible load conditions and working out technical measures allowing the machine to adapt to these conditions within the set level of values of the dominant criteria.

2. ANALYSIS OF SCIENTIFIC RESEARCHES

The idea of adaptation got further development and was considered more thoroughly at solving tasks of controlling open dynamic systems. The most wide-spread approach involves generating equations of kinetics of material systems described by Lagrange equation of second kind [1].

$$D_i L = S_i + u_i, D_i = \frac{d}{dt}\frac{\partial}{\partial \dot{q}_i} - \frac{\partial}{\partial q_i}, i = 1,2,...,n \quad (1)$$

where D_i - differential operator of Euler-Lagrange, $L = T - \ddot{I}$ - Lagrange function of a mechanical system, T - system kinetic energy, $\ddot{I}$ - system potential energy, S_i - vector of generalized forces, q_i - system generalized coordinates. Solving the adaptation problem is based on determination of controlling the target conditions and realization of adaptive algorithm. In overwhelming majority at generating a mathematical model deterministic approaches are considered.

In relation to control systems there considered one of the two types of tasks of a mechanical system adaptive stabilization with respect to the desired law of motion $q_p(t)$ [1]:

1. Passive stabilization. Implies solving the inequality

$$\left\| q(t) - q_p(t) \right\|^2 + \left\| \dot{q}(t) - \dot{q}_p(t) \right\|^2 < \delta, \quad (2)$$

where t - time, $\delta > 0$ - required accuracy of controlling the system movement.

2. Optimal stabilization. In this case it is required to meet conditions (2) at simultaneous minimization of the composite function of the control system quality

$$I(x, u, \tau, \overline{\tau}, t) \to \min_{u(x,\overline{\tau}) \in u}, \quad (3)$$

The presented composite function can describe possible energy, power, time and other types of consumption [1].

In work [2] the authors draw attention to the fact that the vast number of dynamic systems are essentially nonlinear. At that the impact of environment on the object under study is often uncontrolled and uncertain.

On the basis of analysis of nonlinear dynamic systems behavior, the authors propose a new approach to the problem of synthesis of the adaptive control system [2]. It is suggested to use achievement of the desired dynamic states as control objectives, which excludes analysis in accordance with the known Lyapunov stability conditions. Thus, to solve the problems of adaptive control in systems with non-equilibrium and unstable target dynamics of a broad class of nonlinear dynamic systems, it is necessary to describe nonlinear dynamic systems in a language that does not require precise knowledge of differential equations of the object itself, as well as a mathematical apparatus to analyze compounds of such objects [2]. Principles and limitations in the problem of adaptive controller synthesis follow from the analysis of function spaces of the object state. For developing mathematical models of the objects and describing the objective control functions in conditions of nonlinearity and uncertainty, according to the authors, it is necessary to apply the apparatus of fuzzy mathematics. This approach to the synthesis of adaptive control systems is new and requires further research. Works by V.A. Meshcherjakov [3, 4] are an example of implementing the new approaches to EMM adaptive control. The author reasonably states that for developing EMM adaptive control, it is necessary to rely on information about dynamics of EMM working processes. For this purpose two approaches should be

*Corresponding author: valeriy_shevchenko_2013@mail.ru

developed. The first one is based on developing analytical models of working processes elements and combining them into a general simulation model. Such approach is based on a priori information about EMM design. The second approach to simulation of EMM working processes is based on identification of the working processes that allows creating adaptive dynamic models on the basis of experimental data characterizing parameters of such processes. The specified approach makes it possible to identify and simulate hidden dependencies between the parameters of the working processes without full information about EMM design and the environment characteristics [4]. The author gives preference to the second approach and proposes to simulate EMM working processes by means of self-learning neural network dynamic model [3].

Ideas proposed by V.A. Meshcherjakov suggest, first of all, availability of a real machine and carrying out a complex of experimental trials to "teach" the developed neural network dynamic model. In the case studies realizing the author's developments, the control objectives are simplified and practical. Thus, at analyzing the process of moving soil by a motor-grader, the criterion of maintenance of the maximum traction power is suggested to be the control objective [5]. When blading and grading the earth road bed the target control criterion is minimizing deviation of the working attachment vertical coordinates from the designed values. To implement the control action, a hydraulic actuator of the working attachment control and regulation of EMM motion speed are most commonly used.

Such an approach does not take into account the fact that for essentially nonlinear dynamic systems, which EMMs are, characteristic with a smooth variation of the parameters is a manifestation of bifurcational phenomena as well as processes of dynamic chaos generated by the machine itself. The considered adaptive control principles in most of the mentioned situations can only partially ensure the specified level of complex quality indicators characterizing EMM operational properties.

3. FACTORS CAUSING CHANGE OF EMM LOADING CONDITONS

To develop a strategy of EMM adaptation to external loading conditions, it is necessary to determine factors causing changes in characteristics of acting external loadings. The analysis of operation conditions of earth-moving machinery shows that there are several such factors. The most important of them are physical and mechanical properties of the working environment, accidental influence of the operator on the machine work as well as the parameters of the working process itself. The latter are determined by a number of peculiarities and aspects.

For improving the efficiency of earth-moving machines, they are used to perform various working operations. At that, each operation is characterized by its own loading conditions. For example, at performing operations of cutting and transporting soil and materials, external loadings are reliably described as a random process [6]. At the same time, at implementation of working operations associated with unsteady movement both of the machine and its working attachment, the loading conditions can be rather precisely described as the determined dynamic process [7].

In figures 1 and 2 oscillograms of variation in time of the horizontal effort on the motor-grader blade corresponding to the specified processes are presented. The given graphs demonstrate that speed characteristics of the implemented work process have a considerable impact on the loading conditions. Some authors point to the fact that with increase in the speed the resistance to digging increases as well, but none of them pays attention to changes in loading conditions [8, 9]. The graphs show variation in time of the horizontal component of digging resistance when performing the same operation but at different speeds. It should be noted that the specified speeds are recommended to perform typical working operations.

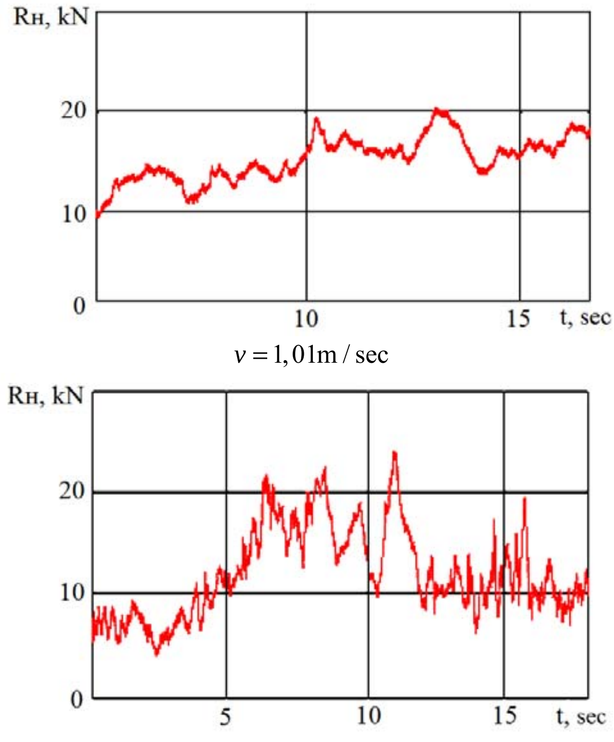

$v = 1,21\text{m} / \text{sec}$

Figure 1: Oscillograms of variation in time of the horizontal component of resistance to soil digging by a motor-grader

The important factor for determining conditions of EMM loading is the method of performing one and the same working operation but using different techniques. Thus, for instance, digging discrete material by a single-bucket front-end loader can be performed by various techniques:

– movement of the working attachment in horizontal direction due to realization of the maximum tractive force and mass inertia of the machine;

– movement of the machine in the horizontal direction at a simultaneous boom swing;

– deepening of the work attachment in a pile of material at a simultaneous bucket swing;

– combining several of these techniques.

Each technique forms its own condition of EMM loading.

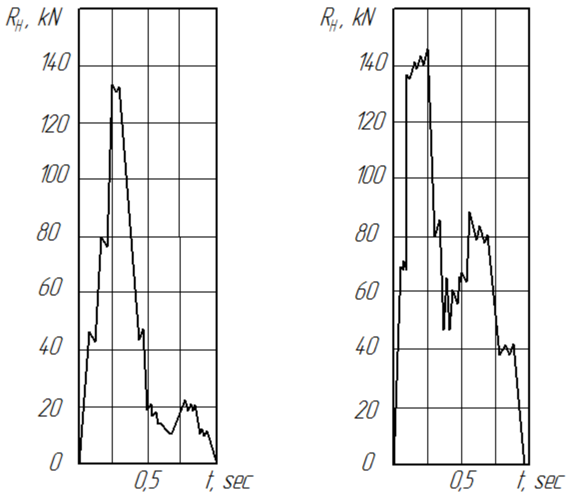

$v = 1,01\text{m/sec}$ $v = 1,21\text{m/sec}$

Figure 2: The horizontal loading on the motor-grader blade at hitting a boulder

Another factor influencing the formation of loading conditions is changing the direction of the external load resultant. At different stages of the operational cycle the machine takes up different types of loading. Thus, at digging soil, forces of work resistance on the working attachment (mainly horizontal loadings are taken into account) are prevailing. While at the transportation mode the dominant are vertical weight and inertial loadings. The conducted experiments showed that at transportation modes the stress motion acting in EMM main metal construction are comparable with stresses occurring in the digging modes and sometimes exceed them.

The type of working attachment installed on EMM has a significant impact on external loading conditions. Taking into consideration that one of perspective directions of EMM development is common use of various replaceable working attachment, a wide range variation of acting loadings should be expected. So, it is recommended to use not less than 30 replaceable working attachment for motor-graders, and more than 100 - for single-bucket front-end loaders. The machine designed for implementation of standard working operations by its working attachment, in real conditions at its replacing will automatically be subject to a new, not taken up before, condition of loading.

Largely, EMM loading conditions are determined by its design features. Being an essentially nonlinear dynamic system consisting of a number of basic units (engine, transmission, chassis, metal construction, working attachment and control systems), each of them having its own dynamic characteristics and complicated interrelations, in conditions of real operation the machine can by itself, without the operator intrusion, vary loading conditions of each unit [10, 11]. In the course of experiments with the medium motor-grader at performing operations, during which blocking of the main working attachment was carried out (the blade deepening into the soil at a speed until the complete stopping down of the machine) there was noticed occurrence and development of uncontrolled oscillating process in individual machine units, Figure 3. It is important, to our opinion, that the oscillations were developing in the machine units not simultaneously. Thus, in a number of experiments the development of oscillating processes was noticed in the metal construction and the hydraulic actuator of the blade control, when the transmission worked in the design mode and vice versa.

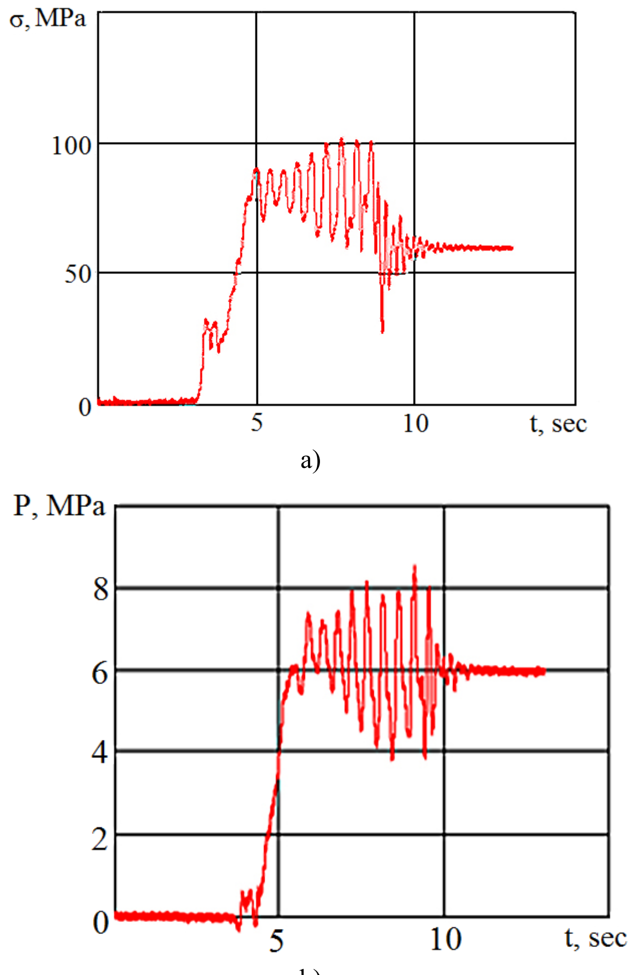

Figure 3: Oscillograms of variation in time of primary stress in the centre girder (a) and pressure of the hydraulic fluid in the main blade hydraulic lift-cylinders (b)

Growth of working operation speed significantly increases the probability of occurrence and development of uncontrolled spontaneous oscillations in individual units. With an initial vehicle speed of up to 0.8 m/sec in conditions of movement close to locking of the working attachment, oscillatory processes of self-excited type in the motor-grader systems were not registered at all. If the operating speed is about 1.2 m/sec and higher, the probability of occurrence and development of such processes increases up to 100%. Modern techniques of EMM design do not imply studying loading conditions of the kind and most often do not consider constructive measures allowing to avoid them.

4. THE GENERAL BLOCK SCHEME OF THE PROCESS OF EMM ADAPTATION TO EXTERNAL LOADING CONDITIONS

Changing the working attachment, type of working operations, stages of the machine working cycle, speeds of the working operation performance, type of the processed material cause changing in loading conditions of both EMM itself and its individual units. The experiments show that variations of frequency and amplitude of the loadings acting in these cases have very wide limits. Such a complex change of loading conditions can lead to changing values of the main performance criteria of the machine: working capacity, reliability indexes, energy and economic parameters, performance index etc. [12, 13]. From our point of view, the problem of EMM adaptation to acting external loadings is that it should meet the specified level of the criteria values regardless of the type and parameters of working operation performed.

On the assumption of the above mentioned remarks, the general block scheme of the adaptation process has the view as it is presented in Figure 4.

The most important element of the scheme is space of EMM dynamic states, which limits are determined by specified values of the machine performance criteria. The space itself includes a miltifactorial complex of acceptable loading conditions satisfying the set level of criteria. It is possible to determine the limits of such space describing the performance criteria by inequations taking into account not only parameters of the working environment and working operations performed but geometrical, kinematic and dynamic parameters of the machine itself.

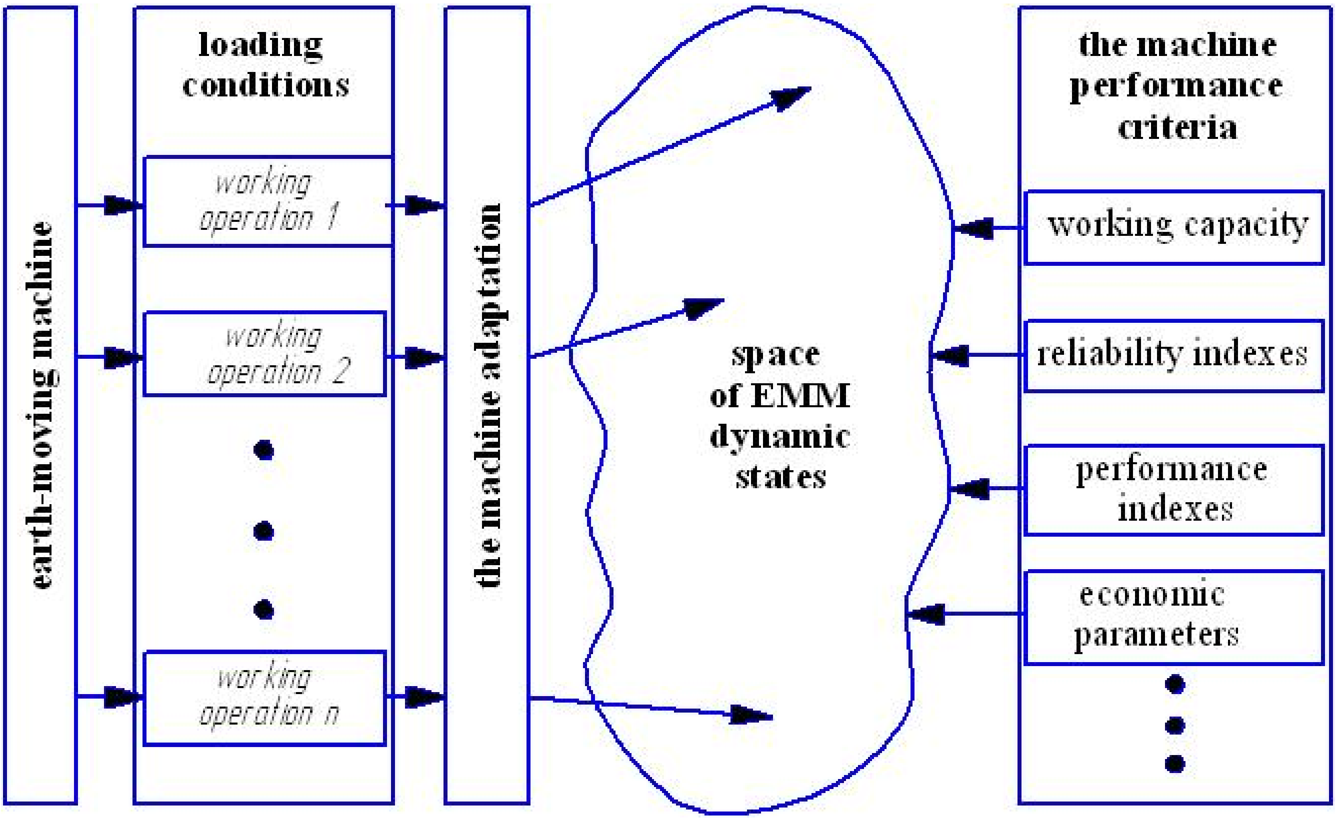

Figure 4: The general block scheme of EMM adaptation to conditions of external loading

Thus, determining limits of EMM space of dynamic states is reduced to solving the task of multicriteria optimization [14]. A significant number of criteria, their inconsistency considerably complicate solving the given task and sometimes make it rather problematic. However, a survey conducted among specialists of operating organizations show that for different types of EMM in different conditions there put forward a limited number of requirements to the machine performance criteria. This allows to allocate several dominant (the most important) ones from the list of criteria and perform all the subsequent mathematical operations only on their basis. In this case the task is simplified to a certain degree.

The very process of adaptation involves changing EMM parameters so that loading conditions both of the machine and its units corresponded to the designated space of dynamic states.

For realizing the adaptation process two approaches can be used: analytical and experimental one.

The analytical approach suggests development of a generalized dynamic model of EMM presented as a system of differential equations of motion. Choice of adjustable EMM parameters and the limits of their variation are based on qualitative and numerical analysis of the developed generalized model. In view of a great variety of EMM models and substantial volume of computation, realization of this approach is possible only at development of a specialized software support.

The experimental approach allows realizing the machine adaptation "on the fly", in the process of implementing a certain working operation. Problems of such approach are reduced to solving the following tasks:

– development of data measuring system with a reasonable number of data sources (sensors) and determination of places for their installation for complete description of loading conditions of EMM and its units;

– constructive provision of a set of the machine parameters, which variation has the greatest impact on loading conditions;

– intellectualization of the adaptation system, which lies in developing self-learning bundled software allowing in conditions of impact of random loads with determinate trend to make prompt rational decisions on EMM modifications within the set of the adjustable parameters.

Thus, technical realization of the adaptation system will allow rapid adaptation of mass-produced EMM in correspondence with conditions of their loadings.

5. CONCLUSIONS

Loading conditions of EMM and its units is determined by a number of factors, the main of which are: the worked material parameters; type and kinematic parameters of the working operation performed; geometric, kinematic and dynamic parameters of the machine itself.

The complex of performance criteria of the machine allows determining the space of the machine acceptable dynamic states meeting the specified values of the criteria.

The main task of the machine adaptation is transformation of its geometrical, kinematic and dynamic parameters allowing irrespective from the type and method of performing working operations to ensure a guaranteed matching with the space of the EMM acceptable dynamic states.

REFERENCES

[1] Тертычный-Даури В.Ю. Адаптивная механика. – 2-е изд., перераб. и доп. – М.: Изд-во «Факториал Пресс», 2003. – 464 с.

[2] Тюкин И.Ю., Терехов В.А. Адаптация в нелинейных динамических системах. – М.: Издательство ЛКИ, 2008. – 384 с.

[3] Мещеряков В.А. Нейросетевая динамическая модель рабочего процесса землеройной машины // Межвузовский сборник трудов молодых ученых, аспирантов и студентов. Омск: СибАДИ, 2004. – Вып. 1, ч. 1. – с. 135-141.

[4] Мещеряков В.А. Адаптивное управление рабочими процессами землеройно-транспортных машин. – Автореф. дис. на соиск. уч. степени доктора технических наук. – Омск, 2007. – 42 с.

[5] Бузин Ю.М. и др. Пути повышения эффективности работы автогрейдеров. – Ж. «Строительные и дорожные машины». - № 10. – 1986. – с. 2-3.

[6] Федоров Д.И. Рабочие органы землеройных машин. - 2-е изд., перераб. и доп. – М.: Машиностроение, 1989. – 368 с.

[7] Наукові основи створення високоефективних землерийно-транспортних машин / Кириченко І.Г., Назаров Л.В., Нічке В.В. та ін. – Харків: ХНАДУ, 2003. – 588 с.

[8] Ничке В.В. Надежность прицепного и навесного оборудования тракторов. – Харьков: Вища шк. Изд-во при Харьк. ун-те, 1985. – 152 с.

[9] Завьялов Л.М., Завьялов М.А., Кузнецова В.Н. Взаимодействие дорожных и строительных машин с контактной средой: Монография. – Омск: Изд-во «Полиграфический центр КА11», 2011. – 370 с.

[10] Проектирование машин для земляных работ / Под ред. А.М. Холодова. – Харьков: Вища шк. Изд-во при Харьк. ун-те, 1986. – 272 с.

[11] Ксеневич И.П. Аспекты проектирования сложных вероятностных нелинейных динамических неголономных систем. – Ж. «Тракторы и сельскохозяйственные машины». – 2007. - № 8

[12] Брауде В.И., Семенов Л.Н. Надежность подъемно-транспортных машин. – Л.: Машиностроение, Ленинградское отд-ние, 1986. – 183 с.

[13] Краснокутський В.М., Якість будівельних і дорожніх машин / Краснокутський В.М., Пімонов І.Г., Пімонов Г.Г. – Харків: ХНАДУ, 2011. – 276 с.

[14] Дубров Ю.А., Травкин С.И., Якимец В.Н. Многокритериальные модели формирования и выбора вариантов систем. – М.: Наука, Гл. ред. физ.-мат. лит., 1986. – 296 с.

Increasing the Efficiency of the Operation of the Batch-type Earth-moving Machines at the Expense of Using the Pneumatic Storage System

Leonid Khmara[1], Anton Kholodov[2,*]
[1]Mechanical Faculty, Department of Road Building Machines, Prydniprovs'ka State Academy of Civil Engineering and Architecture,
[2]Mechanical Faculty, Department of Road Building Machines, Kharkiv National Automobile and Highway University (KhNADU)

This paper presents the cyclograms of power distribution and the schemes of distribution of power flows for the work cycle of bulldozers, scrapers and graders equipped by pumped hydrostorage systems.

Key words: Accumulator, Energy, Hydraulic drive, Power, Power flow

INTRODUCTION

At the present time not mechanized, heavy and labour-intensive work can hardly be found in the road building, municipal or agricultural sector. In all the mentioned industries earthmoving machines (EMM) are used. One of the main issues at large output volumes is the cost of the manufactured products. The cost of fuel, which is nowadays continuously increasing, has a direct impact on the cost of products. Therefore, in the epoch of progressing energy crisis the possibility to reduce fuel consumption at set productivity of a vehicle or increase its productivity at set fuel consumption is of growing interest. In this regard the major and primary task facing the creators of earthmoving machines in the next decade will be increasing of their efficiency and competitiveness on the global market. The basic performance characteristics of earthmoving machines are working capacity, fuel, materials and energy consumption, reliability, social adjustment (safety, human factor and environmental performance) and as a consequence, the cost of the manufactured products and the performed work.

In this connection the urgent and perspective direction is considered to be advancing EMMs efficiency due to increase of their working capacity and decrease of fuel consumption that brings to reduction of the cost of manufactured products.

ANALYSIS OF PUBLICATIONS

The analysis of achievements of industrial construction technology allows to allocate a number of the main directions of development and researches in the field of earthmoving equipment, methods to intensify its operation and increase its efficiency. These directions are substantially predetermined by general provisions of mechanical engineering development.

The first direction covers problems of increasing reliability and competitiveness of such machines and mass-produced complexes as well as machines to be introduced [1]. The second direction includes problems of improvement of the drive and hydraulic systems of the machines work process control [5, 6, 7, 8, 9, 11]. The third direction is characterized by works on automation and ways of earthmoving machines robotization. The fourth direction is connected with problems of improvement of the machines functional properties and perfection of their working attachment on the basis of achievements in technology and fundamental sciences as well as creation of heavy machines and machines for construction works in space-limited environment [1]. The fifth direction characterizes one of the most important tendencies in development of construction and road mechanical engineering as a branch providing production of new equipment and includes problems of using the means and methods of automated design and research of the machines in the course of their creation and operation.

The carried out analysis of works on increasing the efficiency of earthmoving equipment and methods of energy storage shows that:

– at present recommendations on development of earthmoving equipment with the energy storage system on the basis of hydro-pneumatic accumulators are lacking. The existing methods either consider possibility of installation of such systems on carrying and lifting machines to accumulate the energy of the load moving down [9, 10] or consider flywheel systems [5], which are rather inconvenient to be used on hydraulically operated EMMs for they accumulate the mechanical instead of hydraulic energy. To choose the effective storage system further researches are required;

– studies of interrelations between traction characteristics, geometrical and weight parameters of EMMs and operation of the hydro-pneumatic accumulating system are not highlighted in the publications [7]. There are no common criteria describing parameters of the hydro-pneumatic accumulating system in the traction and energy accumulation mode with EMMs working conditions and their technical specifications;

– there are no information on influence of the hydro-pneumatic accumulators operation mode on that one of the machine working attachment.

PURPOSE AND TASKS

The purpose of the work is increasing EMMs efficiency due to storage of the energy accumulated in hydro-pneumatic accumulators at transportation modes to improve their working capacity at the expense of reducing the cycle time and fuel consumption through using the accumulated energy in the digging mode.

Corresponding author: Kharkiv National Automobile and Highway University, anton_kholodov@mail.ru

For achievement of the set purpose it is required to solve the following tasks:

– to determine the character of power distribution in the work cycle for EMMs of cyclic operation on the basis of the existing theoretical research and the conducted field research of pumped hydrostorage systems [2, 3, 4];

– to develop theoretical justification for using of the pumped hydrostorage systems on EMMs.

THEORETICAL JUSTIFICATION OF USING PUMPED HYDROSTORAGE SYSTEMS ON EMM

At using the hydrostorage systems in the bulldozer work cycle, the stage-by-stage engine power demand will change (Fig. 1) and redistribution of the power flows will take place (Fig. 2).

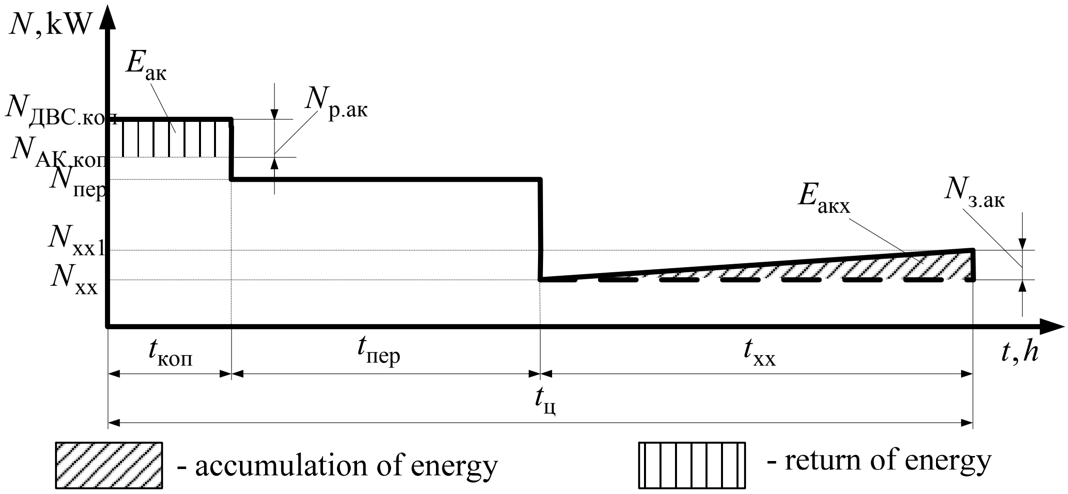

Figure 1: The work cycle of a bulldozer with application of a pumped hydrostorage system: $E_{ак}$ – energy spent by the accumulator at the stage of digging; $N_{р.ак}$ – power spent by the accumulator at the stage of digging; $E_{акх}$ – energy accumulated at idle running; $N_{з.ак}$ – power accumulated at idle running; $N_{ДВС.коп}$ – ICE power at digging operation without application of the pumped hydrostorage system; $N_{АК.коп}$ – ICE power at digging operation with application of the pumped hydrostorage system; $N_{пер}$ – ICE power at earth handling; $N_{хх1}$ – power spent at idle running with application of the pumped hydrostorage system; $N_{хх}$ - power spent at idle running without application of the pumped hydrostorage system; $t_{коп}$ – time of excavation; $t_{пер}$ – travel time; $t_{хх}$ – time of idle running; $t_{ц}$ – cycle time.

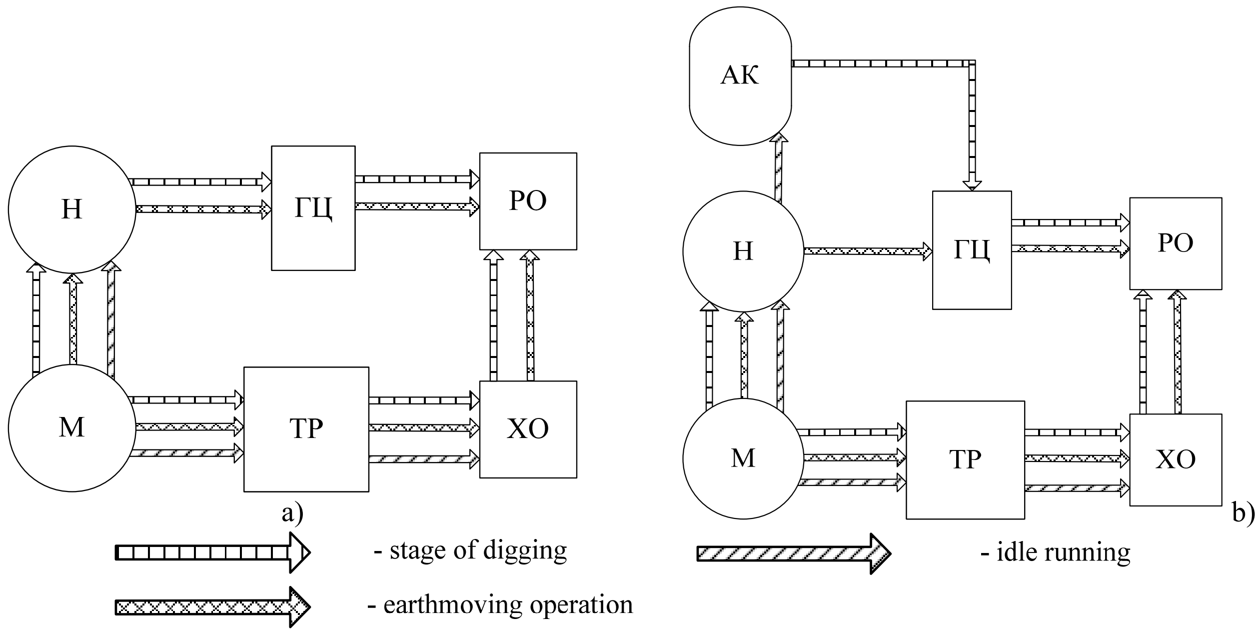

Figure 2: The scheme of energy flows in a bulldozer power unit during the work cycle: a – bulldozer of a conventional design; b – bulldozer with a pumped hydrostorage system; M – engine; TP – bulldozer power train; H – hydraulic pump; ГЦ – hydraulic cylinder; PO – working implement; AK – accumulator

The ICE power in the work cycle is distributed to powers spent on the power trains $N_{тр}$ and the hydraulic system $N_{гс}$

$$N_{ДВЗ} = N_{гс} + N_{тр}\,. \qquad (1)$$

The power spent on the hydraulic system should be stored in the hydraulic accumulator at the idle running

$$N_{гс} = N_{ак}. \tag{2}$$

At that the ICE power, making allowance for losses, will be completely transmitted to the bulldozer power train

$$N_{ДВЗ} = N_{тр}. \tag{3}$$

Thus, the power spent on digging will have 2 components

$$N_{коп} = N_{р.ак.} + N_{ДВЗ_{max}}. \tag{4}$$

To perform the useful yield on the blade penetration with the help of hydro-pneumatic accumulators (HPA), it is necessary that the accumulated energy $E_{ак}$ corresponded to the energy $E_{гц}$ spent on this operation by the basic hydraulic system unit.

$$E_{ак} = E_{гц}. \tag{5}$$

The HPA discharge time is equal to the time of the blade penetration

$$t_з = t_{р.ак}. \tag{6}$$

We set down

$$N_{ак}\, t_з = N_ц\, t_з. \tag{7}$$

The power required for the hydraulic cylinder is related to the pump power as follows

$$\frac{N_н}{\eta_н} = \frac{N_ц}{\eta_{гс}}, \tag{8}$$

where $N_н$ – hydraulic pump power; $N_ц$ – power required for the hydraulic cylinder; $\eta_н$ – total efficiency of the hydraulic pump; $\eta_{гс}$ – total efficiency of the hydraulic system.

The HPA power spent on digging operations must equal to the pump power at the same operation. On this basis we can set down

$$\frac{N_н}{\eta_н} = \frac{N_{ак}}{\eta_{гс}} = \frac{N_ц}{\eta_{гс}}. \tag{9}$$

One of the main parameters of the pumped hydrostorage system is a required liquid supply, i.e. the volume of the HPA working chamber. Theoretically it must be equal to the hydraulic cylinder volume upon condition of the maximally extended cylinder rod

$$V_{ак} = V_ц. \tag{10}$$

But during the bulldozer work cycle the cylinder rod does not always move to the maximal possible position. This factor depends on the cut layer height $h_з$. The HPA volume should take account of losses. And proceeding from the HPA operation specific feature, it must keep the fluid volume ΔV_0 being completely discharged.

At the stage of the energy accumulation it is necessary to control the fluid residue in the HPA at a given time interval.

Let us consider the powers $N_н$ and $N_ц$

$$N_н = Q_н\, p_н, \tag{11}$$

where $Q_н$ – hydraulic pump consumption; $p_н$ – hydraulic pump output pressure

$$N_ц = R_ц\, \vartheta_ш. \tag{12}$$

Let us present the force on the cylinder rod as

$$R_ц = A_п\, p_н. \tag{13}$$

The speed of the piston movement makes

$$\vartheta_ш = l_ш / t_з, \tag{14}$$

where $l_ш$ – piston movement; $t_з$ – time of the blade deepening.

The blade deepening time is the time of the HPA providing the required fuel volume equal to

$$t_з = \frac{T - G_б\,(f \pm i)}{a_1\, k_K\, B\, \vartheta_з}, \tag{15}$$

where a_1 – coefficient of influence of the soil type and the machine design on the deepening trajectory; $\vartheta_з$ – blade deepening speed.

The blade deepening speed is equal to

$$\vartheta_з = \vartheta_ш\, k_{кз}, \tag{16}$$

where $k_{кз}$ – coefficient taking into account drive connection between the cylinder rod and the blade.

Using (3.23) – (3.25) we can set down

$$\frac{Q_н}{\eta_{гс}}\, t_з = \frac{A_п\, l_ш}{\eta_{гс}}. \tag{17}$$

on the basis of

$$\frac{Q_н}{\eta_{гс}}\, t_з = V_ц, \tag{18}$$

where $V_ц$ – fluid volume to be supplied to the hydraulic cylinder at the deepening stage.

The HPA working chamber volume is calculated considering the volume of fluid consumed by the hydraulic cylinder. Taking into account that the HPA is to supply to the hydraulic cylinder the fluid supply $V_ц$ we can set down

$$V_{ак} = V_ц = \frac{A_п\, l_ш}{\eta_{гс}}. \tag{19}$$

The obtained value $V_{ак}$ can be considered the minimum permissible volume, thus, for the system reliability the HPA working volume must be equal to

$$\Delta V = 2 V_{ак}. \tag{20}$$

The volume of the accumulator working chamber is directly proportional to the number of cylinders of the driven equipment control

$$\Delta V_{ак} = n_ц\, \Delta V, \tag{21}$$

where $n_ц$ – number of cylinders with the same volume.

The amount of the energy accumulated in the battery must be sufficient for ensuring performance of the hydraulic drive of the driven equipment control and the bucket dump

$$E_{ак} = E_{зн} + E_{зр}. \tag{22}$$

The power spent on the work implement hydraulic drive is

$$N_{з.ак} = N_{р.ак1} + N_{р.ак2}. \tag{23}$$

For ensuring high efficiency of graders and motor graders it is necessary to seek for reduction of the work cycle time, i.e. to work at the highest possible speeds of motion. Also it is necessary to achieve increase in volume of soil in the prism moved by the blade. However, it is not efficient to overload the machine, for it can cause skidding of caterpillars of the tractor towing the grader or of the grader driving wheels. The undercarriage skidding results in wear increase, excessive loss of working time, constant need to throw the clutch and change gears, as well as considerable reduction of the equipment working capacity.

The operation sequence of graders, motor graders and scrapers during construction and shaping of unpaved roads is identical and has a cyclic character as that of bulldozers. The proposed pumped storage system can be used for motor graders, scrapers to reduce the work cycle time at the expense of decreasing the load on the ICE in the modes of the working attachment deepening and shanking out thereby directing all the power to the machine power train, i.e. ensures working at high speeds. Thus, stage-by-stage power input of the machine can be changed (Fig. 3, 5) and energy flows redistributed (Fig. 4, 5)

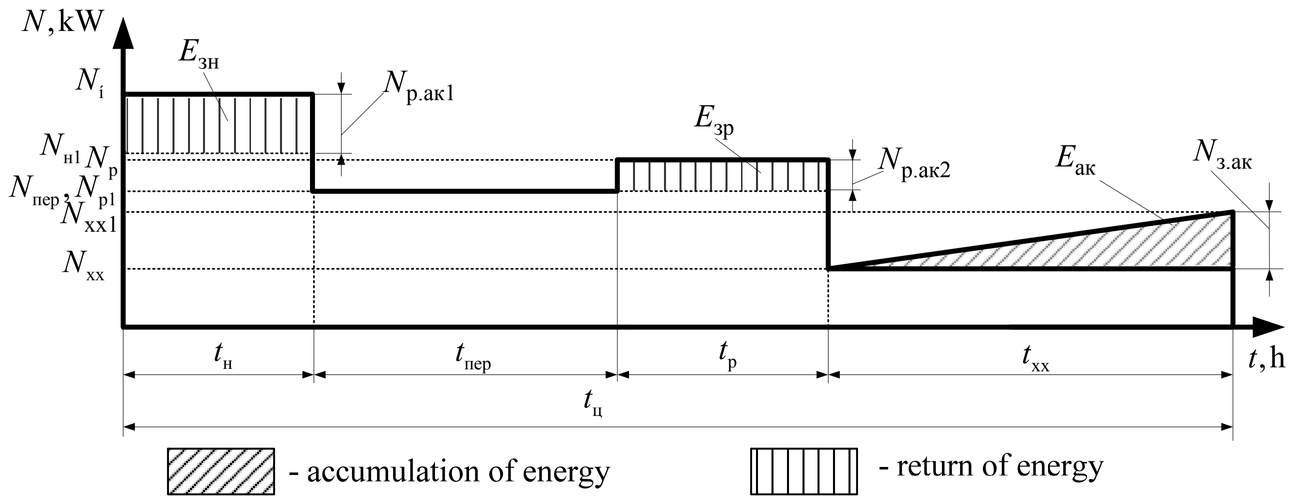

Figure 3: The work cycle of a scraper with a pumped hydrostorage system: $N_н$ - power consumed at filling of the scraper bowl without application of the pumped hydrostorage system; $N_р$ и $N_{р1}$ – powers spent by the ICD on the scraper dump with and without application of a pumped hydrostorage system correspondingly; $N_{р.ак1}$ and $N_{р.ак2}$ – powers spent by the accumulator on the hydraulic drive of the working attachment at its filling and dumping correspondingly; $E_{зн}$ и $E_{зр}$ – energies spent on the hydraulic drive of the working attachment at its filling and dumping correspondingly; $t_н$ – time of the bowl filling; $t_р$ – time of the bowl dumping

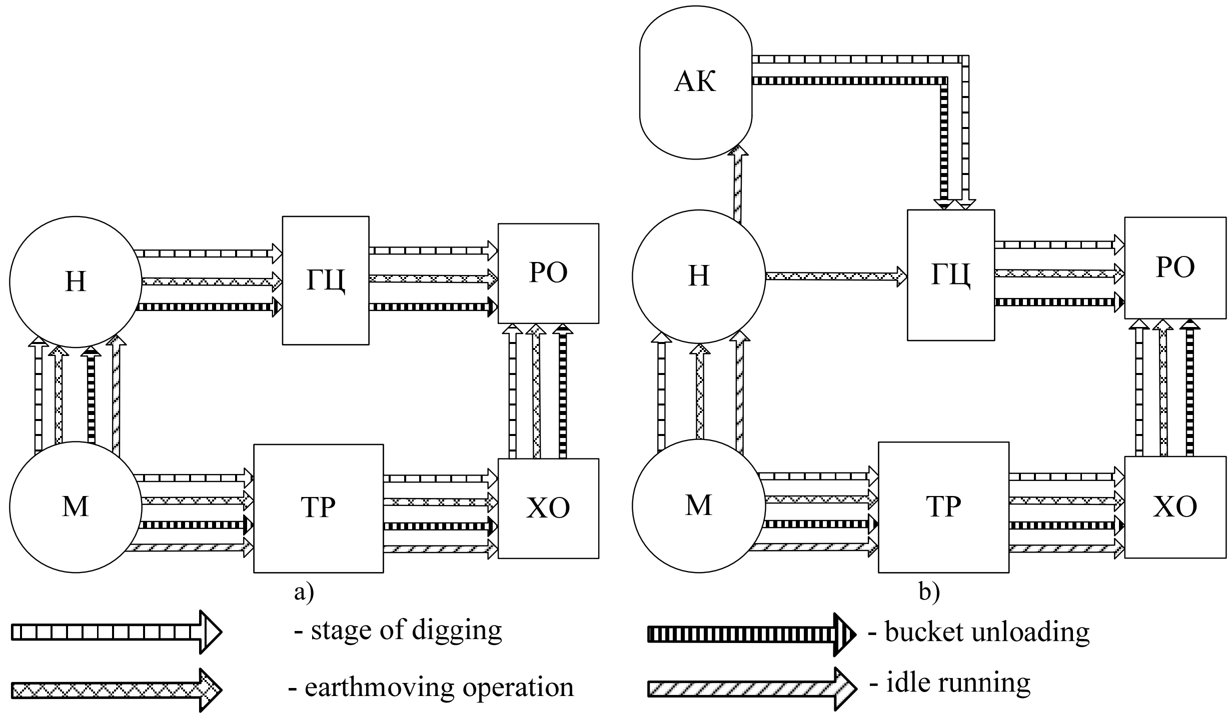

Figure 4: The scheme of energy flows in a scraper power unit during the work cycle: a – scraper of a conventional design; b – scraper with a pumped hydrostorage system; M – engine; TP – scraper power train; H – hydraulic pump; ГЦ – hydraulic cylinder; PO – working implement; АК – accumulator

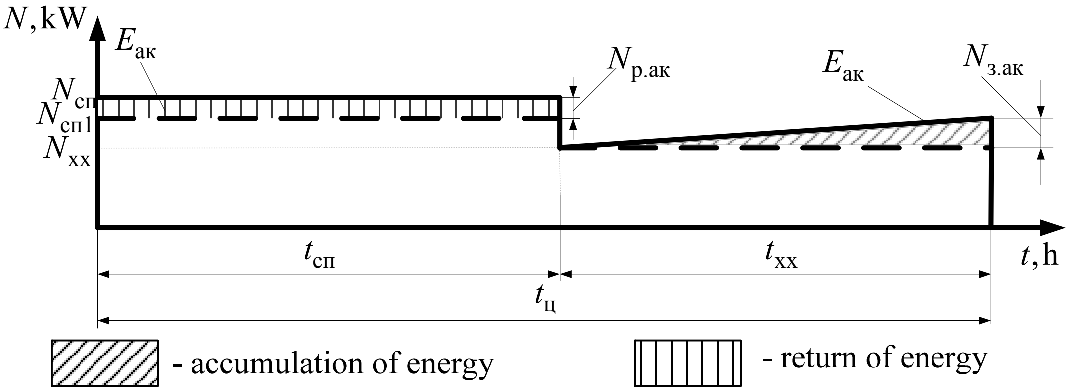

Figure 5: The work cycle of a motor grader with a pumped hydrostorage system: $N_{сп}$, $N_{сп1}$ – power spent by the ICE at cutting and handling of soil by the working attachment with and without application of a pumped hydrostorage system correspondingly; $t_{сп}$ – time of soil cutting and handling

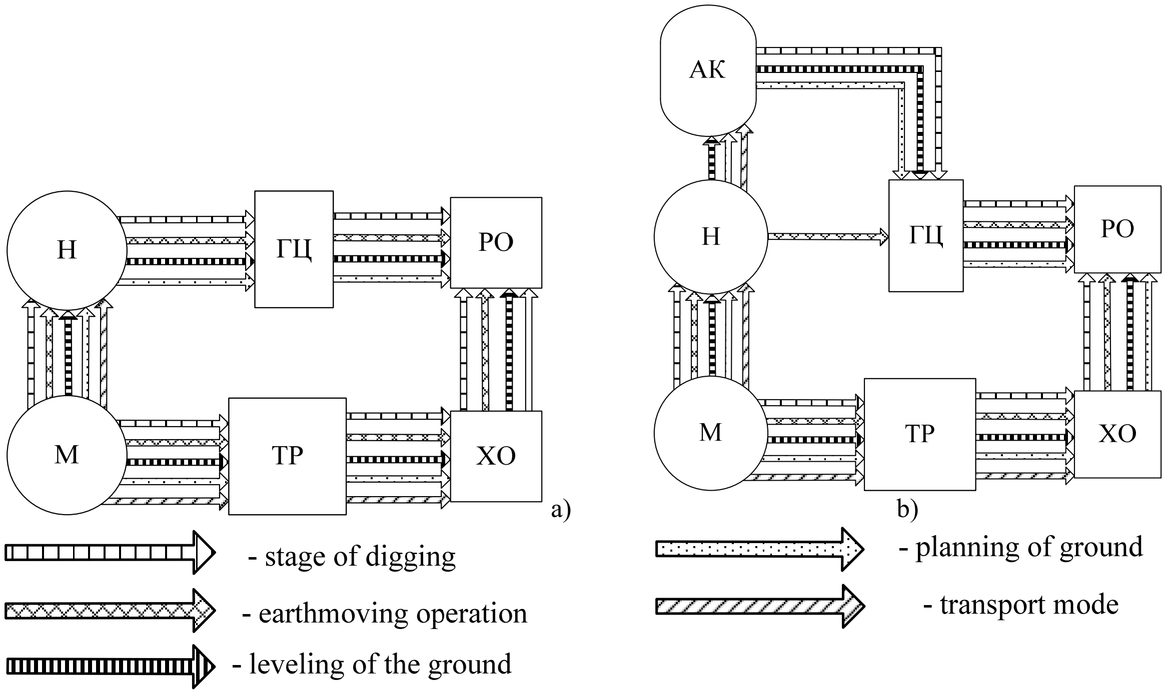

Figure 6: The scheme of energy flows in a bulldozer power unit during the work cycle: a – motor grader of a conventional design; b – motor grader with a pumped hydrostorage system; M – engine; TP – motor grader power train; H – hydraulic pump; ГЦ – hydraulic cylinder; PO – working implement; АК – accumulator

It is also possible that the energy stored in the hydraulic accumulator will supplement the ICE energy, which will allow for increasing the machine working capacity. In the case of the machine skidding most of the energy can be distributed to the power train and the power accumulated in the HPA transmitted to the hydraulic system, thereby decreasing the power spent by the ICE on hydraulic system and increasing the power transmitted to the bulldozer power train. According to the research data the power input on the hydraulic system depending on the type of the power train drive makes up to 50% of the ICE power.

CONCLUIONS

1. For the first time there have been presented a schematic diagram of energy flows for EMMs of cyclic operation – bulldozers, scrapers, motor graders equipped with a pumped hydrostorage system, which operation principle is in breaking the energy flow from the power unit to the working attachment in the digging mode and using the energy of hydraulic accumulators.

2. The theoretical studies demonstrated that application of pumped hydrostorage systems based on hydropneumatic accumulators allows to decrease a set output of the power unit on average for bulldozers by 4-6 %, scrapers by 5-6 %, motor graders by 4-7 %.

3. The choice of the hydro-pneumatic accumulator unit parameters is influenced by such construction and technical characteristics of the machine as the drawbar category, the number and volume of the hydraulic cylinders, nominal and maximal pressure in the hydraulic system.

4. There have been obtained formula allowing to determine characteristics of the pumped hydrostorage system for the given parameters of EMMs: the hydro-

pneumatic accumulator volume is calculated by the expression $\Delta V_{\text{ак}} = n_{\text{ц}} \Delta V$; the precharge pressure $p_{нач} = \left(\frac{n}{zn-1}\right)^{\frac{n}{n-1}} p_{\max}$; the charging time $t_з = t_{\text{хх}} = \frac{\Delta V_{\text{ак}}}{Q_{\text{н}}}$.

REFERENCES

[1] L.A. Khmara "Application of Accumulators of Potential Energy in Construction Machinery (on the Example of the Bucket Excavator)" Construction. Materials Science. Mechanical Engineering: Collection of Scientific Papers "Intensification of Work processes of Construction and Road Machines", PGASA, Dneproperovsk (Ukraine), Vol. 33. – pp.17–33, (2005)

[2] L.A. Khmara and A.P. Kholodov, "Increasing the Efficiency of Bulldozers by Means of the Pumped Hydrostorage System", Construction and Road Machines, Vol. 3, pp. 33 – 37, (2012)

[3] L.A. Khmara, A.P. Kholodov and A.V. Yaryzhko, "Experimental Research of the Pumped Hydrostorage System", Collection of Scientific Papers: Construction. Materials Science. Mechanical Engineering, Vol.63, PGASA, Dneproperovsk (Ukraine), pp. 69 – 78, (2011)

[4] L.A. Khmara and A.P. Kholodov "Trials of the Bulldozer Equipped with the Energy Storage System", Collection of Scientific Papers: Construction. Materials Science. Mechanical Engineering, PGASA, Dneproperovsk (Ukraine), Vol. 63, pp. 61 – 69, (2011)

[5] N.V. Gulia "The Inertial Car Engines", Transport, Moscow (Russia), (1974)

[6] V.M. Volotskij, "The Vehicle Hydraulic Drives and their Components", Apprenticeship Course, Gidroeleks, Kharkov (Ukraine), (1995)

[7] T.V. Aleksejeva, "The Hydraulic Drive and Hydroautomatic Equipment of the Earth Moving Machines", Machinostroenije, Moscow (Russia), (1966)

[8] T.V. Aleksejeva, Yu.V. Remizovich and V.G. Sherman, "Application of the Energy Storage Principle in the Earth Moving Machine Controlling System", Research and Trial of Road and Construction Machines: Collection of Scientific Papers, SibAHI, Vol. 1, pp. 70–75, (1969)

[9] V.F. Shcherbakov "The Regenerative System of the Hydraulic Drive of Earth Moving Machines, Construction and Road Machines, Vol. 9, pp. 49-51, (2008)

[10] V.F. Shcherbakov "The Energy-Efficient Hydraulic Drive of Construction and Road Machines", Vol. 10, pp. 1–2, (2011)

[11] R.T. Dann "The Revolution in Flywheels", Machine Design, May 17 1973, pp.130-135 (1973)

Fracture Analysis of the Hydraulic Truck Crane ATLAS 3006

Mile Savković[1*], Milomir Gašić[1], Nebojša Zdravković[1], Goran Bošković[1], Goran Pavlović[2]
[1] University of Kragujevac, Faculty of Mechanical and Civil Engineering Kraljevo, Dositejeva 19, 36000 Kraljevo (Serbia)
[1] Colpart d.o.o-Beograd, Ćirovljeva 5, 11030 Beograd, (Serbia)

This paper presents the analysis of a fracture due to the local increase in stress at the point of connection between the hydrocylinder and the first segment of the truck crane boom. The connection between the hydrocylinder support and the body of the first boom segment is accomplished by welding. The first part of the paper defines the relevant load for calculation of the hydrocylinder support, by using the manufacturer's data to perform analytical calculation of the critical section. It is followed by the FEM analysis and fatigue analysis, for the most unfavourable load case. It has been established that the critical value of stresses is at the point of connection between the hydrocylinder support and the structure of the first boom segment. Experimental testing has shown that the fracture did not occur due to an error in the material and that the material type is adequate for this type of structure. The superposition of negative influences: fatigue of the material and a pronounced difference in material thicknesses in the cross section at the point of fracture are the main causes of damage of the hydraulic truck crane structure.

Keywords: Hydraulic truck crane, Truck crane boom, Fracture analysis, FEM analysis

1. INTRODUCTION

The hydraulic truck crane ATLAS 3006 (Figure 1) is used for lifting and transportation of loads with the mass $Q_{min}=1120\ kg$ at the largest reach ($L_{max}=6080\ mm$), i.e. $Q_{max}=3650\ kg$ at the smallest reach ($L_{min}=1920\ mm$). The main structure of the crane consists of the crane column, two jointed segments and one telescopic segment. Another two telescopic segments can be added to the crane. The crane which is the subject of research in this paper does not have additional telescopic segments built-in. The mass of the crane ATLAS 3006, with the complete installation and oil in its hydrocylinders, is 1245 kg. The nominal pressure of the hydraulic installation is $p_n=175$ *bar*, and the maximum operating pressure can be $p_n=225$ *bar*. At the moment of damage of the mentioned crane, the operating pressure of the hydraulic installation was set to $p_n=170$ *bar*.

Figure 1. *Hydraulic truck crane Atlas 3006*

The hydraulic truck crane ATLAS 3006, which is the subject of research in this paper, is located at the Electricity Distribution Company Kruševac and is used for work in very difficult conditions, for mounting and dismounting elements of power transmission lines and long distance lines so that it is mostly engaged for field work. The mentioned working conditions are difficult because it often lifts loads that are at the limit or exceed the values defined by the carrying capacity diagram. It is also used for tightening power lines, and there are no precise data about the values of forces that load the crane structure. The life and proper functioning of such a crane considerably depend on the operator himself, i.e. how much he adheres to the recommendations for its proper exploitation.

After more than 12 years of crane exploitation, during a regular overhaul, certain damages at the first jointed segment of the crane were noticed. This damage is at the point of connection between the hydrocylinder and the segment (detail "A" - Figure 2).

Figure 2. *Point of the fracture initiation in the crane Atlas 3006*

Hydraulic truck cranes mostly perform difficult operations and their loads are dynamic and stochastic, which is a frequent cause of failures that may have catastrophic consequences [1-6]. However, even when

*Corresponding author: savkovic.m@mfkv.kg.ac.rs

they are not catastrophic, they certainly result in huge financial losses.

For the purpose of saving, the user himself, without any previous detailed analysis of the causes of damage, solved the problem of repairing the damage in the truck crane boom by welding at the point of cracking. The damaged plates were connected by butt welding. After the repair, the crane was returned to exploitation.

After more than 3 years of exploitation of the repaired crane, a fracture (Figure 3) occurred at the point where it had been repaired.

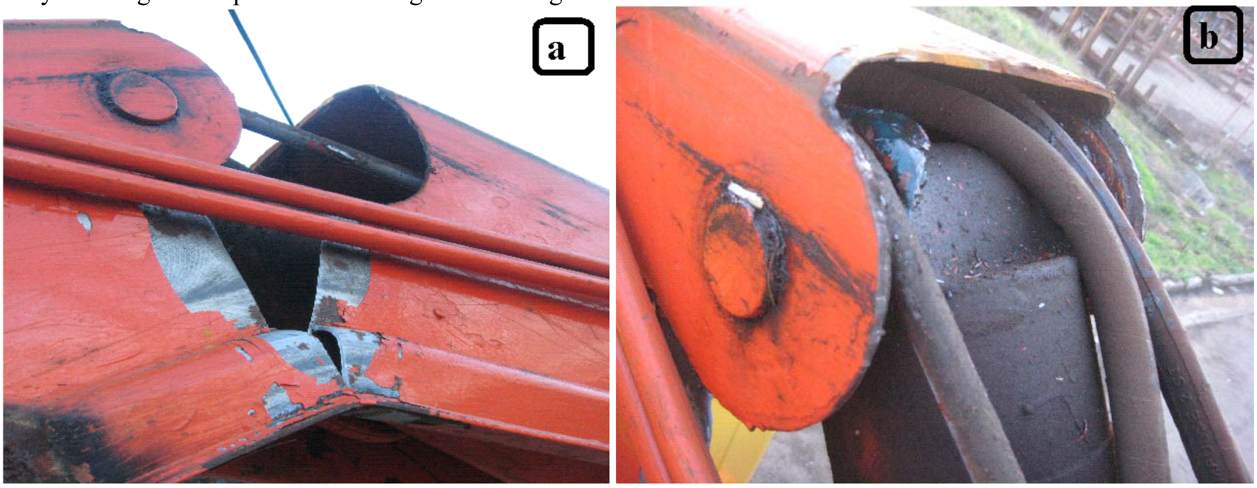

Figure 3. *Point of the boom fracture in the telescopic truck crane ATLAS KRAN 3006 a) lateral side; b) upper side;*

2. ANALYSIS OF THE MATERIAL USED FOR THE BOOM OF THE HYDRAULIC TRUCK CRANE ATLAS 3006

In the first phase, an experimental procedure was performed and it covered testing of the mechanical properties and chemical composition of the material as well as the visual examination of the fracture surface. The results of examination of the chemical composition of the samples taken at the point of fracture are presented in Table 1.

The results of examination of the samples taken at the point of fracture showed that the chemical composition and mechanical properties corresponded to the quality of steel NIOVAL 47 (P460NL1). For obtaining better mechanical properties and removal of resudual stresses during welding, that material is subjected to the process of thermal treatment. More precise data about the type of material and its physical and chemical properties were obtained based on [7-9].

Table 1. Results of examination of the chemical composition of the samples taken at the point of fracture

Elements %		**C**	**Si**	**S**	**P**	**Mn**
Prescribed values	from	max	max	max	max	max
NIOVAL 47 (P460NL1) (DIN 1.8915)	to	0.20	0.60	0.020	0.030	1-1.7
Values obtained by testing		**0.14**	**0.41**	**0.013**	**0.011**	**1.08**

Table 2. Results of examination (determination) of the mechanical properties of the material

Examined material		**$R_{p0,2}$ (N/mm^2)**	**R_m (N/mm^2)**	**A_5 (%)**
Prescribed values	from	510*	680*	**min**
	to	800*	975*	21
Sample 1		**717**	**762**	**15.2**
Sample 2		**726**	**772**	**15.3**
Sample 3		**715**	**760**	**15.3**

(*According to [7], for thermally treated steel)

The fracture analysis clearly shows the fatigue fracture initiation which occurred in the transition zone between the weld and the base material as well as at the point of joining the plates with a large difference in thicknesses (Figure 3).

The performed experimental procedure of testing the chemical composition and mechanical properties of the material, as well as the visual examination of the fracture surface indicate that the fracture did not occur due to an error in the material.

3. ANALYSIS OF THE BOOM STRESS IN THE HYDRAULIC TRUCK CRANE ATLAS 3006

The analysis of the stress state of the hydraulic truck crane ATLAS 3006 was carried out by applying the finite element method (FEM). The model was formed on the basis of catalogue documentation and the additional measurements performed at the crane itself (Figure 4).

Papers [10-13] deal with damages of heavy-duty machines. In addition to metallographic examination, the FEM analysis is used for obtaining characteristic values of stresses and establishing the causes of damage..

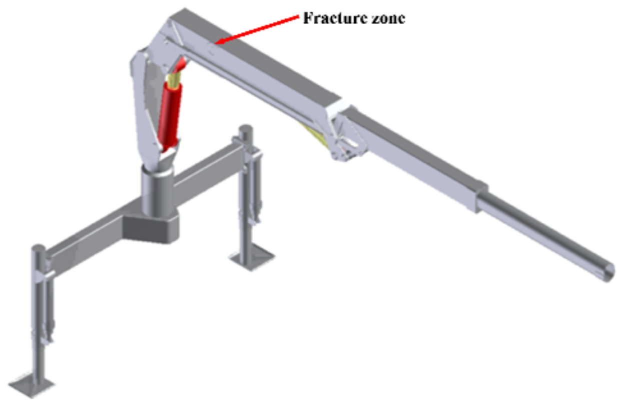

Figure 4. *Model of the hydraulic truck crane ATLAS 3006*

The 3D model of the hydraulic truck crane was built by synthesis of all structural parts (Figure 4). The model represents a continuum discretized by 10-node tetrahedral elements for the purpose of creating an FEM model (64036 nodes and 33060 elements). The first segment of the jointed boom of the truck crane was particularly taken out and analysed (Figure 5).

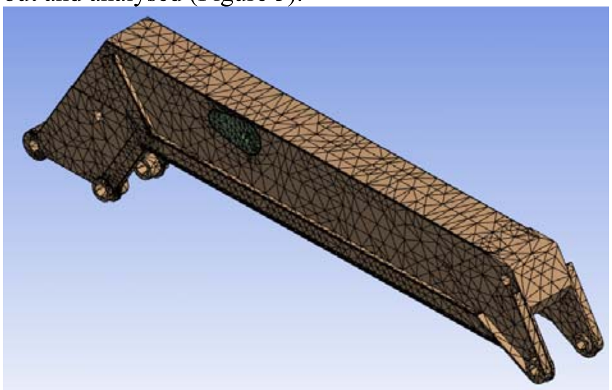

Figure 5. *First segment of the boom of the hydraulic truck crane ATLAS 3006*

The manufacturer's data about the value of maximum load and the data about the mass of crane elements were used for the analysis of loads of the hydrocylinder support for lifting the second segment. The scheme of loading of the first segment of the crane boom is shown in Figure 6.

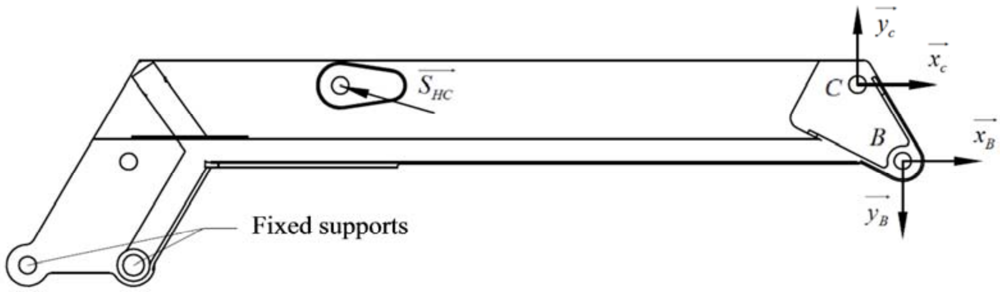

Figure 6. *Scheme of loading of the first segment of the boom in the hydraulic truck crane ATLAS 3006*

The analysis of stresses of the jointed segment of the boom was carried out for two load cases:

- case I - the telescope is extended to the maximum, the reach is maximum, the payload $Q = 11.2\,kN$
- case II - the telescope is extended to the maximum, the reach is minimum, the payload $Q = 36.5\,kN$

The loads due to the dead weight are the same in both cases, i.e.:

$Q_{s1} = 1{,}12\,kN$ - the load due to the weight of the boom extension and the telescopic segment

$Q_{s2} = 1{,}15\,kN$ - the load due to the boom weight.

The stress state for case I is more unfavourable than for case II.

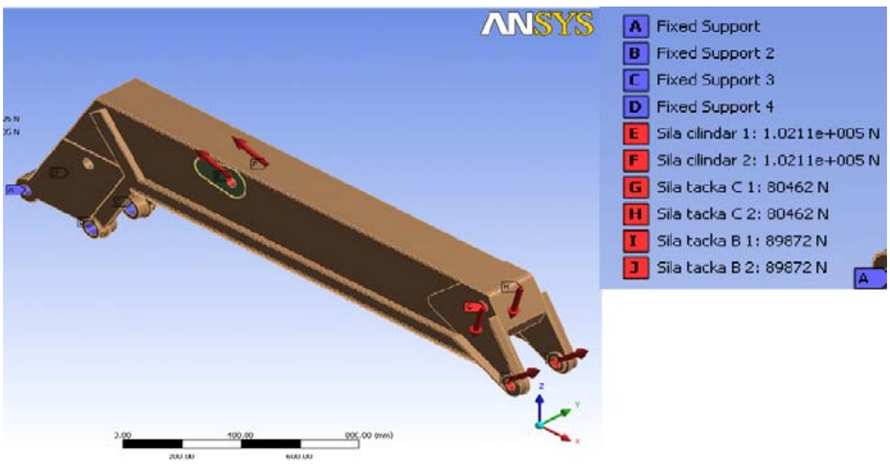

Figure 7. *Scheme of loading of the first segment of the boom in the hydraulic truck crane ATLAS 3006*

The obtained values of loads at the characteristic points (Figure 5) are:

$x_B = 139,44\,kN$; $y_B = -113,42\,kN$; $x_C = -41.8\,kN$;

$y_C = -155,4\,kN$; $S_{HC} = 204,22\,kN$;

The obtained values of loads were used in the calculation model created in the software package ANSYS (Figure 7).

The uniaxial stress field, according to the Huber-Hencky-von Mises hypothesis, for load case I, is presented in Figs. 8 and 9.

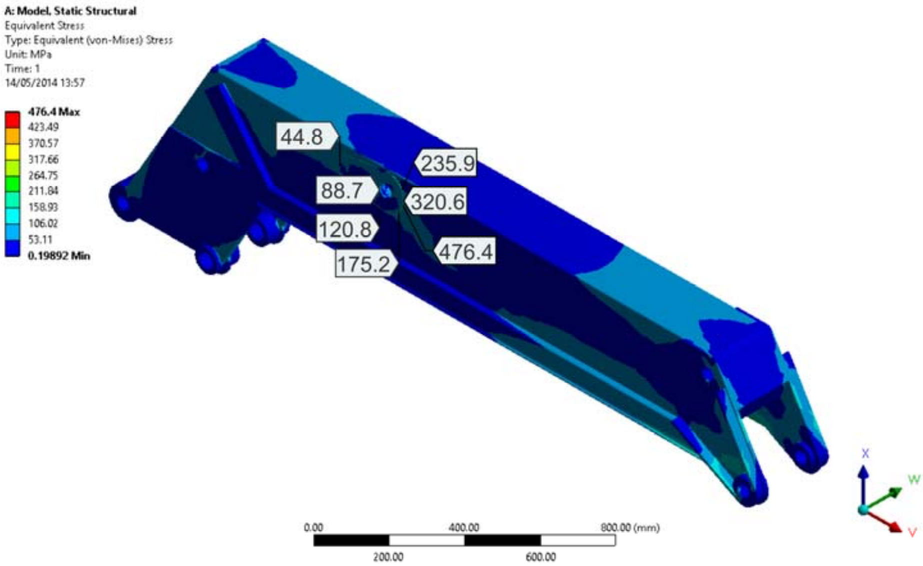

Figure 8. *Stress state of the first segment of the boom with characteristic values*

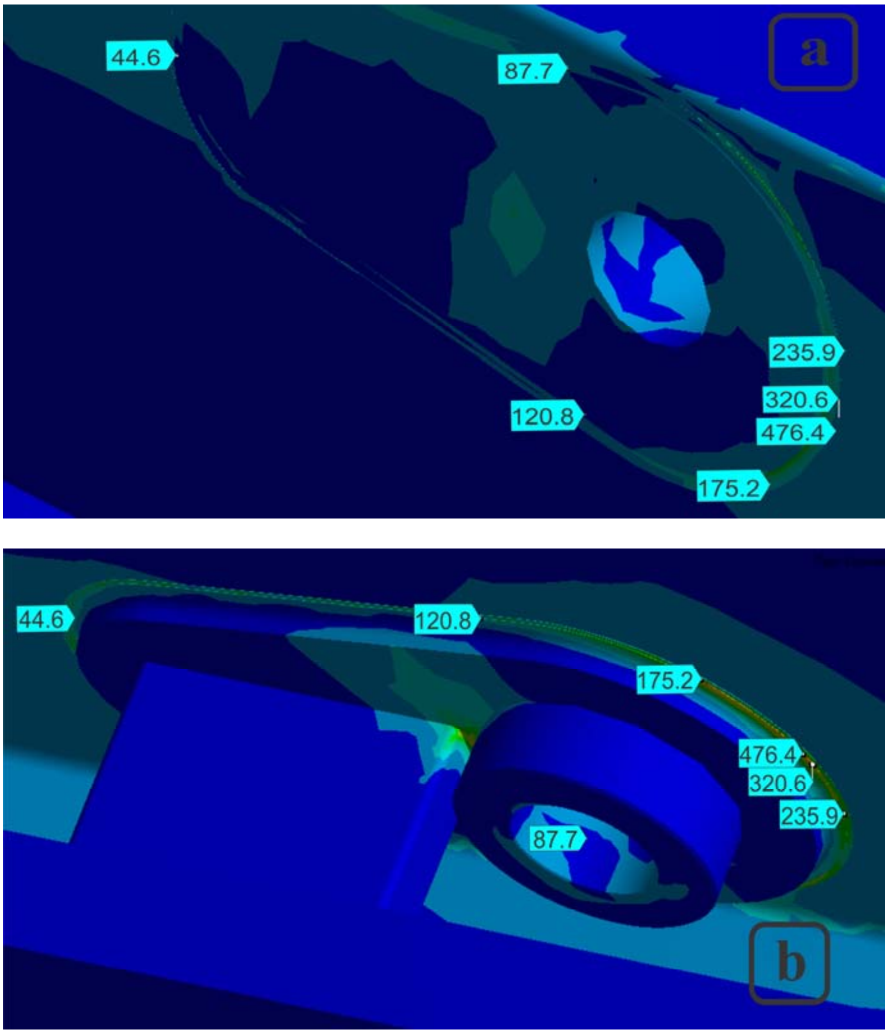

Figure 9. *Stress state at the point of connection between the hydrocylinder and the first segment: a) outer side b) inner side*

The characteristic values of the analysed segment of the truck crane boom obtained by the finite element method are shown in Table 3 and Table 4.

Table 3 – Characteristic values of stresses in the weld zone

Measuring point	1	2	3	4	5	6	7
$s_{i,max}(MPa)$	476.4	320.6	235.9	175.2	120.8	87.7	44.6
$s_{i,min}(MPa)$	428.8	288.5	212.3	157.7	108.7	78.9	40.1
$s_{mean}(MPa)$	381.1	256.5	188.7	140.2	96.6	70.2	35.7
$s_a(MPa)$	47.6	32.1	23.6	17.5	12.1	8.8	4.5

Table 4 – Characteristic values of stresses in the zone of base material

Measuring point	1	2	3	4	5	6	7
$s_{i,max}(MPa)$	350.4	309.3	286.8	218.6	94.5	81.2	68.5
$s_{i,min}(MPa)$	315.3	278.4	212.3	196.7	85.1	73.1	61.6
$s_{mean}(MPa)$	280.2	247.5	188.7	174.8	75.7	65.0	54.7
$s_a(MPa)$	35.1	30.9	28.7	21.9	9.4	8.1	6.9

The analysis of fatigue fracture was carried out by using the Goodman diagram. Based on the results of chemical and mechanical testing of samples of the material in the zone of fracture of the first segment of the boom, the values of tensile strength of the weld material are read and then written on the abscissa of the Goodman diagram.

The value of yield stress of the weld material is calculated as follows: $R_e = 0.66 \cdot Rm = 0.66 \cdot 772 \approx 509\,MPa$

In Figs. 9 and 10, the yield limit is represented by the line E-F (. For the weld, the value of yield stress is $R_e = 509\,MPa$, and for the base material, based on the results of testing, it is $R_e = 726\,MPa$.

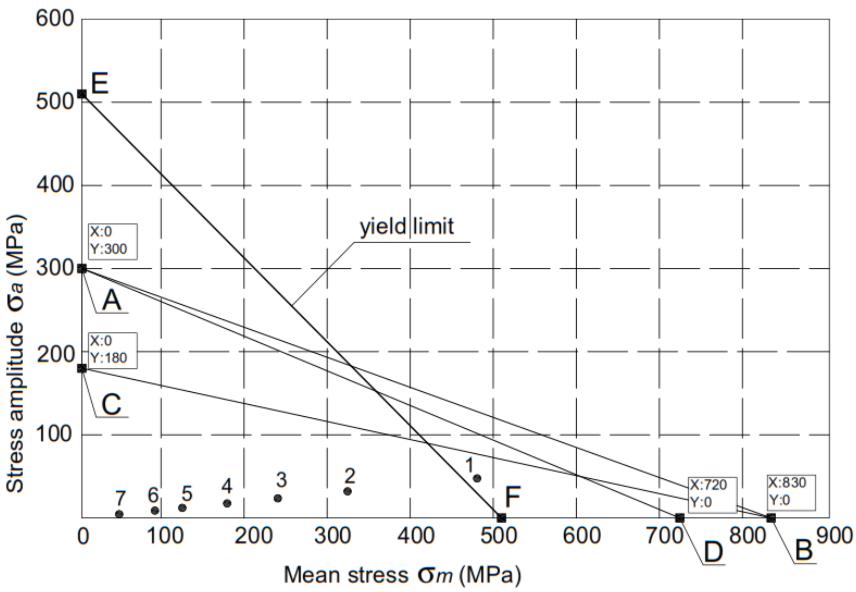

Figure 9. *Goodman diagram in the weld zone*

The characteristic values of the working stresses obtained by the finite element method are presented in Table 3 and Table 4. The minimum recommended value of the stress amplitude is $\sigma_a = 300\,MPa$ [9,14-15], where the minimum value of tensile strength in the weld is $\sigma_m = 830\,MPa$ [7], and in the base material, based on the data from testing of the material, $\sigma_m = 730\,MPa$. These values are presented by points A and B, and they represent the fatigue boundary line. However, for real exploitation conditions, this line must be corrected.

The minimum recommended value of the stress amplitude [7] is: $\sigma_a = 300\,MPa$. For real exploitation conditions, in compliance with the recommendations [7,8], the corrected minimum value of the stress amplitude ($\sigma_{a,m} = 180\,MPa$) was defined, whereas the minimum value of tensile strength was established experimentally (Table 2) and it is $\sigma_{m,m} = 730 MPa$.

These values are denoted with points C and D (Figs. 9 and 10) and they define the modified boundary of the Goodman diagram.

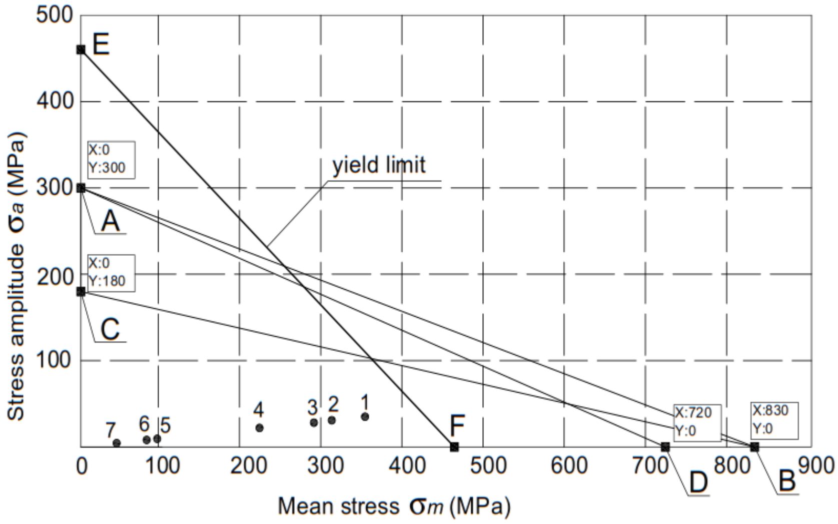

Figure 10. *Goodman diagram for the base material*

The characteristic values for testing the boom of the telescopic truck crane for fatigue are denoted with numbers from 1 to 7 in the diagrams. All values of the corresponding working stresses were obtained by the finite element method – by using the software package ANSYS.

In Fig. 9, the mentioned points (1-7) are below the line A-B, which represents the fatigue boundary, while in Fig.10 the point 1 exceeds the fatigue boundary and thus fatigue safety is not provided.

The line C-D was chosen to be the relevant fatigue line and in the first diagram in Figure 3.9 the point 1 does not exceed this boundary, but in the diagram in Fig.10 this boundary is already exceeded in terms of the position of the point 1 in the diagram.

4. CONCLUSION

On the basis of the presented research results, the following conclusions can be made:

- The chemical composition and mechanical properties of the material of the truck crane structure correspnd to the steel NIOVAL 47 (P460NL1**,** DIN 1.8915).
- The chemical composition and mechanical properties of the material of the boom are within the prescribed limits, so it can be concluded that the cause of damage is not an error in the material.
- Based on the results of the FEM analysis, it can be concluded that the highest values of stresses are at the point of connection between the hydrocylinder and the boom.
- The safety factor of the truck crane boom in the characteristic section for the most unfavourable load case is:

$$S = \frac{\sigma_y}{\sigma_{eq,\max}} = \frac{730}{476.4} = 1.53$$

- The critical value of stresses in the weld exceeds the fatigue boundary line. Therefore, fatugue failure safety is not provided, which was proved by the FEM analysis.
- The truck crane boom was not repaired in a prescribed and adequate manner. Such jobs should be entrusted to the companies which are specialized for that type of activity.

ACKNOWLEDGEMENTS

A part of this work is a contribution to the Ministry of Science and Technological Development of Serbia funded Project TR35038

REFERENCES

[1] A.A. Marquez, P. Venturino, J.L. Otegui, *Common root causes in recent failures of cranes,* Engineering Failure Analysis, Elsevier, 2014.

[2] D. Kovacevic, I. Budak, A. Antic, A. Nagode, B. Kosec, *FEM modeling and analysis in prevention of the waterway dredgers crane serviceability failure,* Engineering Failure Analysis, Elsevier, 2013.

[3] E. Rusinski, A. Iluk, K. Malcher, D. Pietrusiak, *Failure analysis of an overhead traveling crane lifting system operating in a turbogenerator hall,* Engineering Failure Analysis, Elsevier, 2013.

[4] W. Ost, P. D. Baets, W. D. Waele. Pietrusiak, *Failure of a large ball bearing of a dockside crane,* Engineering Failure Analysis, Elsevier, 2003.

[5] P. Swuste, *A 'normal accident' with a tower crane? An accident analysis conducted by the Dutch Safety Board,* Safety Science, Elsevier, 2013.

[6] F. Frendo, *Analysis of the catastrophic failure of a dockside crane jib,* Engineering Failure Analysis, Elsevier, 2013.

[7] K. T. Rie & W. Kohler, *Effect of microstructure on LCF-behaviour of steels in high pressure hydrogen environment,* Proceedings of the 4th European Conference on Fracture(ECF4), Leoben, Austria, 1982.

[8] J. Vojvodič Tuma, D.Kmetič & R. Celin, *A 490 yield stress steel for liquified-gas vessels,* Proceedings of the International Conference on Advances in Structures: (ASSCCA '03), Sydney, Australia, 22-25 June 2003.

[9] Key to Steel – online version, Verlag Stahlschlüssel, Germany, 2014

[10] Mile Savković, Milomir Gašić, Dragan Petrović, Nebojša Zdravković, Radmila Pljakić, *Analysis of the drive shaft fracture of the bucket wheel excavator,* Engineering Failure Analysis, Elsevier, 2012.

[11] Rusinski E., Harnatkiewicz P., Kowalczyk M., Moczko P., *Examination of the causes of a bucket wheel fracture in a bucket wheel excavator,* Engineering Failure Analysis, Elsevier, 2010.

[12] Savković M., Gašić M., Arsić M., Petrović R., *Analysis of the axle fracture of the bucket wheel excavator,* Engineering Failure Analysis, Elsevier, 2011.

[13] Brian McDonald, Bernard Ross, Robert A. Carnahan, *The Bellevue crane disaster,* Engineering Failure Analysis, Elsevier, 2011.

[14] *Shigley's Mechanical Engineering Design*, Eighth Edition, McGraw-Hill, 2006.

[15] V. B. Bhandari, *Design of Machine Elements*, 3rd Edition, Tata McGraw Hill Education Private Limited, 2010.

Application of the Numerical Methods for Dynamic Analysis of Transportsystems with Rope

Jovan Vladić[1], Dragan Živanić[1*], Igor Džinčić[2], Radomir Đokić[1], Anto Gajić[3]
[1] Faculty of Technical Sciences, University of Novi Sad, Novi Sad, Serbia
[2] Faculty of Forestry, University of Belgrade, Belgrade, Serbia
[3]Mine and Thermal Power Plant, Ugljevik, Republic of Srpska

Solving differential equations oscillation structure with steel ropes creates serious difficulties for large and complex systems, like ropeways, elevators, belt conveyors, etc., exposed to different impulse force. The problem occurs in solving the system of differential equations in the so-called closed form. Therefore, in such situations, looking solutions by numerical methods. The method is based on the assumption that the velocity of propagation deformation of the system is small compared to the velocity of propagation of elastic waves (velocity of sound). This condition is met in the case of a relatively small distance between the concentrated mass. There are a significant difference in the analysis of the dynamic behavior of vertical and horizontal rope. The paper presents the possibilities of applying numerical methods for analysis of monocable ropeways.

Keywords: monocable ropeways, numerical method

1. INTRODUCTION

Modern ropeways perform highly effective transport on short and middle-scale distances (2÷50 km), and are applied in transportation of people and material especially at mountainous and unreachable regions.

Ropeways is technical systems are composed from a great number of elements. Because of permanently changing loads of ropes during vehicles moves, and periodical changing ″usefuls″ loads, on ropeways does not exist stationary work, then dynamic occurrences very expressive.

Figure 1: Ropeway

Numerical methods are studied in the continuous process of finite number of sufficiently small time interval. In these small time intervals can be a function of time (coordinates, displacement, velocity, force, ...) approximated by expressions. Then, the integration is done in every elementary interval, with the integration of the results in the previous interval taken as the starting time for the next interval. In this concept, use two general methods:

- method of direct integrals and
- method of stacking the main oscillation forms.

The method of direct integrals consists in replacing the differential equations of small oscillations of the system, the system of algebraic equations with unknown increments of coordinates. This is accomplished by the displacements (generalized coordinates), velocity and acceleration functions in small time intervals can be replaced with approximate functions, and then introduced into the system of differential equations and their integration performed. The term „direct“ integration is related to the fact that do not perform the operation of the system of equations, but just integrals. Today used three methods for direct integration:

- central difference method,
- Wilson's ″theta″ method and
- Newmark's method.

Newmark presented family one step integration method for solving structural dynamics problems, as well for impact and for seismic (current) load, [1]. Over the last 50 years, Newmark's method was applied for the dynamic analysis of a large number of engineering structures derived. The method is at that time was repaired and modified by many other researchers.

Numerical methods are suitable for use in the dynamic analysis of ropeways. The method is based on the assumption that the longitudinal and transverse waves propagated independently of each other. This requirement is adequately met in the case of short duration (a small time interval) because the propagation velocity of longitudinal waves is significantly higher than the speed of propagation of transverse waves. There are many possible applications of this method of analysis. It is used when considering the dynamic behavior of the ropeways, where the large and small forces involved in the rope when eg. starting and braking is very important to analyze the behavior of the whole system.

The arbitrary mass m_i (weight concentrated rope) forces acting in the rope, gravity and arbitrary external force, fig. 2, and the following equality is valid:

*Corresponding author: Faculty of Technical Sciences, Trg D.Obradovica 6, Novi Sad, zivanic@uns.ac.rs

$$m_i \cdot \vec{a}_i = \vec{S}_i + \vec{S}_{i+1} + \vec{R}_i \qquad (1)$$

where it is:

$\vec{a}_i$ - acceleration vector of concentrated mass m_i,

$\vec{S}_i, \vec{S}_{i+1}$ - force in the rope on the left and right of the concentrated mass m_i,

$\vec{R}_i$ - resultant external force acting on the mass m_i, for example, consequence of the presence of hooked up the vehicles on the rope.

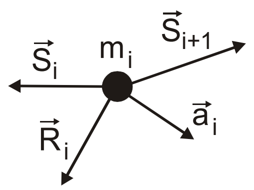

Figure 2: The forces acting on an arbitrary concentrated mass m_i

If the application of numerical method in the previous equation, and if with u_i present movement, with v_i velocity and with a_i acceleration of arbitrary concentrated mass in time point t, then these values at time point $t + \Delta t$ can be calculated by:

$$u_i(t+\Delta t) = u_i(t) + \Delta t \cdot \left(v_i(t) + \frac{1}{2} \cdot \Delta t \cdot a_i(t) \right) \qquad (2)$$

$$S_i(t+\Delta t) = c_i(t+\Delta t) \cdot [u_{i+1}(t+\Delta t) - u_i(t+\Delta t)] \qquad (3)$$

$$a_i(t+\Delta t) = \frac{[S_i(t+\Delta t) - S_{i-1}(t+\Delta t)] + R_i(t+\Delta t)}{m_i(t+\Delta t)} \qquad (4)$$

$$v_i(t+\Delta t) = v_i(t) + \frac{1}{2} \cdot \Delta t \cdot (a_i(t) + \cdot a_i(t+\Delta t)) \qquad (5)$$

The time increment Δt is calculated by:

$$\Delta t = \frac{\Delta x}{c_L} \qquad (6)$$

where it is:

Δx - the distance between neighboring concentrated masses (vehicles), which are assumed to be constant,

c_L - propagation velocity of longitudinal waves in a rope, which is also a constant.

Thus the calculated value for Δt means that the size of any renewed (or recalculated) after a specified time interval. Time increment Δt (step time), depending on the speed of propagation of longitudinal waves in a rope, and on the distance between the vehicles. When analyzing the dynamic behavior of the vehicle, it may be inferred that the amount $\Delta t = 0{,}001 \div 0{,}002\, sec$. This method of integration is extremely consistent, stable and easy to use. [2]

2. THE DYNAMIC MODEL OF THE ROPEWAYS

The described method will be used to define the kinematic and dynamic parameters of the monocable ropeways with two fields, at startup, fig. 3.

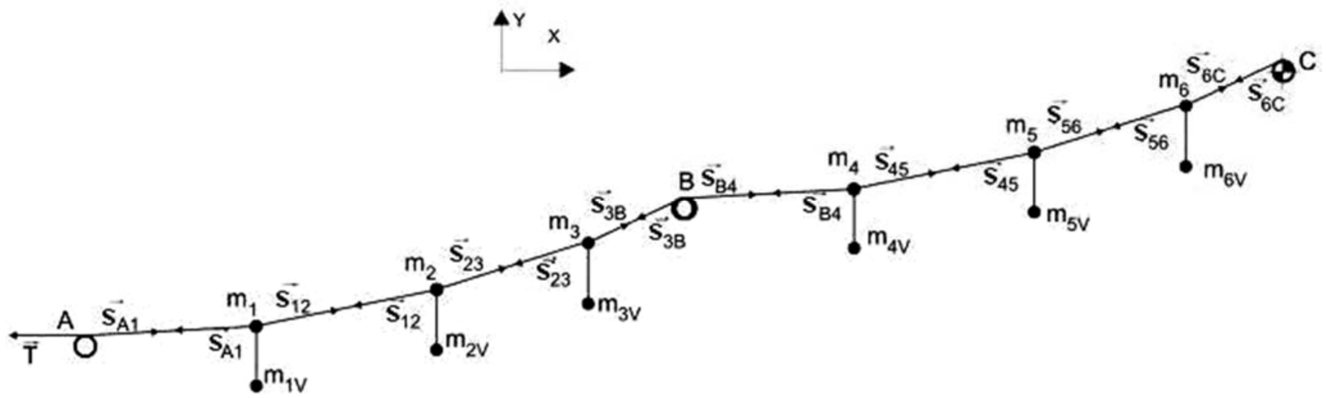

Figure 3: The dynamic model of the ropeways with two fields

Model ropeways with two fields and three vehicles on the field, will allow analysis of non-stationary behavior of the vehicle modes. In doing so, there will not be seen vehicles go through the supports which means that during the entire simulation in both fields constant number of vehicles (3). [4]

In the support A acts weights T, which ensures that the lift (rope and vehicles) takes up the position specified in [3], and that forces in the rope have a values determined by static calculation. In the support C is set up the drive mechanism.

2.1. Time point $t = t_0$

In the the initial time point $t = t_0 = 0$, values speed v_{Xi} and v_{Yi}, acceleration a_{Xi} and a_{Yi} at all points are the same and are 0. Positions of points x_i and y, the forces in the the rope X_{iL}, X_{iD}, Y_{iL} and Y_{iD}, and the inflection angles α_{iL} and α_{iD} corresponding to values for standby (is given in the [3]).

2.2. Time point $t = t_1 = t_0 + \Delta t$

In the time point $t = t_1 = \Delta t$, in the point C appears components of the acceleration in the x and y direction, in a stationary coordinate system set in the support A, the following:

$$a_{XC}(t_1) = a_C(t_1) \cdot \cos \alpha_{CL}(t_1)$$

$$a_{YC}(t_1) = a_C(t_1) \cdot \sin \alpha_{CL}(t_1)$$

wherein in the parentheses indicates the time point at which a given size is calculated.

Acceleration causes displacement at point C, which is:

$$\Delta x_C(t_1) = a_{XC}(t_1) \cdot \frac{\Delta t^2}{2}$$

$$\Delta y_C(t_1) = a_{YC}(t_1)\cdot\frac{\Delta t^2}{2}$$

Speed of rope displacement at point C is:

$$v_{XC}(t_1) = a_{XC}(t_1)\cdot\Delta t$$
$$v_{YC}(t_1) = a_{YC}(t_1)\cdot\Delta t$$

Moving the rope over the point C causes a change in the length of the rope in the section 6C, which causes a change (increment) of force in the rope in this segment, which is:

$$\Delta X_{6C}(t_1) = c_{6C}(t_0)\cdot\Delta x_C(t_1)$$
$$\Delta Y_{6C}(t_1) = c_{6C}(t_0)\cdot\Delta y_C(t_1)$$

where it is:

$$c_{6C}(t_0) = \frac{E\cdot A}{\sqrt{[x_C(t_0)-x_6(t_0)]^2+[y_C(t_0)-y_6(t_0)]^2}}$$

stiffness of the rope in the section 6C at time point $t = t_0$,

$E = 0,5 \div 1,4\cdot 10^5\ MPa$ - modulus of elasticity of the rope,

A - metal cross-sectional area of the rope.

New values of the force on the part 6C are:

$$X_{6C}(t_1) = X_{6D}(t_1) = X_{CL}(t_1) = X_{6C}(t_0)+\Delta X_{6C}(t_1)$$
$$Y_{6C}(t_1) = Y_{6D}(t_1) = Y_{CL}(t_1) = Y_{6C}(t_0)+\Delta Y_{6C}(t_1)$$

The values of all parameters (position, velocity, acceleration, force) in other points (1, 2, 3, 4 and 5) are the same like at time point $t = t_0$.

2.3. Time point $\mathrm{t} = \mathrm{t}_2 = \mathrm{t}_0 + 2\cdot\Delta\mathrm{t}$

The time interval is chosen to disturbance comes from point C to point 6. Therefore, at time point $t = t_2$, due to change of rope force in the section 6C, the acceleration occurs at point 6, whose components are (Figure 4):

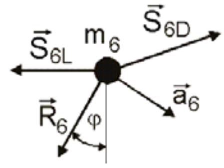

Figure 4: The forces acting on the mass m_6

$$a_{X6}(t_2) = \frac{\Delta X_{6D}(t_2)-\Delta X_{6L}(t_2)-R_{X6}(t_2)}{m_6(t_2)}$$
$$a_{Y6}(t_2) = \frac{\Delta Y_{6D}(t_2)-\Delta Y_{6L}(t_2)-R_{Y6}(t_2)}{m_6(t_2)}$$

where it is:

$$\Delta X_{6L}(t_2) = \Delta Y_{6L}(t_2) = 0$$

increment rope force in the x and y direction, on the left side of the vehicle 6 at time point t_2,

$$R_{X6}(t_2) = R_6(t_2)\cdot\cos\varphi_6(t_2)$$

components of the external force because of the presence (oscillation) of the vehicle in the x directions, at time point t_2,

$$R_{Y6}(t_2) = R_6(t_2)\cdot\sin\varphi_6(t_2)$$

components of the external force because of the presence (oscillation) of the vehicle in the y directions, at time point t_2,

$\varphi_6(t_2)$ - angle of the external force R_6 with respect to the vertical axis, at time point t_2.

$$m_6(t_2) = \frac{Q_6(t_1)}{g} = q_U\cdot\left[\frac{w}{2}+\frac{1}{2}\cdot\sqrt{[x_C(t_1)-x_6(t_1)]^2+[y_C(t_1)-y_6(t_1)]^2}\right]$$

concentrated mass consisting of the top weight of the vehicle and the reduced mass of the rope,

$q_U[N/m]$ - weight per meter of the rope,

w - distance between vehicles.

Calculating the value of the components external force $R_{X6}(t_2), R_{Y6}(t_2)$ requires an analysis of all the forces acting on point 6, respectively vehicle 6, figure 5. According D'Alembert's principle, of non-free material point, it is necessary at each time point geometric sum of the active forces, reaction links and inertial forces to be in equilibrium. It should also be noted that the vehicle m_{6v} performs relative motion, and the concentrated mass m_6 performs a portable motion, with the acceleration at time t_2, which is $\vec{a}_6(t_2)$.

Acting on the mass m_{6v} of the transmission force (Coriolis force of inertia), which can be presented via the tangential and normal components. Finally, according D'Alembert's principle, can write the following equation, figure 5:

equilibrium of forces in the x – direction:

$$\sum X = 0 \ \Rightarrow$$
$$m_{6V}\cdot a_{X6V} + F_{T6}\cdot\sin\varphi + R_6\cdot\cos\varphi = F_{N6}\cdot\cos\varphi$$

equilibrium of forces in the y – direction:

$$\sum Y = 0 \ \Rightarrow$$
$$m_{6V}\cdot a_{Y6V} + m_{6V}\cdot g + F_{N6}\cdot\sin\varphi + F_{T6}\cdot\cos\varphi = R_6\cdot\sin\varphi$$

the sum of moments at point 6 is equal 0:

$$\sum M_6 = 0 \ \Rightarrow$$

$$m_{6V}\cdot g\cdot l_V\cdot\sin\varphi + m_{6V}\cdot a_{Y6V}\cdot l_V\cdot\sin\varphi + F_{T6}\cdot l_V + m_{6V}\cdot a_{X6V}\cdot l_V\cdot\cos\varphi = 0$$

where it is:

$F_{N6} = m_{6V}\cdot l_V\cdot\dot{\varphi}^2$ - normal component of the inertial force,

$F_{T6} = m_{6V}\cdot l_V\cdot\ddot{\varphi}$ - tangential component of the inertial force,

l_V - the distance between the masses m_{6V} and m_6.

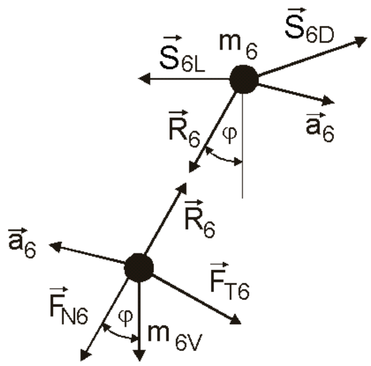

Figure 5: The forces acting on the masses m_6 and m_{6V} at time point t_2

Precalculated the acceleration of point 6, causes movement of the rope, and move the point 6:

$$\Delta x_6(t_2)=\left(v_{X6}(t_1)+\frac{a_{X6}(t_1)\cdot\Delta t}{2}\right)\cdot\Delta t$$

$$\Delta y_6(t_2)=\left(v_{Y6}(t_1)+\frac{a_{Y6}(t_1)\cdot\Delta t}{2}\right)\cdot\Delta t$$

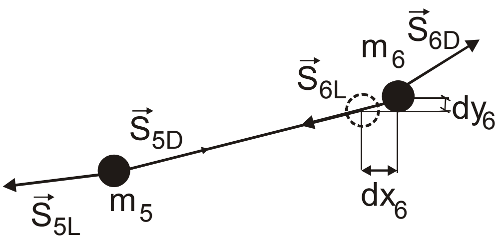

Figure 6. Movement in point 6 at time point t_2

Now the new position of point 6 is:

$$x_6(t_2)=x_6(t_1)+\Delta x_6(t_2)$$

$$y_6(t_2)=y_6(t_1)+\Delta y_6(t_2)$$

Appropriate speed of points 6 is:

$$v_{X6}(t_2)=v_{X6}(t_1)+\frac{1}{2}\cdot\Delta t\cdot\left[a_{X6}(t_2)+a_{X6}(t_1)\right]$$

$$v_{Y6}(t_2)=v_{Y6}(t_1)+\frac{1}{2}\cdot\Delta t\cdot\left[a_{Y6}(t_2)+a_{Y6}(t_1)\right]$$

Movement of point 6 causes a change in force in the rope section 5-6, which is:

$$\Delta X_{56}(t_2)=c_{56}(t_1)\cdot\left[\Delta x_6(t_2)-\Delta x_5(t_2)\right]$$

$$\Delta Y_{56}(t_2)=c_{56}(t_1)\cdot\left[\Delta y_6(t_2)-\Delta y_5(t_2)\right]$$

where it is:

$\Delta x_5(t_2)=0$ - movement of point 5, along the x-axis at time point t_2,

$\Delta y_5(t_2)=0$ - movement of point 5, along the y-axis at time point t_2,

$$c_{56}(t_1)=\frac{E\cdot A}{\sqrt{\left[x_6(t_1)-x_5(t_1)\right]^2+\left[y_6(t_1)-y_5(t_1)\right]^2}}$$ -

stiffness of the rope in section 5-6, at time point t_1.

New values of force in section 5-6 is:

$$X_{56}(t_2)=X_{5D}(t_2)=X_{6L}(t_2)=X_{56}(t_1)+\Delta X_{56}(t_2)$$

$$Y_{56}(t_2)=Y_{5D}(t_2)=Y_{6L}(t_2)=Y_{56}(t_1)+\Delta Y_{56}(t_2)$$

The values of all parameters (position, velocity, acceleration, force) in other points (1, 2, 3 and 4) are the same like at time point $t=t_0$.

2.4. Time point $t=t_3=t_0+3\cdot\Delta t$

Change of forces in section 5-6, which occurred at time t_2, causing acceleration of point 5, whose components:

$$a_{X5}(t_3)=\frac{\Delta X_{5D}(t_3)-\Delta X_{5L}(t_3)-R_{X5}(t_3)}{m_5(t_3)}$$

$$a_{Y5}(t_3)=\frac{\Delta Y_{5D}(t_3)-\Delta Y_{5L}(t_3)-R_{Y5}(t_3)}{m_5(t_3)}$$

where it is:

$\Delta X_{5L}(t_3)=\Delta Y_{5L}(t_3)=0$ - increment rope force in the x and y direction, on the left side of the vehicle 5 at time point t_3,

$$m_5(t_3)=\frac{Q_5(t_2)}{g}=q_U\cdot\frac{1}{2}\cdot\left[\sqrt{\left[x_6(t_2)-x_5(t_2)\right]^2+\left[y_6(t_2)-y_5(t_2)\right]^2}+\sqrt{\left[x_5(t_2)-x_4(t_2)\right]^2+\left[y_5(t_2)-y_4(t_2)\right]^2}\right],$$

concentrated mass at point 5 consisting of the top weight of the vehicle and the reduced mass of the rope

$R_{X5}(t_3)=R_5(t_3)\cdot\cos\varphi_5(t_3)$ - components of the external force because of the presence (oscillation) of the vehicle 5 in the x direction, at time point t_3,

$R_{Y5}(t_3)=R_5(t_3)\cdot\sin\varphi_5(t_3)$ components of the external force because of the presence (oscillation) of the vehicle 5 in the y directions, at time point t_3,

$\varphi_5(t_3)$ - the angle of the external force R_5 with respect to the vertical axis, at time point t_3.

Calculating the value of the components external force $R_{X5}(t_3), R_{Y5}(t_3)$ requires an analysis of all the forces acting on point 6, respectively vehicle 6, figure 7. There are valid all the observations which are mentioned in behavior analysis of point 6 at time point t_2, followed by:

equilibrium of forces in the x – direction:

$$\sum X=0\ \Rightarrow$$

$$m_{5V}\cdot a_{X5V}+F_{T5}\cdot\sin\varphi+R_5\cdot\cos\varphi=F_{N5}\cdot\cos\varphi$$

equilibrium of forces in the y – direction:

$$\sum Y=0\ \Rightarrow$$

$$m_{5V}\cdot a_{Y5V}+m_{5V}\cdot g+F_{N5}\cdot\sin\varphi+F_{T5}\cdot\cos\varphi=R_5\cdot\sin\varphi$$

the sum of moments at point 5 is equal 0:

$$\sum M_6=0\ \Rightarrow$$

$$m_{6V} \cdot g \cdot l_V \cdot \sin\varphi + m_{6V} \cdot a_{Y6V} \cdot l_V \cdot \sin\varphi + F_{T6} \cdot l_V + m_{6V} \cdot a_{X6V} \cdot l_V \cdot \cos\varphi = 0$$

where it is:

$F_{T5} = m_{5V} \cdot l_V \cdot \ddot{\varphi}$ - tangential component of the inertial force,

$F_{N5} = m_{5V} \cdot l_V \cdot \dot{\varphi}^2$ - normal component of the inertial force,

l_V - the distance between the masses m_{5V} and m_5.

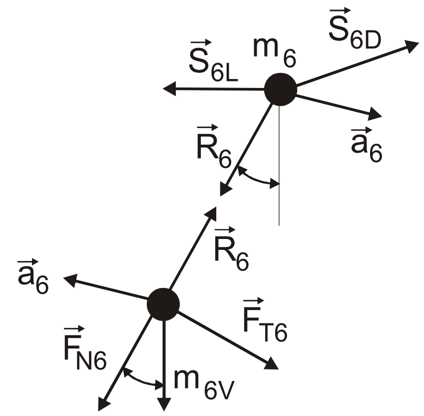

Figure 7: The forces acting on the masses m_5 and m_{5V} at time point t_3

Precalculated the acceleration of point 5, causes movement of the rope, and move the point 5:

$$\Delta x_5(t_3) = \left(v_{X5}(t_3) + \frac{a_{X5}(t_3) \cdot \Delta t}{2} \right) \cdot \Delta t$$

$$\Delta y_5(t_3) = \left(v_{Y5}(t_3) + \frac{a_{Y5}(t_3) \cdot \Delta t}{2} \right) \cdot \Delta t$$

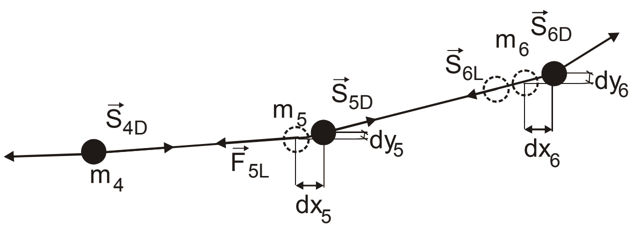

Figure 8: Movement in points 5 and 6 at time point t_3

Now the new position of point 5 is:

$$x_5(t_3) = x_5(t_2) + \Delta x_5(t_3)$$

$$y_5(t_3) = y_5(t_2) + \Delta y_5(t_3)$$

The corresponding velocity of point 5 is:

$$v_{X5}(t_3) = v_{X5}(t_2) + \frac{1}{2} \cdot \Delta t \cdot [a_{X5}(t_3) + a_{X5}(t_2)]$$

$$v_{Y5}(t_3) = v_{Y5}(t_2) + \frac{1}{2} \cdot \Delta t \cdot [a_{Y5}(t_3) + a_{Y5}(t_2)]$$

Movement of point 5 causes a change in the force on the rope in section 4-5, which is:

$$\Delta X_{45}(t_3) = c_{45}(t_2) \cdot [\Delta x_5(t_3) - \Delta x_4(t_3)]$$

$$\Delta Y_{45}(t_3) = c_{45}(t_2) \cdot [\Delta y_5(t_3) - \Delta y_4(t_3)]$$

where it is:

$\Delta x_4(t_3) = 0$ - movement of point 4, along the x-axis at time point t_3,

$\Delta y_4(t_3) = 0$ - movement of point 4, along the y-axis at time point t_3,

$$c_{45}(t_2) = \frac{E \cdot A}{\sqrt{[x_5(t_2) - x_4(t_2)]^2 + [y_5(t_2) - y_4(t_2)]^2}}$$

stiffness of the rope in section 4-5, at time point t_2.

New values of force in section 4-5 is:

$$X_{45}(t_3) = X_{4D}(t_3) = X_{5L}(t_3) = X_{45}(t_2) + \Delta X_{45}(t_3)$$

$$Y_{45}(t_3) = Y_{4D}(t_3) = Y_{5L}(t_3) = Y_{45}(t_2) + \Delta Y_{45}(t_3)$$

The values of all parameters (position, velocity, acceleration, force) in other points (1, 2 and 3) are the same like at time point $t = t_0$.

Point 6 continuing movement according to law movement which was applicable at time t_2, and that would generally be described by the following equations:

$$a_{X6}(t_{I+1}) = \frac{\Delta X_{6D}(t_{I+1}) - \Delta X_{6L}(t_{I+1}) - R_{X6}(t_{I+1})}{m_6(t_{I+1})}$$

$$a_{Y6}(t_{I+1}) = \frac{\Delta Y_{6D}(t_{I+1}) - \Delta Y_{6L}(t_{I+1}) - R_{Y6}(t_{I+1})}{m_6(t_{I+1})}$$

$$v_{X6}(t_{I+1}) = v_{X6}(t_I) + \frac{1}{2} \cdot \Delta t \cdot [a_{X6}(t_{I+1}) + a_{X6}(t_I)]$$

$$v_{Y6}(t_{I+1}) = v_{Y6}(t_I) + \frac{1}{2} \cdot \Delta t \cdot [a_{Y6}(t_{I+1}) + a_{Y6}(t_I)]$$

$$\Delta x_6(t_{I+1}) = \left(v_{X6}(t_I) + \frac{a_{X6}(t_I) \cdot \Delta t}{2} \right) \cdot \Delta t$$

$$\Delta y_6(t_{I+1}) = \left(v_{Y6}(t_I) + \frac{a_{Y6}(t_I) \cdot \Delta t}{2} \right) \cdot \Delta t$$

$$\Delta X_{6C}(t_I) = c_{6C}(t_{I-1}) \cdot \Delta x_C(t_I)$$

$$\Delta Y_{6C}(t_I) = c_{6C}(t_{I-1}) \cdot \Delta y_C(t_I)$$

$$X_{6C}(t_I) = X_{6D}(t_I) = X_{CL}(t_I) = X_{6C}(t_{I-1}) + \Delta X_{6C}(t_I)$$

$$Y_{6C}(t_I) = Y_{6D}(t_I) = Y_{CL}(t_I) = Y_{6C}(t_{I-1}) + \Delta Y_{6C}(t_I)$$

It is the acceleration on the support C defined by characteristics of driving mechanism, and the velocity at which the rope passes over the support is:

$$v_{XC}(t_{I+1}) = v_{XC}(t_I) + \frac{1}{2} \cdot \Delta t \cdot [a_{XC}(t_{I+1}) + a_{XC}(t_I)]$$

$$v_{YC}(t_{I+1}) = v_{YC}(t_I) + \frac{1}{2} \cdot \Delta t \cdot [a_{YC}(t_{I+1}) + a_{YC}(t_I)]$$

Continuing the analysis begin in subsequent points in time, can define the laws of motion for all elements of the monocable ropeway. Solving procedure, algorithm and computer program based on the application of numerical method are given in [1].

3. CONLUSION

Numerical integration method is suitable for use in dynamic analysis of monocable ropeways. The method is based on the assumption that the longitudinal and transverse waves propagated independently of each other. This requirement is adequately met in the case of short duration (a small time interval) because the propagation velocity of longitudinal waves is significantly higher than the speed of propagation of transverse waves.

This method is used to determine the kinematic and dynamic characteristics of monocable ropeways with two fields. Model monocable ropeways with two fields and three vehicles on the field, allowed the analysis of non-stationary behavior of the vehicles, where there is also some limitations.

4. REFERENCES

[1] P. Pavić, "Development of procedures for the study of static and dynamic behavior of the monocable ropeways", PhD Thesis, Faculty of technical sciences, Novi Sad, (2006)

[2] J. Vladić, "The development of computational methods for the analysis of static and dynamic behavior of the ropeways", PhD Thesis, Faculty of technical sciences, Novi Sad, (1989)

[3] D. Živanić, "Automation procedures for static and dynamic analysis of monocable ropeways", master's thesis, Faculty of technical sciences, Novi Sad, (2006)

[4] J. Vladić and D. Živanić, "Modeling ropeways on computer", Proceedings of International Conference on constructing, shaping and design КОД2006, Palić, Serbia, May 30-31, pp.157-162 (2006)

The Development of Hydrostatic Drive Transmissions of Wheel Loaders

Jovan Pavlović[1*], Dragoslav Janošević[1], Vesna Jovanović[1], Saša Petrović[2]
[1] Faculty of Mechanical Engineering, Department of Material Handling Systems and Logistics, University of Niš, Niš (Serbia)
[2]Ministry of Defence, Department of Logistics (J-4) of SAF Belgrade (Serbia)

In this paper is defined the process of analysis and synthesis of hydrostatic drive transmission of wheel loader. It is defined general calculation of transmission from which was developed program for the modular design. The basic requirements of transmission designing are related to the given drawbar pull and maximum ground speed with the choice of available transmission components produced by leading manufacturers.

Keywords: Wheel loaders, modular design, hydrostatic drive transmission

1. INTRODUCTION

The basic function of a loaders of all sizes, is cyclic transport of bulk materials, that is achieved by general configuration of the kinematic chain consisting of: the back part L_1 (Fig. 1a) and the front part L_2 of moving mechanism and manipulator with an arm L_3 and the bucket L_4.

For the drivetrain of the loaders there are used hydrodynamic and hydrostatic drive transmission, and for the manipulators drive there are used a mechanisms with hydrostatic actuators. General concept of the hydrostatic drive transmission of loader consists of: diesel engine 1 (Fig. 1b), hydraulic pump 2, hydraulic motor 3, gearbox 4, axle 5 and tires 6. Depending on the size of loader, general conception of hydrostatic transmission is performed by following version: V_1 (Fig.1b) – with one hydraulic pump and one hydraulic motor, directly linked to axle, for loaders with power of 60 kW (Fig . 1c); V_2 - with one hydraulic pump, one hydraulic motor and gearbox, directly connected to the axle, for loaders with power of 90 kW; V_3 - with one hydraulic pump, two hydraulic motors and two-stage gearbox, for loaders with power of 150 kW and V_4 - with one hydraulic pump, two hydraulic motors and multi-stage gearbox, for loaders with power of 250 kW [1] [2].

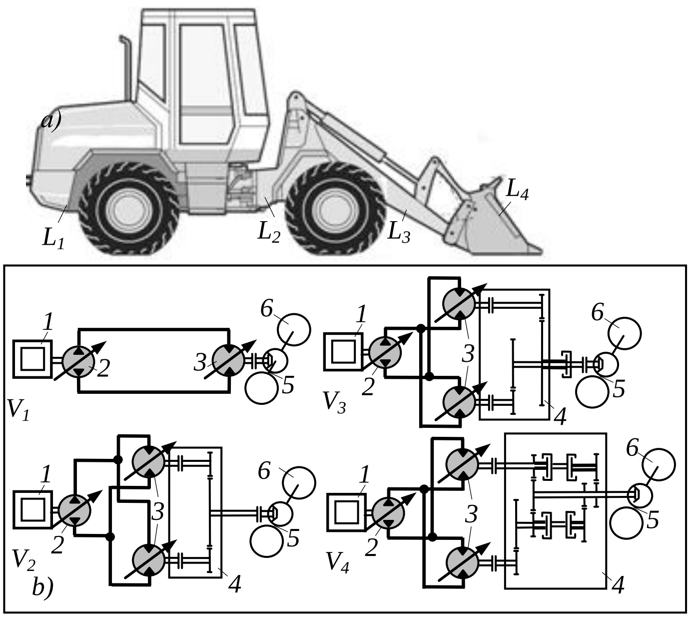

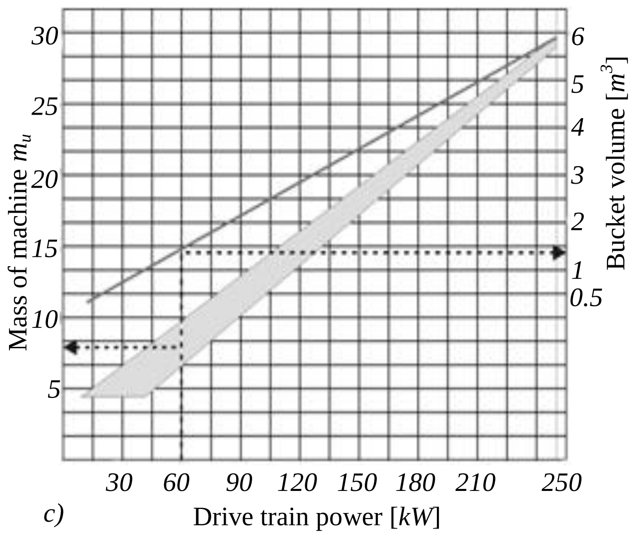

Fig. 1. Wheel loader: a) kinematic chain, b) conceptual solutions of hydrostatic transmissions, c) correlation diagram of the basic parameters[1][2]

2. CALCULATION OF HYDROSTATIC TRANSMISSIONS

The selected conceptual design of hydrostatic transmission of loader, for which is given a calculation, consists of: diesel engine 1 (Fig. 2a), hydraulic pump 2 with variable specific flow, one or two hydraulic motors 3 with specific variable flow, two-stage or three-stage gearbox 4, driveshaft 5, axel 6 and tire 7.

The initial parameters that is set up at calculation of transmission, belong to the following parameters:

$$P_n = \{V, b_4, k_z, \alpha_z, v_{t\,max}\} \tag{1}$$

where are: V - volume of bucket, b_4 - bucket width, k_Z - the characteristics of the grabbed materials, α_z - maximum angle of the motion path incline of loader, v_{tmax} - maximum transport speed. Based on the given set of parameters P_n there are determined the parameters of the machine and the size of transmission components that define the next set of sizes:

$$E_n = \{m, N_{en}, q_{pmax}, q_{mmax}, q_{mmin}, i_{mi}, i_o, r_d\} \tag{2}$$

where are: m - mass of machine, N_{en} - maximum power of diesel engine, q_{pmax} - maximum cubic displacement of the hydraulic pump, q_{mmax} - maximum cubic displacement of hydraulic motor, q_{mmin} - minimum cubic displacement of hydraulic motor, i_{mi} - gear ratios of the gearbox, i_o - gear ratio of the axle, r_d - dynamic radius of the tire.

*Corresponding author: Faculty of Mechanical Engineering, Aleksandra Medvedeva 14 18000 Niš, Serbia, jovan.mfn@gmail.com

2.1. The choice of diesel engine

For drive train of the loader there are used diesel engines, which choice are based on the required maximum power of the machine from condition of moving at maximum speed on a flat surface and from conditions of grabbing materials.

To determine the maximum power of diesel engine, first is need to determine the weight of machine from condition of stable motion (no-slip) at grabbing materials on a flat surface (Fig. 2b):

$$m \geq \frac{W_x}{g(\mu_p - f)} \tag{3}$$

where are: W_x - horizontal resistance of digging, μ_p - coefficient of the tire grip on the surface, f - coefficient of rolling resistance of tires, m - mass of the machine.

Horizontal resistance of digging - penetration of bucket in land is determined by the equations:

$$W_x = K_k \cdot b_4 \cdot h \tag{4}$$

where are: K_k - specific resistance of digging for the current category of land, b_4 - bucket width, $h = (0.10 \div 0.12)\sqrt[3]{V}$ - thickness land determined from dependence of the bucket volume.

Required power of diesel engine at motion of machine at continuous maximum transport speed on a horizontal way is:

$$N_{e1} = W_{fr} \cdot v_{t\,max} \frac{k_e}{\eta_t} \tag{5}$$

where are: W_{fr} - rolling resistance, k_e - the coefficient of increase of diesel engine's power for drive of other devices and systems that work at machine motion, η_t - efficiency of transmission drive of machine.

Rolling resistance of machine at motion on a horizontal way is:

$$W_{fr} = f \cdot gm \tag{6}$$

Required power of the diesel engine at horizontal penetration of bucket in material way by continuous transport speed is:

$$N_{e2} = W_{kk} \cdot v_r \frac{k_e}{\eta_t} \tag{7}$$

where are: W_{kk} - resistance of movement at horizontal penetration of bucket in material by continuous transport speed, v_r - movement speed of machine at horizontal penetration of bucket in material.

$$W_{kk} = W_{fr} + W_x \tag{8}$$

Based on maximum required power $N_e = max\{N_{e1}, N_{e2}\}$, from catalog of specialized manufacturers, it can be selected the size of the diesel engine.

2.2. The choice of transmission components

The axles are determined by the static and dynamic transport capacity. Maximum static load of axles occurs at digging when it comes to raising the rear wheel of loader (Fig. 2b), so that the total load is transferred to the front wheels and the front axles.

The boundary resistance W_y of digging cause uplift of rear wheels $Y_1 = 0$, and can be determine from the condition of the static stability of the machine for a possible line of front wheels turnover:

$$W_y = \frac{gm \cdot x_t}{x_w} \tag{9}$$

where is the maximum static load Y_{2s} of front axle equal:

$$Y_{2s} = mg + W_y \tag{10}$$

where are: x_t - the coordinate of center of mass of whole machine, x_w - the coordinate of the position of tooth top of bucket.

The maximum dynamic load of axles occurs when machine is moving with a full bucket of the grabbed materials where is:

Dynamic load of rear axle:

$$Y_{1d} = \frac{g(m \cdot x_t - V \cdot \rho_z \cdot x_z)}{a} \tag{11}$$

Dynamic load of front axle:

$$Y_{2d} = g(m + V \cdot \rho_z) - Y_{1d} \tag{12}$$

where are: ρ_z - the density of the grabbed materials with bucket whose volume is V, x_z - the coordinates of the position of the center of mass of the grabbed materilas when machine is moving, a - wheelbase of wheels.

According to the calculated loads it can be selected axles from catalog of specialized manufacturers so that the calculated loads is bigger than the allowable loads on axles, whereby each model that is chosen can have ratio in the interval $i_o = \{i_{omin}, i_{omax}\}$.

The choice of tire is based on: the maximum static load of tires:

$$Y_{ps} = \frac{Y_{2s}}{2} \tag{13}$$

and a maximum dynamic load of the tire:

$$Y_{pd} = \frac{max\{Y_{1d}, Y_{2d}\}}{2} \tag{14}$$

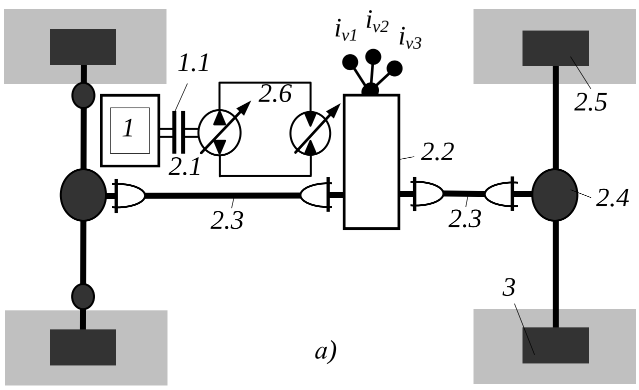

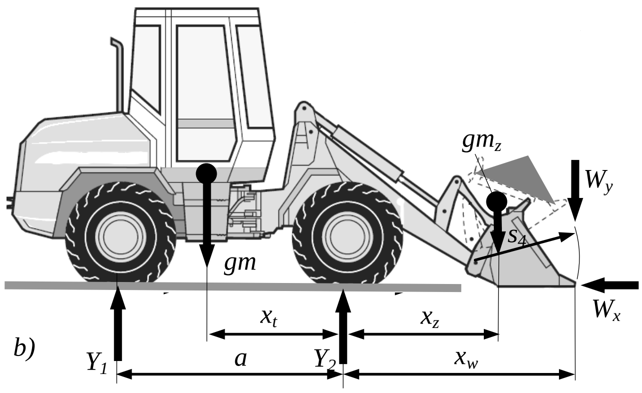

Fig. 2 Wheel loader: a) the concept of hydrostatic transmissions, b) resistance of digging and ground reaction

According to the calculated load and from manufacturer's catalogs it can be selected size of the tire, with the corresponding dynamic radius r_d and with the condition that the calculated load is less than the allowable loads for the adopted level of air pressure in the tire.

Gearbox of transmission can be selected from the catalog of the manufactures, based on the maximum possible torque moment M_m on input shaft of gearbox:

$$M_m = \frac{r_d \cdot W_{kk}}{i_o \cdot i_{m\,max} \cdot \eta_{m1} \cdot \eta_o} \tag{15}$$

and the maximum possible number of revolutions n_m on the input shaft of gearbox:

$$n_m = \frac{30}{\pi} \frac{v_{t\,max}}{r_d} i_{m\,min} \cdot i_o \tag{16}$$

where are: η_{m1} - efficiency of gearbox (first gear), η_o - efficiency of axles, i_{mmax}, i_{mmin} - appropriate ratio of gearbox of transmission.

Each selected model of gearbox can be performed with a determined number of gear ratios in the interval $i_m = \{i_{mmin}, i_{mmax}\}$.

2.3. The choice of hydraulic components

Size of hydraulic pump is determined by the hydraulic power N_h. For a hyperbolic dependence of the hydraulic pump parameters (pressure and flow) at the regulation according to criteria of constant hydraulic power (Fig. 3), we can write the equality:

$$N_h = \frac{p_p \cdot Q_p}{60 \cdot \eta_{pv} \cdot \eta_{pm}} = \frac{p_k \cdot Q_k}{60 \cdot \eta_{pv} \cdot \eta_{pm}} = \frac{p \cdot Q}{60 \cdot \eta_{pv} \cdot \eta_{pm}} = const \tag{17}$$

where are: p_p , Q_p - pressure and flow respectively at the beginning of hydraulic pump regulation (where is $Q_p=Q_{max}$), p_k , Q_k - pressure and flow at the end of hydraulic pump regulation (where is $p_k = p_{max}$), p, Q - the pressure and flow in the range of hydraulic pump regulation.

The range of hydraulic pump regulation e can be determined as ratio:

$$e = \frac{p_{max}}{p_{min}} \tag{18}$$

Determining the maximum flow Q_{max} of hydraulic pump that corresponding to flow $Q_p=Q_{max}$ at the beginning of the regulation:

$$Q_{max} = \frac{60 \cdot N_h \cdot e}{p_{max}} \cdot \eta_{pv} \cdot \eta_{pm} \tag{19}$$

by whome is determined the required maximum displacement q_{pmax} of hydraulic pump:

$$q_{p\,max} = \frac{1000 \cdot Q_{max}}{n_p \cdot \eta_{pv}} \tag{20}$$

where are: n_p – number of revolution of pump (for the first step of the calculation can be taken: $n_p = n_{en}$, e = 2.3-2.6).

According to the calculated value of the maximum displacement q_{pmax} it can be selected, based on the catalog of the manufacturers, size of hydraulic pump.

Size of hydraulic motor is defined by a maximum displacement of hydraulic motor q_{mmax} which is determined from the condition that the current pulling force F_{max} of machines reached at: maximum pressure p_{max} of hydraulic pump, the maximum displacement q_{mmax} of hydraulic motor and gear ratio of gearbox i_{m1} which is used at operating speeds.

Required maximum torque M_{max} on wheels at maximum drawbar pull can be computed as:

$$M_{max} = r_d \cdot F_{max} \tag{21}$$

From the condition that the required torque M_{max} of wheels is bigger than maximum torque of hydraulic motor M_{mmax}:

$$M_{m\,max} = \frac{(p_{max} - p_o) q_{m\,max}}{2\pi} \eta_{mm} = \frac{M_{max}}{i_{m1} \cdot i_o \cdot \eta_m \cdot \eta_o} \tag{22}$$

we can determine the required maximum displacement q_{mmax} of hydraulic motor:

$$q_{m\,max} = \frac{2\pi \cdot M_{max}}{(p_{max} - p_o) \cdot i_{m1} \cdot i_o \cdot \eta_{mm} \cdot \eta_m \cdot \eta_o} \tag{23}$$

where are: M_{max} - the maximum torque of wheels of loader determined on the maximum resistance of movement [Nm].

Based on the calculated values q_{mmax} it can be selected from the catalog of the manufacturer [6], size of motors. Required minimum displacement q_{mmin} of hydarulic motor is determined from the condition that the machine achieve the desired maximum transport speed v_{tmax} at: maximum flow of hydrulic pump Q_{max}, minimum cubic displacement q_{mmin} of hydraulic motor and gear ratio of gearbox i_{m2} used at transport speed of machine.

Maximum number of revolution of hydraulic motor n_{mmax} occurs when the machine has a maximum transportation speed:

$$n_{m\,max} = \frac{v_{t\,max}}{r_d} \cdot \frac{30}{\pi} \cdot i_{m2} \cdot i_o \le n_{md} \tag{24}$$

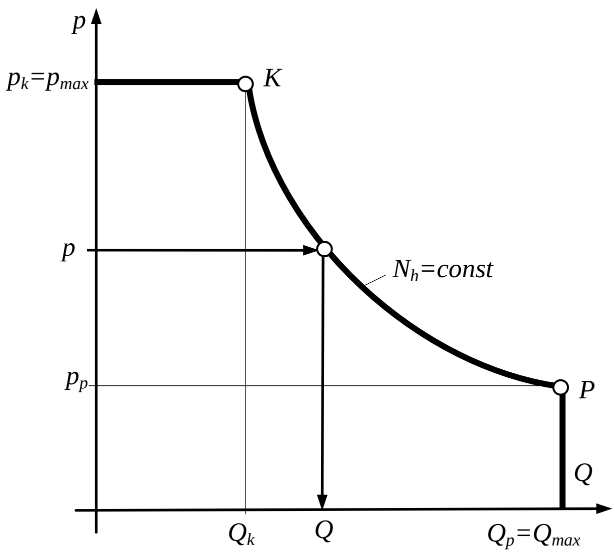

Fig. 3 Diagram of regulation of hydraulic pump's parameters based on criteria of constant power

where are: n_{md} - maximum number of revolution of hydraulic motor which is given in the catalog of the manufacturer of hydraulic motors.

The maximum number of revolution of motor is achieved at maximum flow Q_{max} of hydraulic pump:

$$Q_{max} = \frac{q_{m\,min} \cdot n_{m\,max}}{1000 \cdot \eta_{mv}} \tag{25}$$

so that required minimum displacement q_{mmin} of hydraulic motor is:

$$q_{m\,min} = \frac{1000 \cdot Q_{max}}{n_{m\,max}} \cdot \eta_{mv} \tag{26}$$

2.4. Determination of drawbar pull diagram

The drawbar pull diagram gives the dependence of the pulling force F_i and the speed v_i of the machine for the proper gear ratio. Speed of motion v_i and pulling force F_i for any conditions of work in the range of regulation of hydraulic pump and for any gear ratio of gearbox had value:

$$v_i = r_d \cdot \frac{1000 \cdot Q}{q_m} \cdot \eta_{mv} \frac{1}{i_{mi} \cdot i_o} \cdot \frac{\pi}{30} \tag{27}$$

$$F_i = \frac{1}{r_d} \frac{(p - p_o) \cdot q_m}{2\pi} \eta_{mm} \cdot i_{mi} \cdot i_o \cdot \eta_m \cdot \eta_o \tag{28}$$

where are: v_i, F_i - speed and pulling force respectively, p, Q - pressure and its corresponding flow of hydraulic pump respectively (depending on the criteria of regulation of hydraulic pump), q_m - cubic displacement of hydraulic motor (changes within borders q_m=[q_{mmax}, q_{mmin}] if is variable cubic displacement of hydrulic motor).

At determining the drawbar pull characteristics, for certain cubic displacement q_m of hydraulic motor and ratio of gearbox i_{mi}, there is change of pressure of hydraulic pump within borders p = [0, p_{max}]. For each value of the selected pressure p there is determined the appropriate flow rate Q of hydraulic pump depending on the characteristics of regulator of hydraulic pump.

For example, for hydraulic pump with regulation by the criteria of constant hydraulic power (Fig. 3) with the change of pressure p, flow Q of hydraulic pump, according to equation (17), following values can be computed as:

for pressure within borders p = [0, p_p] the flow is:

$$Q = Q_{max} = \frac{60 \cdot N_h \cdot \eta_{pv} \cdot \eta_{pm}}{p_p} \tag{29}$$

for pressure within borders p = [p_p , p_k] the flow is:

$$Q = \frac{60 \cdot N_h \cdot \eta_{pv} \cdot \eta_{pm}}{p} \tag{30}$$

According to the calculated speed of movement and pulling force F_i it can be defined drawbar pull diagram (Fig.5a,b) of machine [3].

3. PROGRAM

Based on the above given calculation there was developed program for determination the basic parameters of the machine and components of hydrostatic transmission of loader.

At the entrance on the program is given: the file of parameters of loader bucket UD1 (Fig. 4), the file of parameters of material UD2 and file of parameters of the machine UD3.

Based on the input parameters, the program first determines the necessary power and weight of machines according to which is selected: size of diesel engine, from the file DDM [4] of available diesel engines and components of moving mechanism - the drive axle and tires, from file DKM [5] [6] of available components.

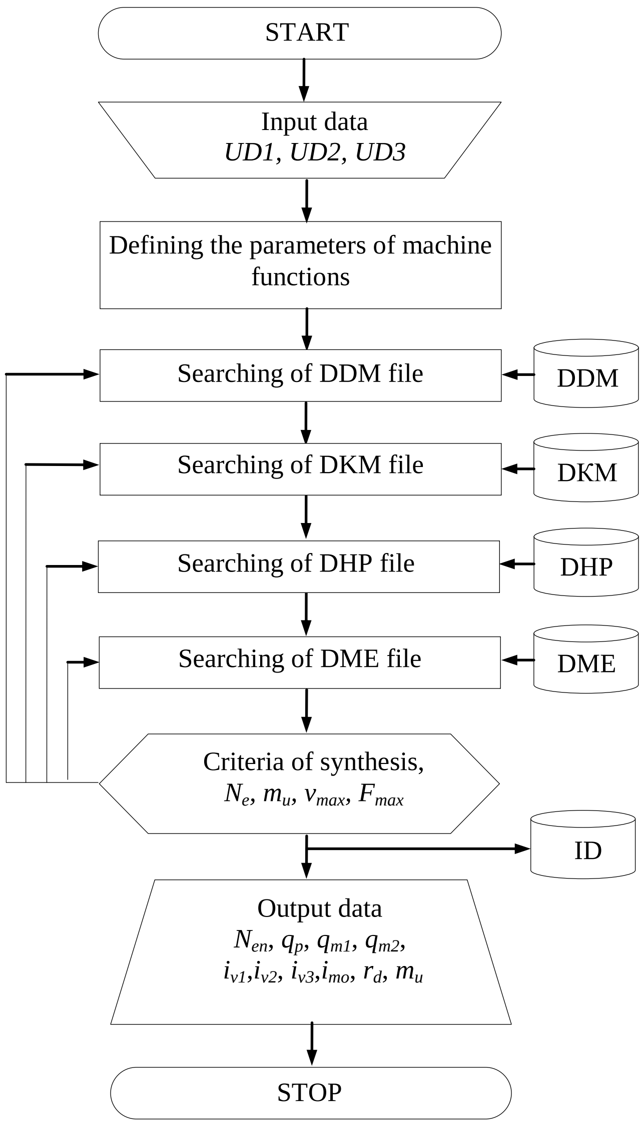

Fig. 4 Algorithm of program

Hydraulic pump and hydraulic motor are selected from condition of speed and maximum pulling force, by searching file DHP [7] of available hydraulic pump and file DME [8] of available integrated solutions of motors and gearbox.

Iterative search of all files, programs from a set of alternative solution through the imposed constraints stands out possible solutions of loader transmission. Constraints are related to the allowed deviations of given drawbar pull characteristics compared to drawbar pull characteristics that enables each variant of transmission.

3.1. Example

Using the developed program there were done research with the aim to replace the hydrodynamic transmission of the loader ULT - 160 [9] with hydrostatic transmission, there is given a input parameters (Table 1) corresponding to the size of the loader ULT – 160. Based on the input parametars, program is searched next files: 35 models of diesel engine, 15 models of motion mechanisms, 12 models of hydraulic pump and 25 models of integrated solutions of gearbox and hydraulic motor, and there is separated possible solutions in table T2.

From the set of possible variants $N=DDM \cdot DKM \cdot DHP \cdot DME=157500$ there were selected variants (Table 1)

Based on the size of the components obtained from optimal synthesis, there were done graphical analysis of obtained alternative solutions (Fig. 5).

For this analysis we are observing drawbar pull diagrams (Fig. 5) with regard to an ideal hyperbolic dependence of the pulling force *F* and the speed of motion *v*.

Table 1: Input parameters

Name of parametar	Bucket volume $V\ [m^3]$	Bucket width $b_4\ [m]$	Max. transportation speed $v_{tmaxx}\ [km/h]$	Speed on climb $v_u\ [km/h]$	Operating speed $v_r\ [km/h]$	Acceleraton time $t_u\ [s]$
Size	2,7	2,7	40	4	2,7	3

Table 2: Output file of program

N_{en} [kW]	q_p $[cm^3]$	q_{m1} $[cm^3]$	q_{m2} $[cm^3]$	i_{v1} [-]	i_{v2} [-]	i_{v3} [-]	i_{mo} [-]	r_d [m]	m_u [kg]
123	145,3	56,1	56,1	6,1	3,03	1,34	25,267	0,681	13797
123	110,4	56,1	90,0	6,1	3,03	1,34	20,210	0,711	13797

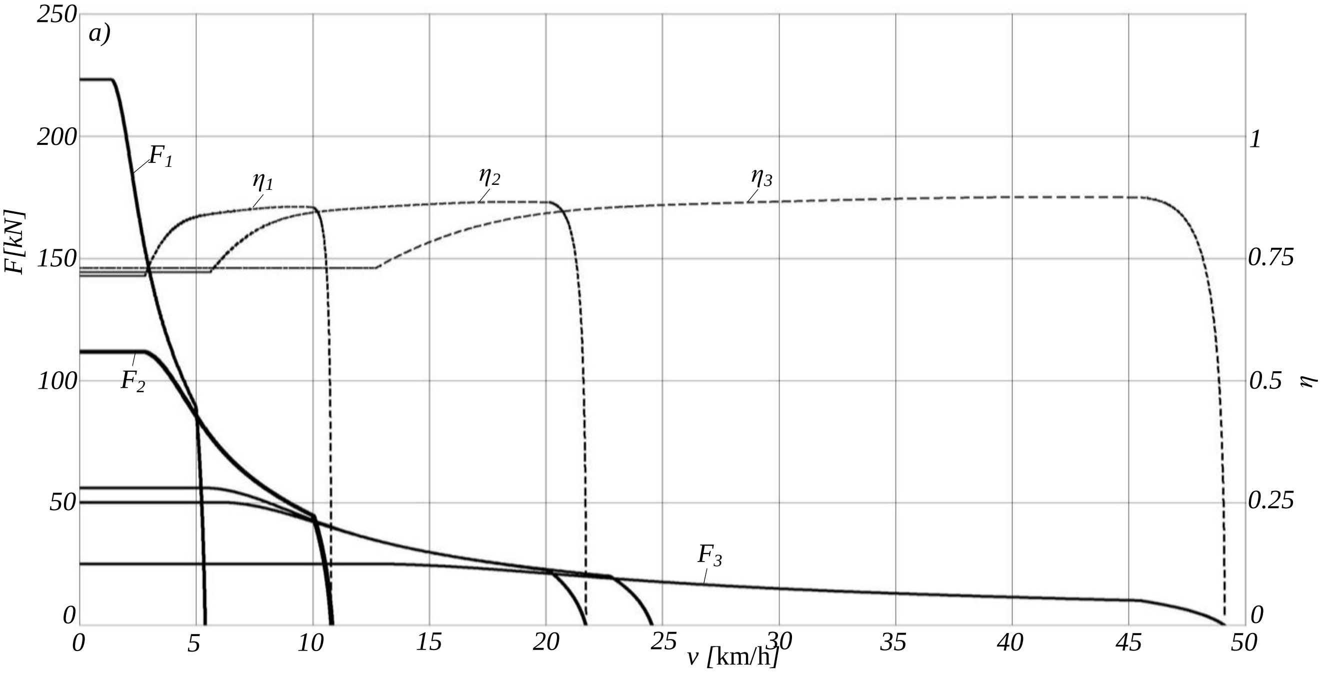

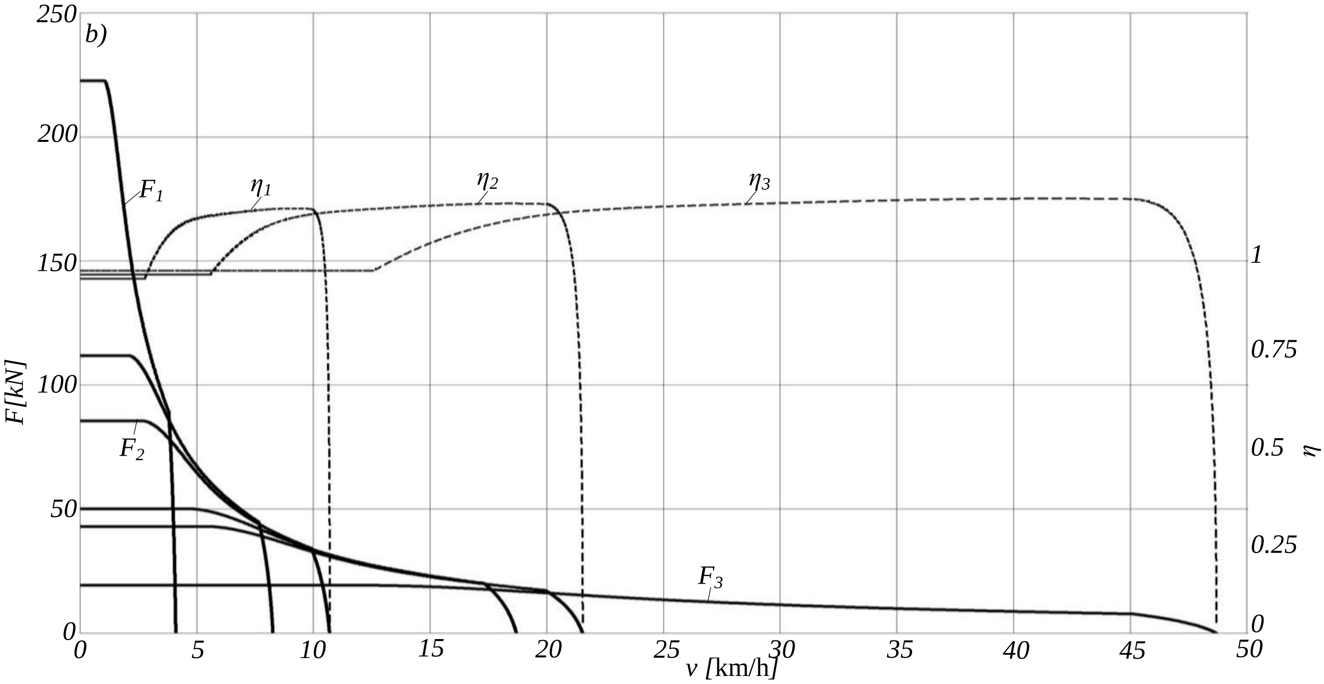

Fig. 5 Drawbar pull diagrams: a) variant I, b) variant II [10]

4. CONCLUSION

Conducted researches indicate that there are many reasons for the increasing use of hydrostatic transmissions for mobile machines, which are reflected in the following benefits and opportunities: easy regulation of drawbar pull characteristics, modular design, the possibility of a hydraulic brake, hydraulic differential option, simply limit of overload, simply and easily manage the movement. Beside that, the leading specialized manufacturers of mobile hydraulics developed a different conceptual solution of hydrostatic system for certain types of mobile machines for which choice is necessary to know the basic parameters of the machine.

Hydrostatic transmission have drawbar pull characteristics close to ideal hyperbolic dependence due to easy regulation of hydrostatic power parameters (flow and pressure) of transmissions. At higher speeds and lower pulling forces (which corresponds to the transport conditions of the machine), the level of efficiency η_1, η_2, η_3 of hydrostatic transmissions have high value. Compared to the speed of motion, on diagram can be showen that at low speeds of motion can be achieved higher pulling force.

ACKNOWLEDGEMENTS

This paper is result of technological project "Theoretical and experimental researches of dynamics of transport mechanical systems", No. TR35049, supported by Ministry of Education, Science and Technological Development of the Republic of Serbia

REFERENCES

[1] D. Janošević, Projektovanje mobilnih mašina, Faculty of Mechanical Engineering University of Niš, ISBN 8680587443, 9788680587448, Niš (2006)

[2] R. Paoluzzi, L. G. Zarotti, "The minimum size of hydrostatic transmissions for locomotion" Journal of Terramechanics, Vol. 50, pp. 153–164 (2013).

[3] K. Rydberg, "Hydrostatic Drives in Heavy Mobile Machinery –New Concepts and Development Trends", Sae Transactions; Vol. 107(2), pp. 232-238 (1998)

[4] http//www.cummins.com, official site of the company Cummins

[5] http//www.zf.com, official site of the company ZF Transmission

[6] http//www.michelin.com/, official site of the company Micheline

[7] http//www.boschrexroth.com, official site of the company Rexroth Bosh

[8] http//www.dana.com, official site of the company Dana

[9] Manual for operation and maintenance of wheel loader ULT – 160, Technical service industry IMK 14 Oktobar Kruševac, (1986)

[10] J. Pavlović, "Istraživanje i razvoj hidrauličkih transmisija mobilnih mašina", master thesis, Faculty of Mechanical Engineering, University of Niš, (2012).

About Choosing the Right Computational Model for FEA Stress Analysis of Drilling Rigs and Well Servicing Structures in Oil Industry

Radoslav Simić[1*], Nikola Brkljač[2]
[1]NIS a.d., NAFTAGAS Tehnički Servisi D.O.O, Zrenjanin (Serbia)
[2]Faculty of Technical Sciences, University of Novi Sad (Serbia)

The paper presents computational models for FE static structural analysis of stress-deformation states of mobile rig for servicing wells in oil industry. In order to assess impacts of the introduced approximations on the calculation results of computational models, simulations of different ways for defining load on crown of the mast were performed by considering the impact of changes in direction and position of vectors representing reaction rope forces of hoist mechanism due to the moving crown of the mast. The impact of preload in static ropes on calculation results is considered for two different inclination of the mast. FEM analyses of representative computational models were performed using linear and nonlinear second-order theory and corresponding calculation results are given comparatively.

Keywords: Service rig, Computation model, FEA

1. INTRODUCTION

Results obtained from the computational model represent more or less approximate estimate of response of structure to the load action, primarily due to the (1) approximations made during the design of computational model and (2) discrepancies between produced and designed construction. In addition to these two groups of sources that lead to discrepancies between the results of the calculations and the actual behaviour of the structure, in practice is also possible that variety of other errors, which accompany design of structures. Clearly, the task of the designer is to fully understand and consciously controls their impact on the calculation results. By discussing the shortcomings of computational models of engineering structures, Dvornik and Lazarević among other state: "… we need to know that in all phases of modeling and calculation occur large errors, even when everything is done the best it could be and when formally looking everything is right". At the end they conclude: "For complex problems 'templates' are not sufficient, so today, as well as in the era without computers, the knowledge, experience and intuition of good engineer are essential.", [1].

Considering the importance of selecting an effective computational model which provides a comprehensive analysis of structural response to load's action, in the framework of this paper is considered the impact of certain approximations on the quality of results obtained using the given computational model.

2. DESCRIPTION OF SERVICE RIG

2.1. Description of the service rig

The mast with the maximum rated static hook load of 500 kN is situated on the load-bearing frame of an auxiliary chassis, which is connected to the main chassis of the truck. Auxiliary chassis is welded assembly with the main task to provide sufficient rigidity and stability for the work of the service rig. The chassis is equipped with necessary supports for load-bearing structure of the mast in transport and work position as well as with elements to install an engine, draw-works with transmission, supports of hydraulic cilinders and other equipment. On the front and back side of the chassis are hydraulic cylinders that are used to elevate the chassis with the mast on an appropriate height.

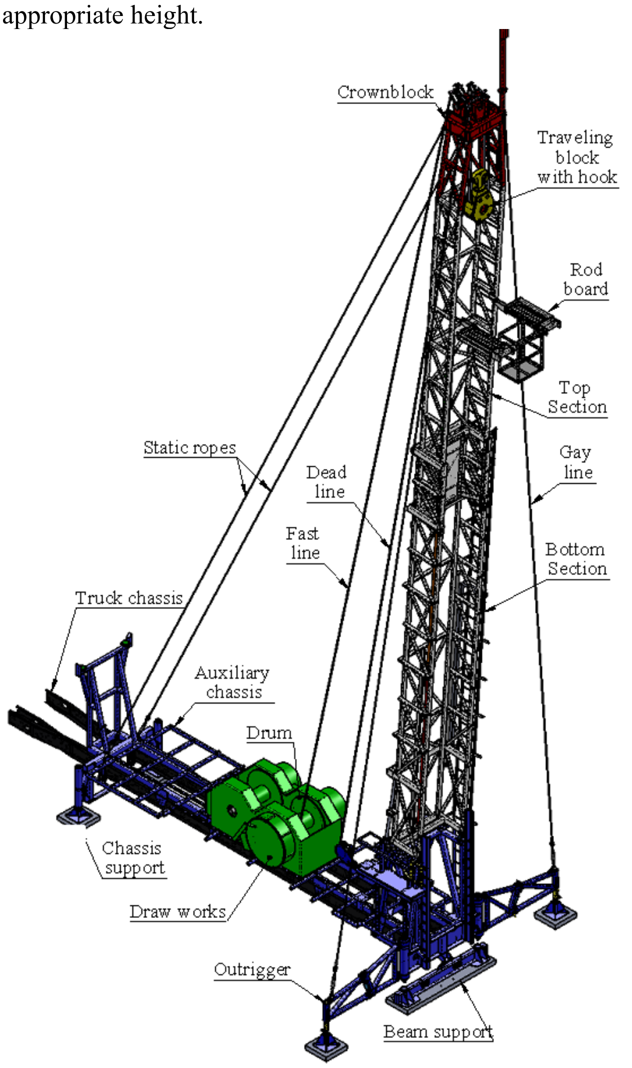

Figure 1 Service rig with mast in working position.

All cilinders are equipped with support legs which have an appropriate area in order to provide a reliable support for

*Corresponding author: Bulevar cara Lazara 98, 21000 Novi Sad, radoslav.simic@nis.eu

the chassis. Two static ropes ϕ16mm are from the one side connected to the lugs welded on the auxiliary chassis, and the other side of the ropes is connected to the lugs on the crown of the mast. The mast of the rig is projected as free standing, without clasic wind gaylines with anchors in the ground. In order to provide resistance to horizontal forces originating from the wind and prevent overturning, at the back side of the chassis on both sides are frames equipped with support legs. The frames are connected to chassis and equipped with the appropriate mechanism which places them in the working or transport position. At the end of the outriggers on the top side there are connections with the end of the rope. The second end of the rope is connected to crown of the mast. Working position of the mast is illustrated in Figure 1. The mast consists of two sections. The bottom section of the mast has two lugs on the back side for connection of the mast with the supporting structure of the auxiliary chassis.

In the transport position mast is horizontal and the top section of the mast is placed inside the bottom section. Erection of the mast into vertical position is performed with two hydraulic cylinders with rotation around back lugs of bottom section for the angle of 94.17°. In the operating position mast is sloped for 4.17 º relatively to the vertical axis.

After erection of the mast, top section is telescoped with the hydraulic plunger cylinder to the proper height and then the mechanism is used to pull the pin and perform the locking of the top with the bottom section. In the operating position the top and the bottom section have some overlap (Figure 2).

2.2. Description of the computational FE model

According to 2D documentation that is generated from the 3D CAD models, geometry of computational models was made using the preprocessor for FE analysis. The relevant passing of beam axis welded to each other is taken into account. In order to provide appropriate evidence of strength, stiffness and stability, the geometry is discretized with linear beam elements which include warping and shear deformation in line with the Timoshenko theory.

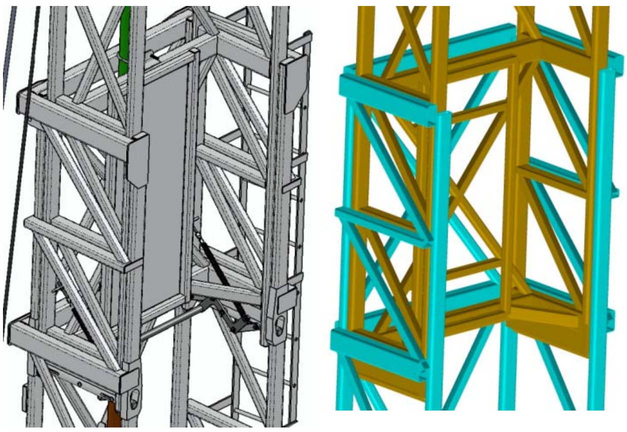

Figure 2. Overlap of top and bottom section of the mast.

All pinned connections are modeled with revolute joints, including geometry of lug as conical plate with suitable thickness, in order to simulate adequate rigidity of joints. The front supports of the mast legs on the substructure are modeled as spherical joints with no moment resistance (Figure 3).

Relationship between stresses and deformation is considered as linear with a modulus of elasticity of steel equal to E=2.1x10^5 MPa and Poisons ratio ν=0.3. Modulus of elasticity of ropes is modeled with E_r= x10^5 MPa.

All Ropes are modeled as "spar" elements in order to transmit only axial tension forces.

Overlaps of sections (Figure 2) are modeled with appropriate coupled degree of freedom on potential contact point pair between the beams of the top and the bottom section of the mast in direction normal to the mast axis. The top section is considered as cantilevered in the bottom section of the mast. The transmission of the forces parallel with the mast axis is prevented at the pins where the sections are connected. Geometry of the rod board is also modeled, and it is connected with the crown with ropes and with the mast using revolute joint.

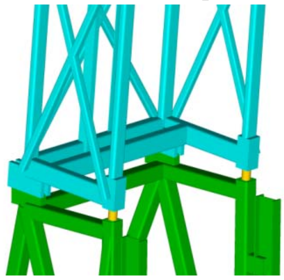

Figure 3 Supports of mast to auxiliary chassi.

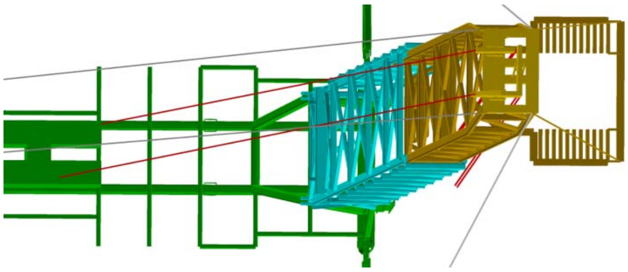

Figure 4 Appearance of modeled ropes in the computational model of the service rig.

Geometry of sheave on the crown is included in the model with approximate rigidity and is modeled with beams connected to the crown with revolute joint and on the other side with the rope that is modeled as the "spar" element with the resistance only to axial tension force. Length of the beam corresponds to the radius of the sheave.

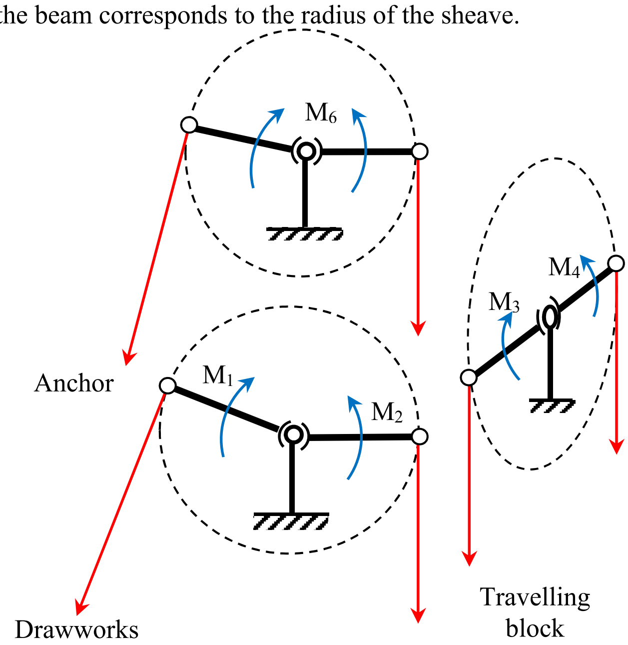

Figure 5 Simulation of load on the crown/block.

The rope ends, from the fast line and the dead line sheave, are connected to the corresponding nodes on the tangent of the drum of drive-works (fast line) and anchor point (dead line), respectively. Rope ends towards the traveling block are vertical and connected to the points above well.

The changes in the direction and position of spar element, which is used for modeling of the fast line, due to the rotation of the drum and sheave are neglected. All ropes of hoisting system are modeled as elements with the resistance only for tension.

To simulate the changes of the direction of rope forces during the deformation of crown-block, loads on the crown are applied as appropriate moment on elements used to simulate revolute joints of the sheaves (Figure 5). All ropes of hoist mechanism are also modeled as beams with ability to receive only axial tension forces.

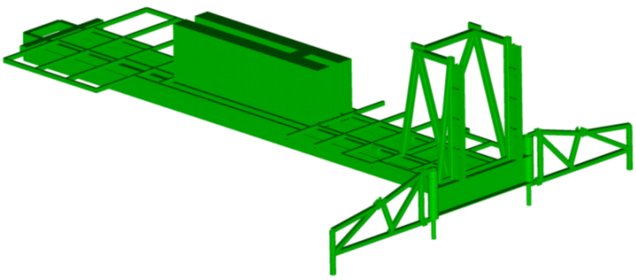

Figure 6 FE model of chassis.

Geometry of draw-works is modeled with approximate rigidity in order to appropriately describe mass and position of structure on the chassis. Load-bearing beams of the main chassis of the truck and auxiliary chassis are also modeled in accordance with defined geometry. Supports of the chassis at the front and the back side are defined with spherical joints in corresponding points.

Figure 7 a.) Computation FE model, b.) 3D CAD model of the service rig.

2.3. Load cases

The load cases for computational model of the Self-propelled service rig are defined in accordance with the relevant specification of American Petroleum Institute, (API), i.e. Specification for drilling and well servicing structures 4F, [1].

Table 1 Calculation load cases in accordance with the API Spec. 4F.

Combination Load cases:	1	2	3 ÷ 7	8 ÷ 12	13 ÷ 17	18	19	20
Maximum rated static Hook load 500 kN + TE	x	x	x					
Dead weight	x	x	x	x	x	x	x	x
Rod board load (max load 32 kN)		x	x	x				
Operating wind speed (33 knots)			x (5)			x(1)	x(1)	
Unexpected wind speed (60 knots)				x (5)				
Expected wind speed (75 knots)					x (5)			
Transportation load case							x	
Mast Erection						x		
(1) – one direction of wind , (5) – five different directions of wind load								

Load case 1: Maximum rated static Hook load with dead load of the mast (without Wind load);

Load case 2: Maximum rated static Hook load with dead load of the mast and maximum load on rod board (32 kN);

Load case 3 - 7: Maximum rated static Hook load with dead load of the mast, load on rod board (32 kN) and Wind load with speed 33 knots from five directions;

Load case 8 - 12: Dead load of the mast and other equipment, load on the rod board (32 kN) and unexpected wind load with speed of 60knots from five directions;

Load case 13 - 17: Expected Wind load with the speed of 75 knots from five directions with dead load of mast;

Load case 18: Transportation load cases with dead load of the mast on the supports of the auxiliary chassis with the wind speed of 33 knots in normal direction to the mast;

Load case 19: Mast erection with two hydraulic cylinders with the wind speed of 33 knots from direction normal to the mast;

Load case 20: Dead weight of the mast with equipment.

For all load cases on the Hook, a quazistatic case of moving load and different forces in the ropes due to the friction resistance forces in sheave bearing and efficiency of wire ropes is considered.

According to API RP 9B [3], the efficiency of wire ropes is defined as:

$$\eta = \frac{C^p - 1}{C^s \cdot p \cdot (p-1)} \tag{1}$$

C - Factor of friction (1.04- Roller bearing, 1.09 – Plain bearing);
p - Number of rope parts supporting load;
S - Number of revolving sheaves.

$$W = Q + G \tag{2}$$

$$F_f = \frac{W}{p \cdot \eta}$$

Q - Load lifted; G - Weight of traveling block;
W - Maximum rated static hook load.

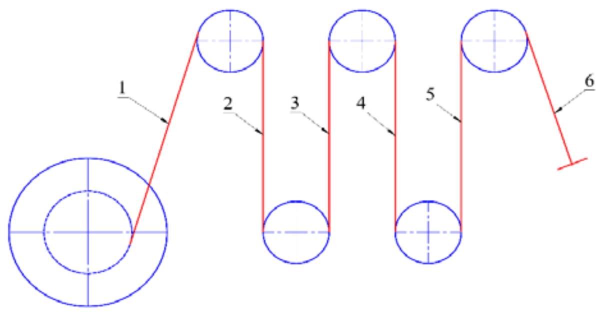

Figure 8 The chart of wire rope reevings.

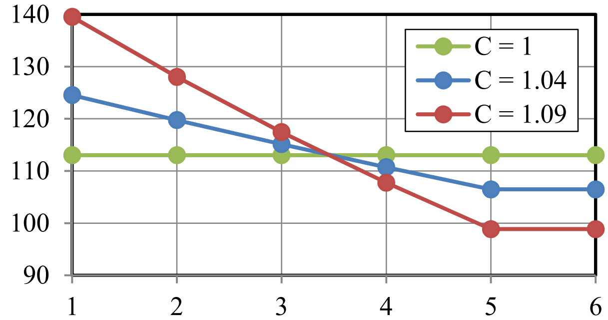

Figure 9 Differences in rope forces due to different friction coefficient “C” used in eq. (1).

Wind loads are considered from five different directions for three different intensities. Wind speed W_1=33 knots is the wind load defined as the operating wind and that load is applied in Load combinations 3-7 (Table 1) with the maximum rated Hook load of 500 kN, dead weights and the rod board load of 32kN.

Wind speed W_2 = 60 knots, is the unexpected wind load and it is applied in load cases 8-12 in combination with the dead load and setback load, without Hook load.

Wind speed W_3=75 knots is defined as expected wind speed and is applied in load cases 13-17, with dead load, without rods in setback and without hook load.

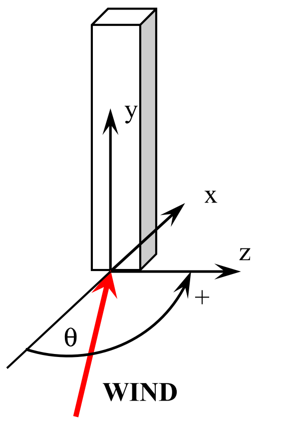

Figure 10 Global coord. system of the mast.

Considered wind actions are defined through the wind load vectors with directions defined in global coordinate system of the mast (Figure 10), along the x-axis (θ=0°) in positive direction towards the back side of the mast, i.e. from the chassis towards the mast. Next four directions are defined by incrementally changing the angle θ in positive angle direction with the step size of 45°.

Pretension force in static ropes is not defined. Weight of the equipment on the mast and truck chassis (axles, wheels, cabin and other equipment) is defined as appropriate mass load.

2.4. Calculation results

Static structural nonlinear analyses are performed for all defined load cases (Table 1) and calculated results from load cases 1-17 are presented in this paper.

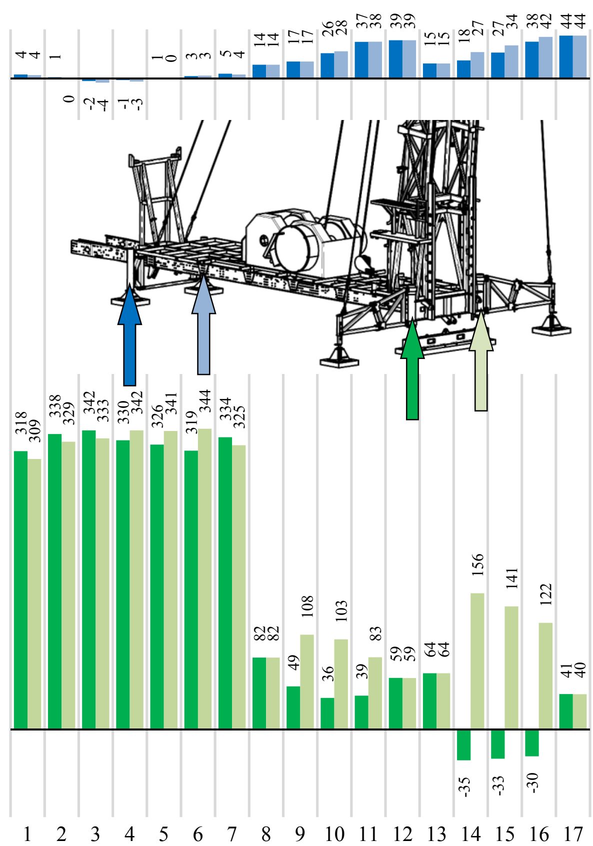

Figure 11 Reaction forces of chassis (kN), calculated for 17 load cases defined in Table 1.

Results presented in Figure 11, show reaction forces of chassis on the ground and because of existing negative values for some load cases due to insufficient weight of the rig, it is necessary to make analyses of overturning and sliding of the rig due to horizontal forces from wind, changing mass or considering to include prevention of vertical and horizontal movement of chassis support.

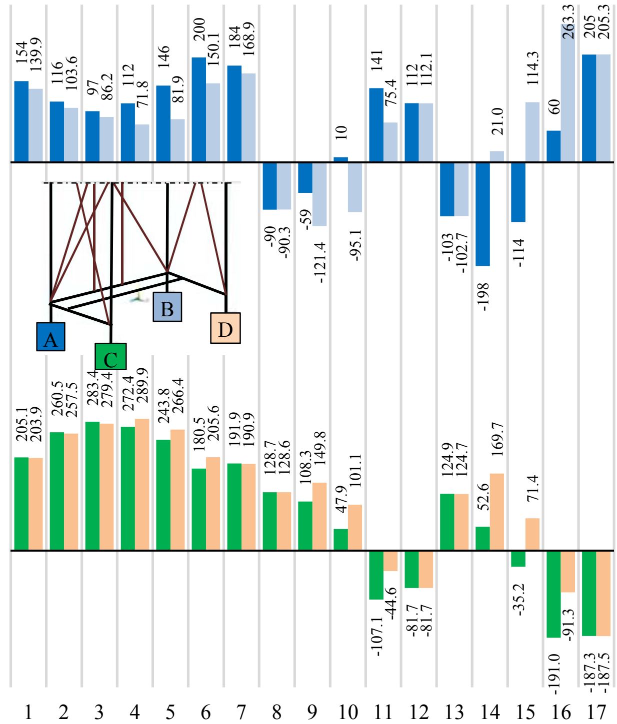

Figure 12 Reaction forces of Mast to auxiliary chassis(kN)

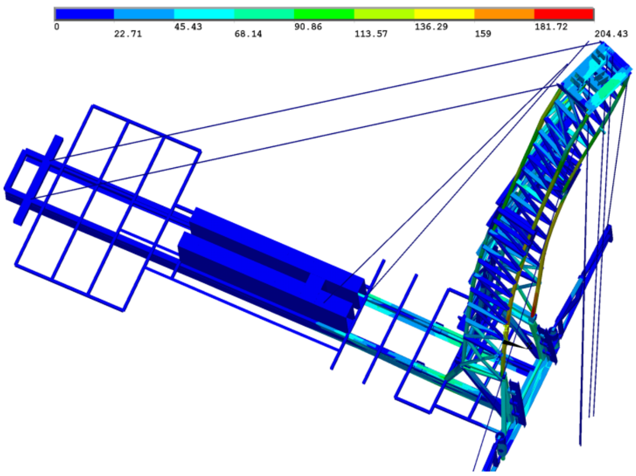

Figure 13 Von Misses stresses (MPa), on whole load bearing structure of the service rig, computed for load case 4.

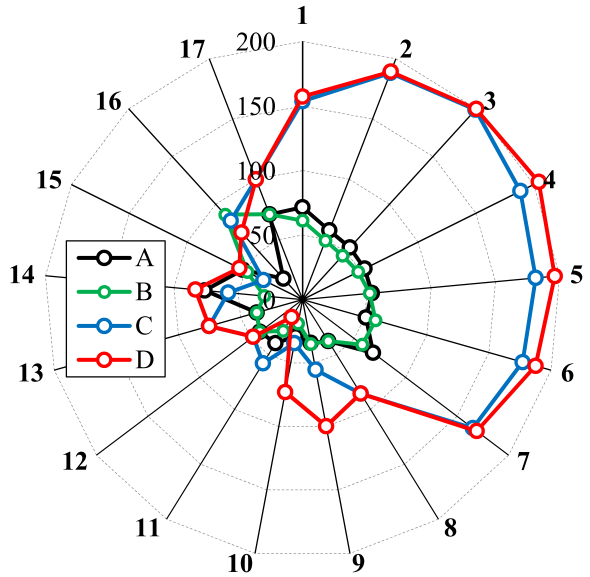

Figure 14 Von Misses stresses (MPa), in vertical beams of Mast bottom section, computed for 17 load cases.

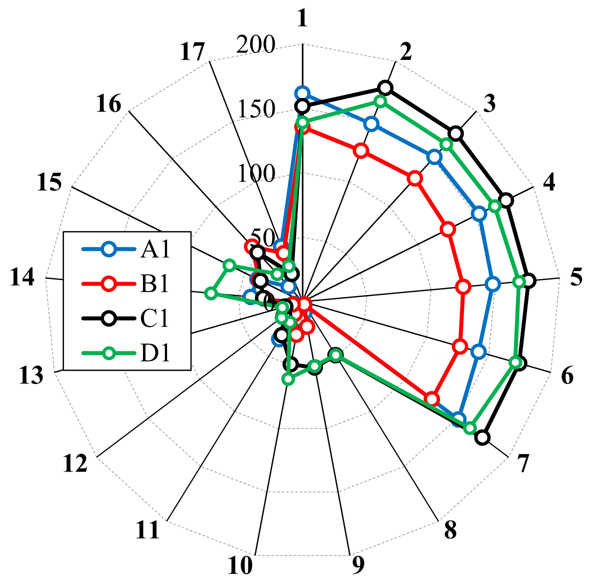

Figure 15 Von Misses stresses (MPa), in vertical beams of top section of the mast, computed for17 load cases.

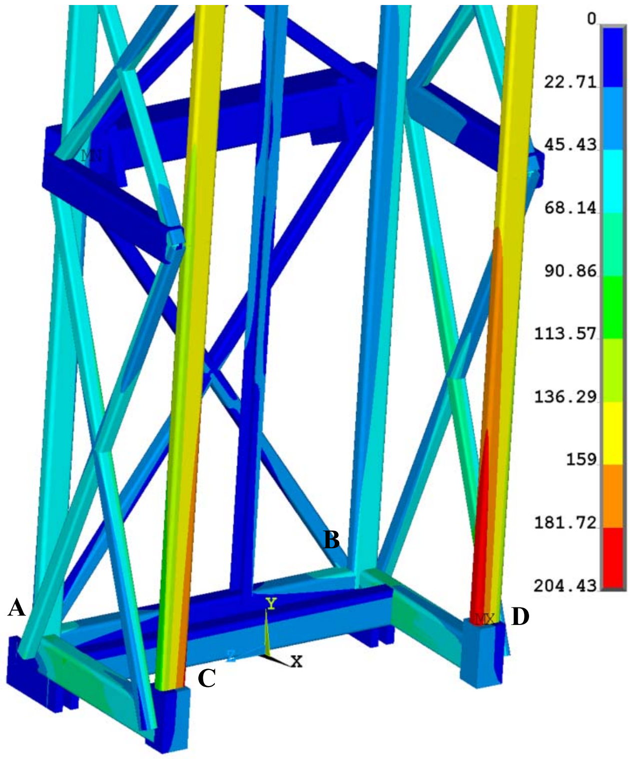

Figure 16 Detail on bottom section of the mast with maximum von Misses stresses (MPa), computed for load case 4.

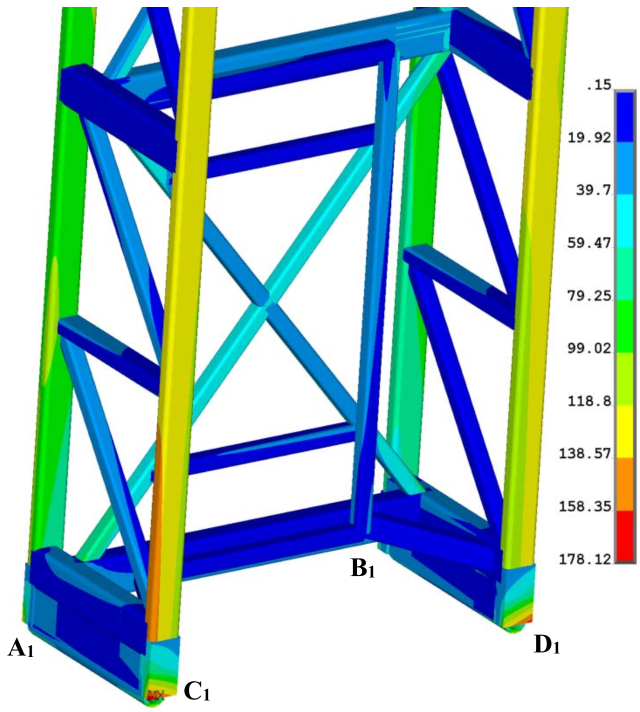

Figure 17 Detail on top section of the mast with maximum von Misses stresses (MPa), computed for load case 4.

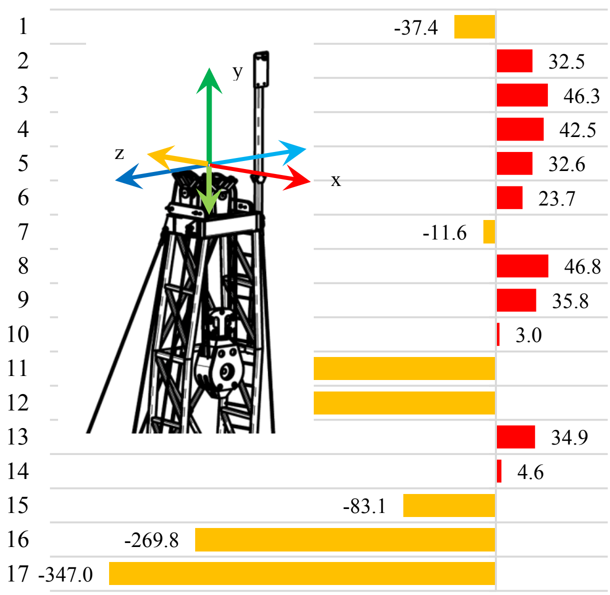

Figure 18 Displacements of crown of the mast in x-direction (mm), calculated for load cases 1-17.

3. ABOUT APPROXIMATIONS IN COMPUTATIONAL FE MODELS

Computational FE model on the basis of which in the previous section an analysis of the stress and deformation state of the load-bearing structure of the service rig is performed, represents one of many different ways in which the geometry, boundary conditions and loads can be modelled. In the general case, the designer has a wide selection of various finite elements which can be used for discretization and calculation of structure. The use of beam elements for FEM calculation of this type of load-bearing structures, according to the authors opinion, certainly has the advantage and is recommended especially for the mast structure, which represents spatial truss whose constituent elements are beam girders with one dimension significantly larger than the dimensions of their cross-section. Having in mind the existence of complex geometric details in structure, as are the mast crown and truck chassis, which represent a complex welded assembly in space, for this kind of structure parts is recommended to use spatial finite elements. Despite the significant development of methods for discretization of spatial geometry in software packages for FE analysis and the different options for importing structure's three-dimensional geometry from CAD programs, the issue of the relationship between the required accuracy of the calculation results, the speed of calculation and the optimal use of available computing resources is still present. The development of various theoretical assumptions embedded in the formulation of various types of finite elements was in the direction to be able to offer designer an adequate element for discretization and efficient calculation, with as small as possible approximation to the state of actual structure.

Guided by the recommendations, knowledge and his own experience, the engineer is one that needs to make the correct choice from the available tools for discretization, modelling of boundary conditions and calculation methods, and ensure that the computed values do not deviate significantly from the actual ones.

In order to contribute to the development of computational models for the analysis of structures of this type, in this paper are created several computational models that introduce certain approximations which could be used by the designer. One part of the analysis is dealing with the evaluation of the level of discrepancy of the calculation results due to the "errors " that may arise in the process of defining loads in computational model, and the other aspect of the analysis is referred to the influence of neglecting certain effects imposed on the structure and the choice of calculation method.

a.) Analysis of actual load on the mast structure as a result of forces in the ropes of hoist mechanism.

b.) Analysis of the influence of pretension of static ropes on the stress-strain state of the mast for the cases of different mast slope angles.

c.) Analysis of the differences between results obtained by linear and non-linear calculation methods.

Table 2 Computation models

Model Name	Ropes directions[1]	Fast line position[2]	Factor for sheave friction[6]	Fast line position on Drum[3]	Change dir. of ropes[4]	Mast angle (deg)	Pretension in static ropes (kN)	Load cases	Performed static analysis[5]
M1.1	I	A	1	F	×	4.17	0	1-17	L/N
M1.2	II	A	1	F	×	4.17	0	1-7	L/N
M1.3	II	B	1	F	×	4.17	0	1-7	L/N
M1.4	II	B	R	F	×	4.17	0	1-7	L/N
M1.5	II	B	R	D	×	4.17	0	1-7	L/N
M1.6	U	B	R	F	✓	4.17	0	1-17	N
M1.7	U	B	R	D	✓	4.17	0	1-7	N
M1.8	U	B	P	F	✓	4.17	0	1-7	N
M1.9	U	B	P	D	✓	4.17	0	1-7	N
M1.10	U	B	1	F	✓	4.17	0	1-7	N
M1.11	U	B	1	D	✓	4.17	0	1-7	N
M1.12	U	B	R	F	✓	4.17	5.3	1-7	N
M1.13	U	B	R	F	✓	4.17	10	1-7	N
M1.14	U	B	R	F	✓	5.56	0	1-7	N
M1.15	U	B	R	F	✓	5.56	5.3	1-7	N
M1.16	U	B	R	F	✓	5.56	10	1-7	N

[1] Direction of fast line rope force from (Figure 19)
U – ropes are modeled
[2] Position of fast line end of rope on drum (Figure 20)
[3] A – Center of sheave (drum),
B – Tangent to sheave(drum),
[4] Change of force direction in ropes due to deformation
[5] L – Linear analysis, N – Nonlinear analysis
[6] R – Roller Bearing (1.04), P – Plain bearing (1.09)
Factor "S" in Equation.1

M1.1: Direction of fast line rope force vector is defined defined on the crown-block and chassis, from center of the drum to the center of fast sheave. Rope force from the dead line of the rope is defined with direction originating from the center of dead sheave on crown to the anchor on auxiliary chassis. Fast line force is defined in center of sheave and center of drum. Dimensions of the sheaves and the drum are neglected. Aproximations are made for the direction and the position of these rope force vectors.

M1.2: Direction of the fast line rope force vector is defined from tangent of fast line sheave to the tangent of the drum. Force is defined in the center of the drum and the center of fast line sheave. Aproximations of rope force vector position are made.

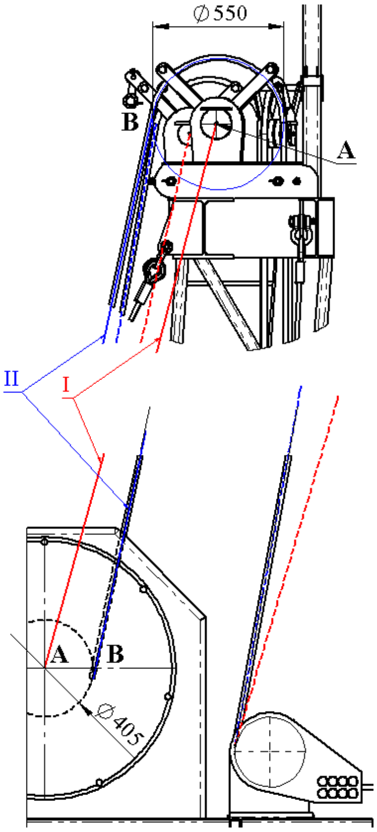

Figure 19 Review of different direction and position of vector forces from fast line end of rope, defined in computation models (Table 2).

M1.3: Direction of the fast line rope force vector is defined from tangent of fast line sheave to the tangent of the drum. Positions of force vectors on the fast line end and the dead line end are defined in the tangent of the corresponding sheaves. Position of the force on the second end of fast line rope is defined as tangent of the drum, and the other end of the dea line rope is defined in anchor point of the auxiliary chassis.

M1.4: Forces from ropes are defined without aproximation in directions and positions, in the same way as in the model M1.3. Forces are defined in the corresponding nodes on crown and chassis. Model includes changes of force intensities in ropes due to the friction on sheave when using roller bearing.

M1.5: Forces from ropes are defined without aproximation in directions and position, in the same way as in the model M1.3. Forces are defined in the corresponding nodes on crown and chassis. Model includes changes of intensities of forces in ropes due to the friction on sheave when using roller bearing, and also change of the fast line rope force vector direction due to movement of the fast line end of the rope on the drum.

M1.6: Ropes of hoist mehanism are modeled with "spar" elements in real position in relation to the drum, sheaves, dead line anchor and well. Differences in the intensity of rope forces due to the friction on sheaves when roller bearing is used are included.

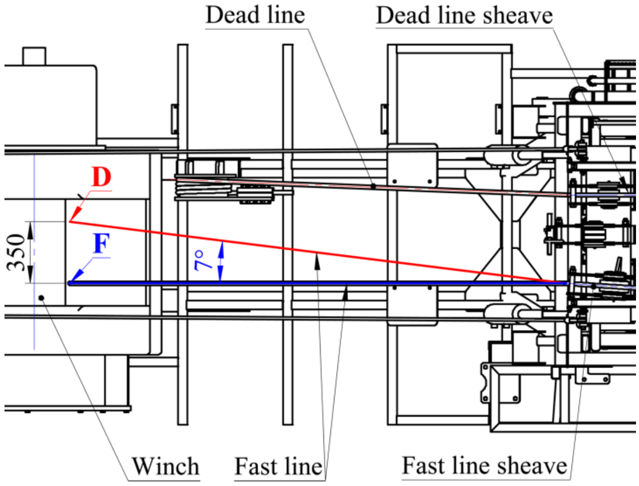

Figure 20 Simulated positions of fast line on the drum of the drawworks

3.1. Comparative results of analysed computation models calculated for Load case 1 (Table 1).

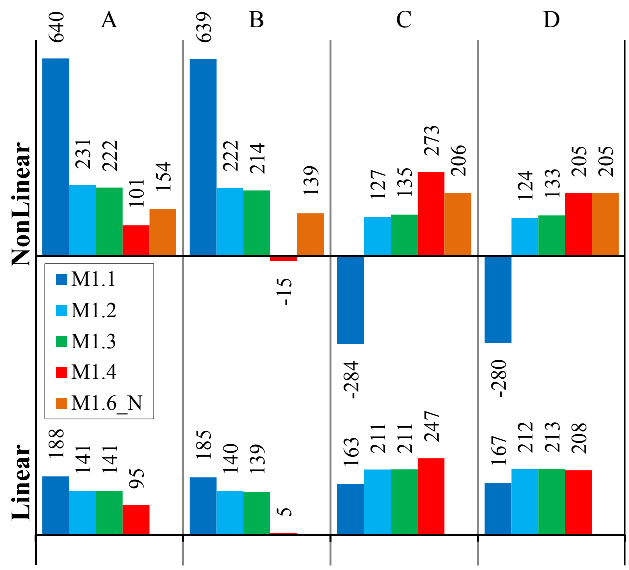

Figure 21 Diagram of mast reaction forces (kN) to the auxiliary chassis, in points A, B, C and D (Figure 14), calculated using four FE models M1.1, M1.2, M1.3, M1.4 linear and nonlinear and M1.6 only nonlinear.

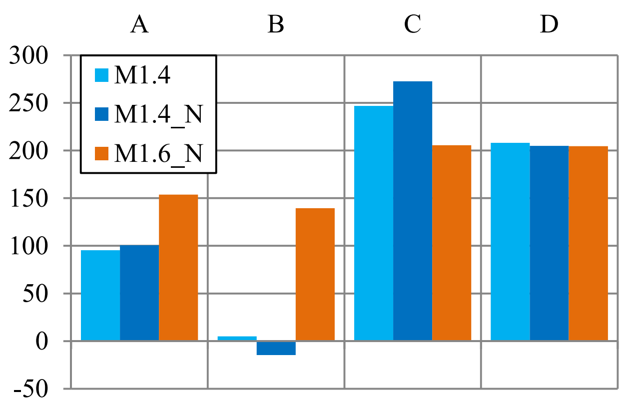

Figure 22 Diagram of mast reaction forces (kN) to the auxiliary chassis, in points A, B, C and D (Figure 14), due to different approach of modeling load forces on crown (Model M1.4 L/N and M1.6N)

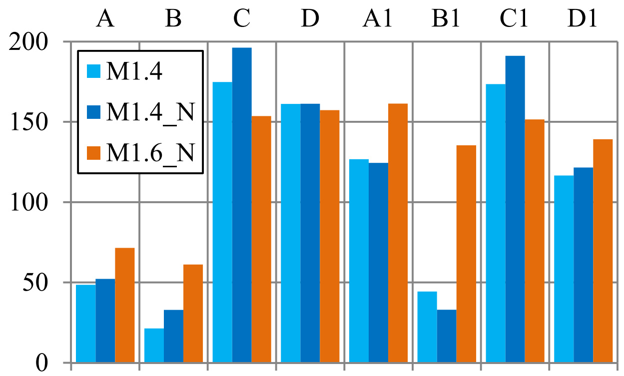

Figure 23 Diagram of Von Misses stresses (MPa), in considered points (Figure 14,14) on botom and top section of the mast, due to different approach of modeling load forces on crown using FE model M1.4 L/N and M1.6N.

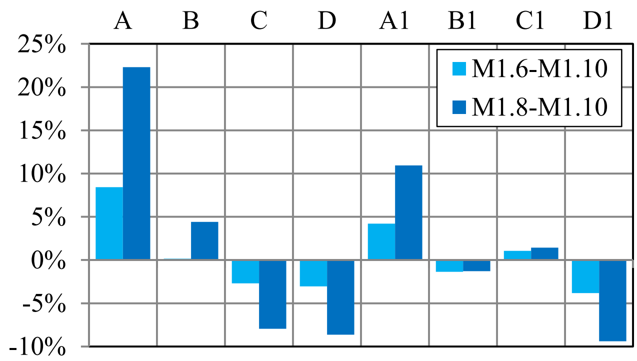

Figure 24 Diagram of procentual changes of stresses in considered points (Figure 14,14) of top and bottom section of the mast, due to quasistatic load with different friction resistance of sheaves, using FE models (M1.6 – Roller bearing, M1.8 – Plain bearing) and compared to static load with equal force in ropes (M1.10), calculated nonlinear with modeled ropes.

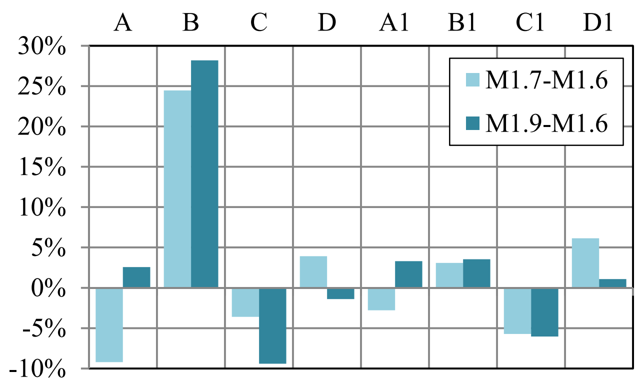

*Figure 25 Diagram of procentual changes of stresses in considered points (Figure 14,14)of top and bottom section of the mast, with quasistatic loading, due to change position of fast line to point »D« on drum (**Error! Reference source not found.**) and two different friction resistance of sheaves, using FE models (M1.7 – position »D« with roller bearing, M1.8 – Plain bearing) and compared with FE model M1.6 – position »F« with roller bearing, calculated nonlinear with modeled ropes.*

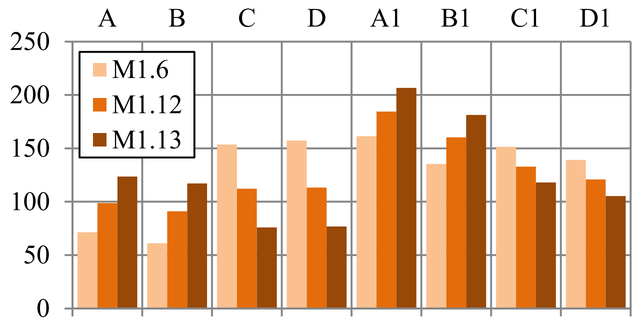

Figure 26 Diagram of Von Misses stresses (MPa), in considered points (Figure 14,14) on bottom and top section of the mast ,due to different pretension load in static ropes defined in FE models (Table 2), M1.6 – no pretension, M12 – pretension with 5.3kN and M.13 – pretension with 10kN, calculated nonlinar with mast angle 4.17º.

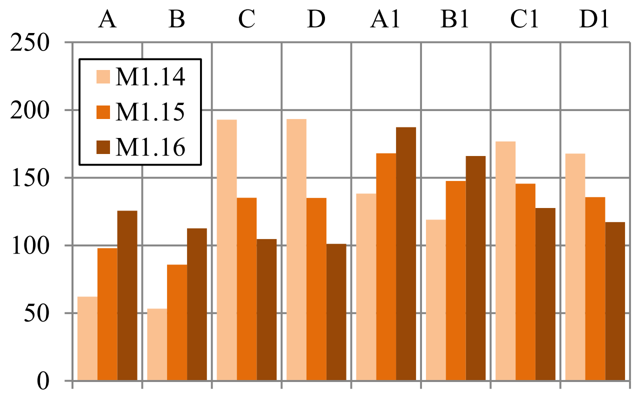

Figure 27 Diagram of Von Misses stresses (MPa), in considered points (Figure 14,14) on botom and top section of the mast, due to different pretension load in static ropes defined in FE models (Table 2)M1.14 – no pretension, M15 – pretension with 5.3kN and M.16 – pretension with 10kN, calculated nonlinar with mast angle 5.56º.

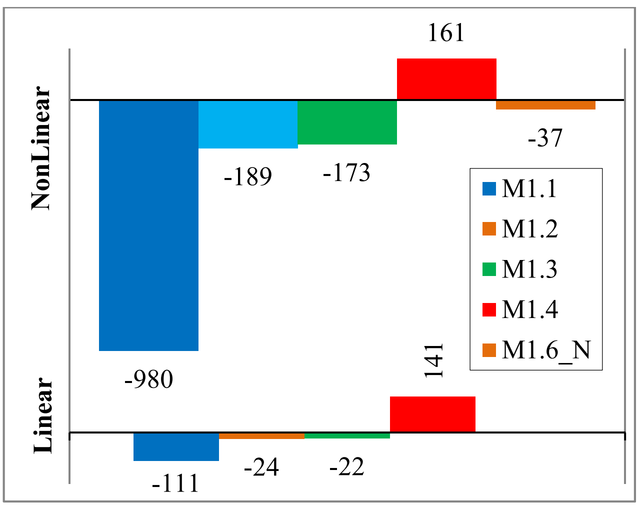

Figure 28 Diagram of displacements of mast crown (mm), calculated using FE models (Table 2), M1.1 L/N, M1.2 L/N, M1.3 L/N, L1.4 L/N and L1.6 N (L-Linear, N – Nonlinear).

4. CONCLUSION

Considering approximation of the directions and positions of the force vectors of the fast line rope defined in computational models M1.1, M1.2, M1.3 and M1.4, it can be concluded that there exist significant differences in the support reaction forces of the mast to the auxiliary chassis (Figure 20 and 21).

Considering the impact of changes in the direction of ropes' force vectors due to the moving of the crown of the mast (moving is caused by the resultant force acting on the top of the mast), from Figure 21 and Figure 22, which present significant differences in reaction forces and Von Misses stresses, respectively, it can be concluded that changes of the ropes' force vectors due to the displacements of the crown has to be considered in FE calculation model.

Considering quasi-static loading with different forces in ropes due to the friction on sheaves, in Figure 26 is shown 22% increase of stresses in vertical beam of the mast bottom section compared to the static loading, and it can be concluded that it would be necessary to include the quasi-static load case in computational FE model.

Considering change of the force direction due to the change of the fast line rope position on the drum of drive-works, in Figure 24 is shown 25% increase of Von Misses stresses in the vertical beam of the mast bottom section compared to the case corresponding to the fast line rope position on the opposite side of the drum, so it can be concluded that the change of the fast line rope position on the drum should be taken into account when designing appropriate computational model.

Analysing changes in calculation results due to the different angle of the mast, in Figure 25 and Figure 26 is shown that it is very important to consider pretensions in ropes because of their significant impact to the distribution of stresses and reaction forces on the front and back vertical beams (legs) of the mast at the bottom top section.

5. REFERENCES

[1] J. Dvornik and D. Lazarević, "Manjkavosti proračunskih modela inženjerskih konstrukcija," *Građevinar,* vol. 57, no. 4, pp. 227-236, 2005.

[2] American Petroleum Institute (API), API Spec. 4F Specification for Drilling and Well Servicing Structures, Washington: API, 2013.

[3] API (American Petroleum Institute), "API RP 9B, Use of Wire Rope for oilfield Services," API, Washington, 2000.

Road-Holding Ability of the Motor Grader in the Process of Performing Work Operations

Valery A. Shevchenko[1], Olexandra M. Chaplygina[2*], Zhanna P. Beztsennaya[3]
[1]Cand. Eng. Sc., Associate Professor, Department of Construction and Road Machines, Kharkiv National Automobile and Highway University, Kharkiv (Ukraine).
[2*]Post-graduate student, Department of Construction and Road Machines, Kharkiv National Automobile and Highway University, Kharkiv (Ukraine).
[3]Senior Lecturer, Department of Foreign Languages, Kharkiv National Automobile and Highway University, Kharkiv (Ukraine).

Most of the operations performed by the motor grader are carried out with asymmetric loading on the blade. Eccentrically applied load results in displacement of the machine from a rectilinear motion path. Deviation from the initially set path causes the necessity for the machine to perform several passes. Consequently, the productivity falls, traction qualities of earth-moving machines deteriorate, the time for processing the site increases, thus, increasing the economic costs.

The conducted field research allowed estimating the impact of such parameters as the excavated soil condition, the implement specifications, dynamic and kinematic parameters, characterizing the performed work operation, on indexes of the motor grader road-holding ability. The data obtained permit developing constructive measures to improve the motor grader road-holding ability under eccentric external loading.

Keywords: Motor grader, road-holding ability, lateral loading

1. INTRODUCTION

The main working operations of a motor-grader are blading and grading of the road bed, handling and distribution of soil and construction materials. When performing the mentioned operations, depending on working conditions, it is recommended to position the main blade of the grader at the working angle of 90º – 45º (at digging drain ditches of about 40º – 20º) and the angle of obliquity in the vertical plane of 0º – 18º (at slope leveling - up to 60º) [1].

Such positioning of the blade with respect to the main path of the machine motion results in formation of a complex spatial scheme of its loading. In particular, except for the longitudinal horizontal component of digging resistance there arise additional lateral and vertical forces. Influence of the latter results in the motor-grader deviation from the straight-line trajectory in the course of the working operation implementation.

In practice, to ensure the course stability the operator should continually adjust the machine position. Nevertheless, loss of the course stability results in decreasing the performance indexes of the working operations, the need to make additional trips. Ultimately, this leads to a drop in productivity, increase in cost of the work performed and the specific fuel consumption.

2. ANALYSIS OF PUBLICATIONS

A whole series of developments has been devoted to the problem of road holding ability of earth-moving machines. Their distinctive feature is analysis of the machine path of motion under the impact of lateral loadings such as centrifugal force, arising in the process of the machine movement at making a turn; gravitational component, arising at movement on the support surface with a transverse grade; the lateral component of the resistance resultant on the working attachment.

The problem of road holding ability was considered more thoroughly in respect of the machine movement at making a turn. In his research M. Podrigalo determines the road-holding ability coefficient (see Table 1.1), which is similar both for the front and rear axles. It depends mainly on dynamic forces acting on the machine at turning. [2].

In researches by Ya. Povzner there noticed that the road-holding ability coefficients for the front and rear axles are different (see Table 1.2). The wheel stability is directly proportional to its slip angle and the slip resistance coefficient [3].

Ya. Farobin, analyzing the problem of wheel slippage, developed an equation of balance of lateral forces and characterized the road-holding ability by the transverse stability coefficient of the vehicle (see Table 1.3), depending on its geometric parameters [4].

V. Knoroz, unlike the previous investigators, developed the coefficient of the wheel lateral slip resistance, which depends on the lateral slip angle and the lateral force acting along the wheel axle (see Table 1.4) [5].

In agricultural mechanical engineering mainly operation of the machine on a slope has been studied. Basically, all the indexes of the road-holding ability depend on the machine weight, the angle between the horizontal plane and the plane of the slope where the machine is located.

V. Bulgakov, M. Usenko, V. Prishl'ak developed in their work a machine equilibrium condition directly proportional to its mass and coefficient of the lateral adhesion of the propelling device with the ground (see Table 1.5) [6].

*Corresponding author: Kharkiv National Automobile and Highway University, olexandrachaplygina@gmail.com

T. Tsygankov marks out the limiting coefficient of traction depending on the longitudinal base of the machine (see Table 1.6) [7]. I. Dontsov considers movement of an agricultural machine equipped with front working attachment, paying special attention to oscillatory and dead-beat stability of the front implement itself (see Table 1.7) [8].

A number of scientific researches are devoted to theoretical analysis of the wheel motion under the impact of lateral force. In works by V. Gus’kov, I. Ksenevich there pointed out that the slip resistance coefficient is inversely proportional to relations of the abovementioned force and the slip angle (see Table 1.8) [9]. A. Petrov, at analyzing the process of the wheel rolling, proposes to take into account changes in the longitudinal velocity due to slipping. The wheel lateral displacement is neglected by the author (see Table 1.9) [10].

A number of authors (see Table 1.10) [11] believe that at describing a machine with a steering frame, parameters characterizing the road-holding ability are insignificant.

Researches conducted in the field of earth-moving equipment allow stating that coefficients characterizing the road-holding ability directly depend on ultimate loads acting on the blade cutting edge at loss of stability (see Table 1. 11 – 12) [12, 1].

For tracked vehicles this coefficient is characterized by the ratio of the moment of keeping the machine from turning to the moment of its turning. (see Table 1. 13) [13].

In the wheel theory Ye. Malinovskij describes the inverse proportion of the pneumatic tire slip angle and relation of the slip and velocity (see Table 1.14) [14].

Table 1: Parameters characterizing the road-holding ability.

Number	Author	Dynamic model	Road-holding ability parameter
1	M. Podrygalo	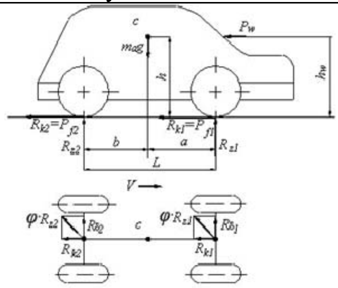	Slip coefficient: $$K_{yc\grave{o}} = \frac{b}{a} \cdot \frac{R_{\delta 1}}{R_{\delta 2}},$$ where a, b – coordinates of projection of the vehicle mass center to the horizontal plane; $R_{\delta 1}, R_{\delta 2}$ – cornering force of the road on the wheels of the front and rear axles;
2	Ya. Povzner	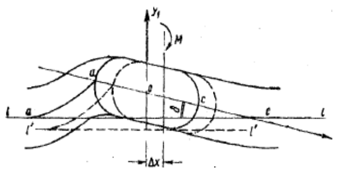 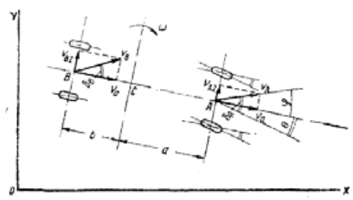	The wheel stability equation: $$Y = k \cdot \delta,$$ where k – slip resistance coefficient; δ – slip angle Slip coefficient of the vehicle wheels $$K_B = \left(\frac{dY_B}{d\delta_B}\right)_{\delta_B = \delta_{Bp}},$$ $$K_A = \left(\frac{dY_A}{d\delta_A}\right)_{\delta_A = \delta_{Ap}},$$ where δ_B, δ_A - angles between the attitudes of velocities V_B, V_A and the planes of the wheels; Y_B, Y_A - dependencies between the slip angle of the vehicle axles (front and rear) and the cornering force.
3	Ya. Farobin A. Litvinov	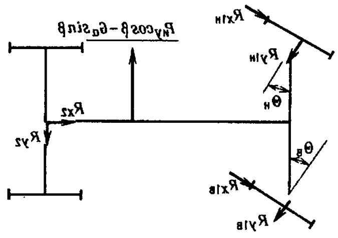	Conditions, under which there arise the wheels slipping is calculated by the equation of balance of lateral forces and the road reacting force: $P_{uy} \cdot \cos\beta - G_a \cdot \sin\beta = \sum R_y,$ where $\sum R_y = \sum R_{\acute{o}\hat{a}} + \sum R_{yi}$ - sum total of projection on the lateral axis of reacting forces, acting on the wheels. The coefficient of the vehicle transverse stability $$\eta_{\ddot{\imath}\acute{o}} = \frac{B}{2h_g},$$ where B – wheel spacing of the vehicle h_g – arm from the gravitational center position in the vertical plane.

4	V. Knorz	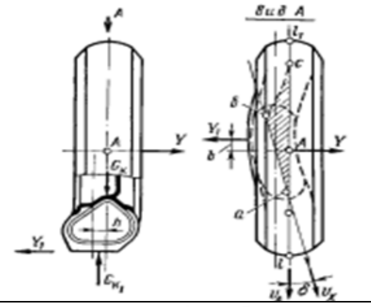	The slip resistance coefficient $$k_y = \frac{dY}{D\delta},$$ where δ – slip angle; Y – lateral force acting along the axle.
5	V. Bulgakov M. Usenko V. Ghishl'ak	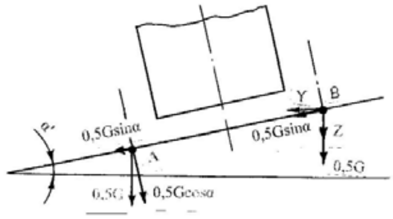	Condition of equilibrium: $$0,5\varphi G \cdot (1+\sin\alpha) \geq 0,5G\sin\alpha,$$ where G – mass of the two-wheel tractor, acting on the wheels; φ – coefficient of the lateral adhesion of the tire with the round; $0,5G\sin\alpha$ – lateral force causing the lower wheel move down the slope.
6	T. Tsygankov	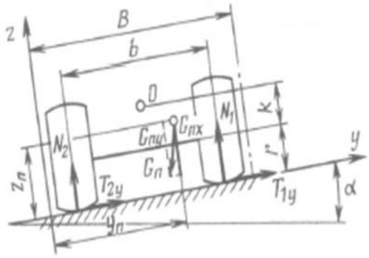	The limiting adhesion coefficient: $$K_{tn} = \frac{(L-0,5\psi_{\ddot{\imath}})}{t_1},$$ $$tg\alpha_{\ddot{\imath}} = \frac{\delta_1(2L-\psi_n)}{\delta_2+\psi_n},$$ where L - longitudinal base; $\psi_{\ddot{\imath}}, t_1, \delta_1, \delta_2$ - additional function.
7	I. Dontsov	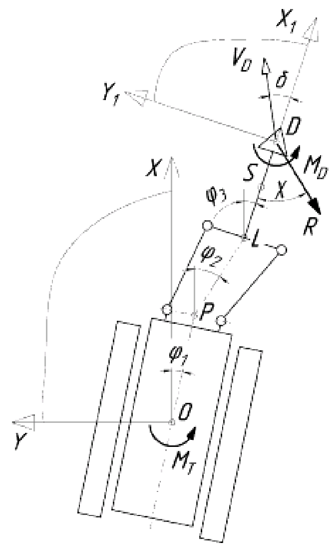	Conditions of the front implement stability: $$a_2 = \alpha_0 Rl\frac{[1+(1-u)\rho]^2}{V_0} > 0$$ $-$oscillatory stability; $$a_3 = -Rl[(1-u)^2\alpha_0\rho + (1-u)(\alpha_0-1)+1] > 0$$ $-$dead $-$ beat stability; where α_0 - force parameter, characterizing vectoring X of the resultant R and changing in the resultant moment M_D of the implement resistance proportionally to the changing of the angle δ R - resultant vector and resultant moment of the resistance forces with the reduction centre in point D; l - distance from point P to the line of hitching the links to the implement, where the point is positioned; u - hitch attachment ratio; ρ - dimensionless ratio between the given length of the implement and the length of the link; V_0 - initial motion speed.

8	V. Petrov	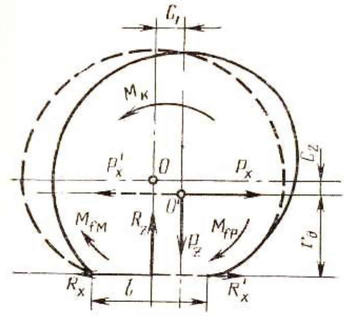	The wheel skidding velocity: $v_{á} = (r_{êí} - r_{ê}) \cdot \omega,$ where $r_{êí}$ – radius of the wheel circle perimeter; $r_{ê}$ – radius of the wheel rolling; ω – wheel angular velocity. The skidding coefficient: $s_{á} = \frac{(r_{êí} - r_{ê})}{r_{êí}}.$
9	V. Gus'kov I. Ksenevich	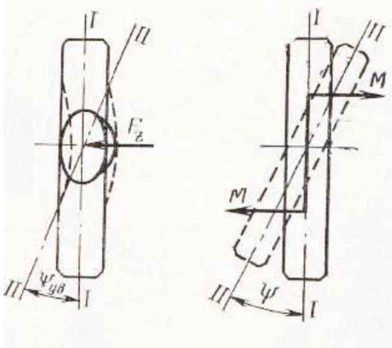	The slip resistance coefficient in the case of application of the lateral force F_z to the wheel axle: $K_{óâ} = \frac{F_z}{\varphi_{óâ}},$ where $\varphi_{óâ}$ – slip angle. The tire angular deformation is characterized by the cornering stiffness coefficient: $K_{\varphi} = \frac{M}{\varphi},$ where M – moment arising in the tire loaded by the normal force; φ – angle characterizing the cornering stiffness.
10	Yu. Br'anskij M. Griff A. Naumov A. Skokan	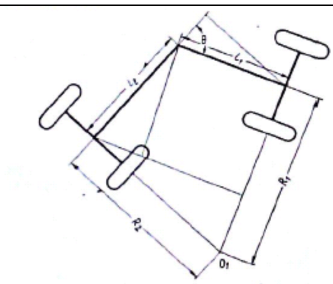	When describing the machine behavior at turning, longitudinal and sideways sliding are not taken into account as well as slipping, which is considered insignificant.
11	T. Aleksejeva K. Artemjev A. Bromberg.	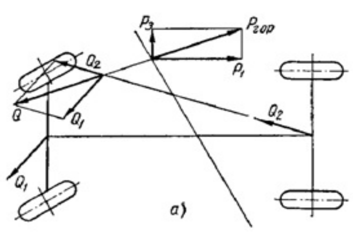	$k_x = \frac{P_1}{P_{1\max}},$ where P_1 – limiting component of the ground reaction on the blade, which does not result in loss of course stability at the specified weighing (the given value of G_2) $P_{1\max}$ – limiting component of the ground reaction on the blade, which does not result in the loss of course stability at the most favorable weighing (the most favorable value of G_2)
12	K. Sevrov	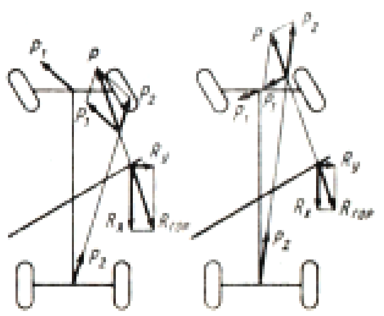	The coefficient of the course stability degree: $K_x = \frac{R_x}{R_{x\max}},$ where R_x – the greatest longitudinal component of the ground reaction on the blade; $R_{x\max}$ – the greatest longitudinal component of the ground reaction on the blade at the most favorable weighing on the axles.

13	A. Koval'	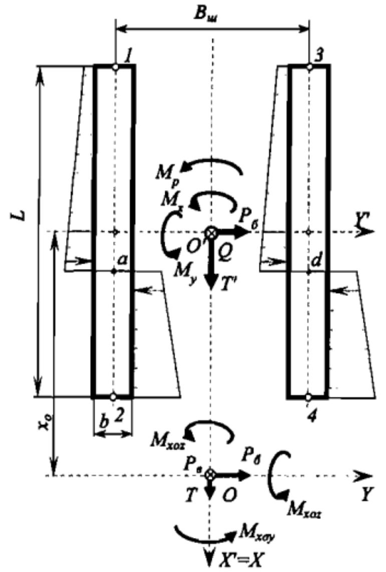	The road-holding ability of earth-moving machines is estimated according to the value of the course stability coefficient: $$k_{\grave{e}c} = \frac{\grave{I}_{\grave{i}\eth}}{\grave{I}_{\eth}} > 1,$$ where $\grave{I}_{\grave{i}\eth}$ - moment of keeping the machine from turning; $\grave{I}_{\eth}$ - turning moment
14	Ye. Malinovskij	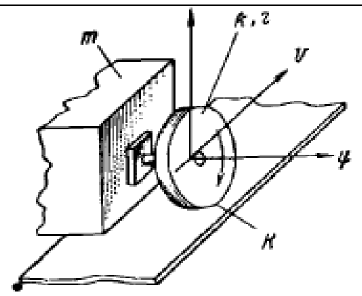	The coefficient of the pneumatic tire slip k is assumed to be known. Thus, the slip angle is: $$\delta = \frac{\dot{y}}{v},$$ where $\dot{y}$ – lateral displacement; v – velocity.

Summing up the result, it is possible to determine three main areas of mechanical engineering, where much attention is paid to research of the machine road-holding ability: transport equipment, agricultural and earth-moving machinery, which in their turn have own specifics in approaches to estimation of the road-holding ability parameters (see Fig.1).

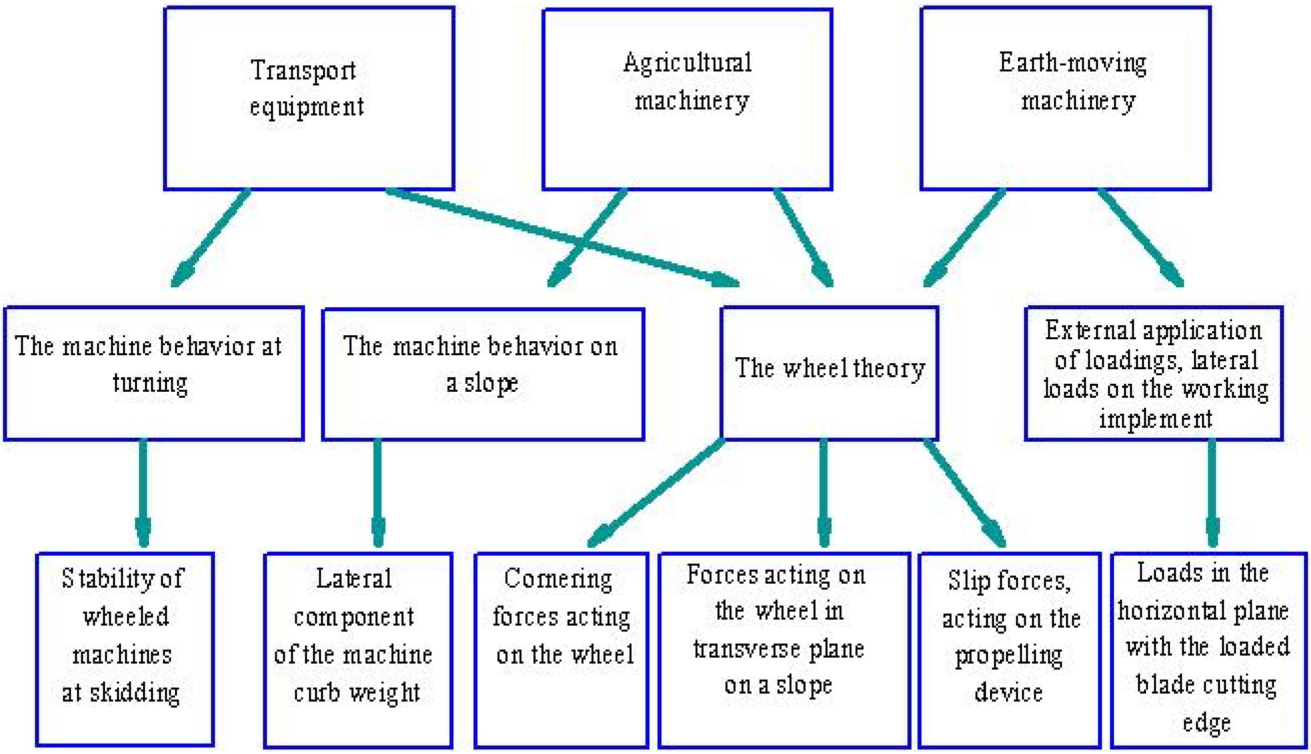

Figure 1: Area of analizing the road-holding ability parameters

3. PURPOSE AND TASKS OF THE RESEARCH

The research purpose is experimental estimation of impact of the moto-grader working process parameters on the road-holding ability parameters.

4. RESEARCH OF THE MOTOR-GRADER ROAD-HOLDNG ABILITY PARAMETERS

To achieve the set purpose in conditions of the Testing ground of Kharkive National Automobile and Highway University there were prepared and conducted field researches with the motor-grader ДЗк – 251. At carrying out the tests the process of cutting soil of category II with the main blade end in the form of cross-section cut layer. The relative degree of the soil humidity was about 19 – 25%. The initial speed of the motor-grader and the blade angular displacement in the plane were chosen as variable paramenters (Table 2).

Table 2: Levels of the factors variation.

Variable values	Symbol	Unit of measurement	Levels of the factor variation
The angle of the blade positioning in the plane	α	gr.	45º
			90º
			135º
The maching velocity	V	m/sec	1.01
			1.4
			1.57

The parameters of the factors were set on the basis of the values recommended for main working modes of the motor-grader. In the course of the experiments it was noticed that loss of the motor-grader road-holding ability results from the front axle slipping (Fig. 2).

Figure 2: *The machine movement in the course of the experiment*

At this the machine path of motion consists of straightways and thesection where the motor-grader turning takes place (Fig. 3).

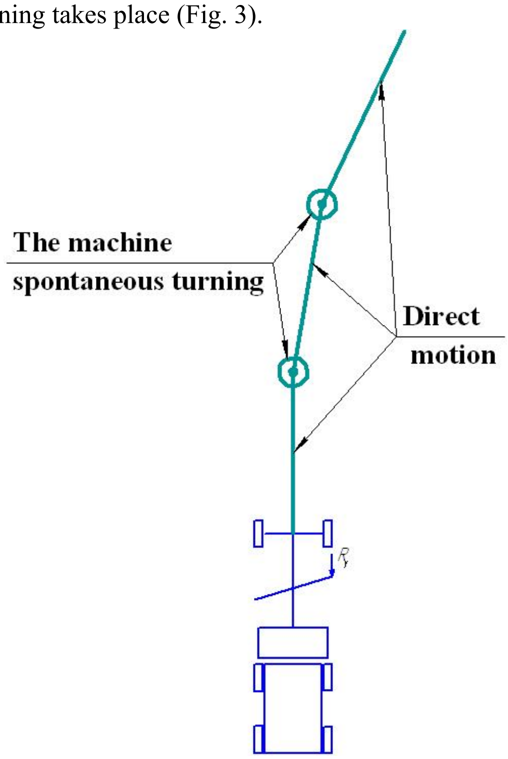

Figure 3: *The scheme of the machine motion*

Measuring the lateral displacement and turning angle with respect to the machine's longitudinal axis were made according to the scheme (Fig. 4.)

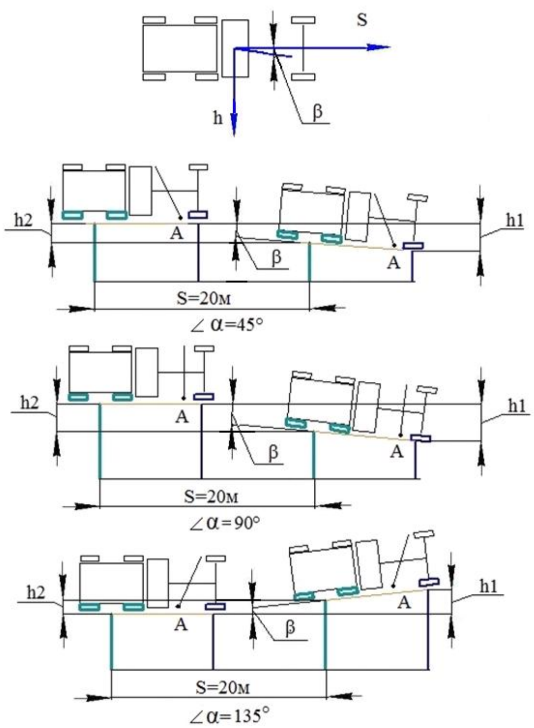

Figure 4: *The scheme of measuring the parameters characterizing the motor-grader road-holding ability*

Point A designates the blade edge, by which the soil cutting is performed. The data of measurements corresponding to the coordinat system are presented in Table 3.

Table 3: Parameters characterizing the motor-grader road-holding ability

Experimantal data		Displacement, m		β – angle of the machine turning
α, gr.	V, m/sec	h_1– front wheels	h_1– rear wheels	
45	1.01	3.471	2.575	47°44'
	1.4	0.339	0.764	22°26'
	1.57	0.160	0.228	3°57'
90	1.01	0.339	0.299	2°17'
	1.4	1.454	1.352	6°4'
	1.57	2.411	2.306	6°5'
135	1.01	1.427	1.329	5°50'
	1.4	0.937	0.674	17°6'
	1.57	0.287	1.567	65°31'

The experimental data analysis shows that on the face length of 20 m limiting lateral displacements of the front axle make 3.5 m and of the rear axle – 2.6 m. The angle of turning of the machine's longitudinal axis correspondingly equals 20º – 65º. Cutting with the leading blade end results in the machine displacement and turning to the side of the applied load. In the case when cutting is performed with the back blade end, results in the machine displacement and turning to the opposite direction.

Processing of the obtained data with the help of MATLAB software allowed recieving a number of regressional relationships presented in Table 4

Graphic interpretation of the obtained results is presented in Figures 5 – 7 in the form of the machine path of motion at changable factors.

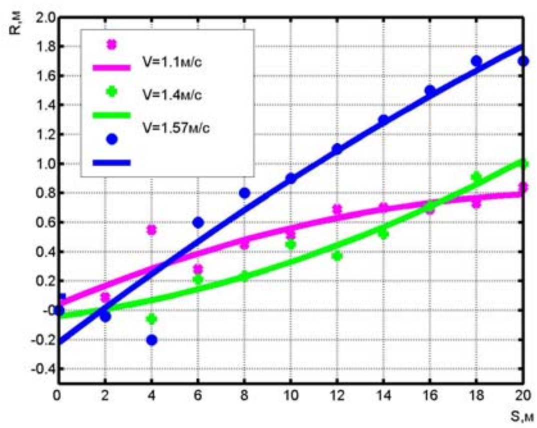

Figure 5: The curve of regression equation at the working angle of α=45°

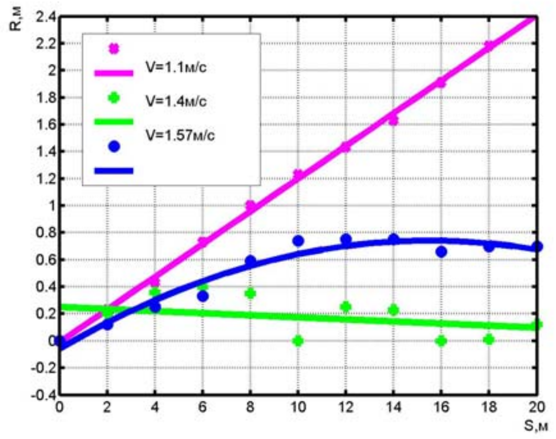

Figure 6: The curve of regression equation at the working angle of α=90°

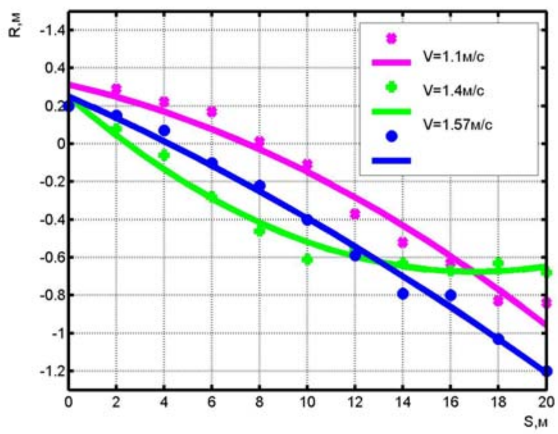

Figure 7: The curve of regression equation at the working angle of α=135°

Table 4: Parameters characterizing the motor-grader path of motion

Angle of the blade adjustment	Velocity, m/sec	Displacement value, m										
		0	2	4	6	8	10	12	14	16	18	20
90°	1.01	0	0.09	0,55	0.28	0.45	0.51	0.69	0.7	0.69	0.73	0.84
	1.4	0	0	-0,06	0.21	0.23	0.45	0.37	0.52	0.71	0.91	1
	1.57	0	-0.4	-0,2	0.6	0.8	0.9	1.1	1.3	15	1.7	1.7
45°	1.01	0	0.23	0,43	0.73	1	1.23	1.43	1.63	1.91	2.18	2.43
	1.4	0	0.2	0,36	0.4	0.35	0.2	0.25	0.23	0	0.01	0.12
	1.57	0	0.12	0,25	0.33	0.59	0.74	0.75	0.75	0.66	0.7	0.7
135°	1.01	0	0.09	0,02	-0.03	-0.19	-0.31	-0.57	-0.72	-0.83	-1.03	-1.04
	1.4	0	-0.12	-0,26	-0.48	-0.66	-0.81	-0.76	-0.83	-0.87	-0.83	-0.88
	1.57	0	-0.05	-0,13	-0.3	-0.42	-0.6	-0.79	-0.99	-1	-1.23	-1.4

Table 4 (continuation) Parameters characterizing the motor-grader path of motion

Angle of the blade adjustment	Velocity, m/sec	Regression equation
90°	1.01	$R = -0.0014 + 0.0664S + 0.0406S^2$
	1.4	$R = 0.0016 + 0.0210S - 0.0410S^2$
	1.57	$R = -0.0010 + 0.1206S - 0.2193S^2$
45°	1.01	$R = 0.1210 - 0.0100S$
	1.4	$R = -0.0076 + 0.2509S$
	1.57	$R = -0.0033 + 0.1032S - 0.0576S^2$
135°	1.01	$R = -0.0017 - 0.0287S + 0.1121S^2$
	1.4	$R = 0.0032 - 0.1088S + 0.0495S^2$
	1.57	$R = -0.0009 - 0.0561S + 0.0517S^2$

The analysis of the results showed that the second-degree regression equation gives the most accurate description of the machine motion. Thus, at increasing the speed from 1.01 to 1.57 m/sec the lateral displacement had a random character, in some cases there was observed its growth proportionally to the speed, in other cases at low rates of speed the value of displacement rose. There were not observed any strict regularities of changes in the motor-grader road holding ability in relation to changes in the machine speed. High values of the experimental data can be explaned by high humidity of the surface layer of soil , low coefficient of adhesion of the propelling device with the ground, high slip coefficient.

5. CONCLUSIONS

On the basis of the review we can argue that main reasons for the machine loss of its course stability and deviation from the specified path of motion are lateral forces arising at performing working operations: centrifugal forces and gravitational components applied to the machine mass center, as well as influence of an eccentrically applied resistance resultant on the working implement.

On the basis of the field research we can conclude that for the most accurate description of road-holding ability parameters of earth-moving machinery, namely a motor-grader, it is expedient to use two parameters: lateral displacement and angle of the machine turning with respect to the longitudinal axis.

The motor-grader speed has insignificant influence on formation of its course stability. During the experiment there were not observed any strict regularities of chngings in the road-holding ability parameters in relation to changing in the machine speed.

The most considerable influence on the motor-grader parameters of road-holding ability has the angle of the blade positioning in the plane. Cutting with the laeding or back ends of the blade results in changing the direction of lateral displacement, which are within the limits: at cutting with the leading end 0.12 – 2.43 m; at cuting with the back end 0.8 – 1.4 m; at the working angle 90^o the eccentric application of the rolling resistance causes the lateral displacement of 0.8 – 1.7 m at the face length of 20 m.

REFERENCES

[1] Севров К.П. Автогрейдеры. Конструкции, теория, расчет / К.П. Севров, Б.В. Горячко, А.А. Покровский. – М. – Машиностроение, 1970. – С. 95–121

[2] Устойчивость колесных машин при заносе и способы ее повышения / [Подригало М.А., Волков В.П., Доброгорский М.В., Степанов В.Ю.]. . – Харьков: Изд-во ХНАДУ, 2006. – 335 с.

[3] Теория устойчивости автомобиля / Певзнер Я.М. — М.: Машгиз, 1947, 156 с.

[4] Литвинов А.С. Автомобиль: Теория эксплуатационных свойств [учебник для вузов]/Литвинов А. С, Фаробин Я.Е — М.: Машиностроение, 1989. – 240 с.

[5] Работа автомобильной шины / Под ред. В. И. Кнороза . — М. : Транспорт, 1976. — С. 137–150.

[6] Теоретичне дослідження роботи пристрою для стабілізації руху мотоблоку на схилі / Булгаков В.М., Усенко М.В., Пришляк В.М // Збірник наукових праць Віницького національного аграрного університету. – 2012. – № 10 т. 2 (59) – С.50 – 53.

[7] Цыганков Т.В. Поперечная устойчивость самоходной машины с балансирной подвеской / Т.В.Цыганков // Тракторы и сельхозмашины. – 1991. – № 1 – С. 22 – 23.

[8] Донцов И.Е Повышение курсовой устойчивости машинно-тракторного агрегата с фронтальным орудием (ФМТА) / И.Е Донцов // Вестник КрасГАУ. – 2008. – № 2 – С. 209 – 215.

[9] Гуськов В.В. Вопросы качения, тягового и мощностного баланса колеса / В.В.Гуськов, И.П.Ксеневич // Тракторы и сельхозмашины. – 1986. – № 8 – С. 22 – 25.

[10] Петров А.В Узловые вопросы теории качения пневматического колеса / В.А.Петров // Тракторы и сельхозмашины. – 1986. – № 8 – С. 18 – 22.

[11] Брянский Ю.А. Кинематика поворота машин с шарнирно сочлененной рамой / Ю.А.Брянский, М.И.Грифф, А.В.Наумов, А.И.Скокан // Строительные и дорожные машины. – 1970. – № 2 – С. 15 – 17.

[12] Дорожные машины. Машины для земляных работ / [Алексеева Т.В., Артемьев К.А., Бромберг А.А. и др.]; [Изд. 3-е, перераб. и доп.]. — М.: Машиностроение, 1972. — 504с.

[13] Коваль А.Б. Визначення умов забезпечення курсової стійкості універсальних землерийних машин : автореф. дис. на здобуття наук. ступеня канд. техн. наук : спец. 05.05.04 «Машини для земляних, дорожніх і лісотехнічних робіт» / А.Б. Коваль. – Дніпропетровськ, 2014. – 21 с.

[14] Малиновский Е.Ю Синтез уравнений движения и анализ динамических механизмов строительных и дорожных машин / Е.Ю.Малиновский // ВНИИСТРОЙДОРМАШ. – 1977. – № 75 – С. 3 – 14/

5D Modelling of Mechanical Systems

Kudryavtcev E.M.
The Moscow State Building University (Russia)

It is offered the new approach to complex research of mechanical systems with use of a certain set of modern computer systems - 5D modelling. This approach provides high level of complex research of mechanical systems, including and presentation of received results. It is especially important at the earliest design stages of mechanical systems.

Keywords: Mechanical system, modeling, dynamic analysis, final-element analysis

1. INTRODUCTION

It is known, that wrong technical decisions at early design stages of mechanical systems can entail serious expenses at all subsequent stages of life cycle of a product.

Estimation of cost of correction of one error at various stages preparation of manufacturing (Gartner Group):

- 1 $ - preliminary design phase;
- 10 $ - design stage;
- 100 $ - manufacturing of a breadboard model of a product;
- 1000 $ - industrial equipment designing;
- 10000 $ - equipment manufacturing;
- 100000 $ - prototype serial production;
- 1000000 $ - serial production.

2. MODELLING STAGES

5D modelling of mechanical systems includes three stages:

1) creation of three-dimensional model (3D) of mechanical system, for example, in system KOMPAS-3D, Solid Works, etc. [1 - 8];

2) modelling of functioning of mechanical system in time (the dynamic analysis +1D), for example, in system UMExpress (the Universal mechanism), UM 7.0, etc.;

3) research of the intense deformed condition of mechanical system taking into account loadings defined at the previous stage (the is final-element analysis +1D), for example, in system APM FEM or APM Structure 3D [9], etc.

Process of complex modelling has iterative character, with possibility of transition to any of above listed stages of modelling. For example, presence of other-wordly pressure in separate elements of mechanical system, can demand serious changes in three-dimensional model of system - the first stage of modelling or to change a system operating mode - the second stage of modelling. It, finally, after several iterations it will allow to create the highly effective mechanical system,.

For example, in the course of the dynamic analysis of three-dimensional model of mechanical system there can be inadmissible levels of the resonance oscillations. It can demand serious changes in a system operating mode - the second stage of modelling or to return to the first stage and to spend corresponding modernisation of three-dimensional model etc. The process of operational development of model of a product can occupy some iterations.

3. CREATION 3D MODEL

Creation of a three-dimensional model of mechanical systems can be carried out with the use of various CAD systems: AutoCAD, Solid Work, Solid Edge, Inventor, T-Flex, APM Win Machine, KOMPAS-3D, etc.

5D modelling of mechanical systems is the execution by the system the KOMPAS-3D, last versions of firm ASCON. It is connected, first of all, by this system to provide complete support of systems of ESKD, SPDS and ISO. Besides, it has a satisfactory quantity of libraries of fragments, models and applied libraries, which by 10 times facilitate performance of designer and researcher [5 - 8].

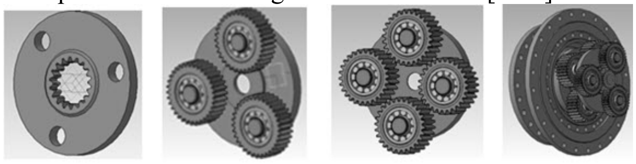

Figure 1: Samples parts and assemblage

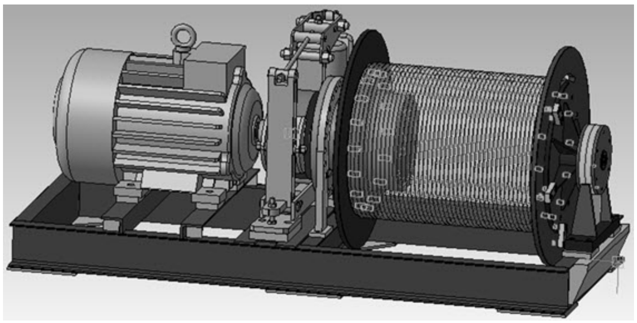

Figure 2: Sample mechanical system

4. CREATION AND RESEARCH DYNAMIC MODEL

For carrying out static, kinematics and dynamic calculations of mechanical systems we used systems Universal mechanism (UMExpress), which is built directly in system the KOMPAS - 3D, or UM-7. These systems can to have completely parametrized objects.

UMExpress changes a configuration of mechanical system and such parameters, as the sizes of links, factors in expression of forces, etc. This system actually changes of parameters of mechanical systems without a repeated conclusion of the equations of movement. The equations are deduced in the full symbolical form, and corresponding parameters are included into them in the form of identifiers.

*Corresponding author: The Moscow State Building University, sdm@mgsu.ru

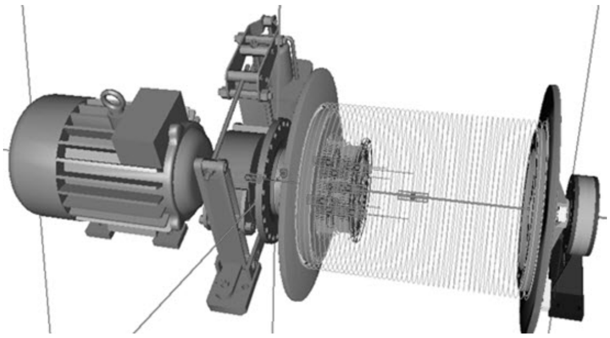

Figure 3: Sample mechanical system in UMExpress

To reduce time of performance of the static, kinematics and dynamic analysis the designer are used by so as;
- to transform an assemblage tree to a set of bodies by association of details that allows to reduce number of incorporated bodies in 10 times;
- to spend completion of the kinematics scheme by visual addition or removal of necessary hinges;
- to create graphic images of springs, etc. power elements if there is such necessity;
- to set power interactions between bodies, etc. actions.

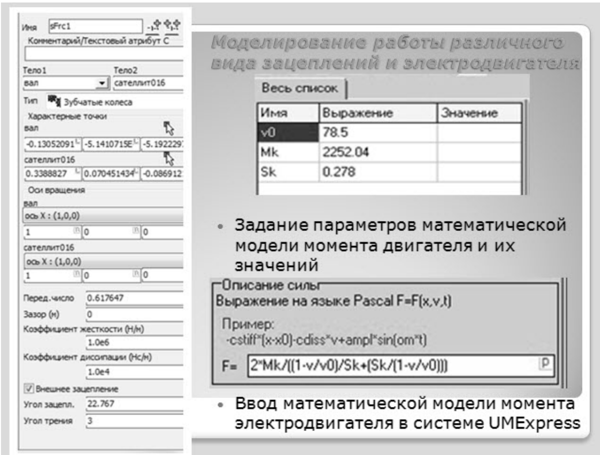

Figure 4: Sample installations of the parameter points

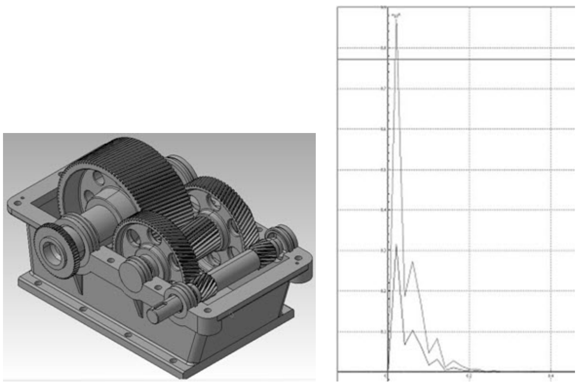

Figure 5: Some research results (interacting forces in the toothings)

The use of program complex UMExpress (the Universal mechanism) allows:
- <u>*to simplify process of creation of dynamic models*</u> and their numerical analysis, having made accessible modelling of dynamics of systems of bodies to a wide range of engineers-researchers and designers;
- <u>*as much as possible to lower cost of design workings out*</u> that will allow to transform it into mass software product (tool) of the expert;
- *to prepare the mass user* for use of more difficult and functionally full similar programs, including programs UM (see <u>www.umlab.ru</u>);
- <u>*automatically to create avi file*</u>.

5. CREATION AND RESEARCH DYNAMIC MODEL

Research of the is intense-deformed condition of the most loaded knots of mechanical systems by a finite-element method (FEM) by us it was carried out in system APM FEM, which has been built in system the KOMPAS 3D. However, it can be executed and by means of other systems, for example, Mechanical Desktop Power Pack [8], APM Structure 3D [9], etc.

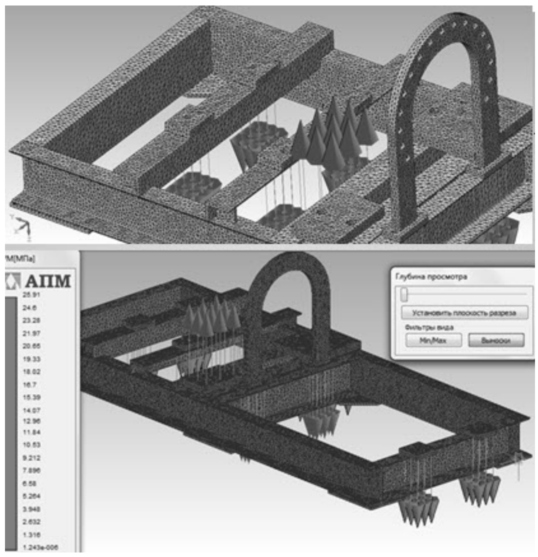

Figure 6: Some research results

Each of FEM systems allows to put loadings of various types to three-dimensional model, to specify boundary conditions, to create an is final-element grid and to execute calculation. Thus procedure of generation of final elements, drawing up of systems of the equations and their decision is spent automatically. As a rule, such systems allows to spend following kinds of calculations:
- static calculation;
- calculation on stability;
- calculation of own frequencies and forms of fluctuations;
- thermal and other kinds of calculations.

The use of program complex APM FEM allows:
- <u>*to simplify process of creation of is final-element models*</u> <u>*and their numerical analysis*</u>, having made accessible carrying out of research of the is intense-deformed condition of various knots СиПТМ to students and a wide range of engineers-researchers and designers;
- <u>*as much as possible to lower cost of design workings out*</u> that will allow to transform APM FEM into mass software product (tool) of the expert;
- <u>*to prepare the mass user*</u> for use of more difficult and functionally full similar programs, including АПМ Structure 3D (see APM WinMachine).

6. CONCLUSION

5D modeling of mechanical systems provides high level of complex research, including and presentation of received results. It is especially important at the earliest design stages of mechanical systems. As is shown above, the wrong technical decision at early design stages of mechanical system can entail serious expenses at all subsequent stages of life cycle of a product.

[1]. Kudryavtcev E.M. Computer-aided design systems of cars and the equipments. The Textbook for high school. M: Publishing house ASV, 382 p. (2013)

[2]. Kudryavtcev E. M. Execution of final qualifying work on the computer: the manual for high school. M: Publishing House "Bastet", 240 p. (2013)

[3]. Kudryavtcev E.M. Fundamentals of the computer-aided design: The Textbook for high school. M: Publishing centre "Academy", 304 p. (2011)

[4]. Kudryavtcev E.M. KOMPAS-3D V10. 2 v. M: DMK Press. 1184 p. (2008)

[5]. Kudryavtcev E.M. Modelling, designing and calculation of mechanical systems. M: DMK Press, 400 p. (2008)

[6]. Kudryavtcev E.M. Practical work on KOMPAS-3D V8: Machine-building libraries. M.: DMK Press, 440 p. (2007)

[7]. Kudryavtcev E.M. Machine-building designing Mechanical Desktop. M.: DMK Press, 432 p. (2006)

[8]. Zamrii A.A. Designing and calculation by a method of final elements of three-dimensional designs in the environment of APM Structure 3D. M: Publishing house APM, 208 p. (2004)

New Effective Machine for Rolling Holes During Installing Underground Communications in Urban Construction

A.I.Dotsenko[1],*
[1]National Research Moscow State University of civil engineering

Designed and tested a new machine for installing underground communications in urban construction . Its benefits : environmental security , the absence of harmful effects of dynamic , high performance, cost-effectiveness..

Keywords: installing underground communications, methods, raskatchik, optimal parameters

1. INTRODUCTION

Installing underground communications of different function (gas and water supply system, sewerage, heating systems, electricity and communications cables, etc) in the conditions of city construction often produce under the exiting roads and railways, tramways, city street and the squares, buildings and structures for what the special closed installation methods are used.

The most common methods of closing laying underground communication are now horizontal mechanical drilling , piercing and punching . In the Moscow State Construction University (MSCU) at the chair Department of Technology, mechanization and operation of urban roads for this purpose developed a new more effective machine for rolling holes.

2 . SUMMARY OF MAIN METHODS INSTALLING UNDERGROUND COMMUNICATIONS

Method of horizontal drilling lay under automobile and the railroads pipelines and protective cases for placement of working pipelines in them, cables and other communications. Machines, working by this principle, provide laying in soil I-IV of category of pipes casings under pipelines with a diameter of 325 … 1420 mm with the maximum length of laying 40 … 60m. Speed of a driving choose according to specific conditions of work, namely: 2 … 5,5m/hour at an object construction in soil of average density and 1,8 … 3,5m/hour – in heavy soil.

When laying pipes by *a piercing method* formation of holes carry out due to radial replacement and soil consolidation (without its development) a laid pipe or working body. Distinguish a piercing mechanical and a vibropiercing at what the last is used more often.

Vibropiercing apply when laying pipelines in sandy and sandy water-saturated soil in which it is impossible to receive a steady hole and therefore the mechanical piercing is strongly complicated or almost impossible because of big resistance of movements of the pipe clamped by soil. Vibropiercing lay pipes with a diameter up to 426 mm at the length up to 25 … 50m. Speed of a driving depends on soil conditions and diameter of a laid pipe and corresponds on the average 20 … 60m/h.

Method of punching carry out laying in soil I-III of categories of steel pipelines with a diameter of 529 … 1720 mm, and as combined ferroconcrete collectors of casting appointment to length of 60 … 80m. At punching the pipeline (case) press into the soil massif the open end supplied with a ring knife, and the soil arriving in a head link, develop and delete via the laid pipeline in the mechanized way. As the punching devices used hydraulic jacks.

Driving speed for a method of punching depends on physicomechanical properties of soil, diameter and extent of the pipeline, power of jacks and as from a way of development and removal of soil and averages 0,5 … 1,5m/hour.

Selecting the optimal closed installation methods defined geometrical dimensions , purpose and depth of laying communications, location , extent and soil conditions it runs, character recut structures and existing communications .

3 . CLOSED INSTALLING UNDERGROUND COMMUNICATIONS BY MACHINE FOR ROLLING HOLES.

In MSCU at the chair of Technology, mechanization and operation of urban roads a new, more effective machine for rolling holes, is developed for closed installation underground communications[2,3]. This machine is called raskatchik soil and can be used for forming the horizontal , vertical and deviated holes.

Rolling holes represents continuous process of creation of a cylindrical cavity by deformation and concentrating of soil by the unrolling mechanism. This mechanism (the unrolling device) consists of the several conic skating rinks freely rotating on an axis. The axis of skating rinks is located under a corner and displaced concerning a device axis, so - that, at device rotation, skating rinks rotate on a spiral. At rotation and axial moving of the unrolling device, skating rinks form a hole. Each skating rink enters into the site of a hole unrolled by the previous skating rink, and thus increases diameter of a hole. The earth is condensed in a radial vector and round a hole the dense zone in diameter equal to 3-4 diameters of a hole is formed. Formation of a hole by skating rinks of the unrolling device is identical to compression by group of

*Corresponding author: National Research Moscow State of Civil Engineering, Moscow, 129337, Yaroslavl highway,26

skating rinks of a surface of the earth so, that each subsequent skating rink is heavier, than previous.

Unlike traditional methods of creation of holes in the earth where the destroyed breed is taken out on a surface, the unrolling device creating a hole in the earth, condenses breed in hole walls. It allows receiving a steady cylindrical hole in which communications of different function can be laid.

There are 3 principal parts of machine for rolling holes (Fig.l):

1. power unit (oil tank);
2. drilling unit with remote control;
3. working body (raskatchik soil).

Advantages machine for rolling holes:

a. lack of vibration and noiselessness of a driving of holes;
b. the possibility of the formation of large diameter holes (up to 1 m) and a length of up to 50m ;
c. the high speed of a driving(10 ... 20m/hour) .

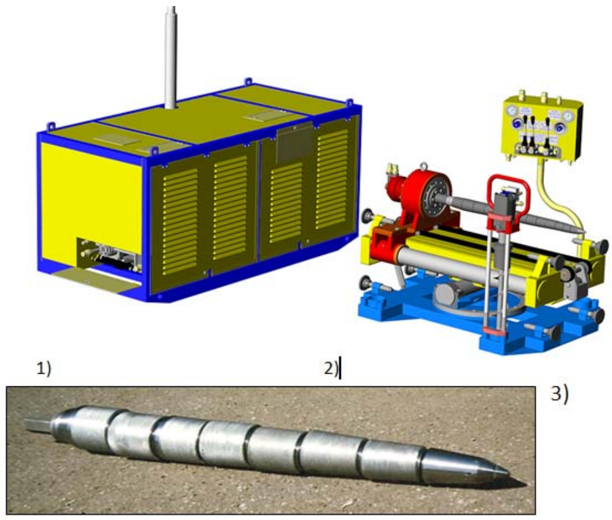

Fig.1 Machine for rolling holes.

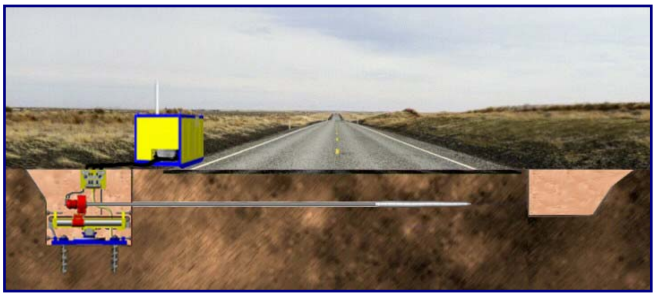

Fig.2 Creation of holes by the rolling device.

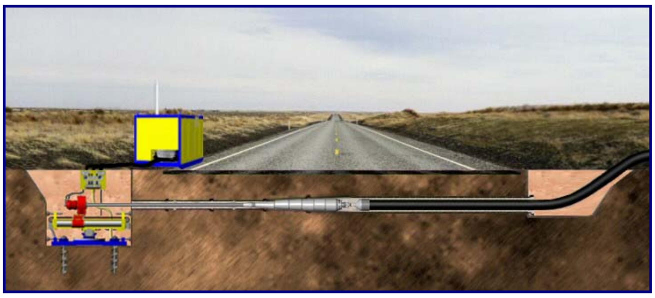

Fig.3 Renewal of pipelines with use of the rolling device.

The machine can operate in crowded urban conditions to form holes without removing the soil.
Closed pipelines, cables, replacement of old pipes (Figure 2.3) - this is a list of major works carried out using raskatchik .

4. CONCLUSION

Conducted in a production environment testing machine for rolling holes show its performance and identified a number of advantages compared with other similar machines, namely:

1. Environmental safety, quietness, lack of harmful effects on the dynamic service staff and the environment;
2. Higher productivity due to the fact that during the formation of the holes is no extraction of soil outwards and reduced cycle time;
3. Significant economic effect due to the low energy consumption of the process rolling and labor.

REFERENCES

1. Dotsenko AI Drones VG Construction machinery M., Infra-M, 2014.
2. Patent of the Russian Federation for the invention № 2379429 " Raskatchik leader to form a well in the ground". Priority from 14.11.2008. (Authors: AI Dotsenko , Bobilev AL)
3 . PATENT OF THE RUSSIAN FEDERATION FOR THE INVENTION № 238687 " RASKATCHIK TO FORM A HOLES IN THE GROUND". PRIORITY FROM 14.11.2008. (AUTHORS: AI DOTSENKO ,

Kinematics Computational Modelling of Self-Erecting Tower Cranes' Erection Mechanism

Cătălin Frăncu[1*], Marian Dima[1]
[1] Technical University of Civil Engineering Bucharest

This paper presents a method to build the forward kinematics model of the 1 DOF erection mechanism of the self-erecting tower crane. For building the forward kinematics, the MBS (multi body system) method is used since is adequate for computer aided studying. The results of the study show the variations of positions, velocities, and accelerations of the characteristic points in the erecting and lowering stages.

Keywords: self-erecting cranes; forward kinematics; MBS

1. INTRODUCTION

The self-erecting cranes are generally used in construction sites for handling relatively small loads, but also in tight spaces and sites with difficult access figure 1.

The main characteristic of these cranes is that their metal structure is part of a planar mechanism with bars, having one degree of mobility using it on the construction site for self-erecting it from the folded state, prepared for transport, figure *1a*, to normal working state, figure *1b* in a short time on the order of minutes.

Some other specific characteristics of these cranes are as follows: nominal load is between 400 and 8000 kg, hoisting height is between 14 and 37 meters, maximum radius is between 15 and 50 m [1].

The crane used in the calculus example is Potain Igo 36

.

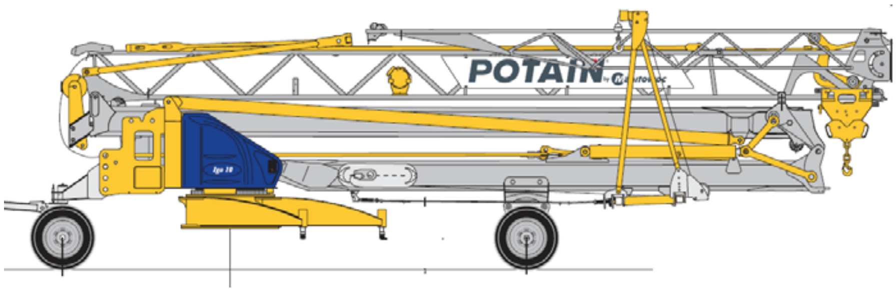

a)

b)

Figure 1: Self erecting crane; a) self-erecting crane in transport state; b) erected self-erecting crane

*Corresponding author: Technical University of Civil Engineering 122-124 Lacul Tei Blv., Bucharest, Romania, francu@mail.utcb.ro

2. DESCRIPTION AND WORKING

The structure of this type of crane is composed of: chassis, tower and jib. The tower is composed of 2 sections hinged together, lower tower 3 and upper tower 2 respectively. At the end of the erection, the 2 sections of the tower are locked together, figure 2c. The jib is composed of 2 sections hinged together 6 and 7 and according to the required maximum radius, can be used only the first section 6 or both sections. The relative position between the jib and the vertical tower is maintained by the backstays T1 which is linked to the chassis and T2 linked to the boom.

The self-erecting mechanism is composed of the four bar linkage AJDB with the coupler JD fixed to the upper tower and the follower BD fixed to the lower tower. To this mechanism is attached the dyad EHK which is linked to the lower tower in E and to the upper tower in K. Driving of the mechanism is done using a hydraulic cylinder mounted between the joint C, which belongs to the lower tower, and joint H of the dyad EHK. Changing the length of the hydraulic cylinder sets into motion the four bar linkage, by rotating the lower tower counter clockwise, figure 2a, from horizontal position to vertical position. In the same time, through the dyad EHK, the upper tower is rotating in relation to the lower tower clockwise from horizontal to vertical.

Unfolding the jib is done in 2 stages. In the first stage, the jib is folded over the upper tower and moves along with it until the backstays T1 and T2 are fully stretched. The second stage begins and consists in the relative rotation of the jib in relation to the upper tower around the joint L counter clockwise, rotation due to backstays T1 and T2.

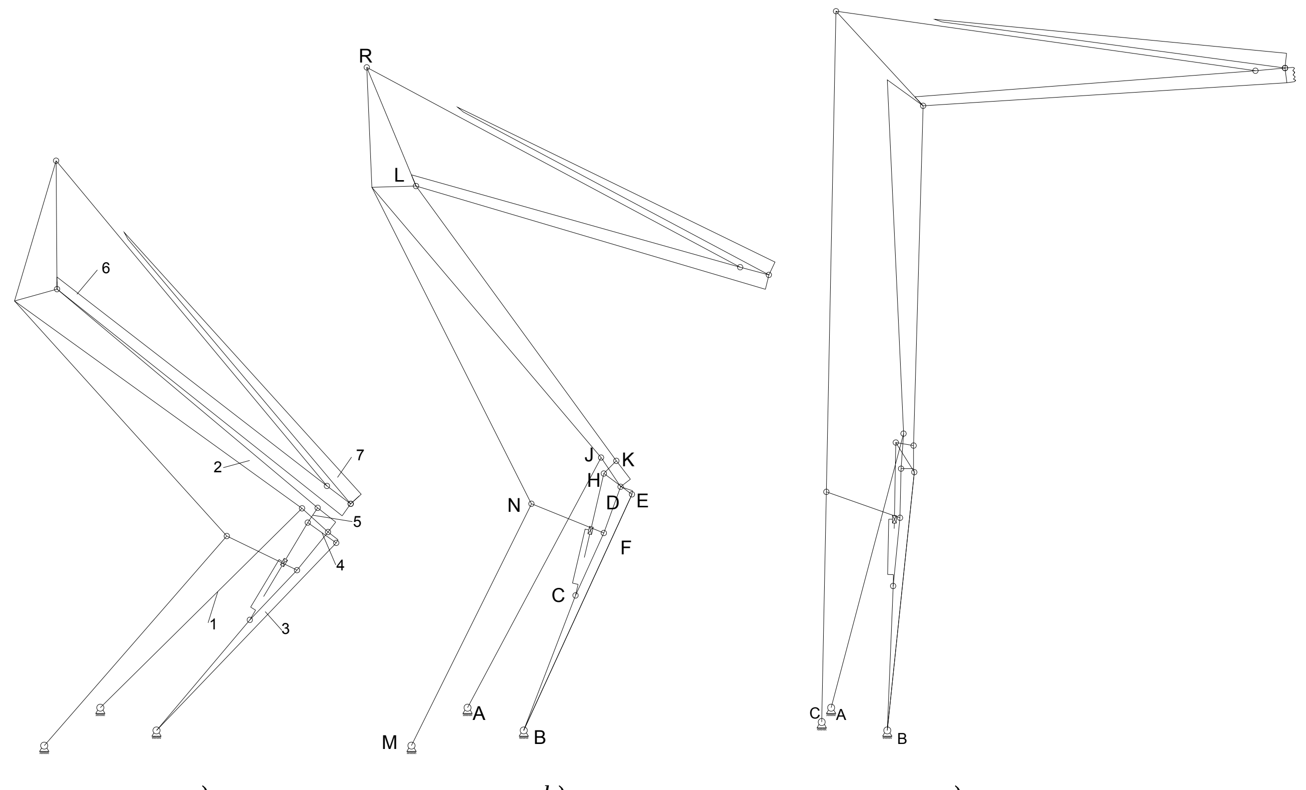

Figure 2: The self-erecting crane in various stages of erection a) the time before the backstays are fully stretched; b) after the backstays are fully stretched; c) at the end of erection;

3. KINEMATIC STUDY OF THE SELF-ERECTION MECHANISM

3.1. Method presentation

For the kinematic study of the self-erecting mechanism, having the kinematic scheme presented in figure 3a, the MBS (Multi Body System) method was chosen [2,3], expressing the geometrical constraints equations in Cartesian coordinates.

The required number of geometrical constraints equations, $\emptyset_i(q)$ is determined with the equation:

$$3(n-1)-\emptyset_i(q)=M \quad (1)$$

The number of kinematic constraints, $\emptyset_j(t)$, must be equal to the mobility M of the mechanism.

The generalized coordinates q represent the coordinates of the origins of the mobile reference frames and their orientations in relation to the fixed reference frames and n represent the number of kinematic elements of the mechanism.

Determining the positions of the characteristic points corresponding to the joints and orientations of the kinematic elements is carried out by solving the system of geometrical and kinematic constraints.

$$\emptyset(q,t)=0 \quad (2)$$

Determining the velocities of the characteristic points and the angular velocities of the kinematic elements is carried out by differentiating against time of the system of geometrical and kinematic constraints (2). Doing the differentiation is obtained:

$$\frac{\partial\emptyset(q,t)}{\partial q}\frac{\partial q}{\partial t}+\frac{\partial\emptyset(q,t)}{\partial t}=0 \qquad (3)$$

The equation can be written as follows:

$$\emptyset_q(q,t)\cdot\dot{q}=-\emptyset_t(q,t) \qquad (4)$$

From equation (4) by multiplying to the left with the inverse of the Jacobian matrix $\emptyset_q(q,t)$ we obtain the column vector of velocities:

$$\dot{q}=-\left(\emptyset_q(q,t)\right)^{-1}\cdot\emptyset_t(q,t) \qquad (5)$$

Determining the accelerations of the characteristic points and the angular accelerations of the kinematic elements is carried out by differentiating against time of the system of equations (3). Doing the differentiation is obtained:

$$\frac{\partial\emptyset(q,t)}{\partial q^2}\left(\frac{\partial q}{\partial t}\right)^2+\frac{\partial\emptyset(q,t)}{\partial q}\frac{\partial^2 q}{\partial t^2}+\frac{\partial^2\emptyset(q,t)}{\partial t^2}=0 \qquad (6)$$

The equation can be written as follows:

$$\emptyset_q(q,t)\cdot\ddot{q}=-\emptyset_{qq}(q,t)\cdot\dot{q}^2-\emptyset_{tt}(q,t) \qquad (7)$$

From equation (7) by multiplying to the left with the inverse of the Jacobian matrix $\emptyset_q(q,t)$ we obtain the column vector of accelerations:

$$\ddot{q}=-\left(\emptyset_q(q,t)\right)^{-1}\cdot\left(\emptyset_{qq}(q,t)\cdot\dot{q}^2+\emptyset_{tt}(q,t)\right) \qquad (8)$$

3.2. Kinematic study of self-erection mechanism for the first stage of erection

For this stage of working, the kinematic scheme of the mechanism is presented in figure 2*a*. The mechanism is composed of 6 elements and driven by the hydraulic cylinder CH. In these conditions the mobility of the mechanism is M=1, and the number of geometrical constraints equations is $\emptyset_i(q)=14$

3.2.1. Attaching the reference frames to the kinematic elements and expressing the absolute coordinates

To each of the elements is attached its own reference frame in relation to which the coordinates of the characteristic points of the element are expressed, these characteristic points being the point corresponding to the joints and the centres of gravity, figure 3.

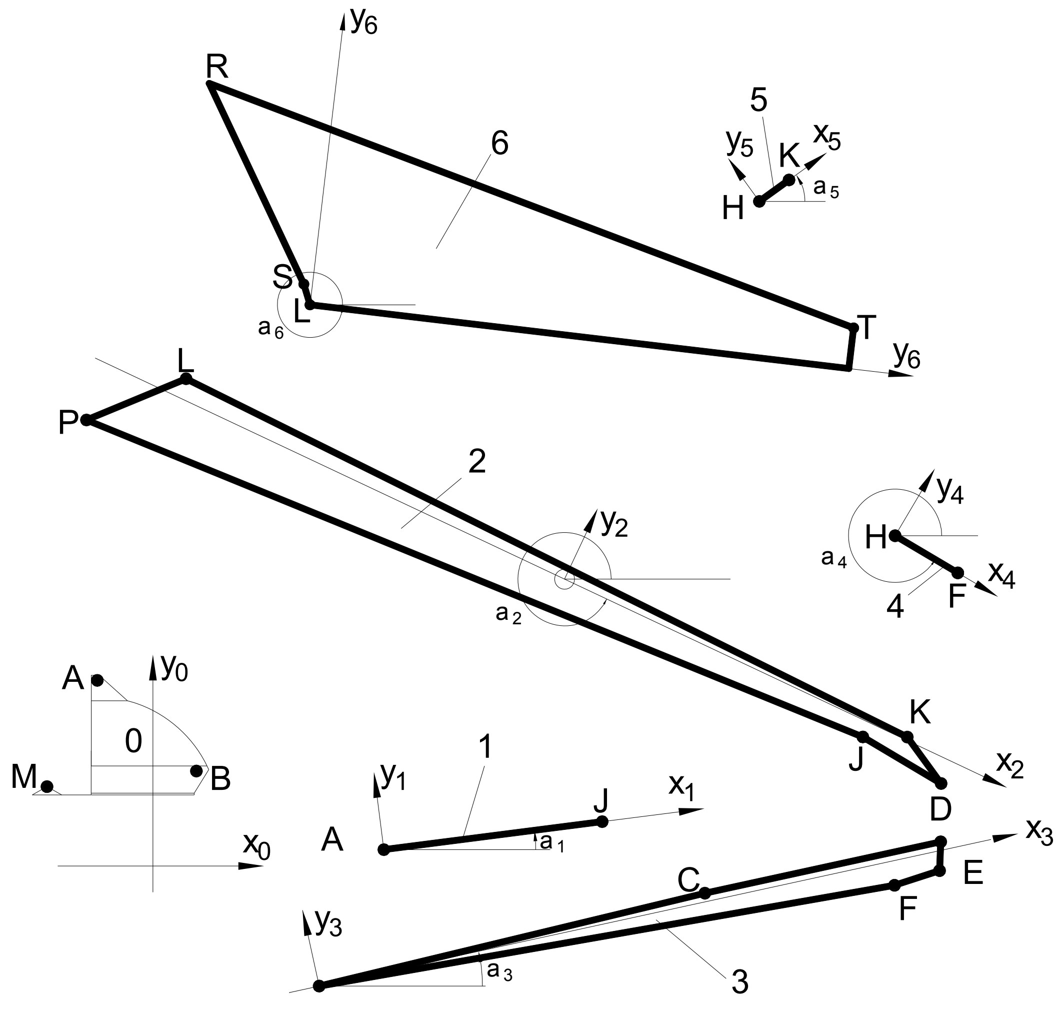

Figure 3: Reference frames attached to the kinematic elements in the first stage of erection

The absolute coordinates of the characteristic points of the kinematic elements related to the fixed reference frame are obtained by expressing the position and orientation of the mobile reference frame linked to the kinematic element in relation to the fixed reference frame attached to the base of the mechanism according to the following relations:

$$
\begin{aligned}
&\begin{pmatrix} xJ1 \\ yJ1 \end{pmatrix} = \begin{pmatrix} x1 \\ y1 \end{pmatrix} + \begin{pmatrix} \cos(\alpha1) & -\sin(\alpha1) \\ \sin(\alpha1) & \cos(\alpha1) \end{pmatrix} \cdot \begin{pmatrix} xJ1m \\ yJ1m \end{pmatrix} \\
&\begin{pmatrix} xD2 \\ yD2 \end{pmatrix} = \begin{pmatrix} x2 \\ y2 \end{pmatrix} + \begin{pmatrix} \cos(\alpha2) & -\sin(\alpha2) \\ \sin(\alpha2) & \cos(\alpha2) \end{pmatrix} \cdot \begin{pmatrix} xD2m \\ yD2m \end{pmatrix} \\
&\begin{pmatrix} xJ2 \\ yJ2 \end{pmatrix} = \begin{pmatrix} x2 \\ y2 \end{pmatrix} + \begin{pmatrix} \cos(\alpha2) & -\sin(\alpha2) \\ \sin(\alpha2) & \cos(\alpha2) \end{pmatrix} \cdot \begin{pmatrix} xJ2m \\ yJ2m \end{pmatrix} \\
&\begin{pmatrix} xK2 \\ yK2 \end{pmatrix} = \begin{pmatrix} x2 \\ y2 \end{pmatrix} + \begin{pmatrix} \cos(\alpha2) & -\sin(\alpha2) \\ \sin(\alpha2) & \cos(\alpha2) \end{pmatrix} \cdot \begin{pmatrix} xK2m \\ yK2m \end{pmatrix} \\
&\begin{pmatrix} xL2 \\ yL2 \end{pmatrix} = \begin{pmatrix} x2 \\ y2 \end{pmatrix} + \begin{pmatrix} \cos(\alpha2) & -\sin(\alpha2) \\ \sin(\alpha2) & \cos(\alpha2) \end{pmatrix} \cdot \begin{pmatrix} xL2m \\ yL2m \end{pmatrix} \\
&\begin{pmatrix} xC3 \\ yC3 \end{pmatrix} = \begin{pmatrix} x3 \\ y3 \end{pmatrix} + \begin{pmatrix} \cos(\alpha3) & -\sin(\alpha3) \\ \sin(\alpha3) & \cos(\alpha3) \end{pmatrix} \cdot \begin{pmatrix} xC3m \\ yC3m \end{pmatrix} \\
&\begin{pmatrix} xD3 \\ yD3 \end{pmatrix} = \begin{pmatrix} x3 \\ y3 \end{pmatrix} + \begin{pmatrix} \cos(\alpha3) & -\sin(\alpha3) \\ \sin(\alpha3) & \cos(\alpha3) \end{pmatrix} \cdot \begin{pmatrix} xD3m \\ yD3m \end{pmatrix} \\
&\begin{pmatrix} xE3 \\ yE3 \end{pmatrix} = \begin{pmatrix} x3 \\ y3 \end{pmatrix} + \begin{pmatrix} \cos(\alpha3) & -\sin(\alpha3) \\ \sin(\alpha3) & \cos(\alpha3) \end{pmatrix} \cdot \begin{pmatrix} xE3m \\ yE3m \end{pmatrix} \\
&\begin{pmatrix} xF3 \\ yF3 \end{pmatrix} = \begin{pmatrix} x3 \\ y3 \end{pmatrix} + \begin{pmatrix} \cos(\alpha3) & -\sin(\alpha3) \\ \sin(\alpha3) & \cos(\alpha3) \end{pmatrix} \cdot \begin{pmatrix} xF3m \\ yF3m \end{pmatrix} \\
&\begin{pmatrix} xE4 \\ yE4 \end{pmatrix} = \begin{pmatrix} x4 \\ y4 \end{pmatrix} + \begin{pmatrix} \cos(\alpha4) & -\sin(\alpha4) \\ \sin(\alpha4) & \cos(\alpha4) \end{pmatrix} \cdot \begin{pmatrix} xE4m \\ yE4m \end{pmatrix} \\
&\begin{pmatrix} xH4 \\ yH4 \end{pmatrix} = \begin{pmatrix} x4 \\ y4 \end{pmatrix} + \begin{pmatrix} \cos(\alpha4) & -\sin(\alpha4) \\ \sin(\alpha4) & \cos(\alpha4) \end{pmatrix} \cdot \begin{pmatrix} xH4m \\ yH4m \end{pmatrix} \\
&\begin{pmatrix} xK5 \\ yK5 \end{pmatrix} = \begin{pmatrix} x5 \\ y5 \end{pmatrix} + \begin{pmatrix} \cos(\alpha5) & -\sin(\alpha5) \\ \sin(\alpha5) & \cos(\alpha5) \end{pmatrix} \cdot \begin{pmatrix} xK5m \\ yK5m \end{pmatrix} \\
&\begin{pmatrix} xH5 \\ yH5 \end{pmatrix} = \begin{pmatrix} x5 \\ y5 \end{pmatrix} + \begin{pmatrix} \cos(\alpha5) & -\sin(\alpha5) \\ \sin(\alpha5) & \cos(\alpha5) \end{pmatrix} \cdot \begin{pmatrix} xH5m \\ yH5m \end{pmatrix}
\end{aligned}
\tag{9}
$$

3.2.2. The set of the equation system of geometrical and kinematic constraints

Obtaining the set of the equation system of geometrical and kinematic constraints is carried out by imposing the conditions of coincidence for the characteristic points of the joints from the kinematic scheme figure 2*a*. We obtain the following:

$$
\begin{aligned}
&xA = -767 \\
&yA = 2560 \\
&xB = 600 \\
&yB = 1310 \\
&\begin{pmatrix} xJ1 \\ yJ1 \end{pmatrix} = \begin{pmatrix} xJ2 \\ yJ2 \end{pmatrix} \\
&\begin{pmatrix} xD2 \\ yD2 \end{pmatrix} = \begin{pmatrix} xD3 \\ yD3 \end{pmatrix} \\
&\begin{pmatrix} xE3 \\ yE3 \end{pmatrix} = \begin{pmatrix} xE4 \\ yE4 \end{pmatrix} \\
&\begin{pmatrix} xK2 \\ yK2 \end{pmatrix} = \begin{pmatrix} xK5 \\ yK5 \end{pmatrix} \\
&\begin{pmatrix} xH4 \\ yH4 \end{pmatrix} = \begin{pmatrix} xH5 \\ yH5 \end{pmatrix}
\end{aligned}
\tag{10}
$$

To these constraints, the kinematic constraint is added:

$$CH := CHmin + v \cdot t \tag{11}$$

3.2.3. Positions study

Taking into account the equations (10) and (11) the equations system (2) becomes:

$$
\begin{aligned}
&x1 + xJ1m\cos(\alpha1) - yJ1m\cdot\sin(\alpha1) - x2 - xJ2m\cos(\alpha2) + yJ2m\cdot\sin(\alpha2) = 0 \\
&y1 + xJ1m\sin(\alpha1) + yJ1m\cdot\cos(\alpha1) - y2 - xJ2m\sin(\alpha2) - yJ2m\cdot\cos(\alpha2) = 0 \\
&x2 + xD2m\cos(\alpha2) - yD2m\cdot\sin(\alpha2) - x3 - xD3m\cos(\alpha3) + yD3m\cdot\sin(\alpha3) = 0 \\
&y2 + xD2m\sin(\alpha2) + yD2m\cdot\cos(\alpha2) - y3 - xD3m\sin(\alpha3) - yD3m\cdot\cos(\alpha3) = 0 \\
&x3 + xE3m\cos(\alpha3) - yE3m\cdot\sin(\alpha3) - x4 - xE4m\cos(\alpha4) + yE4m\cdot\sin(\alpha4) = 0 \\
&y3 + xE3m\sin(\alpha3) + yE3m\cdot\cos(\alpha3) - y4 - xE4m\sin(\alpha4) - yE4m\cdot\cos(\alpha4) = 0 \\
&x2 + xK2m\cos(\alpha2) - yK2m\cdot\sin(\alpha2) - x5 - xK5m\cos(\alpha5) + yK5m\cdot\sin(\alpha5) = 0 \\
&y2 + xK2m\sin(\alpha2) + yK2m\cdot\cos(\alpha2) - y5 - xK5m\sin(\alpha5) - yK5m\cdot\cos(\alpha5) = 0 \\
&x4 + xH4m\cos(\alpha4) - yH4m\cdot\sin(\alpha4) - x5 - xH5m\cos(\alpha5) + yH5m\cdot\sin(\alpha5) = 0 \\
&y4 + xH4m\sin(\alpha4) + yH4m\cdot\cos(\alpha4) - y5 - xH5m\sin(\alpha5) - yH5m\cdot\cos(\alpha5) = 0 \\
&x5 + xH5m\cos(\alpha5) - yH5m\cdot\sin(\alpha5) - CH\cdot\cos(\beta) - x3 - xC3m\cos(\alpha3) + yC3m\cdot\sin(\alpha3) = 0 \\
&y5 + xH5m\sin(\alpha5) + yH5m\cdot\cos(\alpha5) - CH\cdot\sin(\beta) - y3 - xC3m\sin(\alpha3) - yC3m\cdot\cos(\alpha3) = 0
\end{aligned}
\tag{12}
$$

The equations system (12) consists of 12 equations because the first 4 equations in (10) are embedded in the others and the kinematic constraint equation (11) was projected by the axes of the fixed reference frame.

In this stage the point R is considered belonging to the upper tower because the jib is resting on the upper tower superior. The coordinates of this point are required of determining the beginning of the second stage of the erection, which is the detachment of the jib from the upper tower. Mathematically this detachment can be expressed as follows:

$$
\begin{aligned}
&RPN < T3 - \text{stage } 1 \\
&RPN = T3 - \text{stage } 2
\end{aligned}
$$

3.2.4. Velocities study

By differentiating the equations (12) and pushing the results in equation (4) the equation system for velocities becomes:

$$\begin{pmatrix} A & -1 & 0 & C & 0 & 0 & 0 & 0 & 0 & 0 & 0 & 0 \\ B & 0 & -1 & D & 0 & 0 & 0 & 0 & 0 & 0 & 0 & 0 \\ 0 & 1 & 0 & E & I & 0 & 0 & 0 & 0 & 0 & 0 & 0 \\ 0 & 0 & 1 & F & J & 0 & 0 & 0 & 0 & 0 & 0 & 0 \\ 0 & 0 & 0 & 0 & K & -1 & 0 & O & 0 & 0 & 0 & 0 \\ 0 & 0 & 0 & 0 & L & 0 & -1 & P & 0 & 0 & 0 & 0 \\ 0 & 1 & 0 & G & 0 & 0 & 0 & 0 & -1 & 0 & S & 0 \\ 0 & 0 & 1 & H & 0 & 0 & 0 & 0 & 0 & -1 & T & 0 \\ 0 & 0 & 0 & 0 & 0 & 1 & 0 & Q & -1 & 0 & U & 0 \\ 0 & 0 & 0 & 0 & 0 & 0 & 1 & R & 0 & -1 & V & 0 \\ 0 & 0 & 0 & 0 & M & 0 & 0 & 0 & 1 & 0 & W & Y \\ 0 & 0 & 0 & 0 & N & 0 & 0 & 0 & 0 & 1 & X & Z \end{pmatrix} \cdot \begin{pmatrix} \omega1 \\ vx2 \\ vy2 \\ \omega2 \\ \omega3 \\ vx4 \\ vy4 \\ \omega4 \\ vx5 \\ vy5 \\ \omega5 \\ \omega CH \end{pmatrix} = \begin{pmatrix} 0 \\ 0 \\ 0 \\ 0 \\ 0 \\ 0 \\ 0 \\ 0 \\ 0 \\ 0 \\ -vx \\ -vy \end{pmatrix} \tag{13}$$

in which we have the following substitutions:

$A = -xJ1m\sin(\alpha1) - yJ1m\cdot\cos(\alpha1)$
$B = xJ1m\cos(\alpha1) - yJ1m\cdot\sin(\alpha1)$
$C = xJ2m\sin(\alpha2) - yJ2m\cdot\cos(\alpha2)$
$D = yJ2m\cdot\sin(\alpha2) - xJ2m\cos(\alpha2)$
$E = -xD2m\sin(\alpha2) - yD2m\cdot\cos(\alpha2)$
$F = xD2m\cos(\alpha2) - yD2m\cdot\sin(\alpha2)$
$G = -xK2m\sin(\alpha2) - yK2m\cdot\cos(\alpha2)$
$H = xK2m\cos(\alpha2) - yK2m\cdot\sin(\alpha2)$
$I = xD3m\sin(\alpha3) + yD3m\cdot\cos(\alpha3)$
$J = yD3m\cdot\sin(\alpha3) - xD3m\cos(\alpha3)$
$K = -xE3m\sin(\alpha3) - yE3m\cdot\cos(\alpha3)$
$L = xE3m\cos(\alpha3) - yE3m\cdot\sin(\alpha3)$
$M = xC3m\sin(\alpha3) + yC3m\cdot\cos(\alpha3)$
$N = yC3m\cdot\sin(\alpha3) - xC3m\cos(\alpha3)$
$O = xE4m\sin(\alpha4) + yE4m\cdot\cos(\alpha4)$
$P = yE4m\cdot\sin(\alpha4) - xE4m\cos(\alpha4)$
$Q = -xH4m\sin(\alpha4) - yH4m\cdot\cos(\alpha4)$
$R = xH4m\cos(\alpha4) - yH4m\cdot\sin(\alpha4)$
$S = xK5m\sin(\alpha5) + yK5m\cdot\cos(\alpha5)$
$T = yK5m\cdot\sin(\alpha5) - xK5m\cos(\alpha5)$
$U = xH5m\sin(\alpha5) + yH5m\cdot\cos(\alpha5)$
$V = yH5m\cdot\sin(\alpha5) - xH5m\cos(\alpha5)$
$W = -xH5m\sin(\alpha5) - yH5m\cdot\cos(\alpha5)$
$X = xH5m\cos(\alpha5) - yH5m\cdot\sin(\alpha5)$
$Y = CH\cdot\sin(\beta)$
$Z = -CH\cdot\cos(\beta)$

3.2.5. Accelerations study

Differentiating the Jacobian matrix $\emptyset_q(q,t)$ according to the equation (8) and doing the calculus the equations system for accelerations is obtained:

$$\begin{pmatrix} A & -1 & 0 & C & 0 & 0 & 0 & 0 & 0 & 0 & 0 & 0 \\ B & 0 & -1 & D & 0 & 0 & 0 & 0 & 0 & 0 & 0 & 0 \\ 0 & 1 & 0 & E & I & 0 & 0 & 0 & 0 & 0 & 0 & 0 \\ 0 & 0 & 1 & F & J & 0 & 0 & 0 & 0 & 0 & 0 & 0 \\ 0 & 0 & 0 & 0 & K & -1 & 0 & O & 0 & 0 & 0 & 0 \\ 0 & 0 & 0 & 0 & L & 0 & -1 & P & 0 & 0 & 0 & 0 \\ 0 & 1 & 0 & G & 0 & 0 & 0 & 0 & -1 & 0 & S & 0 \\ 0 & 0 & 1 & H & 0 & 0 & 0 & 0 & 0 & -1 & T & 0 \\ 0 & 0 & 0 & 0 & 0 & 1 & 0 & Q & -1 & 0 & U & 0 \\ 0 & 0 & 0 & 0 & 0 & 0 & 1 & R & 0 & -1 & V & 0 \\ 0 & 0 & 0 & 0 & M & 0 & 0 & 0 & 1 & 0 & W & Y \\ 0 & 0 & 0 & 0 & N & 0 & 0 & 0 & 0 & 1 & X & Z \end{pmatrix} \cdot \begin{pmatrix} \varepsilon1 \\ ax2 \\ ay2 \\ \varepsilon2 \\ \varepsilon3 \\ ax4 \\ ay4 \\ \varepsilon4 \\ ax5 \\ ay5 \\ \varepsilon5 \\ \varepsilon CH \end{pmatrix} = -\begin{pmatrix} AA & -1 & 0 & CC & 0 & 0 & 0 & 0 & 0 & 0 & 0 & 0 \\ BB & 0 & -1 & DD & 0 & 0 & 0 & 0 & 0 & 0 & 0 & 0 \\ 0 & 1 & 0 & EE & II & 0 & 0 & 0 & 0 & 0 & 0 & 0 \\ 0 & 0 & 1 & FF & JJ & 0 & 0 & 0 & 0 & 0 & 0 & 0 \\ 0 & 0 & 0 & 0 & KK & -1 & 0 & OO & 0 & 0 & 0 & 0 \\ 0 & 0 & 0 & 0 & LL & 0 & -1 & PP & 0 & 0 & 0 & 0 \\ 0 & 1 & 0 & GG & 0 & 0 & 0 & 0 & -1 & 0 & SS & 0 \\ 0 & 0 & 1 & HH & 0 & 0 & 0 & 0 & 0 & -1 & TT & 0 \\ 0 & 0 & 0 & 0 & 0 & 1 & 0 & QQ & -1 & 0 & UU & 0 \\ 0 & 0 & 0 & 0 & 0 & 0 & 1 & RR & 0 & -1 & VV & 0 \\ 0 & 0 & 0 & 0 & MM & 0 & 0 & 0 & 1 & 0 & WW & YY \\ 0 & 0 & 0 & 0 & NN & 0 & 0 & 0 & 0 & 1 & XX & ZZ \end{pmatrix} \cdot \begin{pmatrix} \omega1 \\ vx2 \\ vy2 \\ \omega2 \\ \omega3 \\ vx4 \\ vy4 \\ \omega4 \\ vx5 \\ vy5 \\ \omega5 \\ \omega CH \end{pmatrix}^2 - \begin{pmatrix} 0 \\ 0 \\ 0 \\ 0 \\ 0 \\ 0 \\ 0 \\ 0 \\ 0 \\ 0 \\ 0 \\ 0 \end{pmatrix} \tag{14}$$

in which we have the following substitutions:

$AA = yJ1m\cdot\sin(\alpha1) - xJ1m\cos(\alpha1)$
$BB = -xJ1m\sin(\alpha1) - yJ1m\cdot\cos(\alpha1)$
$CC = xJ2m\cos(\alpha2) + yJ2m\cdot\sin(\alpha2)$
$DD = xJ2m\sin(\alpha2) + yJ2m\cdot\cos(\alpha2)$
$EE = yD2m\cdot\sin(\alpha2) - xD2m\cos(\alpha2)$
$FF = -xD2m\sin(\alpha2) - yD2m\cdot\cos(\alpha2)$
$GG = yK2m\cdot\sin(\alpha2) - xK2m\cos(\alpha2)$
$HH = -xK2m\sin(\alpha2) - yK2m\cdot\cos(\alpha2)$
$II = xD3m\cos(\alpha3) - yD3m\cdot\sin(\alpha3)$
$JJ = xD3m\sin(\alpha3) + yD3m\cdot\cos(\alpha3)$
$KK = yE3m\cdot\sin(\alpha3) - xE3m\cos(\alpha3)$
$LL = -xE3m\sin(\alpha3) - yE3m\cdot\cos(\alpha3)$
$MM = xC3m\cos(\alpha3) - yC3m\cdot\sin(\alpha3)$
$NN = xC3m\sin(\alpha3) + yC3m\cdot\cos(\alpha3)$
$OO = xE4m\cos(\alpha4) - yE4m\cdot\sin(\alpha4)$
$PP = xE4m\sin(\alpha4) + yE4m\cdot\cos(\alpha4)$
$QQ = yH4m\cdot\sin(\alpha4) - xH4m\cos(\alpha4)$
$RR = -xH4m\sin(\alpha4) - yH4m\cdot\cos(\alpha4)$
$SS = xK5m\cos(\alpha5) - yK5m\cdot\sin(\alpha5)$
$TT = xK5m\sin(\alpha5) + yK5m\cdot\cos(\alpha5)$
$UU = xH5m\cos(\alpha5) - yH5m\cdot\sin(\alpha5)$

$$VV = xH5m\sin(\alpha 5) + yH5m\cdot\cos(\alpha 5)$$
$$WW = yH5m\cdot\sin(\alpha 5) - xH5m\cos(\alpha 5)$$
$$XX = -xH5m\sin(\alpha 5) - yH5m\cdot\cos(\alpha 5)$$
$$YY = CH\cdot\cos(\beta)$$
$$ZZ = CH\cdot\sin(\beta)$$

3.3. Kinematic study of self-erection mechanism for the second stage of erection

For this stage of working, the kinematic scheme of the mechanism is presented in figure 2*b*. The mechanism is composed of 10 elements and driven by the hydraulic cylinder CH. In these conditions the mobility of the mechanism is M=1, and the number of geometrical constraints equations is $\emptyset_i(q) = 26$

3.3.1. Attaching the reference frames to the kinematic elements and expressing the absolute coordinates

In this stage are valid the systems attached to the §3.2.1, plus reference frames are attached to the kinematic elements that in the first stage were not working, figure *4*.

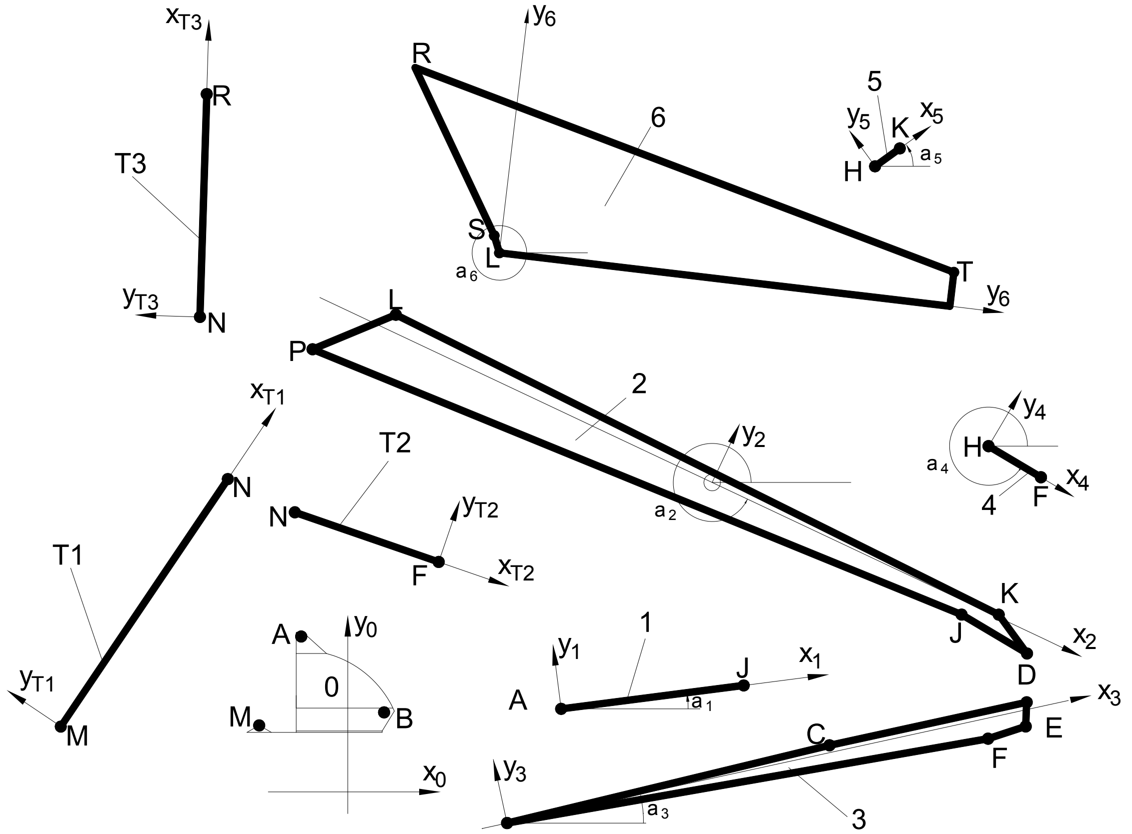

Figure 4: Reference frames attached to the kinematic elements in the second stage of erection

The absolute coordinates of the characteristic points of the newly introduced kinematic elements are determined like in the §3.2.1:

$$\left.\begin{array}{l}
\begin{pmatrix} xL6 \\ yL6 \end{pmatrix} = \begin{pmatrix} x6 \\ y6 \end{pmatrix} + \begin{pmatrix} \cos(\alpha 6) & -\sin(\alpha 6) \\ \sin(\alpha 6) & \cos(\alpha 6) \end{pmatrix} \cdot \begin{pmatrix} xL6m \\ yL6m \end{pmatrix} \\
\begin{pmatrix} xS6 \\ yS6 \end{pmatrix} = \begin{pmatrix} x6 \\ y6 \end{pmatrix} + \begin{pmatrix} \cos(\alpha 6) & -\sin(\alpha 6) \\ \sin(\alpha 6) & \cos(\alpha 6) \end{pmatrix} \cdot \begin{pmatrix} xS6m \\ yS6m \end{pmatrix} \\
\begin{pmatrix} xR6 \\ yR6 \end{pmatrix} = \begin{pmatrix} x6 \\ y6 \end{pmatrix} + \begin{pmatrix} \cos(\alpha 6) & -\sin(\alpha 6) \\ \sin(\alpha 6) & \cos(\alpha 6) \end{pmatrix} \cdot \begin{pmatrix} xR6m \\ yR6m \end{pmatrix} \\
\begin{pmatrix} xT6 \\ yT6 \end{pmatrix} = \begin{pmatrix} x6 \\ y6 \end{pmatrix} + \begin{pmatrix} \cos(\alpha 6) & -\sin(\alpha 6) \\ \sin(\alpha 6) & \cos(\alpha 6) \end{pmatrix} \cdot \begin{pmatrix} xT6m \\ yT6m \end{pmatrix} \\
\begin{pmatrix} xMT1 \\ yMT1 \end{pmatrix} = \begin{pmatrix} xT1 \\ yT1 \end{pmatrix} + \begin{pmatrix} \cos(\alpha T1) & -\sin(\alpha T1) \\ \sin(\alpha T1) & \cos(\alpha T1) \end{pmatrix} \cdot \begin{pmatrix} xMT1m \\ yMT1m \end{pmatrix} \\
\begin{pmatrix} xNT1 \\ yNT1 \end{pmatrix} = \begin{pmatrix} xT1 \\ yT1 \end{pmatrix} + \begin{pmatrix} \cos(\alpha T1) & -\sin(\alpha T1) \\ \sin(\alpha T1) & \cos(\alpha T1) \end{pmatrix} \cdot \begin{pmatrix} xNT1m \\ yNT1m \end{pmatrix} \\
\begin{pmatrix} xFT2 \\ yFT2 \end{pmatrix} = \begin{pmatrix} xT2 \\ yT2 \end{pmatrix} + \begin{pmatrix} \cos(\alpha T2) & -\sin(\alpha T2) \\ \sin(\alpha T2) & \cos(\alpha T2) \end{pmatrix} \cdot \begin{pmatrix} xFT2m \\ yFT2m \end{pmatrix}
\end{array}\right| \quad (15)$$

$$\left.\begin{array}{l}
\begin{pmatrix} xNT2 \\ yNT2 \end{pmatrix} = \begin{pmatrix} xT2 \\ yT2 \end{pmatrix} + \begin{pmatrix} \cos(\alpha T2) & -\sin(\alpha T2) \\ \sin(\alpha T2) & \cos(\alpha T2) \end{pmatrix} \cdot \begin{pmatrix} xNT2m \\ yNT2m \end{pmatrix} \\
\begin{pmatrix} xNT3 \\ yNT3 \end{pmatrix} = \begin{pmatrix} xT3 \\ yT3 \end{pmatrix} + \begin{pmatrix} \cos(\alpha T3) & -\sin(\alpha T3) \\ \sin(\alpha T3) & \cos(\alpha T3) \end{pmatrix} \cdot \begin{pmatrix} xNT3m \\ yNT3m \end{pmatrix} \\
\begin{pmatrix} xRT3 \\ yRT3 \end{pmatrix} = \begin{pmatrix} xT3 \\ yT3 \end{pmatrix} + \begin{pmatrix} \cos(\alpha T3) & -\sin(\alpha T3) \\ \sin(\alpha T3) & \cos(\alpha T3) \end{pmatrix} \cdot \begin{pmatrix} xRT3m \\ yRT3m \end{pmatrix}
\end{array}\right|$$

3.3.2. The set of the equation system of geometrical and kinematic constraints

The new set of geometrical constraints is obtained by adding to the constraints set (10) the geometrical constraints according to the coincidence conditions for the characteristic points of newly introduced according to figure 2b, we obtain:

$$
\begin{gathered}
yM := 1095 \\
xM := -1461 \\
\begin{pmatrix} xL2 \\ yL2 \end{pmatrix} = \begin{pmatrix} xL6 \\ yL6 \end{pmatrix} \\
\begin{pmatrix} xFT2 \\ yFT2 \end{pmatrix} = \begin{pmatrix} xF3 \\ yF3 \end{pmatrix} \\
\begin{pmatrix} xNT1 \\ yNT1 \end{pmatrix} = \begin{pmatrix} xNT2 \\ yNT2 \end{pmatrix} \\
\begin{pmatrix} xNT3 \\ yNT3 \end{pmatrix} = \begin{pmatrix} xNT1 \\ yNT1 \end{pmatrix} \\
yT3 + xNT3m \cdot \sin(\alpha T3) + yNT3m \cdot \cos(\alpha T3) - T3 \cdot \sin(\alpha T3) - \\
-(y2 + xL2m \cdot \sin(\alpha 2) + yL2m \cdot \cos(\alpha 2)) + \sqrt{xR6m^2 - yR6m^2} \cdot \sin(\alpha 6) = 0 \\
(xT3 + xNT3m \cdot \cos(\alpha T3) - yNT3m \cdot \sin(\alpha T3)) - T3 \cdot \cos(\alpha T3) - \\
-(x2 + xL2m \cdot \cos(\alpha 2) - yL2m \cdot \sin(\alpha 2)) + \sqrt{xR6m^2 - yR6m^2} \cdot \cos(\alpha 6) = 0
\end{gathered} \tag{16}
$$

The kinematic constraint (11) is the same

3.3.3. Positions study

Taking into account the equations (16) and (11) the equations system (2) becomes:

$$
\begin{gathered}
x1 + xJ1m \cdot \cos(\alpha 1) - yJ1m \cdot \sin(\alpha 1) - x2 - xJ2m \cdot \cos(\alpha 2) + yJ2m \cdot \sin(\alpha 2) = 0 \\
y1 + xJ1m \cdot \sin(\alpha 1) + yJ1m \cdot \cos(\alpha 1) - y2 - xJ2m \cdot \sin(\alpha 2) - yJ2m \cdot \cos(\alpha 2) = 0 \\
x2 + xD2m \cdot \cos(\alpha 2) - yD2m \cdot \sin(\alpha 2) - x3 - xD3m \cdot \cos(\alpha 3) + yD3m \cdot \sin(\alpha 3) = 0 \\
y2 + xD2m \cdot \sin(\alpha 2) + yD2m \cdot \cos(\alpha 2) - y3 - xD3m \cdot \sin(\alpha 3) - yD3m \cdot \cos(\alpha 3) = 0 \\
x3 + xE3m \cdot \cos(\alpha 3) - yE3m \cdot \sin(\alpha 3) - x4 - xE4m \cdot \cos(\alpha 4) + yE4m \cdot \sin(\alpha 4) = 0 \\
y3 + xE3m \cdot \sin(\alpha 3) + yE3m \cdot \cos(\alpha 3) - y4 - xE4m \cdot \sin(\alpha 4) - yE4m \cdot \cos(\alpha 4) = 0 \\
x2 + xK2m \cdot \cos(\alpha 2) - yK2m \cdot \sin(\alpha 2) - x5 - xK5m \cdot \cos(\alpha 5) + yK5m \cdot \sin(\alpha 5) = 0 \\
y2 + xK2m \cdot \sin(\alpha 2) + yK2m \cdot \cos(\alpha 2) - y5 - xK5m \cdot \sin(\alpha 5) - yK5m \cdot \cos(\alpha 5) = 0 \\
x4 + xH4m \cdot \cos(\alpha 4) - yH4m \cdot \sin(\alpha 4) - x5 - xH5m \cdot \cos(\alpha 5) + yH5m \cdot \sin(\alpha 5) = 0 \\
y4 + xH4m \cdot \sin(\alpha 4) + yH4m \cdot \cos(\alpha 4) - y5 - xH5m \cdot \sin(\alpha 5) - yH5m \cdot \cos(\alpha) = 0 \\
x5 + xH5m \cdot \cos(\alpha 5) - yH5m \cdot \sin(\alpha 5) - CH \cdot \cos(\beta) - x3 - xC3m \cdot \cos(\alpha 3) + yC3m \cdot \sin(\alpha 3) = 0 \\
y5 + xH5m \cdot \sin(\alpha 5) + yH5m \cdot \cos(\alpha 5) - CH \cdot \sin(\beta) - y3 - xC3m \cdot \sin(\alpha 3) - yC3m \cdot \cos(\alpha 3) = 0 \\
x2 + xL2m \cdot \cos(\alpha 2) - yL2m \cdot \sin(\alpha 2) - x6 - xL6m \cdot \cos(\alpha 6) + yL6m \cdot \sin(\alpha 6) = 0 \\
y2 + xL2m \cdot \sin(\alpha 2) + yL2m \cdot \cos(\alpha 2) - y6 - xL6m \cdot \sin(\alpha 6) - yL6m \cdot \cos(\alpha 6) = 0 \\
xT2 + xFT2m \cdot \cos(\alpha T2) - yFT2m \cdot \sin(\alpha T2) - x3 - xF3m \cdot \cos(\alpha 3) + yF3m \cdot \sin(\alpha 3) = 0 \\
yT2 + xFT2m \cdot \sin(\alpha T2) + yFT2m \cdot \cos(\alpha T2) - y3 - xF3m \cdot \sin(\alpha 3) - yF3m \cdot \cos(\alpha 3) = 0 \\
xT1 + xNT1m \cdot \cos(\alpha T1) - yNT1m \cdot \sin(\alpha T1) - xT2 - xNT2m \cdot \cos(\alpha T2) + yNT2m \cdot \sin(\alpha T2) = 0 \\
yT1 + xNT1m \cdot \sin(\alpha T1) + yNT1m \cdot \cos(\alpha T1) - yT2 - xNT2m \cdot \sin(\alpha T2) - yNT2m \cdot \cos(\alpha T2) = 0 \\
xT3 + xNT3m \cdot \cos(\alpha T3) - yNT3m \cdot \sin(\alpha T3) - xT1 - xNT1m \cdot \cos(\alpha T1) + yNT1m \cdot \sin(\alpha T1) = 0 \\
yT3 + xNT3m \cdot \sin(\alpha T3) + yNT3m \cdot \cos(\alpha T3) - yT1 - xNT1m \cdot \sin(\alpha T1) - yNT1m \cdot \cos(\alpha T1) = 0 \\
yT3 + xNT3m \cdot \sin(\alpha T3) + yNT3m \cdot \cos(\alpha T3) - T3 \cdot \sin(\alpha T3) -(y2 + xL2m \cdot \sin(\alpha 2) + yL2m \cdot \cos(\alpha 2)) + \\
+ \sqrt{xR6m^2 - yR6m^2} \cdot \sin(\alpha 6) = 0 \\
(xT3 + xNT3m \cdot \cos(\alpha T3) - yNT3m \cdot \sin(\alpha T3)) - T3 \cdot \cos(\alpha T3) -(x2 + xL2m \cdot \cos(\alpha 2) - yL2m \cdot \sin(\alpha 2)) + \\
+ \sqrt{xR6m^2 - yR6m^2} \cdot \cos(\alpha 6) = 0
\end{gathered} \tag{17}
$$

By solving this equations system can be determined the coordinates of the characteristic points and rotations of the kinematic elements.

3.3.4. Velocities study

By differentiating the equations (17) and pushing the results in equation (5) the equation system for velocities becomes:

$$\begin{pmatrix}
A&-1&0&C&0&0&0&0&0&0&0&0&0&0&0&0&0&0&0&0&0&0\\
B&0&-1&D&0&0&0&0&0&0&0&0&0&0&0&0&0&0&0&0&0&0\\
0&1&0&E&I&0&0&0&0&0&0&0&0&0&0&0&0&0&0&0&0&0\\
0&0&1&F&J&0&0&0&0&0&0&0&0&0&0&0&0&0&0&0&0&0\\
0&0&0&0&K&-1&0&O&0&0&0&0&0&0&0&0&0&0&0&0&0&0\\
0&0&0&0&L&0&-1&P&0&0&0&0&0&0&0&0&0&0&0&0&0&0\\
0&1&0&G&0&0&0&0&-1&0&S&0&0&0&0&0&0&0&0&0&0&0\\
0&0&1&H&0&0&0&0&0&-1&T&0&0&0&0&0&0&0&0&0&0&0\\
0&0&0&0&0&1&0&Q&-1&0&U&0&0&0&0&0&0&0&0&0&0&0\\
0&0&0&0&0&0&1&R&0&-1&V&0&0&0&0&0&0&0&0&0&0&0\\
0&0&0&0&M&0&0&0&1&0&W&Y&0&0&0&0&0&0&0&0&0&0\\
0&0&0&0&N&0&0&0&0&1&X&Z&0&0&0&0&0&0&0&0&0&0\\
0&1&0&A1&0&0&0&0&0&0&0&0&-1&0&G1&0&0&0&0&0&0&0\\
0&0&1&B1&0&0&0&0&0&0&0&0&0&-1&H1&0&0&0&0&0&0&0\\
0&0&0&0&E1&0&0&0&0&0&0&0&0&0&0&0&1&0&O1&0&0&0\\
0&0&0&0&F1&0&0&0&0&0&0&0&0&0&0&0&0&1&P1&0&0&0\\
0&0&0&0&0&0&0&0&0&0&0&0&0&0&0&K1&-1&0&Q1&0&0&0\\
0&0&0&0&0&0&0&0&0&0&0&0&0&0&0&L1&0&-1&R1&0&0&0\\
0&0&0&0&0&0&0&0&0&0&0&0&0&0&0&M1&0&0&0&1&0&S1\\
0&0&0&0&0&0&0&0&0&0&0&0&0&0&0&N1&0&0&0&0&1&T1\\
0&0&0&C1&0&0&0&0&0&0&0&0&0&0&I1&0&0&0&0&0&0&U1\\
0&0&0&D1&0&0&0&0&0&0&0&0&0&0&J1&0&0&0&0&0&0&V1
\end{pmatrix}
\cdot
\begin{pmatrix}
\omega 1\\ vx2\\ vy2\\ \omega 2\\ \omega 3\\ vx4\\ vy4\\ \omega 4\\ vx5\\ vy5\\ \omega 5\\ \omega CH\\ vx6\\ vy6\\ \omega 6\\ \omega T1\\ vxT2\\ vyT2\\ \omega T2\\ vxT3\\ vyT3\\ \omega T3
\end{pmatrix}
=
\begin{pmatrix}
0\\0\\0\\0\\0\\0\\0\\0\\0\\0\\-vx\\-vy\\0\\0\\0\\0\\0\\0\\0\\0\\0\\0
\end{pmatrix}
\tag{18}$$

in which we have the following substitutions:

$A1 = -xL2m\sin(\alpha 2) - yL2m\cdot\cos(\alpha 2)$

$B1 = xL2m\cos(\alpha 2) - yL2m\cdot\sin(\alpha 2)$

$C1 = xL2m\sin(\alpha 2) + yL2m\cdot\cos(\alpha 2)$

$D1 = yL2m\cdot\sin(\alpha 2) - xL2m\cos(\alpha 2)$

$E1 = xF3m\sin(\alpha 3) + yF3m\cdot\cos(\alpha 3)$

$F1 = yF3m\cdot\sin(\alpha 3) - xF3m\cos(\alpha 3)$

$G1 = xL6m\sin(\alpha 6) + yL6m\cdot\cos(\alpha 6)$

$H1 = xL6m\cos(\alpha 6) + yL6m\cdot\sin(\alpha 6)$

$I1 = -\sin(\alpha 6)\cdot\sqrt{xR6m^2 - yR6m^2}$

$J1 = \cos(\alpha 6)\cdot\sqrt{xR6m^2 - yR6m^2}$

$K1 = -xNT1m\sin(\alpha T1) - yNT1m\cdot\cos(\alpha T1)$

$L1 = xNT1m\cos(\alpha T1) - yNT1m\cdot\sin(\alpha T1)$

$M1 = yNT1m\cdot\cos(\alpha T1) - xNT1m\sin(\alpha T1)$

$N1 = -xNT1m\sin(\alpha T1) - yNT1m\cdot\cos(\alpha T1)$

$O1 = -xFT2m\sin(\alpha T2) - yFT2m\cdot\cos(\alpha T2)$

$P1 = xFT2m\cos(\alpha T2) - yFT2m\cdot\sin(\alpha T2)$

$Q1 = yNT2m\cdot\cos(\alpha T2) - xNT2m\sin(\alpha T2)$

$R1 = yNT2m\cdot\sin(\alpha T2) - xNT2m\cos(\alpha T2)$

$S1 = xNT3m\sin(\alpha T3) - yNT3m\cdot\cos(\alpha T3)$

$T1 = xNT3m\sin(\alpha T3) + yNT3m\cdot\cos(\alpha T3)$

$U1 = T3\cdot\sin(\alpha T3) - xNT3m\sin(\alpha T3) - yNT3m\cdot\cos(\alpha T3)$

$V1 = xNT3m\cos(\alpha T3) - T3\cdot\cos(\alpha T3) - yNT3m\cdot\sin(\alpha T3)$

3.3.5. Accelerations study

Differentiating the Jacobian matrix $\emptyset_q(q,t)$ according to the equation (8) and doing the calculus the equations system for accelerations is obtained:

$$\begin{pmatrix}
A&-1&0&C&0&0&0&0&0&0&0&0&0&0&0&0&0&0&0&0&0&0\\
B&0&-1&D&0&0&0&0&0&0&0&0&0&0&0&0&0&0&0&0&0&0\\
0&1&0&E&I&0&0&0&0&0&0&0&0&0&0&0&0&0&0&0&0&0\\
0&0&1&F&J&0&0&0&0&0&0&0&0&0&0&0&0&0&0&0&0&0\\
0&0&0&0&K&-1&0&O&0&0&0&0&0&0&0&0&0&0&0&0&0&0\\
0&0&0&0&L&0&-1&P&0&0&0&0&0&0&0&0&0&0&0&0&0&0\\
0&1&0&G&0&0&0&0&-1&0&S&0&0&0&0&0&0&0&0&0&0&0\\
0&0&1&H&0&0&0&0&0&-1&T&0&0&0&0&0&0&0&0&0&0&0\\
0&0&0&0&0&1&0&Q&-1&0&U&0&0&0&0&0&0&0&0&0&0&0\\
0&0&0&0&0&0&1&R&0&-1&V&0&0&0&0&0&0&0&0&0&0&0\\
0&0&0&0&M&0&0&0&1&0&W&Y&0&0&0&0&0&0&0&0&0&0\\
0&0&0&0&N&0&0&0&0&1&X&Z&0&0&0&0&0&0&0&0&0&0\\
0&1&0&A1&0&0&0&0&0&0&0&0&-1&0&G1&0&0&0&0&0&0&0\\
0&0&1&B1&0&0&0&0&0&0&0&0&0&-1&H1&0&0&0&0&0&0&0\\
0&0&0&0&E1&0&0&0&0&0&0&0&0&0&0&0&1&0&O1&0&0&0\\
0&0&0&0&F1&0&0&0&0&0&0&0&0&0&0&0&0&1&P1&0&0&0\\
0&0&0&0&0&0&0&0&0&0&0&0&0&0&0&K1&-1&0&Q1&0&0&0\\
0&0&0&0&0&0&0&0&0&0&0&0&0&0&0&L1&0&-1&R1&0&0&0\\
0&0&0&0&0&0&0&0&0&0&0&0&0&0&0&M1&0&0&0&1&0&S1\\
0&0&0&0&0&0&0&0&0&0&0&0&0&0&0&N1&0&0&0&0&1&T1\\
0&0&0&C1&0&0&0&0&0&0&0&0&0&0&I1&0&0&0&0&0&0&U1\\
0&0&0&D1&0&0&0&0&0&0&0&0&0&0&J1&0&0&0&0&0&0&V1
\end{pmatrix}
\cdot
\begin{pmatrix}
\varepsilon 1\\ ax2\\ ay2\\ \varepsilon 2\\ \varepsilon 3\\ ax4\\ ay4\\ \varepsilon 4\\ ax5\\ ay5\\ \varepsilon 5\\ \varepsilon CH\\ ax6\\ ay6\\ \varepsilon 6\\ \omega T1\\ axT2\\ ayT2\\ \varepsilon T2\\ axT3\\ ayT3\\ \varepsilon T3
\end{pmatrix}
= -
\begin{pmatrix}
AA&0&0&CC&0&0&0&0&0&0&0&0&0&0&0&0&0&0&0&0&0&0\\
BB&0&0&DD&0&0&0&0&0&0&0&0&0&0&0&0&0&0&0&0&0&0\\
0&0&0&EE&II&0&0&0&0&0&0&0&0&0&0&0&0&0&0&0&0&0\\
0&0&0&FF&JJ&0&0&0&0&0&0&0&0&0&0&0&0&0&0&0&0&0\\
0&0&0&0&KK&0&0&OO&0&0&0&0&0&0&0&0&0&0&0&0&0&0\\
0&0&0&0&LL&0&0&PP&0&0&0&0&0&0&0&0&0&0&0&0&0&0\\
0&0&0&GG&0&0&0&0&0&0&SS&0&0&0&0&0&0&0&0&0&0&0\\
0&0&0&HH&0&0&0&0&0&0&TT&0&0&0&0&0&0&0&0&0&0&0\\
0&0&0&0&0&0&0&QQ&0&0&UU&0&0&0&0&0&0&0&0&0&0&0\\
0&0&0&0&0&0&0&RR&0&0&VV&0&0&0&0&0&0&0&0&0&0&0\\
0&0&0&0&MM&0&0&0&0&0&WW&YY&0&0&0&0&0&0&0&0&0&0\\
0&0&0&0&NN&0&0&0&0&0&XX&ZZ&0&0&0&0&0&0&0&0&0&0\\
0&0&0&AA1&0&0&0&0&0&0&0&0&0&0&GG1&0&0&0&0&0&0&0\\
0&0&0&BB1&0&0&0&0&0&0&0&0&0&0&HH1&0&0&0&0&0&0&0\\
0&0&0&0&EE1&0&0&0&0&0&0&0&0&0&0&0&0&0&OO1&0&0&0\\
0&0&0&0&FF1&0&0&0&0&0&0&0&0&0&0&0&0&0&PP1&0&0&0\\
0&0&0&0&0&0&0&0&0&0&0&0&0&0&0&KK1&0&0&QQ1&0&0&0\\
0&0&0&0&0&0&0&0&0&0&0&0&0&0&0&LL1&0&0&RR1&0&0&0\\
0&0&0&0&0&0&0&0&0&0&0&0&0&0&0&MM1&0&0&0&0&0&SS1\\
0&0&0&0&0&0&0&0&0&0&0&0&0&0&0&NN1&0&0&0&0&0&TT1\\
0&0&0&CC1&0&0&0&0&0&0&0&0&0&0&II1&0&0&0&0&0&0&UU1\\
0&0&0&DD1&0&0&0&0&0&0&0&0&0&0&JJ1&0&0&0&0&0&0&VV1
\end{pmatrix}
\cdot
\begin{pmatrix}
\omega 1\\ vx2\\ vy2\\ \omega 2\\ \omega 3\\ vx4\\ vy4\\ \omega 4\\ vx5\\ vy5\\ \omega 5\\ \omega CH\\ vx6\\ vy6\\ \omega 6\\ \omega T1\\ vxT2\\ vyT2\\ \omega T2\\ vxT3\\ vyT3\\ \omega T3
\end{pmatrix}^2
-
\begin{pmatrix}
0\\0\\0\\0\\0\\0\\0\\0\\0\\0\\0\\0\\0\\0\\0\\0\\0\\0\\0\\0\\0\\0
\end{pmatrix}
\tag{19}$$

in which we have the following substitutions:

$$AA1 = yL2m\sin(\alpha2) - xL2m\cos(\alpha2)$$
$$BB1 = -xL2m\sin(\alpha2) - yL2m\cos(\alpha2)$$
$$CC1 = xL2m\cos(\alpha2) - yL2m\sin(\alpha2)$$
$$DD1 = xL2m\sin(\alpha2) + yL2m\cos(\alpha2)$$
$$EE1 = xF3m\cos(\alpha3) - yF3m\sin(\alpha3)$$
$$FF1 = xF3m\sin(\alpha3) + yF3m\cos(\alpha3)$$
$$GG1 = xL6m\cos(\alpha6) - yL6m\sin(\alpha6)$$
$$HH1 = yL6m\cos(\alpha6) - xL6m\sin(\alpha6)$$
$$II1 = -\cos(\alpha6)\cdot\sqrt{xR6m^2 - yR6m^2}$$
$$JJ1 = -\sin(\alpha6)\cdot\sqrt{xR6m^2 - yR6m^2}$$
$$KK1 = yNT1m\sin(\alpha T1) - xNT1m\cos(\alpha T1)$$
$$LL1 = -xNT1m\sin(\alpha T1) - yNT1m\cos(\alpha T1)$$
$$MM1 = -xNT1m\cos(\alpha T1) - yNT1m\sin(\alpha T1)$$
$$NN1 = yNT1m\sin(\alpha T1) - xNT1m\cos(\alpha T1)$$
$$OO1 = yFT2m\sin(\alpha T2) - xFT2m\cos(\alpha T2)$$
$$PP1 = -xFT2m\sin(\alpha T2) - yFT2m\cos(\alpha T2)$$
$$QQ1 = -xNT2m\cos(\alpha T2) - yNT2m\sin(\alpha T2)$$
$$RR1 = xNT2m\sin(\alpha T2) + yNT2m\cos(\alpha T2)$$
$$SS1 = xNT3m\cos(\alpha T3) + yNT3m\sin(\alpha T3)$$
$$TT1 = xNT3m\cos(\alpha T3) - yNT3m\sin(\alpha T3)$$
$$UU1 = T3\cdot\cos(\alpha T3) - xNT3m\cos(\alpha T3) + yNT3m\sin(\alpha T3)$$
$$VV1 = T3\cdot\sin(\alpha T3) - xNT3m\sin(\alpha T3) - yNT3m\cos(\alpha T3)$$

3.4. Obtained results

Based on the equations (12), (13), (14), (17), (18), (19) a program was written in a high-level programming language and the results are presented as following:

- in figure 5a are presented the positioning angles of the kinematic elements 1, 2, 3 and 6 against time and in figure 5b are presented the trajectories of the characteristic points A, J, D, B, C, H, L and M in relation to the fixed reference frame
- in figure 6a are presented the angular velocities of the kinematic elements 1, 2, 3 and 6 and in figure 6b are presented the variation diagrams of the characteristic points velocities D, J, C, H and L,.
- in figure 7a L are presented the angular accelerations of the kinematic elements 1, 2, 3 and 6 and in figure 7b are presented the variation diagrams of the characteristic points accelerations D, J, C, H and.

The unit system used in representing the diagrams is as follows: mm for coordinates, radians for angles and seconds for time.

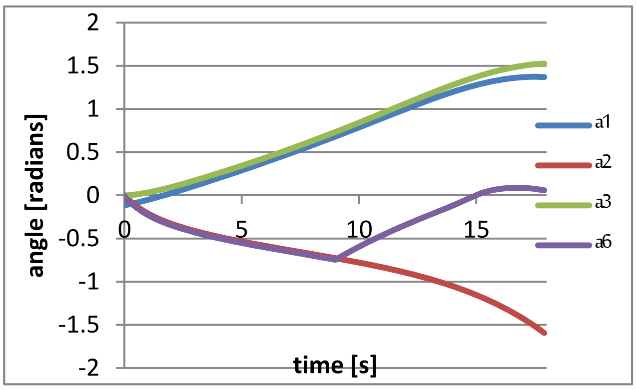

a)

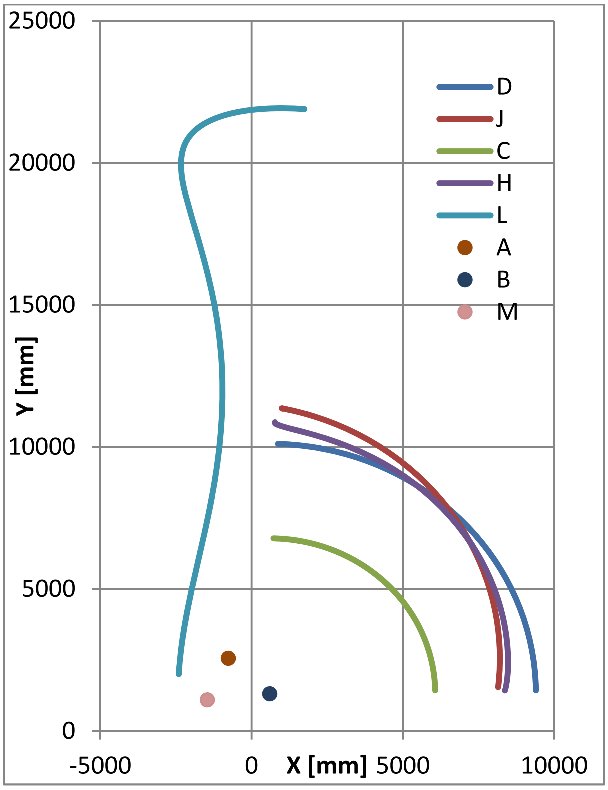

b)

Figure 5: Positions study; a) angles of elements; b) trajectories of characteristic points

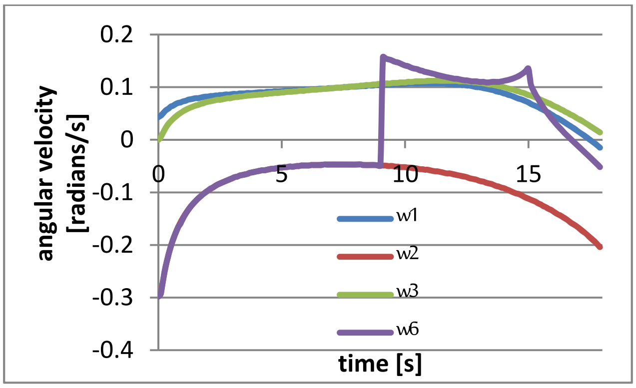

a)

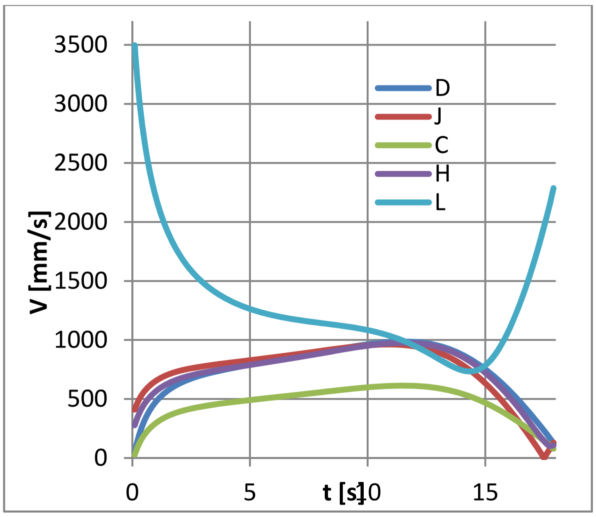

b)

Figure 6: Velocities study; a) angular velocities of elements; b) velocities of characteristic points

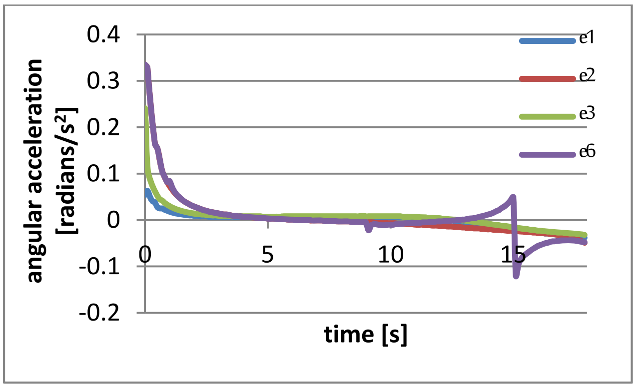

a)

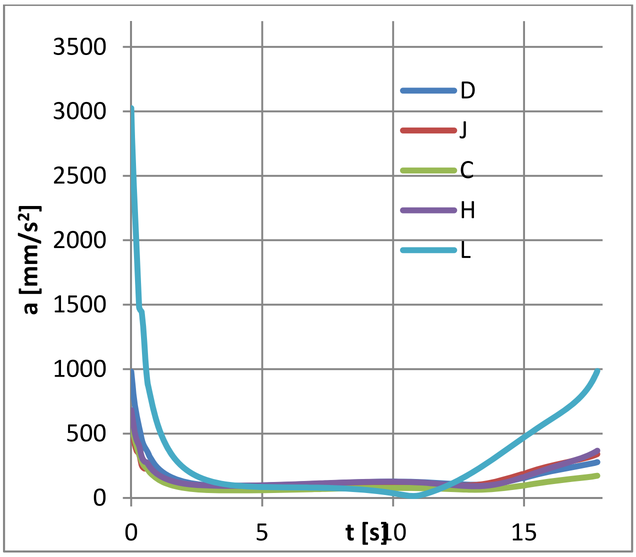

b)

Figure 7: Accelerations study; a) accelerations of characteristic points; b) angular accelerations of elements

4. CONCLUSIONS

- The chosen method in this paper for the kinematic study of the self-erecting mechanism of self-erecting cranes is applied separately for the 2 stages of the erection process because the number of elements that are working in motion transmission is different from one stage to the other.
- In this method cable type flexible kinematic elements are modelled, after their tensioning, in the shape of rigid bars.
- For every category of kinematic parameters positions, velocities, accelerations respectively, is written one equations system (12), (13), (14) or (17), (18), (19) and by solving these we obtain all the coordinates, velocities, accelerations, linear or angular, of all kinematic elements of the mechanism
- The positions study carried out on the mechanism of this type of crane is useful for determining the workspace required on the construction site for the erection of the crane.
- The results of the velocities and accelerations studies are required for determining the equation of motion and reactions in the joints of the erection mechanism of the self-erecting crane

REFERENCES

[1] *** - Commercial brochure MANITOWOC POTAIN Igo 10

[2] B. Fabien, "Analytical System Dynamics", Springer, (2009), ISBN-13: 978-0-387-85605-6

[3] E. J. Haug, "Computer aided Kinematics and Dynamics of Mechanical Systems", Allyn and Bacon, (1989) ISBN-13: 978-0-205-11669-0

Research and the Creation of Energy-Efficient Vibration Machines Based on the Stress-Strain State of Metal and Technological Environments

Nazarenko I.I. [1,*], Sviderski A.T. [1], Ruchinski N.N. [1], Dedov O.P. [1]
[1]Kyiv National University of Construction and Architecture, Kiev

Improving efficiency and reducing energy and metal vibrators is one of the key tasks of modern basic research and work based on a scientific idea, which is that the study of the mathematical model of the vibration system is determined by taking into account the internal structure of the subsystem as a single, despite their different physical nature and structure.

Proposed methodological approach makes it possible to comprehensively consider the energy components of the system, thus defining "comfortable" situation behavior of the system with maximum impact energy on the course of any process based on the use of vibration. The study model is represented as a combination of focused energy machine and environment based on the stress-strain state of metal vibrators and processed technological environments. The study model is represented as a combination of focused energy machine and environment based on the stress-strain state of metal vibrators and processed technological environments.

Proposed new design scheme vibrators with minimal energy consumption to perform the.

Keywords: *vibrosystem, distributed parameter system, contact vibration force, efficiency vibrating machines.*

Vibration machines are widely used in various industries to perform a significant amount of technological processes. A common feature of this class is the vibration effect on the material being processed, resulting in material changes its properties, thus providing an appropriate process.

Despite the different physical properties of vibrators and processed materials, they are subject to a single vibration process and in general mathematical descriptions of the systems are complex structures. Determination of physical and mathematical models of such systems is usually carried out separately for machinery vibration action and processed materials. Metal construction machines modeled usually solids with concentrated loads. Environment that is processed, depending on the model properties, manifested in a vibratory action: elastic, elastoplastic, viscoplastic. Difference between these models is the adoption of various laws dissipative characteristics: dry friction, amplitude-dependent friction, frequency-dependent friction.

The effectiveness of the vibration machine can be estimated given technology parameters and modes of vibrations on the processed material that can be realized by careful selection of the calculated mathematical models that adequately reflect the real movement of the vibration system.

In this paper we put forward a scientific idea, which is that in the study of a mathematical model of the process of the vibration system "machine - environment" should be determined by taking into account the internal structure of these subsystems as a single, despite their different physical nature and structure. This methodological approach makes it possible to consider a comprehensive energy components of the system, thus defining "comfortable" situation behavior of the system with maximum impact energy on the course of any process. The computational model is represented as a combination of focused energy machine and environment, provided that the maximum transfer of energy to perform technical operations sealing materials.

One of the main tasks of research vibrosystem have the choice of rheological model of the manufacturing environment. In rheology, there are two concepts: "perfectly elastic body" and "non-viscous liquids" [2]. In the first case, the tension is achieved immediately, and residual stress isotropic liquid is independent of the state of flow, so that the liquid is not able to build and maintain a voltage offset. Between the boundary condition of the bodies in nature there is a great variety of bodies of intermediate character, among which there are three idealized models of intermediate materials perfectly elastic body (Hook); ideally viscous fluid (Newtonian); perfectly plastic body (Saint Wenan). To describe the actual materials and apply simple ideal body that have only one physical and mechanical properties and are interconnected in parallel or sequentially. So were the models: Kelvin-Voigt, Maxwell, Bingham, Shvedova and others whose use due regard to certain properties [2].

Based on the physics of the process, such as compaction of concrete mix, changes its properties from the initial to the final state seal possible to obtain generalized (synthesized) model (Fig. 1), depending on the stage of consolidation and has some or other properties.

Ease of this structural model is that for the selected criteria (time compression, process rate and the ratio of the working body acceleration to the acceleration due to gravity) it is possible to describe the process and determine the resulted contact vibration force that is part of the workflow.

To determine the motion of the system, the environment model was introduced a system with distributed parameters as:

*Corresponding author: Kyiv National University of Construction and Architecture, Kiev, i_nazar@i.ua

$$\frac{\partial^2 u\,(z,\,t)}{\partial\, z^2} = \frac{\rho^*(z,\,t)}{E^*\,(z,\,t)} \cdot \frac{\partial^2 u\,(z,\,t)}{\partial t^2} \qquad (1)$$

Fourier coefficients for the function $u\,(z,\,t)$ - longitudinal movement of the current section of the column treated with fluctuations, this movement depends on the position (Z) of the cross section (coordinates) and the time t;

$\rho^*(z,\,t)$ - medium density;

$E^*(z,t)$ - complex modulus.

Law of deformation under stress environment

$$\sigma = E^*\varepsilon = (E' + iE'')\varepsilon \qquad (2)$$

where E', E'' - components of complex modulus;

i - imaginary unit, indicating a shift $\pi/2$ between E' and E'';

ε - deformation of the medium.

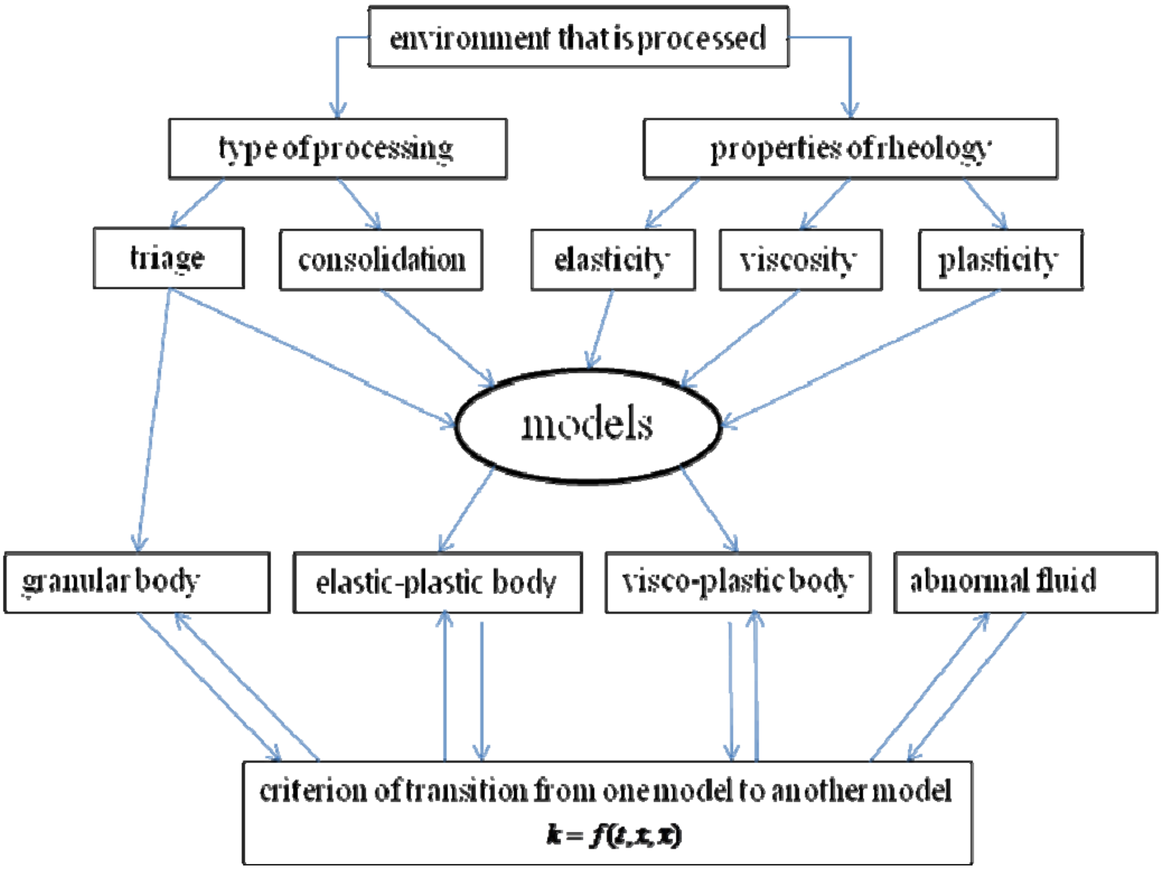

Fig. 1. Structural model of "environment - type of processing"

If we accept the general law of force application

$$F(t) = \sum_{n=-\infty}^{+\infty} F_n e^{in\omega t} \qquad (3)$$

where $\omega = 2\pi/T;\ n = \pm 1; \pm 2;\ F_n = F_n^* = \int_{-\tau/2}^{\tau/2} F(\tau)e^{-in\omega t}d\tau$,

then the solution of the original equation, according to the Fourier method can be represented by a function

$$U(z,t) = \sum_{n=-\infty}^{+\infty}\left(U_{1n}e^{k_n z} + U_{2n}e^{-k_n z}\right)e^{in\omega t} \qquad (4)$$

In the cited paper [1] defines a model for linear discrete systems vibrosistem. Currently, more and more are beginning to apply nonlinear systems [3]. To assess their effectiveness, consider unbalanced law of motion (Fig 2).

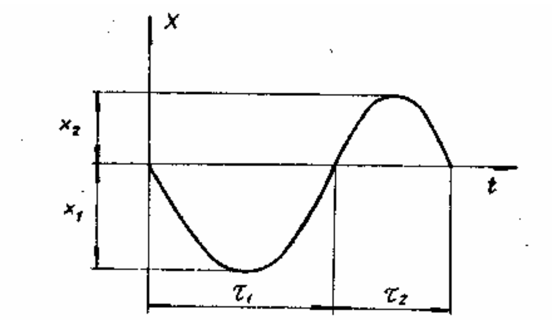

Fig. 2. The law of motion of the shock-vibration system

$$x^*(t) = \begin{cases} -x_1 \sin\left(\dfrac{\pi}{\tau_1} t\right), 0 \le t \le \tau_1; \\ x_2 \sin\left(\dfrac{\pi}{\tau_2} t\right), \tau_1 \le t \le \tau_2. \end{cases}, \qquad (5)$$

Here x_1, x_2 – amplitude of oscillation of the working bodies in the times of movement: T, τ_1, τ_2.

If the period features $x^*(t) \in T$, then it can be represented as a Fourier decomposition:

$$x^*(t) = \sum_{n=-\infty}^{+\infty} x_n e^{in\omega t}; \; \omega = 2\pi / T, \quad (6)$$

where x_n – Fourier coefficients for the function (6).

To find the reaction medium under the law of motion (5) use a slightly different approach than the harmonic mode. Define separate reactive and active components support environment for a visual representation of ideas and merits of the method. We start with the argument that the reactive component of the reaction medium can be represented according to Newton's law in the:

$$R_c = -m_c \ddot{x}, \quad (7)$$

where $\ddot{x}$ – acceleration of the contact zone.

On the other hand the power of resistance of the medium:

$$R_c = -ES \frac{\partial U}{\partial z}|_{Z=0}, \quad (8)$$

де $\frac{\partial U}{\partial z}|_{Z=0}$ – deformation of the contact material layer.

To determine the acceleration $\ddot{x}$ write the original wave equation with respect to acceleration:

$$\chi = \frac{\partial^2 u}{\partial t^2}|_{Z=0} = c^2(1+i\gamma)\frac{\partial^2 U}{\partial z^2}|_{Z=0}, \quad (9)$$

Comparing (7) and (8), and taking into account (9), we obtain:

$$m_c' = \frac{-ES\frac{\partial u}{\partial z}|_{Z=0}}{c^2(1+i\gamma)\frac{\partial^2 u}{\partial z^2}|_{Z=0}}, \quad (10)$$

Thus, the problem of the reactance, rather factor m_c', which has the dimension of mass determines reactance is reduced to finding the deformation $\frac{\partial u}{\partial z}$ and its derivative $\frac{\partial^2 u}{\partial z^2}$ on the boundary z = 0 in the implementation of the law of motion (see Fig. 2). From (4) we can determine the deformation

$$\frac{\partial u}{\partial z}|_{Z=0} = (\alpha_1 + i\beta_1)[U_{1n} - U_{2n}],$$

$$\frac{\partial u}{\partial z}|_{Z=h} = 0; \; U_{1n}e^{h(\alpha_1+i\beta_1)n} - U_{2n}e^{-h(\alpha_1+i\beta_1)n} = 0 \quad (11)$$

$$U_{1n}/U_{2n}e^{-2h(\alpha_1+i\beta_1)_n},$$

Then the derivative of strain:

$$\frac{\partial^2 u}{\partial z^2}|_{Z=0} = (\alpha_1 + i\beta_1)[U_{1n} - U_{2n}], \quad (12)$$

Now substitute the expressions (11) and (12) into (10) we have:

$$m_c' = -\frac{PS}{(\alpha_1+i\beta_1)} \cdot \frac{\sum_{n=-\infty}^{+\infty} nU_{2n}\left(\frac{U_{1n}}{U_{2n}} - 1\right)e^{in\omega t}}{\sum_{n=-\infty}^{+\infty} n^2U_{2n}\left(\frac{U_{1n}}{U_{2n}} + 1\right)e^{in\omega t}} = \frac{PS}{(\alpha_1+i\beta_1)} \cdot \frac{\sum_{n=-\infty}^{+\infty} nU_{2n}\left[1 - e^{2h(\alpha_1+i\beta_1)n}\right]e^{in\omega t}}{\sum_{n=-\infty}^{+\infty} n^2U_{2n}\left[1 - e^{2h(\alpha_1+i\beta_1)n}\right]e^{in\omega t}}, \quad (13)$$

Taking the boundary conditions: $\frac{\partial U}{\partial Z}|_{Z=h} = 0$ i $U|_{Z=0} = x(t)$ and expansion of the function (6), we obtain:

$$\sum_{n=-\infty}^{+\infty} U_{2n}\left[1 + e^{2h(\alpha_1+\beta_1)n}\right]e^{in\omega t} = \sum_{n=-\infty}^{+\infty} x_n e^{in\omega t},$$

Тоді

$$U_{2n} = x / \left[1 + e^{-2h(\alpha_1+\beta_1)n}\right], \quad (14)$$

Using (13) has a formula for determining m_c' the type of:

$$m_c' = \frac{PS}{(\alpha_1+i\beta_1)} \frac{\sum_{n=-\infty}^{+\infty} nx_n th[h(\alpha_1+i\beta_1)n]e^{in\omega t}}{\sum_{n=-\infty}^{+\infty} n^2 x_n e^{in\omega t}}, \quad (15)$$

Since it is known, що $\dot{x}^*(\gamma) = i\omega x^*(t)$; $\ddot{x} = -\omega^2 x^*(t)$ and assuming that the amplitude of the higher harmonics less than the first harmonic to the adopted law of motion (5), we obtain the following transformation: if $0 \le t \le \tau 1$

$$m_c' = \frac{2\rho Sth[h(\alpha_1+i\beta_1)\tau_1]}{(\alpha_1+i\beta_1)(\tau_1+\tau_2)}, \quad (16)$$

при $0 \le t \le \tau_1$

$$m_c' = \frac{2\rho Sth[h(\alpha_1+i\beta_1)\tau_2]}{(\alpha_1+i\beta_1)(\tau_1+\tau_2)}, \quad (17)$$

Separating the real part in the formulas (16) and (17), we find the true value m_c':

при $0 \le t \le \tau_1$

$$m'_c = \frac{2\rho S(\alpha_1 sh2\alpha_1 h + \beta_1 \sin 2\beta_1 h)\tau_1}{(\alpha_1^2 + \beta_1^2)(ch2\alpha_1 h + \cos 2\beta_1 h)(\tau_1 + \tau_2)}, \quad (18)$$

при $\tau_1 \le t \le T$

$$m'_c = \frac{2\rho S(\alpha_1 sh2\alpha_1 h + \beta_1 \sin 2\beta_1 h)\tau_2}{(\alpha_1^2 + \beta_1^2)(ch2\alpha_1 h + \cos 2\beta_1 h)(\tau_1 + \tau_2)}, \quad (19)$$

Comparing the dependences (18) and (19) with those found previously, we see that for $\tau_1 = \tau_2$ (symmetric law of motion) depending on the definition of reactance are equal. The accepted assumption of the superiority of the first harmonic of the following has made it possible to estimate the difference in analytical expressions for the reactive component in the implementation of the harmonic and shock-vibration (18) and (19) the nature of the movement. And the second. The ways of determining the reaction medium on the motion of the machine does not require finding the coefficients that characterize the boundary conditions in explicit form, which can significantly simplify making progress. Moreover, the opportunity to assess the continual movement of the medium in the implementation of complex laws of motion with preservation of wave processes. Now generalize the task to determine the reactance contribution in case more high harmonics and taking into account that each harmonic is also a phase φ. Then the expression (15) will have the

$$m'_c = \frac{\frac{ESk_{1n}}{\omega^2}\sum_{n=1}^{\infty}\sum_{n=1}^{\infty}(-n^2\omega^2)x_{1n}e^{i(n\omega t+\varphi_n)}th\frac{k_{1n}h}{n}}{\sum_{n=1}^{\infty}\sum_{n=1}^{\infty}(-n^2\omega^2)x_{1n}e^{i(n\omega t+\varphi_n)}}, \quad (20)$$

From (20) that depends m'_c on time t, the pulse shape (x_{1n}, φ_n), medium in height direction vibration h and frequency ω.

After transformation relationship (20) we obtain an expression for the equivalent reactance:

$$R_p = -m'_c \ddot{x}, \quad (21)$$

where

$$m'_c = \frac{\frac{ES}{\omega^2}\sum_{n=1}^{\infty}\sum_{n=1}^{\infty}(-n^2\omega^2)\sqrt{\mu^2+\nu^2}\cos\left[n\omega t + arctg\left(-\frac{dn}{\alpha n}\right)\right]\frac{N_{11}}{n}}{\sum_{n=1}^{\infty}\sum_{n=1}^{\infty}(-n^2\omega^2)\sqrt{\mu^2+\nu^2}\cos\left[n\omega t + arctg\left(-\frac{dn}{\alpha n}\right)\right]}$$

Here

$$N_{11} = \frac{\alpha_{11} sh(2\alpha_{1n}h) - \beta_{11}\sin(2\beta_{1n}h)}{ch(2\alpha_{1n}h) + \cos(2\beta_{1n}h)},$$

$$\alpha_{1n} = \frac{n\omega}{c_в \sqrt[4]{1+\gamma^2}}\cos\left[\frac{1}{2}arctg(-\gamma)\right], \quad (22)$$

$$\beta_{1n} = \frac{n\omega}{c_в \sqrt[4]{1+\gamma^2}}\sin\left[\frac{1}{2}arctg(-\gamma)\right].$$

Now it is possible to identify and resistance by taking the second part of equation (9)

$$R_a = iES\gamma\frac{\partial U}{\partial z}\Big|_{Z=0}, \quad (23)$$

Equating this force equivalent viscous drag force $F_c = b\ddot{x}$, we have:

$$\begin{aligned} R_a &= i\gamma ES\sum_{n=1}^{\infty}k_{1n}th(k_{1n}h)x_{1n}e^{in\omega t} = \\ &= \frac{ES\gamma}{\omega}\sum_{n=1}^{\infty}ink_{11}\omega th(k_{1n}h)x_{1n}e^{in\omega t}, \end{aligned} \quad (24)$$

By analogy with the method of the reactance (24) can be written as:

$$\begin{aligned} &\frac{ES\gamma}{\omega}\sum_{n=1}^{\infty}ink_{11}\omega th(k_{1n}h)x_{1n}e^{in\omega t} = \\ &= в_{экв.}\sum_{n=1}^{\infty}i`n\omega x_{1n}e^{in\omega t} \end{aligned}, \quad (25)$$

where the coefficient of equivalent resistance:

$$в_{экв.} = \frac{\frac{ES\gamma}{\omega}\sum_{n=1}^{\infty}\sum_{n=1}^{\infty}nk_{11}th(k_{1n}h)x_{1n}e^{in\omega t}i\omega}{\sum_{n=1}^{\infty}in\omega x_{1n}e^{in\omega t}} = \frac{\frac{ES\gamma}{\omega}\sum_{n=1}^{\infty}\sum_{n=1}^{\infty}nk_{11}th(k_{1n}h)x_{1n}e^{in\omega t}}{\sum_{n=1}^{\infty}nx_{1n}e^{in\omega t}}. \quad (25)$$

By carrying out the procedure for the separation of the real and imaginary parts of (25), we obtain coefficient of resistance the medium:

$$в_{экв.} = \frac{\frac{ES\gamma}{\omega}\sum_{n=1}^{\infty}n\sqrt{\mu_n^2+\nu_n^2}\cos\left[n\omega t + arctg\left(-\frac{dn}{\alpha n}\right)\right]N_{11}}{\sum_{n=1}^{\infty}n^2\sqrt{\mu_n^2+\nu_n^2}\cos\left[n\omega t + arctg\left(-\frac{dn}{\alpha n}\right)\right]} \quad (26)$$

The dependences (21) and (26) define reactive and active resistance fluctuations taking into account the higher harmonics. It is possible to use the coefficients m'_c, $в_{экв.}$ in the equations of motion of hybrid dynamical systems, which include a focus settings of the operating parameters of the processed and distributed environments and to evaluate the effectiveness of machine design.

The main indicator of the effectiveness of vibration is energy that is transferred from the treated environment working body. Thus, knowing the energy of the contact zone and the nature of the medium in any subsequent layer, we can assess the ability of the environment to accept certain levels of energy depending on the vibration parameters.

The formula works in the contact zone for one oscillation period $T = \frac{2\pi}{\omega}$:

$$A_k = \int R_0^a \dot{x}\sin\alpha_0\cos\omega dtdt \quad (27)$$

where R_0^a - the contact force (reaction medium), reflecting a dynamic equilibrium of forces; $\dot{x}$ - speed of fluctuations in contact zone; α_0 - angle between the directions of displacement of the contact zone and the reaction medium.

Taking the law of motion (see Fig. 2), provided that $\omega = \frac{2\pi}{t_n}$ - average frequency of the process R_H, R_P - the amplitude of the corresponding reactions in the process, we write the expression of useful energy ΔW, which refers to a unit volume V:

$$\Delta \overline{W}_{num} = \frac{\Delta W}{V} = \frac{R\Delta x t_H}{\rho S \Delta x t_H} = \frac{R\Delta x \omega_{cp}}{2\pi\rho S\alpha}, \qquad (28)$$

ρ, S - density and cross-sectional area of the processed medium;

$$\Delta W_{num} = \frac{1}{t_H}\int_0^{t_H} R dt \frac{\omega_{cp}}{2\pi\rho S\alpha} = \frac{\omega^2{}_{cp}}{4\pi^2\rho S\alpha^2}\int_0^{\alpha t_H} R dt. \qquad (29)$$

Change the contact force can be represented by the dependence:

$$R(t) = -R_H \sin\left\{\frac{\pi t}{tn(1-\alpha)}\right\} \qquad (30)$$

From (30) it follows that $\alpha = 1/2$, $R_H = R_P$ the motion and the investigated layer is quasiharmonic. When taking into account (30), expression (29) is transformed to the form

$$\Delta W_{num} = \frac{\omega^2{}_{cp}}{4\pi^2\rho S\alpha^2}\int_{t_H(1-\alpha)}^{t_H}\left\{-R_H \sin\left[\frac{\pi t}{t_H(1-\alpha)}\right]\right\}dt = \qquad (31)$$
$$= \frac{R_H \omega_{cp}(1-\alpha)}{\pi^2\rho S\alpha^2}\cos^2\left[\frac{\pi}{2(1-\alpha)}\right].$$

Examining (31) we obtain the extremum condition:

$$tg\left[\frac{\pi}{2(1-\alpha)}\right] = \frac{(\alpha-2)(1-\alpha}{\pi d}. \qquad (32)$$

Solving the transcendental equation (32), we find that the maximum energy transfer for a given law of variation of (30) is possible with $\alpha = 1/3$. Thus, while providing value, obtained asymmetry signal maximum possible impact created the conditions for the maximum value of the energy goes into compressing the investigated volume of the mixture.

Conclusion

1. Proposed a method for the study of joint motion of the vibration machine - environment based on consideration of the stress-deformation state in the contact zone and the conditions of interaction between the two subsystems.
2. Establishing laws depending vibratory motion study on the analytical determination of stresses and deformations in the contact zone machine – environment.
3. Defined performance criteria based on vibro synergistic approach of maximum energy transfer to the environment, which is processed

References:

1. Nazarenko I.I., Sviderski A.T., Ruchinski N.N., Dedov O.P., Design of New Structures of Vibro-Soching Building Machines dy Internal Characteristics of Oscillating Sistem, Hfvy Vfchinery HM 2011, B session, pp. 1-4, 2011.
2. Назаренко І.І. Прикладні задачі теорії вібраційних систем (2-е видання) / Назаренко І.І. – К.: Видавничий Дім "Слово". 2010. – 440 с.
3. Назаренко І.І. Вібраційні машини і процеси будівельної індустрії / Назаренко І.І. – К.:КНУБА, 2007. – 203 с.

Top Tier Technology in Subway Tunnelling Using a Mechatronic Driving Shield

Ioan Bărdescu[1*], Amelitta Legendi (s) [2]
[1+2] Faculty of Technological Equipment, Department of Construction Machinery and Mechatronics
Technical University of Civil Engineering Bucharest-Romania

The paper presents comparatively three underground drilling technologies for subway circular tunnels using three driving shields: D_1-6,5 m walking Semi-mechanized one; D_2-6,55 m electro-hydraulic Mechanized one; D_3 6,5 m Mechatronic one using performant control means (laser, computer, Wolfram knives…). In each of these cases apart, the paper makes references to some assemblies and components, and submits the values of the essential parameters.

Keywords: Subway Tunnel, Mechatronic drilling shield, Underground drilling technology, Mechatronics, Shield pilot

1. INTRODUCTION

The shield accomplishes underground drilling for *subway circular tunnels*, as well as the gallery coating with precast *concrete tunnel arches*. The technology consists also in the soil transportation through the drift and its discharge at the end of the tunnel, this last technological activity being done using grab equipment on excavator.

There are introduced three underground drilling technologies for subway circular tunnels using three driving shields: D_1-6,5 m *walking Semi-mechanized* one (generation 1); D_2-6,55 m *electro-hydraulic Mechanized* one driven by classical means (generation 2); D_3 6,5 m Mechatronic one using performant control means (generation 3).

For the mechatronic shield an *application* is presented, namely at Bucharest-Romania subway, the 5th artery, *the 1st section, Eroilor-Drumul Taberei*.

2. TECHNOLOGY WITH D 6,5 m WALKING SEMI-MECHANIZED SHIELD

The semi-mechanized technology symbolized as PTM5-858-76, was *projected and applied in Romania* in 1976 for the Bucharest subway. The paper's first author was the project manager in charge. [1]

2.1. D 6,5 m Semi-mechanized shield

This shield consists in 3 essential subassemblies: *main body-knife cover* assembled at the front side in the drilling sense and *erector*, pressing ring assembled at the rearwards (Figure 1).

The shield disposes of a *self-propelling system*, electric, with hydraulic jack (32 pcs.) disposed on the erector's outline, each jack developing a 1500 N force. The soil is manually dug, using some *mechanisms, sustained*, and drilling tools carrier (hydraulic hammer, bit, chisel, shovel…). The two technological activities of hydraulic propulsion and manual assisted drilling gave the shield's name *semi-mechanized*.

The underground advancing system gave its name of *mole*, used in practice.

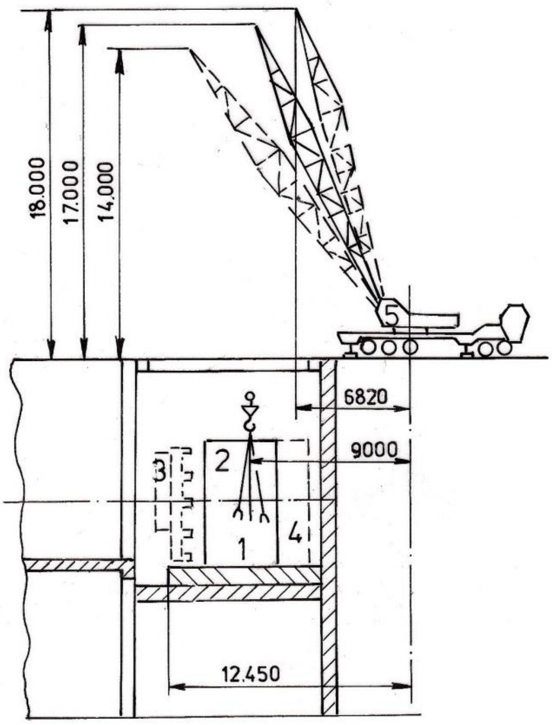

Figure 1: Half assemblage of the central body, (with hydraulic press)

1. central body inferior part; 2. central body superior part; 3. pressing ring -erector; 4. knife; 5. 143 t arm auto-crane on tyres

2.2. Technological solutions for other subassemblies and elements

During the subway tunnel projecting and drilling process many problems occurred claiming a great number of *technological solutions* to be studied. Some of these solutions and the resolution ways are presented below.

- *Over-sized transport* and launching in the subway well tunnel;
- Due to the oversizing and heavy weighing problems , but also due to the absence of large capacity mechanized means, the technological solution for transport, launching and assembling of *the two halves at the main body* shield cover in the well were established and implemented;
- Some *raising devices* for all subassemblies and component elements were projected;

*Romania, București, str. Târgu Neamț, nr. 22, sector 6, Bl. 27, Sc. 1, Et. 5, Ap. 31, cod. 062059, OP 74, e-mail: amelitta.legendi@gmail.com.

- M*etallic sledges* for the shield's mounting support were projected (6 pcs × 6 m length);
- In order to assemble *the two halves of the main body* some 135° spinning devices were projected in the well;
- *The launching well* was technological conceived for 8,5 m width and 22 m length (Figure 2).

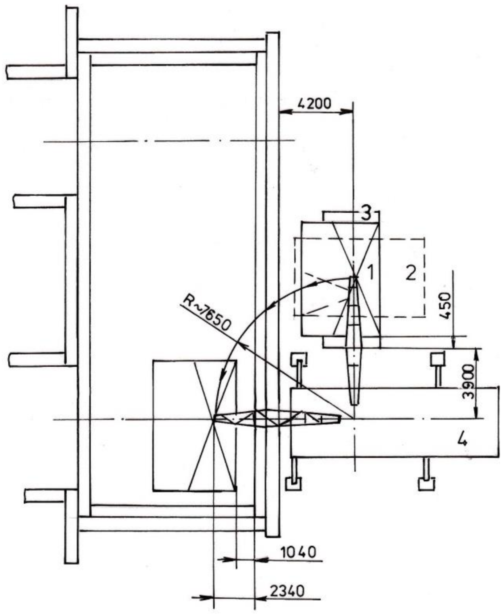

Figure 2: Launching central body in the well, inferior part
1. *central body inferior part*; 2. *central body superior part rotated in the launching position after being raised from the trailer; 3. 60 t trailer; 4. 143 t tired auto-arm-crane*

- A *mechanized crushing system for the drilled soil*, transportation, processing and positioning the tunnel *arches* in the erector's area for assembly was conceived;
- A 143 t mobile arm crane for transportation and launching the two halves of the body-cover in the well was used.

2.3. Means to direct the shield advancing process

The shield's trajectory displacement was ensured by high precision *optical instruments*.

The trajectory adjustments, when necessary, were done with *hydraulic presses*.

A classic solution was conceived to aim *to stop the shield's spinning during the drilling process*.

3. TECHNOLOGY WITH D 6,55 M ELECTRO-HYDRAULIC MECHANIZED SCHIELD

The PTM 15-634-76 technologic project treated solutions regarding the transportation-launching in the tunnel well of an electro-hydraulic mechanized shield having a much greater mass (380 t) than the semi-mechanized one, establishing so more efficient solutions using either portal cranes especially projected, or large capacity mobile arm-cranes. In this project, the paper's first author was the project manager in charge to. [2]

3.1. Shield's main subassemblies

● *The main body*, also named *shield cover*, imposed following up on the Romanian designer, that transportation and launching in the well is to be realized using the single casting main body (Figure 3). From several studied solutions, only two were developed: the first, two portal cranes 2×115 t-12, the second, a 300 t arm mobile crane, stalled on a special working deck. The first solution was adopted, being more efficient, both technically and economically.

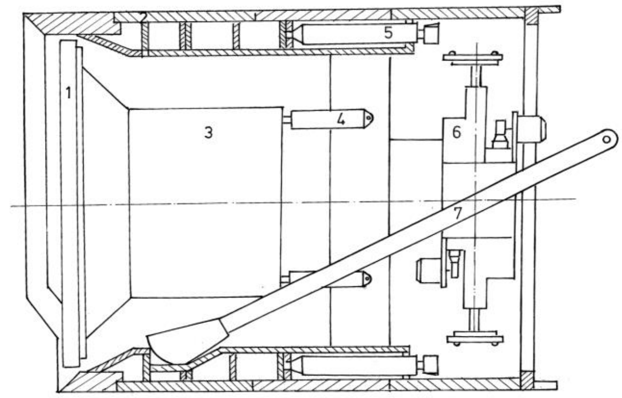

Figure 3: Electro-hydraulic mechanised shield:
1. cutting head; 2. main body-cover; 3. cutting head rotating mechanism; 4. cutting head advance presses; 5. shield's advance presses; 6. erectile mechanism; 7. drag elevator

● *The cutting head* consists in a rigid frame, fixed on the rotation mechanism. 12 *press plates* and 12 *oscillating knives* are fixed on the frame. The knife's cutting edges are manufactured of 12 plates of high-alloyed steel.

● *The erector* raises the tunnel arch on the railway truck and fixes it on the outline, thus building a circular tunnel.

● *The mechanism for fixing, raising and assembling* the tunnel arches is composed of a rigid frame on which two rings are independently spinning, each being driven by a hydraulic cylinder. The tunnel arches are picked up from the car of the sledge train, is *raised* and is *laid* on the gallery's outline, thus building the gallery's strength structure.

● *The rotating mechanism* of the cutting head consists in *8 hydraulic linear motors*, with double effect.

● *The advance mechanism* of *the cutting head* is composed of 4 *hydraulic motors* with double effect, which are pushing the cutting head and its rotating mechanism on a 550 mm distance. The cutting head displacement speed: 20-40-60 mm/min.

● *The shield's pushing mechanism*. The advancement of the whole shield is assured by 32 hydraulic linear motors with double effect, rigidly assembled in the central cover.

● *The drag elevator*. The soil dislocated by the mill's knives is laid in the cutting head tank, raised up and then falls down on the conveyor belt that carries it out the shield.

3.2. The sledge train

The sledge train is composed of *5 metallic sledges* towed one to another (4 pcs×7,5 m + 1 pc×2,5 m). The whole train of sledges, *40 m long*, is *towed by the shield* through two *hydraulic cylinders*. The train displacement is realised *by sliding* on *a rolling tracks with reels.*

The first 4 sledges carry on above a belt conveyor each in order to evacuate the resulting soil after drilling. *Within sledges* there are *two rolling tracks* serving the displacement of the railway trucks for the *tunnel arches transport.* (Figure 4)

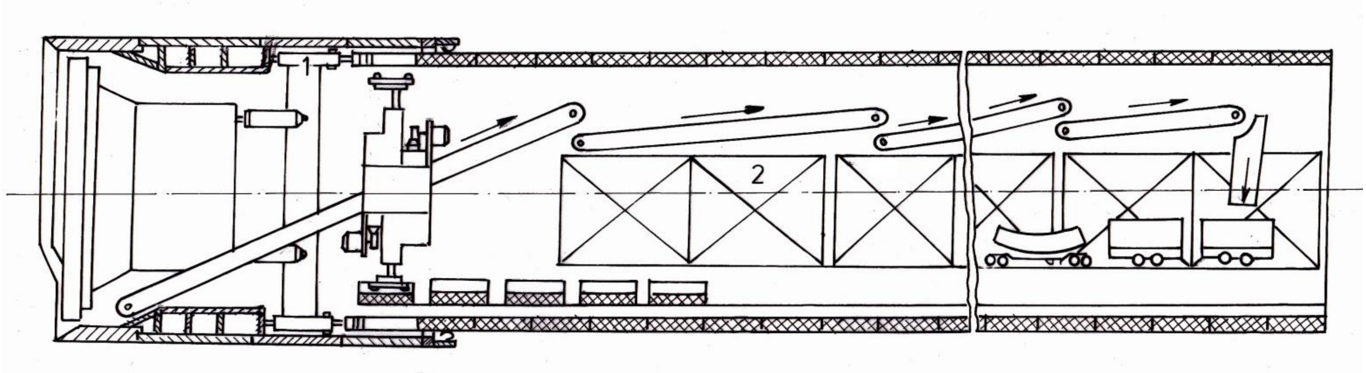

Figure 4: Technological system of mechanized electro-hydraulic shield D 6, 55 m
1. shield-assembly; 2. Sledge-train

The largest part of the hydraulic and electric gear is placed on the sledge-train (Control panel, hydraulic motors, electric transformers, and electric cables necessary for the installation’s functioning).

4. TECHNOLOGY WITH MECHATRONIC SHIELD D = 6,5 M

4.1. State of the art technology, in-line formation, terminology

This state of the art drilling technology is mostly made out of *multinational operational teams* organized in working units. These teams are equipped with mechatronic shields of generation 3 and special machinery, complementary, for *drilling* technologies in-tunnel *transport* and *soil-lifting* at the surface, where the end of the subway gallery can be found as well. The hereby presented technology has imposed and adopted a specific terminology, in theory and in practice, for instance, shield pilot, *shield cockpit nacelle*, pilot directly conducted team, complementary works teams.

The *mechatronic shield* moves, through sliding, on an auxiliary field made up from metallic sledges. (Figure 5)

Figure 5: Mechatronic shield working on the subway section Eroilor-Drumul Taberei

The pilot’s working space is a *cockpit nacelle* situated on the outside, on the left-hand side of the shield. The pilot manoeuvres the shield, assisted by *five persons* with precise determined tasks, established through a tunnel drilling procedure with mechatronic shield (Figure 6).

Figure 6. pilot cockpit nacelle, D 6,5 mechatronic shield

The soil that has been dug out is moved towards the end of the gallery, where it is lifted by a grab equipped excavator and loaded in tip lorries. The tip lorries transport the dirt in a deposit authorized by the municipality.

4.2. Application at the Bucharest, Romania subway

The particular application refers to the 5^{th} artery Drumul Taberei – Pantelimon, with a total length of 6 km, and only the 1^{st} section respectively, Eroilor – Drumul Taberei [4].

The constructing firm brought in 2 mechatronic shield named Saint Varvara and Saint Filofteia.

First tunnel of the artery, Academia Militară – Orizont, was dug *by Saint Varvara shield* within 15 days (25^{th} September 2013- 10^{th} November 2013). The official drilling record was set at 27m of tunnel/ day. On 16^{th} of April 2014 the new record was set at 43m of tunnel/day.

The team of the shield pilot is a *multinational one* comprised of Romanians, Italians, Portuguese and Spaniards. The shield pilot is an Italian named Nicodeno Giovani. The manager of the team is of Japanese nationality.

Underground, in the working space, besides the 5 persons that assist the pilot, some 12 other persons are assisting the shield and another 30 persons responsible for miscellaneous activities. The works usually take place 6 days a week, with a compulsory break of one day for technological inspection (Sunday). The work is usually done in 4 shifts of 6 hours each. The temperature inside the tunnel is of 32°C.

Figure 7: Cutting head D 6.5m mechatronic shield, used at Eroilor-Drumul Taberei thoroughfare

1. main body; 2. cutting head; 3. knives mill

4.3. Performance and mechatronic elements

Knives of *Wolfram steel* as component element of the shield’s cutting head.

Laser rays to protect the shield against deflection from the initial imposed track.

Computer for the centralized carrying out of all commands and the correlation of all technological component activities, *planimeter, altimeter*.

The tunnelling shield is disposing of the most modern *technical equipment*.

5. TECHNOLOGIES USED FOR THE FRIST SECTION OF THE EROILOR-DRUMUL TABEREI SUBWAY

The Bucharest subway system construction started in 1976 and was partially opened in 1979. In November 2014 it is the 35th anniversary since the first subway started working. The drilling of the subway galleries was achieved with the *semi-mechanized shield* designed and manufactured in Romania. Moreover, the technologic project for transport, the launching in the well, and also the University subway station completion, in closed fosse, were designed by the Construction Institute in Bucharest [1 și 2].

5.1. Technologies with mechatronic shield TBM

For building the 5th artery of the Bucharest subway system, *the most novel technology of subway gallery excavation* is used. This is done by employing similar mechatronic shields as the ones used in the New-York subway system construction.

The D 6,5 mechatronic shield, also known as a super-shield, is mostly referred to by the construction engineers as TBM (Tunnel Boring Machine) or “Mole”.

Due to an international constructing tradition of naming the employed mechanisms with Saints name, the shields were named accordingly *Saint Varvara* and *Saint Filoftea* respectively. A third shield that is going to be used will be named *Saint Parascheva*. These Saints are said to be the guardians of both the shields and the labour workers.

5.2. The gallery section Eroilor-Râul Doamnei

First section where the excavation has begun is Eroilor-Râul Doamnei with a length of over 6 km. The mechatronic shield, or the super-shield, having a total diameter of d = 6,5 m, has gone underground at the *AcademiaMilitară –Răzoare* subway station, having a spatial orientation facing Drumul Taberei (Figure 8).

Figure 8. Mechatronic shield launched in the subway station-well Academia Militară

1. main-body cover; 2. cutting head rotating mechanism; 3. cutting head knives

First drillings were done at the Academia Militară subway station, facing Orizont direction.

The two schields, Saint Varvara and Saint Filoftea respectively, were launched in the well-station at Academia Militara subway station using *tyred arm-cranes* of large capacity. Each shield has 2 lifting eyes on both sides of the metallic cover, where the lifting devices using steel cables and hooks can manouvre the shield. The stances of the lifting eyes are calculated depending on the *center of gravity of the shield's wieght* (Figure 9).

Three shield related technological activities can be distinguished, which contribute to the completion of the subway tunnel.

- The construction of the *pushing devices* and that of the *basis* for installing the *primary tunnel arching concrete rings* for encasing the drilled galleries;
- *The fliting of the shield in thrusting position through the structure wall*, approximately 50 cm;
- The activation of the assembly of *mechanisms* for drilling and for installing the prefabricated concrete tunnel arches.

5.3. Subassemblies, mechanisms, and systems for the mechatronic shield TBM.

The most important subassemblies and mechanisms are highlighted [6].

- *Cutting knives carrier* (8 in total);
- *Main body* shield cover;
- *Group of hydraulic cylinders* for forming the *lead-shield*;
- System of permanent *sustainability* of the *excavation field*;

Figure 9. Two mechatronic shields launched at Academia Militara subway well-station, in a ready-to-drill stance of the two circular tunnels.

1. subway station; 2. & 3. shields; 4. Shield attaching device; 5. Lifting-eyes

- *Erector*-grabbing, lifting and positioning mechanism for prefabricated concrete tunnel arches, 6 pieces on a tunnel ring;
- Mechatronic systems for controlling the shield lead-direction drilling parameters: *planimeter, altimeter, computer* and electronic components that assure a *precise guidance of the trajectory*, as well as immediate *corrections* of the shield’s stance;
- *Electro-mechanic equipment* for *injecting filling and sealing material on the extrados of the tunnel arching ring,* which is created during the excavation and fixing process.
- Compressed-air equipment and associated components for pressuring the excavation chamber and for both the inner and outer communication of this chamber; this way the pressure is consistently maintained for sustaining the working place.

The cutting head of the mechatronic TBM shield has 8 knife-teeth of large dimensions and are made out of Wolframm steel.

The 2 shields are functioning at the same time in the two tunnels, however there’s a *distance delay* of 500m between the two of them.

5.4. The sledge train

The mechatronic shield executes the drilling alongside the sledge train which is comprised of *6 sledges towed to one another*. The sledges are represented under the form of metallic constructions with latticed members [2].

The whole sledge train is towed by the shield using two *hydraulic cylinders*. *The movement of the sledge train* is realised through *gliding* on a *rolling way using reels.* For maintaining the train on its track and for assisting it on curves, the sledges are laterally guided by *reels*.

The first four sledges are provided with a belt above them so that it would facilitate the evacuation of the drilled soil.

Inside the sledges, at the lower part, *two rolling ways are provided,* on which both the *barrows for transporting the arches* and the barrows for evacuating the drilled soil are circulating.

On the sledge train, again at the lower part, most of the *hydraulic and electric device* can be found, which is vital for the proper functioning of the installation: Hydraulic motors, control panels, electrical transformers, and electric cables.

The hydraulic installation is positioned on the 1st and 2nd sledge, and on the 3rd sledge the *electronic installation with its accessories* are positioned [6].

5.5. Essential shield parameters

For a partial comparison between the TBM mechatronic shield and the mechanized electro-hydraulic shield (EHS), some values are presented in the table below:

Table 1: Shield parameters

No.	Technic Parameter	UM	Shield type	
			TBM	EHS
1	Excavation Diameter	m	6,57	6,55
2	Shield length (cutting mill, cover, erector)	m	7,450	10,45
3	Shield total weight	t	376	380
4	No. shield’s pushing cylinders	Pcs.	2×1 Pcs.	2×16 Pcs.
5	Pushing force	MN	42,6	
6	Cutting head travel	mm	550	550
7	Speed	m/day	20-40	30
8	Shield & sledge train length	m	70	50
9	Installed power	kW	2000	2150

6. TECHNOLOGIES, MECHANISMS AND DEVICES FOR TRAILERS AND CRANES

6.1. Launching wells for single casting shields.

Regarding the construction of the launching well, the *trailer positioning platforms* and the *keying cranes*, it is indicated that the shield should only be launched in areas where *subway station are under construction.*

The dimensions of the well are on average 12 m long ×8,6 m width x 18 m depth.

6.2. Working platforms at the launching spot

For trailers, special platforms are made, which would have the capacity of absorbing both the weight of the trailer and the weight of the shield. Concerning the single casting shields with trailer 400 t (105 t+380 t).

For cranes, a special *keying* platform is made, which would have the capacity of absorbing the charge of the *crane*'s weight and also the shield's weight; in this case, it is compulsory that the maximum charge that can be sustained on a keying platform is calculated, which should also be taken into account when the keying platform is designed. The working platforms should, as much as possible, be conceived in modulated construction.

At the same time, the working platform at the launching spot should insure the positioning of the equipment, the radius of manoeuvring and entering at the launching well of the technological train; the launching well is also prone to different buttresses and reinforcements.

6.3. Transport means and cranes

The transportation of the single casting shield weighing 380 tons was studied in two ways:

- *A trailer with a total charging capacity of 400 tons*;
- *Two trailers with a capacity of 280 tons each, under coupled working*, T 2×280 t.

For single casting shield transport, special placing devices are mad in order to better place them on the trailers, and to assure the safety of the shield throughout the transport.

The cranes needed for launching the single casting shield of 380 t were studied in three ways:

- Launching with a single mobile arm-crane with a lifting capacity of 400 t;
- Launching with two mobile arm-cranes with a lifting capacity of 300 t each, symbolized MB 2×300 t;
- Launching with two *portal cranes*, with a total lifting capacity of *230 t*; each portal crane has two tackles of 115 t each with a distance of 12 m between its legs, symbolized MP×115t-12 m.

The launching of the 380 t single casting, mechatronic TBM1 shield was done in Academia Militară subway station, București, with two mobile arm-cranes 2×300 t.

The transportation of the single casting shield was done with two trailers 2×280 t.

The lifting mechanism with steel cables was hung by 4 lifting-eyes (2×2) (Figure 9).

6.4. Grabbing and lifting mechanisms

The mechanisms ensuring the grabbing, manoeuvring, transportation and the launching of the shield are project based executed, depending on the *weight and the form of each sub-assembly.*

The special lifting mechanisms are conceived to insure cert stability of the burden, and of the crane, respectively.

A cumbersome problem is that of establishing a precise centre of gravity of the shield's weight and of the other technological subassemblies.

Regarding the single casting mechanized shield the *more significant charge* is on the *cutting head*, where the oscillating knives can be found (over 50 t), the rotation and lead mechanism of the shield (over 100 t).

Lifting eyes/ ears. The lifting mechanism grips onto the shield's lifting ears. They can be placed either one ear on each of the two longitudinal sides of the shield, seldom used case, or *two ears on each of the longitudinal sides of the shield*. The technological solution provided with two lifting ears on each side is the most common used method, since it is the most secure one. In this case, *the placement of the lifting ears was done towards the front side of the shield*, a distance of under 3.5 m between the lifting ears being imposed.

The uplifting of the shield is done using *closed beams*, which insures the uniformity of efforts for each *lifting mechanism* and has the advantage obtaining surcharge only on the vertical axis.

For a proper grip of the shield onto the closed beams, steel cables are most commonly used, otherwise chains are used.

The ears or lifting eyes are usually attached to the shield through soldering; after the shield's launching the ears are being cut off for fear not to hamper the normal trajectory and functioning of the shield.

7. LIFTING AND WELL-LAUNCHING TECHNOLOGY FOR SINGLE CASTING SHIELD WITH TWO COUPLED PORTAL CRANES MP2×115T-12 M

In many countries with traditional subway projects, the most common method of well-launching a single casting shield is by using two portal cranes.

At the mechanized electro-hydraulic shield EHS 6,55m and 380t (Table 1) a *portal crane* was designed 2 × 115 t-12 (Figure 10) [2].

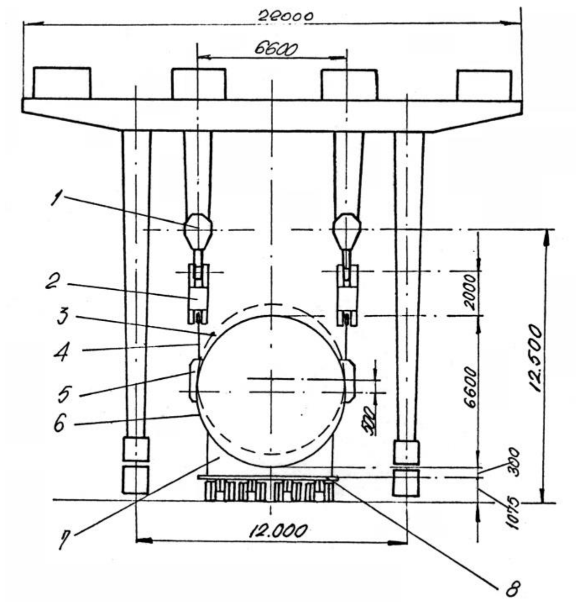

Figure 10. Portal crane 2×115t-12 m when taking over a single casting shield off a trailer for well-launching.

1. lifting mechanism muffle; 2. Lifting beam ; 3. Shield lifted by 500 mm; 4. Cable ear-device; 5. Soldered ear; 6. Single casting shield on trailer; 7. Placement device for shield on trailer; 8. Large capacity trailer.

The two portal cranes of 230 tons each, when working coupled the lower part is *being stiffened up* with a *closed beam* griped onto with two bolts on each crane. This *enhances the stability of the cranes* and afterwards it ensures a quick decoupling.

The rolling ways of the portal cranes are positioned depending on the axis of the shield, and with the longitudinal axis of the trailer, respectively.

All technologies, mechanisms and devices presented in the 6^{th} section, were realized through the CTM 15-6343-77 project. [2]

The access and positioning platforms for the trailers, under the alternative of well-launching the shield through portal cranes hold more advantages, than the alternative of using arm-cranes.

Amongst other advantages, it has to be mentioned that: it holds a shorter well-launching time span, larger stability, certain safety conditions when lifting and mounting the shield, quick mounting and un-mounting and simple transport, since it is constructed through subassemblies of lighter weights, which in turn requires transportation and lifting means of smaller capacities.

CONCLUSIONS

(1) The presented subway solutions do not exclude one another because some of them are economical efficient in drilling tunnel-channels for piping, road transport routes ashore, etc.

(2) The passenger and merchandise transport solutions are efficient and safe.

(3) The subway projects realized up today are a real challenge in improving hereinafter the technological execution means and mainly those driving the shield during the technological process.

(4) The shield works with more associated machinery, such as: Sledge train, Extrados material injection equipment, etc.

(5) For the activation of the shield, launching-wells need to be executed, working platforms, lifting mechanisms, etc.

(6) As alternative for the mobile arm-cranes, the portal cranes are proposed, holding more advantages from both an economic and technological point of view.

REFERENCES

[1] I. Bărdescu, project and collective manager, "Technologic assembling project with mobile arm cranes for launching in the tunnel's well the D 6,5 m semi-mechanized shield ", The Institute of Constructions Bucharest, Faculty of Technological Equipment, 1976.

[2] I. Bărdescu, project and collective manager, "Study of technological solutions in launching the mechanized shield with portal crane CTM 15-6343-76", The Institute of Constructions Bucharest, Faculty of Technological Equipment, 1977.

[3] Cox, Rey and Morris Neil, Field, James, "The 3×7 wonders of the ancient, medieval and modern world", Officina Nova, Club of Hungarian Book Printing House, Budapest, 2000, ISBN 9635472714.

[4] M.P. Pârvu, "Whithin the subway entrails Drumul Taberei-Bucharest", Evenimentul Zilei Journal, 11 November 2013.

[5] *** http://www.click.ro, "Train capsule pushed ahead throughout magnetic attraction", 13 April 2014.

[6]*** http://www.b365.ro/metrorex-super-cartitele-incep-sa-foreze-in-tunelurile-magistralei-5-de-metrou-de-la-1-iulie_190640

Free Vibrations of the Planar Gantry-like Structures

Vlada Gašić*, Aleksandar Obradović, Nenad Zrnić
University of Belgrade, Faculty of Mechanical Engineering, Belgrade (Serbia)

This paper deals with eigenfrequencies of distributed-parameter system within the form of gantry-like structure with cantilever part. The individual members of the structure-framework are assumed to be governed by the transverse vibration theory of Euler-Bernoulli beam. It is obtained postulation of frequency equation while solutions are obtained numerically with in-house software, for several cases of structures. Also, it is done finite element postulation of the gantry-like structure as discrete-parameter system for analyzing the free undamped vibrations. Thus, it stands for two folded presentation. It is done verification of postulated algorithms.

Keywords: Gantry crane, Free vibration, Modal analysis

1. INTRODUCTION

Structural dynamics is always needed when complete behaviour of structure has to be analyzed. It is very important for design of bridges, buildings and high-performance cranes. Nowadays, we have a permanent tendency towards constant improvement of performances of machines and systems in general, including their increase in size [1]. However, the mass and the stiffness of the structure are not always in suitable proportion which requires good understanding of structural dynamic characteristics.

The orientation here is towards gantry-like structures as at gantry cranes. Especially, this group of cranes are important for container terminals because of importance of container transportation in world economy.

Figure 1: Rail mounted gantry crane at container terminal

From the main producers of the container RMG cranes (Konecranes, Liebherr, Kuenz) one can found the current level of main performances, Table 1.

Table 1: RMG container crane performances

Span	22...70 m
Cantilever	up to 21 m
Height	up to 28 m
Capacity	up to 50 t

The first step in structural dynamic is always modal analysis. Approximate expressions for fundamental symmetric and antisymmetric frequencies of symmetric portal frame can be obtained buy the Reyleigh method [2], useful for simplifying the vibration formulation of beams. Laura, Filipich [3] dealt with the determination of the fundamental frequency in the case of antisymmetric modes of a frame elastically restrained against translation and rotation, carrying concentrated masses. Blevins [4] presented formulas for determination of fundamental frequencies for symmetric portal frame, for first symmetric and first antisymmetric mode, according to frequency equation presented with trigonometric-hyperbolic functions. Furthermore, frequencies of non-regular frames were investigated by Bolotin, Kiselev [5,6], with slope-deflection method. But, even that process of gaining frequency equation was defined, finding solutions were difficult because of its transcendental nature involving trigonometric and hyperbolic functions. Nowadays, state-of-the-art computer routines enable solution of frequency equation of in-plane vibrations of structural system of portal crane i.e. non-regular frame. Such routine is given here symbolically with software Mathematica, Wolfram. Also, nowadays, modal analysis with commercial FEM software are widely used for determination of frequencies of various structures [7]. The most common structural dynamics problems include vibration excitation, blast and shock, wind and earthquake loads. In vibration excitation analysis one is primarily concerned with avoiding resonance, usually at a few frequencies. In this case, modal analysis is generally used to calculate a small number of eigenfrequencies, e.g. vibrations of machine parts and machine foundations.

This paper deals with analysis of in-plane vibrations of the structural system of gantry-like structures with cantilever part, which is improvement of the model given in [8]. First, it is obtained frequency equation for distributed-parameter system of the structure and then the eigenfrequencies and mode shapes with finite element model in basic form. Solutions are verified against each other.

2. MATHEMATICAL MODEL

The main structural parts of gantry-like structure are main girder, pier leg and shear leg. The main girder has span part of length L and cantilever part with length Lp. The different heights for legs, H,h, are used solely for generalization of the framework, despite the fact that in

*Corresponding author: vgasic@mas.bg.ac.rs

almost all the cases legs of the gantry cranes are mounted on the same level. The geometric set of this postulation is given on Figure 2a.

Presented model is the planar framework which assumes that main structural parts are beams having uniform properties along their lengths. For other types of structures it can be applied with proper idealization of elements. The individual members of the frame, Figure 2, are assumed to be governed by the transverse vibration theory of an Euler-Bernoulli beam. Neglecting the axial and shear deformation and rotatory inertia effects can be done because of known structural behaviour of gantry cranes. Individual elements are made of same material (steel).

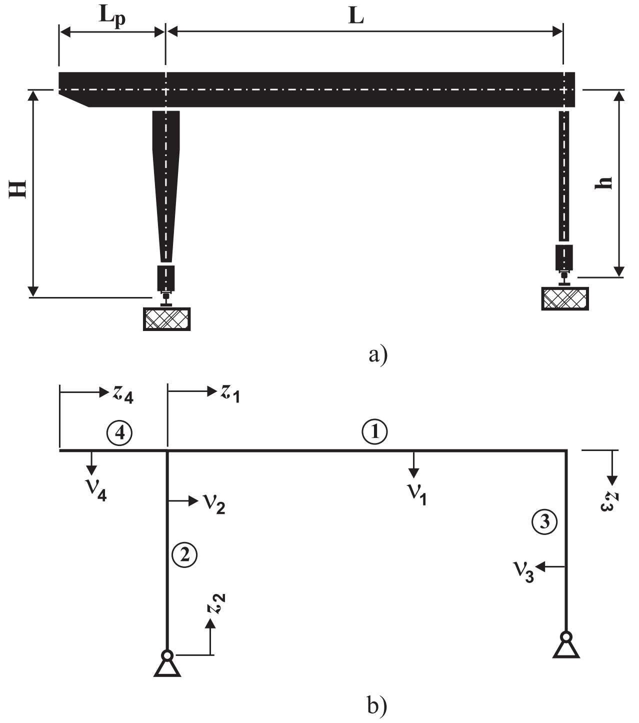

Figure 2: Mathematical model of gantry-like structure as distributed-parameter system

The partial differential equation for free transverse undamped vibrations of each element has the following form

$$\frac{\partial^2 v_i}{\partial t^2}+\frac{EI_i}{\rho A_i}\frac{\partial^4 v_i}{\partial z_i^4}=0 \quad (i=1,2,3,4) \tag{1}$$

with postulation as

$$v_1=v_1(z_1,t)=Z_1(z_1)\cdot T(t) \quad 0\le z_1\le L \tag{2}$$

$$v_2=v_2(z_2,t)=Z_2(z_2)\cdot T(t) \quad 0\le z_2\le H \tag{3}$$

$$v_3=v_3(z_3,t)=Z_3(z_3)\cdot T(t) \quad 0\le z_3\le h \tag{4}$$

$$v_4=v_4(z_4,t)=Z_4(z_4)\cdot T(t) \quad 0\le z_4\le L_p \tag{5}$$

where A_i represent section area, I_i is moment of inertia, ρ is density and E is Young's modulus.

The mode shapes are presented throughout Krylov functions

$$Z_i(z_i)=G_i\mathbf{S}(k_iz_i)+B_i\mathbf{T}(k_iz_i)+C_i\mathbf{U}(k_iz_i)+D_i\mathbf{V}(k_iz_i)$$
$$(i=1,2,3,4) \tag{6}$$

The time function is presented as

$$T(t)=X\cos(\omega t)+Y\sin(\omega t) \tag{7}$$

where circular frequency is

$$\omega=k_i^2\sqrt{\frac{EI_i}{\rho A_i}} \quad (i=1,2,3,4) \tag{8}$$

One can formulate the boundary conditions for the model under study as following.

The pinned joint at element 2 gives

$$Z_2(0)=0 \tag{9a}$$

$$-EI_2Z_2^{''}(0)=0 \tag{9b}$$

The pinned joint at element 3 gives

$$Z_3(h)=0 \tag{9c}$$

$$-EI_3Z_3^{''}(h)=0 \tag{9d}$$

Free end of element 4 gives

$$-EI_4Z_4^{''}(0)=0 \tag{9e}$$

$$-EI_4Z_4^{'''}(0)=0 \tag{9f}$$

The joints of elements 1 and 3, along with joints of element 1, 2 and 4 give following

$$Z_1(L)=0 \tag{9g}$$

$$Z_1^{'}(L)=Z_3^{'}(0) \tag{9h}$$

$$-EI_1Z_1^{''}(L)=-EI_3Z_3^{''}(0) \tag{9j}$$

$$Z_1(0)=0 \tag{9k}$$

$$Z_4(L_p)=0 \tag{9l}$$

$$Z_2^{'}(H)=Z_1^{'}(0) \tag{9m}$$

$$Z_4^{'}(L_p)=Z_1^{'}(0) \tag{9n}$$

$$-EI_1Z_1^{''}(0)=-EI_2Z_2^{''}(H)-EI_4Z_4^{''}(L_p) \tag{9o}$$

$$Z_2(H)=-Z_3(0) \tag{9p}$$

Finally, most important condition is equilibrium of shear forces at the top of the legs with inertial force developed in the main girders elements by sideway motion which provides the condition

$$-(\rho A_1L+\rho A_4L_p)\ddot{v}_3(0,t)=EI_2v_2^{'''}(H,t)+EI_3v_3^{'''}(0,t) \tag{9r}$$

which becomes

$$(\rho A_1L+\rho A_4L_p)Z_3(0)\omega^2=EI_2Z_2^{'''}(H)+EI_3Z_3^{'''}(0) \tag{10}$$

Afterwards, one may obtain a set of 16 homogenous system of equations with unknown guantities, G_i, B_i, C_i, D_i (i=1,2,3,4) and non-trivial solution of determinant of coefficients must be equal to zero.

From (8) one may express frequency parameters of every element with

$$k_i=k_1\sqrt[4]{\frac{A_iI_1}{A_1I_i}} \tag{11}$$

and set up the postulation of frequency equation which is very complex because of combination of special functions and numerous parameters such as A_1, A_2, I_1, L, H ....

The form as

$$f(k_1)=0 \tag{12}$$

don't allows analytical solution but only numerical one. Here, it is solved with state-of-the-art software Mathematica. Upon the finding the solutions for k_1 one may calculate the frequencies with (8) and

$$f=\frac{\omega}{2\pi} \tag{13}$$

2.1. Numerical results

It is determined first 3 frequencies for the adopted cases of gantry-like structures. Main geometric parameters are set with L and H, while it is assumed that L_p=0,25 L and that H=h. Due to the fact that design of main girder is first step in design of a crane, the static characteristics of main girder are used as start point. They are determined with design recommendations for flexible and rigid case. The cantilever part is the same as span part of main girder.

The variation of parameters are given with following expressions

$$\alpha = \frac{I_1}{I_2}, \beta = \frac{I_1}{I_3}, \gamma = \frac{A_1}{A_2}, \delta = \frac{A_1}{A_3} \tag{14}$$

The results are given in Table 2.

Table 2. First 3 frequencies of the adopted gantry-like structures

L = 30 m **H = 18 m**				I_1= 0.024 m^4 A_1= 0.07 m^2			I_1= 0.05 m^4 A_1= 0.09 m^2		
α	γ	β	δ	**f₁** [Hz]	**f₂** [Hz]	**f₃** [Hz]	**f₁** [Hz]	**f₂** [Hz]	**f₃** [Hz]
1	1	1	1	1.57	7.58	15.69	2.00	9.65	19.97
1	1	10	2	1.12	6.49	10.34	1.43	8.27	13.16
10	2	10	2	0.69	5.25	10.11	0.88	6.68	12.87
10	2	50	4	0.54	5.09	6.64	0.68	6.48	8.45

L = 40 m **H = 20 m**				I_1= 0.05 m^4 A_1= 0.09 m^2			I_1= 0.13 m^4 A_1= 0.11 m^2		
α	γ	β	δ	**f_1** [Hz]	**f_2** [Hz]	**f_3** [Hz]	**f_1**[Hz]	**f_2** [Hz]	**f_3** [Hz]
1	1	1	1	1.45	5.76	12.57	2.12	8.41	18.34
1	1	10	2	1.03	4.92	10.26	1.50	7.18	14.96
10	2	10	2	0.65	3.90	9.67	0.95	5.70	14.10
10	2	50	4	0.51	3.77	6.70	0.74	5.51	9.81

L = 45 m **H = 18 m**				I_1= 0.07 m^4 A_1= 0.1 m^2			I_1= 0.18 m^4 A_1= 0.14 m^2		
α	γ	β	δ	**f_1** [Hz]	**f_2** [Hz]	**f_3** [Hz]	**f_1** [Hz]	**f_2** [Hz]	**f_3**[Hz]
1	1	1	1	1.74	5.40	12.08	2.36	7.34	16.38
1	1	10	2	1.23	4.61	11.52	1.67	6.25	15.67
10	2	10	2	0.81	3.58	9.86	1.13	4.88	13.66
10	2	50	4	0.63	3.44	9.11	0.85	4.66	12.34

3. FINITE ELEMENT MODEL

The previous chapter offers free vibrations of the gantry-like structure as distributed-parameter system. Even that results are the closest to the *exact* solutions, one may respect the fact that discrete-parameter system analysis is widely accepted approach for this kind of problems [9]. It is especially needed for structures with complex form which can't be easily simplified to SDOF system or beam models. The gantry-like structures as in this paper are the end form for consideration with distributed-parameter system. Any additional structural parts would demand discrete-parameter analysis.

Here, the discrete model of the gantry-like structure is shown at Figure 3, with same geometric set as previous.

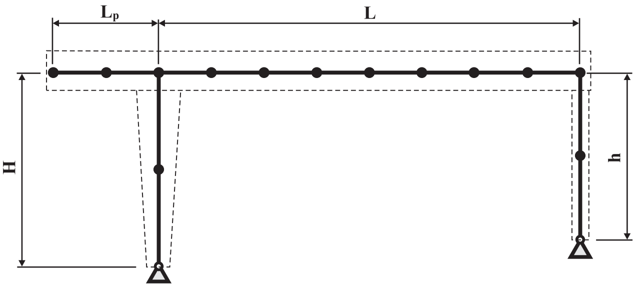

Figure 3: Discrete-parameter system of gantry-like structure

The main girder is divided into the 10 elements and legs into 2 elements, each. This can be described as enough level of discretization.

It is used the finite element method, in basic form, for postulation of the discrete-parameter system. The FE model is shown in Figure 4 and is consisted of 15 nodes and 14 elements. The length of elements (l_n) are the same for same construction part.

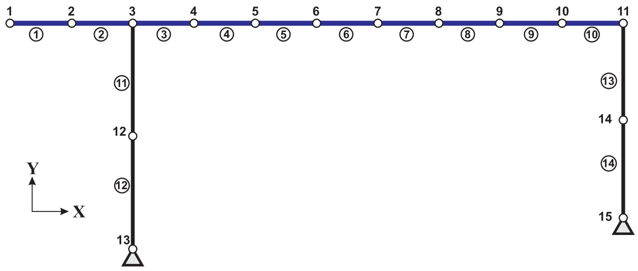

Figure 4: FE model of the gantry-like structure

Every node has 3 DOF's, horizontal displacement, vertical displacement and planar rotation. This is starting postulation for creating property matrices.

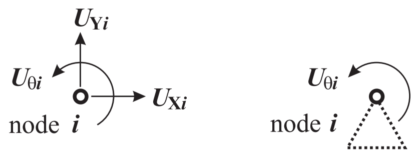

i = 1-10, 12,14 $\quad$ i = 13,15

Figure 5: Nodal displacements

The restrained translations of pinned joints are not included in postulation of problems of any kind.

Thus, vector of structural displacements becomes

$$\mathbf{U} = \{U_{X1} \quad U_{Y1} \quad U_{\theta 1} ... U_{\theta 12} \quad U_{\theta 13} ... U_{\theta 14} \quad U_{\theta 15}\}^T \tag{15}$$

The discretization of the framework (Fig. 4) is done by using FEM, with plane-frame elements [10].

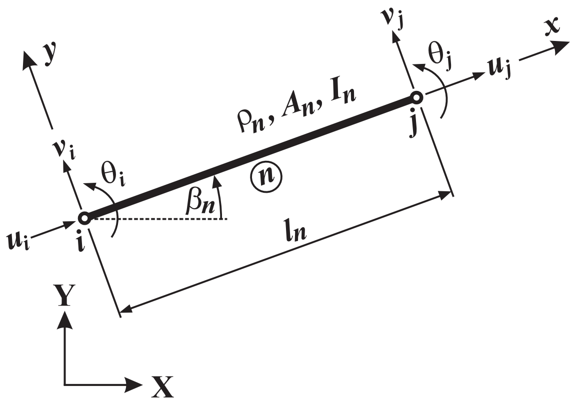

Figure 6: The local and global system of plane-frame element

This postulation gives following matrices, stiffness and mass matrix, respectively, in element local coordinate system.

The element stiffness matrix can be obtained by

$$\mathbf{k}_n = \begin{bmatrix} \frac{EA_n}{l_n} & 0 & 0 & -\frac{EA_n}{l_n} & 0 & 0 \\ 0 & \frac{12EI_n}{l_n^3} & \frac{6EI_n}{l_n^2} & 0 & -\frac{12EI_n}{l_n^3} & \frac{6EI_n}{l_n^2} \\ 0 & \frac{6EI_n}{l_n^2} & \frac{4EI_n}{l_n} & 0 & -\frac{6EI_n}{l_n^2} & \frac{2EI_n}{l_n} \\ -\frac{EA_n}{l_n} & 0 & 0 & \frac{EA_n}{l_n} & 0 & 0 \\ 0 & -\frac{12EI_n}{l_n^3} & -\frac{6EI_n}{l_n^2} & 0 & \frac{12EI_n}{l_n^3} & -\frac{6EI_n}{l_n^2} \\ 0 & \frac{6EI_n}{l_n^2} & \frac{2EI_n}{l_n} & 0 & \frac{6EI_n}{l_n^2} & \frac{4EI_n}{l_n} \end{bmatrix}$$

The element mass matrix is

$$\mathbf{m}_n = \frac{\rho_n A_n l_n}{420} \begin{bmatrix} 140 & 0 & 0 & 70 & 0 & 0 \\ 0 & 156 & 22l_n & 0 & 54 & -3l_n \\ 0 & 22l_n & 4l_n^2 & 0 & 13l_n & -3l_n^2 \\ 70 & 0 & 0 & 140 & 0 & 0 \\ 0 & 54 & 13l_n & 0 & 156 & -22l_n \\ 0 & -13l_n & -3l_n^2 & 0 & -22l_n & 4l_n^2 \end{bmatrix}$$

The transformation matrix to global coordinate system is

$$\mathbf{T}_n = \begin{bmatrix} \cos\beta_n & \sin\beta_n & 0 & 0 & 0 & 0 \\ -\sin\beta_n & \cos\beta_n & 0 & 0 & 0 & 0 \\ 0 & 0 & 1 & 0 & 0 & 0 \\ 0 & 0 & 0 & \cos\beta_n & \sin\beta_n & 0 \\ 0 & 0 & 0 & -\sin\beta_n & \cos\beta_n & 0 \\ 0 & 0 & 0 & 0 & 0 & 1 \end{bmatrix}$$

3.1. Overall stiffness matrix

The global stiffness matrices for the main girder elements are the same as local stiffness matrices, while leg elements are obtained with transformation matrix for angle of $3\pi/2$, which give

$$\mathbf{K}_n = \mathbf{k}_n \text{, } n\text{=1-10} \tag{16}$$

$$\mathbf{K}_n = \mathbf{T}_n{}^T \mathbf{k}_n \mathbf{T}_n \text{, } n\text{=11-14} \tag{17}$$

Adjustment with all the DOF's and with combination of element stiffness matrices give [11]

$$[K_{st}]_{45x45} = \sum_1^{14} \mathbf{K}_n \tag{18}$$

Overall stiffness matrix of the structure, which includes only free structural displacements, is now obtained with

$$\mathbf{K}_{st} = [K_{st}]_{41x41} \tag{19}$$

3.2. Overall mass matrix

Similarly, the global mass matrices of elements are obtained as

$$\mathbf{M}_n = \mathbf{m}_n \text{, } n\text{=1-10} \tag{20}$$

$$\mathbf{M}_n = \mathbf{T}_n{}^T \mathbf{m}_n \mathbf{T}_n \text{, } n\text{=11-14} \tag{21}$$

Adjustment with all the DOF's give

$$[\mathbf{M}_{st}]_{45x45} = \sum_1^{14} \mathbf{M}_n \tag{22}$$

Overall mass matrix of the structure becomes

$$\mathbf{M}_{st} = [\mathbf{M}_{st}]_{41x41} \tag{23}$$

3.3. Free undamped vibrations

The governing equation of the free undamped vibration of the MDOF system is known as [12]

$$\mathbf{M}_{st}\ddot{\mathbf{U}}+\mathbf{K}_{st}\mathbf{U}=0 \tag{24}$$

where $\ddot{\mathbf{U}},\mathbf{U}$ are acceleration and displacement vectors of the system, respectively.

Frequency equation becomes

$$\left\|\mathbf{K}_{st}-\omega^2\mathbf{M}_{st}\right\|=0 \tag{25}$$

which gives a set of 41 circular frequencies for the system, while frequency is calculated as

$$f_i=\frac{\omega_i}{2\pi} \tag{26}$$

The given algorithm is also programmed in software Mathematica.

4. VERIFICATION

Verification of the given algorithm is done with finite element model in correlation with mathematical model with distributed-parameter system.

The adopted FE model has following characteristics: L=30 m, H=18 m, I_1=0,024 m^4, A_1=0,07 m^2 and other characteristics are done to comply with (14), following $\alpha=1$, $\beta=10$, $\gamma=1$ and $\delta=2$. It is obtained frequencies of f_1=1,122 Hz, f_2=6,45 Hz, f_3=10,386 Hz, f_4=15,43 Hz ...

For this case on can found only slight differences from the suitable case from Table 2.

Figure 7 shows the first 2 mode shapes of this structure.

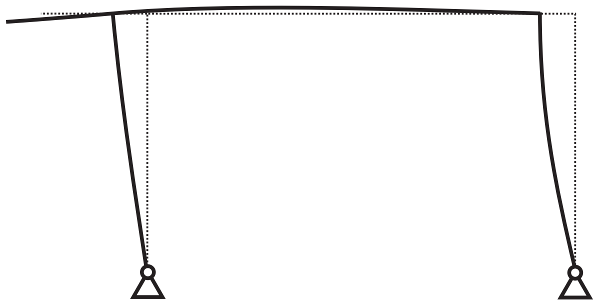

a)

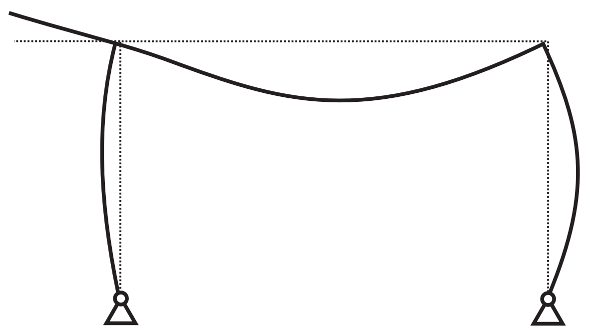

b)

Figure 7: a) 1st mode shape, f_1=1,12 Hz, b) 2nd mode shape, f_2=6,45 Hz

The character of mode shapes from Figure 7 describe the typical behaviour of gantry-like structure where 1st mode represent sideway motion of the structure and 2nd mode represent bending of the main girder and legs.

5. CONCLUSION

The paper is dealing with modal analysis of gantry-like structures. First part is devoted to modelling of these structures as distributed-parameter systems. It is obtained frequency equation for free vibrations and solution is obtained with numerical software for several cases.

The main advantages of this approach are:

- the results are closest to *exact* solutions of eigenfrequencies
- it is easy to track the influence of any structural parameter on natural and other frequencies of the structure

The biggest drawback is cumbersome mathematical expressions with special functions and graphically oriented tracking of solutions, but this should be the cost for gaining the *exact* solutions. Consideration of only transversal vibrations is quite suitable approximation for this kind of structures.

The second part deals with title problem with finite element method in basic form. With plane frame elements one can set the model of the framework as discrete-parameter MDOF system. The modal analysis is performed with basic matrix algebra.

The main advantages are:

- simple mathematical apparatus is needed to postulate the problem
- this approach is practically unavoidable when response of structures due to general dynamic loading is needed
- it is more flexible to the changes of framework element characteristics

The basic drawback is that the influence of some structural parameter is not so *visible* on eigenfrequencies analysis and require more detailed consideration.

Authors deliberately didn't show the modal analysis with commercial FEM software. The 2 mentioned concepts in this work serve as starting point of analysis of dynamic behaviour of gantry-like structure as well for validation of modal analysis results performed with commercial FEM.

ACKNOWLEDGEMENTS

This work is a contribution to the Ministry of Science and Technological Development of Serbia funded project TR 35006.

REFERENCES

[1] Zrnić N.Đ., Gašić V.M., Bošnjak S.M.,"Dynamic responses of a gantry crane system due to a moving body consisted as moving oscillator", Archives of Civil and Mechanical Engineering (2014), http://dx.doi.org/10.1016/j.acme.2014.02.002 (Article in press)

[2] FILIPPOV, A.P., "Vibration of deformable systems" (in Russian), Moscow, 1970

[3] FILIPICH, C.P., LAURA, P.A., "In-plane vibrations of portal frames with end supports elastically restrained against rotation and translation", Journal of Sound and VIbration, pp 467-473, (1987)

[4] BLEVINS, R., "Formulas for natural frequency and mode shape", New York, 1979

[5] BOLOTIN, V.V., "The dynamic stability of elastic systems", San Francisco, (1964)

[6] KISELEV, V.A., "Dynamics and stability of structures" (in Russian), Third edition, Moscow, 1980

[7] Liu, G.R., Quek, S.S.: "The finite element method, a practical course", Butterworth-Heinemann, 2003.

[8] Gašić, V., Obradović, A., Petković, Z., "Mathematical modelling of the in-plane vibrations of portal cranes with FEM verification", Machine Design 2009, Novi Sad, Serbia, pp. 121-126,(2009)

[9] PAZ, M., LEIGH, W., "Structural dynamics: theory and computation", Fifth edition, Kluwer, (2004)

[10] Spyrakos, C., Raftoyiannis, J., "Linear and nonlinear finite element analysis in engineering practice", Algor Publishing Division, (1997)

[11] Przemieniecki, J.S., "Theory of matrix structural analysis", McGraw-Hill, NY, (1985)

[12] Clough, R.W., Penzien, J., "Dynamics of structures", McGraw-Hill, NY, (1993)

[13] http://www.wolfram.com/mathematica/

Optimization of the Box Section of the Main Girders of the Bridge Crane for the Case of Placing the Rail in the Middle of the Top Flange

Goran Pavlovic[1*], Milomir Gasic[2], Mile Savkovic[2], Radovan Bulatovic[2], Nebojsa Zdravkovic[2],
[1]Colpart d.o.o., Belgrade (Serbia)
[2]Faculty of Mechanical and Civil Engineering Kraljevo, University of Kragujevac, Kraljevo (Serbia)

This paper considers the problem of optimization of the box section of the main girder of the bridge crane for the case of placing the rail in the middle of the top flange. Reduction of the girder mass is set as the objective function. The method of Lagrange multiplier was used as the methodology for approximate determination of optimum dependences of geometrical parameters of the box section. The criterion of strength were applied as the constraint function. The analysis of the optimization results and the solutions was the basis for recommendations which are significant for designers during construction of cranes.

Keywords: Box section, Bridge crane, Lagrange multiplier, Optimization, Strength

1. INTRODUCTION

The main task in the process of designing the carrying structure of the bridge crane is determination of optimum dimensions of the main girder box section. The mass of the main girder has the largest share in the total mass of the bridge crane, so it is very important to perform its optimization in order to reduce the total costs of manufacturing the whole carrying structure. That is the reason why the selection of the optimum shape and geometrical parameters which influence the reduction of mass and costs of manufacturing is the subject of research of a lot of authors ([2], [3], [5], [7], [8], [9], [10], [11], [12], [14], [15], [16], [17] and [18]).

Most authors set permissible stress or two constraint functions: permissible stress and permissible deflection as the constraint function.

The analysis of cost structure for manufacturing metal structures made in [2], showed that the participation of material costs in the total costs is the largest (30-73) %, and that the other costs are lower**.**

Having in mind all the above mentioned results and conclusions, the aim of this paper is to define optimum values of geometrical parameters of the box girder cross-section that will lead to the reduction of its mass.

2. MATEMATHICAL FORMULATION OF THE OPTIMIZATION PROBLEM

The task of optimization is to define geometrical parameters of the cross section of the girder as well as their mutual relations, which result in its minimum area.

Minimization of the mass corresponds to minimization of the volume, i.e. the area of the cross section of the girder, where the given boundary conditions must be satisfied. The area of the cross section primarily depends on: height and width of the girder, thickness of plates and their mutual relations.

The optimization problem defined in this way can be given the following general mathematical formulation:
minimize $f(\boldsymbol{X})$ subject to $g(\boldsymbol{X}) \le 0$.

where:
$f(\boldsymbol{X})$ the objective function,
$g(\boldsymbol{X}) \le 0$ the constraint function,
$\boldsymbol{X} = \{x_1, ..., x_D\}^T$ represents the design vector made of D design variables. Design variables are the values that should be defined during the optimization procedure.

In this paper optimization for the criterion of strenght:

$$g = \sigma_{\max} - \sigma_k \le 0 \qquad (1)$$

where:
$\sigma_{\max}$ - the calculation stress,
σ_k - the permissible stress.

The Lagrange function is defined in the following way:

$$\Phi = A + \lambda \cdot g \qquad (2)$$

$$\frac{\partial \Phi}{\partial b} = 0; \frac{\partial A}{\partial b} + \lambda \cdot \frac{\partial g}{\partial b} = 0 \qquad (3)$$

$$\frac{\partial \Phi}{\partial h} = 0; \frac{\partial A}{\partial h} + \lambda \cdot \frac{\partial g}{\partial h} = 0 \qquad (4)$$

$$\frac{\partial \Phi}{\partial \lambda} = 0; \Rightarrow g = 0 \qquad (5)$$

3. OBJECTIVE AND CONSTRAINT FUNCTIONS

3.1. Objective function

The objective function is represented by the area of the cross section of the box girder (Fig. 1). The paper treats two optimization parameters *(h, b)*. The wall thicknesses t_1 and t_2 are not treated as optimization parameters for the purpose of simplification of the procedure. Their values were adopted in accordance with the recommendations of crane manufacturers [6].

$$A(h,b) = f(h,b) = \frac{2}{s} \cdot (e \cdot b \cdot h + h^2) \qquad (6)$$

where:
$e = \frac{t_1}{t_2}$ - the ratio between thicknesses of plates at the flange and at the web,

* Corresponding author: Colpart d.o.o, Kirovljeva 5, 11030 Belgrade, Serbia, goranthepavlovic@yahoo.com

$s = \frac{h}{t_2}$ - the ratio between the height and thickness of the plate at the web,

$k = \frac{h}{b}$ - the ratio between the height and width of the girder.

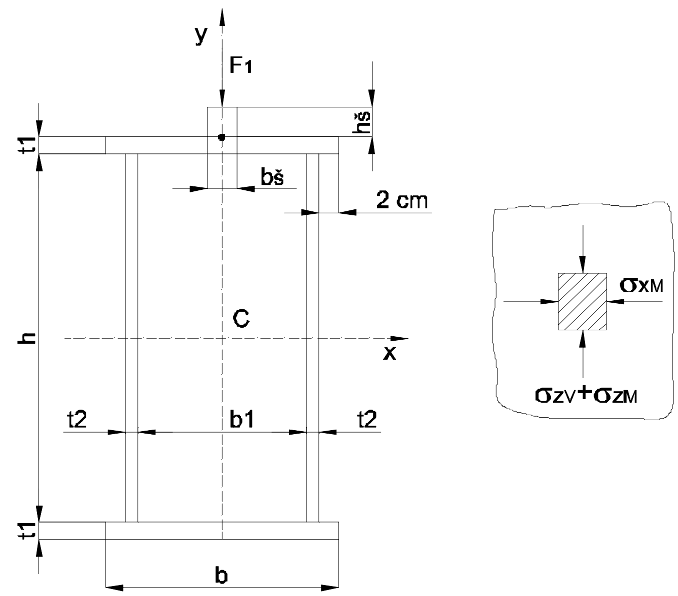

Figure 1: The box section of the main girder of the bridge crane

To know the optimal value of the ratio between the height and width of the girder *k* is of particular significance for the designer, especially in the initial design phase.

The expressions for the moments of inertia around the *x* and *y* axes are:

$$I_x = \frac{1}{6}\cdot\frac{h^4}{s} + \frac{1}{2}\cdot e\cdot b\cdot\frac{(s+e)^2}{s^3}\cdot h^3 \tag{7}$$

$$I_y = \frac{1}{6}\cdot e\cdot\frac{h}{s}\cdot b^3 + \frac{1}{2}\cdot\frac{h^2}{s}\cdot\frac{(f\cdot b\cdot s + h)^2}{s^2} \tag{8}$$

where:

$f = \frac{b_1}{b} < 1$ - the ratio between the distance of web plates and the width of flange plates of the box girder.

Since the expressions for the moments of inertia *(I_x, I_y)* and the section moduli *(W_x, W_y)* are complex, it is common to take approximate values of expressions by neglecting the members of the lower order ([8], [16] and [18]):

$$W_x = \alpha_x\cdot h\cdot A \tag{9}$$

$$W_y = \alpha_y\cdot b\cdot A \tag{10}$$

where:

α_x, α_y - the dimensionless coefficient of the resistance moment of inertia for the *x* and *y* – axes.

The coefficient α_x are obtained from the conditions of equality of the equation (7) and the expression (9) and relation between moment of inertia and section moduli:

$$\alpha_x = \frac{k + 3\cdot e}{6\cdot(e+k)} \tag{11}$$

By repeating the procedure for the section moduli for the *y* – axis, the following values of coefficient are obtained:

$$\alpha_y = \frac{3\cdot k\cdot f^2 + e}{6\cdot(e+k)} \tag{12}$$

3.2. Constraint function

The maximum equivalent stress which occurs in the main girder of the bridge crane for the case of placing the rail in the middle of the top flange is under the rail (Fig. 1). The constraint function according to this criterion is:

$$\sigma_{max} = \sqrt{(\sigma_{zV}+\sigma_{zM})^2 + \sigma_{xM}{}^2 - (\sigma_{zV}+\sigma_{zM})\cdot\sigma_{xM}} \le \sigma_k \tag{13}$$

Partial conditions must also be fulfilled:

$$\sigma_z = \sigma_{zV} + \sigma_{zM} \le \sigma_k \tag{14}$$

$$\sigma_{xM} \le \sigma_k \tag{15}$$

where:

$$\sigma_k = \frac{f_y}{\nu_1} \tag{16}$$

where:

f_y - the minimum yield stress of the plate material,

ν_1 - the factored load coefficient for load case 1,

σ_{zM} - the normal stress due to local bending in the longitudinal direction of the girder,

σ_{xM} - the normal stress due to transverse bending of the web plate.

$$\sigma_{zV} = \frac{M_{cv} + c\cdot A}{\alpha_x\cdot h\cdot A} \tag{17}$$

where:

M_{cv} - the bending moment in the vertical plane,

c – the coefficient of influence of the dead weight of the girder on the bending moment.

Local bending of the plate and occurrence of a biaxial state of normal stresses arise due to the contact between the rail and the web plate during passage of the trolley.

The normal stress due to local bending in the longitudinal direction of the girder, which is obtained on the basis of equality between rail deformations and the web plate is:

$$\sigma_{zM} = \frac{6\cdot K_3\cdot N}{t_1^2} \tag{18}$$

The normal stress due to transverse bending of the web plate is:

$$\sigma_{xM} = \frac{6\cdot K_2\cdot N}{t_1^2} \tag{19}$$

where:

N - the part of the maximum force of wheel pressure which, due to rail rigidity, goes for the plate and depends on the ratio a_1 / b_1 (Fig. 2),

K_2, K_3 - the dimensionless coefficients,

a_1 - the distance between short vertical stiffeners.

At the very beginning it is necessary to analyze certain ratios of geometrical parameters.

$$a_1 = \frac{a}{3} = \frac{2\cdot h}{3} \tag{20}$$

The following ratio is observed:

$$\frac{a_1}{b_1} = \frac{2\cdot h}{3\cdot b_1} = \frac{2\cdot k}{3\cdot f} \tag{21}$$

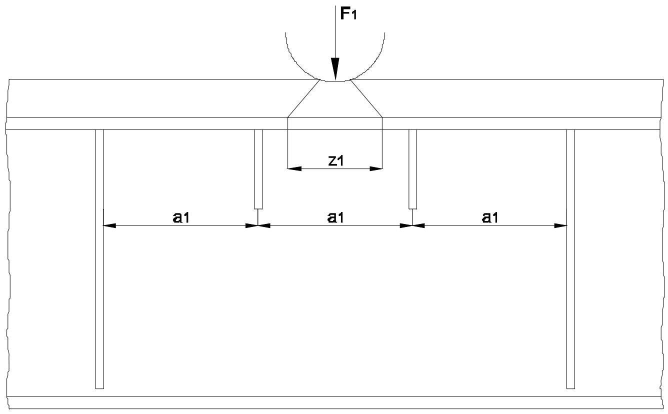

Figure 2: Action of the wheel on the rail of the main girder of the bridge crane

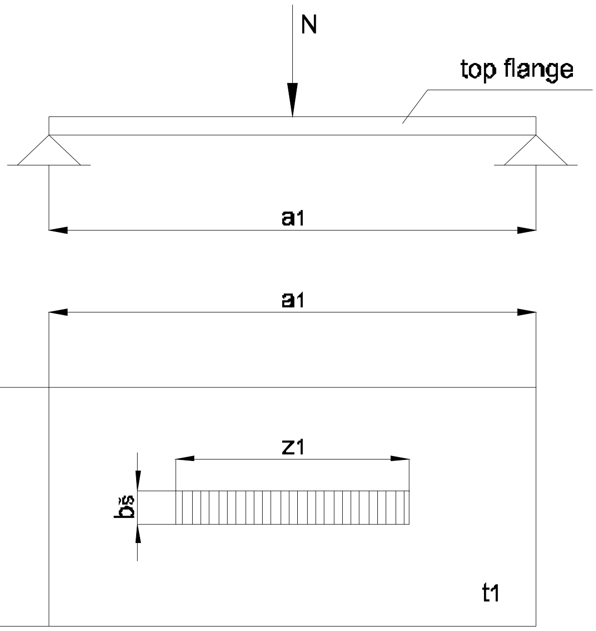

Figure 3: The zone of distribution of a part of the maximum force of wheel pressure

As in this case K=2÷3, f<1, it follows that this ratio is higher than 1, i.e. it is obtained that $a_1 > b_1$, i.e. the force N is taken according to the formula (22).

$$N = \frac{\gamma \cdot F_1}{1 + \dfrac{96 \cdot b_1^{\,2} \cdot I_{\check{s}1} \cdot K_1}{a_1^{\,3} \cdot t_1^{\,3}} \cdot \dfrac{1}{c_o}} \tag{22}$$

where:

γ - the coefficient of the classification class of the bridge crane [1],

F_1 - the maximum force of pressure of the wheel on the main girder of the bridge crane ,

$c_o \approx 1$ - the coefficient which depends on the manner of connecting the rail to the flange,

$I_{\check{s}1}$ - the moment of inertia of the rail for its own axis,

K_1 - the coefficient which depends on the ratio a_1 / b_1.

The members of the formula (22) will now be analyzed.

It is seen that this ratio depends both on k and on f. As the limit for the expected values of k is known, it is necessary to consider the values taken for the parameter f.

$$f = 1 - \frac{2 \cdot k \cdot b + 4 \cdot s}{s \cdot b} \tag{23}$$

As f is treated as constant, it is necessary to adopt a mean value of it.

As f depends on the slenderness s, mean values will be adopted, so that s = 210 is taken for S235 , s = 170 is taken for S355 , and a mean value will be taken for k=2.5.

The following value of the parameter f is adopted for the expected range of values of the width b.

$f_{sr} = 0.87$ - for S355 , $f_{sr} = 0.88$ - for S235 . It is seen that these values are approximate.

Now the ratio a_1 / b_1 should be analyzed.

$$\frac{a_1}{b_1} = \frac{2 \cdot k}{3 \cdot f} = 1.53 \div 2.3 \tag{24}$$

For this interval of ratio values, the approximate value of the coefficient K_1 can be adopted, and its value is $K_1 \approx 0.176$, where deviations of this value with the upper and lower limits are smaller than 5%, [13].

The same will now be done for the coefficients K_2 and K_3. Their dependence is little more complex in relation to the previous coefficient. These coefficients depend both on the ratio a_1 / b_1, and the ratios $b_{\check{s}} / b_1$ and z_1 / b_1, where:

$$z_1 = 2 \cdot h_{\check{s}} + 5\,cm \tag{25}$$

where:

z_1 - the width of the zone of action of the wheel on the rail (Fig. 3),

$h_{\check{s}}$ - the height of the rail,

$b_{\check{s}}$ - the width of the rail.

In order to treat the coefficients K_2 and K_3 as constant and not variable values (which would considerably complicate the model), it is adopted that the rail is of a square cross section, where $h_{\check{s}} = b_{\check{s}}$ and it is adopted that $b_{\check{s}} \approx b/8$, as the carrying capacities higher than Q=16t are not observed.

The ratio $b_{\check{s}} / b_1$ is now observed.

$$\frac{b_{\check{s}}}{b_1} = \frac{b}{8 \cdot f \cdot b} = \frac{1}{8 \cdot f} < 0,2 \tag{26}$$

$$\frac{z_1}{b_1} = \frac{2 \cdot h_{\check{s}} + 5}{b_1} = \frac{b_1 + 20 \cdot f}{4 \cdot f \cdot b_1} \tag{27}$$

Taking into account the spans, carrying capacities and classification classes that are analyzed in this case, the expected values for b_1 will be found in the following range $b_1 = 30 \div 45\,cm$. In that case, the ratio z_1 / b_1 is within the following limits: $z_1 / b_1 = 0.456 \div 0.400$, [13].

For this interval of ratio values, the approximate value of the coefficient K_2 can be adopted, and its value is $K_2 \approx 0.213$, where deviations of this value with the upper and lower limits are smaller than 5%. The situation is similar for the coefficient K_3 and its value is $K_3 \approx 0.149$, [13].

These deviations can be tolerated because exceeding of stresses up to 10% is tolerated, according to [4].

The members of the formula (22) are further observed.

It is now necessary to consider the expressions for stresses (18) and (19), which should be written as functions of *h* and *b*, i.e. the ratio N/t_1^2.

The following ratio is observed first:

$$Kn = \frac{27 \cdot K_1 \cdot f^2 \cdot s_1^3}{64^2 \cdot c_o} \tag{28}$$

where:

$$s_1 = \frac{s}{e} \tag{29}$$

By replacing in the expression (22), it is obtained that:

$$N_1 = \frac{N}{t_1^2} = \frac{F \cdot h^4}{h^6 + Kn \cdot b^6} \tag{30}$$

where:

$$F = \gamma \cdot F_1 \cdot s_1^2 \tag{31}$$

The expressions (18) and (19) now become:

$$\sigma_{zM} = 6 \cdot K_3 \cdot N_1 = \frac{6 \cdot K_3 \cdot F \cdot h^4}{h^6 + Kn \cdot b^6} \tag{32}$$

$$\sigma_{xM} = 6 \cdot K_2 \cdot N_1 = \frac{6 \cdot K_2 \cdot F \cdot h^4}{h^6 + Kn \cdot b^6} \tag{33}$$

The constraint functions in this case have the following forms:

$$g_{11} = \sqrt{(\sigma_{zV} + \sigma_{zM})^2 + \sigma_{xM}^2 - (\sigma_{zV} + \sigma_{zM})\sigma_{xM}} - \sigma_k \le 0 \tag{34}$$

$$g_{12} = \sigma_{zV} + \sigma_{zM} - \sigma_k \le 0 \tag{35}$$

$$g_{13} = \sigma_{xM} - \sigma_k \le 0 \tag{36}$$

By applying the well-known method of Lagrange multipliers to the expression (34), it is obtained that:

$$\frac{\partial A}{\partial b} \cdot \frac{\partial g_{11}}{\partial h} = \frac{\partial A}{\partial h} \cdot \frac{\partial g_{11}}{\partial b} \tag{37}$$

After rearrangement, it is obtained that:

$$\left[2(\sigma_{zV} + \sigma_{zM}) - \sigma_{xM}\right]\left[\left(\frac{\partial \sigma_{zV}}{\partial h} + \frac{\partial \sigma_{zM}}{\partial h}\right)\frac{\partial A}{\partial b} - \left(\frac{\partial \sigma_{zV}}{\partial b} + \frac{\partial \sigma_{zM}}{\partial b}\right)\frac{\partial A}{\partial h}\right] = \left[(\sigma_{zV} + \sigma_{zM}) - 2\sigma_{xM}\right]\left(\frac{\partial \sigma_{xM}}{\partial h}\frac{\partial A}{\partial b} - \frac{\partial \sigma_{xM}}{\partial b}\frac{\partial A}{\partial h}\right) \tag{38}$$

By applying the well-known method of Lagrange multipliers to the expression (35), it is obtained that:

$$\frac{\partial A}{\partial b} \cdot \frac{\partial g_{12}}{\partial h} = \frac{\partial A}{\partial h} \cdot \frac{\partial g_{12}}{\partial b} \tag{39}$$

i.e.:

$$\left(\frac{\partial \sigma_{zV}}{\partial h} + \frac{\partial \sigma_{zM}}{\partial h}\right) \cdot \frac{\partial A}{\partial b} = \left(\frac{\partial \sigma_{zV}}{\partial b} + \frac{\partial \sigma_{zM}}{\partial b}\right) \cdot \frac{\partial A}{\partial h} \tag{40}$$

By applying the well-known method of Lagrange multipliers to the expression (36), it is obtained that:

$$\frac{\partial A}{\partial b} \cdot \frac{\partial g_{13}}{\partial h} = \frac{\partial A}{\partial h} \cdot \frac{\partial g_{13}}{\partial b} \tag{41}$$

i.e.:

$$\frac{\partial \sigma_{xM}}{\partial h} \cdot \frac{\partial A}{\partial b} = \frac{\partial \sigma_{xM}}{\partial b} \cdot \frac{\partial A}{\partial h} \tag{42}$$

Based on the obtained expressions, it is seen that if the relations (40) and (42) are fulfilled simultaneously, then the equality (38) is also satisfied.

It is now necessary to solve the previous equations. If we start from the simplest equation (42), it is obtained that:

$$\frac{\partial N_1}{\partial h} \cdot \frac{\partial A}{\partial b} = \frac{\partial N_1}{\partial b} \cdot \frac{\partial A}{\partial h} \tag{43}$$

The partial derivatives have the following values:

$$\frac{\partial N_1}{\partial b} = \frac{\partial}{\partial b}\left(\frac{F \cdot h^4}{h^6 + Kn \cdot b^6}\right) = -6F\frac{Kn \cdot h^4 \cdot b^5}{(h^6 + Kn \cdot b^6)^2} \tag{44}$$

$$\frac{\partial N_1}{\partial h} = \frac{\partial}{\partial h}\left(\frac{F \cdot h^4}{h^6 + Kn \cdot b^6}\right) = -F\frac{2h^6 - 4Kn \cdot b^6}{(h^6 + Kn \cdot b^6)^2}h^3 \tag{45}$$

By replacing in (43) and using the known relation (46), [18]:

$$\frac{\partial A}{\partial b} / \frac{\partial A}{\partial h} = e \tag{46}$$

it is obtained that:

$$e \cdot k_{\sigma 3}^6 - 3 \cdot Kn \cdot k_{\sigma 3} - 2 \cdot e \cdot Kn = 0 \tag{47}$$

Solving the equation (47) results in obtaining the optimum coefficient of the ratio between the height and width of the girder $k_{\sigma 3}$ in relation to the partial condition of the strength criterion.

By replacing this value in the constraint equation (36), the optimum height $h_{\sigma 3}$ in relation to the partial condition of the strength criterion is obtained:

$$h_{\sigma 3} = \sqrt{\frac{6 \cdot K_2 \cdot F \cdot k_{\sigma 3}^6}{\sigma_k \cdot (k_{\sigma 3}^6 + Kn)}} \tag{48}$$

$$b_{\sigma 3} = \frac{h_{\sigma 3}}{k_{\sigma 3}} \tag{49}$$

Let us now observe the equation (40):

$$\frac{\partial \sigma_{zV}}{\partial b} \cdot \frac{\partial A}{\partial h} + \frac{\partial \sigma_{zM}}{\partial b} \cdot \frac{\partial A}{\partial h} = \frac{\partial \sigma_{zV}}{\partial h} \cdot \frac{\partial A}{\partial b} + \frac{\partial \sigma_{zM}}{\partial h} \cdot \frac{\partial A}{\partial b} \tag{50}$$

The partial derivatives have the following values:

$$\frac{\partial \sigma_{zV}}{\partial b} = -\frac{M_{cv}}{\alpha_x \cdot h \cdot A^2} \cdot \frac{\partial A}{\partial b} \tag{51}$$

$$\frac{\partial \sigma_{zV}}{\partial h} = -\frac{M_{cv}}{\alpha_x \cdot h \cdot A^2} \cdot \frac{\partial A}{\partial h} - \frac{M_{cv} + c \cdot A}{\alpha_x \cdot h^2 \cdot A} \tag{52}$$

$$\frac{\partial \sigma_{zM}}{\partial b} = -36K_3 \cdot F \cdot \frac{Kn \cdot h^4 \cdot b^5}{(h^6 + Kn \cdot b^6)^2} \tag{53}$$

$$\frac{\partial \sigma_{zM}}{\partial h} = -12K_3 \cdot F \cdot \frac{h^6 - 2 \cdot Kn \cdot b^6}{(h^6 + Kn \cdot b^6)^2}h^3 \tag{54}$$

Further rearrangement results in (55):

$$\frac{M_{cv} + c \cdot A}{\alpha_x \cdot h^2 \cdot A} \cdot \frac{\partial A}{\partial b} = \frac{12 \cdot K_3 \cdot F \cdot h^3}{(h^6 + Kn \cdot b^6)^2} \cdot \left[Kn \cdot h \cdot b^5 \cdot \frac{\partial A}{\partial h} - (h^6 - 2 \cdot Kn \cdot b^6) \cdot \frac{\partial A}{\partial b}\right] \tag{55}$$

The constraint equation (35) can be written in the form (56):

$$\frac{M_{cv} + c \cdot A}{\alpha_x \cdot h \cdot A} + \frac{6 \cdot K_3 \cdot F \cdot h^4}{h^6 + Kn \cdot b^6} = \sigma_k \tag{56}$$

Solving the system of nonlinear algebraic equations (56) and (55) results in obtaining the optimum height $h_{\sigma 2}$ and width $b_{\sigma 2}$ in relation to the partial condition of the strength criterion.

The principal equation (38) is now observed:

$$\frac{2(\sigma_{zV}+\sigma_{zM})-\sigma_{xM}}{(\sigma_{zV}+\sigma_{zM})-2\sigma_{xM}}\cdot\left[\left(\frac{\partial\sigma_{zV}}{\partial h}+\frac{\partial\sigma_{zM}}{\partial h}\right)\frac{\partial A}{\partial b}-\left(\frac{\partial\sigma_{zV}}{\partial b}+\frac{\partial\sigma_{zM}}{\partial b}\right)\frac{\partial A}{\partial h}\right]=\frac{\partial\sigma_{xM}}{\partial h}\frac{\partial A}{\partial b}-\frac{\partial\sigma_{xM}}{\partial b}\frac{\partial A}{\partial h} \tag{57}$$

The partial derivatives have the following values:

$$\frac{\partial\sigma_{zV}}{\partial b}=-\frac{M_{cv}}{\alpha_x\cdot h\cdot A^2}\cdot\frac{\partial A}{\partial b} \tag{58}$$

$$\frac{\partial\sigma_{zV}}{\partial h}=-\frac{M_{cv}}{\alpha_x\cdot h\cdot A^2}\cdot\frac{\partial A}{\partial h}-\frac{M_{cv}+c\cdot A}{\alpha_x\cdot h^2\cdot A} \tag{59}$$

$$\frac{\partial\sigma_{zM}}{\partial b}=-36\cdot K_3\cdot F\cdot\frac{Kn\cdot h^4\cdot b^5}{(h^6+Kn\cdot b^6)^2} \tag{60}$$

$$\frac{\partial\sigma_{zM}}{\partial h}=-12\cdot K_3\cdot F\cdot\frac{h^6-2\cdot Kn\cdot b^6}{(h^6+Kn\cdot b^6)^2}\cdot h^3 \tag{61}$$

$$\frac{\partial\sigma_{xM}}{\partial b}=-36\cdot K_2\cdot F\cdot\frac{Kn\cdot h^4\cdot b^5}{(h^6+Kn\cdot b^6)^2} \tag{62}$$

$$\frac{\partial\sigma_{xM}}{\partial h}=-12\cdot K_2\cdot F\cdot\frac{h^6-2\cdot Kn\cdot b^6}{(h^6+Kn\cdot b^6)^2}\cdot h^3 \tag{63}$$

By replacement in the previous expression, the following equation (64) is obtained:

$$\begin{aligned}&\frac{12F\cdot h^3}{(h^6+Kn\cdot b^6)^2}\cdot\left(3Kn\cdot h\cdot b^5\cdot\frac{\partial A}{\partial h}-(h^6-2Kn\cdot b^6)\cdot\frac{\partial A}{\partial b}\right)\cdot\left(K_4\frac{M_{cv}+c\cdot A}{\alpha_x\cdot h\cdot A}+2K_5\cdot\frac{6F\cdot h^4}{h^6+Kn\cdot b^6}\right)=\\&=\frac{1}{h}\cdot\frac{\partial A}{\partial b}\left[2\left(\frac{M_{cv}+c\cdot A}{\alpha_x\cdot h\cdot A}\right)^2+K_4\frac{M_{cv}+c\cdot A}{\alpha_x\cdot h\cdot A}\cdot\frac{6F\cdot h^4}{h^6+Kn\cdot b^6}\right]\end{aligned} \tag{64}$$

where:

$$K_4=2\cdot K_3-K_2 \tag{65}$$

$$K_5={K_2}^2-K_2\cdot K_3+{K_3}^2 \tag{66}$$

The constraint equation (34) can be written in the form (67):

$$\left(\frac{M_{cv}+c\cdot A}{\alpha_x\cdot h\cdot A}+\frac{6\cdot K_3\cdot F\cdot h^4}{h^6+Kn\cdot b^6}\right)^2+\left(\frac{6\cdot K_2\cdot F\cdot h^4}{h^6+Kn\cdot b^6}\right)^2-\left(\frac{M_{cv}+c\cdot A}{\alpha_x\cdot h\cdot A}+\frac{6\cdot K_3\cdot F\cdot h^4}{h^6+Kn\cdot b^6}\right)\cdot\left(\frac{6\cdot K_2\cdot F\cdot h^4}{h^6+Kn\cdot b^6}\right)={\sigma_k}^2 \tag{67}$$

Solving the system of nonlinear algebraic equations (57) and (67) results in obtaining the optimum height $h_{\sigma 1}$ and width $b_{\sigma 1}$ in relation to the partial condition of the strength criterion.

As it can be seen, there are three different solutions. In order to analyze which one is the most optimum one, it is necessary to have graphical representation of the obtained solutions in the same plane.

4. NUMERICAL REPRESENTATION OF THE RESULTS OBTAINED

The functions (14), (15) and (16) depending on *h* and *k*, read:

$$\begin{aligned}&f_{11}(h,k)=4{\alpha_x}^2{\sigma_{dop}}^2(e+k)^2(k^6+Kn)^2h^6-4c^2(e+k)^2(k^6+Kn)^2h^4-24\alpha_xK_4cF(e+k)^2k^6(k^6+Kn)h^3-\\&-4(e+k)k\left[sM_{cv}c(k^6+Kn)^2+36{\alpha_x}^2K_5F^2(e+k)k^{11}\right]h^2-12\alpha_xK_4sM_{cv}F(e+k)k^7(k^6+Kn)h-s^2{M_{cv}}^2k^2(k^6+Kn)^2\geq 0\end{aligned} \tag{68}$$

$$f_{12}(h,k)=2\alpha_x(e+k)(k^6+Kn)\sigma_{dop}h^3-2c(e+k)(k^6+Kn)h^2-12\alpha_xK_3F(e+k)k^6h-skM_{cv}(k^6+Kn)\geq 0 \tag{69}$$

$$f_{13}(h,k)=\sigma_{dop}(k^6+Kn)h^2-6K_2Fk^6\geq 0 \tag{70}$$

These functions will be presented in the *k*-*h* plane, where it is necessary to fulfil certain boundary conditions:

$$k\geq\frac{s\cdot f}{65\cdot e}\cdot\sqrt{\frac{R_e}{23.5}} \tag{71}$$

$$h\geq\frac{b_1\cdot k}{f} \tag{72}$$

The function (71) relates to the condition of stability of the top flange, whereas (72) relates to the technological possibilities of manufacturing the box section.

The optimum point in this diagram will be the lowest point that fulfils the above mentioned conditions and constraints.

This will be illustrated through the following examples.

The following diagrams (Fig. 4 – Fig. 7) will show how the curves f_{11}, f_{12} and f_{13} change depending on the classification class and selection of materials according to this criterion, where it will be adopted, for illustration, that the span is *L*=20m and the carrying capacity is *Q* = 12,5t.

The following initial data will be adopted: *e*=1.33, for S235 : *s*=210, *f*=0.88, and for S355 : *s*=170, *f*=0.87.

The diagrams (Fig. 4 and Fig. 5) show how the curves f_{11}, f_{12} and f_{13} change according to the strength criterion, for classification class 1, where it is adopted that the base material is S235 (Fig. 4) and S355 (Fig. 5).

It is seen to which extent the selection of base material influences the shapes of the curves f_{11}, f_{12} and f_{13}, which is seen from (Fig. 4 – Fig. 7).

The diagrams (Fig. 6 and Fig. 7) show how the curves f_{11}, f_{12} and f_{13} change according to the strength criterion, for classification class 2, where it is adopted that the base material is S235 (Fig. 6), i.e. S355 (Fig. 7). It is seen to which extent the selection of base material influences the shapes of the curves f_{11}, f_{12} and f_{13}, as well as the change of classification class, which is seen from these diagrams.

It is seen from the previous diagrams that in these cases the optimum point according to the strength criterion will be in the intersection of the vertical line of the function (71) and the function (69).

The results from the previous examples will be shown in Table 1. The solutions were obtained in the software package MathCad.

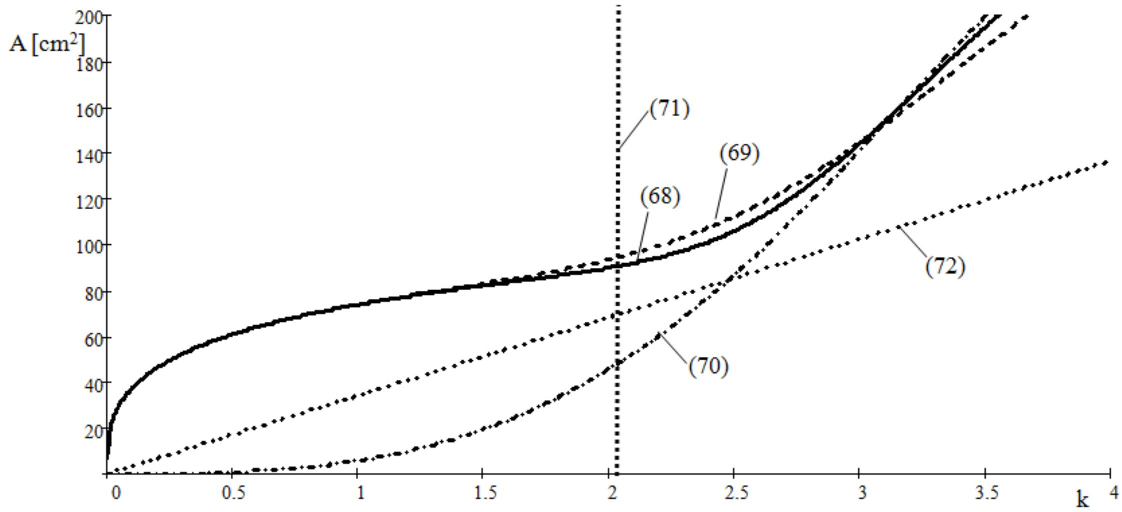

Figure 4: Comparative analysis of optimum values

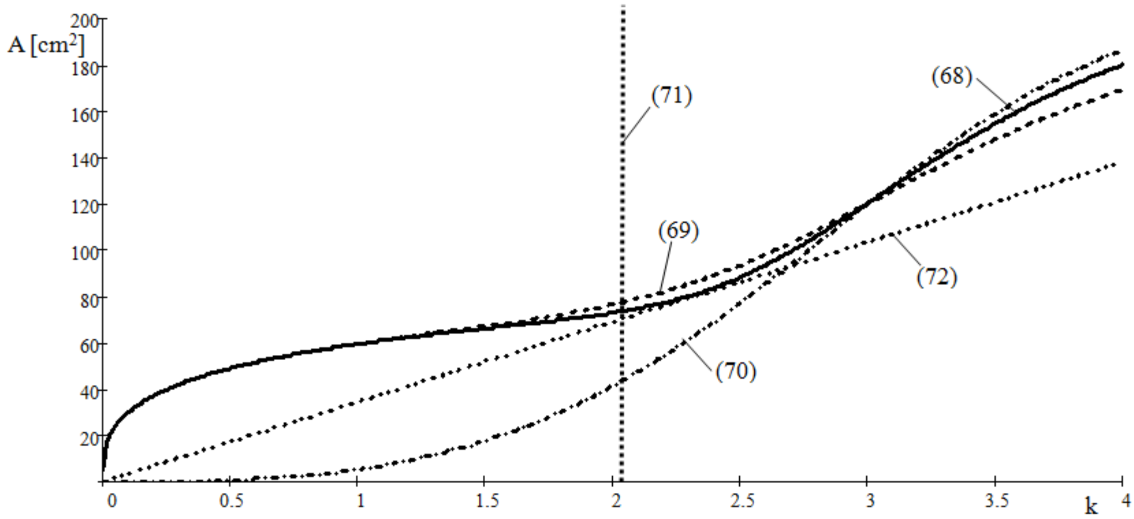

Figure 5: Comparative analysis of optimum values

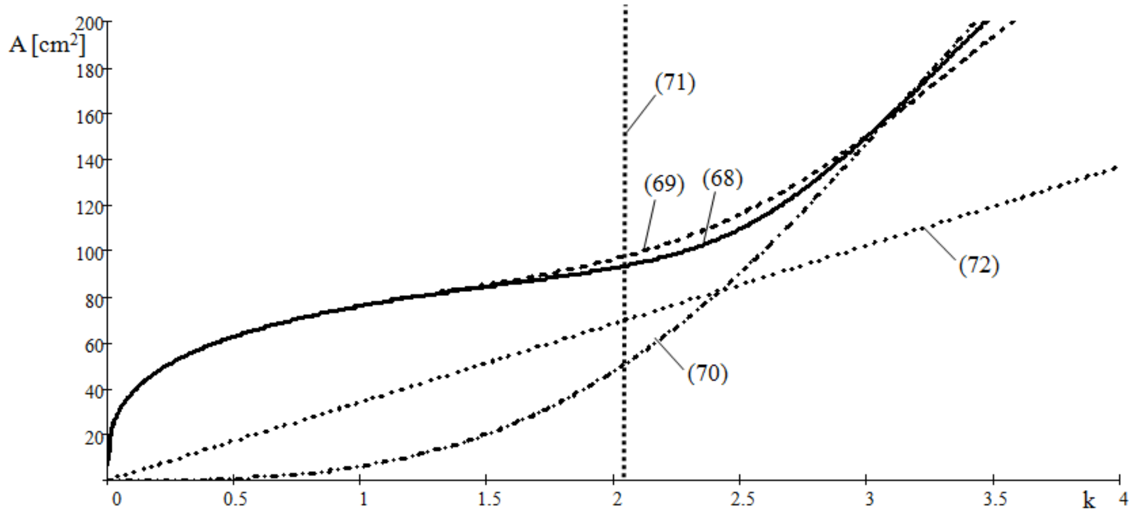

Figure 6: Comparative analysis of optimum values

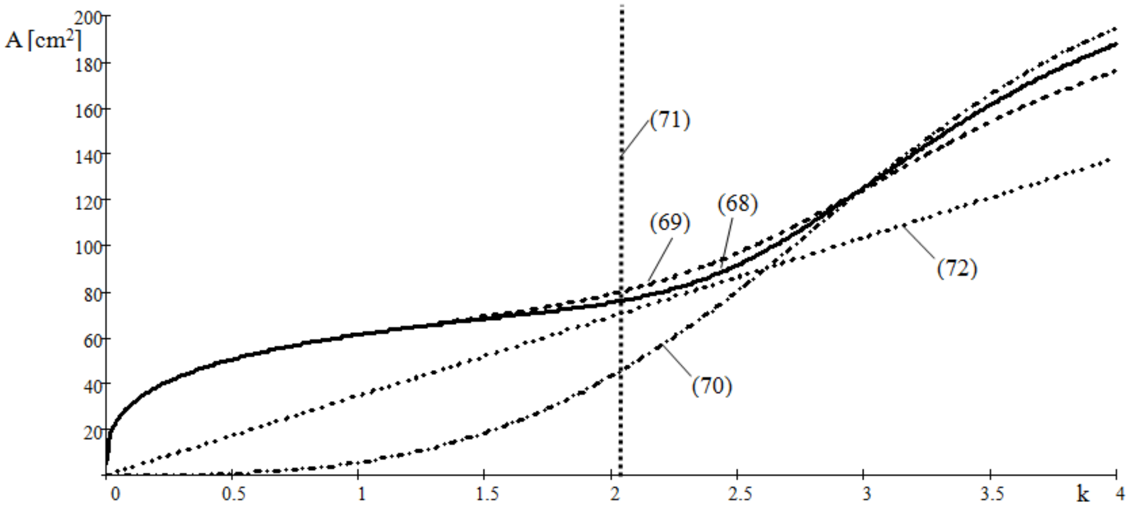

Figure 7: Comparative analysis of optimum values

Table 1: Values of optimum parameters

Material	f_{11}		f_{12}		f_{13}		Optimum		Cl. class
	k	*h(cm)*	*k*	*h(cm)*	*k*	*h(cm)*	*k*	*h(cm)*	
S235	2,821	127.05	1.518	83.20	6.184	330.03	2.133	97.26	***1***
	2.806	130.64	1.512	85.49	6.184	344.01	2.133	100.30	***2***
S355	2.685	98.70	1.457	66.36	5.441	216.62	2.098	79.00	***1***
	2.670	101.40	1.451	68.18	5.441	225.80	2.098	81.47	***2***

5. CONCLUSION

The paper defined optimum dimensions of the box section of the main girder of the bridge crane for the case of placing the rail in the middle of the top flange in an analytical form, by using the method of Lagrange multipliers, according to criterion of strength.

It was shown that the proper selection of girder height and plate thickness can considerably influence the reduction in the cross sectional area at the same time satisfying all constraint functions.

The results were obtained in explicit form, which is very favourable for discussion of solutions as well as for consideration of influences of individual geometrical parameters and their ratios. Comparison of the obtained results with certain solutions of bridge cranes shows that the obtained cross sectional areas are smaller, which verifies the optimization results.

In addition, the usage of the method of Lagrange multipliers is justified because the optimization results are obtained in analytical form, which allows getting conclusions about influences of particular parameters and further researches toward mass reduction.

The results obtained may be of great use to the engineer-designer, particularly in the first phase of the design procedure when the basic dimensions of the main girder of the bridge crane, as its most responsible part, are defined.

The conclusion is that further research should be directed toward a multicriteria analysis where it is necessary to include additional constraint functions, such as: lateral stability, local stability of plates, deflection dynamic stiffness, material fatigue, influence of manufacturing technology, optimization of the ratio of plate thicknesses, types of material, conditions of crane operation.

ACKNOWLEDGEMENTS

A part of this work is a contribution to the Ministry of Science and Technological Development of Serbia funded Project TR35038.

REFERENCES

[1] JUS M.D1.050 Standards for cranes, Yugoslav Institute for Standardization, Belgrade (Serbia), (1968)

[2] J. Farkas, Optimum design of metal structures, Akademiai KIADO, Budapest (Hungary), (1984)

[3] J. Farkas, Economy of Higher-Strength Steels in Overhead Travelling Cranes with Double-Box Girders, J. Construct, Steel Research 6: 285-301, (1986)

[4] JUS U.E7.145/1987, Noseće čelične konstrukcije spojene zakovicama i vijcima - Tehnički uslovi, Yugoslav Institute for Standardization, Belgrade (Serbia), (1987)

[5] K. Jarmai, Decision Support System on IBM PC for Design of Economic Steel Structures Applied to Crane Girders, Thin-Walled Structures, 10: 143-159, (1990)

[6] Catalogues, And as-built projects of Serbian crane manufacturers, IMK 14 Oct., MIN, ILR, (Serbia), (1996)

[7] J. Farkas, K. Jarmai, Analysis and optimum design of metal structures, Balkema, Rotterdam (Holland), (1997)

[8] R. Šelmić, R. Mijailović., Optimization of trapezium cross-section in structures, Facta iniversitatis mechanical engineering, Vol. 1, N5/1998, pp. 555–564, Niš, (Serbia), (1998)

[9] K. Jarmai, J. Farkas, Optimum cost design of welded box beams with longitudinal stiffeners using advanced backtrack method, Structural and Multidisciplinary Optimization, 21:52–59, (2001)

[10] J. Farkas, L.M.C. Simoes, K. Jarmai, Minimum cost design of a welded stiffened square plate loaded by biaxial compression, Structural and Multidisciplinary Optimization, 29:298–303, (2005)

[11] J. Farkas, Structural optimization as a harmony of design, fabrication and economy, Structural and Multidisciplinary Optimization, 30:66–75, (2005)

[12] M. Savković, Optimization of Complex Cross Sections of Structures of Autocrane Booms (Optimizacija složenih poprečnih preseka konstrukcija strele autodizalice). (IMK-14- Research and Development) IMK -14- Istraživanje i razvoj 20-21(1) pp. 41:45, (Serbia) (2005)

[13] D. Ostrić and S. Tošić, *"Dizalice"*, Institute for Mechanization of the Faculty of Mechanical Engineering of the University in Belgrade, Belgrade, (Serbia), (2005)

[14] J. Farkas, K. Jármai, J.A. Snyman, Global minimum cost design of a welded square stiffened plate supported at four corners, Structural and Multidisciplinary Optimization, 40:477–489, (2010)

[15] M. Gašić**,** M. Savković, R. Bulatović, R. Petrović, Optimization of a pentagonal cross section of the truck crane boom using Lagrange's multipliers and differential evolution algorithm**,** Meccanica. Online First 13 August 2010. doi:10.1007/s1 1012-010-9343-7 (2010)

[16] G. Pavlović, M. Savković, N. Zdravković, Optimization of box-girder cross-section of the main bridge cranes according to the criteria of lateral stability (Optimizacija kutijastog poprečnog preseka glavnog nosača mosne dizalice prema kriterijumu bočne stabilnosti), IMK – 14 Research and Development (IMK – 14 Istraživanje i razvoj), (Serbia) (41), 4/2011, (2011)

[17] M. Gašić**,** M. Savković, R. Bulatović, R., Optimization of trapezoidal cross section of the truck crane boom by Lagrange's multipliers and by differential evolution algorithm (DE), Strojniški vestnik – Journal of Mechanical Engineering 57, 4:304-312, (2011)

[18] M. Savković, M. Gašić, D. Ćatić, R. Nikolić, Pavlović G., Optimization of the box section of the main girdre of the bridge crane with the rail placed above the web plate, Structural and Multidisciplinary Optimization, DOI: 10.1007/s00158-012-0813-5, (2012)

Optimal Synthesis of the Driving Mechanism of Basket Articulated Trucks

Dragoslav Janošević[1*], Jovan Pavlović[1], Vesna Jovanović[1], Predrag Milić[1]
[1]Univerzitet u Nišu, Mašinski fakultet u Nišu

This paper presents a general mathematical model of the dumper on which basis was developed the program for the optimal synthesis of kinematic and dynamic simulation for driving mechanism of basket articulated trucks. Synthesis is determine the required size of hydro-cylinder drive mechanism and the optimal coordinates of the joints which hydro-cylinder linked for thrust-motional mechanism and basket articulated trucks. In simulation are defined parameters as: position, angular velocity and acceleration lifting of basket, the volume of material and the position of the center of mass of the material in the basket, the forces in the joints of the drive mechanism, the required torque and power of lifting baskets. As an example is given the results of the synthesis and analysis of drive mechanism to lifting the basket of the articulated trucks capacity 24000 kg.

Keywords: articulated trucks, basket drive mechanism

1. INTRODUCTION

A trucks are transport machines that are used for cyclic transport of bulk and unit materials in civil and mining industry, prevalence. By conception of a kinematic chain there are rigid and articulated trucks. The rigid trucks have kinematic chain that is consists of two members: a moving mechanism L_1 (Fig.1a) and a bucket L_2 that are connected like kinematic pair with horizontal rotary joint. The articulated trucks have kinematic chain that is consists of three members: a front L_1 (Fig. 1b) and a rear L_2 part of moving mechanism that are connected with vertical joint on the rear part of moving mechanism and basket L_3 [1].

Lifting, unloading of basket and its lowering in a loading position is realized with the a drive mechanism of basket that is at the rigid and articulated trucks consists of kinematic pair: the supporting-moving member and the basket that are connected with hydro-cylinders. The drive mechanism of rigid trucks can be with one or two three-stage or four-stage telescopic hydro-cylinders c_2 (Fig.1a) with bidirectional effect. The drive mechanisms of basket at articulated trucks have two differential hydro-cylinders c_3 (Fig.1b) of bidirectional effect. The hydrostatic system of hydro-cylinders, have working pressure from *22* up to *25 MPa*. In this paper, there is a procedure of optimal synthesis of basket drive mechanism of articulated trucks [2].

2. SYNTHESIS OF BASKET DRIVE MECHANISM

At the optimal synthesis of busket drive mechanism of articulated trucks there is necessary to determined, based on setted objective function and constraint, parameters of hydro-cylinders: a diameters of pistons and rods, motion of the hydro-cylinder at begin and at end and coordinates of joints in which are hydro-cylinders are connected for the supporting-moving member and the basket,

For synthesis of busket drive mechanism of articulated trucks, there is developed a general mathematical model of machine based on physical model. (Fig.2). The articulated truck is consider in its absolute coordinate system OXYZ, where is each member L_i of kinematic chain defined in its local coordinate system $O_ix_iy_iz_i$, with set of parameters [3]:

$$L_i = \{\vec{e}_i, \vec{s}_i, \theta_{ip}, \theta_{ik}, E_{io}, \vec{t}_i, m_i\} \quad \forall \; i = 1,2,3 \qquad (1)$$

where is: $\boldsymbol{e_i}$ - unit vector of joint axis with whom is

a)

b)

Fig.1 Kinematic chain: a) rigid truck, b) articulated truck

*Corresponding author: Faculty of Mechanical Engineering, Aleksandra Medvedeva 14 18000 Niš, Serbia, janos@masfak.ni.ac.rs

connected with previous member of kinematic chain, $\mathbf{s}_i$ - kinematic length of the member L_i, θ_{ip},θ_{ik} - boundary generalized coordinates of the member position at begin and at end in respect to previous member, E_{io} - subset of a geometric values that are determined shape of the member, $\mathbf{t}_i$ – position vector of centar of mass of member, m_i - mass of member.

With the subset of geometric values of basket E_{3o}, there is determined volume of basket.

The objective function of the optimal synthesis of drive mechanism of articulated truck basket is defined with aim to in whole scope of basket unloading, with the change of position angle θ_3 from start values θ_{3p} to end values θ_{3k}, have minumum value of needed force F_{c3} in hydro-cylinder.

$$f \to min\, F_{c3} \tag{2}$$

An area of drive mechanism optimization of trucks basket is determined by set of values:

$$E = \{E_{A2}, E_{A3}, E_{c3}\} \tag{3}$$

where are: E_{A2},E_{A3} - boundary area of the possible position of joints coordinates A_2, A_3 with whome are the drive hydro-cylinders connected to the moving mechanism and basket of trucks, E_{c3} - data file of the parameters of the standard differential bidirectional hydro-cylinder.

The constraints of optimization are related to condition:

$$\begin{aligned} 2c_{3p} - c_{3k} &\le c_{3c} \\ F_{c3} &\le F_{c3i} \end{aligned} \tag{4}$$

where are c_{3p},c_{3k} – length of the hydro-cylinder in starting and ending postion of basket, c_{3c} - construction constant of hydro-cylinder, F_{c3i} - force that is determined from the condition of elastic stability (non-buckling) of hydro-cylinder

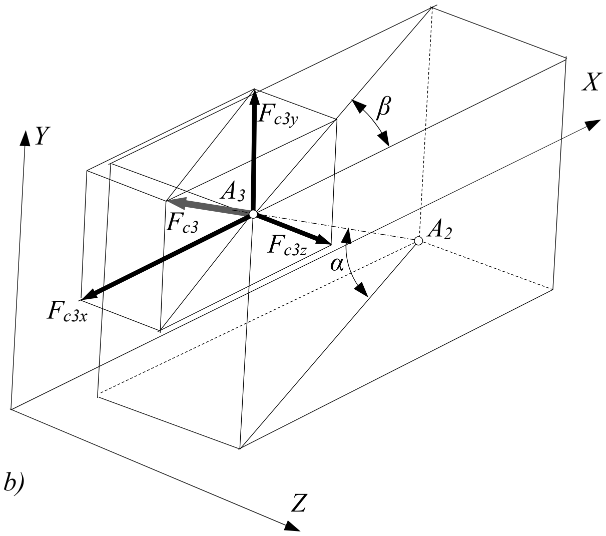

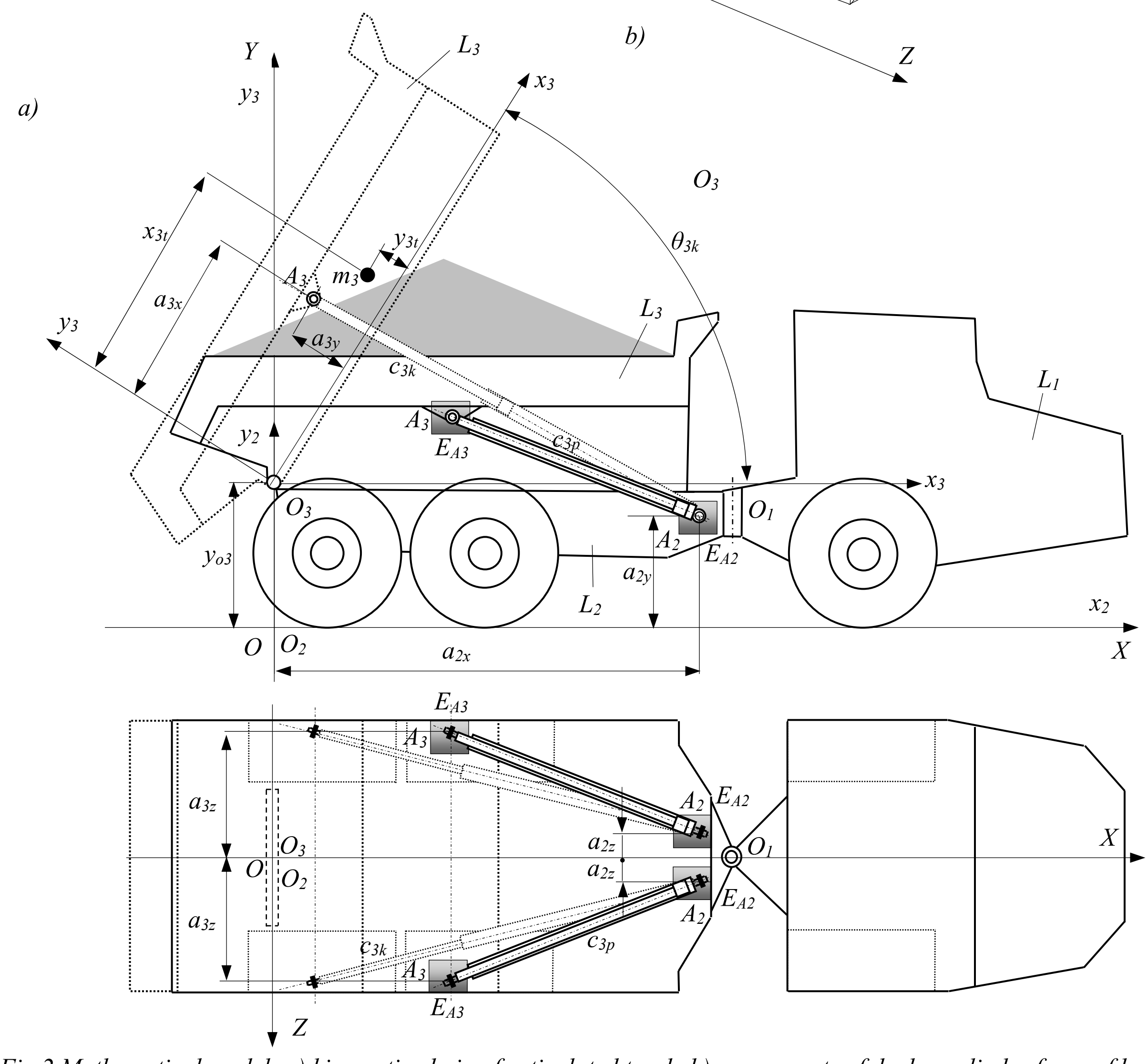

Fig.2 Mathematical model: a) kinematic chain of articulated truck, b) components of hydro-cylinder force of basket drive mechanism of articulated truck

2.1. Mathematical model

With the mathematical model there are defined dependences of parameters which enable a simulation of unloading of basket. Whereby, by the function of basket unloading time, there is determined next values: position angle θ_3 of basket L_3, motion of hydro-cylinder c_3, volume of the materials and basket, torque and needed power of the basket mechnism, force, velocity and needed flow of pulling hydro-cylinder.

According to the adopted general trapezoidal cyclical model of an angular velocity change of basket, there is determined maximum value of angular velocity $\dot{\theta}_{3m}$ of basket lifting [3]:

$$\dot{\theta}_{3m} = \frac{2(\theta_{3k} - \theta_{3p})}{(t_{32} + t_{33}) - t_{31}} \tag{5}$$

where are: t_{31} - duration time of an acceleration of basket, t_{32} - deceleration beginning time and t_{33} - time of a operation ending apropos the unloading of basket.

According to the maximum value of angular velocity of basket there are defined, in each time of the unloading operation of basket, angular velocity $\dot{\theta}_3$:

$$\dot{\theta}_3 = \begin{cases} \dfrac{\dot{\theta}_{3m}}{2}\left(1 - cos\dfrac{t}{t_{31}}\pi\right), & \forall\, 0 \le t \le t_{31} \\ \dot{\theta}_{3m}, & \forall\ \ t_{31} \le t \le t_{32} \\ \dfrac{\dot{\theta}_{3m}}{2}\left[1 + cos\left(\dfrac{t - t_{32}}{t_{33} - t_{32}}\right)\pi\right], & \forall\ t_{32} \le t \le t_{33} \end{cases} \tag{6}$$

and the angular acceleration $\ddot{\theta}_3$ of basket:

$$\ddot{\theta}_3 = \begin{cases} \dfrac{\dot{\theta}_{3m}}{2}\dfrac{\pi}{t_{31}} sin\dfrac{t}{t_{31}}\pi, & \forall\, 0 \le t \le t_{31} \\ 0, & \forall\ \ t_{31} \le t \le t_{32} \\ -\dfrac{\dot{\theta}_{3m}}{2}\dfrac{\pi}{t_{33} - t_{32}} sin\left(\dfrac{t - t_{32}}{t_{33} - t_{32}}\right)\pi, & \forall\ t_{32} \le t \le t_{33} \end{cases} \tag{7}$$

The needed forces in drive hydro-cylinders when basket is unloading:

$$F_{c3} = \frac{M_{o3z}}{r_{c3}} \tag{8}$$

where are: M_{o3z} - the total torque of basket drive mechanism, r_{c3} - transfer function of drive mechanism.

The total torque of basket drive mechanism is equal to a sum of static and dynamic torque of basket and material for the axis of joint O_3z_3 (Fig.1):

$$M_{o3z} = gm_3 \cdot x_{t3} + gV_m\rho_m \cdot x_{tm} + (J_{3z} + J_{mz}) \cdot \ddot{\theta}_3 \tag{9}$$

where are: m_3 - mass of basket, V_m - volume of materials in basket, ρ_m - density of materials x_{t3}, x_{tm} - coordinates of the center of mass of basket and materials in basket, J_{3z}, J_{mz} - moments of inertia of the basket and materials, that is in basket.

According to the model of basket unloading, there is regard the change of materials volume when it is change angle of basket inclination. Whereby it can be take that basket in starting position accomplish maximum volume of bulk homogeneous materials with certain boundary natural slope angle φ_{gz}.

With the change of basket position in respect to horizontal for the angle θ_3 it come to change of angle that is form by upper edge of the materials in basket in respect to natural slope angle φ_{gz}.

A characteristik angles for following the position of basket apropos following the materials in basket are angle of material slope above flank sides φ_{nk} and angle of materials in basket φ_{nz}. By following this angle in respect to natural slope angle of materials, it can be insight four characteristik phase of change of basket loading position.

In the first phase angle of material above flank sides φ_{nk} (Fig.3a) is less than boundary natural slope angle φ_{gz}. In this case, the material is not came out from the basket apropos its volume stays unchanged.

In second phase of the consideration of basket position, angle of material above flank sides φ_{nk} (Fig.3b) is great than boundary natural slope angle φ_{gz}.

In this case there is change in material volume in basket apropos material volume above basket flank sides, while volume of material in basket is unchanged.

In third phase the material angle that is in basket φ_{nz} (Fig.4a), is equal to the material boundary angle φ_{zg}. In this the volume of material above basket flank sides is equal to zero while volume of materials that is in basket is unchanged.

In fourth phase, angle of materials that is in basket φ_{nz} (Fig.4b) is great than the material boundary angle φ_{zg}. In this case there is come to changing of the materials volume

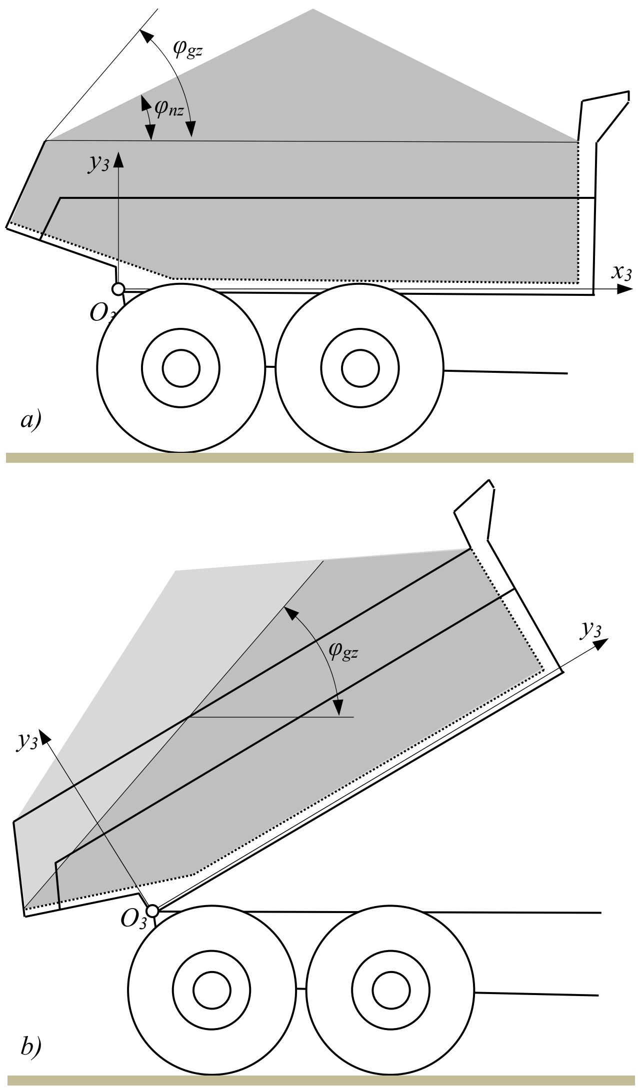

Fig.3 First and second phase of basket unloading

that is leftover in basket, and its position of center of mass, that will be until the basket slope angle φ_2 is not become equal to material boundary angle φ_{zg} when basket is completely empty. The transfer function of drive basket mechanism is defined with equation (Fig.1б):

$$r_{c3} = x_{A3}\sin\alpha + (y_{A3} - y_{O3})\cos\alpha \cdot \cos\beta \quad (10)$$

$$\alpha = \arcsin\frac{y_{A3} - y_{A2}}{\left[(z_{A3} - z_{A2})^2 + (x_{A3} - x_{A2})^2\right]^{0,5}} \quad (11)$$

$$\beta = arctg\frac{z_{A3} - z_{A2}}{x_{A2} - x_{A3}} \quad (12)$$

where are: y_{O3},x_{A2},y_{A2},z_{A2},x_{A3},y_{A3},z_{A3} - coordinates of the joint O_3, A_2 and A_3 in the absolute coordinate system of the mathematical model of trucks.

An alowed force of hydro-cylinder of the drive mechanism of basket is determined from the condition of elastic stability of hydro-cylinder:

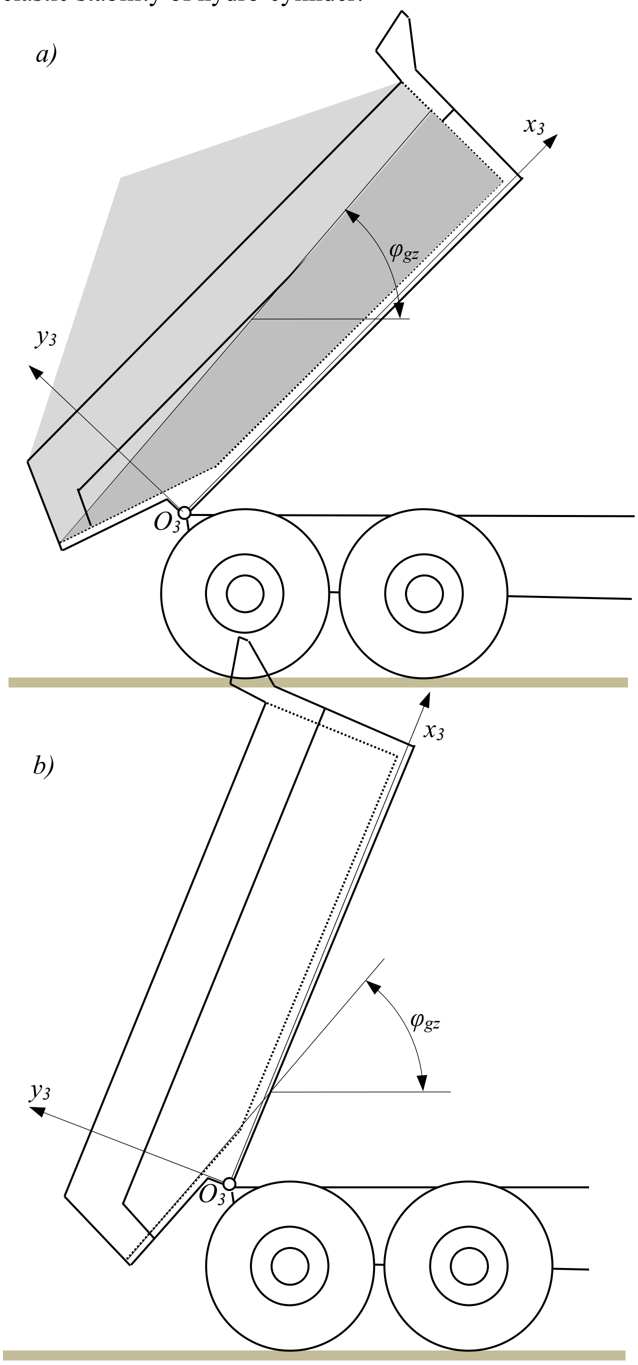

Fig.4 Third and fourth phase of basket unloading

$$F_{c3i} = \frac{\pi^2 E \cdot I}{\nu \cdot c_3^2} \quad (13)$$

where are: E, I - elastic modul and moment of inertia of the materials and cross section of hydro-cylinder's rod, υ – degree of assurance from the hydro-cylinder's buckling, c_3 - length of the hydro-cylinder.

According to the equation 8, the optimization objectiv function of drive mechanism of basket can be defined with aim that in whole area of changing of basket lifting angle, transfer function have minimum value.

$$f \rightarrow \max r_{c3} \quad (14)$$

3. PROGRAM FOR SYNTHESIS OF THE BASKET DRIVE MECHANISM

By using the defined mathematical model it had been developed program for optimal syntesis of drive mechanism of articulated trucks basket. The program provides simulation of unloading the materials from basket and determination off all needed parameters on based who is defined the drive mechanism of basket.

For program initial values it has been given a data files in which are the parameters of kinematic chain members and the hydrostatic system of drive mechanism, like as condition, criteria, area and constraints of the optimization.

For the condition of simulation it has been given total duration time of the basket unloading operation with time's intervals of acceleration and deceleration of the hydro-cylinder's rod.

For the area of optimization it has been defined the boundary ranges E_{A2},E_{A3} (Fig.1) in which are possible changes of the joint coordinates of hydro-cylinder on supporting-moving member and basket. An inner part of the program is file data E_{c3} of bidirectional effect hydro-cylinders with parameters that defined its values and characteristik: diameter of the piston and rod and construction constant. For the criteria it has been given alowed minimum value of the positive difference of the drive's torque and the torque of basket drive mechanism in whole range of unloading.

The algoritam of program provides that first, by willing step, from the range of optimization E_{A2},E_{A3} determined coordinates of the hydro-cylinder's joints which are connected to the supporting-moving member and the basket, and then to determined diameter of the piston and the rod, then the starting and ending length of hydro-cylinder. The aim of all of this is to defined one from many possible variant solutions of the drive mechanism

By the cyclic change of time and by willing number of basket position, in the whole range of movement, it has been computed the static and dynamic parameters of one possible variant solution of the drive mechanism. On ending of program there are abstract just the variant solutions which satisfied given constraints and criteria of optimization. As an example, by using developed program, it has been computed synthesis of the basket drive mechanism of articulated trucks which mass is *21000 kg* (without load) and volume of basket is *15 m*^{3}. The given parameters of condition, constraints and area of optimization at synthesis of the basket drive mechanism are given in Table 1 and Table 2.

Table 1: Parameters of synthesis condition and constraints

Name of parameter	Value
Starting angle of basket position	$\theta_{3p}=0^o$
Ending angle of basket position	$\theta_{3k}=70^o$
Acceleration ending time of basket	$t_{31}=1\ s$
Deceleration starting time of basket	$t_{32}=8\ s$
Unloading time of basket	$t_{33}=10\ s$
Max. pressure of hydro-cylinders	$p=25\ MPa$
Elastic modul	$E=2{,}1\ 10^{11} N/m^2$
Buckling degree of assurance	$\upsilon=3{,}5$

Table 2: Parameters of optimization area

Optimization area	Coordinates	*min*	*max*
E_{A2}	$x_{A2}\ [mm]$	4300	4500
	$y_{A2}\ [mm]$	1200	1400
	$z_{A2}\ [mm]$	400	500
E_{A3}	$x_{A3}\ [mm]$	1700	1900
	$y_{A3}\ [mm]$	600	800
	$z_{A3}\ [mm]$	1300	1400

The part of obtained results of the synthesis of basket drive mechanism of truck is given on diagrams (Fig. 5)

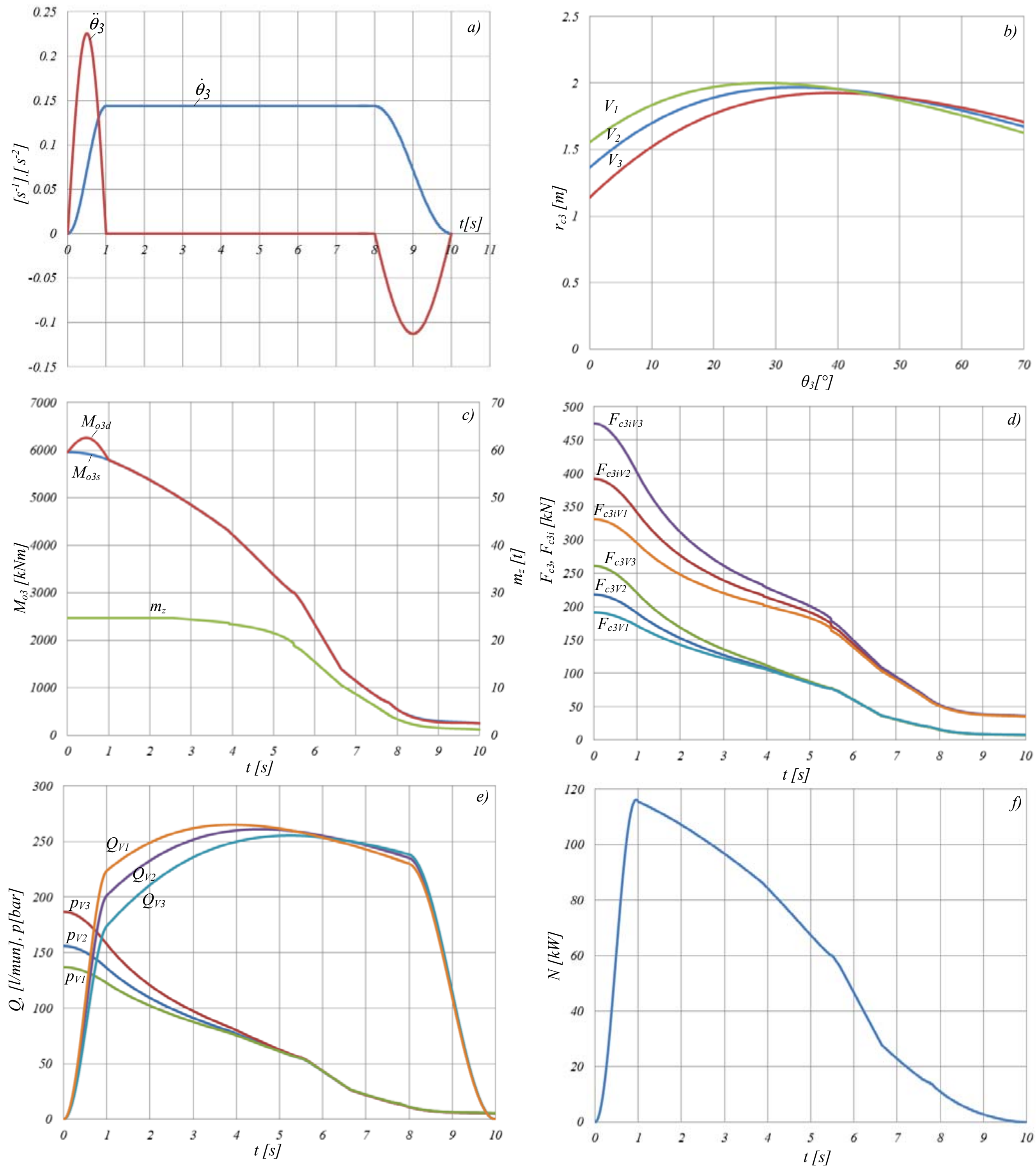

Fig.5 Synthesis of basket drive mechanism of truck: a) angular velocity and angular acceleration of basket, b) transfer functions of variant solutions, c) torque, d) forces in hydro-cylinders and critical forces, e) pressure and flow of hydro-cylinders, f) needed power of basket drive mechanism

The conditions of movement at simulation of lifting of articulated truck’s basket is given by setted change of the angular velocity $\dot{\theta}_3$ (Fig.5a) and the angular accelartion $\ddot{\theta}_3$ (Fig.5b) of basket in the function of duration of basket unloading cycle. For the certain increase step of duration of basket unloading cycle there is determined the change of static M_{o3s} (Fig.5b) and dynamic M_{o3d} torque of the drive mechanism and the change of mass m_z of material that is in basket. Diagrams shows that some great difference of the static and dynamic torque is when basket is lifting while mass of material in basket of truck starts to rushly unloading at the half of cycle.

By the changing and choosing the values in area of optimization there are abstract possible solution of the basket drive mechanism that are satisfied given constraints and setted criterias of the optimization. The abstract possible solution of drive mechanism have same values of the hydro-cylinder: diameter of piston/rod $D_3/d_3=140/90$ *mm*, but different transform functions r_{c3} (Fig.5c), apropos diferent joint coordinates which are connected with members of kinematic chain. According to the defined objectiv function, optimal solution of the basket drive mechanism presents variant V_1 which have maximum value of the transform function, apropos the minimum value of needed force F_{c3} (Fig.5d) in the hydro-cylinders during basket unloading cycle. For the possible variant solutions, with progam it can be determined needed pressure p (Fig. 5e), flow Q (Fig.5e) and power N (Fig.5f) of hydrostatic system that feeds hydro-cylinders of basket drive mechanism

4. CONCLUSION

The obtained analysis, which one part is given in this paper, shows that the general model of the drive mechanism of articulated trucks is built by kinematic pair consists of: supporting-moving member - basket of articulated truck, that are connected with the rotary joint of fifth class with one degree of freedom that is realised with acting of the pairs of bidirectional hydro-cylinders as actuators of hydrostatic system.

For the synthesis of basket drive mechanicm and based on defined mathematical model, there is developed program that provides the optimal defining (choice) of the mechanism parameters: the sizes of hydro-cylinders, the hydrostatic drive system and the coordinates of joints with whome is hydro-cylinders connected on the supporting-moving member and the basket.

For the area of optimization on beginning of program there is the given space in which are possible changes of the joint coordinates and the data file of standard bidirectional hydro-cylinders. The objective function is defined with the maximum value of tranfer function of of drive mechanism in whole range of the basket unloading

ACKNOWLEDGEMENTS

This paper is result of technological project "Theoretical and experimental researches of dynamics of transport mechanical systems", No. TR35049, supported by Ministry of Education, Science and Technological Development of the Republic of Serbia

REFERENCES

[1] Ž. Đorđević : *Analiza i sinteza pogonskih mehanizama dampera,* master thesis, Faculty of Mechanical Engineering, University of Niš, (2008).

[2] S. Anđelković*: Istraživanje i razvoj inženjerskog, industrijskog i ergonomskog dizajna zglobnog dampera,* master thesis, Faculty of Mechanical Engineering, University of Niš, (2012).

[3] D. Janošević: *Projektovanje mobilnih mašina*, Faculty of Mechanical Engineering University of Niš, ISBN 8680587443, 9788680587448, Niš (2006)

[4] Industrija 14. Oktobar - Kruševac: *Priručnik za ru-kovanje i održavanje dampera D22,* Kruševac, (1987).

[5] Articulated Dump Truck HM 300-2, *Materials and specifications are subject to change without notice*. KOMATSU is a trademark of Komatsu Ltd. Japan.

[6] Thomas H. L., Brian B. C., Ole M., Michael R. H., *Optimization of Front Axle Suspension System of Articulated Dump Truck*, The 1st Joint International Conference on Multibody System Dynamics, May 25–27, Lappeenranta, (2010).

Numerical Analysis of Elevator Ropes Vibration with Time Varying Length

Jovan Vladić[1*], Radomir Đokić[1], Anto Gajić[2], Dragan Živanić[1]
[1]Faculty of Technical Sciences, University of Novi Sad, Serbia
[2]Mine and Thermal Power Plant, Ugljevik, Republic of Srpska

Electric drive elevators represent a special group of transport machines for vertical lifting of a load with stressed dynamic features. The dynamic characteristics of the elevator car system play a very important role in elevator engineering.

Consideration of passengers travelling problems in an elevator car represents the study of complex processes and procedures. Nowadays, high ride quality of elevators is demanded. Besides modern elevator cars, we must provide the low vibration and noise levels.

Elevator’s dynamic models of hoist ropes whose length varies with time due to the up and down movement of the elevator car are presented in this paper. Also, longitudinal vibrations of elevator system’s elastic elements (steel ropes) were considered. Based on the dynamic law, equations of motion for the end of a rope wound on the driving pulley were established. Mathematical models are formed and expressed through differential equations of motion. For solving of the mathematical models of steel ropes vibration (systems of partial differential equations), we used in consideration of different boundary conditions at the end of a rope wound on the driving pulley and at the place of a rope conection with the elevator car. Using adequate mathematical programs (matlab) and implementing appropriate numerical methods, the procedures for solving of motion’s differential equations are presented in the paper.

Keywords: Steel ropes, elevators, mathematical models, numerical analyis

1. INTRODUCTION

A dynamic model with three degrees of freedom is usually used when setting a dynamic load in the case of vertical hoisting by a driving pulley. The model is applicable with small heights and low hoisting velocities. The rope weight is not really important in such cases.

However, when the rope weight is not to be neglected, e.g. at low hoisting velocities and great heights, a model with an indefinite number of degrees of freedom is applied, and the boundary conditions are set at the points where the rope comes and gets off the pulley and they are also set for the places where the cabin is hung, or actually the counterweight. On the other hand, at big hoisting heights, a bigger capacity usually requires higher velocities, over 2 m/s (express elevators). Bearing that in mind, it is necessary to adopt a dynamic model which includes the influence of changing the free rope length on its dynamic behavior, which leads us to an oscillatory system with changeable stiffness ($c = EA/l$).

Defining a dynamic model with changeable parameters is much more complex in comparison to defining the previous models, especially if we take into consideration the changeable boundary conditions and the steel rope slipping at the points where it comes and gets off the driving pulley.

At great lifting heights and great lifting velocities, a dynamic model is applied which considers the influence of changing the free rope length in relation to its dynamic behaviour [2], [7] and [8] where different solutions are applied for solving the partial differential equations of movement for the cabin side and the counterweight side. Besides, in [2] there is an analysis of a connection problem between longitudinal and transversal oscillations of the steel rope in exploitation facilities in mining ("Köppe" system).

Ref. [5] shows the problem of longitudinal oscillations and stability of movement of an elastic string with concentrated masses.

For solving partial differential equations of a hyperbolic type in the function of one space coordinate and time, a module has been developed ("hpde" function) which is applicable for a MATLAB software package.

Model developing and elevator process simulations have enabled us to define its behavior during exploitation,. i.e. secure the efficiency in choosing the best solutions, which includes reducing the negative factors to the minimum.

2. ELEVATOR MODEL WITH GREAT HEIGHTS AND MEDIUM LIFTING VELOCITIES

This group embodies elevators with the lifting velocity up to 2 m/s and it embodies the greatest number of passenger elevators in skyscrapers. The problem can be modelled as a system with an infinite number of degree of freedom (longitudinal stick oscillation) with suitable boundary conditions.

Forming of differential equations of rope oscillations (rope with constant length) is to be done through considering one side (the side of the cabin), so basically one examines longitudinal oscillations of a stick with the length equal L [1] and [7], Fig. 1. By representing the rope as a Calvin’s model, it can be written that:

$$S(x,t) = E \cdot A \cdot \frac{\partial}{\partial x} \cdot \left[u(x,t) + b \cdot \frac{\partial u(x,t)}{\partial t} \right] \qquad (1)$$

with:
E – elasticity modulus, Pa
A – rope cross-section, m^2

*Corresponding author: Faculty of Technical Sciences, Trg Dositeja obradovića 6, Novi Sad, Serbia, vladic@uns.ac.rs

u – rope elastic deformations, m
b – damping coefficient, s [9]

Based on de Lambert's principle, it can be written by observing the equilibrium of the elementary rope part:

$$\frac{q}{g}\cdot\frac{\partial^2 u(x,t)}{\partial t^2}=E\cdot A\cdot\frac{\partial^2}{\partial x^2}\left(u(x,t)+b\cdot\frac{\partial u(x,t)}{\partial t}\right)+q \quad (2)$$

with:
q – rope weight pro meter, N/m

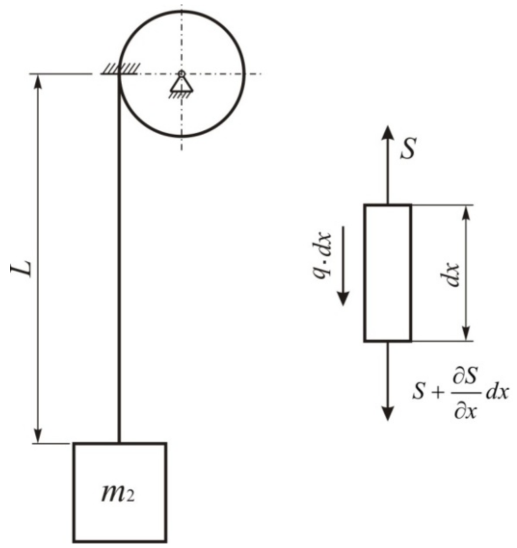

Figure 1: Oscillation of a rope with constant length

If one observed oscillation around the equilibrium position (position of static equilibrium), where $v(x,t)$ marks distance from a equilibrium position, and $u(x,0)=u_{st}$ elongation of the rope caused by its own weight, the differential equation for oscillations of the rope with constant length would look like this [1]:

$$\frac{\partial^2 v}{\partial t^2}=\frac{g\cdot E\cdot A}{q}\cdot\frac{\partial^2}{\partial x^2}\left(v+b\cdot\frac{\partial v}{\partial t}\right) \quad (3)$$

Solution of the equation (3) will be searched in a form of two functions which are functions of only one variable:

$$v(x,t)=X(x)\cdot T(t) \quad (4)$$

After differentiation of the expression and incorporation into the equation (3), two ordinary differential equations are obtained:

$$\begin{aligned}&\ddot{T}+b\cdot k^2\cdot C^2\cdot\dot{T}+k^2\cdot C^2\cdot T=0\\&X''+k^2\cdot X=0\end{aligned} \quad (5)$$

with:

$C^2=\frac{g\cdot E\cdot A}{q}$ – propagation velocity of an elastic wave.

These are well known equations for oscillations of a homogeneous beam with constant cross section, which is restrained on one side, and connected with mass on the other side [11].

Solution to the second equation has the following form:

$$X(x)=A_1\cdot\cos(k\cdot x)+A_2\cdot\sin(k\cdot x) \quad (6)$$

The constants A_1 and A_2 and the frequency equation are defined from limiting conditions:

a) For $x=0$, based on Fig. 1, elongation equals zero, $u(0,t)=0$, so the first boundary condition is $v(0,t)=0$.

b) For $x=L$, the second boundary condition is:

$$\frac{Q}{q}\cdot\left(\frac{\partial^2 v}{\partial t^2}\right)_{x=L}=-E\cdot A\cdot\frac{\partial}{\partial x}\left(v+b\cdot\frac{\partial v}{\partial t}\right)_{x=L} \quad (7)$$

A complete solution of the system of regular differential equations (5), and therefore the equation (3) as well, is given in [9]. A frequency equation of rope oscillations with the load on its back end, in the case when a driving pulley is standing still, is obtained by using the second boundary condition. After some time, we get a frequency equation like this:

$$\beta\cdot tg(\beta)=\alpha \quad (8)$$

with:

$$\beta=k\cdot(L-l),$$
$$\alpha=\frac{q\cdot(L-l)}{Q}.$$

It is possible to find solutions for the mentioned equation, when there are different weights of the rope and load. The equation has infinite amount of roots, so the number of own circular frequencies is infinite, too. In practice, the most important items are the first (basic) oscillation form and the lowest (basic) oscillation frequency. Based on an analysis for different weight connections between a free jib of the rope, and cabin weight, where at elevators we have $(\alpha<<1)$, with satisfying accuracy one can say that the basic oscillaton form is a straight line, i.e. the movement of rope points is the linear function of their distance from the point of rope arriving at the pulley, which is applied in the shown work situations.

3. ELEVATOR MODEL WITH GREAT HEIGHTS AND VELOCITIES OF LIFTING (EXPRESS ELEVATORS)

It is a group of contemporary passenger models (Bujr Khalifa, a building in Dubaii with the height of 828 metres, with over 160 floors. It has 57 elevators which do not go throughout the whole building. They are divided into three groups - till the 43rd, 76th and 123rd floor. The fastest elevator has a velocity of 18 m/s and the exploitation facilities in mining (the biggest velocity is 20 m/s and the pitch depth is 1 km at the most). For these elevators, the previously mentioned models are not suitable because of the fact that during lifting, by diminishing the free movement of a free rope jib, the basic parameter of a dynamic model is drastically changed – stiffness (EA/l). Based on that, a suitable dynamic model for describing dynamic behaviour of devices with a driving pulley in application at elevator drive and for forming differential equations of movement according to [8] is shown in Fig. 2. Such a model should be applied for elevators with high lifting velocities without the machine room (a small free rope length in the upper station), while for the express elevator it is necessary because of the parametric oscillations (a change in a free rope length) which can cause unstable movement and unpermitted load of elevator supporting elements with big consequences (tearing the rope, human victims and material damage).

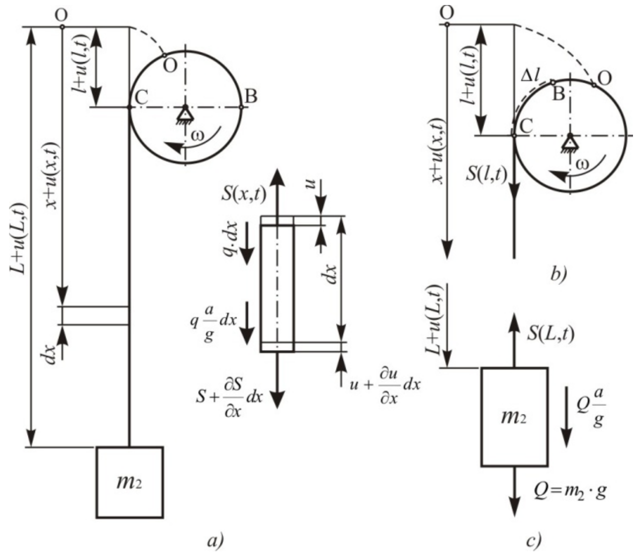

Figure 2: Dynamic elevator model with boundary conditions: a) on a pulley without slipping, b) on a pulley with slipping, c) on a cabin [8]

Just as in the previous example, the equilibrium equation of the elementary rope part is:

$$\frac{q}{g}\cdot\frac{\partial^2 u(x,t)}{\partial t^2}=E\cdot A\cdot\frac{\partial^2}{\partial x^2}\cdot\left[u(x,t)+b\cdot\frac{\partial u(x,t)}{\partial t}\right]+q\cdot\left(1\pm\frac{a}{g}\right) \qquad (9)$$

with:

a – driving mechanism acceleration, m/s^2.

As a boundary condition at the meeting point of a rope and a driving pulley out of the equlibrium of elements, Fig. 2a, we get:

$$M_m=\frac{R}{i\cdot\eta}\cdot E\cdot A\cdot\frac{\partial}{\partial x}\cdot\left[u(l,t)+b\cdot\frac{\partial}{\partial t}u(l,t)\right]+J_r\cdot\frac{a\cdot i}{R} \qquad (10)$$

with:

M_m – driving motor torque, Nm

i – gear ratio

η – driving mechanism efficiency

J_r – moment of inertia of rotating masses, reduced to the motor shaft, kgm^2

R – driving pulley radius, m.

In equation (10), the articles in the brackets are not constant, but they depend on the length, that is, the velocity of rolling the rope onto a pulley: $u(l,t)$ and $\frac{\partial u(l,t)}{\partial t}$. The size of deformation on the rolled part of the rope can be defined with integration for the observed time period according to:

$$u(l,t)=\int_0^t\frac{\partial u(l,t)}{\partial x}\left(\frac{dl}{dt}\right)\cdot dt \qquad (11)$$

with:

l – the rope part rolled on a pulley, m

$\frac{dl}{dt}$ – the velocity of rolling the rope (lifting), m/s.

Expression (11) shows the case when the rope sliding on a driving pulley is neglected. The problem is greatly complicated because of elastic sliding of the rope on a driving pulley (Δl), Fig. 2b, where the above expression can be written as:

$$u(l,t)=\int_0^t\frac{\partial u(l,t)}{\partial x}\left(\frac{dl}{dt}-\frac{d}{dt}(\Delta l)\right)\cdot dt+\Delta l\cdot\frac{\partial u(l,t)}{\partial x} \qquad (12)$$

with:

$\frac{d}{dt}(\Delta l)$ – velocity of elastic sliding, m/s.

Boundary condition on the connection point of rope and cabin, Fig. 2c, is:

$$Q=E\cdot A\cdot\frac{\partial}{\partial x}\left(u(L,t)+b\cdot\frac{\partial u(L,t)}{\partial t}\right)+\left(\frac{Q}{g}\cdot\frac{\partial^2 u(L,t)}{\partial t^2}-a\right) \qquad (13)$$

An analytical solution of a system of differential equations with uncholomos boundary conditions is extremely complicated, and it demands application of different procedures shown in [6] and [8].

It is noticeable that the analysis scheme (modelling and solving mathematical models) is complex because it is essential to form adequate dynamic models with acceptable simplifications for various kinds of elevators according to their specific characteristics. Analytical solutions of a closed form are possible only for the simplest of cases, so numerical procedures have been applied lately, i.e. suitable software packages for dynamic analysis, such as MATLAB-Simulink, ADAMS, Mathcad, Mathematica etc.

4. NUMERAL PROCESS AND ELEVATOR OPERATING SIMULATIONS

Based on the previous analysis it can be deduced that it is possible to apply with satisfying accuracy the elevator models with reduced cabin masses, counterweight and elements of driving mechanism with the rope models. At the express elevators, a rope can be seen as a visco-elastic body with varying stiffness. The rope stiffness changes in the function of change of the free rope length, and the basic oscillation form is an approximatelly straight line. However, sliding between the ropes and a driving pulley in the coming point is neglected.

Modelling of movement can be done in various ways through models of driving mechanisms. These are the ways:

- Defining the function for changing the number of revolutions of electrical motor (through the velocity of a driving pulley),
- Defining acceleration on a driving pulley,
- Assigning driving force depending on the way of releasing a driving motor, Fig. 3a,
- Modelling of a driving moment on the rotor of an electrical motor through a "static characteristic", Fig. 3b etc.

Modelling of a driving moment, i.e. driving force, is complicated because it depends on the features of the driving motor, i.e. electromagnetic flux, balance masses, (especially of the first shaft, and the way of control (direct motor supply, motors with one or two velocities, control via frequency regulator...). These influences are defined in electronics through a system of six differential equations which describe the interdependence of mechanical and electric parameters.

It is most common to approximately define the amount of driving force in the transferring operating regime [6], depending on the way of releasing the driving motor, based on these relations:

$P(t) = P_0 = \text{const.}$, Fig. 3a (p. 1)

$P(t) = P_0 \cdot \left(1 - \frac{t}{t_1}\right)$ – soft drive regime, Fig. 3a (p. 2)

$P(t) = P_0 \cdot \left(1 - \frac{t^2}{t_1^2}\right)$ – medium drive regime, Fig. 3a (p. 3)

$P(t) = P_0 \cdot \left(1 - \frac{t^4}{t_1^4}\right)$ – rigid drive regime, Fig. 3a (p. 4)

with:

t_1 – acceleration time, s

P_0 – pulled force (moment), N

More precisely, but analytically more difficult, the driving moment can be defined by a so-called "static characteristic of an electrical motor" in the velocity function, or number of revolutions – P=f(v). The moment characteristic of an asynchrone machine in Fig. 3b, has this form according to [4]:

$$M = \frac{q}{2 \cdot \pi \cdot f} \cdot U^2 \cdot p \cdot \frac{\frac{R_r^{'}}{s}}{\left(R_s + \frac{R_r^{'}}{s}\right)^2 + \left(X_{\gamma s} + X_{\gamma rk}^{'}\right)^2} \tag{14}$$

with:

q – number of phases

$f = 50$ – network frequency, Hz

U – change of voltage, V

p – number of pole pairs

s – slip

R_s – stator resistance, Ω

$R_r^{'}$ – narrowed down rotor resistance, Ω

$X_{\gamma s}$ – reactance of overflowing of stator, Ω

$X_{\gamma rk}^{'}$ – narrowed down reactance of rotor overflowing, Ω.

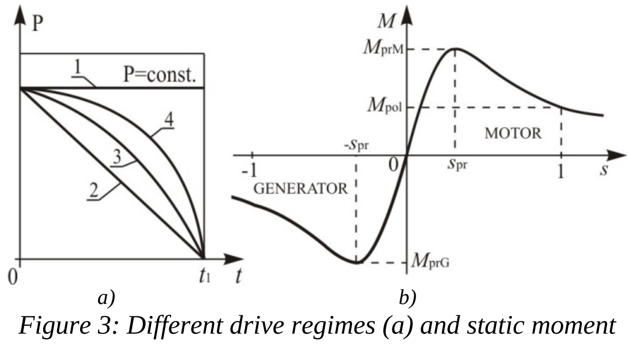

Figure 3: Different drive regimes (a) and static moment characteristic of an asynchronous machine as a function of slip (b), [4]

This paper represents the case of asigning movement through a change in the number of revolutions of electrical motor and defining acceleration on a driving pulley. In such cases a simulation of dynamic behaviour of elevator elements is performed for different operating regimes (acceleration, stationary movement and breaking).

4.1. Defining the change in number of revolutions on a driving pulley

Setting the movement at elevators is a problem which is not easily and simply solved. Most software does not contain tools for representing the supporting rope - driving pulley system. In such cases one has to use a combination of existing tools in order to get satisfying results. After various attempts of movement, several suitable solutions emerged. Setting a function for chanaging the number of revolutions of an electrical motor can be seen as setting a function for changing the position of a certain marker on the rope in the direction of lifting the cabin. That enables setting a translatory movement on a translatory or cilindric joint, which can simply model the connection of a rope to a driving pulley.

Description of a movement in time can be assigned in many ways, although a combination of commands *If* and *Step* is the most often applyed The *If* command has the following inscription:

IF (expression1: expression2, expression3, expression 4).

Expression1 is actually a variable in a movement function, which is time in this case. If *expression1* is less than a zero, the function equals *expression2*. If it equals zero, the function is equal to *expression3* and when it is bigger than zero, it equals *expression4*.

Step command defines the *Step* function, which is approximately like Heaviside function with a cube polynome.

This equation defines *Step*:

$$Step = \begin{cases} h_0 & : x \le x_0 \\ h_0 + (h_1 - h_0) \cdot \left[\frac{x - x_0}{x_1 - x_0}\right]^2 \cdot \left\{3 - 2 \cdot \left[\frac{x - x_0}{x_1 - x_0}\right]\right\} & : x_0 < x < x_1 \\ h_1 & : x \ge x_1 \end{cases}$$

Step command format goes like this:

STEP (x, x_0, h_0, x_1, h_1)

with:

x – independent variable,

x_0 – real variable which defines h value where the *step* function begins,

x_1 – real variable that defines h value where the *step* function ends,

h_0 – the *step* function value at the beginning,

h_1 – the final value of the *step* function.

It should be noted that the movements can be given by displacement, by velocity or acceleration, depending on what is easier to define at a specific moment. In this paper, movements are defined by a *Step* function and the *If* command through a big velocity of the driving pulley.

5. MOVEMENT SIMULATION RESULTS GIVEN THROUGH A CHANGE IN THE NUMBER OF REVOLUTIONS IN AN ELECTRICAL MOTOR

The case: Lifting the cabin with a carrying capacity of 1000 kg, at a velocity of 20 m/s, for the lifting height of 500 m, and a damping of 1 Ns/mm.

Function of change of cabin lifting velocity is represented like this:

IF(time-24:step(time,0,0,8,20000), step(time,24,20000,32,0), step(time,24,20000,32,0))

When the time is less than 8 s, then the velocity changes according to the step function, in a way that at the beginning the velocity equals zero, and within 8 s the velocity is 20 m/s. After that the cabin moves at a velocity of 20 m/s for the following 16 s. Then the breaking starts. This part in the previous expression is represented by another *step* function according to which the velocity of 20 m/s at 24 s, changes to 0 mm/s at 32 s.

The mass oscillating at the cabin side is $m_2 = 1000$ kg. The simulation result is shown in the following figures. Fig. 4 represents a pulley velocity through which the movement was given, as well as the change in cabin acceleration in cases when rope stiffness is a constant and a variable with reducing the free length at the side of the cabin. Fig. 6 shows how the amplitude of cabin oscillations significantly increases in the part where the change of stiffness is great.

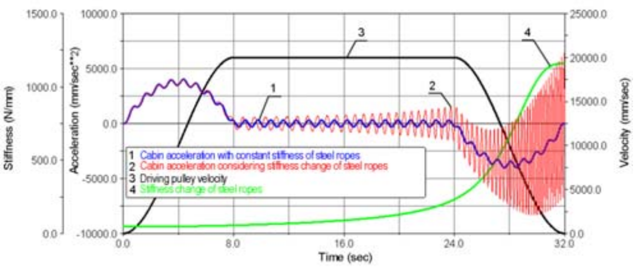

Figure 4: Diagram of change of ample pulley velocity and acceleration with a constant and varying rope stiffness

Fig. 5 represents the change of the cabin position during simulation, as well as the change in acceleration when the damping in ropes is considered. The figure shows that in the part where the cabin stops, an increase in oscilation frequency occurs, which is directly related to a significant increase in stiffness in that part.

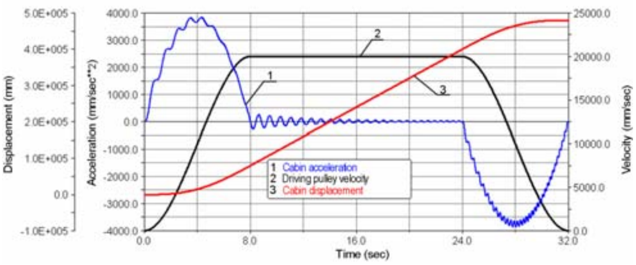

Figure 5: Diagram of the change in cabin position and acceleration considering inner friction within the ropes

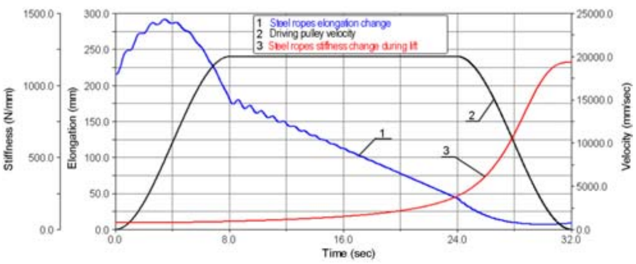

Figure 6: Diagram of change in rope stiffness and elongation during a simulation when the lifting height is 500m

Besides the change in stiffness of driving ropes in Fig. 6, there is also represented an elongation of ropes which is changed with the change in free length at the cabin side.

6. CONCLUSION

The paper represents the procedures and methods of elevator modelling, depending on their features, with the application of numerical methods and contemporary software packages. The represented elevator models enable to grasp the most influential parametres which occur during their exploitation.

The models provided in the paper enable simulations of elevator behaviour with a defined pulley movement (control through the number of revolutions of an electrical motor). Based on the previous analysis, we came to the conclusion that:

It is possible to analyse the influence of weight of the cabin, cabin load, lifting height, rheological rope features (E, A, b, c,...) influences of various movement diagrams (the defined movement through a control system).

It is possible to authentically simulate the movement of a driving pulley, in accordance with the control system of a real elevator,

At greater lifting heights, one must take into consideration the influence of the change in stiffness, because it strongly influences the size of dynamic load, especially at high movement velocities and low inner friction, i.e. damping,

Simulation results can be used for determining control parameters (determining an optimal moment of change from accelerated to stationary movement and breaking), aiming at decreasing the dynamic load,

The given simulations make it possible to determine the critical lifting velocity (through varying it) depending on the relations between the change of stiffness and the size on inner friction within ropes.

ACKNOWLEDGEMENTS

This paper is part of the research included in the project *Theoretical-experimental dynamic researches of transporting mechanical systems*, supported by the Ministry of Science and Technological Development of the Republic of Serbia. The authors would like to thank the Ministry for the financing of this project.

REFERENCES

[1] R. Đokić, "Development of analitic-numerical procedures for determining of elevator's dynamic behaviour", Master thesis, Faculty of Technical Sciences, Novi Sad, (2010)

[2] S. Kaczmarczyk, W. Ostachowicz, "Transient vibration phenomena in deep mine hoisting cables", Journal of Sound and Vibration, 262, p. 219–244, (2003)

[3] H. Kimura, H. Ito, T. Nakagawa, "Vibration analysis of elevator rope (Forced vibration of rope with time-varying length)", Journal of Environment and Engineering, Vol. 2, No. 1, pp. 87-96, (2007)

[4] E. Levi, V. Vučković, V. Strezoski, "Fundamentals of electrical engineering (Power converters)", Faculty of Technical Sciences Novi Sad, (1996)

[5] M. Pakdemirli, A.G. Ulsoy, "Stability analysis of an axially accelerating string", Journal of Sound and Vibration, 203, 5, pp. 815-832, (1997)

[6] В. Ф. Столярчук, "Dynamic of Vertikal Lifting", University of L'viv, 1965. (org. in Russian)

[7] J. Vladić, "Contribution to the determination of security against slipping of dinamicaly loaded rope in the system of power transmission through driving pulley",

Master thesis, Faculty of Technical Sciences, Novi Sad, (1982)

[8] J. Vladić, P. Malešev, R. Šostakov, N. Brkljač, "Dynamic analysis of the load lifting mechanisms", Strojniški vestnik, 54, 10, pp. 655-661, (2008)

[9] J. Vladić, R. Đokić, M. Kljajin, M. Karakašić, "Modelling and simulations of elevator dynamic behaviour", Tehnički vjesnik/Technical Gazette, Vol. 18, No. 3, Slavonski Brod, pp. 423-434, (2011)

[10] J. Vladić, R. Đokić, "Dynamic simulations and type of electrical elevators models", Machine Design, Vol. 4, No. 4, ISSN 1821-1259, pp. 219-224, (2012)

[11] B. Vujanović, "Theory of oscilations", University of Novi Sad, (1995)

The Influence of Structure Anchoring on Eigenvalues and Translations

Goran Radoičić[1*], Miomir Jovanović[1], Ivan Savić[2]
[1]Faculty of Mechanical Engineering/Department of Transport Engineering and Logistics, University of Niš

This paper presents the investigation of dynamic and static behaviour of a heavy frame structure. Two models of the same type of real crane are considered. The free-standing and anchor model were simultaneously developed for the research purpose. By modal analysis, the characteristic eigenfequencies were extracted. Conclusions on the propagation field of eigenvalues were adopted in the case study of both models. The influence of tower height and anchoring on static deflection i.e. translation of the structure under load was also considered in the scope of the paper. The paper provides certain limitations in terms of applied tower heights. Normal modes analysis and static testing of both models were carried out using FEM technology.

Keywords: Frame structure, eigenfrequency, translation

1. INTRODUCTION

The tower crane height can be changed by adding corresponding frame sections. For assembling the tower crane on a building site, the crane boom is installed so as to initially satisfy the maximal nominal range. Then, the crane tower is also erected to the maximal necessary hoisting height.

It is interesting to observe the same tower crane with more different heights. Since it is very difficult to provide the experimental research for more of the same type real cranes with different heights at a time, the numerical FEM analysis is applied alternatively. By this analysis, the discrete values of own parameters for selected heights of the tower crane are computed. On the basis of these analyses, we can see how the change of design influences static (translations) and dynamic (eigenvalues, vibration period) behaviour of high and heavy structures,i.e. how own static and dynamic parameters depend on the geometry of these machines. Such structural analysis is an integral part of the support structures design because it often leads to the geometry redesign of the structure in accordance with the values of own parameters.

In civil engineering there is a practice to install the local safety connection i.e. anchor device from a crane to a building under construction. It is usually called anchoring. The crane anchoring to the building is performed in order to increase the crane stability. These safety connections are usually realized in two points of a building at the same selected height. Manufacturers give recommendations to the prevention of incidents in the use of a crane with large hoisting heights, which contain the description of safety connection. However, an anchoring problem should be considered from the point of vibrating comfort. Hence, it should be explored how the anchoring contributes to the vibrating comfort and if the anchor point height influences the quantity of strain energy (deformation work).

2. THE DEVELOPMENT OF A THEORETICAL MODEL TO ANALYSE THE STRUCTURE

The equation of motion for an un-damped linear system is expressed in the matrix form, Eq. (1), while free vibrations have the harmonic form, Eq. (2).

$$[M]\cdot\left\{\ddot{q}\right\}+[K]\cdot\left\{q\right\}=\left\{0\right\}, \tag{1}$$

$$\left\{q\right\}=\left\{\Phi\right\}_i\cdot\cos\omega_i\cdot t \tag{2}$$

Eigenvalues (frequencies) and eigenvectors of a model are determined in normal modes analysis. For each eigenvalue, which is proportional to a natural frequency, there is a corresponding eigenvector, or mode shape. For solving the free un-damped vibratory movement, the normal modes analysis uses the frequency equation as follows:

$$\left|[K]-\omega^2\cdot[M]\right|\cdot\left\{\Phi\right\}=\left\{0\right\}, \tag{3}$$

In Eq. (3), there are the mass matrix [M], the structural stiffness matrix [K], the i^{th} natural circular frequency in radians per unit time ω_i and the i^{th} eigenvector $\{\Phi\}$ representing the mode shape of the i^{th} natural frequency.

This study considers the results of numerical analyses for the developed FEM model of the real frame crane structure POTAIN 744E. In the study, the discrete crane model with 17.6 m of height measured from the ground to the lower jib belt was initially used. For modelling the entire structure, 1146 nodes and 1667 finite elements were used, [1, 2]. Three types of finite elements were applied. Thus, the beam element, with 6 degrees of freedom in each of nodes, was used for the description of frame structure. For the description of boom pendants the rod element was used. The reinforced concrete footing was modelled by the 8-node solid elements. For modelling several different tower heights, a group of elements – the tower section was used. The addition of the tower sections corresponds to the procedure of a real crane erection to a certain height.

*Corresponding author: PUC Mediana Niš, str. Mramorska 10, Niš, goran.radoicic@jkpmediana.rs

Figure 1 shows the anchor model of the tower crane (Model "b"). This model has a safety connection, where *L* is the length and *h* is the height of this connection. Other labels in Fig. 1 are: the tower height *H* under the boom in the position without load, the maximal boom range L_{max}, the deflection Δz in global vertical direction and the load *Q*.

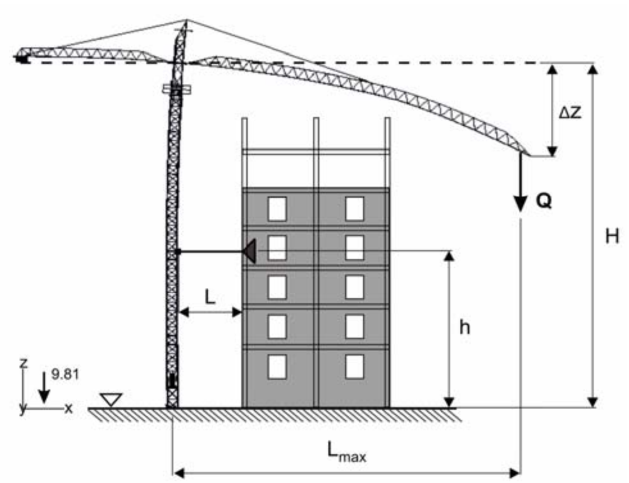

Figure 1: Anchor model of crane

Besides the anchor model (Model "b"), the paper simultaneously considers another model. This is the model of crane freely supported by own concrete footing on the ground (Model "a" - free-standing model), Fig. 2. The point of added connection – the anchoring point is placed on the height *h*=29.7 m from the ground and the normal distance *L*=4 m from the tower, Fig. 2. The tower height *H* is changeable in the range from 17.6 to 51.3 m by adding appropriate tower sections. All tower heights in Fig. 1 are selected for the investigation. The anchor device is simplistically shown, Fig. 2, by a normal tie rod and a joint connection just placed on the building. The anchor connection length *L* depends on the building geometry and working area availability. The anchor connection height *h* depends on the crane and building height. Other solutions of the anchoring with different anchor connection heights *h* and distances *L* can also be applied in practice, Fig. 3.

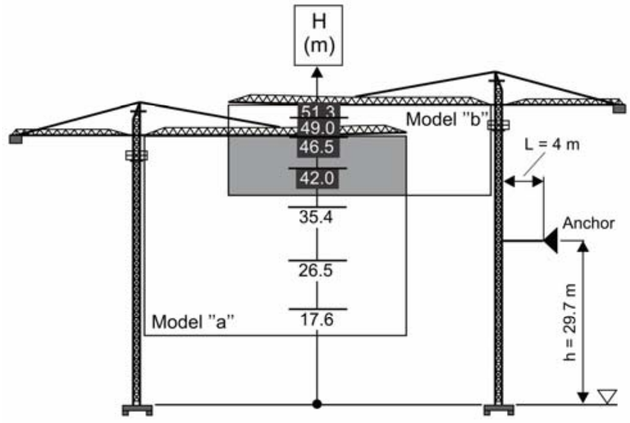

Figure 2: Two crane models for testing

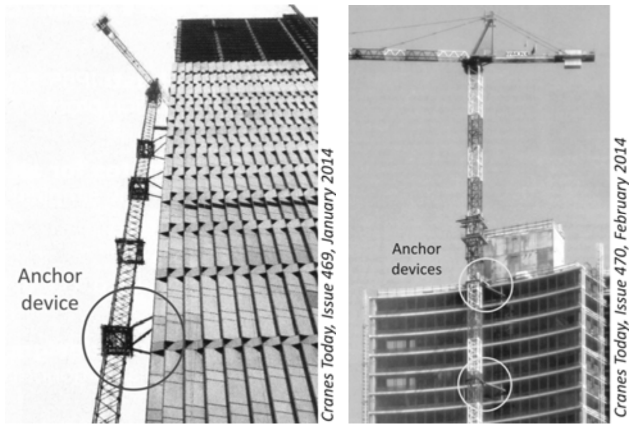

Figure 3: Some solutions for crane anchoring

Table 1: Eigenfrequency [*Hz*]

Mode shape	The Model "a" tower height in metres					The Model "b" tower height in metres			
	17.6	26.5	35.4	42	46.5	42	46.5	49	51.3
1	0.1687	0.1417	0.1243	0.1148	0.1096	0.1596	0.1462	0.1436	0.1228
2	0.4749	0.3826	0.3026	0.2535	0.2257	0.2798	0.2439	0.2297	0.2136
3	0.5596	0.4647	0.3505	0.2821	0.2456	0.4299	0.3880	0.3737	0.3472
4	1.5444	0.9879	0.7552	0.6638	0.6210	0.8854	0.8632	0.8857	0.8456
5	1.6342	1.1370	0.9669	0.9149	0.8932	1.5556	1.1753	1.0593	0.9399
6	2.0274	2.0229	2.0190	2.0160	2.0139	1.8912	1.8821	2.0154	1.8783
7	2.5162	2.5064	2.5034	2.5021	2.5015	2.4827	2.4729	2.4795	2.3142
8	2.7747	2.7744	2.7725	2.7376	2.6081	2.6545	2.5558	2.5062	2.4855
9	3.0221	2.8901	2.8275	2.7821	2.7778	2.8441	2.8263	2.7771	2.7989
10	3.4109	3.3877	3.3677	3.3449	3.1596	3.4206	3.1187	3.0499	2.9500

3. THE PROPAGATION FIELD OF EIGENVALUES

Seven tower heights *H*, for normal modal analysis, were selected. Five of them, from the range *H*=17.6÷46.5m, were used in order to determine the eigenvalues development trajectory of the model "a" as well as four heights from the range *H*=42÷51.3 m in the modal analysis of the model "b". On that occasion, the research of modal shapes for the two tower heights, *H*=42 m and *H*=46.5 m, and both models (free-standing and anchor model) was performed. Modal analysis of both crane models was performed using the software MSC FEMAP/NASTRAN [3]. The *Lanczos* real eigenvalue extraction method was used to determine eigenvalues. The first hundred mode shapes of both models were extracted by this method. The first ten eigenfrequencies from Table1 were taken for further analysis.

Fig. 4 provides an insight into periods of vibration and eigenfrequencies comparatively. In the figure on the right, the development trajectories of the own circular frequencies ω for the model "a" (free-standing model) and different tower heights *H*, are shown. Starting from the lowest (*H*=17.6 m) to the highest height (*H*=46.5 m), the eigenfrequency ω had a non-linear decrease. Among them, the circular frequency ω_4, Fig. 4, had the largest total decrease for the entire range of heights. This decrease takes value:

$$\Delta\omega_4 = \left| \frac{\omega_4^{H_5} - \omega_4^{H_1}}{\omega_4^{H_1}} \right| \cdot 100 = 56.79\% \qquad (4)$$

Follow the eigenfrequency decrease $\Delta\omega_3$=56.11% and $\Delta\omega_2$=52.46%. In the case of modal shapes with lower frequencies ω_2, ω_3 and ω_4, the strain energy is the most expressed. Thus, these frequencies are used to calculate the damping matrix, which requires the choice of two dominant frequencies for transient analysis, [4].

Two interesting mode shapes with frequencies ω_6 and ω_7, whose values are almost equal for all heights *H*, can be seen in Fig. 4. In these cases, the overall geometry had a more important influence to the vibration than the tower height. For these mode shapes, with the increase of tower height, the total decrease of frequency is calculated and amounted to $\Delta\omega_6$=0.66% i.e. $\Delta\omega_7$=0.58%. The strain energy was mainly distributed to the vertical translations of the hoisting jib in the case of *mode 6*, as well as to the torsion of hoisting and counter jib in the case of *mode 7*.

The first lowest circular frequency ω_1 corresponds to the rotation of the entire structure around the vertical *z*-axis for all heights *H* and the models. This basic frequency of torsional vibrations was experimentally identified in the investigation [5]. A larger vertical deflection Δz corresponds to the modal shapes of frequencies ω_2 and ω_4 for the model "a", i.e. ω_3 and ω_5 for model "b". These are the shapes which imply the highest axial force and stress in the structure.

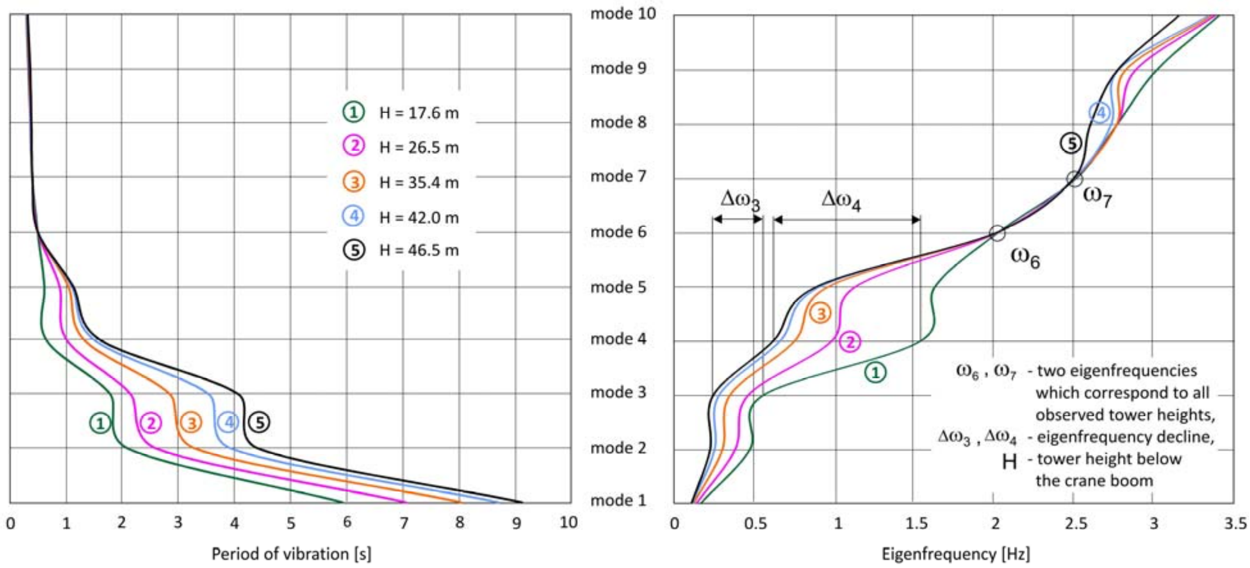

Figure 4: Periods of vibration and eigenfrequencies for the first ten mode shapes of the Model "a"

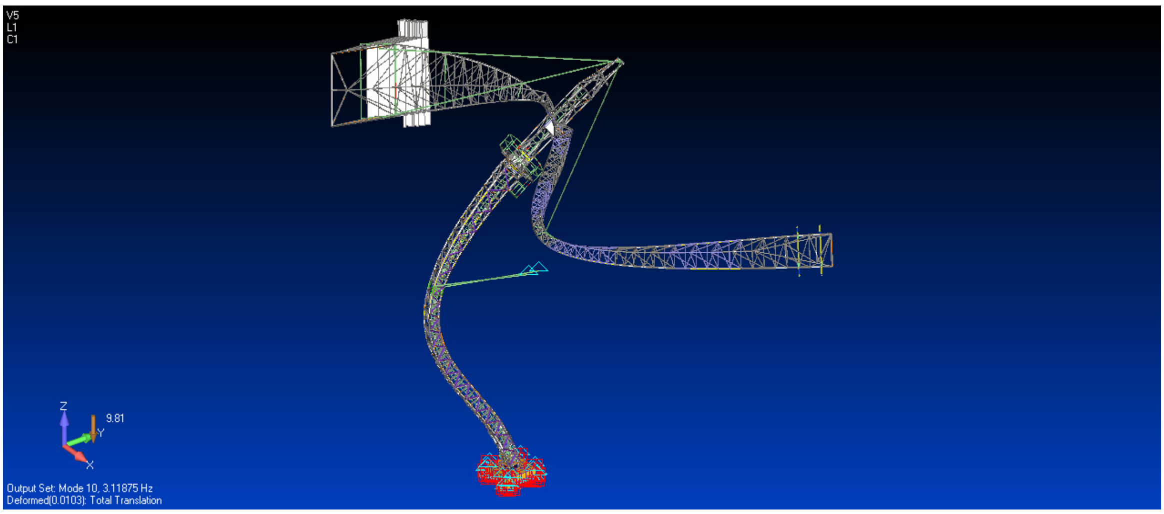

Figure 5: Anchor model, H=46.5 m, h=29.7 m, Mode 10, ω_{10}=3.11875 Hz

Fig. 5 shows an interesting mode shape, *mode 10*, which justifies the existence of the anchor connection because the strain energy of crane, in this mode, caused the lateral translation of frame mast structure. This mode also characterizes a torsional property of boom and counter-boom vibrations. The anchor connection in Fig. 5 allows three degrees of freedom in the two connection points as three rotations around global axes (pinned connection).

Fig. 6 shows another interesting own shape of vibration, *mode 20*. It is about the same model and tower height H. The strain energy is distributed to incite the bending of the structure. The period of vibration is short, T_{20}=0.138 s.

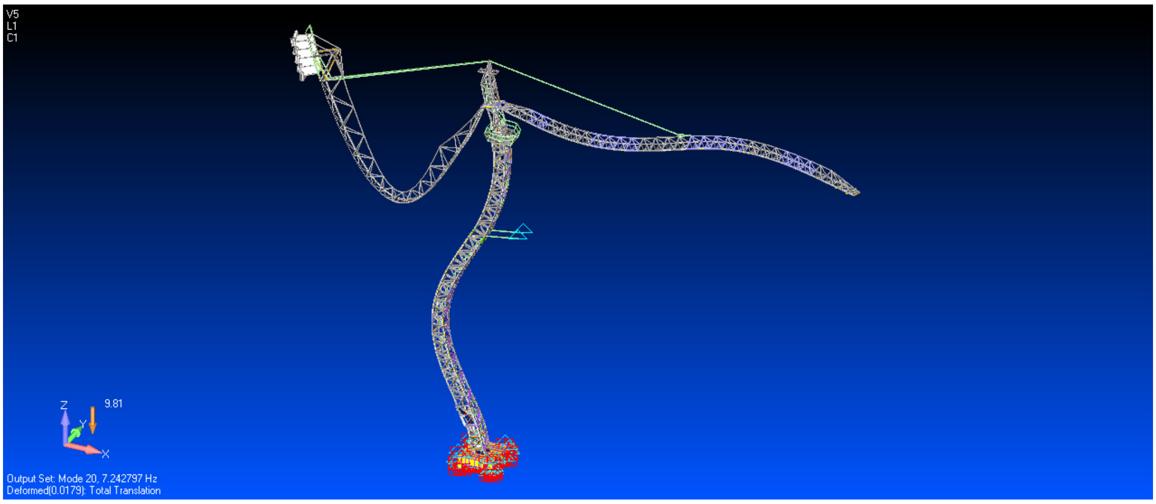

Figure 6: Anchor model, H=46.5 m, h=29.7 m, Mode 20, ω_{20}=7.242797 Hz

The analysis of two crane models indicates significant differences of eigenvalues. In Fig. 7, we can see the differences of eigenfrequencies for the two identical applied heights, h=42 m and h=46.5 m. The eigenvalues of the anchor model, for a few basic mode shapes, are higher in relation to the free-standing model up to the fifth mode shape. For example, the lowest frequency of tower rotation ω_1 is increased by 39% in the case of height of h=42 m of the anchor model, which leads to a faster damping of structural vibration (i.e. period of vibration had a shorter duration).

Fig. 7, on the right, shows the darker area of frequency change trend (trend-line area) with the increasing tower height. This is the area of non-recommended tower heights to use. Actually, the tower heights formed by adding the tower sections in this area should be avoided.

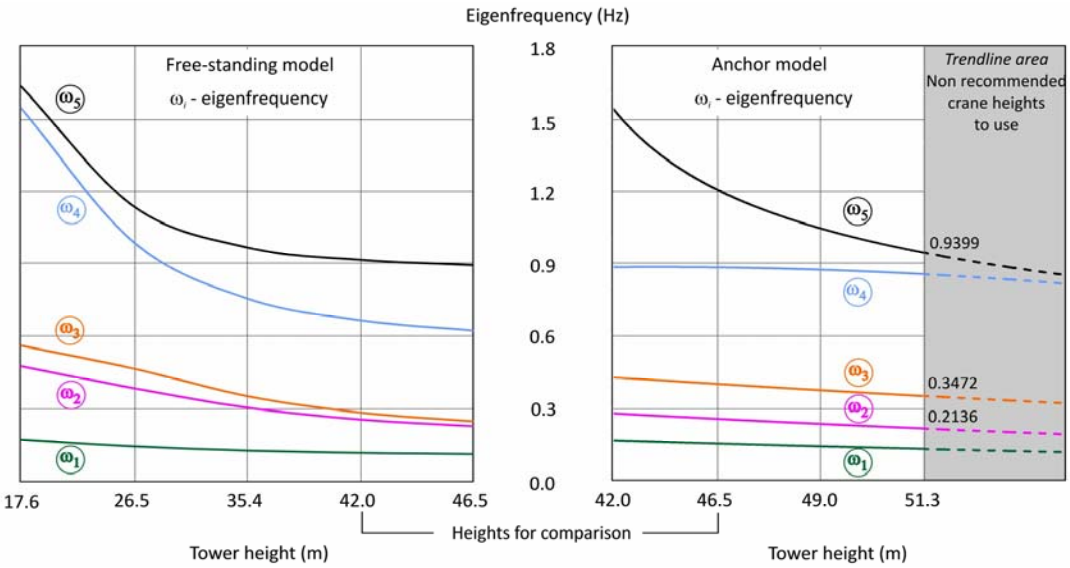

Figure 7: Eigenfrequency decrease depending on the increase of tower height

4. A TRANSLATION ANALYSIS OF THE STRUCTURE UNDER LOAD

The geometrically-linear numerical analysis is verified by the experimental results with the deviations of translation less than 1.5% in relation to the nonlinear analysis, [1]. Hence, the static change of boom deflection in function of the tower height using the linear static analysis in the MSC FEMAP/NASTRAN software [3] is further required. The deflection of free boom end Δz for different tower heights H under the effect of limit static load Q=23.5 KN at the longest boom reach L_{max}=45m is required.

The obtained results are shown in the total translation diagram, Fig. 8. The vertical translation in z global direction here is the dominant translation. The curves a and b, in the diagram, represent the total translations of the hoisting boom free end for the free-standing model (curve a) and the anchor model (curve b). By changing the tower height H, the curves a and b change their values. Three areas of solution for the applied tower heights in the total translation diagram, Fig. 8, were identified. From left to right, the first height area is applied to the free-standing model of the crane. The limited height of this area is H=46.5 m (white area). It follows the anchor area (slightly darker). The beginning of this area corresponds to the crane manufacturers recommendation according to which the anchoring for tower heights H>40m should be used (actually, the first following height in the diagram is 42 m). Greater heights (H>46.5 m) from those declared by the manufacturers in the research are numerically tested. Generally, the boom deflection Δz is higher for the free-standing crane model at all tower heights.

According to the diagram in Fig. 8, more pronounced total translations in both models can be expected for the heights from the darkest area (H=49÷53.5m). This is also an expected domain of the pronounced dynamic sensitivity with significant translation amplitudes and longer periods of vibration. The results of analysis indicate the reduction of static deflections of the structure up to 15% by anchoring the crane at the height of $h\approx30$ m. Although the anchoring of cranes at heights of H<40 m should not apply, the study includes the computation of boom translations to lower tower heights as well as the heights which were increased by adding a number of the tower sections.

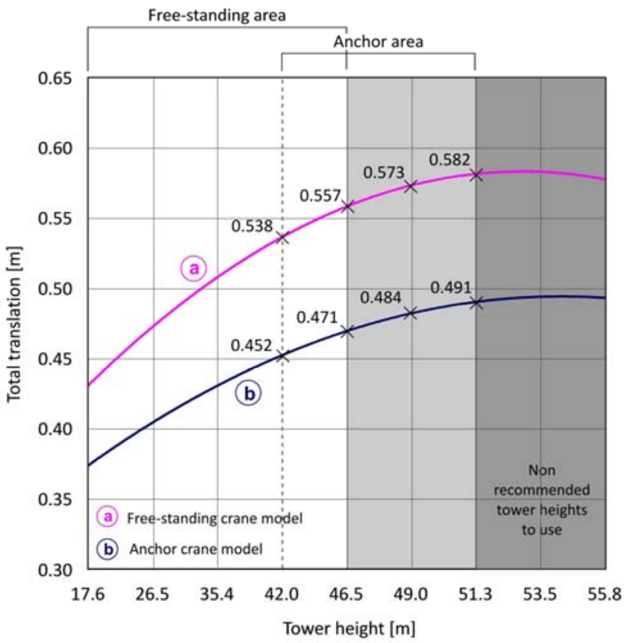

Figure 8: Total translation diagram

With this approach, the total translation trends were determined. Thus, the curves a and b, Fig. 8, were completely determined. The tower heights from the darkest area in the diagram, Fig. 8, are not recommended for use due to the significant enlargement of the structural mass of the crane. The use of these heights can jeopardize the general structure stability in incidental situations or due to overload.

The question of optimal anchor height h of the lateral crane connection to a building in terms of crane behaviour at external excitation can also be an interesting point. Having in mind the recommendation for minimal tower height of the anchored crane, in this paper the anchor height h=29.7 m, Fig. 2, was tested. The anchor height h i.e. anchoring point place is practically always conditioned by the current built height of the building.

CONCLUSION

1. Design changes, in terms of the tower and anchor height, can really influence the eigenvalues of heavy lifting machines.
2. By anchoring the tower crane, the static deflections of structure in the most expressed deformation areas are reduced up to 15%.
3. At the same time, the kinematic anchor connections are elements for providing the structure stability and the design solutions which contribute to the vibration comfort quality. By the theoretical solution of connection, depending on the two selected crane tower heights of 42 and 46.5 m, the period of vibration is decreased up to 40% in relation to the free-standing crane model (calculated as $T = 1/\omega$ on the basis of data from Table 1).
4. By numerical calculating of eigenvalues, two principles are defined: 1) "higher height" = "lower frequency", 2) "anchoring" = "less strain energy". The first principle indicates the increase of elastic translations and periods of vibration depending on the increase in crane height. The second principle indicates that smaller deformation work and faster vibration damping of the entire system are achieved by anchoring.
5. On the basis of the previously conducted simulations, we can formulate another principle as: "higher anchor place" = "less strain energy".
6. The adding of tower sections is limited by the permissible own mass of the crane and structural stresses. The increase in the number of the tower sections leads to the general instability of the structure.
7. The influence of different anchor heights of the kinematic couple of crane and building on static and dynamic parameters of the crane at different tower heights will be the subject of future research.

ACKNOWLEDGEMENTS

The paper is a part of the research carried out under project TR35049. The authors would like to thank the Ministry of Education and Science of the Republic of Serbia for their support.

REFERENCES

[1] M. Jovanović, G. Radoičić, G. Petrović and D. Marković, “Dynamical models quality of truss supporting structures”, Facta Universitatis – Series Mechanical Engineering, Vol. 9(2), pp. 137-148, (2011)

[2] G. Radoičić and M. Jovanović, “Experimental identification of overall structural damping of system”, Strojniški vestnik – Journal of Mech. Eng., Vol. 59(4), pp. 260-268, (2013)

[3] ***, “MSC Nastran Version 68 - Basic Dynamic Analysis”, MSC - Software Corporation, Santa Ana, USA, http://www.mscsoftware.com, (2004)

[4] T. Rose, “An approach to properly account for structural damping, frequency-dependent stiffness/damping, and to use complex matrices in transient response”, Worldwide Aerospace Conference & Technology Showcase, presentation no. 6, *www.mscsoftware.com/events/aero2002/partner/index.cfm* , (2002)

[5] M. Jovanović, G. Radoičić and D. Marković, “Theoretical and experimental identification of the base mode of torsional vibrations of tower crane“, Proceedings of XX International Conference on „Material Handling, Construction and Logistics“, Belgrade, 3-5 October 2012, pp. 95-100

Theoretical Aspects of Zip Line Analysis

Mircea Alamoreanu[1], Andrei Vasilescu[2]*
[1]Faculty of Technological Equipment, Department of Construction Equipments, Technical University of Civil Engineering Bucharest, Romania
[2] Faculty of Engineering in Foreign Languages, Department of Structural Mechanics, Technical University of Civil Engineering Bucharest, Romania

Cableway installations are used for a long time in areas with rugged terrain and differences in level. The technology of using ropeway conveyors or cable spans was also introduced to transport timber, ore bucket, or to deliver food, mail and even ammunition for military troops. Such systems proliferated now-a-days to transport also people by aerial tramway, cable cars, ropeway (Japanese), aerial tram, gondolas, open chairlifts, ski lifts, etc. Generally those installations are equipped with one or two track cables and a haulage rope. If the weights are small, mono-cable detachable system has only one cable that does the work of supporting and also propelling. The popularity of steel cable zip lines being used for recreational activities continues to grow all over the world. The noun of "zip line" is synonymous with those of wire rope, zip wire, aerial runway (United Kingdom), aerial rope slide, death slide, flying fox (Australia, New Zealand), Tyrolean traverse, foefie slide (in South Africa).

The paper refers to zip lines (entertainment facilities for eco-adventure tourists), with one opening and one carrier cable. The movement of mobile load is done by gravity to travel from the top to the bottom station of the inclined cable. The carrier cable dimensioning problems are associated with the evaluation of the speed of the mobile load with the arrival station. The estimated speed is necessary to establish the pre-stressed tension in the cable and the using of an adequate braking system. Finally, the paper presents a study-case.

Keywords: Steel Wire Ropes, Riccati Differential Equation, Study-case

1. INTRODUCTION

The cable transport is used for a long time, being the most economical way of transportation in rough areas, for the most part mountainous regions. When transporting materials there are used ropeways and funicular cranes (construction sites of dams, viaducts, etc.). For the people are used: cable cars, chairlifts, ski lifts etc., generically called funiculars. These latter are usually used in mountain recreation areas, but it selves do not provide the recreational pleasure. Instead, installations for the zip line, although initially arisen as a means of individual transport, lately spread mainly for recreation, reaching, under certain conditions and configurations to be considered as facilities for the practice of sport extreme.

Cableway installations are traditionally equipped with one or two cables called carriers, constituting flexible path for trolleys, cabs etc. There is another tractor cable for moving loads upward portions of the route, but also to control the speed. Cableway installation can have a single cable for small loads and small and medium distances, cumulating the role of the carrier cable and the role of tractor cable.

Zip line installations are not equipped with a tractor cable. The mobile load is suspended from a small trolley roller and the movement is gravitational due to the level difference between departure station and the arrival station. Thus the problem of mobile load input speed in the arrival station becomes a problem to be treated very carefully.

There are two cases of interest. The first situation occurs in systems with large slope and large spans. In this case the speed is limited to an admissible value so that the person arrived at the station to be able to stop single, possibly assisted. If it is desired higher speed, this speed should be limited to a value below the permitted value by the brake system used.

A second situation of interest is the small load (such as children) on installations with small differences in level and small openings. In these cases the speeds must be small, but sufficient for crossing the trail and to ensure the entrance in the arrival station. Of course, these two aspects must be resolved when no wind is, but also when the wind is acting in the direction of movement or in the opposite direction.

In what concerns the carrier cable the problems are: cable choice of many types offered by manufacturers, choice of pretension force during assembly to ensure the maximum deflection in exploitation, as well as the dimensioning calculation and strength check of the worst case in operating conditions and also, under the conditions of non-use. We note that such facilities are subject to European standard EN 15567-1 and 15567-2 [1].

Nowadays, there are many approaches using finite element method (FEM) analysis to study the dynamic behavior of a steel cable of zip line. For instance, the study [2] evaluated the structural safety of zip line using a nonlinear finite element analysis, but external variables such as wind and temperature were not considered. To model the external conditions in FEM analysis is not an easy task.

That explains that we consider a classical theoretical analysis including a number of factors that affect speed: slope of the cable, weight of the rider, weather considering wind at your back or wind in your face, temperature. We included sag analysis for rider and ice conditions.

*Corresponding author: Technical University of Civil Engineering, 124 Bvd Lacul Tei, Bucharest, Romania, andrei.vasilescu@utcb.ro

2. ASPECTS ON CALCULATING THE CARRIER CABLE [3], [4]

It is known that the form it takes the chain or cable assumes under its own weight when supported only at its ends, is called the catenary curve whose equation is $y = ch(x/k)$. Here $k = H/q$ is the curve parameter, q is the distributed weight of the cable, and H is the horizontal component of tension in the cable, which is constant throughout its length. In engineering practice, the catenary is approximated by a parabola to solve the problem of flexible cable charged with one or more concentrated loads. Using "parabola method", the problem is significantly simplified in the sense that it offers analytical solutions easy to use in the current calculations. Errors in usual cases are technically acceptable (of the order of a few percentages).

2.1. Design Loads

We considered three types of design loads:

- The weight of the carrier cable $q = m\,g/\cos\beta$
- Load due to the mobile payload $Q = Mg$
- Clear ice (frost) weight $q_c = m_c\,g/\cos\beta$.

2.2. Relations of Computing in the Baseline Situation (the Assembly of Installation)

The scheme for calculation is shown in Figure 1.

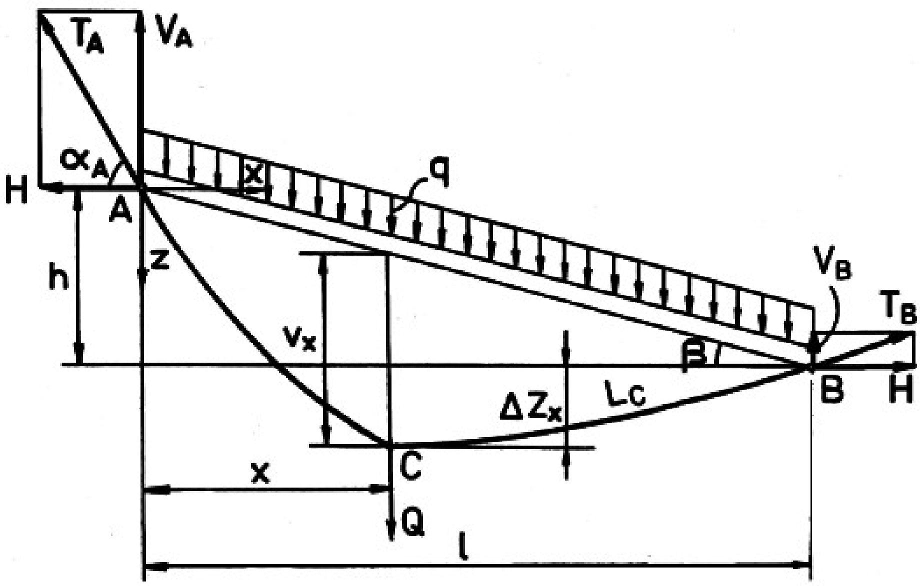

Figure 1: The scheme for calculating: the tensions, the deflection and the carrier cable length, applying "parabola method"

The relationships for the calculation of the quantities of interest are the following (the meanings of notations are shown in Figure 1:

$$\begin{cases} v(x) = \dfrac{qx(l-x)}{2H\cos\beta} + \dfrac{Qx(l-x)}{Hl} \\ v_{\max} = v(l/2) = \dfrac{ql^2}{2H\cos\beta} + \dfrac{Ql}{4H} \end{cases} \quad (1)$$

$$V_{A,B} = \frac{ql}{2\cos\beta} + \frac{Q(l-x)}{l} \pm Htg\beta \quad (2)$$

$$T_{A,B} = \sqrt{H^2 + V_{A,B}^2} \quad (3)$$

$$L_c = l + \frac{h^2}{2l} + \frac{q^2 l^3}{24H^2\cos^2\beta} + \frac{x(l-x)}{2lH^2} \cdot Q\left(Q + \frac{ql}{\cos\beta}\right) \quad (4)$$

In the absence of loading should be considered $Q = 0$, and for the case of clear ice formation $q \to (q + q_c)$.

2.3. The Influence of the Variation of the Load Factors and Environmental Parameters

Variation of load factors and ambient temperature causes variations of tensions, length and deflections in the cable. We assume that the installation was carried out at a temperature t_m and in the cable the tension is T_m. In other loading conditions, denoted q_x, Q_x and temperature t_x, the tension T_x is the real solution of the algebraic equation of the third degree:

$$T_x^3 + \left(\frac{EF}{L} \cdot \frac{A_m}{T_m^2} + \varepsilon \Delta t_x \cdot EF - T_m\right) T_x^2 - \frac{EF}{L} \cdot A_x = 0 \quad (5)$$

In this equation we noted: E - the Young's modulus, F - the sectional area of the cable, $L = l/\cos\beta$ (length of the chord AB from Figure 1), ε - the coefficient of linear expansion of steel, $\Delta t_x = t_x - t_m$, and A_m, A_x are the load factors in the two cases:

$$A_{m,x} = \frac{q_{m,x} l^3}{24\cos^3\beta} + \frac{x(l-x)}{2l\cos\beta} \cdot Q_{m,x}\left(Q_{m,x} + \frac{q_{m,x} l}{\cos\beta}\right) \quad (6)$$

Usually, at the assembly phase $Q_m = 0$.

Observation.

1. The designer has all the data involved in the coefficients of (5), as well as those of the expression (6), but he has less data sufficiently accurate for the modulus of elasticity of the cable.

Specialized literature recommends the following values ([3], [4]): $E = 1.6 \cdot 10^5 MPa$ for simple cables and $E = 1.0 \cdot 10^5 MPa$ for double cables. But these are approximate values. The real values depend essentially on constructive characteristics of steel wire ropes [5], but manufacturers do not provide always such data in the product catalogs.

2. The effort in the cable depends by the difference of the temperature during mounting and the temperature of exploitation. So it becomes necessary for the installer to measure and to record it, so that the designer must have solid data for final verification.

2.4. Case Study

The main results obtained by the authors in designing a facility that will be located in the town Raşnov, county Braşov, Romania, will create an image of the influence concerning the variation of aforementioned factors.

The parameters involved are: opening $l = 400.34m$, level difference between the two stations $h = 58.21m$, average altitude of the facility 800m, maximum payload mass $M = 125kg$, temperature specified for mounting the installation $t_m = 18^o C$, operating temperature limit $t_{\min} = 8^o C$, $t_{\max} = 38^o C$, the minimum temperature in the area $-25^o C$. It proposes the use of a spiral strand cable Φ12 35(W) x 7 / 1960 Superflex, made by CASAR Drahtseilwerke Saar GmbH, having: $F = 73.8mm^2$, $m = 0.62kg/m$, minimum breaking load $S_r = 101.16\ kN$, where it was considered $E = 1.0 \cdot 10^5 MPa$.

Pretension when mounting the installation is expected to do so $H = 6.0kN$.

Figure 2 shows the typical curves of operation (less than the partial payload), and Table 1 contains the values of interest.

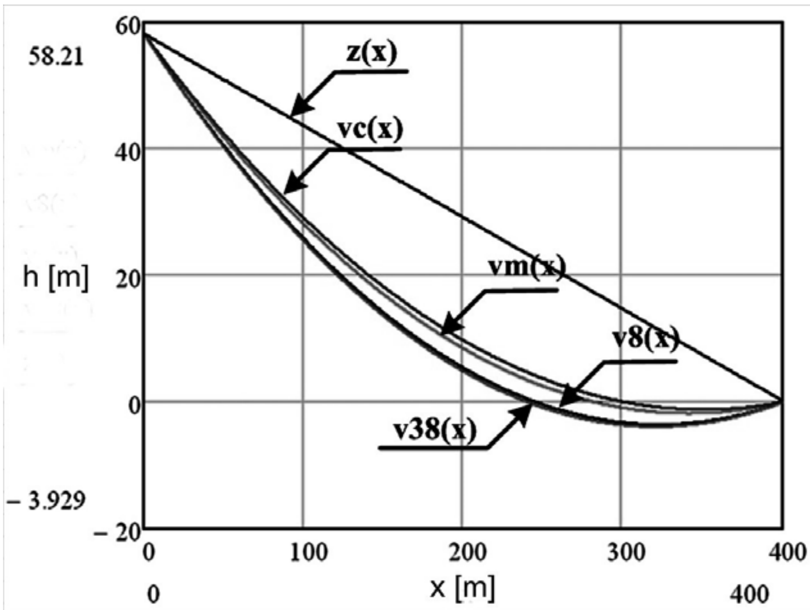

Figure 2. The curves v(x) of carrier cable in accordance with the characteristic conditions (Indices of v(x): m – mounting, 8, 38 – temperatures in degrees C, c – clear ice)

Table 1. The values of quantities of interest in characteristic conditions

Conditions of calculation		H	T_A	$v_{\max}$	L_c
Load	Temperature (°C)	kN	kN	m	m
q	18	6.0	6.362	20.73	407.383
q+Q	8	10.372	10.904	23.82	408.351
q+Q	38	10.155	10.688	24.33	408.515
q	-25	6.215	6.575	20.01	407.240
$q+q_c$	-2	24.891	26.704	24.45	408.514

The values in the first line correspond to the reference situation, when the load Q is considered at the midspan. The table shows that, in this case, the maximum cable tension occurs under the appearance of clear ice (layer thickness 2.5 cm). This is explained by the fact that facility opening is large and the mass deposited of clear ice is sensitive larger than the mass of the cable and mobile load; indeed $m_c \cong 1.7kg/m$ and $M_c = m_c L_c = 694kg$.

3. CINEMATIC ASPECTS; DETERMINING THE SPEED OF MOBILE LOAD AT THE ENTRANCE IN THE ARRIVAL STATION

3.1. Theoretical Considerations

The trajectory of the mobile load is a parabola (1). From the mechanical point of view, the model is the dynamics of the constrained particle with friction, in the gravitational field; it is about plane motion with scleronomic constraints. This approach presents real difficulties in finding the analytical expression of the law of motion. Therefore it will be dealt with in a simplified way, assuming that the movement is not the parabolas of the type shown in Figure 2, but the chord AB (Figure 1), so we can consider the incline plane. The scheme of forces is shown in Figure 3.

Forces in dynamic equilibrium are: active force $G\sin\beta$, rolling resistance force W_r, the aerodynamic drag force W_a and inertia force F_i. The rolling resistance force is $W_r = w \cdot G\sin\beta$, where w is the coefficient of rolling resistance.

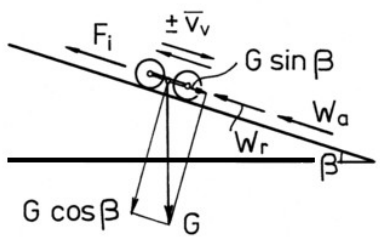

Figure 3. Scheme to establish the law of motion of mobile load

The aerodynamic drag force has the expression

$$W_a = c_a A_v \rho^H \frac{u^2}{2}$$

where c_a is the mobile load drag coefficient, A_v the area of the mobile load projected onto the plane perpendicular to the direction of movement, ρ^H - the density of air at the altitude H of installation, and u – the relative speed.

$$u = v - v_v \tag{7}$$

v is the speed of mobile load, and v_v - wind speed component in the direction of movement of the load; this component will be considered positive if it acts in the direction of movement, and negative, acting to the contrary.

The equation of dynamic equilibrium of the mobile load is

$$G\sin\beta - W_r - W_a = F_i$$

Taking into account the expression of the forces involved and dividing by m – (load mass), therefore we have

$$\dot{v} + ku^2 = g_1$$

It is assumed that during the motion of mobile load between departure and arrival stations, the wind does not change neither the intensity nor direction. Obvious $\dot{v}_v = 0$, and $\dot{u} = \dot{v}$. The differential equation of motion becomes

$$\dot{u} + ku^2 = g_1 \tag{8}$$

This is a Riccati type differential equation. Initial condition is $v(0) = 0$ (payload starts without initial speed), therefore

$$u(0) = -v_v \tag{9}$$

(8) is solved by changing the function

$$u(t) = \frac{1}{z(t)} + u_p$$

u_p is a particular solution of the equation with the right-hand side. It is found easily

$$u_p = \sqrt{g_1/k} \tag{10}$$

The general solution of (8) is

$$u(t) = \frac{1}{Ce^{\tau t} - k/\tau} + u_p\,, \tag{11}$$

where $\tau = 2ku_p = 2\sqrt{g_1 k}$. From (7) and (11) we obtain the speed expression of the mobile load

$$v(t) = \frac{1}{Ce^{\tau t} - k/\tau} + u_p + v_v \tag{12}$$

The limit value of the speed $(t \to \infty)$ is

$$v_{\lim} = \lim v(t) = u_p + v_v \tag{13}$$

By using the initial condition $v(0) = 0$ and (13), is found the expression of the constant of integration

$$C = \frac{k}{\tau} - \frac{1}{v_{\lim}} \tag{14}$$

Thus the problem is solved. In what concerns speed limit, it is found that it depends on the presence and action of the wind direction:

- wind in the direction of motion: $v_{\lim} = \sqrt{g_1/k} + v_v$
- wind opposite of motion: $v_{\lim} = \sqrt{g_1/k} - v_v$
- no wind: $v_{\lim} = \sqrt{g_1/k}$

In the latter situation (no wind), the speed expression of the mobile load becomes

$$v^o(t) = \frac{e^{\tau t} - 1}{e^{\tau t} + 1} \cdot \frac{\tau}{2k} \tag{15}$$

Comment 1.

If the wind acts in the opposite direction of movement, it is possible that $v_{\lim} < 0$, that which happens if $v_v > \sqrt{g_1/k}$. This means that mobile load does not start from the departure station. Actually, in the departure station launch angle is not β, but $\alpha_A > \beta$, so that the wind speed at which the load not start, should be determined replacing in expression of g_1, the angle β by the angle α_A. On the other hand, there may be a risk for the small load (children) to stop during the movement (the mobile load weight occurs in the expression of k, to the denominator). Therefore, there could be situations where the minimum value of the moving load must be enforced.

In order to establish the speed with which mobile load enters in the arrival station, the following procedure is followed: first is integrated the expression (12) of the mobile load speed. We obtain the space law. Thus

$$s(t) = \frac{1}{k}\left(\ln\frac{Ce^{\tau t} - k/\tau}{C - k/\tau} - \tau t\right) + \left(u_p + v_v\right)t \tag{16}$$

Then, we determine the travel time t_p from the condition $s(t_p) = L_c$. This is a equation with the unknown t_p. The carrier cable length is calculated from (10), considering $x = l/2$. Finally, the speed value is calculated using (12): $v_i = v(t_p)$.

Comment 2.

If the speed of entry into the station is high (i.e. if it exceeds 12 to 15 km/h), it is necessary to use a suitable braking system, or the facility operation should be restricted to certain wind speeds. In the case of facilities with steep slopes and large openungs it is necessary to check if the speed of the mobile load enters in the arrival station, is within the limits of efficiency of the braking system. Finally, the acceleration of the mobile load is obtained by deriving the speed expression:

$$a(t) = \dot{v}(t) = \frac{-C\tau e^{\tau t}}{\left(Ce^{\tau t} - k/\tau\right)^2} \tag{17}$$

Comment 3.

Neglecting air resistance force, (8) loses the term ku^2. Acceleration is constant (equal to g_1) and depends only on the angle of inclination β. The movement of mobile load is similar to the free fall in a gravitational field with g_1 acceleration.

3.2. Case study

The theoretical results above will be applied to the facility dealt in section 2.4. The study will be considering minimum operating temperature ($t_{\min} = 8^o C$), because in these conditions the tensile force of the cable is greater.

The input data are: $w = 0.0175\, N/N$, $c_a = 1.1$, $A_v = 1.2m^2$, $\rho^H = 1.0084\, kg/m^3$ (at the altitude $H = 800m$), and $L_c = 408.351m$, according to Table 1.

It follows: $g_1 = 1.147\, m/s^2$, $k = 5.324 \cdot 10^{-3}\, m^{-1}$ and $\tau = 0.156 s^{-1}$.

In the absence of wind, the speed limit is $v^o_{\lim} = 14.676\, m/s \approx 52.8\, km/h$, and the travel time resulting is $t_p = 36.654s$.

The speed with which mobile load enters in the arrival station is $v(t_p) = 14.58\, m/s \approx 52.5\, km/h$. The mode of variation of space, speed and acceleration of the mobile load is shown in Figure 4.

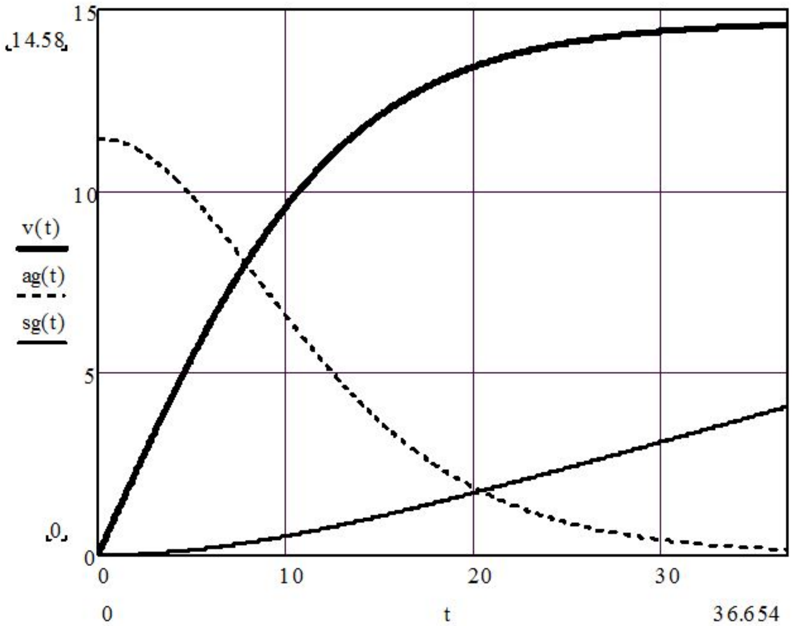

Figure 4. The curves: space sg(t) - thin line, speed v(t) - thick line, and acceleration ag(t) - dashed line

To highlight the clear appearance of the variation of the three cinematic quantities on the same representation, it was necessary to use the following scale factors: $sg(t) = 10^{-2} s(t)$ and $ag(t) = 10a(t)$.

From the graph it is found that the length of the path is large, and the speed of the load mobile practically reached the limit, as confirmed by reducing the acceleration to zero. In this case it becomes compulsory to use a braking device, and to limit the use of the facility for wind speeds in the direction of movement of a maxim no more than 10 *km/h.* It follows the necessity to mount an anemometer.

By neglecting air resistance (see Comment 3), the duration of crossing the trail becomes $t_p = 25.64s$, i.e. approx. 30% lower. It follows the error committed by neglecting it.

4. CONCLUSIONS

1. In case of the zip line, the movement of the mobile load is gravitational. In contrast, to the usual cableway installations, the zip lines require a suitable kinematics' study, for all operating characteristic conditions, particularly in the presence of wind.

2. At large openings and steep slopes, the speed of the load becomes large. The stabilization of this speed is determined by the air resistance. Neglecting the air resistance can not be accepted.

3. In what concerns the conditions for checking the resistance of the carrier cable is required to consider clear ice formation.

4. Manufacturers of the steel wire ropes (cables) for use in cableway installations should provide data on the elastic modulus of the cables.

REFERENCES

[1] ***** - EN 15567-1:2007, “Sports and recreational facilities – Ropes courses”, Part 1: Construction and safety requirements, (2007)

[2] B. S. Ju, J.S. Kim, W.Y. Jung, “Structural Safety Evaluation of Zip-Line Due to Dynamic Impact Load”, World Academy of Science, Engineering and Technology International Journal of Civil, Architectural Science and Engineering Vol: 7(10), (2013)

[3] Barat, I.E., Plavinskii, V.I. - Kabelnâe kranî , Maşinostroenie, Moskva, (1964)

[4] N. Simion, Funiculare, Ed.Tehnică, Bucureşti, (1958)

[5] R. Judge, Z. Yang, S.W. Jones, G. Beattie; “Full 3D finite element modelling of spiral strand cables”, Construction and Building Materials, Vol. 35(10), pp. 452–459, (2012)

Tip-Over Stability of Crawler Cranes with Moveable Counterweights

Huasen Liu[1,2], William Singhose[2*], Wenming Cheng[1]
[1] Mechanical Engineering, Southwest Jiaotong University, Chengdu (China)
[2]Woodroff School of Mechanical Engineering, Georgia Institute of Technology, Atlanta (USA)

A movable counterweight can change the mass center of a crawler crane to keep the crane in balance as the machine moves heavy payloads. Unfortunately, if the movable counterweight is moved to the wrong position, then the crane can tip over in a catastrophic accident that can injure workers or damage equipment. As a result, the stability of such crawler cranes is crucial for efficient and safe operation. This paper investigates the tip-over stability of a crawler crane with a moveable counterweight using static stability criteria. In order to find the appropriate position of the movable counterweight, the overturning moment-index in both the forward and backward directions of the crane are investigated. A stability safety factor method for crawler cranes is used to calculate the suitable position of the movable counterweight. The maximum and the minimum safe positions of the counterweight are investigated while the crawler crane is rotated 360 degrees about a vertical axis.

Keywords: tip-over stability, crawler crane, overturning moment, crane safety

1. INTRODUCTION

Mobile cranes are very important in shipyards, construction, ports, wind farms, and manufacturing. However, they pose a significant tip-over hazard. Furthermore, as such cranes get taller, the required counterweight must be increased. This makes the cranes more expensive and harder to transport. In order to decrease the required counterweight, crane manufacturers have been developing cranes with moveable counterweights.

The counterweight on a crane provides balancing forces so that the crane does not tip over as it picks up and moves heavy payloads. Moveable counterweights provide several advantages in terms of weight, mobility, and ease of use when compared to similar cranes with fixed counterweights. A crane with a moveable counterweight uses less total mass for its counterweight because it can move the weight to various locations to counterbalance the load. Given the lower counterweight mass, the crane is easier to move, both from one job site to another and around any given job site. A moveable counterweight also improves ease of operation because counterweight mass does not need to be added and removed as the payloads alternate from heavy to light.

Moveable counterweights for heavy machinery have been well documented for about 100 years. For example, Figure 1 shows a boom crane patented in 1922. The counterweight D is in a retracted position near the center of the crane. Figure 2 shows the crane with its counterweight extended out the back to provide more resistance to forward tipping. This movement occurs when the boom is lowered, or a larger load is on the hook. Another example of an early crane with a moveable counterweight is shown in Figure 3. The figure is a reproduction from a 1932 patent and shows a back view of the crane. As the boom 10 is lowered, the attached payload creates a large sideways tipping moment to the left. Therefore, as the boom is lowered, the counterweight 21 is moved further to the right side to counterbalance the sideways tipping moment.

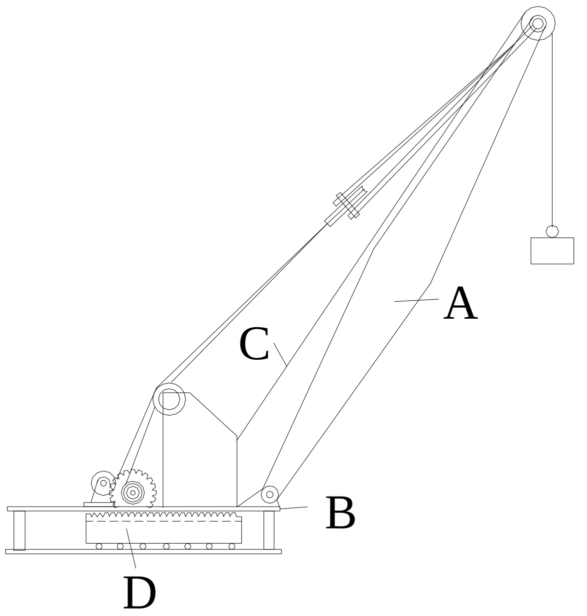

Figure 1: Crane with Moveable Counterweight Patented by Wigglesworth, Counterweight Retracted [1].

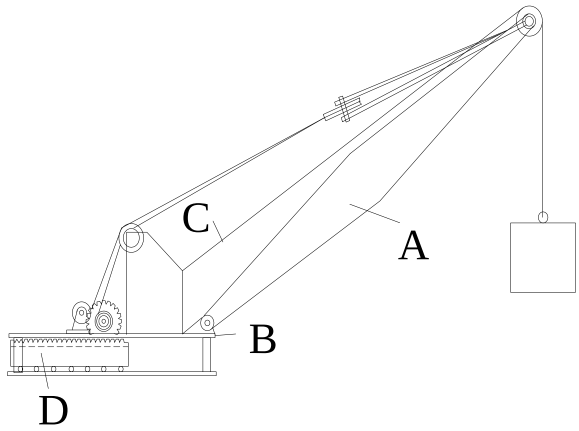

Figure 2: Wigglesworth Boom Crane with Counterweight Extended [1].

*Corresponding author: The George W. Woodruff School of Mechanical Engineering, Georgia Institute of Technology, Atlanta, GA 30332-0405, singhose@gatech.edu

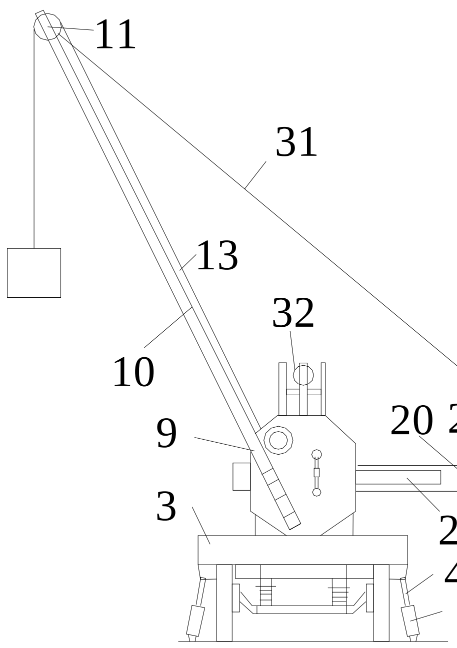

Figure 3: Crane with Moveable Counterweight Patented by Cohen-Venezian [2].

There have been many investigations of the tip-over stability of cranes. Neitzel [4] reviewed available information on crane-related injuries, and gave recommendations for improving crane injury prevention and future crane safety research. Jeng [6] introduced two indices, a moment-index and a force-index, to quantify the tendency of tip-over behaviour of mobile cranes. He also examined the bearing capacity of outriggers. Papadopoulos and Rey [5,7] used the force-angle stability measure, which is easily computed and is sensitive to changes in center of mass height, to provide a human operator with an indication of proximity to tip over.

In [8], a small-scale cherry picker was constructed to investigate the dynamics and stability of these machines. Vibration-control techniques were used to improve system response. Furthermore, tip-over of a mobile manipulator was determined as a function of inertia, gravity, and acceleration [11]. An online fuzzy logic self-motion planner was used to generate desired motions in a real-time manner.

In [9], tip-over stability of a mobile crane considering the payload oscillations was investigated. The comparison between the static stability and the full-dynamic stability revealed that a simple semi-dynamic analysis provides good approximations for the tip-over stability properties. A dynamic model for the control of a flexible mobile crane wherein only the boom of the crane was assumed to be flexible was derived by Kiliçaslan [10]. The goal was determination of safe loads to prevent tipping of a mobile crane. Ghasempoor [12] pointed out that the amount of the impact energy that can be sustained by a vehicle without tipping-over, can be used to compute the potential of tipping-over by vehicles that carry manipulators. Lee [13] investigated a fuzzy logic roll stability control system to prevent the rollover of sport utility vehicles.

More recently, Korayem [14] derived a kinematic and dynamic models of the mobile manipulator. The maximum payload path for a specified payload was generated using an optimal control approach. Zhaofa [15] studied a scheme for stability monitoring of large-scale hoisting transfer equipment. The hydraulic leg force was measured by a weight sensor to judge safety for the hoisting equipment. Abo-Shanab and Sepehri [16] developed a simulation model for studying the tip-over stability of a typical heavy-duty hydraulic log-loader machine. Their results showed that the flexibility at the manipulator joints due to the hydraulic compliance improved the machine stability.

The design and control of a crane with moveable counterweights is more complex than cranes with fixed counterweights. The counterweight must be moved in coordination with both the configuration of the crane and the weight of the attached load. In order to achieve this counterbalancing effect, the crane must be equipped with sensors that measure at least the boom angle, the position of the counterweight, and the mass of the attached load. This sensor information is then used by a control system that automatically adjusts the counterweight position.

In this paper, the tip-over stability of crawler cranes using a moveable counterweight is investigated. A method that is based on the force-angle stability margin measure is proposed to determine the stability. The overturning moment-index in both the forward and backward directions are used as the tip-over critical conditions. In order to determine the safe position of the counterweight, a multi-body representation of the crane is developed. The results show how the maximum and the minimum safe positions of the movable counterweight change in different working conditions.

2. STABILITY MARGIN

There are three traditional methods to determine the stability of a crane, a) calculate the sum of all the torques acting toward the overturning side, b) calculate the stability factor（the ratio of steady torque and overturning torque), and c) demarcate the rated lifting capacity by different critical loads. However, the crawler crane structure is quite complex and acted on by multiple forces, including inertial forces, gravitational loads, wind loads and so on. Therefore, we use a method that is based on the force-angle stability margin measure to determine the stability of the crawler crane. Figure 4 shows the general geometry of the system with a horizontal plane formed by the possible tip-over axes.

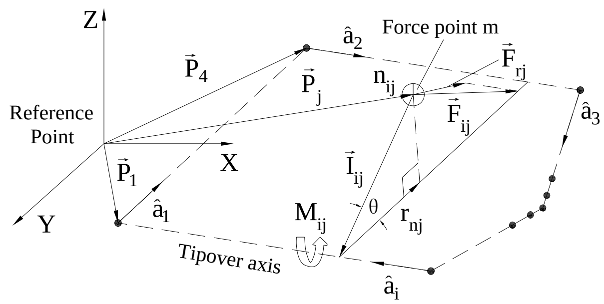

Figure 4: Tip-over Stability Margin Geometry

In Figure 4, $\vec{P}_i$ represents the vector from a reference point to the i^{th} ground contact point, defined as

$$\vec{P}_i = [\ P_x \quad P_y \quad P_z\ ]_i^T \qquad i = \{1, \cdots, n\} \quad (1)$$

And $\vec{a}_i$ denotes the location of the i^{th} point where forces are applied to the structure. The i^{th} possible tip-over axis, which is an edge of the base of the crane, is given by

$$\vec{a}_i = \vec{P}_{i+1} - \vec{P}_i \qquad i = \{1, \cdots, n-1\} \qquad (2)$$

$$\vec{a}_n = \vec{P}_1 - \vec{P}_n \qquad (3)$$

Defining $\hat{a}_i = \vec{a}_i / |\vec{a}_i|$, the i^{th} tip-over normal $\vec{I}_{ij}$ that passes through the j^{th} force point is obtained by subtracting $\left(\vec{P}_{i+1} - \vec{P}_j\right)$.

$$\vec{I}_{ij} = \left(I - \hat{a}_i \hat{a}_i^T\right)\left(\vec{P}_{i+1} - \vec{P}_j\right) \qquad (4)$$

Where I is the 3x3 identity matrix.

For a given tip-over axis, $\vec{a}_i$, the effective part of the force $\vec{F}_{rj}$ that provides the tip-over moment is given by

$$\vec{F}_{ij} = \left(I - \hat{a}_i \hat{a}_i^T\right)\vec{F}_{rj} \qquad (5)$$

Therefore, the tip-over moment M_i for the tip-over axis $\vec{a}_i$ is

$$M_i = \sum_{j=1}^{m} \vec{F}_{ij} \times \vec{I}_{ij} + \sum_{j=1}^{m} n_{ij} \qquad (6)$$

Where m is the number of forces, including the gravitational loads, the wind forces etc. The tip-over moments for all tip-over axes are

$$\begin{bmatrix} \vec{I}_{11} & \vec{I}_{12} & \cdots & \vec{I}_{1j} \\ \vec{I}_{21} & \vec{I}_{22} & \cdots & \vec{I}_{2j} \\ \vdots & \vdots & \ddots & \vdots \\ \vec{I}_{i1} & \vec{I}_{i2} & \cdots & \vec{I}_{ij} \end{bmatrix} \times \sum_{j=1}^{m} \begin{bmatrix} \vec{F}_{ij} \\ \vec{F}_{ij} \\ \vdots \\ \vec{F}_{ij} \end{bmatrix} + \sum_{j=1}^{m} \begin{bmatrix} n_{ij} \\ n_{ij} \\ \vdots \\ n_{ij} \end{bmatrix} = \begin{bmatrix} M_1 \\ M_2 \\ \vdots \\ M_i \end{bmatrix} \quad (7)$$

In order to keep the crawler crane stable, all of the tip-over moments must be nonnegative values. Otherwise, the crawler crane will tip-over along the axis that has a negative value.

3. CASE STUDY

3.1. Model schematics

Figure 5 illustrates a representative model of a crawler crane with a moveable counterweight. The model is composed of a crawler base structure, m_1, a rotational boom arm, m_2, a mast, m_3, a moveable counterweight m_4, and a suspension cable with a payload mass, m_5. The base is modelled as a thin plate with a mass of m_1 and has a center of gravity at the center of the base. The boom arm and the mast can be rotated through a slew angle β about a vertical axis located at the center of the crawler. The boom has a length of L_2. Its center of mass is located at the middle of the boom arm. The boom is elevated at an angle ϕ_1 and the mast is elevated ϕ_2. Its length and mass are L_3 and m_3, respectively. The counterweight is moveable to keep the crawler crane balanced and its position is measured by L_4.

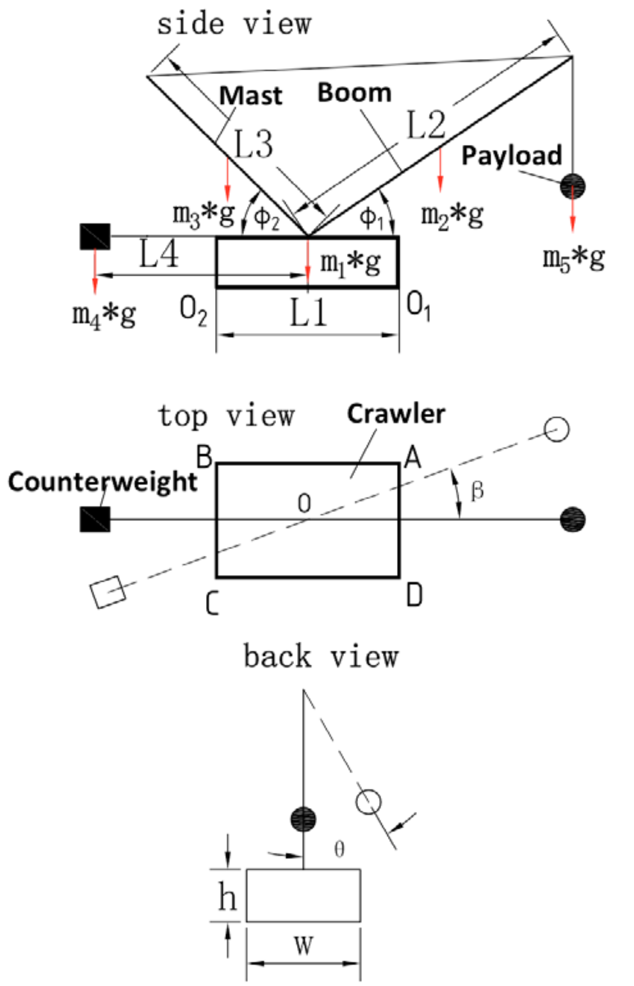

Figure 5: Schematic Diagram of a Boom Crane with a Moveable Counterweight

Considering the planar view of the crane model shown in Figure 5, the crane can tip-over forward about the tip-over axis AD, or tip backward over the tip-over axis BC. The moments creating a forward tip are:

$$M_1 = \sum_{j=1}^{5} \vec{F}_{1j} \times \vec{I}_{1j} + \sum_{j=1}^{5} n_{1j} = m_2 g\left(\frac{L_2 \cos(\phi_1) - L_1}{2}\right)\cos\beta$$
$$+ m_3 g\left(\frac{L_3 \cos(\phi_1) + L_1}{2}\right)\cos\beta + m_4 g(L_4 + L_1)\cos\beta$$
$$+ m_1 g\frac{L_1}{2} - m_5 g\left(L_2 \cos(\phi_1) - \frac{L_1}{2}\right)\cos\beta \qquad (8)$$

Where $\vec{F}_{11}$ is the main body gravitational force, $\vec{F}_{12}$ is the boom gravitational force, $\vec{F}_{13}$ is the mast gravitational force, $\vec{F}_{14}$ is the counterweight gravitational force, $\vec{F}_{15}$ is the payload gravitational force.

Now consider the possibility of tipping backwards about the tip-over axis BC. The overturning moment M_3 for the tip-over axis BC is:

$$M_3 = \sum_{j=1}^{5} \vec{F}_{3j} \times \vec{l}_{3j} + \sum_{j=1}^{5} n_{3j} = m_3 g(\frac{L_3\cos(\phi_1) - L_1}{2})$$
$$+ m_2 g(\frac{L_2\cos(\phi_1) + L_1}{2}) + m_5 g(L_2\cos(\phi_1) + \frac{L_1}{2})$$
$$+ m_1 g\frac{L_1}{2} - m_4 g L_4 \qquad (9)$$

The stability condition is $M_1 > 0$ and $M_4 > 0$. Therefore, simplifying (8) and (9), we get

$$m_4 g(L_4 + L_1)\cos\beta > m_5 g(L_2\cos(\phi_1) - \frac{L_1}{2})\cos\beta - m_1 g\frac{L_1}{2}$$
$$+ m_2 g(\frac{L_2\cos(\phi_1) - L_1}{2})\cos\beta - m_3 g(\frac{L_3\cos(\phi_1) + L_1}{2})\cos\beta$$
$$(10)$$

$$m_4 g L_4 \cos\beta < m_2 g(\frac{L_2\cos(\phi_1) + L_1}{2})\cos\beta + m_1 g\frac{L_1}{2}$$
$$+ m_5 g(L_2\cos(\phi_1) + \frac{L_1}{2})\cos\beta - m_3 g(\frac{L_3\cos(\phi_1) - L_1}{2})\cos\beta$$
$$(11)$$

Given (10) and (11), we can calculate the range of counterweight positions that stabilize the crane.

3.2. Test configuration of a mobile boom crane

In order to decrease the required counterweight, crane manufacturers have been developing cranes with moveable counterweights. A CC2800 Terex crawler crane with a movable counterweight is shown in Figure 6. The geometric parameters and constants for the crane are listed in Table 1.

Table 1: Parameters and Baseline Configuration of the Terex CC 2800 Crawler Crane

Nomenclature	Item	Numerical data
φ_2	Angle of mast	60deg
w	Width of base	8.4m
h	hight of base	1.5m
L_1	Length of base	10.33m
L_2	Length of boom	100m
L_3	Length of mast	30m
m_1	Mass of base	300t
m_2	Mass of boom	80t
m_3	Mass of mast	40t
m_4	Counterweight mass	200t
m_5	Mass of payload	50t

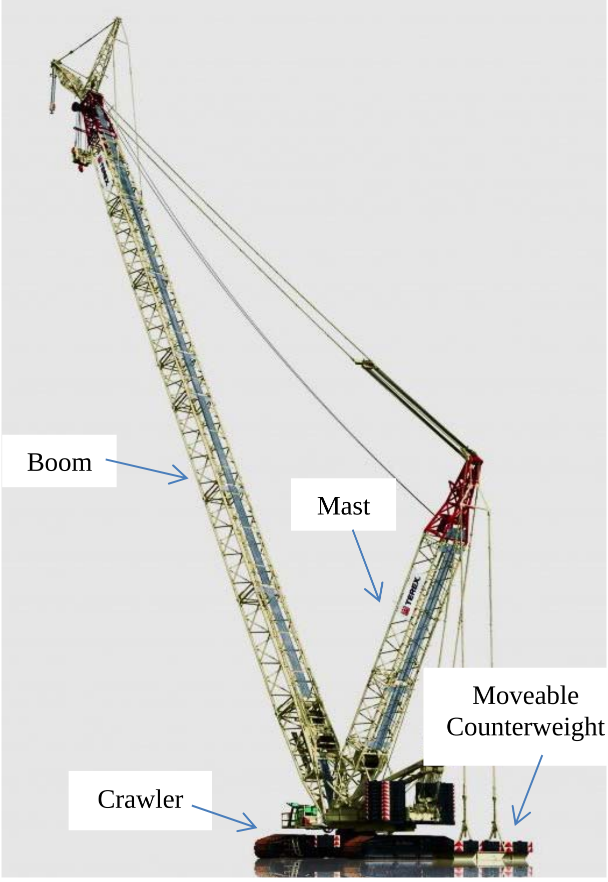

Figure 6: Terex CC 2800 (www.sterettequipment.com/terex-cc-2800)

In order to investigate the stability, the length of the boom and the mass of payload were fixed. The mass of the payload was set to 120t. The luffing angle and the position of the counterweight were changed. Figure 7 shows an example result of the static stability analysis. The polar plot shows tip-over stability for all slewing angle configurations when the luffing angle is 60°. The shortest possible position of the moveable counterweight is shown in Figure 7 when the mass of the moveable counterweights are 150t, 200t, and 300t.

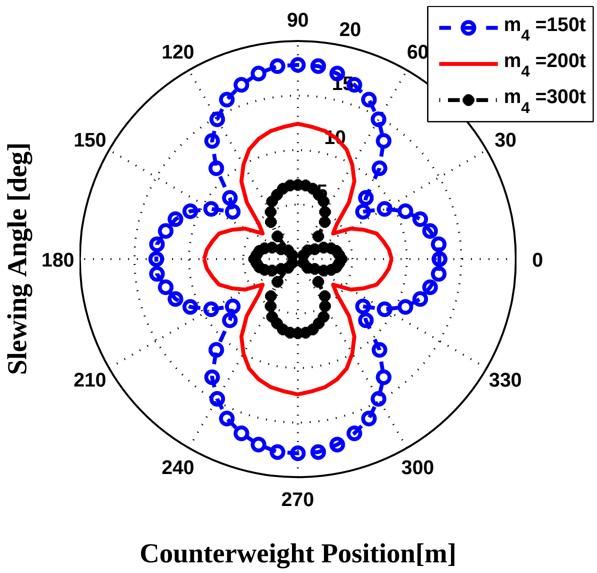

Figure 7: Forward Tip-over for ϕ_1=60°

As the mass of the counterweight increases, it does not have to be extended as far to counterbalance the load. Therefore, the minimum positions for the 300t weight are much smaller than for the 100t weight.

The tip-over backward condition can be triggered if the payload suddenly detaches from the crane. Figure 8 shows the maximum position of moveable counterweight that causes backward tip-over when the mass of the payload is zero. The heavier the mass of the moveable counterweight is, the greater the risk of the crane tipping over backward.

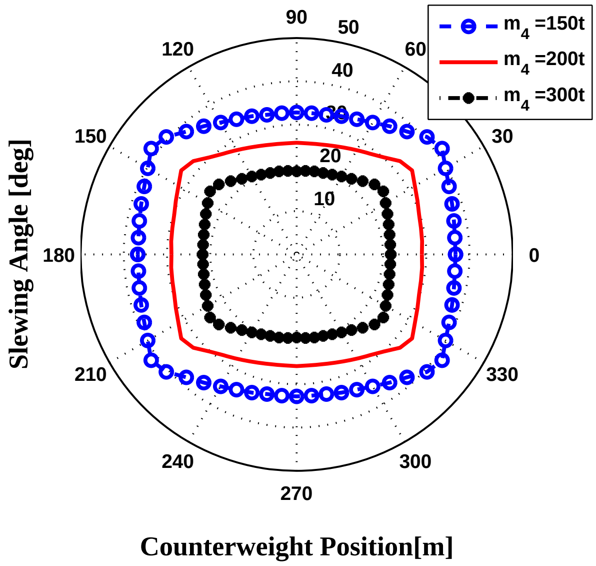

Figure 8: Backward Tip-over for ϕ_1=60°

Figures 9 shows the minimum and the maximum positions of the counterweight when the mass of counterweight is 200t and the luff-angle is 60°. When the slew angle is 90°, the smallest permissible counterweight region is A, while the longest possible counterweight region is B. If the stable region of the counterweight is larger, then the crane will be more stable in a practical sense. Therefore, when the slew angle is 90°, the crane is in the most dangerous position.

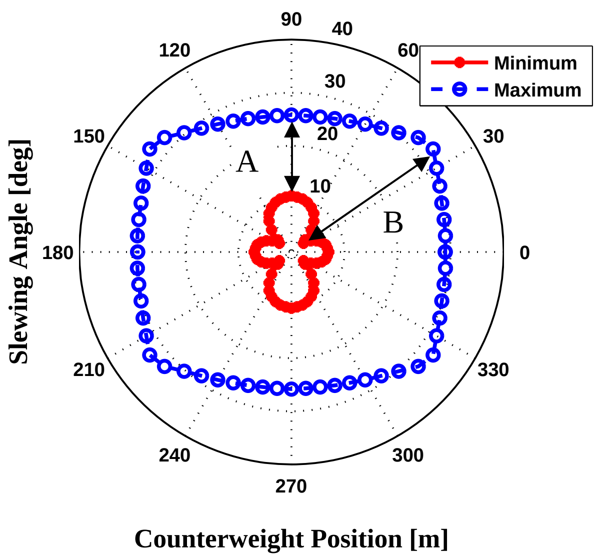

Figure 9: Backward and Forward Tip-over

For a constant counterweight mass, the shortest position of the counterweight is shown in Figure 10. The payload is 60t, and the luffing angles are 35°, 40°, and 45°. With decreasing luff angle, the shortest possible positions of the moveable counterweight also become greater. Compared with the luff angle of 35°, the shortest possible positions of the moveable counterweight is near half of that when the luff angle is 45°. The shortest possible positions of the moveable counterweight are minimized when the boom is directed toward the corner of the crawler base, and they are maximum when the boom is perpendicular to the edge of the crawler base.

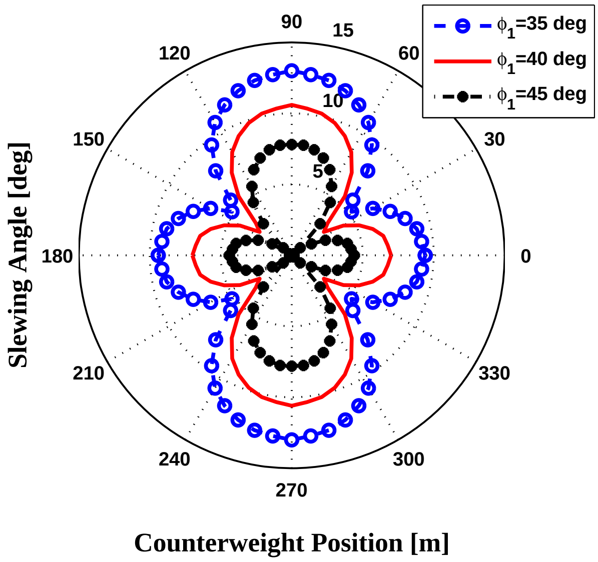

Figure 10: Forward Tip-over for m_5=200t

Figure 11 shows the maximum position of the moveable counterweight that causes backward tip-over when the mass of the payload is zero and the mass of the counterweight is 100t. The positions are given for luffing angles of 30°, 40°, and 60°. As the luff angle gets larger, the crane becomes more stable and the counterweight does not have to be moved as far.

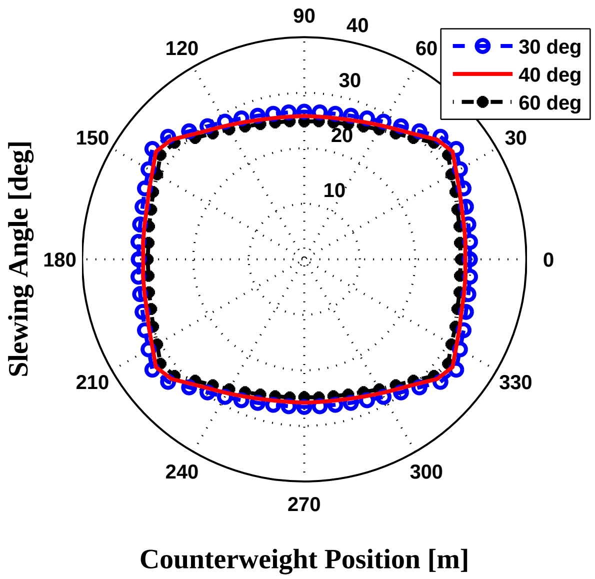

Figure 11: Forward Tip-over for m_5=100t

Figure 12 shows the minimum and the maximum positions of the counterweight when the mass of the counterweight is 200t and the luff angle is 40°. When the slew angle is 90°, the shortest counterweight region is A, while the longest counterweight region is B. Therefore, when the slew angle is 90°, the crane is in its most dangerous position. The shortest possible positions of the moveable counterweight occur when the boom is directed toward the corner of the crawler base, and they are longest when the boom is perpendicular to the edge of the crawler base.

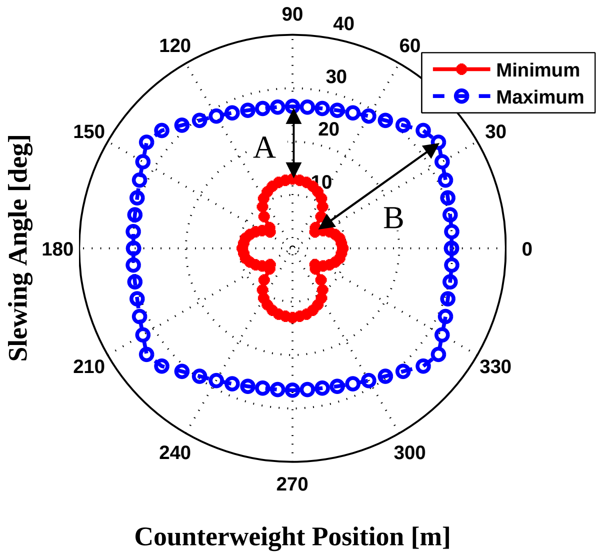

Figure 12: Backward and Forward Tip-over for ϕ_1=40°

In order to find the varying pattern of the center of the mass location, the mass of counterweight and the position of the counterweight were investigated. Figure 13 shows the center of mass of the crawler crane when the mass and the position of the counterweight are varied. If the center of mass location is larger than 4m, then the crawler crane will tip over backward. If it is less than -4m, then the crawler crane will tip over forward.

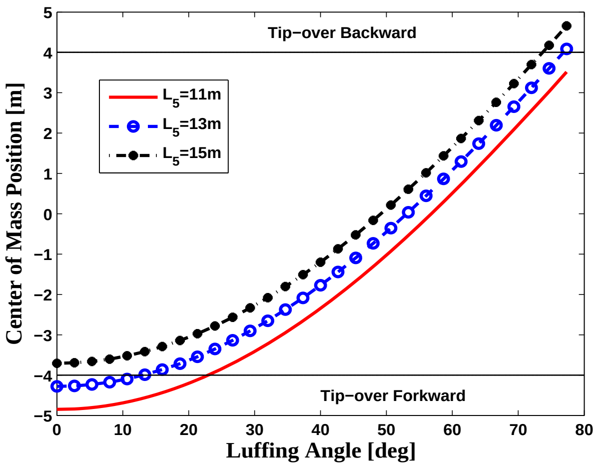

Figure 13: Backward and Forward Tip-over for ϕ_1=60°

When the mass of the counterweight changing, the center of the mass location is also affected. Figure 14 shows the center of mass location when the mass of the counterweight is 100t, 200t, and 300t. If the mass of counterweight is 100t, then the tip-over forward moment is greater than the stability moment when the luffing angle is less than 40°. Otherwise, in order to keep the crawler crane stable, the luffing angle needs to be larger than a threshold value.

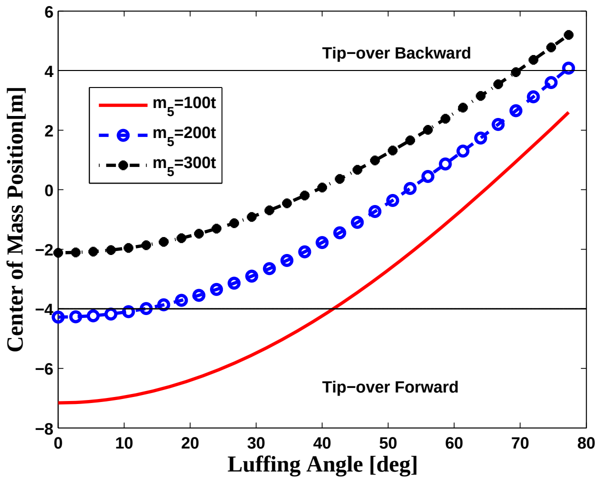

Figure 14: Center of Mass Location for L_5=13*m*

When the crane slews from 0° to 360°, the center of mass location will change as shown in Figure 7 and Figure 10. The luffing angle also effects the center of mass location as shown in Figure 13 and Figure 14. Combining those two factors, we get the 3D surface shown in Figure 15. Figure 15 shows the center of mass location when the mass of the counterweight is 200t. There are four troughs and four bulges on the curved surface. The shortest possible positions of the moveable counterweight occur when the boom is near the corner of the crawler base. They are largest when the boom is perpendicular to the edge of the crawler base. Figure 16 shows the maximum counterweight position for the backward tip-over conditions.

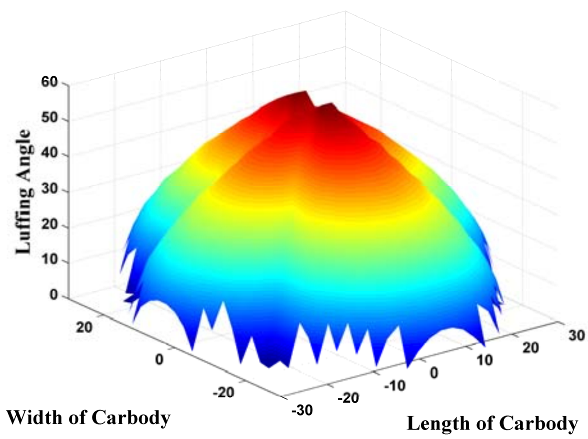

Figure 15: *Forward Tip-over* for m_5=200*t*

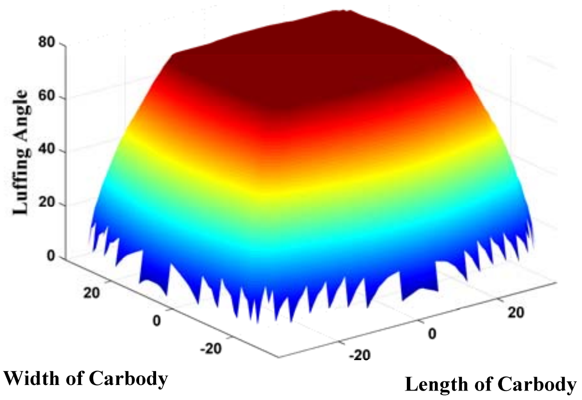

Figure 16: *Backward Tip-over* for m_5=200*t*

4. CONCLUSIONS AND FUTURE WORK

Mobile cranes are very useful; however, they pose a significant tip-over hazard. Because these cranes are getting taller, the required counterweight has been increasing significantly. This makes the crane more expensive and harder to transport. Mobile cranes equipped with moveable counterweights provide numerous advantages. However, their tip-over stability properties are more complicated than traditional cranes. Therefore, care must be taken to understand the tip-over stability and develop a control system that properly measures the state of the crane and positions the counterweight at the appropriate location. This work presented a measure of the tip-over stability margin for crawler crane with a moveable counterweight. The tip-over moment for all possible tip-over axes were calculated. In order to keep the crane balanced, all tipping over moments should be positive. The position of the counterweight is adjusted to make the crawler crane stable when the boom angle changes. Results show that the stable region for the position of the moveable counterweight changes significantly as a function of the crane configuration and its payload mass.

Because crawler cranes are influenced by wind forces and movements of the base, future work should pay attention to the dynamic model of the crawler crane. Apart from that, the automatic control system of the counterweight position should be designed to make it feasible to control.

REFERENCES

[1] E. Wigglesworth, "Improvements in or relating to cranes," GB Patent 190,594, Dec. 28, 1922.

[2] C. Cohen-Venezian, "Crane," US Patent 1,877,373, Sept. 13, 1932.

[3] D. Perch and K. Porubcansky, "Mobile lift crane with variable position counterweight," US Patent 7,546,928, June 16, 2009.

[4] Neitzel, Richard L., Noah S. Seixas, and Kyle K. Ren. "A review of crane safety in the construction industry." Applied Occupational and Environmental Hygiene 16.12 (2001): 1106-1117.

[5] Papadopoulos E, Rey D. A new measure of tip-over stability margin for mobile manipulators. January 1, 1996;

[6] Jeng S, Yang C, Chieng W. Outrigger force measure for mobile crane safety based on linear programming optimization. Mechanics Based Design of Structures And Machines [serial online]. April 1, 2010;38(2):145-170.

[7] Papadopoulos, E. E., & Rey, D. A. (2000). Force-angle measure of tipover stability margin for mobile manipulators. Vehicle System Dynamics, (1), 29. doi:10.1076/0042-3114(200001)33:1;1-5;FT029

[8] Maleki E, Pridgen B, Singhose W, Glauser U, Seering W. Educational use of a small-scale cherrypicker. International Journal Of Mechanical Engineering Education [serial online]. April 1, 2012;40(2):104-120.

[9] Rauch A, Singhose W, Fujioka D, Jones T. Tip-over stability analysis of mobile boom cranes with swinging payloads. Journal Of Dynamic Systems, Measurement And Control, Transactions Of The ASME [serial online]. January 1, 2013;135(3)

[10] Kiliçaslan S, Balkan T, Ider S. Tipping loads of mobile cranes with flexible booms. Journal Of Sound And Vibration [serial online]. June 17, 1999;223(4):645-657.

[11] Li Y, Liu Y. Real-time tip-over prevention and path following control for redundant nonholonomic mobile modular manipulators via fuzzy and neural-fuzzy approaches. Journal Of Dynamic Systems, Measurement And Control, Transactions Of The ASME [serial online]. December 1, 2006;128(4):753-764.

[12] Ghasempoor A, Sepehri N. A measure of stability for mobile manipulators with application to heavy-duty hydraulic machines. Journal Of Dynamic Systems, Measurement And Control, Transactions Of The ASME [serial online]. September 1, 1998;120(3):360-369.

[13] Lee Y, Yi S. Rollover prevention for sport utility vehicle using fuzzy logic controller. Proceedings Of SPIE - The International Society For Optical Engineering. January 1, 2005;6042 I(ICMIT 2005: Control Systems and Robotics)

[14] Korayem M, Azimirad V, Nikoobin A, Boroujeni Z. Maximum load-carrying capacity of autonomous mobile manipulator in an environment with obstacle considering tip-over stability. International Journal Of Advanced Manufacturing Technology. January 1, 2010;46(5):811-829.

[15] Zhaofa Z, Feng L, Xianxiang H. Safety monitoring method of hoisting equipment based on pressure measuring. 2007 8Th International Conference On Electronic Measurement And Instruments, ICEMI [serial online]. January 1, 2007;(2007 8th International Conference on Electronic Measurement and Instruments, ICEMI):2504-2507.

[16] Abo-Shanab R, Sepehri N. Tip-over stability of manipulator-like mobile hydraulic machines. Transactions Of The ASME. Journal Of Dynamic Systems, Measurement And Control. June 1, 2005;127(2):295-301.

Kinematics of the Truck Mounted Hydraulic Cranes

Boris Jerman[1*], Jurij Hladnik[1], Vlada Gašić[2], Miloš Đorđević[2]
[1]Faculty of Mechanical Engineering, University of Ljubljana, Ljubljana (Slovenia)
[2]Faculty of Mechanical Engineering, University of Belgrade, Belgrade (Serbia)

Truck mounted hydraulic cranes are widely used in the timber and in the waste disposal industry. They have a specific design, where dead weight, size in the folded position and the position of the gripper in the folded position are of particularly importance. Functionality of the crane is therefore expressed with load handling capabilities and also with the functionality during road transportation of the payload, when the crane is in the folded position on the truck. For handling of heavier loads, nowadays mainly two types of cranes are used - the K cranes and the Z cranes. The main advantage of the K cranes is higher load capacity in comparison with the Z cranes when cranes of approximately the same weight are compared. On the other hand the main advantage of the Z cranes is their capability of folding in position, transvers to truck length. In the paper the kinematics of the mechanisms of the characteristic size K and Z cranes are analysed and mutually compared. The main accent is on the discussion about their load capacity.

Keywords: Hydraulic Cranes, Crane Mechanisms, Kinematics, Cranes Folded Position, Weight, Load Capacity

1. INTRODUCTION

Generally speaking, cranes are large and heavy structures, movable in different ways. Optimization of their structure is in general oriented toward savings during the production process. Smaller final weight of an overall structure also brings up smaller energy consumption during crane operations. When truck mounted hydraulic cranes are in question the overall weight of the crane is even more important, because it presents part of the allowed truck load capacity and therefor smaller mass means more of the payload and s. All the mentioned imply smaller costs and better sustainability of the transport machine.

Optimization of the overall crane weight requires optimization of the structure and of the mechanisms. For the fatigue optimization of the structure, for example, the investigation of the crane dynamics is important. The scientific articles are dealing with the control strategies for load-swing suppression (linear motion [1-10], slewing [1, 11, 12]) and with the payload swinging and its influence on the loading of a crane’s structure ([13-18]). On the other hand the optimization of the mechanisms primarily involves static and kinematic analysis.

A study of the hydraulic truck mounted cranes and possible improvements to their performance is a study with a real-life application, because these types of cranes are widely used in timber and in the waste disposal industry which are both growing industries. The operation of these cranes involves three main motions: the slewing motion of the crane arm around the vertical axis, the radial movement of the load suspension point (folding or stretching of the boom and the jib) and the hoisting of the load (luffing of the arm). In this paper a kinematic analyses of the crane arm mechanism of the hydraulic truck mounted cranes for the timber and the waste disposal industry are introduced. The performances of the mechanisms of two most common types of such cranes are compared. The cranes of two European producers are chosen for the analyses.

2. TRUCK MOUNTED HYDRAULIC CRANES

There are two main families of truck mounted hydraulic cranes. The first family presents the large boom cranes with luffing arm consisting of one regularly telescopic boom mounted on the slewing platform (figure 1). The cranes of the other family are often called lorry cranes. They are smaller and they consist of the slewing pillar on which the arm containing the boom and the jib is attached (figure 2). The arm can perform luffing motion and can also fold.

Figure 1: Truck mounted hydraulic boom crane
(Source: http://en.wikipedia.org/wiki/File:Truck_crane.jpg, 29.05.2014)

Figure 2: Hydraulic Lorry crane
(Source: http://www.tslvanguard.co.uk/lorry-cranes, 29.05.2014)

*Corresponding author: Faculty of Mechanical Engineering, University of Ljubljana, Ljubljana, boris.jerman@fs.uni-lj.si

In the paper the second family of truck mounted hydraulic cranes is taken under the consideration, which are widely used in the timber and in the waste disposal industry. They have a specific design, where dead weight, size in the folded position and the position of the gripper in the folded position are of particularly importance. Functionality of the crane is therefore expressed with load handling capability and also with the functionality during road transportation of the payload, when the crane is in the folded position on the truck.

For handling of heavier loads, nowadays mainly two types of cranes are used - the K cranes and the Z cranes which differs mainly due to the design of the arm mechanism which enables different folding modes and on the other hand influence the crane's payload capacity. The main advantage of the K cranes is higher load capacity in comparison with the Z cranes when cranes of approximately the same weight and reach are compared. On the other hand the main advantage of the Z cranes is their capability of folding in position, transvers to truck length, which in the contrast to the K cranes ensures that during the transport of the loaded or empty crane the crane arm is removed from the truck hopper (figure 3 and 4).

Figure 3: Arm of the K-crane rests on the payload

(*Source: http://holz.fordaq.com/fordaq/news/ElmiaWood_Evolution_revolution_1457.html?Printable=yes, 29.05.2014*)

Figure 4: Z-crane's arm is folded behind the cab

(*Source: http://www.hiab.co.uk/Products/Forestry-and-recycling-cranes/Product-page/?parentProductGroupId=51949&productGroupId=51964&productId=51975, 29.05.2014*)

In the paper the kinematics of the mechanisms of the K- and Z-cranes of two known European manufacturers are analysed and mutually compared. The main accent is on the discussion about their load capacity regarding the maximum available hydraulic cylinder loading.

The hydraulic lorry cranes for manipulating timber and scrap and for recycling assignments are usually denoted with the typified designation, consisting of letters and numbers. The first part of the designation is a letter which denotes the cranes manufacturer. The second part is a number, which loosely indicates the nominal load capacity in kN m. The third part is a letter, which presents the type of the crane mechanism. K- type cranes are usually designated with letter K or L and Z type cranes are denoted with letter Z. For the analysis the cranes of the characteristic nominal load capacity of 120 are chosen.

3. NUMERICAL ANALYSES

For the execution of the analyses of the mechanisms the numerical modelling in the Adams software is chosen. Four models presented in table 1 are analysed.

Table 1: Designation of the crane models

	K-type crane	Z-type crane
Manufacturer "a"	Model Ka (also denoted as Model 1)	Model Za (also denoted as Model 3)
Manufacturer "b"	Model Kb (also denoted as Model 2)	Model Zb (also denoted as Model 4)

The numerical models are introduced in figure 5. They consist of the following rigid beams: rotating pillar, luffing boom and telescopic jib. Individual beams are mutually connected with hinges. The relative position of the beams is controlled by hydraulic cylinders. In the model the rotation of the pillar around the vertical axis is not modelled as isn't the stretching of the telescopic jib. The mass of the crane elements is ignored since the research is focused on the influence of the payload.

The cranes mechanisms are loaded with unite force and the forces in the hydraulic cylinders are observed during the folding of the reach of the arm - reducing the payload lever length. In that manner the multipliers of the forces, produced in the hydraulic cylinders by the payload weight along its radial movement are calculated, which present an important indicator of the quality of the mechanism design.

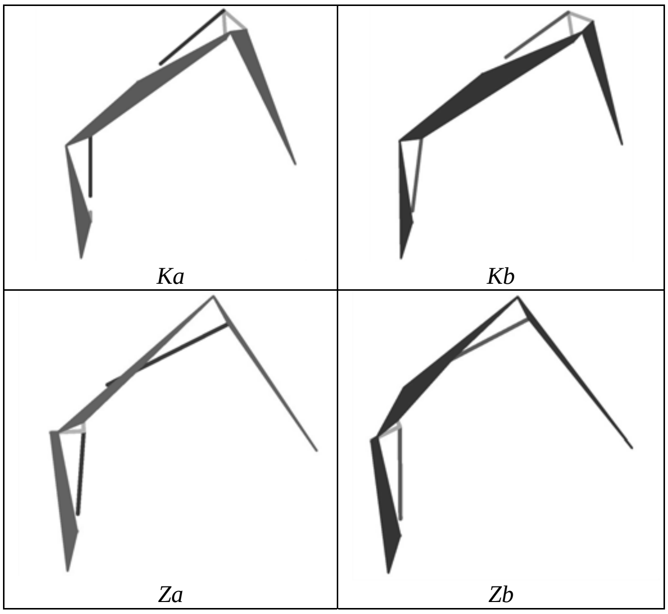

Figure 5: Numerical models of mechanisems of the cranes Ka, Kb, Za and Zb

4. RESULTS

The following results are shown for all four discussed cranes mechanisms for the horizontal radial movement of the load suspension point, located in the pillar height.

Cylinder 1 is the cylinder between the pillar and the boom, whereas cylinder 2 is between the boom and the jib.

4.1. Model Ka (№ 1)

Numerical model Ka represents the 120K crane of the manufacturer a. The force multiplier (in regard to the payload force) in the hydraulic cylinders 1 and 2 in the subordination to the arm reach are shown in diagrams in figures 6 and 7.

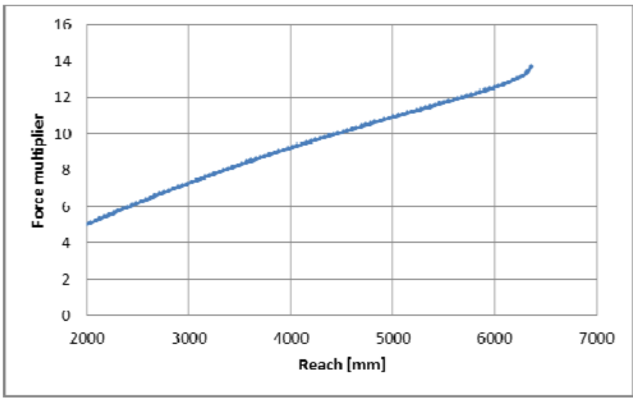

Figure 6: Reaction force in cylinder 1 of the Ka model

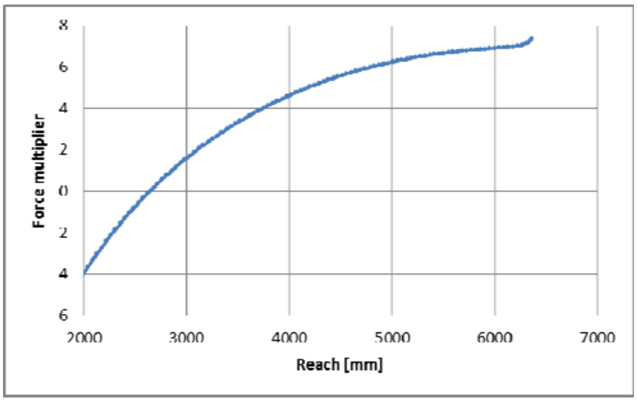

Figure 7: Reaction force in cylinder 2 of the Ka model

From the figure 6 can be seen that the force in the cylinder 1 has almost linear dependency regarding the reach elongation. The force multiplier spans from 5 at reach of 2 meters to almost 13 at reach of 6 meters. Positive multiplier values represent compression forces in the cylinders.

On the other hand from the figure 7 the highly nonlinear dependency of the force multiplier for the cylinder 2 can be observed. The force multiplier spans from -4 at reach of 2 meters to 6 at reach of 6 meters. Negative multiplier values represent tension forces in the cylinders. Tension in the cylinder 2 in the first part of the radial movement of the load suspension point is expected, because of the position of the jib as is shown in figure 8.

Figure 8: Position of the Ka model mechanism where tension forces in cylinder 2 are expected

4.2. Model Kb (№ 2)

Numerical model Kb represents the 120K crane of the manufacturer b. The force multiplier (in regard to the payload force) in the hydraulic cylinders 1 and 2 in the subordination to the arm reach are shown in diagrams in figures 9 and 10.

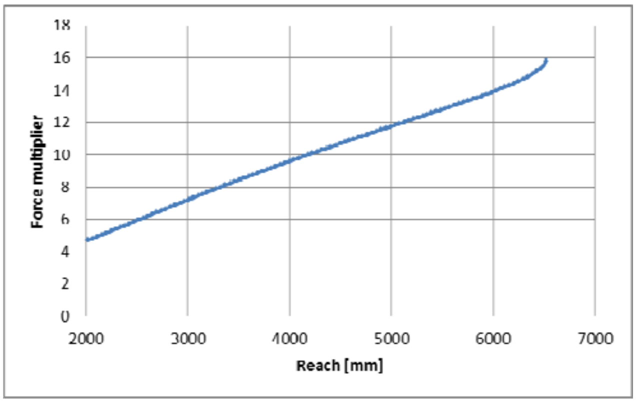

Figure 9: Reaction force in cylinder 1 of the Kb model

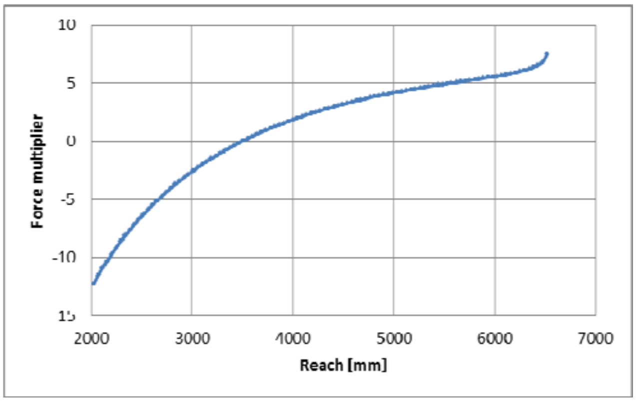

Figure 10: Reaction force in cylinder 2 of the Kb model

From the figure 9 can be seen that the force in the cylinder 1 has almost linear dependency regarding the reach elongation. The force multiplier spans from 4.8 at reach of 2 meters to 14 at reach of 6 meters. The same payload on the same reach presents greater loading of the hydraulic cylinder 1 of the crane Kb than of Ka.

From the figure 10 the highly nonlinear dependency of the force multiplier for the cylinder 2 can be observed. The force multiplier spans from -12.2 at reach of 2 meters to 7.5 at reach of 6 meters. Also in the case of cylinder 2 the same payload on the same reach presents greater loading of the hydraulic cylinder of the crane Kb than of Ka.

The characteristics for the force multiplier for the cylinder 1 and 2 are qualitatively very similar when crane of the manufacturer a and b are compared.

4.3. Model Za (№ 3)

Numerical model Za represents the 120Z crane of the manufacturer a. The force multiplier (in regard to the payload force) in the hydraulic cylinders 1 and 2 in the subordination to the arm reach are shown in diagrams in figures 11 and 12.

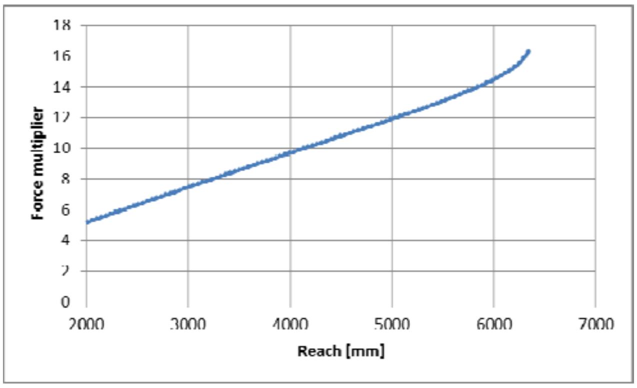

Figure 11: Reaction force in cylinder 1 of the Za model

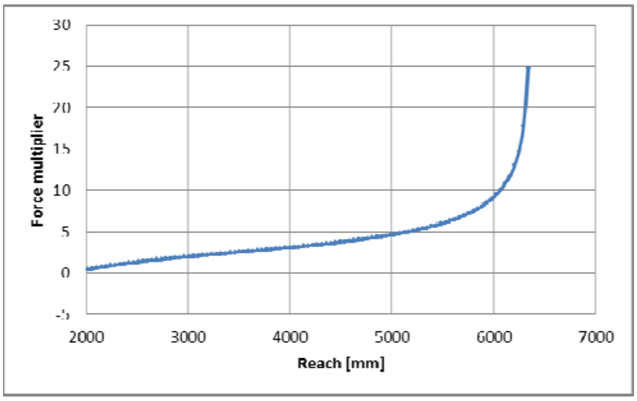

Figure 12: Reaction force in cylinder 2 of the Za model

From the figure 11 can be seen that the force in the cylinder 1 has almost linear dependency regarding the reach elongation. The force multiplier spans from 5.3 at reach of 2 meters to 14.7 at reach of 6 meters.

From the figure 12 the highly nonlinear dependency of the force multiplier for the cylinder 2 can be observed. The force multiplier spans from 0.6 at reach of 2 meters to 9.5 at reach of 6 meters. Beyond that reach the force multiplier increasing very fast and therefore this part of the mechanism working zone is not optimal.

4.4. Model Zb (№ 4)

Numerical model Zb represents the 120Z crane of the manufacturer b. The force multiplier (in regard to the payload force) in the hydraulic cylinders 1 and 2 in the subordination to the arm reach are shown in diagrams in figures 13 and 14.

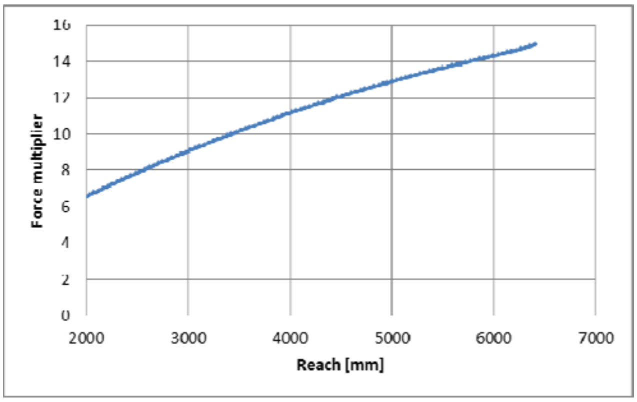

Figure 13: Reaction force in cylinder 1 of the Zb model

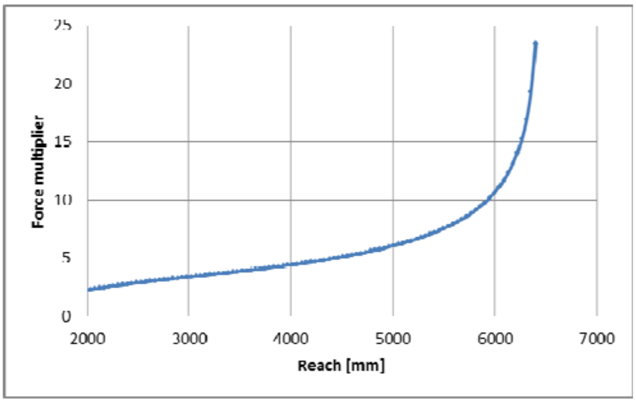

Figure 14: Reaction force in cylinder 2 of the Zb model

From the figure 13 can be seen that the force in the cylinder 1 has almost linear dependency regarding the reach elongation. The force multiplier spans from 6.8 at reach of 2 meters to 14.4 at reach of 6 meters. The same payload on the same reach presents for the major part of the span greater loading of the hydraulic cylinder 1 of the crane Kb than of Ka.

From the figure 14 the highly nonlinear dependency of the force multiplier for the cylinder 2 can be observed. The force multiplier spans from 2.4 at reach of 2 meters to 11.1 at reach of 6 meters. Also in the case of cylinder 2 the same payload on the same reach presents greater loading of the hydraulic cylinder of the crane Kb than of Ka.

5. COMPARISON OF THE RESULTS

For more efficient relative comparison of individual observed cranes mechanisms the curves of the force multipliers for the cylinder 1 are shown on the graph in figure 15 and for the cylinder 2 in the figure 16.

5.1. Force multipliers for the cylinder 1

In the figure 15 the force multipliers of the cylinder 1 of the crane models from № 1 to № 4 are shown. Solid lines present K-type of crane mechanisms whereas dashed lines present Z-type of crane mechanisms. Bold lines present cranes of the manufacturer a and thin lines present cranes of the manufacturer b.

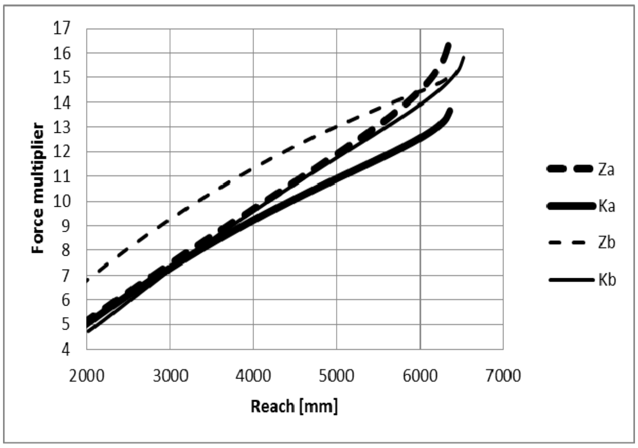

Figure 15: Comparison of the reaction forces in cylinder 1 for different crane types

From the figure 15 the following can be clearly concluded. The Z-crane of the manufacturer b has the less favourable loading of the cylinder 1, which is the cause of higher loading of the pillar and boom elements too. The Z-crane of the manufacturer a is the second less favourable regarding the criterion of the cylinder 1 loading but it is, on the other hand, very close to the characteristic of the K-crane of the manufacturer b. The K-crane mechanism of the manufacturer a is the most appropriate regarding the observed criterion, because the average force and the maximum force are having the lowest values.

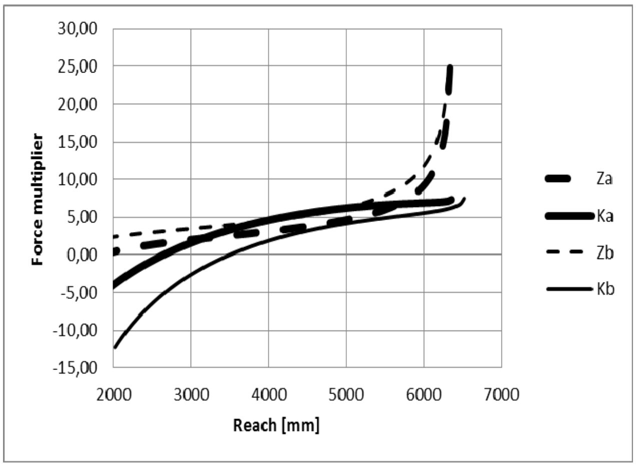

Figure 16: Comparison of the reaction forces in cylinder 2 for different crane types

5.2. Force multipliers for the cylinder 2

In the figure 16 the force multipliers of the cylinder 2 of the crane models from № 1 to № 4 are shown. Solid lines present K-type of crane mechanisms whereas dashed lines present Z-type of crane mechanisms. Bold lines present cranes of the manufacturer a and thin lines present cranes of the manufacturer b.

From the figure 16 the following can be concluded. The Z-crane of the manufacturer b has the less favourable loading of the cylinder 2 too, which is the cause of higher loading of the boom and jib elements. The Z-crane of the manufacturer a is the second less favourable regarding the criterion of the cylinder 2 loading in the beginning and at the end of the span but it is, on the other hand, in the middle part of the span, more favourable than the K-crane of the manufacturer a. The K-crane mechanism of the manufacturer b has the lowest value during the whole span, but the attention must be drown toward its high negative value at small reach. Because of that the K-crane mechanism of the manufacturer a is the most appropriate regarding the observed criterion again, because the force multiplier has the lowest average value as well as much more favourable value during the smaller span.

6. CONCLUSION

Truck mounted hydraulic cranes are widely used in the timber and in the waste disposal industry. For handling of heavier loads, nowadays mainly two types of cranes are used - the K cranes and the Z cranes. In the paper the kinematics of the mechanisms of the characteristic size of 120K and 120Z cranes are analysed and mutually compared. The main accent is on the discussion about their relative load capacity defined trough the loading of hydraulic cylinders. It is assumed that the mechanism is more optimal if the needed force multiplier is smaller.

Both crane mechanism types were analysed and cranes of two manufacturers were taken into account and therefor four different cases were studied.

It was discovered that the Z-crane of the manufacturer b has the less favourable loading of the cylinder 1 during the studied motion, the Z-crane of the manufacturer a is the second less favourable and that the K-crane mechanism of the manufacturer a is the most appropriate, because the average and the maximum force multipliers are the lowest in that case.

It was further find out, that the Z-crane of the manufacturer b has the less favourable loading of the cylinder 2 too. The Z-crane of the manufacturer a is again the second less favourable. On the other hand it should be noted that in the middle part of the span, these characteristics are more favourable than the K-cranes characteristic of the manufacturer a. The K-crane mechanism of the manufacturer b has the lowest value of the cylindr 2 loading during the whole span, but attention must be drown toward its high negative values at small reach. Because of that the K-crane mechanism of the manufacturer a is more appropriate regarding the second criterion too, because the force multiplier has the lowest average value as well as much more favourable value during the smaller span.

REFERENCES

[1] Abdel-Rahman, E.M.; Nayfeh, A.H.; Masoud, Z.N. Dynamics and Control of Cranes: A Review. // Journal of Vibration and Control, 2003, 9, 863-908.

[2] Lee, H. A new design approach for the anti-swing trajectory control of overhead cranes with high-speed hoisting. // International Journal of Control, 2004, 77(10), 931-940.

[3] Oguamanam, D.C.D.; Hansen, J.S. Dynamics of a three-dimensional overhead crane system. // Journal of Sound and Vibration. 2001, 242(3), 411-426.

[4] Bartolini, G.; Pisano A.; Usai E. Second-order sliding-mode control of container cranes.// Automatica. 2002;38:1783-90.

[5] Yavin, Y.; Kemp, P.D. The application of extended inverse dynamics control. // Computers and Mathematics with Applications, 2000, 40, 669-677.

[6] Zrnić, N.; Hoffmann, K.; Bošnjak, S. Modelling Of Dynamic Interaction between Structure and Trolley for Mega Container Cranes. // Mathematical and Computer Modelling of Dynamical Systems, Vol. 15, No. 3, 295-311, 2009.

[7] Zrnić, N.; Bošnjak, S.; Hoffmann, K. Parameter sensitivity analysis of non-dimensional models of quayside container cranes. // Mathematical and Computer Modelling of Dynamical Systems, Vol. 16, No. 2, 145-160, 2010.

[8] Zrnić, N.; Gašić, V.; Obradović, A.; Bošnjak, S. Appropriate modeling of dynamic behavior of quayside container cranes boom under a moving trolley. // Springer Proceedings in Physics 139, Vibration problems ICOVP 2011, pp. 81-86, 2011, Springer.

[9] Gašić, V.; Zrnić, N.; Obradović, A.; Bošnjak, S. Consideration of Moving Oscillator Problem in Dynamic Responses of Bridge Cranes. // FME Transactions, Vol. 39, No. 1, pp. 17-24, 2011.

[10] Vladić, J.; Đokić, R.; Kljajin, M.; Karakašić, M. Modelling and simulations of elevator dynamic behaviour (Preliminary notes). // Tehnički vjesnik - Technical Gazette, Vol. 18 No. 3, 2011.

[11] Glossiotis, G.; Antoniadis, I. Payload sway suppression in rotary cranes by digital filtering of the commanded inputs. // Proceedings of the Institution of Mechanical Engineers, Part K, Journal of Multi-body Dynamics, 2003, 217(2), 99-109.

[12] Spathopoulos, M.P.; Fragopoulos, D. Pendulation control of an offshore crane. // International Journal of Control, 2004, 77(7), 654-670.

[13] Gašić, V.; Zrnić, N.; Rakin, M.; Consideration of a moving mass effect on dynamic behaviour of a jib crane structure. // Tehnički vjesnik - Technical Gazette, Vol. 19 No. 1, 2012

[14] Ghigliazza, R.M.; Holmes, P. On the dynamics of cranes, or spherical pendula with moving supports. // Int. J. of Non-Linear Mechanics. 2002, 37, 1211-1221.

[15] Jerman, B.; Podržaj, P.; Kramar, J. An Investigation of Slewing-Crane Dynamics During Slewing Motion - Development and Verification of a Mathematical Model. // International Journal of Mechanical Sciences, 2004, 46(5), 729-750.

[16] Wu, J.J.; Whittaker A.R.; Cartmell, M.P. The use of finite element techniques for calculating the dynamic response of structures to moving loads. // Computers and Structures. 2000, 78, 789-799.

[17] Jerman, B. An enhanced mathematical model for investigating the dynamic loading of a slewing crane. // Proc. Inst. Mech. Eng., C J. mech. eng. sci., 2006, letn. 220, št. 4, str. 421-433.

[18] Jerman, B.; Kramar, J. A study of the horizontal inertial forces acting on the suspended load of slewing cranes. // Int. j. mech. sci.. [Print ed.], 2008, letn. 50, št. 3, str. 490-500.

Determining the Forward Kinematics Model of a Bucket Excavator's Digging Equipment

Dima Marian[1*], Francu Catalin[1*] , Ghelmeci Radu[1]
[1]The Faculty of Technological Equipment, Technical University of Civil Engineering, Bucharest (Romania)

This paper presents a method to build the forward kinematics model of a bucket excavator's digging equipment. The applied method is the one used for the industrial robots' mechanisms and uses Denavit-Hartenberg convention

Keywords: Forward kinematics; bucket excavator; Denavit-Hartenberg

1. INTRODUCTION

One of the development paths in construction robotics and automation is to automate and robotize existing equipment [1, 2]. Automating and robotizing construction equipment assumes the modelling of the equipment and also its technological process from the kinematic and dynamic point of view. In order to create the model, there are in the specialty literature well-known methods, each of which is oriented to some particular technical field. For construction machinery it's useful to be considered like being composed of 2 parts, the chassis / mobile platform / carrying module and the work equipment, respectively. The first part can be modelled by analogy with mobile robots and the second part by analogy with industrial robots.

Figure 1: Excavator

The work equipment of the bucket excavator, figure 1, can be considered as an open loop kinematic chain composed of the following kinematic elements: undercarriage, boom, stick and bucket and the joints between these elements can be considered driving joints. For example, the driving mechanism with a hydraulic cylinder between boom and stick is considered as being part of the driving joint that connects the 2 elements, transforming it from driven joint to driving joint. Taking these into account, the bucket excavator's digging equipment has 4 degrees of mobility all of them are revolute. These transformations are carried out in order to study the kinematics of this mechanism with the method used for positioning and orientation mechanisms of the industrial robots.

The problem of forward kinematic modelling can be formulated as follows: knowing the variables of the driving joints we need to find out the position and orientation of the end-effector. The forward kinematics model has 2 major uses. First one is for determining the workspace of the equipment, and the second one is for determining the inverse kinematic model.

2. METHOD PRESENTATION

In this method to every kinematic element is attached a reference frame according to the *Denavit-Hartenberg* [3] convention. For the open loop kinematic chain composed of consecutive kinematic elements *i-2, i-1, i* and *i+1* and the kinematic joints linking the elements, figure 2, the choosing of the reference frames linked to the elements *i-1* and *i* is carried out as follows:

1. direction of the z_{i-1} axis that link the element *i-1* to *i* is the joints axis;
2. x_{i-1} axis is linked to the element *i-1* and is chosen to the common normal of the z_{i-1} and z_{i-2} axes oriented from O_{i-2} to O_{i-1};
3. Similarly the axis x_i is chosen as common normal of the rotation axes z_{i-1} and z_i oriented from O_{i-1} to O_i;
4. The origins of the reference frames are chosen in the intersection points between the common normal and the axis of the revolute joint, respectively O_{i-2} and O_{i-1};
5. The name of the joint is given by the highest order of the elements that complete the joint.
6. The y axes are chosen so that the reference frame is orthogonal.

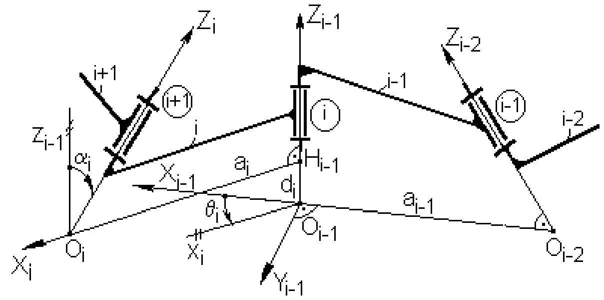

Figure 2: The Denavit-Hartenberg convention

The geometrical parameters which entirely describe any revolute or translational joint in the kinematic chain are as follows:

*Corresponding author: Technical University of Civil Engineering 122-124 Lacul Tei Blv., Bucharest, Romania, francu@mail.utcb.ro

θ_i	Is the joints angle from axis x_{i-1} to axis x_i, measured counter clockwise, around axis z_{i-1}
d_i	Is the distance from the origin O_{i-1} to the intersection of the axis z_{i-1} with axis x_i, measured along the axis z_{i-1}
a_i	Is the distance from the intersection of the axis z_{i-1} with x_i to the origin O_i,measured along the axis x_i (or the least distance between z_{i-1} and z_i axes)
α_i	Is the angle between the z_{i-1} axis with the axis z_i, by rotating it around x_i axis counter clockwise.

The transition from reference frame "*i-1*", attached to the element *i-1*, to the reference frame "*i*", attached to the element *i*, is carried out as follows:

1. rotation around z_{i-1} axis by angle θ_i, in order to overlap the x_{i-1} axis with x_i;
2. a translation along the axis z_{i-1} with the distance d_i,which brings the origin O_{i-1} in the intermediate position H_{i-1} (fig.2);
3. a new translation along the x_{i-1} axis by the a_i distance, thus overlapping the origin O_{i-1} to O_i;
4. finally a second rotation around x_i axis by an α_i angle, in order to overlap z_{i-1} axis with z_i.

Each one of these 4 movements can be expressed using an elementary rotation or translation matrix and the resulting movement being the product of the matrices:

$$
{}_{i-1}T^{i} = Rot(z_{i-1},\theta_i)\cdot Trans(z_{i-1},d_i)\cdot Trans(x_{i-1},a_i)\cdot \cdot Rot(x_i,\alpha_i) \quad (1)
$$

Doing the multiplication of the elementary matrices:

$$
\begin{pmatrix} \cos(\theta_i) & -\sin(\theta_i) & 0 & 0 \\ \sin(\theta_i) & \cos(\theta_i) & 0 & 0 \\ 0 & 0 & 1 & 0 \\ 0 & 0 & 0 & 1 \end{pmatrix} \cdot \begin{pmatrix} 1 & 0 & 0 & 0 \\ 0 & 1 & 0 & 0 \\ 0 & 0 & 1 & d_i \\ 0 & 0 & 0 & 1 \end{pmatrix} \cdot \begin{pmatrix} 1 & 0 & 0 & a_i \\ 0 & 1 & 0 & 0 \\ 0 & 0 & 1 & 0 \\ 0 & 0 & 0 & 1 \end{pmatrix} \cdot \begin{pmatrix} 1 & 0 & 0 & 0 \\ 0 & \cos(\alpha_i) & -\sin(\alpha_i) & 0 \\ 0 & \sin(\alpha_i) & \cos(\alpha_i) & 0 \\ 0 & 0 & 0 & 1 \end{pmatrix} \quad (2)
$$

The transition matrix from the reference frame "*i-1*", attached to the element *i-1*, to the reference frame "*i*", attached to the element *i*, is obtained:

$$
{}_{i-1}T^{i} = \begin{pmatrix} \cos(\theta_i) & -\sin(\theta_i)\cdot\cos(\alpha_i) & \sin(\theta_i)\cdot\sin(\alpha_i) & a_i\cdot\cos(\theta_i) \\ \sin(\theta_i) & \cos(\theta_i)\cdot\cos(\alpha_i) & -\cos(\theta_i)\cdot\sin(\alpha_i) & a_i\cdot\sin(\theta_i) \\ 0 & \sin(\alpha_i) & \cos(\alpha_i) & d_i \\ 0 & 0 & 0 & 1 \end{pmatrix} \quad (3)
$$

The said transition matrix (3) sets the position and orientation of the reference frame "*i*", attached to the element *i* in relation to the reference frame "*i-1*", attached to the element *i-1*.

3. ATTAINING THE FORWARD KINEMATIC MODEL OF THE BUCKET EXCAVATOR'S DIGGING EQUIPMENT

3.1 Attaching reference frames

The kinematic scheme of the bucket excavator's digging equipment is presented in figure 3. In the figure were noted: *1* – upper carriage, *2* – boom, *3* – stick, *4* – bucket. These elements are linked between them through joints B, C and D, also the upper carriage is linked to the under carriage through Joint A. According to the method presented in the previous chapter, considering the under carriage being the element „*i-2≡0*" the O_0z_0 axis is vertical with the positive side going up and going through point A. For simplifying the calculus the origin O_0 is chosen in point A.

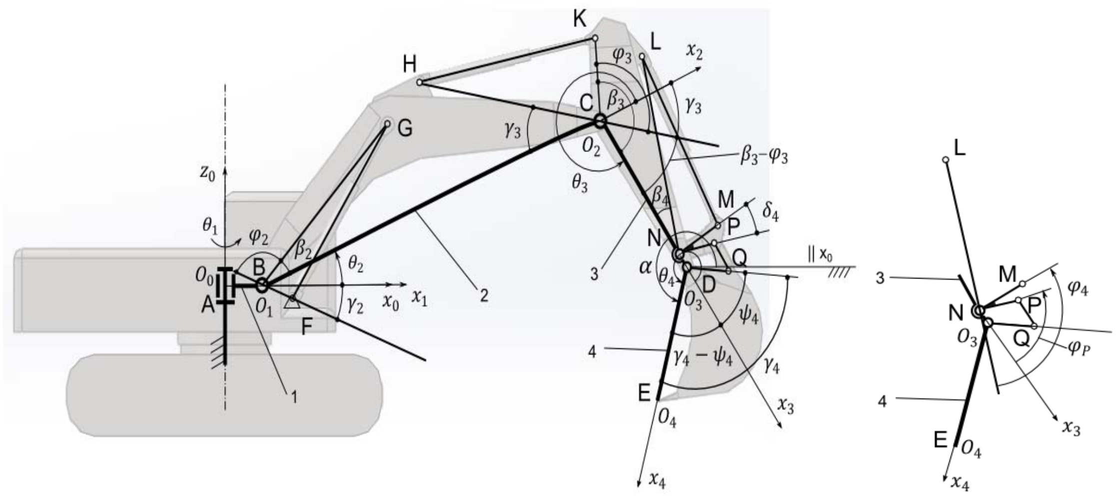

Figure 3: The kinematic scheme of the bucket excavator's digging equipmen

The axes O_1z_1, O_2z_2, O_3z_3 and O_4z_4 are attached to the upper carriage, boom, stick and bucket going through points A, B, C and D and are normal to the drawing plane and the sense going from the viewer to the drawing. The axis O_1x_1 has its direction and orientation by $\overline{AB}$, axis O_2x_2 has its direction and orientation by $\overline{BC}$, axis O_3x_3 has its direction and orientation by $\overline{CD}$, O_4x_4 has its direction and orientation by $\overline{DE}$. The origins of the reference frames are found to the intersection of the *z* axes with the *x* axes which means that O_1 find itself in point B, O_2 in C, O_3 in D and O_4 in point E. The axis O_0x_0 has its direction in the initial position of the O_1x_1 axis.

3.2. Determining the transition matrices and transformation matrices

The geometrical parameters that describe the kinematic chain are presented in the following table.

Table 1: The geometrical parameters

Joint	θ_i	d_i	a_i	α_i	Variable q_i
A (0-1)	θ_1	0	$l_1 = AB$	90°	θ_1
B (1-2)	θ_2	0	$l_2 = BC$	0	θ_2
C (2-3)	θ_3	0	$l_3 = CD$	0	θ_3
D (3-4)	θ_4	0	$l_4 = DE$	0	θ_4

Replacing in eq. (3) the parameters from table 1, we obtain the following matrices:

$$ {}_0T^1 = \begin{pmatrix} \cos(\theta_1) & 0 & \sin(\theta_1) & l_1\cdot\cos(\theta_1) \\ \sin(\theta_1) & 0 & -\cos(\theta_1) & l_1\cdot\sin(\theta_1) \\ 0 & 1 & 0 & 0 \\ 0 & 0 & 0 & 1 \end{pmatrix} \quad (4)$$

$$ {}_1T^2 = \begin{pmatrix} \cos(\theta_2) & -\sin(\theta_2) & 0 & l_2\cdot\cos(\theta_2) \\ \sin(\theta_2) & \cos(\theta_2) & 0 & l_2\cdot\sin(\theta_2) \\ 0 & 0 & 1 & 0 \\ 0 & 0 & 0 & 1 \end{pmatrix} \quad (5)$$

$$ {}_2T^3 = \begin{pmatrix} \cos(\theta_3) & -\sin(\theta_3) & 0 & l_3\cdot\cos(\theta_3) \\ \sin(\theta_3) & \cos(\theta_3) & 0 & l_3\cdot\sin(\theta_3) \\ 0 & 0 & 1 & 0 \\ 0 & 0 & 0 & 1 \end{pmatrix} \quad (6)$$

$$ {}_3T^4 = \begin{pmatrix} \cos(\theta_4) & -\sin(\theta_4) & 0 & l_4\cdot\cos(\theta_4) \\ \sin(\theta_4) & \cos(\theta_4) & 0 & l_4\cdot\sin(\theta_4) \\ 0 & 0 & 1 & 0 \\ 0 & 0 & 0 & 1 \end{pmatrix} \quad (7)$$

By analogy with the robots mechanisms we can consider that the upper carriage, boom and stick of the excavator along with joints A, B and C are composing the positioning mechanism, having 3 degrees of mobility and the bucket and joint D compose the orientation mechanism having only 1 degree of mobility.

Taking these into account the transformation matrix of the positioning mechanisms is:

$$ {}_0T^3 = {}_0T^1 \cdot {}_1T^2 \cdot {}_2T^3 = \begin{pmatrix} \cos(\theta_1)\cdot\cos(\theta_2+\theta_3) & -\cos(\theta_1)\cdot\sin(\theta_2+\theta_3) & \sin(\theta_1) & \cos(\theta_1)\cdot(l_1+l_2\cos(\theta_2)+l_3\cos(\theta_2+\theta_3)) \\ \sin(\theta_1)\cdot\cos(\theta_2+\theta_3) & -\sin(\theta_1)\cdot\sin(\theta_2+\theta_3) & -\cos(\theta_1) & \sin(\theta_1)\cdot(l_1+l_2\cos(\theta_2)+l_3\cos(\theta_2+\theta_3)) \\ \sin(\theta_2+\theta_3) & \cos(\theta_2+\theta_3) & 0 & l_2\sin(\theta_2)+l_3\sin(\theta_2+\theta_3) \\ 0 & 0 & 0 & 1 \end{pmatrix} \quad (8)$$

And the transformation matrix of the orientation mechanism is eq. (7).

The transformation matrix for the entire mechanism can be obtained by multiplying the transformation matrices of the positioning and orientation mechanisms which is:

$$ \begin{pmatrix} \cos(\theta_1)\cdot\cos(\theta_2+\theta_3+\theta_4) & -\cos(\theta_1)\cdot\sin(\theta_2+\theta_3+\theta_4) & \sin(\theta_1) & \cos(\theta_1)\cdot(l_1+l_2\cos(\theta_2)+l_3\cos(\theta_2+\theta_3)+l_4\cos(\theta_2+\theta_3+\theta_4)) \\ \sin(\theta_1)\cdot\cos(\theta_2+\theta_3+\theta_4) & -\sin(\theta_1)\cdot\sin(\theta_2+\theta_3+\theta_4) & -\cos(\theta_1) & \sin(\theta_1)\cdot(l_1+l_2\cos(\theta_2)+l_3\cos(\theta_2+\theta_3)+l_4\cos(\theta_2+\theta_3+\theta_4)) \\ \sin(\theta_2+\theta_3+\theta_4) & \cos(\theta_2+\theta_3+\theta_4) & 0 & l_2\sin(\theta_2)+l_3\sin(\theta_2+\theta_3)+l_4\sin(\theta_2+\theta_3+\theta_4)) \\ 0 & 0 & 0 & 1 \end{pmatrix} = \begin{pmatrix} n_x & o_x & a_x & p_x \\ n_y & o_y & a_y & p_y \\ n_z & o_z & a_z & p_z \\ 0 & 0 & 0 & 1 \end{pmatrix}$$

which means that the first three columns are the direction cosines of the mobile reference frame, and the last column the coordinates of the mobile reference frame's origin to the end-effector:

$$\begin{aligned}
n_x &= \cos(\theta_1)\cdot\cos(\theta_2+\theta_3+\theta_4) \\
n_y &= \sin(\theta_1)\cdot\cos(\theta_2+\theta_3+\theta_4) \\
n_z &= \sin(\theta_2+\theta_3+\theta_4) \\
o_x &= -\cos(\theta_1)\cdot\sin(\theta_2+\theta_3+\theta_4) \\
o_y &= -\sin(\theta_1)\cdot\sin(\theta_2+\theta_3+\theta_4) \quad (10) \\
o_z &= \cos(\theta_2+\theta_3+\theta_4) \\
a_x &= \sin(\theta_1) \\
a_y &= -\cos(\theta_1) \\
a_z &= 0 \\
p_x &= \cos(\theta_1)\cdot(l_1+l_2\cos(\theta_2)+l_3\cos(\theta_2+\theta_3)+l_4\cos(\theta_2+\theta_3+\theta_4)) \\
p_y &= \sin(\theta_1)\cdot(l_1+l_2\cos(\theta_2)+l_3\cos(\theta_2+\theta_3)+l_4\cos(\theta_2+\theta_3+\theta_4)) \\
p_z &= l_2\sin(\theta_2)+l_3\sin(\theta_2+\theta_3)+l_4\sin(\theta_2+\theta_3+\theta_4))
\end{aligned}$$

Equations (10) represent the forward kinematic model of the bucket excavator's digging equipment through which the position and orientation of the end-effector are set $n_x, n_y, n_z, o_x, o_y, o_z, a_x, a_y, a_z, p_x, p_y, p_z$ as a function of the variables corresponding to the degrees of mobility of the mechanism $\theta_1, \theta_2, \theta_3, \theta_4$.

The position of any point on the bucket in relation to the fixed reference frame is determined by multiplying the transformation matrix (9) with the column vector which gives the coordinates of the point in relation to the mobile reference frame. In particular, the coordinates of the bucket's tooth tip are as follows:

$$\vec{r}_0 = {}_0T^4 \cdot \vec{r}_4 \quad (11)$$

$$\begin{pmatrix} \cos(\theta_1)\cdot\cos(\theta_2+\theta_3+\theta_4) & -\cos(\theta_1)\cdot\sin(\theta_2+\theta_3+\theta_4) & \sin(\theta_1) & \cos(\theta_1)\cdot(l_1+l_2\cos(\theta_2)+l_3\cos(\theta_2+\theta_3)+l_4\cos(\theta_2+\theta_3+\theta_4)) \\ \sin(\theta_1)\cdot\cos(\theta_2+\theta_3+\theta_4) & -\sin(\theta_1)\cdot\sin(\theta_2+\theta_3+\theta_4) & -\cos(\theta_1) & \sin(\theta_1)\cdot(l_1+l_2\cos(\theta_2)+l_3\cos(\theta_2+\theta_3)+l_4\cos(\theta_2+\theta_3+\theta_4)) \\ \sin(\theta_2+\theta_3+\theta_4) & \cos(\theta_2+\theta_3+\theta_4) & 0 & l_2\sin(\theta_2)+l_3\sin(\theta_2+\theta_3)+l_4\sin(\theta_2+\theta_3+\theta_4)) \\ 0 & 0 & 0 & 1 \end{pmatrix}\cdot\begin{pmatrix}0\\0\\0\\1\end{pmatrix}$$

of which

$$\begin{aligned} x_E &= \cos(\theta_1)\cdot(l_1+l_2\cos(\theta_2)+l_3\cos(\theta_2+\theta_3) \\ &+l_4\cos(\theta_2+\theta_3+\theta_4)) \\ y_E &= \sin(\theta_1)\cdot(l_1+l_2\cos(\theta_2)+l_3\cos(\theta_2+\theta_3) \\ &+l_4\cos(\theta_2+\theta_3+\theta_4)) \\ z_E &= l_2\sin(\theta_2)+l_3\sin(\theta_2+\theta_3) \\ &+l_4\sin(\theta_2+\theta_3+\theta_4)) \end{aligned} \tag{12}$$

3.3. The relation between the hydraulic cylinders strokes and variables of the driving kinematic joints

The joints B and C of the equipment’s mechanism are driven directly by the hydraulic cylinders FG and HK and joint D is driven by the hydraulic cylinder LM through the four-bar mechanism NPQD.

According to [4] and using the substitutions in figure 3, between the lengths of the hydraulic cylinders and position angles of the driven bars the following eq. are written:

$$\cos(\varphi_2)=\frac{s_2^2-FB^2-BG^2}{2\cdot FB\cdot BG};\ s_2=FG \tag{13}$$

$$\cos(\varphi_3)=\frac{s_3^2-HC^2-CK^2}{2\cdot HC\cdot CK};\ s_3=HK \tag{14}$$

$$\cos(\varphi_4)=\frac{s_4^2-LN^2-NM^2}{2\cdot LN\cdot NM};\ s_4=LM \tag{15}$$

and for the four-bar mechanism NPQD, with the substitutions:

$$a=\frac{NP^2-PQ^2+DQ^2+ND^2-2\cdot NP\cdot ND\cdot\cos(\varphi_p)}{2\cdot NP\cdot DQ\cdot\sin(\varphi_p)}$$

$$b=\frac{NP\cdot\cos(\varphi_p)-ND}{NP\cdot\sin(\varphi_p)} \tag{16}$$

$$\varphi_p=\varphi_4-\beta_4-\delta_4$$

we obtain

$$\psi_4=\operatorname{acos}\left(\frac{a\cdot b-\sqrt{1+b^2-a^2}}{1+b^2}\right) \tag{17}$$

In these conditions the angular variables of the driving joints B, C and D are as follows:

$$\theta_2=\pi-\beta_2-\gamma_2-\varphi_2 \tag{18}$$

$$\theta_3=2\pi-\beta_3-\gamma_3-\varphi_3 \tag{19}$$

$$\theta_4=2\pi-\gamma_4+\psi_4 \tag{20}$$

4. DETERMINING THE WORK SPACE. EXAMPLE

For the excavator Volvo EC650, [5] and a scale model to 1:50, were determined the following geometrical characteristics:

$l_1=720\,mm$; $l_2=6560\,mm$; $l_3=2750\,mm$; $l_4=2135\,mm$
$FB=674{,}38\,mm$; $BG=3189{,}22\,mm$; $HC=3568{,}923\,mm$; $CK=1275\,mm$; $LN=3099{,}428\,mm$; $NM=780\,mm$; $\beta_2=24{,}39°$; $\gamma_2=38{,}2°$; $\beta_3=149{,}18°$; $\gamma_3=30{,}46°$; $NP=620\,mm$; $PQ=500\,mm$; $DQ=755{,}11\,mm$; $ND=250\,mm$; $\beta_4=20{,}89°$; $\delta_4=18{,}51°$; $\gamma_4=100{,}6°$.

The lengths of the hydraulic cylinders are as follows: $s_2=2624\ldots3714\,mm$; $s_3=2733\ldots4623\,mm$; $s_4=2468\ldots3490\,mm$.

With these values the eq. (13)...(17) are computed, the results are pushed into eq. (18)...(20) and further the eq. (12) are computed. For $\theta_1=0°=ct$ the obtained results are presented in figure 4,*a*. For comparison in figure 4,*b* is presented the work space from the product brochure.

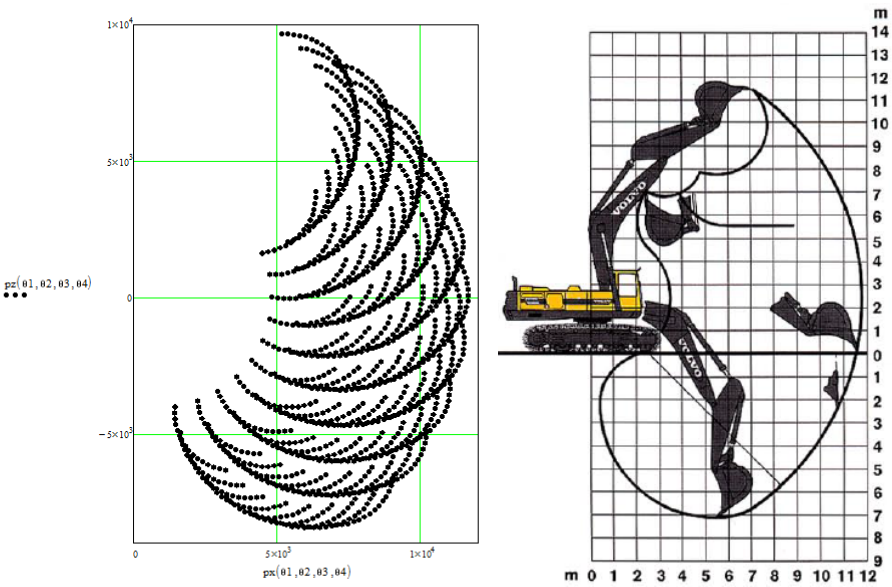

a) *b)*

Figure 4

5. CONCLUSIONS

- The forward kinematic model of the bucket excavator's digging equipment, eq. (10), is determined by analogy with the industrial robots mechanisms and using the Denavit-Hartenberg convention.
- The driving mechanisms with hydraulic cylinders corresponding to axes 2, 3 and 4 were considered as being part of the revolute joints B, C and D, transforming these from driven joint to driving joints. This fact allows that the mechanism to be studied as an open loop kinematic chain.
- The present model regards only the positions study of the kinematic elements. Velocities, accelerations of different points on the elements are determined easily by differentiating some similar eq. like eq. (11).

REFERENCES

[1] "*Robots and automated machines in construction*", IAARC Catalogue, 1998, http://www.iaarc.org
[2] Carlos Balaguer, Mohamed Abderrahim, "*Robotics and Automation in Construction*", InTech Europe, 2008, ISBN 978-953-7619-13-8
[3] Richard S. Hartenberg, Jacques Denavit, "*Kinematic synthesis of linkages*", McGraw Hill, 1964
[4] Raicu, A., Bruja, A., "*Mecanisme*", UTCB, 1996
[5] Brochure "*Volvo Excavators EC140D*"

Case Study of Product Innovation Based on Special Crane Trolley

Zoran Petrovic[1*], Ugljesa Bugaric[2], Dusan Petrovic[2]
[1] Tecon sistem d.o.o., Belgrade (Serbia)
[2] Faculty of Mechanical Engineering Belgrade, Industrial Engineering Department, University of Belgrade, Belgrade (Serbia)

Innovation is generally accepted as key factor for development of every production oriented company. In the case study, development of the new product was analysed – new crane trolley which should replace old one, which is not in the function. Main motive for development of the new product is achieving strategic advantage over competition, since competition couldn't offer such product. Since crane trolley as product already exist in company product portfolio, special trolley is considered as incremental innovation. According to innovation strategy, innovation can be considered as adapted market-pull model, since for this kind of product niche-market was noticed and advantage was achieved. As creative method for idea development mind mapping was used and for innovation creation Stage – Gate innovative model. Result of analyses was new product – crane trolley, which was used for modernization of the crane on HE Matka, Skopje, Former Yugoslav Republic of Macedonia.

Keywords: Innovation, idea development, market-pull model, mind mapping, Stage-gate model, crane trolley

1. INNOVATIONS

Innovations are old almost as human race. In order to survive in hostile surrounding, prehistoric human had to fight for existence and to continually develop tools and weapons for hunting, agriculture, building of the shelters, etc. From theoretical point of view, such developments were primordial innovations.

Beginning of the scientific thought regarding innovations can be pinned to renaissance period. In that manner it is essential to mention work of N. Machiavelli "Prince", written in 1505. [1], and paper of F. Bacon "About innovations" written in 1625. [2]

Word innovations, has its root in Latin word "innovare", which has meaning of creation of something new. Innovation is process of developing idea into something useful for practical consumption – realisation. It can be represented with following expression [3]:

Innovation = theoretical concept + technical innovation + commercial exploitation

Development of innovation theory can be connected with work of J. Schumpeter [4], who defined innovation as main starter of industrial development. According to him, innovations are described as "creative destruction" – rejecting on old concepts in order to define and accept new ones, which were generated through process of innovations.

Thirty years later Uterback and Abernathy [5], defined different approach, in which development of each branch of market is induced by certain, radical, innovation in that field. Although definition of the innovations were not drastically changed over the time, dynamics of innovation development was changing. Drucker was observing innovations as initial force for developing of entrepreneurship [6]. According to him innovation is specific tool of entrepreneur, tool with which he can use change as possibility for different business or service. Porter [7] in his work defined innovations as key concept for development of competitive advantage of company. Nowotny [8], had different approach. Contemporary epoch, he defined as "epoch of fascination and quest for innovations". Fascination on innovations goes so far that some members of scientific community think that taking some psychoactive substances, which are generally used in order to develop cognitive functions of certain clinical patients, can stimulate innovation process [9].

In the Serbian legislation innovation was first mentioned in the Law of innovation activity of Republic of Serbia in 2005. In mentioned law, innovation is described as: "new product, process or technology, or service with unique properties, created in connection with results of scientific research through own or not own concept, idea, or method for its development, which is with certain value introduced to market".

Addition to this law was published in 2010 and in it new definition of the innovation was introduced, according to OECD standard of EU [10]. According to this addition, innovation is defined as: "innovation is successful market use of invention, or new, or significant improvement of product or process, or service, or marketing methodology, or new organizational methodology in business, work organization, or relations of company with its surrounding".

2. CLASSIFICATION OF INNOVATIONS

Main criteria for innovation classification are:
- Nature of innovation,
- Type of innovation (typology).

Nature of innovation has two main subcategories. First subcategory are radical, core innovations and second one are incremental, or evolutive innovations. Regarding typology of innovations, there are numerous different classifications.

One of the first classifications was suggested by Schumpeter:
- Innovation based on new product,
- Innovation based on new method of production,
- Opening of the new market,
- Finding new source of raw materials or components,
- Reorganization of the industry.

*Corresponding author: Tecon Sistem d.o.o., Antifašističke borbe 21 b, 11070 Belgrade, Serbia; zoran.petrovic@tecon.rs

Key types of innovations are ones included in first two types of innovations – innovations based on products and innovations based on new method of production.

Contemporary approach to classification of innovations is coming from Oslo manual, published in 2005, which is core document which gives directions for gathering and interpretation of data about innovations (OECD and Eurostat). [11]

In the manual there are elements of typology with four (five if services are considered as separate element) types of innovation:
- Innovation of product/service,
- Innovation of process,
- Innovation of organization,
- Innovation of marketing.

3. INNOVATION OF THE PRODUCT

Innovation of the product is “introduction of the product/service, which is completely new, or significantly improved – meaning improved characteristics or use” [3].

In the scope of this paper is incremental innovation based on development of the product which performance is changed. Further classification is done according to:
- Products which are improved (better or different performances, or cut costs) with usage of new components or better performance materials,
- Products which consists of numerous of subassemblies or elements and development was achieved by partial change of one or more subassemblies or elements.

One of the frequently asked questions is difference between incremental innovation of the product and product differentiation. Difference is in the fact that in the product differentiation there is no significant change of performance, or cost of materials or components on which product is made of. Or, to be more precise, in the differentiation of the products there is only minor change in technical or aesthetic change in the product.

4. MOTIVE FOR DEVELOPMENT OF THE NEW PRODUCT

There are numerous motives for development of the new product. Most often these motives are strategic in nature, which can provide certain benefits to the company:
- Source of competitive advantage,
- Possibility for improvement or change of strategic course of the company,
- Improvement of corporative image,
- Return of investment and capitalization of results of research and development,
- Improvement of marketing/brand,
- Positive influence on human resource.

It is crucial to emphasise what are key performance elements for development of certain product attributes:
- Design (design and construction of the product),
- Reliability (projection of lifetime of product),
- Quality (components and product),
- Flexibility (adaptiveness and components),
- Simplicity of use,
- Functionality ,
- Price,
- Technical-technological performances.

Based on mentioned above, new products can be classified as:
- Products new to the world (new products for both company and the market),
- New product lines (products new to the company, but not new to the market),
- Addition to new lines (subtype of new product line),
- Development of the product (replacement of existing product with new one),
- Cost reduction (cutting production costs),
- Repositioning (new use of existing product).

5. INNOVATION PROCESS MODELS

Mostly used classification of innovation process models is one proposed by Troth (Table 1). [12]

Table 1: Models of innovation process

Period	Model	Characteristics
1950/60	Technology push	Simple linear-sequence process. R&D are emphasised, market is accepting results from R&D
1970	Market pull	Simple linear-sequence process; market is source of directing of R&D; R&D has reactive role
1980	Coupling model	Integration of R&D and marketing is emphasised
1980/90	Interactive model	Combination of push and pull model
2000	Network model	Knowledge and external integration is emphasised

This is general classification, based on technology development (technology push), or customer related (market pull).

Process innovation models are also classified as:
- Linear-sequence models (phases of innovation process are following each other),
- Simultaneous models (sequence models adjusted to stochastic surrounding),
- Flexible models (adjusted to surrounding, special demands, etc.),
- Integrative models (connecting with surrounding through company strategic development and creation of reversible connection to phases of innovation process),
- Model of innovation diamond (model of support of management to innovation of product),
- Stage-Gate model,
- Model of open innovations.

In order that innovation process can start, it is necessary to generate idea, what and on which way should be developed in order that it can be considered as innovation.

6. IDEA GENERATION

There are lot of different methods and techniques for idea generation. Some of mostly used [3]:
- Creative model for idea generation,
- Model of life cycle,
- Methods of portfolio analyses,
- Predictive methods,
- Methods of strategic evaluation and alternative selection,
- Information support to innovation management.

One of the most used methods is creative model for idea generation. There are lot of techniques which are connected to this subject, but mostly used are [3]:

- Brainstorming (suggesting numerous ideas by expert teams),
- Mind mapping (graphical-symbolic representation of basic concepts),
- Lateral thinking (using non-conventional way of thinking, which would be ignored by everyday logical thinking),
- Inventive problem solving (use of generic solution and external information, supported by creative thinking).

7. RISK IN INNOVATION PROJECTS

Risk management is one of the most important aspects of project management. Innovation, by its nature, can be described as stochastic event, since results are not exact. Risk is connected to possibility and it can be defined as: "possibility that some achievement or project suffers failure and consequences which are outcome of this failure" [13].

Some other authors define risk as: "state in which exist possibility of negative deviation from wanted outcome, which one expects". It can be said that in order that risk can be defined some prerequisite have to be fulfilled: that project has to exist, that it can cause economic damage, it has to be independent and it has to have elements of possibility.

From the definition of the risk, two main elements are derived:

- Possibility of unwanted event happening,
- Consequence of that unwanted event on complete project, financial aspect, labour, property and surrounding.

Risk can be divided on [14]:

1. Financial and non-financial risk – in the field of financial risk exist possibility of financial loss appearance, while in non-financial this possibility is excluded.
2. Static and Dynamic risk – dynamic risk occurs because of change in economic relations, while static risk can be defined as possibility of loss, even if there are no economic changes.
3. Fundamental and special risks – fundamental risk is defined as possibility of loss which can't be divided by it's nature, while special risks are possibility of loss occurrence which are consequences of certain single events.
4. Pure and speculative risk – speculative risk is possibility of gain or loss in the economic transactions, while pure risk is possibility of loss without possibility to gain.

Innovation risks are including following risks [3]:

- Risks in technical sector,
- Risks in marketing sector,
- Risks of interception,
- Risks of time consumption dynamics,
- Risks of obsolescence,
- Risks connected to subjective factors.

In the scope of innovation projects, risks are usually connected to all factors which are important for innovation process. This methodology is connected through analyses of certain phases:

- Determination of risk factors,
- Evaluation of risk factors based on possibility,
- Combination – possible outcomes and possibility of their realization.

8. DEFINING SCOPE OF THE PROJECT – CASE STUDY

Investors request was to modernize old manually driven crane which is used to lift up and down lock on damn on hydro plant Matka in Skopje, FYRM (Figure 1). Modernisation is consisted of replacing old crane trolley with new one, electrically driven. New trolley has following technical characteristics: (Table 2)

Table 2: Main technical characteristics of equipment

Main technical characteristics	Values
Crane location	Mechanical
Nominal value	8 t
Speeds (high/low)	6.0 / 1.0 m/min
Crane rail height from	5 550 mm
Span of the crane	5 410 mm
Length of rails on the crane	5 800 mm
Lifting height	36.0 m
Voltage	400 V, 50 Hz
Control voltage	48 V, 50 Hz
IP Class of electrical	IP 55
Supply	Festoon system
Movement of trolley	Electrical
Working temperature	-5/+40 °C
Maximal humidity	80%
Handling device	Hook with pulley

Problem is that trolley with such characteristics does not exist in company product portfolio, so new innovative solution has to be made. By solving this technical problem company can achieve strategic advantage in this project over the competitors.

Figure 1: Picture of old crane trolley

9. INNOVATION ANALYSES

According to existing company product portfolio and innovation classification and nature of innovation this innovation can be considered as incremental innovation. Crane trolleys exist in company product portfolio, but they don't fit to required technical description which was part of investor demand.

According to type of innovation, this innovation can be considered as product innovation. Motive for innovation of the product is defining market niche, since there is not even one competitor that can offer such product, since they don't have it in their product portfolio. There is also one more strategic advantage, since competitors don't have experience and technical capacity to develop custom product which is needed in this project. According to mentioned above it can be concluded that main reason for new product development is strategic goal of the company – getting competitive advantage.

Essence of innovation is innovation of product performance. Existing crane trolley has to be completely re-engineered, new design has to be made with completely new superstructure construction. Main limitation in design is fact that functionality of the trolley has to remain the same.

According to classification of categories of development of new products, innovation is widening existing lines, or it can be said that it is subtype of existing product line (crane trolley).

If innovation process model is analysed, it can be said that it is adapted market pull model, since in the case of innovation of crane trolley, marketing department is not included in the process (Figure 2).

Figure 2: Addapted market-pull model

Stage Gate model was applied in order to create innovative product (Figure 3).

Based on the market demand (investor demand) technical description of the problem was sent to the company commercial department. After preliminary analyses, it was concluded that there is no standard product in company production portfolio, which can be used to satisfy market demand. Also, additional analyses was conduced, if it is possible to do minor changes to the one of the existing products in order to get adjusted product. It was concluded that there isn't such product which can be improved in that way that it can satisfy all technical demands. Final conclusion was made that it is necessary to develop new product with demanded technical characteristics.

After that business case was analysed. In the business case was stated that there is the need for new product in the situation in which competition doesn't have similar product or has potentials to develop it. It was estimated that it can be considered as monopolistic situation, in which is possible to ask for higher price in order to cover research and development costs, along with cost of developing complete product documentation and product certification and in the end to bring required profit margin.

After analyses of business case, decision is made that company has to go into new product development.

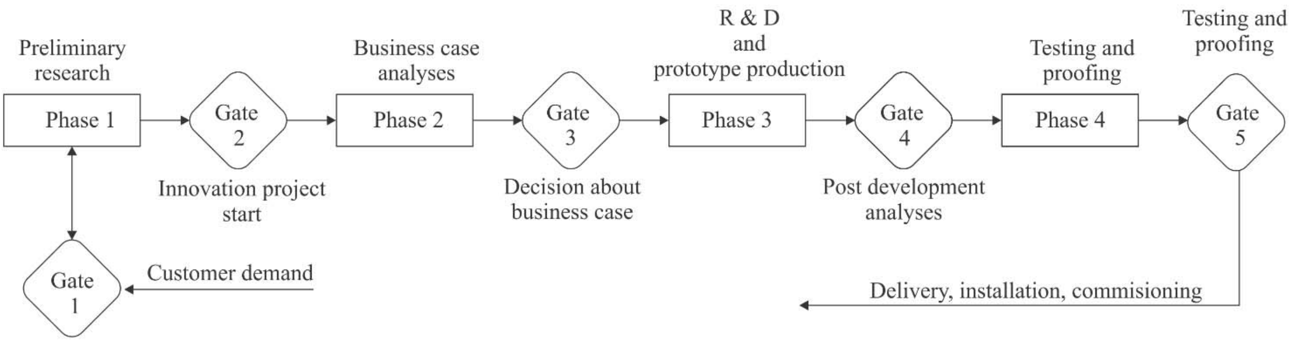

Figure 3: Stage gate diagram of innovation process

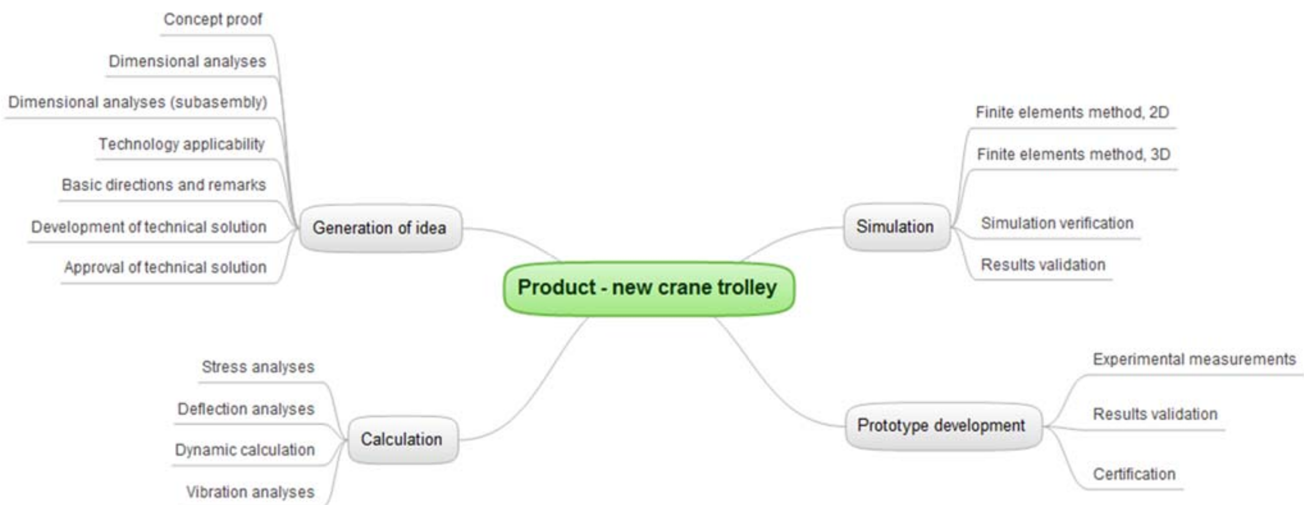

Figure 4: Mind map of idea generation

In the next phase, technical demand was brought to R&D sector in the company. R&D sector made decision based on that for generating idea concept, some of creative methods for idea generation must be used. Method which was used was mind mapping, since it provides fast visual concept of production of new crane trolley (Figure 4).

Process of innovation creation is divided in four basic phases. First phase is development of new idea. Base for development of idea is strongly connected to systematic approach to engineering, or to system engineering.

System engineering has its roots in system approaches to real life problems. According to mentioned fact, four phases of system engineering are defined and they represent activities in system studying.

Phases of system engineering:
- System analyses,
- System synthesis – system design,
- Implementation of the system,
- System operation.

Idea is created in the first two phases of system engineering. System approach means general analyses of physical subject, identification of causes which affect the system and consequences to the subject. After that, boundaries of the system have to be defined, aim of the system work and definition of its required performance.

Next step is anticipation of future system surrounding and formulation of mathematical model (or simulation model), which is used for system operation analyses. On the picture nr. 4, those two phases are given separately, as calculation phase and simulation phase. After this phase, subsystems end elements are defined, as constructive parts of the system.

In the next step analyses of the results is conduced. After that elements of optimised system are defined (both hardware and software) and performance, reliability and some other tests are conduced.

Last step is production of the prototype and its final evaluation. If system doesn't satisfy optimization conditions, it has to be optimised again in order to satisfy initial criteria.

One of the most important analyse are risk analyses and SWAT analysis (Table 3 and Table 4).

Table 3: Innovation risk analyses

	Elements of RBS							Risk evaluation by phases	
Work Breakdown Structure		Innovation team	Budget	Project team	Project management	Development process	Project organization	ΣR	Rank of phases according to risk
	Preliminary research	R=5	R=5	R=5				15	5
	Business case analyses		R=10		R=6			16	4
	Research and development and prototype production	R=5		R=10		R=15	R=8	38	1
	Test and tryouts		R=10	R=7		R=8		25	3
	Delivery, installation and starting			R=8	R=7		R=12	27	2
	ΣR	10	25	30	15	23	20		
	Rank of risk sources	6	2	1	5	3	4		

Table 4: SWOT Analysis

Strengths Strategic position Engineering team Experience Business capacity Production capacity	**W**eaknesses Quick decision making Low analytic High risk taking
Opportunities Special solution development Forming of modular solution which can be used in different future projects Project documentation coordination with different legislation in surrounding countries	**T**hreats Time needed to complete projects Too many employees engaged in the project Standards in FYRM in vertical transport Additional work demanded by investor

Based on SWOT analysis it can be concluded that innovation project of new crane trolley provides excellent strategic position, which derives good sales margin, which is necessary for such special project. This strategic position is achieved through good engineering team which has necessary knowledge and experience. Strength in SWOT analysis is also described by business and production capacity of the company.

Weaknesses are described by fact that essential decisions are made individually (quickly and usually without all necessary analyses conduced). In the field of opportunities is evident that special solution is developed, which is modular and can be used in different projects in the future. Also, opportunity is in forming project documentation which can be developed according to different legislation procedures in different countries. This is important for developing similar projects in surrounding countries, which are also interesting for company future development. One of the most important potential threats is time consumption for development of the new product. Development of new product acquires significant time consumption from employees included in it, so there is possibility that they will fail to finish their everyday work. Also one of the threats is different standards for vertical transport which are applied in FYRM. Also, one of the threats is if investor wants to do additional work, which would lead to additional time and work time consumption.

According to dimensional analyses mathematical model was developed, which is used for further engineering calculations. Same model was later used as base model for FEA analyses. (Figure 5)

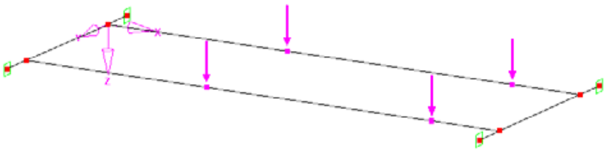

Figure 5: Base for mathematical model of crane trolley

Design of the crane trolley was made based on static and dynamic calculations and dimensional analyses of crane trolley. Such design is presented on Figure 6 in the form of generated 3D model.

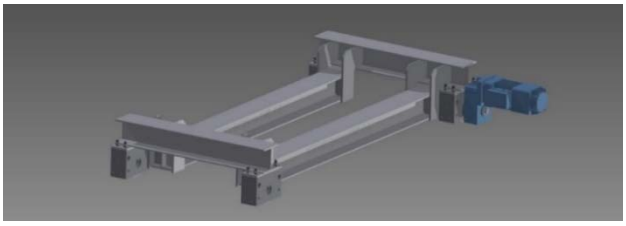

Figure 6: Crane trolley 3d model

According to FEM regulation load of the crane trolley was applied and entering parameters for static and dynamic simulation were introduced. (Figure 7)

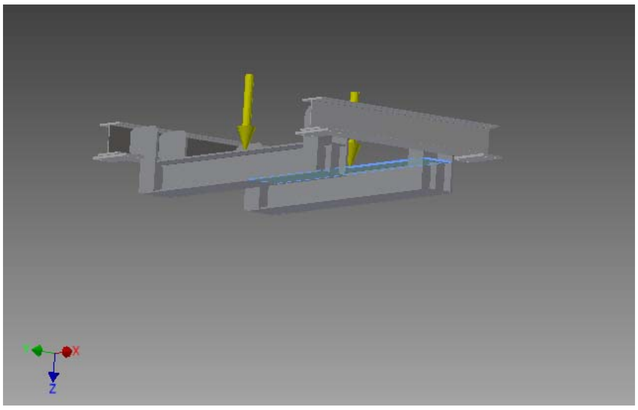

Figure 7: Simulation model

Simulation was started and all main design criteria for steel superstructure were checked (stress, deflection, buckling, torsion buckling, vibrations, etc.). (Figures 8 and 9).

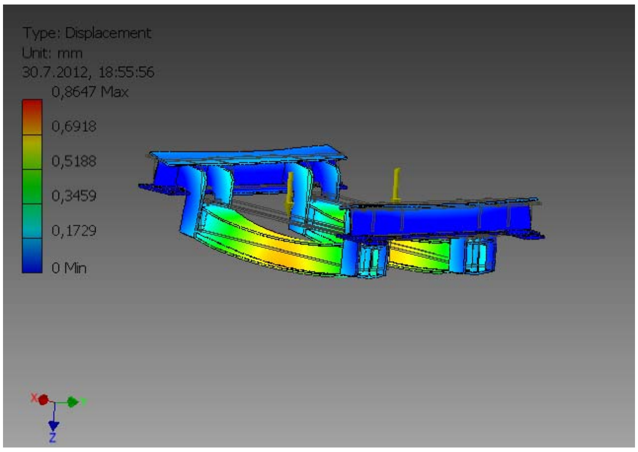

Figure 8: Displecement of the model

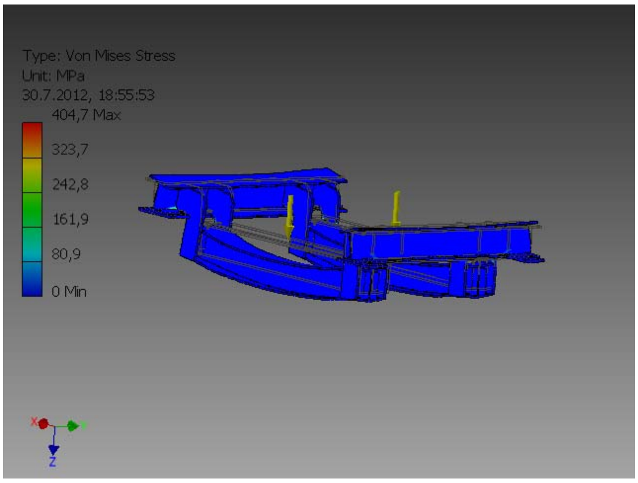

Figure 9: Equivalent stress

Based on results from simulation, prototype of crane trolley was made. Verification of the simulation is done by experimental measurement on prototype.

Table 5: Equipment characteristics

Producer	Hottinger Baldwin Messtechnik, Germany
Type of measurement tape	6/120 K-LY41
Nominal resistance	120 Ω ± 0.35%
Measurement base	6 mm
Maximum measuring voltage	9 V
K factor	2.02 ±1%
Longitudinal sensitivity	-0.1%
Temperature adjustment for steel	α=10.8·10^{-6} 1/°C

Signal change of relative deformation of measurement tapes is processed in measurement-acquisition device Spider8 (producer HBM, Table 5), which is connected to notebook computer. For data acquisition and recording is used software package Catman Express.

Schematic representation of measurement chain is on the Figure 10. Signals are recorded with frequency of 200 samples in second, without filtration.

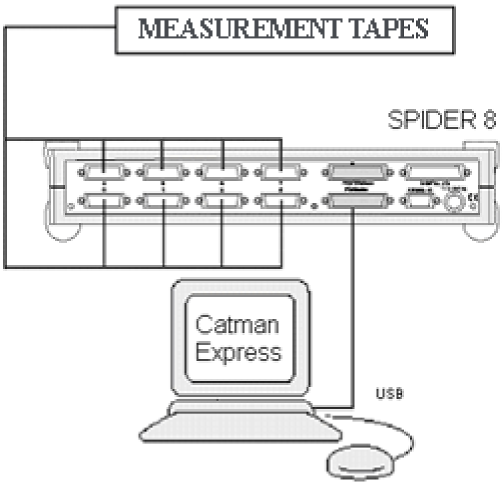

Figure 10: Measurement results of stress on the main girder of the crane trolley

After finished measurement was obtained that deviates from simulation results were less than 0.5%, which is bellow level of statistical error of 5%. According to measurements, validation of the simulation results was made and proposed designed was proved (Figure 11).

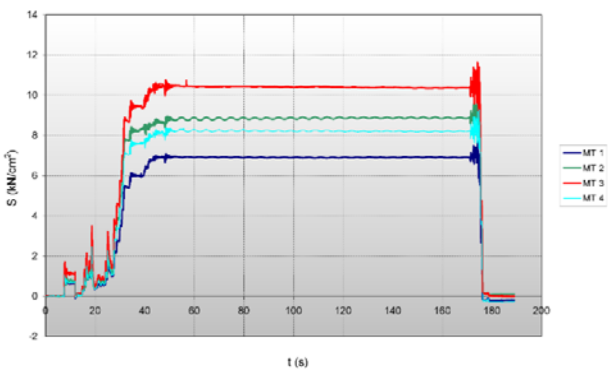

Figure 11: Measurement results of stress on the main girder of the crane trolley

Based on calculation results, results from simulation and experimental research, company applied for CE certification of the product. Final stage in Stage Gate model was delivery and system commissioning (Figure 12). After starting of the system analyses of all system parameters was conduced and it was concluded that new product completely satisfied, by the design and functionality all criteria.

Figure 12: Installation of the equipment

10. CONCLUSION

In the paper was explained innovative approach for development of the new product by using adapted Market-pull innovation model. Basic need for development of new product was market need, which was through R&D department produced as final product.

Classified by nature of the innovation, crane trolley can be fitted in the class of incremental innovation and considering type of innovation it can be fitted in the class of product innovation.

Motive for product development, as concluded is source of competitive advantage, because in existing product pallet such crane trolley doesn't exist. The same situation is with competitors, which alslo dont have such product but they are not in the position to develop it.

For idea generation mind map is used in order to define all steps in product development.

Complete innovation is described by Stage Gate model, which is used later for complete project.

Methodology from system enginieering is used for new product development. Based on proposed methodolgy problem from the real world was transfered to the level of mathematical model, which was used as base for calculation and simulation.

Results from calculation were analysed and trolley structure was dimensioned. Dimensioned model was used as base model for simulation which was used for testing of conceptual structure solution. Based on results from simulation prototype was made which was again used for gathering experimental results from stress analyses as validation of the simulation results.

New product was produced based on proposed methodology for innovation projects. Product was succesfully tested, comissioned and certified, which profeed mentioned methodology used for new product development.

REFERENCES

[1] http://www.constitution.org/mac/prince00.htm

[2] http://www.authorama.com/essays-of-francis-bacon-25.html

[3] B. Stošić, "Menadžment inovacija – inovacioni projekti, modeli i metodi", FON, Beograd (Srbija), (2013)

[4] J. A. Schumpeter, "Capitalism, Socialism, and Democracy", Routledge, New York (USA), (1943)

[5] J.W. Abernathy and J.M. Utterback, "Patterns of industrial innovation", Technology Review, Vol. 80(7), pp. 40-47, (1978)

[6] P.F. Drucker, "Innovation and Entrepreneurship: Practice and Principles", Elsevier Ltd., Oxford (England), (1985)

[7] M.E. Porter, “Competitive strategy”, The Free Press, New York, 1980

[8] H. Nowotny, "The Quest for Innovation and Cultures of Technology, Cultures of Technology and the Quest for Innovation", Oxford (New York) pp. 1-38, (2006)

[9] H. Greely, et al., "Towards Responsible Use of Cognitive Enhancing Drugs", Healthy Nature, Vol. 465, pp. 702-705, (2008)

[10] "Zakon o inovacionoj delatnosti", Službeni glasnik RS, br. 110/2005 i 18/2010.

[11] "Oslo Manual: Guidlines for Collecting and Interpreting Innovation Data - 3rd Edition", Joint Publication, OECD, Eurostat, (2005)

[12] P. Trott, "Innovation Management and New Product Development", Prentice Hall, London (England), (2008)

[13] E. Vaughan and T. Vaughan, "Osnovi osiguranja – Upravljanje rizicima", MATE, Zagreb (Hrvatska), (1995)

[14] L. Barjaktarović, "Upravljanje rizikom", Singidunum, Beograd (Srbija), (2009)

Simplified Life Cycle Assessment of a Conveyor Belting

Miloš Đorđević[1*], Nenad Zrnić[1], Boris Jerman[2]
[1]Faculty of Mechanical Engineering/Department of Material Handling, Constructions and Logistics, University of Belgrade
[2] Faculty of Mechanical Engineering/Department of Engineering Design and Transportation Systems, University of Ljubljana, Slovenia

This paper deals with the simplified life cycle assessment (LCA) of a bucket wheel excavator (BWE) conveyor belting. Belting is the most important component of a belt conveyor. Simplified LCA was conducted with the Ecodesign Assistant (EA) and the Ecodesign PILOT (EP) software tools. Conveyor belting was recognised as ABE hybrid type product, whose 'raw material', 'manufacture' and 'end of life' stages are significant in its life cycle. After the second iteration, the conveyor belting was recognised as a 'raw material' and 'manufacture' intensive product. Further analysis considered strategies for possible product improvement suggested by the EP tool.

This particular analysis of conveyor belting is part of a complete LCA of the BWE belt conveyor which should provide a basis for establishment of the methodology for conducting LCA studies of a BWE or similar types of belt conveyors.

Keywords: Simplified Life Cycle Assessment, Ecodesign Assistant, and Conveyor Belting

1. INTRODUCTION

Belting is the most vital component of the belt conveyor and an element characterised by the lowest life. It participates with 50-60% in total investment costs of a belt conveyor [1]. This particular belting is the main component of a belt conveyor which is constituent element of the BWE SchRs 1201. Since BWEs consume large amounts of electric energy, and the belt conveyor is a part of this large system, any contribution to its energy efficiency and minimisation of energy consumption leads to significant energy and cost savings and towards sustainability.

For terms such as life cycle, LCA and product types please refer to [2, 3], and for terms such as sustainability, sustainable development, energy efficiency and energy saving to [2, 4].

The analysis presented herein was conducted through several iterations using EA and EP software [5, 6]. Initial results had shown that conveyor belting was an ABE hybrid type product. After refining, the second iteration led to an AB hybrid type product, which is ‘raw material’ and ‘manufacture’ intensive. Improvement strategies recommended by EP in first and second iteration were almost identical. The third iteration comprised more detailed energy input calculation during 'manufacturing' stage. However, product type and recommended improvement strategies remained as they were in the second iteration.

2. DESCRIPTION OF THE PRODUCT

The product analysed in this paper was the BWE SchRs 1201 conveyor belting type EP 500/3. The belting properties must ensure sufficient tensile strength and adequate flexibility in both longitudinal and transverse directions as well as sufficient life. Typical conveyor belting is a multilayer flat composite [1]. Thus, it is consisted of top and bottom rubber covers and rims and carcass (core). This particular belting carcass is consisted of 3 reinforcing textile plies made of polyester (warp yarns) and polyamide (weft yarns), see Figure 1. Rubber cover grade is N (natural rubber). Belt length is 16 m, with belt width of 1.6 m and troughing angle of α=30°. Belt speed is v=3.9 m/s.

Estimated conveyor belting life was 5.5 years.

Determined functional unit of the product was transportation of 3465 m^3/h of brown coal.

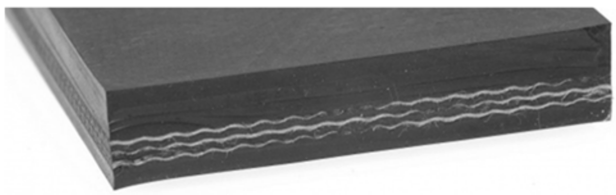

Figure 1: EP 500/3 conveyor belting cross section

3. THE FIRST ITERATION OF ANALYSIS WITH ECODESIGN ASSISTANT

3.1. Raw Material Stage

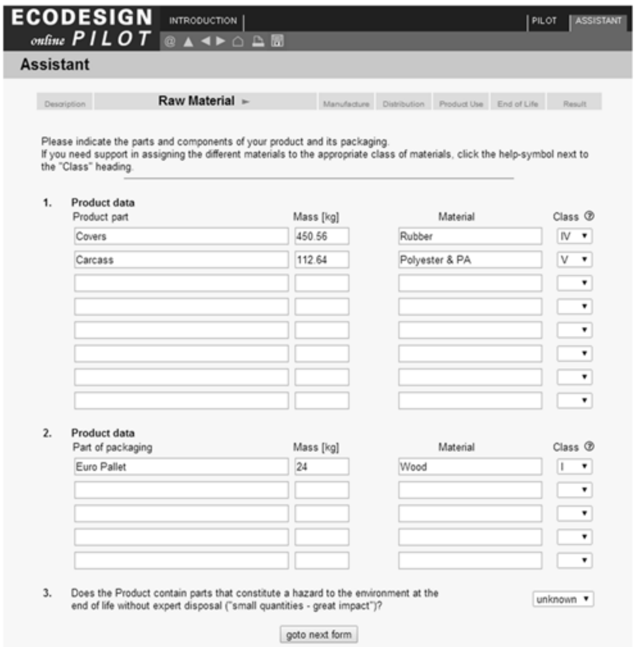

Figure 2: Raw material stage form

*Corresponding author: Kraljice Marije 16, 11000 Beograd 35, mddjordjevic@mas.bg.ac.rs

For purpose of the analysis with EA, the product was divided into following structural parts:

- covers,
- carcass, Figure 2.

Total belting weight was 563.2 kg.

Material classes for each part of the product are determined in correlation with EA material class table [6]. At this point it was assumed that returnable euro pallet was used for packaging.

3.2. Manufacturing Stage

The manufacturing process differs for various types of beltings, but it is commonly comprised of:

- making of a basic rubber compound,
- making of cover sheets from raw rubber batches by calendering or extrusion (injection moulding),
- confectioning the rubber sheets with tensile member (adding reinforcing plies),
- curing in a press - vulcanization.

Making of a basic rubber compound is achieved by mixing rubber with carbon black (a form of paracrystalline carbon that has a high surface-area-to-volume ratio), plasticizers, chemicals and vulcanizing agents in mixing unit [7].

During the calendering process raw rubber batches are run through the rollers, while high temperature and pressure are applied as well. Since the injection moulding consumes more energy than calendering it was considered here as manufacturing process for raw rubber cover sheets.

Confectioning the rubber sheets with tensile member is a repeatable process dependant on a number of reinforcing plies. During this process, rubber sheets are run through the rollers alongside with reinforcing plies. Confectioning process is performed on the same machines as in calendering process [7].

Vulcanization involves the curing process in a press at temperature of 150 °C and pressure of 1.2 MPa (for EP belting) [8].

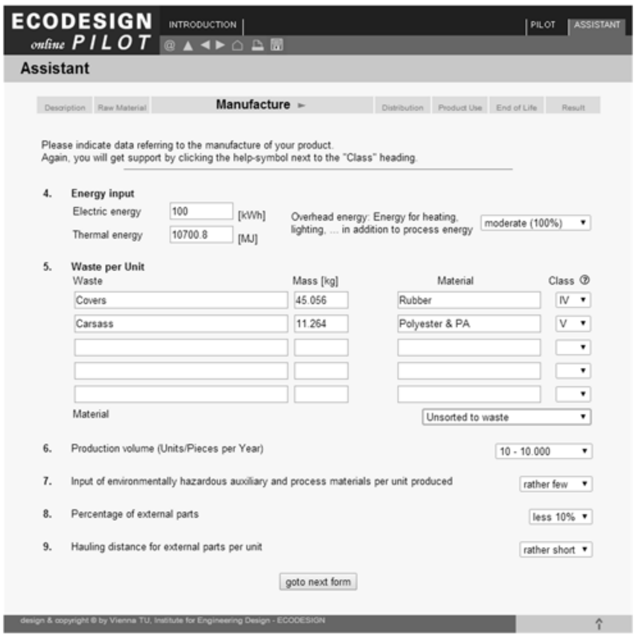

Figure 3: Manufacturing stage form

In absence of specification data for all of the machines in this production chain, the calculation of consumed energy in manufacturing stage was limited to a calculated energy needed for injection moulding of rubber sheets and vulcanization of 16 m of belting, Figure 3.

Calculated thermal energy input was 10700.8 MJ in accordance with specific energy consumption (SEC) of hydraulic injection moulding machine of 19.0 MJ/kg [9] and previously determined total weight of the belting of 563.2 kg.

The average electric energy input for vulcanizing 16 m of belting was aproximately 100 kWh in accordance with vulcanizing machine power requirements which were 30 kW and its production rate of 0.04-4.7 m/min [8, 10].

Waste material per unit was estimated to be 10% of the part's mass and it was dumped unsorted to waste. It was summarised for all rubber parts and presented with a single value. This issue will be improved during the second iteration.

The amount of energy required for heating and lighting was estimated as moderate. The estimated production volume was 10-10000 units per year. Percentage of external parts was 'less 10%'. Hauling distance per unit was determined as 'rather short'. Input of environmentally hazardous auxiliary and process materials per unit produced was assumed to be 'rather few'.

3.3. Distribution Stage

Since the production facility is situated close to the place of product utilization, the average transportation distance for product distribution was estimated to be 20 km. The product was transported by truck. Euro pallet was recognized as returnable packaging.

3.4. Product Use Stage

Electrical motor is the only component of a belt conveyor which consumes electric energy. Therefore belting does not need any material or energy input per use. Calculated use frequency of belting was 325 uses per year. The only thing that could be discussed here is possible material spillage as a waste material per use. That issue was not considered here.

3.5. End of Life Stage

Figure 4: End of life stage form

The disposal of different parts of the product has been considered at the 'end of life' stage. Here, it has been assumed that no parts will be reused, reconditioned or recycled. This is the worst case scenario. Only euro pallet was recognized as returnable packaging intended for reuse, see Figure 4.

3.6. Result

Conducted analysis resulted in an ABE hybrid type product, see Figure 5. 'raw material', 'manufacture' and 'end of life' stages are significant.

Figure 5: Result of the first iteration

Four main improvement strategies were suggested:

- S2 – Reducing material inputs,
- S3 – Reducing energy consumption in production process,
- S5 – Avoiding waste in the production process,
- S19 – Recycling of materials,

and 10 secondary improvement strategies:

- S1 – Selecting the right materials,
- S4 – Optimizing type and amount of process materials,
- S6 – Ecological procurement of external components,
- S9 – Optimizing product use,
- S10 – Optimizing product functionality,
- S11 – Increasing product durability,
- S15 – Improving maintenance,
- S16 – Improving reparability,
- S17 – Improving disassembly,
- S18 – Reuse of product parts.

Each one of the listed improvement strategies is followed by adequate checklists of the EP.

4. THE SECOND ITERATION OF ANALYSIS WITH ECODESIGN ASSISTANT

Most of the forms in the second iteration are identical to forms from the first one. Only the forms that distinguish from the first iteration will be presented here.

4.1. Raw Material Stage

Belting is usually wound on a wooden core and wrapped with polypropylene strips and placed on a euro pallet. Thus, a wooden core was added as a part of packaging in the second iteration of the analysis, see Figure 6. Core diameter was 250 mm with 110 mm square hole and length equal to belt width (1600 mm). The wood density is approximately 500 kg/m^3. Polypropylene strips were neglected.

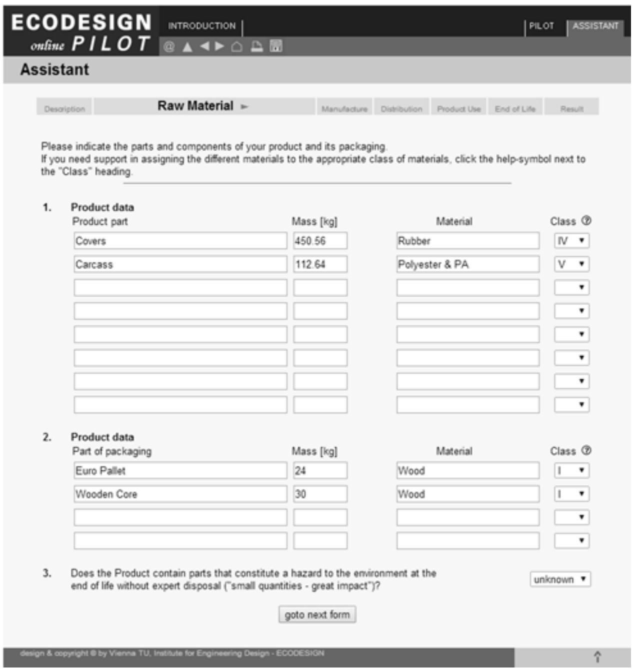

Figure 6: Raw material form for the second iteration

4.2. Manufacturing Stage

Compared to the first iteration waste material is being partially recycled here.

4.3. End of Life Stage

The conveyor beltings are the second largest rubber waste problem after the used tyres. Previously, disposal to landfill was presumed. Instead of dumping, the rubber conveyor belting can be reconditioned. Thus, the energy and resources needed for virgin (primary) rubber production could be saved. Conveyor belting reconditioning involves removal of a worn belting surface with special buffing machine and then re-application of the new rubber top and bottom covers followed by the re-vulcanization of the entire belting. According to this procedure, the scraped worn rubber is disposed to landfill or it could be recycled, while the belting carcass is being reused, see fig 7.

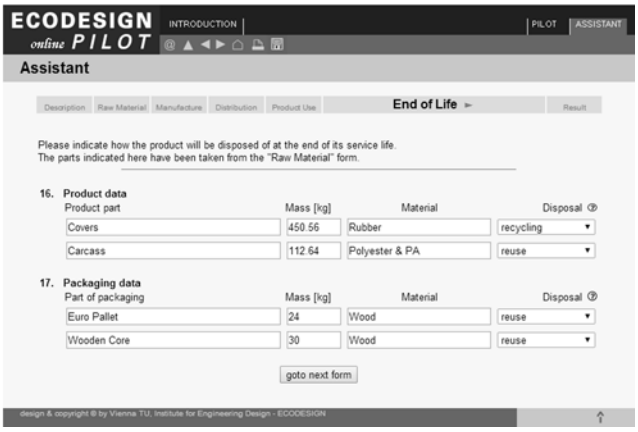

Figure 7: End of life stage form for the second iteration

4.4. Result of the Second Iteration

Because of the changes made in ‘end of life’ stage, the second iteration of the analysis resulted in an AB hybrid type product. The differences between the recommended improvement strategies in the second iteration compared to the first one were the absence of one main improvement strategy – S19, while the improvement strategy S5 became the secondary improvement strategy. However, the improvement strategy - S19 was already covered by the changes made in the ‘end of life’ stage referred to reconditioning of the belting, see Figure 8.

Figure 8: Result of the second iteration

5. THE THIRD ITERATION OF ANALYSIS WITH ECODESIGN ASSISTANT

Further analysis involved a more detailed calculation of thermal and electric energy consumption during the ‘manufacture’ stage. The additional calculation comprised the mixing mill and the confectioning process power requirements. As already stated, the confectioning process is performed on calendering machines.

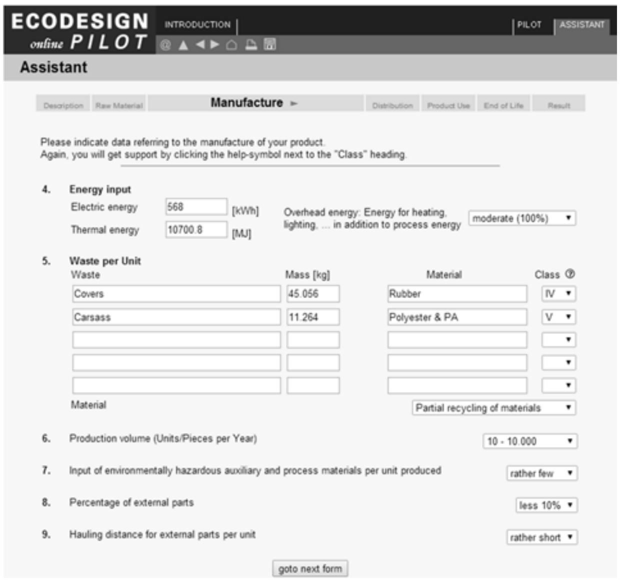

Figure 9: Manufacturing stage form for the third iteration

Appropriate mixing mill models for the production of 450.56 kg of rubber compound for 16 m of belting were SHDX-MM 22 "X60" and SHDX-MM 26 "X84" [11]. Batch capacity range for the first model was 90-110 kg and 160-180 kg for the second model. Mixing time per batch was 45 min. Thus, the average energy consumption for making the basic rubber compound was aproximately 450 kWh.

Since this particular belting has 3 reinforcing plies, the confectioning process has to be repeated 3 times. According to [8], the energy consumption range needed for the calendering 16 m long belting was 0.7-16.4 kWh. The average value of 6 kWh multiplied by 3 cycles resulted in the energy consumption of 18 kWh.

According to the previous calculations, the electric energy consumption has increased by 468 kWh. Therefore, the total electric energy consumption has risen to 568 kWh.

5.1. Result for the Third Iteration

Although the total electric energy consumption was increased, the ‘result’ form remained identical as it was in the second iteration. The belting product type as well as the recommended improvement strategies remained unchanged.

6. ANALYSIS WITH ECODESIGN PILOT

The improvement strategies provided by EA were further considered within EP. They are not presented in this paper entirely. Instead, they are discussed as tasks, measures and recommendations which are to be conducted in order to improve the product's functionality and energy efficiency, as well as environmental performance.

The final iteration resulted in two main strategies, see Figure 8. Since they have the highest priority, they will be considered first.

When it was considered if the product was made of recycled material, it has been concluded that it was not. This could be easily improved by specifying the use of a secondary rubber and carcass materials, Figure 10. On the other hand, the secondary rubber, polyester and polyamide do not have the same properties as virgin materials. Really recyclable material as a secondary material preserves the characteristics of a virgin material to a sufficient degree (if necessary by adding a new material). Therefore, the use of secondary materials in this case should be carefully considered before approval.

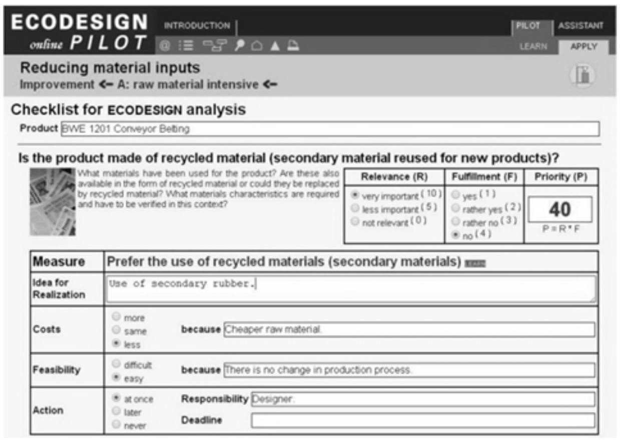

Figure 10: Highest priority task for the main improvement strategy S2

During the second iteration, the reconditioning of the belting has been taken into account. Recycling rate could be maximised by recycling scraped worn rubber (top and bottom cover). In that way there can be formed closed material cycle. The higher the recycling rate the greater the benefit for the environment and the higher economical efficiency of the overall process of reconditioning and/or recycling. Also, demand on resources and waste production can be reduced by using recycled materials.

Unfortunately, for proper functioning conveyor belting has to be a multilayer flat composite. Composite structure of the belting makes forming of closed material cycle difficult. Thus, composite structure of the belting is its main advantage and main disadvantage at the same time. Some improvements could be made by special design of beltings, but this is usually connected with much higher investment costs.

The use of toxic substances should be avoided during 'Manufacture' stage. Thus rubber compounds should not be made of oils containing polycyclic aromatic hydrocarbons (PAHs), and substances listed in Annex XIV of the Regulation No 1907/2006 (REACH) and listed in the Candidate List of substances of very high concern (SVHC) [12].

Although rubber cover material grade is N (natural rubber) and its environmental impact is minimal, it is desirable to examine different bio-polymers for possible application in the belting production. Particular attention should be paid to anti-friction properties and the belting surface quality in general.

Conveyor belting is extremely exposed to soiling and wear, which can cause very adverse effect on material transportation and conveyor functioning in general. Therefore, conveyors are usually equipped with plows and/or other belt cleaning devices. It is of great importance that these cleaning devices work properly, as well as they are adequately selected, which is a very delicate issue. If not, increased wear or even belting damage could occur. Besides belt cleaning devices, preventing material build-up forming could be accomplished by application of an adequate belting surface. Therefore, investigation of different materials with good wear and tear as well as sticky material repellent properties could be worth an effort. In order to identify the best materials for belting production, the investigation based on multi-criteria analysis should be applied [1].

Since belting is exposed to increased wear it could be labelled or equipped with some sort of indicators of remaining service life. This should be implemented alongside adequate maintenance concept. Common maintenance concepts are:

- Reactive or breakdown maintenance – 'run it till it breaks' concept,
- Preventive maintenance or time-based maintenance,
- Predictive maintenance or condition-based maintenance,
- Pro-active maintenance and
- Reliability-centered maintenance.

Maintenance costs are directly related to chosen maintenance concept [13]. An adequate maintenance concept should provide high level of reliability. Use of protection and belt tracking devices may contribute to increased reliability. The weak point of the belting is its splicing. Therefore, special attention should be paid to the belting splice and its realization.

Elastic properties of the coverings have no great impact on the flexibility (elasticity) of the belting. On the other hand, the number of reinforcing plies and their thickness has essential impact on the elasticity and thickness of the entire belting [1]. By achieving the adequate stiffness of the belting, the indentation rolling resistance as well as the flexure resistance of the belt could be minimised. Thus, a so-called energy saving belt could be produced. This kind of belting can save significant amounts of energy during its phase of utilization. Besides that, it could have significantly prolonged life because of the same reason.

Belting production procedures differ from one to another manufactures, but they are always similar and the difference in energy consumption in this stage depends mostly on the used machines. Speaking of energy efficiency, it could be improved by using state-of-the-art machines for each of the production processes. This increases the investment costs, but can result in reduced utilization costs on a long term base. Another way to achieve energy efficient manufacture is through constant monitoring and optimization of the process parameters by means of computerized process control.

When considering minimization of overall energy consumption of the production site, the analysis of energy flows and concomitant costs should be done. One possible approach to a reduction of the overall energy consumption consists in cascading the utilization of heat at different temperature levels; another one is using combined heat and power plants (CHP) for the generation of heat and electricity. By reusing the waste heat as process heat efficiency levels of more than 80% can be realized [6].

Waste in the production process could be avoided by closing the material cycle. It can be done through material separation and recycling during the production process. Reuse and recycling of rubber products, as well as recycling procedures are described in [2].

7. CONCLUSION

Particular issues considered within this paper were recycling and similar procedures, energy saving beltings, material build-up and wear reduction, investigation of possible application of new or different of type materials into production process, maintenance and protective devices, energy efficiency and possibilities for energy consumption reduction during the production stage.

Recycling and reconditioning issues could be solved by closing material cycles at the 'End of Life' and during production stage.

Certain improvement could be achieved by selecting or engineering the materials with superior characteristics regarding environmental performance, dirt repellence and wear resistance. Also material properties could ensure sufficient stiffness/flexibility of the belting and result in energy-saving belt.

Possible energy savings and energy efficiency improvements during the production stage were analysed. State-of-the-art machines, heat management and constant monitoring systems were proposed as a possible solution for this issue.

Analysis in EP has shown that energy and, consequently, cost savings, as well as environmental improvements, could be accomplished by conducting provided recommendations. Complete LCA analysis is needed to provide more precise data and better recommendations and solutions.

Further research will be focused on investigation of the different types of drive systems and accessories as well as on connecting [3], [4] and [14] with this paper and with each other. This should provide insight into environmental performance and other characteristics of complete belt conveyor system and serve as a basis for the complete LCA of a belt conveyor.

ACKNOWLEDGEMENTS

This work is a contribution to the Ministry of Education, Science and Technological Development of Republic of Serbia funded project TR 35006.

REFERENCES

[1] K. Czaplicka, “Eco-design of Non-metallic Layer Composites with Respect to Conveyor Belts”, Mater. Des., Vol. 24, pp. 111-120, (2003).

[2] N. Zrnić, M. Đorđević, “Dizajn i Ekologija: Održivi Razvoj Proizvoda”, Faculty of Mechanical Engineering, Belgrade (Serbia), (2012).

[3] M. Đorđević, N. Zrnić and M. Pantelić, “Simplified Life Cycle Assessment of a Return Belt Conveyor Idler“, Proceedings of 11th International Conference on Accomplishments in Electrical and Mechanical Engineering and Information Technology - DEMI 2013, Banja Luka (BiH), 30th May – 1st June 2013, pp. 201-206, (2013).

[4] N. Zrnić, M. Langerholc, B. Jerman, M. Đorđević, “Conveyor Design Optimization as the Provision of Sustainability”, Proceedings of the XX International Conference MHCL'12, Belgrade (Serbia), 3rd – 5th October 2012, pp. 107-112, (2012).

[5] W. Wimmer, R. Züst, “Ecodesign PILOT – Product Investigation, Learning and Optimization Tool for Sustainable Product Development”, Kluwer Academic Publishers, Dordrecht (The Netherlands), (2003).

[6] www.ecodesign.at

[7] http://www.conveyorbeltguide.com/

[8] http://chaoguangyue.en.alibaba.com

[9] A. Thiriez, T. Gutowski, “An Environmental Analysis of Injection Moulding”, Proceedings of the 2006 IEEE - International Symposium on Electronics and the Environment, San Francisco (USA), 8th-11th May 2006, pp. 1-7, (2006).

[10] http://www.alibaba.com/product-detail/Rubber-Conveyor-Belt-Vulcanizing-Press-Machine_612259302.html

[11] www.slachhydratecs.com/rubbermixingmill.html

[12] https://fttwolbrom.com.pl/offer/3/28

[13] M. Pantelić, Lj. Papić, J. Aronov, “Maintainability and Safety Engineering of Excavator Units”, The Research Center of Dependability and Quality Management DQM, Prijevor (Serbia), (2011).

[14] M. Đorđević, N. Zrnić, B. Jerman, “Simplified Life Cycle Assessment of Belt Conveyor Drive Pulley”, The Fifth International Conference "Transport And Logistics - TIL 2014", article in press.

Selection of the Basic Parameters of General Purpose Telescopic Belt Conveyor

Rodoljub Vujanac[1*], Nenad Miloradovic[1]
[1]Faculty of Engineering, University of Kragujevac, Kragujevac, Serbia

In this paper, a new type of telescopic conveyor is described. Importance of telescopic transport of materials and goods is underlined. General types of this kind of conveyors and their application are discussed. Mobile and fixed telescopic conveyors are described, as well as their optimal use in real exploitation conditions. The technical properties and classifications are given in the paper. The telescopic conveyor is standardized according to the rules in the area of use of the telescopic transports in the process of unloading and loading. By changing its position in all directions and variation of the length of a telescope, very efficient and flexible transport is achieved.

Based on project demands, a proposal for final design of telescopic conveyor for application in warehousing and logistics departments is given.

Keywords: telescopic belt conveyor, basic parameters, types

1. INTRODUCTION

The development of transport equipment has the goal of shortening the time of the transport of goods and to significantly reduce the participation of human labour. Modern transport equipment has developed to the extent that participation of human labour is reduced to coordinating the modern systems by means of command desks. However, it is not always possible to solve everything by means of modern transport systems [1, 2]. It is not often possible to avoid physical work. But even under those circumstances, progress has been made in the development of conveyors which shorten the time of transport and reduce the participation of human labour.

Namely, it is the one kind of conveyors which has to find its use in big distribution centres, factories, as well as in big railway junctions, which have a high frequency during loading and unloading of goods from the means of transport. These are telescopic conveyors. This type of conveyors is related to one-way transport, i.e. it is related to the loading and unloading where much time was spent because the operations were carried out by a man, with considerable energy consumptions. Introducing the pallet into the transport systems mitigated and shortened these aggravating factors in the transportation. However, it was not often necessary for a whole pallet to be transported from the distribution centre, but only a part of the pallet, so the problems of loading or unloading begin to occur because certain amount has to be brought, loaded, unloaded, carried away, etc [3, 4, 5].

For these reasons, and having the humanization of work in mind, an idea occurred about development of the telescopic conveyors.

2. PURPOSE OF TELESCOPIC CONVEYOR

The development of telescopic conveyors is derived from the work it is intended to perform - therefore the purpose of the telescopic conveyors. It is often necessary to carry out unloading, loading or reloading from one means of transport to another in a short period of time. That means that more transport workers and additional means of transport have to be engaged.

It is not often possible, so big losses caused by waiting occur, which cannot easily be reimbursed. These are the parameters needed for a conveyor which can solve this problem by flexibility, efficiency and reliability during the work process. Telescopic conveyor gives the optimal results in one-way transport by changing its position in all directions and by changing the length of a telescope. So, its purpose is to partly or completely replace human labour, to reduce the number of physical transport workers, to shorten time of loading, unloading or reloading of the goods from one means of transport to another. With its light construction and design solution, it produces very good results when handling it. Justification of such conveyor in the domestic market is obvious.

In our country, the presence of this type of conveyor is unknown. However, in western countries the absence of this kind of conveyor cannot be imagined even in small distribution centres. Having in mind that it is often necessary to carry out the operation of loading or unloading of bigger means of transport, the presence of this type of conveyor is becoming more and more justified.

Telescopic conveyors found use in all branches of industry which have the high frequency of entrance and exit of goods. The particular use is in distribution centres, railway junctions, in food industry, etc.

They easily and reliably fit into systems of other conveyors, so this characteristic only expands the range of application of telescopic conveyors.

For distribution centres with high frequency, more telescopic conveyors can be combined by type and kind.

The particular use of telescopic conveyors is envisaged in the transport of single pieces load, so called bulky packages, in the transport of barrels into trucks, in transport of sacks during the loading and unloading the truck, wagons and containers, in transport of bottles (for example, while loading the trucks with bottles of gas for household use), and so on.

*Corresponding author: Faculty of Engineering, University of Kragujevac, Sestre Janjic 6, Kragujevac, Serbia, vujanac@kg.ac.rs

3. DIVISION

Having in mind the purpose of the telescopic conveyors, they can be divided in the following groups:

- Fixed telescopic conveyors,
- Partially mobile telescopic conveyors,
- Mobile telescopic conveyors.

3.1. Fixed telescopic conveyors

When we speak about fixed telescopic conveyors, we refer to conveyors which do not have the possibility of changing the position relative to the floor. That is, they are fixed to the floor by feet of the telescopic conveyor, as given in Figure 1.

Figure 1: Fixed telescopic conveyor

3.2. Partially mobile telescopic conveyors

These conveyors are mobile only in one direction relative to the floor. That is, they move on rails fixed to the floor. These conveyors can serve more vehicles during which they move linearly in regard to the vehicles, Figure 2. The movement of the telescopic conveyor can be manual or motorized, depending on the needs of the purchaser.

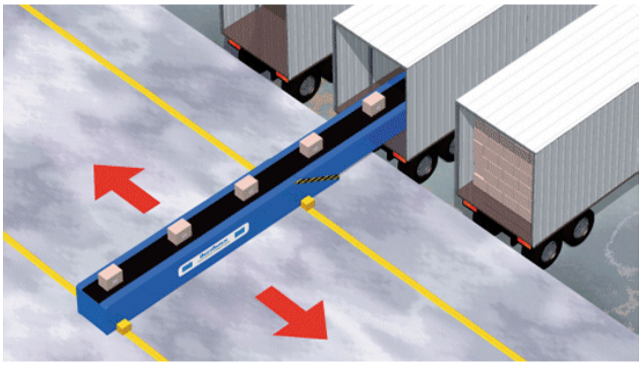

Figure 2: Partially mobile telescopic conveyor

3.3. Mobile telescopic conveyors

Figure 3: Mobile telescopic conveyor

These telescopic conveyors can move in all directions.

Namely, these are the conveyors on wheels which can move around their vertical axis, so they can be manually moved in all directions in relation to the vehicle – the means of transport, which is being loaded or unloaded, see Figure 3.

4. TYPES

Having considered the problems of the use of the telescopic conveyors, and in relation to the length of the means of transport, relation of the telescopic conveyor and transport vehicle, the following types can be determined:

- SINGLE,
- DUPLEX,
- TRIPLEX,
- QUADRIPLEX.

4.1. Single telescopic conveyors

Telescopic conveyor type SINGLE, Figure 4, contains one telescope, i.e. with one pull-out element (which means with one element for change of the length of the line). As their length of extraction is limited due to the stability, these conveyors are used for smaller transport vehicles. The extraction length is 3 meters maximum (Label LTT–1 in Table 1).

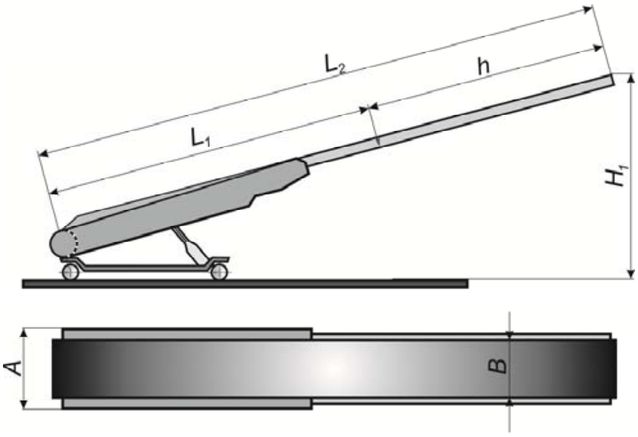

Figure 4: Single telescopic conveyor LTT–1

Considering that this type of telescopic conveyor can be used to serve transport vehicles of greater length, it is produced in one modification with a part that bends so that the telescopic part can follow the depth of the vehicle, Figure 5 (Label HTT–1 in Table 1).

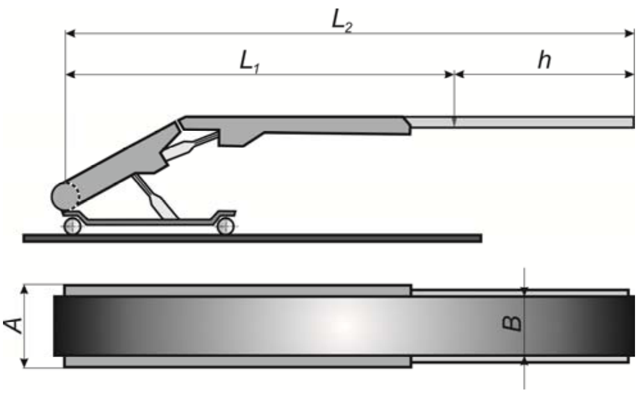

Figure 5: Single telescopic conveyor HTT–1

4.2. Duplex telescopic conveyors

Telescopic conveyor type DUPLEX, Figure 6 is equipped with two telescopes, i.e. two elements which can be continually extracted. Two elements replace the work length of the line (Label LTT–2 in Table 1).

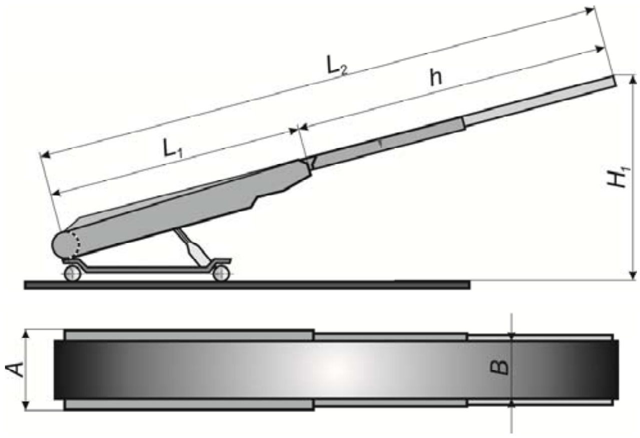

Figure 6: Duplex telescopic conveyor LTT–2

Considering that this type of telescopic conveyor can be used to serve transport vehicles of greater length, it is produced in one modification with a part that bends so that the telescopic part can follow the depth of the vehicle, Figure 7 (Label HTT–2 in Table 1).

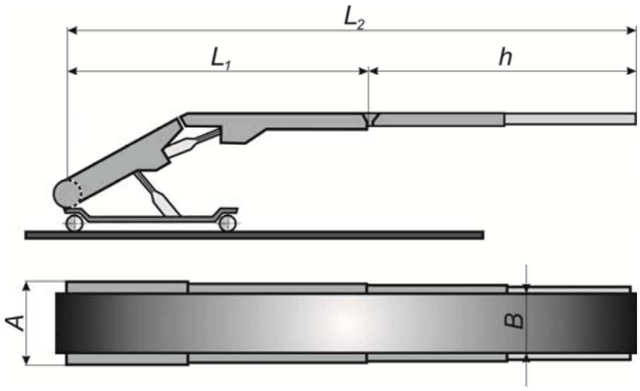

Figure 7: Duplex telescopic conveyor HTT –2

4.3. Triplex telescopic conveyors

Telescopic conveyor type TRIPLEX, Figure 8 is equipped with three telescopes, i.e. three elements which can be continually extracted. Three elements replace the work length of the line (Label LTT–3 in Table 1).

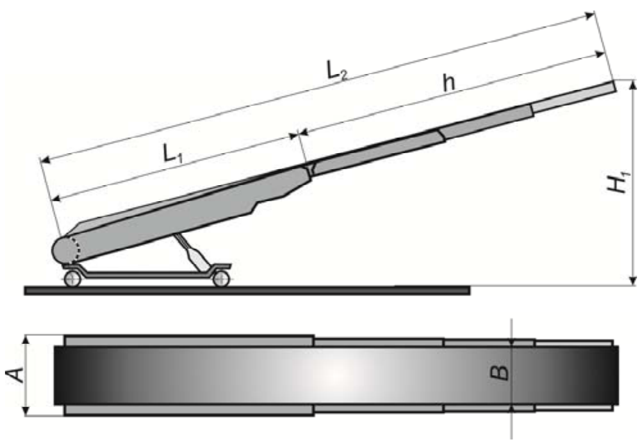

Figure 8: Triplex telescopic conveyor LTT–3

Considering that this type of telescopic conveyor can be used to serve transport vehicles of greater length, it is produced in one modification with a part that bends so that the telescopic part can follow the depth of the vehicle, Figure 9 (Label HTT–3 in Table 1).

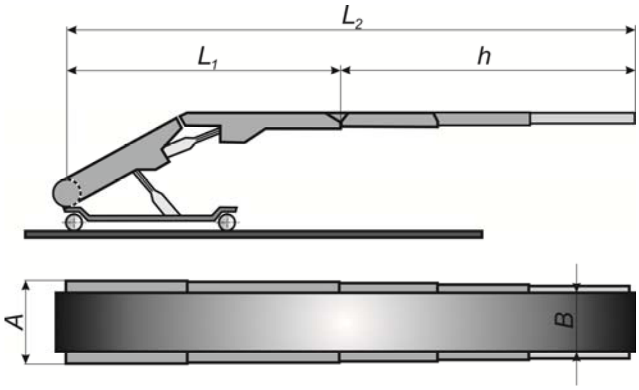

Figure 9: Triplex telescopic conveyor HTT –3

4.4. Quadriplex telescopic conveyors

Telescopic conveyor type QUADRIPLEX, Figure 10 is equipped with four telescopes, i.e. four elements which can be continually extracted. Four elements replace the work length of the line (Label LTT–4 in Table 1).

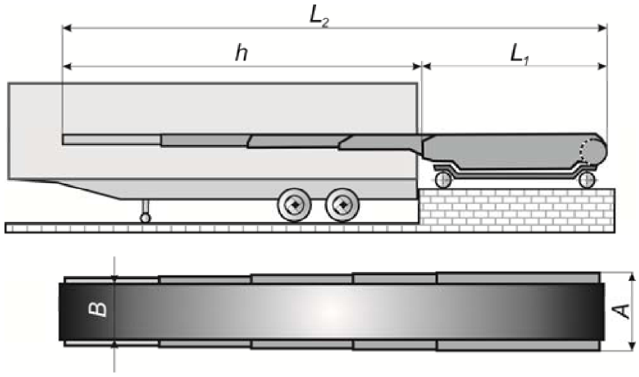

Figure 10: Quadriplex telescopic conveyor

5. TECHNICAL DESCRIPTION AND CHARACTERISTICS OF THE TELESCOPIC CONVEYORS

The trend of development of transport equipment goes towards the faster and more efficient transport. In the system of transporting goods, we can distinguish the following stages: loading, the stage of transport, and unloading.

We can have an effect on all stages so that the costs of transports are minimal. By various methods of linear programming, we reach optimal results which mathematically minimize the costs of transport. Here we dealt with means which should reduce the costs with their efficiency. By combining the technological solutions during the handling or monitoring of the technological process, conveyors, in global technological system, give the best results in terms of rationalization of the production, transport, as well as the cost of the entire technological process.

Telescopic conveyor, introduced as a new type of line conveyors, continues its development of improving the technological process in system of more efficient shipping of the final goods.

We will try to show, by presenting the technical description of the telescopic conveyor, the economic justification of the conveyor being present on our market. First we will discuss the mobility of the whole conveyor.

When we talked about the division of telescopic conveyors, we took into consideration the relation between the conveyor and the floor, so we divided them into three types. Fixed conveyors are strictly fixed to one spot for loading and unloading, i.e. their purpose is for very frequent distribution centres where the change of the place of the conveyor is not necessary.

Rail conveyors are fixed to the rails and can move only on rails. Control of the movement of the conveyor can be manual and motorized.

Mobile conveyors can move in all directions. The wheels are rotary so that the direction of the conveyor in relation to the vehicle can be easily changed. During working mode, the wheels are fixed.

The change in the height of the end of the telescopic conveyor is the second important characteristic which affects the efficiency of the conveyor. By changing the height of the end of the conveyor, we significantly influence the use of the energy of the transport worker because his work is reduced to approximately static stacking of the load on a vehicle.

The change in the length of the end of the telescopic conveyor is the third important characteristic which affects the efficiency of the transport. By changing the length, as well the height, the transport worker reduces his physic part of work to a minimum.

By describing the flexibility of the telescopic conveyor, we conclude that the transport worker’s physical part of work is reduced to minimum, which is very significant for the humanization of human labour.

Controlling the telescopic conveyors is very simple, easy and safe. Telescopic conveyor has double commands which are located at the ends of the conveyor, i.e. at the beginning and at the end, so that the transport worker has the commands within reach. The commands are produced in accordance with the valid norms for this kind of conveyors.

Due to telescopic booms, the telescopic belt conveyors have their own advantages over conventional conveyors.The state of the art designs of telescopic belt conveyors are said to facilitate minimum fatigue to labor, minimum manpower, and optimum speed.

The drive of the conveyor is electric (380 V and 50 Hz).

Technical data are given in the table 1.

Based on project demands regarding transport capacity and transport speed (capacity of 50 kg/m and speed of 30 m/min), the final solution of telescopic conveyor was proposed. Selection was made based on a number of advantages regarding faster working, less fatigue, low manpower, low labour cost.

Graphical presentation of the design is given in Figure 11.

Table 1: Technical data

Type / Characteristics	SINGLE		DUPLEX		TRIPLEX		QUADRIPLEX
	LTT-1	HTT-1	LTT-2	HTT-2	LTT-3	HTT-3	LTT-4
	linear	hinged	linear	hinged	linear	hinged	linear
L_1 [mm] - length in assembled position	5250	6250	5250	7000	5250	5250	5250
L_2 [mm] - length in extracted position	8250	9500	10250	11000	14250	13250	15250
h [mm] - extraction	3000	3000	5000	4000	9000	6000	10000
B_1 [mm] B_2 [mm] - lane width B_3 [mm]	500 650 800	500 650 800	500 650 800	500 650 800	500 650 800	500 650 800	500 650 800
A [mm] - conveyor width	808 968 1118	808 968 1118	868 1028 1178	868 1028 1178	928 1088 1238	928 1088 1238	968 1148 1298
H [mm] - conveyor height	800	800	800	800	850	850	900
α [°] - lifting angle	12	12±9	12	12±9	15	15±9	18
H_1 [mm] - max height of the raising of the free end	2500	2000±475	2175	2338±630	3800	3350±950	4300
G [kg] - conveyor weight	1000	1150	1200	1350	1400	1550	1800
Capacity 50 kg/m Speed 30 m/min							

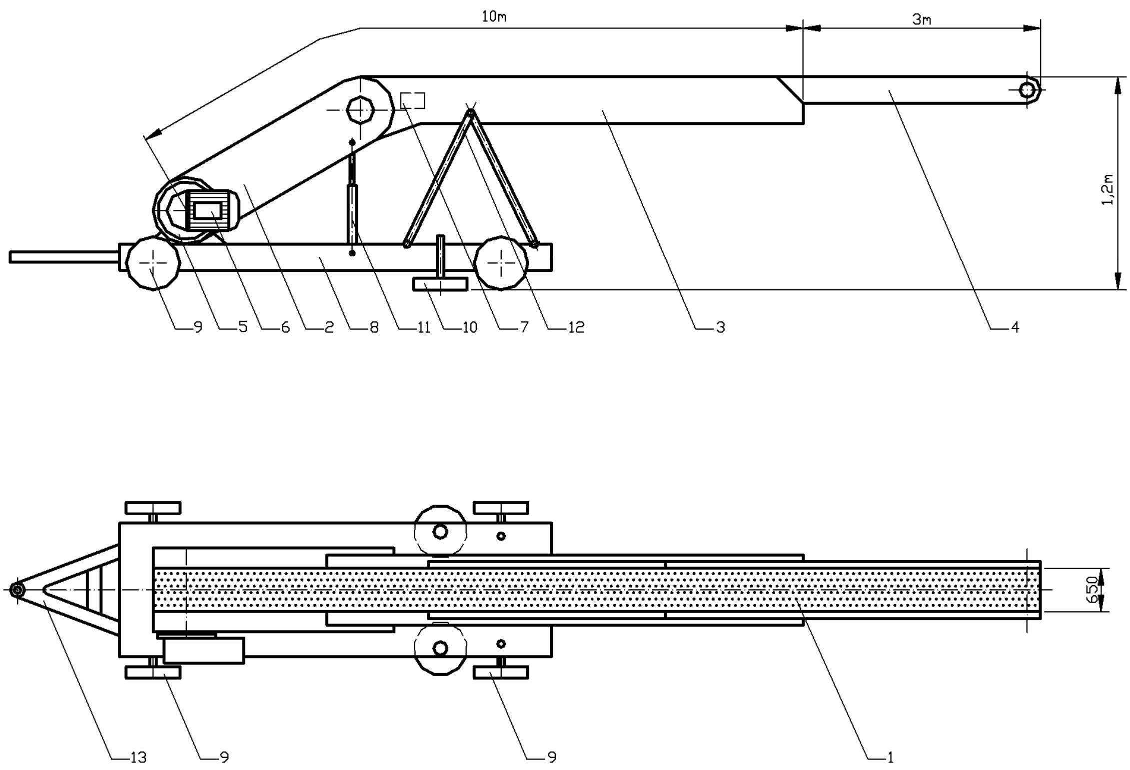

Figure 11: Adopted solution of the telescopic conveyor

Positions in Figure 8 are as follows:

1 – conveyor belt,
2 – inclined frame,
3 – hinged carrier,
4 – telescope,
5 – drum,
6 – belt drive unit,
7 – telescope drive unit,
8 – trolley,
9 – wheels,
10 – supports,
11 – hydraulic cylinder for inclined frame lifting,
12 – side carriers,
13 – hitch.

6. CONCLUSION

A wide selection of telescopic conveyors enables a wide range of application. Having in mind that in the technical solution the humanization of human labour was in the first place, this is still a motive for development of all types and kinds of telescopic conveyors. As the constructive solutions are simple and suitable, the economic justification of the telescopic conveyor is obvious.

With the regard to the situation in the regulations, where every slowdown is charged, with the emergence of the telescopic conveyors the cost of goods not being unloaded from wagons and trucks is being reduced.

REFERENCES

[1] R. Vujanac, R. Slavkovic and N. Miloradovic, "Warehouse Solution in The Phermaceutical Institution of Montenegro Montefarm Podgorica", International Conference "Civil Engineering – Science and Practice" - GNP 2006, Žabljak, (Montenegro), February 20th – 24th 2006, pp. 953-958, (2006)

[2] R. Vujanac , D. Maksimovic, N. Miloradović, and R. Slavković, "Reconstruction of vertical reciprocating conveyors with straddle carriage into four post carriage", 19th International Conference on Material Handling, Constructions and Logistics – MHCL'09 Belgrade, (Serbia) October 15th – 16th, 2009, pp. 99-102, (2009)

[3] R. Vujanac, N Miloradovic and R Slavkovic, "Radio shuttle racking – new generation of high density storage system", The 7th International Scientific Conference Research and development of mechanical elements and systems - IRMES 2011, Zlatibor, (Serbia), April 27th - 28th, 2011, pp. 205-208, (2011)

[4] R. Vujanac, R. Slavkovic, M. Blagojevic and N. Miloradovic, "Autosatmover – new solution for automatic multi – depth pallet storage system", The Seventh International Symposium KOD 2012 Machine and Industrial Design in Mechanical Engineering, Balatonfüred, (Hungary), May 24th – 26th, 2012, pp. 139-142, (2012)

[5] R. Vujanac, D. Maksimovic, and R. Slavkovic, "Self-supported Warehouse Structure Completely Built of Racking Pallet Racking System", 4th International Conference "Civil Engineering – Science and Practice" - GNP 2012, Žabljak, (Montenegro), pp. 899-904, (2012)

'Design-in' Faults - the Reason for Serious Drawbacks in High Capacity Bucket Wheel Excavator Exploitation

Nebojša B. Gnjatović[1,*], Goran Z. Milojević[1], Ivan Lj. Milenović[1], Aleksandar Z. Stefanović[1]
[1]University of Belgrade - Faculty of Mechanical Engineering

This paper describes the failure analysis results of undercarriage and superstructure vital subassemblies, which led to periodical stoppage and eventually total collapse of the bucket wheel excavator (BWE) SchRs 1760, once the machine with the highest theoretical capacity operating on the overburden excavation in open pit mine "Kolubara" - Serbia. It is conclusive that the main cause of two wheel bogie structural failure, described as case 1, is its insufficient strength during the action of lateral forces which are dominantly applied during the BWE curve travel. Case 2 analyses the support structure of portal tie-rods failure which was the consequence of superposition of the negative effects caused by inadequate shaping and dimensioning of the support assembly for given load conditions, as well as influences of defects of the metal weld structure. Both of the described failures are caused by the design-in faults.

Keywords: Bucket wheel excavator, Failure analysis, Finite element analysis

1. INTRODUCTION

Bucket wheel excavator (BWE) SchRs 1760, Fig. 1, was put into exploitation during the year 1989. At that time it was the machine with the highest theoretical capacity of 6100 m^3/h operating on the overburden excavation on open pit mine "Kolubara" – Serbia.

Figure 1: BWE Sch Rs 1760

Ever since the beginning, the exploitation of this BWE was followed by frequent breakdowns of its crawler travelling mechanisms vital subassemblies, especially crawler chain links [1] and two wheel bogies (TWB), Fig. 2. During three years period, from 2001 to 2003, fifty-one two wheel bogie bodies and forty-nine track wheel axles with nuts were manufactured and substituted [2].

Complex substitution procedure, which is done on site in extremely harsh working conditions consists of hole digging (4m length, 3m with and 0.8m depth), crawler chain release, positioning of the excavator above the hole, leaning the damaged TWB on specially designed lifting tool, dismantling, descending and extracting the old and positioning and attaching the new construction, followed by chain tensioning, as presented in [3]. Estimated duration of this operation is about eight hours, during which, the excavator cannot be functional.

Defect inspection showed that the majority of TWB structures suffered the same problems, plastic deformation and crack occurrence in the vertical plate clamping zone and shearing of the axle nut. Frequent failures, followed by the same problems detected during maintenance procedures were the main reason for comprehensive structural integrity analysis of the TWB construction. Diagnosis of the cause of the TWB structure failure will be presented in this paper as Case 1.

Figure 2: Typical failure of the TWB structure

On 3rd of December 2005, after merely sixteen years of exploitation, a heavy accident caused the total collapse of the machine, Fig. 3. Revitalization process, which included dismantling of the complete BWE structure, transport to the erection site, repair and manufacturing of almost every part of the superstructure, erection, testing and putting back to service, lasted for almost five years. On 22nd of October 2010, BWE SchRs 1760 was, once again, included into the production process. Direct expenses in terms of material and labour were estimated to be around fifteen million Euros.

*Corresponding author: Faculty of Mechanical Engineering, Kraljice Marije 16, Belgrade, Serbia, ngnjatovic@mas.bg.ac.rs

However, indirect losses, caused by the BWE's downtime considerably exceed revitalization costs, having in mind that one hour of machine exploitation is valued at 11000 € to 15000 €.

Figure 3: BWE Sch Rs 1760 after the collapse

Damage diagnostics, conducted immediately after the breakdown, concluded that the straightforward cause of the BWE collapse is the failure of the end eye connection of the support of the right portal tie-rod, Fig. 4, which will be analyzed as Case 2 of this paper.

Figure 4: Broken-down support of the right portal tie-rod: (a) element on the counterweight arm and (b) broken-away part.

2. CASE 1 – TWO WHEEL BOGIE FAILURE

Two wheel bogie (TWB) presents the vital part of BWE crawler carrying structure. It distributes the load statically determinate to the individual wheels and also provides the necessary freedom of movement of the travel wheels to adapt to undulating ground conditions in travel direction [4].

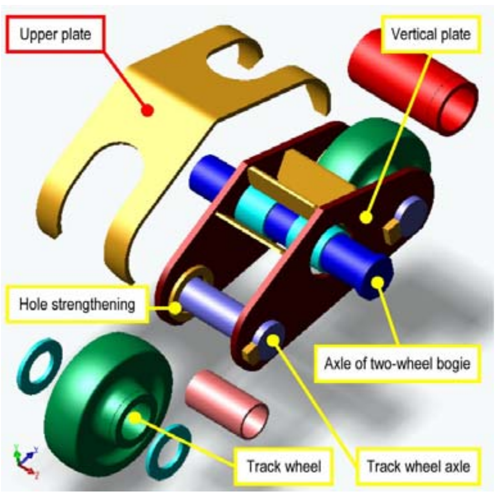

Figure 5: 3D model of the bucket wheel excavator Krupp 1760 TWB

Fig. 5 shows the main TWB subassemblies. It can be observed that there is no connection between the vertical plates in the TWB structure under the hole for bedding the track wheel axles. On the other hand, based on the looks of the TWB damaged structure, shown in Fig. 2, it is conclusive that the main cause of its failure is insufficient strength during the action of lateral forces which are dominantly applied during the BWE curve travel [5]. The verification of this conclusion is done by applying the linear FEA.

Load analysis of the TWB structure is carried out according to the recommendations given in [6,7]. The track wheel is affected by the average vertical load for maximum load on the crawler track $R_{z,m,max}$ = 384.3 kN and the corresponding horizontal load $H_{ym,max}$ = 230.6 kN, as presented in [8].

In order to simulate the behaviour of the TWB structure predefined by the project documentation, a model which includes the track wheel axles was analyzed. Lateral forces act on one vertical plate - annular surfaces of the holes' strengthening, blue coloured surfaces, whereas track wheel axles are loaded by vertical forces and bending moments (M_L) gained by a reduction of lateral forces, Fig. 6.

One of the main problems detected in the process of defect inspection was, as previously stated, shearing of the axle nut, which leads to the appearance of a relatively great axial gap between the TWB vertical plates and the track wheel axle subassemblies. In this case, an FE model was created by supposing that the lateral forces act only on one vertical plate, while the second is the support in the corresponding direction, Fig. 7.

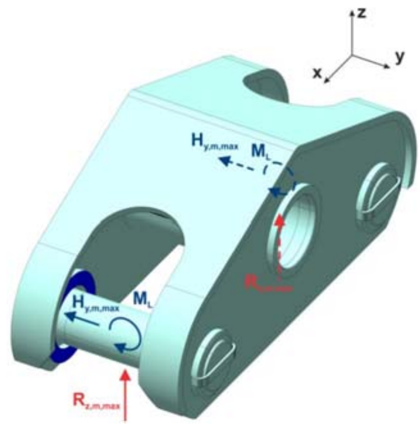

Figure 6: Loading of the TWB structure model which includes the track wheel axles subassemblies

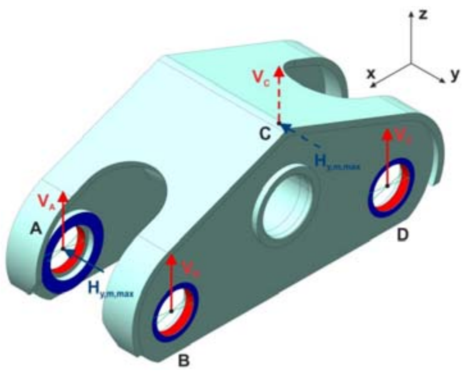

Figure 7: The TWB structure loading in case of an axial gap between the vertical plate and the track wheel axles subassemblies

The maximum calculated stress values appear in the vertical plate clamping zone. Distribution of von Misses stresses in the critical zone is shown in Fig. 8, while averaging of the calculation stress values along the upper plate thickness is done according to [8].

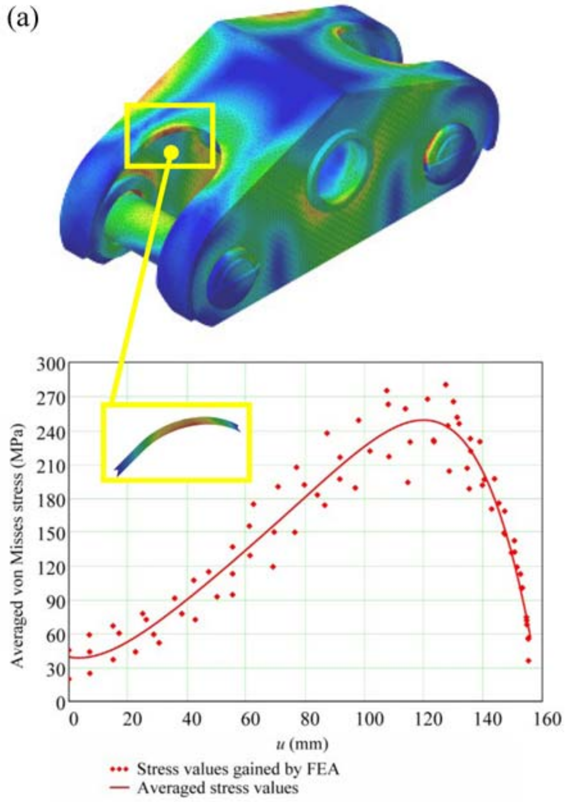

(a) track wheel axle included

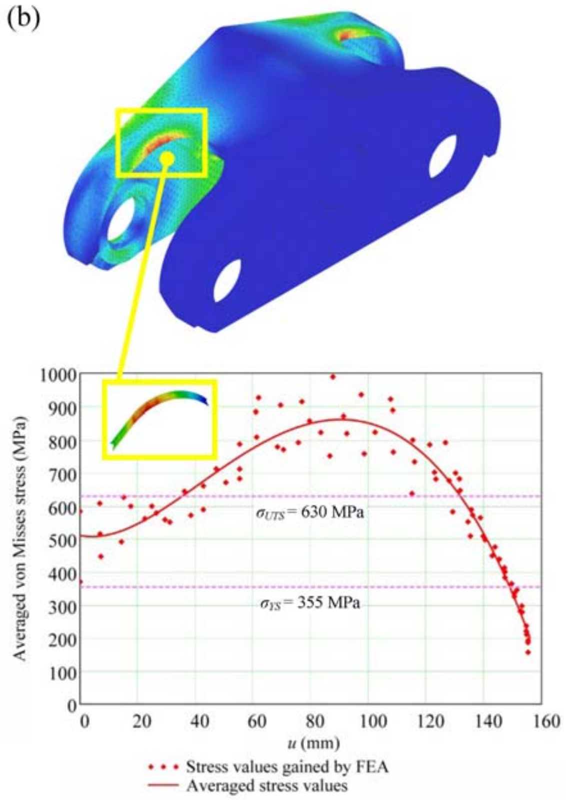

(b): without track wheel axle

Figure 8: Distribution of averaged von Misses stresses in critical zones

If the track wheel axles are included in the model of the TWB structures, the maximum averaged von Misses stress (MAvMS) for the original (249 MPa) TWB structure is lower than the minimum yield stress value (σ_{YS}=355 MPa for steel quality grade S355J2G3). But, if track wheel axles do not distribute the lateral loads, MAvMS (862 MPa) for the original TWB structure is considerably greater than the ultimate tensile strength (σ_{UTS}=630 MPa). This fact fully explains the occurrence of cracks in the case of an axial gap between the TWB structure and the track wheel axle subassemblies.

The authors of this paper strongly suggest the conservative approach to calculating the TWB structure, using models which do not include the track wheel axles, since it provides sufficient TWB carrying capacity even in the case of unforeseen loads, the appearance of which is quite possible having in mind the extremely hard working conditions.

3. CASE 2 –FAILURE OF THE PORTAL TIE ROD END EYE CONNECTION

The portal tie-rods supports, Fig. 9, are the vital parts of BWE structure. By means of tie-rods (rope diameter 110 mm), they accept a part of the BWB and portal loads and transmit it onto the counterweight boom. At the same time they are supports of the rope system drum for BWB hanging. The straightforward cause of BWE collapse, as it was previously stated, is the failure of the end eye connection of the support of the right portal tie-rod (Fig. 4).

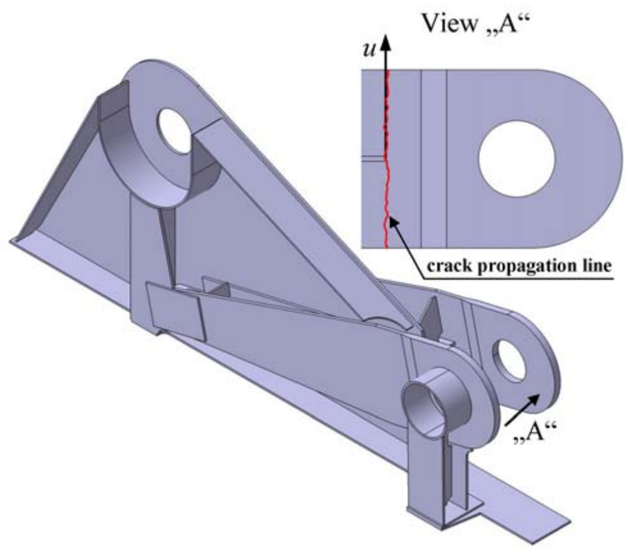

Figure 9: 3D model of the support of the right portal tie-rod

In order to detect the reason of the end eye connection failure it was necessary to calculate the stress state of the eye assembly, conduct visual, metallographic and SEM inspection of the crack surface and determine chemical composition and mechanical properties of the end eye connection plate.

The identification of the portal tie-rod support stress state is done by applying linear finite element method (FEM).

The load analysis of the support of the portal tie-rod is carried out according to the rules given in the German code [6], based on which the considered BWE was designed. The intensities of forces in the portal tie-rods (F_{TR}) are defined for four characteristic load cases (LC) that are: H1 (F_{TR} = 2980 kN), H2 (F_{TR} = 3755 kN), HZ1 (F_{TR} = 4040 kN) and HZS1 (F_{TR} = 4260 kN).

Maximum value of uniaxial stress, calculated according to the Huber–Hacky–von Misses hypothesis, is obtained in the left eye, in the zone of its connection with the lengthwise supporting plate, Fig. 10.

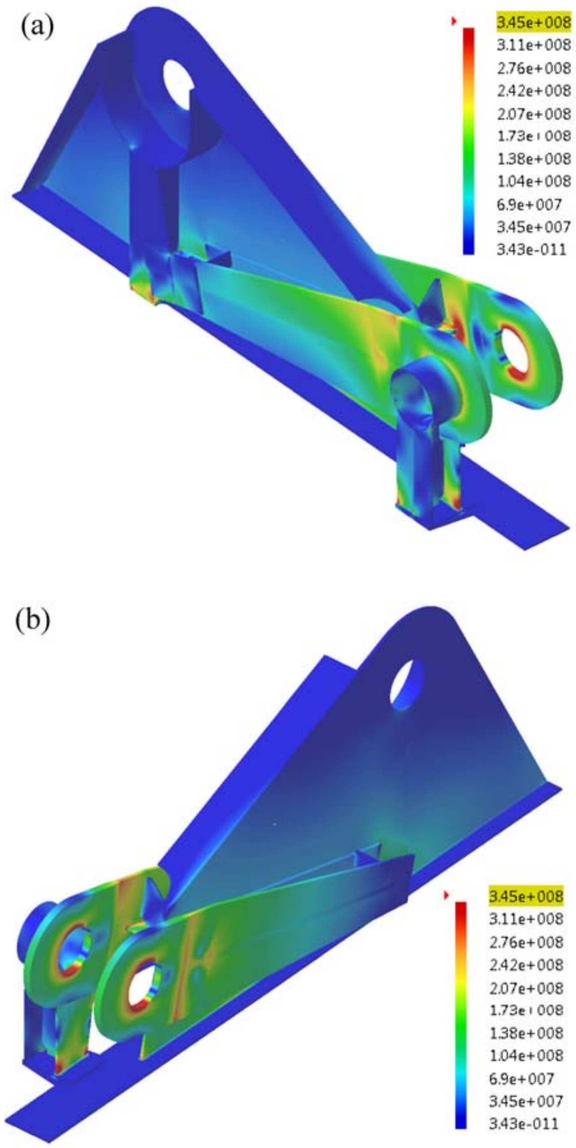

Figure 10: Uniaxial stress field of the portal tie-rod support structure for LC HZS1: (a) right side view and (b) left side view (values higher than yield stress are red coloured)

Distribution of von Misses stresses in the critical zone, as well as calculation stress values along the crack initiation and propagation line are shown in Fig. 11. The maximum von Misses stress (MvMS) values and the permissible stress intensities (PSI) for all analyzed load cases are presented in Tab. 1.

Table 1: MvMS and PSI for all analyzed load cases

Load case	MvMS [MPa]	PSI [MPa]
H1	508	230
H2	640	230
HZ1	689	260
HZS1	726	288

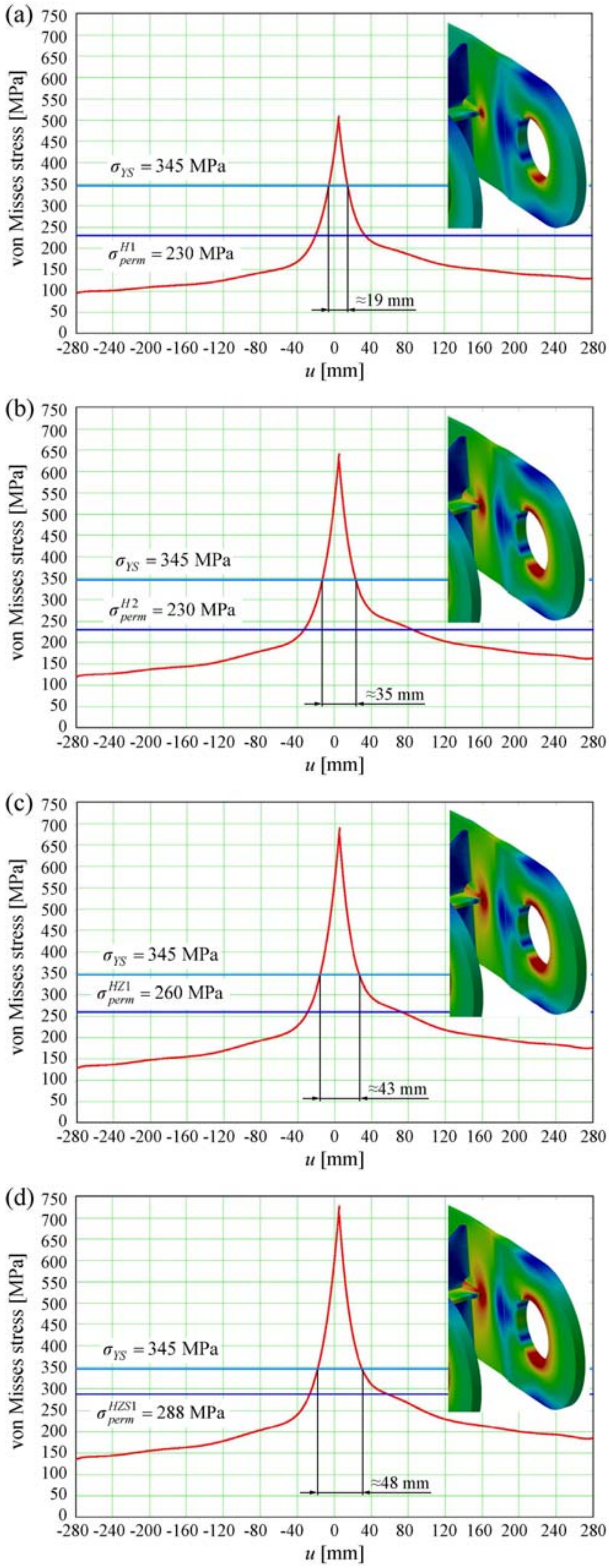

Figure 11: Distribution of von Misses stresses alonge the crack propagation line: (a) LC H1, (b) LC H2, (c) LC HZ1, (d) LC HZS1 (values higher than yield stress in stress field figures are red coloured)

Presented results point out the following:

- Due to the prompt incursion of the lengthwise supporting plate into the eye structure and the proximity of the location where the load is applied, the pronounced stress concentration occurs in the failure zone of the eye;

- In all load cases maximum von Misses stresses are considerably greater than permissible stress values (2.2 times for LC H1; 2.8 times for LC H2; 2.7 times for LC HZ1 and 2.5 times for LC HZS1);
- The reserve of elasticity is also depleted, since MvMS are 1.5, 1.9, 2.0 and 2.1 times greater than yield stress value (σ_{YS} = 345 MPa for steel quality grade S355J0 and plate thickness of 20 mm, [9]) for load cases H1, H2, HZ1 and HZS1 respectively;
- The size of the high stress state zone (values higher than yield stress intensity) is expanding with the increase of load intensity from 19 mm for LC H1 up to 48 mm for LC HZS1.

The high stress state of the designed support structure of portal tie-rods, conjugated with the detrimental effects of the welding seam (not welded through root, porosity, inclusions) perpendicular to the force direction, as presented in [10] and dynamic character of loads, is the principal reason of the end eye connection failure and the BWE collapse.

4. CONCLUSION

The natural tendency towards permanently improving the performance of the BWE, especially their capacities and mobility, as well as harsh deadlines which are always present, have not always been adequately followed by design procedures and manufacturing technologies. This statement is substantiated by various accidents and failures of carrying structures as described and analysed in [11–14]. Digging drives and their vital parts [15–17] and especially travelling mechanisms [18–22] and belonging substructures, are also exposed to failure occurrence in extreme exploitation conditions.

There are four main reasons for the collapse of a high-capacity earthmoving and lifting/conveying machines: ‘design-in’, ‘manufacturing-in’, ‘operating-in’ and ‘environment-in’ defects [23]. Common denominators to all failures of high performance machines are very high financial losses caused by production delays, which often significantly exceed financial losses caused by direct material damage.

Failures of the two vital undercarriage and superstructure subassemblies of the BWE 1760 caused periodical stoppage and eventually total collapse of the machine. The amount of damage, caused by downtime of the machine, which lasted for more than five years, is very hard to estimate, since besides negative repercussions it had on coal excavation, it also influenced the power production in Serbia.

The ‘design-in’ faults should not always be detected through forensic engineering, after the occurrence of failure. The amount of these faults should be significantly reduced by reanalysing the largest structures in earth based technology, such as bucket wheel excavators, using newly developed calculation methods such as the finite element analysis.

ACKNOWLEDGEMENTS

This work is a contribution to the Ministry of Education, Science and Technological Development of Serbia funded project TR 35006.

REFERENCES

[1] S. Bošnjak, D. Momčilović, Z. Petković, M. Pantelić, N. Gnjatović, “Failure Investigation of the Bucket Wheel Excavator Crawler Chain Link”, Eng. Fail. Anal., Vol. 35, pp. 462–469, (2013)

[2] M. Pantelić, R. Spasojević, “Experimental Testing Original and Reconstructed Cart for Bucket Wheel Excavator KRUPP SchRs 1760/5x32 Transport Mechanism”, Proceedings of 7th International Conference “Dependability and Quality Management DQM-2004”, Belgrade (Serbia),16-17 June 2004, pp. 68-79, (2004)

[3] M. Pantelić, M. Nekić, R. Spasojević, “Techno-Economical Analysis of Failure Maintenance Mechanism of Transport Systems of KRUPP Schrs 1760/5x32 Bucket Wheel Excavator”, Proceedings of 8th International Conference “Dependability and Quality Management DQM-2005”, Belgrade (Serbia),15-16 June 2005, pp. 133-141, (2005)

[4] W. Durst, W. Vogt, “Bucket Wheel Excavator”, Clausthal-Zellerfeld: Trans Tech Publications, (1989)

[5] S. Bošnjak, Z. Petković, N. Zrnić, M. Pantelić, A. Obradović, “Failure Analysis and Redesign of the Bucket Wheel Excavator Two-Wheel Bogie”, Eng. Fail. Anal., Vol. 17, Issue 2, pp. 473-485, (2010)

[6] DIN 22261-2. Bagger, Absetzer und Zuzatsgeräte in Braunkohlentagebauen. Teil 2: Berechnungsgrundlagen. Deutsches Instituts für Normung, Berlin, (1998)

[7] L. Der Rasper, Sshaufelradbagger als Gewinnungsgerat. Clausthal-Zellerfeld: Trans Tech Publications, (1975)

[8] S. Bošnjak, Z. Petković, N. Gnjatović, I. Milenović, B. Jerman, “Impact of the Track Wheel Axles on the Strength of the Bucket Wheel Excavator Two-Wheel Bogie”, Techical Gazette, Vol. 20, Issue 5, pp. 803-810, (2013)

[9] EN 10025-2. Hot rolled products of structural steel – Part 2: Technical delivery conditions for non-alloy structural steels, European committee for standardization, (2004)

[10] S. Bošnjak, N. Zrnić, A. Simonović, D. Momčilović, “Failure Analysis of the End Eye Connection of the Bucket Wheel Excavator Portal Tie-Rod Support”, Eng. Fail. Anal., Vol. 16, Issue 3, pp. 740–750, (2009)

[11] E. Rusiński, J. Czmochowski, A. Iluk, M. Kowalczyk, “An Analysis of the Causes of a BWE Counterweight Boom Support Fracture”, Eng. Fail. Anal., Vol. 17, Issue 1, pp. 179–191, (2010)

[12] S. Bošnjak, Z. Petković, N. Zrnić, G. Simić, A. Simonović, “Cracks, Repair and Reconstruction of Bucket Wheel Excavator Slewing Platform”, Eng. Fail. Anal., Vol. 16, Issue 5, pp. 1631–1642, (2009)

[13] S. Bošnjak, M. Pantelić, N. Zrnić, N. Gnjatović, M. Đorđević, “Failure Analysis and Reconstruction Design of the Slewing Platform Mantle of the Bucket Wheel Excavator O&K SchRs 630”, Eng. Fail. Anal., Vol. 18, Issue 2, pp. 658-669, (2011)

[14] P. Jovančić, D. Ignjatović, M. Tanasijević, T. Maneski, “Load-Bearing Steel Structure Diagnostics on Bucket Wheel Excavator, for the Purpose of Failure Prevention”, Eng. Fail. Anal., Vol. 18, Issue 4, pp. 1203–1211, (2011)

[15] E. Rusiński, P. Harnatkiewicz, M. Kowalczyk, P. Moczko, “Examination of the Causes of a Bucket Wheel Fracture in a Bucket Wheel Excavator”, Eng. Fail. Anal., Vol. 17, Issue 6, pp. 1300–1312, (2010)

[16] M. Savković, M. Gašić, M. Arsić, R. Petrović, “Analysis of the Axle Fracture of the Bucket Wheel Excavator”, Eng. Fail. Anal., Vol. 18, Issue 1,pp. 433–441, (2011)

[17] M. Arsić, S. Bošnjak, N. Zrnić, A. Sedmak, N. Gnjatović, “Bucket Wheel Failure Caused by Residual Stresses in Welded Joints”, Eng. Fail. Anal., Vol. 18, Issue 2, pp. 700–712, (2011)

[18] D. Dudek, S. Frydman, W. Huss, G. Pękalski, “The L35GSM Cast Steel – Possibilities of Structure and Properties Shaping at the Example of Crawler Links”, Arch. Civ. Mech. Eng., Vol. 11, Issue 1, pp. 19–32, (2011)

[19] S. Bošnjak, M. Arsić, N. Zrnić, Z. Odanović, M. Đorđević, “Failure Analysis of the Stacker Crawler Chain Link”, Proc. Eng., Vol. 10, pp. 2244–2249, (2011)

[20] Y. Zhi-wei, X. Xiao-lei, M. Xin, “Failure Investigation on the Cracked Crawler Pad Link”, Eng. Fail. Anal., Vol. 17, Issue 5, pp. 1102–1109, (2010)

[21] M. Arsić, S. Bošnjak, Z. Odanović, M. Dunjić, A. Simonović, “Analysis of the Spreader Track Wheels Premature Damages”, Eng. Fail. Anal., Vol. 20, pp. 118–136, (2012)

[22] M. Savković, M. Gašić, D. Petrović, N. Zdravković, R. Pljakić, “Analysis of the Drive Shaft Fracture of the Bucket Wheel Excavator”, Eng. Fail. Anal., Vol. 20, pp. 105–117, (2012)

[23] S. Bošnjak, Z. Petković, G. Milojević, V. Mihajlović, “The Design – in Faults as a Causes of the High Performance Machines Failures”, Proceedings of VII International Conference “Heavy Machinery HM 2011”, Vrnjačka Banja (Serbia), 29 June-2 July 2011, pp. 55-60, (2011)

The Equations of Motion of the Crane with Loading-unloading Trolley on the Slewing Platform

Spasoje Trifković [1*], Milomir Gašić [2], Nebojša Radić[1], Miroslav Milutinović[1]
[1] Faculty of Mechanical Engineering East Sarajevo, University of East Sarajevo, East Sarajevo (Bosnia and Herzegovina)
[2]Faculty of Mechanical and Civil Engineering in Kraljevo, University of Kragujevac, Kraljevo (Serbia)

Dynamic processes of cranes can be sufficiently accurate described by systems of differential equations, where the experiment on real object is replaced with experiment on the equivalent dynamic model. The study of the dynamic behavior of the cranes is very important in terms of precise determination of stress state, as well as the other characteristics of the elements and supporting structures. Dynamic loads of the cranes occur during periods of non-stationary operating regimes of any of its mechanisms. Mathematical model of the crane with loading - unloading trolley on the slewing platform is made in this paper. According calculated mathematical model, formulation of oscillations of elastic systems using the Lagrange equations, is given here.

Keywords: Rotary crane, Dynamic processes, Equations of motion

1. INTRODUCTION

In order to include all loads when designing and modernization of the cranes with loading-unloading trolley on slewing platform, general method for dynamic analysis of their metal structures is proposed.

Problem of dynamic behaviour of cranes was considered in [1÷6]. Oscillations in the metal structure, which is a system with an infinite number of degrees of freedom, will be discussed as oscillating of elastic system with a finite number of degrees of freedom. Because of that the mass of the construction is replaced by one or several reduced masses, whereby the system must have a minimum number of degrees of freedom. Replacing the existing masses of construction with the reduced masses comes from the assumption of dynamic equivalence of both systems.

The rigidity of the elements of the mechanism is considerably higher than the rigidity of metal construction. Thus the flexibility of solid transfer components can be neglected, without reducing accuracy of calculations of the metal construction. This is confirmed by the experimental data of the tensometer testing of the hoist and movement mechanisms. When considering the mathematical model own structural damping is neglected because of its relatively small influence.

2. DYNAMIC MODEL OF CRANE

Based on analysis of construction of cranes with loading-unloading trolley on slewing platform, a mathematical model of their metal construction as elastic dynamic system is made (Fig. 1). We will consider the metal construction of cranes as an eight-mass system with thirteen generalized coordinates. The given mathematical model is general for all types of cranes with loading-unloading trolley on slewing platform and it corresponds to the real working conditions of metal construction, because it includes all elements of the system elasticity and has a minimal number of degrees of freedom.

We will consider the case of simultaneous operation of all the basic mechanisms of crane: the movement of the bridge, trolley movement, lifting and rotation. System of equations of motion of the metal structure in general form is obtained, and it can be defined practically all possible cases of the crane operation.

3. MATHEMATICAL FORMULATION OF THE OSCILLATIONS

As shown in Fig. 1, there are two coordinate systems on the mathematical model. One of them is the $0_n X_n Y_n Z_n$ with the coordinate origin in 0_n, and it is fixed. The other coordinate system is $0XYZ$ with the coordinate origin in 0, and it moves together with the masses m_7. Origin of the coordinate system $OXYZ$ is chosen as the middle of the left beam of the bridge in the position of equilibrium of elastic system. The axis X is directed horizontally along the span of the bridge to the side of the right beam of the bridge. The axis Z is directed horizontally along the beam of the bridge, and the axis Y is directed vertically on the underside of the crane.

The reduced masses are:

- m_1 - mass of the left beam of the bridge (without beam ends), presented in the middle of the bridge;
- m_2 - mass of the right beam of the bridge (without beam ends), presented in the middle of the bridge;
- m_3 - part of the mass of the gripping device, related to the left half of the bridge;
- m_4 - part of the mass of the gripping device, related to the right half of the bridge;
- m_5 - part of the mass of the gripping device, which is reduced to the upper end of the gripping devices;
- m_6 - mass of cargo and part of the mass of horizontal overhanging beam;
- m_7 - beam ends mass and part of the the reduced mass of the bridge.

*Corresponding author: Vuka Karadžića 30, East Sarajevo, Bosnia and Herzegovina, trifkovic_yahoo.com

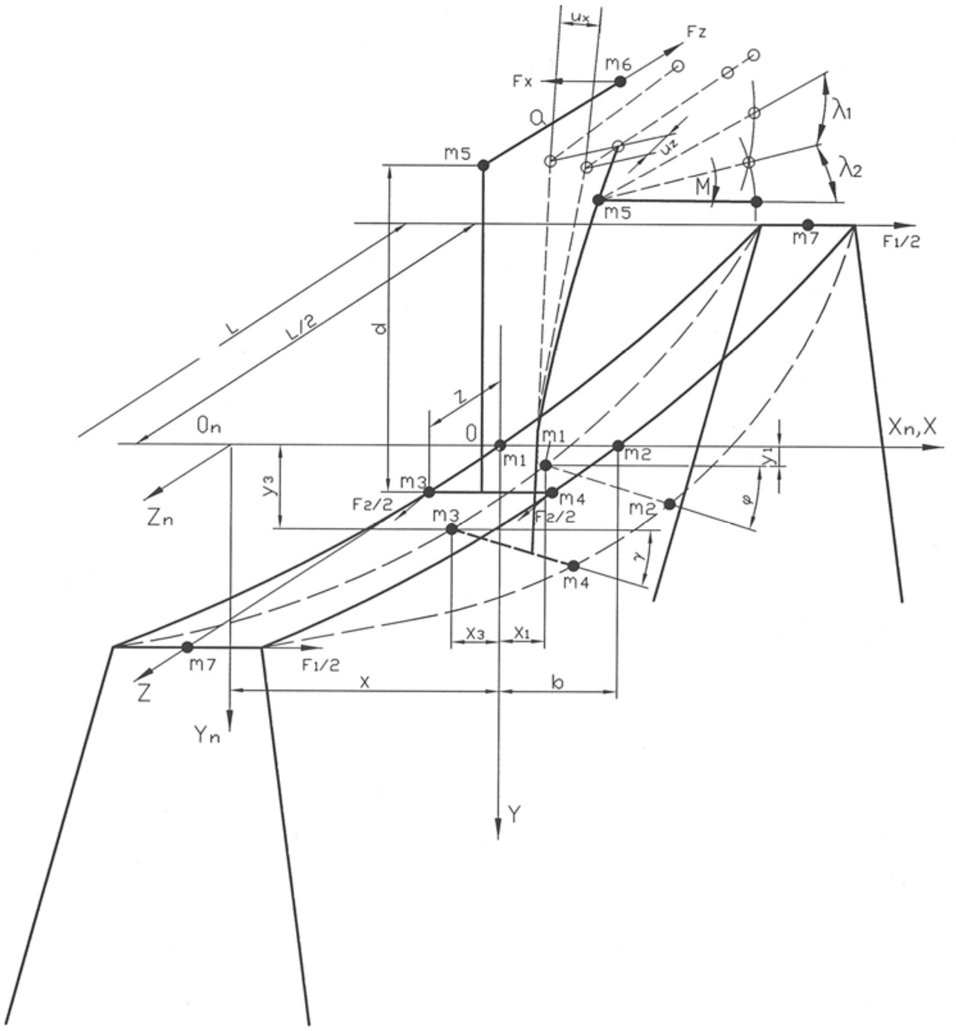

Figure 1: The multi-mass model of a crane with loading-unloading trolley on slewing platform

Generalized coordinates are:

- x - horizontal movement of point 0 along axis X from fixed point O_n;
- x_1 - horizontal movement of mass m_1 along axis X from point O;
- y_1 - vertical movement of mass m_1 along axis Y from point O;
- φ - angle between the reduced masses m_1 and m_2;
- x_3 - horizontal movement of mass m_3 along axis X from point O;
- y_3 - vertical movement of mass m_3 along axis Y from point O;
- z - horizontal movement of mass m_3 along axis Z from point O;
- γ - rotation angle of trolley;
- d - vertical movement of masses m_5 and m_6;
- u_x - movement of the upper end of the vertical overhanging beam along axis X;
- u_z - movement of the upper end of the vertical overhanging beam along axis Z;
- λ_2 - rotation angle of the horizontal overhanging beam in the swing;
- λ_1 - rotation angle of the horizontal overhanging beam around vertical overhanging beam.

The generalised non-conservative forces:

- F_1 - force of the the bridge movement mechanism;
- F_2 - force of the the trolley movement mechanism;
- M - moment on the horizontal overhanging beam;
- F_x i F_z - force components at the end of the horizontal overhanging beam.

For deriving the differential equations of motion, the second-order Lagrange equations of the following form were used. Basis for the mathematical model shown in Fig. 1,:

$$\frac{d}{dt}\left(\frac{\partial E_k}{\partial \dot{q}}\right)-\frac{\partial E_k}{\partial q}+\frac{\partial E_P}{\partial q}=Q_q \tag{1}$$

where
$q=f(x,x_1,y,\varphi,x_3,y_3,z,\gamma,d,u_x,u_z,\lambda_2,\lambda_1)$-independent generalised coordinates;

E_k i E_p- kinetic and potential energy of the elastic system.

$$E_k = \frac{1}{2}a_{00}\dot{x}^2 + a_{01}\dot{x}\dot{x}_1 + a_{04}\dot{x}\dot{x}_3 + a_{07}\dot{x}\dot{\gamma} + a_{09}\dot{x}\dot{u}_x + a_{0\cdot12}\dot{x}\dot{\lambda}_1 +$$
$$+\frac{1}{2}a_{11}\dot{x}_1{}^2 + \frac{1}{2}a_{22}\dot{y}_1{}^2 + a_{23}\dot{y}_1\dot{\varphi} + \frac{1}{2}a_{33}\dot{\varphi}^2 + \frac{1}{2}a_{44}\dot{x}_3{}^2 + a_{47}\dot{x}_3\dot{\gamma} +$$
$$+ a_{49}\dot{x}_3\dot{u}_x + a_{4\cdot12}\dot{x}_3\dot{\lambda}_1 + \frac{1}{2}a_{55}\dot{y}_3{}^2 + a_{57}\dot{y}_3\dot{\gamma} + a_{58}\dot{y}_3\dot{d} +$$
$$a_{5\cdot11}\dot{y}_3\dot{\lambda}_2 + \frac{1}{2}a_{66}\dot{z}^2 + a_{6\cdot10}\dot{z}\dot{u}_z + a_{6\cdot12}\dot{z}\dot{\gamma} + \frac{1}{2}a_{77}\dot{\gamma}^2 + a_{78}\dot{\gamma}\dot{d} +$$
$$a_{79}\dot{\gamma}\dot{u}_z + a_{7\cdot11}\dot{\gamma}\dot{\lambda}_2 + a_{7\cdot12}\dot{\gamma}\dot{\lambda}_1 + \frac{1}{2}a_{88}\dot{d}^2 + a_{8\cdot11}\dot{d}\dot{\lambda}_2 + \frac{1}{2}a_{99}\dot{u}_x^2 +$$
$$a_{9\cdot12}\dot{u}_x\dot{\lambda}_1 + \frac{1}{2}a_{10\cdot10}\dot{u}_z^2 + a_{10\cdot12}\dot{u}_z\dot{\lambda}_1 + \frac{1}{2}a_{11\cdot11}\dot{\lambda}_2 + \frac{1}{2}a_{12\cdot12}\dot{\lambda}^2{}_1.$$

$$E_p = \frac{1}{2}c_{11}x_1^2 + c_{14}x_1x_3 + \frac{1}{2}c_{22}y_1^2 + c_{23}y_1\varphi + c_{25}y_1y_3 +$$
$$c_{27}y_1\varphi + \frac{1}{2}c_{33}\varphi^2 + c_{35}\varphi y_3 + c_{37}\varphi\gamma + \frac{1}{2}c_{44}x_3^2 + \frac{1}{2}c_{55}y_3^2 +$$
$$c_{57}y_3\gamma + \frac{1}{2}c_{77}\gamma^2 + \frac{1}{2}c_{88}d^2 + \frac{1}{2}c_{99}u_x^2 + \frac{1}{2}c_{10\cdot10}u_z^2 + \frac{1}{2}c_{12\cdot12}\lambda_1^2.$$

Generalized forces are obtained using virtual displacements:

1) $Q_x = F_1 + F_x + m_6 a\cos\lambda_1\ddot{\lambda}_1;$
2) $Q_{x1} = 0;$
3) $Q_{y1} = 0;$
4) $Q_\varphi = 0;$
5) $Q_{x3} = F_x + m_6 a\cos\lambda_1\ddot{\lambda}_1;$
6) $Q_{y3} = -(m_5 + m_6)\ddot{d}$;
7) $Q_z = F_2 + F_z + m_6 a\sin\lambda_1\ddot{\lambda}_1;$
8) $Q_\gamma = -F_x d - \frac{1}{2}(m_5 + m_6)b\ddot{d} - m_6 ad\cos\lambda_1\ddot{\lambda}_1;$
9) $Q_d = -(m_5 + m_6)\ddot{d};$
10) $Q_{ux} = -F_x - m_6 a\cos\lambda_1\ddot{\lambda}_1;$
11) $Q_{uz} = F_z + m_6 a\sin\lambda_1\ddot{\lambda}_1;$
12) $Q_{\lambda2} = M + m_6 a\ddot{d};$
13) $Q_{\lambda1} = -F_x a - (I_5 + m_6 a^2)\ddot{\lambda}_1.$

Replacing concrete data in the (1) gives system of equations (2):

1) $a_{00}\ddot{x} + a_{01}\ddot{x}_3 - a_{04}\ddot{x}_3 + a_{07}\ddot{\gamma} + a_{09}\ddot{u}_x + a_{012}\ddot{\lambda}_1 = Q_x;$

2) $a_{10}\ddot{x} + a_{11}\ddot{x}_1 + c_{11}x_1 + c_{14}x_3 = 0$

3) $a_2\ddot{y}_1 + a_{23}\ddot{\varphi} + c_{22}y_1 + c_{23}\varphi + c_{25}y_3 + c_{27}\gamma = 0;$

4) $a_{32}\ddot{y}_1 + a_{33}\ddot{\varphi} + c_{32}y_1 + c_{33}\varphi + c_{35}y_3 + c_{37}\gamma = 0;$

5) $a_{40}\ddot{x} + a_{44}\ddot{x}_3 + a_{47}x\ddot{\gamma} + a_{49}u_x + a_{4\cdot12}\ddot{\lambda}_1 + c_{41}x_1 + c_{44}x_3 = Q_{x3};$

6) $a_{55}\ddot{y}_3 + a_{57}\ddot{\gamma} + a_{58}d_1 + a_{5\cdot11}\ddot{\lambda}_2 + c_{52}y_1 + c_{53}\varphi + c_{55}y_3 + c_{57}\gamma = Q_{y3};$

7) $a_{66}\ddot{z} + a_{6\cdot10}\ddot{u}_z + a_{6\cdot12}\ddot{\lambda}_1 = Q_z;$

8) $a_{70}\ddot{x} + a_{74}\ddot{x}_3 + a_{75}\ddot{y}_3 + a_{77}\ddot{\gamma} + a_{78}\ddot{d}_1 + a_{79}\ddot{u}_z + a_{7\cdot11}\ddot{\lambda}_2 + a_{7\cdot12}\ddot{\lambda}_1 + c_{72}y_1 + c_{73}\varphi + c_{75}y_3 + c_{77}\gamma = Q_\gamma;$

9) $a_{85}\ddot{y}_3 + a_{87}\ddot{\gamma} + a_{88}\ddot{d}_1 + a_{8\cdot11}\ddot{\lambda}_2 + c_{88}d = Q_d;$

10) $a_{90}\ddot{x} + a_{94}\ddot{x}_3 + a_{97}\ddot{\gamma} + a_{99}\ddot{u}_x + a_{9\cdot12}\ddot{\lambda}_1 + c_{99}u_x = Q_{ux};$

11) $a_{10\cdot6}\ddot{z} + a_{10\cdot10}\ddot{u}_z + a_{10\cdot12}\ddot{\lambda}_1 + c_{10\cdot10}u_z = Q_{uz};$

12) $a_{11\cdot5}\ddot{y}_3 + a_{11\cdot7}\ddot{\gamma} + a_{11\cdot8}\ddot{d} + a_{11\cdot11}\lambda_2 = Q_{\lambda2};$

13) $a_{12\cdot0}\ddot{x} + a_{12\cdot4}\ddot{x}_3 + a_{12\cdot6}\ddot{z} + a_{12\cdot7}\ddot{\gamma} + a_{12\cdot9}\ddot{u}_x + a_{12\cdot10}\ddot{u}_z + a_{12\cdot12}\ddot{\lambda}_1 + c_{12\cdot12}\lambda_1 = Q_{\lambda1}.$

Where

a_{ik} -mass coefficients

c_{ik} -stiffness coefficients

i -number of equations

k -number of independent variable

1) $a_{00} = M;\quad a_{01} = m_1 + m_2$;
$a_{04} = m_3 + m_4 + m_5 + m_6$; $a_{07} = -(m_5 + m_6)d$;
$a_{012} = -m_6 a\cos\alpha$.

2) $a_{10} = a_{01}$; $a_{11} = m_1 + m_2$; $c_{11} = 2c_{1r}$;
$c_{14} = c_{4r} + c_{2r}$;

3) $a_{22} = m_1 + m_2$; $a_{23} = m_2 b$; $c_{22} = 2c_1$;
$c_{23} = c_1 b$; $c_{25} = c_4 + c_2$; $c_{27} = \frac{1}{2}(c_4 + c_2)b;$

4) $a_{32} = a_{23}$; $a_{33} = m_2 b^2$; $c_{32} = c_{23}$; $c_{33} = c_1 b^2$;
$c_{35} = \frac{1}{2}(c_4 + c_2)b;\quad c_{37} = \frac{1}{2}(c_4 + c_6)b;$

5) $a_{40} = a_{04}$; $a_{44} = m_3 + m_4 + m_5 + m_6$;
$a_{47} = -(m_5 + m_6)d$; $a_{4\cdot12} = -m_6 a\cos\lambda_1$;
$a_{49} = -(m_5 + m_6)$; $c_{41} = c_{14}$; $c_{44} = 2c_{3r}$;

6) $a_{55} = m_3 + m_4 + m_5 + m_6$;

$a_{57} = \frac{1}{2}(2m_4 + m_5 + m_6)b$; $a_{58} = m_5 + m_6$;

$a_{5\cdot 11} = -m_6 a$; $c_{52} = c_{25}$ $c_{53} = c_{35}$; $c_{55} = 2c_3$;

$c_{57} = 2c_3 b$;

7) $a_{65} = m_3 + m_4 + m_5 + m_6$; $a_{6\cdot 10} = m_5 + m_6$;

$a_{6\cdot 12} = -m_6 a \sin\lambda_1$;

8) $a_{70} = a_{74} = a_{07}$; $a_{75} = a_{57}$;

$$a_{77} = (4m_4 + m_5 + m_6)\frac{b^2}{4} + (m_5 + m_6)d^2;$$

$$a_{78} = \frac{1}{2}(m_5 + m_6)b; \quad a_{79} = (m_5 + m_6)d;$$

$$a_{7\cdot 11} = -\frac{1}{2}m_6 ab; \quad a_{7\cdot 12} = -\frac{1}{2}m_6 al\cos\lambda_1;$$

$c_{72} = c_{27}$; $c_{73} = c_{37}$; $c_{75} = c_{57}$; $c_{77} = c_3 b^2$;

9) $a_{85} = a_{88} = a_{58}$; $a_{87} = a_{78}$; $a_{8\cdot 11} = -m_6 a$;

$$c_{88} = \frac{EF}{d};$$

10) $a_{90} = a_{94} = a_{09}$; $a_{97} = a_{79}$; $a_{99} = m_5 + m_6$;

$$a_{9\cdot 12} = -ma\cos\lambda_1; \quad c_{99} = \frac{3EI_z}{d^3}$$

11) $a_{10\cdot 6} = a_{10\cdot 10} = a_{6\cdot 10}$; $a_{10\cdot 12} = -m_6 a \sin\lambda_1$;

$$c_{10\cdot 10} = \frac{3EI_x}{d^3};$$

12) $a_{11\cdot 5} = a_{11\cdot 8} = a_{5\cdot 11}$; $a_{11\cdot 7} = a_{7\cdot 11}$;

$a_{11\cdot 11} = m_6 a^2$;

13) $a_{12\cdot 0} = a_{12\cdot 4} = a_{0\cdot 12}$; $a_{12\cdot 6} = a_{6\cdot 12}$; $a_{12\cdot 7} = a_{7\cdot 12}$;

$a_{12\cdot 12} = I_5 + m_6 a^2$; $a_{12\cdot 9} = a_{9\cdot 12}$; $a_{12\cdot 10} = a_{10\cdot 12}$;

$$c_{12\cdot 12} = \frac{GI_p}{d}.$$

4. CONCLUSION

In the paper, a model of a crane with loading-unloading trolley on the slewing platform with eight mass and with thirteen degrees of freedom is presented. Lagrange equations were used to derive the equations of motion. The obtained system of equations (2) represents the movement of the metal construction of the crane with loading-unloading trolley on the slewing platform. On that basis, we can calculate real constructions of cranes as separate individual cases. The system enables determination of the dynamic loads that acting on a metal structure in separate and simultaneous operation of all the mechanisms of cranes in different periods of operating. For the calculation of real objects it is necessary to include their models. These models need to correspond as much as possible to the real exploitation conditions and need to be simple in order to avoid complex calculations.

REFERENCES

[1] Nenad. Đ. Zrnić, „INFLUENCE OF TROLLEY MOTION TO DYNAMIC BEHAVIOUR OF SHIP-TO-SHORE CONTAINER CRANES“, Doctoral dissertation, University of Belgrade, Faculty of Mechanical Engineering, Belgrade, (Serbia), (2005)

[2] Slobodan. B. Tošić, "Dinamičko ponašanje mosnih kranova, u zavisnosti od krutosti pojedinih mehanizama i delova noseće konstrukcije", Doctoral dissertation, University of Belgrade, Faculty of Mechanical Engineering, Belgrade, (Serbia), (1989)

[3] Vlada. M. Gašić, „ Dynamic interaction between the structure and the trolley of high performance gantry cranes“, Doctoral dissertation, University of Belgrade, Faculty of Mechanical Engineering, Belgrade, (Serbia), (2012)

[4] N. Zrnić, V. Gašić, A. Obradović, S. Bošnjak, „Appropriate modeling of dynamic behavior of quayside container cranes boom under a moving trolley“, Springer Proceedings in Physics 139, Vibration problems ICOVP 2011, pp. 81-86, 2011, Springer.

[5] J.J.Wu, A. R.Whittaker, M. P. Cartmell, „The use of finite element techniques for calculating the dynamic response of structures to moving loads“, Computers and Structures, 78, 6(2000), pp. 789-799.

[6] V.Gašić, N. Zrnić, M. Rakin, „Consideration of a moving mass effect on dynamic behaviour of a jib crane structure“, Technical Gazette, 19, 1(2012), pp. 115-121.

The Kinematic and Dynamic Analysis of the Hydraulic Excavators

Vesna Jovanović[1], Dragoslav Janošević[2], Jovan Pavlović[3]
[123]Faculty of Mechanical Engineering, /Transport and logistic, University of Niš, Niš (Serbia)

In this paper is defined a general mathematical model for a kinematic and dynamic analysis of hydraulic excavator with backhoe attachment. The mathematical model of the excavator is based on the Newton - Euler 's dynamic equations . In addition, it will be given an algorithm of developed software based on the defined mathematical model that allows a kinematic and dynamic analysis of the excavator based on the experimentally measured quantities of the excavator at work in exploitative conditions. The measured values of the situation is related to the position of the kinematic chain and the parameters of the drive system of the excavator . An example will be given the results of kinematic and dynamic analysis of the hydraulic excavator weight of 16000 kg .

Keywords: hydraulic excavators, kinematic and dynamic

1. INTRODUCTION

The primary function of the hydraulic excavator is cyclic transport of land in a given workspace. Excavators auxiliary functions are many. Besides the intermittent transport of land, excavators can also perform intermittent transportation and other materials and items of work, then, leveling, breaking and surface compaction, demolition of old buildings and other structures.

Their function hydraulic excavators of all sizes performed with various configurations kinematic chain of the machine whereby the first member is thrust-motional mechanism (which may be the caterpillar or tires) and the last member of the chain are the tools of various shapes (buckets, grapples, hammers, material handlers).

The paper presents the kinematic and dynamic analysis of hydraulic excavators with backhoe attachment based on experimental measurements during the cycle of the machine work in exploitative conditions.

For each member of the chain are obtained following kinetic quantity: angular velocity and angular acceleration and linear velocity and linear acceleration, while the dynamic parameters related to the inertial forces which is determined by Newton's second law, and moments of inertial forces which is determined by Euler's dynamic equations.

2. MATEMATICKI MODEL

The mathematical model has been developed according to measured parameters state of the excavator in exploitative conditions of excavator caterpillar BGH 600C, production IMK 14 Octobar - Krusevac, mass 16000 kg and power 70 kW with beachoe attachment, bucket capacity of 0.6 m^3. The measured parameters state of the excavator refers to the size of the parameters state of kinematic chain and excavator drive mechanism (Table 1)

Mathematical model relates to the five-member configuration of the excavator kinematic chain comprising: thrust-motional mechanism L_1 (Fig. 1), rotating platform L_2, and a three-member planar manipulator with: boom L_3, stick L_4 and bucket L_5. Member of the kinematic chain L_i model is defined in its local coordinate system $O_i x_i y_i z_i$, with values set [1]:

$$L_i = \left\{ \hat{\bar{e}}_i, \hat{\bar{s}}_i, \hat{\bar{t}}_i, m_i, \hat{J}_i \right\} \tag{1}$$

where: $\hat{\bar{e}}_i$ - joint axis unit vector O_i by which are segment L_i linked for previous segment L_{i-1}, $\hat{\bar{s}}_i$ - the position vector of the joint center O_{i+1} by which are segment L_i linked for of the joint center O_{i+1} by which are segment L_i linked for to the following segment L_{i-1} (the vector intensity s_i represent kinematic length of segment), $\hat{\bar{t}}_i$ - the position

Table 1 Measured quantities of the state of the kinematic chain and excavator drive mechanisms

Measuring spot	Name of the measured quantity	Symbol	Dimension
M1	Lifting of the support and movement mechanism	c_1	*m*
M2	Platform rotation angle	c_2	^{o}
M3	Boom hydraulic cylinder motion	c_3	*m*
M4	Stick hydraulic cylinder motion	c_4	*m*
M5	Bucket hydraulic cylinder motion	c_5	*m*
M6	Pressure in one duct of the hyd. motor for platform rotation drive	p_{21}	*MPa*
M7	Pressure in other duct of the hyd. motor for platform rotation drive	p_{22}	*MPa*
M8	Pressure in the boom hydraulic cylinder on the piston side	p_{31}	*MPa*
M9	Pressure in the boom hydraulic cylinder on the connecting rod side	p_{32}	*MPa*
M10	Pressure in the stick hydraulic cylinder on the piston side	p_{41}	*MPa*
M11	Pressure in the stick hydraulic cylinder on the connecting rod side	p_{42}	*MPa*
M12	Pressure in the bucket hydraulic cylinder on the piston side	p_{51}	*MPa*
M13	Pressure in the bucket hyd. cylinder on the connecting rod side	p_{52}	*MPa*

*Vesna Jovanović: Faculty of Mechanical Engineering, A. Medvedeva 14, Niš, vesna.nikolic@masfak.ni.ac.rs

vector of centre of mass segment, m_i - segment mass, $\hat{J}_i$ - tensor of moment inertia of members. Vectors marked caps apply to local and no cap on the absolute coordinate system.

For the observed position of the configuration of the kinematic chain excavators, the transfer matrix used to transfer the vector quantities from the local coordinate system $O_i\, x_i\, y_i\, z_i$ of member L_i to the absolute coordinate system $OXYZ$ [1]:

$$A_{10} = \begin{vmatrix} \cos\theta_1 & -\sin\theta_1 & 0 \\ \sin\theta_1 & \cos\theta_1 & 0 \\ 0 & 0 & 0 \end{vmatrix}, \tag{2}$$

$$A_{20} = \begin{vmatrix} \cos\theta_1 \cos\theta_2 & -\sin\theta_1 & -\cos\theta_1 \sin\theta_2 \\ \sin\theta_1 \cos\theta_2 & \cos\theta_1 & -\sin\theta_1 \sin\theta_2 \\ \sin\theta_2 & 0 & \cos\theta_2 \end{vmatrix}, \tag{3}$$

$$A_{i0} = \begin{vmatrix} \cos\varphi_i \cos\theta_2 & -\sin\varphi_i & -\cos\varphi_i \sin\theta_2 \\ \sin\varphi_i \cos\theta_2 & \cos\varphi_i & -\sin\varphi_i \sin\theta_2 \\ \sin\theta_2 & 0 & \cos\theta_2 \end{vmatrix}, \tag{4}$$

$\forall i = 3,4,5;$

where: $\varphi_3 = \theta_1 + \theta_3\,;\ \varphi_4 = \theta_1 + \theta_3 + \theta_4\,;\ \varphi_5 = \theta_1 + \theta_3 + \theta_4 + \theta_5$, and the transfer matrix used to transfer the vector quantities from the absolute coordinate system to the local coordinate system:

$$A_{oi} = A_{io}^T \tag{5}$$

The kinematic values of the kinematic chain members are: linear v_i and angular velocity ω_i and linear a_i and angular accelerations ε_i of chain member L_i, and they are determine relative to an absolute coordinate system with recursive equations:

$$\vec{\omega}_i = \vec{\omega}_{i-1} + \dot{\theta}_i\, \vec{e}_i \tag{6}$$

$$\vec{\varepsilon}_i = \vec{\varepsilon}_{i-1} + \ddot{\theta}_i \vec{e}_i + \left(\vec{\omega}_{i-1} \times \dot{\theta}_i \vec{e}_i\right) \tag{7}$$

$$\vec{v}_i = \vec{v}_{i-1} + \left(\vec{\omega}_{i-1} \times \left(\vec{s}_{i-1} - \vec{t}_{i-1}\right)\right) + \left(\vec{\omega}_i \times \vec{t}_i\right) \tag{8}$$

$$\vec{w}_i = \vec{w}_{i-1} + \left(\vec{\varepsilon}_{i-1} \times \left(\vec{s}_{i-1} - \vec{t}_{i-1}\right)\right) + \vec{\omega}_{i-1} \times \left(\vec{\omega}_{i-1} \times \left(\vec{s}_{i-1} - \vec{t}_{i-1}\right)\right) + \left(\vec{\varepsilon}_i \times \vec{t}_i\right) + \vec{\omega}_i \times \left(\vec{\omega}_i \times \vec{t}_i\right) \tag{9}$$

where: $\dot{\theta}_i, \ddot{\theta}_i$ - the angular velocity and angular acceleration of member L_i in joint O_i.

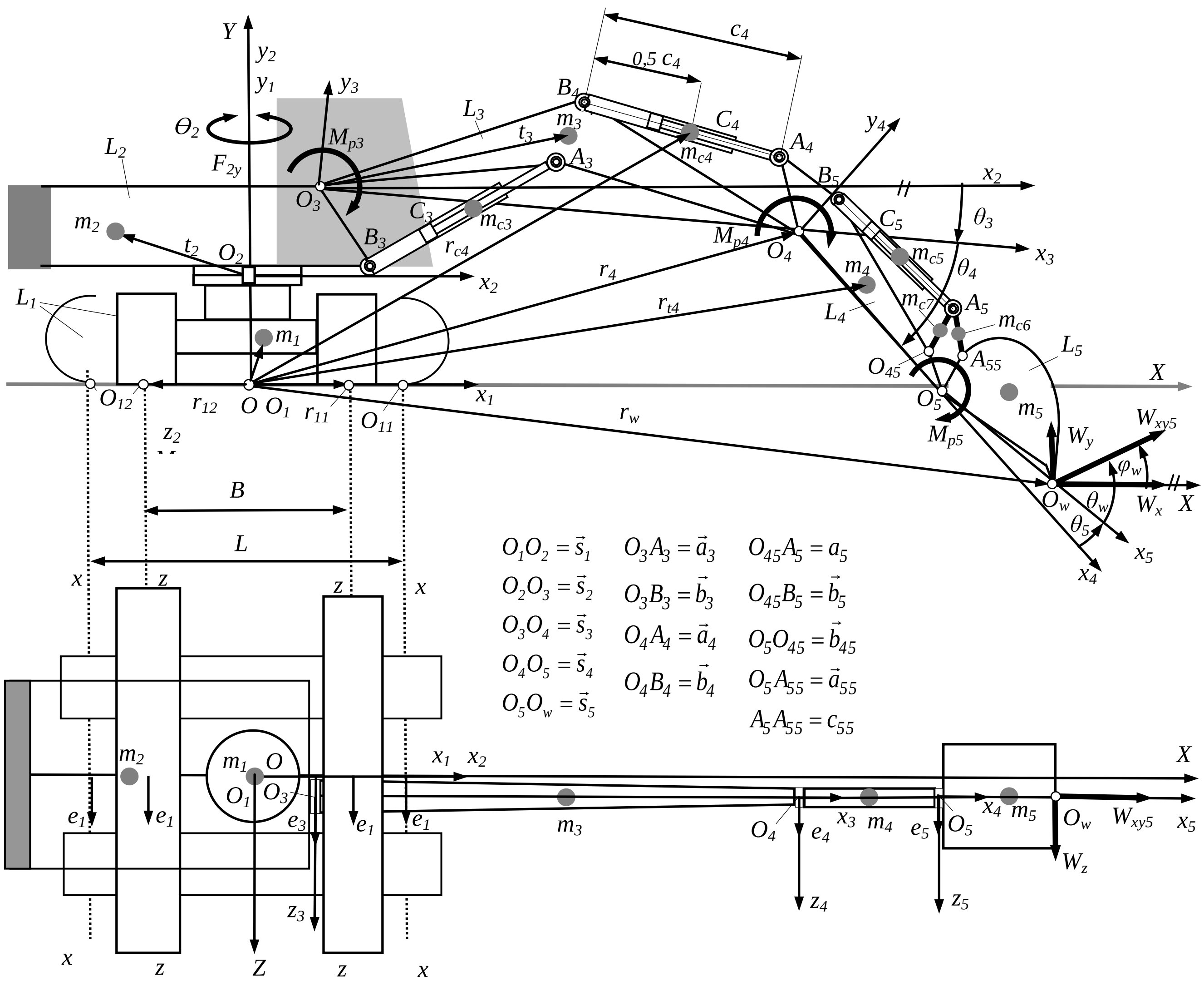

Figure 1 The mathematical model of a hydraulic excavator with bachoe attachment

Quantities of angular velocities and angular accelerations of the excavator kinematic chain members are determined on the basis of the double numerical differentiation by using the equations :

$$\dot{\theta}_i = \frac{\theta_{i(t+\Delta t)} - \theta_{i(t-\Delta t)}}{2\Delta t} \qquad (10)$$

$$\ddot{\theta}_i = \frac{\theta_{i(t+2\Delta t)} - 2\theta_{i(t)} + \theta_{i(t-2\Delta t)}}{4\Delta t^2} \qquad (11)$$

where: $\theta_{i(t)}$ – the generalized coordinate in the moment t of the duration of the digging operation, $\theta_{i(t+\Delta t)}$, $\theta_{i(t-\Delta t)}$, $\theta_{i(t+2\Delta t)}$, $\theta_{i(t-2\Delta t)}$ – the generalized coordinates (angles) in the moment of time which is larger or smaller for one or two intervals of time Δt than time t, Δt – the interval of time between the two subsequent measurements of quantities.

Dynamic quantities of member L_i are: innate force F_i, which is determined by Newton's second law:

$$\vec{F}_i = -m_i \vec{w}_i \qquad (12)$$

and the moment of innate forces M_i, which is determined by Euler's dynamic equations:

$$\hat{\vec{M}}_{ui} = -\hat{J}_i \hat{\vec{\varepsilon}}_i + \left(\hat{\vec{\omega}}_i \times \hat{J}_i \hat{\vec{\omega}}_i\right); \quad \vec{M}_{ui} = A_{io} \hat{\vec{M}}_{ui} \qquad (13)$$

3. ANALYSIS

According to the previously defined mathematical model for kinematic and dynamic analysis of the hydraulic excavators, it is necessary to measure the quantities of state (Table 1) of the excavator kinematic chain in operation under real-exploitation conditions.

Based on algorithm (Fig. 2), a program is developed to process and analyze the measured quantities using a computer. By employing the measured quantities c_i,p_{i1},p_{i2} as input data, the program first determines, in the function of the duration of the work cycle, the geometric and kinematic quantities: generalized coordinates θ_i,

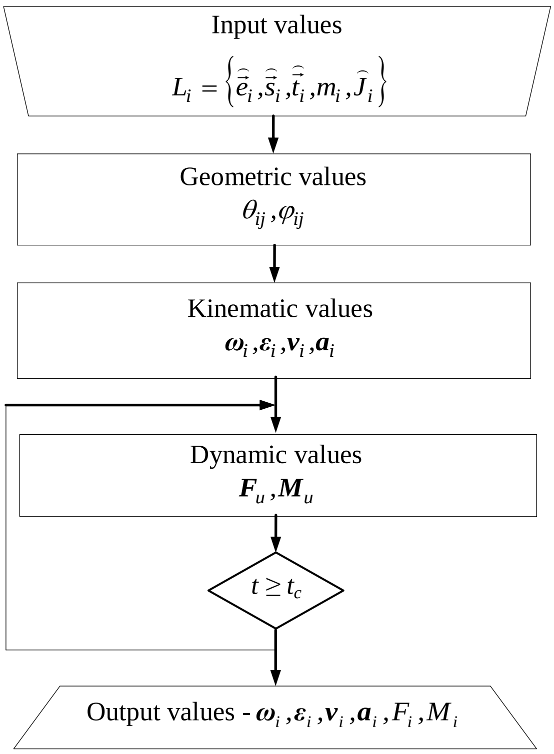

Figure 2 Algorithm of developed program

coordinates of joint centers and mass centers of chain members, angular velocities $\dot{\theta}_i$ and angular accelerations $\ddot{\theta}_i$, and linear v_i and angular ω_i velocity and linear w_i and angular ε_i acceleration for the mass center of the excavator kinematic chain members. The program further determines dynamic quantities: inertial forces F_{ui} and moment M_{ui} of chain members.

As an example, kinematic and dynamic analysis of excavator was carried out from the results of the excavator caterpillar BGH 600C, production IMK 14 Octobar - Kruševac, mass 16000 kg and power 70 kW with backhoe attachment, bucket capacity of 0.6 m^3. Tags, terms and dimensions measured values are given in Table 1. Initial state of the measured values is defined on a horizontal surface overlap of thrust-motional mechanism, with the parallel plane of symmetry manipulator and longitudinal plane of symmetry thrust-motional mechanism, when indrawn piston rod of hydraulic cylinder, and disburdened driving mechanisms. Of the total number of measurements in this study where selected and analyzed measurement for full working cycle witch content excavatirng, transporting, unloading and returning. Part of the results obtained are given in diagrams (Fig. 3) measured and specified size in a function of time duration of the whole cycle of work.

Diagrams stroke (Fig.3a) actuator drive mechanisms show that the manipulative tasks of testing performed with the movement of all three members of the manipulatorsby changing thestrokecylinder of boom c_3 (Fig. 3a) and stroke cylinder of stick $c_4$with the largest movement achieved bucket cylinder c_5. Sometimes when moving the stick there was a trajectory correction in cases when encountering an obstacle or, is caught of land steak was so large that bucket and hand digging force could not overcome created resistance digging. At the beginning and end of the digging (digging time is 6 sec.) there was a uplift (moving) thrust-motional members c_1 (Fig. 3a).

Transfer of land is carried out simultaneously by moving the boom and slewing platform excavator while unloading land is running stick of manipulator. The angle of rotation platform was relatively small θ_2 (Fig.3a) due to the action of lateral resistance digging Wz (Fig.1), whereby the hydraulic fluid acts as a hydraulic spring.

In operation of digging a gradual increase in pressure in the working lines of the drive mechanism stick of p_{41} and p_{51} (Fig. 3c) drive mechanism bucket, and return the drive mechanism boom p_{32} (Fig 3b). Pressure rises to a maximum value, at which are held for some time, and there is a decrease in the end of operation of digging. Sometimes the digging operation, due to the interruption of the excavation process, is occurring with abrupt changes of pressure in the actuators. A jump of pressure comes in lines hydromotor of slewing platform drive p_{21} and p_{22} (Fig. 3b) at the beginning of the rapid rotation of the platform from digging plane to plane excavation unloading and vice versa.

Unlike the process of digging in the open kinematic chain configuration, excavators, changes of pressure in the actuator lines have an oscillatory character. Amplitude changes in pressure to first appear at the end of the excavation process and beginning the transfer of land to be continued when emptying buckets.

Diagrams (Fig. 4a,b) the angular velocity and angular acceleration shows that the boom and stick have small changes in the valuesof angular velocity ($\dot{\theta}_3, \dot{\theta}_4$) and angular acceleration($\ddot{\theta}_3, \ddot{\theta}_4$) with respect to the angular velocity bucket ($\dot{\theta}_5$), and angular acceleration bucket ($\ddot{\theta}_5$), whose were extremely high values occurred at the end of the digging operations when closing full bucket. Character of the changes of angular velocity is close to triangular or trapezoidal shape because members of the kinematic chain manipulators with accelerated phase at the beginning, and slow motion at the end of each operation.

The diagram (Fig. 4c) shows the size of the dynamic and static forces in the joint O_3, where F_{3r} represents the resultant force.

The effect of dynamic size is expressed in the uplift thrust-motional members. Bouncy increase of force in a short interval, occurs at the beginning of the operation of transfer of material when the pressure in the pressure line drive mechanism boom p_{31} (Fig 3c) increased rapidly.

Certain load torque drive mechanism of bucket M_5 and stick M_4 (Fig. 4d) as diagrams show, the biggest, in the operation of digging, when acting mainly in a positive direction. In the boom mechanism, biggest load torque M_3 occurs most often when the digging operation, provided that the same operations are changing direction. The difference between the static load torques, determined using static and dynamic load torque is determined based on the dynamic mathematical model, appeared in the open configuration of the excavator.

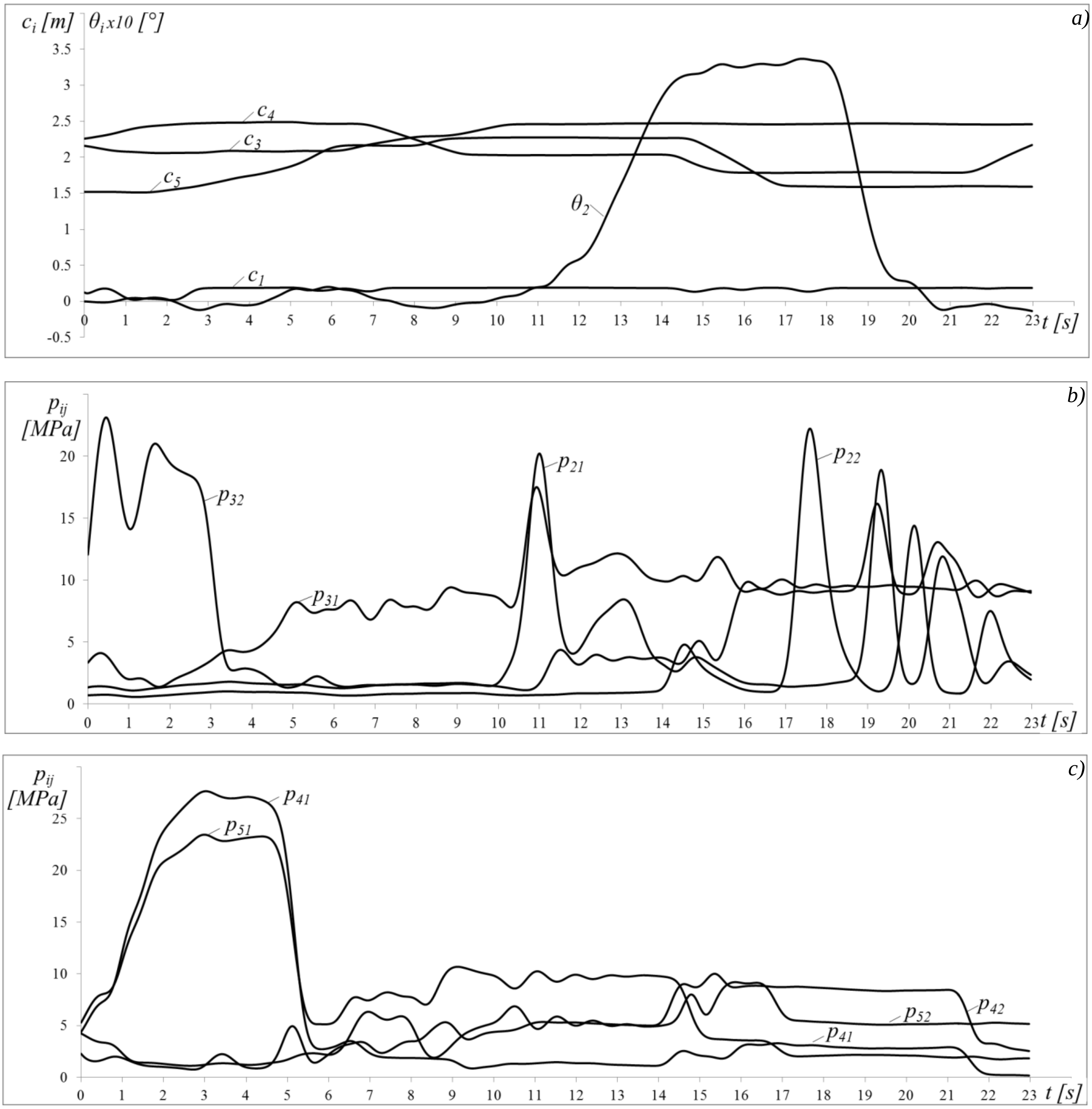

Figure 3 Diagrams of measured values: a) moving thrust – motional segment c_1 and stroke hydraulic cilinder c_3, c_4, c_5 and he angle of rotation of the platform θ_2; b) pressure in the lines actuator drive mechanism slewing platform p_{2i}, drive mechanism boom p_{3i} ; c) pressure in the lines actuator drive mechanism stick p_{4i} and bucket p_{5i}

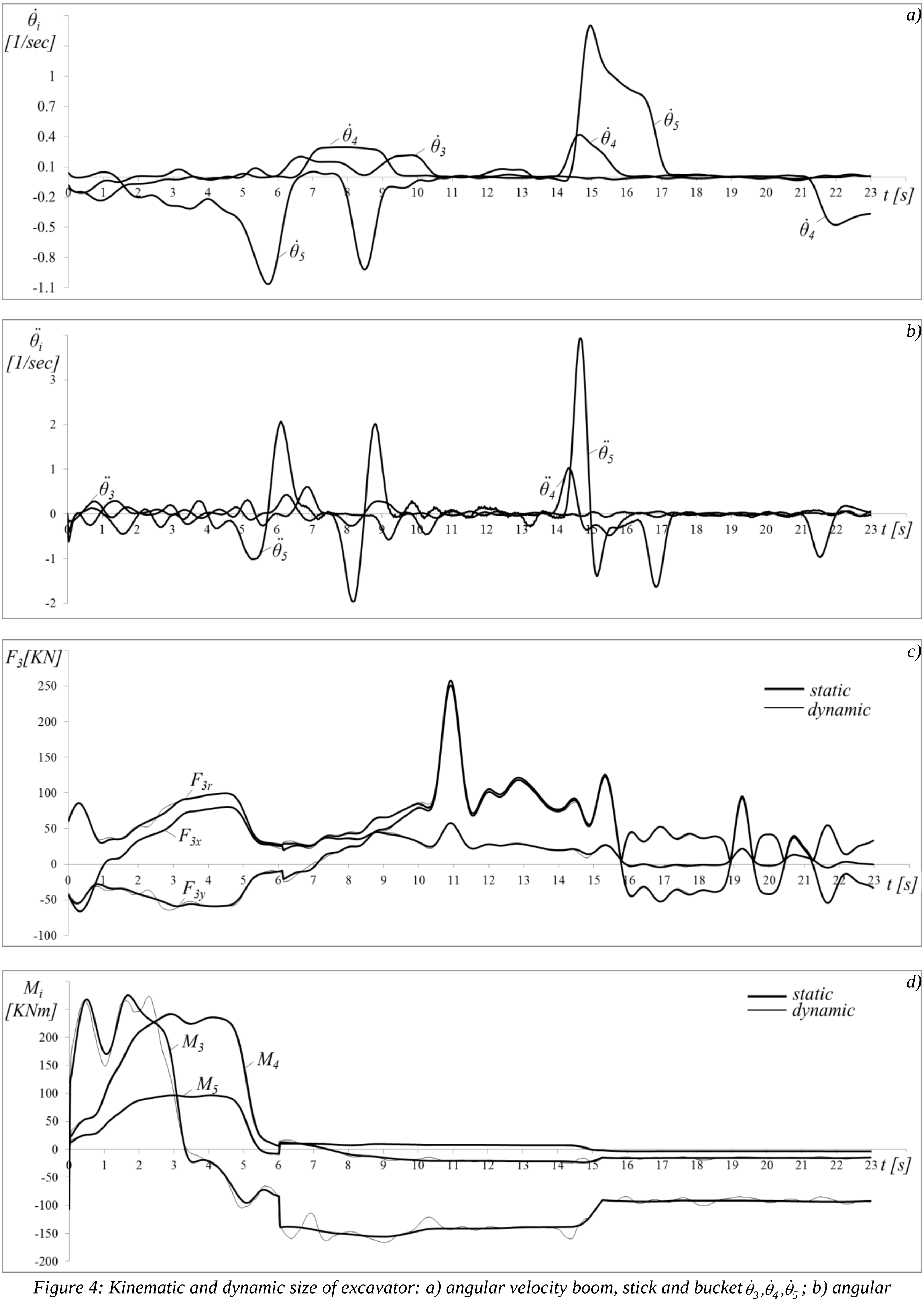

Figure 4: Kinematic and dynamic size of excavator: a) angular velocity boom, stick and bucket $\dot{\theta}_3, \dot{\theta}_4, \dot{\theta}_5$; b) angular acceleration boom, stick and bucket $\ddot{\theta}_3, \ddot{\theta}_4, \ddot{\theta}_5$; c) static and dynamic forces in the joint O_3 ; d) Static and dynamic M_3, M_4, M_5 load torque of driving mechanisms boom, stick and bucket

This occurs most often at the beginning of the operation of transfer of land at startup boom, when expressed dynamically influence, whether due to movement members of kinematic chain excavator, on load torque mechanisms. The dynamic effect is small due to the movement of members of the kinematic chain of excavator in the process of digging, because the process of digging occurs relatively slowly. The slight difference in the mechanism of boom occurs because raising a platform.

4. CONCLUSION

This paper presents the research results of kinematic and dynamic size of the hydraulic excavators with backhoe manipulator. Results were obtained by analysing the measured size of the state of operation of the excavator exploitation conditions, using the developed static and dynamic mathematical model of excavator.

Comparative analysis of the results shows that between static and dynamic quantity of state of excavator little difference in the operation of digging because of the relatively slow movement of members kinematic chain excavator with the operation.

ACKNOWLEDGEMENTS

The paper was done within the project TR 35049 financed by the Ministry of Education and Science of the Republic of Serbia.

REFERENCES

[1] D. Janošević, Projektovanje mobilnih mašina, Univerzitet u Nišu, Mašinski fakultet (2006)

[2] V. Jovanović, D. Janošević, N. Petrović, " Analysis of axial bearing load of a rotating platform drive in hydraulic excavators", Tehnički vjesnik/Technical Gazette, No.2, Vol.21., p. 263-270, (2013)

[3] D. Janosevic, R.Mitrev, B. Andjelkovic, P. Petrov "Quantitative measures for assessment of the hydraulic excavator digging efficiency ", Journal of Zhejiang University-SCIENCE A (Applied Physics & Engineering) No.13, Vol12, p. 926–942, (2012)

[4] J. Maciejewski, A. Jarzebowski, W. Trampczynski, "Study on the efficiency of the digging process using the model of excavator bucket", Journal of Terramechanics. Vol.40, p. 221–233, (2004)

SESSION B

PRODUCTION TECHNOLOGIES

Identification of Supporting Elements Dynamics of Production Machines Using Dynamics of Rigid Bodies System

Radomir Slavković[1*], Ivan Milićević[1], Nedeljko Dučić[1], Marko Popović[1], Zvonimir Jugović[1]
[1]Faculty of technical Science, Čačak, University of Kragujevac, Serbia

Modern design of the production machines treats the suspending parts as a crucial element of the effective vibration isolation. Therefore the suspending items are specifically developed and subjected to extensive tests before applied on real objects. These elements ensure accurate levelling and appropriate vibration damping. Usually selection of inadequate support element causes intensive disturbing effects in machining. The paper presents dynamics analysis of the production machine suspended on flexible mountings. The overall analysis is conceived on a rigid body dynamics. This method enables selection of an optimal supporting configuration. Further on such an effective suspension design prevents a need for expensive monitoring of the dynamic characteristics of the mechanical system, i.e. production machine and supports. The paper explores dynamics of a real, flexibly supported production machine. Results are obtained with the assistance of the "SUPPORT" software, which development is based on modal analysis theory.

Keywords: machine production, dynamics analysis, transfer function, software

1. INTRODUCTION

Technical requirements for the contemporary products quality, as well the compliance towards environmental protection regarding vibration and noise, imposed intensive research and development in machine tools dynamics. Focus of the machine dynamics studies is kept on spectrum signature and vibration severity during the machining process.

As an inevitable side effect of machining arise vibrations. They cannot be totally eliminated, though significantly reduced to an acceptable level by appropriate methodology of vibroisolation. For that reason, a core aspect of the analysis is addressed to casing dynamics, shaft and bearing dynamics, transmitting items and other components of the tool machine. A machine tool can be submitted to either active or passive insulation from the vibrations. Both the cases should be studied under vibration insulation.

Simulations and modelling are the crucial techniques for successful solving machine tool dynamics, throughout Finite Element Method (FEM), Rigid Body Simulation Method (RBS) or a Combination of FEM and RBS. Altintas et al. (2005) presented structural analysis of the machine tools implementing finite element models and their experimental calibration techniques. Multi-body dynamic allow integrated simulation of machine kinematics, structural dynamics and control techniques, as discussed in [1]. Kono et al. (2010) developed Axis Construction Kit (ACK) in order to evaluate the configuration of machine tools. The ACK supports rigid body simulations and simple elastic body simulations [2]. Anayet et al. (2009) presented a consecutive procedure in experimental and analytical modal analysis applied in structural dynamic evaluation processes of a vertical machining centre [3]. Dhupia et al. (2006) presented kinematic and dynamic abilities of the machine, including the experimental frequency response functions (FRFs) and computed stability lobes of the machine in different configurations [4]. Lorenzer et al. (2009) presented efficient modelling and analysis of different machine configurations using encapsulated sub-models, called predefined structural module models [5]. Kono et al. (2010) presented a software tool which allows the evaluation of the performance and compliance with the design requirements for machine structure at an early stage of development [6]. Law et al. (2013) presented computationally efficient methodology which improves a dynamic performance of the machine tool even at the design stage [7].

The researches, discussed above in this paper justify the use of Rigid Body Simulation Method (RBS) in the dynamic analysis of the machine tool-support. Unlike the mentioned research, this paper reveals a new methodology aiming on the software for the simulation of dynamic characteristic of the elastic support. The validity of the created software has been confirmed by the site measurements.

2. DYNAMICS OF A MECHANICAL SYSTEM

The first step in machine tool dynamic analysis is a structural modal analysis regarding one or more of three modelling methods:

a) Structure modelling by the lump masses;
b) Structure modelling by the finite elements; and
c) Structure modelling by the continuous beam.

Dynamic analysis of the machine tool, laid on a flexible mounting, is substantially based on a structure modelling by the box-shaped continuous beam. Substructure consists of other box-shaped beams of different densities. Their density depends on a size, shape, number and disposition of various items – gears, spindles, joints, holders, casing walls etc., [9, 11,]. Fig. 1 shows the example of machine tool, modelled by the set of four rigid bodies.

*Corresponding author: 65 St. Save street, e-mail: radomir.slavkovic@ftn.kg.ac.rs

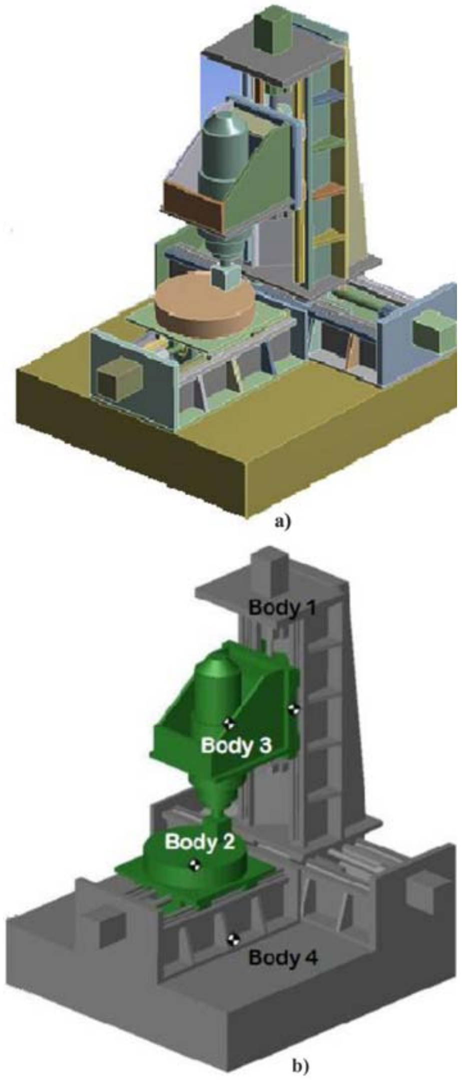

Figure 1: a) Model of machine tool; b)model of machine tool with rigid bodies

2.1. Differential equations

The machining system laid on flexible mountings in operation obeys the damped oscillations motion. This motion is described by the Eq. (1), [8, 10].

$$\boldsymbol{M}\ddot{\boldsymbol{\delta}} + \boldsymbol{B}\dot{\boldsymbol{\delta}} + \boldsymbol{C}\boldsymbol{\delta} = \boldsymbol{F} \tag{1}$$

Where the symbols denote:

$\boldsymbol{M}$ – mass matrix of the rigid body system; $\boldsymbol{B}$ – elastic-viscous damping matrix; $\boldsymbol{\delta}$ – vector of generalized coordinates of rigid bodies inertia centres;

$$\boldsymbol{\delta} = \left(\mathrm{x}_1, \mathrm{y}_1, \mathrm{z}_1, \boldsymbol{\varphi}_{\mathrm{x}1}, \boldsymbol{\varphi}_{\mathrm{y}1}, \boldsymbol{\varphi}_{\mathrm{z}1}, ..., \mathrm{x}_\mathrm{N}, \mathrm{y}_\mathrm{N}, \mathrm{z}_\mathrm{N}, \boldsymbol{\varphi}_{\mathrm{xN}}, \boldsymbol{\varphi}_{\mathrm{yN}}, \boldsymbol{\varphi}_{\mathrm{zN}}\right)^\mathrm{T}$$

$\dot{\boldsymbol{\delta}}$ – vector of generalized velocities of rigid bodies inertia centres; $\ddot{\boldsymbol{\delta}}$ – vector of generalized acceleration of rigid bodies inertia centres; $\boldsymbol{C}$ – matrix of stiffness of elastic-viscous joints ; $\boldsymbol{F}$ – vector of generalized forces.

If the vector $\boldsymbol{\delta}$ gets replaced with vector $\boldsymbol{\psi} = \boldsymbol{\psi}_0 \mathrm{e}^{\lambda_\phi t}$ expressed by Eq. (2), the Eq. (1) transforms into the Eq. (3):

$$\boldsymbol{\psi} = (\dot{\boldsymbol{\delta}}, \boldsymbol{\delta})^\mathrm{T}, \; \dot{\boldsymbol{\psi}} = (\ddot{\boldsymbol{\delta}}, \dot{\boldsymbol{\delta}})^\mathrm{T} \tag{2}$$

$$\boldsymbol{A}\dot{\boldsymbol{\psi}} + \boldsymbol{D}\boldsymbol{\psi} = \boldsymbol{F} \tag{3}$$

i.e. reduced dynamics equation, [6, 12] in which:

$$\boldsymbol{A} = \begin{pmatrix} \boldsymbol{0} & \boldsymbol{M} \\ \boldsymbol{M} & \boldsymbol{B} \end{pmatrix} \tag{4}$$

$$\boldsymbol{D} = \begin{pmatrix} -\boldsymbol{M} & \boldsymbol{0} \\ \boldsymbol{0} & \boldsymbol{C} \end{pmatrix} \tag{5}$$

$$\boldsymbol{F} = \left(\boldsymbol{0F}, \boldsymbol{F_f}\right)^\mathrm{T} \tag{6}$$

$$\boldsymbol{0F} = \left(\boldsymbol{0F}\right)_{1,\boldsymbol{i}} = 0 \; (\mathrm{i}=1,2,.....\mathrm{n})$$

$$\boldsymbol{F_f} = \left(\boldsymbol{F_f}\right)_{1,\mathrm{i}} \; (\mathrm{i}=1,2,.......\mathrm{n}) \tag{7}$$

Where symbols denote: n – degrees of freedom; $\boldsymbol{A}$ – reduced mass matrix; $\boldsymbol{D}$ – reduced stiffness matrix, and $\boldsymbol{F}$ – load vector; λ_ϕ – natural (eigen) frequencies; $\boldsymbol{\psi_0}$ – initial vector.

The basic elements of mechanical systems which form these matrices are given in Figure 2.

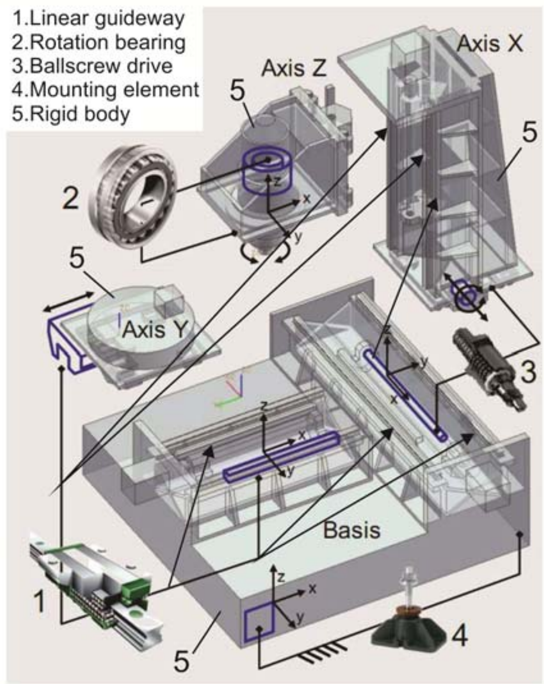

Figure 2: Elements of mechanical systems for the creation of dynamic matrices

2.2. Modal analysis

Modal analysis presented in this paper is based on the concept of a reduced dynamic equation of free damped oscillations (3), [11, 14].

An effective transformation of the dynamic Eq. (3) is accomplished applying a multiplication by the inverted matrix $\boldsymbol{A}^{-1}$. This yields the following (8):

$$\boldsymbol{A}^{-1}\boldsymbol{A}\dot{\boldsymbol{\psi}} + \boldsymbol{A}^{-1}\boldsymbol{D}\boldsymbol{\psi} = \boldsymbol{0} \tag{8}$$

If $\boldsymbol{E}$ stands for a unit matrix and $\boldsymbol{K} = -\boldsymbol{A}^{-1}\boldsymbol{D}$, then (18) transforms into (9):

$$\left(\boldsymbol{K}^{-1} - \Lambda_\phi \boldsymbol{E}\right)\psi_0 = \boldsymbol{0} \tag{9}$$

The system of Eq. (19) has a nontrivial solution for $\boldsymbol{\psi}_0$ if:

$$\det\left(\boldsymbol{K}^{-1} - \Lambda_\phi \boldsymbol{E}\right) = 0 \tag{10}$$

Solving the system of Eq. (10) an outcome contains n-pairs of eigenvalues (11):

$$\left.\begin{aligned} \Lambda_{\phi j} &= \theta_j \pm i \cdot \nu_j \ (j = 1,2,.......n) \\ \lambda_{\phi j} &= \frac{1}{\Lambda_{\phi j}} \ (j = 1,2........n) \end{aligned}\right\} \tag{11}$$

The calculus might be conducted considering a high, low or zero damping rate. The low damping rate brings the complex conjugates of the eigenvalues (λ_ϕ) into machine tool dynamics. In that case system generates minor oscillations around the stable equilibrium position. The structure should remain non-symmetric throughout modelling, to evade appearance of multiple roots. Fortunately real structures are intrinsically asymmetric, which ease the analysis. Introduction of the system of Eq. (9) into eigenvalue relation (11) results with n-pairs of eigenvectors (12),

$$\boldsymbol{\psi}_0 = \boldsymbol{\kappa} \pm i \cdot \boldsymbol{\varphi} \tag{12}$$

$\boldsymbol{\kappa}$ and $\boldsymbol{\varphi}$ are real and imaginary part of the original vector. If the solutions of the Eq. (9) are different complex conjugates, then the reduced mass matrix $\boldsymbol{A}$ and reduced stiffness matrix $\boldsymbol{D}$ can be transferred into a diagonal form. Hereby the Eq. (3) turns into global coordinates (16). The transformation is performed deploying the following matrices: modal complex conjugates $\boldsymbol{\mu}_\phi$, eigenvectors $\boldsymbol{\psi}_0$, and eigenvalues λ_ϕ, in the following manner:

$$\left.\begin{aligned} \boldsymbol{\psi}_{0z}(\lambda_{\phi r}) &= \boldsymbol{\mu}_{\phi zr} \ (z = 1,2,.....2n), \ (r = 1,2,....2n) \\ \boldsymbol{\mu}_{\phi zr} &= \boldsymbol{\mu}_{\phi R zr} + i\boldsymbol{\mu}_{\phi I zr} \end{aligned}\right\} \tag{13}$$

Introducing a global coordinate vector $\boldsymbol{q}$ presented by (14) and (15):

$$\boldsymbol{\psi} = \boldsymbol{\mu}_\phi \boldsymbol{q} \tag{14}$$

$$\boldsymbol{\mu}_\phi = \left(\boldsymbol{\mu}_{\phi z1}, \boldsymbol{\mu}_{\phi z2}, ...\boldsymbol{\mu}_{\phi z2n}\right) \ z = 1, 2, .., 2n \tag{15}$$

Involving the values from above into the Eq. (3) and multiplying it on the left hand side by $\boldsymbol{\mu}_\phi{}^T$, yields a new Eq. (16),

$$\boldsymbol{G}\dot{q} + \boldsymbol{H}q = \boldsymbol{\mu}_\phi{}^{\mathrm{T}} \boldsymbol{F} \tag{16}$$

Where the symbols denote:

$\boldsymbol{G} = \boldsymbol{\mu}_\phi{}^{\mathrm{T}} \boldsymbol{A} \boldsymbol{\mu}_\phi$ – reduced diagonal mass matrix,

$\boldsymbol{H} = \boldsymbol{\mu}_\phi{}^{\mathrm{T}} \boldsymbol{D} \boldsymbol{\mu}_\phi$ – reduced diagonal stiffness matrix,

$\boldsymbol{q}$ – global coordinate vector.

Thus the eigenvalues are obtained as (17)

$$\lambda_{\phi i} = -\frac{(\boldsymbol{H})_{i,i}}{(\boldsymbol{G})_{i,i}} \ (i = 1,2,.....2n) \tag{17}$$

2.3. Transfer function

Transfer function (18) [13] comprises the relation between Laplace z - coordinate ψz(iΩ) and p – Laplace transformation of the excitation force $F_p(i\Omega)$.

$$\left[W(i\Omega)\right]_p^z = \frac{\psi_z(i\Omega)}{F_p(i\Omega)} = \sum_{r=1}^{2n} \frac{\mu_{\phi pr}\mu_{\phi zr}}{(\boldsymbol{G})_{rr}(i\Omega - \lambda_{\phi r})} \tag{18}$$

As eigenvalues and vectors are considered as complex conjugates in this paper, the Eq. (18) transforms into the Eq. (19)

$$\left[W(i\Omega)\right]_p^z = \sum_{r=1}^{2n} \frac{\left(\mu_{\phi R_{pr}} + i \cdot \mu_{\phi I_{pr}}\right)\left(\mu_{\phi R_{zr}} + \mu_{\phi I_{zr}}\right)}{(\boldsymbol{G})_{rr}\left[i\Omega - (\theta_r + i \cdot \nu_r)\right]} \tag{19}$$

Where the following symbols denote: $\mu_{\phi Rpr}$, $\mu_{\phi Ipr}$, $\mu_{\phi Rzr}$, $\mu_{\phi Izr}$ – real and imaginary part of respective vectors, θ_r, ν_r – real and imaginary part of eigenvalues, $(\boldsymbol{G})_{rr}$ – diagonal members of the reduced diagonal mass matrix, $\boldsymbol{\Omega}$ – excitation force frequency. For the convenience of analysis if $n < p \le 2n$, the displacements are deployed, otherwise, when $p \le n$ the velocities are deployed. The stated frequency properties refer to the inertia centres of each rigid body of the modelled structure.

The coefficient of disturbances transfer from the machine to the floor is presented by the (20):

$$K_{py} = \frac{\left|F_{yi}\right|}{\left|F_p\right|} = \frac{\left|c_{yi} \cdot y_i + b_{yi} \times \dot{y}_i\right|}{\left|F_p\right|} \ (i = 1,2,.....N_s) \tag{20}$$

Where symbols denote: F_{yi} – the force transferred vertically to the floor via i - support, F_p – p-coordinate orientated disturbance, K_{py} – coefficient of the vertical disturbance transfer, c_{yi} – stiffness of the vertical i-support , b_{yi} – damping of the vertical i-support, N_s – number of flexible mountings on the floor, y_i – displacement of the supporting point i, and $\dot{y}_i$ – velocity of the point i. In the zones where the coefficient $K_{py} < 1$ an increase in vibrations has not been detected, which consequently means the suspension functions successfully.

According to the presented dynamic analysis, the software 'SUPPORT' is developed, which flowchart is given in Fig.3.

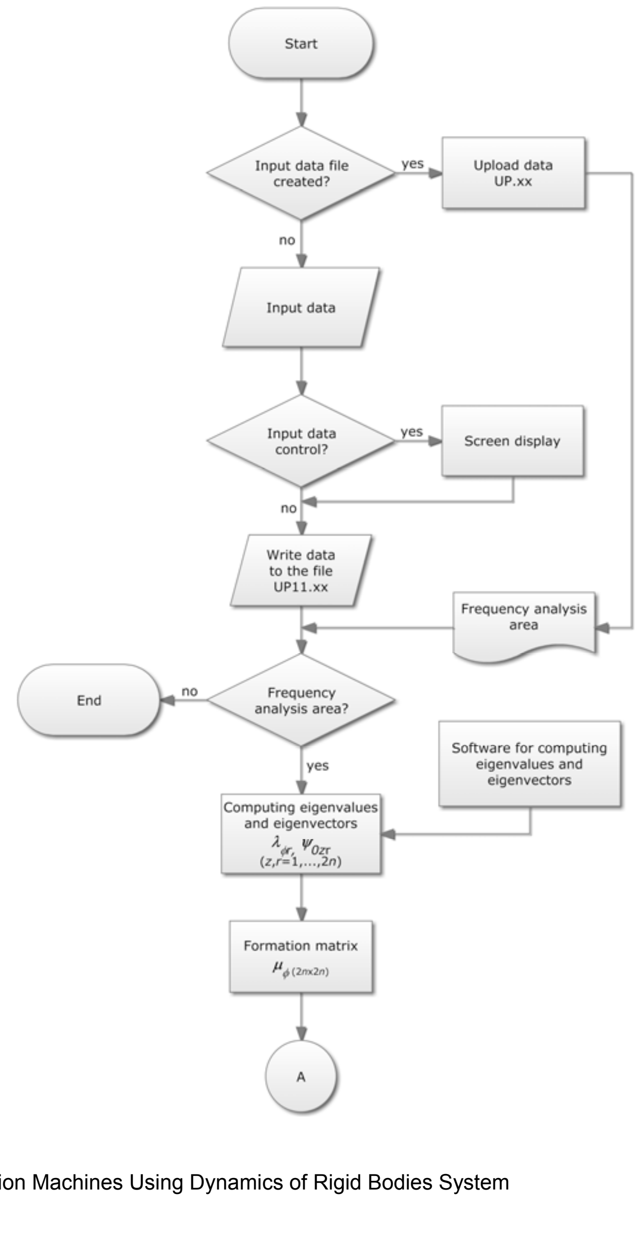

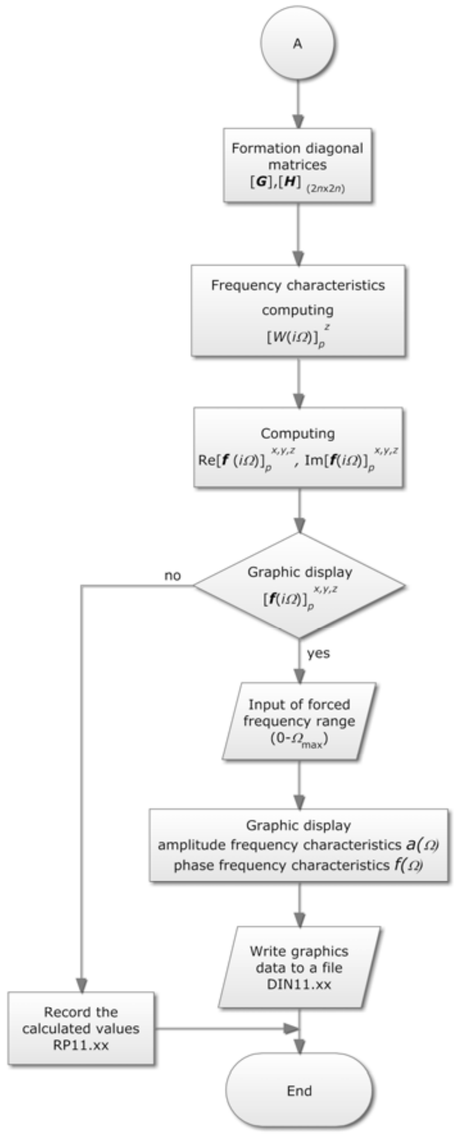

Figure 3: SUPPORT software algorithm

3. APPLICATION OF SUPPORT SOFTWARE

The results of dynamic analysis by software application SUPPORT are given on the example of founding universal milling machine KB KNUTH 2500. The machine and the discretized model are shown in Figure 4. Machine of mass m = 12000 kg, was placed on the ground via six elastic supports with stiffness $c_x=c_y=1E+06$ N/m, $c_z=2E+06$ N/m, and damping $b_x=b_y=b_z=1.5E+03$ Ns/m.

Figure 4a: Machine tool

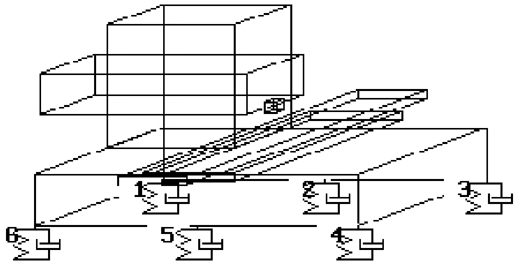

Figure 4b: Discretized model

The first three major oscillation modes of discretized model are shown in Figure 5.

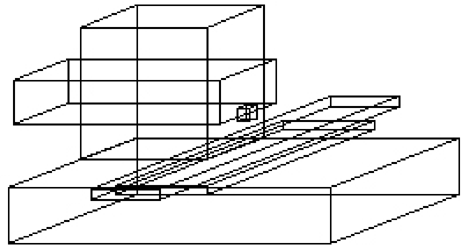

f_{01} = 4.87 Hz

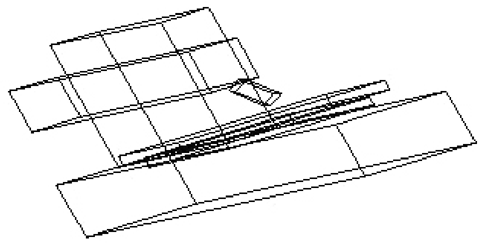

f_{02} = 6.43E+02 Hz

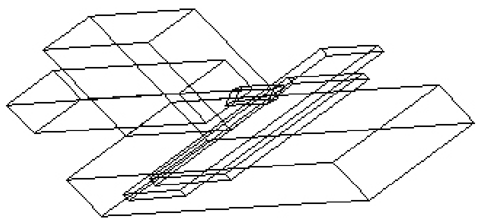

f_{03} = 7.36E+02 Hz

Figure 5: The first three major oscillation modes of modeled structure

The dynamic characteristics of the displacements in the vertical direction at the point of support 1, in the interval 0-700 Hz, are given in Figure 6.

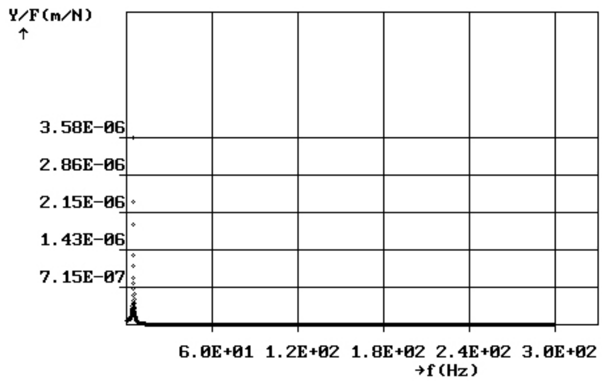

a)

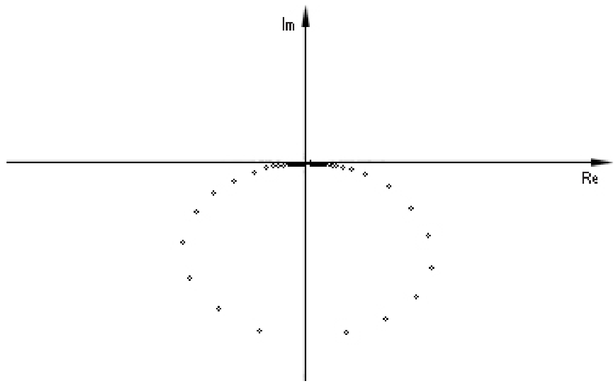

b)

Figure 6: The dynamic characteristics of the displacements in the vertical direction at the point of support 1, a) amplitude frequency and b) amplitude phase characteristics

The dynamic characteristics of the oscillation velocity in the vertical direction at the point of support 1 are given in Figure 7.

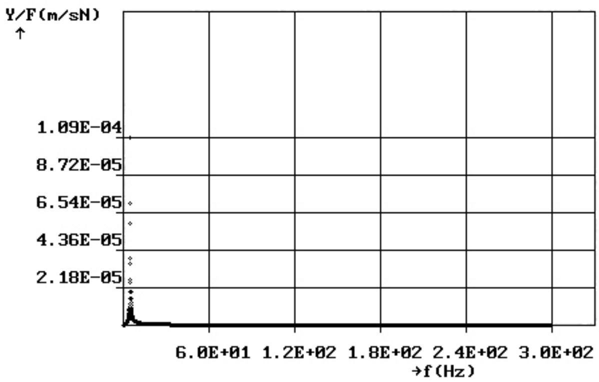

a)

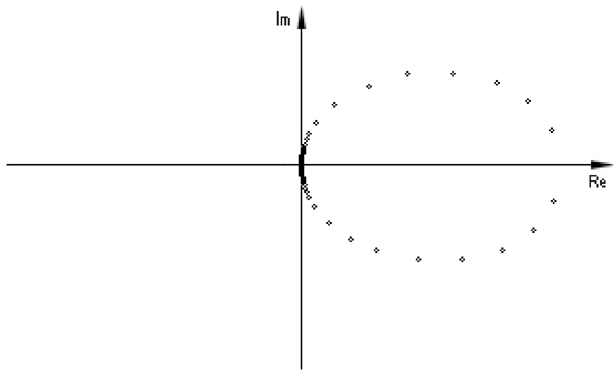

b)

Figure 7: The dynamic characteristics of the of the oscillation velocity in the vertical direction at the point of support 1, a) amplitude frequency and b) amplitude phase characteristics

From the results of dynamic analysis can be seen that in a real working range of the machine (10-60) Hz has no significant disturbances to be transmitted to the ground of the machine.

In case of intensive functioning machines in the field below 5 Hz machine should be placed on the supports with greater stiffness and damping. The process of dynamic analysis can be repeated with the new selected supports.

4. CONCLUSION

Based on a modal analysis that has been conducted throughout this paper, the SUPPORT software for the simulation of machine tool support dynamics, has been developed. This dedicated software is inspired by a theory of Multi-body dynamics, as well as the software IWF Axis Construction Kit (Institute of Machine Tools and Manufacture, ETH-Zurich) aimed for the simulation of the Machine tool dynamics. The software has been used in the first stage of selecting the elastic supports for the machine tool, deployed in the simulation of the dynamic behavior of any possible type of elastic support. Such an approach enables the selection of the most appropriate supports by their dynamic characteristics. Also, most probably, after setting the machine up on the supports chosen by this method, it would be unnecessary to adjust or verify applied suspension. Referring to the site measurements the software results diverge within (2-13%), which is a good convergence according to common engineering practice. The real operating range of the machine is (10-60) Hz, thus the frequency characteristic, in the machining process does not intensify the vibrations which can be transmitted over the support to the soil, i.e. the coefficient of the transmissibility is Kp<1. Further researches are planned to point on discrete models and sub-models, providing to the SUPPORT software a larger applicability on models with extended rate in degrees of freedom.

REFERENCES

[1] Altintas, Y.; Brecher, C.; Weck, M.; Witt, S. Virtual machine tool. // Annals of the CIRP. 54(2), (2005), pp.115.

[2] Kono, D.; Lorenzer, Th.; Weikert, S.; Wegener, K.: Evaluation of modelling approaches for machine tool design. // Precision Engineering. 34, (2010), pp. 399–407.

[3] Anayet, U. P.; Waleed, F. F.; Nurul, A. K. M.; Loh, S. K. Dynamic Modal Analysis of Vertical Machining Centre Components. // Advanced in Aciustic and Vibration. (2009). URL: http://dx.doi.org/10.1155/2009/508076.

[4] Dhupia, J.; Powalka, B.; Katz, R.; Ulsoy, G. A. Dynamics of the arch-type reconfigurable machine tool. // International Journal of Machine Tools & Manufacture. 47, (2007), pp. 326–334.

[5] Lorenzer, T.; Weikert, S.; Wegener, K. Efficient Modelling and Simulation of Reconfigurable Machine Tools Using Predefined Structural. // 3rd International Conference on Changeable, Agile, Reconfigurable and Virtual Production, 2009.

[6] Kono, D.; Lorenzer, Th.; Weikert, S.; Wegener, K Comparison of Rigid Body Mechanics and Finite Element Method for Machine Tool Evaluation. // Institute for Machine Tools and Manufacturing (IWF), Zurich, Switzerland, 2010.

[7] Law, M,; Altintas, Y.; Phani, A. S. Rapid evaluation and optimization of machine tools with position-dependent stability. // International Journal of Machine Tools & Manufacture. 68, (2013), pp. 81–90.

[8] Bishop, R. E. D.; Gladwell, M. L.; Michaelson, S. The Matrix Analysis of Vibration. // Cambridge University Press, 2008.

[9] Krodkiewski, J. Mechanical Vibration. The University of Melbourne, Department of Mechanical and Manufacturing Engineering, 2008.

[10] De Silva, C.W. Vibration and shock handbook. CRC Press, Taylor & Francis Group, 2005.

[11] Wenqing, Y.; Guangming, W.; Rongying, S.; Hongxing, H.; Dynamic equations of a multi-stage isolation system. // Int J Adv Manuf Technol. 34, (2007), pp. 1053–1061.

[12] Slater, J.C.; Inman, D.J. Transfer Function Modeling of Damping mechanisms in Distributed Parameter Models. // Mechanics Research Communications. 20(4), (1993), pp. 287-292.

[13] Kalajdzic, M. The Finite Elements Method. Faculty of Mechanical Engineering, University of Belgrade, 1984.

[14] Gawronski, W. Dynamics and Control of Structures: A Modal Approach. Springer-Verlag New York, Inc., 1998.

New Concept of Multi-Agent CAPP System in Inteligent Manufacturing Systems

Ljubomir Lukić, Mirko Djapić, Aleksandra Petrović[1], Veda Kilibarda[2]
[1]Faculty of Mechanical and Civil Engineering in Kraljevo, University of Kragujevac (Serbia)
[2]Belgrade Business School, Belgrade (Serbia)

Modern computer technology has been widely applied in the field of production engineering, design and construction, engineering calculations and analysis, generating NC code, while application of CAPP systems (computer-aided process planning) is still at initial development phase in the area of production processes design in manufacturing systems. The biggest problem in development of CAPP systems for industrial applications is modeling knowledge in the field of metal-cutting(processes.

This paper explores the modeling of technical expertise in metal-cutting processes in a form suitable for the development of CAPP system in intelligent manufacturing systems using agent-oriented software technologies. Focusing on the selection of tools and cutting parameters in the design of machining operations, we first introduce the ontology for the knowledge domain, and then in that context identify and analyze some of the challenges that CAPP presents to the multiagent system architect. In particular, we investigate interactions between operation design and setup design, examine issues arising from global impacts of local decisions in plan construction, and discuss differences between software agents and humans in comparable planning roles. The analysis leads to several multiagent design patterns that help capture domain-specific know-how and integrate it into efficient team behavior.

Keywords: Inteligent manufacturing systems, Multi-agent systems, CAPP systems, CNC systems, Technology design

1. INTRODUCTION

An effective solution for the engineering task of globally planning distributed flexible production while cutting metal can be realized by applying multi-agent architecture [1], as a new area of artificial intelligence [2]. With such systems, distributed computer agents of different specializations work cooperatively to generate a machining plan. The basis for developing a multi-agent CAPP system is formalizing technological knowledge, from technological work piece analysis, clamping, choice and order of technological operations to designing all the technological parameters of the manufacturing process and generating an NC program for tool paths during the cutting process [3], which occurs in intelligent technological systems (IMS).

2. CURENT STATE OF RESEARCH

Of late, experts dealing with looking for an efficient solution for the complex problem of planning globally distributed flexible production see a solution in applying multi-agent architecture [4], a special area of artificial intelligence that has been rapidly developing for the past years. With these systems, distributed computer agents of different specializations work cooperatively to generate a machining plan [5], [6]. Starting from the complexity of the planning the machining process and impossibility of one centralized expert system resolving such a substantial problem, eminent authors [7] had proposed a distributed environment for developing the CAPP system. Their system, CoCAPP has characteristic multi-agent architecture and is completely autonomous, meaning that it is developed independently from existing CAD/CAM systems. The CoCAPP system is projected for a simple integration with CAD/CAM systems; it's flexible to accept new technologies and methods, it can be distributed in multiple different machining centers, it's operative, modular and easily extendible. This system is one of the best known CAPP systems based on multi-agent architecture developed up till now, in the area of designing production technologies in the field of manufacturing by cutting [4]. CoCAPP as well as all other modern CAPP systems that were discussed, is characterized by a fixed multi-agent architecture where each agent has clearly defined expert knowledge for performing a specific activity within the planning process.

This paper shows the research results [8] for the development of a multi-agent model of designing CNC technologies, realized in flexible and intelligent technological systems [1].

3. BASES OF DESIGNING METAL MACHINING PROCESS BY CUTTING, BASED ON INTELLIGENT SOFTWARE AGENTS

Modern CAD, CAM and CAPP systems are based on the Machining feature concept, on which is also based the production strategy for planning clamping, designing the cutting process technology, choosing the cutting tool, designing clamping accessories. A machining feature is a technological form of processing, a parameterized geometrical body to which, apart from natural geometrical attributes have also been assigned the attributes of position, orientation, geometrical tolerance, material qualities, quality of the contact surface between the parameterized geometrical body and the rest of the machining part, as well as references to other technological types of machining within the work piece model (Figure 1).

Engineering the machining plan in technological processes of manufacturing metal by cutting, has some very significant aspects of complexity [9], which must be resolved in a multi-agent CAPP system.

*Corresponding author: Faculty of Mechanical and Civil Engineering in Kraljevo, lukic.lj@mfkv.kg.ac.rs

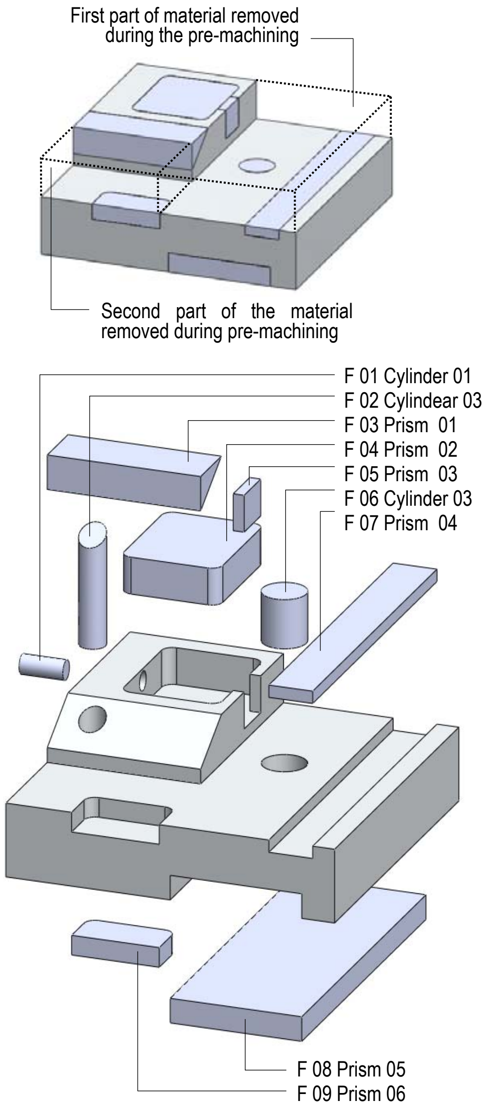

Figure 1: Machining feature and transformation of the raw material throughout the machining process

Combinatory complexity – Generating a processing plan requires the best choice in every step of the decision-making process, which can always be performed in a number of different ways, which for instance leads to a large number of variants when choosing the cutting tool for one and the same technological operation when a machining feature is being processed (Figure 2).

Technological complexity – Identifying the machining feature requires technological know-how for selecting cutting tools, defining the cutting geometry of the tool blade, defining process parameters, planning clamping, designing accessories for clamping and choosing the optimization strategy for global surveillance of all technological indicators of the machining processes in IMS (Figure 3, Figure 4).

Logical complexity – Choice of machining parameters in one step of independent decision making can have an indirect influence on the decisions in the next steps, for instance choice of cutting depth and feed has a direct impact on the intensity of the cutting forces that can be of a satisfactory level from the aspect of dynamic stability of the machining centers, but can be of high intensity for the clamping accessories (Figure 5).

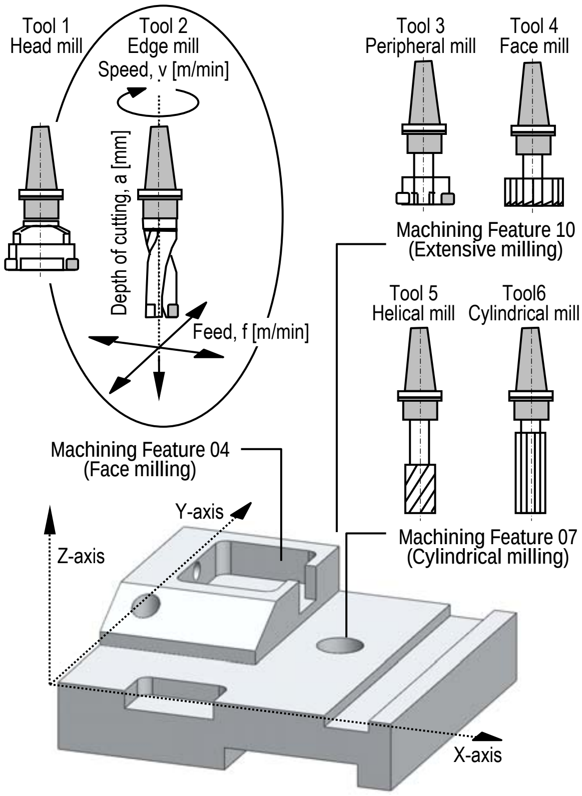

Figure 2: Combinatory complexity in engineering the technological process

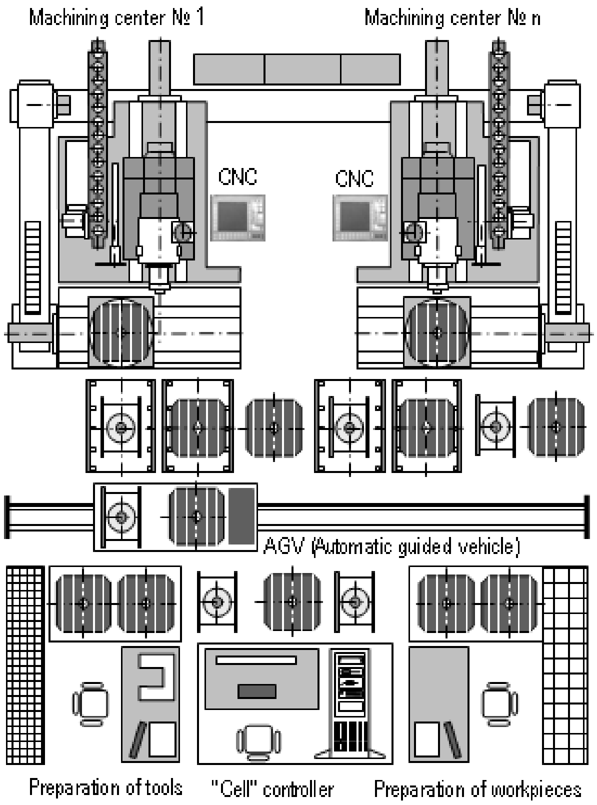

Figure 3: IMS – Inteligent manufacturing system

Social complexity – Communication and coordination requirements are greater from the CAPP system for the distributed organization of modern production, because the sources of technological know-how are even more dispersed between diverse organizations and countries with linguistic, cultural, administrative and other systems differences.

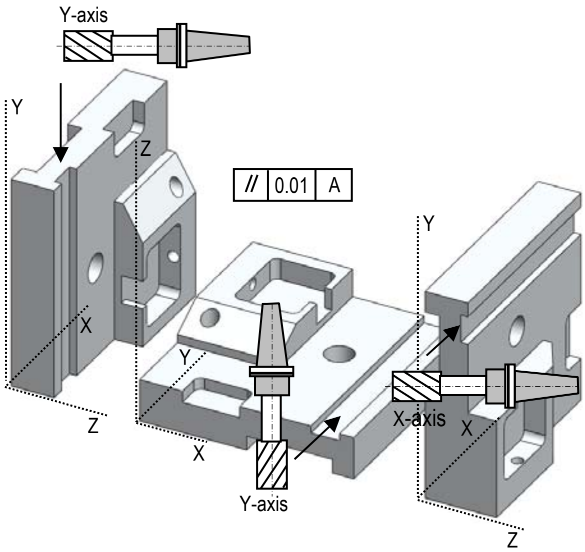

Figure 4: Technological complexity in engineering the machining plan

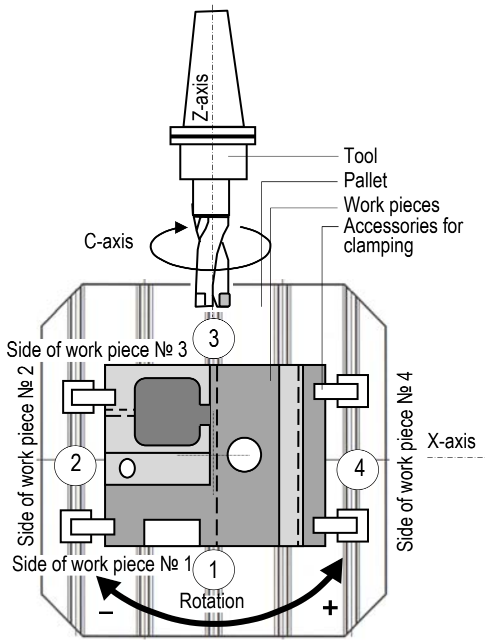

Figure 5: Logical complexity in designing the clamping and order of technological operations

The empirical nature of knowledge on phenomenological occurrences in metal machining processes – Knowledge of the technologies for metal cutting processes are based on empirical and laboratory research in combination with the analytical methods of testing machining parameters, expanding the available know-how base to a wider number of users with the assistance of Internet technologies.

Difficult formalizing of reasoning – engineer, expert immediately discusses the real options when engineering the machining plan, however, intuitive, qualitative and approximate reasoning of a human is difficult to formally express and efficiently emulate with an automated computer system.

4. MULTI-AGENT TEAM FOR ENGINEERING A MACHINING PLAN IN CUTTING PROCESSES

A multi-agent team for engineering a machining plan performs five abstract agent roles that are defined as elements of the metamodel for cooperative planning [1]. These are: the organizer, engineer, evaluator, strategist and interagent (Figure 6).

The organizer gives instructions to individual agent groups or independent agents, decides on activities for making plan elements, selects evaluation methods and plan optimization strategy and it also approves the machining plan.

The designer engineers elements of the machining plan based on technological competence and its specialization in certain phases of designing the technological process.

The evaluator calculates the values of performance indicators of the machining plan based on metrics for plan evaluation (calculates the total machining time for clamping in order to optimally plan the transport process and use the machining centers.

A strategist uses evaluation results to determine and suggest how to optimize the current version of the machining plan.

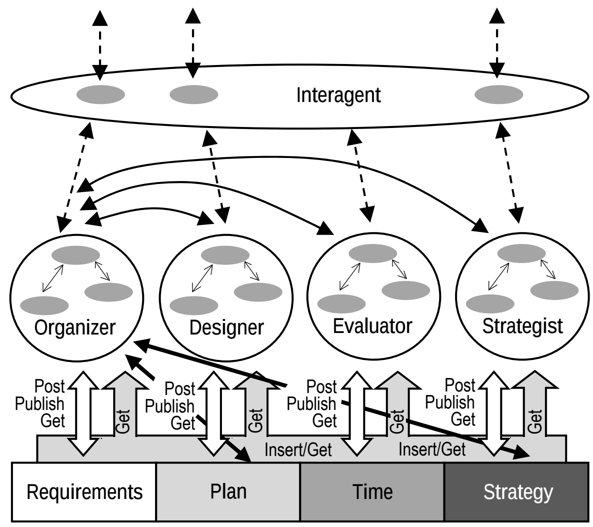

Figure 6: General architecture of a multi-agent CAPP system for designing the machining plan in cutting processes

The interagent is an active, intelligent interface according to some other segment of the production process (specialized roles like the CAD interagent or the interagent distributor are necessary to provide the dynamic interaction of the plan team with other elements of production [15].

Formally the CAPP plan multi-agent team is made up of four people

$$T = (Roles, Kom, A, \alpha)$$

where:

- *Roles*, a set of agent role instances,
- *Kom* = (*E, Prot*), communication model comprised of environment *E* and a set of protocols *Prot* with which define the mutual interactions of agent role instances and environment instances,
- *A*, is a set of agents, members of the multi-agent team and
- α: *Role* $\rightarrow$ *A,* replication, role assignment.

The main feature of rational agents is their mental state. The features of the mental state of an agent, member of the plan team for the CAPP system, reflect domain-specific knowledge and assigned role within the plan team [10]. When describing the mental states and mutual interactions of a multi-agent plan team of the CAPP system, we use the paradigm Belief-Desire-Intention [11], [4]. This entails:

- Combined beliefs,
- Combined wishes and intentions,
- Personal beliefs,
- Personal intentions,
- Relationship between combined and personal beliefs-wishes-intentions.

Defining the mental state of individual agents and agent groups is done with primitive operators (Figure 7).

(Bel i φ)	agent i believe that it is φ
(Goal i φ)	agent i has goal φ
($\tau = \tau'$)	term τ is equal to term τ'
($i \in g$)	agent i isa member of agent group g
(Agts a g)	agent group g needs to perform a series of actions a
A φ	φ applies on all paths of temporal stub A
(Happens a)	the next action that will happen is a

(M-Bel g φ**)**	agent group g believes in φ
(M-Goal g φ**)**	agent group g has goal φ
(J-Commit g φ ψ χ c**)**	agent group g has a combined commitment to goal φ in relation to motivation ψ, with preconditional χ, and custom c

Figure 7: Primitive operators of modal logic for defining the mental state of the agent and group of agents

In order to develop the agent team model, we use multi-modal logic [11]. The environment model of a multi–agent CAPP system is presented with a time tree where traveling through the tree represents the potential histories, states and environments.

A tree has its own start, the moment when the plan organizer (OP) puts the task of planning into the environment, and the end is defined by accepting a version of the CAPP system plan. Tree nodes are the environment states. Branches, representing branching over time, are marked with primitive actions that transform one state into another. Each of these primitive actions is associated with an agent or agent team [12], [13].

5. PROCEDURE FOR DEFINING THE WORK ALGORYTHM OF A MULTI_AGENT TEAM

To define the algorithm the necessary lingual elements are defined that together with graphic symbols make up an extension of standard UML activity diagrams when designing the machining plan (Figure 8).

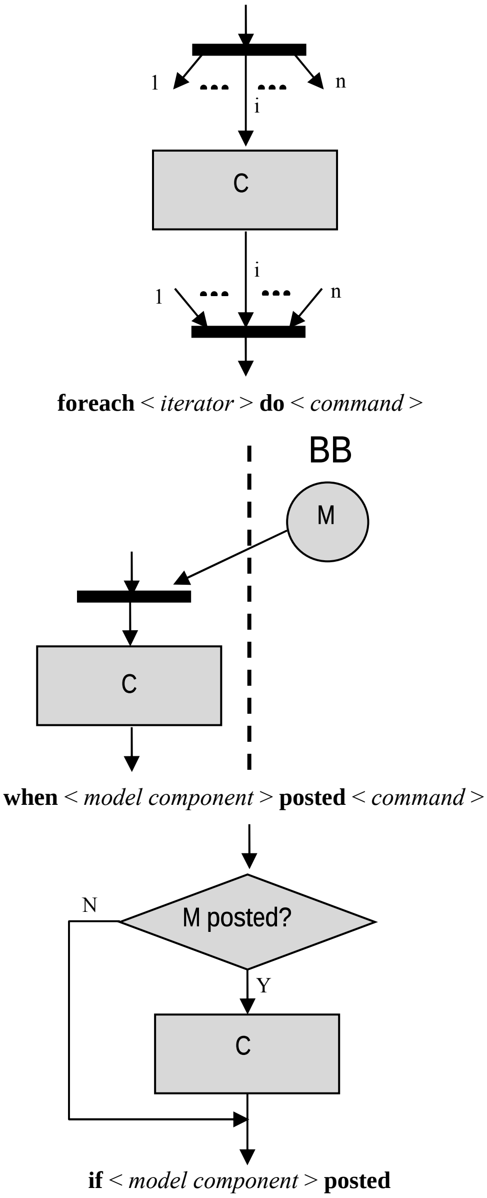

Figure 8: UML activity diagram element and pseudo code language

Apart from standard lingual elements, like ***while*** and ***for*** loops, in this pseudo code are introduced commands used for external synchronization with information being received from the blackboard. In that way, a command with syntax “**when** *m* **posted** *C*” stops the work of the agent while component *m* is not posted on the blackboard, and then continues executing *C*. The agent subscribed to component *m*, may, once having executed the ***get*** instruction, take the information from the component. Command “**when** *m* **published** *C*” has a similar meaning to command “**when** *m* **posted** *C*” except that it’s not necessary for the agent to execute command ***get*** because the value of the component is in variable *m*.

The versions of these commands that do not block executions are conditional commands "**if** *m* **posted** C_1 [**else** C_2]" and "**if** *m* **published** C_1 [**else** C_2]", where the part in square brackets is a possible option. With these commands the agent executes expression C_1 if *m* was either posted or published on the blackboard and if not, and there is no **else** option, it prolongs its normal execution flow. The existence of option **else** conditions first the execution of C_2 then the continuation of the normal flow. Another important command "**foreach** $i \in S$ **do** C^m", is actually a loop with multiple concurrent multithreaded loops that usually end on the same processor.

6. DESIGNONG THE PROCESSING PLAN

When generating the initial version of the processing plan all the agents to which have been assigned specialist roles of engineers and which make up the project sub-team have been directly included, and they are:

- Designer of the Machining Feature Model (DMFM),
- Designer for Clamping (DC),
- Designer of Clamping Accessories (DCA),
- Designer of Machining Types Model (DMMT),
- Designer of the Machining Processes Method Model (DMMPM),
- Designer for the Selection of Cutting Tools (DSCT) and
- Designer for Tool Settings (DTS).

The basic characteristics of the generative way of designing the machining plan by a multi-agent plan team from the viewpoint of decision-making activities can be summarized as follows:

1. Decisions when recognizing the machining feature.
2. Decision when choosing machining process types.
3. Decisions when designing clamping.

The task of planning the machining process can be presented as an assortment of four elements

$$T = (A, C, E, R),$$

where A is the assortment, C is the configuration of the manufacturing system, *E* the evaluation metrics and R requests. Decision making problems must be observed simultaneously in order to design an optimal solution for the machining plan for the posed technological task in conditions when the planning process becomes a combinatory problem [14], [15].

The Machining feature model (MFM) of the work piece is an integration element of all activities that preclude the production process, such as generating the work piece plan, generating the project of the clamping tools and tool plan.

In order to generate the work piece performance design (DPW) the agent uses project models from the combined environment to which he gets by perceiving the common environment.. By using personal beliefs and know-how of the rules for determining material accessories for the machining process. DMFM defines its wishes and intentions to find a favorable solution for projects of the raw material, by determining the processing accessories and generating the machining feature model (MFM), based on recognizing the elementary features that through the clamping process must be turned into chips of metal by respecting the STEP standard. It uses machining parameters to define wishes for determining geometrical shapes and material volume that needs to be removed from the raw material in order to get the shape defined by the project. It expresses intentions by decomposing the total volume into the machining feature, such as the through-hole, blind hole, ring, notches of different shapes, stepped slits etc. that can be processed with operations for removing metal chippings – i.e. drilling, chipping or milling.

Since the solution can come in several variations, MFM, DMFM publishes one of the solutions for any project model from the assortment into the space of combined beliefs while it places alternative solutions into the area of personal beliefs. Recognizing the shape and generating MFM is not a single step, but in the optimization process can be repeated, which is why alternative solutions are kept.

While DMFM is looking for a favorable solution for MFM_i, the DCA updates personal beliefs on the information about MPW_i that will enable him to achieve its purpose of determining the appropriate surfaces of the raw material for locating and clamping the work piece, i.e. the reference surfaces necessary when placing the work piece onto the work table of the machine. From multiple possible solutions, the DCA opts for one adequate solution which it posts on the BB, thereby updating the combined beliefs of the plan team. After having found favorable solutions for MFM_i, DMFM selects one and posts it on the BB, while it stores other solutions into its personal beliefs for potential future use. The machining type model (MMT) is created by copying individual machining features and their relations from MFM into one or more technological operations based on the type of the machining feature (hole, slot and so on), dimensions, tolerances and quality of the processed surface on the work piece that borders with the technological shape. Thus, for example, for the technological shape of a hole the size of 20 mm without tolerance or quality of the processed surface, the type of process used will be drilling, while in the case of a defined tolerance and quality of the processed surface center drilling-drilling-enlarging or central drilling- drilling-reaming can be used. For each technological shape, DMMT first determines the type of process (chipping, drilling and/or milling) and type of the technological operation inside the processing type, such as for instance vertical chipping or peripheral chipping (Figure 8). For this purpose the agent uses a knowledge database formed based on the model of the technological work piece processing by cutting. By using the information from an updated storage of personal beliefs about the technological shape concerned, DMMT creates wishes containing the possible types of technological operations. When forming wishes it uses know-how about the available technological system providing the feasibility of the technological operation.

To design a processing plan is required the cooperative work of several agents: organizer-strategist (OS), designer of the machining feature model (DMFM), designer of clamping (DC) and designer of model of machining types (DMMT) which work together through a blackboard (BB). Agent DMMPM has activities concerning the selection of the cutting tool (characterized by its geometry, tool material), cutting speed and feed when cutting during a given type of technological operation, work piece material and tool type.

```
agent Designer of Model of Machining Types {
    when DT posted {
        get n =BB.size of product range from 𝒜;
        get BB.machining constraints from C ;
        get BB.team goals from ℛ;
        make design criteria for machining;
    }
    foreach i ∈ {1 . . . n} do {
      when MTOi posted
         get Fi =BB.a set of index feature (MFMi);
      for f ∈ Fi do {
         get BB.descriptionof the feature(f);
         make MMT(f);
      }
      make MMTi ;
      post BB.MMTi ;
    }
}
```

Figure 9. An example of the agent algorithm pseudo code designer of machining types model (DMMT)

Numerous alternative possibilities for choosing the parameters on the level of individual operations generate a very large space for potentially satisfactory solutions, but in the agent team there must be such a decision making order to avoid a detailed elaboration of inadequate solutions. It's very important to notice as early as possible for example the incompatibility of the suggested type of technological operation and solution for clamping accessories so as not to overstep permitted forces, in order to repeat the selection of adequate machining parameters.

7. CONCLUSIONS

The further course of research refers to modeling the mental state of individual agents and agent teams, connected to the CAPP domain and its specifics. Of particular interest is research on the development of suitable learning methods that would rely on previous agent experiences and reasoning methods of agents-experts, to quickly get to the desired goal. This entails the modeling of intuitive reasoning and deduction based on the experience of particular significance for planning metal processing by cutting. From a research point of view, we need to formally specify the mental states of agents by using multi-modal logic and develop learning modules alongside the existing knowledge databases for cutting processes.

One course for future research refers to multi-agent methodology in particular. When it comes to the environment in which the agents exist, two approaches are possible for their modeling. In one approach, the environment is modeled as a passive component, while in the other it is modeled as an active component of the multi-agent team. This vagueness comes from a lack of efficient mechanisms for software modeling of the environment, which also represents a research challenge. Apart from researching the necessary mechanisms for an efficient distribution of the environment, we need to bear in mind the mobility of software agents across the internet.

REFERENCES

[1] D.Polajnar, "Multi-agent model designing of CNC technologies in intelligent manufacturing systems", PhD Dissertation, University of Kragujevac, Faculty of Mechanical Engineering in Kraljevo (2010).

[2] D.Polajnar, Lj. Lukic and, V. Solaja, "An expert system for the design of cutting processes in FMS", Proc. of Factories of the future CARS & FOF'94 conf., Ottawa, Canada, August 21-24 (1994).

[3] D.Polajnar, J. Polajnar, Lj. Lukic and M. Djapic, "Complexity Challenges in CAPP Systems and Promises of Multi-Agent Technology", Proceedings The Sixth Triennial International Conference "Heavy Machinery HM 2008", Kraljevo, 24-29 June 2008, pp.F.19-P.24.

[4] M.Wooldrige, An Introduction to MultiAgent Systems, Wiley (2009).

[5] Lj. Lukic, "Flexible Manufacturing Systems – Structure, construction, control and technology", Monographs, University of Kragujevac, Faculty of Mechanical Engineering of Kraljevo (2008).

[6] W.J.Zhang and S.Q.Xie, "Agent technology for collaborative process planning: a review", The International Journal of Advanced Manufacturing, 3(2007), pp.41-71.

[7] F.L.Zhao, S.K.Tso and P.S.Y.Wu, "A cooperative agent modeling approach for process planning", Computers in Industry, 41(2000), pp.83-97.

[8] Lj.Lukic, D.Polajnar and V.Solaja, "A Yugoslav approach to decision support for optimization of FMS technologies", In Annals of the CIRP, vol. 40 (1991)1, pp. 99–102.

[9] V.Solaja, M.Dimitric and Lj.Lukic, "On the Two Cases of Yugoslav Attempts in Adaptive Control", Robotics & Computer Integrated Manufacturing 4(1988)1/2, pp.241-244.

[10] D.Polajnar, J.Polajnar and Lj.Lukic, "Metamodel Abstractions of Agent Roles in Cooperative Process Planning", Proc. IEEE SMC Int. Conf. on Distributed Human-Machine Systems, (2008), pp. 77-82.

[11] A.Rao and M.Georgeff, "BDI-agents: from theory to practice", Proceedings of the First International Conference on Multiagent Systems, San Francisco (1995), pp.185-204.

[12] F.Zambonelli, N.Jennings and M.Wooldridge, "Developing multiagent systems: The methodology", ACM Transactions Software Engineering Methodology, 12 (2003)3, pp 317-370.

[13] C.Carrascosa, J.Bajo, V.Julian, J.Corchado and V.Botti, "Hybrid multi-agent architecture as a real-time problem-solving model", Expert Systems with Applications, 34 (2008)1, pp 2-17.

[14] P. Dutta, N.Jennings and L.Moreau, "Cooperative information sharing to improve distributed learning in multi-agent systems", Journal of Artificial Inteligence Research 24 (2005), pp. 407–463.

The Use of Biologically-inspired Algorithms for the Optimization of Machining Parameters

Goran Miodragović[1]*,, Radovan Bulatović[2], Slobodan Ivanović[1], Marina Bošković[2]
[1] College of Applied Professional Mechanical Studies , Trstenik (Serbia)
[2] The Faculty of Mechanical and Civil Engineering in Kraljevo of the University in Kragujevac, Kraljevo (Serbia)

This paper proposes the application of biologically -inspired algorithms to determine optimal parameters of metal cutting . The objective functions are operation time, cost per product, and surface roughness. Model of metal cutting is non-linear , constrained problem.As an example of biologically -inspired algorithm for solving optimization problems , in this paper we have applied the Cuckoo search algorithm , and the Firefly algorithm. Contemporary analysis of these two methods , as well as their hybridization and the experimental results show that the use of biologically -inspired algorithms is applicable to parameter problems optimization of metal cutting.

Keywords: Cuckoo Search algorithm, Firefly algorithm, Hybridization, Machining parameters, Non-linear optimisation, Optimization

1. INTRODUCTION

Economical machining has always held an important place in determining the machining parameters. In practice, technologists and operator on the machine selected processing parameters on the basis of either their experience or using information from a database or from catalog of tools. However, there is rarely such values do often do guarantee the effectiveness of data processing or minimal processing costs. Processing costs minimization involved in how to determine includes the cutting speed, step and depth of cut, which will give optimum results.

When setting these parameters, special attention is given to the constraints that are characteristic for the chosen method of cutting, or that are determined by the machining method, machine tools, tools and workpiece. These constraints, among others, includes: a tool - resistance; cutting force, required cutting power, the stability of the cutting zone, temperature field in the cutting zone, dimensional accuracy, surface quality, as well as the relationship between rough and finish machining.

There are a number of methods to deal with techno-economic optimization of machining parameters. Some of these methods are concerned only with the machining in single pass. Parameters which have to be optimized, in this case, are the cutting speed and the feed rate. It is assumed that in this single pass, estimated depth of cut which is at the same time the maximum possible, what in most cases is not so. In other methods, the optimized parameters are either the number of passes (at a constant depth of cut) or the cutting depth per pass and cutting speed and feed rate. For this method of optimization (cost minimization or profit maximization), there are a variety of techniques, such as differential calculus, regression analysis, linear programming, geometric programming and stochastic, computer simulation.

Some of these methods do not consider previously mentioned constraints, because a large number of constraints complicates the problem of optimization of machining parameters using classical (deterministic) methods. Deterministic methods are used in cases where the objective function has no several local minima, there is no point where the gradient is not defined, or where the objective function is continuous. In situations where the objective function has many local minima, where there are a points where the gradient is not defined, and the objective function is discontinuous, heuristic methods such as genetic algorithms, simulated annealing, particle swarm optimization, Cuckoo Search algorithm, the Firefly Algorithm are used.

Heuristics means the way when we use trial and error to come to an acceptable solution. Metaheuristics algorithms represent a more advanced type of heuristic algorithms. These algorithms use a certain compromise between the random and local search. Metaheuristics algorithms have two important features: the intensification and diversification. Diversification means the search at the global level, while the intensification is based on the search at the local level. Algorithms are divided into the algorithms based on population and algorithms based on trajectory.

In this paper, we propose the use of hybrid algorithm, the firefly and cuckoo searches in optimizing the parameters of metal cutting.

2. FIREFLY ALGORITHM

Firefly algorithm was first developed by Xin-She Yang, 2007a. [1]. This algorithm is inspired by the behaviour and movement of fireflies in nature. Yang showed the superiority of this algorithm over the existing traditional optimization algorithms. Yang believes that each swarm can be associated with a Lévy flight. Thus, Lévy flight firefly algorithm is formulated.

2.1. The behaviour of fireflies

There are about 2000 species of fireflies and they mainly inhabit temperate and tropical regions. Most of them produces a brief flash that creates a beautiful sight in the sky. Method of sowing is characteristic of each

*Corresponding author: College of Applied Professional Mechanical Studies Trstenik, Radoja Krstića 19, 37240 Trstenik, Serbia, mijac037@yahoo.com

species. Basic functions of sowing are attracting partners (communication) and to attract potential victims. Also, seeding can be a warning sign. Females respond to a unique method of sowing the male within the same species. In some species the females can mimic the way planting other species in order to lure and ate males.

Planting firefly can be formulated as a method for the realization of the objective function optimization.

2.2. Explanation of the algorithm

Firefly algorithm can be considered as metaheuristics algorithm based on the swarm of fireflies and inspired by sieving. It is presented as an iterative procedure based on the numerical population. Factors interact with each other by means of sowing (natural light) which allows them to search the premises of the objective function . Appropriates it is a solution in which factor - firefly glowing in proportion to its quality, in the considered problem. Each firefly attracts partners, regardless of sex, and thus build the search space, which is much more efficiently searched.

It is necessary to define two key things in this algorithm: first the changes in planting and second the attraction, [1].

In the simplest case, sifting fireflies, and at a certain location x can be written as:

$$I(x) \propto f(x) \tag{1}$$

The appeal of β is relative and it varies with the distance r_{ij}, between firefly i and j. In addition, the intensity decreases with seeding distance from the source, because the absorption is carried out in air. We can see that the attraction varies in proportion to the degree of absorption. The intensity of planting varies inversely proportional to the law:

$$I(r)=I_s / r^2 \tag{2}$$

where I_s is the intensity of the light source. The intensity of screening and (r) varies with distance r monotonically and exponentially . For a given environment with a fixed absorption coefficient of light will be:

$$I = I_0 e^{-\gamma r} \tag{3}$$

where I_0 is the intensity of the actual planting . The value of γ represents the change in attractiveness with increasing distance from the switch. The parameter γ is an important part in determining the speed and convergence behaviour of the algorithm with the firefly. There are two limiting cases when $\gamma \to 0$ and $\gamma \to \infty$. When $\gamma \to 0$ the attraction has a constant value of $\beta = \beta_0$. In the case when $\gamma \to \infty$ attraction is close to zero, corresponding to a completely random search. In many embodiments typically ranges from 0.01 to 100.

To avoid the singularity at $r = 0$ in the expression using Gaussian I_s/r^2 formula:

$$I = I_0 e^{-\gamma r^2} \tag{4}$$

The attractiveness of a firefly is proportional to the intensity of screening and can be defined by the equation:

$$\beta = \beta_0 \cdot e^{-\gamma r^2} \tag{5}$$

where is r the distance between two of the firefly and β_0 is their attraction when $r = 0$.To calculate the exponential function takes longer than the computation rate $1/(1+r^2)$. Therefore, if necessary, the previous relation can be approximated as:

$$\beta = \frac{\beta_0}{1+\gamma r^2} \tag{6}$$

The characteristic distance is based on the last two relations can be defined as $A = 1/\gamma$. Above this value the attraction is significantly changed.

The reality is attractive function $\beta(r)$ monotonically decreasing and can be represented as:

$$\beta(r) = \beta_0 e^{-\gamma r^m} \tag{7}$$

For fixed γ characteristic distance becomes :

$$\Gamma=\gamma^{-1/m} \to 1,\ m \to \infty \tag{8}$$

The distance between two of the firefly i and j x_i and x_j, respectively , is defined as the distance Descartes :

$$r_{ij} = \left\| x_i - x_j \right\| = \sqrt{\sum_{k=1}^{d} \left(x_{i,k} - x_{j,k} \right)^2} \tag{9}$$

where x_i , k-th component of the spatial coordinates x_i the i-th switch.

The movement of i-th firefly is attractive another more brilliant firefly j and is defined as :

$$x_i = x_i + \beta_0 e^{-\gamma r_{i,j}^2} \left(x_j - x_i \right) + \alpha \varepsilon_i \tag{10}$$

In equation (10) the second member is determined on the basis of attractiveness , while the third member is random (random) character. In the third article mentioning a vector random variable ε_i which is taken from a Gaussian or uniform distribution .

In accordance with the above principles can be established optimization algorithm firefly , Figure 1., [1].

```
Start
  The objective function f (x), x = (x1, ..., xd) T
  Generating population firefly xi (i = 1, 2, ..., n)
  Define the absorption coefficient γ sowing
  while (t <MaxGeneration)
     For i = 1: n (n all firefly)
       For j = 1:i ( n all firefly )
          The intensity of the sowing Ii xi determined by f (xi)
          If (Ij> Ii)
             Move firefly i towards j firefly
               using equation (10)
          end
          Attractiveness varies with distance r via
          exp [-γr2]
          Generate new solutions and update intensity sowing
       End of j
     End of i
    Sort fireflies and find the current best
  End of while loop
  Results and observations
End
```

Figure 1: Pseudo code. Optimization firefly algorithm

3. CUCKOO SEARCH ALGORITHM

Cuckoo Search (CS) is also metaheuristics optimization algorithm, inspired by the biological behavior of a cuckoo searching for a nest where they can lay their eggs. This algorithm, as proposed by Yang and Deb.

3.1. The behavior of Cuckoo

Cuckoo lay their eggs in the nests of other birds and bird hosts take care of the egg, and then chicken. Cuckoo usually chooses birds nest in which eggs are already set, so you can be sure that the first chicken hatched from an egg chicken. Some species are adapted to the cuckoo lay their eggs in the nests of other birds, so their eggs are very similar to the eggs of birds of the host. When hatched cuckoo chick, it instinctively pushed out of the nest eggs or chicks bird host in order to receive all the food from the new "parents" . In addition cuckoo can mimic the call of birds species in whose nest is located. If, finally, the bird hosts realize that it is in their set are the cuckoo's nest, they either remove or abandon the nest.

3.2. Explanation of the algorithm

In this optimization algorithm, each nest represents a potential solution. The cuckoo reproduction process in the algorithm is simplified by three rules, [4]:

1. Each cuckoo lays an egg in a randomly chosen nest;
2. The best nests carry over to the next generation of cuckoos;
3. The number of available host nests is fixed (limited), and the egg laid by a cuckoo is discovered by the host bird with a probability pa, which ranges [0,1]. Birds can detect only the worst nests so that they are losing from the population.

CS has a simple algorithm, and its code is given in Yang and Deb (2010), [4]. The initial population of nests with the size n, which are randomly distributed over the search space, is generated first. The randomly chosen initial solutions of design variables are defined in the search space by the lower and upper boundaries.

The new nest, for example *i-th*, is generated according to the following law

$$x_i^{(t+1)} = x_i^{(t)} + \alpha \otimes \text{Lévy}(\lambda) \tag{11}$$

where $\alpha>0$, is the step size whose value depends on the optimization problem, and t is the current generation. Step size is multiplied by the random numbers with Lévy's distribution, and such random motion is called Lévy flight.

In this research work [4] a Levy flight in which the step-lengths are distributed according to the following probability distribution:

$$Le'vyu = t^{-\lambda} \quad 1 < \lambda \le 3. \tag{12}$$

In standard CS algorithm [4], parameters p_a and α are very important in fine tuning of solution vector and appropriate selection of their values can result to the global solutions. However, values of these parameters are constant in the standard CS algorithm, Fig. 2.

Valian et al. (2013), [5], have introduced dynamic changes of these parameters in each generation, in solving complex engineering problem. If the value of probability p_a is small, and the value of parameter α, which represents step size, is large, such values can result in very slow convergency in CS algorithm. Otherwise, if the value of p_a is large and the value of α is small, the speed of convergence is very fast and algorithm can not find the best solution.

The idea of ICS algorithm is that these parameters are adjustable in each generation, because in that way better solutions of algorithm can be achieved.

```
Begin
The objective function f(x), x=(x1,x2,...,xd)^T
Generate initial population of
   n host nest xi (i=1,2,...,n)
While (t < MaxGeneration) or (stop Criterion)
      Get a cuckoo randomly by Lévy flights
      Evaluate its quality/fitness Fi
      Choose a nest among n (say. J) randomly
      If (Fi > Fj)
            Replace j by the new solution
      End If
      A fraction (pa) of whore nests are abandon
      And a new ones are built
      Keep the best solutions (or nests with quality solutions)
      Rank the solutions and find the current best
End while
```

Figure 2: Pseudo code. Optimization Cuckoo search algorithm

4. HYBRID OPTIMIZATION ALGORITHM (CUCKOO SEARCH AND FIREFLY)

Hybridizing algorithm means are combination of analyzed optimization algorithms (Cuckoo search and Firefly algorithm).

In this paper, the proposed algorithm is obtained so that the Cuckoo search algorithm implements part of Firefly algorithm. In the classical Cuckoo search algorithm, Fig 2, when is reached the probability of finding the worst nest (p_a), it nest is leaving and these nest is assigned a new value for a random distribution. In the proposed algorithm, instead of "abandoning" the worst nests, reducing the probability of finding the worst nests installing firefly algorithm, Fig. 3. In other words, "bad nest" is replaced with the best firefly.

```
Begin
The objective function f(x), x=(x1,x2,...,xd)^T
Generate initial population of
   n host nest xi (i=1,2,...,n)
While (t < MaxGeneration) or (stop Criterion)
      Get a cuckoo randomly by Lévy flights
      Evaluate its quality/fitness Fi
      Choose a nest among n (say. J) randomly
      If (Fi > Fj)
            Replace j by the new solution
      End If
         Firefly algorithm
      Keep the best solutions (or nests with quality solutions)
      Rank the solutions and find the current best
End while
```

Figure 3: Pseudo code. Hybrid Optimization Cuckoo search & FireFly algorithm

5. OPTIMIZATION MODEL

The main objectives in the optimization of machining processes are reducing processing costs, increasing productivity and profits. Of course, it is possible to combine these goals and then approaches to solving optimization problems with multiple objectives. By accessing the optimization problem, it is necessary to acquire the necessary knowledge about the process. To set the optimization model it is necessary to define: the objective function, the function of the process conditions, functions and limitations of optimization criteria. In machining processes, the most common functions of the state are: force (resistance) cutting, cutting power, cutting temperature, tool wear, tool life and surface quality. As the objective function: processing time, processing costs, processing accuracy, productivity, cost, profit are usually taken Restrictions relating to performance of machine tools, tools and work piece are set as function limitations [10]. The criteria of optimization are usually: minimization of time and processing costs or maximizing productivity and profits or maximum surface quality, Fig. 3.

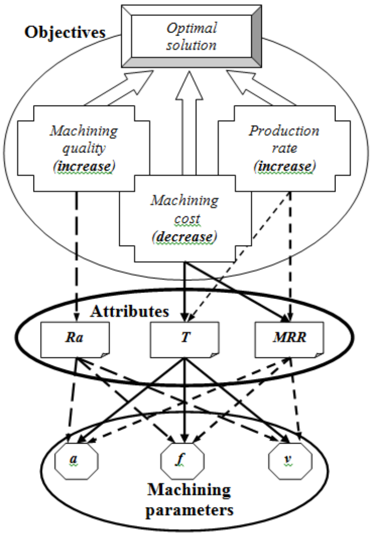

Figure 3: Representation structure of the objectives, attributes and cutting parameters

Without going into the details of generating optimization models, as a base for verification of the proposed hybrid optimization algorithm, a model that aims to reduce costs and processing time is presented and raise productivity,.

The parameters that can be optimize are cutting speed (v), feed rate (a) and the cutting depth (a), [10].

5.1. Operation time

Operation time is measured as the entire time necessary for the manufacture of a product (T_P). It is the function of the material removal rate (*MRR*) and of the tool life (*T*) [10]:

$$T_P = T_S + V_{RM} \cdot \frac{1 + \frac{T_C}{T}}{MRR} + T_i \tag{13}$$

where is T_s the tool set u time, T_C the tool change time, T_i idle time between two consecutive cuts, *T* tool life and V_{RM} the volume of the removed material. In some cases the T_s, T_C, T_i and V_{RM} are constants so that *T* is the function of *MRR* and *T*.

The material removal rate can be calculated using the following equation [10]:

$$MRR = 1000 \cdot v \cdot f \cdot a \tag{14}$$

where is *v* the cutting speed, *f* feeding rate and *a* cutting depth.

The tool life is measured as the average time between the tool changes or tool sharpenings. The relation between the tool life and the parameters is expressed with the well known Taylor's formula [10]:

$$T = \frac{k_T}{v^{a_1} \cdot f^{a_2} \cdot a^{a_3}} \tag{15}$$

where k_T, a_1, a_2 and a_3, are constants relevant to a specific tool-workpiece combination [10].

5.2. Operation cost

The operation cost (C_P) can be expressed as the cost per product, as follows [10]:

$$C_P = T_P \cdot \left(\frac{C_t}{T} + C_l + C_0 \right) \tag{16}$$

where is T_P necessary time for the manufacture of a product, *T* tool life, C_t the tool cost, C_l the labour cost and C_0 overhead cost.

5.3. Cutting quality

The most important criterion for the determination of the surface quality is roughness [10]:

$$R_a = k \cdot v^{k_1} \cdot f^{k_2} \cdot a^{k_3} \tag{17}$$

where k_1, k_2, k_3, and *k* are constants relevant to a specific tool-workpiece combination.

5.4. Constrains

Space solutions to be scanned in the search for the optimum conditions when routing is limited by technological and practical requirements relating to the installed power of machines (*P*), the maximum cutting force (*F*), the available range of steps (f_{min} - f_{max}) and cutting speeds (v_{min} - v_{max}) on the machine and the maximum, a_{max}, and minimum, a_{min}, cut depth.

$$P = \frac{F \cdot v}{6122 \cdot \eta} \tag{21}$$

where *F* is the cutting force, *v* cutting speed , η efficiencies.

As we mentioned feed rate and speed must match the range of the selected machine and cutting depth can not exceed a given range:

$$f_{\min} \le f \le f_{\max} \tag{22}$$

$$v_{\min} \le v \le v_{\max} \tag{23}$$

$$a_{\min} \le a \le a_{\max} \tag{24}$$

5.5. The objective function

The task here is to find the optimum cutting conditions involving the same three decision variables: speed (v), feed rate (f), and cut depth (a). The objectives are operation time, cost per product, and surface roughness, which all must be minimized for a better machining operation.

In the case of many incomparable and contradictory objectives the ideal solutions satisfying all requirements are very rare. In order to ensure the evaluation of mutual influences and the effects between the objectives it is recommendable to determine the multi-attribute function of the manufacturer (*F*) representing the company's/ manufacturer's overall preference. The following manufacturer's implicit value function [10,13] is selected:

$$F = 0.42 \cdot e^{-0.22 \cdot T_P} + 0.36 \cdot e^{-0.32 \cdot C_P} + 0.17 \cdot e^{-0.26 \cdot R_a} + \frac{0.05}{1 + 1.22 \cdot T_P \cdot C_P \cdot R_a} \tag{25}$$

6. THE EXPERIMENTAL RESULTS

The machining operation considered here is a turning process of machining a cast steel blank using NC lathe with a HSS cutting tool. The multi-objective formulation is given below [10,13]:

{following three objective functions

Minimize $F_1(x) = T_P(x)$

Minimize $F_2(x) = C_P(x)$

Minimize $F_3(x) = R_a(x)$

are replaced with single objective function}

Minimize $F(T_P, C_P, R_a)$ from Eq. (25)

subject to $g_1(x) = 1 - \dfrac{P(x)}{P_{\max}} \geq 0$

$$g_2(x) = 1 - \frac{F(x)}{F_{\max}} \geq 0$$

$70 \leq v \leq 90$ (m/min)

$0.1 \leq f \leq 2$ (mm/rev)

$0.1 \leq a \leq 0.5$ (mm)

$P_{max} = 5\ kW$

$F_{max} = 230\ N$

where:

$$T_P(x) = 0.12 + 2313.76 \cdot \left(\frac{1 + \frac{0.26}{T(x)}}{MRR(x)} \right) + 0.04$$

$$C_P(x) = \left(\frac{13.55}{T(x)} + 0.39 \right) \cdot T_P(x)$$

$$R_a(x) = 1.001 \cdot (v^{0.0088} \cdot f^{0.3232} \cdot a^{0.3144})$$

$$T(x) = 1575134.21 \cdot (v^{-1.7} \cdot f^{-1.55} \cdot a^{-1.22})$$

$$MRR(x) = 1000 \cdot v \cdot f \cdot a$$

$$F(x) = 1.38 \cdot f^{1.18} \cdot a^{1.26}$$

$$P(x) = 0.000626 \cdot v \cdot f^{0.24} \cdot a^{0.11}$$

$$x = [x_1\ x_2\ x_3] = [v\ f\ a]$$

6.1. Cucko search algorithm

Algorithm parameters that are used to solve this problem are:

- The number of chest is $n=280$
- The value of probability is $p_a=0,75$
- The number of iteration is $N=500$.

The parameters and the results obtained in solving the optimization problem are shown in the Table 1.

Table 1: Values of objective function, project variables and constraints for cutting parameters optimization

Project variables	The values
$x_1 = v$	77.2232 [m/min]
$x_2 = f$	1.8704 [mm/rev]
$x_3 = a$	4.6863 [mm]
Objective function ***F***	***0,9007***
Constraints	
g_1	0,9909
g_2	0,9922

The values of the particular objective function for which a minimum was searched are given in Table 2.

Table 2: Values of objective functions

Objective function	The values
T_P	0.1634 [min]
C_P	0.1033[€/piece]
R_a	2,0694 [µm]

6.2. Firefly algorithm

Algorithm parameters that are used to solve this problem are:

- The number of fireflies *is n=40*
- The step size is $\alpha=2.5$
- The attraction is $\beta=0.2$
- The parameter γ from equation (3) is $\gamma=1$

Table 3 and Table 4 show the results obtained from Firefly optimization algorithm. As noted, the obtained results are slightly worse than results which we obtained from Cuckoo search algorithm.

Table 3: Values of objective functions

Project variables	The values
$x_1 = v$	70.9737 [m/min]
$x_2 = f$	0,6558 [mm/rev]
$x_3 = a$	2.1327 [mm]
Objective function ***F***	***0,9271***
Constraints	
g_1	0,9939
g_2	0,9984

Table 4: Values of objective functions

Objective function	The values
T_P	0.1833 [min]
C_P	0.0744[€/piece]
R_a	1.1056 [µm]

6.3. The hybrid algorithm

The results of optimization received by using hybridized algorithm, given in Table 5. and Table 6., are the better than result obtained with Cuckoo search algorithm and Firefly Algorithm. This is because instead of rejecting "bad" nests, the part of Firefly algorithm which refer to attract fireflies is used.

Table 5: Values of objective functions

Project variables	The values
$x_1 = v$	90 [m/min]
$x_2 = f$	2 [mm/rev]
$x_3 = a$	5 [mm]
Objective function ***F***	***0,8929***
Constraints	
g_1	0,9938
g_2	0,9984

Table 6: Values of objective functions

Objective function	The values
T_P	0.1626 [min]
C_P	0.1247[€/piece]
R_a	2,1611 [µm]

Results graphical representation of the objective function F is shown in Fig. 4, respectively, presentation the individual objective function TP, CP and R_a is shown in Fig. 5.

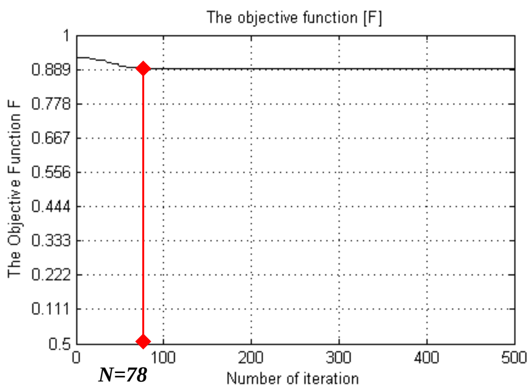

Figure 4:The Objective function F(T_P, C_P, R_a)

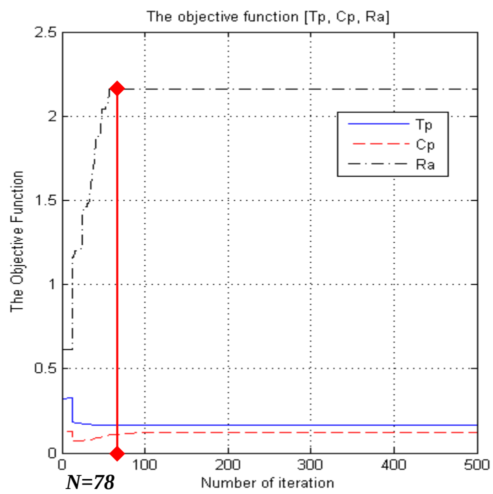

Figure 5:The Objective functions:

TP(v, f, a), CP(v, f, a), Ra(v, f, a)

From Fig. 4. and 5. it can be noticed that after 78 iterative passages algorithm reached optimal solution. The speed of convergence depends of the selected parameter (p_a), so that its variation may slow or speed up the convergence.

7. CONCLUSION

This paper describes a biologically - inspired algorithms for the optimization of cutting parameters. It is also shown attempt of hybridization of these two algorithms: Cuckoo search and Firefly algorithm. The obtained results showed that hybrid Cuckoo & Firefly algorithm gives the better result, than Cuckoo search and Firefly algorithm.

This paper also showed that hybridization is possible, but it is necessary to be caution when combining optimization algorithms, because in addition to a satisfactory solution, small dispersion of received results is needed during the iterative process.

The future researches and development of hybrid algorithm should go towards achieving better and optimal results with shortening the search time. In this sense, it is necessary to do some modifications of the algorithm and the improvement of existing code.

REFERENCES

[1] Yang XS, "Firefly Algorithms for Multimodal Optimization", Stochastic Algorithms: Foundations and Applications, SAGA 2009, vol. 5792, pp. 169-178 (2009).

[2] Yang XS, "Engineering optimization: an intoduction with metaheuristic applications", John Wiley & Sons, (2010).

[3] R. Bulatović, G. Bošković, M. Savković , M. Gašić, "Improved Cuckoo Search (ICS) algorthm for constrained optimization problems", Latin American Journal of Solids and Stuctures, 2014, vol. 11, no. 8, pp. 1349-1362, (2014).

[4] Yang, X.S., Deb, S., "Engineering Optimisation by Cuckoo Search", International Journal of Mathematical Modelling and Numerical Optimisation, vol 2(4), 330-343., (2010).

[5] Valian, E., Tavakoli, S., Mohanna, S., Haghi, A., "Improved cuckoo search for reliability optimization problems", Computers & Industrial Engineering, vol. 64, 1, pp. 459-468, (2013).

[6] Talbi E, "Metaheuristics: from design to implementation.", Hoboken, New Jersey: John Wiley & Sons, (2009)

[7] Gandomi AH, Yang XS, Alavi H.A. "Cuckoo search algorithm: a metaheuristic approach to solve structural optimization problems", Engin with comput, 2013, vol. 29, pp. 17-35

[8] Saibal K. Pal, C.S Rai i Amrit Pal Singh, "Comparative study of Firefly Algorithm and Particle Swarm Optimization for Noisy Non-Linear Optimization Problems", I.J.Intelligent Systems and Applications

[9] Miodragović G, Bošković M, "The use of the firefly algorithm for solving problems of applied mechanics". IMK-14 - Istraživanje i razvoj, vol. 19, pp. 56-61, (2013)

[10] D. Kalyanmoy, D . Rituparna, "Hybrid Evolutionary Multi-Objective Optimization of Machining Parameters", Engineering Optimization, vol 44, Issue 6, pp. 685-706,2012.

[11] F. Cus and J. Balic, "Optimization of cutting process by GA approach", Robotics and Computer-Integrated Manufacturing, vol. 19(1-2), pp.113–121, 2003.

[12] B. Malakooti, J. Wang, E.C. Tandler, "A sensor-based accelerated approach formulti-attribute machinability and tool life evaluation", International Journal of Production Research, vol. 28, pp. 2373-2392, (1990).

[13] U. Zuperl, F. Cus, "Optimization of Cutting Conditions During Machining by Using Neural Networks", International Conference on Flexible Automation and Intelligent Manufacturing 2002, Dresden, German, (2002).

Machining Parameters Influence on Cutting Force Used for Tool Path Optimization in End Milling

Aleksandra Petrović[1*], Ljubomir Lukić[1], Marina Pljakić[1]
[1]Faculty of Mechanical and civil engineering in Kraljevo, University of Kragujevac, Serbia)

Tool path in contour milling needs to satisfy geometric criterion by adjusting the shape to the feature to be machined as well as other criteria in terms of cutting forces, tool wear intensity and desired surface quality. Researchers developed various cutting force models which take into account cutting force dependence on machining parameters such as cutting depth, feed rate and cutting speed. Some of this parameters directly depend of tool path geometry, so selection of tool path indirectly influences on cutting force, tool wear and surface finish.

This paper presents overview of existing cutting force models for end milling and analysis of machining parameters which are used. Cutting force model capability to describe influence of tool path dependent parameters is used for selection and adaptation of model for further research in tool path optimization.

Keywords: Cutting forces, Cutting process, Machining parameters, Tool path

1. INTRODUCTION

The metal cutting process involves forces that influence the deformations in the primary and secondary shear zones, the cutting temperature, the process stability, the part quality, and the tool conditions. One of the main objectives of studying the machining process is to predict the cutting forces, which is a necessary exercise in many engineering applications [1].

Cutting force is one of machining process parameter which is relatively easy to monitor quantitatively, and is directly connected to tool conditions. Most research has been related to cutting force regulation, with objectives roughly categorized into (1) enhancing machining efficiency while avoiding tool damage, and (2) suppressing chatter [2]. Abruptly increasing cutting force on a tool may damage it or cause unexpected wear. If cutting force is below an "appropriate" level, assumed to be known, machining efficiency is improved by raising it. This is a common control objective in many past researches.

Prior to designing a control system, it is necessary to evaluate the reliability and accuracy of the cutting force model which will be used for this purpose.

2. CUTTING PROCESS MODELLING

All metal cutting operations share the same principles of mechanics, but their geometry and kinematics may differ from each other [3].

In general, the cutting process is a result of the dynamic interactions between the machine tool, the cutting tool and the workpiece. Therefore, its mathematical description should take into account its:

- Kinematics,
- Dynamics,
- Geometry of the chip formation and
- Workpiece mechanical and thermo-dynamical properties [4].

Although cutting operations are commonly three dimensional and geometrically complex, the simple case of two-dimensional orthogonal cutting is usually used to explain the general mechanics of metal removal. In orthogonal cutting, material is removed by a cutting tool that is perpendicular to the direction of relative tool-workpiece motion.

Figure 1 shows schematic representations of orthogonal and oblique cutting processes where the cutting velocity (v) is perpendicular to the cutting edge in orthogonal cutting, where as in oblique cutting, it is inclined at an acute angle to the plan normal to the cutting edge [3].

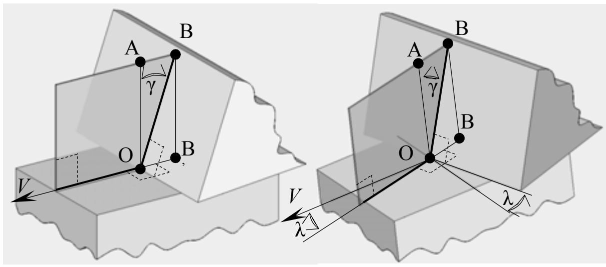

Figure 1: Geometries of orthogonal and oblique cutting processes

Three deformation cutting zones are distinguished in the chip generation process (Figure 2):

- Primary shear zone: As the edge of the tool penetrates into the workpiece, the material ahead of the tool is sheared over the primary shear zone to form a chip.
- Secondary shear zone: The shared material, the chip, partially deforms and moves along the rake face of the tool, which is called the secondary deformation zone or secondary shear zone.
- Tertiary zone: Is the friction area, where the flank of the tool rubs the newly machined surface.

Along the twentieth century researchers have tried to develop an adequate model to explain metal removal phenomena and predict three fundamental aspects: chip shape, forces and cutting temperatures. However nowadays does not exist a totally accepted model [4].

*Corresponding author: Dositejeva 19, 36000 Kraljevo, Serbia, petrovic.a@mfkv.rs

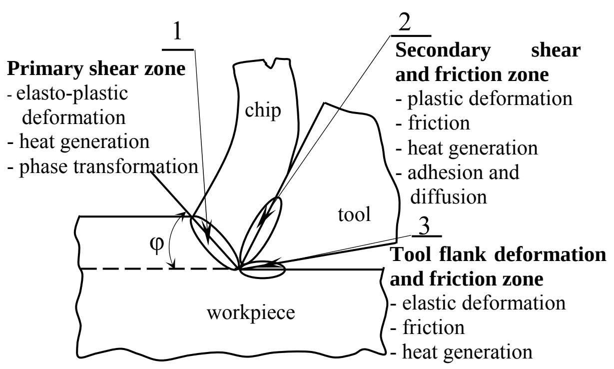

Figure 2: Deformation zones and physical phenomena [4]

2.1. Merchant's force model

One basic model of chip formation was developed by Merchant. Merchant's force diagram is an orthogonal cutting model that assumes the shear zone to be a thin plane. This circle is restricted to a model of orthogonal two-dimensional metal cutting.

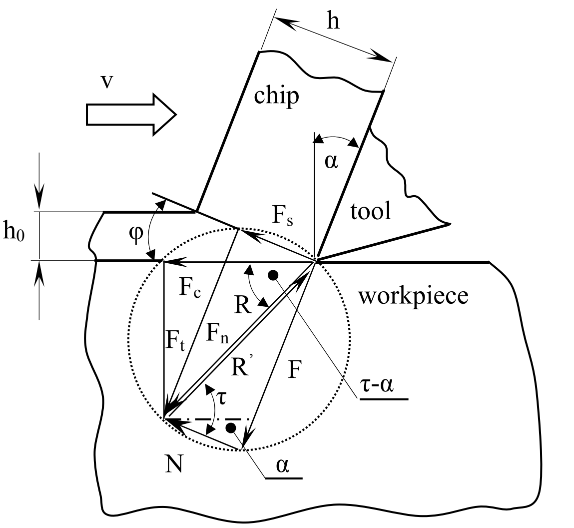

Figure 3: Merchants force diagram [5]

Where,
v: cutting velocity
Fc: cutting force
Ft: thrust force
F_s: shearing force
F: friction force
F_n: normal shear force
N: normal force to the rake face
R: resultant force coming from the workpiece and action on the chip
R': resultant force coming from the cutting tool
φ: shear angle
α: rake angle
τ: friction angle
h: chip width
h_0: initial depth of cut

The resultant force coming from the workpiece R is compensated by the resultant force coming from the cutting tool R′ and is formed from the cutting F_c and thrust F_t forces.

The key variable in Merchant's approach is the shear angle, Φ. The optimum shear angle Φ is calculated following the principle of minimum energy.

$$\phi = \frac{1}{4}\pi - \frac{\tau}{2} + \frac{\alpha}{2} \tag{1}$$

Merchant developed an elegant model and despite of the fact that this approach has not correlated too well with the experimental results, this research left a significant impact in the field [4].

2.2. Oxley predictive model

Two zones of shearing are identified as: primary shearing zone (which is centered on plane AB) and secondary shearing zone along the tool chip interface which are shown as plastic zones in Figure 4.

The primary shear zone is assumed to be parallel sided of finite thickness where from one side the material flows inside the shear zone from the workpiece at room temperature and normal conditions and from the other side the deformed material leaves the shearing zone and forms into chip. The parameter c is used to represent the relative length of the primary shear zone with respect to the thickness of the primary shear zone, and given as:

$$c = \frac{l}{\Delta S_2} \tag{2}$$

Oxley's model is presented to calculate the main parameters like c, δ and shear angle Φ [6].

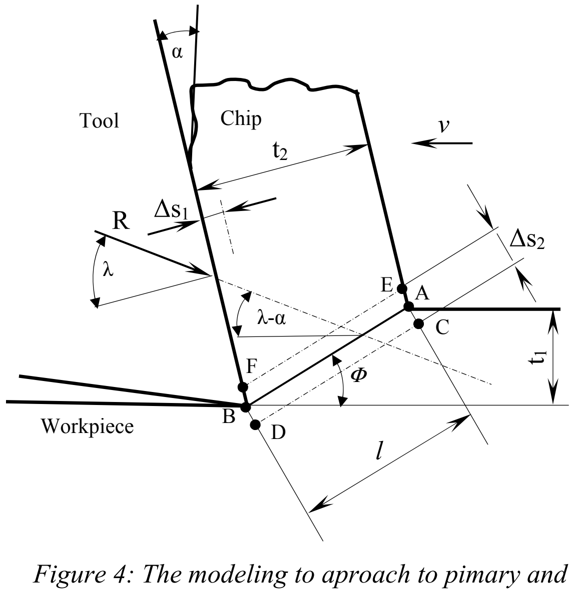

Figure 4: The modeling to aproach to pimary and secondary shear zones [6]

Using slip line field theory for the primary shear zone, the shear lines parallel to plane AB are identified as alpha slip lines. Oxley was able to formulate the hydrostatic pressure difference between points A and B of the shear plane AB assuming the constant shear strength, temperature and strain rate along an alpha line AB.

2.3. Material Model Selection

In recent years, the researchers in high velocity impact analysis have carried out an extensive amount of characterization of material properties at high strain rates and temperature. The Johnson-Cook constitutive model is one of such model developed by Johnson in 1983, which takes into account temperature and strain rate [6]. According to this model, the flow stress is given by:

$$\sigma = \left(A + B\varepsilon^n\right)\left(1 + C\ln\left(\frac{\dot{\varepsilon}}{\dot{\varepsilon}_0}\right)\right)\left(1 - \left(\frac{T - T_r}{T_m - T_r}\right)^m\right) \quad (3)$$

Here, T_r and ε_0 are the reference temperature (room temperature) and strain rates respectively. T_m is the melting temperature.

In the previous section of cutting force modelling, the effect of plastic deformation with high strain, strain rates and temperature and change in material properties are modelled for extracting the cutting coefficient representing the physical interaction of milling tool and workpiece material

However, the geometric aspect of the milling tool-workpiece interaction is not been taking care adequately. Contact between tool and workpiece is assumed to be constant while it may vary along the tool path depending upon the in-process geometry.

This contact zone between the tool and the instantaneous in-process geometry is usually known as cutter workpiece engagement (CWE) zone. The engagement zone and cutting force in milling are related because the cutting action of the helical cutting edge depends upon the engagement area and its location along the axis of rotation of the cutting tool [6].

3. CUTTING FORCE MODELLING IN END MILLING

In the milling process, material is removed from a workpiece by a rotating tool, which has one or more cutting teeth. While the tool rotates, it translates in the feed direction x. Cutting forces are acting on the cutting edge in axial, radial and tangential direction. In milling process with cylindrical end mill axial force is usually neglected.

The tangential and radial forces on the tool are denoted by F_t and F_r, respectively in Figure 5. The parameters shown are the spindle speed n, the chip load f_z, the axial depth of cut a_p and the radial depth of cut a_e.

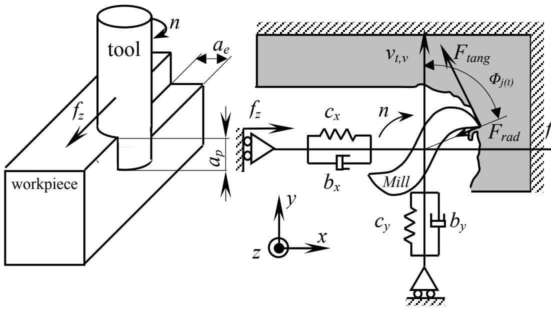

Figure 5:Schematic representation of the milling process [7]

In cutting force modelling in end milling spindle toolholder- tool combination is modelled as a 2-dof mass-spring-damper system in x- and y-direction with spring constants c_x and c_y and damping constants b_x and b_y, respectively.

Cutting forces are modelled related with chip thickness at different ways:

Linear function:

$$F_{tj} = a_p\left(K_{tc}h_j(t) + K_{te}\right)g_j\left(\phi_j(t)\right),$$
$$F_{rj} = a_p\left(K_{rc}h_j(t) + K_{re}\right)g_j\left(\phi_j(t)\right) \quad (4)$$

Exponential function:

$$F_{tj} = g_j\left(\phi_j(t)\right)K_t a_p h_j(t)^{x_F},$$
$$F_{rj} = g_j\left(\phi_j(t)\right)K_r a_p h_j(t)^{x_F} \quad (5)$$

Combination of linear and exponential function:

$$F_{tj} = a_p\left(K_{tc}h_j(t)^{x_F} + K_{te}\right)g_j\left(\phi_j(t)\right),$$
$$F_{rj} = a_p\left(K_{rc}h_j(t)^{x_F} + K_{re}\right)g_j\left(\phi_j(t)\right) \quad (6)$$

The angle that tooth j makes with the normal direction y is described by $\Phi_j(t)$:

$$\phi_j(z) = \phi + j\phi_p - \psi \quad (7)$$

$$\psi = \frac{2tg\beta}{D}z \quad (8)$$

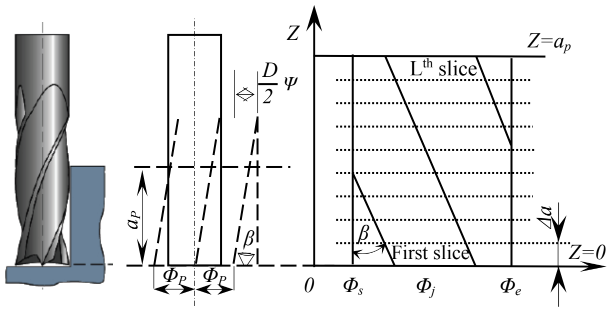

Figure 6: Geometry of a helical end mill [8] *here D denotes the diameter, β is the helix angle and Φp is the pitch angle*

The function g_j describes whether a tooth is in or out of cut:

$$g_j\left(\phi_j(t)\right) = \begin{cases} 1, & \phi_s \le \phi_j(t) \le \phi_e \wedge h_j(t) > 0, \\ 0, & else \end{cases} \quad (9)$$

Where, Φ_s and Φ_e are the entry and exit angle of the cut.

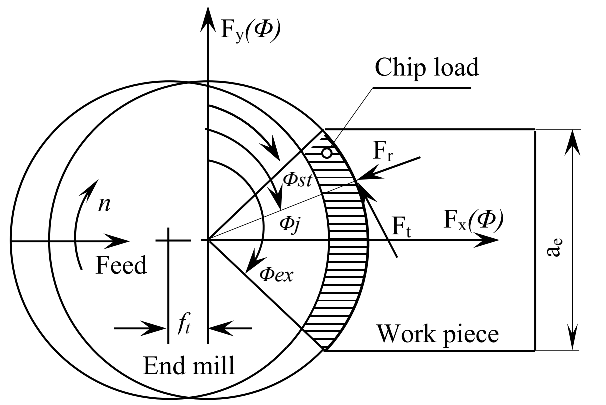

Figure 7: Chip formation phenomenon in milling operation [8]

Herein, the parameters K_{tc}, K_{rc}, K_{te} and K_{re} are parameters that can be determined experimentally. The cutting forces are separated as edge (e) and cutting (c) components: an edge force component due to rubbing or ploughing at the cutting edge, represented by K_{te} and K_{re} on a unit width of cut basis, and a cutting force component due to shearing at the shear zone and friction at the rake face, represented by K_{tc} and K_{rc}. These parameters are dependent on each material tool combination. However, it is possible to estimate these parameters from orthogonal cutting data, this approach needs orthogonal tests for the orthogonal to oblique cutting transformation.

When considering these coefficients as constant or as a linear function of chip thickness, integration along the cutting edge is possible. Nevertheless, when a power function is used, which generally leads to better results, numerical methods are needed.

The determination of chip thickness is a key factor for accurate simulation of cutting forces. It is calculated as the distance between two consecutive trajectories of the cutting flutes on the workpiece. These trajectories may deviate from their nominal values owing to runout, cutter deflection, thermal errors or tool wear, among others [9].

Chip thickness:

$$h_j(t) = h_{j,stat}(t) + h_{j,dyn}(t) \qquad (10)$$

The difference between the current and previous wavy surface is denoted as the dynamic chip thickness:

$$h_{j,dyn}(t) = \left[\sin\phi_j(t)\cos\phi_j(t)\right]\left(\underline{v}_t(t) - \underline{v}_t(t-\tau)\right) \qquad (11)$$

$$\tau = \frac{60}{zn} \qquad (12)$$

Herein, n is the spindle speed in revolutions per minute (rpm) and z the number of teeth.

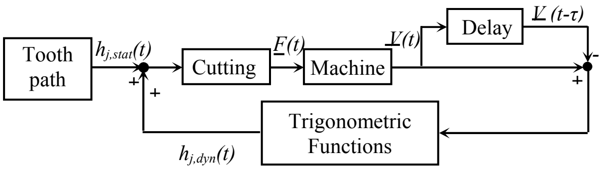

Figure 8 Block diagram of the milling [7]

Milling is a variable cutting process where chip thickness varies periodically. For circular tooth path (real tooth path is trochoidal, but effect of the trochoidal tooth path model becomes relevant when considering low immersion levels –when the ratio a_e/D is small):

$$h_{j,stat}(t) = f_z \sin\phi_j(t) \qquad (13)$$

With f_z the chip load in mm/tooth and Φj(t) the rotation angle of the j-th tooth of the tool with respect to the y (normal) axis.

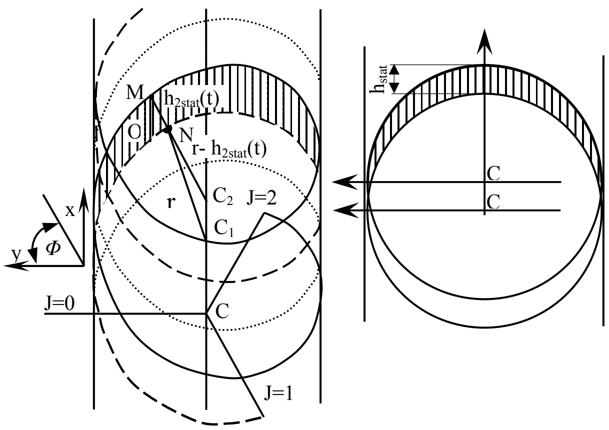

Figure 9:Trochoidal and circular tooth path

For trochoidal tooth path:

$$h_{j,stat}(t) = r - r\cos\left(\frac{\theta f_z \cos\phi_j(t)}{f_z\cos\phi_j(t) + \theta r}\right) + \left(\frac{f_z\theta r}{f_z\cos\phi_j(t) + \theta r}\right)\sin\phi_j(t) \qquad (14)$$

$$\tau_j = \frac{\hat{\tau}\theta r}{f_z\cos\phi_j(t) + \theta r} \qquad (15)$$

Where θ is the angle between two subsequent teeth given by:

$$\theta = \frac{2\pi}{z} = \hat{\tau}\cdot\Omega \qquad (16)$$

Where Ω is the spindle speed in rad/s.

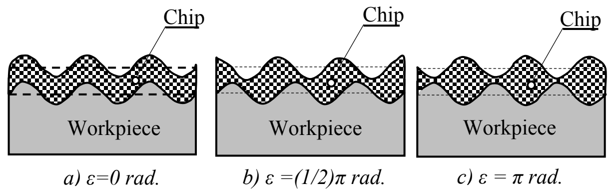

Figure 10: Effect of relative phase diference of subsequent tooth passings on chip [7]

There is a non-uniform distribution of chip thickness along the cutting edge in contact with the workpiece. Each point on the cutting edge has a different angular position, and therefore, it will cut different chip thicknesses. The chip load variation along the active length of the cutting edge implies the variation of the resultant cutting forces.

In this case, numerical integration is generally used to obtain the cutting force acting on a flute. The cutting edge is segmented into elemental discs, and the resultant force acting on a flute is the sum of the forces acting on each elemental disc. The contributions of all cutting edges are summed to obtain the total forces acting on the tool.

The new model for milling force estimation developed by Perez [9] is based on the average chip thickness for the engaged flute. The average chip thickness is calculated for the flute engagement angle, Φ_{pr}. This angle is the projection of the active length of the cutting flute on the xy-plane. This is the flute length which engages the material for that particular tool–workpiece interaction from the first point, located by φ_1, to the last contact point, located by φ_2.

It is possible to use this model to estimate the cutting forces when special cuts are done in variable conditions. To evaluate the efficiency in determining the cutting forces under non-uniform machining conditions, the proposed method is used for estimating the entry of the cutter into the workpiece until it reaches total engagement. Both entry and exit angles vary in each cutter revolution and the cutting force profile varies accordingly.

3.1. Mechanics of Cutting Model

In the mechanics of cutting approach, force coefficients are determined from analytical models of oblique cutting with the following procedure:

- Shear angle (φ_c), average friction angle (β_a) and shear yield stress (τ_s) are evaluated experimentally from orthogonal cutting experiments (turning tests). During the orthogonal cutting experiments, chip thickness and tangential and feed forces are measured. Chip thickness is measured with a micrometre and cutting forces are measured with a cutting force dynamometer.

• The following assumptions are made: the orthogonal shear angle is equal to the normal shear angle in oblique cutting ($\varphi_c \equiv \varphi_n$); normal rake angle in oblique cutting is equal to the rake angle in orthogonal cutting ($\alpha_r \equiv \alpha_n$); the chip flow angle is equal to the oblique angle ($\eta \equiv i$); the friction coefficient (βa) and shear yield stress (τ_s) are the same in both orthogonal and oblique cutting operations for a given speed, chip load and cutting tool-workpiece material combination.

• Cutting force coefficients are expressed as [10]:

$$K_{tc} = \frac{\tau_s}{\sin\phi_n} \frac{\cos(\beta_n - \alpha_n) + tgi\,tg\eta \sin\beta_n}{\sqrt{\cos^2(\phi_n + \beta_n - \alpha_n) + tg^2\eta \sin^2\beta_n}}$$

$$K_{rc} = \frac{\tau_s}{\sin\phi_n \cos i} \frac{\sin(\beta_n - \alpha_n)_n}{\sqrt{\cos^2(\phi_n + \beta_n - \alpha_n) + tg^2\eta \sin^2\beta_n}}$$

$$K_{ac} = \frac{\tau_s}{\sin\phi_n} \frac{\cos(\beta_n - \alpha_n) tgi - tg\eta \sin\beta_n}{\sqrt{\cos^2(\phi_n + \beta_n - \alpha_n) + tg^2\eta \sin^2\beta_n}} \qquad (17)$$

Mostly, orthogonal cutting experiments are repeated for a range of cutting speed, rake angle and uncut chip thickness to prepare a database for certain cutting tools and workpiece materials. The values of shear angle, average friction angle and shear yield stress are further used to determine force coefficients using the oblique cutting model presented by (17). Oblique cutting transformation using basic orthogonal parameters can predict the force coefficients before the cutting tool is manufactured.

3.2. Mechanistic Model

The identification of force coefficients from time consuming orthogonal cutting tests is not a feasible and practical approach. In such cases, a mechanistic approach is used for quick calibration of cutting tools. For a given cutting tool and workpiece material, the mechanistic approach for force coefficient identification has the following steps:

• A set of slot cutting (full immersion) experiments are conducted at different feed rates. Spindle speed and axial depth of cut are kept constant during the experiments.

• The cutting forces in feed, normal to feed and axial directions are measured with a cutting force dynamometer. The total force per spindle revolution is collected and divided by the number of flutes of the cutting tool to avoid the influence of run out in the machine tool.

• Force coefficients are then identified by equating the experimentally evaluated average cutting forces to analytically derived average milling force expressions for slot milling. The average cutting forces per tooth period are presented as [3]:

$$\overline{F}_x = -\frac{NA_p}{4} K_{rc} f_t - \frac{NA_p}{\pi} K_{re}$$

$$\overline{F}_y = +\frac{NA_p}{4} K_{tc} f_t + \frac{NA_p}{\pi} K_{te}$$

$$\overline{F}_z = +\frac{NA_p}{\pi} K_{ac} f_t + \frac{NA_p}{2} K_{ae} \qquad (18)$$

Here, F_x, F_y and F_z are the average cutting forces per tooth period in feed, normal to feed and axial directions respectively, f_t is the feed rate and A_p is the selected axial depth of cut.

• The average cutting forces can be expressed by a linear function of feed rate as:

$$\overline{F}_q = \overline{F}_{qc} f_t + \overline{F}_{qe} \qquad (q = x, y, z) \qquad (19)$$

The average cutting forces at each feed rate are measured and cutting components (F_{qc} and F_{qe}) are estimated by linear regression of the data. Using equations (17) and (18) cutting force coefficients are evaluated by:

$$K_{tc} = +\frac{4\overline{F}_{yc}}{NA_p} \quad and \quad K_{te} = +\frac{\pi\overline{F}_{ye}}{NA_p}$$

$$K_{rc} = -\frac{4\overline{F}_{xc}}{NA_p} \quad and \quad K_{re} = -\frac{\pi\overline{F}_{xe}}{NA_p}$$

$$K_{ac} = +\frac{\pi\overline{F}_{zc}}{NA_p} \quad and \quad K_{ae} = +\frac{2\overline{F}_{ze}}{NA_p} \qquad (20)$$

This procedure is repeated for each combination of cutting tool geometry and workpiece material. Force coefficients are directly calibrated for an existing cutting tool with the mechanistic model.

Most mechanistic models are based on the average force measurement, whose accuracy is affected by the charge leakage and drifting associated with the use of piezoelectric sensors. It is thus advisable to identify the pressure coefficients at low cutting velocities.

When the cutting pressure coefficients are identified at low cutting velocities, some phenomena (e.g., material softening, chip segmentation, etc.), which only appear at high cutting speeds, are not considered [1].

4. TOOL LIFE INFLUENCE ON CUTTING FORCE

A basic problem with model-based systems (feed forward) for cutting process control approach is its poor adaptability to machining process changes. The most important process change is the progress of tool wear. Figure 11 shows the trade-off between machining efficiency and tool life. Generally, speeding up material removal to enhance machining efficiency often shortens tool life, increasing tool cost, meaning efficiency is often sacrificed for tool life. Practical machining places various constraints on this relationship, for example, on machining time to meet the manufacturing deadline. Another example is where machining is required to be finished using a single tool only, often done in die and mold machining.

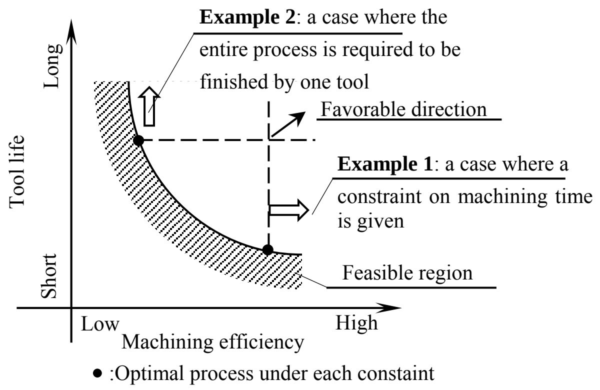

Figure 11: Trade-off between machining efficiency and tool life [2]

In end milling processes, cutting force generally increases as the tool wear progresses [2]. In tool condition monitoring (TCM), algorithms to detect excessive tool wear from cutting force have been drawing attention for years.

Ibaraki [2] used a set of simple cutting test to prove correlation between tool wear and cutting forces. Figure 12 shows cutting forces (their mean values over one path) measured by using a piezoelectric three-component dynamometer. This experiment show that the progress of tool wear is strongly correlated to cutting force in the normal to feed direction.

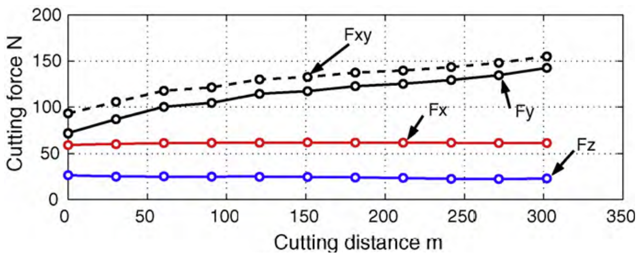

Figure 12 Cutting forces in the straight side cutting test (Fx: in feed direction, Fy: in direction normal to feed, Fz : in axial direction) [2]

To estimate the tool wear progress from cutting force, the influence of machining conditions and tool path geometries must be separated. It can be done by using a process model to relate machining conditions to cutting force.

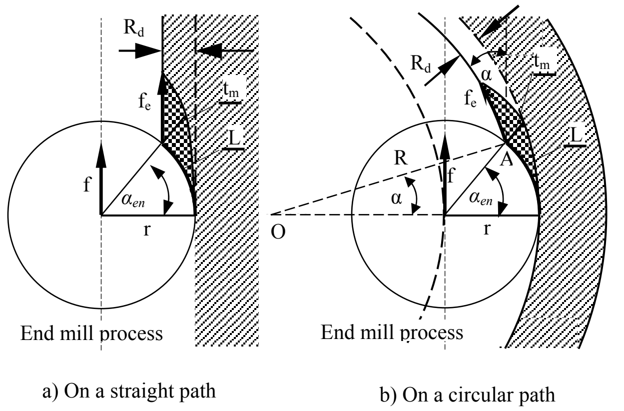

Figure 13: Schematics of end milling process[2]

In [2] model which gives the cutting force in XY plane, F, as a function of t_m, the maximum undeformed chip thickness, and L, the arc length of cutting engagement (see Figure 13, where R_d: radial depth of cut, r: tool radius, f : feed per tooth, α_{en}: engagement angle, and R: curvature radius at cutting point) is used:

$$F = F_0 + \beta_1 X_1 + \beta_2 X_2 + \beta_{11} X_1^2 + \beta_{22} X_2^2 + \beta_{12} X_1 X_2 \qquad (21)$$

Where $X_1 = (t_m - t_{m0})/\delta_{tm}$, $X_2 = (L - L_0)/\delta L$. t_{m0}, δ_{tm}, L_0, and δL represent constant central values.

The coefficient F_0 can be seen as the normalized cutting force for machining conditions corresponding to $X_1 = X_2 = 0$. It represents the influence of tool wear progress in cutting force, excluding the influence of tool path geometry and machining conditions.

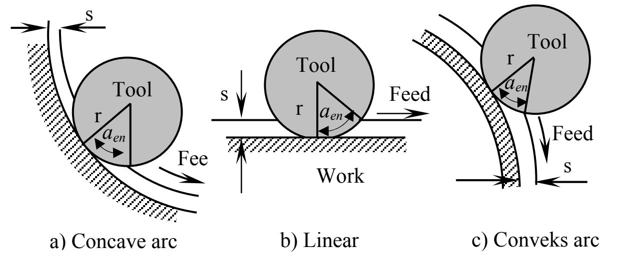

Figure 14: Variation in cutting engagement for different tool path geometries in 2D end milling [11]

Feedrate scheduling and tool path modification approaches are usually used to regulate cutting force.

Among in-process machining parameters, feedrate is the easiest to manage. Ibaraki [2] used this approach illustrated in Figure 15.

Regulating feedrate to suppress cutting force variation may not effectively avoid tool damage, especially in high-speed milling.

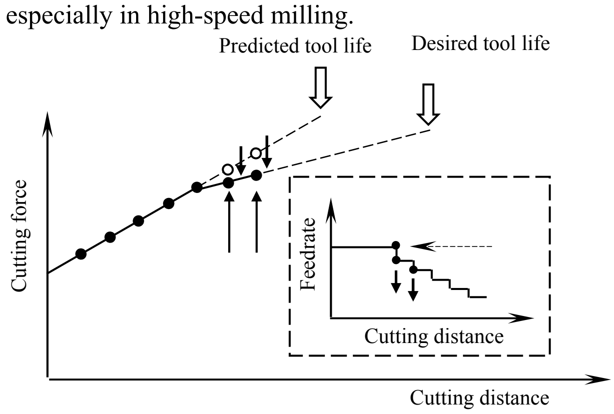

Figure 15: Concept of tool life control through cutting force control [2]

Compared to feedrate scheduling, tool path modification approaches to regulate cutting force have been less explored.

5. TOOL PATH AND CUTTING FORCE

The tool path generation is usually purely geometric in nature, which leads to a variation of radial depth of cut especially at sharp corners. The usual problems encountered due to this variation are: (1) left over material at corners (2) sudden tool breakage, which leads to choosing worst scenario cutting conditions in manufacturing practices.

From the machine dynamics and cutting tool point of view, the variation in the cutting load affects the tool life as well as the machine tool condition itself. Conventional tool path based approaches such as spiral milling although they insure smooth tool paths; they result in a high variation of the radial depth of cut, which influences the tool load and machine dynamics. For the general cases, there are two popular approaches mentioned in the literature to find the solution for the cutting load variation problem along the machining tool path: feed rate scheduling and tool path strategies. The approach to adapt or modify the tool path for achieving a constant load is independent from the cutting tool diameter, length, number of flutes and work piece material.

Dhanik [6] develop a recursive method and algorithms which avoids the leftover material at the corners and minimizes the variation of radial depth of cut at each level of contour milling and consequently tries to maintain the same cutting conditions specified as the starting cutting parameters which are favorable for process reliability, part quality and tool life. Other methods for maintaining a constant cutting load are analysed in [12].

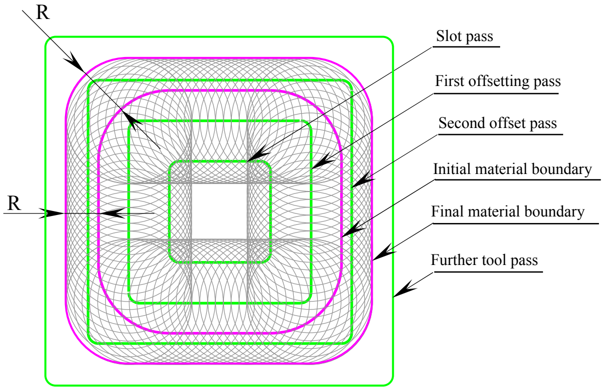

Figure 16: Conception of Tool Path Modification[6]

6. CONCLUSION

In this paper cutting force modelling is analysed in order to determine which model is suitable for force representation for optimization of tool path with minimizing cutting force and tool wear. First, general approach for cutting force modelling is presented, and then milling force models are analysed. There are a lot of influencing factors related with cutting force, starting with phenomena in cutting zone, through cutting engagement zone, static and dynamic chip thickness, chatter occurrence, tool wear etc. All cutting force models have coefficients which are determined experimentally and related with tool- workpiece material selection. Usually this experiments are conducted in special conditions (slot milling) and are not suitable enough for working conditions (low immersion angle). Model used in [2] is taking into account a tool wear, and shows good applicability for low immersion angles which makes it a good candidate for using in high speeding milling modelling.

Force control through tool path adaptation or modification is feed forward method for ensuring minimisation of cutting force and tool wear. Based on this cutting force research and tool path analyses in previous work [12], future investigation will be directed to modification of cutting force model for use in tool path optimization.

ACKNOWLEDGEMENTS

The authors would like to express their gratitude to the Ministry of Education and Science of the Republic of Serbia for their support to this research through the project TR37020.

REFERENCES

[1] I. Zaghbani and V. Songmene, "A force-temperature model including a constitutive law for Dry High Speed Milling of aluminium alloys," *J. Mater. Process. Technol.*, vol. 209, no. 5, pp. 2532–2544, Mar. 2009.

[2] S. Ibaraki and T. Shimizu, "A long-term control scheme of cutting forces to regulate tool life in end milling processes," *Precis. Eng.*, vol. 34, no. 4, pp. 675–682, Oct. 2010.

[3] Y. Altintas, *Manufacturing Automation: Metal Cutting Mechanics, Machine Tool Vibrations, and CNC Design*, Illustrate. Cambridge University Press, 2012.

[4] G. Quintana i Badosa, "Stability lobes diagram identification and surface roughness monitoring in milling processes." Universitat de Girona, Girona, Spain, 2010.

[5] M. E. Merchant, "Mechanics of the Metal Cutting Process. I. Orthogonal Cutting and a Type 2 Chip," *J. Appl. Phys.*, vol. 16, no. 5, pp. 267–275, 1945.

[6] Sandeep DHANIK, "NC Tool Path Evaluator and Generator for High Speed Milling," vol. 4533. ÉCOLE POLYTECHNIQUE FÉDÉRALE DE LAUSANNE, Lausanne, Switzerland, p. 201, 2009.

[7] R.P.H. Faassen, "Chatter prediction and control for high-speed milling:modelling and experiments." Technische Universiteit Eindhoven, Eindhoven, Netherlands, p. 144, 2007.

[8] S. Aggarwal, "Part Programming to Realize Chatter Free and Efficient High Speed Milling," EPFL, Lausanne, Switzerland, 2012.

[9] H. Perez, E. Diez, J. J. Marquez, and A. Vizan, "An enhanced method for cutting force estimation in peripheral milling," *Int. J. Adv. Manuf. Technol.*, vol. 69, no. 5–8, pp. 1731–1741, Jul. 2013.

[10] E. Budak, Y. Altintaş, and E. J. A. Armarego, "Prediction of Milling Force Coefficients From Orthogonal Cutting Data," *J. Manuf. Sci. Eng.*, vol. 118, no. 2, p. 216, May 1996.

[11] A. Matsubara and S. Ibaraki, "Monitoring and Control of Cutting Forces in Machining Processes: A Review," *Int. J. Autom. Technol.*, vol. 3, no. 4, pp. 445–456, 2009.

[12] A. Petrovic, Lj.Lukic, M. Bjelic, M. Pljakic, "Optimal tool path modeling in contour milling process," 36th International Conference on Production Engineering, Kopaonik, 2013, pp 263-270

.

Marketing Oriented Organizational Culture as Prerequisite for TQM Implementation: The Case Study of Serbian Mechanical Industry

Ljiljana Pecić[1], Milan Kolarević[2]
[1]College of Applied Professional Mechanical Studies Trstenik, Serbia
[2]Faculty of Mechanical and Civil Engineering in Kraljevo, University of Kragujevac, Kragujevac, Serbia

The purpose of this paper is to propose a tool for determining the right moment for introducing radical changes aimed at implementing TQM in a company. As we know, there is a huge number of companies that dismiss benefits of TQM implementation. This is especially important for companies which come from undeveloped countries and countries in transition, as Serbia is. In this paper, a survey questionnaire was used to identify the quality of marketing orientation of organizational culture within 20 companies working within mechanical industry in Serbia. The questionnaire was used for all managerial levels and workers and it proved that there is no big difference in orientation among different levels organizational within a company. According to the fact that Serbia is a country in which consensus economics used to have a long tradition (almost till the end of XX century), these findings are very important to its further development.

Keywords: Organizational Culture, Marketing Orientation, TQM, contractual economy

1. INTRODUCTION

Many studies have supported the positive link between an organization's culture and financial performance. What many leaders do not realize is that behaviour drives organization performance. By modifying their architecture, organization can eliminate or minimize negative behaviours and foster positive ones. The net result of all this research is that focusing on culture is not another leadership fad, it is a good business.

What is organization culture?

From an organization stand point, culture is defined as a prevalent norms, values and behaviours held by the vast majority of employees. A company's culture influences everything it does. It is the core of what the company is really like, how it operates, what it focuses on, and how it treats customers, employees and shareholders. As a lot of researches show, culture is a driver of business performance [1].

Today's business is not about selling or proving customer service. It is well known that business excellence in companies is realized through implementation of the concept of total quality management (TQM). ISO officially defines TQM as a way of managing an organization which aims at continuous participation and co-operation of all its members in the improvement of quality in order to achieve customer's satisfaction, long-term profitability of the organization and benefit of its members, in accordance with requirements of the society.

That is why resources in such cultures are totally utilized [2, 3]. Benefit comes in all segments of business: fewer defects, reduced rework and lead times, lower inventory levels, cost reduction, and higher level of customer satisfaction [4,5].

TQM is a culture in an organization committed to total customer satisfaction through continuous improvement. On the other hand, the world's most successful business leaders agree that corporate culture, if correctly aligned with the external environment, is the glue that ensures long-term organizational success. Former IBM CEO Lou Gerstner, who led its spectacular transformation from a products company to a service organization, says: " I came to see, in my time at IBM, that culture isn't just one aspect of the game-it is a game"[6].

When we come to the point to identify fundamental strategy of running business, most companies follow an orientation that matches one of the following categories: product- oriented, sales-oriented or market oriented. Nowadays we have a situation that lot of companies have implemented those standards, but they dismissed benefits from implementation- better business results.

We believe that reason for such situation lies in the fact that this implementation did not become a part of daily life and behaviour of employees in the company and that the old way of thinking stood in their habbits, even because of the economic situation some good practices become less important and forgotten.

In this paper we are going to try to clarify terms TQM, organizational culture and market orientation and to prove that in Serbian metal industry exists strong organizational culture, but on conservative marketing level, and that level of marketing orientation do not depend of education level, work experience and company, but is the result of long period under contractual economy.

2. LITERATURE OVERVIEW

The organizational culture or what is known as the "organization values and personality" was not given the natural interest before the second half of the twentieth century. The 1970s era had witnessed an increasing interest in this concern and culminated in 1990s.[**7].**

*Corresponding author: College of Applied Professional Mechanical Studies Trstenik, Radoja Krstića 19, 37240 Trstenik, ljiljana.pecic72@gmail.com

Between 1990 and 2007 more than 60 research studies covering 7,619 companies and small business units in 26 countries have found that market culture and business performance are strongly related. This positive correlation is identified by more than 35 performance measures, including return of investment, revenue growth, customer retention, market share, new product sales and employee performance [8]. The evidence provides executives with empirical basis for embracing a strong market culture as a means to creating a competitive advantage for their firms and the superior business performance results.

For example, Kotter and Hasket [9] reported that firms with performance-enhancing cultures grew their net income 765 percent between 1977 and 1988, as compared with 1 percent for firms without performance –enhancing culture over the same period.

Nowadays, when world became one global village connected with the modern communication methods, achieving business excellence and good business parameters become impossible for any country and any company which stays in isolation of changes [10].

In the wake of the interest and attention to the organizational culture, the TQM concept emerged, which is one of the most important, pioneer, intellectual and philosophical concepts that gained broad attention by the managerial specialists, professionals, researches and academics, who are, particularly interested in the development and improvement of the production performance of the different organizations [11]. The TQM concept is one in which the thoughts and vision vary, depending on the viewing angle by the researches. But this depends of objectives, which organizations are seeking to achieve. Achieving customer satisfaction through the interaction between all effective parties of the organization is the common for all visions.

TQM is defined as "creation of a remarkable culture in performance, where all the organization's individuals are continuously working to achieve the customer's expectations and the work performance with the achievement of the quality at the best possible level, or with high effectiveness and at the shortest possible time [12]. If we now look on organizational culture as a key to organizational success [13] and achieve TQM business excellence, than market orientation of organizational culture may be defined as "the organizational environment that most effectively and efficiently generates the behaviour necessary for the creation of superior values for buyers [14]**.**

Market orientation is the focus of a firm that treats marketing as a cross-functional responsibility where meeting customer needs is an overriding priority for the entire organization [15]. Day [16] holds that market orientation is a combination of a customer orientation and competitor orientation, while Gallagher et al. [17] have created ***6Cs Model of Market Culture*** and that model is based on: *creating of superior customer value, profitability*, *customer insight*, *cross-functional team approach*, *collaborative value networks*, *creiteria for decision making* and *CEO leadership*.

3. PROBLEM IDENTIFICATION

Lot of companies in the world did not succed on the road to achieve business excellence and TQM. Now, if we assume that company's culture influences everything it does, it is clear that if you want to achieve TQM business excellence in the era of globalization, you have to be marketing oriented.

For businesses in underdeveloped economies, which are numerous, this is very important. They have to find a way how to get to the market, but simply, problems related to their successful business operations are much more complex. Problems in developing world economies have mainly four-dimensional character [18]:

- lack of quality marketing practices,
- lack of adequate technological equipment,
- lack of adequate financial means, and
- lack of satisfactory management behavior.

For economies in transition, there is another important issue – the noted presence of political and economic instability.

It is clear that for successful implementation, the challenges undertaken in the underdeveloped world economies, especially those in transition, need to have a more comprehensive methodological approach than the ones applied in developed economies.

The following paragraphs deal with evaluating the state of marketing orientation of organizational culture in 20 companies within Serbian mechanical industry: all companies are nowadays independent entities, whereas in the recent past they used to be a part of the giant IHP Prva Petoletka in Trstenik (PPT – the field of hydraulics and pneumatics, which gives to almost all of them the prefix PPT). Nineteen companies are currently undergoing the process of restructuring.

4. DESCRIPTION OF THE COMPANIES SUBJECTS OF THE RESEARCH

Industry of hydraulics and pneumatics Prva petoletka (*PPT*) in Trstenik is nowadays a complex business system consisting of 18 independent economic entities which are working under the supervision of the Serbian Government and are behaving as elements of a holding (as they used to be one. However, there is a bulk of persisting problems). It was founded on 23rd March 1949, and in 1989 it had the workforce of about 15,000 people and about $400 million in sales (about $200 million were exports outside former Yugoslavia). In the late eighties, it was a holding company with 23 mutually interrelated companies, some of which were established to support the system (called internals) and some were solely production units (in the fields both of hydraulics and pneumatics). All companies were directed to each other and acted as supplementary units.

The 1990s brought dramatic changes in economic practice. The great Eastern market broke down, where *PPT* and had realized the largest volume of its export business. This change was followed by a drastic reduction of home market. It further caused changes in political and economic systems, as well as social and economic restructuring. Although unprepared, these companies were forced to compete on the global market, where there was no place for consensus economics.

At the beginning of 1996, PPT initiated the project of its total process organization. The aim of this process was to enable a breakthrough on the world market where the best world companies were successfully doing their business. The presented settling in *PPT* started to produce positive results from the very beginning.(Fig.1) There were some changes in management as already mentioned and the arrival of modern, market-oriented management resulted in obvious business improvement.

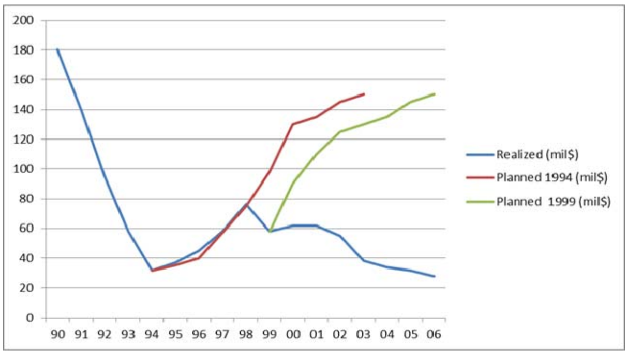

Figure1: Relations between planned and achieved realization from 1990 till 2006

However, sanctions on Yugoslavia were imposed, the country was bombed and the company suffered the loss of 80 working days in 1999.

At the end of 1999, the change of the CEO was followed by some changes in the top management as well. *PPT* was restored to former frameworks which shook development results achieved in the initiated recovery process. All activities concerning ISO 9000 implementation and total process organization stopped. Very soon, these measures proved to be wrong. However, it was impossible to correct the error that was made. The trend of changing company leaders continued for a whole decade, which led to organizational and operational chaos in the company.

Such a misfortunate situation did not finish till the end of 2010, when the company was divided into 20 component parts. Although most of these companies had certified QSs, business operations have been getting ever worse. The greatest paradox was the fact that *PPT-Kočna tehnika AD* was in the worst position, although only in 1998 it was one of the most successful companies in the mechanical industry of both Serbia and former Yugoslavia (as a recognition of its success, it got an Oscar for quality - the most prestigious reward for quality in former Yugoslavia). At the end of 1998 the *PPT* system had approximately 12,000 employees, whereas at the end of 2010 it had 4,343 workers and almost the same technology park (*Energetika* became a public company and *FUD Brus* was facing bankruptcy).

The Serbian Government, aware of the importance of these companies for the industry of Serbia, has launched a project for their recovery and this paper presents the first part of the work methodology called company reengineering, developed with the purpose to help companies implement TQM philosophy and get much better business parameters.

5. THE TOOL FOR IDENTIFYING THE EXISTING MARKETING ORIENTATION OF AN ORGANIZATIONAL CULTURE

In order to identify the present level of the organizational culture in terms of marketing orientation of *in those 20 companies* (taking into account tradition and their business history) and find what the starting point for the project is, it was first necessary to make the appropriate questionnaire, which would provide the answer to the key question: what the direction of our business is. The questionnaire was based on MARK – PLAN questionnaire (Mark-Plan, 2003). This poll list was used to conduct the research in companies, in terms of determining management orientation, i.e. weather it is *production, sales* or *market.*

The questionnaire was structured in such a way that the answers to previously mentioned issues led to conclusion about the state of organizational culture in terms of marketing orientation. The structure of the questionnaire is given in Table 1 [18], and provided answers are grouped in such a way that they unequivocally point to three possible orientations. The questionnaire was compiled from these 15 questions with the options given in a way that would prevent routine answering. The data collected from anonymous respondents in the interview were: degree of professional education, years of working experience and their occupation.

The structure of questions led to the conclusion that a market-oriented company implies "the way employees behave towards business realization and towards the environment", or "the way the company perceives itself and its environment".

For scoring the survey, the points scale was adopted where a response is scored 0 points for indicating production orientation, 5 points for indicating technological orientation, and 10 points for indicating marketing orientation.

In the context of the survey results, the marketing orientation of a company can be described as:

- advanced (121-150 points),
- barely satisfactory (91-120 points),
- conservative (61-90 points),
- bad (31-60 points), and
- hopeless (0-30 points).

Table 1: The structure of questions

Company orientation/ questions	Production orientation	Sales orientation	Market orientation
1. Which existing problem should be given the highest priority? ***(problem identification)***	Production	Sales	Meeting consumer needs
2. It would be possible to revive the company if… ***(Vision of fate)***	The State provides adequate support	Market behavior becomes more regular	Customer needs are met in a quality way
3. Apart from the CEO, the second most important function in the company is… ***(identification of the most important role in a company)***	Technical Manager	Commercial Manager	Marketing Manager
4. What should special attention be paid to? **(*How do you see yourself in the future)***	Production Performance	Sales Performance	Meeting customers' requirements
5. The basic goal of the company for all employees is gaining…	Quality performance of assigned tasks	Profitability	Long-term perspective
6. From the external point of view, it is very important for the company to develop…	A good relationship with respective power centers (*characteristics of a consensus economics*)	A good relationship with business partners (*lower supply, higher sales)*	Quality image in the market
7. From the ***marketing*** point of view, it is very important for the company to do…	Active public appearance and promotion	Promotion in the market and attraction of users' attention	Communication with target groups
8. The company ***communicates with the external public***…	Through formal notices	By providing information to media	By using different means intended to target groups
9. From a managerial point of view, who makes ***internal public?***	The most influential human factors	Authoritative representatives of interested groups	All employees
10. Management communicates with the internal public through…	Formal notices or posting notices on bulletin boards	The information service	Direct contacts related to specific issues with interested groups
11. Top management of the company consists of…	the members representing current centers of power	experts in specific professional areas	experts in corporate management
12. The primary factor for the successful operation is …***(type of exchange)***	Production of quality products and goods	As cheaply buy and produce, and as dearly sell	Quality to meet customer needs
13. The following is a sign of management goodwill…	Highlighting individual contributions generated from operations	Periodical awards and commendations	Adherence to company's mission
14. Achieved success in business is expressed through...	The level of achieved production volume	The range of achieved market presence	The level of gained market position
15. The company would do business more successfully if there is … **(*vision of solution*)**	Better production equipment	Satisfactory current assets	Higher quality of human resources

6. DATA COLLECTION, PROCESSING AND ANALYSIS

6.1 Data collection

The starting point of the research was to collect data using surveys on the representative sample of employees in every company. The survey was conducted in the period from the beginning of December 2010 to the end of March 2011. The number of interviewed workers was 2729 from the total of 3600 employed in those companies. The Workers took questionnaires to the home, and the following day they were left in the boxes, kept by delegated people.

6.2 Data processing

The results gained from processing collected data are presented in Table 2. Data processing was done in the following way: answers of all employees were recorded, and then the percentage for each given response was calculated. Description of the used procedure is given in [18]. Points for each question are obtained by summing-up the product of the number of points that every question bares with the percentage that every answer has gained (percentages are made decimal numbers). The overall number of points for the survey was obtained by adding up the points given to all questions.

Tabel 2: Average Points per Company

Company	Number of respondents	Points
Armature	236	71,25
Cilindri	180	78,67
Energetika	71	59,93
Fud Brus	225	77,40
Hidraulika	237	68,02
Holding	20	64,00
Ind.pneumatika	200	76,15
Inženjering	117	71,28
Ishrana	24	74,79
Kočna tehnika	328	72,65
Namenska	380	67,99
NIC	4	53,75
Obezbeđenje	49	80,71
PPT NP	105	72,57
PPT promet	159	72,45
Remont i energetika	103	76,00
Servoupravljači	171	81,14
TMO	16	74,38
Transport	12	78,33
Zaptivke	92	78,64

The *Prva petoletka* system, i.e. all companies together, won 73 points.

On figure 5 it can be seen distribution of all average points obtained per company, educational level and working experiance.

Table 3: Results obtained by educational level

Education Level	percentage of employees	Points
1	0.73%	81,50
2	2.24%	71,07
3	26.53%	75,06
4	43.20%	72,23
5	5.57%	74,01
6	13.01%	73,28
7	8.68%	72,97

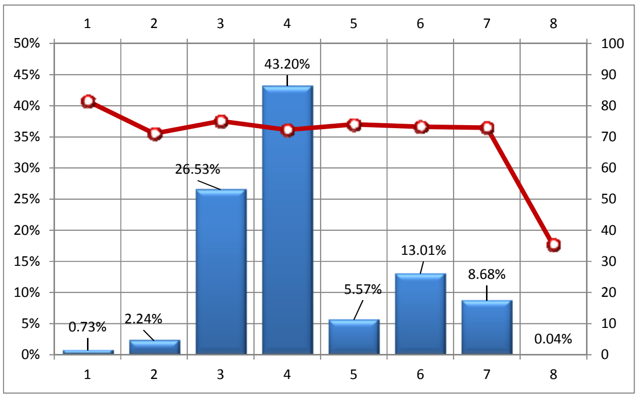

Figure 3: Average points per educational level

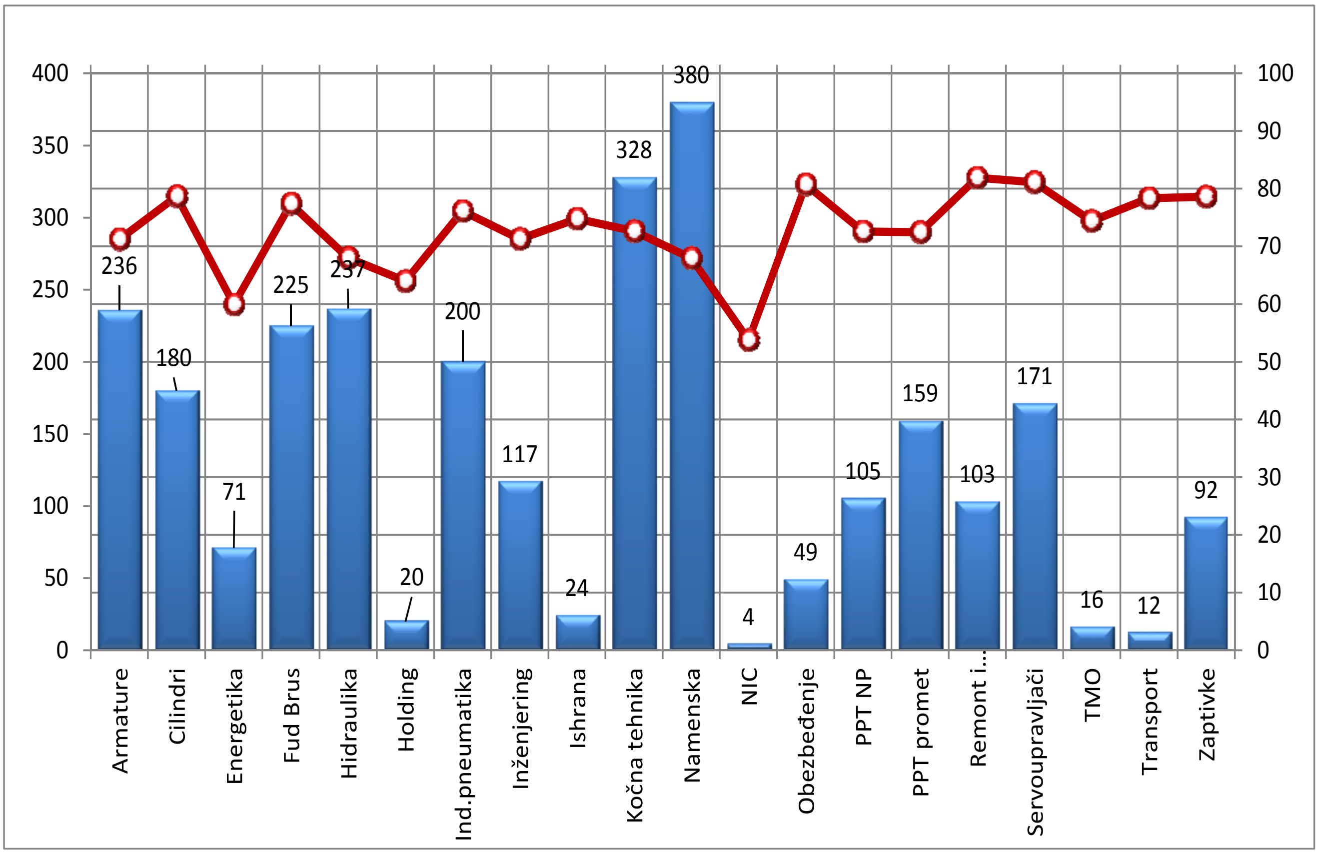

Figure 2: Average points (red line) and number of respondents (blue pillar) per company

Table 4: Results obtained by working experience

Working experience	percentage of employees	Points
0-5	8.72%	71,11
6-10	8.17%	71,12
11-15	10.00%	78,70
16-20	9.78%	76,25
21-25	24.11%	73,22
26-30	28.58%	71,92
31-35	9.75%	73,52
36-40	0.88%	66,46

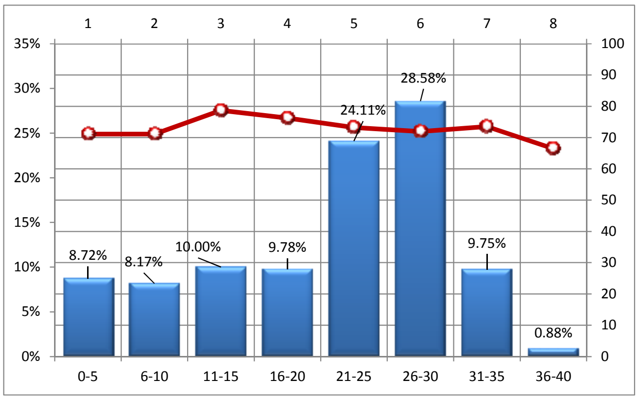

Figure 4:Results obtained by working experience

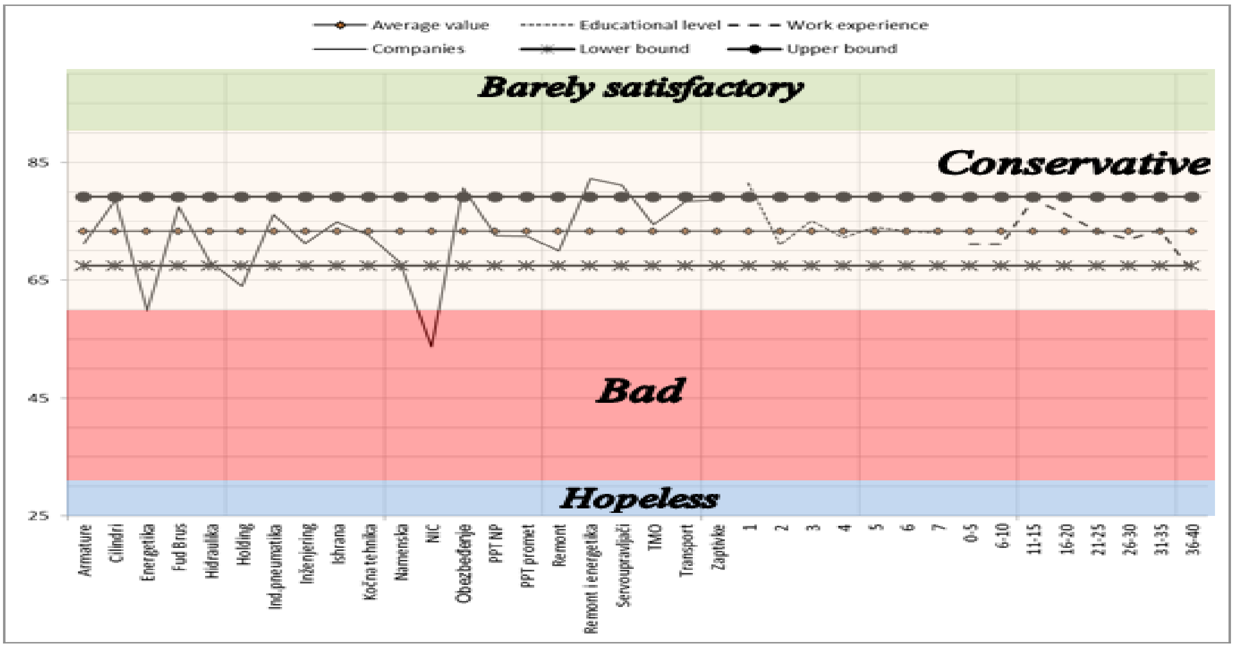

Figure. 5: Number of reached points per company, work experiance and level of education

6.3 5.3 Data analysis

The given results show that companies have "conservative" marketing orientation of organizational culture (hardly satisfactory level of marketing orientation). Results show that Servoupravljaci has the highes number of points and that company has the best business results. Analyzing points received according to the level of educaion, it is very disturbing that employees with first level of education have the highes number of points (81,5), while the best educated level has 72,97 points.

The analysis was done by using software Design Expert v.8.0.7.1. After eliminating the rough mistake, the analysis was done by using 2692 guestionnares.

The level of marketing orientation was analysed through dependence of three independent variables:

- **A** – level of education (SSS)
- **B** – years of working experience (GRS), and
- **C** –size of a company (number of employees (NZ)

Main data and coded values are presented in tabel 5.

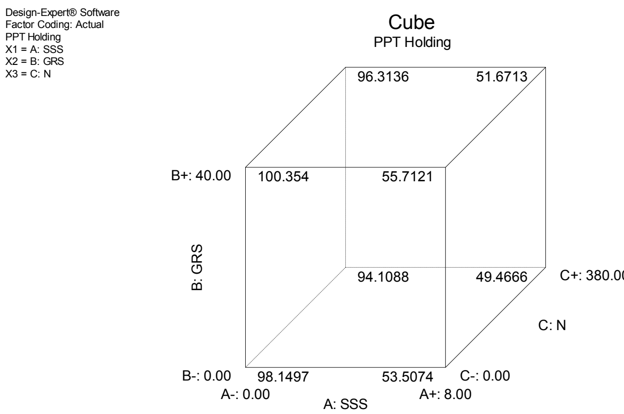

Figure 6: Coded values of analysed variables

Tabel 5: Design Summary

Factor	Name	Type	Min	Max	Coded	Values	Mean	Std. Dev.
A	SSS	Numeric	1	8	-1.00=0.00	1.000=8.00	4.2455	1.3195
B	GRS	Numeric	0	40	-1.00=0.00	1.000=40.00	21.2184	9.0242
C	NZ	Numeric	4	380	-1.00=0.00	1.000=380.00	217.7154	98.9784

Response	Name	Obs	Min	Max	Mean	Std. Dev.	Ratio	Trans	Model
Y1	IHP PPT	2692	30	120	72.72845	18.39110691	4	None	Linear

After ANOVA analysis (Analysis of Variance) enforcement, it has been found that between dependent variable and analysed variables exist correlation and that it could be described with linear model.

Tabel 6: ANOVA for Response Surface Linear Model

Source	Sum of Squares	Degrees of Freedom	Mean Square	F Value	p-value (Prob > F)	
Model	11552.847	3	3850.949	11.519	< 0.0001	significant
A-SSS	727.575	1	727.575	2.176	0.1403	
B-GRS	161.931	1	161.932	0.484	0.4865	
C-NZ	10414.783	1	10414.783	31.152	< 0.0001	
Residual	898631.653	2688	334.312			
Lack of Fit	527787.936	772	683.663	3.532	< 0.0001	significant
Pure Error	370843.717	1916	193.551			
Corr Total	910184.500	2691				

The Model F-value of 11.52 implies the model is significant. There is only a 0.01% chance that a "Model F-Value" this large could occur due to noise.

The "Lack of Fit F-value" of 3.53 implies the Lack of Fit is significant. There is only a 0.01% chance that a "Lack of Fit F-value" this large could occur due to noise.

Std. Dev.	18.28421097
Mean	72.72845468
C.V. %	25.14038151
PRESS	901299.0534
R-Squared	0.012692863
Adj R-Squared	0.011590958
Pred R-Squared	0.009762248
Adeq Precision	13.83249764

The "Pred R-Squared" of 0.0098 is in reasonable agreement with the "Adj R-Squared" of 0.0116,

"Adeq Precision" measures the signal to noise ratio. A ratio greater than 4 is desirable. Our ratio of 13.832 indicates an adequate signal.

Final Equation in Terms of Coded Factors:

n = 73.41058 - 1.58576*A - 0.54681*B - 3.78052*C

Final Equation in Terms of Actual Factors ie. final equation of chosen regresion model is:

n = 79.3237 - 0.3964*A - 0.0273*B - 0.0199*C

It can be seen that coefficients of the analyzed variables are negative, which indicates on negative trend, i.e, decrees of depending variable with the growth of each independent variable. The same can be seen from the space diagrams given on figures 7 to 11.

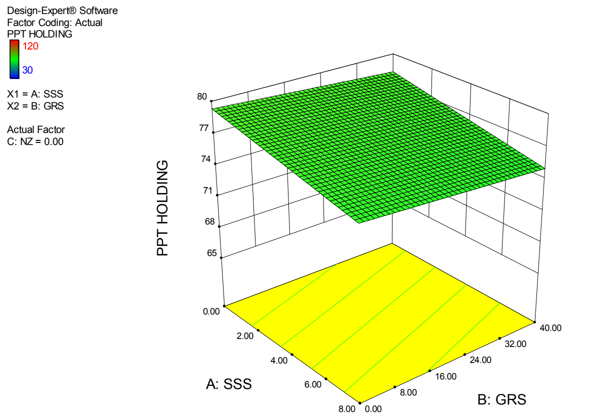

Figure 7: Analysed variable dependence of SSS and GRS for NZ=0

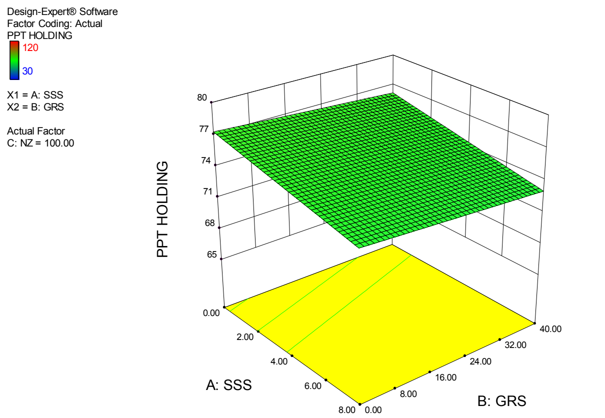

Figure 8: Analysed variable dependence of SSS and GRS for NZ=100

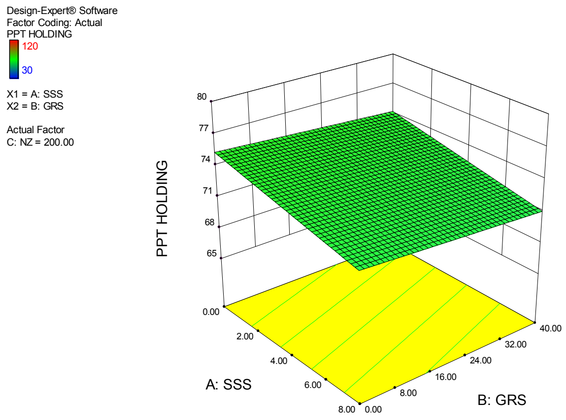

Figure 9: Analysed variable dependence of SSS and GRS for NZ=200

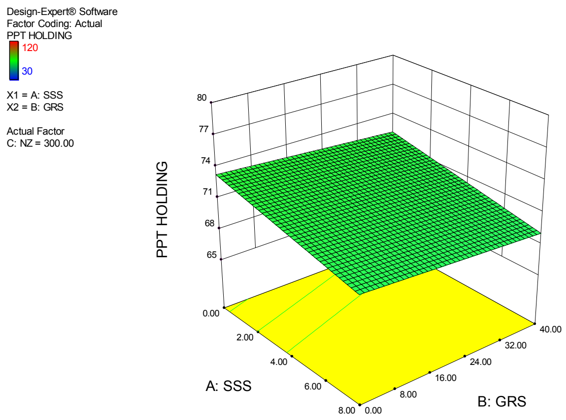

Figure 10: Analysed variable dependenceof SSS and GRS for NZ=300

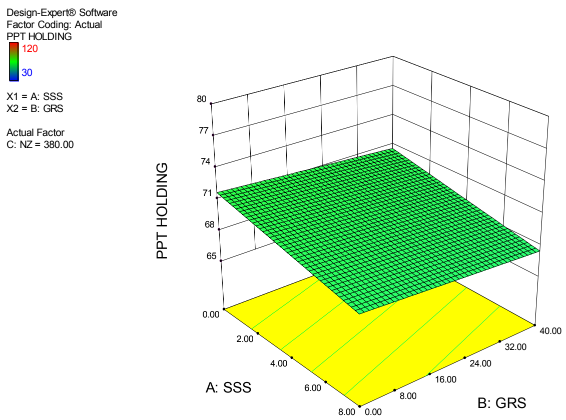

Figure 11: Analysed variable dependence of SSS and GRS for NZ=380

7. CONCLUSION

The aim of the conducted study was to prove that the precondition of a successful implementation of changes leading to TQM is having quality market orientation or having high quality organizational culture that is marketing oriented. Before implementing TQM principles, the organizational culture is to be examined by organizational development practitioners [19]. If there is such an organizational culture in a company, then it would be possible to establish a complete and balanced business structure with long-term marketing orientation where it would be likely to achieve quality total process organization striving to TQM realization. Otherwise, these ventures are difficult to achieve. For all those companies which found themselves in such a situation, it is necessary to implement the appropriate company re-engineering.

The obtained results become clearer if we know the history of the companies included into the research. A deeper analysis shows that due to the long-lasting presence of consensus economics in Serbia, its principles are still present in thoughts of most employees. A more dangerous fact is that these principles are cherished by top management as well. The analysis has also shown that political influence should be eliminated from business, as it significantly slows the changes and distracts the implementation of changes to be based on scientific thought. This problem could be solved through the process of education of all levels of hierarchy.

The real reason companies such as ex *PPT* companies are poor business systems nowadays, despite the fact that they got certificates for their QSs in the last ten years, is that they failed in implementing marketing oriented principles, i.e. marketing management into their organizational structures and behavior.

The attitude advocated by the paper is that a successful process organization aiming at implementing TQM could be achieved only with the companies having a complete and totally ballanced business structure which is marketing oriented. Any other situation would not give a satisfactory quality of this process. The reason is that the activities contributing to successful satisfaction of market requirements would not be done at a quality level.

REFERENCES

[1] S.Gallagher, C. Brown and L. Brown,"A Strong Market Culture Drives Organizational Performance and Success," Employment Relations Today, pp.25-31(2008)

[2] A.Gunasekaran,.,(1999), Enablers of total quality management implementation on manufacturing: a case study", Total Quality Management, Vol.40, pp.987-96

[3] M.A Youssef, J. Boyd, and E.Williams, " The impact of total quality management on firms responsiveness: an empirical analysis", Total Quality Management,Vol.7 No.1, pp.127-44, (1996)

[4] Salegna, G., and Fazel, F.,(2000), " Obstacles to implementing quality", Quality Progress, Vol.33, No.7, pp.53-7

[5] Mosadghrad. A.M, (2006), "The impact of organizational culture on successful implementation of total quality management,

[6] Gerstner, L.V, (2002), " Who says elephants can 't dance? Inside IBM's historic turnaround, New York: HarperCollins,pp. 181-182

[7] F.A.Bourini, M. Ghaith, Al- Abdallah and A. Abou-Moghli, "Organizational Culture and total Quality Management", International Journal of Business and Management, Vol.8, No.24, pp. 95-106, (2013)

[8] S.Gallagher, Brown, C. Brown, "A strong market Culture drives Organizational Performance and Success", Employment Relations Today, Willey Periodicals, pp. 25- 31, (2008)

[9] J.P.Kotter and J.L.Haskett, "Coprorate Culture and Performance", New York, The Free Press, (1992)

[10] Al- Farhran, "Organzational Culture and Administrative Development in the Jordanian Public Sector Institutions", The Jordanian Journal, Vol 6/1, (2003),

[11] F.A.Bourini, M. Ghaith, Al- Abdallah and A. Abou-Moghli, "Organizational Culture and total Quality Management", International Journal of Business and Management, Vol.8, No.24, pp. 95-106, (2013)

[12] Zaidan, "Philosophy and Work Entrance", Total Quality Management, First Edition,(2009)

[13] Swais, "Relationship between the Organizational Culture and TQM Application in the Algerian Public Oil Companies (Case Study) " , Derast, Administrative Sciences, Vol. 38, No.2, (2011)

[14] T.J., Peters and R.H.Waterman,"In Search of Excellence", Harper&Rowe, Sydney, (1982)

[15] S.F.Slater and J.C.Narver, "Market Orientation and the Learning Organization", Journal of Marketing, Vol.59/3, pp.63-74, (1995)

[16] S. G.Day, "Market driven strategy:Processes for Creating Value". New York: The Free Press, (1990)

[17] S.Gallagher, Brown, C. Brown, "A strong market Culture drives Organizational Performance and Success", Employment Relations Today, Willey Periodicals, pp. 25- 31, (2008)

[18] Pecić, Lj., Klarin,M., Trifunović, D., Dašić, P., "Marketing-oriented organizational culture and implementation of total quality management The case study of Prva petoletka, Metalurgia International, Vol. 18 No. 6 pp.121-126, (2013a)

[19] S. Pool, W., (2000), "The learning organization: motivating employees by integrating TQM philosophy in a supportive organizational culture", Leadership &Organization Development Journal, Vol. 21 No.8, pp. 373-8

Recognizing MAG Process Parameters on the Basis of the Sound Emitted

Marina Pljakić[1*], Miomir Vukićević[1], Milan Kolarević[1], Mišo Bjelić[1]
[1] University of Kragujevac, Faculty of Mechanical and Civil Engineering in Kraljevo, Dositejeva 19, Kraljevo, Serbia

Manufacturing companies and enterprises are faced with two big challenges: accomplishing constant product quality with a lower price. These are the conditions for survival of production in the increasing competition both at the regional and global levels. Another very important characteristic of manufacturing systems is the flexibility and agility of manufacturing processes because companies are forced to respond to market demands where buyers' wishes must be particularly satisfied. Furthermore, this requires efficient manufacturing systems focused on automation, computers and software.

Development of robotic welding systems is indeed impressive and that technology nowadays represents one of the leading branches in the application of industrial robots. The scientific challenge is contained in the tendency to make the performances of technological equipment approximate to human capabilities or even surpass them.

During a welding process, sound is emitted as one of the physical and natural phenomena. This phenomenon is treated with attention by using modern measuring equipment, i.e. directed microphones which allow separation of sound emission of the process from the total emission.

Control of robots based on visual, acoustic and energy feedbacks represents the basis for their further development and application in this technology.

Keywords: welding, robots, control, noise, feedback

1. ACOUSTICS

1.1. Term acoustics

If it is necessary to give a definition at the very beginning, then it can be said that acoustics is the science of sound. It covers the study of sound generation, its propagation in different environments and effects it causes in an environment. During its long-standing development, acoustics has passed through the process of expansion from a purely theoretical science to a science applied in broad fields of engineering. In recent times, acoustics has expanded even to the fields beyond physics and engineering, such as the functions of the sense of hearing, human speech... On the other side, the specific field of acoustics refers to development of electro-acoustic transducers as sensors and noise generators. It is a synthesis of various disciplines, such as mechanics, micro-mechanical engineering, technology of materials...

1.2. Definition of sound

Acoustics is the science of sound, and the definition of sound which is nowadays most generally accepted and which covers all its forms reads: sound is any time variable mechanical deformation in the elastic environment.

The accent in the definition of sound is on the time variability of elastic deformations. Namely, it is possible for deformations in material environments to be time invariable and as such, they are not sound. This, for example, refers to various forms of plastic deformations of materials.

Such a definition is not quite connected with human empirical experiences of sound and one can easily guess that it covers a lot of physical phenomena that are far from human perception, i.e. human empirical knowledge of sound phenomena. Exactly that mechanical nature of sound is important for understanding the nature of sound phenomena and many practical problems that arise from sound application. Hence, all the phenomena related to sound, e.g. sound radiation, propagation, ... are, by their physical nature, mechanical phenomena. [4]

1.3. Sound in engineering

If the view is narrowed only to the fields of engineering disciplines, acoustics covers different practical aspects of application of sound in life, including the theoretical bases for sound as a physical phenomenon, to the extent necessary for understanding and use of sound phenomena in possible applications.

In the field of action which is understood in this way there are several aspects where sound appears as a subject of engineering interest. It can be said that three types of sound are dominant:

- a means of communication,
- an ecological topic, and
- a tool.

Basically, speech is an acoustic phenomenon and all principles to which it is subjected result from that. Another very specific form of communication by means of sound is music as a field of artistic action of sound. In communication, there are circumstances when the sound wave is used as the carrier of information on the same principles as the electromagnetic wave in radio technique.

Excessive sound energy may jeopardize the health of people by its action, and therefore sound has become one of inevitable topics within the ecological action in modern society.

In different circumstances, sound assumes the role of a tool in the form of an active or passive means. The role of active tool is realized through the execution of a certain operation or a special function, and the passive role is realized through registration and analysis of sounds that

*Corresponding author: Faculty of Mechanical and Civil Engineering Kraljevo, 36000 Kraljevo, Serbia, pljakic.m@mfkv.kg.ac.rs

occur spontaneously and thus form information or complete some working operations.

1.4. Energy and information aspects of sound

Each engineering use of sound is reduced to sound as energy in space or as signal.

When sound is observed as signal, then it is a carrier of information, Figure 1.1. Excitation of the acoustic transmission system from the figure is sound pressure or sound power, which depends on the circumstances.

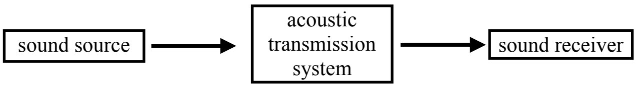

Figure 1: Information block diagram of acoustics phenomena

In the engineering fields in which sound is observed as signal, human sense of hearing frequently appears at the end of the acoustic transmission system, at the point of receiver, which is represented by the block diagram, Figure 2.

Although there are different physical models, sound as energy and sound as signal are combined in engineering conditions, because both aspects are important for the problem.

1.5. Term acoustic image

The ultimate result of hearer's perception is a complex impression, i.e. complex sound. The expression "sensation" is used and it denotes everything that makes a response to the excitation of a sense. In case of the sense of hearing, the sensation is composed of a multitude of received sound information. The mechanism of the sense of hearing serves as a mediator, and the sensation arises in the consciousness of the hearer and is called "acoustic image", Figure 2. [6]

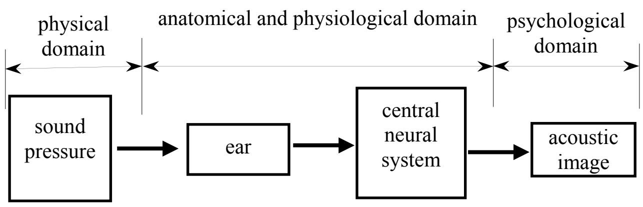

Figure 2: Relation between acoustic field and acoustic image

1.6. Noise

Sound can be simple or complex. Simple sound is a pure harmonic change, with one constant frequency. Complex sound is a complex periodical change which consists of several components with different frequencies. The first component with the basic frequency represents the basic harmonic, whereas the others are higher harmonics. [3]

Figure 3 shows time functions and the corresponding amplitude-frequency spectra of simple and complex sounds and noise.

The basic values that characterize sound are its intensity, pitch and timbre. Sound intensity represents, at a certain point in the acoustic field, energy which, in the unit of time, passes through the unit of area which is perpendicular to the direction of sound propagation. Pitch, where tone represents simple sound, is defined by frequency. Timbre is characteristic of complex sound, and it is defined by the number of higher harmonics and their intensities. [3]

A machining system represents, in a general case, a complex source of noise. Noise, due to its physical properties and nature, is connected with the operation regime, rigidity, variability of load, manner of machine support... The main sources of noise in a machining system are:

- machine/device with its sources in the whole kinematic system, and
- the machining process.

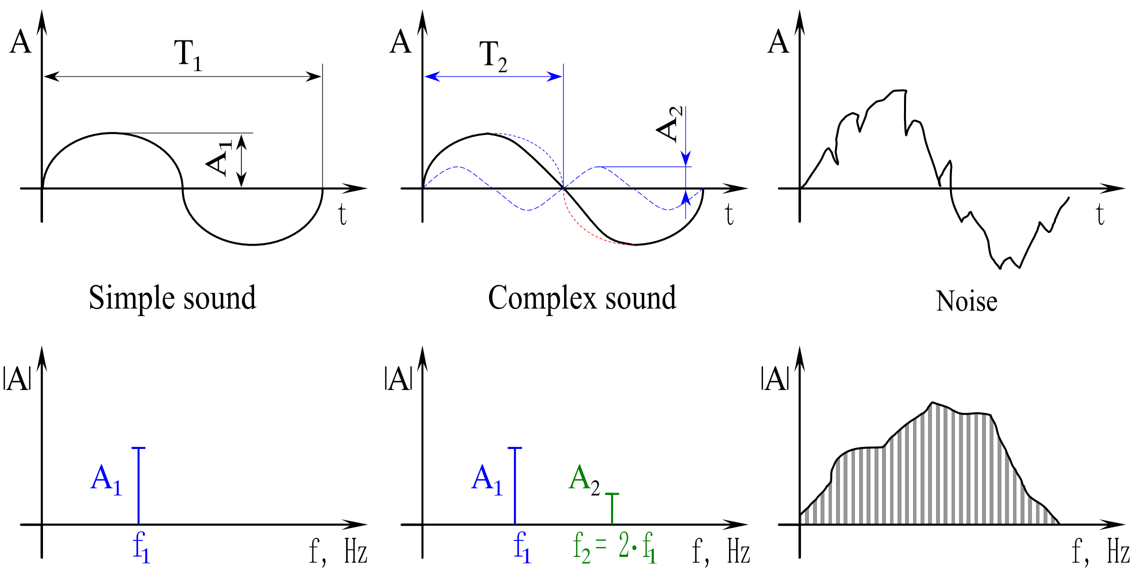

Figure 3: Time functions and frequency spectra of simple and complex sounds or noise [3]

2. SPATIAL DIMENSIONS OF ACOUSTICS IMAGE

In the transmission of sound information to the hearer or the measuring instrument-sensor, one of the information components is the information about the space with sound sources.

For the hearer, all sources of sound which he can recognize are at the point where the speaker is placed, and spatial information are reduced only to reverberation**,** which, in a reduced way, gives the image of the space with sound sources.

In direct hearing of a sound source, two global levels of spatial information that are integrated into a unique whole can be recognized in the acoustic image which then arises in the consciousness of the hearer:

sound comes from individual sound sources, i.e. localization of the places in space with sound sources whose sounds are recognized, and

- integrated information about the space where the hearer and sound sources are, which is often called "acoustic ambience".

Transmission of sound information on audio systems starts, as a rule, by placing a microphone in the input acoustic environment. The first step in that job is generation of adequate signals which will, together as a package, also carry the information about the space. It is realised by the application of several microphones placed in an appropriate way in the space of the input acoustic environment.

information about directions from which direct

3. CHARACTERISTICS OF THE GMEL WELDING PROCESSS

3.1. Principle

When it is established, the electric arc is maintained, and the electrode wire is uniformly introduced/added (automatic-alectromotor, rollers for flattening, drawing and/or pushing the wire). Shortening of the electrode is the consequence of its melting (consumption).

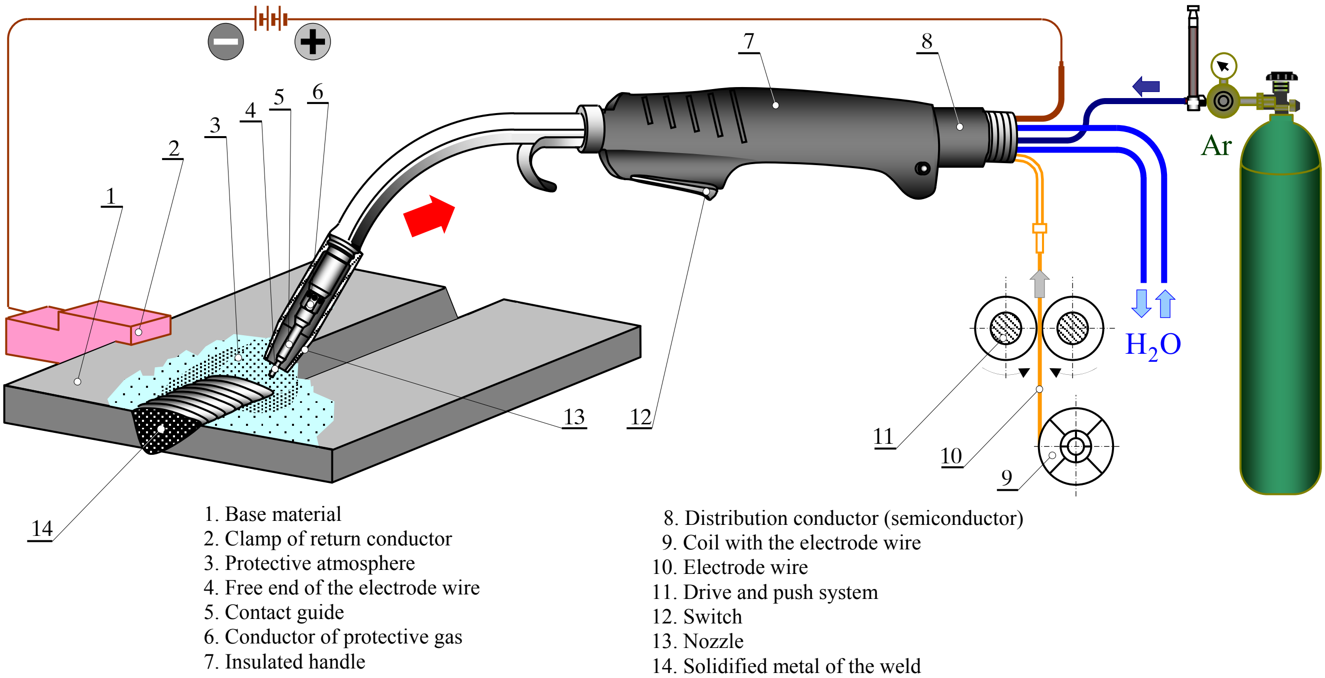

Figure 4: Schematic presentation of the GMEL process

The created mixture of molten metals of the electrode and the workpieces makes a weld pool, which, during the cooling period, turns into the solidified metal of the weld.

During the whole process, the weld zone is covered with protective gas whose task is to prevent air penetration whose components produce harmful chemical links with liquid and/or heated base and additional metal.

Therefore, this process is defined as the process of creation of permanent joint by applying heat energy of activation accomplished by transformation of electrical energy by means of the electric arc formed between the base material and the electrode wire (additional material) in the zone of protective atmosphere of inert or active gas or mixtures of technical gases, Figure 3.[2]

3.2. Application

Production welding, surfacing and repair welding of most metal material. In welding, there are numerous ways of expressing the effectiveness of the process. It is most frequently done by means of deposit (kg/h), in certain conditions the indicators are the intermittence of process, the time used for subsequent cleaning of welds and the surrounding area... GMEL is applied for welding profiles, sheets and pipes whose wall thickness is 1÷20 mm (in some cases far above those thicknesses when it is economically and technologically justified). Originally, it is a semi-automatic process, but it is very often used as an automatic and robotic procedure.

According to the degree of automation, GMEL process is:

- semi-automatic; automatic bringing of the electrode wire to the zone of electric arc, manual control of the welding gun, i.e. additional material and electric arc,
- completely mechanized; application of mechanical systems for planar or spatial guiding of the welding gun, i.e. electric arc and the workpiece,
- automated; besides the previously mentioned, it covers the application of system for automatic guiding of the process (regulation of process parameters) and all other systems of the process on the basis of computer application,
- robotic; the process is led by computers with the application of robot.

The GMEL process is used for welding low carbon, low alloyed and stainless steels with the thicknesses 1÷30 mm. For the thicknesses $\delta>4$ mm, welding is performed in several passes.

GMEL processes are used for welding non-ferrous metals, particularly for:

- aluminium and its alloys,
- magnesium and its alloys,
- copper and its alloys,
- titanium...

GMEL only terminologically differs from the common and standardized term MIG/MAG because there is no technical difference between them – the difference is only in the type of utilized protective atmosphere. As modern industry mainly uses gas mixtures, it is the reason to apply the mentioned terminological difference.

3.3. Parameters

Although it is common to divide the welding process parameters into primary and secondary ones, here they are mentioned without making such a difference:

- $U_z = 16\div26$ V, the welding voltage,
- $U_0 = 60$ V, the open circuit voltage (most frequently),
- $I_z = 80\div180$ A, and more than 500 A, the current intensity,
- $j_z = 100\div200$ A/mm^2, even more than 450 A/mm^2 – the current density,
- $V_z = 2\div4$ mm/s $= 7.2\div14.4$ m/h, the welding speed,
- $d_0 = 0.7\div4$ mm, the electrode wire diameter,
- $\eta = 75\div85\%$, the energy efficiency.

For welding by the GMEL process, JSEP is most often used. It accomplishes a stable electric arc, uniform transfer of additional material, reduction of losses in material due to splashing and bigger depth of penetration. JSEN is more rarely applied because the electric arc becomes unstable, despite the increase in the melting coefficient, except for welding of light weight metals and in surfacing. The application of alternating current is avoided because of the intermittent electric arc in every semi-cycle and its difficult renewal, especially if the cathode is sufficiently cooled. [2]

4. MAN OR ROBOT?

The dilemma indicating by this title has resulted from the necessity of planning an experiment which can be realized at a robotic or conventional work post.

The correlation of kinematic schemes of manipulators (mechanical structure of the robot) and the welding processes for which they are intended or suitable, is presented in Figure 5. Various jobs are covered by manipulators with basic translatory motions (Descartes coordinate system). They are mostly applied in the field of welding both for positioning of workpieces and for positioning of executive bodies, i.e. welding guns. When the latter domain is in question, i.e. welding robots, their manipulators are, to the largest extent, realized on the basis of spherical and polar coordinate systems. Manipulators with the cylindrical coordinate system have primary application in positioning workpieces. [1] [5]

From the aspect of comparative characteristics of man and robot, the advantage is given to robot because it possesses better characteristics:

- precision in the execution of operations,
- repeatability of operations,
- willing-physiological character...

5. CURENT RESEARCH

The use of noise as a feedback element in control systems is based on the analogy of welder's role in the welding process and the facts that he uses the sense of hearing in order to estimate the state of the process. Enabling the robot control system to make decisions on the basis of change of sound emission of the welding process represents a significant scientific challenge and has a great practical importance.

The aim of planned research is the elaboration of methodology for procession of sound emitted during the realization of the considered process which provides the control system with quality information for the purpose of establishing corrections of development and maintenance of the process in the desired state. That aim is accomplished by establishing a correlation between three groups of characteristics of the process: sound emission characteristics, values of the main parameters of the process and qualitative indicators of the process.

The achieved results of the research should increase the levels of knowledge about the possibilities of using sound in control processes as well as encourage other researchers to use their ideas in order to add to the developed methodology.

6. EPILOGUE

The challenge set by this paper is contained in the ambition of engineering copying of nature, which is, in this case, reduced to recognizing human characteristics that could be mapped to an artificial object, i.e. robot. Those goals can be achieved when certain scientific and technical possibilities are reached.

The result of the research should be a robot enabled to "hear", which would imitate one of the human abilities. As the robot has already been enabled to "see", and also to feel, the sense of hearing is another human ability it would be provided with.

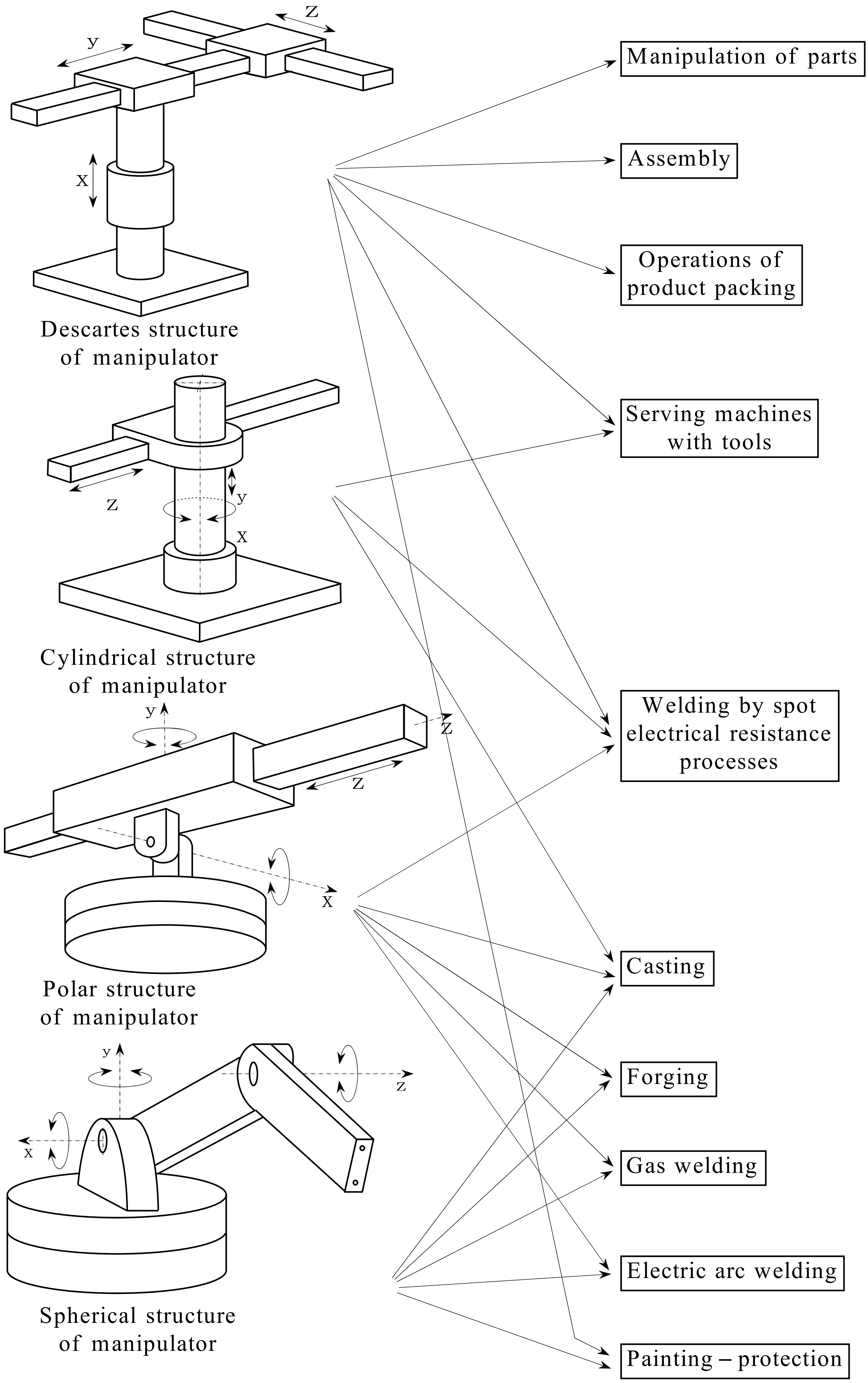

Figure 5: Schematic presentation of main types and condition of manipulator application

ACKNOWLEDGEMENTS

This paper is realized within the project TR 37020 funded by the Ministry of Education, Science and Technological Development.

REFERENCES

[1] Vukićević, M., “Uređaji i pribori u zavarivanju”, ISBN 978–86–82631–60–6, COBISS.SR–ID 191158284, Mašinski fakultet Kraljevo, Kraljevo, 2012

[2] Vukićević, M., „Tehnologije spajanja materijala“, Udžbenik u štampi, Fakultet za mašinstvo i građevinarstvo u Kraljevu, 2014

[3] Kalajdžić, M., “Tehnologija mašinogradnje“, Mašinski fakultet u Beogradu, 2002

[4] Mijić, M., „Audio sistemi“, Akademska misao, Beograd, 2011

[5] Pires, J. Norberto, „Welding Robots: technology, system issues and applications“, ISBN-10: 1852339535, Springer-Verlag London Limited 2006

[6] Pravica, P., Drinčić, D., „Elektroakustika“, VISER, Beograd, 200

Application of Sub Matrixes for Phase Process Optimization of Linear Programming

Milan Kolrević[1], Vladan Grković[1], Nenad Kolarević[2], Zvonko Petrović[1], Miloje Rajović[1]
[1]Faculty of Mechanical and Civil Engineering in Kraljevo, University of Kragujevac, Kraljevo, Serbia
[2]Faculty of Mechanical Engineering, University of Belgrade, Belgrade, Serbia

The problem of optimization of a multiphase production process by the linear programming method is very frequent in manufacturing practice. Instead of a classical solution to the problem, by creating constraint equations per production phase, the paper proposes the methodology of application of sub matrixes for solving the complex mathematical model of the problem in a matrix form.

The method is illustrated in the example of an optimization process of manufacturing and assembly of a hydraulic valve for regulation of pressure and flow, which is intended for installation on hydraulic bar feeders for CNC machines. Problem is solved by MatLab software package.

Keywords: Phase process, linear programming, optimization, sub matrixes

1. INTRODUCTION

In contrast to the single-phase production process in which the final products are directly produced from semi-finished products, multiphase process can be divided into several single-phase processes, interrelated and conditioned by the given constraints.

The number of levels of multiphase process breakdown is determined by objective conditions such as technology production process and assembly of the product, although breakdown can sometimes be also due to subjective decisions [1] [2].

The paper [2] discusses programming of multiphase processes that can be mathematically solved by linear programming method. The procedure of forming a mathematical model to optimize multiphase process is present in the example of manufacturing and assembly of hydraulic valves for regulating pressure and flow, which is designed for installation on hydraulic feeders from rod material for CNC machines.

The task consists of the following procedure [2]: it is necessary to program the multi-phase production process in order to produce the optimal amount of control valves from available quantity of semi-finished product and standard parts while at the same time profit from the sale of the valve is maximum. Market limitations in the amount of product placement do not exist.

2. MATHEMATICAL MODEL

The mathematical model in its matrix form reads:
It is necessary to maximize the objective function:.

$$\mathbf{max\ F(X) = d\ X} \tag{1}$$

with satisfying the constraints with respect to available quantities:

$$\mathbf{M\ X \le B} \tag{2}$$

and the non-negativity condition:

$$\mathbf{X \ge 0} \tag{3}$$

For the given example [2], the matrices **M** , **X** and **B** read:

$$X = \begin{bmatrix} x_1 \\ x_2 \\ x_3 \\ x_4 \\ x_5 \\ x_6 \\ x_7 \\ x_8 \\ x_9 \\ x_{10} \\ x_{11} \\ x_{12} \\ x_{13} \end{bmatrix} \qquad B = \begin{bmatrix} 10026,24 \\ 38,733 \\ 12,255 \\ 6,456 \\ 53,36 \\ 38,142 \\ 22,694 \\ 500 \\ 600 \\ 500 \\ 700 \\ 500 \\ 600 \\ 1000 \\ 700 \\ 0 \\ 0 \\ 0 \\ 0 \\ 0 \\ 0 \\ 0 \\ 0 \\ 0 \\ 0 \\ 0 \\ 0 \end{bmatrix}$$

*Corresponding author: Dositejeva 19, 36000 Kraljevo, Serbia, kolarevic.m@mfkv.kg.ac.rs

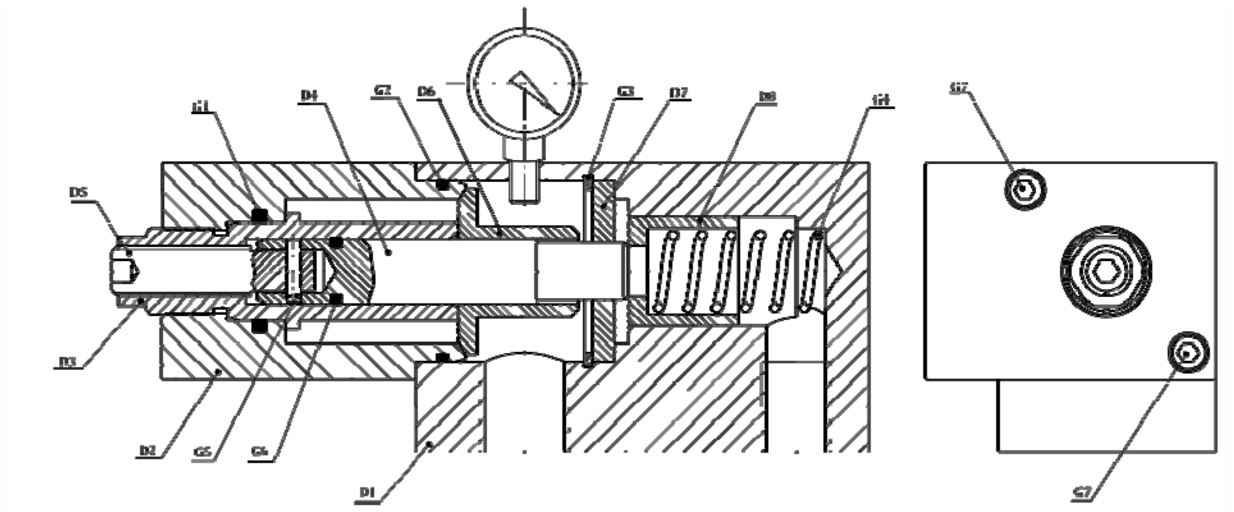

Fig. 1. Assembly structure of the product

$$
\mathbf{M} = \left[\begin{array}{cccccccc|ccc|c|c}
4{,}888 & 3{,}459 & 0 & 0 & 0 & 0 & 0 & 0 & 0 & 0 & 0 & 0 & 0 \\
0 & 0 & 0{,}646 & 0 & 0 & 0 & 0 & 0 & 0 & 0 & 0 & 0 & 0 \\
0 & 0 & 0 & 0{,}219 & 0 & 0 & 0 & 0 & 0 & 0 & 0 & 0 & 0 \\
0 & 0 & 0 & 0 & 0{,}097 & 0 & 0 & 0 & 0 & 0 & 0 & 0 & 0 \\
0 & 0 & 0 & 0 & 0 & 0{,}534 & 0 & 0 & 0 & 0 & 0 & 0 & 0 \\
0 & 0 & 0 & 0 & 0 & 0 & 0{,}191 & 0 & 0 & 0 & 0 & 0 & 0 \\
0 & 0 & 0 & 0 & 0 & 0 & 0 & 0{,}199 & 0 & 0 & 0 & 0 & 0 \\
\hline
0 & 0 & 0 & 0 & 0 & 0 & 0 & 0 & 0 & 1 & 0 & 0 & 0 \\
0 & 0 & 0 & 0 & 0 & 0 & 0 & 0 & 0 & 1 & 0 & 0 & 0 \\
0 & 0 & 0 & 0 & 0 & 0 & 0 & 0 & 0 & 0 & 1 & 0 & 0 \\
0 & 0 & 0 & 0 & 0 & 0 & 0 & 0 & 0 & 0 & 1 & 0 & 0 \\
0 & 0 & 0 & 0 & 0 & 0 & 0 & 0 & 1 & 0 & 0 & 0 & 0 \\
0 & 0 & 0 & 0 & 0 & 0 & 0 & 0 & 1 & 0 & 0 & 0 & 0 \\
0 & 0 & 0 & 0 & 0 & 0 & 0 & 0 & 0 & 0 & 0 & 0 & 2 \\
0 & 0 & 0 & 0 & 0 & 0 & 0 & 0 & 0 & 0 & 0 & 0 & 1 \\
\hline
-1 & 0 & 0 & 0 & 0 & 0 & 0 & 0 & 0 & 0 & 1 & 0 & 0 \\
0 & -1 & 0 & 0 & 0 & 0 & 0 & 0 & 0 & 1 & 0 & 0 & 0 \\
0 & 0 & -1 & 0 & 0 & 0 & 0 & 0 & 1 & 0 & 0 & 0 & 0 \\
0 & 0 & 0 & -1 & 0 & 0 & 0 & 0 & 1 & 0 & 0 & 0 & 0 \\
0 & 0 & 0 & 0 & -1 & 0 & 0 & 0 & 1 & 0 & 0 & 0 & 0 \\
0 & 0 & 0 & 0 & 0 & -1 & 0 & 0 & 1 & 0 & 0 & 0 & 0 \\
0 & 0 & 0 & 0 & 0 & 0 & -1 & 0 & 0 & 0 & 1 & 0 & 0 \\
0 & 0 & 0 & 0 & 0 & 0 & 0 & -1 & 0 & 0 & 1 & 0 & 0 \\
\hline
0 & 0 & 0 & 0 & 0 & 0 & 0 & 0 & -1 & 0 & 0 & 1 & 0 \\
0 & 0 & 0 & 0 & 0 & 0 & 0 & 0 & 0 & -1 & 0 & 1 & 0 \\
0 & 0 & 0 & 0 & 0 & 0 & 0 & 0 & 0 & 0 & -1 & 0 & 1 \\
\hline
0 & 0 & 0 & 0 & 0 & 0 & 0 & 0 & 0 & 0 & 0 & -1 & 1
\end{array}\right]
$$

It can be noted that the matrix of coefficients **M**, the matrix of variables **X** and the matrix of constraints **V** consist of several sub matrixes. In the given example, the matrix **M** is of dimension p x q and is composed of p x q = 5 x 4 = 20 sub matrixes. If the following marks are introduced:

- i – the number of different semi-finished products
- j – the number of standard parts
- k – the number of parts fabricated in first phase
- l – the number of sub-assemblies fabricated in second phase
- m – the number of main assemblies fabricated in third phase
- n – the number of products
- s – the number of phases

Main matrix **M** can be present in the following shape:

$$
\mathbf{M} = \left[\begin{array}{c|c|c|c}
M_{11} & M_{12} & M_{13} & M_{14} \\
\hline
M_{21} & M_{22} & M_{23} & M_{24} \\
\hline
M_{31} & M_{32} & M_{33} & M_{34} \\
\hline
M_{41} & M_{42} & M_{43} & M_{44} \\
\hline
M_{51} & M_{52} & M_{53} & M_{54}
\end{array}\right] \begin{array}{c} q \\ \\ \\ \\ p \end{array}
$$

wherein matrix dimension are

$$p = s+1$$

$$q = s$$

The generating of sub matrixes of matrix **M** can be performed in the following manner:

a) The formation of the first column of matrix **M** from its sub matrixes is as follows

Sub matrix $\mathbf{M_{11}}$ is of dimension *i* x *k* , sub matrix $\mathbf{M_{21}}$ is of dimension *j* x *k*, sub matrix $\mathbf{M_{31}}$ is of dimension *k* x *k*, sub matrix $\mathbf{M_{41}}$ is of dimension *l* x *k*, sub matrix $\mathbf{M_{51}}$ is of dimension *m* x *k*. For presented example [2] these matrixes are:

$$M_{11} = \begin{bmatrix} 4,888 & 3,459 & 0 & 0 & 0 & 0 & 0 & 0 \\ 0 & 0 & 0,646 & 0 & 0 & 0 & 0 & 0 \\ 0 & 0 & 0 & 0,219 & 0 & 0 & 0 & 0 \\ 0 & 0 & 0 & 0 & 0,097 & 0 & 0 & 0 \\ 0 & 0 & 0 & 0 & 0 & 0,534 & 0 & 0 \\ 0 & 0 & 0 & 0 & 0 & 0 & 0,191 & 0 \\ 0 & 0 & 0 & 0 & 0 & 0 & 0 & 0,199 \end{bmatrix}_i^k$$

$$M_{21} = \begin{bmatrix} 0 & 0 & 0 & 0 & 0 & 0 & 0 & 0 \\ 0 & 0 & 0 & 0 & 0 & 0 & 0 & 0 \\ 0 & 0 & 0 & 0 & 0 & 0 & 0 & 0 \\ 0 & 0 & 0 & 0 & 0 & 0 & 0 & 0 \\ 0 & 0 & 0 & 0 & 0 & 0 & 0 & 0 \\ 0 & 0 & 0 & 0 & 0 & 0 & 0 & 0 \\ 0 & 0 & 0 & 0 & 0 & 0 & 0 & 0 \\ 0 & 0 & 0 & 0 & 0 & 0 & 0 & 0 \end{bmatrix}_j^k$$

$$M_{31} = \begin{bmatrix} -1 & 0 & 0 & 0 & 0 & 0 & 0 & 0 \\ 0 & -1 & 0 & 0 & 0 & 0 & 0 & 0 \\ 0 & 0 & -1 & 0 & 0 & 0 & 0 & 0 \\ 0 & 0 & 0 & -1 & 0 & 0 & 0 & 0 \\ 0 & 0 & 0 & 0 & -1 & 0 & 0 & 0 \\ 0 & 0 & 0 & 0 & 0 & -1 & 0 & 0 \\ 0 & 0 & 0 & 0 & 0 & 0 & -1 & 0 \\ 0 & 0 & 0 & 0 & 0 & 0 & 0 & -1 \end{bmatrix}_k^k$$

$$M_{41} = \begin{bmatrix} 0 & 0 & 0 & 0 & 0 & 0 & 0 & 0 \\ 0 & 0 & 0 & 0 & 0 & 0 & 0 & 0 \\ 0 & 0 & 0 & 0 & 0 & 0 & 0 & 0 \end{bmatrix}_l^k$$

$$M_{51} = \begin{bmatrix} 0 & 0 & 0 & 0 & 0 & 0 & 0 & 0 \end{bmatrix}_m^k$$

b) The formation of the second column of matrix **M** from its sub matrixes for given example is as follows

$$M_{12} = \begin{bmatrix} 0 & 0 & 0 \\ 0 & 0 & 0 \\ 0 & 0 & 0 \\ 0 & 0 & 0 \\ 0 & 0 & 0 \\ 0 & 0 & 0 \\ 0 & 0 & 0 \end{bmatrix}_i^l \quad M_{22} = \begin{bmatrix} 0 & 1 & 0 \\ 0 & 1 & 0 \\ 0 & 0 & 1 \\ 0 & 0 & 1 \\ 1 & 0 & 0 \\ 1 & 0 & 0 \\ 0 & 0 & 0 \\ 0 & 0 & 0 \end{bmatrix}_j^l$$

$$M_{32} = \begin{bmatrix} 0 & 0 & 1 \\ 0 & 1 & 0 \\ 1 & 0 & 0 \\ 1 & 0 & 0 \\ 1 & 0 & 0 \\ 1 & 0 & 0 \\ 0 & 0 & 1 \\ 0 & 0 & 1 \end{bmatrix}_k^l \quad M_{42} = \begin{bmatrix} -1 & 0 & 0 \\ 0 & -1 & 0 \\ 0 & 0 & -1 \end{bmatrix}_l^l;$$

$$M_{52} = \begin{bmatrix} 0 & 0 & 0 \end{bmatrix}_m^l;$$

c) The formation of the third column of matrix **M** from its sub matrixes for given example is as follows

$$M_{13} = \begin{bmatrix} 0 \\ 0 \\ 0 \\ 0 \\ 0 \\ 0 \\ 0 \end{bmatrix}_i^m; \quad M_{23} = \begin{bmatrix} 0 \\ 0 \\ 0 \\ 0 \\ 0 \\ 0 \\ 0 \\ 0 \end{bmatrix}_j^m; \quad M_{33} = \begin{bmatrix} 0 \\ 0 \\ 0 \\ 0 \\ 0 \\ 0 \\ 0 \\ 0 \end{bmatrix}_k^m;$$

$$M_{43} = \begin{bmatrix} 1 \\ 1 \\ 0 \end{bmatrix}_l^m; \quad M_{53} = \begin{bmatrix} -1 \end{bmatrix}_m^m;$$

d) The formation of the fourth column of matrix **M** from its sub matrixes for given example is as follows

$$M_{14} = \begin{bmatrix} 0 \\ 0 \\ 0 \\ 0 \\ 0 \\ 0 \\ 0 \end{bmatrix}_i^n; \quad M_{24} = \begin{bmatrix} 0 \\ 0 \\ 0 \\ 0 \\ 0 \\ 0 \\ 2 \\ 1 \end{bmatrix}_j^n; \quad M_{34} = \begin{bmatrix} 0 \\ 0 \\ 0 \\ 0 \\ 0 \\ 0 \\ 0 \\ 0 \end{bmatrix}_k^n;$$

$$M_{44} = \begin{bmatrix} 0 \\ 0 \\ 1 \end{bmatrix}_l^n; \quad M_{54} = \begin{bmatrix} 1 \end{bmatrix}_m^n;$$

One can note the following:

- sub matrixes **M12**, **M13** и **M14** are zero matrixes because in phase processes achievement of sub-assemblies, main assemblies and products is not possible just from semi-finished products;
- sub-matrixes **M41**, **M51** и **M52** are also zero matrices because it is not possible to achieve part from sub-assemblies and assemblies, nor is it possible to achieve sub-assembly from main assembly;
- sub-matrixes **M31**, **M42** and **M53** are diagonal matrices wherein the elements on the main diagonal have a value of -1, so they represent a scalar matrices, ie.

$$M_{31} = [-1a]_k^k$$
$$M_{42} = [-1a]_l^l$$
$$M_{53} = [-1a]_m^m$$

which are negative of

$$M_{31} = -E = [-a]_k^k$$
$$M_{42} = -E = [-a]_l^l$$
$$M_{53} = -E = [-a]_m^m$$

The mentioned matrixes can be defined solely on *i, j, k, l, m, n* and *s* values, while the other sub matrixes of main matrix **M** can be formed on the basis of data for each phase of development.

The matrix **X** is a matrix of columns and will have as many sub matrixes as phases in the process that is. *r = s*, so there are 4 sub matrixes in the given example:

$$\mathbf{X} = \begin{bmatrix} X_1 \\ X_2 \\ X_3 \\ X_4 \end{bmatrix}_r^1 ,$$

The number of elements of sub matrixes are:

- for matrix **X1** the number of elements is equal to the number of parts k,
- for matrix **X2** the number of elements is equal to the number of sub-assemblies l,
- for matrix **X3** the number of elements is equal to the number of main assemblies m, and
- for matrix **X4** the number of elements is equal to the number of products n.

Sub matrixes of matrix **X** for given example are:

$$X_1 = \begin{bmatrix} x_1 \\ x_2 \\ x_3 \\ x_4 \\ x_5 \\ x_6 \\ x_7 \\ x_8 \end{bmatrix}_k^1 ; \quad X_2 = \begin{bmatrix} x_9 \\ x_{10} \\ x_{11} \end{bmatrix}_l^1 ;$$

$$X_3 = [x_{12}]_m^1 ; \quad X_4 = [x_{13}]_n^1 .$$

The matrix **B** is also column matrix and consists of *c=s+1* column matrixes:

$$B = \begin{bmatrix} B_1 \\ B_2 \\ B_3 \\ B_4 \\ B_5 \end{bmatrix}_c^1$$

The number of elements of sub matrixes is:

- the number of elements of the matrix **B1** is equal to the number of semi-finished products,
- the number of elements of the matrix **B2** is equal to the number of standard parts,
- the number of elements of the matrix **B3** is equal to the number of parts,
- the number of elements of the matrix **B4** is equal to the number of sub-assemblies,
- the number of elements of the matrix **B5** is equal to the number of main assemblies.

Sub matrixes **B3**, **B4**, **B5**, are zero matrixes, while sub matrix **B1** represents available quantity of semi-finished products and sub matrix **B2** represent available amount of standard parts. For given example these sub matrixes are:

$$B_1 = \begin{bmatrix} 10026,24 \\ 38,733 \\ 12,255 \\ 6,456 \\ 53,36 \\ 38,142 \\ 22,696 \end{bmatrix}_i^1 ; \quad B_2 = \begin{bmatrix} 500 \\ 600 \\ 500 \\ 700 \\ 500 \\ 600 \\ 1000 \\ 700 \end{bmatrix}_j^1 ; \quad B_3 = \begin{bmatrix} 0 \\ 0 \\ 0 \\ 0 \\ 0 \\ 0 \\ 0 \\ 0 \end{bmatrix}_k^1 ;$$

$$B_4 = \begin{bmatrix} 0 \\ 0 \\ 0 \end{bmatrix}_l^1 ; \quad B_5 = [0]_m^1$$

3. PROBLEM SOLVING

For solving the multiphase problem of linear programming with sub matrixes the software package MATLAB is used. For data from the mentioned example program code is written in the following form:

```
i=7;
j=8;
k=8;
l=3;
m=1;
n=1;
s=4;

M11=[4.888 3.459 0 0 0 0 0 0; ...
     0 0 0.646 0 0 0 0 0;...
     0 0 0 0.219 0 0 0 0;...
     0 0 0 0 0.097 0 0 0;...
     0 0 0 0 0 0.534 0 0;...
```

```
    0 0 0 0 0 0 0.191 0;...
    0 0 0 0 0 0 0 0.199;]

M21=zeros(j,k)
M31=-eye(k)
M41=zeros(l,k)
M51=zeros(m,k)

M12=zeros(i,l)
M22=[0 1 0;...
     0 1 0;...
     0 0 1;...
     0 0 1;...
     1 0 0;...
     1 0 0;...
     0 0 0;...
     0 0 0;]
M32=[0 0 1;...
     0 1 0;...
     1 0 0;...
     1 0 0;...
     1 0 0;...
     0 0 0;...
     0 0 1;...
     0 0 1;]
M42=-eye(l)
M52=zeros(m,l)

M13=zeros(i,m)
M23=[0;0;0;0;0;0;0;0]
M33=[0;0;0;0;0;1;0;0]
M43=[1;1;0]
M53=-eye(m)

M14=zeros(i,n)
M24=[0;0;0;0;0;0;2;1]
M34=[0;0;0;0;0;0;0;0]
M44=[0;0;1]
M54=[1]

M=[M11 M12 M13 M14;
   M21 M22 M23 M24;
   M31 M32 M33 M34;
   M41 M42 M43 M44;
   M51 M52 M53 M54;]

B1=[10026.24;38.733;12.255;6.456;53.36;38.1
42;22.696]
B2=[500;600;500;700;500;600;1000;700]
B3=zeros(k,1)
B4=zeros(l,1)
B5=zeros(m,1)
B=[B1;B2;B3;B4;B5]

F=[0 0 0 0 0 0 0 0 0 0 0 0 0 100]'

[x,fval,exitflag,output]=linprog(-
F,M,B,[],[],[],[],[])
```

After the sixth iteration the following solution is obtained:

```
x =
  1.0e+003 *

    1.1322
    1.0206
    0.0577
    0.0560
    0.0632
    0.0813
    0.1648
    0.1026
    0.0560
    0.2317
    0.0762
    0.0560
    0.0560

fval =
 -5.5959e+003

exitflag =
     1
output =
      iterations: 6
       algorithm:   'large-scale:   interior
point'
    cgiterations: 0
```

Therefore, based on the available quantity of semi-finished products and standard parts it is possible to produce 56 units of a product, where the profit of 5.600,00 of monetary units is achieved.

4. CONCLUSION

The paper [2] presents the methodology of a mathematical modeling of the phase process of linear programming in matrix form. Unlike the traditional way of mathematical modeling where for each phase equations of restrictions for certain category of recourses are defined, by applying this methodology it is possible to define the matrixes **X**, **M** and **B** from the summary table, which defines the forming of the product in phases, which significantly reduces errors occurrence in the mathematical modeling process.

For multiphase problems in linear programming that have many constraints and variables, matrixes **X**, **M** and **B** can be expressed by sub matrixes which simplifies the process of mathematical modelling because the majority of sub matrixes can be defined automatically.

Due to limited space, in this paper, four phase production problem is analyzed on practical example only with constraints of the available quantities of semi-finished products and standard parts. For solving the problem MatLab software package is used.

Real practical problems are more complex because products are more complex, requiring a greater number production phases, and mathematical models have more resource constraints such as: labor restriction, the available capacity of machines, market constraints, the available monetary fund and etc.

Further authors efforts will be focused on the software solving of the problem with unlimited number of phases and large number of different types of constraints.

ACKNOWLEDGEMENT

The authors would like to express their gratitude to the Ministry of Education and Science of the Republic of Serbia for their support to this research through the project TR37020.

REFERENCES

[1] Vadnal A., Primjena matematičkih metoda u ekonomiji, Informator, Zagreb, 1980.

[2] Kolarević M., Grković V., Radičević B., Petrović Zv., Model For Optimization Of Phase Processes By The Linear Programming Method, 36th International Conference on Production Engineering, Kopaonik, 2013, pp61-68

[3] Rajović M., Linearna algebra – teorija matrica i linearnih operatora, Akademska misao, Beograd, 2007.

[4] Mamuzić Z., Determinante, matrice, vektori, analitička geometrija, Građevinska knjiga, Beograd, 1974.

Application of the COPRAS Method for Selection of Competitive Non-Conventional Machining Processes

Miloš Madić[1*], Miroslav Radovanović[1], Danijel Marković[2], Goran Petrović[2]
[1]Faculty of Mechanical Engineering in Niš/Department of Production Engineering, University of Niš, Niš, Serbia
[2]Faculty of Mechanical Engineering in Niš/Department of Transport Engineering, University of Niš, Niš, Serbia

Evaluation and selection of competitive non-conventional machining processes (NCMPs) for a given machining application is a multi-criteria decision making (MCDM) problem with many conflicting and diverse criteria. Although a large number of MCDM methods have been proposed to evaluate and select the most suitable NCMP, this paper explores the applicability and capability of complex proportional assessment (COPRAS) method for solving NCMPs selection problems. Two case studies dealing with selection of the most suitable NCMP were selected to illustrate computational procedure and applicability of the COPRAS method. The obtained results have very good correlation with those derived by the past researchers which validates the usefulness of this method while solving complex NCMPs selection problems.

Keywords: Non-conventional machining processes, COPRAS, Decision making

1. INTRODUCTION

Machining of advanced materials having high tensile strength, hardness and heat resistance is much more difficult and in some cases of complex shapes and contours even impossible. From these reasons, during past several decades, there has been a wide application of so called non-conventional machining processes (NCMPs) [1]. By NCMPs there is no direct contact between cutting tool and workpiece material, instead the material is removed based on the use of physical and chemical phenomena i.e. on the use of thermal, electrical, light or chemical energy or a combination of these energies. A particular characteristic of NCMPs is the ability to concentrate large amounts of energy per unit area. The NCMPs fulfill the requirements of high dimensional accuracy and surface finish, high material removal rate, process automation, miniaturization, waste reduction, machining of very complex contours, precision machining of hard-to-reach areas, etc [1, 2].

Thanks to the numerous advantages and unique characteristics NCMPs have evolved continuously over the years. Laser beam machining (LBM), abrasive jet machining (AJM), electrical discharge machining (EDM), wire electrical discharge machining (WEDM), plasma arc machining (PAM), electrochemical machining (ECM), water jet machining (WJM), ultrasonic machining (USM), electron beam machining (EBM), chemical machining (CHM) are now being widely used in industry for material machining.

Due to the presence of complex physical characteristics of various NCMPs along with a dearth of experts in this domain, it becomes quite difficult for a process engineer to select the most appropriate NCMP for a specific machining application. A particular NCMP found suitable under the given conditions may not be equally efficient under other conditions [3]. While selecting a NCMP to be employed, the following aspects are usually considered [4]: (*i*) physical parameters, (*ii*) properties of the workpiece material and shape feature to be machined, (*iii*) process capability and (*iv*) economy.

These aforesaid considerations make the comparison and selection of NCMPs a difficult multi-criteria decision making (MCDM) problem. Tolerance and surface finish, power requirement, material removal rate, cost, efficiency, tooling and fixtures, tool consumption, safety, work material, shape feature are considered as one of the main criteria that influence the NCMP selection for a given machining application.

Various MCDM methods and different optimization procedures have been proposed in literature to make the selection process more objective. In order to evaluate and rank competitive NCMPs, the decision making problem includes selection of relevant criteria, selection of alternative NCMPs, determination of the relative significance of each criterion, weighting the criteria and obtaining of ranking performance.

The past researchers have already applied various MCDM methods like combined analytic hierarchy process (AHP) and technique for order performance by similarity to ideal solution (TOPSIS) [5, 6], AHP method [7], digraph-based approach [4], multi-objective optimization using ratio analysis (MOORA) [8], analytic network process (ANP) [9], data envelopment analysis (DEA) [10], preference ranking organization method for enrichment evaluation (PROMETHEE) and geometrical analysis for interactive aid (GAIA) [3], TOPSIS and fuzzy TOPSIS [11] and evaluation of mixed data (EVAMIX) [12] for ranking and selection of the most suitable NCMP for different machining applications. Despite the development of a large number of MCDM methods, none can be considered as the “super method” appropriate to all decision making situations [13]. As noted by Karande and Chakraborty [3] sometimes it is not possible for the adopted MCDM methods, like AHP, ANP, TOPSIS, DEA etc. to provide optimal solutions to the NCMPs selection problems due to the involvement of the decision makers in pair-wise comparing the performance of different NCMPs with respect to the considered selection criteria. Moreover, some methods are not flexible enough to model the decision makers’ preferences or have complex mathematical computations and require extensive

*Corresponding author: Faculty of Mechanical Engineering in Niš, University of Niš, A. Medvedeva 14, 18000 Niš, Serbia, madic@masfak.ni.ac.rs

knowledge on graph theory, linear programming, etc. [12]. As noted by Hajkowicz and Higgins [14] the ease of understanding of an MCDM method is a primary concern in the choice of whether (or not) it will be used.

This paper focuses on the application of complex proportional assessment (COPRAS) method to help the process engineers in selecting the most suitable NCMP for a given machining application. Two real time case studies were solved using this method and obtained results prove the applicability, usefulness, and accuracy of the COPRAS method while solving complex NCMPs selection problems.

2. MCDM METHODS

Multiple criterion decision making (MCDM) refers to making decisions in the presence of multiple conflicting criteria. A typical MCDM problem consists of four main components: (a) alternatives, (b) criteria, (c) criteria weights or relative importance of each criterion and (d) performance measures of alternatives with respect to criteria. On the basis of aforementioned components a decision matrix (or decision table) is formed (Table 1).

Table 1: Decision matrix in MCDM methods

Alternatives	Criteria			
	C_1	C_2	...	C_n
	w_1	w_2	...	w_n
A_1	x_{11}	x_{12}	...	x_{1n}
A_2	x_{21}	x_{22}	...	x_{2n}
...	...	...	...	...
A_m	x_{m1}	x_{m2}	...	x_{mn}

The decision matrix shows alternatives, A_i (i = 1, 2,…,m), criteria, C_j (j = 1, 2,...,n), criteria weights, w_j (j = 1, 2,...,n) where $\sum_{j=1}^{m} w_j = 1$ and performance measures of alternatives with respect to criteria, x_{ij} (i = 1, 2,…,m; j = 1, 2,...,n). Both X and W may contain either ordinal or cardinal data, or a mix of both. In any case, all the elements in the decision matrix must be normalized to the same units so that all the possible criteria can be considered in the decision problem.

Here it should be noted that criteria can be beneficial (where higher performance measures are preferable) and non-beneficial (where lower performance measures are preferable). Given the decision matrix, decision maker applies certain MCDM method in order to [14]:

- Define the function $r_i = f_1(X,W)$, $R = \{r_1,...,r_n\}$ and provide a rank order of the alternatives and/or;
- Define the function $u_i = f_2(X,W)$, $U = \{u_1,...,u_n\}$ and provide a utility score for each alternative.

In the MCDM process determination of criteria weights is very important. Except the AHP method, other methods do not handle determination of criteria weights. Therefore, combination of AHP with other MCDM methods is very popular approach in decision making process.

3. COPRAS METHOD

The complex proportional assessment (COPRAS) method was developed by Zavadskas et al. [15]. During past years it has been particularly applied for solving a variety of decision making problems within the built environment. In this method, the influence of maximizing and minimizing criteria on the evaluation result is considered separately. The selection of the best alternative is based considering both the ideal and the anti-ideal solutions. The main procedure of the COPRAS method includes several steps [16].

Step 1: Set the initial decision matrix, X:

$$X = \left[x_{ij}\right]_{m\times n} = \begin{bmatrix} x_{11} & x_{12} & \dots & x_{1n} \\ x_{21} & x_{22} & \dots & x_{2n} \\ \dots & \dots & \dots & \dots \\ x_{m1} & x_{m2} & \dots & x_{mn} \end{bmatrix} \tag{1}$$

where x_{ij} is the assessment value of the i-th alternative with respect to the j-th criterion, m is the number of alternatives and n is the number of criteria.

Step 2: Normalization of the decision matrix by using the following equation:

$$R = \left[r_{ij}\right]_{m\times n} = x_{ij} / \sum_{i=1}^{m} x_{ij} \tag{2}$$

Step 3: Determination of the weighted normalized decision matrix, D, by using the following equation:

$$D = \left[y_{ij}\right]_{m\times n} = r_{ij} \cdot w_j,\ i = 1,...,m,\ j = 1,...,n \tag{3}$$

where r_{ij} is the normalized performance value of the i-th alternative on j-th criterion and w_j is the weight of the j-th criterion.

The sum of weighted normalized values of each criterion is always equal to the weight for that criterion:

$$\sum_{i=1}^{m} y_{ij} = w_j \tag{4}$$

Step 4: In this step the sums of weighted normalized values are calculated for both the beneficial and non-beneficial criteria by using the following equations:

$$S_{+i} = \sum_{j=1}^{n} y_{+ij} \tag{5}$$

$$S_{-i} = \sum_{j=1}^{n} y_{-ij} \tag{6}$$

where y_{+ij} and y_{-ij} are the weighted normalized values for the beneficial and non-beneficial criteria, respectively.

Step 5: Determination of the relative significances of the alternatives, Q_i, by using the following equation:

$$Q_i = S_{+i} + \frac{S_{-\min} \cdot \sum_{i=1}^{m} S_{-i}}{S_{-i} \cdot \sum_{i=1}^{m} \left(S_{-\min} / S_{-i}\right)},\ i = 1,...,m \tag{7}$$

where S_{-min} is the minimum value of S_{-i}.

Step 6: Calculation of the quantitative utility, U_i, for the i-th alternative by using the following equation:

$$U_i = \frac{Q_i}{Q_{\max}} \cdot 100\% \tag{8}$$

where Q_{max} is the maximum relative significance value.

As a consequence of Eq. 8, utility values of the candidate alternatives range from 0% to 100%.The greater the value of U_i, the higher is the priority of the alternative. Based on alternative’s utility values a complete ranking of the competitive alternatives can be obtained.

4. CASE STUDIES

In order to demonstrate applicability of the COPRAS method two case studies dealing with selection of competitive NCMPs are considered. In each case study the results obtained using the COPRAS method were compared with the results obtained by previous researchers using different MCDM methods.

4.1. Case Study 1

Yurdakul and Cogun [5] developed an MCDM procedure for NCMPs selection using TOPSIS and AHP methods. The NCMPs selection problem considered five NCMPs (AJM, USM, CHM, EBM and LBM) and seven criteria i.e. tolerance (T), surface finish (SF), surface damage (SD), taper (TR), material removal rate (MRR), work material (WM) and cost (C). Among the considered criteria, MRR and WM are beneficial criteria where higher values are preferred. The decision matrix for the case study is given in Table 2.

In order to determine the criteria weights, Rao [17] applied AHP method and subsequently applied AHP and TOPSIS methods. The criteria weights were obtained as: w_T=0.32, w_{SF}=0.19, w_{SD}=0.04, w_{TR}=0.04, w_{MRR}=0.19, w_{WM}=0.11 and w_C=0.11. The same criteria weights were used by Karande and Chakraborty [3] while applying PROMETHEE method. These criteria weights are also considered here for the subsequent analyzes.

The detailed computational procedure of the COPRAS method for solving the aforestated NCMP selection problem is as follows. By using Eq. 2 the normalized decision matrix is obtained (Table 3). As mentioned earlier, the purpose of normalization is to obtain dimensionless performance values of alternatives with respect to each criterion so that all candidate alternatives can be compared on the equal basis. Subsequently by using Eq. 3 the weighted normalized decision matrix is obtained (Table 4). By applying Eqs. 5 and 6 sums of weighted normalized values are calculated for all alternatives. Subsequently, relative significance (priority) of each alternative was obtained by using Eq. 7 (Table 5). Finally, by using Eq. 8, quantitative utility for each alternative was calculated (Table 6). From Table 6 the ranking of the competitive NCMPs is obtained as USM-LBM-AJM-EBM-CHM. Hence the most appropriate NCMP is USM. LBM is the second choice followed by AJM, and CHM is the last choice. Yurdakul and Cogun [5] also obtained USM as the most suitable NCMP.

The comparison of the derived ranking with the results obtained by previous researchers using different MCDM methods is given in Table 7.

Table 2: Decision matrix for case study 1

	T (mm)	SF (μm)	SD (μm)	TR (mm/mm)	MRR (mm^3/min)	WM	C
Goal	Min	Min	Min	Min	Max	Max	Max
AJM	0.05	0.6	2.5	0.005	50	3	4
USM	0.013	0.5	25	0.005	500	3	5
CHM	0.03	2	5	0.3	40	1	2
EBM	0.02	3	100	0.02	2	3	1
LBM	0.02	1	100	0.05	2	3	1

Table 3: Normalized decision matrix

AJM	0.3759	0.0845	0.0108	0.0132	0.0842	0.2308	0.3077
USM	0.0977	0.0704	0.1075	0.0132	0.8418	0.2308	0.3846
CHM	0.2256	0.2817	0.0215	0.7895	0.0673	0.0769	0.1538
EBM	0.1504	0.4225	0.4301	0.0526	0.0034	0.2308	0.0769
LBM	0.1504	0.1408	0.4301	0.1316	0.0034	0.2308	0.0769

Table 4: Weighted normalized decision matrix

AJM	0.1203	0.0161	0.0004	0.0005	0.0160	0.0254	0.0338
USM	0.0313	0.0134	0.0043	0.0005	0.1599	0.0254	0.0423
CHM	0.0722	0.0535	0.0009	0.0316	0.0128	0.0085	0.0169
EBM	0.0481	0.0803	0.0172	0.0021	0.0006	0.0254	0.0085
LBM	0.0481	0.0268	0.0172	0.0053	0.0006	0.0254	0.0085

Table 5: Relative significance of competitive NCMPs

Q_i	0.1482	0.3844	0.1257	0.1431	0.1988
NCMP	AJM	USM	CHM	EBM	LBM

Table 6: Utility values of competitive NCMPs

U_i	38.5	100	32.7	37.2	51.7
NCMP	AJM	USM	CHM	EBM	LBM

Table 7: Rankings of the competitive NCMP obtained using different MCDM methods

	Yurdakul and Cogun [5]	COPRAS	PROMETHEE and and GAIA Karande and Chakraborty [3]	AHP Rao [17]	TOPSIS Rao [17]
AJM	5	3	3	3	2
USM	1	1	1	1	1
CHM	4	5	5	5	3
EBM	3	4	4	4	5
LBM	2	2	2	2	4

As could be seen from Table 7 application of different MCDM methods consistently yielded USM as the best suited NCMP and these results agree with the findings of Yurdakul and Cogun [5]. It could be observed that COPRAS method gives a perfect match for the competitive NCMPs as PROMETHEE and AHP methods.

4.2. Case Study 2

Chakladar and Chakraborty [6] proposed combined approach using TOPSIS and AHP methods for solving NCMPs selection problems. This case study deals with the selection of the most suitable NCMP that can efficiently machine precision holes on duralumin. The NCMPs selection problem considered nine NCMPs (USM, WJM, AJM, ECM, CHM, EDM, WEDM, EBM and LBM) and ten criteria i.e. tolerance and surface finish (TSF), power requirement (PR), material removal rate (MRR), cost (C), efficiency (E), tooling and fixtures (TF), tool consumption (TC), safety (S), work material (M) and shape feature (F). MRR, E, S, M and F are beneficial criteria where higher values are preferred, while TSF, PR, C, TF, and TC are non-beneficial criteria. The decision matrix of the NCMPs selection problem with criteria weights as determined in [6] is given in Table 8.

Again, by using Eq. 2 the normalized decision matrix is obtained (Table 9). Subsequently by using Eq. 3 the weighted normalized decision matrix is obtained (Table 10). By applying Eqs. 5 and 6 sums of weighted normalized values are calculated for all alternatives. Subsequently, relative significance (priority) of each alternative was obtained by using Eq. 7 (Table 11). Finally, by using Eq. 8, quantitative utility for each alternative was calculated (Table 12).

Table 8: Decision matrix for case study 2

	TSF (μm)	PR (kW)	MRR (mm^3/min)	C	E	TF	TC	S	M	F
Goal	Min	Min	Max	Min	Max	Min	Min	Max	Max	Max
Weights	0.0783	0.0611	0.1535	0.1073	0.0383	0.0271	0.0195	0.0146	0.2766	0.2237
USM	1	10	500	2	4	2	3	1	4	1
WJM	2.5	0.22	0.8	1	4	2	2	3	3	1
AJM	2.5	0.24	0.5	1	4	2	2	3	3	1
ECM	3	100	400	5	2	3	1	3	5	4
CHM	3	0.4	15	3	3	2	1	3	5	4
EDM	3.5	2.7	800	3	4	4	4	3	4	5
WEDM	3.5	2.5	600	3	4	4	4	3	4	5
EBM	2.5	0.2	1.6	4	5	2	1	3	4	1
LBM	2	1.4	0.1	3	5	2	1	1	4	1

Table 9: Normalized decision matrix

USM	0.0426	0.0850	0.2157	0.0800	0.1143	0.0870	0.1579	0.0435	0.1111	0.0435
WJM	0.1064	0.0019	0.0003	0.0400	0.1143	0.0870	0.1053	0.1304	0.0833	0.0435
AJM	0.1064	0.0020	0.0002	0.0400	0.1143	0.0870	0.1053	0.1304	0.0833	0.0435
ECM	0.1277	0.8499	0.1726	0.2000	0.0571	0.1304	0.0526	0.1304	0.1389	0.1739
CHM	0.1277	0.0034	0.0065	0.1200	0.0857	0.0870	0.0526	0.1304	0.1389	0.1739
EDM	0.1489	0.0229	0.3451	0.1200	0.1143	0.1739	0.2105	0.1304	0.1111	0.2174
WEDM	0.1489	0.0212	0.2588	0.1200	0.1143	0.1739	0.2105	0.1304	0.1111	0.2174
EBM	0.1064	0.0017	0.0007	0.1600	0.1429	0.0870	0.0526	0.1304	0.1111	0.0435
LBM	0.0851	0.0119	0.0000	0.1200	0.1429	0.0870	0.0526	0.0435	0.1111	0.0435

Table 10: Weighted normalized decision matrix

USM	0.0033	0.0052	0.0331	0.0086	0.0044	0.0024	0.0031	0.0006	0.0307	0.0097
WJM	0.0083	0.0001	0.0001	0.0043	0.0044	0.0024	0.0021	0.0019	0.0231	0.0097
AJM	0.0083	0.0001	0.0000	0.0043	0.0044	0.0024	0.0021	0.0019	0.0231	0.0097
ECM	0.0100	0.0519	0.0265	0.0215	0.0022	0.0035	0.0010	0.0019	0.0384	0.0389
CHM	0.0100	0.0002	0.0010	0.0129	0.0033	0.0024	0.0010	0.0019	0.0384	0.0389
EDM	0.0117	0.0014	0.0530	0.0129	0.0044	0.0047	0.0041	0.0019	0.0307	0.0486
WEDM	0.0117	0.0013	0.0397	0.0129	0.0044	0.0047	0.0041	0.0019	0.0307	0.0486
EBM	0.0083	0.0001	0.0001	0.0172	0.0055	0.0024	0.0010	0.0019	0.0307	0.0097
LBM	0.0067	0.0007	0.0000	0.0129	0.0055	0.0024	0.0010	0.0006	0.0307	0.0097

Table 11: Relative significance of competitive NCMPs

Q_i	0.1162	0.0886	0.0886	0.1176	0.1156	0.1630	0.1499	0.0772	0.0825
NCMP	USM	WJM	AJM	ECM	CHM	EDM	WEDM	EBM	LBM

Table 12: Utility values of competitive NCMPs

U_i	71.3	54.4	54.3	72.1	70.9	100	91.9	47.4	50.6
NCMP	USM	WJM	AJM	ECM	CHM	EDM	WEDM	EBM	LBM

As could be seen from Table 12 the ranking of competitive NCMP is obtained as EDM-WEDM-ECM-USM-CHM-WJM-AJM-LBM-EBM. EDM is observed to be the most suitable NCMP for this machining application whereas LBM is the least favored.

The same problem was solved by Chakladar and Chakraborty [6], Karande and Chakraborty [3] and Chaterjee and Chakraborty [12] by using combined TOPSIS and AHP method, PROMETHEE and and GAIA, and EVAMIX method, respectively. The ranking performance of the COPRAS method with respect to those derived by past researchers is given in Table 13.

When dealing with complex MCDM problems agreement of MADM methods can be assessed by the Spearman rank correlation coefficient (r_s) which calculates the sums of the squares of the deviations between the different rankings. The formula for the Spearman rank correlation coefficient is [18]:

$$r_s = 1 - \frac{\sum_{i=1}^{n} D^2}{n \cdot \left(n^2 - 1\right)} \tag{9}$$

where n is the number of pairs of ranks and D is the difference between a pair of ranks.

Table 14 represents Spearman's rank correlation coefficients between mentioned methods. High rank correlation between COPRAS and combined TOPSIS and AHP method (0.82), COPRAS and PROMETHEE and GAIA method (0.73) and COPRAS and EVAMIX (0.75) in Table 14 shows the potentiality and suitability of the COPRAS method for solving complex NCMPs selection problems.

Table 13: Rankings of the competitive NCMP obtained using different MCDM methods

	COPRAS	Combined TOPSIS and AHP Chakladar and Chakraborty [6]	PROMETHEE and GAIA Karande and Chakraborty [3]	EVAMIX Chaterjee and Chakraborty [12]
USM	4	5	4	6
WJM	6	8	8	8
AJM	7	9	9	9
ECM	3	2	3	4
CHM	5	4	7	3
EDM	1	1	1	1
WEDM	2	3	2	2
EBM	9	6	5	7
LBM	8	7	6	5

Table 14: Spearman rank correlation coefficients between different MCDM methods

	COPRAS	Combined TOPSIS and AHP	PROMETHEE and GAIA	EVAMIX
COPRAS	–	0.82	0.73	0.75
Combined TOPSIS and AHP		–	0.88	0.9
PROMETHEE and GAIA			–	0.78
EVAMIX				–

5. CONCLUSION

Selection of competitive NCMPs for a given machining application is a complex MCDM problem involving a set of different and opposite criteria. A large number of MCDM methods have been proposed in literature to aid decision makers in systematical selection of the most suitable NCMP. In this paper the application of the COPRAS method is suggested for solving NCMPs selection problems. The obtained results while solving two case studies proved the applicability and accuracy of the COPRAS method while solving complex NCMP selection problems. In both case studies, it is observed that the top-ranked alternatives exactly match with those derived by the past researchers. Furthermore, very high Spearman's rank correlation coefficient values clearly justify the global applicability of the COPRAS method for solving complex NCMP selection problems.

The COPRAS method can simultaneously take into account any number of criteria, both quantitative and qualitative, and offer a relatively simple computational procedure. Application of this method in a wider range of selection problems in real-time manufacturing environment is a future research scope.

ACKNOWLEDGEMENTS

This work was carried out within the project TR 35034 financially supported by the Ministry of Education and Science of the Republic of Serbia.

REFERENCES

[1] D. Lazarević, M. Radovanović, "Nekonvencionalne Metode", Mašinski fakultet u Nišu, Niš, (1994)

[2] J.A. McGeough, "Advanced Methods of Machining", Chapman and Hall, London, (1998)

[3] P. Karande and S. Chakraborty, "Application of PROMETHEE-GAIA Method for Non-traditional Machining Processes Selection", Manag. Sci. Lett, Vol. 2, pp. 2049–2060, (2012)

[4] N.D. Chakladar, R. Das and S. Chakraborty, "A Digraph-based Expert System for Non-traditional Machining Processes Selection", Int. J. Adv. Manuf. Technol, Vol. 43, pp. 226–237, (2009)

[5] M. Yurdakul and C. Cogun, "Development of a Multi-attribute Selection Procedure for Nontraditional Machining Processes". Proc. IMechE Part B: J. Eng. Manuf, Vol. 217, pp. 993–1009, (2003)

[6] N.D. Chakladar and S. Chakraborty, "A combined TOPSIS-AHP-method-based Approach for Non-traditional Machining Processes Selection", Proc. IMechE Part B: J. Eng. Manuf, Vol. 222, pp. 1613–1623, (2008)

[7] S. Chakraborty and S. Dey, "Design of an Analytic-hierarchy-process-based Expert System for Non-traditional Machining Process Selection", Int. J. Adv. Manuf. Technol, Vol. 31, pp. 490–500, (2006)

[8] S. Chakraborty, "Applications of the MOORA Method for Decision Making in Manufacturing Environment", Int. J. Adv. Manuf. Technol, Vol. 54, pp. 1155–1166, (2011)

[9] S. Das and S. Chakraborty, "Selection of Non-traditional Machining Processes using Analytic Network Process", J. Manuf. Syst, Vol. 30, pp. 41–53, (2011)

[10] A. Sadhu and S. Chakraborty, "Non-traditional Machining Processes Selection using Data Envelopment Analysis (DEA)", Exp. Syst. Appl, Vol. 38, pp. 8770–8781, (2011)

[11] T. Temuçin, H. Tozan, J. Valíček and M. Harničárová, "A Fuzzy Based Decision Support Model for Non-traditional Machining Process Selection", Tech. Gazz, Vol. 20, pp. 787–793, (2013)

[12] P. Chatterjee and S. Chakraborty, "Nontraditional Machining Processes Selection using Evaluation of Mixed Data Method", Int. J. Adv. Manuf. Technol, Vol. 68, pp. 1613–1626, (2013)

[13] A. Guitouni and J.-M. Martel, "Tentative Guidelines to Help Choosing an Appropriate MCDA method", Eur. J. Oper. Res, Vol. 109, pp. 501–521, (1998)

[14] S. Hajkowicz and A. Higgins, "A Comparison of Multiple Criteria Analysis Techniques for Water Resource Management", Eur. J. Oper. Res, Vol. 184, pp. 255–265, (2008)

[15] E.K. Zavadskas, A. Kaklauskas, Z. Turskis and J. Tamošaitien, "Selection of the Effective Dwelling House Walls by Applying Attributes Values Determined at Intervals", J. Civil Eng. Manag, Vol. 14, pp. 85–93, (2008)

[16] P. Chatterjee, V.M. Athawale and S. Chakraborty, "Materials Selection using Complex Proportional Assessment and Evaluation of Mixed Data Methods", Mater. and Des, Vol. 32, pp. 851–860, (2011)

[17] R.V. Rao, "Decision Making in the Manufacturing Environment, Using Graph Theory and Fuzzy Multiple Attribute Decision Making Methods", Springer-Verlag, London, (2007)

[18] B.M. King, P.J. Rosopa and E.W. Minium, "Statistical Reasoning in the Behavioural Sciences", Willey, (2010)

Evaluation of Quality and Efficiency of Technologies for Making Axi-symmetrical Profiles – Method of Superiority and Inferiority

Temeljkovski Dragana[1*], Temeljkovski Dragan[1], Nusev Stojanče[2]
[1]Faculty of Mechanical Engineering, University of Nis, Nis (Serbia)
[2]Faculty of Engineering, University St. Kliment Ohridski Bitola, Bitola (Macedonia)

In this paper the method for evaluating superiority, that is, inferiority and quality of the most often used technologies for making tiny axi-symmetrical profiles is applied for the first time. The method of superiority and inferiority is the one used for evaluating quality as well as superiority or inferiority of some natural or engineering-technological value with respect to some other one or of many values of the same kind with respect to one another which is a result of the research done by the author of this paper.

Keywords: Product, Technology, Quality, Superiority, Inferiority, Variable, Comparative Value, Method, State

1. INTRODUCTION

As stated in Ref. [1], the method of superiority and inferiority is the one used for evaluating superiority or inferiority of a given value with respect to some other one or of many values of the same kind with respect to one another which has come into being as a result of the research done by the author of this paper.

The theoretical research has shown that in the process of making compact axi-symmetrical profiles the widest application is, basically, that of the following three technologies:

a) Drawing technology with diverse stress states (two compressive and one tensile) in the deformation zone where, with drawing of circular section, the following is realized:

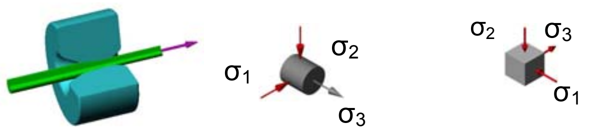

$|\sigma_3| > |\sigma_1| = |\sigma_2|$

Figure 1: Matrix drawing in stationary single-part matrix of full axi-symmetrical profiles and scheme of stress state in the deformation zone

b) Technology of drawing through the system of freely-rotating rolls.

The sliding friction which is present in matrix drawing is replaced by rolling friction whose resistance is incomparably smaller which leads to a considerable reduction of stress in the deformation zone. The rolls get the drive due to the action of axial drawing force over the workpiece (Figure 2.). In the deformation zone the stress state is achieved which is identical to the stress state of drawing of incomparably smaller intensity where the following principle is valid:

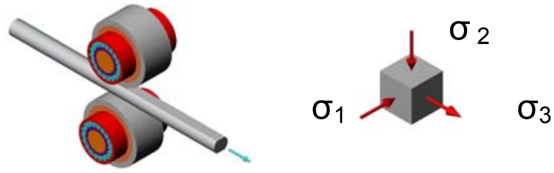

$|\sigma_3| > |\sigma_2| > |\sigma_1|$

Figure 2: Drawing of full axi-symmetrical profile through the system of freely-rotating rolls and scheme of stress State in the deformation zone)

c) Technology of drawing full axi-symmetrical profiles

Drawing of axi-symmetrical profiles in cold state represents a process of flat longitudinal rolling. The orifice of the rolls corresponds to the geometrical shape of the profile's cross section. For the profile drawing process to be realized, the rolling condition must be satisfied. On the workpiece material, through the rolls, two forces are acting (Figure 3.), namely, friction force F_T, between the rolls and the workpiece and the compressive force of roll F_N. As can be seen from the given figure, the horizontal component of friction $\mu F_N \cos\alpha$, which draws in the material into the deformation zone is opposed by the horizontal component of the compressive side of roll $F_N \sin\alpha$.

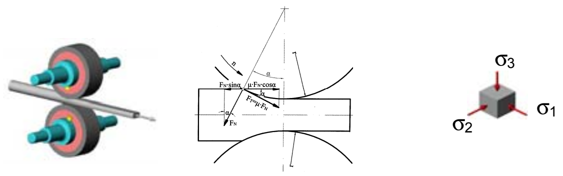

$\sigma2 > \sigma3 > \sigma1$

Figure 3: Rolling axi-symmetrical profiles, mechanical scheme of stress state in the deformation zone, forces on the rolls and the rolling condition

For the rolling process to be carried out, the following condition must be satisfied (1):

$$\mu\, F_N \cos\alpha \;\exists\; F_N \sin\alpha, \text{ i.e. } \mu \;\exists\; \mathrm{tg}\alpha \qquad (1)$$

*Corresponding author: Aleksandra Medvedeva 14, 18000 Nis and draganatemeljkovskiarh@gmail.com

Equation (1) represents the condition of rolling: where: μ - coefficients of contact friction,
α - range angle

Quality of the observed technologies can be shown in the form (2):

$$KV_j = \sum_{k=1}^{m} q_{kj} \cdot p_{kj} \quad (k = 1,2,3...m \quad j = 1,2,... \;...n,) \qquad (2)$$

where: KVj - quality of jth comparative technology,
q_{kj} - kth coefficient of participation of variable k in evaluating comparative technology j,
p_{kj} - kth characteristic of variable given in the form of quantitative parameter of optimality of comparative technology j,
J - jth comparative technology,
m - number of characteristics of variable k given in the form of optimality parameter and
n - number of comparative technologies whose quality is being evaluated.

By analyzing the above-given three technologies, we have defined the following techno-economic and energetic parameters of optimality for the profile making process (Figure 4.). The proposed technology parameters can be written in the form (3).

$$p_{kj} \qquad (k = 1,2,3,... \;...10,; \; j = 1,2,3), \qquad (3)$$

where: k - number of variables, number of observed technology parameters, and
j - number of observed technologies of profile making.

1.1. Limitations in determining optimality of observed profile making technologies

While researching optimality of profile making technologies the limitations are taken into consideration so that to all the above-mentioned technologies, the following is applied:

- The same quality of the basic profile material regarding both mechanical and chemical surface characteristics,
- The same cooling device,
- The same processing system,
- The same material of processing module (tool), the same surface finish and hardness of surface tools' layer,
- The same measuring apparatus for identifying measured process parameters, and,
- The same means for measuring and identifying parameters of the finished product.

In this case, variables Vj represent the above-given technologies and their stress states in the deformation zone while the variables' characteristics are parameters of optimality pkj of the given technologies.

The very process of calculating and evaluating the observed variable by this method is taking place in four steps by making respective decision-making matrices, [3], [4], [5], [6].

Evaluation of efficiency of the discussed technologies, that is, their stress/strain states in the deformation zone is derived in an especially made module of the program package PAPATIP.

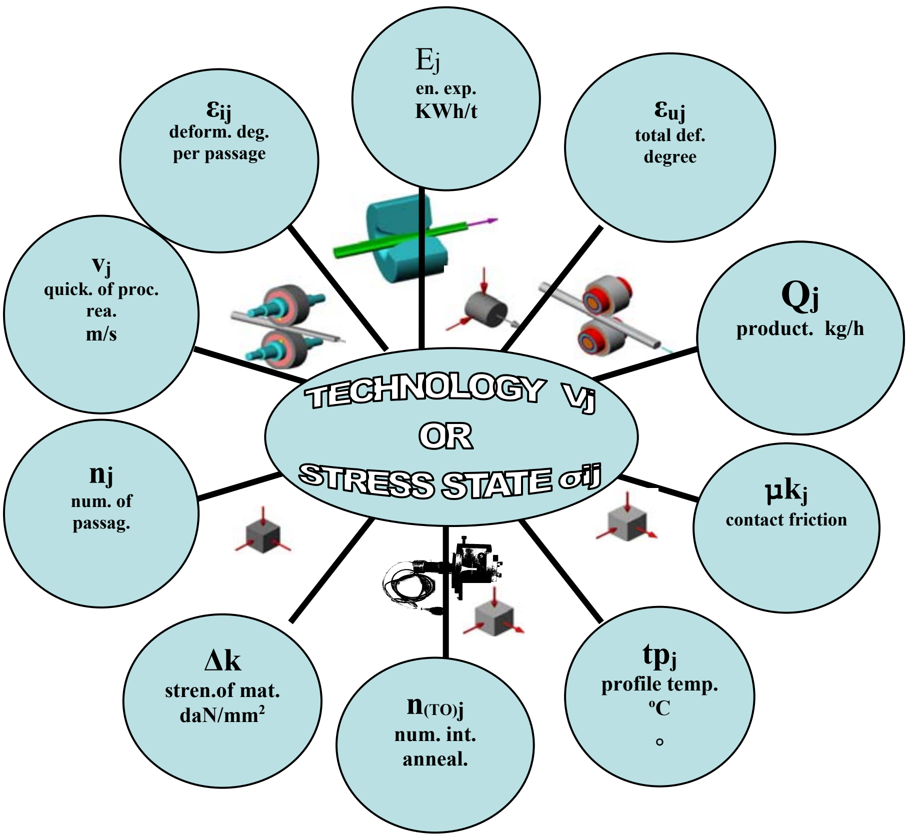

Figure 4: Parameters of technology optimality p_{kj} and defined stress states σ_{ij},, that is, technologies for making v_j profiles

2. FIRST STEP

In Table 1 there is the first step matrix of the given method.

Figure 5. gives a graph of nominal values of parameters of evaluation pkj from Table 1 in the function of the above-given technologies, that is, evaluation variables.

Sums in the last row of the given matrix represent qualities of the observed technologies in the function of optimality variable parameters where coefficients of characteristics are qkj = 1.

If we undertake evaluation and comparison of the given technologies now, the evaluation will refer only to the tenth indicator of optimality – productivity since the other indicators, with respect to productivity, though participating in quality evaluation with 100% of their value, are negligible by their intensity while their impact on the final evaluation in this step is negligible and minor.

Table 1: First step matrix of the method for evaluating efficiency of the technologies and their stress states in the deformation zone in making axi-symmetrical profiles - method of superiority and inferiority.

EVALUATION OF EFFICIENCY OF TECHNOLOGIES FOR MAKING TINY COMPACT AXI-SYMMETRICAL PROFILES

METHOD OF SUPERIORITY AND INFERIORITY

FIRST STEP

N.	PARAMETARS OF EVALUATION	TERMS OPTIMIZA TION	VARIABLE EVALUATION			SUM
			ROLING	DRAWING OF FREELY ROT. ROLLS	MATRIX DRAWING (Rm=Dv/2)	
1	2	3	4	5	6	7
1	MAX. DEFORMATION DEGREE PER PASSAGE	MAX	0,5552	0,396	0,2609	**1,212**
2	MAX. TOTAL DEFORMATION DEGREE	MAX	0,9067	0,835	0,67	**2,412**
3	MAX. QUICKNESS OF PROCESS	MAX	4,5	1	0,5	**6**
4	MIN. NUMBER OF PASSAGES	MIN	4	6	10	**20**
5	MIN. STRENGTHENING OF MATERIAL	MIN	28,7	32	41,1	**101,8**
6	MIN. NUMBER INTEROPERATIO. ANNEALING	MIN	1	2	3	**6**
7	ESTIMATED PROFILE TEMPERATURE	MIN	91	95	152	**338**
8	MIN. CONTACT FRICTION	MIN	0,1107	0,1881	0,2234	**0,522**
9	MIN. ENERGY EXPENDITURE	MIN	12,72	16,43	33,31	**62,46**
10	MAX. PRODUCTIVITY	MAX	2500	860	400	**3760**
		SUM	**2643,49**	**1013,85**	**641,06**	**4298**

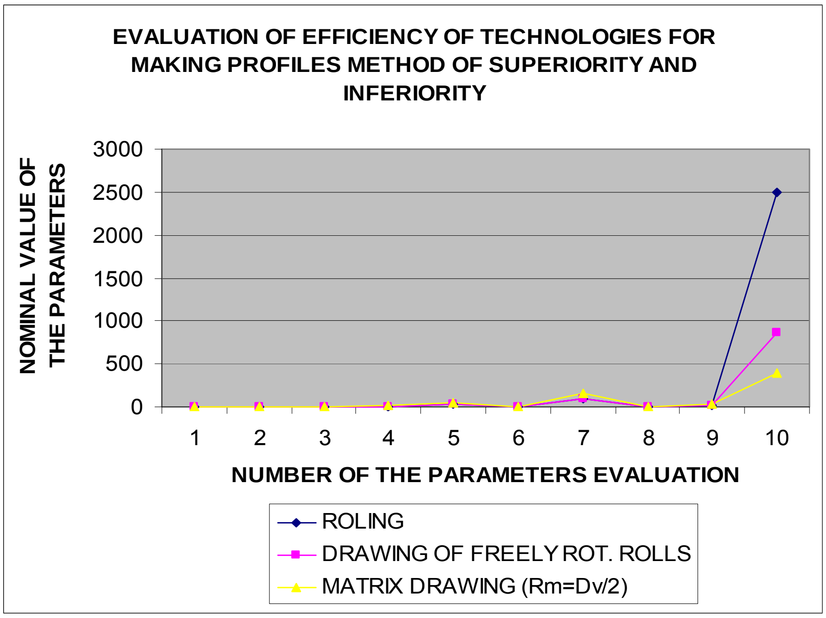

Figure 5: Graph of nominal values of evaluation parameters

3. SECOND STEP

In this step we unify the evaluation parameters, that is, optimality parameters pkj according to optimality condition (column 3 of the given matrix) by using the optimality criteria given in [1][2] so that the given parameters have passed into coefficients of participation of the given characteristic of the optimality indicators in the total evaluation of the given technologies.

Figure 6. presents nominal values of coefficients of optimality parameter characteristics of the given technologies after their optimization and unification in the second step.

From the made matrix in the second step and from Figure 7. it can be seen that in rolling technologies coefficient of characteristic is qkj = 1 in all the above-mentioned optimality indicators which means that this technology is more superior with respect to drawing technologies regarding all optimality indicators of the given technologies.

Table 2: Second Step Matrix

SECOND STEP

N.	PARAMETARS OF EVALUATION	TERMS OPTIMIZA TION	VARIABLE EVALUATION			SUM
			ROLING	DRAWING OF FREELY ROT. ROLLS	MATRIX DRAWING (Rm=Dv/2)	
1	2	3	4	5	6	7
1	MAX. DEFORMATION DEGREE PER PASSAGE	MAX	1	0,71	0,47	**2,18**
2	MAX. TOTAL DEFORMATION DEGREE	MAX	1	0,92	0,74	**2,66**
3	MAX. QUICKNESS OF PROCESS	MAX	1	0,22	0,11	**1,33**
4	MIN. NUMBER OF PASSAGES	MIN	1	0,67	0,4	**2,07**
5	MIN. STRENGTHENING OF MATERIAL	MIN	1	0,9	0,7	**2,6**
6	MIN. NUMBER INTEROPERATIO. ANNEALING	MIN	1	0,5	0,33	**1,83**
7	ESTIMATED PROFILE TEMPERATURE	MIN	1	0,96	0,6	**2,56**
8	MIN. CONTACT FRICTION	MIN	1	0,59	0,5	**2,09**
9	MIN. ENERGY EXPENDITURE	MIN	1	0,77	0,38	**2,15**
10	MAX. PRODUCTIVITY	MAX	1	0,34	0,16	**1,5**
		SUM	**10,00**	**6,58**	**4,39**	**20,97**

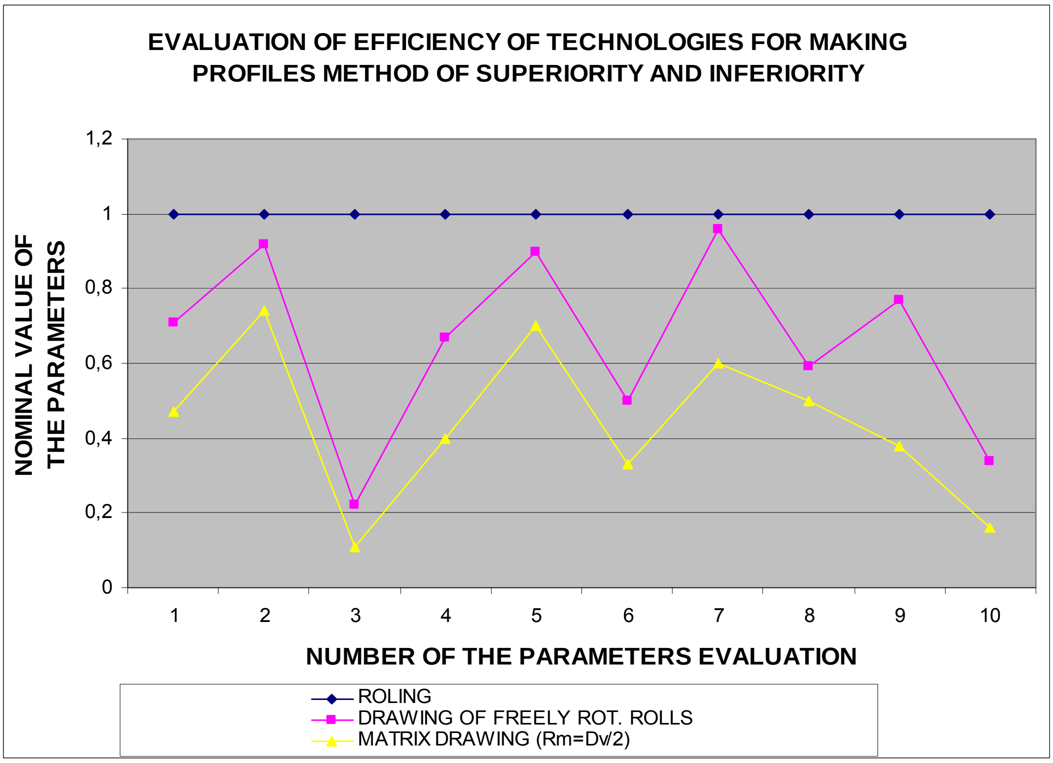

Figure 6: Value of optimality parameter characteristics in the second step of evaluating technologies' quality by the method of superiority and inferiority

4. THIRD STEP

In the third step the coefficients of the variable participation are determined, optimality characteristic qkj in total evaluation of quality of the observed technologies in such a way that each member of the matrix from the previous step is divided by the SUM of the row in which the given member is located; the value obtained in this way is divided by the SUM from the column in which the given matrix member is located,

$$q_{kj} = \frac{\left(\frac{[r_{kj}]_P}{[\sum r_{kj}]_{PR}} \right)}{[\sum r_{kj}]_{PK}} \tag{4}$$

where: P - denotes the previous member,
PR - denotes the previous row and
PK - the previous column.

Figure 7. gives coefficients of quality of optimality indicators qkj and their percentage participation in evaluating quality of the above-mentioned technologies.

As can be seen from the given figure, the percentage participation of any optimality indicator of the given technologies does not exceed the value of 15%. The SUMS in the last row of the given matrix are 1 and they represent the sums of the coefficients of all the characteristics of the optimality indicators of the technology whose quality is being assessed. In this way by the given coefficients of characteristics the participation of the optimality indicators in the process of evaluating the given technologies' qualities is balanced and thus it is ensured for each optimality indicator to have an equal impact upon the final evaluation of the observed technology quality.

Table 3: Third step matrix

THIRD STEP

N.	PARAMETARS OF EVALUATION	TERMS OPTIMIZA TION	VARIABLE EVALUATION			SUM
			ROLING	DRAWING OF FREELY ROT. ROLLS	MATRIX DRAWING (Rm=Dv/2)	
1	2	3	4	5	6	7
1	MAX. DEFORMATION DEGREE PER PASSAGE	MAX	0,092	0,108	0,109	**0,309**
2	MAX. TOTAL DEFORMATION DEGREE	MAX	0,075	0,114	0,141	**0,33**
3	MAX. QUICKNESS OF PROCESS	MAX	0,15	0,055	0,042	**0,247**
4	MIN. NUMBER OF PASSAGES	MIN	0,097	0,107	0,098	**0,302**
5	MIN. STRENGTHENING OF MATERIAL	MIN	0,077	0,114	0,136	**0,327**
6	MIN. NUMBER INTEROPERATIO. ANNEALING	MIN	0,109	0,09	0,092	**0,291**
7	ESTIMATED PROFILE TEMPERATURE	MIN	0,078	0,124	0,118	**0,32**
8	MIN. CONTACT FRICTION	MIN	0,096	0,093	0,12	**0,309**
9	MIN. ENERGY EXPENDITURE	MIN	0,093	0,119	0,09	**0,302**
10	MAX. PRODUCTIVITY	MAX	0,133	0,076	0,054	**0,263**
		SUM	**1,00**	**1,00**	**1,00**	**3,00**

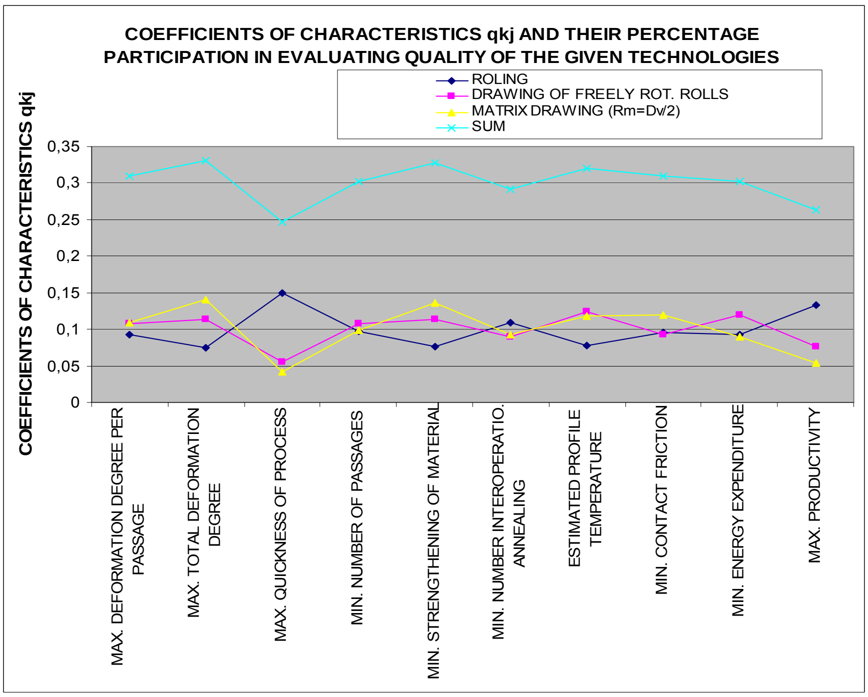

Figure 7: Coefficients of characteristics qkj and their percentage participation in evaluating quality of the given technologies

5. FOURT STEP

In order to obtain the fourth step matrix, it is necessary for each coefficient q_{kj} from the third step matrix to be multiplied by respective nominal value of technology optimality indicator parameter p_{kj} from the first step.

The last sum at the end of each column, that is, sums in the last row of the fourth step matrix represents quality of the observed technologies expressed in numerical value.

From the given Table 4 it is obvious that rolling technology is evaluated by quantitative evaluation 344, drawing technology in freely-rotating rolls with 83 while matrix drawing technology with 50.

Figure 8. gives a graph of quality of the given technologies expressed in numerical indicators in the function of the selected optimality parameters. Of special consideration is a visibly outstanding impact of parameters 5 and 7 (material reinforcement and profile temperature) as parameters that are of considerable influence on the observed technologies' quality.

As has already been stressed, the obtained sum at the end of each column in the fourth step matrix represents quality of the given technology in the function of optimality indicators of the given technologies.

Table 4: Fourth Step Matrix

FOURTH STEP

N.	PARAMETARS OF EVALUATION	TERMS OPTIMIZA TION	BLE EVALUATION			SUM
			ROLING	DRAWING OF FREELY ROT. ROLLS	MATRIX DRAWING (Rm=Dv/2)	
1	2	3	4	5	6	7
1	MAX. DEFORMATION DEGREE PER PASSAGE	MAX	0,051	0,043	0,028	**0,122**
2	MAX. TOTAL DEFORMATION DEGREE	MAX	0,068	0,096	0,094	**0,258**
3	MAX. QUICKNESS OF PROCESS	MAX	0,675	0,055	0,021	**0,751**
4	MIN. NUMBER OF PASSAGES	MIN	0,387	0,64	0,979	**2,006**
5	MIN. STRENGTHENING OF MATERIAL	MIN	2,212	3,655	5,596	**11,463**
6	MIN. NUMBER INTEROPERATIO. ANNEALING	MIN	0,109	0,18	0,276	**0,565**
7	ESTIMATED PROFILE TEMPERATURE	MIN	7,121	11,765	18,012	**36,898**
8	MIN. CONTACT FRICTION	MIN	0,011	0,018	0,027	**0,056**
9	MIN. ENERGY EXPENDITURE	MIN	1,18	1,95	2,985	**6,115**
10	MAX. PRODUCTIVITY	MAX	332,55	65,018	21,533	**419,1**
		SUM	**344,36**	**83,42**	**49,55**	**477,34**
					MINIMUM	
	SUPERIORITY		**9,95**	**1,68**	**1**	
			MAXIMUM			
	INFERIORITY		**1**	**0,24**	**0,14**	
				CONDITIONAL VARIABLES		
	< 1 = INFERIORITY. > 1 =INFERIORITY		**4,13**	**1**	**1,39**	

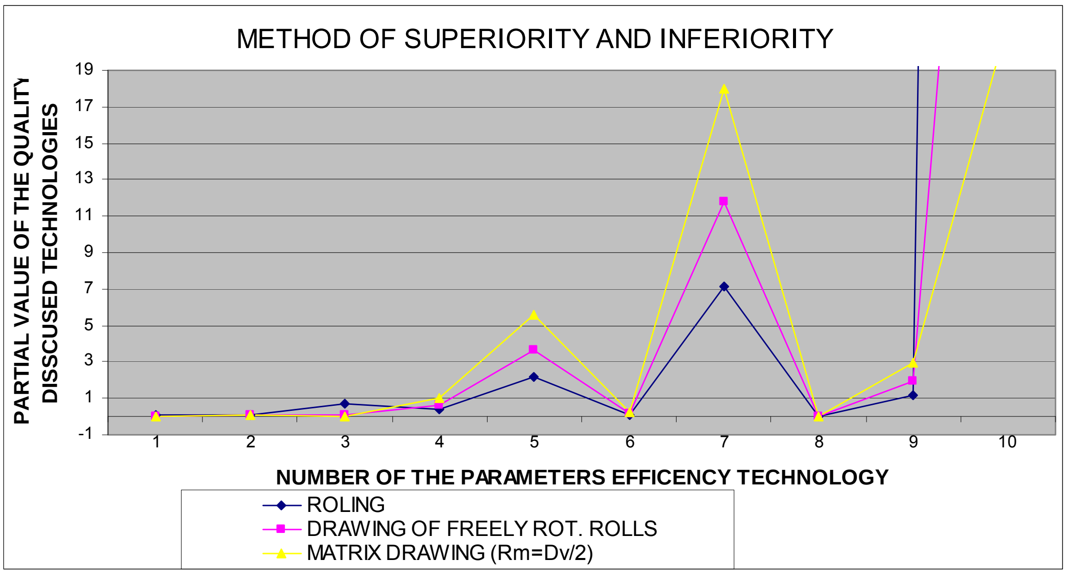

Figure 8: Graph of quality of the given technologies represented by numerical indicators in the function of selected optimality parameters

			MINIMUM
SUPERIORITY	9,95	1,68	1

Figure 9: Detail from fourth step table

	MAXIMUM		
INFERIORITY	1	0,24	0,14

Figure 10: Detail from fourth step table

		CONDITIONAL VARIABLES	
< 1 = INFERIORITY. > 1 =INFERIORITY	4,13	1	1,39

Figure 11: Detail from fourth step table

6. CONCLUSION

Now we can undertake evaluation of the given technologies, that is research of superiority, that is inferiority of one technology with respect to some other one.

If for evaluation we select technology with MINIMAL value of the sum, then by simply dividing all the other sums by the selected sum, we obtain SUPERIORITY of other technologies with respect to the selected one.

Thus rolling technology is 6,95 times while drawing technology in freely-rotating rolls is 1.68 times more SUPERIOR than drawing technology in keyed rolls (Rm = Dv/2).

If for evaluation we select technology with MAXIMAL value of the sum, then by simply dividing all the other sums by the selected sum, we obtain INFERIORITY of other technologies with respect to the selected one.

Thus drawing technology in keyed rolls (Rm = Dv/2) is 0.14 times while drawing technology in freely-rotating rolls is 0.24 times more INFERIOR than rolling technology.

If for evaluation we select drawing technology in freely-rotating rolls, then by simply dividing all the other sums of all the other technologies by the sum of the drawing technology in freely-rotating rolls, we obtain respective values.

If the calculated value is greater than 1, this is SUPERIORITY of this technology with respect to the selected one; if the calculated value is less than 1, this is INFERIORITY of the given technology with respect to the selected one.

Thus, the drawing technology in freely-rotating rolls is INFERIOR with respect to that of rolling for 2.35 times, while it is SUPERIOR to that of drawing in keyed rolls (Rm = Dv/2) for 0.77 times.

As can be seen from the given calculations, the selected variables serving for comparison always have value of 1 while the others are greater or less than 1 depending on whether they are SUPERIOR or INFERIOR to the selected variable. In this way we very simply learn which of them is a comparative variable.

ACKNOWLEDGEMENTS

This paper is part of project TR33040 Revitalization of Existing and Design of New Micro and Mini Hydroelectric Power Plants (from 10 to 1000 kW) on the Territory of Southern and Southeastern Serbia, funded by the Ministry of Education and Science of Republic of Serbia.

REFERENCES

[1] Zrilić R., "Istraživanje zavisnosti tehno-ekonomske i energetske efikasnosti od naponskog stanja pri izradi profila", Doktorska disertacija, Mašinski fakultet, Banja Luka (BIH), September (2004)

[2] Zrilić R., "Matematički model elastičnih deformacija okvira valjačke mašine", Obrada deformisanjem u mašinstvu, Novi Sad (Serbia), September 1987, Vol. 12, Number 1-2, pp. 73-83, (1987)

[3] Popović B., Kamberović B., "Upravljanje kvalitetom" – zbirka rešenih zadataka sa objašnjenjima, Naučna knjiga, Beograd (Serbia), (1987)

[4] Stanić J., "Metod inženjerskih merenja" – osnovne matemaičke teorije eksperimenta, Mašinski falkultet, Beograd (Serbia), (1986)

[5] Norton P., "Visual Basic 6", Kompjuter biblioteka, Četvrto izdanje, SAMS publishing, Svetlost, Čačak (Serbia), (2001)

[6] Temeljkovski D., Popović P., Rančić B., Đekić P., "Evaluation of Product and Production Technologies Quality Method of Superiority and Inferiority", 34th International Conference on Production Engineering, IPCE 2011, pp. 267-270, Niš. (Serbia), (2011)

On the Effect of normal Load and sliding speed on wear under dry Sliding Contact on the Brass (70-30, 60-40)

Dragan Milcic [1*], Amir M. Rashid[1], Boban Anđelković[1], Mustafa Amir Mustafa[2]
[1] Faculty of Mechanical Engineering Niš, Aleksandra Medvedeva 14, 18000 Niš, Serbia
[2]The Iraqi Oil Ministry Baghdad

Purpose of this paper is the investigation on the properties and microstructural changes in load and sliding speed in the brass alloy (70-30) and (60-40) in function of wear rate. Experimental program using pin-on-disc tester has been conducted to investigate the effects of normal load, sliding speed on sliding wear mechanism. The worn surfaces and debris have been examined. Surface examination of the tested samples using scanning electron microscope SEM was used to study the wear particles and the wear surfaces. The results show that the Wear rate increase with increase applied normal load and decrease with increase speed sliding.

.

Keywords: Wear; Brass alloys; normal load; sliding speed

1. INTRODUCTION

The alloys of copper with zinc and brass are the first alloys accompanying the development of mankind. Nowadays, they are widely applied in technology, and next to light metals they belong to the most commonly used alloys in the group of non-ferrous metals. Thanks to the specific properties of brasses they are applied in various domains of industry, among others in civil engineering, armaments industry, aircraft industry, machine building, the production of motor cars, electrical industry, ship building, precision mechanics, and chemical industry and many others, even in the production of musical instruments [1].

These alloys are characterized by a considerable ductility and resistance to corrosion and wear, particularly atmospheric corrosion, corrosion in sea-water and sliding wear. They also display good casting properties. In technology CuZn alloys with a zinc content of 45% are applied. A higher content of zinc in the brass increases their brittleness. The optimal mechanical properties display brass containing about 30% zinc. Those are characterized by considerable plastic properties together with high tensile strength and hardness [2]

Wear is a complex phenomenon. It occurs whenever surfaces come into sliding contact, even in the presence of a lubricant. To the designers and engineers who have to make optimal decisions in situations where tribological considerations are significant, it is important for them to have ready access to information pertaining to the fundamental understanding of the wear processes of interest. Some kind of user-friendly databases would be most helpful here. These databases should be able to provide the appropriate information for materials selection and choice of the suitable (optimal) operating condition—such as contact geometry, speed and environment—for a particular pair of materials in tribological contact[3].

The most common wear model is named Archard's Wear Law [1], although Holm [4] formulated the same model much earlier than Archard. However, Archard and Holm interpreted the model differently. The model has the following general form:

$$V = K\frac{F_N}{H} \quad (1)$$

Where V is the wear volume, K is the dimensionless wear coefficient F_N, is the normal load, H is the hardness of the softer contact surface and s is the sliding distance. Eq.(1) is often reformulated by dividing both sides by the apparent contact area A and by replacing K/H with k Eq.(2):

$$\frac{V}{A} = k\frac{F_N}{A}s \ , \frac{F_N}{A} = p, \ \ \frac{V}{A} = h \xrightarrow{yields} h = k.p.s \quad (2)$$

Where h is the wear depth in m, k is the dimensional wear coefficient in m^2/N, p is the contact pressure in Pa and s is the sliding distance in m, as before. This wear model is widely used. The problems of wear and friction of extremely important because of the negative impact on the accuracy of the sliding parts, in addition to the large material losses caused by wear.researchers studies dry sliding contact due to: 1) In the case of the absence of lubrication the results are clear, 2) The need to direct such results in the field of nuclear power generation. Brass is taught for being gives the results of high-resolution and is used in the broad field of industrial [4].

When sliding copper alloys that basis (such as) on the steel, it is noted that the color of copper covered steel, can change color depending on the type of the alloy. Sometimes is observed that covers the surface of a plate of dark gray or black color when viewed with the naked eye or optical microscope as a result of it contains oxides or its interaction with the environment [5].

If we take the effect of overload, sliding speed and hardness on the dynamic coefficient of friction observe that the dynamic coefficient of friction increases with vertical load when the load is from 1 to 20 N, then take the state of stability. Either in the case of speed, the dynamic coefficint of friction least when increasing speed of 0.1 to 10 mm / sec after this speed it's growing. The relationship dynamic coefficient of friction with hardness, at least whenever it increases the hardness material [6].

*Corresponding author: Faculty of Mechanical Engineering Niš, Aleksandra Medvedeva 14, 18000 Niš, Serbia, milcic@masfak.ni.ac.rc

Observed (Archard) that the wear rate decreases with time in the state lubricated, while the increase in the dry state [7]. There are two cases of wear, the severe wear and mild wear, it is observed that the severe wear is formed when the load hanging high, while mild wear occurs when the load is hanging relatively small[8].

Characterized by the wear severe that the surface becomes rough and the size of debris wearranges between 10 to 100 micrometers, either wear mild shall be surface smooth and the size of debris the wear is less than in the case of wear severe, as it ranges from 1 to 0.01 micrometers, and the debris of the wear is a peel oxidant [9]. Archard has observed that the transition from mild wear to severe wear obtain an increase of load(load), causing severe wear the large damage to material and quick to remove the tops of microroughness on the opposite of what is happening in the mild wear[10]. It was observed that the wear mild in the case of alloy brass (70-30) turns severe wear after a period of time and then a few turns to mild wear, while the alloy brass (60-40) on the content of 2% lead gives severe wear when the load little[8]. Observed (Lancaster) that the rate of wear in the alloy brass (60-40) when the bring temperature from an external source up to (20-600) ^{0}C increases up to 300 ^{0}C, Then at least the rate of wear when you increase the temperature more[5]. That this change in the rate of wear to be accompanied by an increase in contact resistance between the sliding surfaces. Within the limits of temperatures (400-450) ^{0}C a significant increase in contact resistance, and a significant increase in the coefficient of friction is also value (0.6-1)., and an increase in the rate of wear when the temperature is less than 300 ^{0}C be accompanied by a decrease in hardness of the metal, but when (20-120) ^{0}C observed that the hardness of the metal remains constant [5]. The instantaneous temperature generated as a result of sliding surfaces on each other, it increases with speed due to the flow of heat through the metal quickly at high speed less than it is in low-lying speed [11].

2. EXPERIMENTAL PROCEDURE

For the case of touching between the two solid bodies under the influence of vertical load has been the use of a wear (pin-on-disc) designed according to the specifications (ADTM) As shown in Figure (1).The experiments were conducted on the brass alloy (70-30) and (60-40), Been using discs from high carbon steel with a hardness of 300Mpa and diameter and 200 mm each, their chemical composition are respectively presented in tables 1. Examine the sample (pin) after every 10 minutes of running and weight of calculate how much weight loss, and to stop the experiment after an hour per sample. Samples were prepared from brass rod-shaped diameter of 10 mm and a length of 92 mm to suit the specifications of device (pin-on-disc), were refined samples surface roughness (0.25μm C.LA) and surface disc roughness (0.35μm C.LA), Was measured roughness device (Talysurf-Hobson), both hardness alloy brass (60-40), (70-30) and disk respectively (136.4 Mpa), (113.8Mpa) and (300Mpa), Chemical content of both alloys brass shown in Table (1).

Figure 1: Pin-on-disc device

Table (1). Chemical content of brass (60-40) and (70-30)

Components	Cu	Zn	Sn	Pb	Fe	Total	Impurities
Brass 60-40	58.17	40.0	0.051	0.990	0.762	99.973	0.027
Brass 70-30	70.1	29.6	-	-	-	99.7	0.3

2.1. Wear rate measurement

Have been measuring the rate of wear to method the weight, where the sample is weighed before and after the running by the delicate balance of digital (0.0001mg) Type (Mttler HK 160). Of weight lost is calculated wear rate Eq.(3)

$$\frac{dV}{dL} = \frac{W}{\pi.\rho.D.N.T} \tag{3}$$

Where (dV/ dL) is volume the rate of wear, W is weight lost (g), L is Sliding distance (cm), ρ The density of brass(g/cm^3), D is diameter which rotate by the sample(cm), N is sliding speed (rpm), T is sliding time (min).

Experimental program

The program is divided into groups practical for both the alloys, as shown in Table (2).

Wear experiments were carried out for three different normal loads of (6N, 12N and 18N) and three different velocities (95, 250 and 350 rpm) at atmospheric condition. Each test was conducted for at least three repeated times at the same test conditions to ensure the repeatability. The ring surface was abraded before each test with a (P1500) grade emery paper; also, the pin was initially rubbed against the P1500 grade emery paper pasted on the ring to establish a conformal contact of the composite pin with the counterpart (cup).

Table 2: Experimental program

No. experience	Sliding speed (rpm)	Normal load (N)	No. experience	Sliding speed (rpm)	Normal load (N)	Surface roughness (µm)	
						Disc	pin
(70-30) -01	95	18	(60-40) -10	95	18	0.35	0.25
(70-30) -02	95	12	(60-40) -11	95	12		
(70-30) -03	95	6	(60-40) -12	95	6		
(70-30) -04	250	18	(60-40) 13	250	18		
(70-30) -05	250	12	(60-40) -14	250	12		
(70-30) -06	250	6	(60-40) -15	250	6		
(70-30) -07	350	18	(60-40) -16	350	18		
(70-30) -08	350	12	(60-40) -17	350	12		
(70-30) -09	350	6	(60-40) -18	350	6		

3. EFFECT OF THE NORMAL LOAD ON THE RATE OF WEAR

To increase the normal load increases plastic deformation happening at the tops of microroughness and thus increases the density of dislocations, and it gradually becomes brittle material [12]. Due to grouping these dislocations, consisting small gaps, which combine to be small cracks in the surface of the metal, expanding these cracks toward the weak areas to form a large incision, as in Figure (2), the convergence these cracks with each other or with the lines of wear cause the removal of a thin layer of metal, remove easily slide toward the wear debris, as in Figure (3, 4, 5)

Figure 2: Brass sample surface when the vertical load (12N), sliding speed (350 rpm), power magnification (X700)

As well as obtain to break the oxide in the case of high normal load shooting outside the sample surface, leading to an increase in the rate of wear as in Figure (6,7).

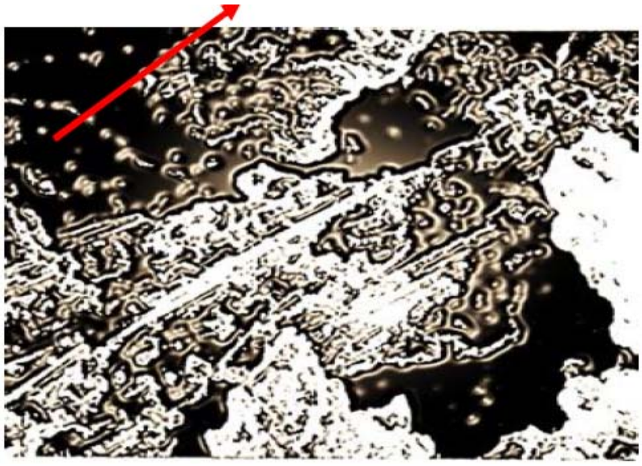

Figure (3).Debris the wear of the alloy brass (60-40) when the normal load (18N), the speed of the slide (95rpm), power magnification (X280).

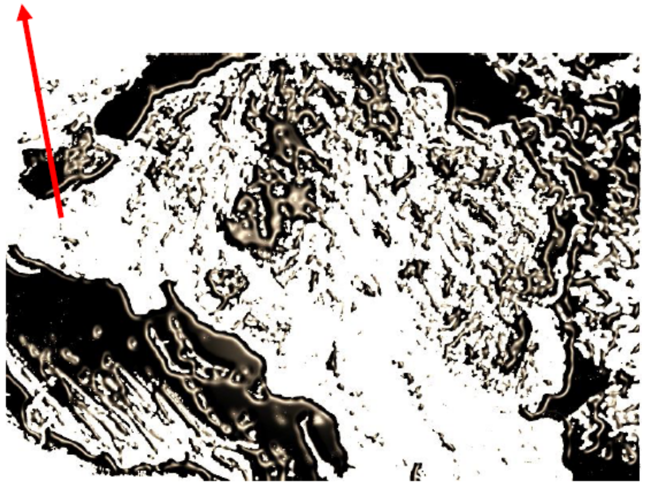

Figure (4).Debris the wear of the alloy brass (60-40) when the normal load (12N), the speed of the slide (350 rpm), power magnification (X280)

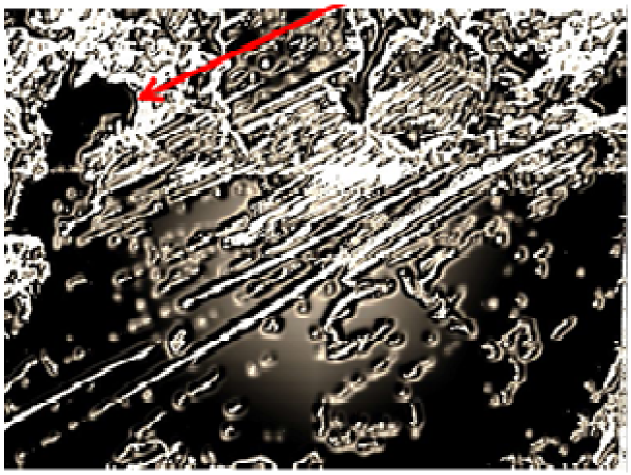

Figure (5).Debris the wear of the alloy brass (60-40) when the normal load (18N), the speed of the slide (350 rpm), power magnification (X280)

Microroughness that adhesion between surfaces of both the slider is heavily dependent on the normal load, In the case of little normal load and during the process sliding consists protective surface film leads to a lack of contact between the two surfaces slide [5], and this force will be required to cut the interconnection happening between the microroughness in less metal atoms and thus leads to a lack in the rate of wear. As in the case of higher normal load former would receive to break the oxide layer, leading to the occurrence of strong metal contact which makes the force required to cut the microroughness related to higher than in the metal atoms and thus an increase in the rate of wear. The increase in the percentage zinc alloy copper - zinc increases the portability of the oxides on the surfaces of contact and therefore break the oxide and thrown to the outside surface of the sample increases in the rate of wear, too, can be seen scattered on the surface oxide in figure (8, 9).

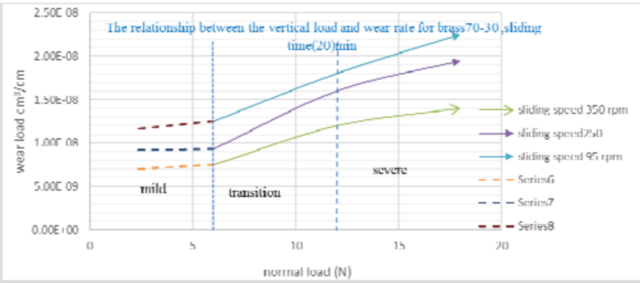

Figure (6).The relationship between the vertical load and wear rate for brss70-30, sliding time 20 min

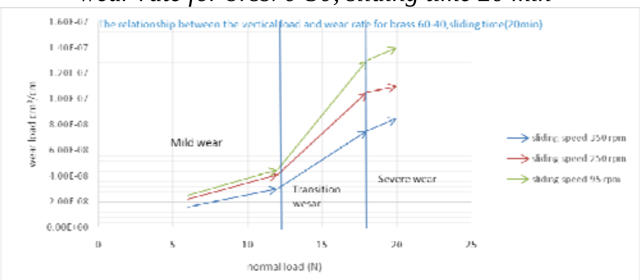

Fig (7).The relationship between the vertical load and wear rate for brass 60-40, sliding time 20 min

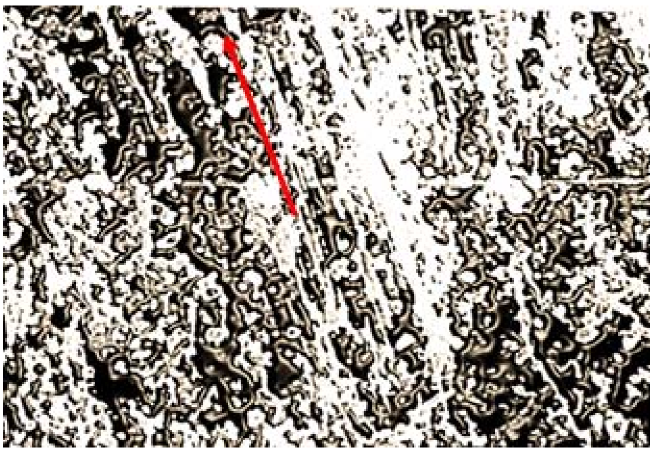

Figure .8: Brass (60-40) sample surface when the vertical load (6N), sliding speed (95 rpm), power magnification (X490)

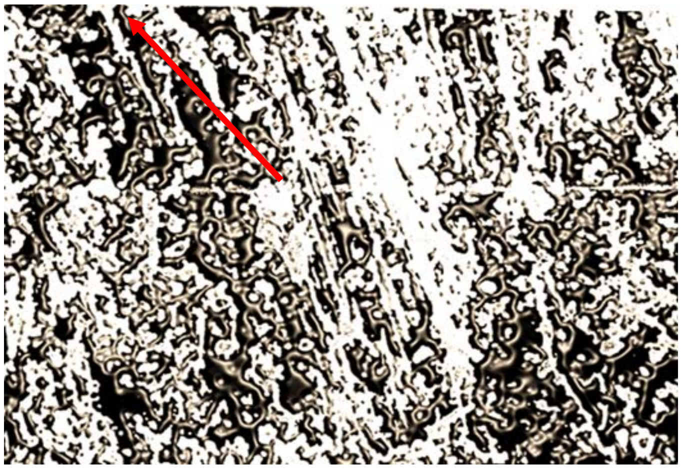

Figure 9: Brass (60-40) sample surface when the vertical load (12N), sliding speed (95 rpm), power magnification (X700)

The increase in the normal load causes fatigue of the surface can be seen when comparing both forms figures (4, 5). The increase in the vertical load causes fatigue of the surface can be seen when comparing both figures, observe where fatigue cracks and clear the debris of wear in the form (4), while it is not shown in the figure (5). From this it is clear that the mechanism of wear varies increase load, when load little oxide is removed from the surface when the shear strength of the oxide less than the shear strength due to normal load, either at conception and receives higher removal of a thin layer of the surface of the metal itself. When comparing both curves (6, 7) is observed there a great difference between the behavior of both alloy as used as the region wear mild disappeared completely in the alloy 70-30 within the range of load user (6-18) N, where it appears at loads less than it also appears in figure (6) the extrapolated part, so it can be divided into two regions, curved transitional wear and severe wear. In the case of alloy brass 60-40 region wear mild perfectly clear within the range of (6-12) N followed by the transitional wear within the loads (12-18) N for the region comes after intense wear. Comparison between both alloys is observed that the carrying capacity of alloy (60 -40) is greater than the capacity of the alloy (70-30), so it can use alloy (60-40) in industrial applications for a certain range of loads and for relatively long periods without a significant loss of material, although the rate of wear to the large than it is in the alloy 70-30.

4. EFFECT OF THE SLIDING SPEED ON THE RATE OF WEAR

The high temperature of both surfaces of the slide when the weather conditions surrounding the increase of the surface portability to oxidant, Given that oxide may act as a lubricant for universe the contacts that occur between the microroughness of sliding surfaces be weaker in the case of a thin oxide layer on the surface of the slider one or both. The leak of heat from the sample surface at velocities of low-lying more than in the case of velocities high[9], and this leads to a lack of softness microroughness in speed low-lying and thus a fusion of partial between microroughness both surfaces slider, and make the force required to cut the contact points greater than in the metal atoms and thus an increase in the rate wear decrease the speed of the slide as shown in Figure (10,11,12,13,14,15).At the confluence clean surfaces adhesion occurs because of the strong the spread of atoms, which leads to the occurrence of cold welding [13] and the occurrence of this strong connection between the contact surfaces lead to increased wear rate.

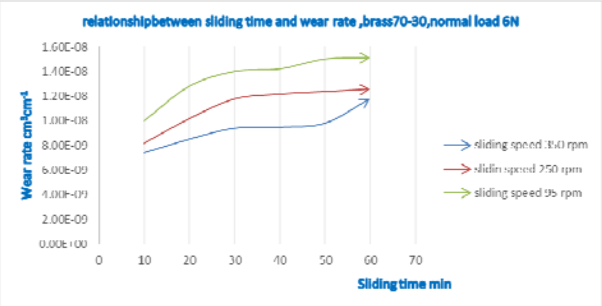

Figure 10:The relationship between sliding time and wear rate for brass 70-30 normal load 6N

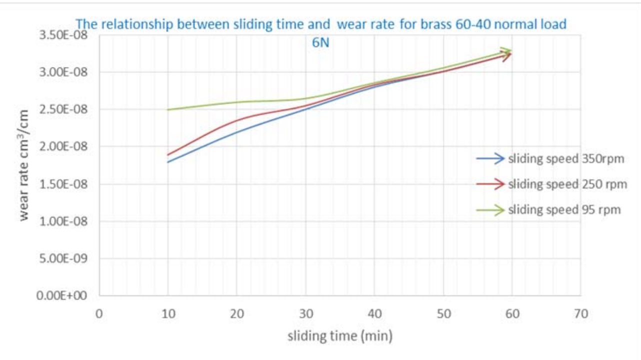

Figure 11:The relationship between sliding time and wear rate for brass 60-40 normal load 6N

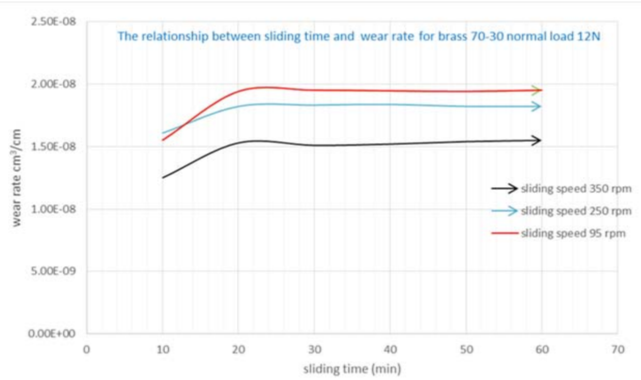

Figure 12:The relationship between sliding time and wear rate for brass 70-30 normal load 12N

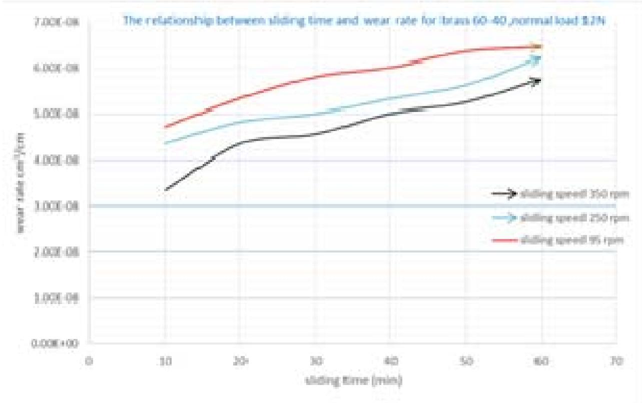

Figure 13:The relationship between sliding time and wear rate for brass 60-40 normal load 12N

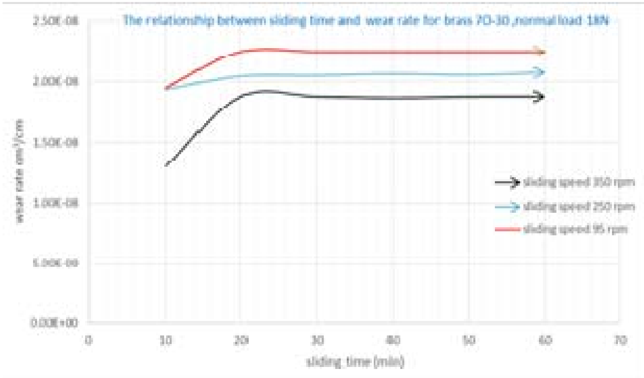

Fgure 14:The reiationship between sliding time and wear for brass 70-30,normal load 18N

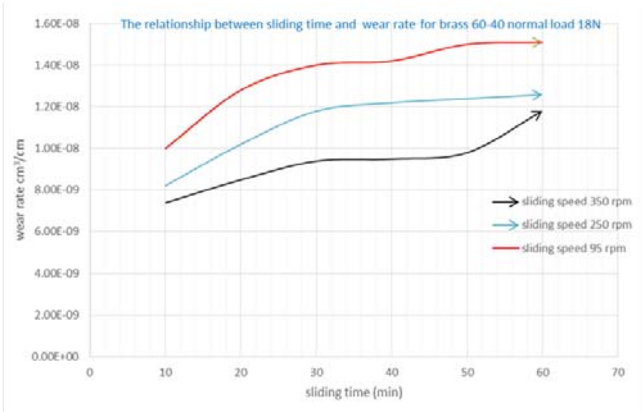

Figure 15:The relationship between sliding time and wear rate for brass 60-40 normal load 18N

CONCLUSIONS

In the case of the sliding surfaces prefer to use elements of intermetallic soft so as to ease the transition from one surface to the other, so that at least the rate of wear. Was found that the alloy brass 70-30 have less wear rate of the alloy brass 60-40. Study a wider range of alloys copper- zinc to study the proportion of zinc on the rate of wear under different conditions, mechanical. Study the effect of surface roughness on the rate of wear.

REFERENCES

[1] R. Nowosielski, "Ductility minimum temperature in selected mono-phase, binary brasses", Journal of Materials Processing Technology 109, pp. 142-153, (2001)

[2] J. Freudenberger, A. Kaumann, H. Klauß, T. Marr, K. Nenkov, V. Subramanya Sarma, L. Schultz, "Studies on recrystallization of single-phase copper alloys by resistance measurements", Acta Materialia, (2010)

[3] D. Tabor, "Status and direction of tribology as a science in the 80's. " In Proc. Int. Conf. Tribology in the 80's, NASA Lewis Research Center, Cleveland, Ohio, pp. 1–17, (1983)

[4] A.D. Sarkar, "Friction and Wear", Academic press Inc. (London), (1980)

[5] P.Heilmann, J.Don,T.C. Sun and D.A.Rigney, "Sliding wear and transfer", Wear, vol 91, pp. 171-190, (1983)

[6] M. O. Mokhtar, M. Zaki and G. S. A.Shawki, "An experimental re-examination of kinetic friction", Tribology international , 26-264, (1979)

[7] J.K. Lancaster, "The influence of temperature of metallic wear", Proc. phys. Soc.70B, pp.112-118, (1957)

[8] T.S. Eyer, "Wear workshop", Brunel–University-Metallurgy department, p.12, (1982)

[9] J. Mqlgaard, "The dry wear of metal as a process in an open wear", Wear, vol. 32, pp. 353-362, (1975)

[10] H.J.F.Archard and W. Hirst, "Hhe wear of metal under unlubricated conditions", Proc. Roy. Soc.A236. pp. 397-410, (1956)

[11] J.F.Archard, "The temperature of rubbing surfaces wear" , Wear, vol. 2, pp. 438-454, (1958)

[12] J.T. AL-Haidary ,N.J.Petchand E.R. Delo Los Rios "The plastic deformation of polycrystals II. Aluminium at 77K0", Philosophical magazine ,A, Vol .47,No.6, pp. 891-902, (1983)

[13] M.O.M.Mokhtar ,M.Zaki and G.S.A.Shawki "Effect of mechanical properties on frictional behaviour of metals", Tribology international , pp. 265-268, (1979)

Implementation of the RCM Methodology on the Example of City Waterworks

Zoran Petrović[1], Zlatan Car[2], Branko Radičević[1*], Leon Šikulec[2], Vladan Grković[1]
[1]Faculty of Mechanical and Civil Engineering in Kraljevo, University of Kragujevac, Kraljevo, Serbia
[2]Fakulty of Engineering, University of Rijeka, Rijeka, Croatia

The paper presents the possibility of application of Reliability Centered Maintenance (RCM) in infrastructure systems, such as waterworks. It introduces the RCM methodology which is adapted to such systems. The RCM methodology offers the best strategy for optimization of preventive maintenance. It covers a new understanding of the way in which the equipment may fail. Failure Modes, Effects and Criticality Analysis (FMECA) was first performed. The most suitable maintenance tasks have been defined for each failure and they belong to one of the four groups: Time-Directed (TD), Condition-Directed (CD), Failure-Finding (FF), Run-to-Failure (RTF). The analysis on the concrete example, a waterworks pumping station, has established that 61% of failures can be prevented by the application of preventive maintenance. The interdisciplinary procedure applied during analyses allows optimization of the existing preventive maintenance in the city waterworks.

Keywords: : RCM methodology, waterworks, preventive maintenance

1. INTRODUCTION

Literature provides numerous examples of succesful application of the RCM methodology: the USA navy and aviation [9], oil industry [10], maintenance of ships and submarines [11], railway [5], different fields of industry [6,7]. There are also certain projects where the results of RCM analysis were not accepted. The Norwegian railway is one of such examples, and this case is probably connected with very ambitious goals of the company [12].

This paper aims at investigation of the possibility of applying RCM in infrastructure systems, such as city waterworks. The pumping station which was the subject of observation, uses traditional preventive maintenance, relying on periodic inspections of certain components of the system. Having the models of large infrastructure systems like railway, RCM analysis was performed on a smaller system – a waterworks pumping station. It had several effects. The insight into the possibility of a more quality way of maintenance in comparison with the existing one was obtained. The interdisciplinary approach used during analysis considered the problems of entire maintenance, and the results of analysis were presented in a way which is completely clear to the maintenance staff and management of the company.

Water supply of the population implies providing high quality water for households, public needs and a part of industry. The quality of drinking water directly influences the health of people and that is why it is regulated by the law. Water supply and public health are the fields which are covered by legal regulations all over the world. Laboratory testing of drinking water is carried out exclusively by authorized health care institutions. In order to satisfy necessary requirements regarding water production and water quality, special attention must be paid to the maintenance of water supply systems.

Not so many people in our country have been introduced to the RCM methodology. One of possible reasons is lagging behind world trends for decades, which has been caused by isolation and sanctions. The second reason can be based on the initial knowledge that reached our country. The end of the eighties of the last century saw the flourishing of the statistical theory of reliability. Everything led to the attitude that only strong computer support and a large database of failures enabled significant optimization of maintenance of large systems. The initial application of RCM was expressed in systems such as civil aviation, atomic energy, navy and aviation, which are representatives of extremely expensive and critical systems. The name itself – reliability centered maintenance contibuted to it, so that it could be easily conluded that it was a methodology that sublimated leading accomplishments of the reliability theory and that it was necessarily based on strong computer support and databases of failures. Today's level of development of RCM shows that the methogology is applied both in military systems and in various branches of economy: metal processing branches, power engineering, mining, oil industry, paper industry, railway, harbour plants, maritime affairs, health care, etc. [15]

2. RCM ANALYSIS – REASONS FOR INTRODUCTION

The term **Reliability Centred Maintenance - RCM** first appeared in 1978, when the leading engineers of the American company United Airlines, Nowland and Heap, gave that name to their report intended for the American army [14]; the report was a thorough presentation of the methodology of improvement of the maintenance process in civil aviation. Nowland and Heap aimed to emphasize, by the title itself, that United Airlines was increasing the reliability of its airplanes.

This method was developed as the product of a real need on the basis of research. In 1960, the Federal Aviation Agency carried out research in the USA with the goal to establish the effectiveness of airplane repair in fixed time intervals. The research resulted in two findings:

*Corresponding author: Dositejeva 19, 36000 Kraljevo, Serbia, radicevic.b@mfkv.kg.ac.rs

- the planned repair had small effects on the total reliability of complex components, except if the component had a dominant failure due to wear
- there are a lot of components for which there are no effective and efficient manners of preventive maintenance.

Such results have basically changed the approach to reliability. For the purpose of solving complex problems, RCM analysis has been divided into phases. A functional model which observes all functions of the system with their functional failures has been developed. Functional failures have been correlated with all failure modes, with their causes and consequences.

The leading theorist of the RCM methodology, John Moubray, has defined RCM as a process which is basically the same as FMECA (Failure Modes, Effects and Criticality Analysis). The difference is that the manufacturer uses FMECA to sum their knowledge about possible failures, and RCM sums the experience gained by the operator and the person in charge of maintenance for many years.

The results achieved by the application of the RCM strategy, in different cases, are as follows [13]:

- reduction of the number of working hours for preventive maintenance by 87%;
- reduction of the total number of working hours for maintenance by up to 29%;
- reduction of costs for intermediate goods for maintenance by up to do 64%;
- increased availability of the equipment and system by up to 15%;
- increased reliability of technical means by up to 100%.

It is a well-known fact from [1], having in mind the experience of the systems for which the RCM methodology was elaborated and where it was implemented, that 60% of failure modes can be prevented by preventive tasks.

Understanding the importance and possibilities of RCM, the International Society of Automotive Engineers (SAE) established the Technical Committee which in 1999 developed the JA1011 standard: Evaluation Criteria for Reliability-Centred Maintenance (RCM) Process. This standard should help all those who want to implement RCM, since it defines guidelines and clarifies a lot of details and activities that are used during the implementation.

2.1. RCM analysis

Before starting a comprehensive RCM analysis and defining requirements, it is necessary to create a detailed catalogue of technological systems which are the subject of maintenance and carry out detailed introduction to the production process. After the realization of these two necessary steps, it is necessary to make seven basic questions/requirements of the RCM concept for every technological system thus defined and give detailed answers to each of them. The seven questions are [17] :

1. Which functions of the equipment are important in current exploitation?
2. What kind of equipment failure may occur?
3. What are the causes of failure occurrence?
4. What happens when a failure occurs?
5. What is the importance of each failure?
6. What can be done to prevent a failure?
7. What should be done if no adequate preventive activity can be found?

1. Which functions of the equipment are important in current exploitation? As the main task of maintenance is to provide proper, i.e. designed operation of equipment, it is necessary that the maintenance staff knows what is expected from individual technological systems, what “normal” operation mode is, and which standard was used to design the equipment. Therefore, the maintenance staff should know which functions of the equipment are important for the foreseen exploitation and hence it is necessary to pose this question first and give a detailed and precise answer to it.

2. What kind of equipment failure may occur? After the introduction to the functions of the equipment, it is logical to make the second question. It is necessary to identify every possible way of interruption of execution of the planned function, and it is done by means of two subquestions: a) – how can the equipment fail in the execution of its function and b) – what may cause unsuccessful execution of the equipment function?

3. What are the causes of failure occurrence? The aim of posing this question is identification of all ways of failure occurrences – non-fulfillment of the foreseen function, in order to identify the things that should be prevented. While carrying out this step, it is necessary to perform a sufficiently detailed analysis in order to avoid the situation when maintenance activities are carried out for the purpose of eliminating consequences, and not causes of a failure. On the other side, it is necessary to pay enough attention to avoid excessive going into details and unnecessary wasting of time and energy of participants in the analysis.

4. What happens when a failure occurs? When every manner of occurrence of failure is identified, it is necessary to identify the consequences of occurrence of each stated manner of failure occurrence: whether the production stops, whether the production process continues to produce waste, whether there is a threat to the environment, whether there is a threat to the health of workers...

5. What is the importance of each failure? The consequence of every failure is certain amounts of time and money that should be spent in order to eliminate the failure. Besides, failures may have additional consequences related to the stopping of production, production of waste, degradation of the environment, workers’ injuries, damage of other parts of the system. Thus, every failure has its time and financial equivalents as well as additional consequences which are sometimes possible and sometimes impossible (or it is extremely complicated) to be expressed in time and financial units. The more “expensive” the consequences, the stronger the need to prevent such a failure, i.e. to find a preventive activity which would eliminate and postpone failure occurrence, or at least alleviate the consequences of that failure. In order to facilitate the work with these terms, RCM has defined four possible groups of consequences: hidden consequences, consequences related to safety and the environment, production consequences and non-production consequences.

6. What can be done to prevent a failure? It used to be understood that all elements, i.e. their failures, are governed by the "bathtub diagram", which is shown in Figure 4.9 and denoted by „A".

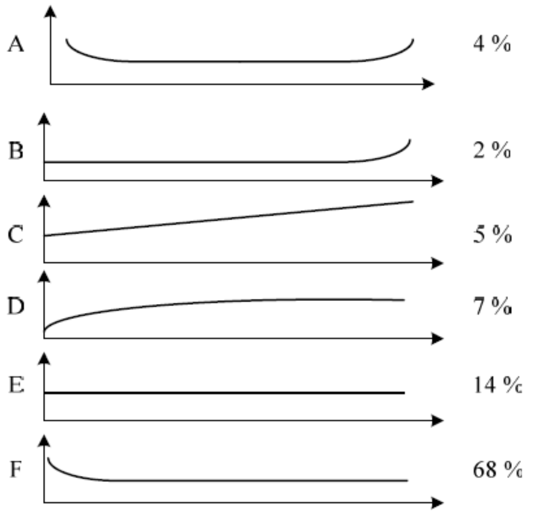

Figure 1. Six forms of failure intensity diagram

However, by monitoring the failure occurrence in civil airplanes, the data presented in the same figure have been obtained and now it can be seen that only 4% of parts have such a shape of the failure intensity curve. The shape of the failure intensity curve designated by "B" have additional 2% elements. As the preventive replacements are carried out at the moment when there is an increased probability of failure due to intensive wear, it means that only these two shape of the failure intensity curve are justified for application of preventive replacements, i.e. in only 6% elements it is justified to carry out preventive replacements; all other preventive replacements have a negative effect on the reliability of the system and the number of failures of that system. Later studies in industrial conditions have shown that between 77 and 92% of failures are not time dependant, i.e. in those cases it is not recommended to perform preventive replacements.

7. What should be done if no adequate preventive activity can be found? There are some cases when it is not possible to find an adequate preventive activity which will prevent failure occurrence and then it is necessary to perform an economic analysis: whether it is economically profitable to let an element fail and then replace it or whether it is necessary to do something so that the failure could have minimum consequences.

RCM has defined four groups of failure consequences and, depending on the group to which consequences of a failure belong, the possibility of treating each failure, i.e. its causes and consequences is searched for. If it is a hidden failure, it is necessary to define the activities for discovering the failure (these activities are widely used in the army, but they are also used in the functions of fire protection). If it is a failure with the consequences related to safety and the environment, it is useful to carry out only the activities that reduce or eliminate the consequences of the failure. If such an activity does not exist, the observed element should be redesigned or it is necessary to change the whole process in which that element participates. In the failures which have only production consequences, it is recommended to perform preventive interventions only when the total costs of those preventive interventions are lower than the costs arising due to the failure of that element. The situation is identical with the failures that do not have direct influence on the production.

In both cases, if it is not possible to find the preventive activity which will reduce the total costs, it is necessary to let that element fail and then replace it. The exception is the situation when the costs arising due to the failure are extremely high and then it is recommended to redesign the element of the whole system.

3. RCM METHODOLOGY

RCM can be regarded as an efficient tool that covers guidelines for executive managers who want to achieve high standards of maintenance. This includes identification of critical equipment and development of optimum maintenance policies based on the reliability data. RCM can be used for formulation of the maintenance strategy for production equipment and for the analysis of functional failures, which includes aspects of the environment and human factors.

The RCM methodology can be presented in 7 steps, which cover one or several activities, as shown in Figure 2.

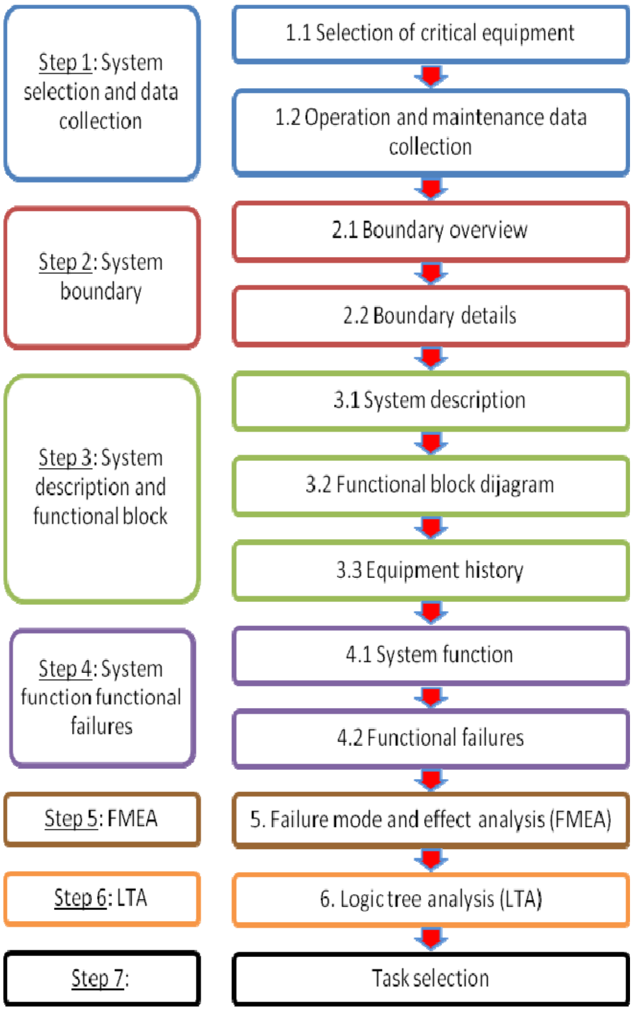

Figure 2. Flow diagram in RCM methodology

3.1. Selection of the system and collection of information

The level at which RCM analysis is performed can be selected as part of a large system or plant. The system is connected to the starting point of the RCM process because there are several failure modes, ranged by their priority due to limited resources of preventive maintenance (PM). Different factors, such as: costs, safety and environment protection can influence selection of the system. Documents such as the scheme of the system and/or block diagram, history of failures of similar equipment or operating instructions should serve as the basis for collecting information about the system.

3.2. Definition of system boundaries

The main equipment included in the system is identified with primary physical boundaries. Precise definition of boundaries is important from two aspects. Firstly, we should make sure that the potentially important functions are not neglected and secondly, the boundary represents a link between the entrance to the system (energy signals, flow...) and the exit from the system (output interfaces). This approach facilitates drawing of the block diagram.

3.3. Description of the system and the functional block diagram

Description of the system and the functional block diagram should provide certain important information that relate to:

a) functional description of the system and its functions, excess functions, protective functions, etc.
b) representative functions of the system
c) input/output interface
d) a list of equipment and functional subsystems
e) history of failures of equipment during the past 2 - 3 years

3.4. Functions and functional failures

Function is a desired activity which should be performed by the equipment or system during a defined time interval. Every system has its primary and secondary functions.

In the process of function identification it is necessary:

- to consider all functions
- to describe the functions by the expressions that contain specific constraints/restrictions
- to describe the functions in the expressions that show what a user needs, and not overall capabilities
- not to combine the functions
- to describe the functions so that the description includes a verb, an object and an applicable constraint/restriction

The importance of this issue is supported by the fact that there are certain standards which give guidelines for identification of important functions. One of those standards is NAVAIR 00-25-403. In addition to definition of important functions, it is necessary to eliminate inconsistent functions.

A functional failure must refer to the defined functions. A functional failure does not have to be a complete loss of a function. It is necessary to point out the functional failures where the effect of function degradation is different from the total loss of function.

3.5. MEA and FMECA analysis

FMEA is the basic procedure for qualitative estimation of technical system reliability. The logical continuation of FMEA is quantification of the corresponding values related to the failures of technical system elements and examination of criticality. Criticality most frequently means a relative measure of consequences of failure modes and the frequency of its occurrence. FMEA and CA make the Failure Modes, Effects and Criticality Analysis – FMECA. Systematic monitoring of failures of elements and creation of a database provides a basis for application of the FMECA procedure. Necessary conclusions for development of corrective measures for the purpose of elimination of noticed weaknesses can thus be drawn.

The existing standards, which refer to the FMEA method, are different. The differences are smaller or bigger, which depends on the standard. They are most often connected with the look of the form for documenting FMEA, terminology, designation of certain values/quantities, etc.

3.6. Logic tree analysis (LTA)

When the lists of failure modes are formed for each component of the system and when the functional dependence among all failure modes of components and functional failures are found, it is necessary to establish the influence of each failure mode at the local level as well as at the levels of system and plant. Such decisions are not at all simple, so the logic tree shown in Figure 3 is used for that purpose.

The failure modes classified in this way can be in one of the following three branches of the logic tree (algorithm, Figure 3):

- Evident
- Safety
- Outage

Classification of the effects of failure modes according to the logic tree analysis puts every failure mode in one of the following 4 groups:

- A – safety problem
- B – outage problem
- C – minor (insignificant) economic problem
- D – hidden failure

This analysis, taking into account a huge number of combinations that can appear when failure modes and their causes are in question, once again confirms the inevitability of creation of a database of failures.

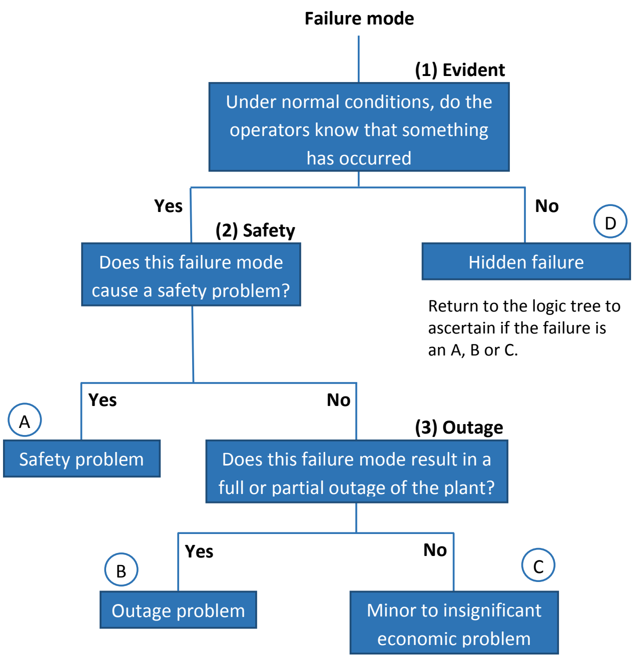

Figure 3. Logic tree analysis

3.7. Classification of maintenance tasks based on the RCM analysis

The aim is to find such a maintenance task which has the highest performance regarding prevention of failure occurrence. If the failure mode cannot be prevented, then the mechanism of failure occurrence should be monitored through a measurable parameter which has its defined dependence with the failure mode during a time interval. If there is no preventive task (activity), or if techno-economic analyses are taken into account, in certain cases it can be decided that the system component (or some of its elements) should operate until it fails.

Potential maintenance tasks belong to one of the 4 possible categories (Figure 4):

- TD – Time – Directed
- CD – Condition – Directed
- FF – Failure Finding
- RTF – Run to Failure

It is necessary to assign a maintenance activity to every failure mode. That activity should prevent the occurrence of the failure mode in the most efficient way or provide maximum reduction of its effect. Every selected type of activity should have its description and details about its periodic repetitions.

4. RCM ANALYSIS ON THE EXAMPLE OF CITY WATERWORKS

City waterworks has been chosen for practical realization of the RCM methodology. As the process of water production is continuous, preventive maintenance has a very important role in the reliability of such systems. Costs of preventive maintenance can be optimized by proper selection and frequency of maintenance tasks.

The first step of the standard RCM methodology is to identify the system which should be analyzed. Potential users of the analysis should always be borne in mind. The company managers and the maintenance staff have different requirements. Therefore, the standard RCM methodology must be modified and adapted to specific requirements of users. Taking into account that the city waterworks is a large infrastructure facility which consists of several sources, pumping stations, tanks and water supply network, Figure 5 proposes the infrastructure organization of the waterworks, which can meet the requirements of the RCM methodology. The levels of details in the RCM methodology are shown at certain organizational levels.

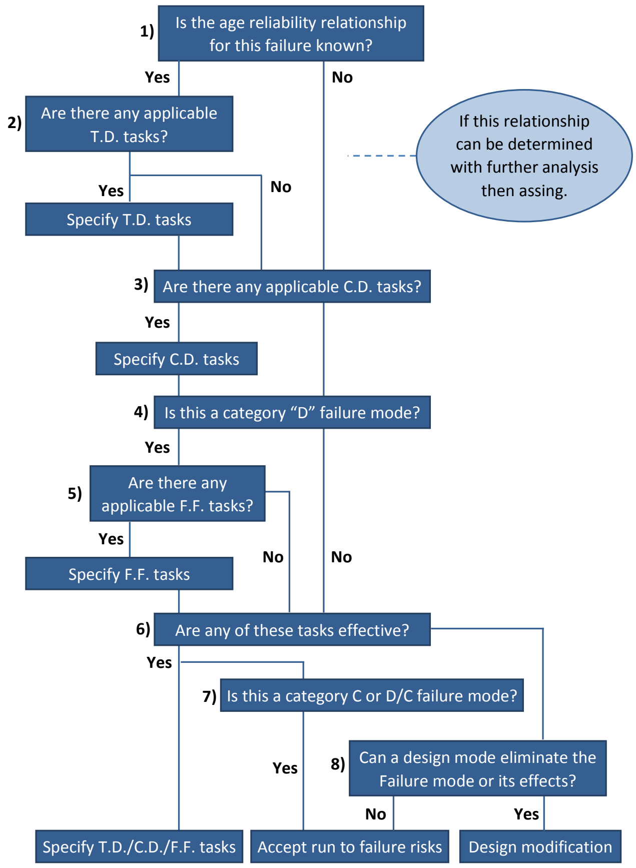

Figure 3. Classification of maintenance tasks based on the RCM analysis

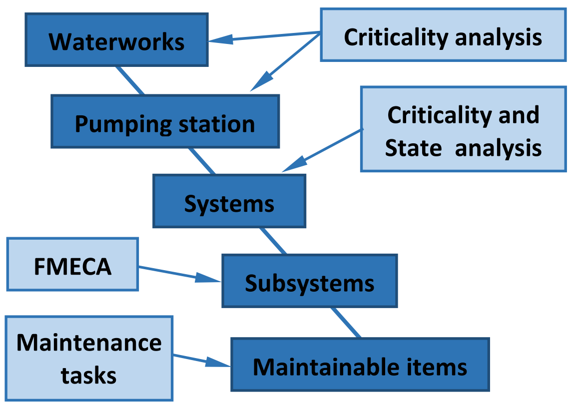

Figure 5. Waterworks infrastructure organization

The waterworks is at the highest level in the structural organization. The criticality analysis establishes the parts of the waterworks which should be covered by the RCM analysis in order to avoid comprehensive analyses at unnecessary points. The pumping stations are the most important parts of the water supply network, so they are given as an obligatory part of the structural organization. For the generality of analysis, when systems are in question, legal regulations that differ from country to country should also be taken into consideration.

The selected pumping station consists of a source and a powerhouse with the pump aggregates and the plant for water chlorination. The powerhouse is located next to the well from which water is taken and directly pumped toward users. The well is dug, with the walls made of compacted concrete.

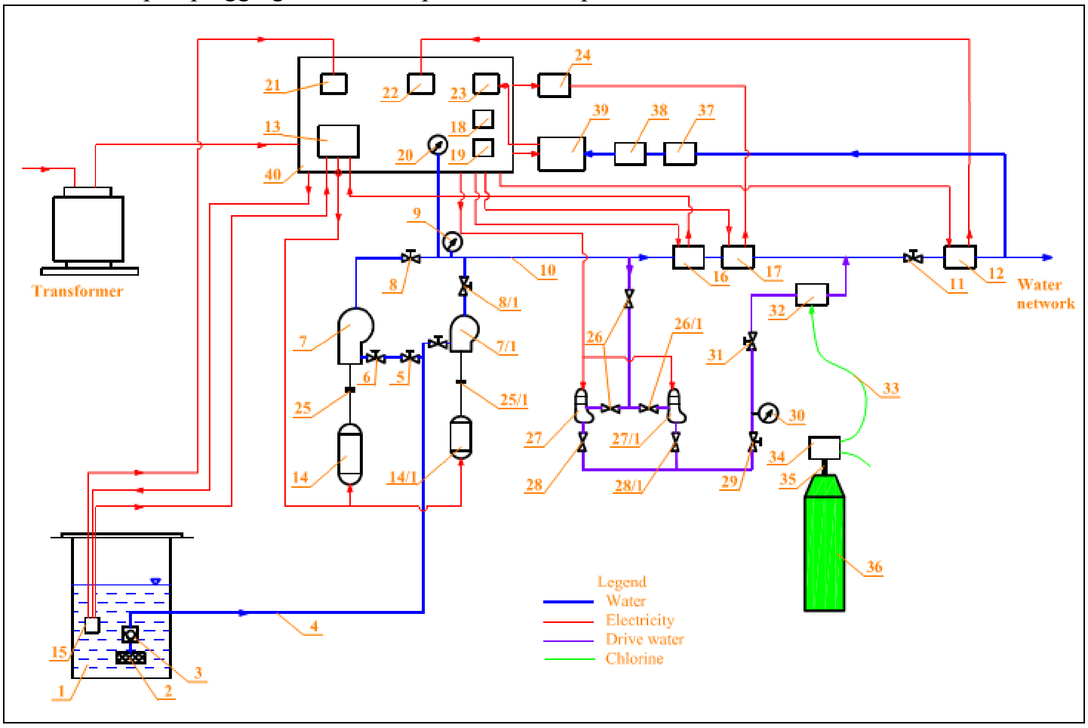

Figure 6. Schematic presentation of the pumping station for water supply

Pumping station consists of the following basic components (Figure 6): 1 - well, 2 – suction chamber, 3 - irreversible valve, 4 - suction pipeline, 5 - valve on the suction branch, 6-tap of the pipeline for filling; 7-centrifugal pump, 8-valve on the pressure pipeline, 9-pressure gauge, 10 pressure pipeline, 11-valve V2, 12-flow meter, 13-frequent regulator, 14-motor, 15-hydrostatic level sensor, 16-pressure transducer, 17-flow transducer, 18-switch with indicator of centrifugal pump; 19 -switch with indicator for booster pump operation, 20-sensor for pressure in the pressure pipeline, 21-sensor for water level in the well; 22-sensor of flow in the pressure pipeline, 23-sensor of chloral level 24- flow indicator; 25-connector, 26-gate valve ; 27-booster pump, 28-valve Z3, 29-valve on the pressure branch of the water flow, 30-gauge of water flow, 31 - valve V3, 32-injector, 33-vacuum hose, 34-vacuum regulator, 35-valve for chlorine ; 36-bottles for chlorine; 37-flow regulator of chlorine analyzer; 38 - pressure regulator of chlorine analyzer; 39-analyzer of free chlorine, 40-distribution cabinet.

There are two centrifugal pumps in the powerhouse, one of them being controlled by a frequency regulator. Both pumps are intake and discharge pumps at the same time. The pumps have parallel connection to the water supply network. The pipe fittings allow simultaneous operation of both pumps. Most frequently only one pump operates, and the other serves as a back-up pump. The pump operation variant depends on the necessary quantity of water and the well yield. For the purpose of increasing energy efficiency, the higher flow pump is controlled by a frequency regulator. The speed regulation system changes the pump characteristic by adjusting the discharge head (generated in the pump) according to the required parameters of the pipeline and the desired flow.

4.1. Selection of the system

Pumping stations are the most important parts of the waterworks system. That is why the pumping station was selected as a subject of the RCM analysis in this example. The pumping station consists of three functional systems: a well, water production and chemical treatment of water. It should be particularly emphasized that some undesirable consequences which can threaten the safety and health of people may occur during chemical treatment of water. In addition, the maintenance costs for the pumping station has the largest share in the total maintenance costs for the waterworks. These are the key reasons for selection of the system.

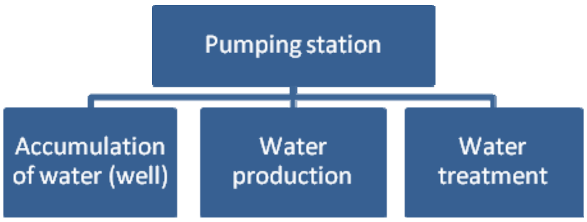

Figure 7. Functional systems in the pumping station

a. Boundaries of the system

In the pumping station, the boundaries of the system are selected in such a way that they cover all important functions which should be performed by the pumping station. The selected boundaries provide a link between the input and output of certain functional systems in the pumping station. At the same time, this represents preparation for the performance of further activities, such as drawing block diagrams.

b. Functional block diagram

If **water production and water treatment** are designated as a system, it can be separated into three functional subsystems:

- drive,
- pumping water
- chlorination of water.

The functional subsystems and their relationships are shown in the block diagram in Figure 8.

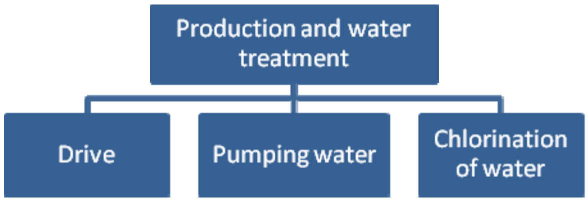

Figure 8. Functional subsystems

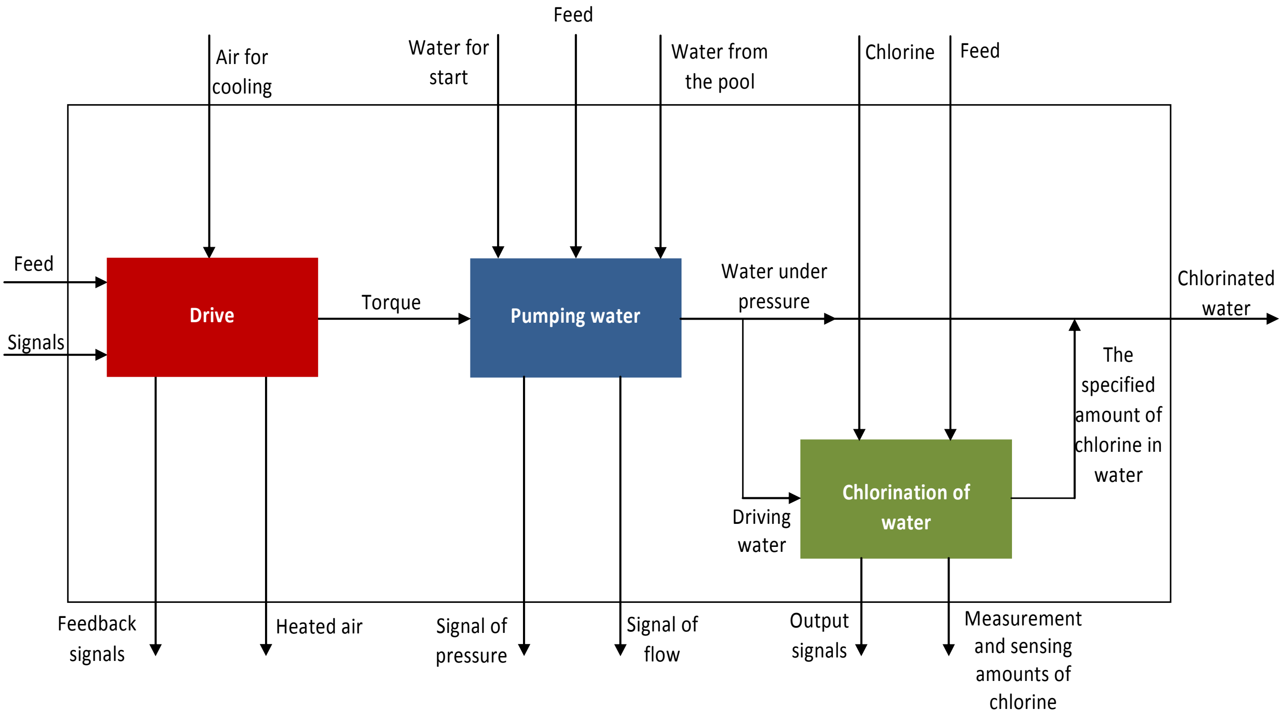

Figure 9. Functional block diagram

4.2. Functions and functional failures

Definition of functions and functional failures is presented in the example of the subsystem for chlorination of water.

For chlorination of water, it is necessary to use the injector for achieving a defined value of subpressure/underpressure, so that the vacuum regulator could provide chlorine flow to the discharge pipeline. Within this subsystem, a very important function is also realized – measuring and inspection of concentration of free chlorine.

Table 1. Functions and functional failures in the subsystem for chlorination of water

Providing the necessary flow of chlorine	Leaking of chlorine
	Insufficient flow of chlorine
	Dropping of the chlorine dosage
Indication of the quantity of chlorine	Indicator on the vacuum regulator shows "empty"
	Quantity of chlorine in water cannot be read
Providing the necessary subpressure/underpressure	Insufficient pressure
Providing operation without disturbing factors	Water in the vacuum installation
Measuring concentration of free chlorine	Insufficient flow of water through the measuring block
	Insufficient electrode current
	Unstable value of chlorine concentration
Providing operating water of the given pressure	There is no flow of operating water to the booster pump
	Flow of water in the discharge pipeline cannot be controlled
	Insufficient pressure of operating water
	Pressure of operating water cannot be inspected

4.3. FMEA

After the data about systems with their subsystems, components of the systems and their failure modes with causes of failures and functions of the systems with functional failures are formed, it is necessary to establish the relationship between functional failures and failure modes of components. This part is the most complex part of the RCM analysis, and it is solved by means of the matrix of interdependences between failure modes of components and functional failures, which is presented in Table 2.

Table 2. Matrix of interdependences between failure modes of components and functional failures

Com. #	Component name	Functional failures													
		3.1.1	3.1.2	3.1.3	3.2.1	3.2.2	3.3.1	3.4.1	3.5.1	3.5.2	3.5.3	3.6.1	3.6.2	3.6.3	3.6.4
23	Sensor of chloral level					X									
26	Gate valve											X			
27	Booster pump			X			X								
28	Valve Z3												X		
29	Valve on the pressure branch of the water flow													X	
30	Gauge of water flow														X
31	Valve V3													X	
32	Injector			X			X	X							
33	Vacuum hose		X												
34	Vacuum regulator	X	X	X	X		X								
35	Valve for chlorine	X													
36	Bottles for chlorine	X													
37	Flow regulator of chlorine analyzer								X		X				
38	Pressure regulator of chlorine analyzer										X				
39	Analyzer of free chlorine								X	X	X				

4.4. LTA

Within the RCM analysis, all functions of the pumping station with its functional failures have been treated. All possible failure modes with their causes have been formed for key components of certain subsystems, such as the electromotor, the centrifugal pump, the injector for chlorination and the vacuum regulator, as well as for a large number of other components. In order not to become too extensive, the paper leaves failure modes for certain components to be further developed.

Table 3. Presentation of the RCM analysis

RCM category	Number
System	1
Subsystems	3
Components	40
Functions	17
Functional failures	37
Failure modes (with causes of failures)	94

Establishing of all necessary relationships required by RCM results in a wide platform for research not only into reliability but also into other indicators which characterize maintenance of a technical system.

Failure modes are classified into two groups:

- Group 1 (A, B, D/A and D/B)
- Group 2 (C, D/C)

Table 4. Categorization of failure modes by groups

	Group 1	Group 2
A – safety problem	4	
B – outage problem	40	
C – minor economic problem		35
D/A - hidden failure / safety problem		
D/B - hidden failure / outage problem	13	
D/C - hidden failure / minor economic problem		2
Total	57	37

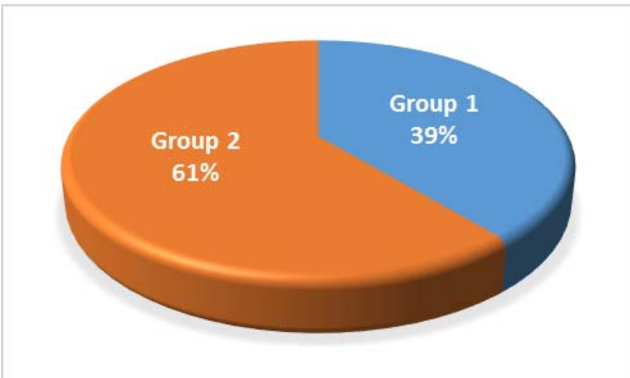

Figure 10. Classification of failure modes by effects

On the basis of the diagram from Figure 10, it can be concluded that 61% of failure modes should be planned for preventive maintenance, and 39% for corrective maintenance.

4.5. Maintenance tasks

Potential maintenance tasks belong to one of the 4 possible categories:

1. TD – Time – Directed
2. CD – Condition – Directed
3. FF – Failure Finding
4. RTF – Run to Failure

When the relationship between the effects of failure modes and maintenance tasks is established, the situation is as shown in Table 5.

Table 5. Relationship between the category of failure modes and maintenance tasks

	TD	CD	FF	RTF	
A –safety problem	4				4
B –outage problem	22	10	3	4	39
C – minor economic problem	20	7	9		36
D/A - hidden failure/ safety problem					
D/B - hidden failure / outage problem	5	2	5	1	13
D/C - hidden failure / minor economic problem	2				2
Total	53	19	17	5	

5. CONCLUSION

Classification of failure modes and maintenance tasks on the example of a pumping station of the waterworks was carried out by applying the algorithms developed in the RCM methodology. The most effective task of preventive maintenance was selected for every failure mode, so that this example also confirms that RCM equally treats all maintenance concepts. RCM is led by safety and costs. The selection of maintenance activities is based on consequences: safety, operational, non-operational and consequences of hidden failures. Safety must be achieved at any costs, and after that costs become a criterion.

By applying the RCM methodology, on the example of a pumping station of the waterworks, and by the analysis of a set of all possible failure modes, it was established that 61% of failures could be prevented or that their effect could be reduced by proper selection and periodic repetition of preventive maintenance tasks. Hence, it can be concluded that city waterworks are suitable systems for application of the RCM methodology. Besides the suitability for application, the other positive effects of RCM application stated in the paper may be expected in these and similar systems. In addition to a series of advantages, the RCM methodology also has its weaknesses, which primarily refer to the length of duration and necessity of software support. RCM analysis on a relatively simple example, such as the pumping station, cannot be successfully realized without computer support.

ACKNOWLEDGEMENT

"Three of the authors (Z.P), (B.R.) and (V.G.) wishes to acknowledge his gratitude to <Ministry of Education and Science of Republic of Serbia> for the support to the research through project grant TR37020."

REFERENCES

[1] Radičević B., Master thesis „Računarska podrška održavanju orijentisanom ka pouzdanosti", The Faculty of Mechanical Engineering Kraljevo, Kraljevo, 2009

[2] Radičević B., Petrović Z., Ivanović S., Georgieva M., „Calculation of failure criticality in Reliability – Centred Maintenance", VII International Scientific Conference Heavy Machinery – HM 2011, Kraljevo, 2011, 17-23, ISBN 978-86-82631-58-3

[3] Radičević B., Petrović Z., Kolarević M., Dinić M., „THE ANALYSIS OF MODE COSEQUENCES AND CRITICALITY AT POTENTIAL FAILURES OF GEAR PUMP", VI International Scientific Conference Heavy Machinery – HM'08, Kraljevo, 2008, str. F.7 – F.12

[4] Radičević B., Petrović Z., Ivanović S., Kolarević M., - „AN EXAMPLE OF APPLICATION OF SOFTWARE FOR ASSESSMENT RELIABILITY DISTRIBUTION", 20th INTERNATIONAL SCIENTIFIC CONFERENCE TRANSPORT 2011- Sofia, Bulgaria, Academic journal, Mechanics Transport Communications, ISSN 1312-3823, isuse 3, 2011, article No 0593, pages VI-113÷118

[5] Carretero J., et al, Applying RCM in large scale systems: a case study with railway networks, Reliability Engineering and System Safety 82 (2003) 257–273

[6] V.S. Deshpande, J.P. Modak, Application of RCM to a medium scale industry, Reliability Engineering and System Safety 77 (2002) 31-43

[7] Abdul-Nour G, et al., A reliability based maintenance policy: a case study. Comput Ind Engng 1998;33(3/4):591–4.

[8] Anderson R., Lewis N., Reliability centered maintenance: Management and engineering methods. The Netherlands: Elsevier; 1990

[9] NAVAIR, Guidelines for the naval aviation reliability-centered maintenance. Direction of Commander, Naval Air Systems Command, USA; 1996.

[10] OREDA Consortium, Reliability data handbook, 3rd ed.; 1997

[11] Schlkins N. Application of the reliability centered maintenance structures methods to ships and submarines. Maintenance June 1996; 11(3)

[12] Vatn J, Hokstad P, Bodsberg L. An overall model for maintenance optimization. Reliab Engng Syst Safety 1996;51:241–57.

[13] Tomas V. Et al., Mogućnosti i problemi primjene suvremenih strategija održavanja u pomorstvu, Pomorstvo, 2005, str. 29 – 41

[14] Stanley, N. F. Heap H. F.: "Reliability-Centered Maintenance", Defense Documentation Center, AD-A066-579, Washington DC, 1979

[15] Aleksić M, Stanojević P., Model revizije koncepcija brodskih sistema I RCM Document Transcript

[16] Islam H. Afefy, Reliability-Centered Maintenance Methodology and Application: A Case Study, Engineering, 2010, 2, 863-873

[17] Razvoj sredstava za rad i koncepcija održavanja, https://www.iim.ftn.uns.ac.rs

Modeling and Numerical Analysis of Wire temperature in GMA welding

Mišo Bjelić[1*], Karel Kovanda[2], Ladislav Kolařík[2], Marie Kolaříková[2], Petr Vondrouš[2]
[1]Faculty of Mechanical and Civil Engineering, University of Kragujevac, Kraljevo, Serbia
[2]Faculty of Mechanical Engineering, Czech Technical University, Prague, Czech Republic

This paper presents a method of modeling the thermal process involved in electrode heating during GMA welding. Numerical model of heat exchange in wire is developed based on the energy conservation laws. Developed model was adopted for computer simulation using successive over-relaxation method.

Keywords: GMAW, temperature, heat transfer, numerical method

1. INTRODUCTION

GMAW process is found widespread use in industry because of the various advantages, among which the most important are the following: cost effectiveness, greater depth of penetration, ability to achieve higher welding speeds, high productivity, etc.

During GMA welding, an electric arc is established between the electrode and the base material. The electrode is at the same time filler material. Whole process takes place in a protective atmosphere of an inert/active gas, Figure 1.

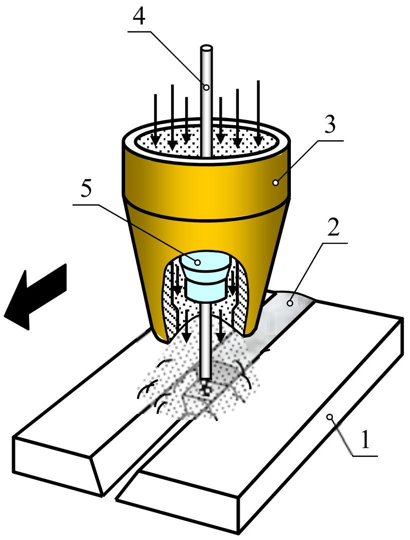

Figure 1: Schematic representation of GMAW; 1. base material, 2. weld bead, 3. nozzle, 4.wire [1]

Many welding processes are based on the rapid change of temperature in the welding zone or in the electrode. At the same time, various physical and chemical processes, such as melting of base and filler materials, metallurgical reactions, crystallization processes, etc. occur simultaneously. In case of GMAW, electrode which moves with speed v_e through contact tip, is heated above the melting point. As the melting of the electrode is important part of GMAW process, it is necessary to be able to predict and simulate the process of electrode heating. First step is to establish a simulation model of the process with appropriate accuracy.
Preparation of computational model can be divided into three phases [2]:

- selection of proper geometric approximation of domain,
- selection of idealized source characteristic,
- setting of the initial and boundary conditions.

As stated before, first step is selection of geometric approximation.

2. GEOMETRIC APPROXIMATION

Propagation of heat during welding, among other things depend on the shape and dimensions of the body. Welded parts can have a very complex shape which greatly complicates the calculations related to the propagation of heat. Therefore, for the calculation of the temperature field is necessary to select simpler geometry which will represent real calculation domain.

For the modelling of the heat transfer in the wire we used model of a rod. Rod represents a body of cylindrical shape, Figure 2. Inside the rod, heat is propagated one – dimensionally. Temperature distribution in the cross sections of rod is even.

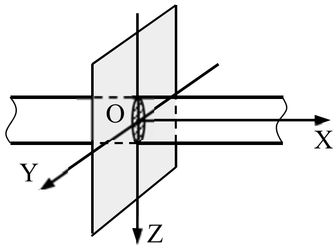

Figure 2. Infinite rod [3]

3. MODELLING OF HEAT PROPAGATION

Modelling of heat propagation inside the rod requires to choose a proper control volume.

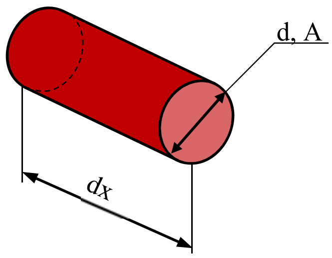

Figure 3. Control volume

*Corresponding author: Dositejeva 19, 36000 Kraljevo, Serbia, bjelic.m@mfkv.kg.ac.rs

In this case, control volume is cylinder of infinitely small length dx and diameter which is equal to diameter of wire, Figure 3.

All inputs and outputs to and from control volume are shown on Figure 4.

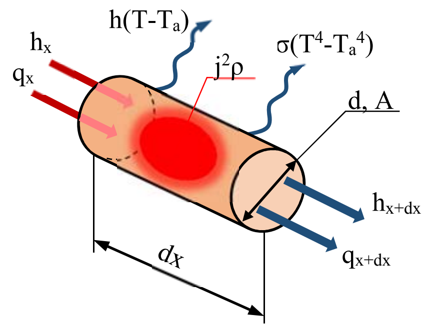

Figure 4. Exchange of heat inside of control volume

It can be seen that exchange of energy inside the control volume is due to heat and mass transfer. Heat transfer is based on conduction, convection and radiation. Exchange of energy due to mass is consequence of the fact that wire is moving with constant speed v_e.

Also, there is a volumetric heat source inside the wire due to Joule heating.

Amount of energy exchanged by heat is equal to:

$$\left(E_{in}-E_{out}\right)_{heat}=\frac{\partial}{\partial x}\left(\lambda\frac{\partial T}{\partial x}\right)Adx-h\left(T-T_a\right)2r\pi dx-\ldots \qquad (1)$$
$$-\varepsilon\sigma\left(T^4-T_a^4\right)2r\pi dx$$

While the amount of energy exchanged due to mass transfer is equal to:

$$\left(E_{in}-E_{out}\right)_{mass}=\dot{m}\left(e_x-e_{x+dx}\right)=-\gamma v_e\frac{\partial(c_pT)}{\partial x}dxA \qquad (2)$$

where:

c_p – specific heat capacity (J/kgK)
γ – density (kg/m^3)
λ – thermal conductivity (W/mK)
h – heat transfer coefficient (W/m^{2}K)
σ – Stefan–Boltzmann constant (W/m^{2}K)
ε – emissivity
e – specific enthalpy
T – temperature of control volume (K)
T_a – ambience temperature (K)
r – radius of wire (m)

Amount of energy that is generated in control volume by Joule effect, Figure 4, can be calculated as:

$$E_{gen}=j^2\rho Adx \qquad (3)$$

where:

j – current density (A/m^2)
ρ – electrical resistivity (Ωm)

Latent heat of melting can be calculated as:

$$E_{lh}=\gamma AdxL\frac{\partial f_l}{\partial t} \qquad (4)$$

where:

L – latent heat of melting (J/kg)
f_l – fraction of liquid phase

Fraction of liquid phase depends on temperature and can be expressed as:

$$f_l=\begin{cases}0 & T<T_s\\ \dfrac{T-T_s}{T_l-T_s} & T_s\le T\le T_l\\ 1 & T>T_l\end{cases} \qquad (5)$$

where:

T_s – solidus temperature (K)
T_s – liquidus temperature (K)

Amount of energy which is used for heating of control volume is equal to:

$$E_{ch}=\gamma Adxc_p\frac{\partial T}{\partial t} \qquad (6)$$

First law of thermodynamics bring us to following equation:

$$\gamma c_p\frac{\partial T}{\partial t}=\lambda\frac{\partial^2T}{\partial x^2}-\gamma c_pv_e\frac{\partial T}{\partial x}-\frac{2h}{r}(T-T_a)-\frac{2\varepsilon\sigma_c}{r}(T^4-T_a^4)-$$
$$-\gamma L\frac{\partial f_l}{\partial t}+j^2\rho$$

Reforming the f_l term, we obtain:

$$\frac{\partial f_l}{\partial t}=\frac{\partial f_l}{\partial T}\frac{\partial T}{\partial t} \qquad (8)$$

By substitution (8) into equation (7) we obtain:

$$\gamma\left(c_p+L\frac{\partial f_l}{\partial T}\right)\frac{\partial T}{\partial t}=\lambda\frac{\partial^2T}{\partial x^2}-\gamma c_pv_e\frac{\partial T}{\partial x}- \qquad (9)$$
$$-\frac{2}{r}\left[h+\varepsilon\sigma_c\left(T+T_a\right)\left(T^2+T_a^2\right)\right](T-T_a)+j^2\rho$$

Introducing following substitutions:

$$c_{eff}=\left(c_p+L\frac{\partial f_l}{\partial T}\right)$$

where:

c_p – equivalent specific heat capacity (J/kgK)

$$h_{ekv}=\left[h+\varepsilon\sigma_c\left(T+T_a\right)\left(T^2+T_a^2\right)\right]$$

where:

h_{ekv}– equivalent heat transfer coefficient

$$j=\frac{I}{r^2\pi}$$

where:

I – welding current (A)

We obtain following non – stationary, second order, partial differential equation:

$$\frac{\partial T}{\partial t}=\alpha\frac{\partial^2T}{\partial x^2}-v_e\frac{\partial T}{\partial x}-\frac{2h_{ekv}}{\gamma c_{eff}r}\left(T-T_a\right)+\frac{I^2\rho}{\gamma c_{eff}\pi^2r^4} \qquad (10)$$

4. NUMERICAL SOLUTION

Equation (10) describes change of temperature along the wire. Analytical solution of equation (10) is connected with many difficulties. Instead, we have used finite difference method.
Partial derivatives are are approximated using central finite differences:

$$\frac{\partial^2 T}{\partial x^2} = \frac{T_{i+1} - 2T_i + T_{i-1}}{\Delta x^2} \tag{11}$$

$$\frac{\partial T}{\partial x} = \frac{T_{i+1} - T_{i-1}}{2\Delta x} \tag{12}$$

$$\frac{\partial T}{\partial t} = \frac{T_i^{n+1} - T_i^n}{2\Delta t} \tag{13}$$

where:

T_i^n – temperature at point i at present time step

T_i^{n+1} – temperature at point i at next time step

By substituting equations (11-13) into equation (1) we obtain:

$$\frac{T_i^{n+1} - T_i^n}{2\Delta t} = \alpha \frac{T_{i+1}^n - 2T_i^n + T_{i-1}^n}{\Delta x^2} - v_e \frac{T_{i+1}^n - T_{i-1}^n}{2\Delta x} - \\ - \frac{2h_{ekv}}{\gamma c_{eff} r}\left(T_i^n - T_a\right) + \frac{I^2 \rho}{\gamma c_{eff} \pi^2 r^4} \tag{14}$$

Equation (14) now becomes:

$$T_i^{n+1} = AT_i^n + BT_{i+1}^n + CT_{i-1}^n + D \tag{15}$$

where coefficients A, B, C, D are equal to:

$$A = \frac{\Delta x^2 \gamma c_{eff} r - 2\alpha \Delta t \gamma c_{eff} r - 2h_{eq} \Delta t \Delta x^2}{\Delta x^2 \gamma c_{eff} r}$$

$$B = \frac{2\alpha \Delta t - v_e \Delta t \Delta x}{\Delta x^2} \qquad C = \frac{2\alpha \Delta t + v_e \Delta t \Delta x}{\Delta x^2}$$

$$D = \frac{4h_{eq} \Delta t T_a r^3 \pi^2 + 2I^2 \rho \Delta t}{\gamma c_{eff} r^4 \pi^2}$$

Necessary conditions for equation (15) in order to get stabile solution are:

$$A \geq 0 \tag{16}$$
$$B \geq 0 \tag{17}$$

From condition (17) we get value of stable grid step:

$$2\alpha \Delta t - v_e \Delta t \Delta x \geq 0 \qquad \Rightarrow \qquad \Delta x \leq \frac{2\alpha}{v_e} \tag{18}$$

Where:

α – thermal diffusivity (m^2/s)

From condition (16) we get value of stable time step:

$$\Delta x^2 \gamma c_{eff} r - 2\alpha \Delta t \gamma c_{eff} r - 2h_{eq} \Delta t \Delta x^2 \geq 0$$
$$\Delta t \leq \frac{\Delta x^2 \gamma c_{eff} r}{2\left(\alpha \gamma c_{eff} r + h_{eq} \Delta x^2\right)} \tag{19}$$

5. BOUNDARY CONDITIONS

Partial differential equation (10) in general have an infinite number of solutions. To obtain the solution which describes the given problem, it is necessary that equation (10) fulfill initial and border conditions. Initial conditions in this case are:

i = 0, T_i = Tct (i = 1,n)

Boundary conditions are shown on Fig. 5.

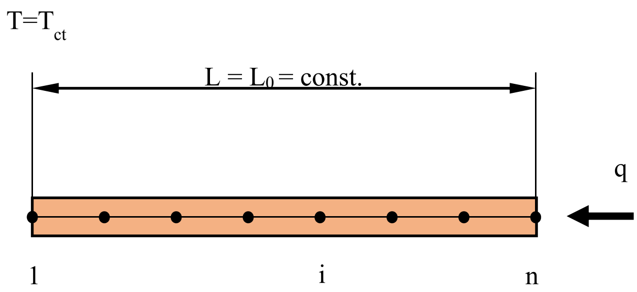

Figure 5. Boundary conditions

The amount of heat that enters at the end of electrode is equal [4]:

$$q = \left(V_a + \phi + \frac{3}{2}\frac{kT}{e}\right) I \tag{20}$$

where:

V_a – anode voltage fall,
ϕ – work function of metal surface,
3kT/2e – thermal energy of electrons.

Boundary condition at the end of electrode are shown at Figure 6.

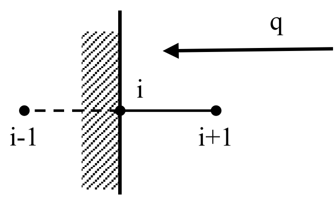

Figure 6. Boundary condition at the end of electrode

Introducing the fictive point i+1, we can express border condition at the end of electrode as:

$$\lambda \frac{T_{n+1}^n - T_{n-1}^n}{2\Delta x} = q \tag{21}$$

$$T_{n+1}^{n} = \frac{2\Delta x}{\lambda} q + T_{n-1}^{n} \tag{22}$$

By substituting equation (22) into equation (15) we obtain:

$$T_n^{n+1} = AT_i^n + (B+C)T_{i-1}^n + E$$

where:

$$E = B\frac{2\Delta x}{\lambda} q + D$$

Now, we have following equations which have to be solved iteratively:

$$T_1^{n+1} = T_{ct} \qquad i=1 \tag{23}$$

$$T_i^{n+1} = AT_i^n + BT_{i+1}^n + CT_{i-1}^n + D \qquad i=2,n-1 \tag{24}$$ 1.

$$T_n^{n+1} = AT_i^n + (B+C)T_{i-1}^n + E \qquad i=n \tag{25}$$

Equations (23-25) are solved iteratively by SOR method in software package MATLAB. Results of simulation are shown at Figure 7. Parameters used for simulation are listed below.

– electrode extension = 0.01 m
– welding current = 150 A
– wire diameter = 0.001 m
– wire speed = 0.1 m/s
– temperature of contact tip = 573 K
– ambience temperature = 293 K
– grid step = 0.0001 m
– time step = 0.0001s

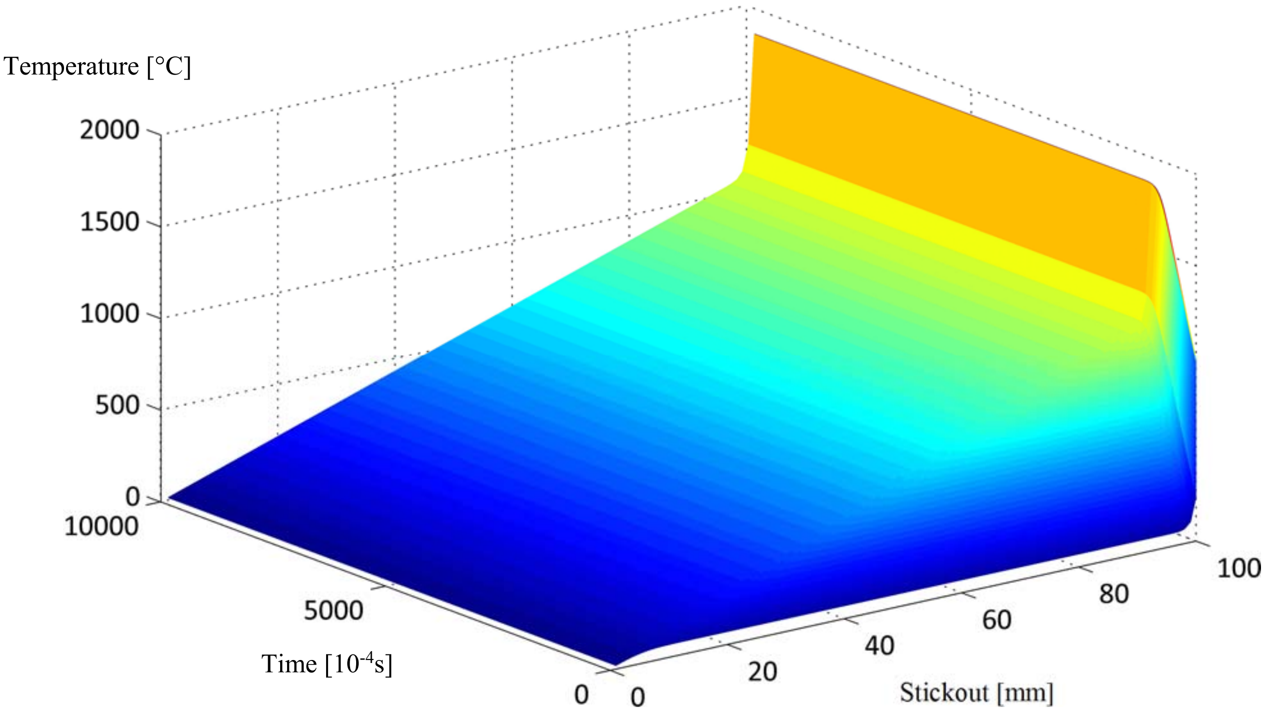

Figure 7. Temperature along the wire

CONCLUSIONS

Results of simulations shows that temperature inside the wire changes nearly linearly from the contact tip to the point near the end of the wire. At the end of wire, the temperature rises sharply as a consequence of arc influence. Achieved temperatures at the end of the wire are higher than melting temperature. Proposed model does not take into account that temperature of contact tip rises from ambient temperature to temperature Tct which is used in simulation as boundary condition. Future research should include solution of this problem in proposed model.

ACKNOWLEDGEMENT

The authors wish to express their gratitude to National CEEPUS Office of Czech Republic for support through project "Concurrent Product and Technology Development - Teaching, Research and Implementation of Joint Programs Oriented in Production and Industrial Engineering".

REFERENCES

[1] Weman K., Welding Processes Handbook, Woodhead Publishing, Cambridge, 2003.

[2] Goldak J.A., Akhlaghi M., *Computational welding mechanics*, New York: Springer, 2005

[3] Николаев Г. А. (ред.), *Сварка в машиностроении. Справочник 1-4,* Машиностроение, Москва, 1978.

[4] Lancaster J., The Physics of Welding, New York: Pergamon, 1986

Complexity in Production Systems

Elvis Hozdić[1*], Emine Hozdić[2]
[1]Faculty of Mechanical engineering, University of Ljubljana, Ljubljana (Slovenia)
[2]Technical faculty of Bihać, University of Bihać, Bihać (Bosnia and Herzegovina)

Complex systems are systems comprised of a large number of elements that effect each other and exchange information. Complexity in the complex production systems occurs because of such interaction. The term complexity can be explained by observing the measure of ambiguity in achieving functional demands. This paper explains the nature of complexity and defines the concept of the terms complications, complexity and chaos. By explaining these terms, two types of complexities in the compley adaptive systems such as structural and operative complexity are perceived.

Keywords: Complex adaptive systems, complexity, enthropy, organisation, stabilisation and self-organisation

1. INTRODUCTION

Several approaches to solving the complexity of production systems can be found in literature. In rough terms, these approaches can be divided into ad-hoc approaches, which refer to the complexity in light of a specific problem, and general theoretical approaches, which are greatly based on the information theory or the foundation of non-linear mechanic.

A complex systems is each system that consists of a higher number of elements, which are arranged into a structure and can exist on several levels. The elements change, but those changes cannot be described with only one rule, or brought down to only one level of thinking. These different levels often contain traits and cannot be anticipated from their actual specifications [1].

2. COMPLEX SYSTEMS

A complex system consists of a high number of basic components. These components can perform dynamic interactions and create higher hiearchical levels. It leads to the description of the system behaviour in general, which cannot be found in the behaviour of the basic component.

Characteristics of complex systems are shown on image 1.

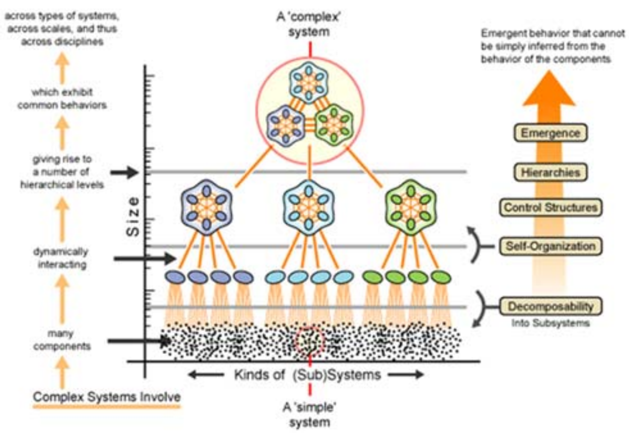

Image 1. Characteristics of complex systems

Complex systems have many autonomous parts, which are able to answer to the initiatives from the environment and also to the inner demands of the self-organisation through levels of inner return connections [3]. The key of these systems is their adjustment in order to improve their functioning. Three levels of adaptation are identified in [4]:

- Optimisation,
- Stabilisation, and
- Selforganisation.

Adaptation of elements of a complex systems reflects in the change of the rules by which the elements operate. Each individual element can be followed by different rules. According to it, each element comes to a decision based on the state of current stimulus from the environment and/or history and the final state of elements. Autonomous elements can be based on the knowledge based on which the business is carried out, independently change the rules, and with it also the goals of their companies. This event is defined solely as – organisation.

Complecity is in general a subjective term, because it cannot be defined well without defining the role of a observer and that which the observer observes. Nevertheless, after the role of an observer and the levels of observance is defined, we can speak of objective dimensions of complexities.

The dynamics of the complex systems can be summarised in eight points [5]:

- Complex systems are opened and exchange material, energy and/or information with the environment;
- A high number (not excessively) of elements in a complex system are mutually non-trivially interacting – in a static case, the system would lose important information on the properties of the system;
- Non-trivial interactions result in inner disturbances, which lead to a coordinated global behaviour;
- The system is with it better organised that before,

*Corresponding author: Hasana Kikića 67 , Velika Kladuša, BiH; e –mail: ehozdic@yahoo.com

- Coordinated global behaviour can be from the perspective of an outside observer in the form of patterns, new behavior occurs;
- Coordination of occurances can appear in the response to the effect of the environment, in that case we can say that the system is adaptive;
- When it comes to the adjustment ot the temporal generational scale, we say that there is an evolution is occuring;
- Created properties reflect in a higher level of observance. The system can also by identified as a new entity which can interact with another system or process, which reflects on the same level.

However, the aforementioned processes are to an extent connected with a causal connection, they occur in a complex system simultaneously. It is important that the strength of the complex system is monitored on several levels, having in mind that the single description of all levels is extremely difficult. As a result, the system can be monitored, but in general, we cannot understand it and operate it in engineering terms. That is the key problem in the science of complexity [6].

Despite a high diversity of the area of the occurence of complex systems, the science of complexity admits that those systems have the same properties. A general overview of theoretical information for the complexity and connected terms, self-organisation, creation, adaption and evolution we find in the works of Prokopenko.

3. THE CONCEPT OF COMPLEXITY IN THE COMPLEX PRODUCTION SYSTEMS

Suh [7] defines complexity as a measure of ambiguity in achieving functional demands. He defines four types of complecity, those being:

- complexity independent of time,
- imaginary complexity independent of time,
- combinatorial complexity dependent of time,
- periodically complexity dependent of time.

3.1. Sources of complexity

Complexity in production systems can be divided into two types, structural and operative, which is significantly different [6][8].

Structural complexity is a characteristic trait of a production system, independent of time. In such production systems, from the perspective of the observer at a certain moment the observance is frozen. The properties of the system are used in determining of complexity.

Structural complexity is in its basis subjective, since it identifies the structure and the determination of the probability of the system in a structural form, depending on the observer. Like termodynamics, a structured production system is equalised with enthropy, which, in a way, speaks about the accuracy of the system despite the unambiguity of the calculated enthropy, or its value, depending on the level of references which are subjectively chosen.

On the other hand, in solving the complexity of operational production systems, the observance is conducted in time, namely, the existence of operational complexity conditioned by time. For such behaviour it is necessary to use dana on the past and the current state of the production system. Operational complexity, such as structures, influence the level of observance. However, it is important that operational complexity is a direct result of control. Control is realised in the production system due to transfer from one state into another in the time interval [6].

The properties of the production system are presented in [8], due to which the production system can be identified as a complex system.
Those properties are:

- absence of a formal methametical description of an object,
- stochasticity,
- intolerance in operating,
- non-stationary behaviour,
- lack of experiment repetition.

3.2. The nature of complexity

There is no universal, precise (e.g.. formal) and widely accepted definition of this term. The source Latin word „complexus“ denotes „intertwined“ quality or something weaved together. In other words, something is complex if it is hard to disassemble into smaller parts. Why a system is complex and to what extent is one of the basic questions in the area of complex systems. Generally speaking, the research activities in the area of complex systems can be divided into three categories: measuring the system complexity, recognising the patterns of adaptivity and evolution, and modeling of complex systems [9].

3.2.1. Complication, complexity, chaos:

In simple conditions for the time being, it is easy to identify a simple system. A complicated system or product is not simple to identify, but it can be ambiguous, for example, a car is a complicated product/system.
A complex system is the one in which there is uncertainty. For example, the development of a car is complicated, it demands engineering work, knowledge of several disciplines, group work in teams, etc. The details are not known entirely to each developing engineer. A complicated system can refer to a system which has many parts, which is somewhat harder to understand, various sizes, and complexity refers to a system which contains uncertainty during the process or crucial development in its design, so the outcome is not entirely predictable or under control.

Complexity can also be on the operational level, such as those during the production, the processes themselves. What is complicated is not necessarily complex, and vice versa, and what is complicated for one person, can be complex for an even less educated individual or a group with less technical knowledge [10]. An example in production is communication by speech between the machines, and it is a complicated phenomenon, which could become chaotic, but not for the work of industrial and academic researchers as well.

In general, in engineering, such as the design of new products and systems, we use science and engineering methos and tools for operating with complexity, turning a problem into operating and controling.

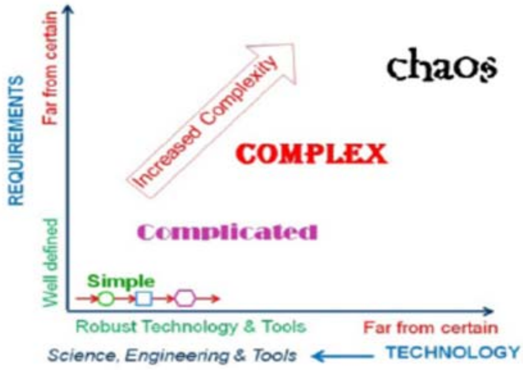

Image 2. Spectrum of complexity [10]

4. TYPES OF COMPLEXITY

The definition of complexity in the approximate approach uses the content of information as a measure of complexity, which is defined as insecurity in achieving functional demands.

Frizelle and Woodcock suggest a method by means of enthropy for measuring complexity in a structural and operational domain in production.

There are two basic types of complexity: structural (static) complexity and operational (dynamic) complexity [10].

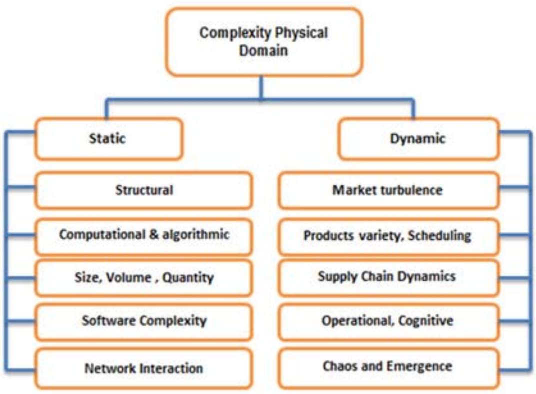

Image 3. Types of complexity in a physical domain [10]

4.1. Structural complexity

Static complexity is based on the attempt of measuring size of the minimal programme ability and static reproduction of patterns in a dana group. It stems from the approach of computational mechanics of pattern discovery which is applied in various fields in the range from molecular systems to commerce [11].

The course of data of infinite length, row, is defined with the equation

$$X = \underbrace{\dots, x_{t-2}, x_{t-1}, x_t}_{\overleftarrow{x}}, \underbrace{x_{t+1}, x_{t+2}}_{\overrightarrow{x}} \quad (1)$$

Causal S_i is defined as a group of elements x for which the probability of x is the same for every x. The group of causal state is marked with S.

Statistic complexity is defined with the expression:

$$C_\mu = -\sum_{S_i \in S} P(S_i) \log_2 P(S_i) \quad (2)$$

Statistic complexity measures the average amount of previously stored memory in the process. In a complex system, more information about the past is stored internally. So, predicting requires more information, and therefore is harder to do.

4.2. Operational (dynamic) complexity

Product complexity is a function of the material, design and special specification for every component inside the product. Complexity of procedure is a function of a product, amount, demands and work environment.

Operational complexity is a function of the production process and refers to the tasks and production logistics. Information and skills are necessary to perform work in the production (the emphasis being on the quality in all aspects) or in production processes (the focus is on the machines, permeability or effectiveness), which is shown on image 4.

For determining operational complexity, ElMaragy and Urbanik introduce the term indeks of complexity OI.

For measuring operational complexity, there have to be two elements: the product and the process [12]. Indeks of operational complexity OI is defined with equations.

$$OI = \left(D_{R\,op,product} + C_{o\,,product}\right) * H_{op,\ product} + \left(D_{R\,op,process} + C_{op\,,\ process}\right) * H_{op,\ process} \quad (3)$$

$$H_{op,\ y} = \log_2\left(N_{op,\ y} + 1\right) \quad (4)$$

where:

$N_{op,y}$ is the total respectively connected amount of elements of products and processes.

The measure of cohesion is the ratio of diversity DR defined as the ratio of sole information and the total information, as is stated in the equation:

$$D_{Rop\,,\ y} = \frac{n_{op,y}}{N_{op\,,y}} \quad (5)$$

where:

$n_{op,y}$ is the amount of individual information

$N_{op,y}$ is the amount of total information of the system or process.

Operational complexity depends on the product and the complexity of the process. Operational complexity measures the transformation which the system went through or the process through „relative effort". On the basis of a product, the course of the process, equipment and other similar points, decisions are made in such a way that the product operations are modernised to respond to certain demands from the environment.

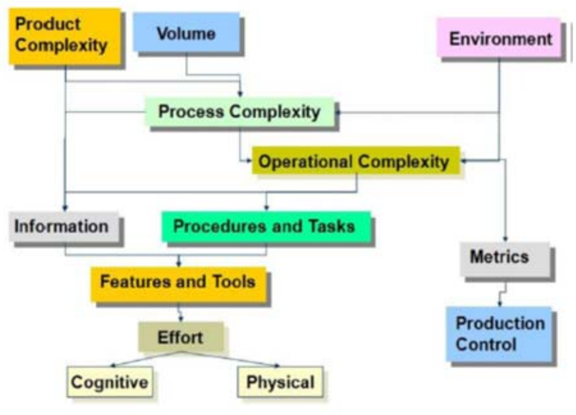

Image 4. Operational complexity [12]

Indeks of complexity points to the differences in complexity (the level of skills stems from there) as a result of versatility of information and amount of products. Indeks of operational complexity is a measure which should be used in modeling of performances. Zhis frame can be applied in any environment, it is a powerful tool from the area of physical, as well as cognitive complexity is applied in a way of simple understanding. It is important when different operational options of the process are being compared [12].

5. MEASURES OF COMPLEXITY OF PRODUCTION SYSTEMS

Wiendahl and Scholtissek in their review article on complexity in production systems state that, in order to better understand and control complexity, it is necessary to develop measures which would quantify complexity in production systems. Those methos can be developed on the principles of Shanon's enthropy, on the principles of Kolmogorov's algorhythmic theory of information, computational mechanics and many other approaches. In this paper, the emphasis is on the enthropy of systems as a measure of complexity in complex production systems.

5.1. Enthropy as measure of complexity

The term of enthropy was first defined in thermodynamics, but later on Wiener broadened it to all other systems. Enthropy in thermodynamics marks the irreversibility of thermal processes and is characterised as the relation between the amount of heat and temperature of the observed system (Q/T). Enthropy is used for defining another law of thermodynamics which states that: "Heat cannot transfer from a body of lower to the body of higher temperature, if at the same time another change is not being performed (or some other work is not being performed – energy) which enables this transfer". Actually, another law of thermodynamics defines the transformation of heat into work and determines that such transformation is not entirely possible.

Generally speaking, enthropy presents a measure of uncertainty of the system and it presents the probability of the transfer from an unlikely state of order into a chaotic or probable state. Therefore, the aim of every system to cross from an arranged state (which is also the least likely state of the system) into a chaotic state, which is also the most probably one, is very clear. In order to make this more clear, let us consider a simple example. Let us observe a cube of ice, which is possible to shape into any form, according to the shape of the container in which the water is frozen. It is possible because in a frozen state, water has a crystal structure which is arranged entirely. In that shape, water has a minimal value of enthropy.

If we leave the cube of ice to melt during time and turn into liquid, there is a small probability that the liquid will form into a proper geometric form. The reason for it is that water in the liquid state represents a system with disordered molecular structure. Then the disorder of the system is minimal and the value of the enthropy of system is maximal [13].

Based on everything previously stated, the point is that all systems, no matter how organised they were, strive during time to cross into a lesser organised state – chaos, namely, they start to work irregularly (as soon as enthropy rises). From that reason, the systems need to be maintained in a desired state, by a permanent control of behaviour and regular operating actions.

The second law presupposes that all systems, including living systems, become less complex or less organised during time, and as such show the elevated level of enthropy, disorder, uncertainty, simplicity, and generally, dissipation.

Introducing information into a system can lead to a more efficient and productive use of energy, therefore to a lower level of enthopy. That way the input of information, as well as input of energy can slow down the rise of system enthropy.

Frizelle and Woodcock were the first to use enthropy of information as a measure of complexity of production systems [14]. They define statistic complexity as

$$H = -\sum_M \sum_{N_j} p_{ij} \log_2 p_{ij} \qquad (6)$$

where:

- p_{ij} is the probability that the value of the system *i* comes into the state *j*.

Efstathiou et.al., 2002. use enthropy as a measure of structural complexity in an expert system for evaluating complexity of complex production systems.

6. CONCLUSION

This paper has given a description of the basic elements of complexity in production systems. Complexity is identified as an unavoidable characteristic of production systems, a characteristic which we have to control. On this path it is necessary to develop measures of complexity to better understand, and with it to control complexities in complex production systems.

Complexity is first the result of interaction between the participants in the complex production systems and as such grows with the development of new production systems such as, for example, the upcoming cyber-physical systems, which represent a basis for the development of new industrial revolution. Further research needs to be directed towards discovering new measures for understanding complexities in production systems in order to understand and control it, and not reduce it.

REFERENCES

[1] D. Kirshbaum, "Introduction to Complex Systems," *Available at: http://www.calresco.org/intro.htm [26.01.2011]*. .

[2] Z. Car, I. Hatono, and K. Ueda, "Reconfiguration of Manufacturing Systems based on Virtual BMS," in *The 35th CIRP International seminar on Manufacturing Systems*, 2002, pp. 15–24.

[3] C. Lukas, "Complex Adaptive Systems - Webs of Delight," *Available at: http://calresco.org/lucas/cas.htm*, 1999. .

[4] K. Iwata, M. Onosato, M. Fuse, Y. Fucuda, and M. Miki, "Manufacturing Systems Evolution: Historical and Structural Aspects of Manufacturing Systems Research," in *Flexible Manufacturing Systems*, 1993, pp. 113 – 127.

[5] M. Prokopenko, F. Boschetti, and A. J. Ryan, "An Information - Theoretic Primer on Complexity, Self - Organization, and Emergence," *Complexity*, vol. 15, no. 1, pp. 11–28, 2009.

[6] R. Vrabič, "Krmljenje avtonomnih obdelovalnih sistemov v proizvodnem okolju." Fakulteta za strojništvo Ljubljana, Ljubljan, 2012.

[7] N. P. Suh, "Complexity in Engineering," *Ann. CIRP*, vol. 54, no. 2, pp. 581 – 598, 2005.

[8] J. Peklenik, "Complexity in Manufacturing Systems," *CIRP J. Manuf. Syst.*, vol. 24, pp. 17 – 25, 1995.

[9] T. Lipić, "Modeliranje i oblikovanje kompleksnih sustava," *Centar za informatiku i računarstvo, Institut Ruđer Bošković, Zagreb*, Zagreb.

[10] P. Butala and A. Sluga, "MORPHOLOGY OF RECONFIGURABLE MANUFACTURING SYSTEMS."

[11] R. Vrabic and P. Butala, "Assessing operational complexity of manufacturing systems based on statistical complexity," *Int. J. Prod. Res.*, vol. 50, no. 14, pp. 3673–3685, Jul. 2012.

[12] W. H. Eimaraghy and R. J. Urbanic, "Assessment of Manufacturing Operational Complexity," no. 2.

[13] I. Mihaljović, Đ. Nikolić, and A. Jovanović, *Opća teorija sistema - inžinjerski menadžment pristup*. Bor: Tehnički fakultet Bor, 2009.

[14] G. Frizelle and E. Woodcock, "Measuring Complexity as an Aid to Developing Operational Strategy," *Int. J. Oper. Prod. Manag.*, vol. 15, no. 5, pp. 26–39, 1995.

SESSION C

CIVIL ENGINEERING AND MATERIALS

Drainage Wells on the Landslide - Sloboda Bridge in Novi Sad

Milinko Vasić[1], Mitar Djogo[1*], Branko Jelisavac[2]
[1]Faculty of Technical Sciences/Department of Civil Engineering, University of Novi Sad, Novi Sad (Serbia)
[2]The Highway Institute, Beograd (Serbia)

This paper presents the results of the investigation of the landslide in the zone of the Sloboda Bridge in Novi Sad. At the time of its completion in 1981, this cantilever-spar cable-stayed bridge was the largest in the world, with a central span of 351 m. In the body of the landslide, the bridge is founded on reinforced concrete piles 27 m in length. The measured depth of movement for the first part of the sliding mass is 26 m, while that of the second one is 35 m. The movement of the landslide is measured by seven built-in inclinometers at depths of up to 80 m. The movements are slight and slow but practically continual. The designed drainage structures consist of the following: two wells with diameters of 6.5 m and depths of 22 m, eight drains with lengths of 45 m and a drainage tunnel linking the pressure chamber and the wells. The drainage structures were constructed with the purpose of draining the groundwater from the 12-m-thick Pliocene sand layers and stopping the flow of groundwater from these layers into the landslide body.

Keywords: Drainage, Landslide, Site investigation

1. INTRODUCTION

The landslide in the area surrounding the Sloboda Bridge has been extremely thoroughly and comprehensively investigated. The landslide presents a threat to the stability of the existing large bridge and this necessitated the implementation of countermeasures to stabilize the landslide (Fig. 1). The bridge was built in 1981 and some investigation was carried out into the landslide. In the course of time as the bridge was being used, this investigation proved to have been inadequate. The countermeasures implemented during the construction of the bridge did not stop the sliding process. In order to find a solution for the problem of sliding, a series of very detailed investigations have been carried out into the landslide since 1990 to the present day and these results have been presented in this paper.

The landslides on the right bank of the Danube in Serbia are large, deep and have very specific features . It is these particular features that are pointed out on the example of the landslide in the area surrounding the Sloboda Bridge, and their specific nature is such that the sliding along the deep sliding planes occurs very slowly, namely at about 1 cm a year. Such small displacements are possible and they occur in other geological surroundings as well, which definitely makes research into this problem an interesting prospect outside of Serbia as well.

In Serbia, landslides of this sort prevail in an area of about 100 km along the right bank of the Danube. Along this stretch of land, there are only small areas which do not have landslides. Such areas with landslides were impossible to avoid, especially during the construction of the Belgrade-Budapest motorway and railroad. Until the present day, there have been many researchers studying this type of landslide [1]. Some researchers put forward hypotheses in their papers explaining the causes of landslides along the Danube. Among the first papers published was that of Lukovic [2]. Peric's [3] hypothesis was based on the premise that the artesian water in the aquiferous sand below the Danube river bed causes soil breakage in the area surrounding the Danube. The next hypothesis is based on the premise that tectonic movement causes the areas with the landslides to rise and that sliding is caused by the faults in the terrain and by tectonic events [4]. This paper has demonstrated that the main causes behind the creation of landslides are: sediments which are mildly tilted towards the Danube; the frequency of low-resistance sediments along which the sliding takes place; the influence of groundwater flowing from the slope part of the terrain into the landslide; the Danube with its deep river bed which erodes the right river bank.

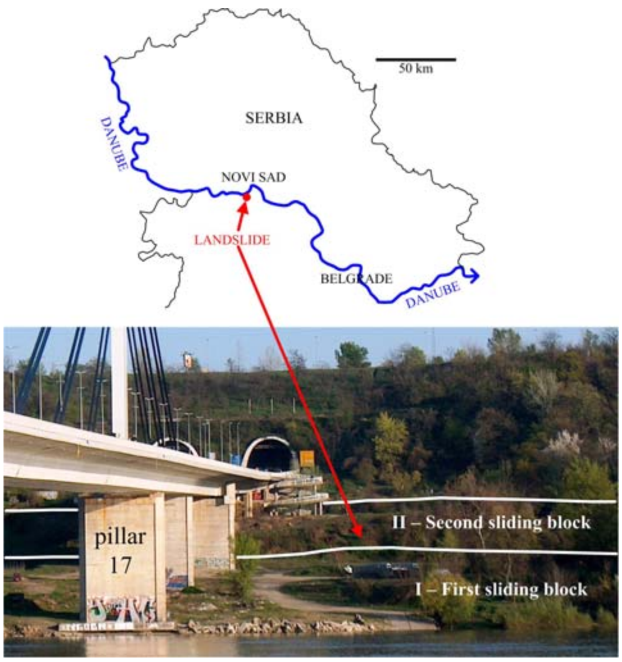

Figure 1: The Danube landslide

Investigations have determined the size of the landslide and the factors that led to it and countermeasures have been proposed to stabilize the landslide [5, 6]. The slow movement of the landslide allows the process to be monitored and measurements to be taken over a long period of time [7]. The detailed investigations and reliable data on the landslide allow the partial implementation of countermeasures and the monitoring of their effect on stabilizing the landslide.

*Corresponding author: Faculty of Technical Sceinces, Trg Dositeja Obradovića 6, 21000 Novi Sad, Serbia, e-mail: mitar@uns.ac.rs

2. METHODS

Apart from charting the terrain and examining satellite images, over sixty boreholes were drilled. The deepest borehole is 104 m in depth. A high-quality continual core was created by drilling. In addition to determining the geological composition of the core and the structural features of the rocky masses within it, all its sliding planes and sliding zones were also accurately documented. Inclinometer structures were installed in seven deep boreholes and measurements of the landslide's movements have been taken since 1992.

New deep boreholes were drilled in the vicinity of the inclinometer boreholes and they were fitted with electric piezometers. Each piezometer measures the porous pressure in the zone of the deep sliding planes and in the two layers of sand which are below the sliding planes. In addition to the seven electric piezometers, over twenty classic piezometers were installed. The piezometers are used to measure groundwater levels four times a year. Following the construction of both drainage wells, each with four drains, the influx of water into the drainage wells was measured and test drainages of both wells were carried out. These measurements lasted 45 days. The measurements were carried out separately for each drain and with all the drains open. During the excavation of the drainage tunnel, all instances of groundwater were documented.

Over 20 cone penetration tests were carried out as well as a large number of laboratory experiments on soil samples.

In order to get a precise cross-section of the Danube river bed, the bottom of the river bed was scanned using echo-sonography.

Geodetic measurements of bridge pillar movements have continuously been carried out since the bridge was built and the data acquired has been compared with the data gathered from the inclinometers.

3. BRIDGE FOUNDATION DATA

On the right bank of the Danube, the pillars of the bridge were founded on relatively deep piles (Fig. 2), except for the final pillar, number 22, which was founded on a raft without piles. Thus, for instance, pylon pillar number 17 had a total of 6 groups of 4, namely 24 piles, 150 cm in diameter and 27 m in depth below the pile cap. Pillars no. 18, 19, 20 and 21 were also founded on piles. The bases of the piles below pylon pillar 17 reach down to the deepest sliding planes. All the other pillars were founded on shallow piles which are situated in the body of the landslide. It is absolutely certain that they did not penetrate the stable base of the landslide (Fig. 3).

As the landslide moves, the pillars of the bridge move along with it. The movements of the pillars are being geodetically measured. Based on these measurements, it is possible to analyze the dynamics by which the landslide and the bridge are moving. Generally speaking, pillars no. 17-21 have moved an average of 6mm/year in the past 28 years. The movements of the bridge pillars and those of the inclinometers have been identical. The results of years of measurement were crucial in making the decision that the unstable slope in the area around the bridge must be stabilized.

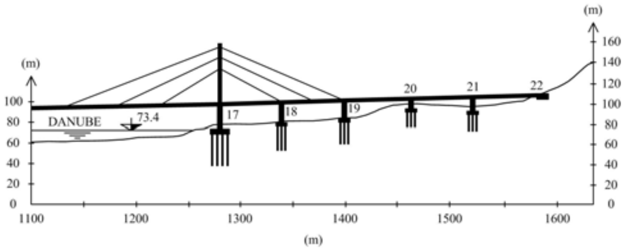

Figure 2: The bridge and the piles on the right bank of the Danube

4. GEOLOGICAL SETTING

Investigatory boreholes ascertained that the stationary-stable part of the terrain, in its deepest part, is made up of shallow-water Pliocene sediments or so-called paludin layers. This was confirmed by the discovery and the identification of certain representative fossil remains. From a lithological viewpoint the sediments are present mainly in gray marl clay and in aleurites which are also gray in color. Sands are substantially less present. Besides the listed sediments also present are coal clay, red marl and lignite layers. All of the listed sediments are clearly layered and are inclined towards the Danube at an angle of 2°-5° (Fig. 3).

The younger part of the Pliocene sediments is without fossil remains and it is likely that it belongs to younger levels of medium paludin layers. In a lithological sense gray and gray-brown clay prevails alongside sandy clay and individual layers of sand and sandy aleurites. To a slightly less extent they contain layers of sandy gravel and individual layers of sandstone. The sand horizon in the youngest part of the Pliocene is of particular importance from the aspect of the goal of the research. It is through these continually developed sand layers that the largest amount of the groundwater flows into the landslide surface and the body of the landslide. Based on data from drainage well DW-1 (Fig. 7) the horizon of Pliocene sand was found at a depth of 7.50-19.40 m. It is consisted of several layers of sandstone partially bound by $CaCO_3$ components and thin inner-layers of clay. However, those clay layers do not represent absolute barriers for the movements of the groundwater.

At its shallowest part or in the zone which is immediately below quaternary sediments, the Pliocene sediments are altered-degraded and enriched with $CaCO_3$ [8, 9]. This area is interesting from the aspect of studying the process of surface decomposition of marl sediments in the distant past, as well as marking the sliding process compared to that age. Likewise, characteristic geological markers may be found in the immediate under-layer of the slide, such as coal clay and red-stripe marl. These have been discovered in all of the borehole cores.

Coal clays are part of the makeup of the Pliocene marl-clay sediments in a very small percentage. They can usually be found in the form of layers or sometimes as thin lenses only a few centimeters or even a few decimeters thick. They can be found in somewhat larger amounts only in the contact zone between the altered and unaltered Pliocene sediments, approximately at an elevation of 44-46 m. Despite their minute presence, their significance and influence on the sliding activities of the terrain are extremely large. As a rule, shearing resistance parameters in that environment show the smallest value and so they represent planes prone to shearing-sliding.

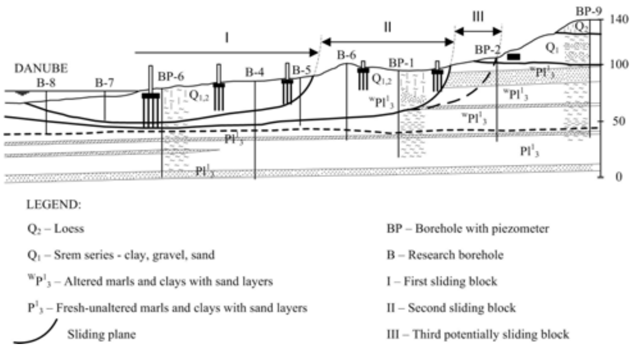

Figure 3: Geotechnical cross-section

Loess represents the youngest sediment in the stable part of the terrain. In borehole BP-9, which was drilled on the loess plane, two horizons of soil loess have been recorded and another layer of fossil soil in between. The thickness of the loess deposits together with the fossil soil is 13.2 m. Loess acted as a stabilizing factor in the old landslides which have been formed on the slope before it had accumulated.

The contact zone between the stable under-layer and the body of the landslide is the sliding zone in which the occasional shearing and sliding of the sliding body occurs. The existence of a sliding zone has been confirmed in all of the boreholes. It is formed largely from coal clay and less from marl and marl clay. The thickness of the zone is several meters, it is intensively fragmented and all of the moving surfaces are extremely smooth. Numerous shallower sliding zones were confirmed in all the boreholes in addition to the deepest sliding zones.

In the wider area of the bridge, the detailed geomorphologic analyses performed have registered no neo-tectonic active faults so their influence on the process of sliding is non-existent.

5. HYDRO-GEOLOGICAL PROPERTIES OF THE TERRAIN

The information about the hydro-geological properties of the terrain has been gathered through the analysis of the measurements by classic and electric piezometers and water-tightness experiments both in laboratory and field conditions. It has been determined with great certainty that a unique aquifer exists in the body of the landslide with variable levels of underground water depending on precipitation, and water inflow from the sand horizons and the background of the landslide together with the activity of the constructed drainage system. From the stable part of the terrain, that is from the background the landslide, the landslide is receiving a significant supply of water from the sand of the Srem series and especially from Pliocene sand horizons which have been found in borehole BP-9 at a depth of 41.30-54.10 m (Fig. 3). This horizon of Pliocene sand has been interrupted by the landslide head scar and the position it has taken up within the body of the landslide is dictated by the sliding process. The presence of three significant layers of sand was confirmed in the deeper parts of the stable terrain, i.e. at borehole BP-6 within the Pliocene. These layers were found at the following depths: 45.80-47.00 m; 57.20-59.20 m; and from 75.90 to approximately 85.0 m. Within all of the three layers of sand electric piezometers have confirmed the presence of groundwater with sub-artesian pressure but only in BP-6 has groundwater with artesian pressure been discovered within the deepest horizon of sand. Practically watertight thick layers of marl and marl clay can be found between the aforementioned layers of sand.

In the newly installed electric piezometers produced by "Soil mechanics" the measuring cells are positioned, as a rule, on three levels. Several measuring cells have been installed into the sliding areas which are several meters in thickness. The measuring cells in the borehole were covered under a certain depth of sand and the remaining space between the measuring cells was insulated by watertight cement-clay material.

6. THE CARACTERISTICS OF THE LANDSLIDE AND ITS MOVEMENTS

The lithogenic composition of the terrain was determined up to a depth of 104 m by the exploratory work that was carried out. Examinations of the cores of the exploratory boreholes as well as measurements with the installed inclinometers determined the boundary between the stable and the unstable terrain [10]. It has been ascertained that the old-fossil landslide used to reach the limit of the unaltered Pliocene sediments (Fig. 3). Loess acted as a stabilizer on the once unstable parts of terrain. The degree of loess degradation determines the degree to which the sliding process could expand along the slope. Besides that, the degraded loess which reaches the activated landslides from the brim of the loess area in the form of delluvial sediments acts unfavorably with its weight on the already activated landslides.

Immediately after the installation of each of the inclinometers, the measurement of the movements began. Measurements were taken four times a year on average starting from 1992 until 2009.

Each of the inclinometers allows measurements through lowering the measuring probe to the bottom of the installed inclinometer structures. During the process of installing the inclinometer tubes, great care was taken to orient them in such a way that one set measured movements perpendicular to the flow of the Danube (A, B) while the other measurement plane was actually parallel to its flow (C, D).

This paper shows only the representative diagram of the movement (Fig. 4) relative to inclinometer BI-3.

One can claim with great certainty that the movements on the inclinometers occur at several different depths. The extent of the movements is different at different depths, but based on cumulative movements, certain main areas and discontinuities can be distinguished where these movements are the greatest. At inclinometer BI-3 the most intensive sliding occurs at depths of around 28 m (elevation 57.7 m). Seen from the A-B measurement plane, the direction of the most extensive sliding is towards the Danube along the sliding planes which are slightly sloped towards the river.

The sliding zones were precisely determined by examining the borehole cores. They are characterized by a highly damaged core, crushed together, with a large number of shearing cracks. It has been concluded that the maximum movements occur along previously registered sliding zones in the borehole cores. The greatest movements occur down the slope perpendicular to the flow of the Danube while smaller movements occur in the upstream or downstream directions of the flow of the Danube.

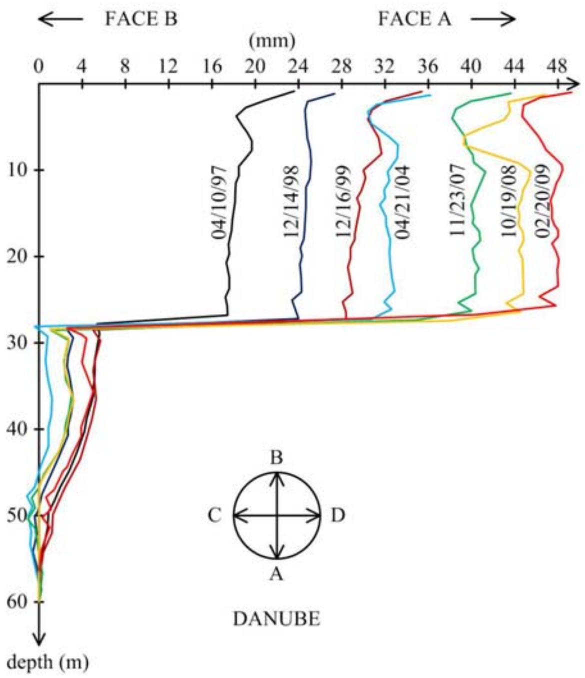

Figure 4: The results of the movement measurements on the inclinometer BI-3

Analyses of the movements of all 7 inclinometers have led to the conclusion that the shallower landslide moves across sliding planes at a depth of around 26 m (BI-6, BI-4, BI-5, BI-3). Inclinometers BI-2 and BI-7 show relatively intense movements across the sliding plane at a depth of around 35 m [11, 12]. The interesting thing is that inclinometer BI-1 registered more intense movements only at a depth of around 10 m. That means that the deep landslide in the area of this inclinometer has still not been activated.

7. REPAIRING THE LANDSLIDE

At the time when the bridge was designed and constructed, from 1976 to 1981, it was a known fact that there were active landslides on the right bank of the Danube. Because of that the bridge was founded on piles and countermeasures were implemented to stabilize the unstable slope. The following work was carried out at the time: evening out the surface terrain; surface channels to drain atmospheric and spring water; a brief drainage. In the course of the exploitation of the bridge, these measures proved to have been insufficient to stop the sliding process.

In 1995 work on stabilizing the landslide resumed according to the new project design. Its fundamental assumptions were based on the results of the more recent detailed geotechnical research and testing which allowed for a very high degree of landslide investigation, which is presented in this paper. The order in which the countermeasures were to be implemented was adapted to meet the following demands:

- it had to be possible for the effects of each countermeasure to be monitored and controlled through the installed inclinometers;
- that the implementation of one countermeasure does not hinder the possibility of observing the effects of subsequent measures;
- that the countermeasures be implemented in stages since the dynamics of the sliding process allows this.

The sliding does not require the simultaneous implementation of all the countermeasures and their immediate and cooperative effects [13]. Such an approach required that the bank revetment should not be constructed first because that would make it impossible to separate the effects of the bank revetment from that of the other countermeasures. Also, it would not be possible to implement the alleviation of the slope during the first stage because that could change the pressure status in the terrain causing the inclinometers to function in somewhat altered conditions. It was quite logical to perform the drainage of the groundwater from the background and partially from the body of the landslide first. Such operations change practically nothing in the morphology of the adjacent terrain and their effects are definitely positive for the following reasons:

- they stop the inflow of the groundwater into the sliding plane and the landslide;
- they prevent the negative effects of hydrostatic and hydrodynamic pressures;
- they cause an increase of the shearing parameters of the soil in certain areas of the landslide.

The repair measures (Fig. 5) consist of three stages:

Stage I-a: the construction of drainage wells DW-1 and DW-2 with 4 drains leading from both wells. The drains will be located in the Pliocene sand. The pressure chambers PC and the wells are connected by the drainage tunnels DT.

Stage I-b: the insertion of drains from the surface terrain into the sandy-gravel sediments (the so-called Srem series) which are below the loess horizons;

Stage II: the construction of the bank revetment and alleviation and evening out of the slope;

Stage III: the construction of six supporting structures consisting of counterforts on the lower level of the slope.

Since the concept of the solution to the problem and the sequence of implementing the countermeasures was established, as the paper shows, almost all of the countermeasures listed in stage I-a were completed. Only the pressure chamber PC-2 and the drainage tunnel DT-2 leading to the well DW-2 (Fig. 5) were not constructed. The groundwater flows into both of the wells through the drainage canals and it is then channeled from DW-1 through drainage tunnel DT-1 into the Danube in a controlled fashion. Bearing in mind that the drainage system leading from DW-2 was not realized, this well has not been performing its function of draining water from the background. Draining the terrain using the entire system in stage I-a was supposed to have completely eliminated the negative effects of the groundwater. Thus, the drainage system from stage I-a needs to be completed as soon as possible.

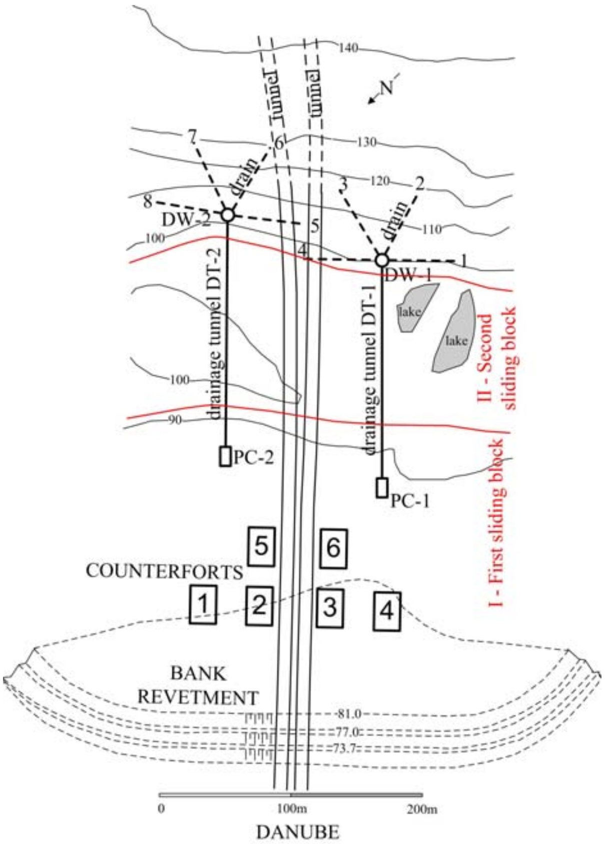

Figure 5: Positioning of the designed countermeasures

The completed drainage wells DW-1 and DW-2 are 22 m deep with an internal diameter of 6.50 m and concrete walls 0.45 m thick. Four drains of 45 m in length lead from each of the wells. The drainage of water from these drainage wells was originally planned to be achieved using deep drainage protected by steel (Larsen) sheet pile sections. A drainage canal 2.7 m wide was to be fitted with a drainage pipe 1400 mm in diameter and the excavation shaft from that pipe to the surface was to be filled in by drainage material made from crushed stone and gravel. But instead of this expensive design of the drainage a new solution was accepted and implemented. From the pressure chamber to drainage well DW-1, laser-guided reinforced concrete pipes were installed. The pipes were 1500/1840 mm in diameter and were installed at a length of 139 m.

Stage II of the slope stabilization also had a design incorporating a bank revetment whose far end would lie in the Danube river bed at a distance of about 75 m from pillar number 17.

Stage III involves six concrete box diaphragms (counterforts) made of reinforced concrete with a rectangular base which is 20 m by 30 m (Fig. 5). The thickness of their walls is about 0.50 m. They span the entire length of the landslide ending in stable terrain. The basic function of concrete box diaphragms is to increase resistance parameters within their area of effect to the shearing of the rocky masses in the sliding area, which occurs as a result of stopping the circulation and inflow of groundwater.

8. TERRAIN DRAINAGE

Comprehensive investigations have determined that significant quantities of groundwater are flowing into the landslide. Groundwater has a significant effect on the sliding process. In order to eliminate that cause of the landslide the terrain was drained. According to the geotechnical cross-section (Fig. 3) the largest amounts of groundwater flow in from the pockets of Pliocene sands whose thickness is about 12 m. The sands are interrupted by the landslide but they are continual in the slope. The purpose of draining the terrain is to channel the groundwater from the sands into the drainage facilities in a controlled manner and to draw it off into the Danube. A number of variant solutions were considered for that purpose: deep drainage trenches; drainage tunnels; watertight clay membranes implemented in deep trenches. Finally, a solution with deep wells and drains leading from the wells was implemented (Fig. 6).

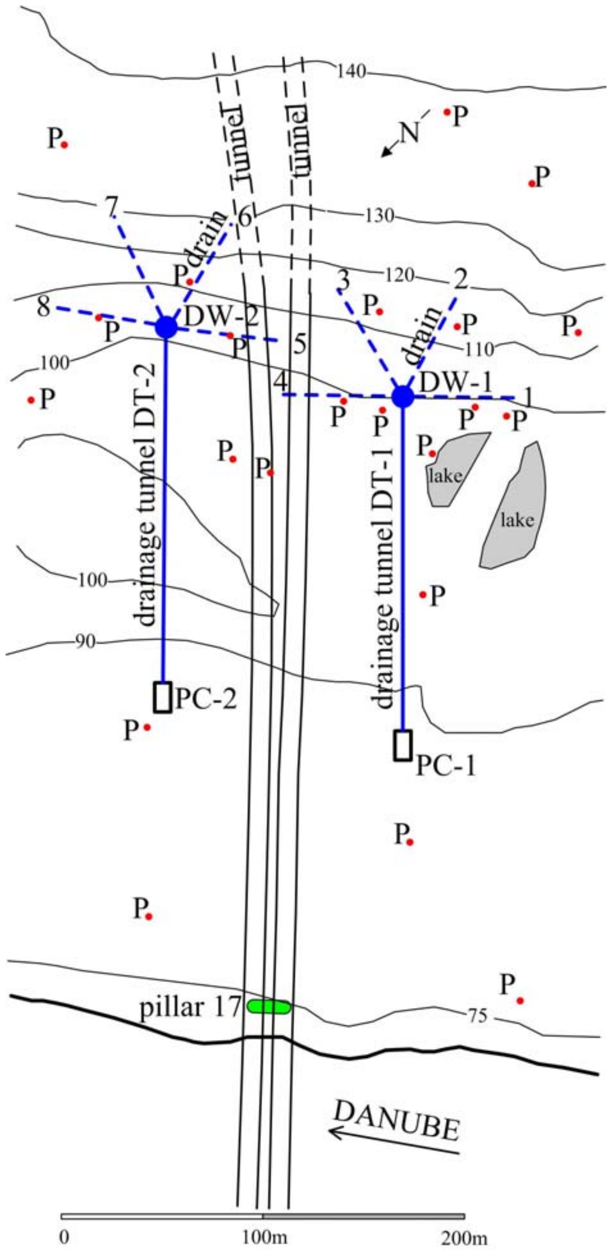

Figure 6: Drainage structures and the distribution of piezometers P

For the purpose of micro-locating the wells, an additional 12 control boreholes and six piezometers had to be implemented. The wells were positioned into the stable area of the terrain with the basic task of draining the water from the undisturbed sand thus stopping the flow of groundwater into the body of the landslide. The wells were founded within the stable marl and as such represent strong structures which contribute to the stability of the terrain. Both of the wells are positioned very close to the main sliding slopes at 47 m upstream and 47 m downstream from the area of the bridge respectively. Thus the wells and the 45 m-long drains stemming from each of them provide total terrain drainage in the area of the bridge along a 200 m stretch.

Both drainage wells were 6.5 m in diameter and 22 m in depth (Fig. 7). They were constructed by using hooks while the concrete segments were installed in stages in situ. At the bottom there was a steel knife of a somewhat larger diameter while the well was being lowered as the excavation process proceeded. The friction of the well casing with the surrounding terrain was reduced by using bentonite. The verticality of the well during the construction was controlled geodetically. The wells were pre-fitted with outlet apertures for the horizontal drains in the layer of aquiferous sand. The construction was locally made more difficult by the appearance of lenses and semi-layers of unevenly hardened sandstone and conglomerates. Those sandstones and conglomerates were making it exceptionally difficult to insert and form the drains. The position and the length of certain drains, especially on well DW-2 were not completed according to design but are substantially shorter. After the well had been lowered to its final depth a process of underwater lining with concrete was performed and the base of the well was formed.

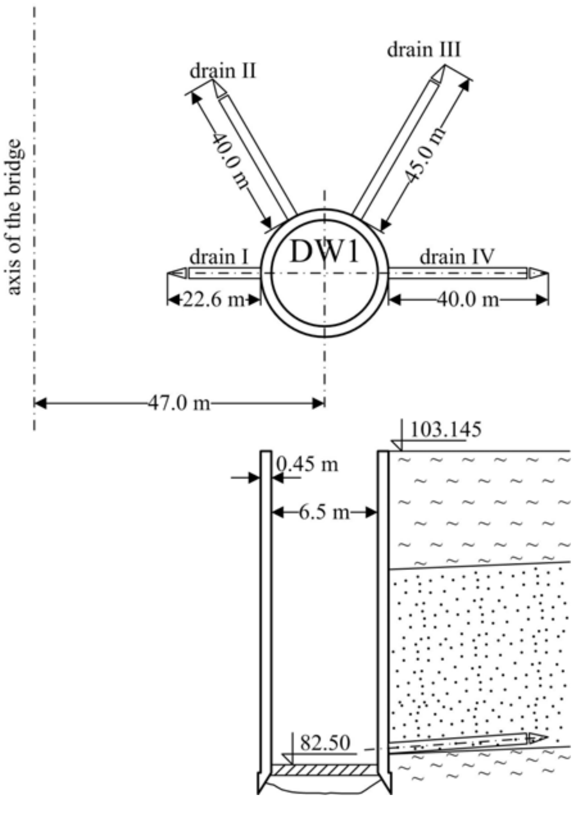

Figure 7: The DW-1 drainage well and its drains

The construction of the drains stemming from the well was performed after the well was completely emptied of water. The drains were constructed in two stages. First was the installation of the protective casing whose head contained orifices for the jets used to hydraulically dig and remove the sand. In the loose sand the installation of the protective casing and the removal of the sand were completed without any problems. Problems arose when hardened sand or sandstone was encountered during the installation of the protective casing and these were impossible to destroy with the jets. The diameter of the protective casing was 500 mm. After the protective casing was installed to the desired length, work began on forming the drains. The drains were made from stainless steel tubes 250 mm in diameter while the space between the tubes and the protective columns was filled by gravel. In the end, the protective columns were removed and the head with the jets remained at the end of the formed drain. Due to high friction, a large number of stainless steel tubes were crumpled and destroyed as the protective casing was being pulled out.

Of the planned 200 m of drains leading from DW-1, only 147.6 m were constructed. In the case of DW-2, this was only 57.6 m out of 200 m. The length of the drains on the DW-1 well is satisfactory which was confirmed in the course of its exploitation. The drains constructed on DW-2 are insufficient so the installation of new drains is planned.

According to the design, the water from the drainage wells will be channeled into the Danube using gravity. This will mostly be accomplished through two drainage tunnels. A 139 m-long drainage tunnel leading away from DW-1 was constructed. It was constructed by pressing prefabricated concrete pipes from the pressure chamber and digging a tunnel using a mole encased in a protective steel case. The pipes were installed using laser guided presses. The work was coordinated in such a way that the mole first penetrated the soil and then the material within the steel casings is excavated and brought up to the surface through a tunnel. The success of installing concrete tubes was confirmed by the fact that the tunnel was constructed in the designed direction from the pressure chamber to the orifice in well DW-1. The tunnel is currently in operation. During the construction of the tunnel certain problems were anticipated in the body of the landslide. Surprises occurred at two points when soft muddy sediments were encountered. The technology used for constructing the tunnel did not allow for any deviation from the planned direction. After some delays in the digging of the tunnel 4 additional boreholes were drilled and 13 additional cone penetration tests were carried out at a distance of 2.5 m from each other. The results of the investigation showed that work on digging the tunnel may proceed. The problems of fluid muddy soil entering the tunnel also confirmed the justifiability of installing the drainage system within the landslide. The two critical points where the fluid muddy materials appeared coincide completely with the areas of the main sliding planes within the landslide.

Drains will subsequently be constructed from the tunnels. That will make them drainage tunnels and not only outlet tunnels, and this will stop the lateral inflow of water into the stabilized area of the landslide.

Plans were also made to press drains from the surface into the sands located between the elevations of 105 m and 110 m. The water from these drains will also be channeled into the Danube using gravity. These drains will be installed into the drainage area stretching 100 m upstream and 100 m downstream from the bridge.

After the construction of the wells and all the drains leading from them, a test drainage was carried out. Tests were performed by measuring the inflow from each of the drains individually and all of them together. During the test, levels of groundwater were measured by observing the lowering of the levels on all of the installed piezometers. After the level of the water within the well stabilized due to the inflow of water from all the drains, test drainage was performed by pumping water from the well. Also the levels of groundwater were measured by the piezometers. The testing lasted for about a month for each of the wells. Fig. 8 shows the reduction of water level in drainage well DW2 by three capacities of the test drainage and a restoration of the water level in the well after the drainage has ended.

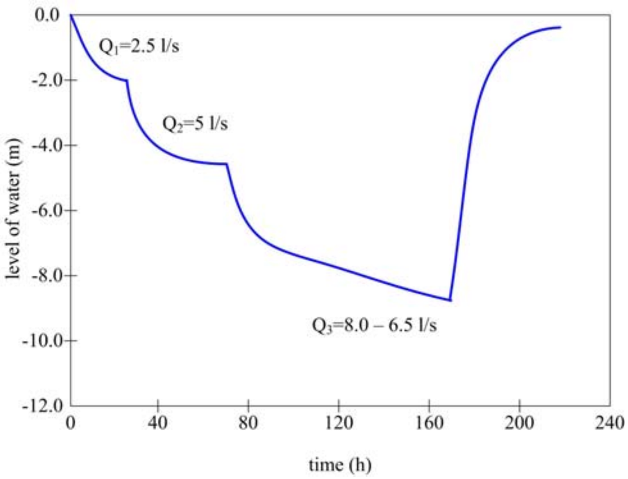

Figure 8: Test drainage in DW-2

The layer of aquiferous sands in which the drains were installed is about 12 m in thickness. On the Danube slope, these sands are interrupted by landslides. In the stable part of the terrain, the aquiferous sand environment is continual. Measurements by piezometers have determined the level of groundwater in the sands containing the drains prior to the test drainage (Fig. 9).

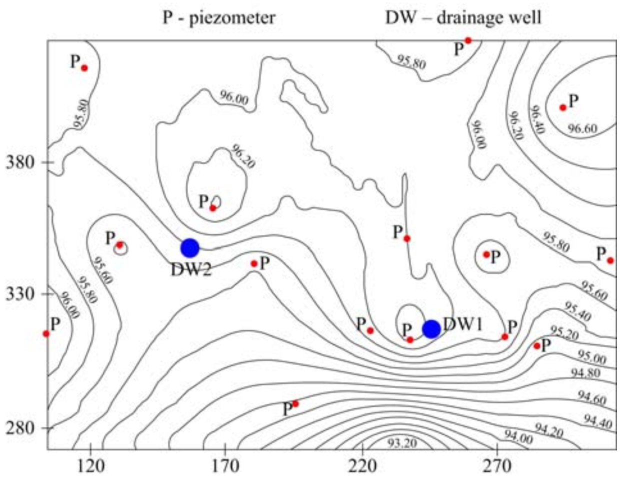

Figure 9: The groundwater isolines prior to the test drainage

After the test drainage was carried out, the reduction in the groundwater levels was measured and the results were shown using isolines in Fig. 10. The isolines refer to the projected decrease in the groundwater levels after a year of drainage. After the test drainages were completed all the drains in drainage well DW1 were opened thus enabling the gravitational drainage of water through drainage tunnel DT1 and towards the Danube. This drainage has been done in the course of several years. The landslide is still active, which has been confirmed by measurements using the installed inclinometers and by geodetic measurements. All this indicates the necessity to continue work on the construction of the drainage system in its entirety.

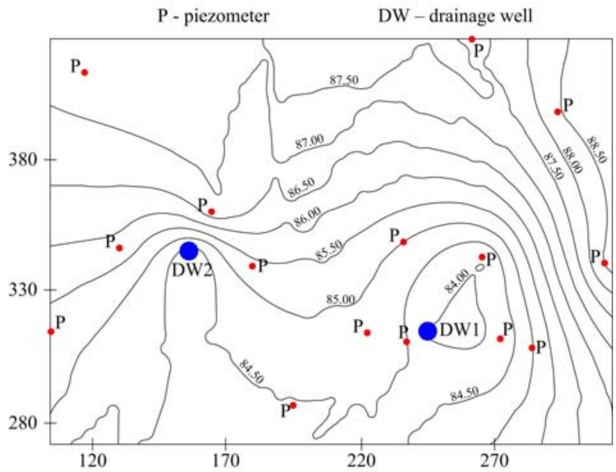

Figure 10: Projected groundwater isolines after pumping for a year

9. CONCLUSION

Based on the detailed and lengthy examination of the large landslide endangering the stability of the Sloboda Bridge on the Danube, the following most important conclusions can be reached:

- The landslide consists of two main sliding blocks at depths of 26 m and 35 m. The geometry of the sliding blocks has been determined on the basis of a large number of field explorations.
- The movements of the two main sliding block are very slow and they average about 6 mm per year. The movements of the sliding blocks are measured using inclinometers, and the movements of the bridge are measured geodetically. The results of these measurements have shown that the landslide and the bridge are moving at the same rate.
- The landslide is predominantly made up of clayey dusty sediments. The instabilities are mainly influenced by the mildly sloping sediments towards the Danube, groundwater and the erosion of the right bank of the Danube.
- Significant amounts of groundwater flow into the landslide from a layer of water-saturated sand whose width is about 12 m. This layer of sand is interrupted by the main sliding planes. The main aim of the drainage is to channel the water from this sand into the Danube in a controlled manner. Test drainages have shown that this can be carried out successfully.
- In landslides of this type, where the movements are slow and long-lasting, monitoring is a compulsory part of the exploration process.

- Slow landslides of this type allow the partial implementation of countermeasures. That is why, in the case of this landslide, it was necessary to implement the drainage system first, and the bank revetment in the Danube river bed and the counterforts will be implemented subsequently, as the need arises.

ACKNOWLEDGEMENTS

This work was financially supported by research grants No. TR36043 and TR37017 of the Serbian Ministry of Science and Technological Development. Also, this work was financially supported by research grant Theoretical, experimental and applied research in area of Civil Engineering of the Faculty of Technical Sciences in Novi Sad.

REFERENCES

[1] Lokin P, Sunaric D, Cvetkovic T, “Landslide in Neogene sediments on the right Danube bank, Yugoslavia,” Fifth international Symposium on Landslide, Lausanne, pp 202-208, (1988)

[2] Lukovic T, “Major Types of Landslides in Our Country and Possibilities of Repairing Them,” Geoloski vesnik, pp 50-60 (in Serbian), (1951)

[3] Peric J, “A Hypothesis Regarding the Origins of the Landslide on the Slope along the Right Bank of the Danube from Vinca to Grocka,” Proceedings RGF, Beograd, pp 35-47 (in Serbian), (1970)

[4] Markovic M, Pavlovic R, Cupkovic T, “Photogeological Research on Landslides on the Right Bank of the Danube,” Yu Symposium on Landslide, Donji Milanovac, pp 143-150 (in Serbian), (1995)

[5] Stevanovic S, Petrovic R, “Repairing the Danube River Bank on the Srem Side at the New Bridge in Novi Sad,” Vode Vojvodine, Novi Sad, pp 437-448 (in Serbian), (1977)

[6] Petrovic R, “A Review of the Construction Countermeasures Planned for Repairing the Landslide at the Sloboda Bridge on the Danube in Novi Sad,” Yu Symposium on Landslide, Donji Milanovac, pp 325-334 (in Serbian), (1995)

[7] Djogo M, Vasic M, Jelisavac B, “Monitoring the Landslide in the Sloboda Bridge Zone in Novi Sad,” Put i saobracaj 1, Beograd, pp 26-38 (in Serbian), (2008)

[8] Petkovic K, Ciculic-Trifunovic M, Pasic M, Rakic M, “Fruska Gora, a Monograph Overview of its Geological Composition and Tectonic Make-up,” Matica Srpska, Novi Sad, p 121 (in Serbian), (1976)

[9] Lokin P, Petricevic M, Vasic M, Janosev Z, “On the Disturbance and Protection of the Geological Medium in Natural Parks with Special Reference to Fruska Gora,” Proceedings on Eighth International Congress, International Association for Engineering Geology and the Environment, Vancouver, pp 2659-2666, (1998)

[10] Lokin P, Vasic M, Sakovic S, Petricevic M, “Landslide along the Danube Bank at Novi Sad, Yugoslavia,” Proceedings of the 7th International Symposium on Landslide, Trondheim, pp 803-808, (1996)

[11] Vasic M, Sakovic S, Lokin P, Jablanovic R, “Results of Measurements by Inclinometers – The Sloboda Bridge Landslide in Novi Sad,” Yu Symposium on Landslide, Donji Milanovac, pp 353-363 (in Serbian), (1995)

[12] Vasic M, Djogo M, Jelisavac B, “Examination of the terrain at the old Sloboda Bridge in Novi Sad and the Restored One after the Bombing,” Proceedings, Zlatibor, pp 37-44 (in Serbian), (2005)

[13] Maksimovic M, “Evaluating Countermeasures on the Example of the Landslide at the Sloboda Bridge in Novi Sad,” Yu Symposium on Landslide, Donji Milanovac, pp 269-278 (in Serbian), (1995)

Microstructural Analysis of Concrete and Cementitous Materials

Milena Rangelov[1, 2*], Jovana Kaličanin[1, 2], Vlastimir Radonjanin[2], Mirjana Malešev[2]
[1]Faculty of Mechanical and Civil Engineering in Kraljevo, University of Kragujevac, Kraljevo (Serbia)
[2]Faculty of Technical Sciences, Department of Civil Engineering, University of Novi Sad, Novi Sad (Serbia)

Abstract: *This paper represents general overview of most significant contemporary methods in concrete and cementitious materials studying. Each method is based on a microstructural examination that leads to conclusions about macrostructure and overall state of material. All of the methods require additional software analysis of captured images. Proper specimen preparation with using advanced options of image processing software can provide quick, automated and accurate analysis. Covered methods are: method of optical microscopy, scanning electron microscopy (SEM), backscattered electron imaging (BSE or BEI method) and X ray computed microtomography. The main focus is on the method descriptions and the possible ways of their application, as well as sample preparation and image processing.*

Keywords: concrete, cement, optical microscope, scanning electron microscope, backscattered electron imaging, X ray microtomography, micro structure, cracks

1. INTRODUCTION

Along with technology development, methods for microstructural analysis have become more powerful and sophisticated. There are many contemporary devices applicable in wide range of scientific research (in geology, medical sciences, biology) that can be successfully applied in structure materials research. Advantages of these contemporary methods are numerous options of devices, such as resolution adjustment, contrast changing, wide range of magnifications etc. This paper covers the following methods: method of optical microscopy, scanning electron microscopy (SEM), backscattered electron imaging (BSE or BEI method) and X ray computed microtomography.

The microscopy has been a powerful tool in study of cement and concrete, since the early development of these materials. It has been first studied by Le Chatellier (1882) and by Travasci (1941) [1]. They were both exploring physical and chemical aspects of cement and concrete, as well as set the foundation for future reasearches. The electron microscope was firstly used by Radczevsky(1939) and Eitel (1942) for studying the process of cement hydratation. It has been successfully used in microcracking investigation since 1980th. Backscattered electron imaging has become well established method of concrete and cement research in last 20 years, for its various options. X ray methods have been used in many fields of material research as powerful, non-destructive method, applicable In sity and with many advanced assets.

This paper covers a few of the most contemporary methods in material examination, their descriptions and some of the possible ways of application. Special attention has been dedicated to specimen preparation and image processing, as technical, yet essential aspects of these studies.

2. METHODS' DESCRIPTION

2.1. Optical microscopy

This method is based on observing and imaging of thin impregnated speciments of mortar, concrete or other materials with light optical microscope. Thickness of speciments and microscope magnification is adjusted by the objectives of study. Very important aspect of this method is specimen preparation [1]. Specimens need to be impregnated with epoxy resin, containing fluorescent due (See the Chapter 3). After the preparation, specimens are subjected to observation in ultraviolet light. Images show the basic material as dark and cracks filled with resin in lighter colors. Fluorescent due in resin provides contrast in images, which is prerequisite for quantitative software analysis.

This technique is often combined with observations In situ, and provides accurate results in terms of estimating structure state.

2.2. Scanning electron microscopy (SEM)

Scanning electron microscope or SEM (Fig. 1) is one of the most versatile instruments in microstructural examining of solid objects [2]. It produces images of samples by scanning it with focused beam of electrons. It provides significant extent of magnifications that range from 100X to 100000X. The great assets of SEM are high resolution and image quality. SEM can reach the resolution up to than 1 nm. Specimens can be observed in various conditions: in vacuum, in wet condition, dried, on high temperatures. In concrete and composite material investigations, specimen impregnation may or may not be required, depending on research objectives.

*Corresponding author: Kopernikova 9, 11000 Belgrade, milenarangelov@hotmail.com

Figure 1- Scanning electron microscope

2.3. Backscattered electron imaging (BSE)

Backscattered electrons are electrons from the incident beam, scattered through large angles, so that they can re-emerge from the specimen. Re-emerged or secondary electrons have lower energy and they form BSE image. The intensity of diffracted electrons is mainly the function of the average atomic number of the certain area. Areas with the lower atomic number have lower diffraction, so they appear darker in the images (and vice versa). If the sample surface is flat and polished, reproducible contrast and high quality of images can be easily attained.

BSE technique has many advantages in microstructural studies, such as visualization of representative cross sections over a wide range of magnifications (from about 20X to 10000X) and reproducibile contrast, depending on atomic number [3]. Low magnifications can be used in observing aggregate arrangements, cement paste and other structural traits. Higher magnifications are helpful in studying morphology of clinker minerals, as well as micro pores. BSE imaging can be combined with information from local chemical microanalysis.

The main limitation of this method is the fact that all the conclusions about material in 3 dimensions are based on observing 2D specimens. As a matter of fact, it is the common flaw of most of the listed techniques. Smaller grains of aggregate have lower probability of being sectioned, which can lead to error in estimation of their quantity. Sections are mainly not equatorial, which leads to imprecise anticipation of particle sizes.

2.4. Computed X ray microtomography

All the methods of imaging using X ray are based on the following: linear attenuation coefficient is a measure of material absorbiton and scattering. It depends mainly on a density and atomic number of material particles. Image is being formed by the difference in attenuation coefficient of the phases or features of specimen encountered with X rays. Formed image represents a two dimensional projection of attenuation characteristics of the examined material.

As mentioned before, majority of microstructural analysis methods are unable to precisely define 3D structure based on images of 2D sections or thin, flat specimens. Sometimes thin samples can be damaged, contaminated or crashed. The method of computed X ray microtomography successfully overcomes all of those limitations. The principle of this method is very similar to medical scanner. The large number of 2D images of material X ray absorbtion is taken at various angles. 3D model is obtained after the computed reconstruction of all of the 2D images (Fig. 2). It is a big advantage, for, as mentioned before, 3D relationship cannot be exactly deducted out of 2D sections.

It is non-destructive method and thus can be applied to many kinds of materials (biological, geological, industrial etc.). This method is highly applicable in examination of processes such as cement hydratation, concrete leaching, strengthening or shrinking etc. One single sample can be examined in many phases so that the whole process can be followed [4]. This reduces statistical estimations and provides more representative results.

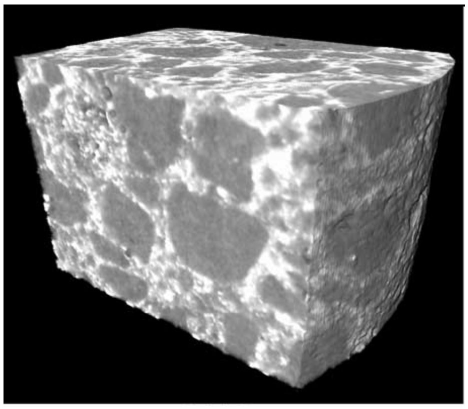

Figure 2- 3D Model of concrete, obtained by computed X ray microtomography

3. SPECIMEN PREPARATION

Speciment preparation is essential part of microstructural analysis. Done properly, it can provide desired contrasts, accurate quantification of significant parameters and correct information about the structure condition. Furthermore, it can provide process automatisation and make it available and efficient [5].

Quantitative examination of microcracks in concrete is important indicator of concrete or mortar condition. In many described techniques and their applications, main focus is on microcracks analysis. Prerequisite for obtaining correct results is capturing and processing a large number of images. To make process simpler and quicker, it is good to prepare specimens so that the entities of interest can be seen in significant contrast opposed to the body of material. Prepared specimens must have sharp edges, flat and polished surfaces.

In the method of optical microscopy, all the specimens are being impregnated with epoxy resin, with addition of fluorescent color (optical fluorescent microscopy). Methods that have been used in the past were based on impregnation of specimens with ink, but the results weren't satisfying. The low viscosity made it impossible for ink to fill the voids and microcracks, but capillary pores only. Thus the new, two stage procedure of epoxy impregnation has been developed [5]. Epoxy resin is very suitable in terms of pores and microcracks filling and preserving microstructure of material. Fluorescent color is added in order to obtain good contrast under ultraviolet light. The process of impregnation has two stages. In the first stage specimen is being cut into thin slices that are being vacuum cleaned, drained, immersed into the ink and finally drained for 24h. In the second stage specimen is being impregnated with coloured epoxy resin in pressure chamber and dried for additional 24 hours. Then excessive impregnate is being removed and specimen polished. The difference between specimens prepared with ink and with two stages process can be seen in a Fig. 3.

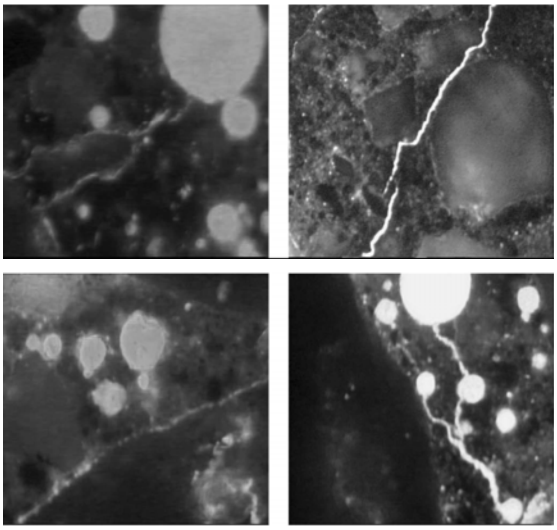

Figure 3- The difference between speciments impregnated with ink only (left) and specimen prepared for optical fluorescent microscopy in two stages (right)

Another inventive method of specimen preparation is impregnation with Wood's metal and is often used in method of scanning electron microscopy. Wood's metal is alloy of bismuth (50%), lead (25%), cadmium (12.5%) and tin (12.5%). It melts at 70ºC and goes through no volume changes in the process of hardening. The Wood's metal has Jung's modulus 9.72 GPa and density of 9.67 g/cm^3. Specimens are being prepared similarly as in previous case. Firstly they are cut into thin slices, cleaned and dried. Then the process of impregnation is being performed in pressure chamber. Specimens are then dried, cooled 3-4h and finally polished [5].

BSE method and X ray microtomography sometimes require epoxy impregnation (no additional fluorescent color needed) and sometimes not, depending on the research objectives. It is important to have clean sample, with sharp edges. X ray methods are very practical in processes examination, for they are non-destructive and it is possible to capture a specimen in many phases of the process. It makes statistical estimations minimal, and obtained results correct.

4. IMAGE PROCESSING

Segmantation is the process during which images are being segmented into meaningful regions, based on intensity of pixels. When segmentation is applied to gray images, gray level of pixels that satisfy certain conditions is set to 1, or otherwise to 0. That is the way of converting image to binary record that is suitable for computed analysis. Each pixel is represented with a single bit that stands for "true" or "false" situation (for instance, microcrack or not). It makes the process of microcracks or other features of interest quantification much easier. After many researches it has been concluded that automated threshold function gives best results (Fig 4) [5].

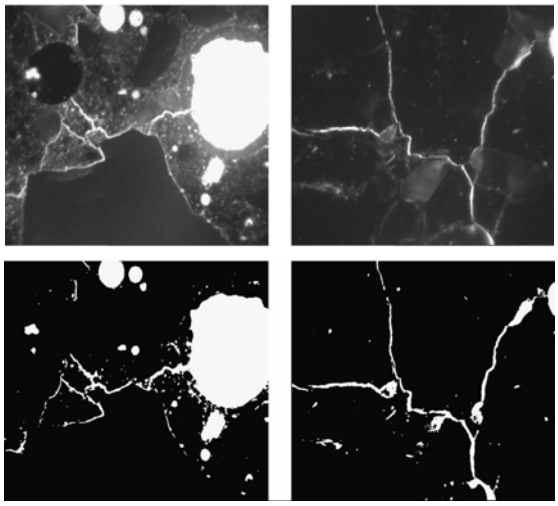

Figure 4- Original gray images (upper) and coverted binary images with authomated threshold function (lower)

It is important to make distinction between the features of interest, for instance between pores and cracks. Software for image analysis has ways of calculating it, using the form factors that represent the ratio between object width and length [5]. Image processing software has many other options, such as measurement of crack width, length, density, angle, distribution, roundness etc.

Despites all the precaution, it is often possible that images contain noise, that can originate from different sources. Sometimes it is caused by contamination, redundant impregnate or damage, inadequate light or contrast. Some noise can be removed in image processing. However, images with too much noise should be removed from the investigation, to prevent the result distortion.

5. METHODS' APPLICATION

5.1. Studying of fire damaged concrete using optical microscopy

The number of building fires has increased in last 50 years and there is a great need for structures that can keep safety and ability to be repired after the influence of fire [6]. Microstructural analysis of fire damaged concrete and other materials includes microcrack examination, mineralogical changing and the estimation of the material and structure condition. These examinations (also known as petrographic examinations) can be applied to masonry structures, mortars, bricks and stone.

Concrete and masonry structures are poor thermal conductors (unlike steel) and incombustible (unlike wood) [7]. However, exposure to high temperatures leads to significant physical, chemical and structural changes, which lead to decrease in capacity of load bearing. Structure is first examined visually In sity, and then the speciments are being taken for further petrographic examination. It is fairly important to check the structure stability and safety at the very beginning. Visual examinations are very useful, but should be supplemented with laboratory analysis. Table 1 represents basic visual directions for the fire damaged concrete structures classification.

Table 1- Simplified visual classification for fire damaged concrete

Class of damage	Visible features					
	Finishes	Color	Spalling	Reinforcement	Cracking	Distorsion
0 (Decoration required)	Unaffected	Normal	None	Unexposed	None	None
1 (Superficial repair)	Some peeling	Normal	Slight	Unexposed	None	None
2 (General repair)	Substantial loss	Pink/red	Moderate	Up to 25% exposed	None	None
3 (Principal repair)	Total loss	Pink/red/ whitish gray	Extensive	Up to 50% exposed	Minor	None
4 (Major repair)	Distroyed	Whitish gray	Total	Up to 50% exposed	Major	Distorted

The strength of fire damaged concrete depends upon the attained temperature, the heating rate and loading. For temperatures lower than 300ºC concrete strength is not severely reduced. Between 300ºC and 500ºC concrete strength rapidly decreases (15-40%) along with structural and mineralogical changes and it is considered that reparation is necessary. The concrete that has been heated in excess of 600ºC is considered structurally useless, for it is losing up to 70% of its initial strength [6], [7].

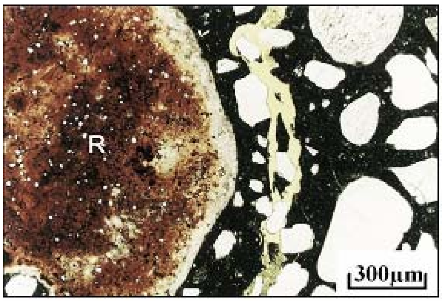

Figure 5- Micrograph of fire damaged concrete; crack induced with high heath and red discoloration od aggregate (letter R)

The colour of concrete changes due to the temperature and it can be accurate indicator of its condition. If the concrete is exposed to temperatures of 300ºC, aggregate grains change their colour to pink or red (Fig 5), along with crack opening and cement paste deterioration. At temperatures over 600ºC, aggregate attains whitish-gray discoloration and cement matrix becomes anisotropic and changes colour to yellow or beige (Fig 6). At the temperatures over 1000ºC, concrete melts and becomes glassy after cooling. Spalling is the first mechanical change that starts to happening and it opens a space for the heat towards the material interior. Cracks are opening along with heating. Different components of composites have different thermal expansion, which induces cracks. That is emphasised on the joints of the concrete and reinforcement bars, for the steel is much better heath conductor. Additional cracks can appear in the process of rapid cooling during the fire-watering [6].

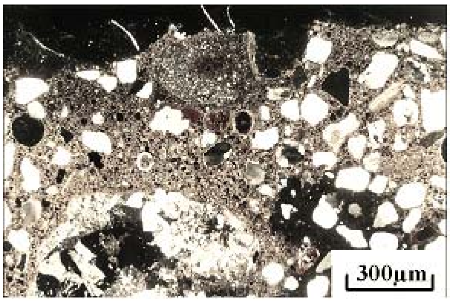

Figure 6- Micrograph of fire damaged concrete- anisotropic structure of cement matrix and yellow discoloration, due to temperatures above 600ºC

All of the above mentioned features can be seen on microscope images and attained temperatures can be estimated very accurately. Visual examinations can sometimes show that structure is not significantly damaged, when microscopic examinations point out differently. Thus it is essential to perform both kinds of investigations, in order to obtain accurate results. Moreover, the costs of petrographic examinations can be paid back many times in cost savings, and choosing good methods of reparation rather than structure demolition [6].

5.2. Identification and quantification of cracks in concrete using optical microscopy

Cracks are weak spots of concrete and structural problems that lead to damage, strength depletion and decreased durability [1]. They can be induced by many causes, either in early stages (temperature changing during hydratation process, unproper curing) or later in exploitation period (leaching, chemical corrosion, fire damage etc.). It is possible to identify and quantify cracks, regardless of their origin. Crack examination can be helpful in determination of structure condition and durability.

Optical fluorescent microscopy is one method of crack examination. Specimens are impregnated with epoxy resin in a way explained in Chapter 3. Figure 7a represents image obtained with optical microscope and ultraviolet light. The body of concrete is darker and cracks filled with epoxy resin lighter. As explained, images are being converted to binary form (Fig 7b). Software for image processing uses special filter, named skeletonization, which converts cracks into single pixel lines (Fig 7c). It makes images more suitable for an automatic processing. The software measures many parameters: length of crack lines, angles, dendrites' lengths, roundness, areas of voids and of material, average width of cracks, crack density etc. These summarised parameters can provide the accurate information about the material condition.

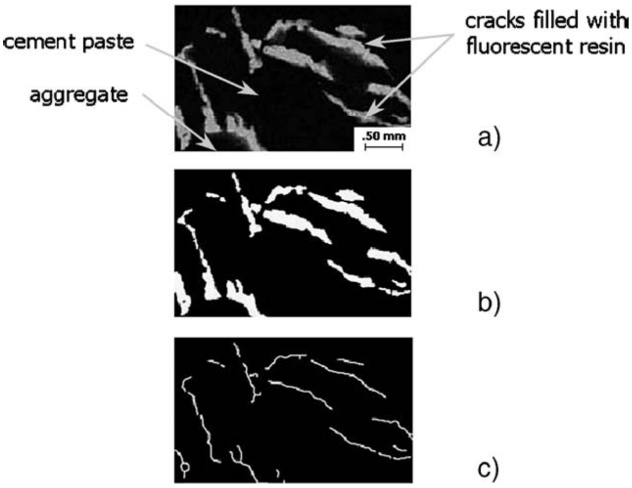

Figure 7- The image processing stages- 7a) original image 7b) binary image after authomated thresholding 7c) binary image after skeletonization

5.3. Analysis of compressive stress induced microcracks in concrete using SEM

Majority of micro analytic methods are focused on crack examination, but this technique can go one step further and describe stress induced microcracks. These examinations are important for showing the structure material in its exploitation conditions and some potential problems in the working life of structure.

Loaded specimens are being impregnated in Wood's metal, as described in Chapter 3. It hardens in 3D form while keeping cracks intact [2]. Wood's metal is especially suitable for this kind of examination, for its low melting temperature, quick hardening and no volumetric changes during the process. Hardened Wood's metal represents crack 3D network in a concrete specimen. Besides of it, parallel experiment should be made on unloaded specimens in order to compare cracks prior to loading and after it. It is also important to determine and quantify pores and voids that originate from the hydration process.

All the specimens have been observed under SEM and images captured. After the software processing, the comparison could be made. It led to the conclusion that cracks in unloaded specimens are narrower, shorter and differently distributed than in loaded ones. Long cracks are very typical for loaded specimens. All the weak spots in unloaded specimens, such as pores, crashed aggregate grains, initial cracks, are becoming starting points for new cracks. Microcracks, pores and voids that appear in hydratation process represent places of new cracks propagation (Fig 8). These cracks were generated due to local tensile strength, tangential to the voids.

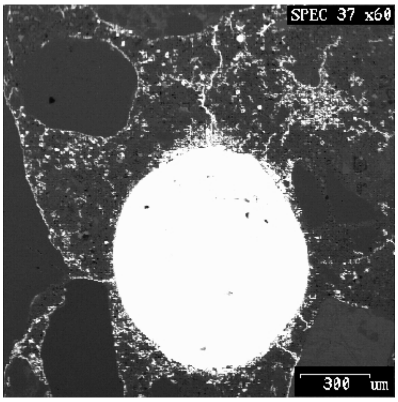

Figure 8- SEM image of microcracks in loaded concrete-microcracks are propagating from the pores

5.4. Determination of water/cement ratio of hardened concrete using BSE

This kind of examination has been already done using method of optical fluorescent microscopy and standardized (Nordtest NT Build 361-1999). BSE technique can be used for this kind of studies as well, and give accurate results.

Studies are performed to concrete samples which w/c ratio is unknown. Laboratorial examination has shown that even small changes in w/c ratio can cause big changes in capilar porosity. Examination of laboratory specimens with known w/c ratio can be used to determine the relation between two parameters: capilar porosity (measured by BSE method) and w/c ratio. It has been concluded that the relation is linear [8]. The specimens of field concrete have been examined for their capillary porosity using BSE method, as described in Chapter 2. The obtained correlation can be applied and results for w/c ratio would follow [8].

5.5. BSE imaging of cementitious microstructures

In spite of very hetherogenic structure of cement paste, it is very important to derive its quantitative measures. BSE method can be used in examination of cementitous paste, concrete and mortar properties and durability [3]. Wide range of magnifications provides ability of observing material configuration, as well as morphology of minerals and the smalles pores.

Cement clinker contains various minerals: C_3S (alite), C_2S (belite), C_3A (aluminate), $Ca_2(Al, Fe)$. During the grinding fracturing goes between the minerals and the resulting cement grains most often contain more than one mineral. It is visible on the BSE images, for all the cement grains appear hetherogenic. Different hydratation zones can also be distinct at the images. Hydratation decreases the average atomic number of area, so hydrated components appear darker. Examinations have shown that hydratation process performs form the outside towards the inside. In first 10 minutes of hydratation, ettringite and amorphous products of cement paste get formed and they separate other grains while making total hydratation impossible. Smallest cement grains (up to 5 μm) get hydrated completely and leave the hollow shells, known as Hadley grains [3]. Figure 9 shows the different components of cement paste on BSE image.

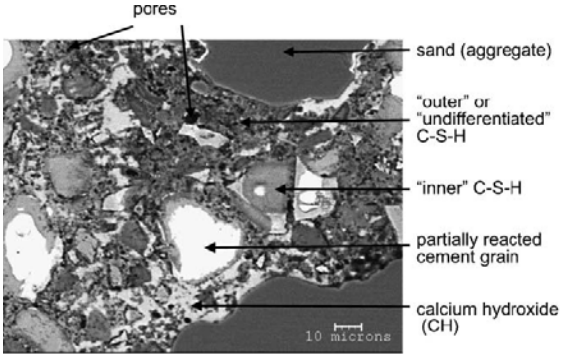

Figure 9- BSE image of cement paste and its minerals

5.6. Examination of the concrete leaching process using computed X ray microtomography

The method of computed X ray microtomography is especially useful in terms of processes monitoring. It can be used to measure the porosity variation in leaching concrete. Leaching is an important process to investigate, for it is related to structure durability. Leaching can be mechanical or chemical. For the experiment, accelerated leaching process can be implemented in laboratory, as a simulation of porosity evolution in time [4].

Specimens can be made in laboratory or sampled In situ, their size and shape depends on the equipment, but they are often cylindric. They are then subjected to the influence of aggressive solution (with low pH value), and monitored in certain time increments.

Firstly, the specimen surface is analysed, for leching starts there and then expands deeper into the body of material. Cement paste deteriorates, while aggregate grains remain mostly intact [4]. Two zones are visible: superficial zone with dissoluted cement paste and sound core, unaffected by the leaching process (Fig 10). Leaching front evolution can be identified and measured. On the cross sections perpendicular to the sample axis it appears that the leaching is almost complete. Leaching front position can be controlled with capturing the cross section parallel to sample axis, which is a great asset of x ray microtomography. Those images prove that the leaching is deep but not complete.

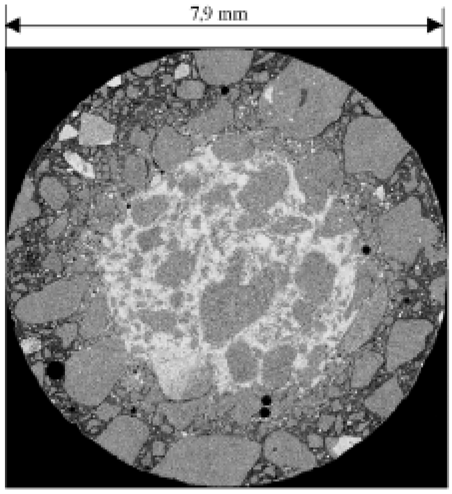

(a)

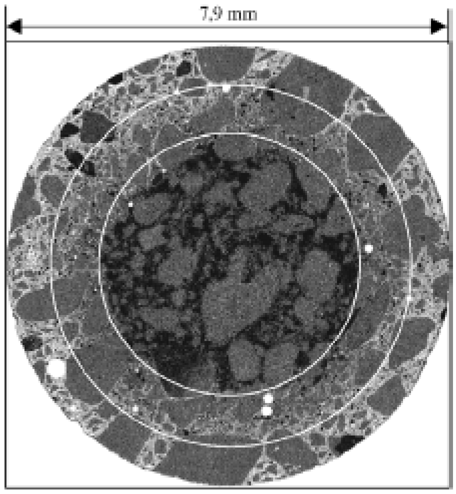

(b)

Figure 10- Cross section perpendicular to specimen axis, initial 2D image (a), negative of the image (b)

6. CONCLUSION

Microstructural analysis methods are the future of the material examination. They are especially useful in concrete and composite material studies. They can be used as a mean of getting better knowing about certain processes, such as concrete leaching, strengthening, shrinking, cracking under loading or chemical treatment, cement hydratation, effects of chemical additives etc. These methods can be used in examination of material samples from the existing structures, in order to determine the structure condition and material durability and strength. Better knowing of materials can result in better decision making and improvements in preparation, building and structure maintaining.

Advance in technology and in software development make these techniques more powerful and practical. Also, they are becoming more efficient and affordable, so that they can be included in regular processes of material investigation. Their costs are significantly lower and can be paid back many times in terms of time, money and resources saving. Reconstructions of objects are excellent way of reusing the existing materials and structures. Another benefits are pollution and waste reduction as well as healthier environment.

ACKNOWLEDGEMENTS

We acknowledge The Faculty of Mechanical and Civil Engineering in Kraljevo, for providing us the opportunity of presenting our work. We would also acknowledge the professors V. Radonjanin, M. Malešev and The Faculty of Technical Sciences in Novi Sad for all the support during the research.

REFERENCES

[1] A. Litorowicz, "Identification and quantification of cracks in concrete by optical fluorescent microscopy," Cement and Concrete Research 36 (2006), pp. 1508-1515

[2] K. M. Nemati, "Fracture Analysis of Concrete Using Scanning Electron Microscopy," Scanning Vol. 19, 6 (1997), pp. 426-430

[3] K. L. Scrivener, "Backscattered electron imaging of cementitious microstructures: understanding and quantification," Cement, Concrete and Composites 26 (2004), 935-945

[4] N. Burlion, D. Bernard, D. Chen, "X-ray microtomography: Application to microstructure analysis of a cementitious material during leaching process," Cement and Concrete Research 36 (2006), pp. 346-357

[5] P. Soroushian, M. Elzafraney, A. Nossoni, "Specimen preparation and image processing and analysis techniques for automated quantification of concrete microcracks and voids", Cement and Concrete Research 33 (2003), pp. 1949-1962

[6] J. P. Ingham, "Application of petrographic examination techniques to the assessment of fire-damaged concrete and masonry structures", Material Characterization 60 (2009), pp. 700-709

[7] B. Georgali, P.E. Tsakiridis, "Microstructure of fire-damaged concrete. A case study," Cement& Concrete Composites 27 (2005), pp. 255-259

[8] S. Sahu, S. Badger, N. Thaulow, R.J. Lee, "Determination of water–cement ratio of hardened concrete by scanning electron microscopy", Cement& Concrete Composites 26 (2004), pp. 987-992

Estimation of Marshall Stability of Steel Fiber Reinforced Asphalt Concrete Using Adaptive Neuro-Fuzzy Inference System

Nihat Morova[1], Sercan Serin[2], Serdal Terzi[1], Mehmet Saltan[1,*], Mustafa Karaşahin[3]
[1]Suleyman Demirel University, Isparta, Turkey
[2]Duzce University, Duzce, Turkey
[3]İstanbul University, Istanbul, Turkey

Steel fibers in asphalt mixtures have been used for improving the stability of pavements. In this study, Marshall Stability (MS) values of steel fiber reinforced asphalt mixture were estimated by using the fiber mixing rates and basic physical properties with an ANFIS (Adaptive Neuro-Fuzzy Inference System) model. For this evaluation, input parameters including different bitumen content, fiber rates and unit weights were used. Thirty three randomly selected input parameters were used as training data and 8 data (residual) were used as testing data. Coefficient of determination (R2) and Total Root Mean Square Error (RMSE) criteria were used for the comparison of experimental results with the results predicted by the model of ANFIS. When predicted and measured values were compared, RMSE and R2 values were obtained as 5.337 and 0.998 for training set, and for the testing set they were obtained as 8.5 and 0.997 respectively.

As a result, Marshall Stability values of steel fiber reinforced asphalt mixture could be predicted practically with very low error rates in a very short time without performing any experiments.

Keywords: Asphalt mixtures, ANFIS, Marshall Stability, Steel fiber

1. INTRODUCTION

Flexible pavements are designed so as to have at least 20 years project life. The current research subjects include the studies focusing on increasing the performance and lifetime of road pavements. For these purposes different kinds of additive materials have been evaluated in asphalt mixtures [1].

The researchers that previously worked on the subject clearly indicated that the use of fiber in the pavements and asphalt mixtures has a strengthening effect. Fibers can be used especially in the mixtures with continuous grading and in Stone Mastic Asphalt (SMA) mixtures in order to overcome the deterioration of asphalt during carriage and construction of the mixture, as well as in asphalt stabilization [2-4]. The use of fibers alters the visco-elasticity characteristics of the mixture [5]; enhances its dynamic modulus [6], enhances sensibility against humidity [7], enhances flow coherence, and provides resistance against the rutting [8-9]; as well as it decreases the amount of reflective cracks in asphalt mixtures and pavement [10-12].

In recent decades, one of the most important and promising research field has been "Heuristics from Nature", an area utilizing some analogies with natural or social systems and using them to derive non-deterministic heuristic methods and to obtain very good results [13-14].

Jang (1993) first proposed the adaptive neural based fuzzy inference system (ANFIS) method and applied its principles successfully to many problems. It identifies a set of parameters through a hybrid learning rule combining the back-propagation gradient descent error digestion and a least squares method. It can be used as a basis for constructing a set of fuzzy IF-THEN rules with appropriate membership functions in order to generate the preliminary stipulated input-output pairs [15].

Kaur and Chou (1999) applied the Neuro-Fuzzy techniques for modeling the highway pavement performance prediction [16]. Also, Göktepe et al (2005) used the ANFIS methodology for backcalculating the mechanical properties of flexible pavements [17].

The main purpose of this paper is to develop an ANFIS methodology for estimation of the Marshall Stability value through steel fibers rate, bitumen content and unit weights.

2. MATERIALS

2.1. Aggregates and Bitumen

Crushed limestone aggregates were used in asphalt mixtures. AC 60/70 asphalt cement was used in asphalt mixtures as bitumen. Aggregate and bitumen material tests were carried out basing on American Codes, in order to obtain the physical and mechanical characteristics of the materials to be used in the mixtures [18].

2.2. Steel Fiber

In this study, Dramix RC-80/60-BN fiber was used. The characteristics of Dramix RC-80/60-BN Steel Fiber: In the denomination of Dramix steel fibers, R and C define the hook and the admixture features of fiber, respectively, while 80 defines the performance class and 60 defines the length of fiber in mm. B stands for Bright. N stands for Low Carbon [18].

2.3. Laboratory Tests

Asphalt mixtures were prepared in accordance with the technical specifications required by Republic of Turkey General Directorate of Highways.

A series of tests were carried out in order to determine the optimum bitumen content. For this reason asphalt mixture samples were produced using 4.50%,

*Corresponding author: Faculty of Engineering/Civil Engineering Department, Suleyman Demirel University, Isparta (Turkey), mehmetsaltan@sdu.edu.tr

5.00%, 5.50%, and 6.00% bitumen contents. As a result of the tests optimum bitumen content was obtained as 5.50%.

As it has been thought that fiber using will change the optimum bitumen content of asphalt concrete, asphalt concrete was prepared in 5.00% and 6.00% percentages of bitumen content as well as optimum 5.50% percentage of bitumen content in all mixtures with and without fibers. Steel fibers were added in different rate of weights (0% - 0.25% - 0.50% - 0.75% - 1.00% - 1.50% - 2.00% - 2.50%) as three samples for each fiber rate and bitumen contents (%5.00, %5.50 and %6.00). Maximum Marshall Stability value was obtained in 5.50% bitumen content and 0.75% fiber addition [18].

3. DEVELOPED ANFIS MODEL DETAILS

In this research, an ANFIS model developed including three inputs, i.e., content of bitumen (COB), rate of fiber (ROF) and unit weight (UW) and an output which is Marshall Stability (MS) as given in Figure 1.

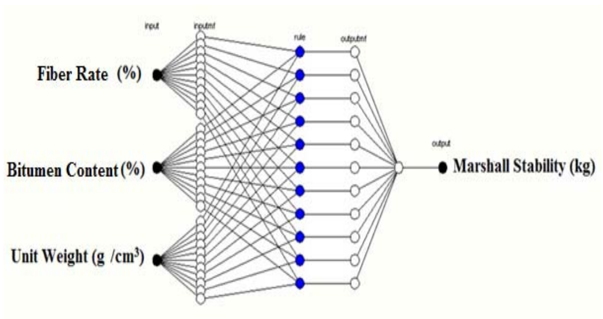

Figure 1: General structure of the model

While developing the model, 33 (about 80%) experimental data were used for training and 8 (about 20%) experimental data were used for testing. The descriptive statistics for the training set of randomly selected 33 data are given in Table 1. After experimenting different learning algorithms with different epochs, best correlations were found through hybrid learning algorithm and 1000 epochs.

Table 1: Descriptive statistics of selected data as training set

Physical prop.	N	Range	Min.	Max.	Mean	Std. Error	Std. Deviation	Variance
Bitumen content (%)	33	1	5	6	5.53	0.065	0.374	0.140
Steel Fiber (%)	33	2	0	2	0.94	0.118	0.679	0.461
Unit Weight (g/cm³)	33	0	2	3	2.49	0.003	0.016	0.000
Marshall Stability (kg)	33	395	717	1112	846.12	20.397	117.170	1.373E4

In the model 14 sinusoidal “gaussmf” membership functions were selected for content of bitumen (COB), rate of fiber (ROF) and unit weight (UW) (Figure 2). All membership functions ranges were used for COB (% 5.00 - % 6.00), for ROF (% 0 - % 2.50) and for UW (2.465-2.515) respectively.

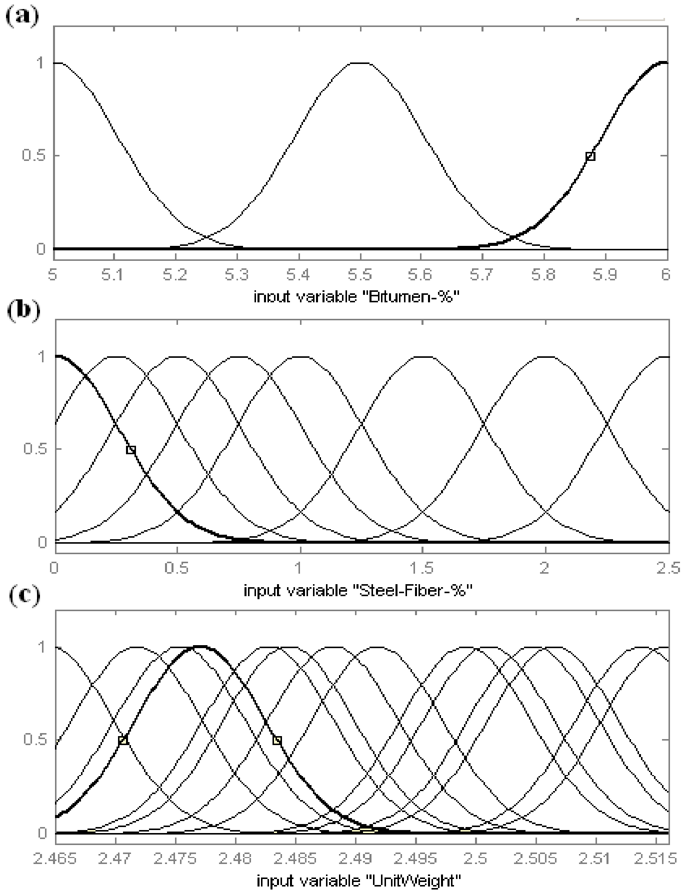

Figure 2: Membership functions of inputs

In the model, 14 rules were defined via the relationship between inputs and output. Table 2 shows the detailed structural properties of model.

Table 2: Detailed structural properties ANFIS model

ANFIS Model Summary	
Number of nodes	118
Number of linear parameters	56
Number of nonlinear parameters	84
Total number of parameters	140
Number of training data pairs	33
Number of checking data pairs	0
Number of fuzzy rules	14
Input	3
Output	1
Type of input member function	Bell-shaped Gauss function
Range of influence	0.2
Squash factor	1.25
Accept ratio	0.5
Reject ratio	0.15

4. RESULTS AND DISCUSSIONS

The adequacy of the developed ANFIS model was evaluated by considering the coefficient of determination (R2) Eq. (1), root mean squared error (RMSE) Eq. (2) and Standard Error of the Estimate (SEE) Eq. (3).

$$R^2 = 1 - \left\{ \left[\sum_{i=1}^{n} (Y_{i(observed)} - Y_{i(model)})^2 \right] \Big/ \left[\sum_{i=1}^{n} (Y_{i(observed)} - Y_{i(mean)})^2 \right] \right\} \quad (1)$$

$$RMSE = \sqrt{\frac{1}{N} \sum_{i=1}^{n} (Y_{i(observed)} - Y_{i(predicted)})^2} \quad (2)$$

$$SEE = \sum_{i=1}^{n} (Y_{i(observed)} - Y_{i(mean)})^2 \quad (3)$$

Where;
n : Total number of data
Yi(observed) : Measured (experimental) Marshall Stability
Yi(model) : Developed model result

Table 3 represents calculated R2, RMSE, SSE and SEE values for training and test groups of developed ANFIS model.

Table 3: Some statistics of Marshall Stability estimation using ANFIS

	R-square	Adjusted R-square	SEE	RMSE
Training Set	0.9980	0.9979	882.9	5.337
Testing Set	0.9971	0.9967	433.3	8.500

Figure 3 and 4 show the model performances of the ANFIS modeling based on the 95% prediction bounds illustrated on the figures and linear curve fitting statistics summarized in Table 3 for training set and testing set respectively.

According to the comparison of the curve fitting statistics, the smallest prediction errors were observed in ANFIS model according to the curve fitting statistics. The RMSE values of the ANFIS model at the training stage is 5.337 In addition, the RMSE values of the ANFIS model at the testing stage is 8.5. All of the statistical values in Table 3 show that the ANFIS model is suitable and predicted the Marshall Stability values very close to the experimental values.

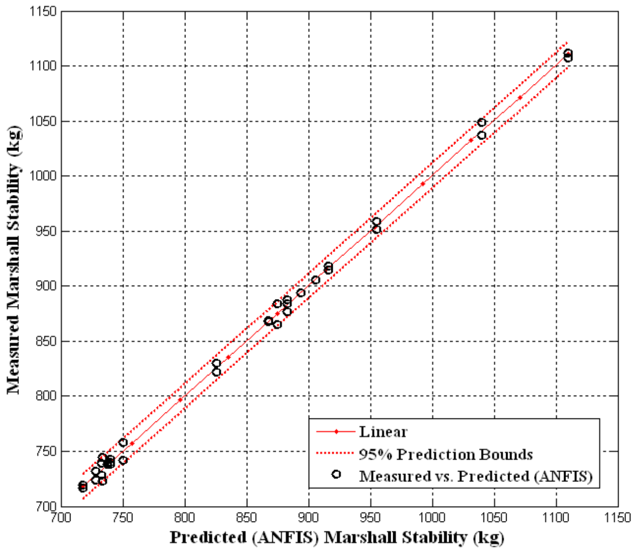

Figure 3: Comparison of experimental Marshall Stability values with the predicted values in the training stage

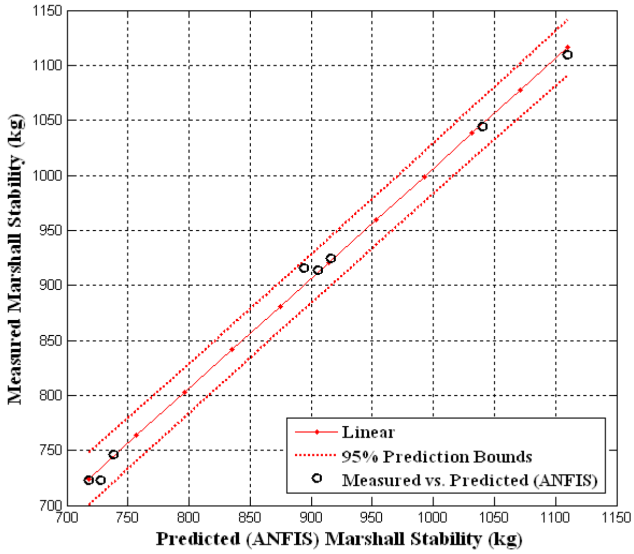

Figure 4: Comparison of the experimental Marshall Stability values with the predicted values in the testing stage

5. CONCLUSIONS

In this paper, ANFIS approach and its prediction capability for Marshall Stability were examined. Steel fibers in asphalt mixtures have been used for improving the stability of pavements. Steel fibers rate, bitumen content, and unit weights were used as input parameters to estimate of the Marshall Stability value.

For training set, 33 samples were randomly selected and the residual data (8 samples) were selected as test set. In the rule base, combinations of various iteration numbers and various membership functions were tried. The best correlation was found with hybrid learning algorithm and 1000 epochs. After finding the best fitting ANFIS model estimation with experimental results, it was compared with each other. The coefficient of determination (R2), root mean square error (RMSE) and standard error of estimation (SEE) were used as comparison criteria.

When predicted and measured values were compared, RMSE and R2 values were obtained as 5.337 and 0.998 for training set, and 8.5 and 0, 9971 for the testing set respectively.

As a result;

- ANFIS method is a useful artificial intelligent tool for the pavement engineering applications.
- The Marshall Stability of samples that are produced with given materials can be predicted quite successfully by the developed ANFIS model.
- Also, engineers and agencies can easily use the formulation of the model, which has been obtained from formulations of selected functions (i.e. summation and activation) used in the ANFIS model and weights of neurons.
- By changing the architecture of ANFIS and the functions, different formulations can be obtained. Also, the developed model produces equations based on the real results, not the assumptions.
- The Marshall Stability can be calculated by using the models built with this methodology.

- It is convenient and easy to use these models for numerical experiments to review the effects of each variable on the mix proportions.

6. REFERENCES

[1] F. Umar, E. Ağar, "Pavement Structure", İstanbul Technical University Civil Engineering Faculty Press, İstanbul, (1991)

[2] H.F. Hassan, S.A. Oraimi, A. Taha, "Evaluation of open-graded friction course mixtures containing cellulose fibers and styrene butadiene rubber polymer." J Mater Civil Eng, 17:416–22, (2005)

[3] J.P. Serfass, J. Samanos, "Fiber-modified asphalt concrete characteristics, applications and behavior." J Assoc Asphalt Paving Technol, 64:193–230, (1996)

[4] P. Peltonen, "Wear and deformation of characteristics of fiber reinforced Asphalt pavements." Construct Build Mater, 5:18–22, (1991).

[5] H. Huang, T.D. White, "Dynamic properties of fiber-modified overlay mixture." Transport Res Rec, 1545:98–104, (2001)

[6] S. Wu, Q. Ye, N. Li, H. Yue, "Effects of fibers on the dynamic properties of Asphalt mixtures." J Wuhan Univ Technol – Mater Sci Ed, 22:733–6, (2007)

[7] B.J. Putman, S.N. Amirkhanian, "Utilization of waste fibers in stone matrix Asphalt mixtures resources." Conserv Recycl, 42:265–74, (2004).

[8] R.S. McDaniel, "Asphalt additives to control rutting and cracking." PHD thesis. Purdue University, Indiana, (2001)

[9] H. Chen, N. Li, C. Hu, Z. Zhang, "Mechanical performance of fibers-reinforced asphalt mixture." J Chang'an Univ (Nat Sci Ed), 24(2):1–5, (2004)

[10] S. Tapkın, "The effect of polypropylene fibers on asphalt performance." Building Environ 2007:1–7, (2007)

[11] D.A. Maurer, G.J. Malasheskie, "Field performance of fabrics and fibers to retard reflective cracking." Geotextiles Geomembranes, 8:239–67, (1989)

[12] C. Huaxin, X. Qinwu, C. Shuanfa, Z. Zhengqi, "Evaluation and design of fiber-reinforced asphalt mixtures." Materials and Design, 30 2595–2603, (2009)

[13] M.E. Emiroglu, O. Kisi, O. Bilhan, "Predicting discharge capacity of triangular labyrinth side weir located on a straight channel by using an adaptive neuro-fuzzy technique." Advances in Engineering Software, 41 (2), pp. 154-160, (2010)

[14] M.A. Mashrei, N. Abdulrazzaq, T.Y. Abdalla, & M.S. Rahman, "Neural networks model and adaptive neuro-fuzzy inference system for predicting the moment capacity of ferrocement members." Engineering Structures, Volume 32, Issue 6, pp. 1723-1734, (2010)

[15] J. Jang, "ANFIS: adaptive-network-based fuzzy inference system." IEEE Transactions on Systems Management and Cybernetics, 23(3), 665–685, (1993)

[16] D. Kaur, E. Chou, "Applying Neuro-Fuzzy Techniques for Intelligent Highway Pavement Performance Prediction Model", Circuits and Systems, 42th Midwest Symposium, Vol 2, 922-924, Las Cruces, NM, USA, (1999)

[17] A.B. Göktepe, E. Ağar, and A.H. Lav, "Comparison of Multilayer Perceptron and Adaptive Neuro-Fuzzy System on Backcalculating the Mechanical Properties of Flexible Pavements", ARI The Bulletin of the Istanbul Technical University, 54 (3), 65-77, (2005)

[18] S. Serin, N. Morova, M. Saltan, S. Terzi, "Investigation of usability of steel fibers in asphalt concrete mixtures." Construction and Building Materials, Volume 36, November, Pages 238–244, (2012)

Geotechnical Conditions for Foundation of Compressor in Velebit

Mitar Djogo[1*], Milinko Vasić[1], Rada Stevanović[1]
[1]Faculty of Technical Sciences/Department of Civil Engineering, University of Novi Sad, Novi Sad (Serbia)

In the process of getting oil and gas from exploitation boreholes of NIS, the large compressor facilities are necessary. Therefore, it is planned to build the compressor in Velebit and the results of soil investigations for it are presented in this paper. The foundation base for each individual compressor has dimensions 5/12m and they'll be placed in the newly built halls. The specifics of geotechnical investigations for compressors are that they must provide a stable foundation soil and also suitable subbase layer directly beneath the machine foundations. Also, because of dynamic machine impacts it is necessary to determine the soil properties for these conditions by soil investigations. The new location for the compressors in Velebit is gently sloped terrain which its flattened part is formed of loess sediments. For the purpose of defining the foundation conditions the exploration drilling holes, penetration and other terrain investigations were carried out to a depth of 13m.

Keywords: Compressor, Founding conditions, Site investigation

1. INTRODUCTION

On the oil field of NIS in Velebit there is one compressor in function now. It is planned to build two new halls because of expanding the volume of the work. In the first hall will be located one compressor and in the other will be located two big compressors side by side. Both halls will be funded on individual footings that are completely independent of machine foundations-compressor. In this paper the fabric halls are not considered. It is written a lot about halls, but in the geotechnical field there is a little contemplation about machine foundations.

The specifics of machine foundations-compressors are that they must have large dimensions, investigations of the terrain have to be sufficient and good, and compressors must carry over to foundations dynamic loads and in the process of designing and building the multidisciplinary is needed. The foundations of the compressors in Velebit have rectangle base and dimensions are B/L=8/12 m. Relatively big dimensions of foundation are the result of the specifics of the vibration displacements and interaction between foundation and the work state of compressor. The foundation depth of compressor is 1.2 m. When design the foundations it is necessary to toughly investigate foundation substrate and especially from stability point of view and due to physical - mechanical characteristics of the soil. The success of designed solution requires team work of geotechnical field, civil engineering, mechanical engineering, electro technique etc.

In Velebit at the location of new halls and compressors terrain is formed of loess sediments. The terrain is slightly sloped toward wide depression plate which emergence is partly related to the process of long exploitation of oil and gas. Namely, on that wide area which is one of the largest oil and gas deposits in Vojvodina, there are large numbers of functional oil and gas boreholes for oil pump from the great depths and for which exploitation the new compressors are needed. In this paper there is no consideration about geotechnical aspects of oil derivation, but only surface layers of terrain in the zone of interactional effects of new halls with the compressors and the terrain.

2. THE RESULTS OF TERRAIN INVESTIGATIONS

The results are based on detailed geotechnical investigations of the terrain on the locations of compressors and halls. There were performed 4 boreholes, 4 cone penetration tests, 5 investigative excavations and adequate laboratory investigations on samples etc. In this paper are shown only the most important results of investigations. Disposition of terrain investigation works is shown in the Figure 1.

Wider area SS-1 in Velebit is relatively proper wavy plane in loess. Namely, around the rim of that plane the vertical cuts with loess are clearly stand out. The heights of these cuts are 7-10 m. Based on performed trial works on micro location of the object it is determinate litogenetic composition of the terrain. Terrain is formed in surface layers of humus, beneath humus is loess, and the deepest layer of terrain is formed of sand deposits. From interaction between object end terrains point of view, the investigated depth of 13.2 m is enough. In the structure of the terrain in the zone B1 it can be single out following geotechnical mediums:

0.00 – 1.00 m – Organic soil
1.00 – 9.20 m – Loess and fossil soil
- 1.0-2.8 m Loess I horizon, sandy silt, easy to crush, dirty yellow color
- 2.8-3.0 m Fossil soil, sandy silt, shades of yellow brown
- 3.0-4.6 m Loess II horizon, with vertical pores width up to 2 mm, with deposits of calcium carbonate with diameter to 2 mm, dirty yellow color
- 4.6-5.2 m Fossil soil, shades of yellow brown color
- 5.2-6.7 m Loess III horizon, with vertical pores in places, width up to 2 mm, dirty yellow color
- 6.7-7.4 m Fossil soil, pores are sporadically width up to 5 mm, shades of yellow brown color

*Corresponding author: Faculty of Technical Sceinces, Trg Dositeja Obradovića 6, 21000 Novi Sad, Serbia, e-mail: mitar@uns.ac.rs

7.4-9.2 m Loess IV horizon, there are in places tin deposits of calcium carbonate silt, loess is dirty yellow color
9.20 – 12.00 m – Sand, very dense, shades of brown grey color

Based on analyze of present medium for all terrain investigations, it can be stated that horizons of loess and fossil soil take turns equally throughout all investigations area similar to what was outlined for B1 zone. Regarding this, it can be surly stated that the loess horizons and fossil soil were emerged as nearly horizontal and that their total thickness increases toward the peak of flattened area. Inclination of terrain is continuous. Characteristic geotechnical profile of terrain is shown in Figure2.

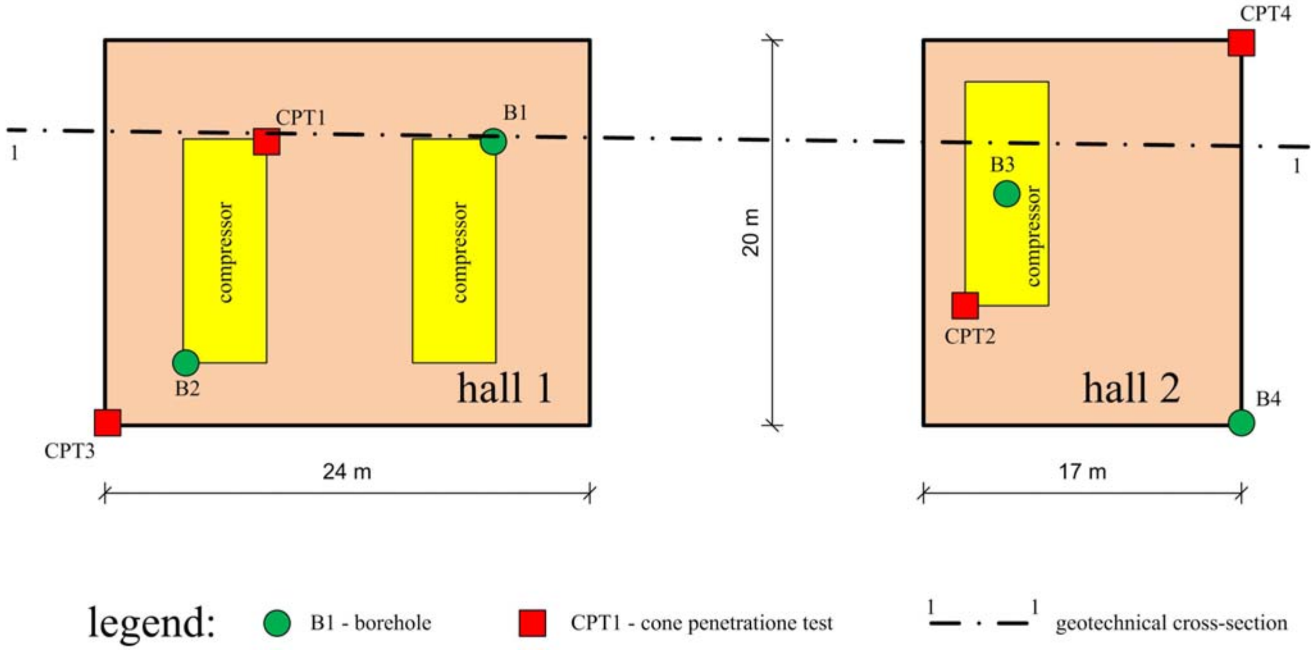

Figure 1: The layout with compressors and the investigation works

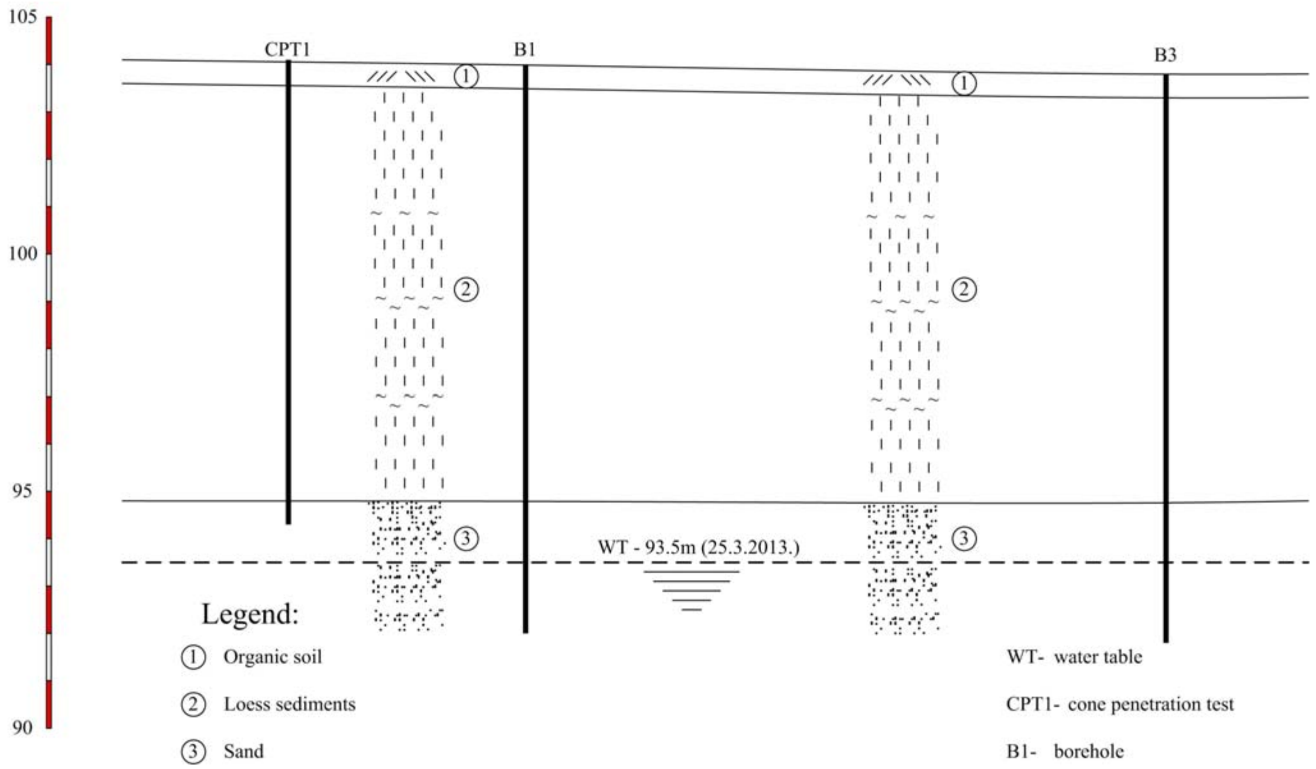

Figure 2: Geotechnical cross-section

In Figure 3 is shown characteristic diagram of cone penetration test.

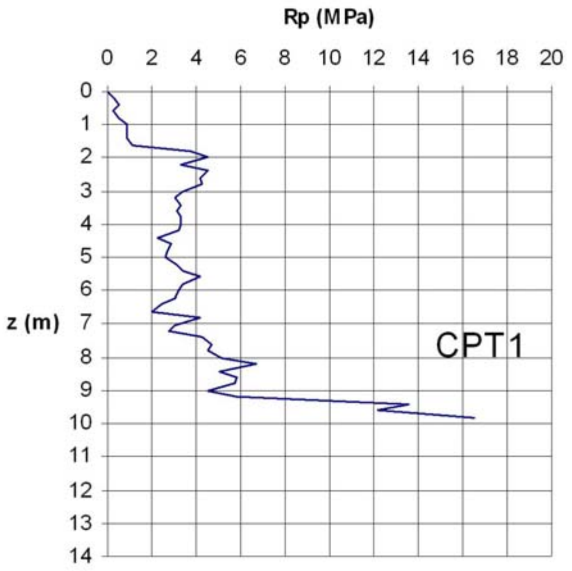

Figure 3: Diagram of cone penetration resistance

Litogenetic composition of terrain, hydro geological properties, conditions and stability of excavation is precisely determined with investigation work. For the purpose of funding the halls and foundations for compressors the bearing capacity and settlement are calculated.

On investigated terrain, in loess soil and sands beneath loess, it is formed unique permanent free aquifer. The depth to the maximum groundwater level is big and is 9m. From the standpoint of building all present objects it is likely that ground water doesn't affect the conditions of building, i.e. the works will be done in dry conditions.

Relevant parameters of shear strength of loess that are defined on the basis of laboratory tests have the following values: the angle of friction of soil is $\varphi = 20^0$ and cohesion is c = 10 kPa. Loess in Vojvodina forms the surface part of terrain on almost one-third of the territory. Numerous tests of loess are done on a large number of samples, on the samples of variable shapes, with samples taken at different depths. The investigations were performed in an extremely large number of objects and for research projects [1]. There are number of published scientific papers on loess investigations and therefore these detailed data are not shown in this paper.

3. FOUNDATION OF COMPRESSOR

Foundations have large dimensions because of the specifics of the work state of compressors. They are located in special halls with base dimensions of 24 x 20 m and 17 x 20 m. From standpoint of geotechnical conditions of funding the compressors foundations, they have to be located in closed halls. Reason for this is in a fact that terrain is formed of loess sediments, with relatively big total thickness that is sensitive to afterward moistening. In many cases, and for different objects (tall buildings, silos, roads, water towers etc.) that are funded in loess, the big damages and inclinations happened because of water infiltration in foundation soil. Characteristic example of bad funding in loess is water tower in Maradik that collapse. Since the compressors in Velebit are located inside halls, its collapse due to water infiltration is not going to happened.

Calculation analysis of bearing capacity and settlement of foundation substrate under the compressor showed that the loess soil have good characteristics. In this paper, these values are not presented with the remark that in the case of water infiltration into the loess soil resistant and deformation characteristics of loess would significantly decrease.

Machine foundations can be classified into three categories [2, 3]:
- Machine foundations with periodical impact such as compressors, strainer, smasher, and piston machines etc.
- Foundations for generators that produces the electricity
- Foundation for forging hammers with mechanical and pneumatic drive

For listed machine foundations the following is necessary:
- Number of natural oscillation of foundation has to be at least 20-25% lower or higher than the full number of machine turn. This can be provided by dimensioning the foundation and with the dense degree of foundation substrate. The foundation is a highly synchronized when the number of natural oscillations of foundation is greater than the full number of machine turn - compressor. The foundation is low synchronized when the number of natural oscillations of foundation is less than the full number of compressor turn; in that case the transient resonant states are possible;
- Has to be determine the value of six individual amplitude of forced oscillations of foundation at the point that is the farthest from the foundation axis of center of gravity and the machine;
- The weight of the foundation has to be much higher than the weight of the compressor;
- The dynamic effects in the foundation substrate, due to the working state of the compressor, has not cause the damage to foundation substrate.

The foundation of the compressor has to be funded on a relatively thick layer of good quality subbase. This means that for the subbase can be used burly stone or burly gravel. Stone is better because of the angular not rounded edges. For compressor in Velebit it was used crushed stone. The two layers of crushed stone are built-in. The first layer of 40 cm thickness on loess is the crushed limestone 31.5/63. This layer is dynamically compacted to achieve $M_s \geq 50$ MPa. On the first layer is embedded second 40 cm layer of crushed stone 31.5/63 by dynamic compaction to achieve $M_s \geq 70$ MPa. Subsoil of loess is compacted before applying the first layer of stone to achieve the criteria $M_s \geq 10$ MPa. It was concerned not to compact the loess at the time of rainfall.

For the purpose of designing the foundation attention was paid to necessary criteria which were defined in this paper. This refers to dependence of mass of the compressor and the foundation, the vibration behavior of the foundation and compressor, and also to the modulus of reaction of foundation substrate. For the foundation design of the compressor the following values of modulus of soil reaction were used:

- Static modulus of soil reaction of subbase layer made of stone is 25 MN/m^3
- Dynamic modulus of soil reaction of subbase layer made of stone is 70 MN/m^3
- Static modulus of soil reaction of loess subsoil is 10 MN/m^3
- Dynamic modulus of soil reaction of loess subsoil is 25 MN/m^3

Dependence of the number of compressor turns, the natural oscillation and amplitude of forced oscillations of the foundation, its dimensions and depth were analyzed when designing the foundation.

4. CONCLUSION

The machine foundations – compressors must be analyzed from the standpoint of dynamic impact of compressor on foundation during the process of design. For many constructions in civil engineering it is common to analyze only static impacts.

Foundations of compressors in Velebit have big dimensions. They are located in hall and that's how their stability and safety is provided. Terrain is formed of loess soil that deflects under afterward water infiltration into foundation soil. The compressors are located in special halls so the water infiltration into foundation soil is not possible.

Negative impact of foundation vibrations onto substrate is partly prevented by placing the quality subbase material. Beneath foundation of compressor in Velebit burly stone is placed with relatively big thickness and increased modulus of soil reaction.

ACKNOWLEDGEMENTS

This work was financially supported by research grants No. TR36043 and TR37017 of the Serbian Ministry of Science and Technological Development. Also, this work was financially supported by research grant Theoretical, experimental and applied research in area of Civil Engineering of the Faculty of Technical Sciences in Novi Sad.

REFERENCES

[1] D. Milović, "Problemi fundiranja na lesnom tlu," Odeljenje tehničkih nauka Vojvođanske Akademije Nauka i Umetnosti, Novi Sad, p. 255, (1987)

[2] M. Debeljković, "Dinamički opterećeni temelji industrijskih mašina u svetlu domaće prakse," Časopis Izgradnja, Vol. 41(9), pp. 11-25, (1987)

[3] V. Aćić, V. Ćurčin, M. Aćić, "Rekonstrukcija temelja konusnih drobilica sa zamenom podloge," Časopis Izgradnja, Vol. 68(3-4), pp. 141-149, (2014)

Knowledge Innovation Trends on a Standardization Platform – in Parallel: Civil Engineering and Railway Engineering

Živadin Micić[1] PhD[*], Slobodan Petrović, M.Sc.Eng.[2]
[1]Faculty of Technical Science Cacak - University of Kragujevac, Cacak (Serbia)
[2]Business Technical College of Vocational Studies, Uzice (Serbia)

The paper presents multi-criteria research and statistical analyses of trends of separated segments per subfields of civil engineering and engineering of railway vehicles. A focus is given to trends in knowledge innovating at the beginning of the second decade of the XXI century. The goal is to provide and improve the resources for quality of knowledge, on the platform of SRPS and ISO standardization. This paper presents the important details (the results) of comparing the trends of knowledge, in the analyzed subfields/ fields classified according to the International Classification of Standards (ICS) or ICS1 = 45 (Railway Engineering) and ICS1 = 93 (Civil Engineering). The directions of further development are presented, and also possibilities of access to the sources of knowledge and obligations, as well as comparisons with the standardization of local (national) and international level, in the same and in all other fields of creative work (for ICS1 = 01 to 99).

Keywords: Knowledge trends, Civil engineering, Railway Engineering, Knowledge innovation, Standardisation

1. INTRODUCTION

According to International Classification for Standards - ICS, civil engineering is a field classified in 12 subfields (ICS2 = 93.xyz), [1], [2]:

1) 93.010 Civil engineering in general,
2) 93.020 Earthworks. Excavations. Foundation construction. Underground works,
3) 93.025 External water conveyance systems,
4) 93.030 External sewage systems,
5) 93.040 Bridge construction,
6) 93.060 Tunnel construction,
7) 93.080 Road engineering,
8) 93.100 Construction of railways,
9) 93.110 Construction of ropeway,
10) 93.120 Construction of airports,
11) 93.140 Construction of waterways, ports and dykes,
12) 93.160 Hydraulic construction.

According - ICS, railway engineering is classified in six sub-fields (ICS2 = 45.xy0), [1], [2]:

1) 45.020 Railway engineering in general,
2) 45.040 Materials and components for railway engineering,
3) 45.060 Railway rolling stock,
4) 45.080 Rails and railway components,
5) 45.100 Cableway equipment,
6) 45.120 Equipment for railway/cableway construction and maintenance.

Standardization and innovations are compatible concepts, based on the trends of knowledge. Standards are binding: at the same time they accelerate technological and organizational changes, improve innovation performances, promote innovative products and services, provide stable references for the development of new solutions and products, [3], [4], [5].

The pace of knowledge innovating and training in professional work is very intensive. Experts are often faced, also in the fields of ICS = 45 and ICS = 93, with the problem to remain competitive, which imposes new, big challenges: Lifelong (continuous) education and maintenance of the knowledge level that is necessary for good quality performance of work. Much of this knowledge has been acquired or completely revised through practice. In this paper, a platform for knowledge innovating is consisted of ISO and SRPS standards, with the aim of knowledge modelling and management. 164 national standardization bodies from all over the world are members of ISO: industrialized countries, developing, countries in transition, [4]. Classification of Standards (ICS) includes 40 hierarchically organized fields of standardization. This paper analyzes the fields ICS1 = 45 and ICS1 = 93.

Standards facilitate and improve the methodology according to PDCA (Plan-Do-Check-Act):

- planning and systematic approach to solving problems,
- dissemination of technologies and best practices, inclusion of all the stakeholders in determining the rules for future research and development, transfer of knowledge and technologies, networking with other industries and main stakeholders in future research, access to new technologies, interoperability of its own with other compatible technologies,
- evaluations and comparison with the best ones, compatibility with other manufacturers,
- providing a platform for innovation, the use of research results [3-7], improvement of products quality, etc.

This paper presents the methodology and analysis of trends and comparisons of innovativeness intensity on the examples of standardization in two fields. The statistical analysis of the results is shown, obtained with our own Web applications [7], developed for the purpose of a comparative analysis and the valuation of

*Corresponding author: Faculty of Technical Science Cacak - University of Kragujevac, Svetog Save 65, 32 000 Čačak, Serbia; micic@kg.ac.rs

international ISO and national SRPS knowledge and obligations. On the examples of ICS1 = 45 and ICS1= 93, the indexes of quantity and knowledge value are presented. The survey also includes all the sub-fields (the total of 6, respectively 12 in the depth of each field), quantitatively, and qualitatively as well. For each sub-field, with the method of a multi-criteria regression analysis, appropriate mathematical relations of knowledge trends, together with the prediction of financial resources, were established. Although all the subfields and the field as a whole were analyzed, the comparisons were made with other fields of work and creativity (40 fields). This paper further presents the results to a lesser extent – as much as the size of this paper allows.

1.1. The objectives of the research and initial hypotheses

The starting hypotheses are proven and **objectives of the research** are implemented in the standardized fields of civil engineering and railway engineering through a PDCA spiral:

H1 - P (Plan) it is possible to predict future resources and financial needs for the valuated units of knowledge and responsibilities for each sub-field (for ICS2 = 45.xy0, 93.xyz) and in the entirety, per subcommittees and development stages of new projects (from a practical side),

H2 - D (Do) research and evaluations of knowledge units allow the formation of explicit mathematical relations, as regression lines of knowledge trends,

H3 - C (Check) it is possible to determine the clear correlations of obligations and knowledge with the intensity of valued knowledge units innovating, on the relations ISO - SRPS

H4 - A (Act) it is possible to define the relations of continuous and discontinuous knowledge innovating of individuals, with the ultimate goal of improving the teamwork (knowledge) and innovating of industrial products on the platform of ISO and SRPS standardization.

2. METHODOLOGY OF RESEARCH

For the research, analysis, systematization and presentation of results, JAVA own software is used [7] – for search of information from the Web site and ISO and SRPS standards. Without this software, the research can not be repeated, and with it, everyday analyses are possible. The software is adaptable to target Web sites for search and comparative analysis of the global ISO, [1] and local SRPS standards, [2].

The software translates all of the original On-line data into databases, in every field and sub-field of creative work. Statistical methodologies, deductive - inductive reasoning methods, predictions and future plannings are applied. With the analysis, all the results from the previous calendar years are distinguished and valuated (in this paper, all the pictures-figures with trend lines on 2014/01/01), for the researched sub-fields and the field as a whole.

2.1. Indexes of sampling and innovativeness

The aforementioned Java application (or Web application) enables efficient statistical analyses, presented through the appropriate quantity indexes of standards ISO and SRPS. In this case, in the fields for ICS1 = 45 and ICS1 = 93: **Iqs** –sampled documents (samples), of which is **Iqp** – number of current published standards (published), **Iqw** – withdrawn from use (withdrawn), **Iqu** –in different development phases (under development) and **Iqd** – deleted projects (deleted).

Parallel for ISO-SRPS, indexes of quantity/ quantity indices (Iq) are defined and specified. In a general case, for the population Iqs, the equation (1) applies:

Iqs = Iqp + Iqw + Iqd + Iqu (1)

Quantity indices (Iq), defined and determined for both ISO and SRPS, refer to: Samples (Iqs), Published (Iqp), Under development (Iqu = Std + Amd + Cor), Withdrawn (Iqw), Deleted (Iqd), **Innovations** (Iqi) – including: Standards (Std), Ammendments (Amd) and Corrections (Cor) (or, Iqi = Iqi(std) + Iqi(amd) + Iqi(cor)).

2.2. Defining trends of innovativeness

The results are graphically presented cumulatively, through the trends, and also through the original mathematical relations:

a) including the quantitative indexes (Iq), indexes of value (Iv) and time aspects, for the entire period of the study research – by years of all the editions;

b) including annual indexes of value (Iv/year and a cumulative index ΣIv), and also financial trend lines, according to the data from all the previous years (or by selecting characteristic years of XXI century) for the formation of the regression equations (for example, yics/ISO and parallel yics /SRPS function (2.1) - (2.4).

$y_{93/ISO/2007-2012/P1} = -32.14\,x + 1020$ (2.1)

$y_{93/SRPS/2007-2012/P1} = 149.6\,x^2 - 239.1\,x + 297.6$ (2.2)

$y_{45/ISO/2007-2012/P1} = -265\ln(x) + 366$ (2.3)

$y_{45/SRPS/2007-2012/P1} = 3019\ln(x) - 3774$ (2.4)

2.3. The intensity of innovativeness

The indexes of time innovativeness intensity (Iti), provide clustering by subfields of work and further periodical updating of knowledge base (KB) and knowledge base system (KBS).

The result is a timely updating of the *Knowledge Base System - KBS*, in the adequate field/subfield of creativity (KBSti/ics ≈ function (Iti)) according to the relation (3) for the model of excellence.

KBSti/ics/C ≈ ∑ (Iti/ics & PiDiCiAi) (3)

Iti periodic frequency is defined on the basis of quantitative indexes Iqi which is in a direct multi-criteria qualitative and financial dependence, according to [3]. The values of periodic checks (Check) of the research for practice: Iti = 0 - annual Check (3.1), Iti = 1 - annual-yearly Check (3.2), Iti = 2 - monthly Check, Iti = 3 - weekly Check or Iti = 4 - daily Checks (3.5), are assigned to this index [3].

$Iti = 0$, for $(Iqu_{ISO} + Iqi_{/SRPS/year}) = 0$ (3.1)

$Iti = 1$, for $1 \le (Iqu_{ISO} + Iqi_{/SRPS/year}) < 10$ (3.2)

$Iti = 2$, for $10 \le (Iqu_{ISO} + Iqi_{/SRPS/year}) \le 50$ (3.3)

$Iti = 3$, for $50 < (Iqu_{ISO} + Iqi_{/SRPS/year}) \le 250$ (3.4)

$Iti = 4$, for $(Iqu_{ISO} + Iqi_{/SRPS/year}) > 250$ (3.5)

$Iti = 5$, for $500 < (Iqu_{ISO} + Iqi_{/SRPS/year}) \le 750$ (3.6)

$Iti = 6$, for $750 < (Iqu/_{ISO}+Iqi_{/SRPS/year}) \le 1000$ (3.7)

$Iti = 7$, $(Iqu_{ISO} + Iqi_{/SRPS/year}) > 1000$ (3.8)

The goal is the establishment of <u>*Decision Support Systems*</u> (DSS) on the platform of clustered subfields of creativity.

2.4. Modelling of DSS - towards excellence

Improving the quality in a PDCA spiral means the integration of at least 12 elements of the model of excellence, for quality management (QMx12, Figure 9 in [3]). In this way, a special methodology is created that facilitates the monitoring of innovativeness trends, and a better control and management and DSS, relation (4).

DSSti/ics/A ≈ ∑ (KBSti/ics/C) & QMx12 (4)

Improving the performance of the products is possible at all stages PiDiCiAi (with distribution of the importance of all 12 elements of excellence, figure 1) from the Plan, <u>through database</u> – KBti and KBSti to DSS.

Figure 1 shows the basic factors of quality management QMx12 (1- Leadership, 2- Organization, ... 9- Resources, ... 12- Results).

For example, in the top-phase (Plan) of a key importance are: 1 - Leadership (professors, teachers, workers, customers, managers, etc.), **organizational and strategic aspects** (element 2 in Figure 1), **resources** in the form of finances (9), which make the organized civil service management more efficient and powerful in relation to individuals.

In the Do-phase, the innovativeness on the platform of standardization, as the platform of a source of knowledge is analyzed, but also the obligation - to the practice and quality of final products.

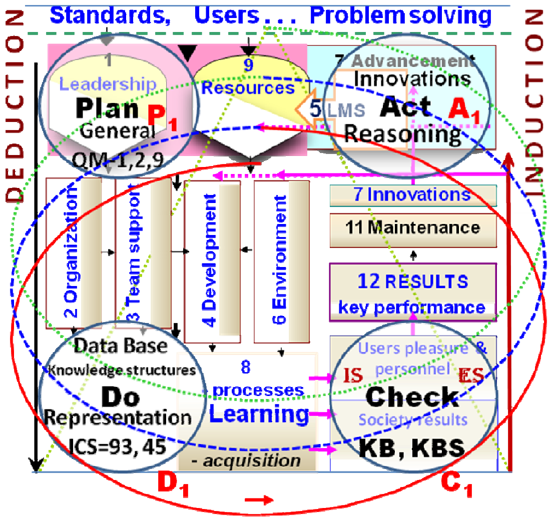

Figure 1: Influential factors in PDCA methodology of innovations

Check-phase allows clustering and comparing the intensity of innovativeness in all the fields of creativity.

Act-phase of improvement gives solutions of possible problems for a new PDCA spiral in the time dimension PiDiCiAi.

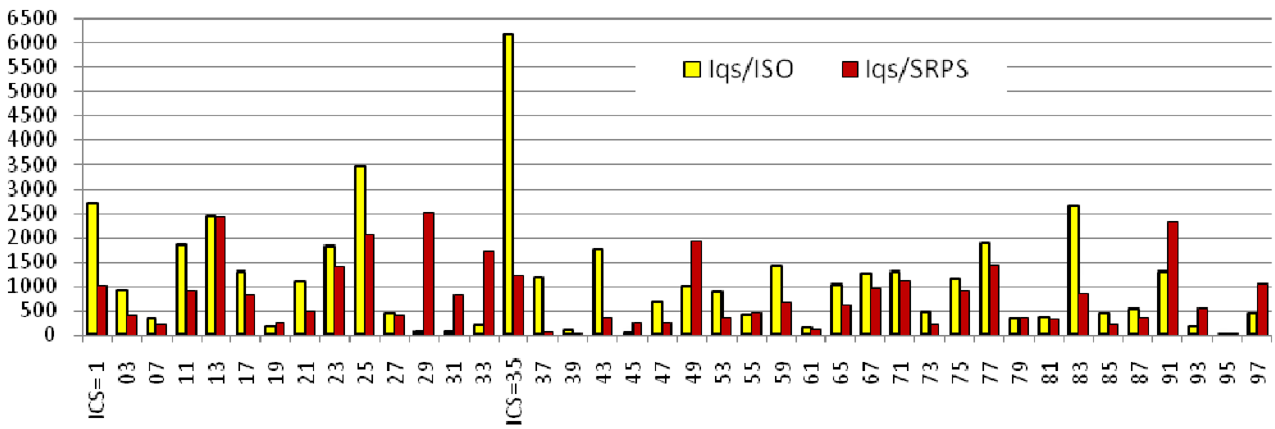

Figure 2: Comparative Analysis of IQS, ISO - SRPS populations of standards (knowledge sources, 01.01.2013)

Table 1: Quantitative indicators, comparative ISO-SRPS for ICS1 = 93 (2014/03/07- X week) (CHF ≈ 100 RSD)

I	ICS2	Samples Iqs		Published Iqp		Under development Iqu		Withdrawn Iqw		Iqp /2013	CHF Iv/2013		CHF ∑Iv	
		ISO	SRPS	ISO	SRPS	ISO	SRPS	ISO	SRPS	SRPS	ISO	SRPS	ISO	SRPS
(1)	(2)	(3)	(4)	(5)	(6)	(7)	(8)	(9)	(10)	(11)	(12)	(13)	(14)	(15)
1.	93.010	2	3	1	3	1	0	0	0	0	0	0	210	103.60
2.	93.020	70	46	52	43	18	2	0	1	0	32	0	3990	1253.18
3.	93.025	30	21	27	17	3	0	0	4	0	0	0	2326	446.55
4.	93.030	31	83	29	52	2	12	0	19	4	172	118.48	2782	1714.04
5.	93.040	4	11	4	9	0	2	0	0	2	0	34.21	458	412.29
6.	93.060	2	9	2	5	0	0	0	4	0	0	0	262	143.91
7.	93.080	28	369	26	310	2	15	0	44	83	364	1693.44	2320	6936.11
8.	93.100	1	93	1	69	0	3	0	21	29	0	633.87	74	2039.53
9.	93.110	0	0	0	0	0	0	0	0	0	0	0	0	0
10.	93.120	0	11	0	10	0	0	0	1	1	0	39.10	0	267.05
11.	93.130	0	5	0	4	0	0	0	1	1	0	23.46	0	77.43
12.	93.160	0	0	0	0	0	0	0	0	0	0	0	0	0
	∑93	168	651	142	522	26	34	0	95	120	568	2542.56	12 422	13 393.69

3. RESULTS

The results show significant quantitative indexes, as well as value indexes on the examples of ISO and SRPS standards. The original mathematical relations and trend lines were derived based on the survey results, and the comparable analyses of standardization and knowledge valuation. According to the graphs of trends, the coefficients of dependence directions of new knowledge were defined and compared to ISO – SRPS.

The results of the analyses (according to the relation (1) and cumulative population of knowledge source on the platform of standardization), can be compared for all the fields of creativity, Figure 2.

In the surveyed field ICS1 = 93, "Problem" is "obvious": ISO maintains $Iqs_{/93/ISO}$ = 168 standards (in the value of $\sum Iv_{/93/ISO}$ = 12 422 CHF, table 1). In parallel, at the same time, $Iqs_{/93/SRPS}$ = 651, $\sum Iv_{/93/SRPS}$ = 13 394 CHF (CHF ≈ 100 RSD) etc.

Table 2: Quantitative indicators, comparative ISO-SRPS for ICS1 = 45 (12/04/2014 - XV week)

I	ICS2	Samples Iqs		Published Iqp		Under development Iqu		Withdrawn Iqw		Iqp /2013	CHF Iv/2013		CHF ∑Iv	
		ISO	SRPS	ISO	SRPS	ISO	SRPS	ISO	SRPS	SRPS	ISO	SRPS	ISO	SRPS
(1)	(2)	(3)	(4)	(5)	(6)	(7)	(8)	(9)	(10)	(11)	(12)	(13)	(14)	(15)
1.	45.020	5	41	2	36	0	4	3	1	1	162	66.47	254	1349.00
2.	45.040		29		24	0	0		2	3		108.70		783.52
3.	45.060	18	265	11	188	0	51	7	26	22	0	490.08	834	6373.04
4.	45.080	11	14	6	5	4	0	2	9	0	0	0	582	128.23
5.	45.100		25		25	0	0		0	0		0		583.40
6.	45.120		7		5	0	2		0	0		0		190.00
	∑45	34	381	18	283	4	60	12	38	27	162	665.25	1670	9516.44

From the results shown in the Table 1 and Table 2, it can be concluded that the local, national knowledge and innovations are much more numerous than the global ones. In some subfields, the analysis is excluded (due to the low level of local innovativeness). It is a cluster for sub-fields of the lowest level of innovativeness (so called "annual", Iti = 0). For access to the sources of knowledge, respectively for the possession of local knowledge, it is necessary to extract $Iv_{/93/SRPS/2014.01}$ = 2542 CHF, which is approximately 4 to 5 times more than the amount of money needed to be allocated for global innovations ($Iv_{/93/ISO/2014.01}$ = 568 CHF) - yearly.

The classified subfields of the second level (ICS2) enable clustering according to the degree of innovativeness in: weekly, monthly and yearly clusters. Clustering (presented in this paper) is closer to the realization of goals in the practice rather than in a theoretical-mathematical way of clustering [8].

3.1. Double-weekly intensity of innovativeness for two parallel fields

Cumulative indexing indicators classify the field **Civil Engineering** (ICS1 = 93) into the "cluster" with a lower intensity of innovativeness – weekly. The field ***Railway Engineering*** is of a similar cumulative (ISO & SRPS) intensity of innovativeness ($Iqu_{/93}$ + $Iqu_{/45}$ = 60 + 64 = 124, towards KB).

Figure 3 shows the summary/cumulative results of the analysis of knowledge sources in the field Civil Engineering**.** We analyzed the trends of knowledge on the platform of standardization in 12 subfields of ICS1 = 93, on March 7, 2014(X weeks 2014) and presented in Fig. 3:

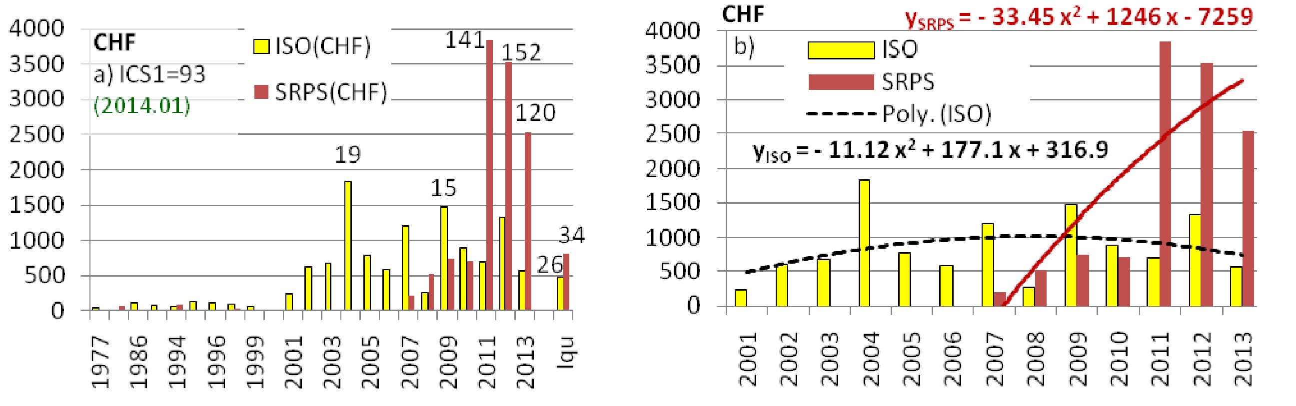

Figure 3: Examples of weekly sources of knowledge on the platform of ISO and SRPS standards (ICS1 = 93)

a) with the currently actual ISO sources since 1977 and SRPS standards since 1981, with the presentation of the valuated quantity standards in the previous years and cumulatively $\sum Iv_{/93}$ – CHF/RSD,

b) with the trend of knowledge and planned (annual) future needs ($Iv_{93/ISO/2014/poly}$ = 616.78 CHF), according to the polynomial relation (93.1).

$$y_{93/ISO/2001\text{-}2013} = -11.12\,x^2 + 177.1\,x + 316.9 \qquad (93.1)$$

The trend line can be seen both as an individual or as a team one, or on the basis of local SRPS or global ISO standardization. Here is the comparison with the trend lines on the platform of SRPS standardization. For example, according to Figure 3b, $Iv_{93/SRPS/2014/poly}$ = 3 500 CHF, respectively according to the separated relation (93.2)

$$y_{93/SRPS/2001\text{-}2013} = -33.45\,x_2 + 1246\,x - 7259 \qquad (93.2)$$

The relation (93.2) refers to the results of a trend analysis of the sources of knowledge on the basis of local SRPS standardization (a trendline of "local" knowledge).

In parallel, Figure 4 shows the summary results of the analysis of the sources of knowledge in the field ***Railway Engineering*** (ICS1 = 45). We analyzed the trends of knowledge on the platform of standardization in six sub-fields for ICS1 = 45, at the end of the XV week of 2014, and presented them in Figure 4:

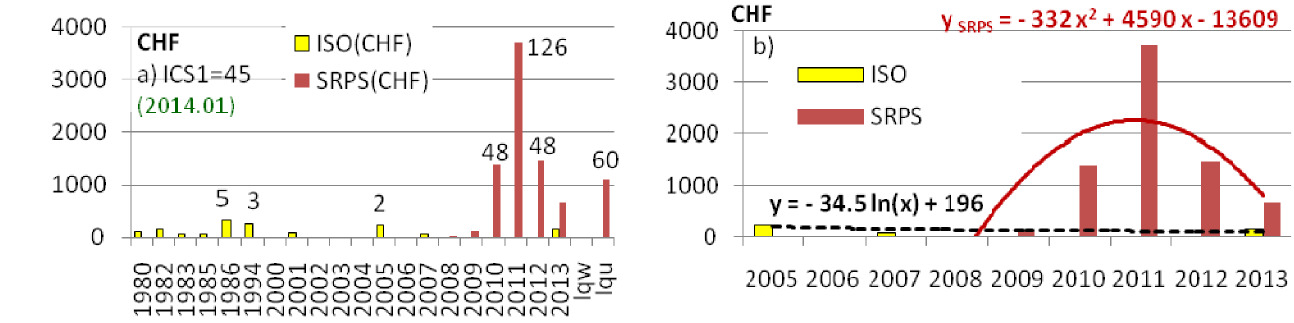

Figure 4: Examples of knowledge sources on the platform ISO and SRPS standards (ICS1 = 45)

a) with the the currently actual ISO sources since 1980 and SRPS standards since 2008, with the presentation of the valuated quantity standards in the previous years and cumulatively $\sum Iv_{/45}$ – CHF/RSD,

b) with the trends of knowledge sources and planned (annual) future needs ($Iv_{45/ISO/2014}$), according to the logarithm relation/expression (45.1).

$y_{45/ISO/2005-2013} = -34.5 \ln(x) + 196$ (45.1)

A trend line based on the local SRPS standardization, for example, according to Figure 4b ($Iv_{45/SRPS/2014}$) has a completely different trend, according to the derived relation (45.2).

$y_{45/SRPS/2008-2013} = -332 x^2 + 4590 x - 13609$ (45.2)

3.2. Subfields of the weekly intensity of innovativeness

Of the mentioned 12 sub-fields (ICS2 = 93.x, Table 1) the subfield VII belongs in a cluster of innovativeness weekly intensity. The examples of the results of the analysis are presented for VII subfield– Road engineering. Figure 5 shows the results of the analysis of knowledge sources in this sub-field for ICS2 = 93.080:

a) with the summarized analyses for all the actual sources of knowledge (ISO and SRPS) in the period from 1981 until 2014.

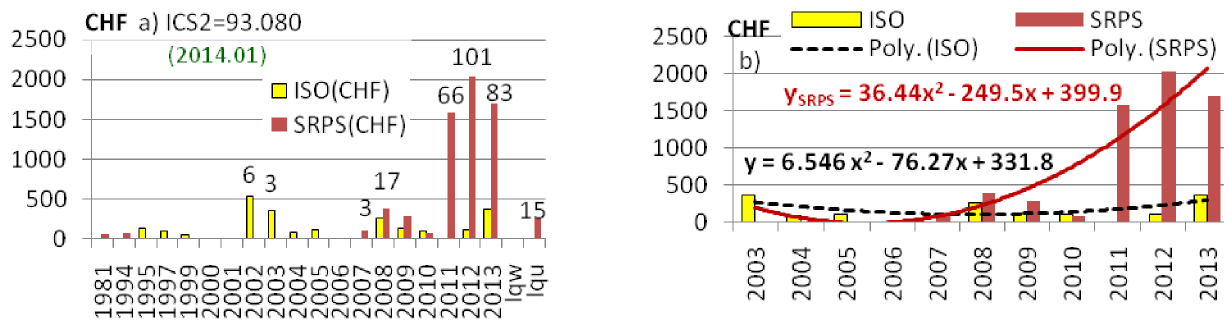

*Figure 5: Results of analysis ISO-SRPS sources of knowledge in the subfield **Road engineering** – (ICS2 = 93.080)*

b) with the trend of planned (annual) needs from y, according to or towards relations (93.3) and (93.4).

$y_{93.080/ISO/2003-2013} = 6.546 x^2 - 76.27x + 331.8$ (93.3)

$y_{93.080/SRPS/2003-2013} = 36.4 x^2 - 249.5 x + 399.9$ (93.4)

In parallel, out of the six mentioned sub-fields (for ICS1 = 45, Table 2) a cluster of weekly intensity of innovativeness includes the subfield III. This paper presents the results of the analysis for this subfield – Railway rolling stock. Figure 6 shows the results of the analysis of knowledge sources in this sub-field for ICS2 = 45.060:

a) with the cumulative analyses for all the actual knowledge sources (ISO and SRPS) in the period from1982 until 2014.

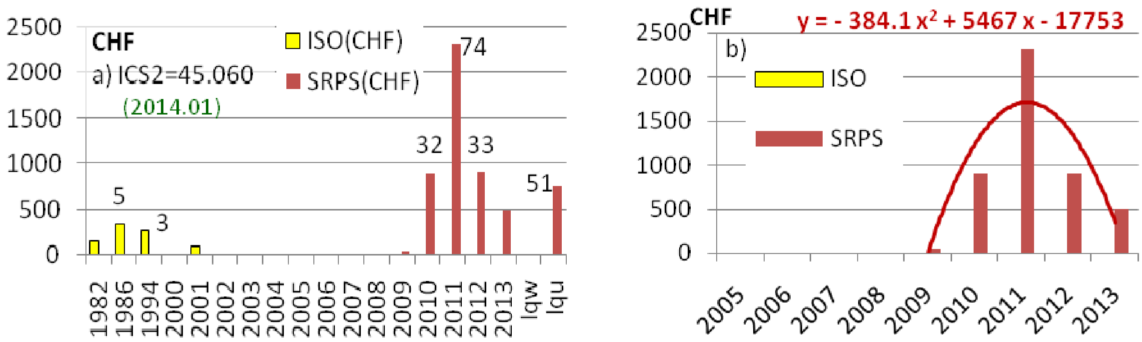

Figure 6: Results of analysis ISO-SRPS sources of knowledge in the subfield Railway rolling stock – (ICS2 = 45.060)

b) with the trend of planned (annual) needs of y, according to the relation (45.3).

$y_{45.060/SRPS/2003-2013} = -384.1x^2 + 5467x - 17753$ (45.3)

3.3. Subfields of monthly innovativeness intensity

Of the mentioned 12 sub-fields (ICS1 = 93) the cluster of monthly innovativeness intensity includes three sub-fields: the second, fourth and eighth (Table 1). Here follows a presentation of the analysis of results in the three above mentioned sub-fields.

3.3.1. Subfield Earthworks. Excavations. Foundation construction. Underground works (ICS2 = 93.020)

Innovativeness in this subfield is different, depending on the platform (ISO-SRPS, Figure 7). At the beginning of the year – 2014/01, there is no obligation from the previous century. Here are the presentations of the analysis results, in Figure 7:

a) with the cumulative analyses until 2014,

b) with a trend of planned (annual) needs of y, according to (93.5) and (93.6).

$y_{93.020/ISO/2003-2013} = -24x^2 + 309.8x + 3.9$ (93.5)

$y_{93.020/SRPS/2003-2013} = -40.8x^2 + 1143x - 4109$ (93.6)

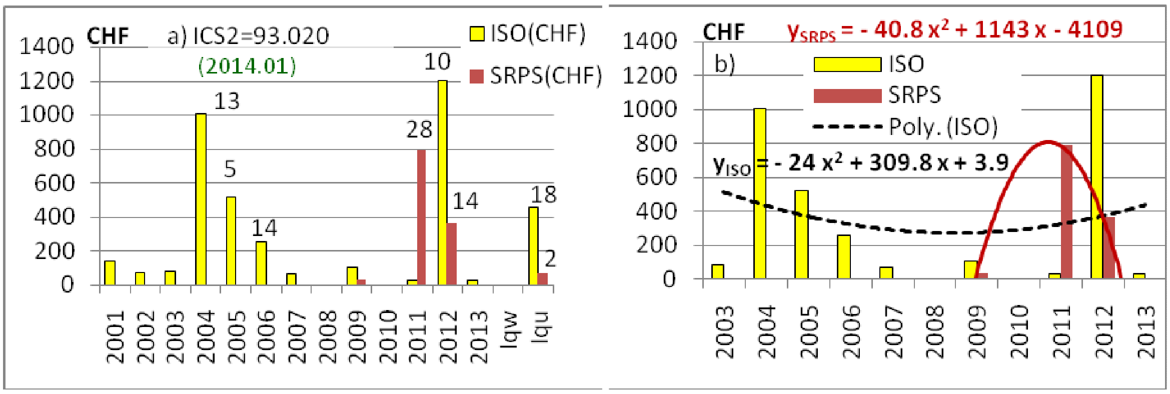

Figure 7: Results of analysis ISO-SRPS sources of knowledge in the subfield – ICS2 = 93.020

3.3.2. Subfield External sewage systems (ICS2 = 93.030)

Figure 8 shows the results of the analysis of knowledge sources in this sub-field External sewage systems, with a situation at the start of the year – 2014/01:

a) with cumulative analyses in the period from 1986 until 2014.

b) with a trend of planned (annual) needs of y, according to (93.7) and (93.8).

$y_{93.020/ISO/2003-2013} = -15.62x^2 + 193.1x - 125.8$ (93.7)

$y_{93.020/SRPS/2003-2013} = -18.96x^2 + 317.1x - 1047$ (93.8)

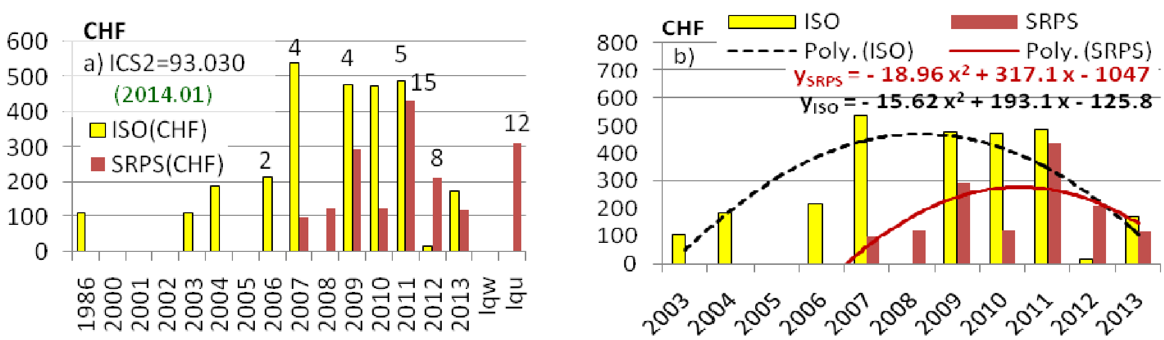

Figure 8: Results of analysis ISO-SRPS sources of knowledge - ICS2 = 93.030

3.3.3. Subfield Construction of railways (ICS2 = 93.100)

Innovativenesses (ISO-SRPS) in this subfield are significantly different. ISO platform is "invisible", Figure 9. At the beginning of the year – 2014/01, there is no obligation from the previous century. Here are the presentations of the analysis results, in Figure 9:

a) with cumulative analyses until 2014,

b) with a trend of planned (annual) needs of y, according to (93.9).

$y_{93.100/SRPS/2010-2013} = -40.8x^2 + 1143x - 4109$ (93.9)

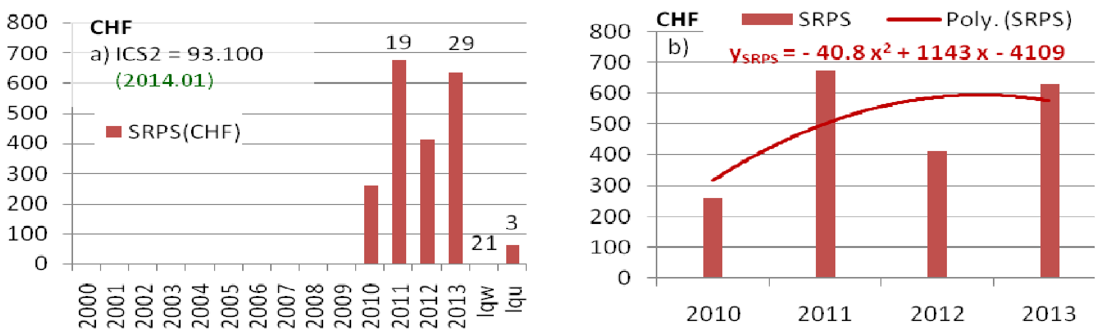

Figure 9: Results of analysis ISO-SRPS sources of knowledge - ICS2 = 93.100

3.4. Subfields of a low innovativeness intensity

Most of the mentioned 12 sub-fields (ICS2 = 93, Table 1) belong to the clusters of low innovativeness intensity (annual and zero level of innovativeness): 1, 5, 6, 9 to 12.

Also, most of the analyzed six subfields (ICS2 = 45, Table 2) belong to the clusters of a low innovativeness intensity (all the subfields except the third, ICS2 = 45.060).

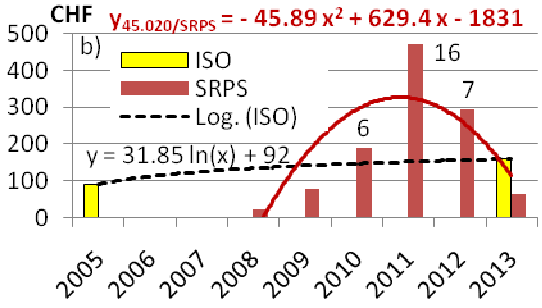

Figure 10: Results of ISO-SRPS sources of knowledge (ICS2 = 45.020)

All the valid sources in the sub-field of Railway engineering in general (ICS2 = 45.020) are from the XXI century, Figure 10.

In Figure 11, a zero intensity of ISO innovativeness is apparent (since 2007 and onwards). Obligations on the platform SRPS standards have been defined for the period 2010-2012. On these SRPS bases there is very low innovativeness intensity (Table 2, Figure 11).

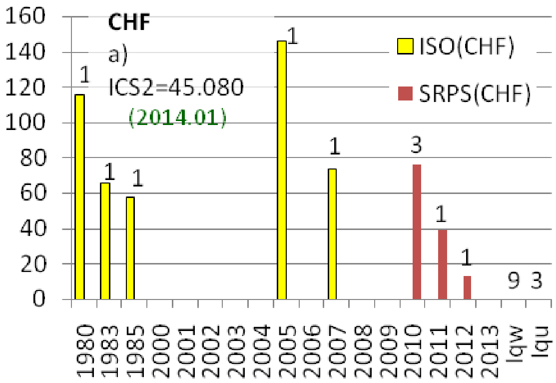

Figure 11: Results of analysis ISO-SRPS sources for subfield (ICS2 = 45.080)

4. DISCUSSION ON RESULTS

The presented methodology allows the comparison of the results with the results in other fields of work and standardized human activities.

The results in the above mentioned fields and subfields are comparable with the results of other published research. For example, in the field of Health protection and safety (ICS1 = 13), according to [9], in the field Manufacturing engineering (ICS1 = 25) according to [4], in the field Electrical Engineering (ICS1 = 29) according to [10], innovativeness in the field IT (ICS1 = 35), according to[3], in the subfield IT applications (ICS2 = 35.240), according to[11]), or for comparison with the already published results in the subfields such as Metallurgy (ICS1 = 77) according to [12]. Previous research and published analyses by certain fields ICS1 [3] to [12], partly facilitate a comparative view of the results of innovativeness towards KBS for ES and new products on the platform of standardization.

The results can be analyzed and trends of knowledge compared in all the fields (and subfields), for example, Information technologies (ICS1 = 35, [3]), Production mechanical engineering (ICS1 = 25, [4]) or Vehicles (ICS1 = 43, [5]).

The planned objectives were achieved, with possible extension of the analysis onto all standardized fields of creativity work. All the initial hypotheses H1 to H4 were proven.

The presented results in the surveyed fields and their subfields provide evidence of all the initial hypotheses with the implementation of the above research objectives (1-4) in PDCA:

1 (P) According to the shown tendencies of development projects, the publications of ISO – SRPS documents, mathematical relations were created and trendlines were presented (from a theoretical side). Also, the selection of adequate trend lines includes the aspects of practice. Based on individual knowledge about the stages of development of new projects (from a practical side), one can predict and plan future resources and financial needs per each sub-field and as a whole.

2 (D) Clear correlations of obligations and knowledge were defined with the annual trends of innovating of valued standardized sources of knowledge, on the relations ISO - SRPS by analyzed fields and subfields:

* for the field **Civil Engineering:** $Iv_{93/ISO/2013} = 568$ CHF per year, according to Table 1 (or $Iv_{/93/ISO/2014} = 616.78$ CHF, according to relation 93.1) – in continuity for ISO units of data base and knowledge (which is comparable to $Iv_{/93/SRPS/2014} \approx 3500$ CHF – according to the trends of SRPS standards in Figure 3b, or the exactly with the relation 93.2, where: $Iqs_{/93/SRPS} = 651$, $Iqp_{/93/SRPS} = 522$, $Iqu_{/93/SRPS} = 34$ etc. An approximate ratio of valued all standardized sources of knowledge is defined, SRPS according to ISO, or numerically $\sum Iv_{/93/SRPS} \approx 13394$ CHF according to $\sum Iv_{/93/ISO} \approx 12422$ CHF, at the beginning of 2014;

* for the field **Railway Engineering**: $Iv_{45/ISO/2013} = 162$ CHF per year, according to Table 2 (or $Iv_{/45/ISO/2014} = 116.56$ CHF, according to the relation 45.1) – in continuity for ISO units of data base and knowledge (which is comparable to $Iv_{/45/SRPS/2014} \approx 0$ CHF by the trends of SRPS standards in Figure 4b, or exactly with the relation 45.2, where: $Iqs_{/45/SRPS} = 381$, $Iqp_{/45/SRPS} = 283$, $Iqu_{/45/SRPS} = 60$ etc). An approximate ratio of all valued standardized sources of knowledge is defined, SRPS according to ISO, or numerically $\sum Iv_{/45/SRPS} \approx 9516$ CHF according to $\sum Iv_{/45/ISO} \approx 1670$ CHF, at the beginning of 2014;

3 (C) The presented and proven level (or intensity) of IT innovativeness (the highest, according to [3]) is comparable to the analyzed fields in this paper (Section 5.1 to 5.7). On the examples of standardisation in all the fields of creative work (figure 1) and with comparative indices, correlations are obvious of quantity indexes (Iqs) and the innovativeness indexes (Iti).

4 (A) The results allow the predictions of future resources, financial needs for valuated units of knowledge and obligations by each sub-group and as a whole, by

subcommittees and development stages of new projects (from a practical side). The relationships are defined between the continuous and discontinuous (cumulative) innovating of the knowledge of individuals, in relation to a team work:

* for the field **Civil Engineering:** $\sum Iv_{/93/ISO}$ = 12422 CHF cumulative, without continuous innovating, for all the standardized ISO and SRPS knowledge in all the above mentioned subfields (or collective), which is comparable to $\sum Iv_{/93/SRPS/} \approx$ 13393 CHF cumulative, without continuous innovating, for all the standardized local knowledge in all the above subfields (local or national - state ...). Thus, the relation/ratio of the overall standardized units of a knowledge base in the researched field (ICS1 = 93), SRPS according to ISO = 13393 according to 12422 (or 1.08 according to one, u CHF), cumulative, for all the standardized knowledge;

* for the field **Railway Engineering:** $\sum Iv_{/45/ISO}$ = 1670 CHF cumulative, without continuous innovating, for all the standardized ISO and SRPS knowledge in all the above mentioned subfields (or collective), which is comparable to $\sum Iv_{/45/SRPS/} \approx$ 9516 CHF cumulative, without continuous innovating, for all the standardized local knowledge in all the above mentioned subfields (local or national - state ...). Thus, the relation/ratio of the overall standardized units of a knowledge base in the surveyed field (ICS1 = 45), SRPS according to ISO = 9516 according to 1670 (or 5.7 according to one, in CHF), cumulative, for all the standardized knowledge.

The results show some significant details of the analyzed standardized units of knowledge in the subfields, from a time aspect. For example, $Iqp_{/93/2013/SRPS}$ = 120, $Iqp_{/45/2013/SRPS}$ = 27. These and other details KBS (from a Check - phase) are necessary for DSS in the Act - phase.

Compared with other papers, dealing with the issue of existence of a standard framework for creation of standards [13], this paper deals with the possibilities of access to standards, with a goal of their implementation for innovating the knowledge in PDCA - [14].

Unlike the papers [15] and [16], which present a comparative analysis of two advanced ICT nations, this paper gives the analyses on the relations of the standards of one nation (SRPS) in parallel or comparatively with the global ISO.

5. CONCLUSIONS

Based on the overall results and indicated analyses in the fields ICS1 = 93 and ICS = 45, and in the corresponding subfields, we conclude about the intensity of innovativeness (quantitatively and qualitatively). Subfields with a higher intensity of innovativeness were parallelly and high valued. Comparison with high-ranked IT fields and mechanical engineering, allows making conclusions for the purpose of necessary continuous innovating of the individual knowledge of each professional.

1 (P) According to the presented trends of development of new projects (from a practical side),the possibilities of predicting future resources, financial needs were researched and presented. From the valuated sources of knowledge, there are the resulting obligations per each of the sub-fields and on the whole (iqu for ISO and SRPS), regardless of the trend lines as mathematical relations.

2 (D) Based on the presented methodology and according to the presented analyses, on the relations of ISO- SRPS platform, as well as for broader comparisons with other fields, there were established mathematical relations and regression trend lines. These were defined: the indices of values (Iv), quantitative indices (Iq): sampled statistics (Iqs), publications (Iqp), the development of new standards (Iqu), decommissioning (Iqw) and deletions (Iqd).

3 (C) For the analyzed sub-fields and the fields as a whole, obvious are the relations and trends of global and local knowledge (on the platforms ISO and SRPS). Access to innovations is far away from individuals, as evidenced by the ratios of value coefficients of the annual innovations (Iv/year), as well as the total value ($\sum Iv$).

4 (A) Providing adequate improvement of knowledge in the processes of products innovating is based on the standards that should be generally available as soon as possible. The model of KBS improvement is based on the defined intensities of innovativeness and elements of QM in PDCA. A time dimension of improvement in the quality spiral is determined by the intensity of innovativeness of a target field / subfield.

ACKNOWLEDGEMENTS

The work presented here was supported by the Serbian Ministry of Education and Science (project III 44006, http://www.mi.sanu.ac.rs/projects/projects.htm#Interdisciplinary).

REFERENCES

[1] ISO/IEC, ISO Store, Standards catalogue, 13: Environment, Healt Protection And Safety, http://www.iso.org/iso/home/store/catalogue_ics.htm, accessed: 2014/03/07 (2014)

[2] ISS - Institute for Standardization of Serbia, Advanced search: http://www.iss.rs/, http://www.iss.rs/standard/advance_search.php, accessed: 2014/03/07 (2014)

[3] Ž. Micić, M. Micić and M. Blagojević, “ICT innovations at the platform of standardisation for knowledge quality in PDCA”, Computer Standards & Interfaces, Vol. 36 (1), pp. 231–243 (2013), http://dx.doi.org/10.1016/j.csi.2013.03.002

[4] Ž. Micić and M. Tufegdžić, “Knowledge trends in the subfields of manufacturing engineering at the platform of ISO/IEC standardization”, Metalurgia International, Vol. XVIII (7), pp 45-50, ISSN 1582-2214 (2013)

[5] Ž. Micić and M. Demić, “Knowledge standardization in road vehicle engineering”, TTEM, Vol. 7 (3), pp. 1281-1288 (2012)

[6] STAIR, “An Integrated Approach for Standardization, Innovation and Research”, CEN, www.cencenelec.eu/news/publications/Publications/STAIR.pdf, accessed: 2014/03/07

[7] Ž. Micić and M. Micić, “Java-software for ISO/IEC standardisation analisys and knowledge assurance in information technology examples”, Technology, Informatics And Education for Learning And

Knowledge Society, 5th International Symposium, Novi Sad, Serbia, pp. 310-322 (2009)

[8] Cluster Analysis, “Ward’s Method”, © 2004 The Pennsylvania State University: http://sites.stat.psu.edu/~ajw13/stat505/fa06/19_cluster/09_cluster_wards.html

[9] Ž. Micić and N. Stanković, “Knowledge trends at the standardization platform of environment, health protection and safety”, 16th International Conference ICDQM-2013, June 27-28. Belgrade, page 519-529 (2013)

[10] Ž. Micić, M. Vujičić and V. Lazarević, “Analysis of Knowledge Base Units within Standardized Electrical Engineering Subfields”, Acta Polytechnica Hungarica, Vol. 11, No. 2, 41-60 (2014)

[11] Ž. Micić, M. Blagojević and M. Micić, “Innovation and knowledge trends through standardisation of IT applications”, Computer Standards & Interfaces, 36(2), 423-434 (2014)

[12] Ž. Micić and N. Stanković, “Knowledge and innovations trends in metallurgy subfields within standardization platform”, Metal. Int. XVIII (8) 154 – 160 (2013)

[13] J. Saltzman, S. Chatterjee and M. Raman, “A framework for ICT standards creation: The case of ITU-T standard H.350”, Information Systems, Volume 33, 285–299 (2008)

[14] T. A. Walasek, Z.Kucharczyk, D. Morawska-Walasek, “Assuring quality of an e-learning project through the PDCA approach”, Archives of Materials Scinence and Engineering, Volume 48, Issue 1, 56-61 (2011)

[15] N. Igari, “How to successfully promote ICT usage: A comparative analysis of Denmark and Japan”, Telematics and Informatics, (2012) http://dx.doi.org.proxy.kobson.nb.rs:2048/10.1016/j.tele.2012.10.001

[16] K. Luu and G. J. Freeman, „An analysis of the relationship between information and communication technology (ICT) and scientific literacy in Canada and Australia”, Computer & Education, Volume 56, Issue 4, 1072–1082 (2011)

Alteration in Mechanical Properties of Porcelain Passing by a Bending Process

Cristiano Fragassa[1*], Ana Pavlovic[1] , Pier Paolo Conti[2], Olivera Erić[3]
[1]Department of Industrial Engineering, University of Bologna, Bologna (Italy)
[2] R.T.C. Ricerca Tecnico Ceramica, Faenza (Italy)
[3] Faculty of Mechanical and Civil Engineering in Kraljevo, University of Kragujevac, Kraljevo (Serbia)

Grès Porcelain stoneware is a ceramic with a compact, hard, coloured and non-porous body. A very prominent patented technology permits to obtained bent porcelain tiles as innovative solutions for a modern architecture. This technology is grounded on a proper combination of heavy machining by cutting tools and secondary firing in a kiln. This paper investigates the alteration in behaviour of porcelain passing by the bending process comparing the mechanical proprieties by flexural, compression and impact tests.

Keywords: Ceramic Industry, Grès Porcelain, Secondary Firing, Experimental Tests,

1. INTRODUCTION

1.1. Grès Porcelain materials

Grès Porcelain stoneware is a ceramic with a compact, hard, coloured and non-porous body. The word "grès" means that the ceramic body of the tile is extremely vitrified, that is to say compact, hence the exceptional great resistance. The result is a lean clay body [1], little refractory, fired in a kiln (at 1200-1400 C°) until it reaches a non-porous vitrification and a complete water-proofing.

The raw materials used for the composition of mixtures from porcelain tiles are of two types [2]: clayey raw materials, which give plasticity to the mixture, and complementary raw materials (not plastic) that include melting minerals and those used for compacting or with structural functions. Of the first group are the clay minerals, as kaolinite and montmorillonite-illitics. The melting minerals, however, are feldspathoids and feldspars, talc, eurits, pegmatite; those more refractory to structural function are quartz and quartzite in gender.

Table 1, Range of percentages for raw elements in most common mixtures of Grés Porcelain stoneware

Elements	**% (in weight)**
SiO_2	**64 – 68**
Al_2O_3	**28 – 21**
$Fe_2O_3 + TiO_2$	**0.3 – 1.0**
$CaO + MgO$	**0.1 – 0.9**
Na_2O	**3.0 – 4.5**
K_2O	**1.4 – 2.9**
Lost in fire	**3.4 – 7.8**

ISO 13006:2012 defines terms and establishes classifications, characteristics and marking requirements for ceramic with special attention to water absorption [1].

1.2. Production technology for Grès Porcelain

The porcelain tiles are obtained by the process of sintering of ceramic clays, feldspar, kaolin and sand. These raw materials are first ground (processed in ceramic slips), then finely atomized until a homogeneous powder particle size suitable for the pressing.

The cooking process takes place at a temperature of about 1150-1250 ° C in long kilns, up to 140 m, where the raw material is gradually brought to the maximum temperature, maintained there for about 25-30 minutes, and cooled gradually to room temperature. The cooking process causes the vitrification of the dough, attributing the typical mechanical and chemical characteristics. During cooking various deformations occur on the matter previously pressed [2]. The size shrinkage after firing is around a 7%.

Grès Porcelain records values of water absorption (i.e. the amount of water that, in particular conditions, the slab can absorb) less than 0.5%, which is among the lowest of all the products for floor and wall.

From this feature also derives the highest degree of resistance to bending [5], that represents the maximum stress that the material, which is subjected to an increasing bending action, can tolerate before breaking down.

The vitrification also leads to a very high abrasion resistance, or the resistance that the surface opposed to the measures connected with the movement of bodies, surfaces or materials in contact with it.

1.3. Advantages in use of Grès Porcelain material

Main advantages in use of Grès Porcelain stoneware for quality architecture and building materials can be summarized as:

- Impact strength and stress resistance
- Wear resistance
- Scratching resistance
- Resistance to frost
- Resistance to chemicals
- Stain resistance

Corresponding author: viale Risorgimento 2, 40133 Bologna, Italy, cristiano.fragassa@unibo.it

2. MODELLING CERAMIC TILES

2.1. Bending technology for Grès Porcelain

Approximately 750 millions square meters of grès porcelain stoneware are produced every year in the World, mainly by Italy (>40%), China, South Asia and Spain, to be used inside or outside buildings [6]. These elements are (almost) entirely commercialized in flat slabs.

On the contrary, a very prominent patented technology [7] permits to obtained practical solutions of bended porcelain tiles, perfect for modern architecture and design. This technology is grounded on a proper combination of machining by cutting tools and secondary firing in a kiln. The line for bending consists of a special kiln, specifically designed to bend the tiles laying down special supports (Fig. 1), and an equipment set which prepares the bend/fold and finishes the piece. This innovative system allows tiles to be bent at variable angles as desired. Prior to this, similar processes were confined to the glass industry. Yet while glass can be modelled when it is still relatively "cool", doing the same with ceramic involves considerably higher temperatures.

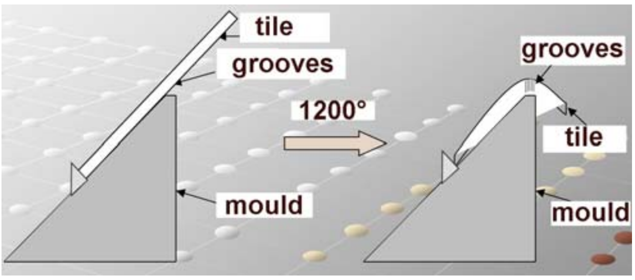

Figure 1: Bending process

Entering in details of the bending technology, the "original" material, usually in the shape of ceramic tiles, is progressively and slowly heated up. This process, known as pyroclastic deformation [8], involves subjecting the tile to an annealing at a temperature lower than that of sintering, between 1160 °C and 1210 °C, but with longer times (160-270 minutes from cold to cold) and thermal gradients smaller compared to traditional cooking. The appearance of the visco-plastic processes within the material at high temperatures allows the tile to recline to support even only due to the force of gravity, allowing to obtain the bending of the tile. This heating phase has to be thermally controlled with high accuracy (Figure 2).

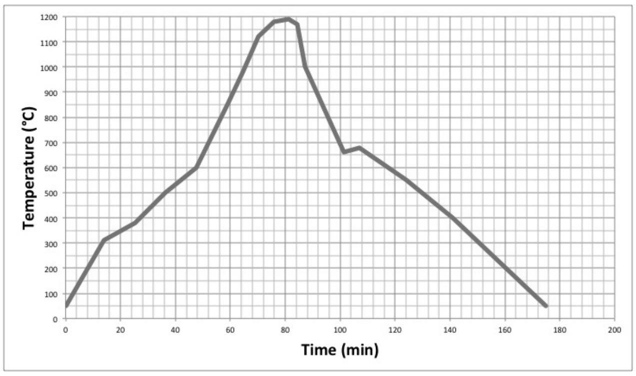

Figure 2: Temperature profile during the bending process

Each profile of temperature is developed and optimized by experience with the aim at permitting to realize each particular angle and curvature. In this way, it is possible to avoid the most relevant phenomena of modification that can occur during the phase of heating and cooling, including geometrical variations or changes in the color of ceramics.

The forming process of the tiles is controlled, in addition to the temperature, also by the application of incisions on the back of the tile [7] that act as guides for bending and the use of media of different shapes and sizes depending on the format to be obtained. The incisions are realized by the appropriate machinery and good precision; the positions and the depth of the incisions are studied by experience on the basis of the type of tile and the type of curvature requested.

As fundamental step of the production cycle, the material has to be placed on special shaped supports (Fig. 3), functionally similar to moulds, that slide inside a roller kiln able to calibrate the thermal period to which the tile must be subjected. Once the preset temperature is reached, the mass of the ceramic material, as described, deforms and adapts perfectly to the template with which it is in contact (Fig. 4). When the tile is cold, it is finished to final dimensions by grinding disc or water-jet.

Figure 3: Tiles before bending process

Figure 4: Tiles after bending process

2.2. Advantages in use of bended porcelain tiles

The potential for the porcelain tile bending technology is enormous and cover large part of the entire world ceramic industry. Ceramic slabs can be shaped to meet specific needs. For example, architects could be able to order specially-shaped tiles to perfectly fit their projects. Main point of application is in the house and its corners. A single ceramic item that has been bent at 90° can, for instance, be used to cover an entire step (Fig. 5, on the left): similarly, it can also act as a floor tile-cum-wall tile to provide an alternative to traditional skirting.

Figure 5: Advanced solutions and design permitted by bending tiles: steps and stairs (left); b) bench seats (right)

These advanced solutions for buildings offer many practical advantages as:

- less installation time and less working on site
- greater area security thanks to the no edges
- better design in products (Fig. 5b4)
- cut of stocks of special pieces
- possibility to differentiate stocks.
- more hygiene for public buildings

Referring to the last aspect, bent tiles eliminates the edges and interstices between wall and floor where dust and dirt often gather. This technical solution is ideal for hospitals and other places where cleanliness and hygiene are fundamental. And it could preserve the positioning of ceramics on the market. In fact, in all Europe, ceramic are going to be progressively banned from hospitals and other public buildings (as schools, airports, shopping centres, etc.) with the aim at eliminating interstices, as referred by UE Rule 852/2004 for hygiene into public buildings [8].

It is worth noting that ISO 13006:2012 [1] is not applicable to decorative accessories or trim, such as edges, corners, skirting, capping, coves, beads, steps, curved tiles. Consequently, ISO 13006:2012 is not applicable to bent ceramic tiles; then, specific rigor has to be reserved to the production and installation of these elements.

Between other features, the necessity to reinforce the bent area of the tile, weakened by grooves, is an important aspect. An efficient recently patented solution fills grooves with a filling material, compatible with the material of which the tile is made. Then it covers the grooves with a flexible strip of incombustible refractory-material, anchors the strip to the surface of the tile, heats the area to be bent up to the softening temperature of the area itself and, finally, cools the modelled tile thus obtained [1].

3. EXPERIMENTAL ANALYSIS

3.1. Materials and Methods

This paper investigates the alteration in the mechanical behaviour of a specific grès porcelain stoneware passing by the pyroclastic deformation as required inside the bending process. Results are obtained comparing mechanical proprieties and resistance by experimental tests. This mechanical characterization was realized on a commercial fine porcelain stoneware, produced by FloorGress and branded as FloorTech®.

Table 2, Technical specifications for grès porcelain stoneware declared by the producer

Specification reference		**Test method**	**Reference value**	**Declared value**
	Water absorbed	ISO-10545-3	<0,5%	< 0,1 %
	Breaking strength	ISO-10545-4	≥1300 |Newton	> 1700
	Bending strength		>35 N/mm^2	> 40

Experimental tests were realized according to the ASTM standards with the aim at evaluating the mechanical properties related to the flexural, compressive and impact behaviour. For each of these 3 tests, two different testing sessions were arranged, involving samples from ceramic tiles before and after the bending process.

To minimize the variability of unexpected factors, samples were obtained by a same lot of ceramics tiles and process parameters (es. times and temperatures) were maintain as constants during the bending process. Adding, many effort at reducing uncertainty, specific attention were used to extract samples from similar zones in the tiles and also to limit the residual stress (related, e.g., to tool cutting processes).

3.2. Experimental Equipment

Test were realized using an INSTRON mod. 8033 servohydraulic testing frame fatigue machine, with a load capacity up to 250 kN. It was equipped with a load cell of 2kN or 25kN according to the specific test and provisional range of loads. Specimens were loaded in control of displacement. Data were acquired by MTS Test Star IIs 2s Digital Controller with an acquisition rate of 10Hz. Grips and fixtures were selected according to the standards.

3.3. Measures and results

For each specimen, tests and calculations permitted to determinate:

– the force-displacement diagram
– the breaking loads and displacements
– the breaking strength and deformation
– the stress-strain diagram

and related mean values/diagrams for samples. These experimental evidences were used to verify alteration in the mechanical proprieties of samples.

4. FLEXURAL TESTS

4.1. Determination of flexural breaking strength

Flexural breaking strength of all ceramic tiles were evaluated in accordance with ISO 10545 [10] by a three point flexural test. It permits the determination of the breaking load, breaking strength and modulus of rupture of a tile by applying a bending force at a specified rate to the centre of the tile, the point of application being in contact with the proper surface of the tile (Fig. 6).

Specifically, the minimum number of test specimens for each sample, diameter of rods, thickness of rubber, overlap of tile beyond the edge supports, were determined according to ISO 10545 (Tab. 3 and 4).

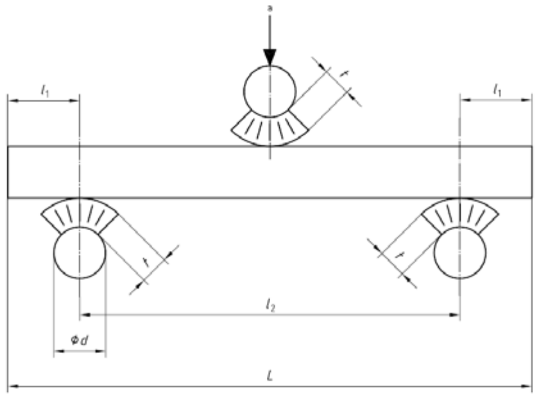

Figure 6: Application of loads to test specimen

Table 3, Technical specifications for application of loads

Diameter of rods	Distance between rods	Overlap of tile beyond supports	Rate of application of force
mm	mm	mm	mm/s
d = 14	50	l_1 = 25	0.005

Table 4, Technical specifications for specimens

Length	Width	Thickness	Samples	Specimens
mm	mm	mm	n.	n.
L = 100	20	9.5	2	7

Specimens were installed on the testing machine with specific care to the correctness of positioning (Fig. 7).

All test on specimens were performed in a single experimental session with the same acquisition rate (10Hz). Loads were applied in control of displacements. Rate of application of force was equal to 0.005 mm/s. According to the ISO 10545,

- breaking load (F_{bl}) is the force necessary to cause the test specimen to break as read from the pressure gauge
- breaking strength (F_{bs}) is the force obtained by multiplying the breaking load by the ratio (span between support rods)/(width of the test specimen)
- bending strength or modulus of rupture (S_{Fbs}) is the quantity obtained by dividing the breaking strength by the square of the minimum thickness along the broken edge (on the base of a rectangular cross-section).

Experimental measures are reported in (Tab. 5, 6); stress-strain curves are reported in (Fig. 8, 9).

Figure 7: Installation of specimens

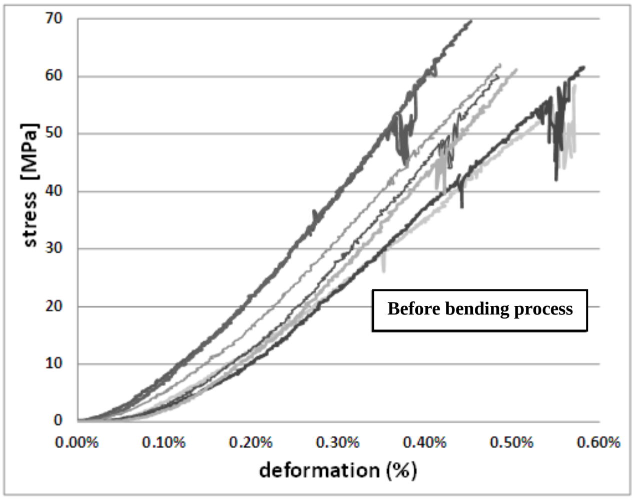

Figure 8: Stress – strain flexural diagrams for specimens extracted before the pyroclastic deformation

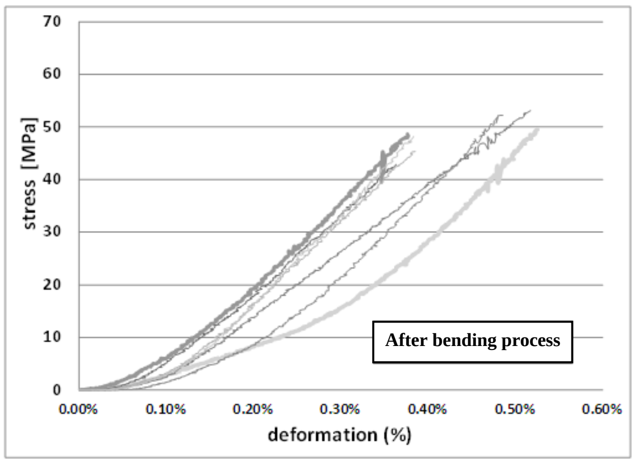

Figure 9: Stress – strain flexural diagrams for specimens extracted after the pyroclastic deformation

Table 5, breaking loads, displacements, strengths and deformations observed from specimens extracted before the pyroclastic deformation of bending

	Load	**Strength**	**Stress**	**Strain**	**Elastic Modulus**
Spec.	kN	kN	MPa	%	MPa
I	1.452	3.630	61.186	0.509	12017
II	1.442	3.605	62.130	0.489	12704
III	1.481	3.703	62.831	0.417	15078
IV	1.668	4.169	69.572	0.454	15312
V	1.442	3.605	60.261	0.495	12174
VI	1.462	3.654	61.608	0.586	10510
VII	1.403	3.507	58.474	0.576	10154
mean	**1.479**	**3.696**	**62.294**	**0.504**	**12564**
st. dev.	*0.087*	0.217	*3.505*	0.061	*2015*

Table 6, breaking loads, displacements, strengths and deformations observed from specimens extracted before the pyroclastic deformation of bending

	Load	**Strength**	**Stress**	**Strain**	**Elastic Modulus**
Spec.	kN	kN	MPa	%	MPa
I	1.158	2.894	48.197	0.383	12572
II	1.010	2.526	45.373	0.416	10894
III	1.158	2.894	48.674	0.413	11779
IV	1.177	2.943	52.286	0.489	10687
V	1.177	2.943	53.082	0.529	10042
VI	1.010	2.526	42.863	0.365	11749
VII	1.167	2.918	49.492	0.529	9348
mean	**1.123**	**2.806**	**48.567**	**0.446**	**11010**
st. dev.	0.077	0.193	3.605	0.068	1110

4.2. Comparing the flexural behaviour

Experimental measures were used to compare mechanical flexural characteristic of grès porcelain before and after the pyroclastic deformation of bending process (Tab. 7). Compared graphs are also detailed (Fig. 10, 11).

Data and graphs shows that the bending process provokes:

- a significant reduction in mechanical resistance (22%) showed by breaking loads and modulus of rupture
- a moderate diminution in ductility and elasticity emerging as reduction in breaking deformation (-11.4%) and elastic modulus (-12.4%)
- a very limited increase in variability of characteristics

At the same time, even considering this alteration, it is evident that:

- breaking strength and bending strength (modulus of rupture) positively exceeds the limits reported in international standards (Tab. 8).

Table 7, deterioration of breaking loads, displacements, strengths and deformations provoked by the pyroclastic deformation of bending

	Load	**Strength**	**Stress**	**Strain**	**Elastic Modulus**
	kN	kN	MPa	%	MPa
Δ	-0.356	-0.890	**-13.728**	-0.001	-1554
%	24.1	24.1	22.0	11.4	12.4

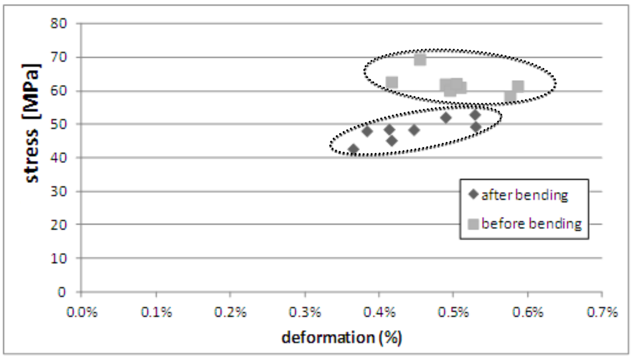

Figure 10: comparing the ultimate stress and strain for specimens extracted after and before the pyroclastic deformation of bending

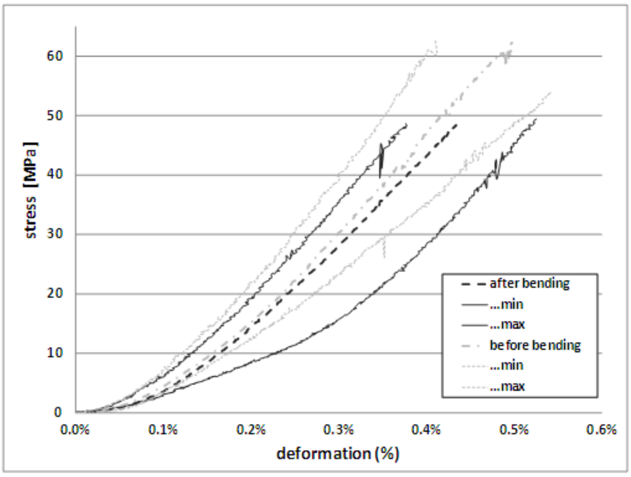

Figure 11: comparing stress – strain diagrams for (some) specimens extracted after and before the pyroclastic deformation of bending

Table 8, comparing breaking strength and bending strength with international standards

Specification reference ISO-10545-4		**Before bending**	**After bending**	**Reference value**
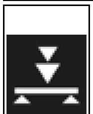	Breaking strength	3696	2806	> 1300N
	Bending strength	62	48	> 35MPa

5. IMPACT TESTS

5.1. Determination of impact resistance

The UNI EN ISO 10545-5 [10] specifies a test method for determining the impact resistance of ceramic tiles by measuring the "coefficient of restitution between two impacting bodies". The determination is obtained by dropping a steel bail from a fixed height onto the test specimen and measuring the height of rebound. In particular, the coefficient of restitution is defined as the relative velocity of departure divided by the relative velocity of approach for the steel ball dropped.

This norm was created with the intent to compare ceramics by a standard procedure. This is the sole procedure referring to impacts on ceramics.

At the same time, it appears not appropriate for a larger utilisation. Specifically it intends to measure the capability of materials, laid on a rigid support, to react to a specific impact (fixed as energy). But it is hard to obtain by ISO 10545-5 in-depth information as, e.g., the minimal impact energy able to create a crack on specimen.

5.2. Drop-weight impacts

With the aim to obtain information on material behaviour respect to an increasing level of impact energy, impact tests were realized by a drop weight methodology.

The advantages of using an instrumented drop-weight impact test are: (1) the initiation and development of damage during impact may be identified from a recorded impact force-time history curve; (2) several impact parameters can be examined; and (3) wide range of incident kinetic energies may be achieved by changing drop height and impactor mass.

5.3. Drop-weight experiments

The experiment consisted of series of drop-weight impact tests performed on ceramic specimens extracted before and after the pyroclastic deformation.

The impact tests were carried out using a drop-weight machine equipped with an electro-optic device, for measurement of initial and final velocity of the impactor, and with a piezoelectric load cell attached to the impactor, for measurement of contact force history. The impactor head had the shape of hemisphere with 12.7mm of diameter. Involuntary multiple collisions were avoided by means of an electromagnetic braking system. A detailed description of the machine can be found in [13]. The impactor mass was 1.22±0.01kg and located to a specific height for its free-fall on specimen.

For each selected height, the free-fall impact speed was easily calculated as $V_0=\sqrt{2gh}$. Considering that the initial impact speed can be only smaller than free-fall impacts peed, it is easy to conclude that the impacts in the experiment may be considered as low-velocity impacts, and treated as quasi-static mechanical processes.

Impacts were repeated with impactor released from the same height until penetration occurred in specimens. Not all specimens were penetrated by impactor.

N. 20 specimens were tested by drop-weight, half extracted before and half after the pyroclastic deformation.

5.4. Comparing the impact behaviour

By the analysis of experimental data from drop-weight tests (Tab. 9), it was possible to estimate between 150 and 155 centimeters the height from which the impactor created a visible crack on ceramic specimens. This value is almost the same for the material before and after the pyroclastic deformation. At the same time, a difference in behavior could be observed. Specimens extracted before the additional thermal treatment on material better resisted to multiple impacts (up to 9 impacts without cracks), when impact energy was slightly lower than the limit of resistance. After treatment, the material was not able to resist to similar impacts and cracks arrived within the 2nd impact. It means that pyroclastic deformation also reduce the resistance to multiple impacts. These considerations remain almost the same if moving the attention from impact height to impact energy.

Table 9, impact tests with heights (in cm.) used for drop-weight and number of repetitions for each specimen extracted before and after the pyroclastic deformation. Some specimens had no crack after multiple impacts (*)

Before bending			**After Bending**		
Spec.	***Height***	***Times***	***Spec.***	***Height***	***Times***
I	500	x1	I	145	x1
II	200	x1	II	140	x2
III	150	x1	III	140	x2
IV	130*	x5	IV	130	x2
V	140	x2	V	145	x2
VI	140*	x6	VI	145	x2
VII	150	x2	VII	150	x3
IIX	145	x2	IIX	155	x1
IX	145	x4	IX	155	x1
X	145*	x9	X	155	x1

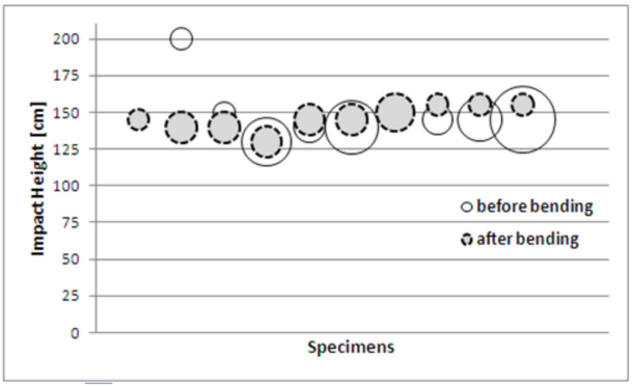

Figure 12: impact tests with heights used for drop-weight. The dimension of circles is proportional to number of ripetitions on specimens

6. COMPRESSIVE TESTS

6.1. The importance of compressive strength

The compressive strength represents the resistance to crushing of a material subjected to load for crushing. Its assessment is of great interest to the materials that are used with structural functions and should therefore be able to withstand considerable loads (i.e. stone and ceramics as common bricks and refractory bricks). Bent tiles are always more frequently as functional components (e.g. steps in stairs). An estimation of compressive strength is mandatory.

6.2. General aspects on tensile and compressive strengths

Ceramics are relatively fragile . The tensile strength of ceramic materials is very variable, ranging from very low values, of less than 0.7 MPa , up to about 7000 MPa of some types prepared under carefully controlled conditions . In any case, a few ceramic materials have the tensile strength exceeding 170 MPa. Moreover, the ceramic materials show a great difference between their tensile and compression; typically the compressive strength is 5 to 10 times higher than the tensile strength, which shows the main differences in advanced ceramic materials [10]. Furthermore, many ceramic materials are hard and have a low toughness (low resistance to dynamic stress), due to the ion-covalent bonds.

6.3. General aspects on hardness and compressive strength

There is strict relation between elastic modulus and hardness of a material and its mechanical strength. The upper limit of the compressive strength of a material is defined as the stress to which it yields (i.e. deformation for sliding along the crystallographic planes). According to this definition of stress, a micro-plastic failure is in relation with the micro-hardness, measured by the Knoop or Vickers methods. In the case of various ceramic materials, the compressive strength corresponds to ½ or ¾ of the stress of failure, calculated by dividing micro-hardness for 3. According to this formulation, a draft estimation for compressive strength can be obtained considering that hardness for Grès Porcelain stoneware, measured by Vickers method, is commonly between 750-830 HV. Consequently, the compressive strength is expected between 125-250 MPa.

6.4. Compressive tests on ceramics

There are not standards or common guidelines used to evaluate the tensile or compressive behavior of ceramics. UNI EN ISO 10545, detailed in 16 parts, specifies a test methods for determining several aspects of ceramics. Compression is not mentioned.

At the same time, the tensile strength of a simple compression in the stone coul be evaluated using the procedure described in the ISO 10545/3 [10], by a standardized vertical compression of specimens (the same as the procedure for the determination of the elastic tensile modulus for stones).

In this paper a complete experimental session for compressive test on ceramic specimens by ISO 10545/3 was also implemented (in completion for other tests). A preliminary evaluation of testing method is proposed.

6.5. Limits respect to the application of standards

N. 2 samples of 10 specimens were realized (from ceramic tiles before and after the bending process). Each sample included N. 10 cubic specimens with nominal dimension a 10x10x10mm. This dimension is lower than the minimal size declared in ISO 10545/3, but represents a possible upper limit in height according to the real dimensions of ceramic tiles

Before testing for compressive strength (Fig. 13), the dimensions of the specimen were measured in several positions and the mean values calculated. The cross-sectional area of the loading faces were calculated. Three measurements of dimensions were made in each of the orthogonal directions (x, y, z). The accuracy of measure was around 5% (higher than the 0.5% limit expressed in ISO 10545/3). Several specimens were ejected considering a relevant difference in dimensions respect to the designated size. The average area of each cube loading face was calculated.

Figure 13: Compressive tests on ceramic specimens

6.6. Stress-strain diagram for fragile materials

The correct determination of the breaking strength by a compressive test in the case of fragile material is not a quite simple task. It has to take in count of additional aspects, as, e.g., the specific failure mechanism (if evident by observations).

In (Fig. 14) are reported stress-strain diagrams representing three different situations:

a. a negligible discontinuity in slope (at 138.5MPa) in a constantly ascending ramp. It represented marginal breaks inside the specimen (e.g. corners) with loss of fragments, evident by observations. Even if facing minor damages, since that moment, the specimen lost its integrity.
b. a discontinuity in slope (at 183.0MPa) with an evident downfall (~20MPa) and a new ascending ramp with similar grade. It represented a significant break in microstructure continuity, also evident observing the specimen and its cracks during the application of load;
c. a complex diagram with a sequence of discontinuities in slope, after the first one (at 171.0MPa), up to the last downfall (to the zero-stress). It represented the complete sequence of multiple fractures up to the definitive crumble.

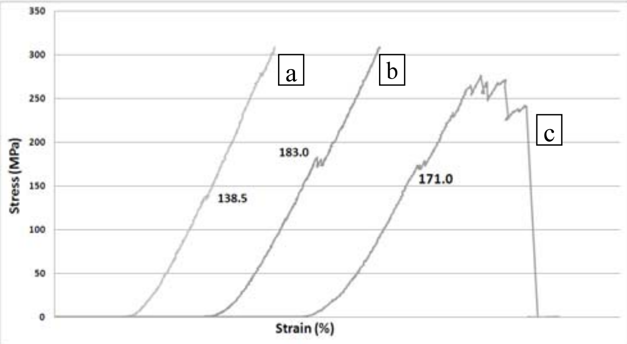

Figure 14: Example of different stress-strain diagrams for compressive tests.

6.7. Determination of flexural breaking strength

Compressive tests were performed on ceramic specimens extracted by tiles before and after the bending process. Measures were realized in a single experimental session. Testing machine was electronically limited with an upper of 25kN in loads (around 200Mpa on speciments). Not all measures releaved by experiments were appropriate for an univocal understanding. Some experimental measures had to be rejected since uncertainty on the failure mode.

A preliminary analysis of specimens is reported in (Fig. 15, 16) and (Tab. 9) where breaking strengths for are evident. In the case of specimens after bending, compressive strengths were in accordance with the expected values (as estimated in [6.3]).

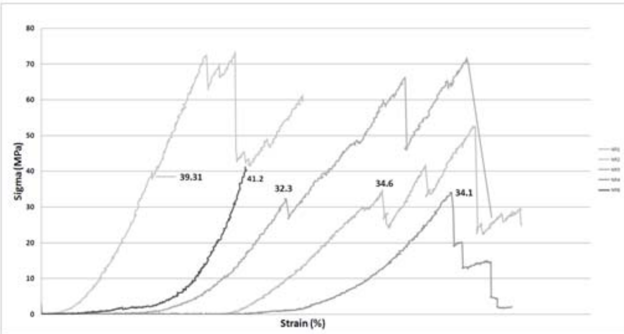

Figure 15: Compressive stress-strain diagrams for specimens extracted before the pyroclastic deformation of bending process

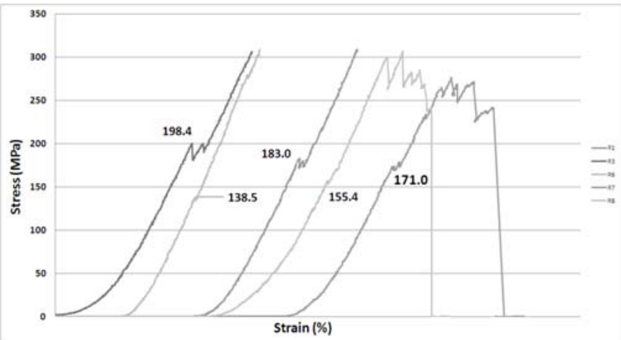

Figure 16: Compressive stress-strain diagrams for specimens extracted after the pyroclastic deformation of bending process

Before bending			After bending		
Specimen	*1st break*	*last break*	Specimen	*1st break*	*last break*
I	39.3	73.2	I	198.4	>300
II	32.3	71.5	II	138.5	>300
III	34.6	52.9	III	183.0	>300
IV	34.1	34.7	IV	155.4	300
V	-	41.2	V	171.0	275
mean	**35.01**	**54.7**	*mean*	**169.3**	>300
	MPa	*MPa*		*MPa*	*MPa*

Table 9, compressive breaking strengths from specimens extracted before and after the pyroclastic deformation

6.8. Comparing the compressive behaviour

Experimental measures were used for a preliminary comparative analysis of compressive behaviour of grès porcelain before and after the bending process. Data suggested that the additional heating treatment, related to the bending process, provokes a net change in the material behaviour. Specifically, referring, for instance, to the stress/strain diagrams:

- lower values for peaks
- smoother curves
- steeper slopes
- less variability in shape

are graphical effects of ceramic pyroclastic deformation.

These evidences could be explained with a general reduction in the grade of brittleness of material. The additional heating treatment, even if realized at lower temperature respect to the sintering, could be relevant in a better compacting of fundamental the elements.

The first breaks, usually evident at very low stress, around 32-45 MPa for untreated materials, and referred to marginal fractures, disappear by this secondary treatment. The zigzag in stress-strain curve, representing the sequence of partial breaks in a nevertheless improving level of stress, also disappear in treated materials. These "new" ceramics appear able to provide a more constant resistance to compressive forces. In other terms, instead to react by means of partial cracks to an increase of loads, after the pyroclastic deformation, the material responds in a more homogeneous way. As a consequence, compressive strengths increase and different trends appear in diagrams.

6.9. Limits of the analysis

For all the experimental evidences listed in the previous paragraph, it could be possible to find theoretical explanations. Some of these justifications could be also related to results from the state of arts. At the same time, there is no any logical reason able to explain the enormous difference between the values of compressive resistance for materials before and after the thermal treatment. The previous characterisations limited this difference to 25%.

Without further evidences, it is obligatory to accept that ISO 10545/3 is not even appropriate for a very draft estimation of compressive behavior of ceramic tiles

7. CONCLUSIONS

Grès Porcelain stoneware is a largely used ceramic material. A very interesting technology permits to obtained innovative solutions by bended porcelain tiles. This technology is able to add new functions to tiles. But a better knowledge on material proprieties is required.

This paper investigated the alteration behaviour of porcelain passing by the bending process comparing mechanical proprieties by bending, compression and impact tests. Specifically, it is possible to affirm that the bending process reduces the mechanical resistance, in the meaning of flexural breaking loads and flexural modulus of rupture, for about 22%. A moderate diminution in elasticity also emerges, together with a change in the behaviour of material, as an increase in fragility during the flexural tests (static response), This information is also confirmed by the impact tests (dynamic response). At the same time, no significant reduction in the resistance to impact is evident.

Adding, this paper highlighted the current limit of international standards if applied to the new class of ceramics that are emerging. At the moment standards consider tiles in their simple role of "covering elements for pavement". While Grès Porcelain tiles, with benefit and advantages, are going to assume a more complex profile of potential applications. Far away from advanced ceramics, bent tiles start to feel its family of ceramics to little. Compressive tests are not ruled by standards, but would be useful for a correct design, use and installation of bent tiles. Even the impact tests, largely used to compare ceramics in a standard way, are not appropriate for in-depth comprehension of mechanical proprieties. The paper started an investigation on the possibility (or the limits) to applied standards coming from other fields of applications. As preliminary results, drop-weight standard methodology appears already appropriate to provide interesting results on impact behaviour of materials or components. On the contrary, compressive test methodologies, largely applied with success in other situations (e.g. on concrete), cannot be used since insuperable limitations.

ACKNOWLEDGEMENTS

Research presented in this paper was supported by the Emilia Romagna Italian Region inside the programme "*From Productive Districts to Technologic Districts - Actions for straightening and orienting the technological productive districts in Emilia Romagna*" and, specifically, for the Materials and of Technologies for Ceramics. The related R&D project, named as "*Setup of products in ceramics with additional functionalities*", is realized by a network of small medium enterprises (*Levikurve, R.T.C. Ricerca Tecnico Ceramica, Keser Italia*), in collaboration with the *University of Bologna* and under the supervision on *Confindustria*, the main organisation representing Italian manufacturing and services companies.

REFERENCES

[1] "Ceramic tiles. Definitions, classification, characteristics, evaluation of conformity and marking" UNI EN ISO 14411:2012 (including UNI EN ISO 13006)

[2] M. Dondi, G. Ercolani, M. Marsigli, C. Melandri, C. Mingazzini, "The Chemical Composition of Porcelain Stoneware Tiles and its Influences on Microstructure and Mechanical Proprieties". Interceram 48 [2], pp. 75-83, (1999)

[3] A. F. Gualtieri, "Thermal Behavior of the Raw Materials Forming Porcelain Stoneware Mixture by Combined Optical and In Situ X-Ray Dilatometry", J. Am. Ceram. Soc. 90, pp 1222-1231, (2007)

[4] A. Salem, S. H. Jazayeri, A. Tucci, G. Timellini, "Influence of Firing Temperature and Soaking Time on Sintering of Porcelain Stoneware Tiles". CFI-Ceram. Forum Int. 80 [9], E66, (2003)

[5] Yu. G. Tkachenko, D. Z. Yurchenko, V. K. Sul'zhenko, G. S. Oleinik, and V. M. Vereshchaka, "Temperature Effect on Bending Strength of Hot-Pressed Boron Carbide Materials", Powder Metallurgy and Metal Ceramics, Vol. 46, Nos. 5-6, 2007

[6] A, Serri, L. Luberto, "23th Statistical Survey on Grès Porcelain", Confindustria Ceramica, Sassuolo (Italy), (2011)

[7] R. Fabbroni, "A Process for Modeling Ceramic Tiles", Patent N. WO/2003/800302, Applicant: Keser Diva Design S.p.A. Faenza (Italy), (2003)

[8] A. M. Bernardi, D. S. Demedeiros, H. G. Riella, "Pyroplasticity in Porcelain Tiles". Mater. Sci. Eng. A427, pp. 316-318, (2006)

[9] "Regulation (EC) 852/2004 on the hygiene of foodstuffs"; Official Journal of the European Union, L 226, 25 June 2004; Volume 47; ISSN 1725-2555

[10] P.P. Conti, "An Improved Method for Bending Ceramic Tiles", Patent N. WO/2014/064720; 01/05/2014; Applicant: Brevetti 2000 Srl, Italy (Italy), (2014)

[11] "Ceramic tiles — Part 4: Determination of modulus of rupture and breaking strength", UNI EN ISO 10545-4:2004

[12] "Ceramic tiles — Part 5: Determination of impact resistance by measurement of coefficient of restitution" , UNI EN ISO 10545-5:1996

[13] Zucchelli, A., Minak, G., Ghelli, D. Low-velocity impact behavior of vitreous-enameled steel plates (2010) International Journal of Impact Engineering, 37 (6), pp. 673-684.

[14] W. A..Dunlay, C. A. Tracy, P. J. Perrone "A Proposed Uniaxial Compression Test for High Strength Ceramics", U.S. Army Materials Technology Laboratory, MTL TR 89-89 (1989)

[15] "Testing hardened concrete — Part 3: Compressive strength of test specimens", UNI EN ISO 12390-1 2002

System for Monitoring the Welding Operation

Olivera Erić Cekić[1*], Radomir Jovičić[2], Branko Zrilić[3], Nebojša Pantelić[3]
[1] University of Kragujevac, Faculty of Mechanical and Civil Engineering, Kraljevo
[2]University of Belgrade, Faculty of Mechanical Engineering Inovation centre, Belgrade,Serbia
[3]FIN IMPORT doo, Belgrade, Serbia

Production of welded structures is complex process which includes a range of activities from construction design to its functional testing and documentation certifying its quality. In order to provide steady and sufficient high quality of welded constructions, standards group EN ISO 3834 prescribes the requirements that must be fulfilled by companies dealing with the production of these structures. The most sensitive operation in the process of welded structures is welding process itself. During the welding process in welded joints can be inserted errors that can later lead to catastrophic construction failure. Therefore, the controls of the welding operation are of particular importance.

This paper presents a system for monitoring, i.e. for continues control of preparation operations for welding and welding process, which significantly reduces the possibility of defects in welded joints, immediately shows the deviation from the given welding parameters, reduces repairs, displays the data on the effectiveness of the device for welding or the entire product line, and makes it easier to identify "bottlenecks" in production.

Keywords: welding process, quality, defects,welded joints, monitoring system

1. INTRODUCTION

Today, reliability and safety standards regarding product and facilities have become increasingly stringent. Due to the fact that welded structures play a significant role, either as finished products (bridges, halls) or as integral parts of other products, machinery, appliances and equipments (boilers, tanks, reactors), the increasingly stringent reliability and safety requirements are set in order to prevent failures and accidents with catastrophic consequences.

The production of welded structures is a complex process that in addition to the quality of structural, technological and project solutions also must ensure optimal conditions for the preparation, production and control of these structures. Therefore, investors around the world access a comprehensive evaluation of technological capabilities and eligibility requirements of manufacturers for their production quality. Standards were introduced in order to harmonize the criteria for this control [1, 2].

These standard requirements, developed for manufacturers of welded structures, depend on the accountability and function, with reference to the required level of construction quality. Since the achieved level of welded structures quality strongly depends on the conditions in which the welding is performed, the standards define the requirements that a manufacturer must meet in order to be recognized by its ability to produce certain types of construction. Enforcement of these requirements is verified by an authorized certificated organization with competent personnel and necessary equipment. Authorized personnel check and evaluate the compliance according to the applicable regulations and provide documentable evidence during testing and evaluation of a facility's capabilities.

According to the Authorized National Body for Company Certification ANBCC (Office-CERT) and European Federation for Welding, Joining and Cutting (EWF) [3], Serbia currently have a small number of certified companies. Due to this fact, Serbian companies leg far behind in terms of competitiveness on global market. The reason for this is that companies in Serbia do not meet the requirements of the standards in the terms of welding quality; therefore the requirements that are defined in standards cannot be met [1, 2].

Contract quality requirements are reviewed in order to prove that a contract is signed within its capabilities i.e. that the manufacturer has the resources and capability to meet the delivery commitments and complete them on time to specification. In order to bind a company to manufacture welded structures, it is desirable and necessary that a manufacturer possess a certificate and credential of qualifications for the production of welded structures, especially when it comes to sophisticated structures such as: pressure vessels, steel structures, lifting equipment, process and energy facilities, shipbuilding, railways, etc. In order to obtain the certificate, the manufacturer must undergo assessment and certification by an authorized organization, e.g. body.

At machinery assessment, it is also carefully verified whether a manufacturer of welded structures has a sufficient number of competent personnel for planning, execution, monitoring and testing of the welding industry (welders, supervisors, technologists, designers, welding coordinators), production area, production and testing equipment, control equipment, transportation equipment, equipment for mechanical and heat treatment, surface protection, etc.

While assessing the manufacturer suitability, the flow of information, materials and documentations accompanying production from conclusion of the contract to the delivery point, should be verified as well. Each of these items must be carefully verified and documented during evaluation process.

*Corresponding author: University of Kragujevac, Faculty of Mechanical and Civil Engineering, Kraljevo, olivera66eric@gmail.com

2. IMPORTANCE OF DAMAGE VALUE IN WELDED JOINTS

Defects in welded joints, or, as referred in literature [4, 5], imperfections in welds, are an integral part of these joints. It is not realistic to expect that welded joints are defect-free welds, no matter how carefully they were welded.

Defects in welding joints can be metallurgical defects and weld formation defects. Metallurgical defect can occur due to wrong selection of raw material, inadequate process control in melting stage of welding joints and an excessive degree of mixing base with an additional material. These defects are manifest in a lack of strength and plasticity, low toughness, high transition temperature in toughness and insufficient resistance of joints against corrosive environment. Defects that can occur during the formation of the welds are results of irregular-shaped weld and insufficiently welded cross section. For example, these defects occur during insufficient or excessive weld reinforcement, excessive convex fillet weld and excessive weld penetration, sharp transition between layers of weld while mixing base material, not penetrated or concave root surface, porosity and cracks.

Defects occurred during formation of weld may reduce the load-bearing cross-section of weld, and cause local concentration of voltage. When voltage becomes greater than tensile strength of the material which surrounds defects, the increased heat inputs cause the cracks formation. It can be concluded that the probability for crack occurrence in welded joints is greater in areas where welding defects exists. Figure 1 and 2 shows the stress concentration coefficients around defects in welded joint of steel S 235JRG2, 10mm thick. Additional material is SG 2 material (M.A.G Welding)[6]. The stress state is determined with the use of Finite Element Method (FEM). Figure 1 show edge cut with depth of 0,5 mm.

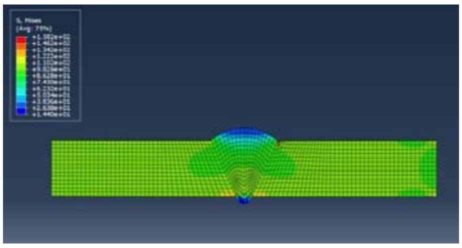

Figure 1: Stress state, edge cut

Figure 2 shows the same welded joint, only now with no penetration on the root, 1mm depth. When tensile stress of 100MPa is acting perpendicular to axis of the weld and thus on the direction of no penetrated root extend, bottom of this defect suffers tensile stress of 214 MPa. Displayed values of heat input on defects represents in fact stress concentration factors, so we can conclude that the local voltage in the vicinity of the defect will be higher if the acting voltage is high.

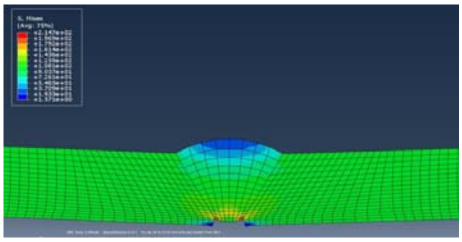

Figure 2: Stress state, no penetration on the root

This penetration depth in edge is acceptable according the highest required quality level for welded joints, as shown in Figure 5. The Figure shows, if tensile stress of about 100 MPa at the edge cut root is acting perpendicular to the axis of the weld and thus to the axis of the edge, the tensile stress of 158 MPa occurs.

The influence of different types of defects on stress concentration factor size is diverse and depends on shape, size and frequency of the defects. Defects with sharp picks, e.g. cracks, small bond strength, no penetration on the root, have higher stress concentration factor then rounded defects, e.g. pores formation, submerged weld surface or weld root. Therefore, with same voltage applied, a stress state ahead of the crack peak is greater than a stress state in vicinity of one pore. In the presence of cracks, fractures of welded joints occur at lower applied voltage than in the presence of pores. Increasing defect dimensions reduces the load-bearing cross-section of the joint and increases the stress concentration factor induced by the presence of defects, which all together results in acting stress reduction which lead to breakage of the welded joint. Increasing frequency of defects also reduces the load-bearing cross-section of the joint and reduces the distance between an individual defects. Reducing the distance can cause stress field overlap in front of some defects, resulting in increased total voltage in zone between defects. This facilitates the breakage of material between defects and leads to their merger, which increases the existing defects and further increases the stress concentration factor.

Therefore, in order to save the stress exerted joint from breakage, it is necessary that welded joint is sharp edge defect-free (cracks, lack of fusion and no penetration in the root) and that the present defects are smaller and less frequent. On the other hand, some types of defect with sharp edges (no penetration in the root, lack of fusion) and the presence of the larger size of defects and their frequency can be tolerated in case of less strained joints.

3. EFFECT OF WELDING PARAMETERS ON DEFECT APPEARANCE

In order to receive welded joints with required, equable and repeatable level of quality, the Welding Procedure Specification (WPS)[7] is made prior to the commencement of the welding for each type of welded joints. These specifications represent an instruction which contains all necessary information required for welding certain type of joint. These data are obtained trough previous testing and welding of larger number of samples. Consistent implementation of Welding Procedure

Specification guarantees that defects in joints, unacceptable to the required quality level, will not occur.

Prior to the commencement of welding, some of defects that occur in welded joints [4] can be avoided with groove preparation proper control, additional material, shielding gas and qualification e.g. proper training of welders, prior to the commencement of welding. However, a number of defects are formed during the welding operation (insufficient welding, lack of fusion, weld reinforcement, submerged weld surface or narrowness of the weld) and take place due to changes in amperage, voltage, welding speed and uses of an electric arc. Figure 3 and 4 shows the surface of joints welded with submerged arc welding procedure (SAW) on steel P 460NL1 thick 14 mm, in manufacturing process of storage tanks for liquid oxygen. Figure 3 a) shows the defect of insufficient penetration in groove weld occurred due to decrease of electric arc voltage in a short time interval during welding. Figure 3 b) shows the defect of insufficient penetration in groove weld occurred due to increased welding speed at some point during welding.

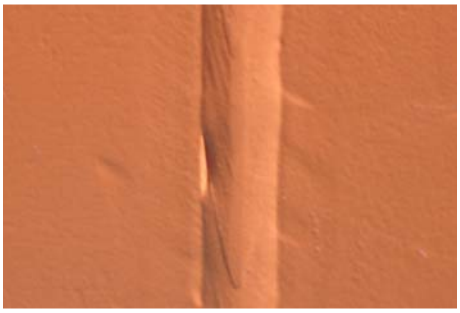

Figure 3: Insufficient penetration in groove weld a) Voltage dropping during welding

Figure 3: b) Increased welding speed during welding

The welding amperage strength and voltage can be monitored on the welding device instruments during welding process, Figure 4. These parameters can be changed during welding process. This is especially a characteristic of M.I.G./M.A.G welding process where changes in welding amperage and arc voltage occur at any stage during welding process, Figure 5. Therefore, it is impossible to get a valid images of an average values of used welding parameters and the given parameters overdraft that can be the cause of the defects in welded joints by visual control of welding parameters on instruments.

Figure 4: Amperage and arc voltage welding

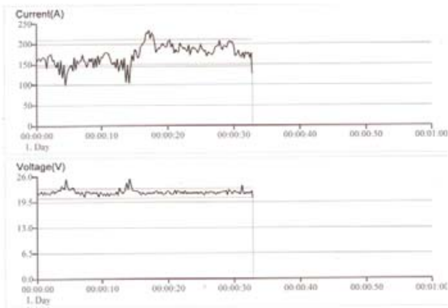

Figure 5: Changes in welding amperage and arc voltage on welding device display during the M.I.G welding process

4 MONITORING SYSTEM FOR ARCQ

Welding standards groups, SRPS EN ISO 3834 and SRPS EN 1090, requires adequate verification that welders with appropriate qualifications have performed welding process using legally regulated additional and supplementary components, and required welding parameters.

a)

b)

c)

d)

Figure 6: a)Data entry for welders b)WPS list entry c)Additional components are not appropriate according to WPS list entry d)Appropriate additional components are used according to WPS list entry

For the majority of welded joints there is no records and evidence they are welded in accordance with welding specifications.

Until now, there was no system that could provide listed records and thus confirms that a derived welded joint meets required quality.

ArcQuality System [8] measure and register welding parameters, register qualifications of welders and additional and supplementary components, and collected information are compared with corresponding information of welding joints from WPS specification list.

This solution provides the necessary welding quality and doesn’t allow variation that may lead to quality problem.

ArcQ System works in the following way:

Before the welding process starts, the welder is connecting to the ArcQ system using a handheld scanner, figure 6. By scanning the identification card barcode, the personal data and professional qualifications of welders are loaded into the system, Figure6 a). Next, the WPS list of specifications for joints to weld barcode is scanned and loaded into the ArcQ system; figure 6 b) and figure 7. The ArcQ system compares the qualifications of welders with required qualifications in accordance with WPS list. This ensures that the qualifications of welders corresponding to WPS list of specifications for joints to weld and that qualification is verified. Selected additional components and shielding gas is also scanned, compared and confirmed, Figure 6 c). The scanner screen, with information accompanied with bright colors, confirms or denied the consistency of existing data from WPS list of specifications, thereby guaranteeing that the welder is informed and, if necessary, required to take corrective measures to avoid the bad quality of welding joints.

Data on the welding parameters are recorded by sensors attached to the welding machine and ArcQ system, Figure 8.

Figure 7: Scanning bar code of WPS List

Figure 8: Sensor for registration of welding amperage and voltage welding

Companies that operate in multiply locations can organize remote sensing database using an innovating system for information exchange - “cloud” based helpdesk, Figure 9. Owing to ability to enter the system and access the information from any location, it is possible to maintain a quality and production management from single place.

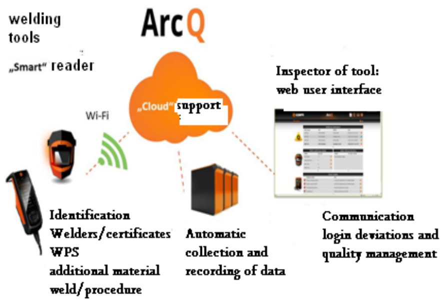

Figure 9: ArcQ System, mode

This gives the possibility to inspector, who controls the large number of welders from a single place, to intervene via web user interface (Figure 10 a) and b)) if corrective measures are necessary or not taken/missed in welding workplace.

Figure 10: ArcQ System, user interface appearence

a) Information on the work of all welders encompassed with ArcQ System

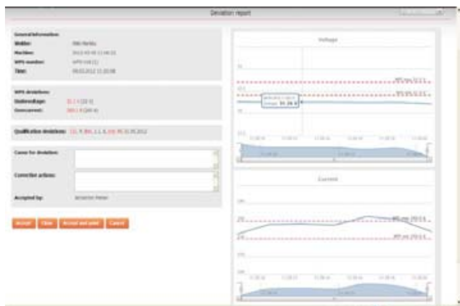

Figure 10: b) Information on the work of one welder

6. CONCLUSIONS

Defects or irregularities in welded joints are integral parts of these joints, and cannot be avoided. Their presences cause a local concentration, i.e. by increasing the voltages which, even when the voltage is in construction, it doesn’t exceed calculated voltage that can lead to structure failure.

Defects in welded joints occur due to deviation from the given welding parameters. Some of these deviation can be promptly detected and thus prevent the occurrence of the corresponding defects. However, some deviations, such as amperage and voltage deviations during M.I.G/M.A.G welding process, cannot be traced due to the fast and frequent changes. Defects, which can occur in this situation, are detected by testing joints with nondestructive method after the welding or are not detected at all. The system warns and registers any deviation from the given parameters and significantly reduces the probability of defect occurrence in welded joints.

ArcQ is monitoring system, i.e. for continuous control of preparation operations for welding and welding process, which significatly reduces the possibility of defects in welded joints and immediatle display the deviation from the given welding parameters, reduces repairs, display data of effectivness directly from welding device, or entire product line, and makes it easer to identify „botllenecks" in production.

REFERENCES

[1] The ISO 3834 (1÷5)-Quality requirements for fusion welding of metallic materials - Part 1: Criteria for the selection of the appropriate level of quality requirements (ISO 3834-1:2005), Part 2: Comprehensive quality requirements (ISO 3834-2:2005); Part 3: Standard quality requirements (ISO 3834-3:2005);Part 4: Elementary quality requirements (ISO 3834-4:2005); Part 5: Documents with which it is necessary to conform to claim conformity to the quality requirements of ISO 3834-2, ISO 3834-3 or ISO 3834-4 (ISO 3834-5:2005)

[2] The EN 1090 is a series of European standards that regulate the fabrication and assembly of steel and aluminium structures, EN 1090-1:2009+A1:2011 CEN/TC 135: Requirements for conformity assessment for structural components (CE Marking), EN 1090-2: 2008+A1:2011 CEN/TC 135: Technical requirements for the execution of steel structures, EN 1090-3:2008 CEN/TC 135 Technical requirements for the execution of aluminium structures

[3] www.ewf.be

[4] Welding and allied processes - Classification of geometric imperfections in metallic materials - Part 1: Fusion welding (ISO 6520-1:2007) CEN/TC 121.

[5] Welding - Fusion-welded joints in steel, nickel, titanium and their alloys (beam welding excluded) - Quality levels for imperfections (ISO 5817:2003)

[6] Catalogue electrodes Jesenice, Jesenice, Slovenia, (2010).

[7] Specification and qualification of welding procedures for metallic materials - Welding procedure specification - Part 1: Arc welding (ISO 15609-1:2004)

[8] Kemppi Arc System 2.0, New Module ArcQuality – самая функциональная система управления качеством сварки, Kemppi ProNews 2012, Kemppi Oy, Finska, p.p. 8 -10 (2012).

Investigation of Steel Properties for Side Frames of Scraper Conveyor

Diana Glushkova[1*], Ye. Voronova[1], Valentina Tarabanova[1], LarisaRak[1]
[1]Kharkiv National Automobile and Highway University, Kharkiv (Ukraine)

On the basis of comparison of steel properties type BRK, 18HGT and 20HGNR for side frames of scraper conveyors pans it was determined that steel BRK does not meet the required level of strength and there was recorded a large spread of properties across the section. The transition to stainless steel was scientifically justified. Of the two investigated types of steel 18HGT 20HGNR the higher set of properties is provided by steel 20HGNR, at quenching of which in soft cooling medium - oil – there is recorded a high level of properties. When welding the side frames of pans made of steel 20HGNR with other parts of the pans, the softening of the subject to wear portions is less than 2 ... 3 HRC.

Keywords: Side frame of the pan, Hardness, Strength, Welding, Hardening, Section.

1. INTRODUCTION

Premature failure of scraper conveyor pans reduces the amount of coal production and condition emergency situations.

Studies of the worn surfaces of pans showed that the pans, and particularly the side frames, are subjected to abrasion during operation. Hardness of the material determines the amount of mutual penetration of asperities of the rubbing surfaces. The authors of works [1, 2] have determined the relationship between the hardness and wear resistance of the test material. The operating conditions specify high requirements to pans material regarding the strength and durability.

Currently, pans are made of steel BRK that is provided by the metallurgical plant "Azovstal". Statistics indicates that the duration of exploitation of pans SP- 87P -81 and CM - 025M is 6-9 months and during that time there's provided transportation of only 300-400 thousand tons of coal at a rate of 650 tons. Here, the service life of the pan is mainly determined by the side frame resistance.

2. STATEMENT OF THE PROBLEM

In connection with the foregoing the objective of the present study was the selection of the material for the side frame of pans by comparing the properties of used and proposed grades of steel. For this purpose it is necessary to analyze the level of properties, the microstructure of side frames after the heat treatment, welding and heat treatment (in this very order these process steps in the manufacture of pans are performed).

Steel BRK, 18HGT and 20HGNR, whose chemical composition is given in Table 1, was used as research material.

Table 1 - Chemical composition of the investigated steel

Steel grade	Content of elements, %								
	C	Mn	Si	Cr	Ni	Ti	B	S	P
Steel BRK	0,29	0,97	0,20	–	–	–	–	0,027	0,027
Steel 18HGT	0,18	0,97	0,30	1,25	0,17	0,050	–	0,019	0,022
Steel 20HGNR	0,20	0,79	0,30	1,05	1,02	–	0,005	0,018	0,021

The methodology of the study was to measure the hardness, strength parameters and the study of microstructure. As there's a direct relationship between the hardness and wear resistance, then according to hardness indicators one can estimate the operational properties of the side frame of pans.

3. RESULTS OF INVESTIGATION AND THEIR DISCUSSION

The study results of steel BRK showed that in hot rolled condition (prior to heat treatment) the spread of hardness values along the perimeter and the cross section of the profile is about 15 HB, and the tensile strength and the flow limit is respectively 27 and 36 MPa. The steel microstructure is ferrite-pearlite.

After the heat treatment, consisting of quenching from 850-870 °C in water and tempering at 200 °C of side frames of pans made of steel BRK, there's observed a

*Corresponding author: 1Kharkiv National Automobile and Highway University, Kharkiv, diana@khadi.kharkov.ua

significant spread of hardness across the cross section of the profile cut out from the pan of current production (Fig. 1). Thus, at the edges of small and large flanges, the thickness of which is 9 and 12 mm, the hardness is, respectively, 444-777 and 320 - 340NV. At junctions of large and small shelves into the wall profile, where the thickness increases approximately 2-fold, the hardness, respectively, decreases to 217 ... 223 HB (Fig. 1 a).

An even greater reduction in hardness is observed with increasing the distance from the edge of the profile (in length). So, at a distance of 300 mm from the edge (at such distance the given hardness should be provided) the latter is slightly different from the hardness of hot rolled profiles and is only 166-217 HB (Fig. 1b).

The results concerning the mechanical properties obtained after appropriate heat treatment in laboratory conditions indicate that in steel BRK after quenching and tempering at 200 and 400 °C there are not provided both the required absolute values, and uniform distribution of strength properties of hardness as well as homogeneity of microstructure along the cross section of the profile.

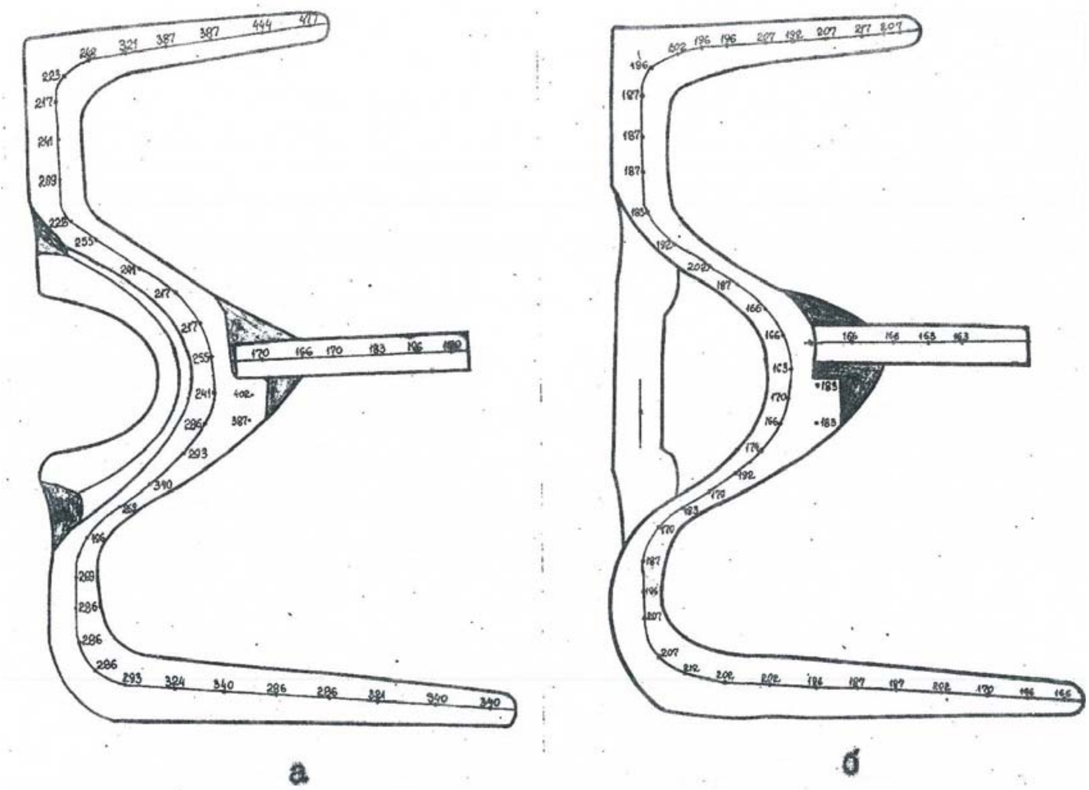

Fig.1. *Hardness (HB) along the cross section of templates of the side frame of the pan made of steel BRK cut from the pan of current production: a - edge profile, b - at a distance of 300 mm from the edge*

If after quenching and low-temperature tempering the tensile strength is 765-1040 MPa (the range of strength values is 275 MPa), then after annealing at the temperature of 400 °C, the level of the tensile strength decreases mainly due to the reduction of the upper limit to 706-905 MPa (variations in strength values is 199 MPa). Similarly, there changes the flow limit. The level of values of the tensile strength is lower than the required level. It is necessary for $\sigma_B \geq 1{,}275$ MPa.

A solid plank is welded to the middle part of the profile (from the non-working surface). The study showed that the heating temperature of the portion of the side frame of the pan, located closest to the welding point, is ~ 300 °C. At the same section the metal in the center (through-thickness) of the profile is heated to ~ 330 °C, and on the surface, somewhat distant from the weld zone, ~ to 250 °C. The minimum heating temperature on the shelf is 120 °C.

Comparison of mechanical properties and the microstructure of the profiles after treatment, including quenching and tempering at 400 °C, as well as heat treatment and welding, demonstrated that the heating of metal during the welding process does not significantly affect the level of hardness, the strength properties of the steel and its microstructure.

However, after welding as well as after heat treatment along the cross section and the length there is observed a large spread in values of properties. As a consequence, the side frame profile of the pan has low wear-resisting properties under operation conditions. The reason for this phenomenon is low hardness penetration of steel. Therefore, the transition to steel was necessary to provide a higher degree of hardness penetration, which is achieved by the introduction of alloying elements that shift the diagram of isothermal decomposition of austenite to the right and reduce the critical quenching rate.

Thus, there were carried out studies on the side frames of pans made of steel 18HGT and 20HGNR. In the hot rolled condition the structure of steel 18HGT is ferrite-pearlite, and that of steel 20HGNR is bainite and some parts of the ferrite have the form of a broken grid along the grain boundaries.

The temperature conditions at the beginning of rolling constitute 1150-1160 °C, and at the end of rolling - 970-990 °C, the speed of rolling is 2.3 m/s.

The hardness of the profile made of steel 20HGNR in the hot rolled condition is 241-262 HB, and the hardness of the profile made of steel 18HGT is lower by 10-20 HB. Given the complexity of the geometric shape of the profile, and the possibility of its buckling during heat treatment there was investigated the level of properties achieved by quenching in a “soft” environment, namely in oil. Studies were carried out simultaneously under cooling in water after tempering. The heat treatment significantly changed the level of properties and the microstructure of the studied types of steel.

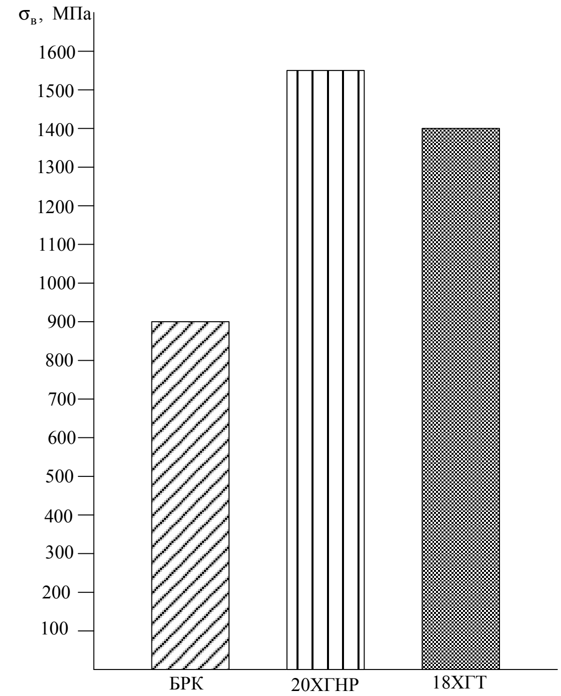

Fig. 2. *Histograms of mean values of rupture strength of steel BRK, 20HGNR, 18HGT after quenching in water and tempering at 200 °C.*

In steel 20HGNR, doped with boron, after quenching in oil the temporary resistance to splitting is at the level of 1430-1440 MPa, and the hardness is 35-39 HRC. Steel 18HGT is significantly inferior according to durability to steel 20HGNR properties after quenching in oil. The temporary resistance is 1030-1020 MPa, the flow limit is by 300-350 MPa lower, and the hardness is by 7-8 HRC lower than in steel 20HGNR.

After water quenching and tempering at 200 °C the rupture strength of steel 20HGNR equals 1480-1550 MPa, the hardness is 42-45 HRC, and that of steel 18HGT is, respectively, 1385-1470 MPa, and - 36-43 HRC.

Fig. 2 shows histograms of mean values of the rupture strength of steel BRK, 20HGNR and 18HGT after water quenching and tempering at 200 °C.

Increase of annealing temperature up to 400 °C leads to a negligible softening of these types of steel, which does not exceed 5-10 % relative to the hardened condition. The studies of hardness after quenching, tempering at 300 °C, and welding of the support bracket and the side frame, the bottom and the side frame imply a slight decline of hardness as compared with the tempered condition.

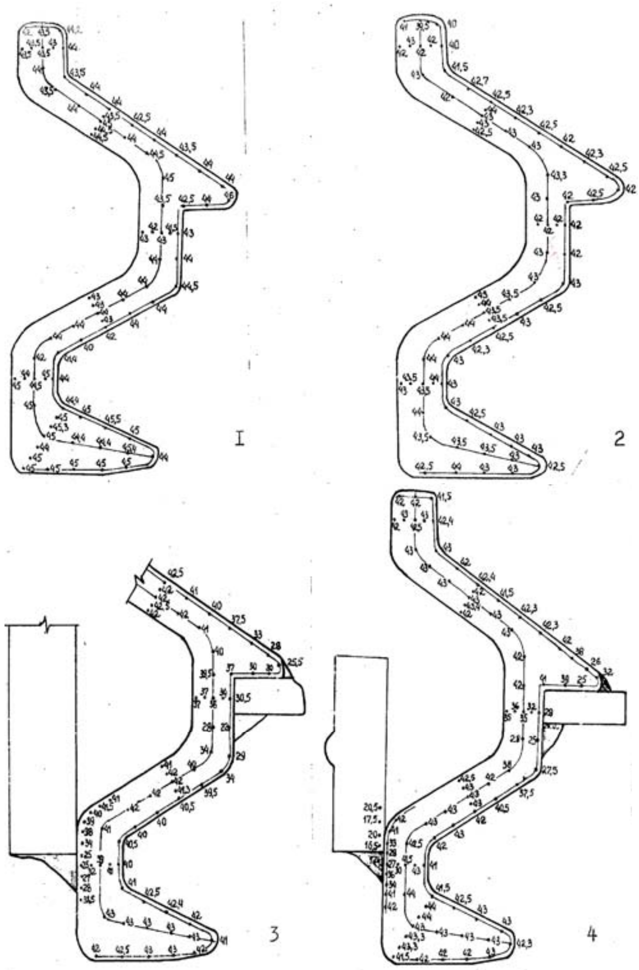

Fig. 3. *Hardness (HRC) in the cross section of the side frame of the pan made of steel 20HGNR after heat treatment and welding: 1 - quenching from 880 °C; 2 - quenching from 880 °C + tempering at 300 °C, 3 - quenching from 880 °C + welding; 4 - quenching from 880 °C + tempering at + 300 °C+welding*

Fig. 3 shows the hardness along the cross section of the side frame of the pan made of steel 20HGNR after heat treatment and welding. The results obtained indicate that reaching of a sufficient level of hardness after quenching over the cross section of the profile the subsequent welding of the hardened profile causes softening of wearable during operation portions no higher than by 3.2 %.

4. CONCLUSIONS

1. After heat treatment and welding of side frames of pans made of steel BRK there is not provided a desired level of durability ($\sigma_B \geq 1275$ МПа), and there is observed unevenness in the distribution of hardness, strength properties over the cross section.

2. Based on the theoretical positions there is explained a big difference of properties across the length of the side frame of the pan made of steel BRK.

3. There was scientifically proven the application of alloy types of steel for side frames of pans.

4. The complexity of the geometric shape of the profile, and the possibility of its buckling during the heat treatment results in the use, during quenching, of a milder cooling medium, which is oil proper.

5. Profiles made of steel 20HGNR when subject to quenching in oil provide a higher level of properties than the sections made of steel 18HGT.

6. At welding, which is one of the process steps for manufacturing of side frames of pans made of steel 20HGNR with other parts of pans, softening of the subject to wear sections does not exceed 2-3 HRC.

7. On the basis of these studies steel 20HGNR can be recommended for manufacture of side frames of pans.

REFERENCES

[1] M Tenenbaum. Wear resistance of construction materials and machine parts in abrasive wear/ M. Tenenbaum. - M.: Mechanical Engineering, 2006. – p.

[2] G. Vinogradov. The mechanism of dry and boundary friction / G. V. Vinogradov. - M.: Mechanical Engineering, 2004. – p. 357. (2011)

Dependence of Mechanical Properties of the Base Metal and Welded Joint of the High Strength Steel S690QL on Elevated Temperatures

Dušan Arsić[1*], Vukić Lazić[1], Andreja Ilić[1], Lozica Ivanović[1],
Srbislav Aleksandrović[1], Milan Đorđević[1]
[1] Faculty of Engineering, University of Kragujevac, 34000 Kragujevac (Serbia)

In this paper is analysed behaviour of mechanical properties of the welded joint and base material of high strength steel S690QL at elevated temperatures. The exposure to elevated temperatures could lead to deterioration of mechanical properties of steel as well as to decreasing of load bearing capacity. Since this steels belongs to a group of steels with exquisite mechanical properties, the aim of this work is to show which is the critical temperature when its mechanical properties are going to worsen. For that purpose, an experimental investigation has been carried out. The specimens were taken both from the welded plate and the base material. The welding was performed with GMAW procedure using two types of filler metals with different mechanical properties for root layer and cover ones. The experiment was performed within the temperature range 20°C to 550°C. The obtained results show the difference with respect to several references, including the European standards, steel producers recommendations and some other researches results. Therefore, studying of mechanical properties of this steel at elevated temperatures is of the utmost importance.

Keywords: High strength steel, S690QL, Welded joint, High temperature, Mechanical properties.

1. INTRODUCTION

With constant advancements in the field of welding technology, there is a growing need for high strength construction steels such as the steel grade S690QL which is analysed in this paper. In order to maintain good weldability, the carbon content in high strength steels has to be as low as possible (max 0.22%) and the steel should have good mechanical properties which would make the welded construction reliable and light. When complex welded constructions are made, especially the ones made of steels of wide cross-sections, the steel is often heated (preheated, additionally heated and tempered), and the process engineers and designers often find themselves in a dilemma concerning the maximum temperatures allowed for this process. In the literature, wide ranges of these temperatures can be found, depending on the thickness of the welded plates i.e., their thickness equivalents. The aim of this experimental paper is to determine the maximum working temperatures at which both base metal (BM) and weld metal (WM) keep thier high strength values.

Dependance of mechanical properties of the base material and welded joints on the temperature has been subject of numerous investigations [1-6]. Due to that, we want do give our contribution to understanding of influence of high temperatures on mechanical properties.

The results shown in the papers [1-4, 6-8] represent a good starting point to understanding the influence of temperature on the base material mechanical properties. However, this influence has not been analysed particularly for the welded joints of high strength steels, which are very sensitive not only to local input of heat that ocurrs during the welding process but also to elevated working temperatures. Due to these reasons we have chosen to perform complex experimental investigations both of the base material and the welded joints. Some of our published papers [9, 10, 11] studied the high steel grade S690QL and certain zones of welded joints from the aspect of mechanic and metallurgical properties. In these papers different welding methods and different filler materials were used in order to find the most suitable welding technology. In the present paper we have chosen the MAG welding method and two different filler materials. The root passage was done using austenitic filler material, and the passes were filled with the filler material of the strength similar to the base material strength. Thus, good ductility of the joint and the minimum stress concentration are achieved, while residual stresses in the welded joints are significantly decreased.

2. SELECTION OF THE MOST SUITABLE WELDING TECHNOLOGY

1.1. Base metal

Since behaviour of the steel S690QL is studied at elevated temperatures, the welded joints have to be welded using the most suitable welding technology. The steel S690QL is produced under special conditions by heating up to the austenite region, rolling and finally by controlled cooling. The steel produced in such a thermo-mechanical treatment process (Quenching + Tempering – Q + T steel) is highly resistant and has good toughness which is maintained even at low temperatures [12]. There are three modifications of this steel that differ only in the guaranteed impact toughness. In fact, all the modifications have the same guaranteed impact toughness of 27 J but different transient temperatures. For the steel grade S690QL it is 47 J at -40°C. The chemical composition and the most important mechanical properties of the steel S690QL are given in Tables 1 and 2 [9, 10, 11, 16].

1.2. Selection of the welding technology

The MAG/MAG method was proposed For welding of the steel grade S690QL the proposed method is MAG/MAG (GMAW/GMAW), and two different filler materials [11, 12] for the root pass and the cover welds were chosen (Tab. 3).

*Corresponding author: dusan.arsic@fink.rs; cmz@fink.rs

Table 1. Chemical composition of the steel S690QL

Steel mark	Require-ment	Chemical composition, %														
		C	Mn	Si	P	S	Cr	Mo	Ni	V	Al	B	Cu	Ti	N	Nb
S690QL	Specified max	0.20	1.50	0.60	0.020	0.010	0.70	0.70	2.0	0.09	0.015	0.005	0.30	0.040	0.010	0.040

Table 2. Mechanical properties of the base metal and the microstructures

Steel mark	Thickness, mm	R_m, MPa	$R_{p0.2}$, MPa	A_5, %	Microstructure
S690QL	4.0 - 53.0	780 – 930	700	14	Interphase tempered structure

Table 3. Chemical composition and mechanical properties of electrode wires [9, 10, 13]

Filler material	Chemical composition, %						Mechanical properties of the pure weld metal			
	C	Si	Mn	Cr	Ni	Mo	R_m, MPa	$R_{p0.2}$, MPa	A_5,%	KV,J
T 18 8 Mn R M 3 (EN ISO 17633-A)*	0.1	0.8	6.8	19	9	-	600 - 630	> 400	> 35	> 60 (+20ºC)
Mn3Ni1CrMo ** (EN 12534)	0.6	0.6	1.7	0.25	1.5	0.5	770 - 940	> 690	> 17	> 47 (-40ºC)
* T 18 8 Mn R M 3	Rutile, highly productive, filled electrode wire for applying root welds in order to increase ductility of the welded joint.									
** Mn3Ni1CrMo	For welding of small grain high strength steels of yield strength up to 690 MPa.									

The MAG/MAG method involves applying the root weld bead in Ar+18% CO_2 shielding gas, using plastic rutile filled electrode wire T 18 8 Mn R M 3 (EN ISO 17633-A) of significantly lower yield stress compared to the base material and applying other weld beads in Ar+18% CO_2 shielding gas with the filler material Mn3Ni1CrMo (EN 12534) of the strength similar to the strength of the base material. The chemical composition and mechanical properties of the filler materials are given in Table 3. The thickness of the welded plates was 15 mm. The applied root pass (1) was partially grooved using a graphite electrode by the arc-air method and a new root weld pass was applied (8) using austenite electrode (Fig. 1). This procedure is carried out in order to correct the mistakes that might have occurred if there was no proper protection from the damaging effect of the air gases.

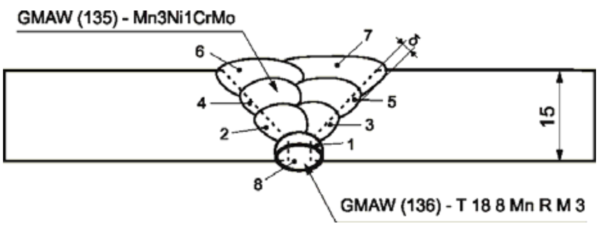

Figure 1. Applying a weld bead using the MAG/MAG method

3. EXPERIMENTAL INVESTIGATION OF THE WELDED JOINTS

The purpose of choosing the most suitable welding technology is to get welded joints whose mechanical and structural properties will resemble the base material properties. The first in order of investigations was tensile testing. Specimens for the tensile testing (Fig. 2), hardness measurement and microstructure testing were prepared according to appropriate standards [14, 15] and used in this paper. Test specimens for the tensile testing were prepared from the base material and from the welded plates. Figure 2 shows the drawing of the test specimens for the tensile testing, and Figures 3 and 4 shows the test specimens before and after the tensile testing [14].

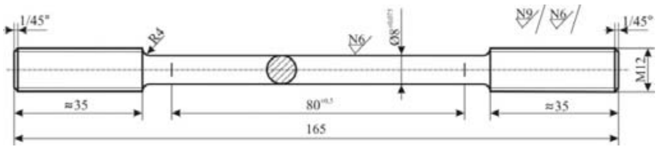

Figure 2. Test specimens for the tensile testing

BM tensile testing specimen

BM test specimen after the testing

Figure 3. Tensile testing specimens made of the base material before and after the testing

WJ tensile testing specimen

WJ test specimen after the testing

Figure 4. Tensile testing specimens made of the base material and welded joints before and after the testing

A homogenous temperature field was formed within the chamber using the controller. Three thermocouples were used to maintain the temperature and a homogenous temperature field. The testing machine with heating chamber on it is shown in figure 5.

Mechanical properties were determined according to the standard that propose all of testing conditions (EN ISO 6892-2) [14].

Figure 5. Zwick Roell Z100 testing machine with a chamber for testing at elevated temperatures

For each testing temperature, two test specimens were prepared, one of the base material and the other of the welded joints. The tests were initially conducted at 20°C, 250°C, 350°C, 450°C (two specimens at every temperature), and then three specimens were tested at 500°C at three more at 550°C. The obtained results are shown in Table 4.

Table 4. Experimental results obtained by tensile testing performed on the specimens made of the base material and the welded joints

Testing temperature, °C	Specimens			
	Base material		Welded joint	
	$R_{p0.2}$	R_m	$R_{p0.2}$	R_m
20	736.6/736.7	793.1/794.3	769.8/779.6	835.5/850.5
250	691.2/702.2	742.8/754.7	715.1/718.9	725.1/785.7
350	665.3/678.9	727.4/748.4	727.9/728.3	804.1/806.3
450	634.2/650.2	718.9/749.4	655.9/671.2	754.5/756.4
500	612.4/617.1/650.2	658.4/662.5/749.4	-	-
550	532.9/547.7/577.3	560.1/583/611.5	-	-

The graphic representations of obtained results are given in form of diagrams (Fig. 6 and 7). The diagrams show two curves for each temperature (for two specimens). The second curve represents the repeated test and it is shifted from the coordinate beginning in order to give a clearer picture.

Testing of the base material has shown that a significant decrease in mechanical properties occurs at the temperatures higher than 450°C (Fig. 6a). With further increase in temperatures this decrease is more and more evident (Table 4 – shaded cells). As for the joints welded using the proposed technology, the decrease in mechanical properties occurs at temperatures higher than 450°C (Fig. 6b). Though an unexpected decrease in mechanical properties and significantly less ductility of the welded joint were registered at the temperature of 250°C, they were attributed to the noticed non-metal inserts in the cross-sections of the broken specimens.

Figure 7 shows histograms of mechanical properties (tensile strength - R_m and yield stress – $R_{p0.2}$) obtained by experimental tensile testing at room and elevated temperatures.

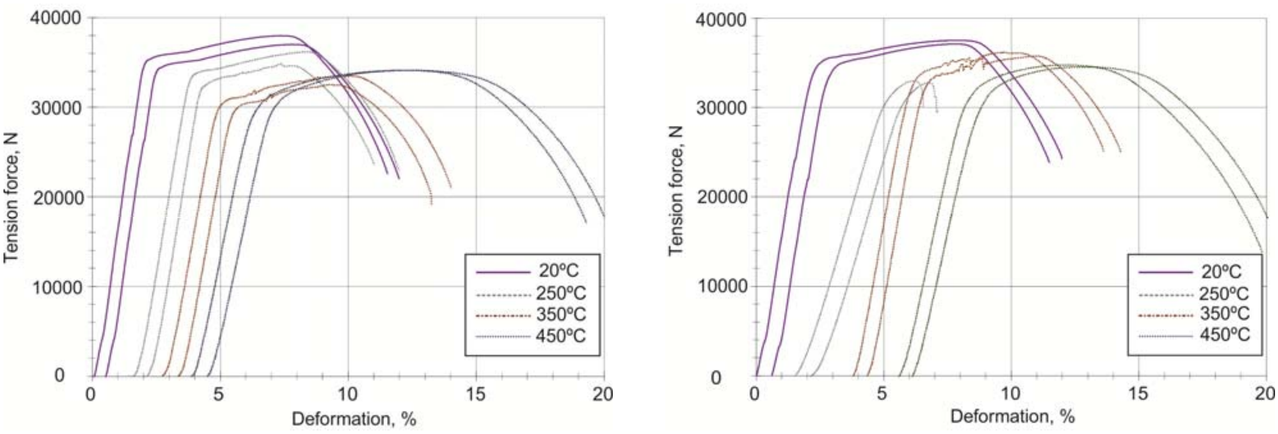

Figure 6. Diagrams of tensile testing for: a) base material and b) welded joints

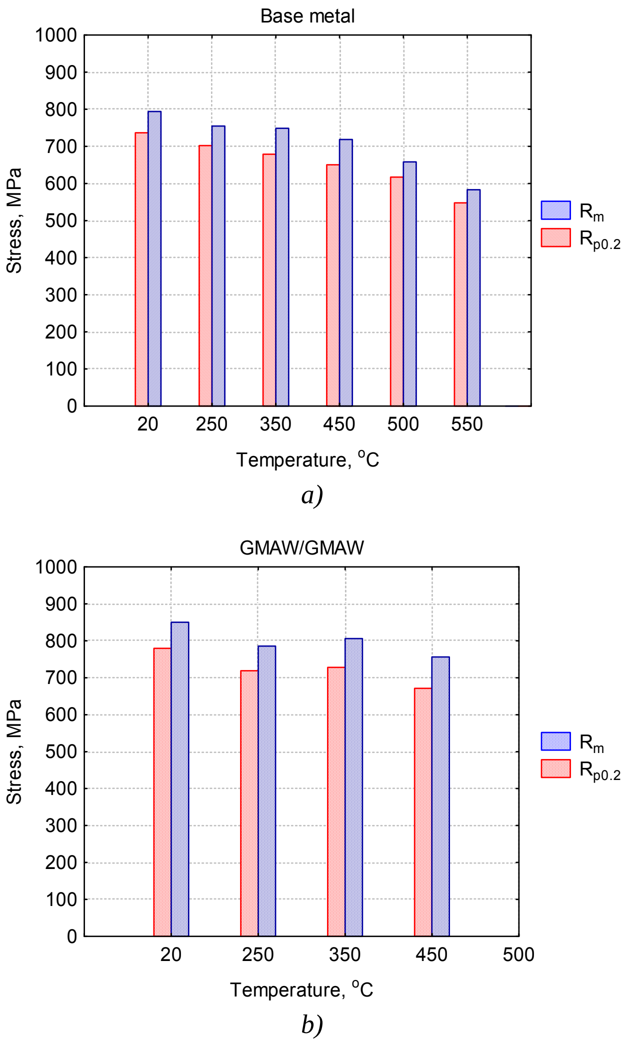

Figure 3. Histograms of the obtained values ($R_{p0.2}$ and R_m) at elevated temperatures for: a) base metal and b) welded joints

After tensile testing investigation of the hardness distribution and the microstructure was performed. The diagram of hardness and microstructure for the characteristic zones of the welded joints obtained using the MAG/MAG welding method is shown an figure 4.

The decrease of hardness in weld metal zone is expected because the selected filler material for applying root welds has austenitic structure and low hardness in order to decrease stress level in the joint and to increase the welded joint plasticity.

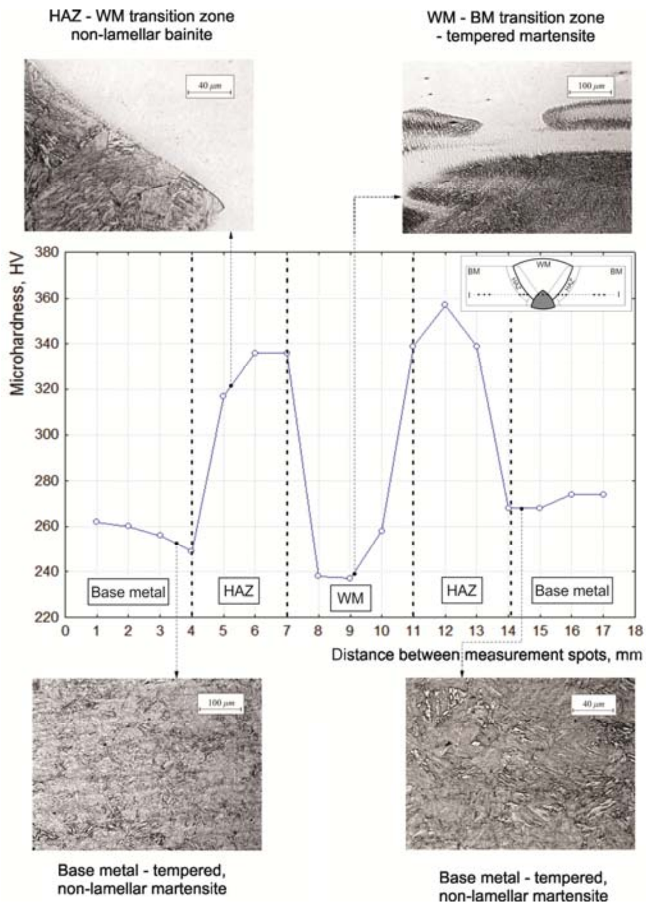

Figure 4. Microhardness distribution and the microstructure for the joint obtained using the MAG/MAG method

4. CONCLUSIONS

The results obtained in this paper show the influence of elevated temperatures on mechanical properties of the steel S690QL. Both the base material and the welded joints obtained using the MAG/MAG method were studied. The base material was tested for the temperature range from 20 to 550°C, while the welded joints were tested for the temperatures in the range from 20 to 450°C.

The obtained experimental results have shown a significant decrease in the yield stress and tensile strength of the base material at temperatures higher than 450°C. The studied welded specimens exhibited a decrease in their mechanical properties at temperatures higher than 450°C. So, the conclusion is that the constructions made of this steel should not be used at temperatures higher than 450°C.

Since the obtained results for the base material and the welded joints have similar results, it can be concluded that the choice of welding technology was right. It also should be emphasized that the choice of welding technology was not a random; a large number of tests was carried out on specimens/models using different welding methods (REL/MAG, MIG/MAG, MAG/MAG), and different filler materials, energy welding parameters as well as other relevant parameters.

In our opinion one should be very careful to choose the right temperature (for preheating, additional heating and tempering) in building welded constructions exposed to dynamic loading. We hope that the results obtained in this paper will be prove useful to process engineers in building welded constructions made of the steel S690QL and in working with them.

REFERENCES

[1] Qiang X., Bijlaard F., Kolstein H.: *Post-fire mechanical properties of high strength structural steels S460 and S690*, Engineering Structures, Pergamon, ISSN 0141-0296, Vol. 35 (2012), pp. 1–10.

[2] Outinen J., Makelainen P.: *Mechanical properties of structural steel at elevated temperatures and after cooling down*, Fire Materials, John Wiley & Sons Ltd. Subsidiary of: John Wiley & Sons, Inc., ISSN 0308-0501, Vol. 28 (2004), pp. 237–251.

[3] Young B., Chen J., Uy B.: *Behavior of high strength structural steel at elevated temperatures*, Journal of Structural Engineering, ASCE, ISSN 0733-9445, Vol. 132 (2006), pp. 1948–1954.

[4] Qiang X., Bijlaard F., Kolstein H.: *Dependence of mechanical properties of high strength steel S690 on elevated temperatures*, Construction and Building Materials, Elsevier BV, ISSN 0950-0618, Vol. 30 (2012), pp. 73–79.

[5] Welding handbook, SSAB Oxelösund AB, Sweden, ISBN: 978-91-978573-0-7, 2009.

[6] Branco M., Ritchie R., Sklenicka V.: *Mechanical Behavior of Materials at High Temperature,* NATO Science Partnership Sub-Series: 3, book, ISBN-13: 9780792341130, Portugal, 1996.

[7] Perry N., Remy L., Petit J.: *Temperature-Fatigue Interaction* Elsevier Science & Technology, book, ISBN-13: 9780080439822, USA, 2002.

[8] Chang K.H., Lee C.H.: *Characteristics of High Temperature Tensile Properties and Residual Stresses in Weldments of High Strength Steels*, Materials Transactions, Japan Institute of Metals, ISSN 1345-9678, Vol. 47, No. 2 (2006), pp. 348-354.

[9] Arsić D.: *Assessment of weldability and the choice of the most suitable welding technology for high strength steel grade S690QL*, Master thesis, Faculty of Engineering in Kragujevac, Kragujevac, 2013.

[10] Lazić V., Aleksandrović S., Nikolić R., Prokić-Cvetković R., Popović O., Milosavljević D., Čukić R.: *Estimates of weldability and selection of optimal procedure for welding of high strength steel*, Steel Structures and Bridges, Procedia Engineering, ISSN 1877-7058, Vol. 40, No.- (2012), pp. 310-315.

[11] Arsić D., Lazić V., Nikolić R., Aleksandrović S., Marinković P., Đorđević M., Čukić R.: *Application of the S690QL class steels in responsible welded structures*, Materials Engineering (MEMI), ISSN 1335-0803, Vol. 20, No. 4 (2013), pp. 174-183.

[12] European standard EN 10025-6:2004 Amendment 1:2009 - Hot rolled products of structural steels. Technical delivery conditions for flat products of high yield strength structural steels in the quenched and tempered condition.

[13] European standard EN 12534:1999 - Welding consumables. Wire electrodes, wires, rods and deposits for gas shielded metal arc welding of high strength steels. Classification.

[14] ISO 6892-2:2011: Metallic materials - Tensile testing - Part 2: Method of test at elevated temperatures.

[15] EN 1043-1:1996: Destructive tests on welds in metallic materials. Hardness testing. Hardness test on arc welded joints. European Committee for Standardization, Brussels.

[16] Arsić, D., Đorđević, M., Lazić, V., Aleksandrović, S., Nikolić, R.: Selecting the optimal welding technology of high strength steel of the S690QL class, 19th International student's seminar SEMDOK 2014, 29 – 31 January, Žilina-Terchova, Slovakia, Proceedings, ISBN 978-80-554-0832-2, pp. 5-9.

SESSION D

AUTOMATIC CONTROL, ROBOTICS AND FLUID TECHNIQUE

Modelling, Simulation and Cascade Navigation Control of a Prototype Cargo Vessel

Erol Uyar[1], Mücahid Candan[2], Nail Akçura[3], Semih Arıkan[4]
[1,2,3,4]Electrical & Electronics Engineering Department, Ege University, İzmir (Turkey)

In this work cascade navigation control of a cargo ship is demonstrated with a prototype model and with Matlab simulation. After theoretical linear modelling of the vessel and cascade route-steering navigation, appropriate master and slave controllers with optimal control parameters are investigated. The results of various alternative controllers and their parameter selections are then compared with each other theoretically and these are demonstrated by a built up ship navigation model. According to the given Route as Master Control Reference, relevant steering is produced as slave control Reference so that the desired route can be achieved.

To demonstrate the Route changes as master control the model ship is mounted on a turning table which is moved by a geared DC motor according to the given reference route and error signal as the difference with the measured feedback position angle. Steering angle is followed then accordingly by a servo motor as slave control which is governed by a micro controller. A PC is used to give the Route reference through HyperTerminal connection and to view the changing data values during control action.

The self-built, open architecture implementation is also considered to be a representative real education model, to demonstrate the effectiveness of various control applications. On the other hand the cost of a non-optimal navigation both as time waste and fuel consumption is emphasized by giving attention to optimal controller selection and design.

Keywords: Navigation, Cascade control, Ship, Modelling, Steering, Route

1. INTRODUCTION

Automatic Control and Instrumentation is an important topic in ship manoeuvring and navigation. To maintain a given course or direction precisely and to obtain economy and security in the navigation the effect of control implementation is authoritative. The navigation and so the steering control structure of a ship is essentially achieved by a cascaded course-rudder control which maintains the ship sailing in a given course as seen in Figure 1.

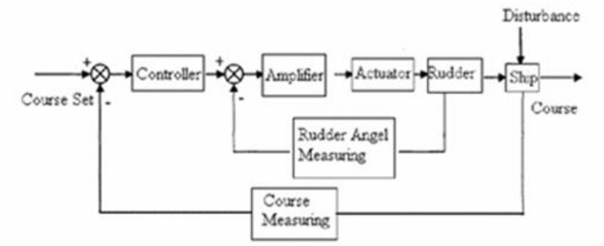

Figure 1: The structure of ship automatic steering

Automatic steering device provides the required ship stability [1], [3] on the scheduled course and reduces unnecessary rudder deflections despite of disturbance effects of waves, wind and currents. Although the navigation control in whole is a non-linear, time varying and uncertain system, it can be modelled and linearized respected to some constrained considerations.

Dynamic motion and analysis of a ship is associated with the knowledge of the couplings between roll, yaw, and sway and this is an important task to improve the manoeuvring ability and modelling. [2]

Generally for description of ship motion four degrees of freedom models are well known, as given by Abkowitz [1] and Chislett and Stom-Tejsen [7], but models describing the interaction between roll sway and yaw have only been scarcely studied.

Son and Nomoto [12] presented a model obtained by combining planar motion mechanism (PMM) test data for lateral motion, using different values of static heel for the model under test, with independent roll motion tests. Källström and Otterson [10] obtained a model by combining a lateral PMM model with theoretical estimates of roll coefficients, using free sailing model tests to calibrate the roll parameters. Perez - Blanke [15] presented models based on experimental results in the unique 4-DOF roll planar motion mechanism (RPMM) facility at the Danish Maritime Institute that allow model testing with full dynamic interaction between motions in roll, sway, yaw and surge.

Although different model publications are presented, [6], [7], [8] in the literature it is still difficult to find a fully-parameterized models. The main contribution of this report is to provide a fully-parameterized non-linear and linear state space models that can be utilized as a basis for analysis and design of ship motion control strategies. The results of a Matlab – Simulink model for cascaded navigation simulation are shown for different actions.

In addition, to demonstrate the results of the obtained linearized model, a built up real like ship navigation model with cascade control is implemented successfully. [11]

2. DYNAMIC POSITIONING - BASIC PRINCIPLES

Motion model of a ship or vessel with acting forces and moments is shown in Figure 2. A seagoing vessel is

*Corresponding author: Ege University, Electrical & Electronics Engineering Department, İzmir, Turkey, erol.uyar@deu.edu.tr

subjected to forces from wind, waves and current as well as from forces generated by the propulsion system.

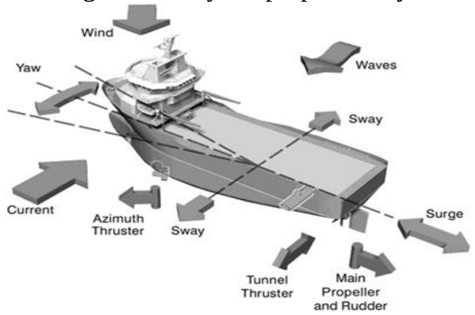

Figure 2: Motion model of a seegoing vessel with acting forces and moments

The vessel's response to these forces, i.e. its changes in position, heading and speed, is measured by the position-reference systems, the gyrocompass and the vertical reference sensors. Reference systems readings are corrected for roll and pitch using readings from the vertical reference sensors. Wind speed and direction are measured by the wind sensors.

The dynamic positioning control system calculates the forces that the thrusters must produce in order to control the vessel's motion in three degrees of freedom - surge, sway and yaw - in the horizontal plane. [8], [9], [14]

The system is designed to keep the vessel within specified position and heading limits, and to minimise fuel consumption [13] and wear and tear on the propulsion equipment. In addition, the control (pos) system tolerates transient errors in the measurement systems and acts appropriately if fault occurs in the thruster units. [5]

For surface ships like vessels course-keeping, speed changing and manoeuvring involve primarily forces, moments and motions acting in all directions in the horizontal plane.(For submarines and undersea vehicles the third direction also comes in play.)

3. EQUATIONS OF MOTION

The basic dynamics of manoeuvring and course-keeping can be described and analysed using Newton's equations of motion. Basic equations in the horizontal plane can be considered first with reference to onset of axes fixed relative to the earth and a second set fixed relative to the ship.

Figure 3 shows typical fixed and moving axed for a surface ship. The path is usually defined as the trajectory of the ship's centre of gravity. Heading refers to the direction (ψ angle of yaw) of the ship's longitudinal axis with respect to one of the fixed axes. The difference between the heading and the actual course (or direction of the velocity vector at the centre of gravity) is the drift or leeway angle β.When the ship is moving along a curved path, the drift angle is thus the difference in direction between the heading and the tangent to the path of the centre of gravity.

There are significant factors that couple the speed of a ship and its path. For example, path changing (turning) and even path keeping (course-keeping) cause involuntary speed reductions. These effects arise from the fact that any misalignment between the x-axis of the ship as shows in Figure 3 and its velocity vector, V, increases the drag force acting on the ship.

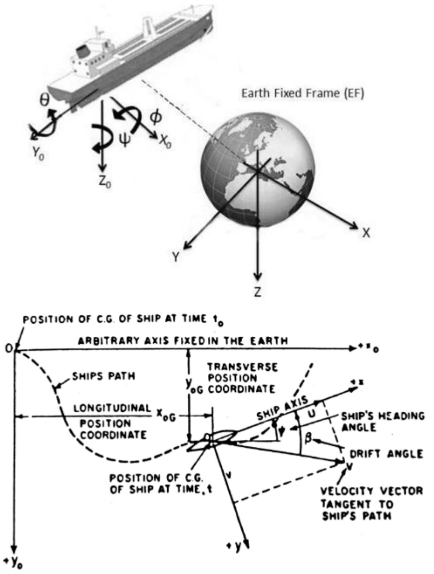

Figure 3: Orientation of fixed and moving axes

The motion of a ship in six degrees of freedom is considered as a translation motion (position) in three directions: surge, sway, and heave; and as a rotation motion (orientation) about three axes: roll, pitch and yaw. To determine the equations of motion, two reference frames are considered: the inertial or fixed to earth frame O that may be taken to coincide with the ship-fixed coordinates in some initial condition and the body-fixed frame O_0— see Figure 1. For surface ships, the most commonly adopted position for the body-fixed frame is such it gives hull symmetry about the x_0z_0-plane and approximate symmetry about the y_0z_0-plane, while the origin of the z_0 axis is defined by the calm water surface The magnitudes describing the position and orientation of the ship are usually expressed in the inertial frame and the coordinates are noted: $[x\ y\ z]t$ and $[\varphi\ \theta\ \psi]t$ respectively, whilst the forces $[X\ Y\ Z]t$, moments $[K\ M\ N]t$, linear velocities $[u\ v\ w]t$, and angular velocities $[p\ q\ r]t$ are usually expressed in the body-fixed frame– see Figure 1. We have used the standard notation given in SNAME (1950).

Let us define the position-orientation vector η with respect to the inertial frame as

$$\eta \triangleq \begin{bmatrix} x & y & z & \phi & \theta & \psi \end{bmatrix}^{\mathrm{T}} \tag{1}$$

And the linear-angular velocity vector ν with respect to the body-fixed frame as

$$\nu \triangleq \begin{bmatrix} u & v & w & p & q & r \end{bmatrix}^{\mathrm{T}} \tag{2}$$

Then, the position-orientation rate vector $\eta^{\cdot}$ is related to ν via:

$$\dot{\eta} = J(\eta)\,\nu \tag{3}$$

$$J\ (\phi,\theta,\psi)=\begin{bmatrix} c(\psi)c(\theta) & -s(\psi)c(\phi)+c(\psi)s(\theta)s(\phi) & s(\psi)s(\phi)+c(\psi)c(\phi)s(\theta) \\ s(\psi)c(\theta) & c(\psi)c(\phi)+s(\phi)s(\theta)s(\psi) & -c(\psi)s(\phi)+s(\psi)c(\phi)s(\theta) \\ -s(\theta) & c(\theta)s(\phi) & c(\theta)c(\phi) \end{bmatrix} \tag{4}$$

$$M_{RB}\dot{\nu}=\tau(\dot{\nu},\nu,\eta)-C_{RB}(\nu)\nu \tag{5}$$

Where M_{RB} is the matrix mass and inertia due to rigid body dynamics, the term $C_{RB}(\nu)\nu$ arise from the coriolis and centripetal forces and moments also due to rigid body dynamics, and $J(\eta)$ is given in (3). The forces and moments vector τ is defined as

$$\tau=\begin{bmatrix} X & Y & Z & K & M & N \end{bmatrix}^{T} \tag{6}$$

And these magnitudes are generated by different phenomena and can be separated into components according to their originating effects:

$\tau=\tau_{hyd}+\tau_{cs}+\tau_{prop}+\tau_{ext}$ where

• hyd: These forces and moments arise from the movement of the hull in the water.

• prop: These forces and moments come from the propulsion system, e.g., propellers and thrusters.

• cs: These forces and moments arise due to the control surfaces (*CS*) like rudder, fins, etc. movement.

• ext: These are the forces and moments acting on the hull due to the environmental disturbances, e.g., wind, currents and waves.

Motions in pitch and heave can generally be neglected in comparison with the other motions for conventional surface ships; thus, ship motion modelling can be considered only 4-DOF: surge, sway, yaw and roll. Therefore, from (6) the following approximations can be made:

$$\dot{\phi}=p \qquad \dot{\psi}=r\cos(\phi) \tag{7}$$

In the sequel we treat only the motion in four degrees of freedom (4-DOF.) For this case, the equations of motion (8) are

$$\begin{bmatrix} m & 0 & 0 & 0 \\ 0 & m & -mz_G & mx_G \\ 0 & -mz_G & I_{xx} & 0 \\ 0 & mx_G & 0 & I_{zz} \end{bmatrix}\begin{bmatrix} \dot{u} \\ \dot{v} \\ \dot{p} \\ \dot{r} \end{bmatrix}=\begin{bmatrix} X \\ Y \\ K \\ N \end{bmatrix}+\begin{bmatrix} m(vr+x_Gr^2-z_gpr) \\ -mur \\ mz_Gur \\ -mx_Gur \end{bmatrix} \tag{8}$$

where m is mass of the ship, I_{xx} and I_{zz} are the inertias about the x_0 and z_0 axes, and x_G and z_G are the coordinates of the centre of gravity *CG* with respect to the body-fixed frame, i.e., $CG=[x_G, 0, z_G]$.

4. NON-LINEAR AND LINEARIZED STATE SPACE MODELS

4.1. Non-linear Model

The non-linear state space model are based on (8), and the models for the forces and moments given in the previous has the general form

$$\dot{x}=H^{-1}f(x,\delta)$$
$$x=\begin{bmatrix} u & v & r & p & \phi & \psi \end{bmatrix}^{T} \tag{9}$$

The model (9) can be further written according the given hydrodynamic model in the following form: Incorporating the time derivatives of the roll and yaw angles given in (7), as Newton's equations of motion

$$\begin{aligned} (m-X_{\dot{u}})\dot{u} &= X^{*}_{hyd}(x)+X_{rudder}(x,\delta)+m(vr+x_Gr^2-z_Gpr) \\ (m-Y_{\dot{v}})\dot{v}-(mz_G+Y_{\dot{p}})\dot{p}+(mx_G-Y_{\dot{r}})\dot{v} &= Y^{*}_{hyd}(x)+Y_{rudder}(x,\delta)-mur \\ -(mz_G+K_{\dot{v}})\dot{v}+(I_{xx}-K_{\dot{p}})\dot{p}-K_{\dot{r}}\dot{p} &= K^{*}_{hyd}(x)+K_{rudder}(x,\delta)+mz_Gur \\ (mx_G-N_{\dot{v}})\dot{v}-N_{\dot{p}}\dot{p}+(I_{zz}-N_{\dot{r}})\dot{r} &= N^{*}_{hyd}(x)+N_{rudder}(x,\delta)-mx_Gur \\ \dot{\phi} &= p \\ \dot{\psi} &= r\cos(\phi) \end{aligned} \tag{10}$$

The matrix H is given by

$$H=\begin{bmatrix} (m-X_{\dot{u}}) & 0 & 0 & 0 & 0 & 0 \\ 0 & (m-Y_{\dot{v}}) & -(mz_G+Y_{\dot{p}}) & (mx_G-Y_{\dot{r}}) & 0 & 0 \\ 0 & -(mz_G+K_{\dot{v}}) & (I_{xx}-K_{\dot{p}}) & -K_{\dot{r}} & 0 & 0 \\ 0 & (mx_G-N_{\dot{v}}) & -N_{\dot{p}} & (I_{zz}-N_{\dot{r}}) & 0 & 0 \\ 0 & 0 & 0 & 0 & 1 & 0 \\ 0 & 0 & 0 & 0 & 0 & 1 \end{bmatrix} \tag{11}$$

4.2. Linearized Model

It is a common practice to decouple the surge equation from the others to analyse the linearized models. Thus, we consider a given service speed u (or the approximation $u\_a\approx (u-U_{nom})/U_{nom})$ and the reduced state vector.

The linearized models are obtained straightforward from (9) as:

$$\dot{z} = H^{-1}\left[\frac{\partial f(z,u,\delta)}{\partial z}\bigg|_{\bar{z},\bar{u},\bar{\delta}} z + \frac{\partial f(z,u,\delta)}{\partial \delta}\bigg|_{\bar{z},\bar{u},\bar{\delta}} \delta\right] = H^{-1}A \quad z + M^{-1}B \quad \delta. \tag{12}$$

The matrix H is now given by (11) without the first row and first column, and to obtain the matrices A and B, the Jacobians in (12) are evaluated at

$$\bar{z} = [0 \quad 0 \quad 0 \quad 0 \quad 0]^{T} \text{ and } \bar{\delta} = 0$$

$$f(x,\delta) = \begin{bmatrix} X^{*}_{hyd}(x) + X_{rudder}(x,\delta) + m(vr + x_G r^2 - z_G pr) \\ Y^{*}_{hyd}(x) + Y_{rudder}(x,\delta) - mur \\ K^{*}_{hyd}(x) + K_{rudder}(x,\delta) + mz_G ur \\ N^{*}_{hyd}(x) + N_{rudder}(x,\delta) - mx_G ur \\ p \\ r\cos(\phi) \end{bmatrix} \tag{13}$$

By using the real data of a container ship given in [15] a linearized ship model is used for the control simulation with Matlab. In the control application all hydraulic forces and moments except rudder are neglected. Assuming a motion in surge direction with initial conditions u_0=8, v_0=0, p_0=0, r_0=0 the linearized state space equations can be obtained as given in (14)

$$\begin{aligned} \dot{u} &= 2.8 * 10^{-6} X \\ \dot{v} &= 8r + 4.6 * 10^{-6} Y - 0.8 * 10^{-6} N + 0.9 * 10^{-6} K \\ \dot{p} &= -0.8 * 10^{-6} Y + 0.4 * 10^{-6} N - 0.1 * 10^{-6} K \\ \dot{r} &= 0.9 * 10^{-6} X - 0.1 * 10^{-6} N + 0.1 * 10^{-6} K \end{aligned} \tag{14}$$

5. CONTROL APPLICATIONS

5.1. Matlab Simulation

According to the linearization of motion equations and investigation of relevant transfer functions a cascade navigation control model in Matlab-Simulink as given in Figure 4 is used for further navigation analysis. Given a reference course direction (yaw angle ψ), the relevant steering (as rudder angle δ) is automatically determined and actuated so that the ship can be brought to reference direction by yaw moment which is produced from the surge- and sway- rudder forces.

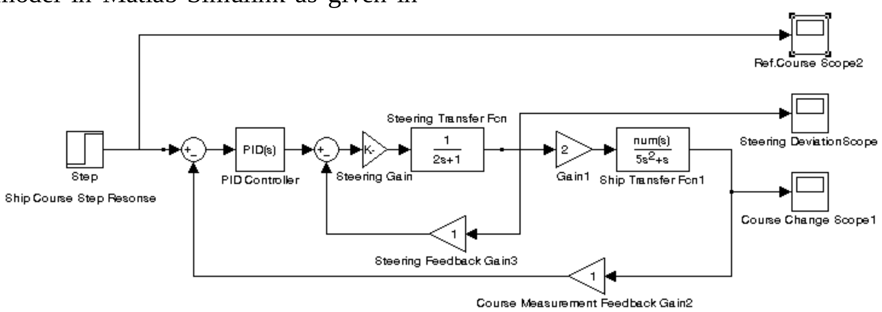

Figure 4: Matlab-Simulink control simulation

Course control (outer loop) being as master control creates the steering reference which works as slave control (inner loop) accordingly. In Figure 5 the time responses of both course and rudder deviations to a given course reference change of 15 degrees are given. PI as master and P controller as slave is applied for the simulation. With appropriate choose of controller parameters, the ship comes to new course after about 65 seconds (response time) as can be seen from recorded curves. Fort the relevant ship this is found as an optimal manoeuvre response comparing with various simulation results evaluated by different control parameters.

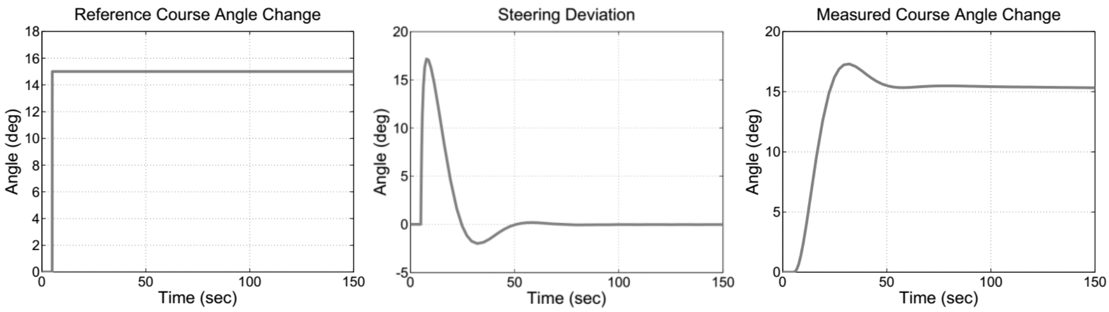

Figure 5: Course change and steering deviation according to a step course change of 15 degrees

6. RESULTS AND CONCLUSIONS

In this paper the modelling and navigation control of a ship is handled. After a brief introduction to basics of ship dynamics (manoeuvring and course-keeping) basic equations of motion in the horizontal plane are derived by using Newton's equation.

In the modelling as mentioned before, motions in pitch and heave are neglected in comparison with the other motions and only the impact of rudder (as hydrodynamic) and inertial forces and moments are taken in to consideration.

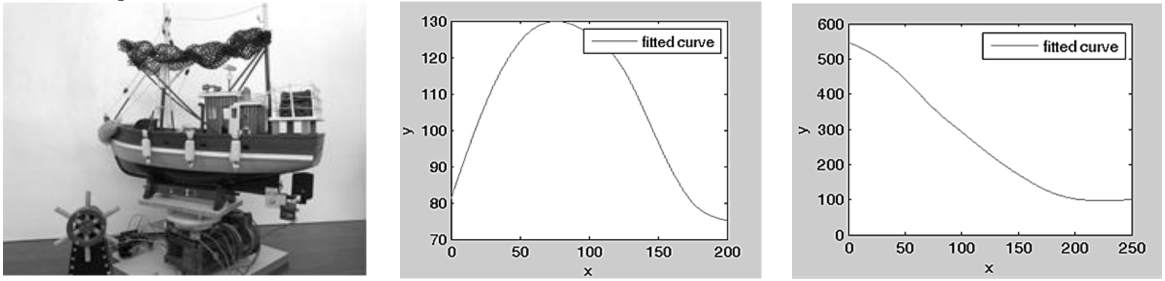

Figure 6: Built-up model and recorded simultaneous steering and course change (reference course angle:20 Degrees)

The forces and moments (left hand side) of the equations of motion (10) are built up four types of forces that act on a ship during a maneuver:

- Hydrodynamic forces acting on the hull and appendages due to ships velocity and acceleration, ruder deflection, and propeller rotation.
- Inertial reaction forces caused by ship acceleration.
- Environmental forces due to wind, waves and currents.
- External forces such as tugs or thrusters.

The first two types of forces generally act in the horizontal plane and involve only surge, sway and yaw responses, although rolling effects (heel) occur in the maneuvering of high-speed ships and the Small Water-plane Are Twin Hull (SWATH) vessels. Hydrodynamic forces fall into two basic categories, those arising from hull velocity through the water (damping forces) and those arising from accelerations through the water (added mass forces). The ship accelerations produced by these and any external forces result in balancing inertial reaction (d'Alembert Forces and Moment), especially when turning.

The effect of a rudder on turning is indirect. Moving the rudder produces a moment that causes the ship to change heading so as to assume an angle of attack (leeway angle) to the direction of motion of the center of gravity. Consequently, hydrodynamic forces on the hull are generated which, after a time, cause a change of lateral movement of the center of gravity. The lateral movement is opposed by the inertial reactions. If the rudder remains at a fixed position, a steady turning condition will evolve when hydrodynamic and inertial forces and moments come into balance.

When in shallow or restricted waters, various complex effects come into play. Interactions between vessels further complicate hydrodynamic and inertial force analysis. These effects are not considered in this work. Further information can be found in [17].

The ship may also be operating and maneuvering in an environment where wind, waves, and current are present. The effect of current is usually incorporated with the hydrodynamic forces by considering the relative velocity between the vessel and the water although studies in restricted water require more careful analysis. Wind and wave forces are generally treated as external forces as described in [17].

Wind velocity is generally unsteady and hence forces and moments due to wind will be time dependent. These forces are generally proportional to the above water area of the ship and the square of the relative velocity between the ship and the wind. Forces and moments also vary with the direction of the wind velocity relative to the ship's axes.

Two distinct types of wave forces act. The steady and slowly varying forces due to second-order wave drift effects are generally more important for ship controllability than the first-order forces, which are of primary importance for sea-keeping. However, the latter can be important for the case of following seas where frequency of encounter is small. Wave drift forces depend primarily on ship length and on the relative magnitudes of wave length and amplitude.

Pitching motion changes the shape of the immersed hull and can therefore have significant effects on the coefficients in the equations of motion, particularly in quartering and following seas.

Finally, tugs and thrusters create effective forces when utilized at relatively slow speeds. The forces they develop are for the most part external to the hydrodynamics of the manoeuvre and are normally treated as independent additions.

The simple case of controllability, assuming a calm open sea without wind, waves, current and external forces can also be considered as described in [17].

The cascade navigation control is further demonstrated with a built up real like model implementation. This is especially thought as a teaching model which emphasizes various control actions and their results. The model consists of a base which is mounted on the shaft of geared DC motor turning a model ship as seen in Figure 6. On the heck of the ship a mini servo motor turning the rudder is mounted. A computer (PC) is used to give the reference course angle via hyper terminal and to realize the control actions of both motors simultaneously a micro controller (Arduino) with written software is applied. The evaluated simulation graphics through computer are reproduced in Figure 6.

As future work linearized state space model can be used to obtain optimal control parameters with application of LQR algorithms. For a desired response tune up modelling with Matlab simulation and parameter selection of PID controller can be investigated. Furthermore the effect of ruder and propulsion forces to the individually states like (u,v,p, r,Ψ and φ) can be investigated by using the state space representation and equations.

REFERENCES

*[1] Abkowitz, M.A., "Lectures on ship hydrodynamics-steering and manoeuvrability", Technical Report Rep. No. Hy-5, Hydro og Aerodynamisk Laboratorium, Lyngby, Denmark, (1975)

*[2] Blanke, M. and A. Christensen, "Rudder roll dumping autopilot robustness to sway-yaw-roll couplings", Proceedings of 10th SCSS, Ottawa, Canada pp. 93–119, (1993)

*[3] Blanke, M. and A.G. Jensen, "Dynamic properties of container vessel with low metacentric height", Technical Report doc. No. R-1997-4173, Dept. of Control Engineering, Aalborg University, Denmark, (1997)

[4] Blanke, M., P. Haals and K.K. Andreasen, "Rudder roll damping experience in Denmark", Proceedings of IFAC work shop CAMS'89, Lyngby, Denmark, (1989)

*[5] Blanke, Mogens, "Ship propulsion losses related to automatic steering and prime mover control", PhD thesis, Servolaboratory, Technical University of Denmark, (1981)

*[6] Chislett, M.S., "The addition of heel-roll servo mechanism to the dmi horizontal planar motion mechanism", Proc. of MARSIM and ICSM, Tokio, Japan, (1990)

*[7] Chislett, M.S. and J. Stom-Tejsen, "Planar motion mechanism tests and full scale steering and maneuvering predictions of a mariner class vessel", Technical Report Rep. No. Hy-6. Hydro og Aerodynamisk Laboratorium, Lyngby, Denmark, (1965)

*[8] T.I. Fossen, "Guidance and Control of Ocean Marine Vehicles", John Wiley and Sons Ltd. New York, US, (1994)

[9] Goodman, A. and M. Gertler, "Planar motion mechanism system", US patent 3052120, (1962)

[10] Källström, C.G. and P. Otterson, "The generation and control of roll motion of ships in closed turns", Proc. 4th-IFAC/IFIP Symposium on Ship Operation Automation, Genova, Italy, (1983)

[11] S. Arikan, E. Uyar, "Built Up Implementation Model for Cascade Ship Navigation", Dipl. Thesis, Ege University, Electrical & Electronics Engineering Department, İzmir, Turkey, (2014)

[12] Son, Kyoung-Ho, and K. Nomoto, "5. On the Coupled Motion of Steering and Rolling of a High-speed Container Ship.", Naval architecture and ocean engineering 20, p.73-83, (1982)

[13] J.van Amerongen, "Adaptive steering of ships - A model reference approach to improved manoeuvring and economic course keeping", PhD thesis. Delft University of Technology, The Netherlands, (1982)

[14] P.G.M. van der Klugt, "Rudder roll stabilization", PhD thesis. Delft University of Technology, The Netherlands, (1987)

[15] T. Perez, M. Blanke, "Mathematical Ship Modeling for Control Applications", Technical Report, (2002)

[17] E. Lefeber, K. Y. Pettersen, and H. Nijmeijer, "Tracking Control of an Underactuated Ship", IEEE transactions on control systems technology, vol. 11, no. 1, (2003)

[17] E. Lefeber, K. Y. Pettersen and H. Nijmeijer, "Tracking Control of an Underactuated Ship", IEEE Transactions On Control Systems Technology, vol. 11, no. 1, January (2003)

[18] R.-Q. Lin, M. Hughes, T. Smith, "Prediction of ship steering capabilities with a fully nonlinear ship motion model. Part 1: Maneuvering in calm water". J Mar Sci Technol, 15:131–142.DOI 10.1007/s00773-010-0084-z, (2010)

Definition of Power and Kinematic Parameters of Full-Flow Hydrostatic Transmission

V.A. Zhulai, V. I. Yenin, E.V. Kozhakin
The Voronezh State University of Architecture and Civil Engineering

Theoretical dependences for determination of the relationship of force and kinematic parameters of hydraulic machines of broken pump hydraulic drive with parallel mains are presented. The problems of theoretical substantiation of different methods for partial blocking of hydro-differential transmission are considered.

Keywords: hydrostatic transmission, calculation of hydrostatic transmission, transport and technological machines

The use of hydrostatic transmissions for the drive of the running gear of transport and technological machines is one of the perspective ways for their improvement and development. Despite the complexity of the design, high cost and increased requirements to the working conditions, these transmissions are finding expanding application in agriculture, road building machines, tractors and in tow trucks. The main advantages of hydrostatic transmissions are flexibility, the ability for transferring the flow of power to different working mechanisms located in remote and difficult to access places, simplicity of controlling, including the reversing, providing the maintenance of the main internal combustion engine under the optimum modes, that makes it possible to increase the capacity and to reduce fuel consumption for transport and technological machines.

Besides, in transmissions of wheeled tractors [1] and road-building machines [2,3,4] more simple in design, full- flow hydrostatic transmissions with one pump and several parallel-connected motors are used. Such transfer is often used as a module for driving two wheels located on the one axis. In this case, the link between the wheels of this axis is hydro-differential, that permits them to move with different speeds in turns and over bumps, but at reducing cross-country capacity and traction qualities. In this case, to improve the passability of the machines, the blocking of hydro-differential link of wheels is needed. A partial blocking of the hydro-differential transmission can be achieved by introducing additional hydraulic resistance into the mains of the drive of one of the wheels, its braking or changing the working volumes of the controlled motors of these wheels [1,5]. To determine the magnitude for the controlling action of any of these blocking methods of such hydrostatic transmission it needs to know the interdependence of their power and kinematic parameters.

Therefore, the task to define the relationship between the power and kinematic characteristics of the full-flow hydrostatic drives with a hydro-differential link is urgent.

Let us consider the operation of a broken pump full-flow hydraulic drive consisting of parallel-switched on motors in steady (static) mode (Fig. 1).

When describing the operation of the above hydraulic drive the following assumptions were taken.

Pump flow is constant, Q = const. All the hydraulic machines are characterized by the following parameters: displacement q_i; torque on the shaft M_i and volumetric rate (supply) Q_i at the rotation frequency of the shaft n_i. In the hydraulic motors mains there are hydraulic resistances caused by the resistance of hydro-motors and by additional ones established, for example, for the purposes of drive regulation (control). The resistance of the mains, as such, is neglected.

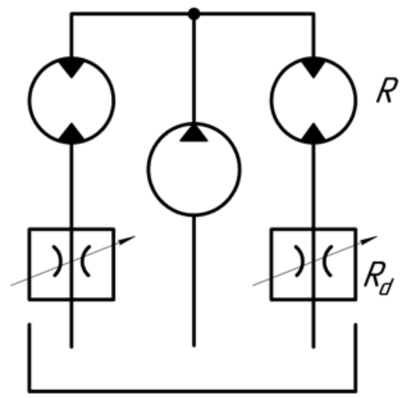

Fig. 1. Schematic diagram of a full-flow hydrostatic drive

For each motor we can write (input) its equivalent hydraulic resistance defined by the relation

$$R_i = \frac{p_i}{Q_i} \tag{1}$$

where p_i - is the pressure difference at the input and output of the *i-th* motor; Q_i - volumetric flow rate of the *i*-th motor.

*Corresponding author: The Voronezh State University of Architecture and Civil Engineering, kzhknzhnj@rambler.ru

Torque M_i on the shaft of the i-th motor is equal to [5]

$$M_i = \frac{q_i\, p_i\, \eta_{ni}}{2\pi} \quad (2)$$

where $\eta_{ni} = \eta_{oi}\, \eta_{mi}$ is the full efficiency of the i-th motor;
η_{oi} - volumetric efficiency of the i-th motor;
η_{mi} - mechanical efficiency of the i-th motor.

$$Q_i = \frac{q_i\, n_i}{\eta_{oi}} \quad (3)$$

from (1) and (2) we obtain the

$$R_i = \frac{2\pi\, M_i\, \eta_{oi}}{q_i^2\, n_i\, \eta_{mi}}. \quad (4)$$

Then, in accordance with the assumptions taken, the full equivalent hydraulic resistance of each main will be equal to

$$R_{\Pi i} = R_i + R_{d\,i}, \quad (5)$$

where R_{di} – additional resistance of the i-th main.
As the motors are parallel-switched on, then in accordance with the method of electromechanical analogies for the considered drive with two mains (i = 1,2), the following equation should be done

$$\frac{1}{R} = \frac{1}{R_{\Pi 1}} + \frac{1}{R_{\Pi 2}} = \frac{R_{\Pi 1} + R_{\Pi 2}}{R_{\Pi 1}\, R_{\Pi 2}}, \quad (6)$$

where R - is full equivalent hydraulic resistance of the drive.

Thus, the pressure p at the output of the above hydraulic pump in view of (6) should be

$$p = Q \frac{R_{\Pi 1}\, R_{\Pi 2}}{R_{\Pi 1} + R_{\Pi 2}}, \quad (7)$$

where Q - pump feed.

In accordance with the assumptions taken and work scheme of the hydraulic drive (Fig. 1), the inlet pressure in both the mains is equal to the output pressure of the pump p. Then, from (1) and (7) it follows that the amount of power consumption of the hydraulic motors (i = 1,2) will be

$$Q_i = \frac{p}{R_{\Pi i}}; \quad Q_1 = Q \frac{R_{\Pi 2}}{R_{\Pi 1} + R_{\Pi 2}};$$

$$Q_2 = Q \frac{R_{\Pi 1}}{R_{\Pi 1} + R_{\Pi 2}}. \quad (8)$$

From the condition of flows continuity there follows the condition of the equality of pump feed and hydro-motors fluid expenditure [5]

$$Q = Q_1 + Q_2. \quad (9)$$

In connection with the fact that in this hydraulic drive the same engines running with equal pressure are used (Fig. 1), we assume their volumetric efficiency and displacements q_i, $\eta = \eta_{m1} = \eta_{m2\,2}$, $q = q_1 = q_2$ to be the same, and taking it into account, we transpose (9)

$$Q\eta = Q_1\, \eta + Q_2\, \eta = q_1\, n_1 + q_2\, n_2 = q\, n, \quad (10)$$

where $n = n_1 + n_2$ is the sum of the rotation frequencies of all the motors.

Then, from (8) taking into consideration (10) we obtain

$$n_1 = n \frac{R_{\Pi 2}}{R_{\Pi 1} + R_{\Pi 2}}; \quad n_2 = n \frac{R_{\Pi 1}}{R_{\Pi 1} + R_{\Pi 2}}. \quad (11)$$

Let us find the relationship between torque M_i and the output shaft rotation frequency n_i of the hydraulic motors in question. For this purpose we will express the full equivalent hydraulic resistance of main (5) in accordance with (4)

$$R_{\Pi i} = \frac{2\pi\, M_i\, \eta_o}{q^2\, n_i\, \eta_m} + R_{d\,i} = \frac{2\pi\, \eta_o}{q_i^2\, \eta_m} \left(\frac{M_i}{n_i} + \frac{q^2\, R_{d\,i}\, \eta_m}{2\pi\, \eta_o} \right)$$

$$= \frac{1}{a} \left(\frac{M_i}{n_i} + a\, R_{d\,i} \right) \quad (12)$$

where $a = \dfrac{q^2\, \eta_м}{2\pi\, \eta_o}$.

Substituting the expression obtained for the full equivalent hydraulic resistance of main (12) into the formula for defining the hydro-motor shaft rotation frequency (11), after the transformation we will receive for each of them

$$n_1 = n\, n_1 \frac{M_2 + a\, R_{d2}\, n_2}{M_1\, n_2 + M_2\, n_1 + a\, n_1\, n_2 \left(R_{d1} + R_{d2} \right)};$$

$$n_2 = n\,n_2 \frac{M_1 + a\,R_{d1}\,n_1}{M_1\,n_2 + M_2\,n_1 + a\,n_1\,n_2\left(R_{d1} + R_{d2}\right)}. \tag{13}$$

The obtained dependences (13) represent a system of equations, and having solved it we can find the relationship between the torque M_i and the output shaft rotation frequency n_i of the first and second hydro-motors.

It is obvious that system (13) has several solutions. Let us examine them.

1. $n_1 = 0$, then $n_2 = n$.
2. Symmetrically $n_2 = 0$, then $n_1 = n$.
3. $n_1 \neq 0$.

In this case, to find the values of n_1 let us transform the first equation of system (13)

$$\begin{aligned} &M_1\,n_2 + M_2\,n_1 + a\,n_1\,n_2\left(R_{d1} + R_{d2}\right) = \\ &n\left(M_2 + a\,R_{d2}\,n_2\right) \end{aligned}. \tag{14}$$

Considering that $n_2 = n - n_1$, we get the equation for n_1

$$\begin{aligned} &-a\,n_1^2\,\left(R_{d1} + R_{d2}\right) + n_1\left[M_2 - M_1 + a\,n\,\left(R_{d1} + R_{d2}\right) + a\,n\,R_{d2}\right] \\ &= n\left(M_2 - M_1 + a\,n\,R_{d2}\right) \end{aligned} \tag{15}$$

or

$$\begin{aligned} &n_1^2 - n_1\left[\frac{M_2 - M_1 + a\,n\,\left(R_{d1} + R_{d2}\right) + a\,n\,R_{d2}}{a\,\left(R_{d1} + R_{d2}\right)}\right] \\ &+ \frac{n\left(M_2 - M_1 + a\,n\,R_{d2}\right)}{a\,\left(R_{d1} + R_{d2}\right)} = 0 \end{aligned}.$$

(16)

Equation (16) has two roots:

$$n_{11} = \frac{\left(M_2 - M_1 + a\,n\,R_{d2}\right)}{a\,\left(R_{d1} + R_{d2}\right)} \quad и \quad n_{12} = n. \tag{17}$$

Changing the values of the torques and additional resistance of the branches it is possible to achieve the desired ratio of the hydraulic motors rotations. At the equality of additional resistance and torques in the mains $n_{11} = n/2$.

Consider the solution of equation (15) for a special case of the absence of additional hydraulic resistance in both the mains - i.e. $R_{d1} = R_{d2} = 0$. Then, (15) takes the form

$$n_1\left(M_2 - M_1\right) = n\left(M_2 - M_1\right). \tag{18}$$

The obtained equation can be solved as follows:

1.1. $M_1 \neq M_2$, then $n_1 = n$;

1.2. $M_1 = M_2$, then n_1 can have any value in the interval from 0 to n.

Such a variant for working conditions of the broken pump hydraulic drive consisting of two hydraulic motors parallel-switched on to the one hydraulic pump is similar to the operation of the mechanical transmission with the symmetric differential when specific values n_1 and n_2 (subject to the fulfillment of the equation $n = n_1 + n_2$) will be governed by the conditions of the machine operation - motion in a straight line or in turning, the magnitude of the traction resistance, soil conditions, and others.

Consider the work of a single-axle wheel mover with such a hydrostatic drive.

Usually, to prevent slipping it needs a partial blocking of the hydro-differential wheels link. As in the work of the mechanical drive with symmetric differential, various lightly braked devices creating an additional moment of the resistance on the one of the sides $M_{d1(2)}$ are introduced into its structure to ensure the equality of $M_1 = M_2$ и $n_1 = n_2$.

This is done by introducing the flow divider (expense), by changing the working volumes of the controlled hydraulic motors, by an additional hydraulic resistance in the mains of each of the wheels or by braking them lightly.

When installing a flow divider (expense) there takes place its dual throttling: throttling by calibrated holes of the entire flow supplied to the drive of the driving axle and additional throttling by the regulating valve of the flow delivered to the skidding wheel, that reduces the overall efficiency of hydrostatic transmission [5]. The method of partial blocking by changing the working volumes of the controlled hydraulic motors of the driving axle is complex and expensive because of the necessity of ensuring the synchronization of the control and high cost of such hydro-machines. The regulation of the hydro-differential transmission by throttling the drive mains of one of the driving wheels or by its lightly braking is a more simple and less expensive method, whose analogs were realized in ABS and ASR systems of mass-produced vehicles [6] .To determine the magnitude of the control effect, in these systems the information about the torque, angular wheels speed and others is used.

The torque on the hydraulic motors drive shafts of the driving wheels will be equal when

$$\begin{aligned} &r_{k1}\,G_1\left[f_{k1} + \psi_1\left(n_1\right)\right] + M_{d1} = \\ &r_{k2}\,G_2\left[f_{k2} + \psi_2\left(n_2\right)\right] + M_{d2} \end{aligned}, \tag{19}$$

where $r_{k\,1(2)}$ - power radius of the corresponding tire;

$G_{1(2)}$ - the force of gravity acting on the corresponding wheel;

$f_{k\,1(2)}$ - the coefficient of resistance to rolling of the corresponding tire;

$\psi_{1(2)}$ - the relative traction force of the corresponding wheel.

Having solved this equation for specific values of the parameters incoming into it, we can define values for n_1 and n_2.

To prevent slipping in the above drives it is common practice to change the amount of the additional resistance moment $M_{d1(2)}$ ensuring the observance of the equality $n_1 = n_2$. To do this, an additional torque is introduced to the wheel having a lower turning force $P_{k\,i} = G_i\left[f_{k\,i} + \psi_i(n_i)\right]$ and accordingly, a greater rotation frequency of n_i. Then the maximum possible torque value on each of the driving wheels, taking into account their equality, will be equal to

$$M_1 = M_2 = M_{\max}\,, \qquad (20)$$

where M_{max} - maximum torque (torque on the wheel lagging behind).

The required value of the torque $M_{d1}(2)$ can be found from equation (19) at specific values of the parameters incoming into it. So, at the equality of additional hydraulic resistances in both the mains, if $M_2 > M_1$, then from (18) follows $n_1 > n/2 > n_2$. To obtain the equality of angular speeds it needs to increase M_1, introducing an additional (braking) resistance moment

$$\begin{aligned} M_{d1} &= r_{k2}\, G_2\left[f_{k2} + \psi_2(n/2)\right] \\ &- r_{k1}\, G_1\left[f_{k1} + \psi_1(n/2)\right] \end{aligned} \qquad (21)$$

when M_{d2}=0.

As an example, let us consider the case when both equally loaded wheels ($r_{k\,1} = r_{k\,2} = r_k$; $G_1 = G_2 = G$; $f_{k\,1} = f_{k\,2}$) move over the surfaces with different traction characteristics ($\psi_1(n_1) \neq \psi_2(n_2)$). Suppose that $n_1 > n_2$. Then, there is a need to introduce an additional braking torque which is equal to

$$M_{d1} = r_k\, G\left[\psi_2(n/2) - \psi_1(n/2)\right]. \qquad (22)$$

when $M_{d2} = 0$.

The elimination of the slippage is done similarly by introducing additional hydraulic resistances to the drive mains. Fig.2 shows the dependences of changing the value of an additional hydraulic resistance in one of the drive mains, necessary observance of the equality $n_1 = n_2$ from the torque on its shaft and the total efficiency of the drive constructed on the basis of solving the system of equations (13).

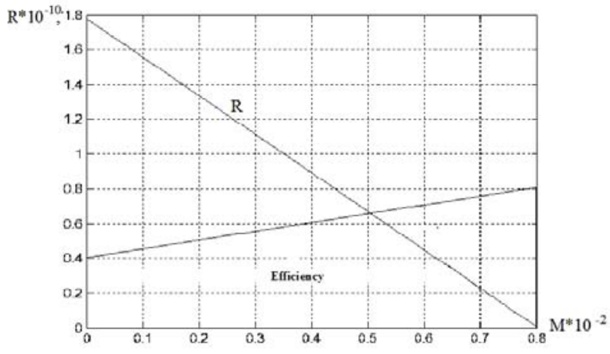

Fig. 2. Dependences of the overall efficiency and additional hydraulic resistance from the torque value in one of the drive mains on its shaft

CONCLUSIONS

Theoretical dependence are obtained to determine the relationship of the power and kinematic parameters of hydraulic machines of the broken pump hydraulic drive with parallel mains.

On the basis of solving the equations obtained the problems of regulating the operation of such drives to ensure the uniformity of hydro-motors rotation frequency are considered. It is established that to ensure the equality of the rotation frequency of the hydraulic motors shafts it needs to maintain the same value of the full equivalent hydraulic resistance of each of the drive mains. Theoretical dependences obtained allow us to examine the work of hydrostatic drives of transport and traction machines movers at different values of their parameters.

Regulating the operation of the hydrostatic drives of the movers can be done by introducing an additional hydraulic resistance into the mains or by additional (braking) resistance moments into the mover.

The introduction of additional hydraulic resistance into the mains reduces the overall efficiency of the hydrostatic drive.

REFERENCES

1. Hydrostatic drives in the transmissions of special self-propelled machines/ Crumbled LN., Golovashkin PP, Shooters A.G. // Bulletin of Moscow state technical University MAMI, 2013. - So 1. № 1. - S. 96-104.

2. Two-axled motor grader GS-10.01/ Linevich V. P, Zhulai V.A. , Serov A.A. // Construction and road machines, 2000. - № 12. - 10 C..

3. Operating modes of controlled hydrostatic transmission in the traction drive power grader/ Zhulai V.A., Yenin V. I, Serov A.A. // Mechanization of construction, 2008. - № 7. - S. 15-16.

4. Research of traction and operation indexes of the grader GS-25.09/ Zhuravlev V.V. Potapov A.P., Zhulai V.A [and other] // Construction and road machines, 2014. - № 1. - N-2 - 5.

5. Petrov V.A. Hydrostatic transmissions of self-propelled machines. M: Mashinostroenie, 1988 - 244 S.

6. Construction of tractors and cars. Training manual / Polivaev I., Vorokhobin A.V., Kostikov A.M. [and other]; edited editorship of Professor I. Polivaev. - S. p.: DOE, 2013. - 288 C.

The Localization of the Robotic Mobile Platforms for Constructions with Laser Tracker and Smarttrack Sensor

Ghelmeci Radu[1*], Dima Marian[1]

[1]The Faculty of Technological Equipment, Technical University of Civil Engineering, Bucharest (Romania)

This paper presents a way in which the localization equipment for the end effector of the industrial robots field of use can be expanded and used for localization of the mobile construction robots. The research paper presents the equipment along with its characteristics, determines the relationships for the localization coordinates by comparison to the forward kinematics of the industrial robot's spherical arm (positioning mechanism in spherical coordinates) and the orientation mechanism with three orthogonal revolute axes and analyses the mobile robot's localization accuracy.

Keywords: Mobile robot, Localization, Localization accuracy, Laser tracker, Smarttrack sensor

1. INTRODUCTION

In this paper, the full localization is defined by the direct or indirect measurement by the instrumentality of sensors for the x, y, z coordinates of the origin and the α, β, γ direction angles of a mobile frame of reference, attached to a mobile object, with respect to fixed frame of reference. The measurements x, y, z, α, β, γ will be further defined localization coordinates.

A mobile construction robot can be considered as being formed by a robotized mobile platform or a carrying module and the robotized work equipment which can be compared to a fixed base industrial robot with respect to the mobile platform, figure 1.

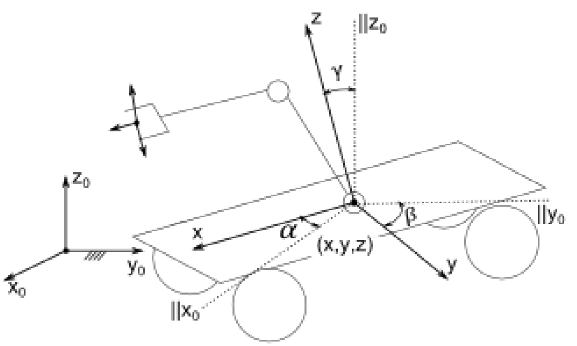

Figure 1: The mobile robot

The programming of such a mobile robot is done based on the inverse kinematics models of the mobile platform and of the work equipment respectively. The inverse kinematics model of the mobile platform is generally deducted [1], starting from the relationships for the nonholonomic constraints expressed in velocities and their integrations cannot be determined in coupled form except the specific cases, such as smooth surface movement and specific trajectories in the straight line, circular arc or zero turn radius [2], often used trajectories in the case of mobile construction robots. For the general situation, the integration is done numerically through odometry and practice has proved that the positioning errors are substantial [3]. The inverse kinematics model for the robotized work equipment does not raise any special problems, being determined through relationships for the holonomic constraints which are expressed in relation to the positions.

According to the working technology, in case of mobile construction robots, two cases can be distinguished. In the first case, the robotic mobile platform is fixed and only the working equipment works; in this case a static localization, carried out after the mobile platform is stopped and before starting the work sequence of the equipment, is required. In the second case, performs the technological process during the movement of the carrying module; in this case is necessary to make a dynamic localization.

On a world scale the experts have designed various sensor systems for the localization of the mobile platforms used in various fields of research [4, 5], some of these can also be used in case of the mobile robots for constructions [6]. One of these is formed by a laser tracker and a "smarttrack" sensor and is further developed.

2. THE LOCALIZATION WITH LASER TRACKER AND SMARTTRACK SENSOR

2.1. The structure of the measurement system of the localization coordinates

The main components of the localization system are as follows[6]:

a) Laser tracker, figure 2,a. This measures in spherical coordinates (azimuth, elevation, distance) the position of the smarttrack sensor with respect to its own frame of reference and it is capable to automatic tracking of the target if moving. The distance is optically measured and the azimuth and elevation are mechanically measured by encoders. The specifications of the laser tracker are presented in table 1.

Smarttrack sensor, figure 2,a. It is capable of self-automatic orientation with respect to laser tracker and measurement of the direction angles (pitch, yaw, roll) of the laser beam, emitted by the laser tracker, with respect to a reference system attached to the fixed mount. The roll angle is optically measured and the pitch and the yaw angles are mechanically measured by encoders. The specifications of the smarttrack sensor are presented in table2.

*Corresponding author: Technical University of Civil Engineering 122-124 Lacul Tei Blv., Bucharest, Romania, ghelmeci@yahoo.com

a)

b)

Figure 2: Laser tracker and smarttrack sensor

Table 1: The specifications of the laser tracker

Parameter	*Specification*
Range of Measurements	100 m
Azimuth	±320°
Elevation	+79°/-59°
Angular Resolution	±0,018 ″
Angular Accuracy	3,5 μm/m
System Resolution	0,1 μm
Maximum Lateral Target Speed	6 m/s
Maximum Acceleration	> 2g
Internal Level Accuracy	±2″
Static Measurement	±10 μm

Table 2: The specifications of the smarttrack sensor

Parameter	*Specification*
Pitch	±55°
Yaw	±140°
Roll	±30°
Tracking distance	40 m
Tracking angular speed	50°/s
Optic centering accuracy	±25 μm
Angular resolution	±3″

2.2. The measurement scheme

In order to attain the full localization of the robotized mobile platform, the laser tracker is put in the origin of the fixed system and the oriented axes with respect to the system of reference with which the attainment of the localization is intended. The smarttrack sensor is mounted on the robotized mobile platform at the known coordinates with respect to the reference system attached to the platform.

The coordinates measured by the two components of the respective system azimuth, elevation, distance, pitch, yaw and roll, show that there is a correspondence between these and the joint variables of a 6 DOF robot, with positioning mechanism in spherical coordinates and orientation mechanism with three orthogonal revolute axes. Therefore, the localization coordinates are determined the same way as the position and the orientation of the end effector of the spherical robot is determined, through the forward kinematics model [1].

Based on the previous reasons, attaching the reference systems in order to determine the localization coordinates is done by using the Denavit-Hartenberg method, therefore in figure 3:

- the fixed frame is chosen with the origin at the intersection of the measurement axes of the laser tracker, the z_0 axis is oriented in according to the vertical direction and is overlapped on the axis of rotation of the laser tracker around which the azimuth is measured in counterclockwise direction; the x_0 axis is located in the horizontal plane and is orientated suitable;
- the system attached to the turret of the laser tracker has the same origin as the fixed system, the z_1 axis is oriented with respect to the rotation axis of the tracker's lens around which the elevation is measured and the x_1 axis is oriented with respect to an optical axis.
- the mobile system attached to the laser tracker's lens has the same origin as the fixed system, the z_2 is oriented along the optical axis with which the z_2 distance is measured and the x_2 is oriented down on the vertical direction;
- the mobile system 3 is attached to the laser beam and has the z_3 axis oriented along it;
- the mobile system 4 is attached on the lens of the smarttrack sensor, has the z_4 axis oriented with respect to the optical axis of it and the roll angle is measured around it;
- the turret of the smarttrack sensor has attached to it system 5 with the z_5 overlapped with the axis of rotation of the turret and around it is measured the pitch angle of the lens rotation with respect to the turret;
- the last reference system is attached on the mount base of the target, it has the z_6 axis oriented on the axis of rotation of the turret with respect to the mount base of the target and around it the yaw angle is measured.

The corresponding Denavit-Hartenberg parameters of the system are centralized in table 3.

Table 3: The corresponding Denavit-Hartenberg parameters of the system

No.		θ_i	d_i	a_i	α_i	q_i
1.	A	θ_1	0	0	270°	θ_1
2.	B	θ_2	0	0	90°	θ_2
3.	C	0	d_3	0	0°	d_3
4.	D	θ_4	0	0	270°	θ_4
5.	E	θ_5	0	0	90°	θ_5
6.	F	θ_6	d_6	0	0°	θ_6

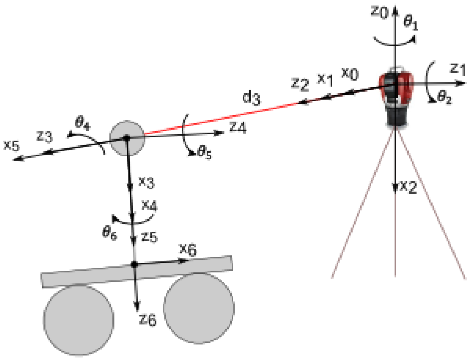

Figure 3: The measurement scheme

2.3. Determining the localization coordinates

Considering a coordinate frame that travels through "the kinematics chain" starting from the $Ox_0y_0z_0$ position to the $Ox_6y_6z_6$ position, the coordinate transformations are thereby written consecutively:

$$T_{i-1}^{i}=\begin{pmatrix} c\theta_i & -s\theta_i c\alpha_i & s\theta_i s\alpha_i & a_i c\theta_i \\ s\theta_i & c\theta_i c\alpha_i & -c\theta_i s\alpha_i & a_i s\theta_i \\ 0 & s\alpha_i & c\alpha_i & d_i \\ 0 & 0 & 0 & 1 \end{pmatrix} \quad (1)$$

in which i= 1...6.

This way, taking into account that α_i are constant and substituting $\sin(\theta_i)=s_i$ and $\cos(\theta_i)=c_i$, the following transformation matrix for the laser tracker results:

$$T_0^3=T_0^1*T_1^2*T_2^3=$$
$$=\begin{pmatrix} c_1c_2 & -s_1 & c_1s_2 & d_3c_1s_2 \\ c_2s_1 & c_1 & s_1s_2 & d_3s_1s_2 \\ -ss_2 & 0 & cc_2 & d_3c_2 \\ 0 & 0 & 0 & 1 \end{pmatrix} \quad (2)$$

for the smarttrack sensor the transformation matrix is obtained:

$$T_3^6=T_3^4*T_4^5*T_5^6=$$
$$=\begin{pmatrix} c_4c_5c_6-s_4s_6 & -c_6s_4-c_4c_5s_6 & c_4s_5 & d_6c_4s_5 \\ c_4s_6+c_5c_6s_4 & c_4c_6-c_5s_4s_6 & s_4s_5 & d_6s_4s_5 \\ -c_6s_5 & s_5s_6 & c_5 & d_6c_5 \\ 0 & 0 & 0 & 1 \end{pmatrix} \quad (3)$$

and for the entire system it is obtained:

$$T_0^6=T_0^3*T_3^6=\begin{pmatrix} r_{11} & r_{12} & r_{13} & r_{14} \\ r_{21} & r_{22} & r_{23} & r_{24} \\ r_{31} & r_{32} & r_{33} & r_{34} \\ 0 & 0 & 0 & 1 \end{pmatrix} \quad (4)$$

Where:

$$\begin{aligned}
r_{11}&=-s_1(c_4s_6+c_5c_6s_4)-c_1c_2(s_4s_6-c_4c_5c_6)\\
&\quad -c_1c_6s_2s_5\\
r_{21}&=c_1(c_4s_6+c_5c_6s_4)-c_2s_1(s_4s_6-c_4c_5c_6)\\
&\quad -c_6s_1s_2s_5\\
r_{31}&=s_2(s_4s_6-c_4c_5c_6)-c_2c_6s_5\\
r_{12}&=c_1s_2s_5s_6-c_1c_2(c_6s_4+c_4c_5s_6)-\\
&\quad s_1(c_4c_6-c_5s_4s_6)\\
r_{22}&=c_1(c_4c_6-c_5s_4s_6)-c_2s_1(c_6s_4+c_4c_5s_6)\\
&\quad +s_1s_2s_5s_6\\
r_{32}&=s_2(c_6s_4+c_4c_5s_6)+c_2s_5s_6\\
r_{13}&=c_1c_5s_2-s_1s_4s_5+c_1c_2c_4s_5\\
r_{23}&=c_5s_1s_2+c_1s_4s_5+c_2c_4s_1s_5\\
r_{33}&=c_2c_5-c_4s_2s_5\\
r_{14}&=d_3c_1s_2+d_6c_1c_5s_2-d_6s_1s_4s_5+d_6c_1c_2c_4s_5\\
r_{24}&=d_3s_1s_2+d_6c_5s_1s_2+d_6c_1s_4s_5+d_6c_2c_4s_1s_5\\
r_{34}&=d_3c_2+d_6c_2c_5-d_6c_4s_2s_5
\end{aligned} \quad (5)$$

From the transformation matrix T_0^6 are identified the coordinates of the origin of the mobile system attached to the mount base of the smarttrack sensor in respect to the fixed system

$$\begin{aligned}
p_x&=r_{14}=d_3c_1s_2+d_6c_1c_5s_2-d_6s_1s_4s_5\\
&\quad +d_6c_1c_2c_4s_5\\
p_y&=r_{24}=d_3s_1s_2+d_6c_5s_1s_2+d_6c_1s_4s_5\\
&\quad +d_6c_2c_4s_1s_5\\
p_z&=r_{34}=d_3c_2+d_6c_2c_5-d_6c_4s_2s_5
\end{aligned} \quad (6)$$

and the direction cosines of the axis of the mobile system with respect to the axis of the fixed reference frame axes

$$\begin{aligned}
n_x&=r_{11}=x_0*x_4=-s_1(c_4s_6+c_5c_6s_4)\\
&\quad -c_1c_2(s_4s_6-c_4c_5c_6)-c_1c_6s_2s_5\\
n_y&=r_{21}=y_0*x_4=c_1(c_4s_6+c_5c_6s_4)\\
&\quad -c_2s_1(s_4s_6-c_4c_5c_6)-c_6s_1s_2s_5\\
n_z&=r_{31}=z_0*x_4=s_2(s_4s_6-c_4c_5c_6)-c_2c_6s_5\\
o_x&=r_{12}=x_0*y_4=c_1s_2s_5s_6-c_1c_2(c_6s_4+c_4c_5s_6)\\
&\quad -s_1(c_4c_6-c_5s_4s_6)\\
o_y&=r_{22}=y_0*y_4=c_1(c_4c_6-c_5s_4s_6)\\
&\quad -c_2s_1(c_6s_4+c_4c_5s_6)+s_1s_2s_5s_6\\
o_z&=r_{32}=z_0*y_4=s_2(c_6s_4+c_4c_5s_6)+c_2s_5s_6\\
a_x&=r_{13}=x_0*z_4=c_1c_5s_2-s_1s_4s_5+c_1c_2c_4s_5\\
a_y&=r_{23}=y_0*z_4=c_5s_1s_2+c_1s_4s_5+c_2c_4s_1s_5\\
a_z&=r_{33}=z_0*z_4=c_2c_5-c_4s_2s_5
\end{aligned} \quad (7)$$

Considering that the smarttrack sensor is mounted on the mobile platform with the O_6 origin situated on its reference point and with the z_6 axis oriented according to the normal of the platform, it results that the localization coordinates have the following expressions:

$$\begin{aligned}
&x(\theta_1,\theta_2,d_3,\theta_4,\theta_5,\theta_6)=p_x=d_3c_1s_2+d_6c_1c_5s_2\\
&\quad -d_6s_1s_4s_5+d_6c_1c_2c_4s_5\\
&y(\theta_1,\theta_2,d_3,\theta_4,\theta_5,\theta_6)=p_y=d_3s_1s_2+d_6c_5s_1s_2\\
&\quad +d_6c_1s_4s_5+d_6c_2c_4s_1s_5\\
&z(\theta_1,\theta_2,d_3,\theta_4,\theta_5,\theta_6)=p_z=d_3c_2+d_6c_2c_5\\
&\quad -d_6c_4s_2s_5\\
&\alpha(\theta_1,\theta_2,d_3,\theta_4,\theta_5,\theta_6)=\mathrm{acos}(n_x)=\\
&\quad =\mathrm{acos}[-s_1(c_4s_6+c_5c_6s_4)\\
&\quad -c_1c_2(s_4s_6-c_4c_5c_6)-c_1c_6s_2s_5]\\
&\beta(\theta_1,\theta_2,d_3,\theta_4,\theta_5,\theta_6)=\mathrm{acos}(o_y)=\\
&\quad =\mathrm{acos}[c_1(c_4c_6-c_5s_4s_6)\\
&\quad -c_2s_1(c_6s_4+c_4c_5s_6)+s_1s_2s_5s_6]\\
&\gamma(\theta_1,\theta_2,d_3,\theta_4,\theta_5,\theta_6)=\mathrm{acos}(a_z)=\\
&\quad =\mathrm{acos}(c_2c_5-c_4s_2s_5)
\end{aligned} \quad (8)$$

2.4. Localization accuracy

The accuracy of the localization of the robotized mobile platform depends on the accuracy with which the localization coordinates $x, y, z, \alpha, \beta, \gamma$ are measured. In their turn, the accuracy of localization coordinates depends on the measurement accuracy of the joint variables azimuth, elevation, pitch, yaw, roll, specified by the system manufacturer [6].

The connection between the two sets of accuracies is attained by Taylor series expansion of the localization coordinates expressions (8) and the maintaining of the expansion terms all the way to degree one. Under these terms, after the derivations execution it results that:

$$\begin{aligned}
\Delta x &= \frac{\partial x}{\partial \theta_1}\Delta\theta_1 + \frac{\partial x}{\partial \theta_2}\Delta\theta_2 + \frac{\partial x}{\partial d_3}\Delta d_3 + \frac{\partial x}{\partial \theta_4}\Delta\theta_4 \\
&\quad + \frac{\partial x}{\partial \theta_5}\Delta\theta_5 + \frac{\partial x}{\partial \theta_6}\Delta\theta_6 \\
\Delta y &= \frac{\partial y}{\partial \theta_1}\Delta\theta_1 + \frac{\partial y}{\partial \theta_2}\Delta\theta_2 + \frac{\partial y}{\partial d_3}\Delta d_3 + \frac{\partial y}{\partial \theta_4}\Delta\theta_4 \\
&\quad + \frac{\partial y}{\partial \theta_5}\Delta\theta_5 + \frac{\partial y}{\partial \theta_6}\Delta\theta_6 \\
\Delta z &= \frac{\partial z}{\partial \theta_1}\Delta\theta_1 + \frac{\partial z}{\partial \theta_2}\Delta\theta_2 + \frac{\partial z}{\partial d_3}\Delta d_3 + \frac{\partial z}{\partial \theta_4}\Delta\theta_4 \\
&\quad + \frac{\partial z}{\partial \theta_5}\Delta\theta_5 + \frac{\partial z}{\partial \theta_6}\Delta\theta_6 \\
\Delta \alpha &= \frac{\partial \alpha}{\partial \theta_1}\Delta\theta_1 + \frac{\partial \alpha}{\partial \theta_2}\Delta\theta_2 + \frac{\partial \alpha}{\partial d_3}\Delta d_3 + \frac{\partial \alpha}{\partial \theta_4}\Delta\theta_4 \\
&\quad + \frac{\partial \alpha}{\partial \theta_5}\Delta\theta_5 + \frac{\partial \alpha}{\partial \theta_6}\Delta\theta_6 \\
\Delta \beta &= \frac{\partial \beta}{\partial \theta_1}\Delta\theta_1 + \frac{\partial \beta}{\partial \theta_2}\Delta\theta_2 + \frac{\partial \beta}{\partial d_3}\Delta d_3 + \frac{\partial \beta}{\partial \theta_4}\Delta\theta_4 \\
&\quad + \frac{\partial \beta}{\partial \theta_5}\Delta\theta_5 + \frac{\partial \beta}{\partial \theta_6}\Delta\theta_6 \\
\Delta \gamma &= \frac{\partial \gamma}{\partial \theta_1}\Delta\theta_1 + \frac{\partial \gamma}{\partial \theta_2}\Delta\theta_2 + \frac{\partial \gamma}{\partial d_3}\Delta d_3 + \frac{\partial \gamma}{\partial \theta_4}\Delta\theta_4 \\
&\quad + \frac{\partial \gamma}{\partial \theta_5}\Delta\theta_5 + \frac{\partial \gamma}{\partial \theta_6}\Delta\theta_6
\end{aligned} \tag{9}$$

$$\begin{aligned}
\Delta x &= \{-d_3 s_1 s_2 - d_6[c_5 s_1 s_2 \\
&\qquad + s_5(c_1 s_4 + c_2 c_4 s_1)]\}\Delta\theta_1 \\
&\quad + [d_3 c_1 c_2 + d_6 c_1(c_2 c_5 - c_4 s_2 s_5)]\Delta\theta_2 \\
&\quad + c_1 s_2 \Delta d_3 - d_6 s_5(c_4 s_1 + c_1 c_2 s_4)\Delta\theta_4 \\
&\quad + \{d_6[c_1(c_2 c_4 c_5 - s_2 s_5) - c_5 s_1 s_4]\}\Delta\theta_5 \\
\Delta y &= \{d_3 c_1 s_2 + d_6[c_1(c_5 s_2 + c_2 c_4 s_5) \\
&\qquad - s_1 s_4 s_5]\}\Delta\theta_1 \\
&\quad + [d_3 c_2 s_1 + d_6 s_1(c_2 c_5 - c_4 s_2 s_5)]\Delta\theta_2 \\
&\quad + s_1 s_2 \Delta d_3 + d_6 s_5(c_1 c_4 - c_2 s_1 s_4)\Delta\theta_4 \\
&\qquad + d_6[c_1 c_5 s_4 \\
&\quad - s_1(s_2 s_5 - c_2 c_4 c_5)]\Delta\theta_5 \\
\Delta z &= [-d_3 s_2 - d_6(c_5 s_2 + c_2 c_4 s_5)]\Delta\theta_2 + c_2 \Delta d_3 \\
&\quad + d_6 s_2 s_4 s_5 \Delta\theta_4 - d_6(c_2 s_5 + c_4 c_5 s_2)\Delta\theta_5 \\
\Delta\alpha &= \frac{c_5 s_1 s_2 + s_5(c_1 s_4 + c_2 c_4 s_1)}{\sqrt{1 - [c_1 c_5 s_2 - (s_1 s_4 - c_1 c_2 c_4)]^2}}\ \Delta\theta_1 \\
&\quad - \frac{c_1(c_2 c_5 - c_4 s_2 s_5)}{\sqrt{1 - [-s_1 s_4 s_5 + c_1(c_5 s_2 + c_2 c_4 s_5)]^2}}\ \Delta\theta_2 \\
&\quad + \frac{s_5(c_4 s_1 + c_1 c_2 s_4)}{\sqrt{1 - [c_1 c_5 s_2 - s_5(s_1 s_4 - c_1 c_2 c_4)]^2}}\Delta\theta_4 \\
&\quad + \frac{c_1(s_2 s_5 - c_2 c_4 c_5) + c_5 s_1 s_4}{\sqrt{1 - [c_1(c_5 s_2 + c_2 c_4 s_5) - s_1 s_4 s_5]^2}}\Delta\theta_5 \\
\Delta\beta &= -\frac{s_5(c_1 c_2 c_4 - s_1 s_4) + c_1 c_5 s_2}{\sqrt{1 - [s_5(c_1 s_4 + c_2 c_4 s_1) + c_5 s_1 s_2]^2}}\Delta\theta_1 \\
&\quad - \frac{s_1(c_2 c_5 - c_4 s_2 s_5)}{\sqrt{1 - [s_1(c_5 s_2 + c_2 c_4 s_5) + c_1 s_4 s_5]^2}}\Delta\theta_2 \\
&\quad - \frac{s_5(c_1 c_4 - c_2 s_1 s_4)}{\sqrt{1 - [s_5(c_1 s_4 + c_2 c_4 s_1) + c_5 s_1 s_2]^2}}\Delta\theta_4 \\
&\quad - \frac{s_1(c_2 c_4 c_5 - s_2 s_5) + c_1 c_5 s_4}{\sqrt{1 - [s_1(c_5 s_2 + c_2 c_4 s_5) + c_1 s_4 s_5]^2}}\Delta\theta_5 \\
\Delta\gamma &= \frac{c_5 s_2 + c_2 c_4 s_5}{\sqrt{1 - (c_2 c_5 - c_4 s_2 s_5)^2}}\Delta\theta_2 \\
&\quad - \frac{s_2 s_4 s_5}{\sqrt{1 - (c_2 c_5 - c_4 s_2 s_5)^2}}\Delta\theta_4 \\
&\quad + \frac{c_2 s_5 + c_4 c_5 s_2}{\sqrt{1 - (c_2 c_5 - c_4 s_2 s_5)^2}}\Delta\theta_5
\end{aligned} \tag{10}$$

The following facts are deducted from the analysis of the relationships (10):

- the accuracies of the localization coordinates are not constant in the measurement range . They are variable according to the θ_1, θ_2, d_3, θ_4, θ_5, θ_6 joint variables and their $\Delta\theta_1$, $\Delta\theta_2$, Δd_3, $\Delta\theta_4$, $\Delta\theta_5$, $\Delta\theta_6$ accuracies;
- the accuracies of the Δx, Δy, Δz, Δα, Δβ, Δγ localization coordinates are not dependent, each on its own of the variables θ_1, θ_2, d_3, θ_4, θ_5, θ_6 of the measurement system.

The manner in which the localization coordinates accuracies is variable in function of each joint variable, for the equipment described in §2.1 is illustrated in figure 4. In order to plot these graphics the nature of the variables has been respected, such as distance or angles. Thereby, in the first six diagrams the variations of localization coordinates accuracies Δx, Δy, Δz, Δα, Δβ, Δγ are presented in function to the θ_1, θ_2, θ_4, θ_5, θ_6 angular variables of the measurement systems and in the last diagram it is shown the variation of the linear coordinate accuracies of the localization as a function of the d_3 distance. The measurement units used in the diagrams are expressed in [m] for the linear coordinates and for linear accuracies and [rad] for the angular coordinates and angular accuracies.

Considering the attained results and the graphic presentations it can be observed that:

- the θ_1, θ_2, d_3 joint variables of the laser tracker have a substantially bigger influence on the accuracy of the localization than the θ_4, θ_5, θ_6 joint variables of the smarttrack sensor.
- the maximum localization error is of approximately 150 μm for the linear coordinates and of approximately $8 * 10^{-6}$ rad or 5 arc seconds for the angular coordinates.

3. CONCLUSIONS

1. By using an equipment made of a laser tracker and a smarttrack sensor, a full localization, static or dynamic, can be made for a mobile construction robot in an area of approximately 40 m.
2. The calculus relationships for the localization coordinates are deducted by analogy with the forward kinematics model of the industrial robot with positioning mechanism in spherical coordinates and orientation mechanism with three orthogonal revolute axes.

   The accuracy with which the localization is performed is sufficient for the construction field, even for the finishing.

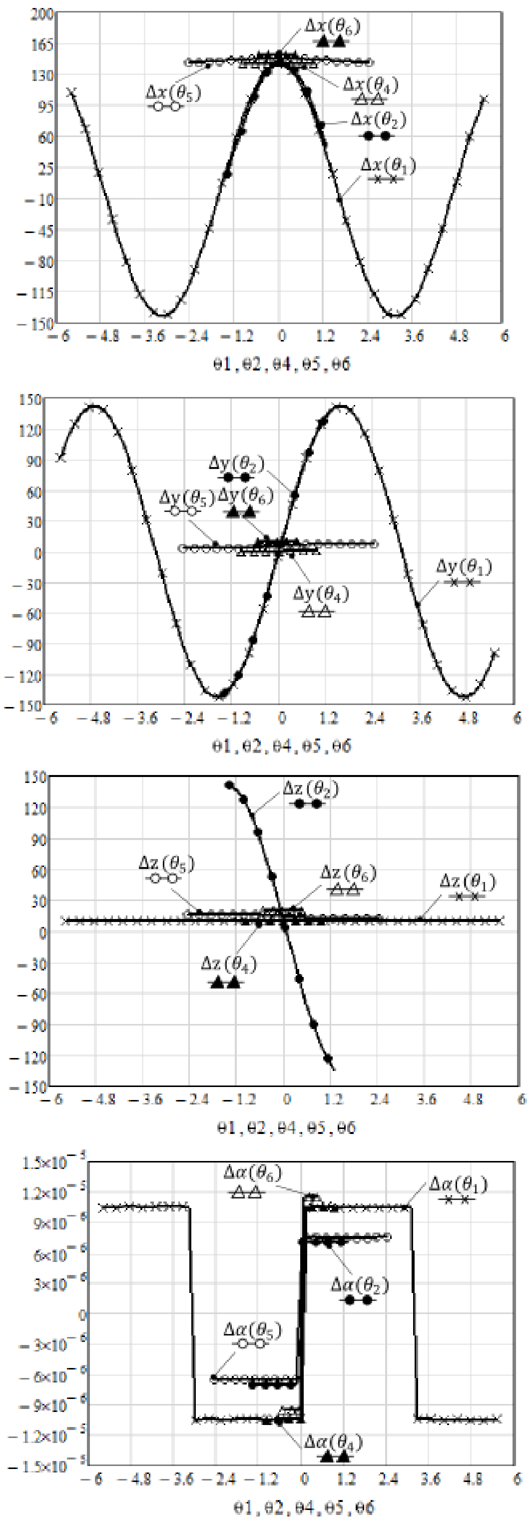

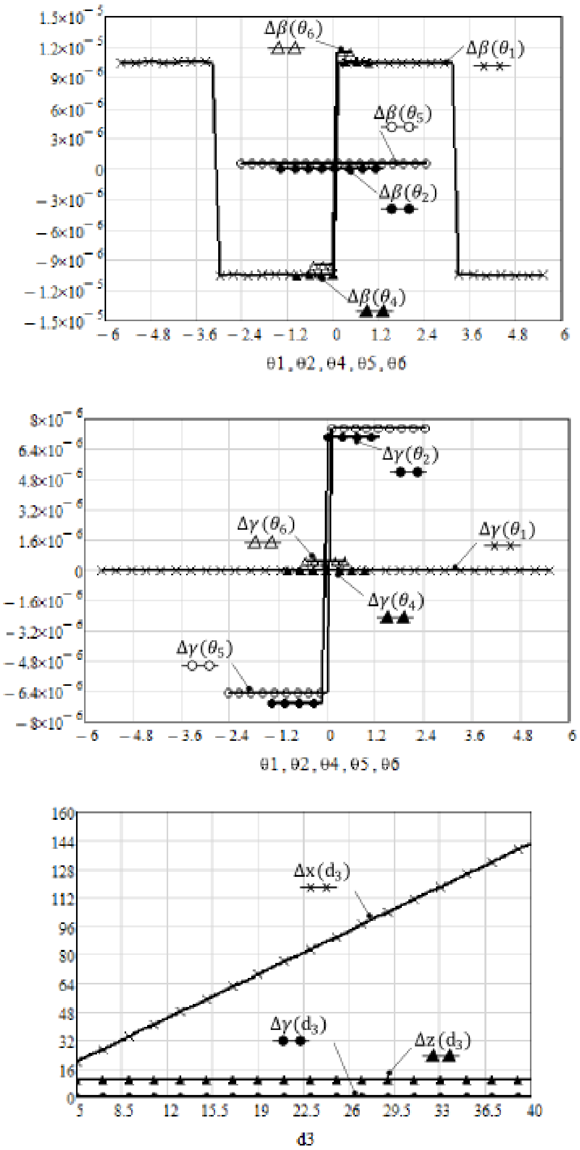

Figure 4: The variation of the accuracy localization

REFERENCES

[1] Siciliano B., Sciavicco L., Villani L., Oriolo G., "*Robotics. Modelling, Planning and Control*", Springer, 2009

[2] Sescu G. C., Tănase N., Vlad M., "*Kinematic model for a portable robotized module navigation*", SRMA2011, Kraljevo, Serbia, 2011

[3] Peter van Turennout, "*Autonomous Motion on Wheels*", Universiteitsdrukkerij T.U. Delft, 1994, ISBN 90 9006530 X

[4] http://www. leica-geosystems.com

[5] http://www.faro.com

[6] http://www.apisensor.com

Comparison of Two Approaches to Identification Process of Condenser in Thermal Power Plant

Novak N. Nedić [1], Saša Lj. Prodanović [2*]
[1]Faculty of Mechanical and Civil Engineering in Kraljevo, University of Kragujevac, Kraljevo (Serbia)
[2] Faculty of Mechanical Engineering East Sarajevo, University of East Sarajevo, East Sarajevo (Bosnia and Herzegovina)

Appropriate mathematical model of process is being emphasized because it affects to possibilities of system analysis and synthesis. Transfer functions of condenser of turbine in the thermal power plant Gacko (B&H) obtained according two different identification methods have been analised and compared in this research. Identification based on input and response of real condenser (i.e. its level as function of time) had been carried out and considered, versus one performed by simulating of relay feedback test in the previous surveys. Final evaluation of the both transfer functions of condenser has been established after tuning of PI controller, which exists in the control system of level in condenser in mentioned power plant, and analysis of system responses. Namely, they were tuned using the same method, i.e. internal model principle (IMP) and their calculated parameters were introduced and simulated in the entire control system to get process responses.

Keywords: Level in condenser, Identification methods, Internal model principle, PI control.

1. INTRODUCTION

Within the all methodologies of system analysis and synthesis, which begin with mathematical model of process, tuning of the controller is one of most important parts. Researches in this paper refer to the defining this model, i.e. identification of the process, that is in some variants necessary for enabling of good controller. There are a lot of approaches in obtaining of process transfer function. Each of them has its minor or major advantages and disadvantages. The quality of process behaviour, as a main topic, depends on abilities researchers and operators to recognize, how features of methods influence (through entire procedure) on the final desired process performance. Some authors, (Åström and Hägglund) prefer relay feedback test, while the others (Ziegler and Nichols) base their identification ways on the real responses [1]. Meaningful overview of this topic can be seen in [2,3]. Surely, modelling using physical postulates shouldn't be neglected.

This survey is focused on the control system of level in condenser of turbine in thermal power plant Gacko. Previous investigations of this system [4,5] were performed in order to enable good system characteristics through the appropriate tuned controller. PI controller is chosen because this type of controllers is the most suitable to the first order processes, how this condenser should be modelled. That is an attempt to obtain PI controller parameters using scientific principles, and thus avoid current practice of tries and mistakes. The idea for this research has appeared after comparing recorded condenser response with its simulated variant obtained using relay feedback test for process identification. It was seen that mathematical model can be derived more accurately, i.e. identification method may be better. Improvement of this procedure will be carried out here. Therefore, two approaches in identification of this condenser will be compared by analyzing responses that will be obtained using simulation. First approach is based on relay feedback test [5], but the second one is combination of data collected from real process response and formulas taken from previous models of this control system that were calculated according physical postulates. Mentioned simulation is performed using block diagram of energy saving strategy that was developed for this control system in [4].

The importance of defining the most representative model of process is bigger because internal model principle (IMP) will be utilized for calculating parameters of PI controller.

2. CONTROL SYSTEM STRUCTURE

Brief explanation of system functioning will be exposed, in order to place this problem into industrial environment. This control strategy was developed and suggested in previous investigations and it is based on use of frequency regulators in order to reduce energy consumption of the entire control system [4].

Level control is performed using two closed-loops, as it shown in Fig. 1. The first one refers to the condensate drainage from the condenser and the second refers to the demineralised (DEMI) water supply.

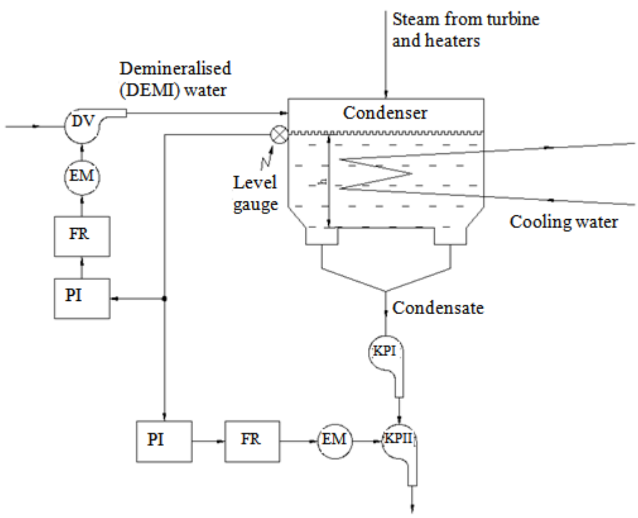

Figure 1: Structural diagram of system for level control in the condenser of turbine [4]

*Corresponding author: Vuka Karadžića 30, East Sarajevo, Bosnia and Herzegovina, sasa.prodanovic@ues.rs.ba

Meaning of the mentioned abbreviations is:

- PI – proportional – integral controller,
- FR – frequency regulator,
- EM – electric motor (asynchronous),
- DV – centrifugal pump for DEMI water supply,
- KP I – centrifugal condense pump first order,
- KP II – centrifugal condense pump second order.

Primary task of this control system is to achieve and hold level in condenser on the reference value $h_{\check{z}}$=120 cm. According structural diagram in the Fig. 1, technical documentation of the thermal power plant Gacko and physical postulates, mathematical model of whole control system has been obtained, i.e. its block diagram has been formed. This block diagram that was composed component by component is shown in Fig. 2 [4,6,7,8,9]. Its simulated responses, obtained after introducing of previously calculated controller's parameters (P and I) into it, will be used for evaluating of identification procedure (process transfer function).

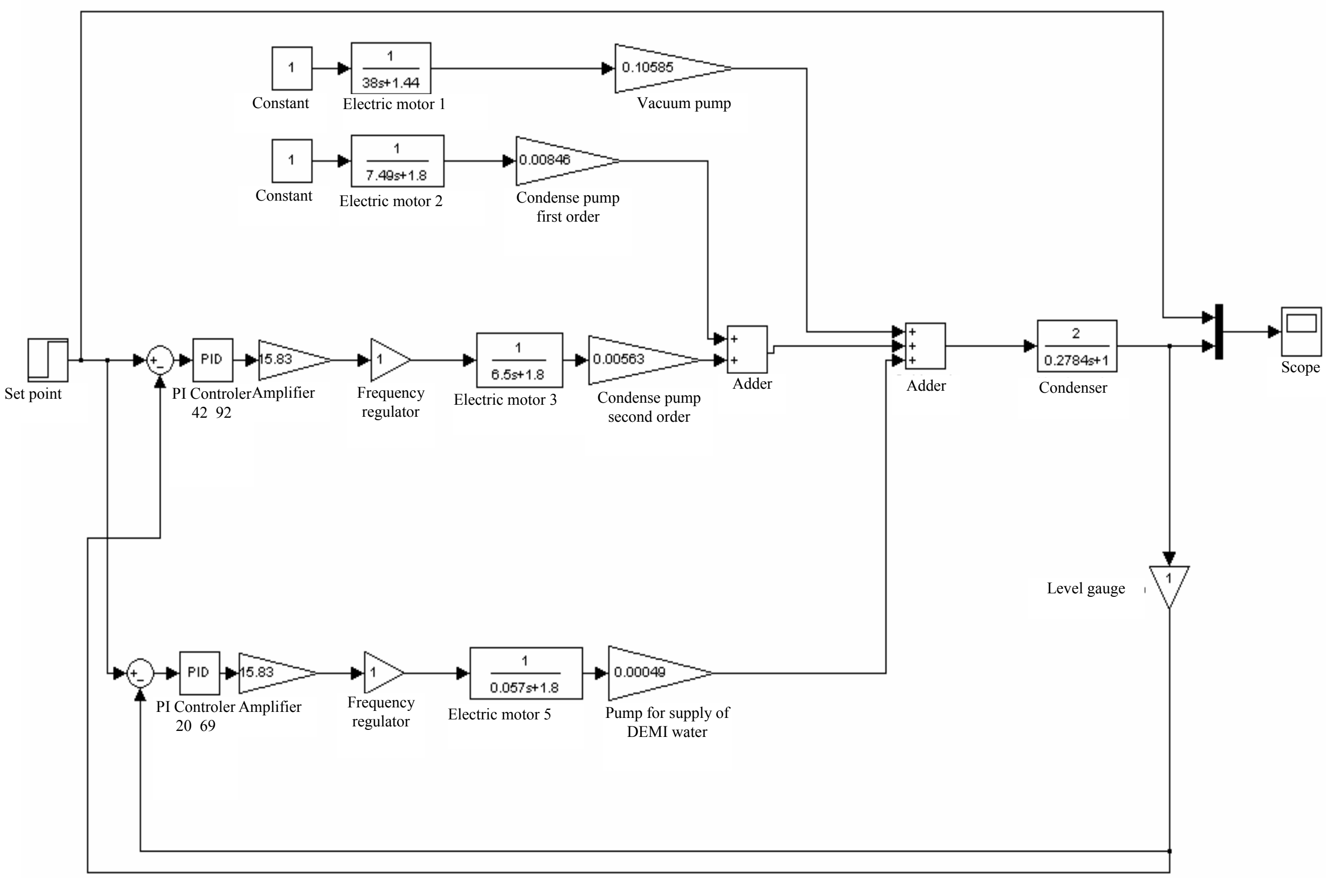

Figure 2: Block diagram of control system of level in condenser of turbine in the thermal power plant Gacko with energy saving strategy [4,6,7,8,9]

3. PROCES IDENTIFICATION AND TUNING OF PI CONTROLLER

This chapter is consisted of two parts. Here will be considered process response (level in the condenser as a function of time), which has been recorded during two different intervals. Both parts include identification procedure according real process response and tuning of PI controller using internal model principle (IMP). Knowing that the process identification in previous surveys has been followed by tuning of PI controller using IMP, as one step in evaluation its quality, here PI controllers will be tuned using the same method. The reason for that is to enable comparison of different methods for process identification. Two graphs of level in the condenser in thermal power plant Gacko has been taken during its exploitation.

3.1. First response

Possibility for recording condenser response is enabling process identification based on data taken from its graph. Response graph for the first case is shown in Fig 3.

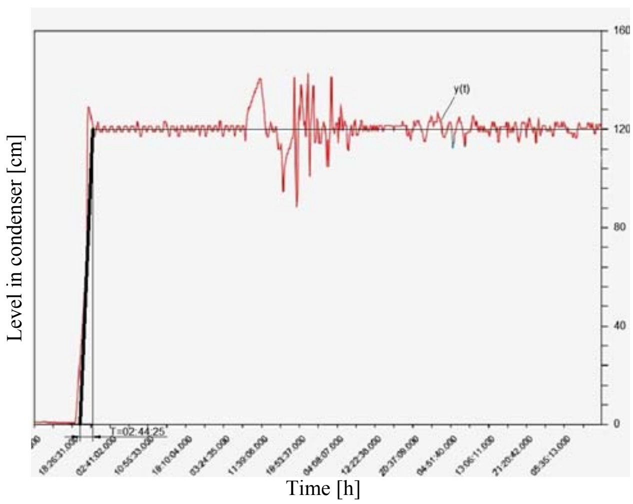

Figure 3: First graph of level in the condenser [9]

Like in previous researches, first-order model (1) has been taken as general model of this process.

$$G(s)=\frac{K}{Ts+1} \quad (1)$$

Meaning of the symbols in this process transfer function is: T – time constant of process and K – process gain.

Graphs in the Fig. 3 and Fig. 4 show that level rises immediately after starting up the entire plant. Because of that, only difference, in regard to model obtained using relay feedback test [5], is referring to the neglecting of dead time L.

Identification procedure, which will be presented here, is consisted of calculation of parameters in (1), i.e. time constant T and gain K. At first, tangent should be put in the point of the maximum slope of curve. Afterward, points of its intersection with stationary values of response before and after influence of step input (starting up the plant) have to be detected. Time between these two points is taken as time constant T of process.

The main specificity of this proposed identification procedure stems from the inability to determine exact process gain by calculating ratio between stationary value of output and input value: $K=\Delta y/\Delta u$. More precisely, input value wasn't shown in graph. Because of that, process gain has been calculated as a sum of gains of the pumps (vacuum pumps, condense pump first order, condense pump second order and pump for supply of DEMI water). Reason for that is their position just in front of the condenser in block diagram, i.e. they have the biggest influence on level in time.

Therefore, here applied method is combination of identification based on real process response (for T) and physical postulates (for K) [4,6,7,8,9].

According graph in Fig. 3, taking into account length ratio and decimal form, time constant is obtained T=2.74 h. Considering block diagram in Fig. 2 process gain is calculated K=0.12, and then mathematical model of process in the first case, i.e. its transfer function $G_1(s)$, is given by:

$$G_1(s)=\frac{0.12}{2.74s+1} \quad (2)$$

3.2. Second response

To enable better model of process another response was recorded and analysed.

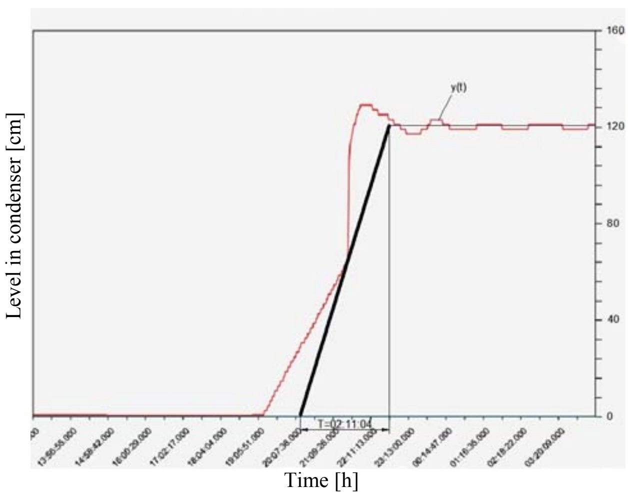

Figure 4: Second graph of level in the condenser [9]

It was done to minimize possibility for making mistake due to unacceptable process behaviour in some case. After observing of Fig. 4, where the second graph is shown, immediately is noticeable that both responses (Fig. 3 and Fig. 4) have similar and good shape.

In this case process gain is same like in first variant of model $G_1(s)$, but time constant slightly deviates and its value is T=2.184 h. Therefore, transfer function $G_2(s)$ obtained from second response (Fig. 4) is represented by:

$$G_2(s)=\frac{0.12}{2.184s+1} \quad (3)$$

3.3. Tuning of PI controller

Characteristic of the IMP is impact of manipulated variable both on object and its model in the controller. Afterward, these two outputs are comparing in real time in order to determine error, based on which, controller adjusts manipulated variable. That is shown in Fig. 5.

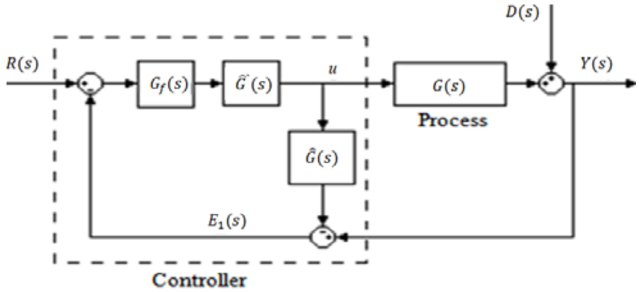

Figure 5: Controller which is based on internal model principle [1]

Where:

- $G(s)$ – process transfer function,
- $\hat{G}(s)$ – model of process,
- $\hat{G}^{`}(s)$ – approximate inversion of process model,
- $G_f(s)$ – filter transfer function,
- u – manipulated variable,
- E_1 – error,
- $D(s)$ – disturbance.

More comprehensive presentation of mathematical apparatus for deriving the forms for the parameters of the PI controller is presented in [1].
Finally it can be written as:

$$K_p(s)=\frac{T}{K\left(L+T_f\right)} \quad (4)$$

$$T_i=T \quad (5)$$

where T_f is time constant of filter.
Time constant of filter has been taken $T_f=T$ [1].

In tuning PI controller based on transfer function $G_1(s)$ (first case) taking into account $T_f(s)$=T=2.74 h following parameters have been calculated: K_p=8.33 (proportional action) and T_i=2.74 h, and afterward K_i=K_p/T_i=3.04 (integral action).

Second case of tuning of PI controller has been carried out using transfer function $G_2(s)$. Here parameters have following values: T_f=T=2.184 h, K_p=8.33, T_i=2.184 h and afterward K_i=K_p/T_i=3.81.

In both calculations process dead time is L=0 because transfer functions $G_1(s)$ and $G_2(s)$ were defined as first order without dead time.

It is known that this tuning method can be automatized too. Hence, this survey represents basis for IMP application in many control loops in thermal power plant Gacko, where computer support for system control and monitoring has already been installed. This fact increases possibilities for its researching in order to improve process characteristics.

4. CHECKING, ANALYSIS AND COMPARISON OF MODELS

As stated before, quality of each model is checking after introducing PI controller's parameters, calculated from exactly that model, into block diagram of entire control system of level in condenser. Knowing the aim of this survey, simulations for three variant of process transfer functions were carried out and considered. Two process transfer functions (cases) has been derived in this paper using identification procedure based on real process responses and partly physical postulates, but third one $G_3(s)$, that was enabled based on relay feedback test as identification way, was taken from [2,5]. This previously investigated model is:

$$G_3(s) = \frac{0{,}645}{0{,}046s+1} e^{-0{,}139s} \tag{6}$$

Obviously it was identified as first-order plus dead time model.

Corresponding parameters of PI controller were tuned using IMP too: K_p = 0,06 and K_i = 1,3. The effects of these parameters were analysed in [5].

4.1. Checking of the models

The goal was to determine which identification procedure is better. In order to get appropriate display, i.e. all responses in one graph, block diagrams from Fig. 2 for three different tuned PI controllers were involved in separated subsystems. As it can be seen in Fig. 6.

In Fig. 6 subsystems 1, 2 and 3 contain PI controllers that have been tuned based on mentioned 1, 2 and 3 identification cases, respectively.

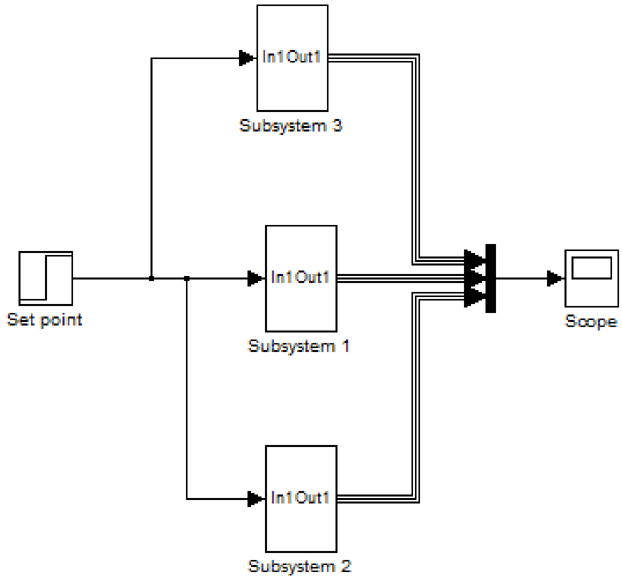

Figure 6: Configuration for simulation of entire control system in three cases

Fig. 7 shows responses of condenser of turbine, i.e. level as a function of time, for three cases of model identification which give three variant of PI controller's parameters.

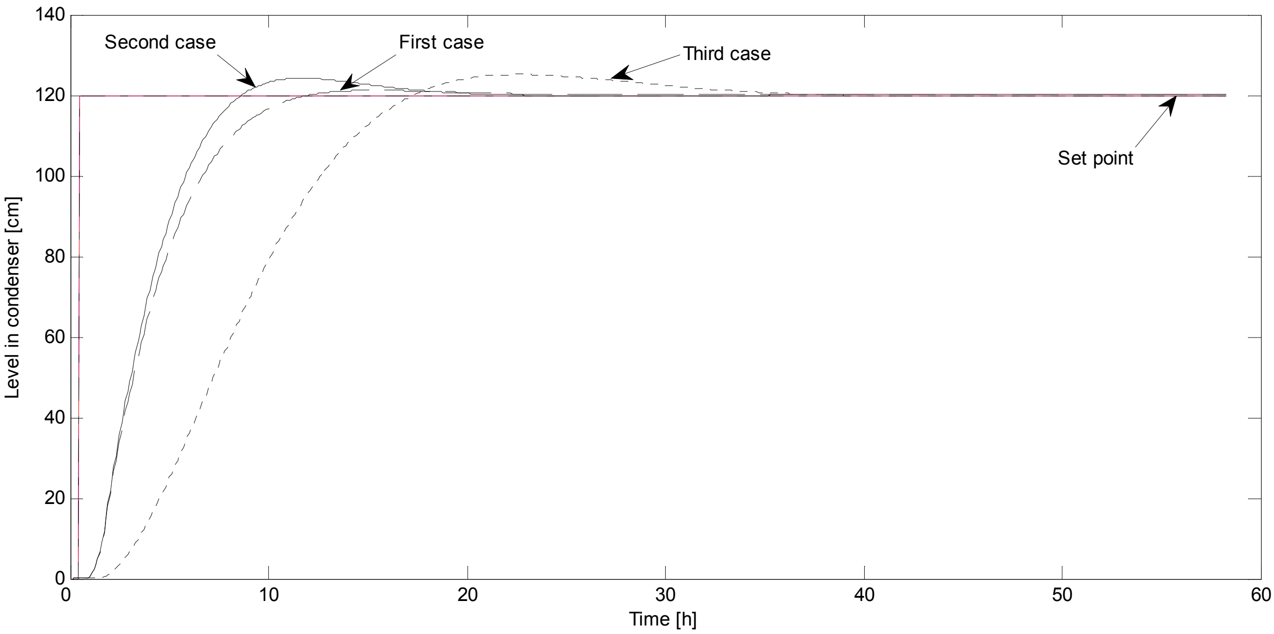

Figure 7: Responses of control system for three cases of model identification

4.2. Analysis of the models

Defining whether some model can be taken as appropriate is based on observation its response and evaluation its deviation from real condenser response. This analysis has purpose to decide whether two models (first and second case) can be taken as represent of identification procedure based on recorded response. This is very important since one can't precisely put tangent on recorded process response, because it don't look like theoretical example, which is shown in Fig. 8. Better say, it is broken line in considered cases (Fig.3 and Fig.4). Mentioned can be the cause of model error that was derived from observed response.

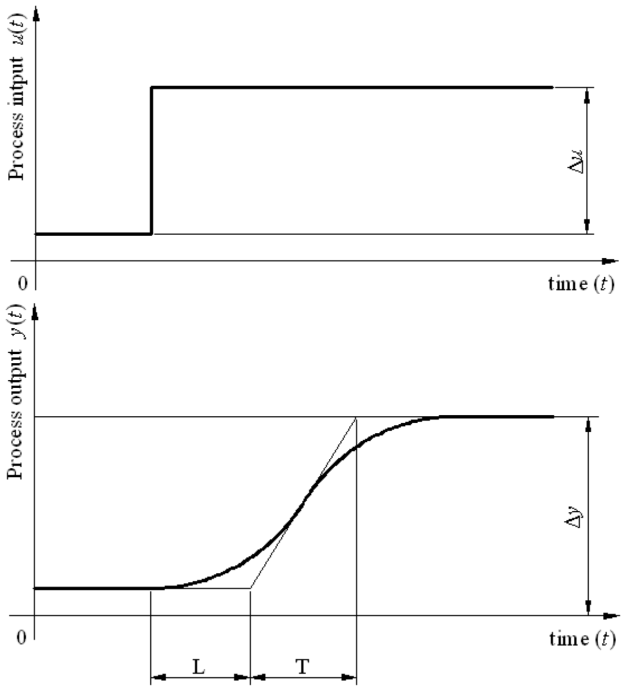

Figure 8: Example for process input and output

After analysis of quality indicators of responses in Fig. 7 it is noticeable that all simulated processes are stable and they have similar shape as recorded responses. More precisely, response for third case has already been known from [5].

4.3. Comparison of the models

In order to get a clearer overview of researches in this paper and enable some contribution to understanding its structure, some connections are given in following Table 1.

Table 1: Some connections in the paper

Identification procedure	Transfer function	Mark on Fig. 7
Based on recorded response and physical postulates	$G_1(s)$	First case
	$G_2(s)$	Second case
Based on relay feedback test	$G_3(s)$	Third case

All of these simulated process outputs have appropriate overshoot, since neither one has value higher than 10%. However, it should be emphasized that in first case is the lowest value of overshoot.

Considering the rising time and time constant it is noticeable that the response in second case is faster than other two responses.

Second case of response has the least value of settling time.

According stated, response in second case has the best performance. It means that transfer function $G_2(s)$ is the best mathematical model of object. Very significant fact is: both simulated responses (and therefore transfer functions $G_1(s)$ and $G_2(s)$), which were obtained using recorded responses and partly physical postulates, have better dynamic and static characteristics than one that was formed based on relay feedback test. Above mentioned states lead to conclusion that identification procedure using recorded real response of object is better than one which use relay feedback test when control system of level in condenser of turbine in thermal power plant Gacko is subject of consideration.

5. CONCLUSIONS

Comparison of recorded condenser response with its simulated variant obtained in [5] has shown that this model do not fully represent dynamic behaviour of object because of it has slower response and longer settling time. New identification way has been suggested here. Validity evaluation of this new method was carried out in three steps: forming of object's transfer functions, tuning of PI controllers based on that models and analysis and comparison of responses which were simulated in block diagram of entire control system of level in condenser that was modelled in previous surveys using physics postulates.

For more comprehensive research, two recorded condenser's responses were considered in order to confirm validity of identification procedure, which involve them as baseline. Therefore, the aim was to define new model of process and compare it with other one which has obtained from different identification procedure.

Determination of best model (transfer function) is important because it has main impact on the accuracy of tuning PI controller according internal model principle, as well as enabling, as good as possible, mathematic model for future researches of this system.

After comprehensive comparison between above explained two identification approaches, it can be concluded that suggested identification procedure, which is based on recorded real condenser response and partly physical postulates, is appropriate for control system of level in condenser in thermal power plant Gacko. This, in addition, leads to conclusion that IMP can be used for tuning of PI controller for this control system of level, but it is necessary to use model of process that is good enough (which has been determined here).

The advantage of this identification approach, beside his accuracy, is avoidance physical introducing of new component, i.e. relay, into control system and eventual causing unpredictable system behaviours during carrying out of relay feedback test (because of default oscillatory state of output). The lack of this procedure is reflected in possible difference between nominal parameters of systems based on which is modelled entire energy saving strategy and its real values in exploitation during recording of condenser's response.

REFERENCES

[1] V. Ž. Filipović, N. N. Nedić, „PID Controllers", University of Kragujevac, Faculty of Mechanical Engineering Kraljevo, Kraljevo, (Serbia), (2008)

[2] C. C. Yu, "Autotuning of PID Controllers", Springer, London, (Grait Britain), (2006)

[3] Q. G. Wang, T.H. Lee, and C. Lin, „Relay Feedback: Analysis, Identification and Control", Springer, London, (Grait Britain), (2003)

[4] S. Prodanović, „Analysis and improvement of control system of condensate level in condenser of turbine in thermal power plant Gacko“, Master Thesis, University of Kragujevac, Faculty of Mechanical Engineering Kraljevo, (Serbia), (2009)

[5] N. N. Nedić and S. Lj. Prodanović, „Some Modifications in the Process Identification and Tuning of Controller of Level in Condenser in Thermal Power Plant“, Proceedings of XI International SAUM Conference on Systems, Automatic Control and Measurements, Niš (Serbia), November 14th-16th, 2012, pp. 382-385, (2012)

[6] D. LJ. Debeljković, G. V. Simeunović, V. S. Mulić, „Mathematical models of objects and processes in automatic control systems“, University of Belgrade, Faculty of Mechanical Engineering, Belgrade, (Serbia), (2006)

[7] D. LJ. Debeljković, A. M. Sićović, G. V. Simeunović, V. S. Mulić, „Mathematical models of objects and processes in automatic control systems, part II“, University of Belgrade, Faculty of Mechanical Engineering, Belgrade, (Serbia), (2006)

[8] D. LJ. Debeljković, V. S. Mulić, G. V. Simeunović, A. M. Sićović, „Mathematical models of objects and processes in automatic control systems, part III“, University of Belgrade, Faculty of Mechanical Engineering, Belgrade, (Serbia), (2007)

[9] Technical documentation of the control system of condensate level in condenser of turbine in thermal power plant Gacko

Harmonic Analysis of a Pneumatic Fixed Orifice

Dragan Piršić [*], Ljubiša Dubonjić, Vladimir Stojanović
[1]Faculty of Mechanical and Civil Engineering in Kraljevo, University of Kragujevac, Kraljevo (Serbia)

Orifices, with constant or variable cross-section areas, are essential components in pneumatic circuits. Dynamic and static characteristics of pneumatic systems depend on their flow characteristics. They have a special role in control components in which are used for mass flow control. In this paper the focus is on pneumatic system consisted of fixed orifices and pneumatic chamber. The characteristics of the fixed orifice are presented in frequency domain. For the purpose of analysis, the sinusoidal input describing function is used, obtained by simulation with nonlinear model.

Key words: fixed orifice, mass flow rate, describing function, Hammerstein model, pneumatic chamber

1. INTRODUCTION

Pneumatic servosystems are widely used in industrial applications because of the favourable performances/price ratio. However, high precision control of such systems is difficult due to their complex physical nature. The main causes of that complexity are: air compressibility, friction between the contact surfaces, nonlinear flow-pressure characteristics of the orifice type restriction and parameter variations [1-3]. In order to solve the problem of design and control of such systems, it is necessary to have better understanding of their nonlinear characteristics. A mathematical model which should clarify the most relevant dynamic and nonlinear behaviour in the pneumatic system is used for that purpose.

Fixed orifices are frequently encountered in pneumatic systems. As the nonlinear characteristics of the orifices reflect in the operation of the whole pneumatic system, they are observed and modelled as a separate subsystems. The paper presents and analyzes the nonlinear mass flow rate characteristics of fixed orifice in frequency domain.

One of the methods of analysis of nonlinear-systems the quasi-linearization method [4, 5]. Linearization in the ordinary sense is not valuable in the case when nonlinearity inputs exceed the limits of acceptable linear approximation or when there is discontinuity at the nominal operating point. The advantages of true linearization are kept in the case of quasi-linearization but there is no limit to the range of input signal magnitudes or to the selection of the operating point. The constraint is that linear description of the system depends on some properties of the input signal. The system description thus depends not only on the system itself, but also on the signals passing through the system (which is a property of nonlinear systems). In other words, quasi-linearization is performed for a certain form of input signal. The problem with nonlinear systems with feedback configurations is in difficult determination of the signal form which occurs on entering the nonlinearity. This is the main constraint of the method. It is not always possible to reduce the nonlinearity input signal to a simple form. The practical solution of the problem is to assume the form of the input signal in advance. In practice, three forms of input signals are used in quasi-linearization [4, 5]: bias, sinusoid and Gaussian process.

The quasi-linear function which approximatively describes nonlinearity is called the describing function (DF). As the design of control systems is frequently realized in the frequency domain, the Sinusoidal Input Describing Function (SIDF) is used in this paper. Assuming that the linear part of the system filters high order harmonics (low-pass filter), every periodic signal is reduced to a basic periodic function on entering the nonlinearity. In the case of memoryless nonlinearity, the SIDF represents the gain which is changed depending on the amplitude of the input signal.

The paper determines the SIDF of the nonlinear mass flow rate characteristic of pneumatic fixed orifice.

2. MASS FLOW-RATE CHARACTERISTIC OF PNEUMATIC FIXED ORIFICE

Fixed orifice characteristics depend on the environment in which a fixed orifice is used. In this paper we consider a pneumatic system consisting of a fixed orifice (Or) and a chamber (Ch) of constant volume (V) as shown in Fig. 1. The system is connected to a variable pressure source (Ps). Downstream pressure P depends on chamber dynamic. The chamber represents a generic load (e.g. actuator chamber) and has a role of low-pass filter. Therefore, it should be noted that the following analysis applies when the fixed orifice is connected to a storage type load.

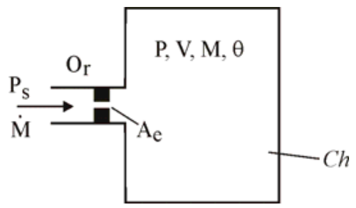

Figure1: Fixed orifice with chamber

The mass flow rate through the restriction can be in sonic or subsonic conditions depending upon the ratio of upstream-downstream pressure. According to the standard theory flow rate through the fixed orifice can be presented

*Corresponding author: Dositejeva 19, Kraljevo 36000, Serbia, prsic.d@mfkv.kg.ac.rs

in the form [6]:

$$\dot{M} = A_e \varphi(P_S, P, \theta_S) \tag{1a}$$

where the function φ is defined as:

$$\varphi(P_S, P, \theta_S) = \begin{cases} C_1 \dfrac{P_S}{\sqrt{\theta_S}} & if \quad \dfrac{P}{P_S} \le P_{cr} \\ C_2 \dfrac{P_S}{\theta_S} \left(\dfrac{P}{P_S}\right)^{\frac{1}{\kappa}} \sqrt{1 - \left(\dfrac{P}{P_S}\right)^{\frac{\kappa-1}{\kappa}}} & if \quad P_{cr} < \dfrac{P}{P_S} \le 1 \end{cases} \tag{1b}$$

while the parameters C_1, C_2 and P_{cr} are determined by:

$$C_1 = \sqrt{\frac{\kappa}{R}\left(\frac{2}{\kappa+1}\right)^{\frac{\kappa+1}{\kappa-1}}}, \quad C_2 = \sqrt{\frac{2\kappa}{R(\kappa-1)}} \qquad P_{cr} = \left(\frac{2}{\kappa+1}\right)^{\frac{\kappa}{\kappa-1}} \tag{1c}$$

If the downstream to upstream ratio is smaller than a critical value P_{cr} (0.528 for air), the flow is sonic and the function of upstream pressure is linear. If the pressure ratio is higher than P_{cr}, the flow is subsonic and depends nonlinearly on both pressures.

It can be seen that the mass flow rate, for a given effective area of restriction (A_e), depends on supply pressure (P_S), upstream temperature (θ_S), and working pressure P. Further, we assume that upstream pressure and air temperature in the chamber are constant (isothermal chamber) and equal to the ambient temperature:

$$\theta = \theta_a = \theta_S = const. \tag{2}$$

The relation (1) is graphically shown in Fig.2 for $A_e = 2.063x10^{-7}\ m^2$ and different values of working pressure. The supply pressure, as exogenous quantity, changes in the interval $\left(P_a < P_S \le 2.5P\right)$.

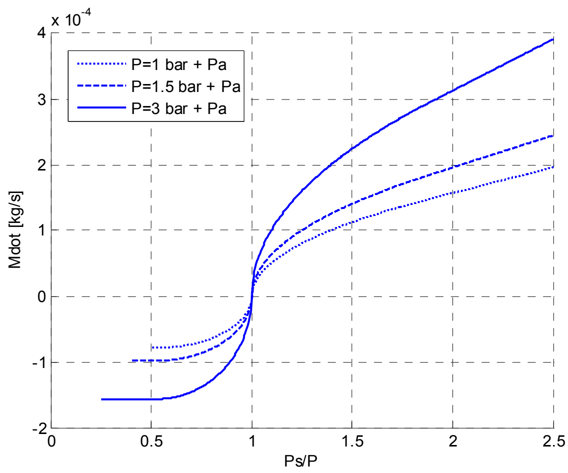

Figure 2: Mass flow rate through fixed orifice

For $P_S > P_a$ and $P_S / P \ge P_{cr}$ (sonic regime) the flow rate through an orifice has a constant value. For $P_{cr} \le P_S / P \le 1/P_{cr}$ (subsonic regime) the flow rate is a nonlinear function of square root-type. For $P_S / P > 1/P_{cr}$ (sonic regime) the flow rate is a linear function of P_S / P. Our objective is to introduce a quasi-linear operator which describe approximately the transfer characteristic of nonlinearity in frequency domain. It should be noted that justification for linearization of the mass flow in a subsonic regime depends on the choice of nominal operating point and the amplitude of the supply pressure P_S. In this paper we determine the describing function of the operating point:

$$P_S / P = 1\,;\ \dot{M} = 0 \tag{3}$$

3. DESCRIBING FUNCTION OF FIXED ORIFICE

Since the descriptive function of fixed orifice depends on the dynamics of the whole system we will first define a mathematical model of the pneumatic system from Fig.1. The dynamics of the pneumatic system can be shown by pseudo bond graph as shown in Fig 3.

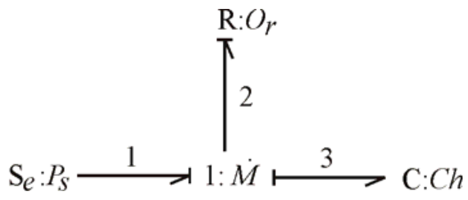

Figure 3: Pseudo bond graph of pneumatic system

A pressure and mass flow are used as energy values. The energy that comes from a constant pressure source (*E*-type source) is partly converted into heat in dissipator *R* and partly goes to the chamber, which represents the storage of *C*-type. The constitutive relation of the dissipator *R* is determined by flow characteristics of fixed orifice. For causality shown in Fig 3 the nonlinear block diagram of the pneumatic system is shown in Fig.4.

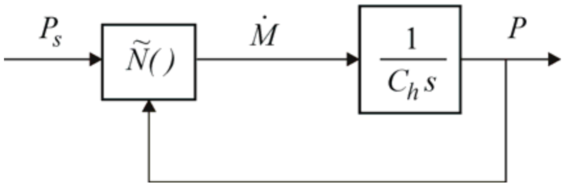

Figure 4: Nonlinear block diagram of pneumatic system

The nonlinearity $\tilde{N}()$ is determined by equations (1). We will now find the parameter C_h. Neglecting the kinetic and potential energy of the gas, based on the first law of thermodynamics, for the chamber we can write:

$$\frac{d}{dt}\left(C_v M \theta\right) = C_p \dot{M} \theta_S - A_h h\left(\theta - \theta_a\right) = C_p \dot{M} \theta \tag{4}$$

Using the state equation for a perfect gas:

$$PV = MR\theta \tag{5}$$

Based on (2), (4) it can be written:

$$C_h \frac{dP}{dt} = \dot{M} \tag{6}$$

where C_h:

$$C_h = \frac{V}{\kappa R\theta} \tag{7}$$

Our goal is that, in frequency domain, we find the appropriate Hammerstein model of the system, as shown in Fig.5.

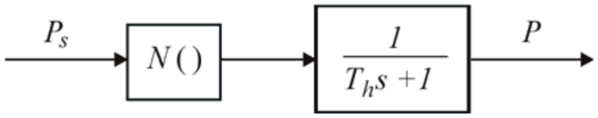

Figure 5: Hammerstein model of pneumatic szstem

Models from Fig.4 and Fig.5 are equivalent in the sense that the second model sufficiently accurate approximates the first model in frequency domain. The model shown in Fig.5 has separated linear dynamics and nonlinearity $N()$ whose describing function we need to determine. The linear part is the first order and the unity-gain. The time constant has the value:

$$T_h = \frac{C_h}{K_L} = \frac{1}{\omega_c} \tag{8}$$

where ω_c is cutoff frequency of linearized frequency characteristics of the pneumatic system.

The amplitude and phase characteristics of the linear part are given by the following equations:

$$A(\omega) = \frac{1}{\sqrt{1+(\omega T_h)^2}} \tag{9a}$$

$$\varphi(\omega) = -\tan^{-1}(\omega T_h) \tag{9b}$$

Now, let us suppose that for a change of exogenous pressure:

$$P_s = P_{sA}\sin(\omega t) \tag{10}$$

a change of the operating pressure P in a stationary regime, is a periodic function that can be approximated by basic harmonics of the Fourier series:

$$P = a_0 + a_1\cos(\omega t) + b_1\sin(\omega t) \tag{11a}$$

or

$$P = a_0 + \sqrt{a_1^2 + b_1^2}\,\sin(\omega t + \varphi) \tag{11b}$$

where

$$a_0 = \frac{1}{2\pi}\int_{-\pi}^{\pi} P\, d(\omega t) \tag{12a}$$

$$a_1 = \frac{1}{\pi}\int_{-\pi}^{\pi} P\cos(\omega t)\, d(\omega t) \tag{12b}$$

$$b_1 = \frac{1}{\pi}\int_{-\pi}^{\pi} P\sin(\omega t)\, d(\omega t) \tag{12c}$$

$$\tan(\varphi) = a_1 / b_1 \tag{12d}$$

Similarly, based on (6) the mass flow through the orifice, in the frequency domain, can be approximated by:

$$\begin{aligned}\dot{M} &= C_h\omega[b_1\cos(\omega t) - a_1\sin(\omega t)] \\ &= C_h\omega\sqrt{a_1^2 + b_1^2}\cos(\omega t + \varphi)\end{aligned} \tag{13}$$

For many mechanical systems, due to the inertial nature, previois assumption is valid, i.e. they have necessary low-pas characteristics. For the system from Fig.4, accuracy of this assumption depends on the values of the time constant C_h of linear dynamics. This assumption is a fundamental condition for the application of SIDF technique, which requires that the input signal to the nonlinear element be essentially in sinusoidal form. The reason is that a limit of all periodic functions after propagation through law-pass linear filter is a sinusoid.

Values of coefficients a_1 and b_1 cannot be found in the analytical form due to the complexity of expressions (1) and (10). For the determination it is used the simulation of *A.C. potentiometer method* [2] for the nonlinear model which is shown in Fig.4. A shematic diagram of this method is shown in figure Fig.6.

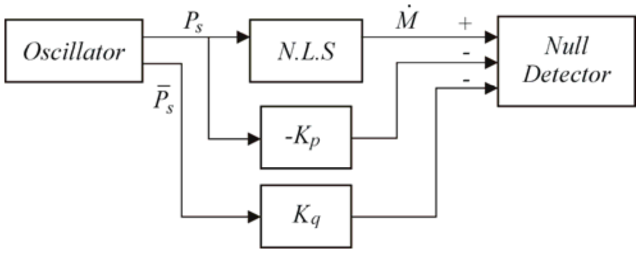

Figure 6: A.C. potentimeter method schematic view

At the oscillator output two signals of frequency ω are generated. One is P_s which is defined by (10) and the other is $\overline{P}_s$ and has the form:

$$\overline{P}_s = P_{sA}\cos(\omega t) \tag{14}$$

The signal P_s is used as the exogenous signal for the nonlinear system (N.L.S). It is recorded the change of variable $\dot{M}$ at the output. Variable gains K_p and K_q are set thus, in a steady state, it holds:

$$\dot{M} \approx K_q\cos(\omega t) - K_p\sin(\omega t) \tag{15}$$

For the determination of optimal values of parameters K_p and K_q the particle swarm optimization method is used [7]. The objective function has the form:

$$OF = (1/2\pi)\int_{0}^{2\pi} e^2 d(\omega t) \qquad (16a)$$

where is:

$$e = \dot{M} - \left[K_q \cos(\omega t) - K_p \sin(\omega t)\right] \qquad (16b)$$

After that, we can determine the value of coefficients in (11):

$$a_1 = K_p P_{sA} / (C_h \omega) \qquad (17a)$$

$$b_1 = K_q P_{sA} / (C_h \omega) \qquad (17b)$$

In Fig.7 the values of coefficients a_1 and b_1 are shown for different frequency and amplitude values of the input signal P_{sA}.

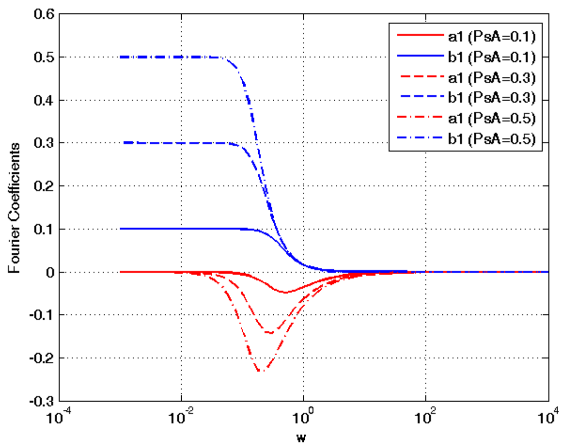

Figure 7:Fourier coefficients

It can be seen that the coefficient a_1 has a negative value in the whole interval for ω and all values of the input signal amplitude. The coefficient b_1 has a positive value. For small values of frequencies ($\omega < 10^{-2}$) we have:

$$a_1 = 0 \text{ i } b_1 = P_{sA} \qquad (18a)$$

which means that a phase shift of the system is equal to zero and a gain is equal to one. For large frequency values ($\omega > 10$) a completely signal attenuation is obtained:

$$a_1 = b_1 = 0 \qquad (18b)$$

The change of pressure P of nonlinear model (Fig.4) and its corresponding approximation (P_{apr}) which is defined by (11a) for $P_{sA} = 0.2$ and $\omega = 0.5$ are shown in Fig.8a.

The mass flow rate ($\dot{M}$) and its corresponding approximation ($\dot{M}_{apr}$) for the pressure change from previous figure are shown in Fig.8b.

The most significant changes of a_1 and b_1 occur on a mean interval. In Fig.9 it is shown the ratio a_1/b_1 on the interval $10^{-1} < \omega < 1$ for different values of P_{sA}.

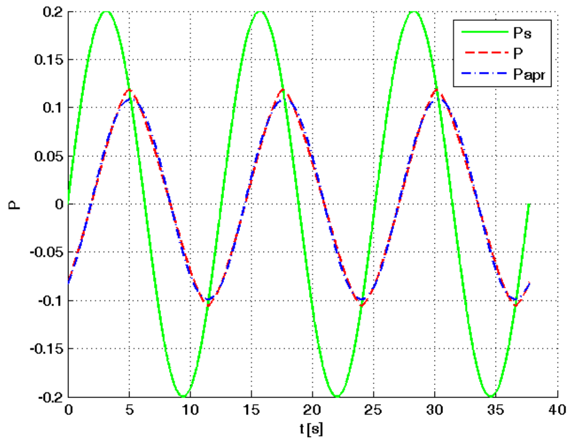

Figure 8a: Simulated pressure and approximation

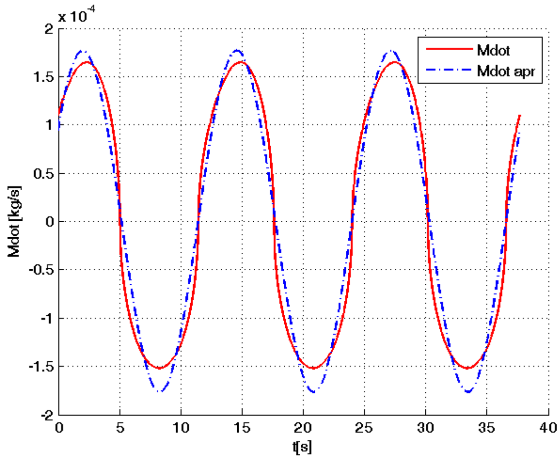

Figure 8b: Simulated mass flow rate and approximation

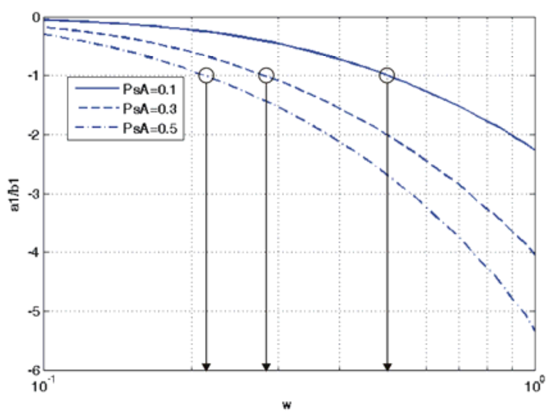

Figure 9: Relationship a_1/b_1

The picture shows the values for ω in which $a_1 = -b_1$. Based on (12d), at these frequencies a phase delay of the system is $-\pi/4$. For $C_h = 8.49x10^{-9}$ [ms^2] the values are obtained:

$$\omega^* = [0.5; 0.28; 0.21] \qquad (19)$$

Figs. 10a and 10b show the frequency characteristics of the whole system.

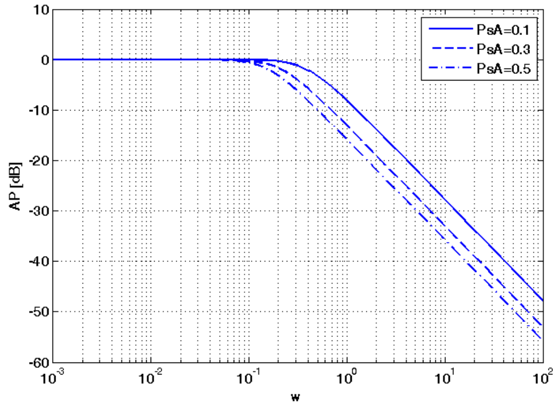

Figure 10a: Amplitude response

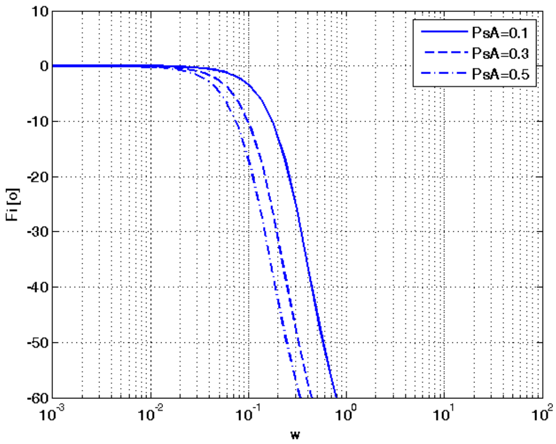

Figure 10b: Frequency response

With amplitude changing of the input signal the time constant of the system is also changed. At higher input amplitude the system becomes slower. It can be seen that the cutoff frequency of the whole system is determined by the cutoff frequency of the linear part (9). This means that the time constant for given amplitudes of the input signal is determined by frequencies (19)

$$T_h = [2;\ 3.57;\ 4.76]\ [\,s\,] \tag{20}$$

For these time constants and the model which is shown in Fig.5 it can be numerically calculated the describing function of nonlinearity $N()$. Fig. 11a shows the module of describing function and the argument depending on the frequency of the input signal is shown in Fig. 11b.

It can be seen that the describing function depends on a frequency of the input signal and its amplitude. Around an inflection frequency the gain decreases and move in the interval [0.8 - 1]. It is also decreased the phase at the interval from 10^0 (phase sequencing) to -3^0 (phase delay).

Nomenclature

$\dot{M}$ - mass flow rate through orifice kg/s

A_e - effective area of restriction m^2

κ - specific heat ratio [.]

R - gas constant $J/(kgK)$

P - absolute pressure Pa

θ - temperature K

Subscripts

a - atmosphere

u - upstream

d - downstream

N - nominal operating regime

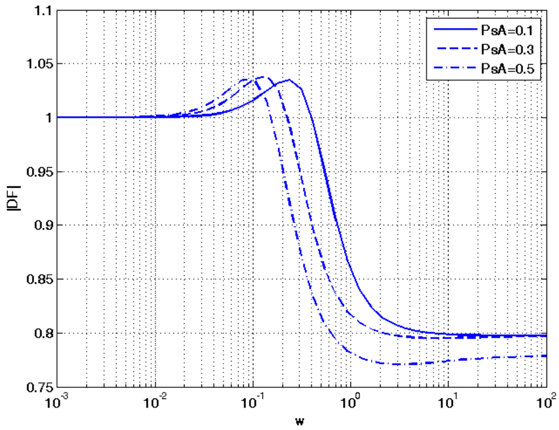

Figure 11a: |DF| - ω dependency

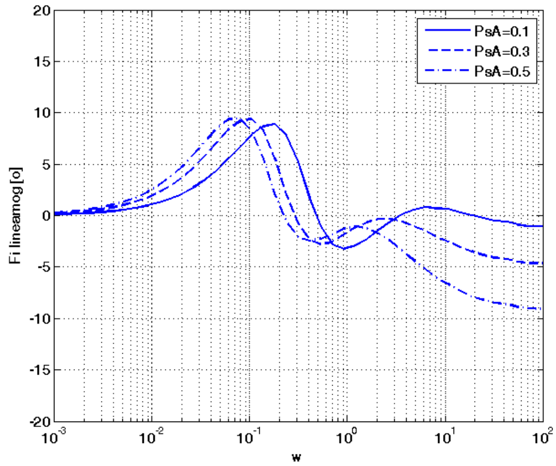

Figure 11b: arg(DF) - ω dependency

4. CONCLUSION

The presented system is a frequent configuration in pneumatic systems. In order to simplify the analysis the initial nonlinear model is transformed into an equivalent Hammerstein model. Instead of nonlinearity of two inputs it is introduced the nonlinearity with a single input. New nonlinearity is described by the describing function. For the determination of describing function simulation results are used. Describing function is dependent on the amplitude and frequencies of the input signal. In addition, the time constant of the linear part is changed with amplitude changing of the input signal.

ACKNOWLEDGMENT

This research has been supported by the Serbian Ministry of Education, Science and Technological Development through project TR 33026. Also, this research has been supported by the European Commission through IPA Adriatic and the project ADRIA-HUB.

REFERENCES

[1] Antonio Carlos Valdiero, Carla Silvane Ritter, Cláudio Fernando Rios, And Marat Rafikov, (2011) Nonlinear Mathematical Modeling in Pneumatic Servo Position Applications, Mathematical Problems in Engineering, Volume, 16pages

[2] João Falcão Carneiro, Fernando Gomes De Almeida, (2011) Undesired Oscillations in Pneumatic Systems, Nonlinear Science and Complexity, Editors Machado, J.A.T., Luo, A.C.J., Barbosa, R.S., Silva, M.F., Figueiredo, L.B., Springer, pp 229-243

[3] N. A. Daw, J. Wang, Q. H. Wu, J. Chen, Y. Zhao, (2003) Parameter identification for nonlinear pneumatic cylinder actuators, Nonlinear and Adaptive Control, LNCIS 281, Editors A. Zinober and D. Owens, Springer-Verlag Berlin Heidelberg , pp. 77-88

[4] Arthur Gelb, Wallace E. Vander Velde, (1969) Multiple-Input Describing Functions And onlinear System Design, McGraw-Hill.

[5] D.P. ATHERTON, (1975) Nonlinear Control Engineering, van Nostrand Reinhold Co. , London.

[6] Anderson, B. W., (1967) The Analysis and Design of Pneumatic Systems, Wiley, New York.

[7] J. Kennedy;R. Eberhart (1995) "Particle swarm optimization" *Proceedings of IEEE International Conference on Neural Networks* IV pp. 1942-1948

Mathematical Modeling, Identifiction and Optimization of Parameters of the Valve Plate of the Water Hydraulic Piston-Axial Pump/Motor

Radovan Petrovic[1,*], Nenad Todic[2], Jelena Zivkovic[3], Zoran Glavčić[2]
[1] University Union Nikola Tesla of Belgrade, Faculty for Strategic and Operational Management,Belgrade, Serbia
[2] Faculty for Mechanical and Civil Engineering, University of Kragujevac, Kraljevo, Serbia
[3] Faculty of Engineering, University of Kragujevac, Kragujevac, Serbia

In the development of application software for mathematical modeling , identification and parameter optimization of the water hydraulic piston axial pump/motor , special attention is paid to the real need for practical engineers . The optimization of seven characteristic parameters of the water hydraulic axial piston pump/motor including: vacuum pressure , the volume of the pressure chamber , the volume of the suction chamber , parietal radius of the inlet opening of the valve plate , the angle for the start of suction on the switchboard , actuating the valve spring stiffness and length of the supply pipeline in order to achieve maximum coefficient times the cylinder. Special attention in this paper is given to optimizing the parietal radius of the inlet opening of the valve plate. Noting here that in the course of optimization and parameter identification of the water hydraulic axial piston pump/motor , automatically creates and displays hundreds of complex 2- D diagrams , which allows the exploration hydrodynamic processes at any time , if necessary, can intervene by changing the input data , wherein the changing the flow identification, and the following optimization .

Keywords: Valve plate, Piston ,Axial, Pump,Motor,

1. INTRODUCTION

For the mathematical modeling of hydrodynamic and dynamic processes in the piston-axial pump/motor (cylinder pumps, suction and pressure chamber, the pressure valve in the high pressure line), adopted the following general assumpti: changes in the quasi-steady state fluid, except in the discharge pipe where there is a heat exchange with the environment; the kinetic energy of the fluid in all of the control region other than the discharge pipe are ignored; leakage of fluid through the gaps (gaps between the piston and cylinder leakage through the valve plate and discharge valve) is quasistationary; processes in the control areas are isothermal or isentropic; field of force (such as gravity) are ignored because they are small in comparison to the inertial forces and the pressure forces. the mathematical model is presented for each element, given the complexity of individual processes and their interdependence and the need for further development of the mathematical model. in this way greatly facilitates modular programming on the computer and further training and monitoring of computer programs. The mathematical model predicted two choices suction or thrust distribution bodies. The physical model investigated axial piston pump comprises distributing the combined working fluids. The working fluid is drawn into the cylinders of the internal cavity of the pump/motor body through the opening of the valve plate and axial holes in the pistons. When working stroke of piston working fluid is released through the pressure valves in the discharge chamber. Contact clip with hair panel at the pump is achieved through a spherical head cut off.

2.MATHEMATICAL MODELING OF FLOW SECTION

Performance of hydrodynamic processes in piston - axial pump/motor is in direct function of the change in flow cross-section distribution bodies Figure 1. Constructive performance distribution organs most often based on the so-called right choice,distribution panel or the selection valve. Modern construction piston - axial pump/motor in the choice of distribution bodies appear in combination valve plate and valves which leads to better results in the suction phase and suppression, and therefore receive a higher volume and overall efficiency of the pump/motor.

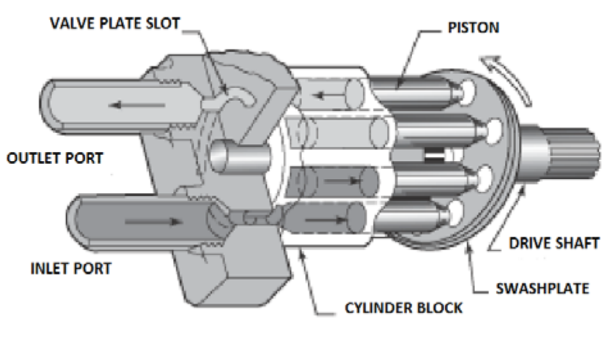

Figure 1. Construction of a piston axial pump/motor

*Corresponding author: radovan4700@yahoo.com

2.1.Determine the size of the opening valve plate

The size of the geometric cross-section of flow through which the fluid is discharged and flows in particular the pump cylinder, the axial position of the aperture in the piston in relation to the opening of the valve plate . The shape of the axial hole in the piston (elliptical or circular) is determined by the size of the angle *(φ_0)*. Geometric flow cross sections are calculated on the basis of analytical expressions derived in function of the angle of rotation for individual intervals in stages suppression, or vacuuming, Figure 2. and Figure 3.

$$A_{do} = \frac{r_o^2}{2}\left[\frac{\pi\alpha}{180} - \sin\alpha\right] \tag{1}$$

or

$$A_{do} = \frac{r_o^2}{2}\left[\alpha - \sin\alpha\right] \tag{2}$$

$$A_o = A_{d0} \tag{3}$$

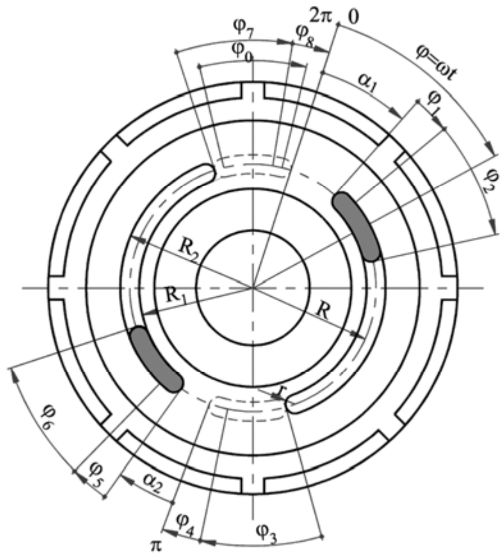

Figure 2. The position of the axial piston hole on the valve plate

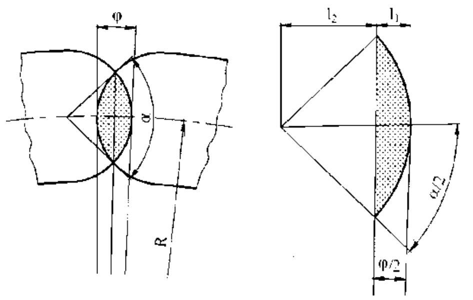

Figure3. Sketch for calculating the geometric flow section of valve plate

$$l_1 = \frac{r\varphi}{2} \qquad l_2 = r_o - l_1 = r_o - \frac{r\varphi}{2} \tag{4}$$

$$\cos\frac{\alpha}{2} = \frac{l_2}{r_o} \Rightarrow \alpha = 2\arccos\left(1 - \varphi\frac{r}{2r_o}\right)$$

(5) $$A_o = r_o^2\left\{2\arccos\left(1-\varphi\frac{r}{2r_o}\right) - \sin\left[2\arccos\left(1-\varphi\frac{r}{2r_o}\right)\right]\right\}$$

(6)

Determination of the second member in the big parenthesis preceding equation is related to the following routes:

$$\sin\delta = \cos\left(\frac{\pi}{2} - \delta\right) = \psi \Rightarrow \delta = \arcsin\psi$$
$$\frac{\pi}{2} - \delta = \arccos\psi; \qquad \arcsin\psi + \arccos\psi = \frac{\pi}{2} \tag{7}$$

$$\sin\delta = \sqrt{1-\cos^2\delta} = \psi$$
$$\cos\delta = \sqrt{1-\sin^2\delta} = \sqrt{1-\psi^2} \tag{8}$$

$$\delta = \arcsin\psi$$
$$\delta = \arccos\sqrt{1-\psi^2} \tag{9}$$

$$\arcsin\psi = \arccos\sqrt{1-\psi^2} \tag{10}$$

$$\sin(\delta_1 \pm \delta_2) = \sin\delta_1\cos\delta_2 \pm \cos\delta_1\sin\delta_2 \tag{11}$$

$$\sin\delta_1 = \psi_1 \qquad \sin\delta_2 = \psi_2$$
$$\cos\delta_1 = \sqrt{1-\psi_1^2} \qquad \cos\delta_2 = \sqrt{1-\psi_2^2} \tag{12}$$

$$\delta_1 = \arcsin\psi_1$$
$$\delta_2 = \arcsin\psi_2 \tag{13}$$

Using Eq. (13) below:

$$\arcsin\psi_1 \pm \arcsin\psi_2 = \arcsin\left(\psi_1\sqrt{1-\psi_2^2} \pm \psi_2\sqrt{1-\psi_1^2}\right) \tag{14}$$

As in the previous equation leads to the following relations:

$$\arccos\psi_1 \pm \arccos\psi_2 = \arccos\left[\psi_1\psi_2 \mp \sqrt{(1-\psi_1^2)(1-\psi_2^2)}\right] \tag{15}$$

By introducing the substitution $\psi_1 = \psi_2 = \psi$ equations become:

$$\arcsin\psi = \frac{1}{2}\arcsin\left(2\psi\sqrt{1-\psi^2}\right)$$
$$\arccos\psi = \frac{1}{2}\arccos\left(2\psi^2 - 1\right) \tag{16}$$

After replacing $\Phi = \varphi\frac{r}{2r_o}; 1-\Phi = \psi; 2\psi^2 - 1 = \delta$ **,** the second member in Eq. (6) becomes

$$: \sin\left[2\arccos\left(1-\varphi\frac{r}{2r_o}\right)\right] = 2\left(1-\varphi\frac{r}{2r_o}\right)\sqrt{\varphi\frac{r}{r_o}\left(1-\varphi\frac{r}{4r_o}\right)}$$

(17)

Finally,

$$A_o = r_o^2\left[2\arccos\left(1-\varphi\frac{r}{2r_o}\right) - 2\left(1-\varphi\frac{r}{2r_o}\right)\sqrt{\varphi\frac{r}{r_o}\left(1-\varphi\frac{r}{4r_o}\right)}\right] \tag{18}$$

interval of the rotation angle φ:

$$\alpha_1 \le \varphi = \omega t - \alpha_1 \le \alpha_1 + \frac{2r_o}{r}$$

2.1.1. Process of suppression

Using the labels in Figure 2 for a certain angle of rotation intervals of φ follows: $\alpha_1 < \varphi < \alpha_3 \Rightarrow \varphi_1 = \varphi - \alpha_1$,

$$Ag(\alpha_1,\varphi) = r^2\left[2\arccos\left(1-\varphi_1\frac{R}{2r}\right) - 2\left(1-\varphi_1\frac{R}{2r}\right)\sqrt{\varphi_1\frac{R}{2r}\left(1-\varphi_1\frac{R}{4r}\right)}\right] \quad (19)$$

If $\alpha_3 < \varphi < \alpha_4 \Rightarrow \varphi_2 = \varphi - \alpha_3$ it folows that:

$$Ag(\alpha_1,\varphi) = \pi r^2 + \frac{1}{2}\varphi_2\left(R_2^2 - R_1^2\right) \quad (20)$$

If : $\alpha_4 < \varphi < \alpha_5$, then

$$Ag(\alpha_1,\varphi) = \pi r^2 + \frac{1}{2}\varphi_0\left(R_2^2 - R_1^2\right) \quad (21)$$

If: $\alpha_5 < \varphi < \alpha_6 \Rightarrow \varphi_3 = \varphi - \alpha_5$, then

$$Ag(\alpha_1,\varphi) = \pi r^2 + \frac{1}{2}\varphi_0\left(R_2^2 - R_1^2\right) - \frac{1}{2}\varphi_3\left(R_2^2 - R_1^2\right) \quad (22)$$

if: $\alpha_6 < \varphi < \alpha_7 \Rightarrow \varphi_4 = \varphi - \alpha_6$, then

$$Ag(\alpha_1,\varphi) = \pi r^2 - r^2\left[2\arccos\left(1-\varphi_4\frac{R}{2r}\right) - 2\left(1-\varphi_4\frac{R}{2r}\right)\sqrt{\varphi_4\frac{R}{2r}\left(1-\varphi_4\frac{R}{4r}\right)}\right] \quad (23)$$

2.1.2. Process of suction

If $\alpha_8 < \varphi < \alpha_9 \Rightarrow \varphi_5 = \varphi - \alpha_8$, then

$$Ag(\alpha_5,\varphi) = r^2\left[2\arccos\left(1-\varphi_5\frac{R}{2r}\right) - 2\left(1-\varphi_5\frac{R}{2r}\right)\sqrt{\varphi_5\frac{R}{2r}\left(1-\varphi_5\frac{R}{4r}\right)}\right] \quad (24)$$

If : $\alpha_9 < \varphi < \alpha_{10} \Rightarrow \varphi_6 = \varphi - \alpha_9$,then

$$Ag(\alpha_2,\varphi) = \pi r^2 + \frac{1}{2}\varphi_6\left(R_2^2 - R_1^2\right) \quad (25)$$

If : $\alpha_{10} < \varphi < \alpha_{11}$, then

$$Ag(\alpha_2,\varphi) = \pi r^2 + \frac{1}{2}\varphi_0\left(R_2^2 - R_1^2\right) \quad (26)$$

If:$\alpha_{11}<\varphi<\alpha_{12} \Rightarrow \varphi_7=\varphi-\alpha_{11}$,then

$$Ag(\alpha_2,\varphi) = \pi r^2 + \frac{1}{2}\varphi_0\left(R_2^2 - R_1^2\right) - \frac{1}{2}\varphi_7\left(R_2^2 - R_1^2\right) \quad (27)$$

If : $\alpha_{12} < \varphi < \alpha_{13} \Rightarrow \varphi_8 = \varphi - \alpha_{12}$,

then

$$Ag(\alpha_2,\varphi) = \pi r^2 - r^2\left[2\arccos\left(1-\varphi_8\frac{R}{2r}\right) - 2\left(1-\varphi_8\frac{R}{2r}\right)\sqrt{\varphi_8\frac{R}{2r}\left(1-\varphi_8\frac{R}{4r}\right)}\right] \quad (28)$$

The size of the angles α_3 to α_{13}, are determined by the following relationships:

$$\alpha_3 = \alpha_1 + 2\frac{r}{R}$$

$$\alpha_4 = \alpha_1 + 2\frac{r}{R} + \varphi_0$$

$$\alpha_5 = \pi - \left(2\frac{r}{R} + \varphi_0\right)$$

$$\alpha_6 = \pi - 2\frac{r}{R}$$

$$\alpha_7 = \pi$$

$$\alpha_8 = \pi + \alpha_2$$

$$\alpha_9 = \pi + \alpha_2 + 2\frac{r}{R}$$

$$\alpha_{10} = \pi + \alpha_2 + 2\frac{r}{R} + \varphi_0$$

$$\alpha_{11} = 2\pi - \left(2\frac{r}{R} + \varphi_0\right)$$

$$\alpha_{12} = 2\pi - 2\frac{r}{R}$$

$$\alpha_{13} = 2\pi \quad (29)$$

The effective flow cross-section of the valve plate

$$A_\mu = A_g\mu \quad (30)$$

2.2. Coefficient of flow distribution orifice

Accurate determination of the coefficient of flow orifice valve plate piston - axial pumps is not possible without their identification, comparison with experimental studies and detailed analysis. When defining the mathematical model adopted are four ways of defining the flow coefficient as follows:

a) flow coefficient by the table,

b) the flow coefficient is determined as a function of pressure p, by the formula:

$$\mu = \mu_0 + \frac{\mu_1}{1-|p_c - p_1|} \tag{31}$$

c) flow coefficient is determined in function of the number of trades n according to the formula:

$$\mu = \mu_0 + \mu_1 \cdot n \tag{31}$$

d) flow coefficient is determined as a function of pressure *p* and number of revolutions *n*

The Eq.(30) through (31) are

$$\mu = \mu_0 + \frac{\mu_1}{1-|p_c - p_1|} + \mu_2 \cdot n \tag{32}$$

In the case of suction, and discharge outlet distribution boards, all the above given expressions receive appropriate indexes "u" - in the case of suction, and "i" when it comes to the discharge opening of the valve plate.

3. OPTIMIZATION OF PARAMETERS OF THE VALVE PLATE OF THE WATER HYDRAULIC PISTON AXIAL PUMP/MOTOR

Comparing the results of the optimized parameters from baseline are obvious requirements that are in the search for the optimal solution structures piston axial pump/motor must approach the analysis of the structure parameters of distribution of working fluid.

The mathematical model predicted two choices suction or thrust distribution bodies. The physical model investigated axial piston pump/motor comprises distributing the combined working fluids. The working fluid is drawn into the cylinders of the internal cavity of the pump/motor body through the opening of the valve plate and axial holes in the pistons. When working stroke of piston working fluid is released through the pressure valves in the discharge chamber. Contact clip with the hair plate at the pump/motor is achieved through a spherical head cut off. The timing circuit in the construction of the investigated axial piston pump is one of the most responsible assemblies and in further consideration of attention to its characteristic parameters. Combined distributing working fluid using a suction valve plate has a major advantage in terms of installing replacement intake valves.

Valve plate is firmly attached to the hair shaft and plate and its junction with axial holes through which the piston is done soaking in the cylinder cavity is achieved through the hydrostatic bearings and spacers rings.

Starting and optimized value of suction pressure indicate a need to increase it to achieve the maximum degree of supply cylinder.

Analyzing the baseline and optimized value of the vertex radius of the suction port of the valve plate R_2 and the angle beginning stages suction α_2 , it can be concluded that further research and development of mathematical models must pay attention to their impact on the level of supply cylinder as the target function.

Identification of the parameters of the working process of axial piston pumps , has been implemented in four stages of identification, for different modes . Table 1 presents the modes with which the optimization is performed.

The optimization of the following parameters : pressure vacuum , the suction chamber volume , the volume of the pressure chamber, the vertex radius of the suction port of the valve plate, angle beginning stages suction, spring stiffness propellant valve and pressure pipeline length .

Optimization of the characteristic parameters was performed for the installation of the hydraulic mode piston axial pump : p = 20MPa and n = 875.6 min -1 (R09) . In Table 2 are given the numerical values of the optimized parameters .

Table 1. Applied modes in experimental research station

No.	Example	Pressure in the cylinder p_c [MPa]	Number of rottions *n*, [min^{-1}]
1.	R03	18	1000
2.	R04	5	800
3.	R05	16	800
4.	R06	18	800
5.	R07	20	800
6.	R08	20	1000
7.	R09	20	875.6

Table 2 Numerical valuable asset of initial and optimized parameters for mode testing with parameters n=875,6min^{-1}, p=20MPa

No.	Parameter	Mark	Unit	Values of parameter	
				Initial	Optimized
1	pressure of suction	P_u	[*Pa*]	2.68E5	3.347E5
2	vol. pressure chamber	V_V	[m^3]	2.81E-4	2.96E-4
3	vol. suction chamber	V_s	[m^3]	5.0E-4	5.04E-4
4	the vertex radius of the suction port of the valve plate	R_2	[*m*]	5.1E-2	4.61E-2
5	angle beginning stages suction	α_2	[^{O}]	29.77	28.4
6	spring stiffness propellant valve	c_v	[*N/m*]	1104.7	1218
7	pipeline length	L_c	[*m*]	1.65	1.462

Parameter optimization of axial piston pump affects the hydrodynamic processes within the pump. Optimization parietal radius hole valve plate directly affect the flow of the board. In Figures 4-8 are shown diagrams flow through the organ distribution of the different modes.

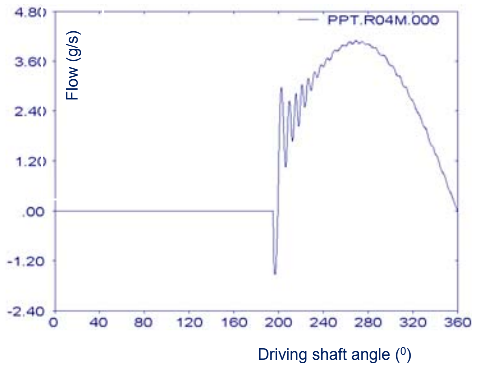

Figure 4. The flow through the valve plate, depending on the angle of the shaft, mode R04,n = 800min^{-1},p=5MPa

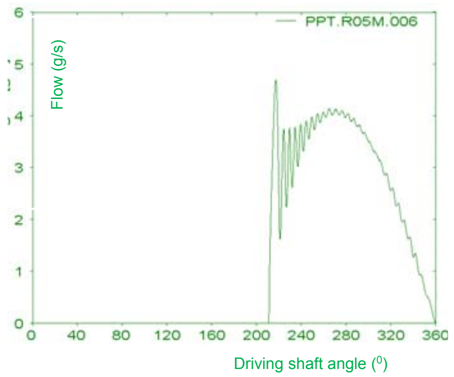

Figure 5. The flow through the valve plate, depending on the angle of the shaft, mode R05,n = 800min^{-1},p=16MPa

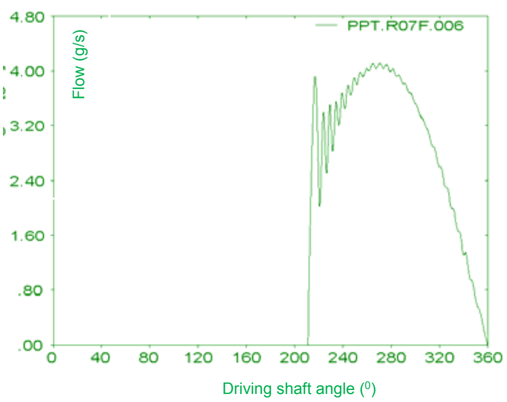

Figure 6. The flow through the valve plate, depending on the angle of the shaft, mode R07,n = 800min^{-1},p=20MPa

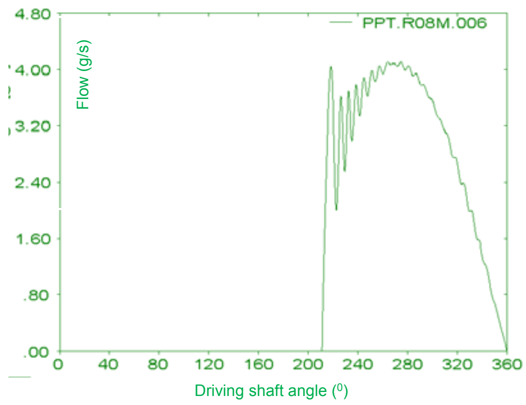

Figure 7. The flow through the valve plate, depending on the angle of the shaft, mode R08,n = 1000min^{-1},p=20MPa

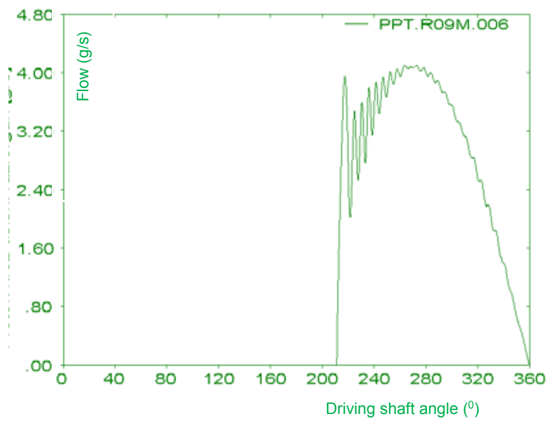

Figure 8. The flow through the valve plate, depending on the angle of the shaft, mode R09,n = 875,6min^{-1},p=20MPa

4.CONCLUSION

The optimization of seven characteristic parameters of the water hydraulic axial piston pump/motor including: vacuum pressure , the volume of the pressure chamber , the volume of the suction chamber , parietal radius of the inlet opening of the valve plate , the angle at the beginning stages of suction ventilskoj board propellant valve spring stiffness and length of the supply pipeline in order to achieve maximum coefficient times the cylinder.

As part of future research in analyzing of the water hydraulic piston axial pump/motor , it is necessary to consider the effects of the flow of working fluid through the gaps in place aglave spherical piston head and seat incline board in this regard extend the mathematical model. Also possible research pulsations in compression and suction to the analysis of noise and noise during operation of axial piston pumps , based on the identified parameters and perform a comparison with the known results of the tests .

The developed program for mathematical modeling, identification and optimization of the water hydraulic axial piston pump/motor , enables the further research of hydrodynamic processes develop the whole family of pumps and motors with an analysis of the advantages and disadvantages of axial piston pumps and motors with fixed and variable flow .

Further research directions are possible in the design of axial piston pumps and motors with inclined cylinder block and dissolving the working fluid by means of the valve plate . The mathematical model in this case was expanded with the dynamics of the cylinder block and hydrodynamic processes in the gap between the cylinder block and valve plate .

5.NOMENCLATURE

A_o	the geometric flow section of valve plate
A_g	geometric flow cross section of the valve plate
A_μ	the effective flow cross-section of the valve plate
n	number of revolutions
p	pressure
p_c	pressure in cylinder
$\|p_c - p_1\|$	pressure drop through the hole distribution valve plate
R,r	radius which defining the geometry of the openings on valve plate
α	angle which defining the geometry of the valve plate
ω	angular velocity of the shaft
φ	the angle of rotation of the shaft
φ_o	angle which defining the geometry of the openings on valve plate
μ	overall coefficient of flow section
μ_0	basic constant flow coefficient distribution boards
μ_1	additional constant flow coefficient openings valve plate

ACKNOWLEDGEMENT

The part of this research is supported by Ministry of Education and Science, Republic of Serbia, Grant TR 32036 and Grant TR 35038.

REFERENCES

[1] R.Petrovic, "Mathematical modeling and identification of multicylindrical axial piston pump parameters", PhD Thesis, Faculty of Mechanical Engineering, Belgrade, 1999. (in Serbian)

[2] M.Bergeman, "Systematische Untersuchung des Geräuschverhaltens von Kolbenpumpen with ungerader Kolbenanzahl", Verlag Mainz, Wissenschaftsverlag, Aachen, 1994.

[3] R.Petrović, "Mathematical Modeling and Experimental Research of Characteristic Parameters of Hydrodynamic Processes in an axial piston Pump", STROJNIŠKI VESTNIK – Journal of Mechanical Engineering, Vol.55, No4, p.224-229 , Univerza v Ljubljani, Fakulteta za strojništvo, Ljubljana, Slovenia,2009.

[4] R.Jankov, "Development of new generation of ultra-fast acquisition and control system ADS 2000", Science and vehicle, Belgrade, (in Serbian).

[5] A.R.Plummer, "Control techniques for structural testing: a review Proc. Instn. Mech. Engrs", Part I, Journal of Systems and Control Engineering, 221(2),139-169, 2007.

[6] J.Ivantysyn,M. Ivantysynova,"Hydrostatic Pumps and Motors. Principles, Design, Performance, Modelling, Analysis, Control and Testing“. First English Edition. New Delhi, India: Akademia Books International,2001.

[7] Z.Glavčić,R.Petrović,"Computer program for mathematical modeling and identification of hydrodynamic processes of a radial piston pump", p.191-198 Volume 1, ISBN 1-932739-14-9, 6th FPNI - PhD Symposium, West Lafayette, Indiana, USA,2010.

[8] M.Haarhaus,H.J. Haas, "Untersuchung neuer Wege zur Geräuschminderung bei Axialkolbenpumpen", Ölhydraulik und Pneumatik 29 , Nr.2 und 3, Germany,1985.

[9] S.Čantrak,Z.Glavčić,R.Petrović,” Modelling of transition process behind the local resistance depending on flow rate circumference component”. *E17-E20 pp, Third International Conference Heavy Machinery – HM ‘02*, 27-30 october 2002, Kraljevo.

[10] R.Petrović, "Systematic research of characteristic parameters of the piston axial pump", poster presentation, III International Fluid Power Conference 2002, Aachen, Germany, 2002.

[11] M. Bergemann,” Noise Problems of Axsial Piston Pumps with odd and even Numbers of Cylinders”. 9th international Fluid power symposium, Chapter 19 of proceedings,STI, Oxford, 1990

[12] M.Haarhaus,“ Geräuschentstehung und Geräuschninderung bei Axialkolbenpumpen in Schrägscheibenbauweise“. *Dissertation TH Aachen.1984*

[14] N.Todic, N. Filipović, R. Petrović, " Modeling of torque with friction effect for water hydraulic axial piston pump/motor", Fourth Serbian (29th Yu) Congress on Theoretical and Applied Mechanics,Vrnjačka Banja,Serbia,2013.

Computer Control on Positioning Stepper Drive – Laboratory Stand

Vasil Dimitrov[1*], Ivan Milenov[1], Emiliya Dimitrova[2]
[1]Faculty of Telecommunications and Electrical Equipment in Transport / Department of Power Engineering and Electrical Equipment in Transport, Todor Kableshkov University of Transport – Sofia (Bulgaria)
[2] Department of Telecommunications and Signalling, Todor Kableshkov University of Transport – Sofia (Bulgaria)

A laboratory stand for control on positioning stepper drive by a personal computer and a microcontroller has been developed. Stepper motors provide a possibility of precise positioning and speed control without using feedback sensors. They are easily adaptable to digital control applications and can be easily controlled by microprocessors – the rotation angle is directly related to the number of input pulses and wide range of rotational speeds can be implemented as the speed of motor shafts rotation is proportional to the pulse frequency. Contemporary stepper motors have an accuracy of 3 – 5% of a step and the error is non-cumulative from one step to the next. These motors are very reliable since there are no contact brushes and the durability of motor operation is simply dependent on the life of the bearing. A high positioning accuracy is possible, even under open-loop control, making the motor simpler and less costly to control.

The stand is built on contemporary devices and offers various possibilities to implement laboratory exercises into practice such as determination of the positioning accuracy, examination on stepper motors, programming of microcontrollers, etc. A number of examinations were made, the proper drive operation was tested and the positioning error was determined.

Keywords: Computer control, stepper motors, positioning

1. INTRODUCTION

Controlled positioning drives are used in many areas of automation technology, robotics and handling systems as well as in the drive technology of production machines and machine tools. The most important requirements to the drives are to ensure high positioning accuracy, safety and reliability. The requirements related to dynamics, speed stability and rigidity necessitate ever increasing gain factors in the control devices. Stepper motors and microcontrollers are involved in many positioning systems and meet these requirements. They perform all indispensable functions and minimize risks that can occur during normal or impaired operation of machines or facilities.

2. BASIC PRINCIPLES OF THE STEPPER MOTOR CONTROL

Stepper motors are electromechanical devices which convert electrical pulses into mechanical discrete angular displacements [1, 2].

Many magnets with alternating poles are arranged around the periphery of the rotor. There are three basic types of stepping motors: permanent magnet, variable reluctance and hybrid. Permanent magnet motors have a magnetized rotor, while variable reluctance motors have toothed soft-iron rotors. Hybrid stepping motors combine aspects of both permanent magnet and variable reluctance technologies. The stator holds multiple windings.

Variable Reluctance Motors usually have three windings connected to a common terminal. Adding more windings (4-th and 5-th) increases the number of poles and for smaller step angles, toothed pole pieces working against a toothed rotor could be used. Variable reluctance motors using this approach are available with step angles close to one degree.

From the viewpoint of electrical and control systems, variable reluctance motors are different from the other types. Both permanent magnet and hybrid motors may be wound using either unipolar windings, bipolar windings or bifilar windings.

The bipolar motor with two phases has one winding per phase (Fig. 1a). The unipolar motor has one winding, with a centred tap per phase (Fig. 1b). The centred tap wires are tied to a power supply and the ends of the coils are alternately grounded. Sometimes the unipolar stepper motor is referred to as a "four-phase motor" (Fig. 1c), even though it only has two phases. It can be used as either unipolar or bipolar according to mode of connecting the windings.

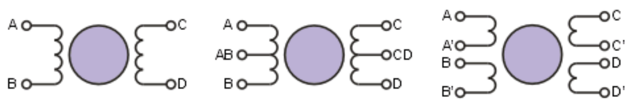

Figure 1: Stepper motors: bipolar, unipolar, four-phase

Each winding in motors with bifilar windings is made up of two wires wound parallel to each other. These motors could be driven as both bipolar and unipolar motors. To use a bifilar motor as a unipolar motor, the two wires of each winding are connected in series and the point of connection is used as a centred-tap. To use a bifilar motor as a bipolar motor, the two wires of each winding are connected in either parallel or series. A parallel connection allows for high current operation, while a series connection allows for high voltage operation.

As all permanent magnet and hybrid motors, unipolar stepper motors operate differently from variable reluctance motors. These motors operate by attracting the north or south poles of the permanently magnetized rotor to the stator poles rather than operating by minimizing the length of the flux path between the stator poles and the rotor teeth where the direction of current flow through the stator windings is irrelevant. Thus in these motors the direction of the current through the stator windings determines what rotor poles will be attracted to which

*Corr. Author's Address: 158 Geo Milev str., 1574 Sofia, Bulgaria, vdimitroff@abv.bg

stator poles. The current direction in unipolar motors is dependent on which half of a winding is energized. Physically, the halves of the windings are wound parallel to one another. Therefore, one winding acts as either a north or a south pole depending on which half is powered.

The full-step angle of a stepper motor can be determined by the relation between the number of rotor poles and equivalent stator poles, and the number of phases:

$$S = \frac{360^o}{N_{ph}.m} = \frac{360^o}{N_p} \quad (1)$$

where: S is the step angle;

N_{Ph} is the number of equivalent poles per phase = number of rotor poles;

m is the number of phases;

N_p is the total number of poles for all phases together.

The control on the rotation angle is performed by application of a series of steps and there are many stepping modes [3]. The following drive modes are the most common ones:

- Wave Drive (1 phase On)
- Full Step Drive (2 phases On)
- Half Step Drive (1 & 2 phases On)
- Microstepping (Continuously varying motor currents).

Only one winding in Wave Drive is energized at any given time according to the following sequence:

$$A \to B \to \overline{A} \to \overline{B} \quad (2)$$

The disadvantage of this drive mode is that only 25% of the total motor winding in the unipolar wound motor and only 50% in the bipolar motor are used at any given time. This means that the maximum torque output from the motor is not reached.

With Full Step Drive two phases are energized at any given time according to the sequence:

$$AB \to \overline{A}B \to \overline{A}\overline{B} \to A\overline{B} \quad (3)$$

Full step mode results in the same angular movement as 1 phase on drive but the mechanical position is offset by one half of a full step. The torque output of the unipolar wound motor is lower than the bipolar motor (for motors with the same winding parameters) since the unipolar motor uses only 50% of the available winding while the bipolar motor uses the entire winding.

Half Step Drive combines both wave and full step drive modes. The stator is energized according to the following sequence:

$$AB \to B \to \overline{A}B \to \overline{A} \to \overline{A}\overline{B} \to \overline{B} \to A\overline{B} \to A \quad (4)$$

The angular movements are half of those in first two drive modes. Half stepping can also reduce the resonance.

With Microstepping Drive the currents in the windings are continuously varying to be able to break up one full step into many smaller discrete steps.

In addition to the steps per revolution, the torque of a stepper motor is the primary feature that determines its suitability for any given application.

Stepper motors have different types of rated torque:

- Holding torque – the torque required to rotate the motor's shaft while the windings are energized.
- Pull-in torque – the torque against which a motor can accelerate from a standing start without missing any steps, when driven at a constant stepping rate.
- Pull-out torque – the maximal value of the motor load at operating speed. The motor stalls or misses steps if the load is greater than Pull-out torque. The maximum frequency at which the motor can operate without losing synchronism is depending on this torque.
- Detent torque – the torque required to rotate the motor's shaft while the windings are not energized.

Stepping motor manufacturers will specify several or all these torques in the data sheets for their motors. However, the pull-in torque offered by a stepping motor strongly depends on the moment of inertia of any load rigidly attached to the motor. The holding torque is the maximum torque that the motor can develop before swinging to a new pole position. It is known that an energized motor has no torque when it is in position; it develops increasing torque as the motor shaft is displaced from its nominal position, i.e. the torque is developed when the magnetic fluxes of the rotor and stator are displaced from each other. The produced torque depends on the step rate, the drive current in the windings and the drive design or type. The magnetic flux intensity and consequently the torque are proportional to the number of winding turns N_w and the current i and inversely proportional to the length l of the magnetic flux path:

$$T_H = \frac{N_w.i}{l} \quad (5)$$

where: T_H is the holding torque;

N_w is the number of winding turns;

m is the current;

l is the length of the magnetic flux path.

A stepper motor is a synchronous electrical motor. This means that the rotor's stable stop position is in synchronization with the stator flux. The rotor is made to rotate by rotating the stator flux, thus making the rotor move towards the new stable stop position. The torque (T) developed by the motor is a function of the holding torque (T_H) and the distance between the stator flux (θ_s) and the rotor position (θ_r), given in electrical degrees:

$$T = T_H.\sin(\theta_s - \theta_r) \quad (6)$$

The relation between electrical (θ_{el}) and mechanical (θ_{mech}) angles is given by the formula:

$$\theta_{el} = \frac{n}{4}.\theta_{mech} \quad (7)$$

where n is the number of full-steps per revolution.

When a stepper motor is driven in Full-Step and Half-Step modes the stator flux is rotated 90°el. and 45°el. respectively every step of the motor. Therefore, compared to Eq. (6) and (7) a pulsing torque is developed by the motor and the torque ripple could cause speed ripple. The reason is that (θ_s - θ_r) is not constant in time due to the discontinuous motion of θ_s. Generating a stator flux that rotates 90° or 45° at a time is simple; just two current levels are required: I_{on} and 0. This can be done easily with all types of drivers. For a given direction of the stator flux, the current levels corresponding to that direction are calculated using the formulas:

$$\begin{aligned} I_A &= I_{\max}.\sin f_s \\ I_B &= I_{\max}.\cos f_s \end{aligned} \quad (8)$$

By combining the I_{on} and 0 values in the two windings, eight different combinations of winding currents could be obtained. This gives eight normal positions corresponding to the flux directions 0, 45, …, 315°el. If the driver can generate any current level from 0 to 141% of the nominal 2-phase-on current I_{on} for the motor, it is possible to create a rotating flux which can stop at any desired electrical position.

If I_A and I_B are sine/cosine pair then T_H is independent of flux direction because it is calculated by the formula:

$$T_H = k.\sqrt{{I_A}^2 + {I_B}^2} \tag{9}$$

It is therefore also possible to select any electrical stepping angle – ¼-full-step, ⅛-full-step or 1/32-full-step for instance. It is not only the direction of flux that can vary, but also the amplitude. Using the torque development formula, it is seen that the effect of microstepping is that the rotor will have much smoother movement on low frequencies because the stator flux, which controls the stable rotor stop position, is moved in a more-continuous way, compared to Full-Step and Half-Step modes. In many applications microstepping can increase system performance, and lower system complexity and cost, compared to full- and half-step drive modes. Microstepping can be used to increase step accuracy and resolution as well as to solve noise and resonance problems.

The natural resonance frequency f_0 of a stepper motor system is determined by the moment of inertia J_T, holding torque T_H (with the selected driving mode and current levels) and number of full-steps per revolution n:

$$f_0 = \frac{\sqrt{\dfrac{n.T_H}{J_T}}}{4.\pi} \tag{10}$$

$$J_T = J_R + J_L \tag{11}$$

where:

J_T is the moment of inertia of the system;

J_R is the moment of inertia of the rotor;

J_L is the moment of inertia of the load.

If the system damping is low, there is an obvious risk of losing steps or generating noise when the motor is operated at or around the resonance frequency. Depending on the motor type, total inertia, and damping, these problems can also appear at or close to integer multiples and fractions of f_0, that is:

$\ldots \frac{1}{4} f_0, \frac{1}{3} f_0, \frac{1}{2} f_0, 2 f_0, 3f_0, 4f_0, \ldots$

Normally the frequencies closest to f_0 give most of problems.

The main reason of these resonances is the discontinuous movement of the stator flux that causes a pulsing energy flow to the rotor. The pulsations excite resonance. The energy transferred to the rotor, when a single step is taken, is in the worst case (no load friction) equal to:

$$E_e = \frac{4.T_H}{n}.\cos(1-\theta_{el}) \tag{12}$$

where:

E_e is the excitation energy transferred to the rotor.

This shows that using Half-Steps instead of Full-Steps reduce the excitation energy to approximately 29% of the Full-Step Energy. If microstepping 1/32-Full-Step mode is used, only 0.1% of the Full-Step energy remains. Therefore by using microstepping drive the excitation energy can be lowered to such a low level that all resonances are fully eliminated. This will improve the movement and will give a sufficient reduction of the noise and vibrations to satisfy the application.

Microcontrollers are good devices for driving stepper motors because they are fast, compatible with the discrete movements of steppers, and can be easily programmed to work with steppers of different types [4]. Some examples of use are precision movements, multi-axis control, sophisticated velocity profiling, and increased fault tolerance. Microcontrollers can also generate the waveforms needed to produce movement in a stepper motor. To control the two phases of the motor, the microcontroller needs four output pins capable of driving four transistors and sinking their gate (base) current of each pin. Most microcontrollers have registers that can be used to control logic levels of an I/O or port pin. For each change in the register state, a change is produced in the waveform that causes the motor to rotate a fixed amount of steps. The period of time required between register states can vary depending upon the motor and the performance desired, but it is usually of the order of milliseconds. If the delay between changes to the register states is too short, the motor will not be able physically to move fast enough to keep up with the register state changes. A delay that is too long could create a motor response with noticeably rigid movements and choppy noises with each step.

In some instances, a microcontroller can provide multiple solutions in a single system because of their ability to be programmed to communicate with other systems or computer while controlling a stepper motor. This is especially advantageous over a dedicated stepper driver that is more difficult to modify and not likely to have full communication capabilities. Because the desired performance of a stepper motor may vary, the algorithm used by a microcontroller to drive a stepper motor is likely to vary as well. Some of these algorithms can become involved and require intimate understanding of the motor, in addition to very organized use of the microcontroller resources.

3. LABORATORY STAND

A laboratory stand for control on positioning stepper drive by personal computer and microcontroller has been built (see Fig. 2). The main elements involved in its configuration are as follows:

- Unipolar stepper motor (windings A1-A2 and B1-B2): $U_N=24V$, $n=200$, $S=1,8°$;
- Microcontroller PIC16F873A [5];
- Transistors 2N3055A – 4 pieces [6];
- Dual driver/receiver MAX232 [7];
- Positive Voltage Regulator 7805 [8];
- Quartz generator (f = 4 MHz);
- Light emitting diodes LEDs – 4 pieces;
- Personal computer: the necessary software is installed and used to set up the positioning drive.

All SMD components are mounted on a circuit board. Where necessary, capacitors and resistors are added. This board is called “Driver” and is fed with 12V DC that corresponds to the nominal voltage of the stepper motor. Four freewheeling diodes are put into a circuit to protect

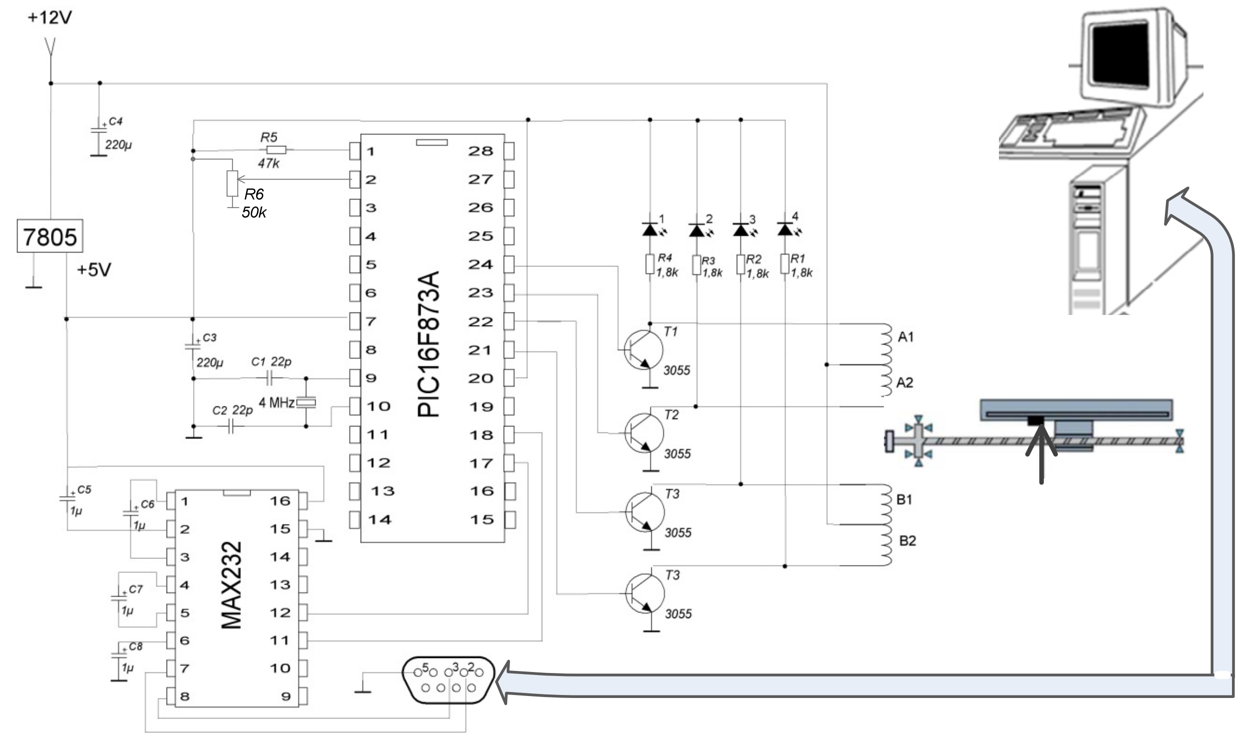

Figure 2: Laboratory stand

the transistors from being damaged by the reverse current of the windings (they are not shown in Figure 2).

The microcontroller PIC16F873A (28-pin package) performs the control on the stepper motor. The required voltage (5V) is provided by Positive Voltage Regulator 7805 in TO-220 package (Output Current up to 1 A).

Four transistors 2N3055A connected to the motor windings A1-A2 and B1-B2 are switched by digital outputs according to the set control program. 2N3055A (60V/15A) is PowerBase complementary transistor especially designed for stepping motor and other switching circuits for inductive loads requiring safe operating area.

Four LEDs (2,5V/25mA) indicate the activated stator winding of the stepper motor in real time.

Stepper motor actuates a benchmark by a gearbox that converts rotary motion into linear with ratio *i = 3:1*, i.e. the laboratory stand is a linear positioning mechanism. The traveled distance is detected by a caliper.

A potentiometer *R6* is connected to the analog input AN0 and can be used for speed control [3, 4, 5]. The slider position corresponds to the period of the output pulses.

The connection between the driver and the personal computer can be established using serial port RS232 and dual driver/receiver MAX232. It includes a capacitive voltage generator to supply TIA/EIA-232-F voltage levels from a single 5V supply. Each receiver converts TIA/EIA-232-F inputs to 5V TTL/CMOS levels.

Microcontroller needs a program previously recorded in its memory. Programming is made by appropriate compiler [9]. This is a sequence of instruction to implement the desired functions. Compilation, translation, simulation and optimization of the program is carried out in the software MPLAB. The electrical connection between the microcontroller and personal computer is done by a programmer, using serial port RS-232.

4. METHODOLOGY AND ALGORITHM OF THE TESTS

A WINDOWS-based computer system is used for control on the drive. The interface COM-Port Reader Writer has to be started and the port number, Baud Rate and Byte Size must be properly set. The distance to be traveled can be set by entering a signed decimal number Z = (0 – 255).

In task Z=050, the stepper motor makes a revolution, and the benchmark travels a distance of S=16.9 mm. This means that in task Z=001, the stepper motor moves four steps and displaces the benchmark with 0.338 mm. One step corresponds to 0.0845 mm respectively. In task Z=255, which is the maximum value, the benchmark will travel a distance of $S_{Tr\_max} = 86.19\ mm$.

Tests are performed in the following sequence. The different values of Z are assigned in increasing order. The distance set point SSP is calculated by the equation:

$$S_{SP} = Z.0{,}338 \tag{13}$$

After execution of the movements of the benchmark, distance travelled S_{Tr} shall be accounted by an electronic caliper. Its accuracy is 25µm [10]. The reduced error ΔS could be calculated by the formula:

$$\Delta S = [(S_{Tr} - S_{SP}) / S_{Tr\_\max}].100{,}\% \tag{14}$$

Test results are shown in Table 1. Then the same examinations are made with decreasing order and the test results are shown in Table 2.

During the tests switching of LEDs has to be monitored. This indicates the alternation of the phases and each movement must finish at one phase (Z is integer and in task Z=001, the stepper motor moves four steps). Thus steps losing can be detected.

Having finished the examinations, the static characteristics of the drive were plotted (see Fig. 3).

Table 1: Test results in positive direction

Z	S_{SP} mm	S_{Tr} mm	ΔS %
21	7.098	7.19	0.107
42	14.196	14.2	0.005
63	21.294	21.38	0.100
84	28.392	28.41	0.021
105	35.49	35.5	0.012
126	42.588	42.6	0.014
147	49.686	49.78	0.109
168	56.784	56.89	0.123
189	63.882	63.98	0.114
210	70.98	71	0.023
231	78.078	78.19	0.130
255	86.19	86.2	0.012

Table 2: Test results in negative direction

Z	S_{SP} mm	S_{Tr} mm	ΔS %
-21	-7.098	-7.19	0.107
-42	-14.196	-14.2	0.005
-63	-21.294	-21.38	0.100
-84	-28.392	-28.41	0.021
-105	-35.49	-35.5	0.012
-126	-42.588	-42.6	0.014
-147	-49.686	-49.78	0.109
-168	-56.784	-56.89	0.123
-189	-63.882	-63.98	0.114
-210	-70.98	-71	0.023
-231	-78.078	-78.19	0.130
-255	-86.19	-86.2	0.012

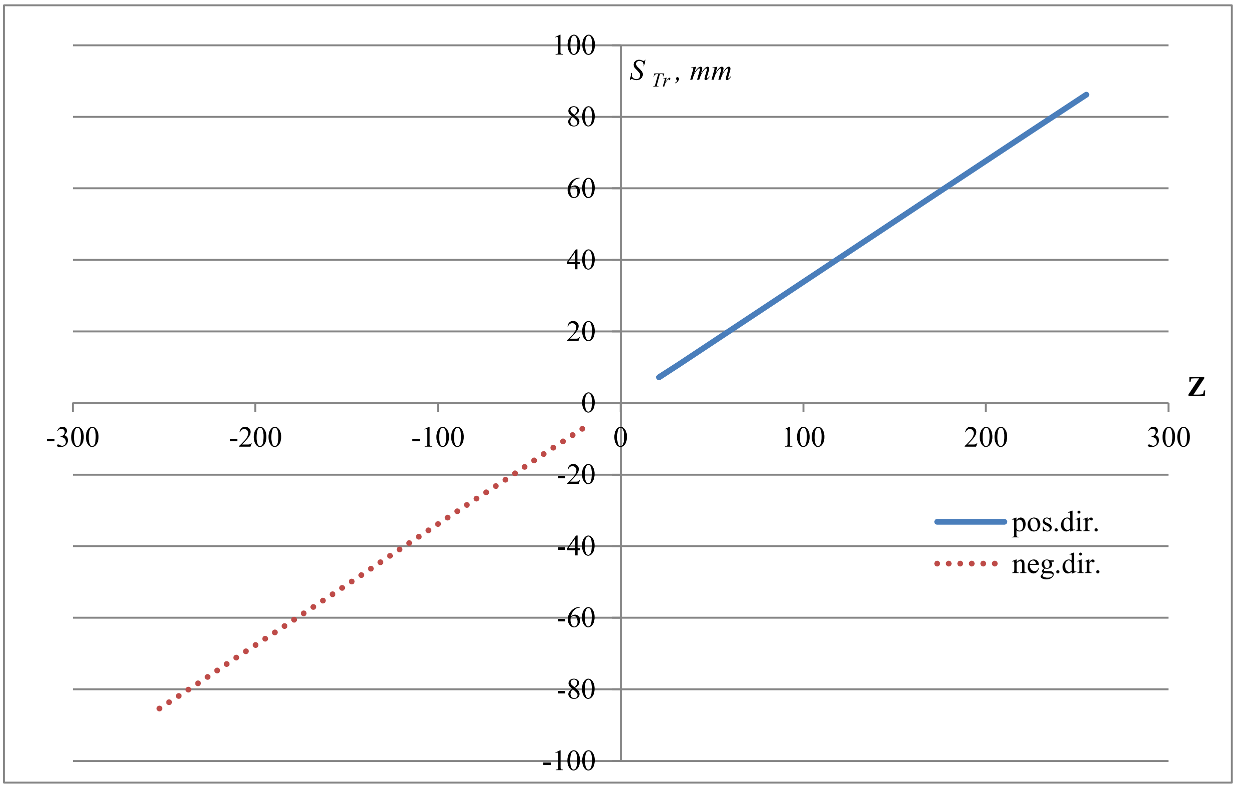

Figure 3: Static characteristic of the drive

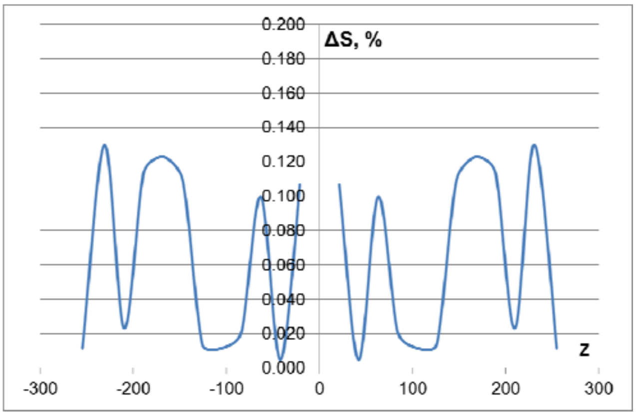

Figure 4: Graphs representing variation of the reduced error ΔS in both directions

A possibility of any load changes is not provided. The motor actuated only the benchmark by the gearbox and the load torque is not very low.

It is seen (Fig. 3) that the characteristic is linear in the both directions and there is no any hysteresis. The reduced error ΔS is very low – it do not exceed 0,14% (see Fig.4). Therefore the drive is correctly set up, the microcontroller is properly programmed and the stand works very well. Thus an experimental verification of the implemented drive is done.

The design methods used are also verified. Similar stepper motors and microcontrollers could be an ideal solution for a variety of applications as positioning drives in automation technology, robotics, process control and machine tool applications.

5. CONCLUSION

The stepper motors can be a good choice whenever controlled movement is required. They could be used with advantage to in control systems that require discrete, easily repeatable movements at moderate to low frequencies as well as in applications where control on the rotation angle, speed, position and synchronism is needed.

Stepper motors suit ideally for measurement and control applications. The step resolution and performance can be improved using a microstepping drive mode.

PIC microcontrollers can perform this mode and drive all different types of stepper motors. These advantages make possible to teach students how to use and program these microcontrollers.

A laboratory stand has been built on the base of a stepper motor and PIC-microcontroller and gives many possibilities of examinations such as determination of the positioning accuracy, study on stepper motors, programming microcontrollers, etc. Students can learn how to optimize drive performance, increase the regulation quality and reduce the positioning error.

This paper presents some experimental tests, which have been carried out, and the comparison made between theoretically deduced dependencies and the results obtained. The stand is used for practical training and research.

REFERENCES

[1] W. H. Yeadon, A. W. Yeadon, “Handbook of Small Electric Motors”, McGraw-Hill, (2001)

[2] “Stepping Motors Fundamentals”, Microchip Technology Inc., (2004)

[3] D.W. Jones, “Control of stepping motors”, University of Iowa, (1998)

[4] M. Grant, “Quick Start for Beginners to Drive a Stepper Motor”, Freescale Semiconductor Inc., (2005)

[5] “PIC16F87XA – 28/40/44-Pin Enhanced Flash Microcontrollers”, Technical specification, Microchip Technology Inc., (2013)

[6] “2N3055A - Complementary Silicon High-Power Transistors”, Technical specification, Motorola, (2006)

[7] “MAX232, MAX232I dual EIA-232 drivers/ receivers”, Technical specification, Texas Instruments, (2013)

[8] “LM78XX / LM78XXA”, Technical specification, Fairchild Semiconductor Corporation, (2013)

[9] Димитров В., Е. Димитрова, Определяне качеството на регулиране при системи за автоматично управление – лабораторен стенд (Dimitrov V., E.Dimitrova, Determining the regulation quality in automatic control systems - laboratory stand), Scientific Conf. UR&US-2013, Proceedings, Vol 52, book 3.2 - Electrical Engineering, Electronics, Automation, "Angel Kanchev" University of Ruse, 2013, ISSN 1311-3321, pp. 153-158

[10] http://www.midwayusa.com/product/417494/hornady-electronic-caliper-6-stainless-steel

Position Control of a Three Degree of Freedom Robot Manipulator

Gökmen Katipoğlu[1], Savaş Takan[2]
[1]Dokuz Eylul University, Computer Engineering Department, İzmir, Turkey
[2]Izmir Institute of Technology, Computer Engineering Department, Izmir, Turkey

Robotics is the area of science which analyzes appliances which are able to perform the desired task, to do physical acts and are supposed to replace man. Meanwhile Robotics is the shared technological area with all basic engineering fields. In order to have an understanding of robots' structure and fields of application, it is essential to use data network of basic engineering (including: mechanical, electrics and electronics, computer and industrial engineering). Robotics is the common outgrowth progressed and developed by all these engineering fields.In analyzing different stages of designing and making a robot one can see that it is the shared result of all engineering fields mentioned above.

Generally speaking, robot is a mechatronic device able to perform pre-determined tasks, in this study gradual development and general design of a hand robot is investigated.

This hand robot can be used for different intents. For instance it can perform as a classification robot. its mechanic structure allows this performance. Five different servo-assisted motors facilitate its movements in any particular way. Since biggest advantage of servo-assisted motors are the ability to make movements in the set angle by controller and high sensitivity. In this study , the movements of limbs in desired angles to desired points are computed using reverse kinematic equations. Atmega 2560 version of Arduino processors is applied as micro-processor. the main advantage of Atmega 2560 is allowing the robot hand to be used for different intents. also existence of different communication protocols which enables writing of different programs is another advantage. process speed of card makes it possible for the robot to perform better and lets the limbs to do desired action at the desired moment. for example if we decide to use it as a classification robot, it will be able to take out the material on the conveyor at the right moment and put them in the pre-determined spot. In the Home position it waits for newly arriving material by going backward. servo-assisted motors are used to make delicate actions like this possible. these motors are corresponded properly by Atmega 2560 to allow proper performance for robot.

Keywords: Forward kinematic, servo motor, arduino, microcontroller

1. INTRODUCTION

Robotics is the shared application area of engineering fields such as aerospace engineering, aircraft engineering, control engineering but it is mostly affected by mechanical electronic and mechatronic engineering fields. Robotics is the field of science which is dealing with developing the technology of electromechanical devices called robots and making it possible to use them in the desired area.

In its history, Ctosibius is accepted as the father of Robotics who has done pioneering projects in century. Ctosibius is the inventor of water clock which is more famous than him. He improved the existing water clock, his water clock was made up of a storage which was filling with water us a special rhythm. As the storage was filled the float inside ascended and the needle on tip of it marked this ascension on a cylinder.

Robotics began mechanical-based and continued with invention of electricity and then with the invention of electrical devices it conjoined electronics. Along with the technological developments, developments happened in robots' function and they started having more part in our daily lives because robots performed the action which they are programmed for directly, the error has been reduced drastically , so they are used to do every day chores or any kind of mass production projects. Even though the first that comes to mind as we hear robot is a device shaped and moving like human, resembling the most famous 'humanoid' robot Honda Asimo, but the features and functions of robot differs.

Robot is a mechanical device with electronic components performing as programmed under human control, nowadays they are mainly used in industrial production. In automotive industry many robots with distinct functioning are exploited. Generally used robots are manipulator type functioning ones. These organ shaped robots are used for functions like welding, assembly and painting.

Issac Asimov's robot series defined robots' creation as a mean of serving human beings. A robot's personal aims can never be preferred to those of human. This is stated as three robotics law. This law is the baseline for the ethical and legal relations among human and robots.

Law of Robotics:

1. a robot may not injure a human being or through inaction allow a human being to come to harm.
2. a robot must obey the orders, given to it by human beings except where such orders would conflict with the first law.
3. a robot must protect its own existence as long as such protection does not conflict with the first or second law.

Robots are electronic devices able to detect their surroundings by their sensors, decide based on these detections perform as the made decision, and move or stop moving their organs as action. According to this definition a car controlled by a key board and linked with parallel

*Corresponding author: gokmen@cs.deu.edu.tr

port to a computer is not a robot. Since it can not decide on its behalf and needs another one to control it. But if the car was able to use computer micro-processors to interpret the data received by sensors, and could make decision because it was able to perform independently would be a robot.

The first attempt to make industrial robot was made in the U.S. after 1950s along with Denavith and Hartenberg’s kinematic calculating methods. In 1960s as a result of Stanford robot institute research different shapes of robots were developed and exploited in industry. Along with American firms like Cincinati Mikron, Westinghouse, Unimation, Japanese firms such as Hitachi, Mitsubishi, Fanuc made their own robots and used them in production line. These resulted in creation of uniquemanipulator types like Puma, Scara, Yasuka- Motoman. Floor- fixed with certain moving space manipulators which worked with open kinematic chain, were robots able to do operations while moving popular as ‘Mobile Robots”.

2. MODELLING OF THE MANIPULATOR

In this study the design of a cartesian type manipulator robot with three free angles on prototype manufacturing with kinematic equations calculation and its supporting software is investigated.

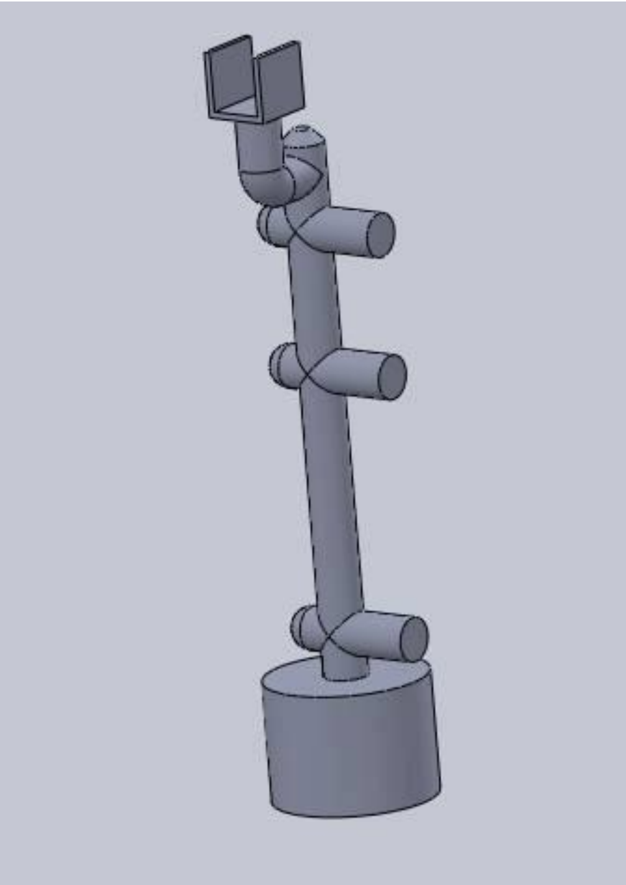

Figure 1. Modelling of the manipulator

Dimensions and kinematics of robot were controlled by developed kinematic method, to do so limb angles were given to check whether the parts reach the calculated point or not. Then using these angles as reference values, robot was run. It was noticed that the extreme points are reached theoretically calculated extreme points and the reference angle is used to run the robot to check whether it reaches the extreme points or it’s nearby and the result was affirmative. Robot’s movements were made by Arduino microprocessor.

3. MICROCONTROLLERS

Microprocessor is a computer system which is combined on a single full circuit. A microprocessor includes CPU (mother board) RAM (random access memory) ROM (read only memory) timer, ADC (analogue digital converter), peripheral units like PWN, IO (input output units). Simple usage and not having a complex essential electric circuit is the main reason of its popularity since it almost has everything needed. Microprocessor is used to simplify complicated actions or automatic controlling. For instance the most basic electronic clocks, automatic washing machines, robots, cameras, LCD monitors, biomedical devices, industrial automation, electronic ticketing systems and the like electronic applications microprocessors are used.

Figure 2 Structure of microcontroller and its components

Three basic actions performed by a microprocessor:

1. receiving various signals from the environment
2. applying the received signals to pre-determined functions
3. using the results of functions in the form of an action in outside world

Arduino data processing is a platform in which all the actions of transmission among various functional units or sending data to interfaces and open-sourced integrated circuit systems and basically programming related to a microprocessor is done.

Figure 3 Arduino Atmel micro-processor cards

4. THE PROCESS OF THE APPLICATION

At the start up of program the servo database is identified which includes information about each servo’s specific timer unit, the number of functioning servos and signals of servos. When identification is done, servos are named. According to servos’ angles the command are defined. In material identification an analogue system which calculates the distance of material on conveyor to check whether it has reached the distance defined as reachable for robot.

Loop waits for start command or‘s’ by the computer. Unless it is not given, sensors will be shut and servos will wait stable. As the letter s was given we entered the if loop and calculated servo motors’ turning angles by using pre-established inverse kinematical locations. Then the in-line commands were written in the program to allow for robot to function fast. In if else loop servo-driver function was called for which with the given servo angles, sets servo motor’s speed. It uses an internal loop to call for database and sends needed signals until gradually the desired angle is realized. Then starting over, waits for new material to reach the desired point. If the letter ’D’ is pressed system take the initial position and waits.

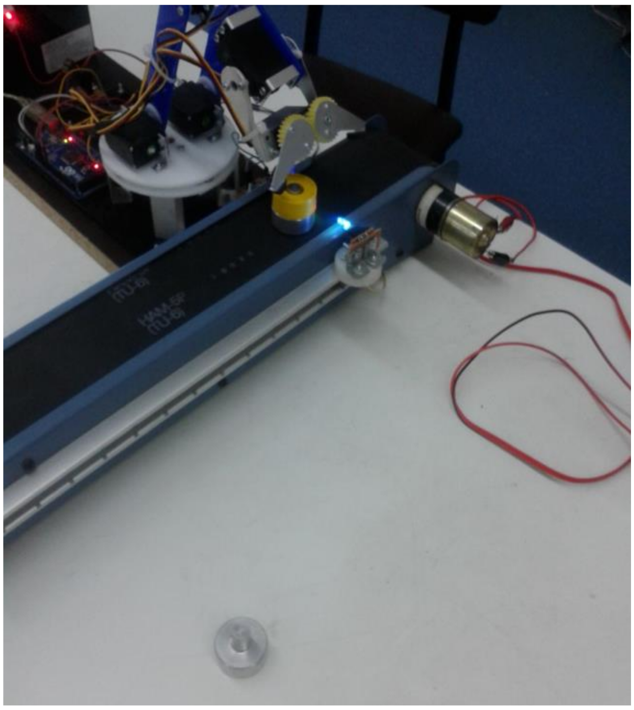

Figure 4. Robot Manipulator recognizes the object

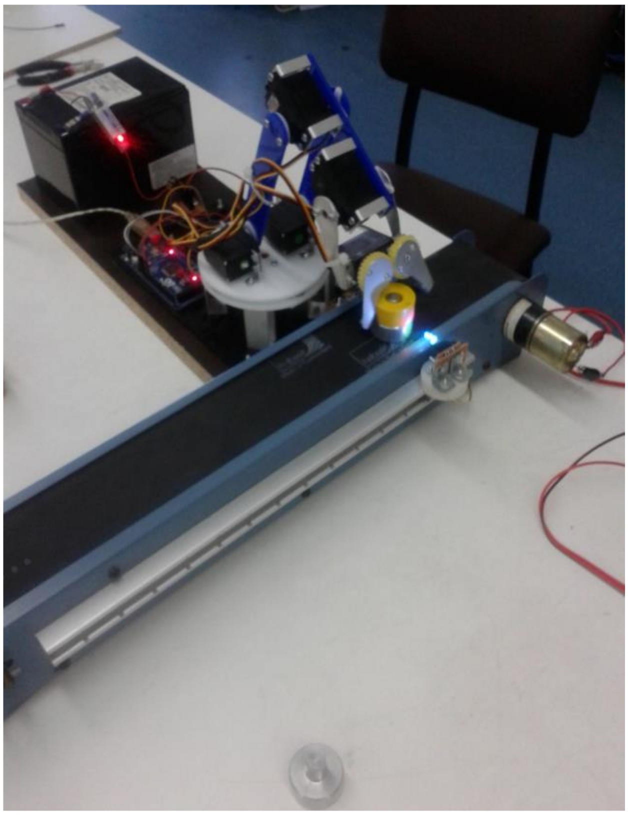

Figure 5. Robot Manipulator grasps the object

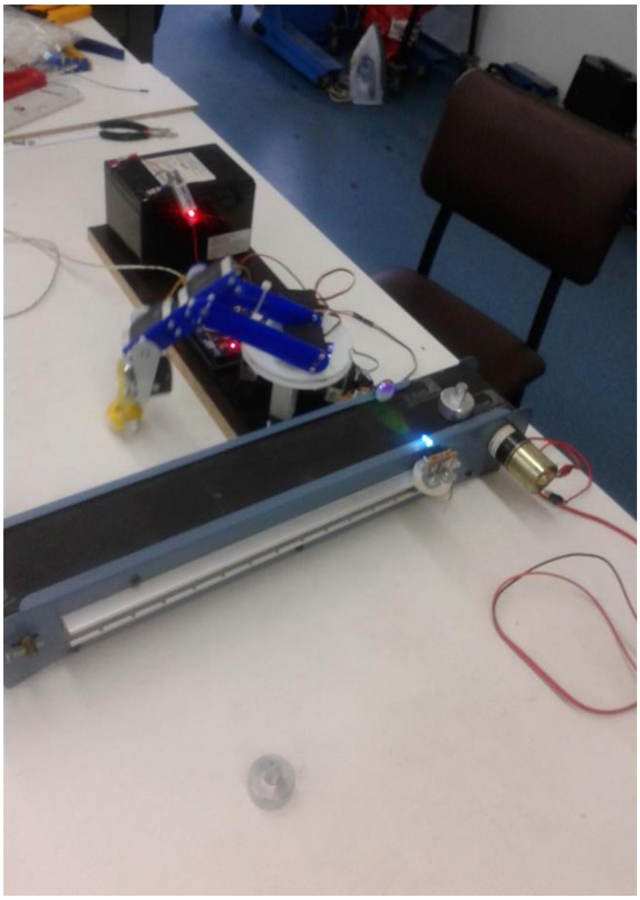

Figure 6. Robot Manipulator moves the object.

ACKNOWLEDGEMENTS

This article is prepared from the mechatronics master thesis called "POSITION CONTROL OF A THREE DEGREE OF FREEDOM ROBOT MANIPULATOR" by Gökmen KATİPOĞLU which is submitted to the Graduate School of Natural and Applied Sciences of Dokuz Eylül University. I would like to express my sincere appreciation to my supervisor Prof. Dr. Erol UYAR for his support and guidance from the beginning to the very end of this study. Under his guidance I had the chance to learn and improve myself in various subjects which I believe will be of great importance in my future academic studies and career.

REFERENCES

[1] Çamoğlu, D. (2011). Bilgisayar kontrollü Robotik, Ankara: Dikey Eksen

[2] Bingül, Z. ve Küçük, S. (2009). Robot kinematiği, İstanbul: Birsen Yayınevi

[3] Kurtoğlu, A. (2011). Robot tekniği, Basım yeri: Papatya Yayınları

[4] Wikipedia (b.t). Robotik, 20 Haziran 2013, http://tr.wikipedia.org/wiki/Robotik

[5] Wikipedia (b.t). Elektrik motoru, 20 Haziran 2013, http://tr.wikipedia.org/wiki/Robotik

[6] Wikipedia (b.t). Servo motor, 20 Haziran 2013, http://tr.wikipedia.org/wiki/Servo_motor

Recursive Estimation of the Takagi-Sugeno Models I: Fuzzy Clustering and the Premise Membership Functions Estimation

Vojislav Filipović[1*], Vladimir Đorđević[1]
[1]Faculty of Mechanical and Civil Engineering, University of Kragujevac, Kraljevo (Serbia)

Fuzzy modelling is an approximation of nonlinear systems by a finite collection of linear systems. On this concept Takagi-Sugeno fuzzy models are based. The procedure for identification of these models include two steps: (a) estimation of membership functions, (b) model parameter estimation. In this paper only the step (a) is considered, where Gustafson-Kessel clustering algorithm is used. The algorithm detects clusters of different shapes. Parameter estimation of the premise membership function is based on the implementation of recursive least squares algorithm. Based on the obtained clusters, recursive least squares algorithm estimates parameters of membership functions. In this paper, it is assumed that the membership functions have triangular shape, performances of the proposed algorithm are demonstrated by simulation.

Keywords: Fuzzy modelling, Fuzzy clustering, Nonlinear systems, Gustafson-Kessel algorithm

1. INTRODUCTION

In general, dynamical model of a system is nonlinear. Identification of this class of systems has been given many attention. Origins of this theory lie in different disciplines: control theory (identification of linear dynamical systems), nonparametric regression and statistics, learning theory, classification theory in pattern recognition, neural networks, fuzzy logic and other disciplines [1]. In this paper is considered the application of fuzzy logic for identification of nonlinear systems. Here will be discussed Takagi-Sugeno models [2]. In these models is used the idea of linearization of nonlinear systems in fuzzy regions of the state space. The structures are obtained, with several linear models. Input space is decomposed into a finite collection of fuzzy regions. The consequent functions describe system behavioural in those regions.

In classic control theory there are approaches that decompose nonlinear model into a finite collection of linear models. Example for that is included angle dividing method [3]. Using this method a finite collection of linear systems is obtained, as a base for further design of the controller. Similar, but more sophisticated methodology is obtained using gap metric concept [4], [5].

Methodologies [3]-[5], as well as the methodology discussed in this paper, are based on fuzzy logic, and they are alternatives to the well-known methodologies for design of controllers for nonlinear systems: feedback linearization [6] and backstepping [7].

The procedure for identification of Takagi-Sugeno models has two steps:

a) Estimation of premise membership functions,
b) Parameter estimation of consequent functions.

In this paper is discussed problem a), while problem b) will be discussed in complete authors' paper [8].

Problem a) is solved using cluster analysis on Cartesian product space of input and output. For cluster analysis is used Gustafson-Kessel fuzzy clustering algorithm. In order to complete the solution of the problem a), after the clusters are defined, it is necessary to determine the parameters of membership functions. It is assumed that membership functions have triangular shape, and their parameters are estimated using recursive least squares algorithm.

The methodology exposed in this paper is demonstrated, thought simulation, on Hammerstein model.

2. TAKAGI-SUGENO MODELS

A nonlinear model $y = f(x)$ can be expressed in the form of Takagi-Sugeno (TS) model based on input-output measurements $\mathbf{u}_k = [u_{1k}, u_{2k}, ..., u_{nk}]^T$ and y_k where k denotes measurements in the k-th moment, and n is the number of regressors in model.

TS model is a combination of logical and mathematical model. Logical rules are consisted of fuzzy premise, and consequent is a mathematical function. The general form of TS model [2]:

$$\mathrm{R}_i : IF\ \mathbf{u}\ IS\ A_i(\mathbf{u})\ THEN\ y_i = \mathbf{a}_i^T \mathbf{u} + b_i; \quad i = 1, 2, \ldots, c \tag{1}$$

where, $\mathbf{u} \in \mathbb{R}^n$ and $y_i \in \mathbb{R}^1$ are inputs and outputs of the system, respectively. Values $a_i \in \mathbb{R}^n$ and $b_i \in \mathbb{R}^1$ are parameters of TS model. R_i is the i-th rule, and c is the number of rules in rule base. A_i is multivariable premise membership function of the i-th rule.

For individual components of vector u, TS model have the following form:

$$\mathrm{R}_i : IF\ u_1\ IS\ A_{i1}(u_1)\ AND ... AND\ u_n\ IS\ A_{in}(u_n)\ THEN\ y_i = \mathbf{a}_i^T \mathbf{u} + b_i;\ i = 1, 2, ..., c \tag{2}$$

Degree of fulfilment of the rule is equal

$$\beta_i(\mathbf{u}) = \prod_{j=1}^{n} \mu_{A_{ij}}(\mathbf{u}) \tag{3}$$

where $\mu_{A_{ij}}(u)$ is the membership function of the fuzzy set A_{ij}.

*Corresponding author: Dositejeva 19, 36000 Kraljevo (Serbia) and v.filipovic@open.telekom.rs

The inference is computed using following formula [2]:

$$y=\frac{\sum_{i=1}^{c}\beta_i(\mathbf{u})\left(\mathbf{a}_i^T\mathbf{u}+b_i\right)}{\sum_{i=1}^{c}\beta_i(\mathbf{u})} \tag{4}$$

From relations (2) and (4) is evident that TS model approximates nonlinear system with finite collection of linear systems.

3. FUZZY CLUSTERING

Fundamental property of measurements for defining clusters is similarity. Therefore, it is necessary to determine the appropriate metrics. Consider an n-dimensional vector of measurements $\mathbf{x}_k=\left[x_{1,k},\, x_{2,k},\dots,\, x_{n,k}\right]^T$, $\mathbf{x}_k\in\mathbb{R}^n$. Set of N measurements is denoted with $\mathbf{X}=\left\{\mathbf{x}_k \mid k=1,2,\dots,N\right\}$ and it is represented in form of an $n\times N$ matrix

$$\mathbf{X}=\begin{bmatrix} x_{1,1} & x_{1,2} & \cdots & x_{1,\mathrm{N}}\\ x_{2,1} & x_{2,2} & \cdots & x_{2,\mathrm{N}}\\ \vdots & \vdots & \ddots & \vdots\\ x_{n,1} & x_{n,2} & \cdots & x_{n,\mathrm{N}}\end{bmatrix} \tag{5}$$

In pattern recognition terminology [10], the columns of matrix $\mathbf{X}$ are called patterns, and the rows are called features or attributes. Matrix $\mathbf{X}$ is called the matrix of patterns or data.

Using exposed, Euclidean distance can be defined as

$$d_2\left(\mathbf{x}_i,\mathbf{x}_j\right)=\left(\sum_{k=1}^{d}\left(x_{i,k}-x_{j,k}\right)^2\right)^{\frac{1}{2}}=\left\|\mathbf{x}_i-\mathbf{x}_j\right\|_2 \tag{6}$$

The more general form of distance is Minkowski distance

$$d_p\left(\mathbf{x}_i,\mathbf{x}_j\right)=\left(\sum_{k=1}^{d}\left(x_{i,k}-x_{j,k}\right)^p\right)^{\frac{1}{p}}=\left\|\mathbf{x}_i-\mathbf{x}_j\right\|_p \tag{7}$$

Practice shows that distance (6) is suitable in a case when clusters are isolated. Distance (6) and (7) express weakness if the features are linearly correlated. Methods based on d_2 and d_p distances cannot distinguish between two groups of observations in the Figure [11].

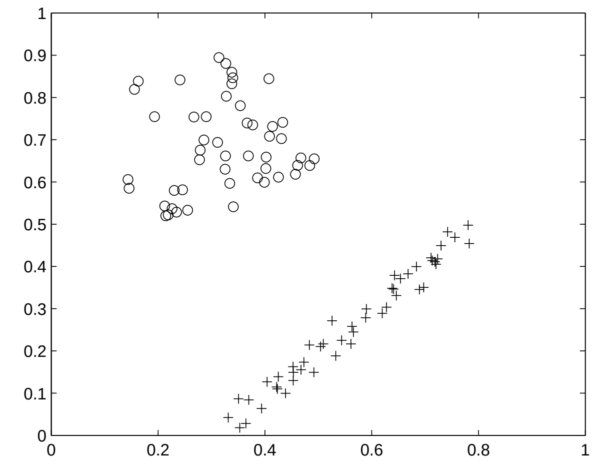

Figure 1: Two different groups of data

In this case Mahalanobis distance is introduced

$$d_M\left(\mathbf{x}_i,\mathbf{x}_j\right)=\left(\mathbf{x}_i-\mathbf{x}_j\right)^T\mathbf{F}^{-1}\left(\mathbf{x}_i-\mathbf{x}_j\right) \tag{8}$$

where $\mathbf{F}$ is a covariance matrix. Using the distance (8) Gustafson-Kessel algorithm is obtained [12].

Gustafson-Kessel clustering algorithm is an iterative optimisation algorithm for minimisation the value of objective function

$$J\left(\mathbf{X};\mathbf{V},\mathbf{U},\{\mathbf{M}_i\}\right)=\sum_{i=1}^{c}\sum_{k=1}^{N}\left(\mu_{i,k}\right)^m D_M^2\left(\mathbf{x}_k,\mathbf{v}_i\right) \tag{9}$$

with constraints

$$\mu_{i,k}\in[0,\ 1];\quad 1\le i\le c;\quad 1\le k\le N \tag{10}$$

$$\sum_{i=1}^{c}\mu_{i,k}=1;\qquad k=1,\dots,N \tag{11}$$

where c is the number of clusters, and m is weighting exponent. The weighting exponent m determines fuzziness of the clusters, and exponent value must be greater than 1. For $m=1$ algorithm performs a hard clustering, a pattern is or is not element of the cluster. With increase of m, the overlap of fuzzy clusters is increased also. Typically, value of m is 2.

In the objective function (9), Mahalanobis distance is replaced with an inner-product norm distance of the form

$$D_{M_i}^2\left(\mathbf{x}_k,\mathbf{v}_i\right)=\left(\mathbf{x}_k-\mathbf{v}_i\right)^T\mathbf{M}_i\left(\mathbf{x}_k-\mathbf{v}_i\right) \tag{12}$$

where $\mathbf{M}_i$ is symmetric and positive-definite norm-inducing matrix.

The arguments of objective function are pattern matrix $\mathbf{X}$, fuzzy partition matrix $\mathbf{U}=\left[\mu_{ik}\right]$, $\mathbf{U}\in\mathbb{R}^{c\times N}$, prototype matrix $\mathbf{V}$ is a set of vector of clusters prototypes (centres) $\mathbf{V}=\left[\mathbf{v}_1,\mathbf{v}_2,\dots,\mathbf{v}_c\right]$, $\mathbf{v}_i\in\mathbb{R}^n$, and $\{\mathbf{M}_i\}$ is the c-tuple of local norm-inducing matrices.

Using the method of Lagrange multiplier is obtained [12] that the objective function have minimal value in case when

$$\mu_{ik}=\frac{1}{\sum_{j=1}^{c}\left(\frac{D_{\mathbf{M}}^2\left(\mathbf{x}_k,\mathbf{v}_i\right)}{D_{\mathbf{M}}^2\left(\mathbf{x}_k,\mathbf{v}_j\right)}\right)^{\frac{2}{m-1}}},\quad \begin{matrix}1\le i\le c\\ 1\le k\le N\end{matrix} \tag{13}$$

and

$$\mathbf{v}_i=\frac{\sum_{k=1}^{N}\left(\mu_{ik}\right)^m\mathbf{x}_k}{\sum_{k=1}^{N}\left(\mu_{ik}\right)^m},\quad 1\le i\le c \tag{14}$$

Matrices $\mathbf{M}_i$ are used as optimisation variables for distance adaptation depending on the layout of data, and as result of optimisation it is obtained the following expression for $\mathbf{M}_i$

$$\mathbf{M}_i=\left[\rho_i\det\left(\mathbf{F}_i\right)\right]^{\frac{1}{n}}\mathbf{F}_i^{-1} \tag{15}$$

where ρ_i are the clusters volumes, and it's value is usually 1.

Fuzzy covariance matrix for the i-th cluster is given by following expression

$$\mathbf{F}_i = \frac{\sum_{k=1}^{N} (\mu_{i,k})^m (\mathbf{x}_k - \mathbf{v}_i)(\mathbf{x}_k - \mathbf{v}_i)^T}{\sum_{k=1}^{N} (\mu_{i,k})^m} \quad (16)$$

Fuzzy covariance matrices contain information of shape and orientation of the cluster. Every cluster can be represented as hyperellipsoid defined by equation

$$(\mathbf{x} - \mathbf{v}_i)^T \mathbf{F}_i^{-1} (\mathbf{x} - \mathbf{v}_i) = 1 \quad (17)$$

Figure 2 shows hyperellipsoid defined by equation (17). The semi-axis of the cluster's hyperellipsoid are the eigenvalues of fuzzy covariance matrix $\mathbf{F}_i$, and directions of the axis are corresponding eigenvectors.

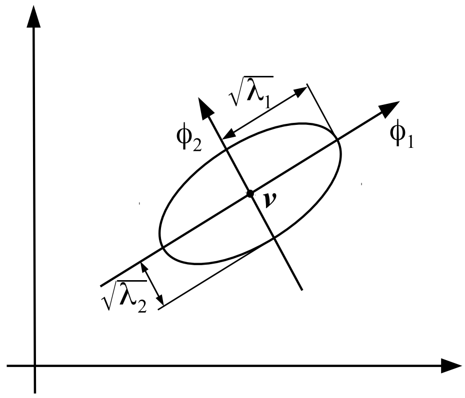

Figure 2: Cluster's hyperellipsoid

Practice shows that Gustafson-Kessel algorithm is suitable method for system identification for several reasons [13]. Since it is based on adaptive distance measure, clusters of different shapes and orientation can be detected. The initialised partition matrix have small influence on results, and also normalisation and standardisation of the data.

On other hand, the large number of clusters and date can result the long execution of algorithm. Also there is singularity problem of covariance matrix in cases when small number of observations is available or when the data are linearly correlated.

The pseudo code for Gustafson-Kessel algorithm is given in following table.

Gustafson-Kessel algorithm

Algorithm inputs are: the pattern matrix $\mathbf{X}$, the number of clusters c, the weighting exponent m, the clusters volumes ρ_i

Initialise random partition matrix $\mathbf{U}^{(0)}$

Do for $l = 1, 2, \ldots$

Compute cluster prototypes:

$$\mathbf{v}_i^{(l)} = \frac{\sum_{k=1}^{N} \left(\mu_{ik}^{(l-1)}\right)^m \mathbf{x}_k}{\sum_{k=1}^{N} \left(\mu_{ik}^{(l-1)}\right)^m}, \quad 1 \le i \le c$$

Compute the cluster covariance matrix:

$$\mathbf{F}_i = \frac{\sum_{k=1}^{N} \left(\mu_{ik}^{(l-1)}\right)^m \left(\mathbf{x}_k - \mathbf{v}_i^{(l)}\right)^T \left(\mathbf{x}_k - \mathbf{v}_i^{(l)}\right)}{\sum_{k=1}^{N} \left(\mu_{ik}^{(l-1)}\right)^m}, \quad 1 \le i \le c$$

Compute distance:

$$\mathbf{M}_i = \rho_i \det(\mathbf{F}_i)^{\frac{1}{n}} \mathbf{F}_i^{-1}$$

$$D_{M_i}^2(\mathbf{x}_k, \mathbf{v}_i) = \left(\mathbf{x}_k - \mathbf{v}_i^{(l)}\right)^T \mathbf{M}_i \left(\mathbf{x}_k - \mathbf{v}_i^{(l)}\right),$$

$$1 \le i \le c, \quad 1 \le k \le N$$

Update the partition matrix:

For $1 \le i \le c$

For $1 \le k \le N$

If $D_{M_i}(\mathbf{x}_k, \mathbf{v}_i) > 0$

$$\mu_{ik}^{(l)} = \frac{1}{\sum_{j=1}^{c} \left(\frac{D_{\mathbf{M}_i}^2(\mathbf{x}_k, \mathbf{v}_i)}{D_{\mathbf{M}_i}^2(\mathbf{x}_k, \mathbf{v}_j)} \right)^{\frac{1}{m-1}}}$$

Otherwise

$$\mu_{ik}^{(l)} = 0 \text{ and } \sum_{i=1}^{c} \mu_{ik}^{(l)} = 1$$

Until $\max\left(\left|U^{(l)} - U^{(l-1)}\right|\right) < \varepsilon$

After the clusters are obtained, in the following procedure the parameters of membership functions need to be estimated.

For estimation of premise membership functions, the clusters need to be projected on premise variables. The projection of clusters on premise variable is point-wise operation. The rows of partition matrix are projected onto original regression values.

In order to get better results, it is necessary to extract linear part of point-wise set of a premise function using α -cut. After that, the extracted linear part needs to be separated in two groups, one group on each side from the centre. Each group is approximated with straight line.

Based on relation (1), the j-th set can be represented as

$$y_{k_j}^j = a^j u_{kj} + b^j = \begin{bmatrix} u_{k_j} & 1 \end{bmatrix} \begin{bmatrix} a^j \\ b^j \end{bmatrix} = \left(\boldsymbol{\varphi}_{k_j}^j\right)^T \boldsymbol{\theta}_{k_j}^j \quad (18)$$

For estimation of parameters of membership functions, a^j and b^j, is used recursive least squares algorithm

$$\hat{\boldsymbol{\theta}}_{k_j}^j = \hat{\boldsymbol{\theta}}_{(k-1)_j}^j + \mathbf{P}_{k_j} \boldsymbol{\varphi}_{k_j} \left(y_{k_j} - \boldsymbol{\varphi}_{k_j}^T \hat{\boldsymbol{\theta}}_{(k-1)_j}^j\right) \quad (19)$$

$$\mathbf{P}_{k_j} = \mathbf{P}_{(k-1)_j} - \frac{\mathbf{P}_{(k-1)_j} \boldsymbol{\varphi}_{k_j}^j \left(\boldsymbol{\varphi}_{k_j}^j\right)^T \mathbf{P}_{(k-1)_j}}{1 + \left(\boldsymbol{\varphi}_{k_j}^j\right)^T \mathbf{P}_{(k-1)_j} \boldsymbol{\varphi}_{k_j}^j} \qquad (20)$$

The initial values are $\hat{\theta}_0^j = 0$ and $P_{0_j} = 10^4 I$.

Once the parameters of both lines are estimated, it is needed to calculate value of premise variable, denoted with β, where lines intersect each other, and also x-intercept of each line, denoted with α and γ.

Now, when all three parameters of fuzzy set are known, the membership function can be defined as normalised point-wise triangular membership function:

$$\mu_{A_{ij}}(x,\alpha,\beta,\gamma) = \max\left(\min\left(\frac{x-\alpha}{\beta-\alpha}, \frac{\gamma-x}{\gamma-\beta}\right), 0\right) \qquad (21)$$

4. SIMULATIONS

The methodology is demonstrated on Hammerstein model, Figure 3.

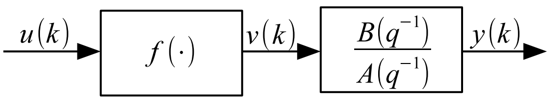

Figure 3: Hammerstein model

Nonlinear function of Hammerstein model is

$$v(k) = u(k) + 0.5u^2(k) + 0.25u^3(k)$$

and polynomials $A(q^{-1})$ and $B(q^{-1})$ are

$$A(q^{-1}) = 1 - 1.6q^{-1} + 0.8q^{-2}$$

$$B(q^{-1}) = 0.85q^{-1} + 0.65q^{-2}$$

As input signal is used following multi-sinusoidal function

$$u_k = 10\sin(0.01\cdot t) + 5\sin(0.1\cdot t) + 2.5\cdot\sin(0.25\cdot t) + \\ +0.75\cdot\sin(t)$$

where $t = 1, 2, \ldots, N$. Figure 4 shows input and output of Hammerstein model.

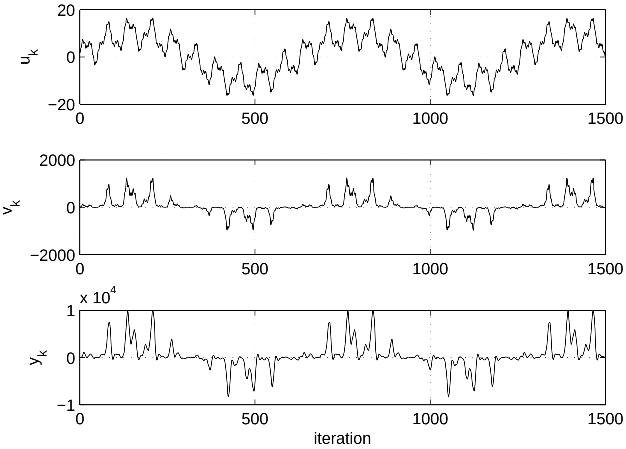

Figure 4: Input and output of Hammerstein model

The Hammerstein model is represented as first-order NARX model,

$$y(k+1) = F\left(y(k), u(k)\right)$$

with following pattern matrix:

$$\mathbf{X} = \begin{bmatrix} y(1) & y(2) & \ldots & y(N-1) \\ u(1) & u(2) & \ldots & u(N-1) \\ y(2) & y(3) & \ldots & y(N) \end{bmatrix}$$

The optimal number of cluster can be find using performance measures [14]. The first performance measure is fuzzy hypervolume and it is defined by:

$$F_{HV} = \sum_{i=1}^{c} \left[\det(F_i)\right]^{\frac{1}{2}} \qquad (22)$$

where F_i are obtained from Gustafson-Kessel algorithm.

The second performance measure is partition density, and given by formula:

$$P_D = \frac{S}{F_{HV}} \qquad (23)$$

where

$$S = \sum_{i=1}^{c} \sum_{j=1}^{N} \mu_{ij}, \\ \forall \mathbf{x}_j \in \left\{ \mathbf{x}_j : \left(\mathbf{x}_j - \mathbf{v}_i\right)^T \mathbf{F}_i^{-1} \left(\mathbf{x}_j - \mathbf{v}_i\right) < 1 \right\} \qquad (24)$$

Both performance measures are calculated for different numbers of cluster, and the results are shown on Figure 5.

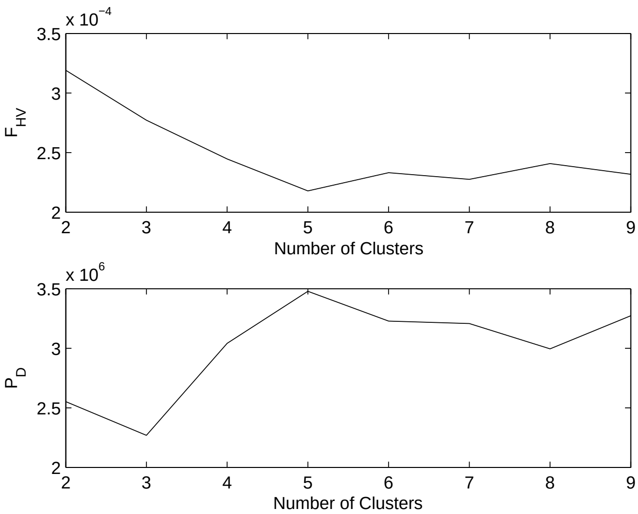

Figure 5: The performance measures: fuzzy hypervolume and partitiom density

The minimum of fuzzy hypervolumes and the maximum of partition densities is when the number of clusters is 5. This is the optimal number of clusters for this first-order NARX model and this matrix of patterns.

Figure 6 shows a premise membership function, obtained by projecting cluster on premise variable. The membership degrees of premise variable are presented with dots. The centre of the membership function is presented with dotted line, and linear approximations of the membership function are presented with dashed lines.

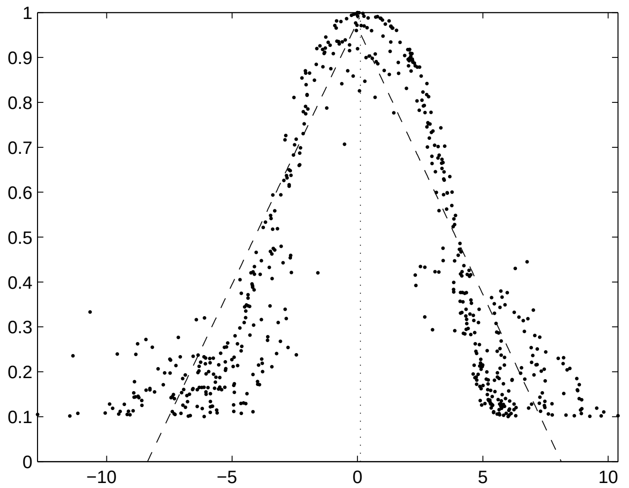

Figure 6: Estimation of membership function

Figures 7 and 8 show normalised estimated membership functions for regressors $u(k)$ and $y(k)$.

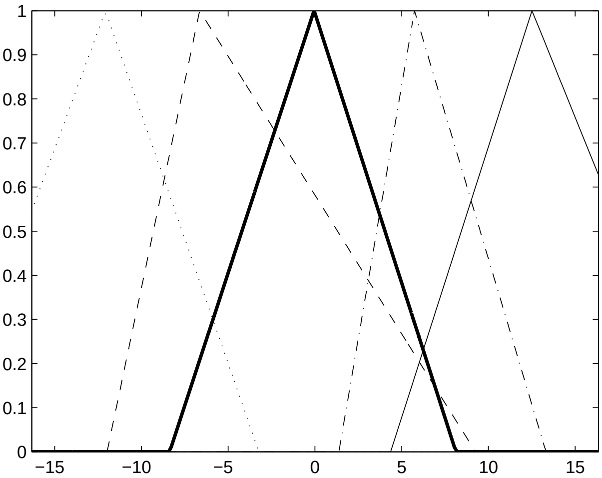

Figure 7: Estimated membership function for $u(k)$

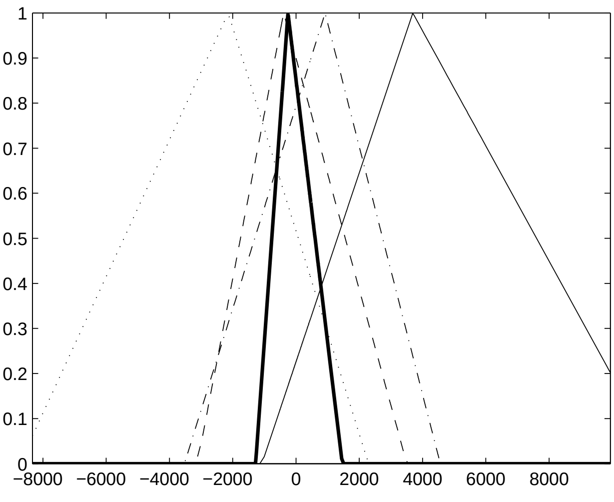

Figure 8: Estimated membership functions for $y(k)$

5. MISCELLANEOUS

In this paper, a methodology for determination of premise membership functions is presented, and its performances are demonstrated through simulation on Hammerstein model. The methodology employs Gustafson-Kessel algorithm to find the clusters, and recursive least squares algorithm to estimates parameters of premise membership functions. The results of this methodology are point-wise triangular membership functions, which are very suitable for use, especially in online applications.

ACKNOWLEDGEMENTS

The authors wish to express their gratitude to the Ministry of Education, Science and Technological Development of the Republic of Serbia for supporting this paper through project TR33026 and project TR33027.

REFERENCES

[1] L. Ljung, "Some aspects of nonlinear system identification," Proceedings of the 14th IFAC Symposium on System Identification, Newcastle (Australia), p. 761-766, (2006)

[2] T. Takagi and M. Sugeno, "Fuzzy identification of Systems and its application to modelling and control," IEEE Transactions on Systems, Man and Cybernetics, Vol. SMC-15, p. 116-132, (1985)

[3] J. Du, X. Zhang and C. Song, "Multi-PID Control of Hammerstein Systems with Input Multyplicity", Proceedings of 30th Chinese Control Conference, Yantai (China), 22-24 July 2011, pp. 303-306, (2011)

[4] O. Galán, J. A. Romagnoli, A. Palazoğlu and Y. Arkun, "Gap Metric Concept and Implications for Multilinear Model-Based Controller Design", Ind. Eng. Chem. Res. Vol. 42, pp. 2189-2197, (2003)

[5] G. Vinnicombe, "Uncertainty and Feedback. H_∞ Loop-Shaping and the ν-Gap metric", Imperial College Press, London (UK), (2000)

[6] A. Isidori, "Nonlinear Control Systems", Springer, Berlin (Germany), (1995)

[7] M. Krstić, I. Kanellakopoulos and P. Kokotović, "Nonlinear and Adaptive Control Design," Wiley, New York, (1995)

[8] V. Filipović and V. Đorđević, "Recursive Estimation of the Takagi-Sugeno Models II: Recursive estimation of fuzzy Hammerstein models," (to be published)

[9] J. Abonyi and B. Feil, "Cluster Analysis for Data Mining and System Identification", Birkhauser, Basel (Switzerland), (2007)

[10] R. O: Duda, P. E. Hart and D. G. Stork, "Pattern Classification", Wiley, New York (USA), (2000)

[11] S. Miyamoto, H. Ichihashi and K. Honda, "Algorithms for Fuzzy Clustering: Methods in c-Mean Clustering with Applications", Springer, Berlin (Germany), (2008)

[12] E. E. Gustafson and W.C. Kessel, "Fuzzy Clustering with a Fuzzy Covariance Matrix," IEEE Conference of Decision and Control including the 17th Symposium on Adaptive Processes, Vol. 17, p. 761-766, (1978)

[13] R. Babuška, "Fuzzy Modeling for Control", Springer Science + Business Media, New York (USA), (1998)

[14] I. Gath and A. B. Geva, "Unsupervised Optimal Fuzzy Clustering", IEEE Transactions on Pattern Analysis and Machine Intelligence, Vol. 11, pp. 773-781, (1989)

Energy Performance Constant Power Motion Control of Robotized Mining Truck

Denis Pogosov
Electronics and Mechatronics Department, Southern Federal University, Rostov-on-Don (Russia)

This paper presents synthesis of a control system of a robotized mining truck with optimization of its energy consumption by arranging a motion control mode in which an internal combustion engine produces a constant power. The paper presents a method for optimize the rotor flux of an electric powertrain induction motor.

Motion control is based on a modified method of the Position-trajectory control. We enlarged the Position-trajectory method to a class of systems which motion is realized with the constant engine power, as well as to a class of systems which have redundant structure.

The introduced solutions are universal about power characteristics of electric machines and to their working mode. This allows the system to control the electric machines with non-hyperbolic characteristics as well as above rated speed without changing the structure of the control system.

Keywords: Mining truck, Robot, Nonlinear control, Constant power motion, Position-trajectory control, Energy performance

1. INTRODUCTION

Designing a robotic control system of heavy mining trucks (MT) with energy optimization is a comprehensive multi-tasking problem. This complexity follows from the structure of the controlled object, which has several elements, that energy optimization is a separate analysis and carried out by different methods, in general.

A typical structure of a tractive drive of MT includes [1] a diesel internal combustion engine (DE), electric powertrain system (EP) and wheeled movers.

Overcoming of rough terrain obstacles, during the movement, requires increasing DE power that is a negative impact on the fuel consumption. From the internal combustion engines theory [2-3] is well known that high dynamics of the engine impair its quality characteristics to reduce the emissions, especially NOx. Reduction NOx emissions most efficiently at a low combustion temperature, which is most easily achieved with constant engine power and constant crankshaft speed. There should be noted that the optimal area of DE is in a neighbourhood of the nominal load point. Just in this optimal area the minimum of fuel consumption is achieved at significantly low engine dynamics. As evidenced by the foregoing causes the task of arrangement a MT movement with constant power and constant DE crankshaft speed, mainly in the nominal point.

Motion with high accuracy on the desired trajectory with constant power of the main engine requires high powertrain dynamics, which leads to the relevant tasks to improve EP efficiency and reduce losses.

2. MATHEMATICAL MODEL OF MINING TRUCK

2.1. Chassis Model

Modern mining trucks have different constructions. Mostly they are presented with a two-axle vehicle with driving rear and steering front axles. At this time actively developed systems with steering-drive axles, for example Belaz 7571 with two and prospective ETF Truck with five steering-drive axles. In this paper we used an universal generalized vector-matrix model of MT for the design of the motion control systems of wide class MT, as well as a simplified model of classic MT chassis for synthesis a control system example and its simulation.

The generalised model in vector-matrix form given as follows [4]:

$$\dot{X} = M^{-1}(L_2\tilde{Q} - F_r - F_N) \tag{1}$$

$$\dot{Y} = \Sigma(P,\gamma) \tag{2}$$

where: Y – is vector of the chassis position P and orientation (yaw) γ, $\Sigma(.)$ – is a nonlinear function of coordinates transformation, L_2 – is matrix of torque-force transformation, X – is vector internal coordinates (of steering angle and driven wheels speed), $\tilde{Q}$ – is vector of internal coordinates derivatives (torque), F_r – is vector of a motion resistance, M – is matrix of mass and inertia parameters, F_N – is vector of immeasurable disturbances.

The simplified model of classic MT chassis is particular case of system (1)-(2) and contains these two equations. We represent the specializing model in vector-matrix form as follows [5-6]:

$$X = [\theta \quad \omega]^T \tag{3}$$

$$Y = [P \quad \gamma]^T \tag{4}$$

$$\dot{P} = rk_{wg}\omega\begin{bmatrix}\cos\theta\cos\gamma - a^{-1}\sin\theta\sin\gamma\\ \cos\theta\cos\gamma + a^{-1}\sin\theta\sin\gamma\end{bmatrix} \tag{5}$$

$$\dot{\gamma} = a^{-1}rk_{wg}\omega\sin\theta \tag{6}$$

$$k_S\ddot{\theta} = U_{st} - hb^{-1}\sin\beta \tag{7}$$

$$M = diag(1, mr) \tag{8}$$

$$L_2 = diag(-r^{-1}k_{wg}^{-1}, 1) \tag{9}$$

$$F_r = f_g mg\left(\cos\alpha\begin{bmatrix}0\\ \cos\beta - \dfrac{h}{a}\tan\alpha\end{bmatrix} + \begin{bmatrix}0\\ \sin\alpha\end{bmatrix}\right) + F_a \tag{10}$$

Corresponding author: D113, Nekrasovskij 44, Taganrog city, Rostov region, Russia and pogosov.den@yandex.ru

where: θ – is steering angle, ω – is driven shaft speed (before wheel gear), r – is the wheel radius, k_{wg} – is the wheel gear ratio, a – is distance between axles, b – is distance between wheels, h – is center of gravity height, m – is MT mass, F_a – is the air resistance, g – is free fall acceleration constant, k_S – is inertial steering constant, U_{st} – is control variable of the steering unit, α – longitudinal (like pitch) angle, β – is lateral (like roll) angle, f_g – is the ground coefficient, $diag(.)$ – is operator to create a diagonal matrix from the operator arguments. No immeasurable disturbances this case.

2.2. Electric Transmission Model

Frequently modern electric powertrains of MT are based on AC induction motors (IM) as a traction drive, AC synchronous generators (SG), as well as inverters with DC link.

High quality control of AC drives is possible by the vector control methods [7-10]. According to the method, all electric units are represent as vectors in the two-dimensional reference frame d, q.

2.2.1. Model of Induction Motor

We represent the model of IM in the d, q frame, that rotating synchronously with the rotor flux, according to the FOC [7-13] method. The model in scalar form given as follows [7-13]:

$$U_d = \sigma L_s \dot{I}_d - \sigma L_s \omega_\Phi I_q + R_1 I_d - L_r^{-2} L_m R_r \Phi \quad (11)$$

$$U_q = \sigma L_s \dot{I}_q + \sigma L_s \omega_\Phi I_d + R_s I_q + L_r^{-1} L_m \omega_\Phi \Phi \quad (12)$$

$$R_1 = R_s + L_r^{-2} L_m^2 R_r \quad (13)$$

$$L_r R_r^{-1} \dot{\Phi} = L_m I_d - \Phi \quad (14)$$

$$Q = 1.5 Z_p L_m L_r^{-1} I_q \Phi - k_f \omega \quad (15)$$

$$\omega_\Phi - Z_p \omega = \frac{L_m R_r I_q}{L_r \Phi} \quad (16)$$

where: U_d, U_q – are stator voltage components in the reference frame, I_d, I_q – are stator currents components in the reference frame, R_s – is the stator resistance, R_r – is the rotor resistance, L_s – is the stator inductance, L_r – is the rotor inductance, L_m – is the mutual inductance, σ – is the motor leakage inductance, Φ – is the rotor flux, Q – is the motor torque, Z_p – is pole pairs quantity, ω_Φ – is the reference frame speed, k_f – is a friction coefficient.

The L_s, L_m, L_r and σ are approximated functions depends on main magnetic flux Φ_m, which estimates by measured voltage and current of the stator and the rotor speed. This is way to take into account the saturation of magnetic system if IM.

2.2.2. Model of Inverter

Hardware implementation of the inverter can be quite different [7-10], so we restricted only by most important relationships.

We assume the inverter as two-stage voltage converter. The first stage is DC link, based on diode rectifiers with capacitance filter. The second stage is self-excited voltage inverter, based on six semiconductor switches.

The inverter realises necessary voltage to IM by vector PWM method. Figure 1 shown the diagram of six base vectors U1-U6, from that realises the necessary vector U.

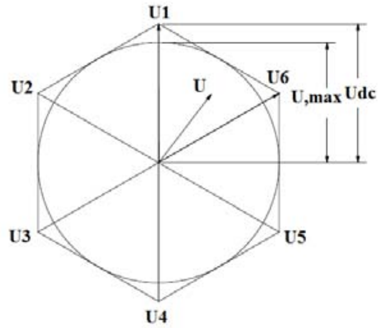

Figure 1: Vector PWM diagram

So, maximal voltage calculated as follows:

$$U_{\max} = \frac{\sqrt{3}}{2} U_{dc} \quad (17)$$

where: $U_{\max}$ – is IM maximal voltage unrestricted by the hexagonal area, U_{dc} – is voltage on DC link.

Software implementation of it can be carried out by variety of known methods [7-8, 10].

Second matter relationship is power loses of the invertor, they are sum of constant and switching loses:

$$P_{loss,inv} = I^2 (R_{sc} + P_{sw} f_{PWM}) \quad (18)$$

where: $P_{loss,inv}$ – is inverter losses, I – is current through inverter, R_{sc} – is semiconductor switch resistance, P_{sw} – is elementary switching resistance correspond to losses (depends on switching time), f_{PWM} – is PWM base frequency.

At the current angles divisible by 30 degrees, the right summand in (18) is equal to zero.

2.2.3. Model of Synchronous Generator

We represent the model of SG in the d, q frame, that rotating synchronously with the rotor. The model in scalar form given as follows [7-13]:

$$U_{gd} = L_{gd} \hat{\dot{I}}_{gd} + L_{gm} \dot{I}_f + R_g I_{gd} + \omega_g L_{gq} I_{gq} \quad (19)$$

$$U_{gq} = L_{gq} \hat{\dot{I}}_{gq} - \omega_g L_{gd} I_{gd} + R_g I_{gq} - \omega_g L_{gm} I_f \quad (20)$$

$$U_f = R_f I_f + L_f \dot{I}_f + L_{gm} \hat{\dot{I}}_{gd} \quad (21)$$

$$Q_{load} = 1.5 Z_{gp} I_{gq} (L_{gm} I_f + L_\Delta I_{gd}) + k_{fg} \omega_g \quad (22)$$

where: U_{gd}, U_{gq} – are stator voltage components in the reference frame, I_{gd}, I_{gq} – are stator currents components in the reference frame, $\hat{\dot{I}}_{gd}, \hat{\dot{I}}_{gq}$ – are estimated stator currents components derivatives in the reference frame, R_g – is the stator resistance, R_f – is the inductor resistance, L_{gd}, L_{gq} – are stator inductance components, L_Δ – is the stator inductance difference, L_{gm} – is the mutual inductance, L_f – is the inductor inductance, U_f –

is inductor voltage, Q_{load} – is the load torque, Z_{gp} – is pole pairs quantity, ω_g – is the reference frame speed, k_{fg} – is a friction coefficient.

This model describes generalized SG with a salient poles rotor, mostly used as EP generators. In particular case of round rotor L_Δ is equal to zero. L_f is a nonlinear function of inductor current. This is way to take into account the saturation of magnetic system of SG.

2.2.4. Coordinates Transformation

Due to the fact that the above models of IM and SG obtained for the two-dimensional reference frame and most real AC electric machines have three phases (some synchronous generators can be six-phase), there is necessary to coordinates transformation from the natural phase system to d,q and vice versa.

The coordinates transformation given as follows [7-8, 10, 14]:

$$R(.) = \begin{bmatrix} \cos(.) & \sin(.) \\ -\sin(.) & \cos(.) \end{bmatrix} \quad (23)$$

$$U_{3IM} = P_S R^{-1}(\gamma_\omega)\begin{bmatrix} U_d & U_q \end{bmatrix}^T \quad (24)$$

$$U_{3SG} = P_S R^{-1}(\gamma_R)\begin{bmatrix} U_{gd} & U_{gq} \end{bmatrix}^T \quad (25)$$

$$P_S = \begin{bmatrix} 1 & -1/2 & -1/2 \\ 0 & \sqrt{3}/2 & -\sqrt{3}/2 \end{bmatrix}^T \quad (26)$$

where: U_{3IM} – is a vector of IM phase voltages, U_{3SG} – is a vector of SG phase voltages, γ_ω – is the angle of IM rotor flux, γ_R – is the angle of SD rotor, $R(.)$ – is a rotation matrix.

Quite similar transformation may be obtained for currents or other variables of the electric machines.

2.3. Diesel Engine Model

A generalised model of DE torque balance in scalar form given as follows [2]:

$$J_e \dot{\omega}_e = M_{ind} - M_{fr} - M_{pump} \quad (27)$$

where: J_e – is the engine inertia, M_{ind} – is the indicated engine torque, M_{fr} – is the friction engine torque, M_{pump} – is the pump torque.

Engine torque components can be represented as follows [2, 14-15]:

$$M_{ind} = \frac{k_F U_F Q_{LHV} R_{gas} T_{im} (e_0 + e_1\omega_e + e_2\omega_e^2)}{\eta_V V_d P_{im}} \quad (28)$$

$$\eta_V = e_3 + e_4\omega_e + e_5\omega_e^2 \quad (29)$$

$$M_{fr} = \frac{1000\, V_d \left(e_6 + e_7\omega_e + e_8\omega_e^2\right)}{2\pi n_R} \quad (30)$$

$$M_{pump} = e_9 P_{im} + e_{10} \quad (31)$$

where: U_F – is a fuel rate, Q_{LHV} – is the fuel lower heating value; R_{gas} – is the gas constant, P_{im} , T_{im} – are pressure and temperature in intake manifold, respectively, V_d – is the engine volume, η_V – is volumetric efficiency, n_R – is number of revolutions for each power stroke per cycle, $k_F, e_0 - e_{10}$ – are constants. We assume measurable of intake manifold pressure and temperature.

3. POWER LOSSES AND OPTIMISATION

We assume two types of energy losses; the first is optimizable losses, the second is not. The efficiency of EP is a nonlinear function of the consumed power. So, to stabilize the power of DE, the control system should use remain energy, exclude all losses.

3.1. IM Energy Losses and Optimisation

Energy optimization techniques of AC motors are concentrated [16-19] on solutions based on the Lagrange approach. In [17, 20] the Lagrange method is used both with the Kuhn-Tucker theorem, that extends the method to cases of constraints set by the inequalities. It is used in [16-17] for synthesis a control of a motor on the boundary modes of operation. Presented in [21] solutions are designed to optimize both components of the stator current or contain extreme conditions where IM is operating at the maximum voltage or current.

Mathematical model of IM with squirrel-cage rotor is represented by (11)-(16). Thus, with respect to (11), (12) and (15) the orthogonal components of the current vector represent IM as a two dimensional object. As follows from (15), I_q component of stator current allows to control IM torque and I_d component allows to flux rotor control, i.e. electromagnetic state of IM. In the case of a constant rotor flux, control of I_q channel allows nearly infinitely fast control of IM torque (15), thereby ensuring a high quick-action performance of a motion control system. However, retention of the rotor flux at a constant (nominal) level is a negative impact on energy consumption. Since the rotor time constant $L_r R_r^{-1}$ has a large value versus σL_s, forced control of Φ will attend energy loss.

For motion control systems is necessary to guarantee a smooth transition from a system with maximum performance properties to a system with maximum energy efficiency properties, predominantly in the intermediate area of operation. This can be achieved by separating the control channels of IM torque and the rotor flux, with a possibility of separate quality of transients on each channel. One matter note there is, this separating is a formal approach, like separating the stator current to two components. So, there is no decomposition of the physical model. For example, in applications where the quick-action is more important than energy efficiency, increasing the transient time of the rotor flux changing, will allow the control system to fast torque control. Tuning the rotor flux to optimal value at long duration thereby will be without energy losses of force of this process. That is, without deterioration of performance characteristics by capture energy from I_q component of stator current during the torque transient.

This necessitates the optimization of some function, which is energy loss function of IM, depending on I_d component of stator current (or the rotor flux) and independent of I_q component. The function may be obtained from the equation of power balance equation, by subtracting therefrom the net power (mechanical work), as well as non-optimizable power losses. We consider total loses and optimizable loses function Λ in steady-state as the following equation [16-18, 20, 22]:

$$P_{loss,IM} = \frac{4}{3}\frac{dW}{dt} + \frac{2}{3}P_{copper} + \frac{2}{3}P_{core} + P_{fr} \tag{32}$$

$$\Lambda = \frac{4}{3}W + \frac{2}{3}P_{copper} + \frac{2}{3}P_{core} \tag{33}$$

$$W = \sigma L_s I_s^2 + L_r^{-1}\Phi^2 \tag{34}$$

$$P_{copper} = (R_s + R_r\frac{L_m^2}{L_r^2})I_s^2 - \frac{R_r}{L_r^2}\Phi^2 \tag{35}$$

$$P_{core} = \frac{L_m^2}{L_r^2}(k_h\left|\omega_\Phi\right| + k_e\omega_\Phi^2)\Phi^2 \tag{36}$$

$$I_s^2 = \frac{\Phi^2}{L_m^2} + \frac{4L_r^2Q^2}{9Z_p^2L_m^2\Phi^2} \tag{37}$$

where: $P_{loss,IM}$ – is total IM losses, P_{copper} – is copper losses of the rotor and the stator, P_{core} – is stator iron losses (at a low sliding core losses of the rotor usually neglected [17]), P_{fr} – is friction and windage losses, W – is the stored energy in the magnetic system of IM, k_e – is eddy currents constant, k_h – is hysteresis constant, I_s – is the Euclidean norm of stator current vector.

The magnetic energy W is the first integral of the magnetic power. Minimizing this is needed to reduce reactive currents.

Using equation (37) we able to represent the function (33) as a function of the rotor flux.

We compute the partial derivative of the function (33) of the rotor flux and given follows equations:

$$\frac{\partial\Lambda}{\partial\Phi} = \frac{4}{3}\frac{\partial W}{\partial\Phi} + \frac{2}{3}\frac{\partial P_{copper}}{\partial\Phi} + \frac{2}{3}\frac{\partial P_{core}}{\partial\Phi} = 0 \tag{38}$$

$$\frac{\partial I_s^2}{\partial\Phi} = \frac{2\Phi}{L_m^2} - \frac{8L_r^2Q^2}{9Z_p^2L_m^2\Phi^3} \tag{39}$$

$$\frac{\partial W}{\partial\Phi} = \sigma L_s\frac{\partial I_s^2}{\partial\Phi} + 2L_r^{-1}\Phi \tag{40}$$

$$\frac{\partial P_{copper}}{\partial\Phi} = (R_s + R_r\frac{L_m^2}{L_r^2})\frac{\partial I_s^2}{\partial\Phi} - \frac{R_r\Phi}{L_r^2} \tag{41}$$

$$\frac{\partial P_{core}}{\partial\Phi} = \frac{2L_m^2}{L_r^2}(k_h\left|\omega_\Phi\right| + k_e\omega_\Phi^2)\Phi \tag{42}$$

Then, we equal (38) to zero and solve the resulting equation:

$$\Phi_{opt} = \sqrt{QL_\Phi(\omega_\Phi, \Phi_m)} \tag{43}$$

where: Φ_{opt} – is the optimal rotor flux, $L_\Phi(\omega_\Phi, \Phi_m)$ – is the nonliner function, aproximated from solving (38).

3.2. SG Energy Losses and Optimisation

We will introduce the SG losses by follows vector-matrix equations:

$$P_{loss,SG} = \frac{3}{2}\left(I_g^T L_g \hat{\dot{I}}_g + I_g^T(R_G + \omega_g L_g D)I_g\right) + k_{fg}\omega_g \tag{44}$$

$$L_g = diag(L_{gd}, L_{gq}) \tag{45}$$

$$P_{loss,f} = R_f I_f^2 + L_f\dot{I}_f I_f \tag{46}$$

where: $P_{loss,SG}$ – is total SG losses, I_g – is vector of stator current, $\hat{\dot{I}}_g$ – is estimated stator current derivative, R_G – is the stator resistance diagonal matrix, $P_{loss,f}$ – is the inductor losses, L_g – is stator inductance matrix, L_{gm} – is the mutual inductance, D – is skew-symmetric matrix.

The windage losses should depend on square-law of a shaft speed, but in this paper they (15), (22), (32), (44) are described as linear functions of correspond electrical machine shaft speed. The reason is, that SG and IM has high power capacity and they usually have units for active cooling. So they have not large impellers for cooling and the windage losses can be approximated by linear functions.

There should be noted about SG optimisation. The components of SG voltage and current in the reference frame are depends on its Euclidean norms and angle between the vector and q axle. The Euclidean norms are fully determined from necessary IM voltage and currents (11), (12) and (17). The angle between I_g and U_g is depend on power factor and skew angle φ, namely:

$$\varphi = \frac{I_dU_d + I_qU_q}{\|I\|\|U\|} - \arctan(\omega_\Phi C_{dc}) \tag{47}$$

where: $\|I\|, \|U\|$ – are Euclidean norms of IM voltage and current, C_{dc} – is capacitance of DC link filter.

The angle between q axes and U_g is depend on load angle $\hat{\theta}_g$, which estimated from the current components, after measure the phases current, we assume. Hence SG is fully determined object, and there is no redundancy, which might have optimised.

3.3. Total losses

The total losses we assume are losses of SG, IM, and the inverter. There we separate the total losses to two types. The first is static losses, which is time independent. The second is dynamic losses, which is time depends.

The static losses equation is get from (17), (18), (32), (35), (36), (44) and (46) and given as follows:

$$P_{loss,static} = I_s^T\tilde{R}I_s + L_3\Phi^2 + k_f\omega + k_{fg}\omega_g + R_f I_f^2 \tag{48}$$

$$\tilde{R} = \frac{3}{\sqrt{3}}\left(R_G + \omega_g L_g D\right) + R_2 \tag{49}$$

$$R_2 = \frac{1}{2}diag(1.5R_1 + R_{sc} + P_{sw}f_{PWM}) \tag{50}$$

$$L_3 = \frac{3}{2}\left(\frac{L_m^2(k_h\left|\omega_\Phi\right| + k_e\omega_\Phi^2) - R_r}{L_r^2}\right) \tag{51}$$

The dynamic losses equation is get from (17), (32), (34), (35), (44) and (46) and given as follows:

$$P_{loss,dynamic} = I_s^T\tilde{L}\dot{I}_s + 2L_r^{-1}\Phi\dot{\Phi} + L_f I_f\dot{I}_f \tag{52}$$

$$\tilde{L} = \frac{3}{\sqrt{3}}L_g + \frac{3}{2}L_S \tag{53}$$

where: L_S – is stator inductance diagonal matrix.

For control synthesis we will use both losses equations (48) and (52).

4. MOTION CONTROL ALGORITHM SYNTHESYS

The control object represented by (1)-(17), (19)-(22), (28)-(31) is essentially nonlinear and multilinked object. There should be noted an impossibility of usage of any linear control system or a systems which working with a decomposed original model of a control object. This is due to the fact, that such systems adequately control an essentially nonlinear objects at significantly narrow area of operation. Thus, for the synthesis of control algorithms, we need the basis control methods of nonlinear and multilinked objects. As such method we choose the Position-trajectory control method [4, 23-26]. This method enables to control the moving objects along on a desired path (trajectory goal) and at a constant speed. Another feature of the method is equality of number of control goals to controlled variables. These present a problem for redundant systems control.

Therefore we supplement the Position-trajectory control method with a motion control with constant power (not just speed) and we supplemented the method with an additional governor of redundant variable (as a sub-goal) in terms of the Position-trajectory control.

4.1. Control goal and control problem definition

We define the control system goal for the synthesis as movement on a trajectory at a desired constant power of traction motor (IM).

We set a trajectory goal of MT by following vector-matrix equation [4], as a function N_1 of external coordinates (4) in implicit form [27]:

$$\Psi_T = \begin{bmatrix} N_1(P) & 0_{2x1} \end{bmatrix}^T \tag{54}$$

We set power consumption at desired level wj at steady state, by the following vector equation, as a function of internal coordinates and their derivatives (2)-(3):

$$\tilde{W} = \begin{bmatrix} 0 & N_2 & N_3 \end{bmatrix}^T \tag{55}$$

$$N_2 = -\left|X\right|^T M\dot{X} + \left|X\right|^T F_R + P_{loss,static} - wj \tag{56}$$

$$N_3 = \Phi^2 - \Phi_{opt}^2 \tag{57}$$

We assume few outputs of control system. The output group is traction side controls, namely steering control (7) and IM voltage (11)-(12), which also used as the inverter control input:

$$U = \begin{bmatrix} U_d & U_q \end{bmatrix}^T \tag{58}$$

The second output group is generation side controls, voltage of SG inductor (21) and fuel rate of DE (28).

We define the desired character of TR motion as a closed-loop system by follows system of vector-matrix equations:

$$\Psi = \Psi_T + A\dot{\Psi}_T \tag{59}$$

$$\tilde{\Psi} = \Psi + T\tilde{W} + T\dot{\Psi} \tag{60}$$

$$\tilde{\tilde{\Psi}} = \tilde{\Psi} + C\dot{\tilde{\Psi}} \tag{61}$$

where: A, T and C – are diagonal matrixes of constant coefficients, which define the desired character of the system action and transient [4, 23-26].

First of all, we present some assumptions, which are taking place in synthesis of the control system.

According to the well-known Lenz principle of the constancy an interlinkage, the resulting magnetic flux cannot change abruptly. Therefore, the rotor flux changes slow, so $\ddot{\Phi} \cong 0$, and then:

$$\dot{\Phi} \equiv L_m \dot{I}_d - J_{Lm}\dot{\hat{\Phi}}_m I_d \tag{62}$$

$$J_{Lm} = \frac{\partial L_m}{\partial \Phi_m} \tag{63}$$

For some minor computations, can be assumed that:

$$\frac{d}{dt}\left(\frac{L_m^2}{L_r^2}\right) \cong 0 \tag{64}$$

Because SG shaft and DE shaft are connected directly $\omega_g = \omega_e$.

According to the Position-trajectory control method [4, 23-26], we differentiate equations (1)-(2) simultaneously with (3)-(10):

$$\dot{Y} = J_{\Sigma X}\dot{X} + J_{\Sigma Y}\dot{Y} \tag{65}$$

$$\ddot{Y} = J_{\Sigma X}\ddot{X} + \Gamma_{\Sigma X}\dot{X} + J_{\Sigma Y}\ddot{Y} + \Gamma_{\Sigma Y}\dot{Y} \tag{66}$$

$$\ddot{X} = M^{-1}(L_2\dot{\tilde{Q}} - \dot{F}_r - \dot{F}_N) \tag{67}$$

$$J_{\Sigma X} = \frac{\partial \Sigma}{\partial X^T}, J_{\Sigma Y} = \frac{\partial \Sigma}{\partial Y^T}, \Gamma_a = \frac{dJ_a}{dt}, a = \Sigma X, \Sigma Y \tag{68}$$

Therefore we differentiate (15) and simultaneously with (62) get the following vector-matrix equation:

$$\dot{\tilde{Q}} = K_{Q5}\begin{bmatrix} U_{st} \\ \dot{I} \end{bmatrix} + K_{Q6}\tilde{Q} + K_{Q7}I \tag{69}$$

$$K_{Q5} = \begin{bmatrix} k_s^{-1} & 0_{1x2} \\ 0 & K_m\begin{bmatrix} L_m I_q & \Phi \end{bmatrix} \end{bmatrix}, K_m = \frac{3Z_p L_m}{2L_r} \tag{70}$$

$$K_{Q6} = \begin{bmatrix} 0 & 0 \\ \dfrac{J_{Lm}\dot{\hat{\Phi}}_m(L_r - 1)}{L_m L_r} & 0 \end{bmatrix} \tag{71}$$

$$K_{Q7} = \begin{bmatrix} 0 & 0 \\ K_m J_{Lm}\dot{\hat{\Phi}}_m & 0 \end{bmatrix} \tag{72}$$

Then, we differentiate (54)-(55) according to (59)-(61) and with substitution of (65)-(67), (69) into the result, and then solving the result equation relative the vector of steering controls and current directive from (69), we obtain follows vector-matrix equation:

$$\begin{bmatrix} U_{st} \\ \dot{I} \end{bmatrix} = -K_0^{-1}(K_1\dot{Y} - K_3F_r - K_{00}\dot{F}_r + K_4\tilde{Q} + \Psi_T + T\tilde{W} + CTK_W + CTK_6 + K_8I + CTK_9) \tag{73}$$

$$K_{00} = CT(AJJ_{\Sigma X} + J_W)M^{-1} \tag{74}$$

$$K_0 = (K_{00} - K_{Z2})K_{Q5} + CTK_{P11} \tag{75}$$

$$K_1 = CTAJJ_{\Sigma Y} + (TA + CA + CT)J + 2CTA\Gamma \tag{76}$$

$$K_2 = (A + T + C)J + (TA + CA + CT)\Gamma + CTA\dot{\Gamma} + \Gamma_{\Sigma Y} + K_1J_{\Sigma Y} \tag{77}$$

$$K_3 = (CTK_{P3} + CTAJ\Gamma_{\Sigma X} + K_1J_{\Sigma Y})M^{-1} \tag{78}$$

$$K_4 = (K_{00} - K_{Z2})K_{Q6} - CTK_{Z3} + K_3 \tag{79}$$

$$K_8 = (K_{00} - K_{Z2})[-k_s^{-1} b^{-1} h \sin\beta \quad 0]^T \tag{80}$$

$$K_9 = (K_{00} - K_{Z2}) \tag{81}$$

$$K_6 = \begin{bmatrix} 0 & (I^T L_g D I + k_{fg})\hat{\omega}_e + (2R_f + L_f) I_f \dot{I}_f + 2L_r^{-2}\Phi^2 (0.75 L_m^2 (k_h + k_e |\omega_\Phi|)\hat{\omega}_\Phi + R_r (L_r^{-1} L_3 - 1)) & 2L_r^{-1} R_r \Phi^2 \end{bmatrix}^T \tag{82}$$

$$K_W = [0_{n-1} \quad -|\dot{X}|^T M\dot{X} + |\dot{X}|^T F_R + |X|^T \dot{F}_R]^T, K_{Z2} = \begin{bmatrix} 0_{2x1} & 0_{2x1} \\ 0 & L_\Phi \end{bmatrix}, \tag{83}$$

$$J_W = [0_{(n-1)x2} \quad -|X|^T M]^T, J = \frac{\partial \Psi_T}{\partial Y^T}, \Gamma = \frac{dJ}{dt} \tag{84}$$

$$K_{Z3} = \begin{bmatrix} 0_{2x1} & 0_{2x1} \\ 0 & J_{L\Phi}\hat{\dot{\Phi}}_m \end{bmatrix}, K_{P3} = \begin{bmatrix} 0 & 0 \\ 0 & k_f \\ 0 & 0 \end{bmatrix}, K_{P11} = \begin{bmatrix} 0 & 0_{1x2} \\ 0 & I^T(\tilde{R} + \tilde{L}) \\ 0 & 0_{1x2} \end{bmatrix}, K_{51} = \frac{2}{L_r}\begin{bmatrix} 0 & 0 \\ (L_3 + 1)\Phi R_r & 0 \\ L_m \Phi R_r & 0 \end{bmatrix} \tag{85}$$

Matrix K_6 is depends on derivative of the static power loss with addition of dynamic power loss and with assumption (64). The terms $\hat{\omega}_e, \dot{I}_f, \hat{\omega}_\Phi$ are estimates of correspond variables and represent their current status before computation as the control terms. In other words, for a discrete system they are previous step data.

The system (73) together with (74)-(85) provides us the steering control and current derivative. The voltage on IM is obtained from:

$$U = L_{IM}\dot{I} + (\omega_\Phi L_{IM} D + R_{IM}) I + K_{IM} \tag{86}$$

$$L_{IM} = diag(\sigma L_s), R_{IM} = diag(R_1, R_s) \tag{87}$$

$$K_{IM} = diag(-L_r^{-2} L_m R_r \Phi, L_r^{-1} L_m \omega_\Phi \Phi) \tag{88}$$

As we described before, voltage (86) is going to the inverter input and be used for follows computation of SG inductor voltage:

$$U_f = \begin{bmatrix} L_f & R_f \end{bmatrix} K_f + \begin{bmatrix} L_{gm} & 0 \end{bmatrix} \hat{\dot{I}}_g \tag{89}$$

$$K_f = K_{G3}^{-1}(U_g - L_g \hat{\dot{I}}_g - R_G I_g - \omega_e L_g D I_g) \tag{90}$$

$$\mathrm{U}_g = \frac{2}{\sqrt{3}} U^T U \bar{R}(\hat{\theta}_g) \tag{91}$$

$$\mathrm{I}_g = I^T I \bar{R}(\hat{\theta}_g + \varphi) \tag{92}$$

$$K_{G3} = \begin{bmatrix} L_{gm} & 0 \\ 0 & -\omega_g L_{gm} \end{bmatrix} \tag{93}$$

$$\bar{R}(.) = [\sin(.) \quad \cos(.)]^T \tag{94}$$

Above equations also compute SG voltage (91) and current (92). DE fuel rate is obtained from:

$$U_F = K_{ICE}(M_{fr} + M_{pump} + J_e \dot{\omega}_e) \tag{95}$$

$$K_{ICE} = \frac{\eta_V V_d P_{im}}{k_F Q_{LHV} R_{gas} T_{im} (e_0 + e_1 \omega_e + e_2 \omega_e^2)} \tag{96}$$

$$\dot{\omega}_e = \frac{3Z_g}{2J_g} I_g^T (K_{G1} K_f + K_{G2} I_g) \tag{97}$$

$$K_{G1} = \begin{bmatrix} 0 & 0 \\ 0 & L_{gm} \end{bmatrix}, K_{G2} = \begin{bmatrix} L_\Delta & 0 \\ 0 & 0 \end{bmatrix} \tag{98}$$

The voltages are known, the currents are measured, SG inductor voltage and current no needed to measure. All estimated units getting the value from numerical computations. So, the control system is fully determined, and basic control outputs are getting from (73), (86), (89) and (95).

5. SIMULATION

Simulation of introduced control algorithms (73)-(98) was accomplished in the software package MATLAB. Because the control object is highly-nonlinear we assume some simplification for better readable of the simulation results.

Chassis MT is presented by (1)-(10) and has the following parameters: weight 8 tons, length 8.0 m, width 2.8 m, inertia is 950 kg·m^2 , radius of the driven wheel is 0.5 m, secondary gear ratio is 1:10. IM is represented by (11)-(16) and have the following parameters: maximum voltage is 1000 V, maximum power is 95 kW, $L_S = L_r = 0.2755$, $L_m = 0.2676$, $\sigma = 0.05683$, $R_r = 0.5625$, $R_s = 0.2755$ and $Z_p = 1$. IM will work on the linear area of its magnetisation characteristic, so all inductances are constant. We neglected the core losses and friction losses. This case the nonlinear function in (43) is a constant and $L_\Phi = 0.4076$.

SG is represent by (19)-(22) with follows parameters: $L_g = 0.25$, $R_g = 0.497$, $L_\Delta = 0$, $Z_p = 1$, $L_f = 0.8$ and $R_f = 2.95$. We neglected the derivatives of current in (19), (20) and SG inductor loses, so the generator is represented as an inertial part. The inverter losses are neglected too.

DE characterization [14] is shown on Fig.2.

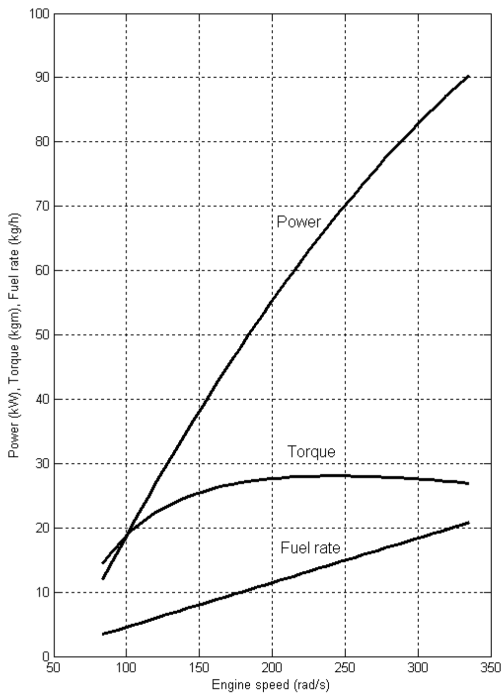

Figure 2: DE characteristics: power (kW), torque (kg•m) and fuel rate (kg/h), all depending on engine speed (rad/s)

The main simulation test is constant power running on a circle. The task of MT motion (54) is the circle of radius 125 m, centred at the origin and the equation (55), corresponding to the stabilization of constant power at level 55 kW. Adjustment matrices coefficients (59)-(61) are equal each other and $A = diag(0.1, 0.3, 1)$. The initial position of the robot is $Y = \begin{bmatrix}125 & 0 & \pi/4\end{bmatrix}^T$ and the robot does not move. Simulation time is 700 s.

Without loss of generality, we represent the motion resistance as a constant equal torque resistance and changing during the test.

The initial resistance is 640 N·m. At 225 s of the simulation, the resistance rises to 740 N·m during 5 s. At 380 s of the simulation, the resistance drop to 540 N·m during 20 s. At 500 s of simulation desired power is changed to 50 kW.

The root-mean-square of position and orientation error should be less than 1 m at steady state of MT operation.

The chassis speed and the torque of the traction IM are shown on Fig. 3 and Fig. 4, respectively. They are shown with comparison with the load torque changes. They are both versus the time.

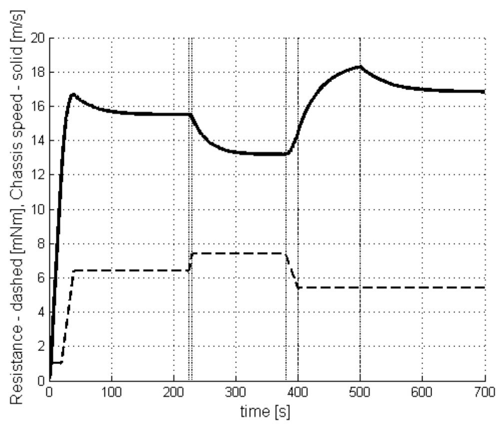

Figure 3: Chassis speed – solid, (m/s) and motion resistance – dashed (mN•m) verus time (s)

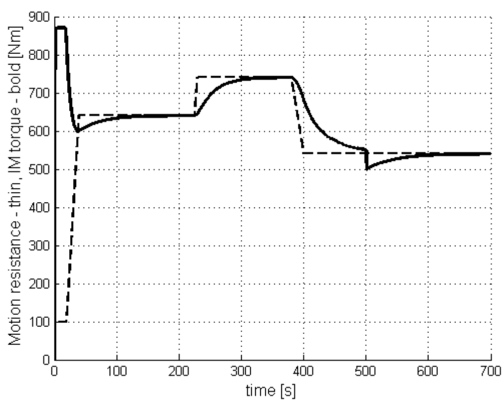

Figure 4: Traction induction motor torque – solid (N•m) and motion resistance – dashed(N•m) verus time (s)

These figures shown the control system (73)-(88) response to unit impact similar that occurs when the vehicle overcoming a hill. Torque change on Fig. 4 at 500 s is result of the desired power change.

The rotor speed and the slip of the traction IM are shown on Fig. 5 and Fig. 6, respectively. They are both versus the time.

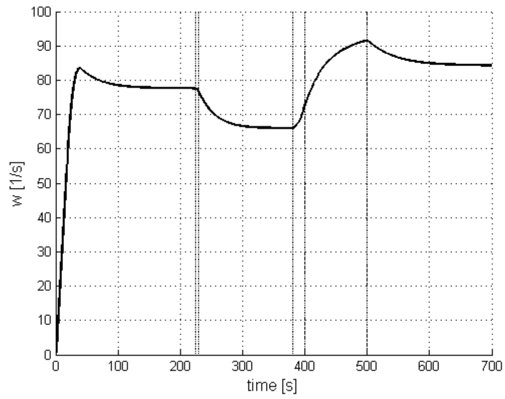

Figure 5: IM rotor rotational speed (1/s) verus time (s)

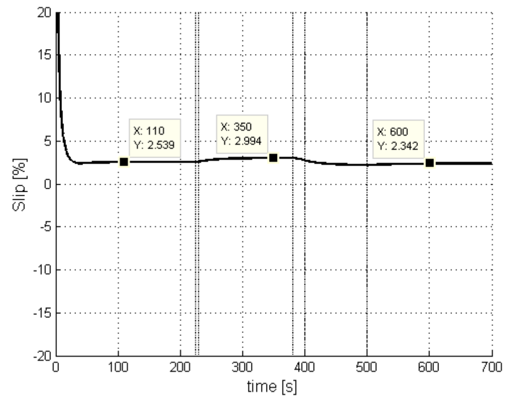

Figure 6: IM slip (%) verus time (s), steady state slips are exact shown for different areas of the test

The slip is under 3% that means well efficiency of IM.

The voltage and current of the traction IM are shown on Fig. 7 and Fig. 8, respectively. They are both versus the time. They are shown in d, q reference frame.

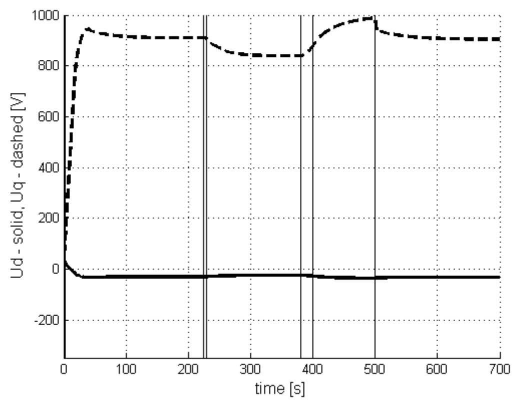

Figure 7: IM voltage (V) in the reference frame d,q verus time (s), d – component is solid, q – component is dashed

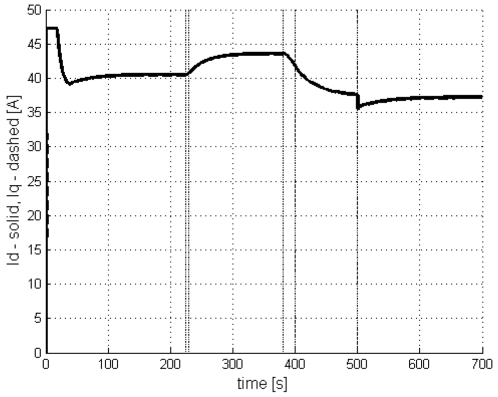

Figure 8: IM current (A) in the reference frame d,q verus time (s), d – component is solid, q – component is dashed

The rotor flux is optimised during the test. The current components are equal that means minimum amplitude of the stator current. It is effect to minimum copper losses and other losses are neglected for this simulation.

The rotor flux is on Fig. 9.

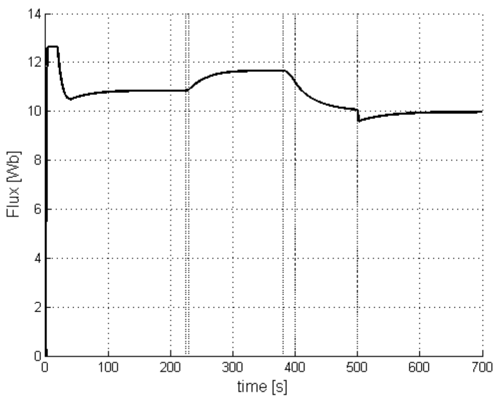

Figure 9: IM rotor flux (Wb) verus time (s)

Power loss of IM is shown on Fig. 10. There is visible a similarity of graphs of current and torque with losses graph. Again, it caused by active losses which are linearly dependent on the current.

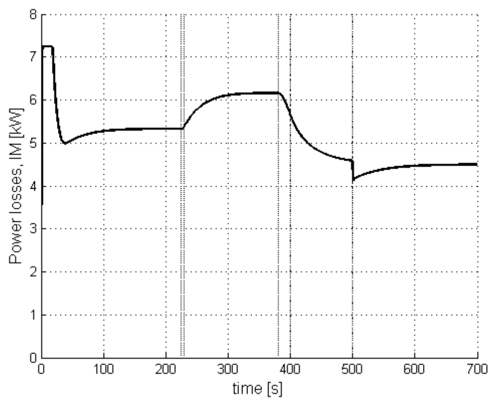

Figure 10: IM power losses (kW) verus time (s)

Consumed power, which is act on the engine shaft is shown on Fig. 11. This power is near to the desired power of the test. The maximum deviation from the desired power is less than 3 rad/s of the engine shaft speed. This is due to the high inertia of the chassis.

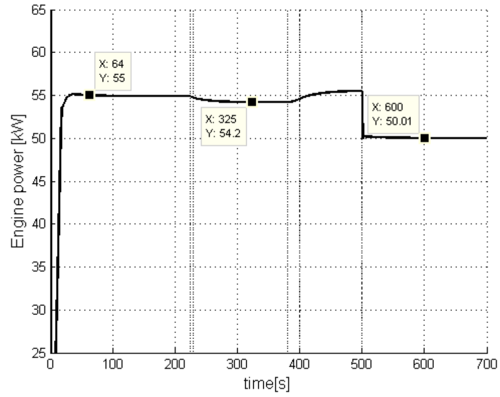

Figure 11: Engine power (kW) verus time (s), deviations are exact shown for different areas of the test

MT trajectory is shown on Fig. 12 and correspond to desired circle with radius of 125 m.

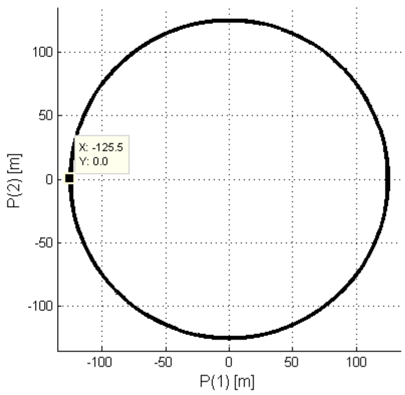

Figure 11: MT trajecotory, deviation is exact shown

The root-mean-square error is 0.86 at steady state, which correspond to the requirements.

6. CONCLUSION

Introduced in this paper solutions extend the Position-trajectory control method for a class of systems, which motion is with a constant power.

The paper introduces solutions to synthesis of nonlinear control algorithms for robotized mining truck equipped with most popular electric transmission.

The solutions are able to optimize energy consumption in the trajectory planning phase of the robot control strategy. This is possible when by taking into account motion resistance changes (parameters of a rough terrain) and as a consequence the necessity of optimization the rotor flux. The introduced solutions are universal about power characteristics of electric machines and to their working mode. This allows the system to control the electric machines with non-hyperbolic characteristics as well as above rated speed without changing the structure of the control system.

The solutions allow to improving the functionality of mobile robots, minimizing fuel consumption without deterioration the quality characteristics, such as accuracy and speed.

ACKNOWLEDGEMENTS

This work was supported by The Russian Federation President grant HS-1557.2012.10, YD-1098-

2013.10, grant of RFBR 13-08-00315 and The Russian scientific foundation grant 14-19-01533.

REFERENCES

[1] A.A. Kuleshov, "Powerful vehicles and excavators mining complexes", Nedra, Moscow (Russia), (1980)

[2] J.B. Heywood, "Internal Combustion Engine Fundamentals", McGraw-Hill, (USA), (1988).

[3] M. Jankovic, I. Kolmanovsky, "Constructive Lyapunov Control Designfor Turbocharged Diesel Engines," IEEE-transactions on Control Systems Technology, Vol. 8, no. 2, pp. 288–299, (2000)

[4] V. Kh. Pshikhopov, M.Yu. Medvedev, "Control of moving objects in structured and unstructured environment", Nauka, Moscow (Russia), (2011)

[5] J.Y. Wong, "Theory of Ground Vehicles", Wiley, (USA), (2008)

[6] C.C. Ward, K. Iagnemma, "A Dynamic-Model-Based Wheel Slip Detector for Mobile Robots on Outdoor Terrain," Robotics, IEEE Transactions on, Vol.24, no.4, pp.821-831, (2008)

[7] V.V. Pankratov, "Vector Control of Induction Motors", NGTU, Novosibirsk (Russia), (1999)

[8] A.A. Usoltzev, "Frequency Control of Induction Motors", ITMO, (Russia), (2006)

[9] A.I. Voldek, "Electric Machienes", Energiya, (USSR) (1978)

[10] A.B. Vinogradov, "Vector Control of AC Motors", IGEU, Ivanovo (Russia), (2008)

[11] I.S. Efremov, "Theory and calculation of electric traction drive", Vysshaja shkola, Moscow (Russia), (1984)

[12] V.I. Klyuchev, "Theory of Electric Drive", Energoatomizdat, (USSR), (1998)

[13] M.G. Chilikin, A. S. Sandler, "General Course of Electric Drive", Energoatomizdat, (USSR), (1981)

[14] D. Pogosov, "Position-Trajectory Control of Advanced Tracked Robots with Diesel-Electric Powertrain," Robot Intelligence Technology and Appl. 2, Vol. 274, pp. 393–403, (2014)

[15] D. Yanakiev, I. Kanellakopoulos, "Engine and Transmission Modeling for Heavy-Duty Vehicles", PATH, (USA) (1995)

[16] Jae Ho Chang, Byung-Kook Kim, "Minimum-time minimum-loss speed control of induction motors under field-oriented control," Industrial Electronics, IEEE Transactions on, Vol.44, no.6, pp. 809-815, (1997)

[17] Adnene Ben Ali, Riadh Abdelati, M. Faouzi Mimouni, R.Dhifaoui, "Maximum-Torque and Maximum-Efficiency Rotor Flux Selection of an Induction Motor in Transient Regime," International Journal of Sciences and Techniques of Automatic control & computer engineering; IJ-STA, Vol. 4, no. 2, pp. 1370-1387, (2010)

[18] S. Lim, K. Nam, "Loss-minimising control scheme for induction motors," Electric Power Applications, IEE Proceedings, Vol.151, no.4, pp.385-397, (2004)

[19] O. Haala, B. Wagner, M. Hofmann, M. Marz, "Optimal current control of externally excited synchronous machines in automotive traction drive applications, " World Academy of Science, Engineering and Technology, International Science Index 81, International Journal of Electrical, Electronic Science and Engineering, Vol. 7(9), pp. 1-7. (2013)

[20] J. Ramirez, C. Canudas de Wit, "Optimal Torque-Flux Control of Induction Motors: Experimental Evaluation," Proc. of the Electrimac congress, Vol. 2, pp. 763-768

[21] O. Wasynczuk, S.D. Sudhoff, K.A. Corzine, J.L. Tichenor, P.C. Krause, I.G. Hansen, and L.M. Taylor, "A Maximum Torque Per Ampere Control Strategy for Induction Motor Drives," IEEE Transactions on Energy Conversion, Vol. 13, no. 2, pp. 163-169, (1998)

[22] D. Rodkin, V. Chenchevoy, V. Ogar, "Determination of losses in steel deep induction motor with its saturated," Kremenchuk Mykhailo Ostrohradskyi National University, Journal Elekromechanichni i energosberegauchi sistemi. Vol. 2 (22) pp. 75-85, (2013)

[23] V.Kh. Pshikhopov, V.A. Krukhmalev, M. Yu. Medvedev, R.V. Fedorenko, S.A. Kopylov, A.Yu. Budko, V.M. Chufistov, "Adaptive Control System Design for Robotic Aircrafts," Robotics Symposium and Competition (LARS/LARC), Latin American, pp. 67-70, 21-27 Oct. (2013)

[24] V. Pshikhopov, N. Sergeev, M. Medvedev and A. Kulchenko, "The Design of Helicopter Autopilot," SAE Technical Paper 2012-01-2098, (2012)

[25] V. Pshikhopov, M. Medvedev, V. Kostjukov, R. Fedorenko et al., "Airship Autopilot Design," SAE Technical Paper 2011-01-2736, (2011)

[26] V.Kh. Pshikhopov, M.Y. Medvedev, "Robust control of nonlinear dynamic systems," ANDESCON, 2010 IEEE, pp.1,7, 15-17 (2010)

[27] D. Pogosov, "Transformation of High-order Spline-functions to implicit form," SWorld conference proceedings 3, Vol. 4, pp. 84–87, (2012)

Design the Digital Internal Model Control of an Electromechanical Positioning System with Controlled Jerk

Mihaylo Y. Stoychitch[1*]
[1]Faculty of Mechanical Engineering, University of Banja Luka, Republic of Srpska, BiH

Abstract. *In this paper design of an electromechanical positioning system that ensures in advance determined and controlled change of the jerk is considered. A system that is formed from a load and an actuating device is used as an object. For the proposed sinusoidal change of the jerk, the appropriate changes of the acceleration, velocity and displacement were found. The control algorithm which ensures the motion of the object with sinusoidal change of the jerk so that the requirements which are related to the maximum values of the acceleration, velocity and displacement are satisfied, is also proposed. As a control system the digital internal model control (IMC) is used. Furthermore the simulation of that system is performed, which is confirmed the proposed theory.*

Keywords: positioning system, internal model control, digital controller, controlled jerk, trajectory planning

1. INTRODUCTION

Positioning systems are often used in the industry as electromechanical drive or to drive of robots. The task of this system is to achieve adequate movement between two arbitrary points, from a point A to a point B, where the system at the initial and the final points is at the idle state. In doing so, we assume that the acceleration and deceleration times are the same, or equivalently, the trajectory is symmetric with respect to the velocity. In order to design such a system it is necessary to solve several problems, such as:

- trajectory planning: determining allowable trajectory and all parameters of motion (jerk, acceleration, velocity, ...) for all degrees of freedom and for each actuating device separately,
- controller design: designing feedback and/or feedforward and/or another kind of a controller that ensures realization of the desired trajectory for each actuating device, even in circumstances when disturbances (internal and/or external) act on the object, and there exists an unmodeled dynamic of the object , and
- other problems, such as: diagnostic, internal checks, communications, etc.

The solutions of the above problems usually are reduced to one actuating unit, assuming that the solutions for the rest units are the same.

Motion of the object (plant) between two points can typically be divided into three phases: acceleration, motion with constant speed, and deceleration. Traditionally, a trapezoidal (or triangular) speed profile has been mainly used. This means that acceleration of the object (for a time t_a) is constant until it reaches the maximum speed, then it keeps this speed (for a time t_v), and it decelerates with a constant deceleration (also, for a time t_a) so that the total time of the movement τ is $\tau = 2t_a + t_v$. One of the main problems with the trapezoidal speed profile is large changes of the jerk, and consequently large inertial forces. Furthermore, that can induce large vibrations of mechanical parts of the system which leads to a large stationary error and too long settling time, that can often be unacceptable for the overall system.

But, there exist several different approaches to improve the performance of these systems, which can be roughly split as:

- Trajectory smoothing or shaping: The result can be very good, but it can leads to a significant increase in execution time of the trajectory. This approach is considered in [3,4,8,10].
- Feedforward control based on plant inversion: This approach gives good results only if the plant model is well known, but with important disadvantage with respect to robustness of the system. Different examples of this approach can be found in papers [3,4,5].
- Feedback control optimization: Since the feedback controller is an integral part of almost all positional systems, then its optimization leads to decrease of the stationary errors and settling time, but at the same time may increase the overshoot and reduce the stability of the closed system. This approach is considered in [2,10,11].
- Combination different types of the controllers: The control system is implemented as a

Corresponding author: (in Serbian language *Михајло Ј. Стојчић*), Vojvode Stepe 75, 78000 Banja Luka,e-mail: stojcicmihajlo@gmail.com

combination of feedforward and feedback controllers. Such control system, in some way, includes advantages of the controllers which are assembled. This approach is considered in [12,13,14] and as analog and as digital type of the control system.

In this paper, as a control system we use the digital Internal Model Control (IMC) with two degrees of freedom. The continuous equivalent of the IMC controller which is used herein, is somewhat modified version of the IMC controller with two degrees of freedom that is proposed and described in detail in [1]. As an object a linear continuous object is used, and we assume that its mathematical model is a perfect representation of actual dynamic behaviour.

Generally, if the object is analog, then there are two different approaches to design digital controllers,[8]. In the first approach, the overall system is considered as analog, then on the basis of advance given requirements is designed an analog controller that is satisfied these requirements and, at the end, this analog controller is transformed to the appropriate digital one. In the second approach, the first, the analog object is transformed into the appropriate digital one, then the total design is moved into discrete time domain, in which we use well known digital techniques. In this paper is used the first approach.

And, at the end of this chapter, a few words about the structure of the paper. The second chapter is related to trajectory planning, that includes: the mathematical model of the object, the laws of changes all the parameters of movement and an algorithm of the trajectory planning. In the third chapter is designed the two degree of freedom IMC digital controller. And, in the fourth chapter simulation of the overall system, using MatLab and SimuLink, is performed. The fifth and sixth chapters include conclusions and references, respectively.

2. TRAJECTORY PLANNING

2.1. Mathematical model of the object

We consider an electromechanical positioning system, Figure 1, where mass m includes masses of all the moving parts (load and actuator). In the initial time $t_0 = 0$, we assume that the values of the jerk j, acceleration a, velocity v and displacement d are zero, i.e. $j(0)= a(0)= v(0)= d(0)= 0$. Force $F(t)$ generated by the actuator must overcome the force of inertia $f_i = ma$ (of all the moving masses) and viscous friction

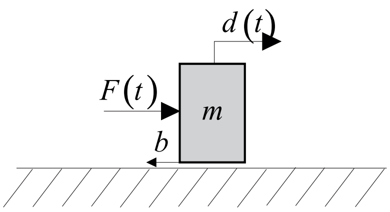

Figure 1. Electromechanical positioning system

force $f_v = bv$. The other frictions (for example Columb frictions) are neglected and their effect is modeled through disturbance $w(t)$, so behaviour of the system is described by the equation:

$$F(t) = m\ddot{d} + b\dot{d} = ma + bv, \quad (1)$$

because the acceleration and velocity are $a(t)= \ddot{d}(t)$ and $v(t)= \dot{d}(t)$ respectively.

After Laplace transformation (all the initial conditions are zero) we obtain the transfer functions of the plant (object), from force to displacement $P_d(s)$

$$F(s) = (ms^2 + bs)D(s) \Rightarrow P_d(s) = \frac{D(s)}{F(s)} = \frac{1}{ms^2 + bs} \quad (2)$$

or, from force to velocity the function $P_v(s)$ (because velocity $V(s)= sD(s)$), as

$$P_v(s)= P(s)= \frac{V(s)}{F(s)}= \frac{1}{ms+b} \quad (3)$$

where $D(s), V(s)$ and $F(s)$ are displacement, velocity and force in complex domain respectively.

2.2. Smoothing trajectory

In order to get little changes of acceleration (trajectory smoothing) we assume sinusoidal change of the jerk as:

$$j(t) = \begin{cases} J\sin\frac{2\pi}{T}t, & t \in [0,T] \\ 0, & t \in [T,t_1], \\ -J\sin\frac{2\pi}{T}(t-t_1), & t \in [t_1,\tau] \end{cases} \quad (4)$$

where: $T = t_a$, $t_1 = T + t_v$ and J are the acceleration time, the time of the start deceleration and the maximum value of the jerk respectively. According to the jerk from (4) and using $a(t) = \int j(t)\,dt + C_a$, we obtain, [11,12], acceleration as

$$a(t) = \begin{cases} \frac{A}{2}\left(1-\cos\frac{2\pi}{T}t\right), & t \in [0,T] \\ 0, & t \in [T,t_1], \\ -\frac{A}{2}\left(1-\cos\frac{2\pi}{T}(t-t_1)\right), & t \in [t_1,\tau] \end{cases} \quad (5)$$

where a relation between the jerk J and the acceleration A is given as $A = \frac{JT}{\pi}$.

From (5), the velocity $v(t)= \int a(t)dt + C_v$ is given as

$$v(t) = \begin{cases} \frac{A}{2}t - \frac{AT}{4\pi}\sin\frac{2\pi}{T}t, & t \in [0,T] \\ \frac{AT}{2}, & t \in [T,t_1], \\ \frac{A}{2}(\tau - t) + \frac{AT}{4\pi}\sin\frac{2\pi}{T}(t-t_1), & t \in [t_1,\tau] \end{cases} \quad (6)$$

and displacement $d(t)= \int v(t)dt + C_d$ as

$$d(t)=\begin{cases}\frac{A}{4}t^2-\frac{AT^2}{8\pi^2}\left(1-\cos\frac{2\pi}{T}t\right), & t\in[0,T]\\ \frac{AT}{4}(2t-T), & t\in[T,t_1]\\ \frac{AT}{4}(2t-T)-\frac{A}{4}(t-t_1)^2+\frac{AT^2}{8\pi^2}\left[1-\cos\frac{2\pi}{T}(t-t_1)\right], & t\in[t_1,\tau].\end{cases} \tag{7}$$

In the equations (5)-(7) the constants of integration C_a, C_v and C_d are determined from initial conditions at appropriate time intervals. Changers of the jerk, acceleration, velocity and displacement at the all time interval ($t\in[0,\tau]$) are shown in the Figure 2.

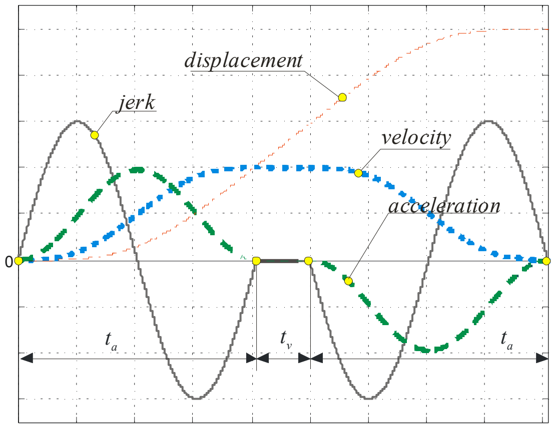

Figure 2. Change of the jerk, acceleration, velocity and displacement at the time interval $[0,\tau]$

From (4) - (7) it is easy to determine the maximum values of the acceleration, velocity and displacement at the time interval [0,T], as:

$$a\left(\frac{T}{2}\right)=\frac{JT}{\pi},\; v(T)=\frac{JT^2}{2\pi},\; d(T)=\frac{JT^3}{4\pi}. \tag{8}$$

2.3. Trajectory planning–algorithm

From a practical viewpoint, it is the best to give the maximum values of jerk J, acceleration A, velocity V and the total displacement D at the beginning of the trajectory planning. These values depend on the possibility of the actuator (force or torque), the application of the positioning system as well as the possibility of the control system. Then it is necessary to determine the shortest time $T=t_a$ and t_v so that given limitations are not exceeded. In this sense, we give the algorithm that follow.

The shortest time within which motion can be performed is calculated from (8) as:

$$D=2\times d(T)=\frac{JT^3}{2\pi}\Rightarrow T=\sqrt[3]{\frac{2\pi D}{J}}. \tag{9}$$

Using this time, the given jerk J and (8) we can calculate the maximum value of the acceleration $a_{\max}$ as, $a_{\max}=JT/\pi$. Now we can test whether $a_{\max}$ exceeds the limit value of the acceleration A. If $a_{\max}\le A$ we continue, but if $a_{\max}>A$ we recalculate T as $T=\pi A/J$. In the similar way we test whether the velocity bound is satisfied. The maximal velocity, from (8), is $v_{\max}=JT^2/2\pi$. Test $v_{\max}\le V$. If this is true we continue, but if it is false we have to recalculate T as $T=\sqrt{2\pi V/J}$. And finally we determine the time t_v as:

$$t_v=\frac{D-\bar{v}T}{\bar{v}}, \tag{10}$$

where velocity $\bar{v}$ is determined as $\bar{v}=\min(v_{\max},V)$. The total time of the movement τ is given as $\tau=2T+t_v$. The above proposed algorithm using flowchart is shown in Figure 3.

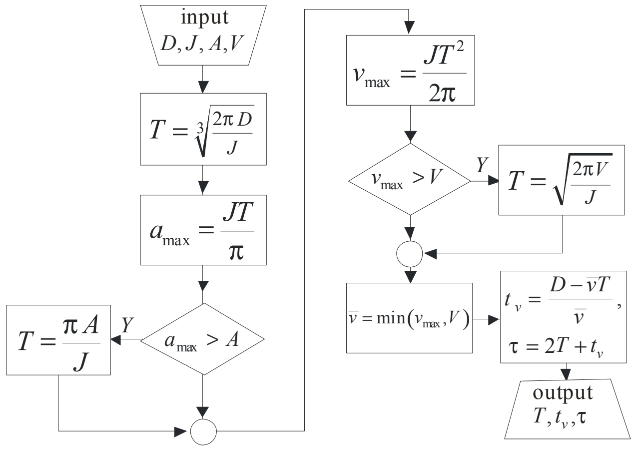

Figure 3. Flowchart of algorithm of the trajectory planning

3. DESIGN OF THE CONTROL SYSTEM

3.1. Configuration of the control system

As already mentioned above, as a control system, we use an IMC controller, which is described in detail in [1]. In this case the IMC with two degree of freedom is used, see Figure 4. The IMC control system in this figure has two inputs: the desired $r(s)$ and real output $y(s)$ and one output, the control $u(s)$. It is composed of: the plant model with transfer function $M(s)$ and two controllers which transfer functions are $Q(s)$ and $L(s)$, that are connected as shown on Figure 4.. The controllers $Q(s)$ and $L(s)$ are independently adjustable, so that the overall control system is called the system with two degrees of freedom.

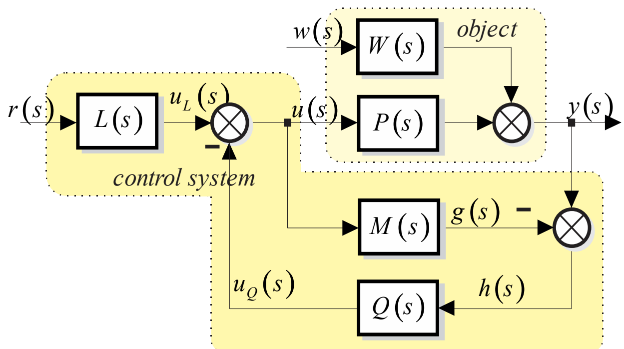

Figure 4. IMC with two degree of freedom

The object model consists of two transfer functions: plant $P(s)$ and disturbance $W(s)$ that are representing dependency of the object output $y(s)$ from control $u(s)$ and disturbance $w(s)$ respectively.

3.2. Change of the output error

The output of the overall system $y(s)$ and the output error $e(s)$ (see Figure 4) in the complex domain are obtained as:

$$\begin{aligned} Lr(s) - Q\left[y(s) - Mu(s)\right] &= u(s) \\ Pu(s) + Ww(s) &= y(s), \end{aligned} \tag{11}$$

from which are obtained: the object output $y(s)$ as

$$y(s) = \underbrace{\frac{PL}{1+Q(P-M)}}_{y_r} r(s) - \underbrace{\frac{W(1-QM)}{1+Q(P-M)}}_{y_W} w(s) \tag{12}$$

and the output error $e(s) = r(s) - y(s)$ as

$$e(s) = \underbrace{\frac{1-QM+P(Q-L)}{1+Q(P-M)}}_{e_r} r(s) + \underbrace{\frac{W(1-QM)}{1+Q(P-M)}}_{e_W} w(s) \tag{13}$$

From the last equation we can see that the output error $e(s)$ has two components: the error $e_r(s)$ due to action of the reference $r(s)$ and the error $e_w(s)$ due to effort of the disturbance $w(s)$. Frome these equation it is easy to conclude that the output error is zero, $e(s) = 0$, if the next conditions are satisfied

$$\begin{aligned} M(s) &= P(s) \\ Q(s) &= M^{-1}(s) \\ L(s) &= Q(s) = M^{-1}(s). \end{aligned} \tag{14}$$

In this case the both parts of errors are zero, $e_r(s) = 0$ and $e_w(s) = 0$, so that the object asymptotically tracks a given reference even though expected or unexpected disturbances act on it.

3.3. Realization of the control system

The control system (Figure 4.) consists of three transfer function that need to be implemented. These functions are: the plant model $M(s)$ and the controllers $L(s)$ and $Q(s)$. In the below we will show the way of realization each of them.

3.3.1. Realization of the plant model $M(s)$

The transfer function of the plant model is given by (3) and (14) ($(s) = P(s)$), so that the transfer function $M(s)$ is

$$M(s) = \frac{1}{ms+b} = \frac{g(s)}{u(s)}, \tag{15}$$

which implies $g(s) = x(s)$, where the auxiliary variable $x(s)$ is given as

$$x(s) = \frac{u(s)}{ms+b} \Rightarrow sx(s) = -\frac{b}{m}x(s) + \frac{1}{m}u(s). \tag{16}$$

The last equations, in time domain and in the state space, becomes as

$$\begin{aligned} \dot{x}(t) &= -\frac{b}{m}x(t) + \frac{1}{m}u(t) \\ g(t) &= x(t). \end{aligned} \tag{17}$$

The realization of these equations using the operating amplifier is given in Figure 5., where the values of the

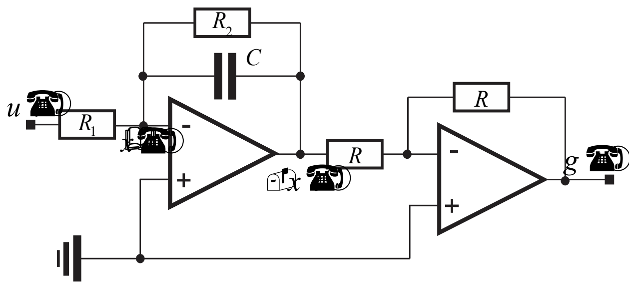

Figure 5. Realization of the plant model

resistors R_1 and R_2 are: $R_1 = \frac{R}{1/m} = mR$ and $R_2 = \frac{R}{b/m} = mR\,/\,b$. The resistor R and the capacity C are chosen so that $RC = 1$ is valid (for example, $R = 1M$ and $C = 1\mu F$ or $R = 100k$ and $C = 10\mu F$), see [9].

3.3.2. Realization of the controller L

The transfer function of controller $L(s)$, using (3) and (14), is

$$L(s) = \frac{U_L(s)}{R(s)} = M^{-1}(s) = P^{-1}(s) = ms + b\,. \tag{18}$$

We got a non-proper transfer functions, that can be realized using differentiation (see [3,4,12]). In the case when the input $r(t)$ is the velocity $v(t)$, $i.e. R(s) = V(s)$, from (18) it is obtained

$$u_L(t) = (ms+b)\frac{1}{s}\dot{v}(t) = \left(m + \frac{b}{s}\right)a(t) = ma + bv\,, \tag{19}$$

where the acceleration $a(t)$ and velocity $v(t)$ are given from (5) and (6). In discrete time domain they are realized

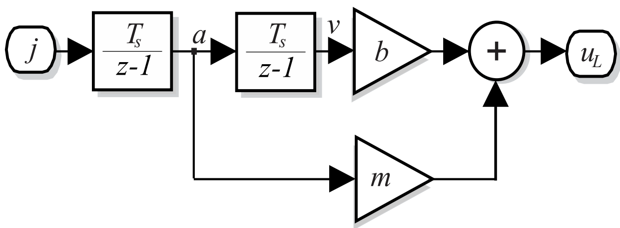

Figure 6. Realization of the controller $L(z)$

by discrete integration of desired change of the jerk and using Euler method, so that are obtained

$$a(k) = a(k-1) + T_s j(k-1)$$
$$v(k) = v(k-1) + T_s a(k-1), \tag{20}$$

where by T_s is denoted the sampling time in [sec].

The realization of this controller is shown in Figure 6.

3.3.3. Realization of the controller Q

The transfer function $Q(s)$ is defined as

$$Q(s) = \frac{U_Q(s)}{H(s)} = M^{-1}(s) = ms + b, \tag{21}$$

Since the controller in this paper is discrete, we have to realize this controller in discrete time domain. Consequently, using backward approximations (when $= \frac{z-1}{zT_s}$, T_s –the sampling time in [sec]), discrete transfer function $Q(z)$ is obtained as

$$Q(z) = \frac{U_Q(z)}{H(z)} = m\frac{z-1}{zT_s} + b = \frac{m}{T_s}\left(1 - z^{-1}\right) + b, \tag{22}$$

so that the output $u_Q(kT_s) = u_Q(k)$ of the controller, in discrete time domain, is defined as

$$u_Q(k) = \frac{m}{T_s}\left[h(k) - h(k-1)\right] + bh(k). \tag{23}$$

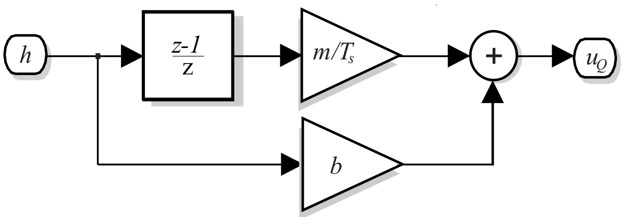

Figure 7. Realization of the controller $Q(z)$

Realization of the discrete transfer function $Q(z)$ is shown in Figure 7.

4. RESULTS OF SIMULATIONS

Simulation of the systems with the controllers (14), the object (3) (the transfer functions $W(s)$ and $P(s)$ are

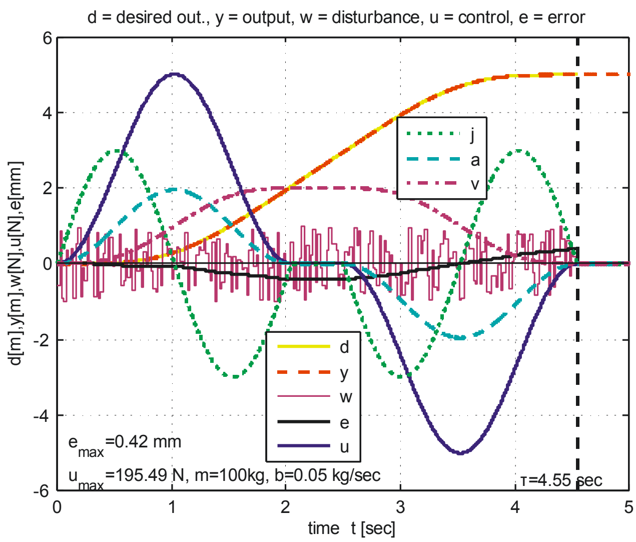

Figure 8. Results simulatoion of the system from Figure 4., for data: m=100kg and b=0.05 kg/sec

the same) and in configuration as in Figure 4. are carried out in Figure 8. As the simulation system we use MATLAB/SIMULINK system that is shown in Figure 9.

In this simulation we use an object whose mass is $m = 100\ kg$ and coefficient of viscous friction b is $b = 0.05\ kg/sec$. The maximum values of the jerk, acceleration, velocity and displacement, respectively, are given and they are: $J = 3\ m/sec^3$, $A = 2\ m/sec^2$, $V = 2\ m/$sec and $D = 5\ m$. In the simulation it is assumed that the sampling time T_s is $1msec.$, $T_s = 10^{-3}sec$ and that the disturbance w is white noise which frequency is $f_w = 125$ and amplitude is 1m, $|w| = 1\ m$. We assume that the disturbance acts in front of the object, so the transfer function $W(s)$ and $P(s)$ are the same, i.e. $W(s) = P(s)$.

5. CONCLUSIONS

In this paper a digital control system is designed that ensures asymptotically tracking a given reference and that rejects all step disturbances. The reference is obtained from the condition that the jerk is changed in a pre-defined manner. As a control system the IMC controller with two degree of freedom is used. An algorithm of the trajectory planning which ensures that the jerk, acceleration, velocity and displacement do not exceed advance defined the maximum values, is also given. The results of the simulation confirm the given theoretical considerations.

ACKNOWLEDGEMENTS

This paper was supported by BANOROB project (Bosnian – Norwegian research based innovation for development of new, environmental friendly, competitive robot technology for selected target groups) .

REFERENCES

[1] C. Brosilow, B. Joseph: "Techniques of Model-Based Control", First edition, Publisher Prentice Hall, (2002)

[2] A. Cervin, J. Eker, Bo Bernhardss-on, Karl-Eric A, "Feedback Feedforward Scheduling of Control Tasks", Real Time Systems (Special Issure on Control Theoretical Approaches to Real Time Computing), To appear in (2002)

[3] Paul Lumbrechts, "Trajectory planning and feedforward design for electromechanical motion systems", Report nr. DCT 2003-08, University of Technology Eindhoven, (2003)

[4] P. Lambrechts, M. Boerlage, M. Steinbuch, "Trajectory planning and feedforward design for electromechanical motion systems", Control Engineering Practice 13 (2005) 145-157, ScienceDirect

[5] V. Cerone, M. Milanese, D. Regruto, "Robust feedforward design for a two-degrees of freedom controller ", System & Control Letters, Volume 56, Issues 11-12, Dec. (2007),pp 736-741

[6] H. Z. Li, Z. M. Gong, W. Lin, and T. Lippa, "Motion profile planning for reduced jerk and vibration residuals", SIMTech technical reports, Vol. 8, No 1, (2007), pp 32-37

[7] Kim Doang Nguyen, Teck-Chew Ng and I-Ming Chen, “On Algorithms for Planning S-curve Motion Profiles”, International Journal of Advanced Robotic Systems, Vol. 5, No 1 (2008), ISSN 1729-8806, pp. 99-106

[8] G.M. Clayton, , S. Tien, A.J. Fleming, S.O.R. Moheimani, S. Devasia, “Inverse feedforward of charge controlled piezopositioners”, Mechatronics 18 (2008) 273–281 , ScienceDirect

[9] M. Y. Stoychitch (in Serbian *Михајло Ј. Стојчић*), „Design of Linear Control Systems” (in Serbian), University of B.Luka, Publisher Faculty of Mechanical Engineering (BiH), (2009)

[10] M. J. Stojčić, B. Knežević, “The controller design for tracking trajectory with controlled jerk”, DEMI 2011 Proceedings, Banja Luka, (2011), pp. 905-911

[11] M. J. Stojčić, B.Knežević, “Design of digital controller that ensures robust tracking trajectory with controlled jerk”, (In Serbian), JUPITER 37 Proceedings, Belgrade (2011), pp. 4-11-4.16.

[12] M. J. Stojčić, “Design of Electromechanical Positioning System with Controlled Jerk”, Haevy Mashinery – HM2011, Proceedings, Kraljevo (2011), pp. 13-17

[13] M. Y. Stoychitch, “Design of an Electromechanical Positioning System with Sinusoidal Change of the Jerk”, Proc. of the Intl. Conf. on Future Trends in Structural, Civil, Environmental and Mechanical Engineering -- FTSCEM 2013, doi:10.3850/ 978-981-07-7021-1_48, pp 35-38, (2013)

[14] M. Y. STOYCHITCH: “Design of a Digital Electromechanical Positioning System with Sinusoidal Change of the Jerk”, Applied Mechanics and Materials Vol. 474 (2014) pp 255-260, © (2014) Trans Tech Publications,Switzerland,doi:10.4028/

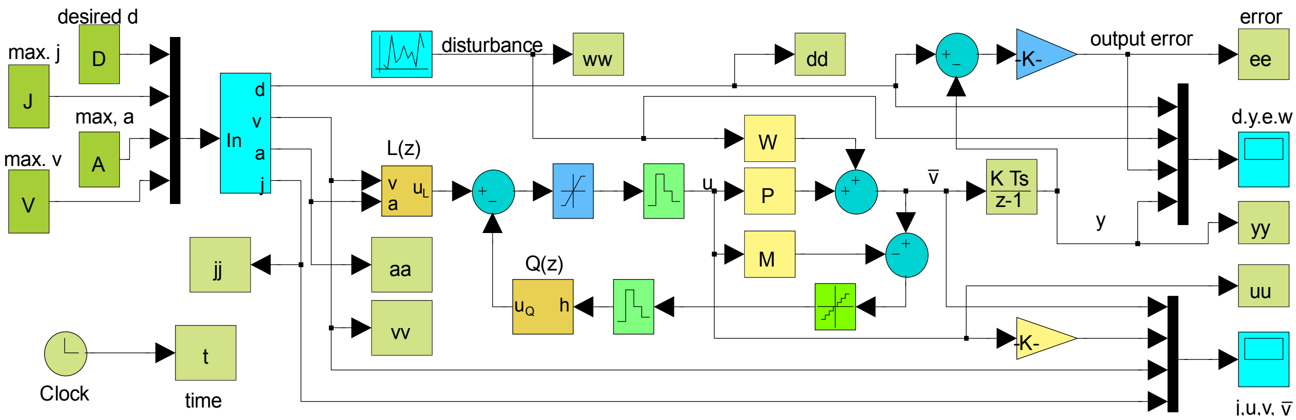

Figure 9. MatLab/SimuLink model of the simulation system from Figure 4.

Design of PID Controllers for High Order Systems

Ljubiša Dubonjić[1], Novak Nedić[1], Dragan Pršić[1]
Faculty of Mechanical and Civil Engineering Kraljevo, University of Kragujevac, Serbia

Abstract: This paper proposes a general method for a PID controller design based on the D-decomposition. The effectiveness of the proposed method is verified by simulation in MATLAB program environment on the example of the high order plant. The simulation results show a good robustness with respect to the unmodeled dynamics, as well as superiority to some methods of a controller tuning. The proposed method is suitable for on line real-time realization and for auto tuning of the PID controller.

Keywords: PID controller, D-decomposition, relative stability, settling time, robustness

1. INTRODUCTION

In spite of all advances in a control of industrial processes in the last 50 years a PID controller is still the most common controller in the industry [1-5]. It is common practice that the PID controller has a hierarchical structure on the lowest level, that is, regardless of the process order the control is performed using the zero-order PID controller. Because of the widespread use of PID controller it is highly desirable to have an efficient method for tuning of controller parameters regardless of the order process [6-9]. This paper proposes the procedure for design of the PID controller for systems of high order. The starting point is a requirement which establishes a direct relation between the IE criterion and the integral gain (the higher the integral gain, the smaller the value of the IE criterion). The result is extended by introducing engineering specifications (settling time and relative stability). It results in a simple and efficient procedure for design of the PI controller for systems of high order.

2. DESIGN PROCEDURE OF PID CONTROLLER

Since the problem of disturbance load rejection is reduced to the minimization of IE criteria, it is also considered in this paper, but engineering constraints are introduced on:

i) relative stability
ii) settling time

This is the basis for development of a simple graphical method based on D-decomposition [9-16].
The transfer function of the PI controller is:

$$W_R = K_p + \frac{K_i}{s} + K_d \cdot s \qquad (1)$$

The transfer function of the process is represented in the form:

$$W_P(s) = \frac{N(s)}{M(s)} = \frac{\sum_{k=0}^{m} b_k s^k}{\sum_{k=0}^{n} a_k s^k}, \quad m \le n \qquad (2)$$

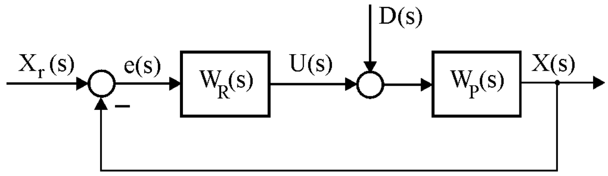

Fig. 1 *Automatic control system*

The characteristic equation of the automatic control system from Fig1 is determined by the equation:

$$f(s) = 1 + W_R(s) W_P(s) = 0 \qquad (3)$$

$$f(s) = 1 + (K_p + \frac{K_i}{s} + K_d s) \cdot \frac{N(s)}{M(s)} = 0 \qquad (4)$$

$$f(s) = s \cdot M(s) + (K_d s^2 + K_p s + K_i) \cdot N(s) = 0 \qquad (5)$$

$$f_1(s) = s \cdot M(s) = \sum_{k=0}^{n} a_k s^{k+1} \qquad (6)$$

By connecting (5) and (6), the final expression for the characteristic equation of the automatic control system in the complex domain is obtained as follows:

$$f(s) = f_1(s) + (K_d s^2 + K_p s + K_i) \cdot N(s) = 0 \qquad (7)$$

Taking into account (7), it is necessary to express the complex number s in a suitable form and use it for establishing the relation between the damping degree ξ and the variable parameters of the controller, K_d , K_p and K_i contained in the characteristic equation (7) for the automatic control system. This is how the area from the “s” plane below the straight line ξ=const. (Fig. 2), is mapped in the area of the corresponding damping coefficient represented by the curve ξ=const., in the parameter plane of tuning parameters of the controller (K_p, K_d) with the condition for observation of the integral gain K_i as a parameter that fulfills the condition of minimum of IE criteria for the corresponding level of the damping coefficient ξ.

*Corresponding author: dubonjic.lj@mfkv.kg.ac.rs

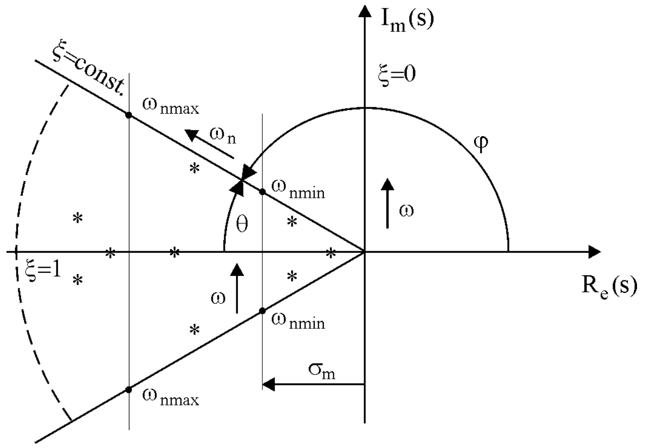

Fig. 2 *Area with the required settling time and relative stability*

Since:

$$s=-\omega_n\xi+j\omega_n\sqrt{1-\xi^2} \tag{8}$$

By connecting (7) with (8) the characteristic equation of the automatic control system obtains the form:

$$f_1(\xi,\omega_n)+\begin{bmatrix} K_d\omega_n^2((2\xi^2-1)-j(2\xi\sqrt{1-\xi^2}))+ \\ K_p(-\xi\omega_n+j\omega_n\sqrt{1-\xi^2})+K_i \end{bmatrix}\cdot N(\xi,\omega_n)=0 \tag{9}$$

$$f_1(\xi,\omega_n)=\alpha(\xi,\omega_n)+j\beta(\xi,\omega_n) \tag{10}$$

where $\alpha(\xi,\omega_n)$ and $\beta(\xi,\omega_n)$ represent the real and imaginary parts of the polynomial $f_1(\xi,\omega_n)$.

$$\alpha(\xi,\omega_n)=\sum_{k=1}^{n}a_{k-1}(-1)^k\omega_n^kT_k(\xi) \tag{11}$$

$$\beta(\xi,\omega_n)=\sqrt{1-\xi^2}\sum_{k=1}^{n}a_{k-1}(-1)^{k+1}\omega_n^kU_k(\xi) \tag{12}$$

$$\beta(\xi,\omega_n)=\sqrt{1-\xi^2}B(\xi,\omega_n) \tag{13}$$

where T_k and U_k are Chebyshev functions of the first and second types for which the following recurrent equations hold:

$$T_{k+1}=2\xi T_k-T_{k-1}\,,\,U_{k+1}=2\xi U_k-U_{k-1} \tag{14}$$

$$T_0=1,T_1=\xi,U_0=0,U_1=1. \tag{15}$$

$$N(\xi,\omega_n)=\gamma(\xi,\omega_n)+j\delta(\xi,\omega_n) \tag{16}$$

where $\gamma(\xi,\omega_n)$ and $\delta(\xi,\omega_n)$ represent the real and imaginary parts of the polynomial $N(\xi,\omega_n)$ and they are determined based on the following equations:

$$\gamma(\xi,\omega_n)=\sum_{k=0}^{m}b_k(-1)^k\omega_n^kT_k(\xi) \tag{17}$$

$$\delta(\xi,\omega_n)=\sqrt{1-\xi^2}\sum_{k=0}^{m}b_k(-1)^{k+1}\omega_n^kU_k(\xi) \tag{18}$$

$$\delta(\xi,\omega_n)=\sqrt{1-\xi^2}D(\xi,\omega_n) \tag{19}$$

By connecting the equation (9) with equations from (10) to (19), after appropriate mathematical transformations and separating the real and imaginary parts, the following system of equations is obtained:

$$\begin{aligned} K_d(\xi,\omega_n)\cdot\omega_n^2\cdot(2\xi^2-1)-K_p(\xi,\omega_n)\cdot\xi\cdot\omega_n &= -\frac{\alpha(\xi,\omega_n)\cdot\gamma(\xi,\omega_n)+\beta(\xi,\omega_n)\cdot\delta(\xi,\omega_n)}{\gamma^2(\xi,\omega_n)+\delta^2(\xi,\omega_n)}-K_i(\xi,\omega_n) \\ 2K_d(\xi,\omega_n)\cdot\omega_n^2\cdot\xi-K_p(\xi,\omega_n)\cdot\omega_n &= -\frac{\alpha(\xi,\omega_n)\cdot D(\xi,\omega_n)-\gamma(\xi,\omega_n)\cdot B(\xi,\omega_n)}{\gamma^2(\xi,\omega_n)+\delta^2(\xi,\omega_n)} \end{aligned} \tag{20}$$

By solving the system of equations at $\omega_n \neq 0,\ 0\le\xi<1$ the expressions for the parameters K_d, K_p and K_i of the PID controller are obtained with the condition that the integral gain fulfills the minimum of IE criteria with the restriction on the corresponding level of the damping coefficient of the closed-loop automatic control system. From the system of equations (20) for $\omega_n=0$ singular straight lines are defined and which are described by the equation:

$$K_i(\xi,0)=0 \tag{21}$$

The graphical interpretation of (20) represents the curve in the parameter plane (K_p-K_d) for the required damping degree with the condition that the integral gain fulfills the minimum of IE criteria. This curve together with the singular straight lines described by (21) represents the closed contour of the region of possible solutions, from which the parameters of PID controller are determined. In the special case N(s) = 1, it follows:

$$\gamma(\xi,\omega_n)=1,\delta(\xi,\omega_n)=0,D(\xi,\omega_n)=0 \tag{22}$$

By using the equation (6.22) the system of equations (20) obtains the following form:

$$\begin{aligned} &K_d(\xi,\omega_n)\cdot\omega_n^2\cdot(2\xi^2-1)-K_p(\xi,\omega_n)\cdot\xi\cdot\omega_n= \\ &=-\alpha(\xi,\omega_n)-K_i(\xi,\omega_n) \\ &2K_d(\xi,\omega_n)\cdot\omega_n^2\cdot\xi-K_p(\xi,\omega_n)\cdot\omega_n=B(\xi,\omega_n) \end{aligned} \tag{23}$$

From the equation (20) it is possible to obtain parameters of PID controllers for all processes described by equation (2).

3. CONTROL OF A PROCESS WITH A LONG TRANSMISSION LINE

In order to show the efficiency of the proposed method for PID controller design we have performed simulations in MATLAB program for transfer function of the process $W_P(s)$:

$$W_P(s)=\frac{1}{\begin{aligned}&5.2\cdot10^{-25}s^{10}+9.23\cdot10^{-22}s^9+9.677\cdot10^{-19}s^8+7.838\cdot10^{-16}s^7+4.592\cdot10^{-13}s^6+2.072\cdot10^{-10}s^5+7.257\cdot10^{-8}s^4+\ldots\\&\ldots+1.755\cdot10^{-5}s^3+2.962\cdot10^{-3}s^2+0.243s+1.248\end{aligned}} \tag{24}$$

The transfer function described by (24), represents a mathematical model of a pump controlled hydromotor, where the variable flow pump and the hydromotor of constant flow are connected by means of a long transmission line [17-19].

Based on the programme created in MATLAB, according to the proposed procedure, the parameters of the PID controller can be determined for the transfer function of the process described by (24), so that the closed loop of the system could possess the required damping coefficient and good settling time.

Figure 3 shows the parameter plane (K_p-K_d) for different values of damping coefficient with the absolute and relative stability limits for corresponding values of the integral gain K_i that fulfill the condition of minimum of IE criteria. From the Fig 3. the parameters of PID controller, that best rejects the load caused by the action of disturbance, are read. The results of the comparative analysis for such selected parameters of the PID controller with performances are shown in Table 1. The comparative analysis of the proposed method was carried out with the Ziegler-Nichols (ZN) and Tyreus Luyben (TL) methods which are very frequent methods of tuning in industrial practice [20-24].

By analyzing the results shown in Table 1, it can be shown that the proposed method gives the best settling time by satisfying requirements of robustness related to the phase margin and gain margin.

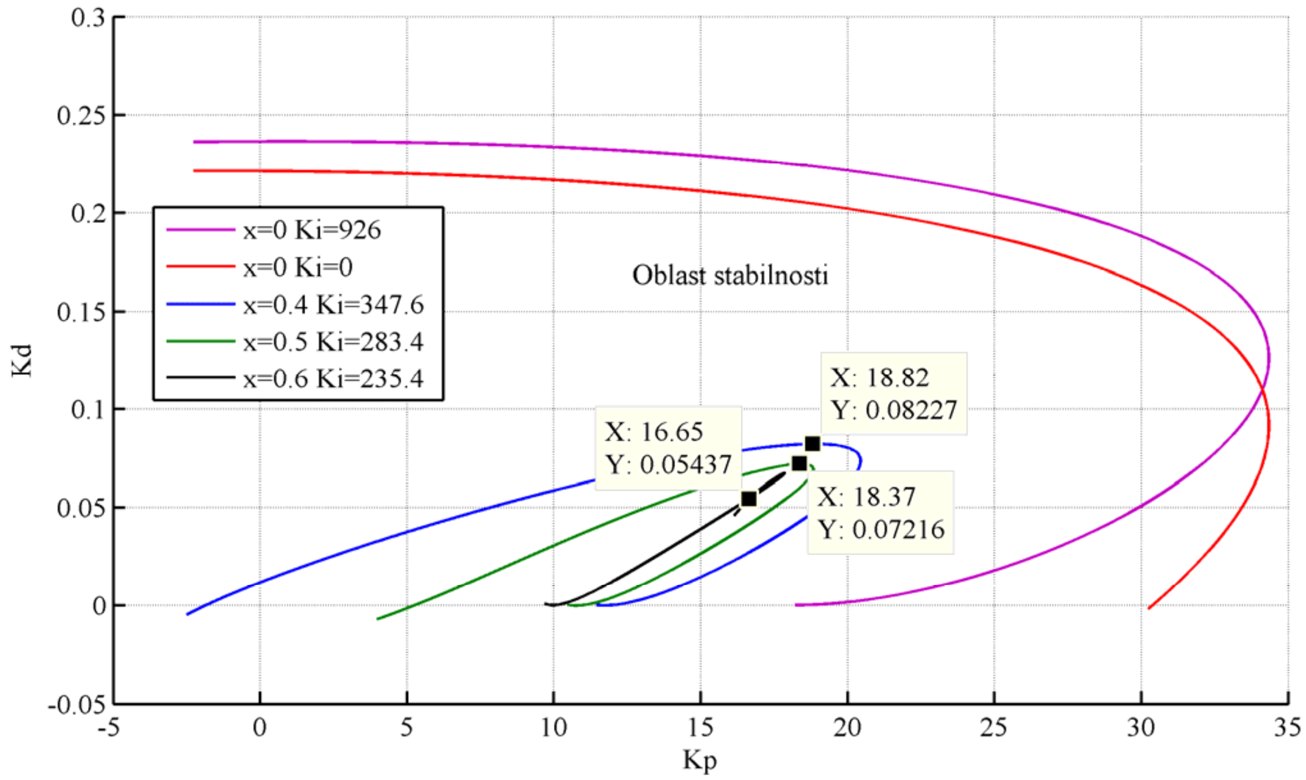

Fig. 3 *Parameter plane for different values of the damping coefficient with relative and absolute stability limits*

Table 1 Comparative presentation of the results of design of the PI controller with performances for three methods

Method	K_p	K_i	K_d	Overshoot (%)	Settling time t_s (ms)	Phase margin φ_m (degrees)	Gain margin g_m
Ziegler-Nichols (ZN)	15.195	633.125	0. 912	40.6	121	34.4	2.06
Tyreus-Luyben (TL)	13.836	130.811	0.105	8	93.4	68	1.83
Proposed method (ξ=0.6)	16.65	235.4	0.0544	30	**83.7**	46	2.06
Proposed method (ξ=0.5)	18.37	283.4	0.07216	40	**83.7**	43	2.06
Proposed method (ξ=0.4)	18.82	347.6	0.08227	42	**83.7**	40	2.04

In Figs. 4 and 5, comparative presentations of system responses, to the action of reference and to the action of load disturbance for three methods of PID controller design, are shown.

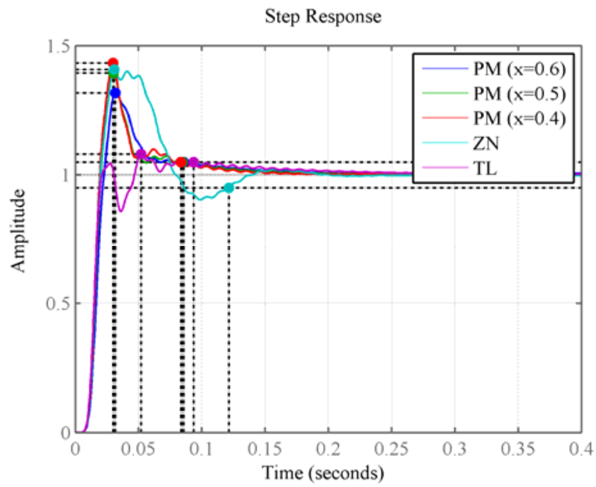

Fig. 4 *Comparative presentation of the system response to the action of reference for three methods*

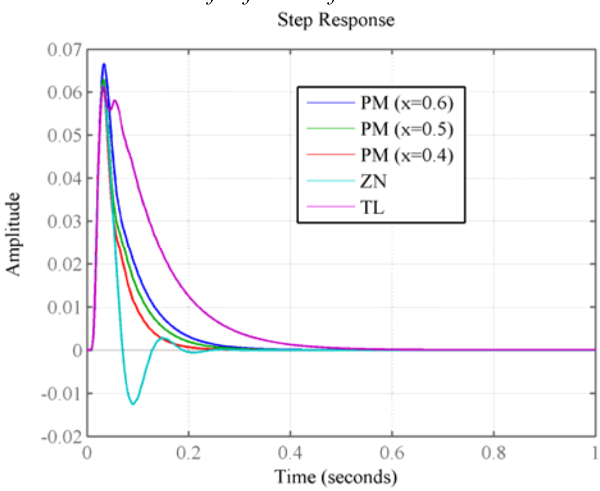

Fig. 5 *Comparative presentation of the system response to the action of load disturbance for three methods*

By using this method design of PID controllers is very efficiently if it is required from the system that has good performances only according to the reference.

By selecting a suitable damping degree value (in this case $\xi = 0.6$), it is first found the frequency range for an appropriate value of the integral gain Ki. A graphical interpretation of a frequency range for this example is shown in Fig. 6.

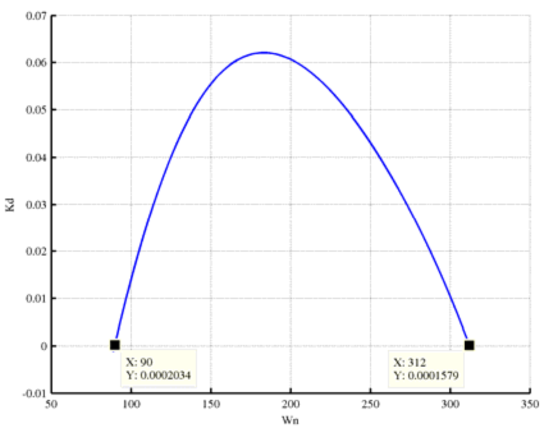

Fig 6. *Choice of the frequency range for damping degree value ξ=0.6 and integral gain value Ki = 57.15*

After selecting the frequency range that is entered in the program based on the system of equations (23) the (Kp-Kd) parameter plane is written, which, in this case, is shown in Fig. 6.

By selecting an appropriate step we find a point in the parameter plane which gives the best settling time with the satisfying requirement that the overshoot is less than a required value of overshoot (in this case 10%).

Obtained values of the parameters of PID controllers for the system with a long transmission line are represented in Fig.7 and they are: Kp=11.83, Ki=57.15 and Kd=0.1126.

For this designed controller a comparative response for the reference for PI and PID controller is shown in Fig.8.

Performances in terms of robustness for PI and PID controller designed by the proposed method are shown in Fig. 9.

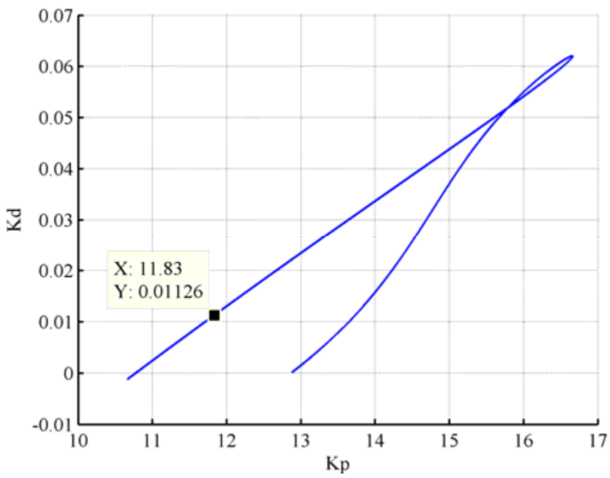

Fig. 7 *Parameter P-D plane for the damping coefficient $\xi = 0.6$ and the value of the integral gain Ki = 57.15*

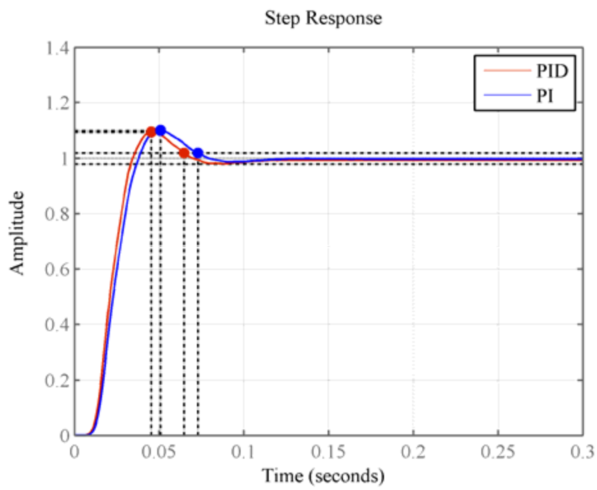

Fig. 8 *Comparative presentation of the system response to the action of reference for the proposed method for PI and PID controller*

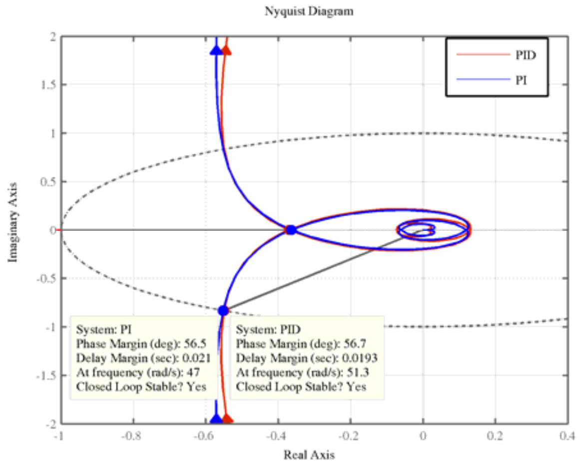

Fig. 9 *Comparative presentation of performance of robustness for PI and PID controller*

A comparative presentation of designed PI and PID controller by the proposed method with complete performances is given in Table 2. Based on the results of comparing PI and PID controller shown in Table 2 it can be concluded that the PID controller for the system described with a long transmission line gives a slightly better performance in response (especially in terms of settling time t_s = 64.7 ms for the PID controller and t_s = 72.8 ms for the PI controller). From the aspect of robustness both controllers give excellent results.

Table 2 Comparative presentation of the PID controller design with the performances of PI and PID controller

Proposed method (ξ=0.6)	K_p	K_i	K_d	Overshot (%)	Settling time t_s (ms)	Phase margin φ_m (degrees)	Gain Margin g_m
PID	11.83	57.15	0.01126	9.45	64.7	56.7	2.74
PI	10.78	57.15	-	9.99	72.8	56.5	2.74

4. CONCLUSION

Based on everything said, we can conclude that it has been developed an efficient and simple graphical methods for design of the PID controller, which achieves high performances for a broad range of linear processes. The process of high order has been considered, in which the variable flow pump controls the hydromotor, where a connection between the pump and the hydromotor is realized by a long transmission line. In comparison with the procedures for tuning of the PID controller proposed in literature, the method described in this paper is characterized by great simplicity and clear engineering specifications. The results of simulations show good robustness in relation to unmodelled dynamics as well as superiority over some other methods of tuning of controllers. The proposed method is suitable for on line real-time realization and for auto tuning of the PID controller.

ACKNOWLEDGEMENTS

This research has been supported by the Serbian Ministry of Education, Science and Technological Development through project TR 33026. Also, this research has been supported by the European Commission through IPA Adriatic and the project ADRIA-HUB.

REFERENCES

[1] D.B. Ender, Process control performance: "Not as good as you think", *Control Eng*., vol.40 (1993), pp.180-185.

[2] W.L. Bialkovski, Dreams and Reality: "A View from Both Sides of the Gap", *Pulp Paper Can*.,vol. 94 (1993), pp. 19-24.

[3] M.A. Hersh, M.A. Johnson, (1997), "A Study of Advanced Control Systems in Workplace", *Control Eng. Practice*, vol. 5 (6), (1997), pp. 771-778.

[4] Yamamoto, S., Hashimoto, I., "Present status and future needs: The view from Japanese industry", (1991) *Chemical Process Control - CPCIV. Proc. 4th Inter. Conf. Chemical Process Control*.

[5] V.Ž. Filipović, N.N. Nedić, (2008), "*PID Controllers*", Faculty of Mechanical and Civil Engineering in Kraljevo, Serbia, Scientific monograph, ISBN:978-86-82631-49-1.

[6] Nedić N., Dubonjić LJ, Filipović V., "Design of constant gain controllers for the hydraulic control system with a long transmission line", *Forschung im Ingenieurwesen*, Vol.75,(4), pp. 231–242.(2011). ISSN:0015-7899

[7] LJubiša Dubonjić, Novak Nedić, Vojislav Filipović and Dragan Pršić, "Design of PI Controllers for Hydraulic Control Systems," *Mathematical Problems in Engineering*, vol. 2013, Article ID 451312, 10 pages, 2013. doi:10.1155/2013/451312, ISNN: 1024-123X

[8] Nedić N., Filipović V., Dubonjić LJ., "Design of Controllers With Fixed Order for Hydraulic Control System With a Long Transmission Line" FME Transactions, Vol. 38 (2), pp. 79-86, (2010). ISSN: 1451-2092

[9] LJ. Dubonjić, "Synthesis of Fixed-Order Controllers for Control Systems with Long Transmission Lines", PhD Thesis, University of Kragujevac (SRB), (2013)

[10] Y.I. Neimark, "Structure of the D-partition of the space of polynomials and the diagram of Vishnegradskii

and Nyquist“, *Dokl Akad Nauk SSSR*, vol. 59, pp. 853-856 (1948). (in Russian)

[11] Y.I. Neimark Search for the parameter values that make automatic control system stable, *Automatica i Telemekhanika*, 9 (3), pp. 190–203 (1948).(in Russian)

[12] D. Mitrovic, Graphical analysis and synthesis of feedback control systems. I—Theory and analysis, II—Synthesis, III—Sampled-data feedback control systems, AIEE Transactions (Application and Industry), 77, pp. 476–496 (1959).

[13] D. Siljak, “Analysis and synthesis of feedback control systems in the parameter plane. I—Linear continuous systems, II—Sampled-data systems“, AIEE Transactions (Application and Industry), 83 pp. 449–466 (1964).

[14] D. Siljak, “Generalization of the parameter plane method“, *IEEE Transactions on Automatic Control*, AC-11 (1), pp. 63–70 (1966).

[15] D. Siljak, Nonlinear systems: “*The parameter analysis and design*“, Wiley, New York (1969).

[16] Gryazina, E.N., Polyak, B.T., “Stability regions in the parameter space: D-decomposition revisited“, *Automatica*, 42 (1), pp. 13-26 (2006).

[17] Nedić N., Dubonjić LJ., “Modeling and Simulation of a Pump Controlled Motor With Long Transmission Lines“ Heavy Machinery HM 08, Kraljevo, (2008).

[18] Nedić N., Dubonjić LJ., Filipović V., "Design of PI Controllers for the Hydraulic Control System with a Long Transmission Line", X Triennial International SAUM Conference on Systems, Automatic Control and Measurements SAUM 2010, pp. 76-80 ISBN 978-86-6125-020-0, Niš, (2010).

[19] Pršić D., Nedić N., Dubonjić LJ., “Modeling and simulation of Hydraulic Long Transmission Line by Bond Graph”, Heavy Machinery-HM 2011, Vol.7,No 3, pp. 41-46, ISBN 978-86-82631-58-3, Vrnjačka Banja, (2011).

[20] Ziegler J.G., Nichols N.B., “Optimum settings for automatic controllers”, Transactions of ASME, 64, pp.759–768 (1942).

[21] Ziegler J.G., Nichols N.B., “Process lags in automatic-control circuits”, Transactions of ASME, 65, pp.433–443 (1943).

[22] Chien K.L., Hrones J.A., Reswick J.B., “On the automatic control of generalized passive systems”, Transactions of ASME, 74, pp.175-185 (1952).

[23] Cohen G.H., Coon G.A., “Theoretical consideration of retorted control”, Transactions of ASME, 75, pp.827-834 (1953).

[24] Tyreus B.D., Luyben W.L., “Tuning PI controllers for integrator/dead time processes”, Ind. Eng. Chem. Res. Vol.31(11) pp. 2628–2631 (1992).

Robust Akaike's Criterion for Model Order Selection

Vladimir Stojanovic[1*], Vojislav Filipovic[1]
[1]Faculty of Mechanical and Civil Engineering in Kraljevo, Department of Energetics and Automatic Control, University of Kragujevac (Serbia)

The paper considers the model order selection (Output Error model) of the system with constant parameters. Ad hoc selection of model order leads to overparametrization or parsimony problem. To avoid these problems, different selection criterions of the model are used: AIC (Akaike Information Criterion), BIC (Bayesian Information Criterion) and FPE (Final Prediction Error Criterion). In this paper, Akaike's criterion is used, which is obtained by minimization of the Kullback-Leibler information distance. The criterion is basically a generalization of the maximum likelihood method. It is assumed that the stochastic disturbance in the model belongs to the class of ε-contaminated distributions. In such conditions the originally proposed AIC criterion cannot be applied. By determining the least favourable probability density for a given class of probability distribution represents a base for design of the robust version of AIC criterion. Simulations illustrate the behavior of the proposed criterion.

Keywords: model order selection, output error model, ε-contaminated distributions, robust Akaike's criterion

1. INTRODUCTION

Obtaining system models based on the fundamental laws of physics is a difficult problem. In order to facilitate the controller design, for the obtained model, different simplifications of the model are performed. Most often it is a procedure of linearization around the equilibrium point. However, there are the systems that cannot be linearized around an equilibrium point, because there is no equilibrium point. If a linear approximation is found, the resulting model will be valid only for a small region around the linearization point. As an alternative approach the design of controllers is largely based on the use of mathematical models that are obtained during the process of system identification [1,2].

Most identification algorithm assume that the model structure is a priori known. As is well known, a fundamental difficulty in statistical analysis is the choice of an appropriate model and determining the order of a model. In recent years, the necessity of introducing the concept of model has been recognized and the problem is posed how to choose the "best approximating" model among a class of competing models with different numbers of parameters by a suitable model selection criterion given a data set. Also, there is presently a great deal of interest in simple criteria represented by parsimony of parameters for choosing one of a set of competing models to describe a given data set. Therefore, the best model is the one with least complexity, or equivalently the highest information. For example, parameter parsimony requires that the smallest number of factors is chosen, such that the corresponding model fits the data. The selection of a parsimonious model, in general, is a nontrivial problem without the aid of model selection criteria.

Several information theoretic criterion have been proposed for structure selection in linear dynamic input output models. The model which minimizes the criterion is then chosen as the best model from the available set. Examples of the classical criterions are the Final Prediction Error (FPE), Akaike's Information Criterion (AIC) and Bayesian Information Criterion (BIC). These techniques find a tradeoff between goodness of fit and model complexity. The performance of an order-selection criterion is optimal if the model of the selected order is the most accurate model in the considered set of estimated models. Note that this is not necessarily the true model order. If the true process is, e.g. tenth-order, where the last six parameters are insignificant, the estimated fourth-order model will be the most accurate.

Used way for deriving model selection criteria is based on the quantification of "how close are" the probability density of the generating model and the probability density of the fitted approximating model. Several coefficients or "measures" have been introduced in the literature for this quantification. The Kullback-Leibler information distance is the most frequently used information theoretic coefficient for measuring divergence or separation between two probability densities [3]. The Akaike's information criterion (AIC) is a commonly used tool for choosing between alternative models [4].

Here, those results are extended on the case when the measurement noise is a non-Gaussian. Justification of this approach was confirmed in practice [5,6]. Namely, in measurements there are rare, inconsistent observations with the largest part of population of observations (outliers). The presence of outliers can considerably degrade the performance of linearly recursive algorithms based on the assumptions that measurements have a Gaussian distribution.

The synthesis of robust algorithms is of primary interest. The synthesis is based on Huber's theory of robust statistics [6]. As a generator of a recursive algorithm, according Huber's theory, it is defined the functional based on the least favourable probability distribution for a given class of probability distribution. Robust recursive algorithms in the identification of

*Corresponding author: stojanovic.v@mfkv.kg.ac.rs

dynamical systems are discussed in [7] while in an area of adaptive control are discussed in [8].

This paper considers the model order selection using robust Akaike's criterion. The recursive algorithm for the OE (output error) model with time invariant parameters have been also discussed. Robustness of the used robust OE parameter estimation algorithm is accomplished by introducing the nonlinear transformation of prediction error (Huber’s function).

The performances of the algorithm are described through simulation results that demonstrate the superiority of the proposed algorithm in relation to the linear algorithm (derived under the assumption that the stochastic noise has a Gaussian distribution).

2. ROBUST PARAMETER ESTIMATION ALGORITHM FOR OE MODEL

The general form of the OE model is

$$y(k)=\frac{B(q^{-1})}{A(q^{-1})}u(k)+e(k) \quad (1)$$

where $u(k)$, $y(k)$ and $e(k)$ are input, output and stochastic noise, respectively. Polynomials $A(q^{-1})$ and $B(q^{-1})$ have the form:

$$\begin{aligned}A(q^{-1})&=1+a_1q^{-1}+\ldots+a_nq^{-n}\\ B(q^{-1})&=b_1q^{-1}+\ldots+b_mq^{-m}\end{aligned} \quad (2)$$

Practical and theoretical studies have shown that in a stochastic model of the system there are some observations that are inconsistent with the largest part of the population (outliers) [5], and that is why the disturbance (measurement noise) $e(k)$ in the model (1) is a non-Gaussian. Hence, the probability density function of the disturbance belongs to approximately normal distribution class:

$$\mathcal{P}_\varepsilon=\left\{p(e):p(e)=(1-\varepsilon)p_1(e)+\varepsilon p_2(e)\right\} \quad (3)$$

in which

$p_1(e)\sim\mathcal{N}(0,\sigma_1^2),\ p_2(e)\sim\mathcal{N}(0,\sigma_2^2)$, $\sigma_2^2\gg\sigma_1^2$.

In other words, the probability density function $p(e)$ represents a mixture of normal (Gaussian) distributions where σ_1^2 and σ_2^2 denote variances. The parameter $0\le\varepsilon<1$ is called the degree of contamination.

Let us introduce an auxiliary model

$$y_M(k)=\frac{B(q^{-1})}{F(q^{-1})}u(k), \quad (4)$$

or in the following form:

$$\begin{aligned}y_M(k)&=-f_1y_M(k-1)-\ldots-f_ny_M(k-n)+\\ &+b_1u(k-1)+\ldots+b_mu(k-m)\end{aligned} \quad (5)$$

Since the parameters $a_i(i=1,\ldots,n)$ and $b_i(i=1,\ldots,m)$ are unknown, their estimates are used, so the output of the auxiliary model is calculated as:

$$\begin{aligned}\hat{y}_M(k)&=-\hat{f}_1\hat{y}_M(k-1)-\ldots-\hat{f}_n\hat{y}_M(k-n)+\\ &+\hat{b}_1u(k-1)+\ldots+\hat{b}_mu(k-m)\end{aligned} \quad (6)$$

Let $\hat{\theta}$ is the estimated vector of OE parameters, and $\varphi(k)$ is the observation vector of OE parameters:

$$\begin{aligned}\hat{\theta}&=[\hat{f}_1,\ldots,\hat{f}_n,\hat{b}_1,\ldots,\hat{b}_m]^T,\\ \varphi(k)&=[-\hat{y}_M(k-1)\ldots-\hat{y}_M(k-n),u(k-1)\ldots u(k-m)]^T\end{aligned} \quad (7)$$

At the moment k, before the estimate $\hat{\theta}(k)$ is known, the prediction of the model is [9]:

$$\hat{y}_M(k)=\hat{\theta}^T(k-1)\varphi(k).$$

The natural definition of the prediction error (residual) is

$$\varepsilon(k)=y(k)-\hat{y}_M(k). \quad (9)$$

The identification criterion (a generator of recursive parameter estimation procedure) is based, according to OE methodology, on the prediction error and has a mathematical form, for systems with constant parameters:

$$\mathcal{J}(\theta)=E\left\{\Phi(\varepsilon(\mathrm{k}))\right\} \quad (10)$$

in which

$$\Phi(\cdot)=-\log p^*(\cdot) \quad (11)$$

In the last relation, $p^*(\cdot)$ represents the least favourable distribution of probability for a given class of probability distribution (3).
This distribution is obtained by using the mathematical machinery of robust statistics [6].

An analytical description of the least favorable probability density $p^*(\cdot)$ is given as follows:

$$p^*(e(\mathrm{k}))=\begin{cases}\dfrac{1-\varepsilon}{2\pi\sigma_1}\exp\left\{-\dfrac{e^2(\mathrm{k})}{2\sigma_1^2}\right\} & |e(\mathrm{k})|\le k_\varepsilon\\[2ex] \dfrac{1-\varepsilon}{2\pi\sigma_1}\exp\left\{-\dfrac{k_\varepsilon}{\sigma_1^2}\left(|e(\mathrm{k})|-\dfrac{k_\varepsilon}{2}\right)\right\} & |e(\mathrm{k})|>k_\varepsilon\end{cases} \quad (12)$$

where k_ε is the Huber function parameter.

The empirical functional for systems with time-invariant parameters has the form (obtained from the relation (10) for sufficiently large k):

$$\mathrm{J}_k(\theta)=\frac{1}{k}\sum_{t=1}^{k}\left\{\Phi(\varepsilon(i))\right\} \quad (13)$$

Expanding $\mathcal{J}_k(\theta)$ in the vicinity of the preceding estimate $\hat{\theta}(\mathrm{k}-1)$ in Taylor series, one obtains:

$$\begin{aligned}J_k(\theta)&=J_k\left(\hat{\theta}(\mathrm{k}-1)\right)+\nabla_\theta J_k\left(\hat{\theta}(\mathrm{k}-1)\right)\left[\theta-\hat{\theta}(\mathrm{k}-1)\right]+\\ &+O\left(\left\|\theta-\hat{\theta}(\mathrm{k}-1)\right\|^2\right)\end{aligned} \quad (14)$$

where

$$\lim_{\|x\|\to\infty} \frac{O\left(\|x\|\right)}{\|x\|} = 0 \tag{15}$$

and $\|\cdot\|$ denotes the Euclidean norm. The desired value $\hat{\theta}(\mathrm{k})$ can be obtained by solving the equation:

$$\nabla_\theta J_k\left(\hat{\theta}(\mathrm{k})\right) = 0 \tag{16}$$

from which one can obtain:

$$\hat{\theta}(\mathrm{k}) = \hat{\theta}(\mathrm{k-1}) - \left[k\nabla_\theta^2 J_k\left(\hat{\theta}(\mathrm{k-1})\right)\right]^{-1}\left[k\nabla_\theta J_k\left(\hat{\theta}(\mathrm{k-1})\right)\right] + \\ + O\left(\left\|\theta - \hat{\theta}(\mathrm{k-1})\right\|\right) \tag{17}$$

Based on the relation (13) it is obtained:

$$J_k(\theta) = \frac{1}{k}\left[\frac{k-1}{k-1}\sum_{i=1}^{k-1}\Phi(\varepsilon(i)) + \Phi(\varepsilon(k))\right] = \\ \frac{1}{k}\left[(k-1)\frac{1}{k-1}\sum_{i=1}^{k-1}\Phi(\varepsilon(i)) + \Phi(\varepsilon(k))\right] \tag{18}$$

or in the form:

$$kJ_k(\theta) = (k-1)J_{k-1}(\theta) + \Phi(\varepsilon(k)) \tag{19}$$

By differentiating the last relation twice one can obtain:

$$k\nabla_\theta^2 J_k(\theta) = (k-1)\nabla_\theta^2 J_{k-1}(\theta) + \Psi'(\varepsilon(k))\varphi(k)\varphi^T(k) \tag{20}$$

where $\Psi(\cdot) = \Phi'(\cdot)$.

Let us assume further that the following assumptions are satisfied:

a) The estimate $\hat{\theta}(\mathrm{k})$ is in the vicinity of the estimate $\hat{\theta}(\mathrm{k-1})$

b) The estimate $\hat{\theta}(\mathrm{k-1})$ is optimal at the instant k-1.

Taking $\theta = \hat{\theta}(\mathrm{k-1})$ in the relation(20), one can obtain:

$$k\nabla_\theta^2 J_k(\hat{\theta}(\mathrm{k-1})) = (k-1)\nabla_\theta^2 J_{k-1}(\hat{\theta}(\mathrm{k-1})) + \\ + \Psi'(\varepsilon(k))\varphi(k)\varphi^T(k) \tag{21}$$

From the assumption a) follows

$$\nabla_\theta^2 J_k(\hat{\theta}(\mathrm{k})) \cong \nabla_\theta^2 J_k(\hat{\theta}(\mathrm{k-1})) \tag{22}$$

Based on this, the relation (21) takes the form

$$k\nabla_\theta^2 J_k(\hat{\theta}(\mathrm{k-1})) = (k-1)\nabla_\theta^2 J_{k-1}(\hat{\theta}(\mathrm{k-2})) + \\ + \Psi'(\varepsilon(k))\varphi(k)\varphi^T(k) \tag{23}$$

Based on the assumption a) it also follows

$$O\left(\left\|\hat{\theta}(\mathrm{k}) - \hat{\theta}(\mathrm{k-1})\right\|\right) = 0 \tag{24}$$

By introducing the notation $\overline{R}(\mathrm{k}) = k\nabla_\theta^2 J_k(\hat{\theta}(\mathrm{k-1}))$ from relations (17) and (23) one can obtain:

$$\hat{\theta}(\mathrm{k}) = \hat{\theta}(\mathrm{k-1}) - \overline{R}^{-1}(\mathrm{k})\left[k\nabla_\theta J_k\left(\hat{\theta}(\mathrm{k-1})\right)\right] \tag{25}$$

$$\overline{R}(\mathrm{k}) = \overline{R}(\mathrm{k-1}) + \Psi'(\varepsilon(\mathrm{k}))\varphi(k)\varphi^T(k) \tag{26}$$

From the assumption b) it follows $\nabla_\theta J_{k-1}(\hat{\theta}(\mathrm{k-1})) = 0$. Based on this condition, and if $\theta = \hat{\theta}(\mathrm{k-1})$ is put in the relation (25), one obtains:

$$k\nabla_\theta J_k(\hat{\theta}(\mathrm{k-1})) = -\Psi(\varepsilon(k))\varphi(k) \tag{27}$$

Finally, based on relations (25) - (27) a recursive algorithm is obtained:

$$\hat{\theta}(\mathrm{k}) = \hat{\theta}(\mathrm{k-1}) + \overline{R}^{-1}(\mathrm{k})\varphi(k)\Psi(\varepsilon(k)) \tag{28}$$

$$\overline{R}(\mathrm{k}) = \overline{R}(\mathrm{k-1}) + \Psi'(\varepsilon(\mathrm{k}))\varphi(k)\varphi^T(k) \tag{29}$$

The algorithm (28) - (29) includes the inverse matrix $\overline{R}^{-1}(\mathrm{k})$. To avoid this let us introduce the matrix $P(\mathrm{k}) = \overline{R}^{-1}(\mathrm{k})$. Using this notation and applying the matrix inversion lemma [1], from (28) and (29), one can obtain the definitive form of a recursive algorithm for identification of dynamic systems with time-invariant parameters:

$$\hat{\theta}(\mathrm{k}) = \hat{\theta}(\mathrm{k-1}) + P(\mathrm{k})\varphi(k)\Psi(\varepsilon(k)) \tag{30}$$

$$\mathrm{P(k)} = P(\mathrm{k-1}) - \frac{P(\mathrm{k-1})\varphi(k)\varphi^T(k)P(\mathrm{k-1})}{\left[\Psi'(\varepsilon(\mathrm{k}))\right]^{-1} + \varphi^T(k)P(\mathrm{k-1})\varphi(k)} \tag{31}$$

$$\varepsilon(\mathrm{k}) = y(\mathrm{k}) - \hat{\theta}^T(\mathrm{k-1})\varphi(k) \tag{32}$$

$$\Psi(x) = \min\left\{|x|, k_\varepsilon\right\}\mathrm{sgn}(x) \tag{33}$$

$$\Psi'(x) = \begin{cases} 1 & |x| < k_\varepsilon \\ 0 & otherwise \end{cases} \tag{34}$$

The function defined by the relation (33) is the Huber function [6]. It is derived for a class of distributions(3). It is shown on the following figure.

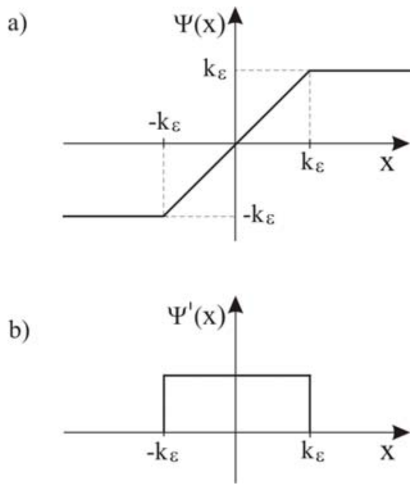

Fig. 1 Nonlinear function of residuals
a) Huber’s function
b) Derivative of Huber’s function

3. ROBUST AKAIKE’S CRITERION

In a general case, a model of system can be described by an assumed probability density function of measurements. This probability density is put in correspondence with the exact probability density measurements. The consistency between two probability densities describes the Kullback - Leibler information distance. By minimization of the information distance it is obtained the criterion for determining the model order [1]. For the given model order this criterion is identical to the maximum likelihood criterion. If it is assumed that the model (1) has constant parameters and a stochastic noise e(k) has a Gaussian distribution, Akaike's criterion has the form:

$$W_A(k) = \sum_{i=1}^{k} \varepsilon^2(i) + p, \quad p = n + m \tag{35}$$

in which k represents a number of measurements and p is a number of parameters. In this paper, it is necessary to define Akaike's criterion for a general case:

a) The system parameters are time-invariant
b) The stochastic noise has a non-Gaussian distribution described by the relation (3)

Based on relations (11) and (12) it is obtained:

$$\Phi\left(\varepsilon(\mathrm{k})\right) = \begin{cases} \dfrac{\varepsilon^2(\mathrm{k})}{2\sigma_1^2} + \ln\dfrac{\sqrt{2\pi}\sigma_1}{1-\varepsilon} & \left|\varepsilon(\mathrm{k})\right| \le k_\varepsilon \\ \dfrac{k_\varepsilon}{\sigma_1^2}\left(\left|\varepsilon(\mathrm{k})\right| - \dfrac{k_\varepsilon}{2}\right) + \ln\dfrac{\sqrt{2\pi}\sigma_1}{1-\varepsilon} & \left|\varepsilon(\mathrm{k})\right| > k_\varepsilon \end{cases} \tag{36}$$

Since in the paper estimation algorithm is based on robust statistics [2], the criterion for the selection of the model structure will be called robust Akaike's criterion. Taking into account conditions a) and b) this criterion has the form:

$$W_{RA}(k) = \sum_{i=1}^{k} \Phi(\varepsilon(k)) + p, \quad p = n + m \tag{37}$$

Based on the point of criterion minimum(37), polynomial orders $A(\cdot,\cdot)$ and $B(\cdot,\cdot)$ are determined.

Remark 1: The criterion (37) determine models collection because when p is determined from minimum of the criterion there are multiple combinations of polynomial orders m and n which satisfy the condition. Because, it is adopted:

$$n = m, \quad p = 2n \tag{38}$$

4. SIMULATION RESULTS

The proposed robust Akaike's criterion has been tested on the following OE model:

$$y(k) = \frac{0.5q^{-1} + 0.3q^{-2}}{1 - 0.7q^{-1} + 0.5q^{-2}} u(k) + e(k) \tag{39}$$

The system identification example, is based on measured 1000 input-output data points obtained during the experiments.

During the simulations, it is assumed that measured noise has non-Gaussian distribution:

$$\mathcal{P}_\varepsilon = \left\{ p(e) = (1-\varepsilon)\cdot\mathcal{N}(0;0.1) + \varepsilon\cdot\mathcal{N}(0;10) \right\}. \tag{40}$$

PRBS signal is used for input signal. Figs. 2 to 4 show noise signal, system input and corresponding system output, respectively.

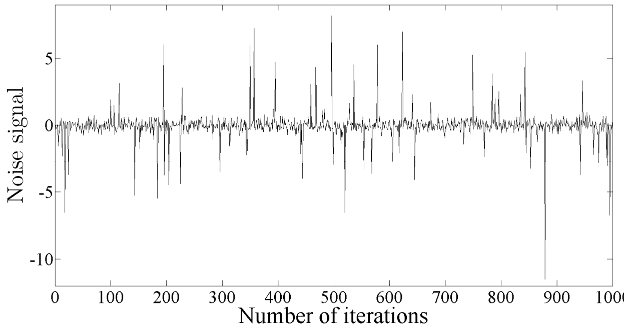

Fig.2 A non-Gaussian noise sequence, $\varepsilon = 0.1$

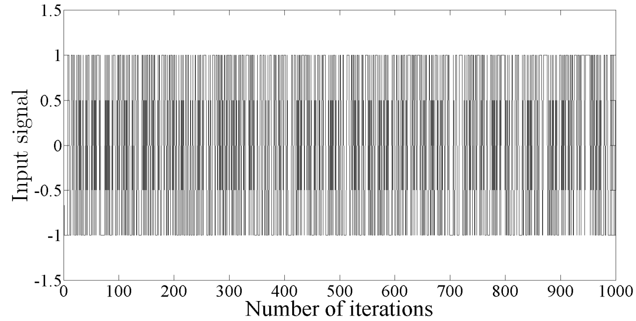

Fig.3. PRBS excitation signal

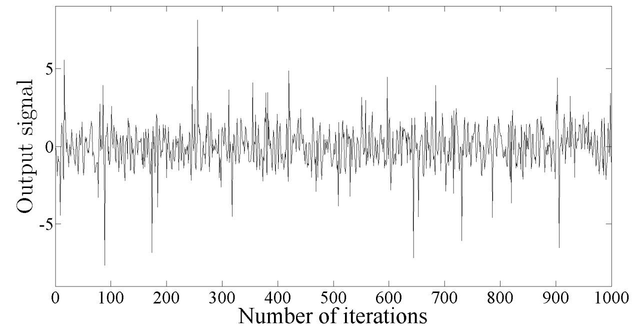

Fig.4. Measured output signal of the system with contamination $\varepsilon = 0.1$

Based on the point of criterion minimum (37), for nine different model orders, it is shown that the observed system can be best described by a second order model, see Fig 5.

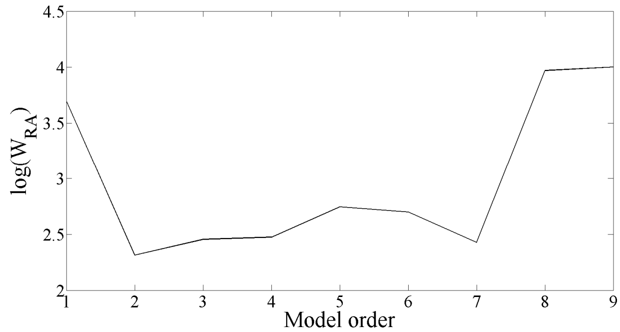

Fig. 5 RAIC criterion for selection of model order

To demonstrate the superiority of the proposed robust OE identification algorithm, a comparison with linear OE identification algorithm [9], when input signal is PRBS signal, is made.

The simulation results are compared in terms of mean square error (MSE), defined by

$$MSE = \ln\left(\mathrm{E}\left\|\hat{\theta}(k) - \theta(k)\right\|^2\right) \tag{41}$$

Figs. 6 to 8 show parameter estimates, and mean square errors.

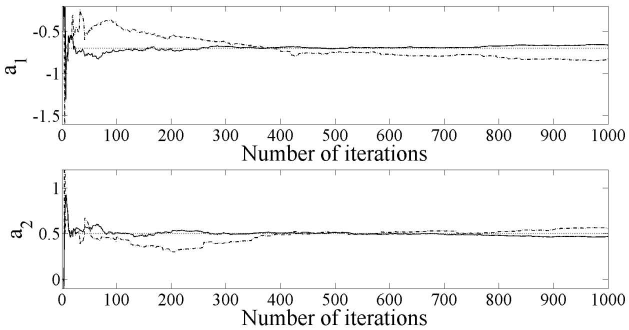

Fig.6. Estimates of parameters a_1 and a_2 obtained in nongaussian noise environment with contamination $\varepsilon = 0.1$ (solid line: Parameter estimates Robust OE, dash-dot: Parameter estimates using linear OE algorithm, dotted line: True parameter values)

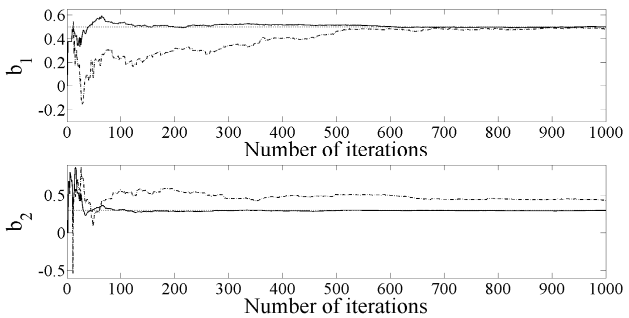

Fig.7. Estimates of parameters b_1 and b_2 obtained in nongaussian noise environment with contamination $\varepsilon = 0.1$ (solid line: Parameter estimates Robust OE, dash-dot: Parameter estimates using linear OE algorithm, dotted line: True parameter values)

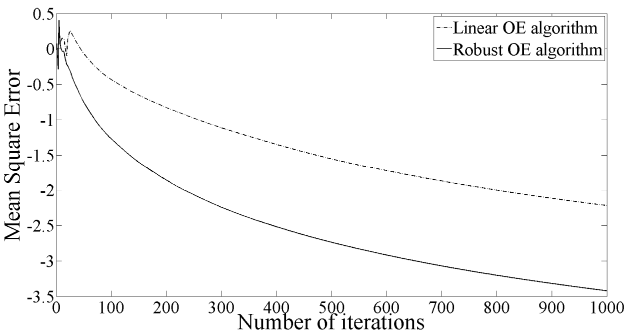

Fig.8. Mean square error, obtained in nongaussian noise environment with contamination $\varepsilon = 0.1$

Figs. 9 and 10 show noise signal and system output respectively, the contamination $\varepsilon = 0.2$.

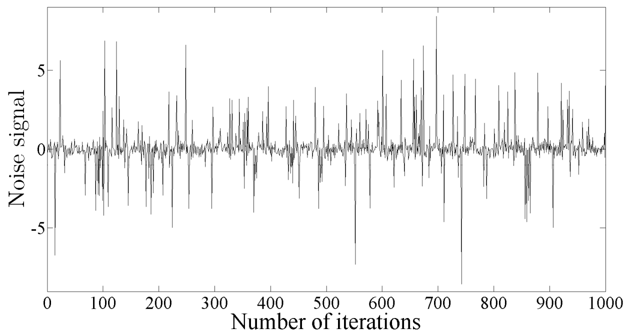

Fig.9 A non-Gaussian noise sequence, $\varepsilon = 0.2$

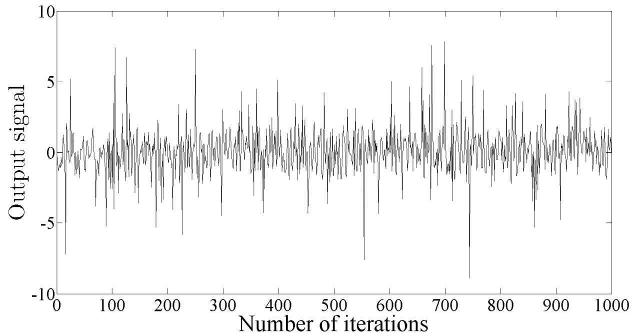

Fig.10. Measured output signal of the system with contamination $\varepsilon = 0.2$

Figs. 11 to 13 show parameter estimates, and mean square errors.

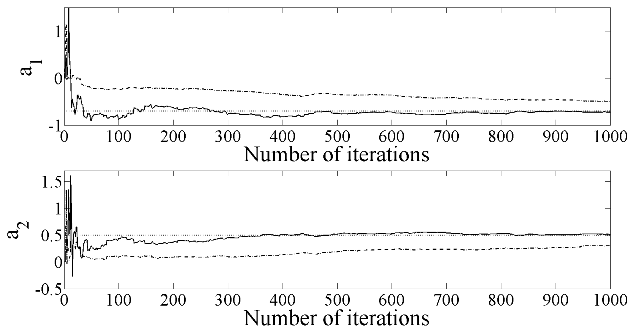

Fig.11. Estimates of parameters a_1 and a_2 obtained in nongaussian noise environment with contamination $\varepsilon = 0.2$ (solid line: Parameter estimates Robust OE, dash-dot: Parameter estimates using linear OE algorithm, dotted line: True parameter values)

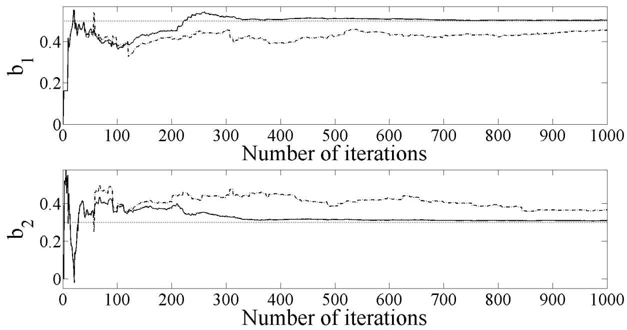

Fig.12. Estimates of parameters b_1 and b_2 obtained in nongaussian noise environment with contamination $\varepsilon = 0.2$ (solid line: Parameter estimates Robust OE, dash-

dot: Parameter estimates using linear OE algorithm, dotted line: True parameter values)

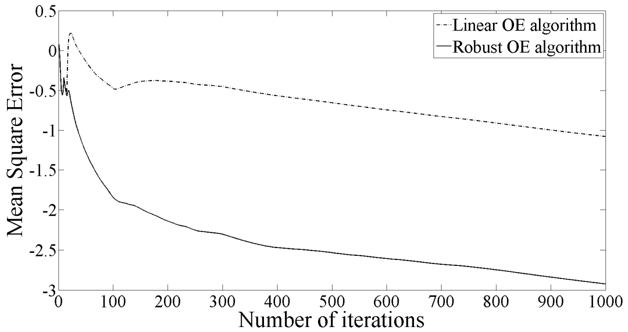

Fig.13. Mean square error, obtained in nongaussian noise environment with contamination $\varepsilon = 0.2$

Comparing Figs. 8 and 13, it can be clearly seen that the superiority of the proposed robust OE algorithm is greater in higher degrees of contamination.

5. CONCLUSION

The basic objective of this paper is to consider how the proposed robust Akaike's criterion copes with the problem of the robust parameter estimation of the time invariant OE model. It assumed that the output measurement of plant is disturbed by Non-Gaussian noise.

The good behavior of proposed robust Akaike's criterion as well as robust identification procedure for OE model is illustrated on the simulation example of the second order model.

ACKNOWLEDGEMENTS

The authors would like to express their gratitude to the Serbian Ministry of Education, Science and Technological Development for supporting this paper through projects TR33026 and TR33027.

REFERENCES

[1] L. Ljung, "System Identification: Theory for the user", 2nd ed., Prentice – Hall, New Jersey (USA) (1999)

[2] T. Söderström, P. Stoica, "System Identification", Prentice – Hall, London (England) (1989)

[3] S. Kullback, R. A. Leibler, "On information and sufficiency," The Annals of Mathematics Statistics, Vol. 22(1), pp. 76–86, (1951)

[4] H. Akaike, "A new look at the statistical model identification", Automatic Control, IEEE Transactions on, Vol. 19(6), pp. 716 – 723, (1974)

[5] V. Barnett, T. Lewis, "Outliers in Statistical Data", 3rd ed. Wiley-Blackwell, New York (USA) (1994)

[6] P.J. Huber, E.M. Ronchetti, "Robust Statistics", 2nd ed., Wiley, New Jersey (USA), (2009)

[7] V. Filipovic, B. Kovacevic, "On robust AML identification algorithm", Automatica, Vol. 30(11), pp. 1775 – 1778, (1994)

[8] V. Filipovic, B. Kovacevic, "On robustified adaptive minimum-variance controller", International Journal of Control, Vol.65(1), pp.117-129, (1996)

[9] I.D. Landau, R. Lozano, M. M'Saad, "Adaptive Control", 1st ed. Springer, Berlin (Germany) (1998)

Simulation Results of Parameter Estimation for a Given ARX Model-system Identification

Sasa Lj. Prodanovic[1]*, Vesna Brasic[2]
[1]Faculty of Mechanical Engineering, East Sarajevo, Bosnia and Herzegovina
[2]Faculty of Mechanical and Civil Engineering in Kraljevo/ Center for the automatic control and fluid technique, University of Kragujevac, Kraljevo (Serbia)

Basis on the system identification are the following principles: collection the set of input and output data in the system work, establishment the forms of possible system model in the form of equations of a model, or in the form of the equation of linear regression and finally adoption of the rule i.e. the criteria according to a possible model of system. It could be accepted like permissible on the basis of the data collected. Based on an algorithm simulation for each individual parameter prediction and its comparison to the exact values of the parameters and it is needed to perform the analysis of the results i.e. the analysis of speed convergence of parameter values obtained by the adopted algorithms to the exact values of the parameters for the ARX model described in this paper. Algorithms which are used for such purposes are the least squares method and the stochastic approximation method .This results will be used in further investigation aimed to the analysis of stochastic approximation algorithm with averaging used in modern approach to system identification

Keywords: system identification, ARX model, least squares method, stochastic approximation method

1. INTRODUCTION

The input-output data are sometimes recorded during the special experiments for system identification, where the user can choose which signal to measure, when to measure, and the type of input signals. The aim of this so called constructed experiment is to enable the choices to allow the experiment to provide data as much information as possible about the system and to be exposed to possible limitations (constraints). The choice of a set of candidate models to represent a suitable option for identification is with no doubt the most important, the most significant and the most difficult task in the procedure of system identification.

It should be noted that a priori knowledge and engineering intuition must be combined with the formal properties of the model. Sometimes the model is made after careful modeling. Then the model with some unknown physical parameters is designed only from the basic laws of physics and the other set of relations. The model that has nothing with the physical relations in the system and use only the adjustment to the data is referred as a black box.

If the model has variable parameters with the physical interpretation, then it is a model called grey box. Generally speaking parametric modelling system is a mapping of inputs and outputs of a some past time moment signed with k-1 and estimation of the output at time k, which is described by the following equation:

$$\hat{y}(k/\theta) = g(\theta, Z^{k-1}) \qquad (1)$$

Here, a vector θ is the final dimensioned vector remanded used to determine the potential value of the parameters. Common types of models are ARX, ARMAX, FIR, State-Space, Multivariable etc. [1]. The task of the system identification is to determine which model is the best for the type of data and the selection is based on some of the adopted criteria. Evaluation of the quality of the model that has been selected based on how the model executes playback of the measured data.

At the end it remains to perform the test of the model validation, and this is the procedure where a model is subjected to testing with respect to data, to comparison to the previous knowledge of the model and to relation to its usefulness. The model can never be accepted as final and real description of the system. It can best be seen as a good enough description of certain aspects that are of particular interest to us in the use of models.

A model of the system is shown by the concrete formula:

$$y(k) - 1{,}5 \cdot y(k-1) + 0.7 \cdot y(k-2) = u(k-1) + 0.5 \cdot u(k-2) + e(k) \qquad (2)$$

This model belongs to a group of linear ARX models. It has a general formula:

$$\begin{aligned} & y(k) + a_1 \cdot y(k-1) + \dots a_n \cdot y(k-n) = u(k-1) + \\ & + b_1 \cdot u(k-2) + b_m \cdot u(k-m) \dots + e(k) \end{aligned} \qquad (3)$$

These equations are called the equations of the model, in which the matrix of adjustable parameters in this case is:

*Corresponding author: Vuka Karadžića 30, 71123 East New Sarajevo, Bosnia and Herzegovina, sasa.prodanovic@maf.unssa.rs.ba

$$\theta=[a_1 \quad a_2 \quad ....a_n \quad b_1 \quad b_2....b_m]^T \tag{4}$$

We also introduce the matrixes:

$$A(q)=1+a_1\cdot q^{-1}+......+a\cdot_n q^{-n} \tag{5}$$

$$B(q)=1+b_1\cdot q^{-1}+......+b_m\cdot q^{-m} \tag{6}$$

As the general form of the linear model described with the expression:

$$y(k)=G(q,\theta)\cdot u(k)+H(q,\theta)\cdot e(k) \tag{7}$$

fe (x, θ) - probability density of the signal e (k), e (k) is a white noise

In this case e (k) is the Gaussian noise and the matrixes G and H are in the form:

$$G(q,\theta)=B(q)/A(q), \quad H(q,\theta)=1/A(q) \tag{8}$$

Graphical scheme of the signal transmission in system described in the framework of this model is shown in the following figure

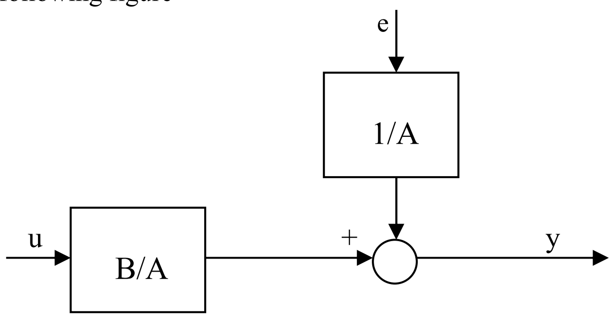

Figure 1: Sheme of the ARX model

Output prediction the system i.e. its estimation follows:

$$\hat{y}(k/\theta)=B(k)u(k)+[1-A(k)]y(k) \tag{9}$$

If we introduce matrix

$$\varphi(k)=[-y(k-1)...-y(k-n) \quad u(k-1)...u(k-m)]^T \tag{10}$$

Now the output evaluation of system i.e. its prediction can be written in the form:

$$\hat{y}(k/\theta)=\theta^T\cdot\varphi(k)=\varphi^T(k)\cdot\theta \tag{11}$$

This feature of the output estimate of the system is very important because on these relationships can make a simple estimate of the matrix θ. This model is called linear regression and matrix φ (k) is called regression matrix.

If it is known some of the coefficients of matrix θ then applies the following equation:

$$\hat{y}(k/\theta)=\varphi^T(k)\cdot\theta+\mu(k) \tag{12}$$

For a given system which is defined by the concrete form (2), where e (k) is Gaussian noise, a random variable with a normal distribution N (0,1).

Our task is to define model of a system in a form:

$$y(k)=\varphi^T(k)\cdot\theta+e(k) \tag{13}$$

with application of following methods for parameter estimation [1]:

1) Recursive least squares method
2) Stochastic approximation

It is necessary to determine which of those two criteria best describes the estimation of the system parameters, suppose that we know the matrix of correct parameters.

$$tetap=[-1.5 \quad 0.7 \quad 1 \quad 0.5]' \tag{14}$$

In the following sections we will see which of the following two algorithms perform best estimate of the system parameters in order to have fastest convergence to the value of accurate parameters and have the least square error and mean square error. This research we will use to compare all results with results given for simulation parameter estimation by method of stochastic approximation with average first used by Polyak [2], which will not be the scope of this article.

2. RECURSIVE LEAST SQUARES METHOD (RLS)

Criteria of recursive least square method is applied on wide problems for which solution is necessary the using of numerical methods. There are a different group of technics and commercial methods for resolving this which requires minimizing problem the following quadratic criteria with the error of predictions:

$$J_N=\frac{1}{N}\sum_{k=1}^{N}\alpha_k\left[y(k)-\theta^T\cdot\varphi(k)\right]^2 \tag{15}$$

Matrix of parameter θ must be estimated in moment so the prediction of parameters $\hat{\theta}(k)$ minimizes the sum of squares between the system output and the output of the estimated model in the range of k measurements. As the criterion (15) is a square criteria, a value $\hat{\theta}(k)$ that minimizes a given amount, obtained from the following equation:

$$\frac{\partial J_N}{\partial\hat{\theta}}=0 \tag{16}$$

This method represents the procedure which could be on line and off line computing of estimated parameters.

The lack of the method with on line parameter computing is that with increasing measuring population z N = {u (i), y (i), i = 1, .. N, and for each measurement z (n +1) = {u (N +1), y (N +1)} the overall budget must be repeated in order to generate new estimates of the parameters with the increasing of computational requirements and the required storage space and computation time, and this method is called no recursive method of least squares.

On the other hand recursive parameter identification method generates a new parameter estimation $\hat{\theta}(k+1)$ based on the previously calculated estimates $\hat{\theta}(k)$ and new information obtained through measurement z (N +1) = {u (N +1), y (N +1)}. In order to obtain recursive algorithms consider the evaluation $\hat{\theta}(k)$

From equations (10) – (16) in Ljung [1] is described the procedure of obatining final form of expression the RLC method which we will use in computing the estimation of system parameters.

$$\hat{\theta}(k)=\hat{\theta}(k-1)+\alpha_k\cdot P(k)\cdot\varphi(k)\cdot\left(y(k)-\varphi^T(k)\cdot\hat{\theta}(k-1)\right) \quad (17)$$

$$P(k)=P(k-1)-\frac{P(k-1)\cdot\varphi(k)\cdot\varphi^T(k)\cdot P(k-1)}{\alpha_k^{-1}+\varphi^T(k)\cdot P(k-1)\cdot\varphi(k)} \quad (18)$$

where $\hat{\theta}(0)=0,\quad P(0)=\alpha\cdot I$, and α is some graet number.In our case we are adopting $\alpha_k=1$.

STOHASTIC APPROXIMATION (SA)

Pošto kriterijum (16) možemo napisati i u sledećem obliku

$$J_N=\frac{1}{N}\sum_{k=1}^{i}\alpha_k\left[y(k)-\theta^T\cdot\varphi(k)\right]^2= \sum_{k=1}^{i}\beta_k\left[y(k)-\theta^T\cdot\varphi(k)\right]^2 \quad (19)$$

That with process of the previous recursive methods based on equation from RLS [1] we write the following equation:

$$\hat{\theta}(k)=\left[\sum_{i=1}^{k}\beta_i\cdot\varphi(i)\cdot\varphi^T(i)\right]^{-1}\sum_{i=1}^{k}\beta_i\cdot\varphi(i)\cdot y(i)= \bar{R}^{-1}(k)\cdot f(k) \quad (20)$$

Where is:

$$\bar{R}(k)=\sum_{i=1}^{k}\beta_i\cdot\varphi(i)\cdot\varphi^T(i) \quad (21)$$

$$f(k)=\sum_{i=1}^{k}\beta_i\cdot\varphi(i)\cdot y(i) \quad (22)$$

The establishment of recursive connection between $\hat{\theta}(k)$ and $\hat{\theta}(k-1)$ has following form:

$$\beta(k,i)=\lambda(k)\cdot\beta(k-1,i),\qquad 0\le i\le k-1$$
$$\beta(k,k)=1 \quad (23)$$

It means that we can write the following assumption:

$$\beta(k,i)=\prod_{j=k+1}^{k}\lambda(j) \quad (24)$$

On the basis of this assumption

$$\bar{R}(k)=\lambda(k)\bar{R}(k-1)+\varphi(k)\cdot\varphi^T(k) \quad (25)$$

$$f(k)=\lambda(k)f(k-1)+\varphi(k)\cdot y(k) \quad (26)$$

Now from (20) using (25) and (26) we receive:

$$\hat{\theta}(k-1)=\bar{R}^{-1}(k-1)\cdot f(k-1) \quad (27)$$

And multiplying the equation (27) on the left with matrix $\bar{R}(k-1)$

$$\bar{R}(k-1)\cdot\hat{\theta}(k-1)=f(k-1) \quad (28)$$

The equation (20) with the insert of (26) and (28) in its becomes:

$$\hat{\theta}(k)=\bar{R}^{-1}(k)\cdot f(k)=\bar{R}^{-1}(k)\cdot\left[\lambda(k)\cdot f(k-1)+\varphi(k)\cdot y(k)\right] \quad (29)$$

$$\hat{\theta}(k)=\bar{R}^{-1}(k)\cdot f(k)=\bar{R}^{-1}(k)\cdot\left[\lambda(k)\cdot\bar{R}(k-1)\cdot\hat{\theta}(k-1)+\varphi(k)\cdot y(k)\right] \quad (30)$$

The insertation of (25) in (30) gives:

$$\hat{\theta}(k)=\bar{R}^{-1}(k)\cdot\left[\left(\bar{R}(k)-\varphi(k)\cdot\varphi^T(k)\right)\cdot\hat{\theta}(k-1)+\varphi(k)\cdot y(k)\right] \quad (31)$$

$$\hat{\theta}(k)=\hat{\theta}(k-1)+\bar{R}^{-1}(k)\cdot\varphi(k)\cdot\left(y(k)-\varphi^T(k)\cdot\hat{\theta}(k-1)\right) \quad (32)$$

$$\bar{R}(k)=\lambda(k)\bar{R}(k-1)+\varphi(k)\cdot\varphi^T(k) \quad (33)$$

These two equations represent recursive stochastic algorithm for calculating the parameters of the system. If we look at equation (31) - (33) we adopt λ = 1 which give the equations (4) and (5). This algorithm we are marking as Stochastic approximation (SA) related to the other algorithms in future work.

$$\hat{\theta}(k)=\hat{\theta}(k-1)+\frac{1}{r(k)}\cdot\varphi(k)\cdot[y(k)-\hat{\theta}^T(k-1)\cdot\varphi(k)] \quad (34)$$

$$r(k)=r(k-1)+\varphi^T(k)\cdot\varphi(k) \quad (35)$$

with the following starting conditions:

$$\hat{\theta}(0) = 0, \qquad r(0) = 1 \tag{36}$$

2.1. Simulation of parameter estimation in comparison with the accurate value in RLS method

By using (17) and (18) with conditions (10) – (14) where signals u(t) and e(t) are Gaussian noises for Monte Carlo simulations [1] of the number of 5000 we receive following simulation results presented in graphical form for the RLS method. The results are obtaining with MATLAB software package [3].

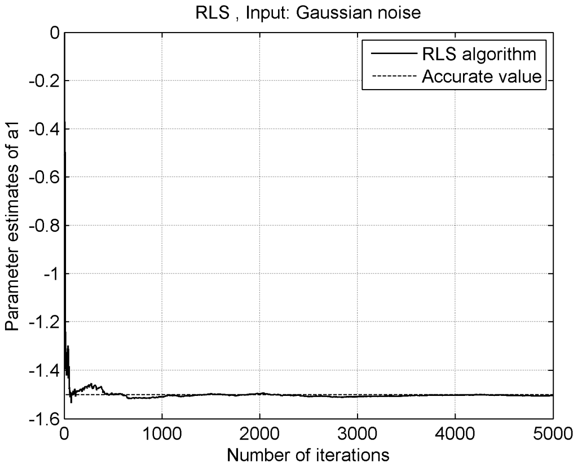

Figure 1. Simulation of parameter prediction for a_1 in comparison with its accurate value in RLS method

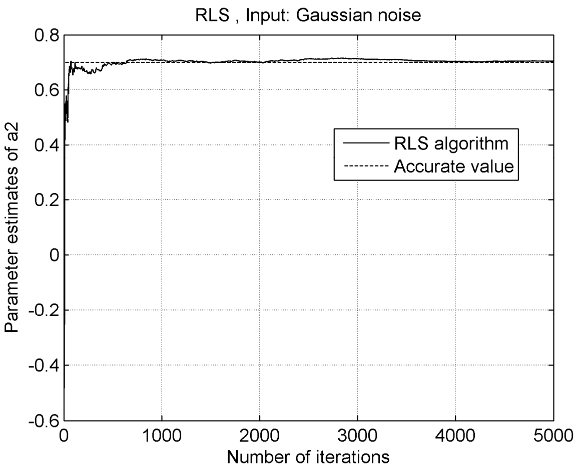

Figure 2. Simulation of parameter prediction for a_2 in comparison with its accurate value in RLS method

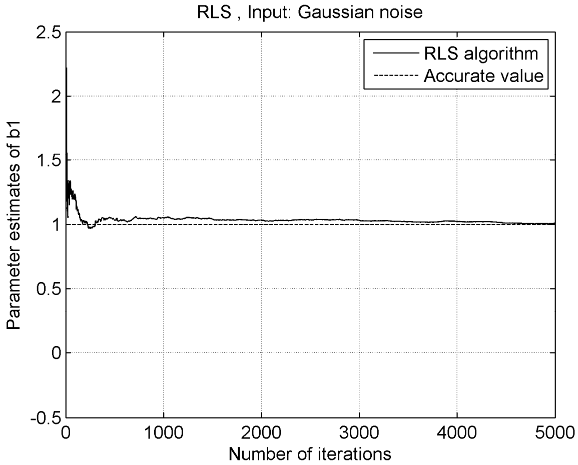

Figure 3. Simulation of parameter prediction for b_1 in comparison with its accurate value in RLS method

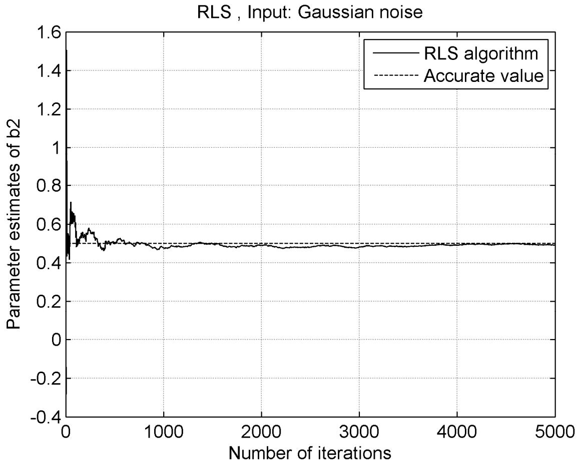

Figure 4: Simulation of parameter prediction for b2 in comparison with its accurate value in RLS method

2.2. Simulation of the parameter estimation in comparison with the accurate value with stochastic approximation method - SA method

Graphical presentations of the results are given:

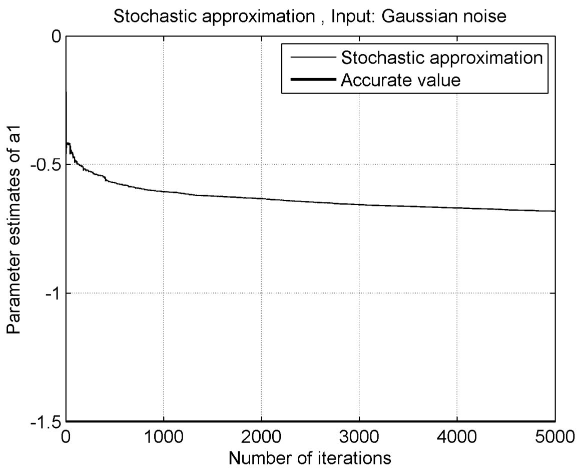

Figure 5. Simulation of parameter prediction for a_1 in comparison with its accurate value in SA method

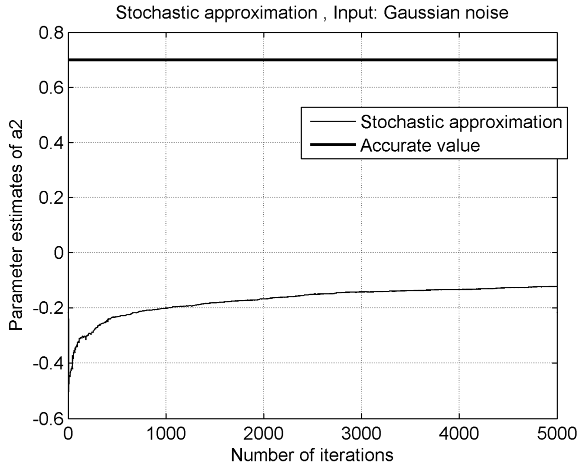

Figure 6: Simulation of parameter prediction for a2 in comparison with its accurate value in SA method

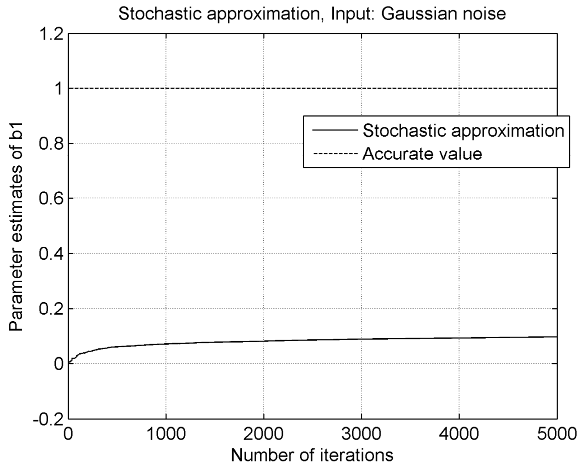

Figure 7. Simulation of parameter prediction for b1 in comparison with its accurate value in SA method

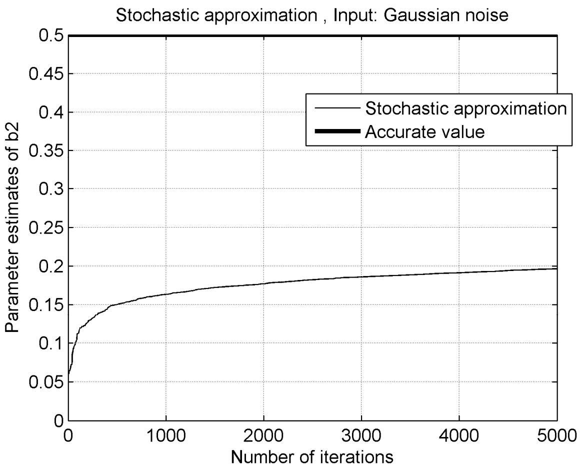

Figure 8. Simulation of parameter prediction for b_2 in comparison with its accurate value in SA

3. GAUSSIAN NOISES E (K) AND U(K)

Signals e(k) and u(k) are the noises with normal density spectres used in the derivation of the estimates of parameters in the given ARX model

The graphical presentations of this signal used like random variables in simulations are given in following pictures.

All simulations and mathematical operation with random variables were done with Math Works software package –MATLAB [3].

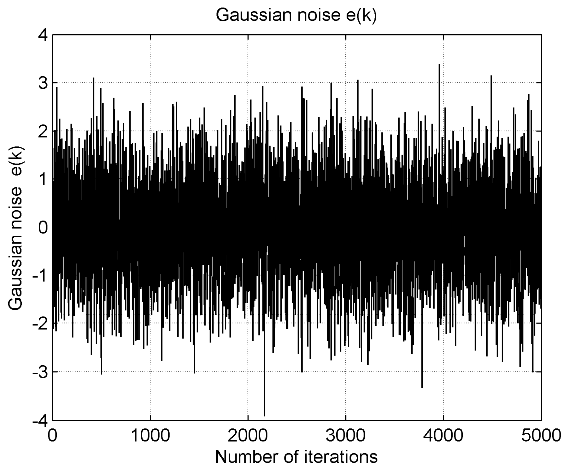

Figure 9: Random variable e(k)

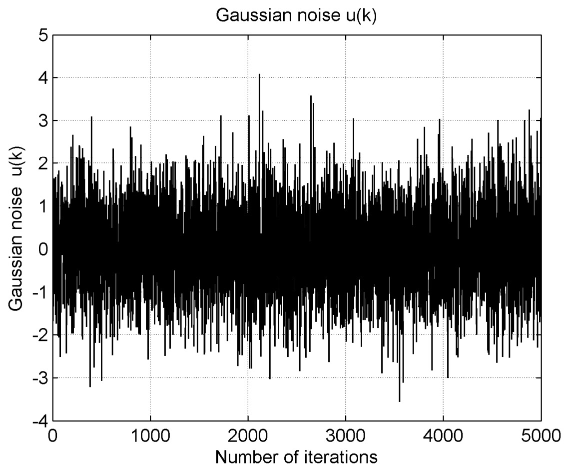

Figure 10: Random variable u(k)

ACKNOWLEDGEMENTS

This article is written in scope of presentation the results and activities of the project „ Bridge technical differences and social suspicions contributing to transform the Adriatic area in a stable hub for a sustainable technological development" with acronym ADRIA – HUB from the IPA ADRIATIC CBC 2007 – 2013 programme.

CONCLUSION

From theoretical considerations it is known that the asymptotic velocity of convergence score lower in stochastic approximation than the recursive least squares method, as can be seen from the examples considered here. From the reason of decreasing the speed of convergence to the accurate value of parameters, in the year of 1990 Polyak [2] proposed stochastic approximation that introduces averaging trajectories obtained by stochastic approximation. The resultant two-stage procedure has the asymptotic rate of convergence similar to a recursive least squares method.

In the future research work we will use that method of stochastic approximation with averaging and all results will present in the article also published in this conference [4]. In that article will be figured the comparing of the RLS, SA and stochastic approximation with averaging across the comparing of parameters simulations , square errors and mean square errors.

REFERENCES:

[1] Ljung, L (1999), System Identification. Theory for the User.Prentice – Hall, New Jersey

[2] Polyak, B.T. (1990) New method of stochastic approximation type. Automation and Remote Control, 51, pp. 937-946

[3] Comuter Software: Gemax Laboratory Solutions, (2009), MATLAB and Simulink, Version:7.8.0.347 (The Language of Technical Computing); Licence Number: 161051; produced by The MathWorks Inc.

[4] Vesna S. Brasic „Comparing the results of stochastic approximation method with averaging related to convenient identification methods“, VIII International Conference “Heavy Machinery-HM 2014”, Zlatibor, 25-28 June 2014.

Comparing the Results of Stochastic Approximation Method With Averaging Related to Convenient Identification Methods

Vesna S. Brašić[1*]
[1] Faculty of Mechanical Engineering Kraljevo/ Center for the automatic control and fluid technique, University of Kragujevac, Kraljevo, Serbia

Modern approach of identification introduces a method called stochastic approximation with averaging. This is done with the intention to investigate the best possible identifications results, which relates only to the method of stochastic approximation. The research we carried out are for four values of α, which describe the extent of required estimate parameter on which is done the averaging. On the basis of simulation for each algorithm separately and comparison of parameter estimation to the exact value of the parameter, it will be determined which of these algorithms faster converge to the exact values of the parameters for a given ARX model. It will also be shown whether these newly introduced algorithms converge better than the recursive least squares. At the end it will appear a conclusion which of these six algorithms has the least square error and mean square error, i.e. performs the best estimate of the system parameters, by using results from the previous researches. To be identification with full procedure it is necessary to make the verification model , i.e. make the comparison of the resulting mathematical model with experimental results , which will not be presented in this paper

Keywords: system identification, ARX model, least squares method, stochastic approximation method

1. INTRODUCTION

Compared to previously processed results of research related to the evaluation of system parameters through algorithms recursive method of least squares (RLS) and stochastic approximation (SA) included in article, published also in this conference [1], our further investigations will be related the stochastic approximation with averaging introduced by Polyak [2]. This method in mathematical terms can be represented by the following steps:

STEP 1

$$\hat{\theta}(k)=\hat{\theta}(k-1)+\frac{1}{\left(r(k)\right)^{\alpha}}\varphi(k)\left[y(k)-\varphi^{T}(k)\hat{\theta}(k-1)\right] \quad (1)$$

$$r(k)=r(k-1)+\varphi^{T}(k)\varphi(k) \quad (2)$$

$$\hat{\theta}(0)=0, \qquad r(0)=1, \qquad 1/2<\alpha<1 \quad (3)$$

STEP 2 (Averaging)

$$\bar{\theta}(k)=\frac{1}{k}\sum_{i=1}^{k}\hat{\theta}(i) \quad (4)$$

From this relation is obtained a recursive form

$$\bar{\theta}(k)=\bar{\theta}(k-1)+\frac{1}{r(k)}\left(\hat{\theta}(k)-\bar{\theta}(k-1)\right) \quad (5)$$

From relations (3) and (5) it follows:

$$\ln\left\|\bar{\theta}(k)-\theta\right\|^{2}$$

$$\ln\left(\frac{1}{k}\sum_{i=1}^{k}\left\|\bar{\theta}(k)-\theta\right\|^{2}\right)$$

$$\bar{\theta}(0)=0\,,\, r(0)=1 \quad (6)$$

In our work it is necessary to:

a) Describe the obtaining of method recursive form represented with equations 1-6
b) Graphically displayed the results

Evaluated parameter for each method is necessary to compare across the simulation results for all methods.

In this article we will detrmine:

The square error of estimation for recrusive least square method and stochastic approximation described in previous article in a following form:

$$\ln\left\|\hat{\theta}(k)-\theta\right\|^{2} \quad (7)$$

and mean square error for the same methods in a form:

$$\ln\left(\frac{1}{k}\sum_{i=1}^{k}\left\|\hat{\theta}(k)-\theta\right\|^{2}\right) \quad (8)$$

*Corresponding author: Dositejeva 19, 36 000 Kraljevio, Republic of Serbia; brasic.v@mfkv.kg.ac.rs

Also we will determine the square error of estimation for shochastic approximation with averaging in a following form:

$$\ln \left\| \bar{\theta}(k) - \theta \right\|^2 \tag{9}$$

And mean square error for the same method in a form:

$$\ln \frac{1}{k} \sum_{i=1}^{k} \left\| \bar{\theta}(k) - \theta \right\|^2 \tag{10}$$

We will also compare the obtaining results of all simulations as for estimated parameters as for obatining errors in all simulations for all methods.

The sofware for simulations will be MATLAB [3] package and the number of Monte Carlo simulations will be Bmk=5000 , described by Ljung [4].

For graphic presentations of the simulations results of stochastic approximation with averaging will be refered to a issue of $\bar{\theta}(k)$

This mehod will be investigated throught the values of α=0.6, α=0.7, α=0.8 and α=0.9 in order to find the best value of α in this method of averaging which could in best way simulate the real values of parameters. With the other words we will determine the prediction of system parameters, since the matrix of accurate values of parameters is known:

$$tetap = [-1.5 \quad 0.7 \quad 1 \quad 0.5]' \tag{11}$$

A describe of this ARX model in equation form and its graphical presentation are given in [1].

In the next sections we will see the simulation results of estimated parameters for the following four algorithms, which at the fastest way converge to the accurate values of parameters:

1. Stochastic approximation with averaging $\alpha = 0.6$
2. Stochastic approximation with averaging $\alpha = 0.7$
3. Stochastic approximation with averaging $\alpha = 0.8$
4. Stochastic approximation with averaging $\alpha = 0.9$

2. SIMULATION THE PARAMETER VALUES

By using equations (1) – (6) and (11) with e(k) and u(k), random Gaussian variables with normal spectral density [4], graphical presentations of obtainig results are looking like follows.

2.1. Stochastic approximation (SA) with averaging $\alpha = 0.6$

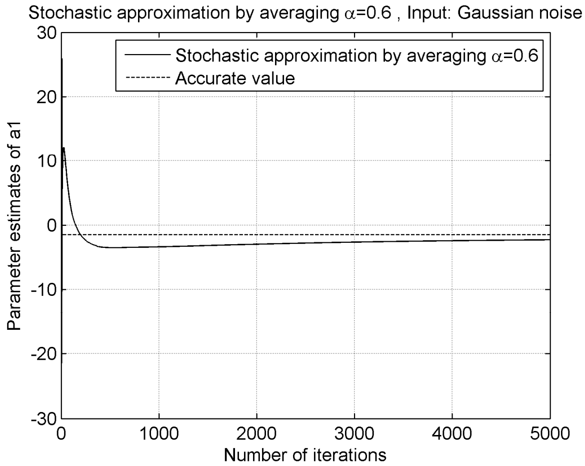

Figure 1: The parameter value of a_1 and its accurate value – SA with averaging α=0.6

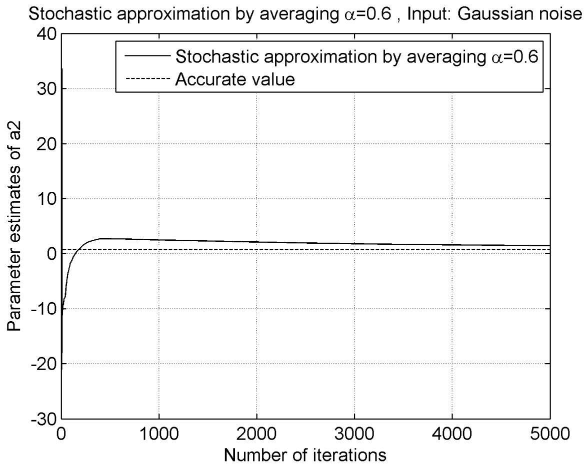

Figure 2: The parameter value of a_2 and its accurate value – SA with averaging α=0.6

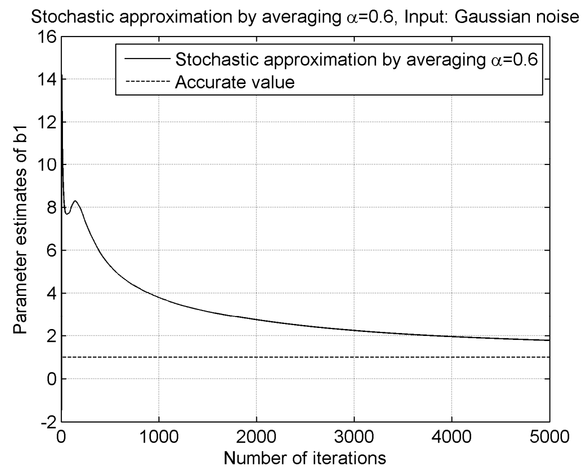

Figure 3: The parameter value of b_1 and its accurate value – SA with averaging α=0.6

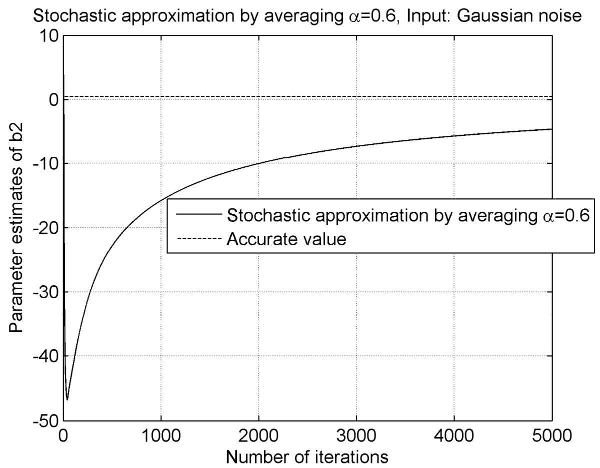

Figure 4: The parameter value of b_2 and its accurate value – SA with averaging α=0.6

2.2. Stochastic approximation with averaging - α = 0.7

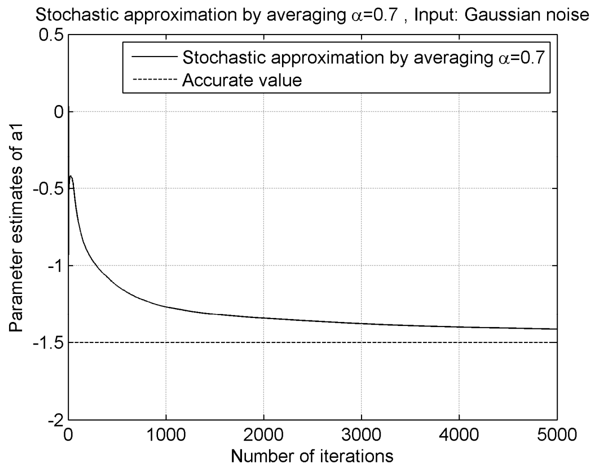

Figure 5: The parameter value of a_1 and its accurate value – SA with averaging α = 0.7

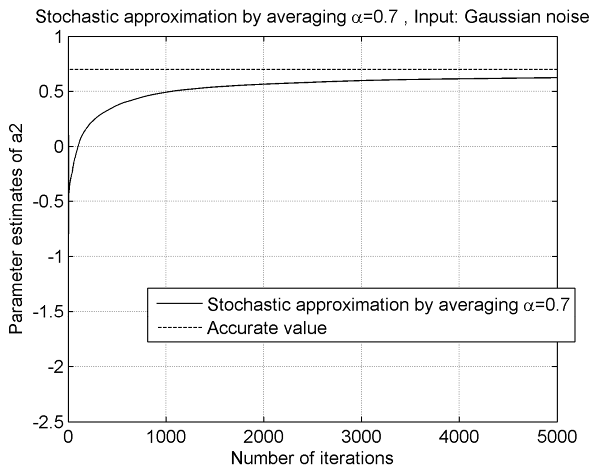

Figure 6: The parameter value of a_2 and its accurate value – SA with averaging α = 0.7

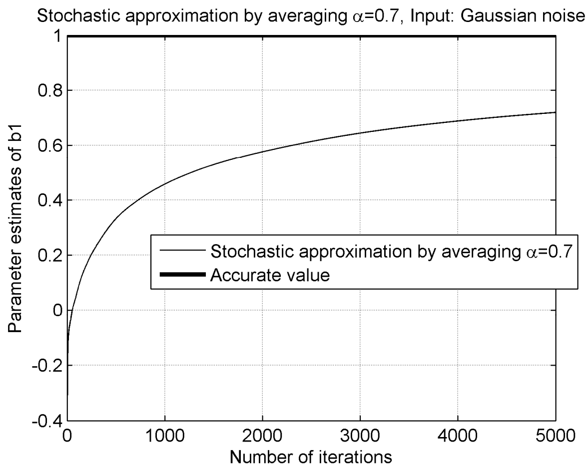

Figure 7: The parameter value of b_1 and its accurate value – SA with averaging α = 0.7

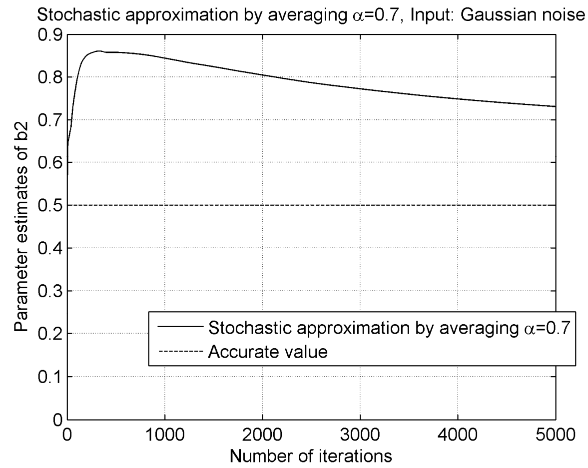

Figure 8: The parameter value of b_2 and its accurate value – SA with averaging α = 0.7

2.3. Stochastic approximation with averaging - α = 0.8

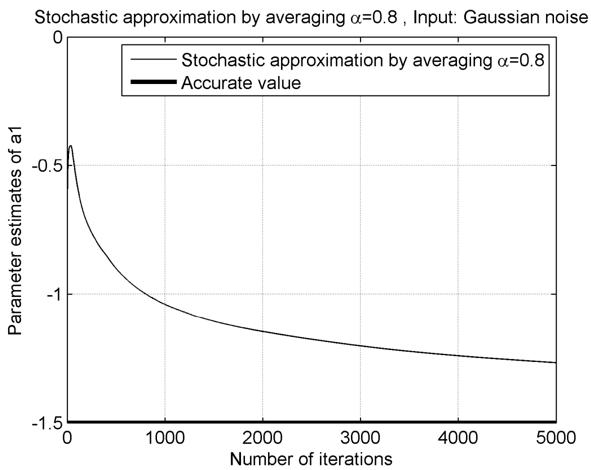

Figure 9: The parameter value of a_1 and its accurate value – SA with averaging α = 0.8

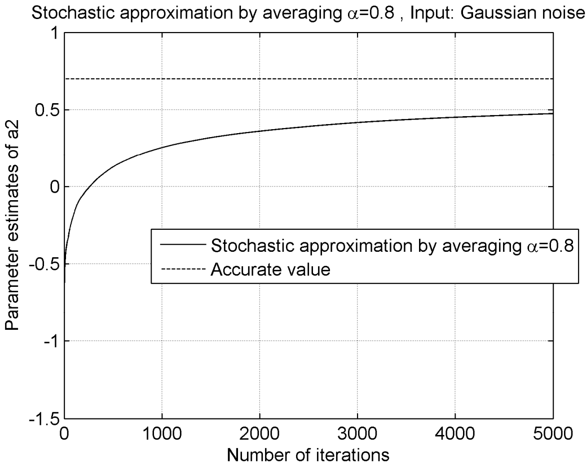

Figure 10: The parameter value of a_2 and its accurate value – SA with averaging $\alpha = 0.8$

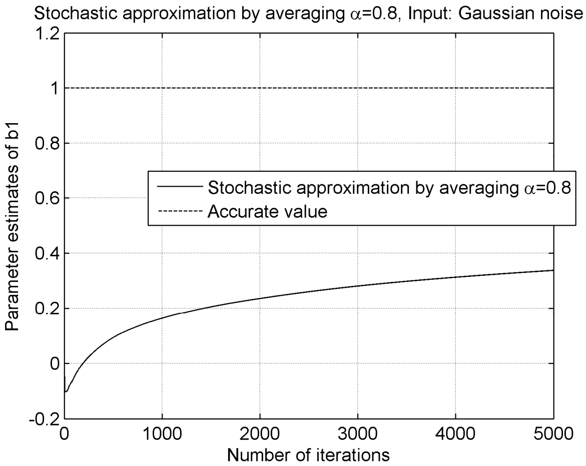

Figure 11: The parameter value of b1 and its accurate value – SA with averaging $\alpha = 0.8$

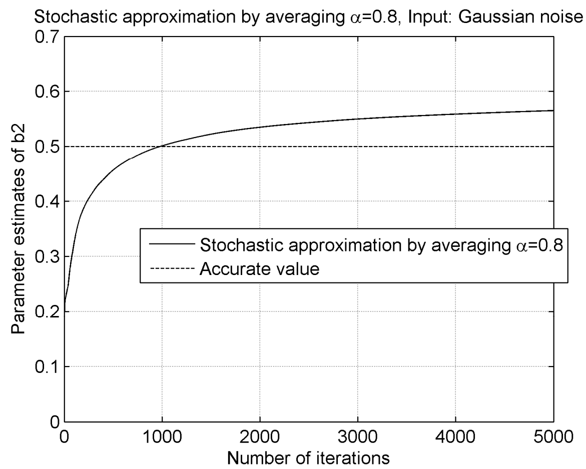

Figure 12: The parameter value of b_2 and its accurate value – SA with averaging $\alpha = 0.8$

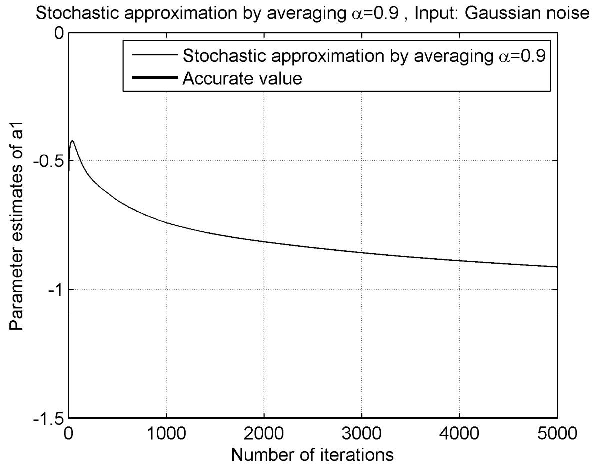

Figure 13: The parameter value of a1 and its accurate value – SA with averaging $\alpha = 0.9$

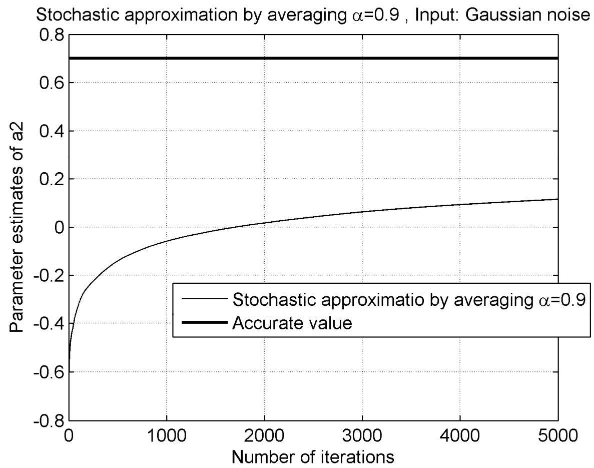

Figure 14: The parameter value of a2 and its accurate value – SA with averaging $\alpha = 0.9$

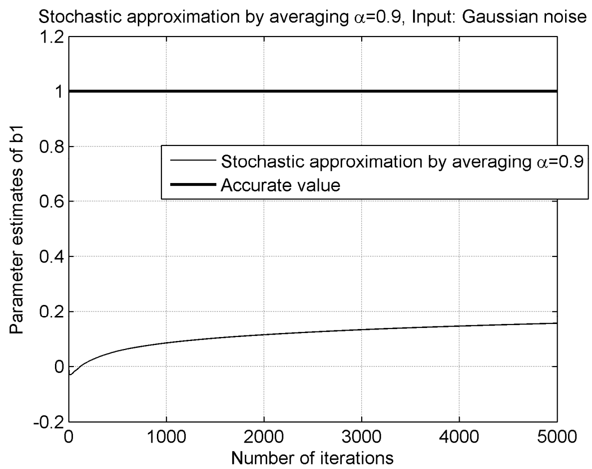

Figure 15: The parameter value of b_1 and its accurate value – SA with averaging $\alpha = 0.9$

2.4 Stochastic approximation with averaging - $\alpha = 0.9$

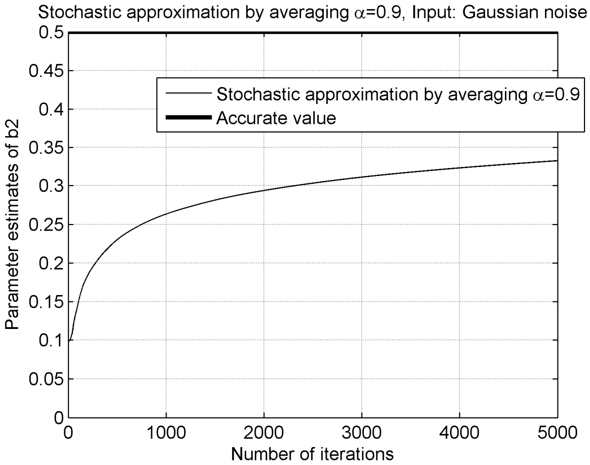

Figure 16: The parameter value of b2 and its accurate value – SA with averaging $\alpha = 0.9$

Since we have results for the same sustem for recrusive least square metod and stochasic approximation we can compare the results from those methods and from these obtainig in present article.

3. COMPARING THE SIMULATIONS RESULTS FOR PARAMETER VALUES

Now we have the simulation results from the six algorithms included the results obtaining from article, published also in this conference [1]. So for this ARX model we can compare the results of identification by stochastic approximation method with averaging with convenient method of identification such as recursive least square method (RLS) and stochastic approximation (SA).

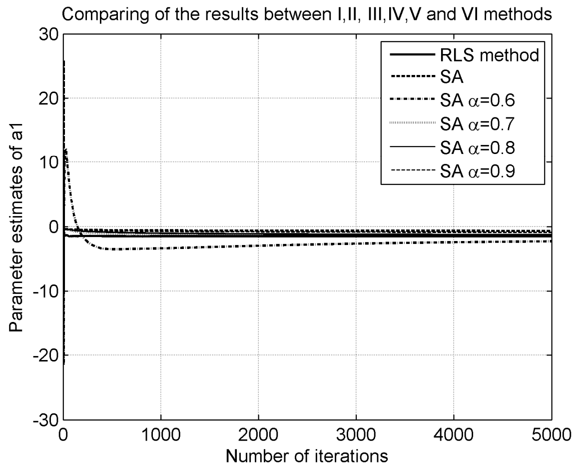

Figure 17: The values of parameter a_1 obtainig with simulations in all algorithms

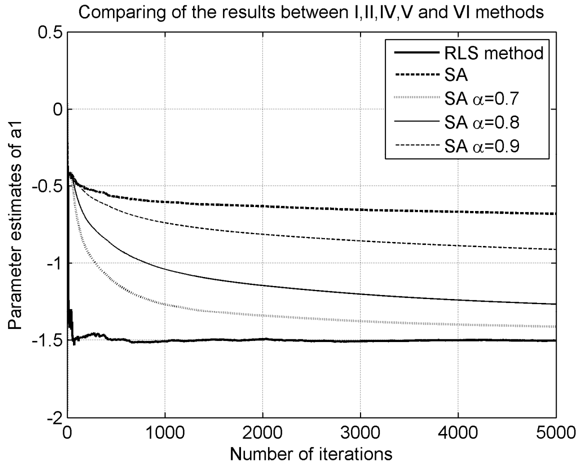

Figure 18: The values of parameter a_1 for the precisions algorithms

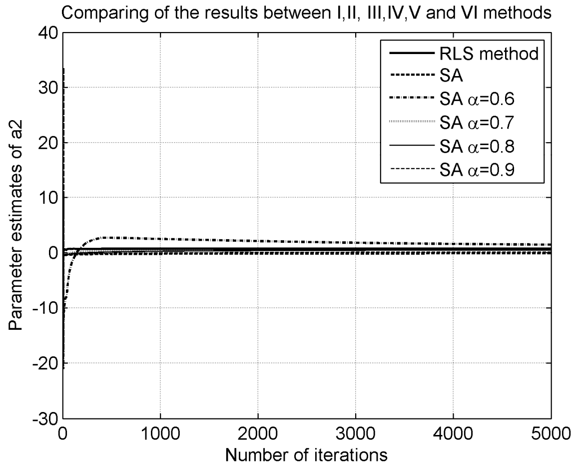

Figure 19: The values of parameter a_2 obtainig with simulations in all algorithms

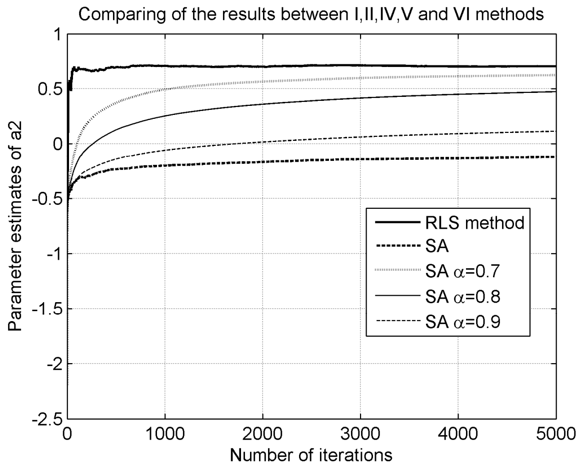

Figure 20: The values of parameter a2 for the precisions simulations in all algorithms

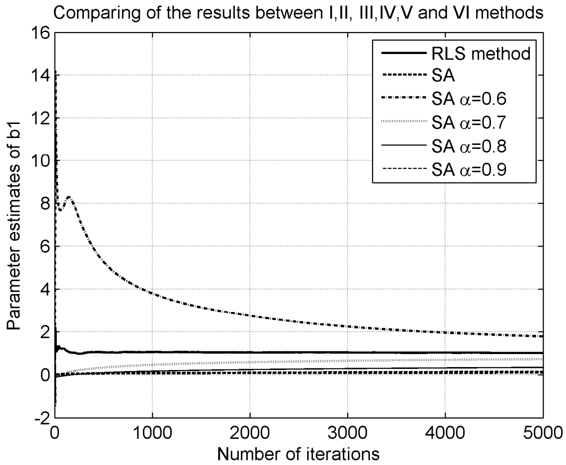

Figure 21: The values of parameter b_1 obtainig with simulations in all algorithms

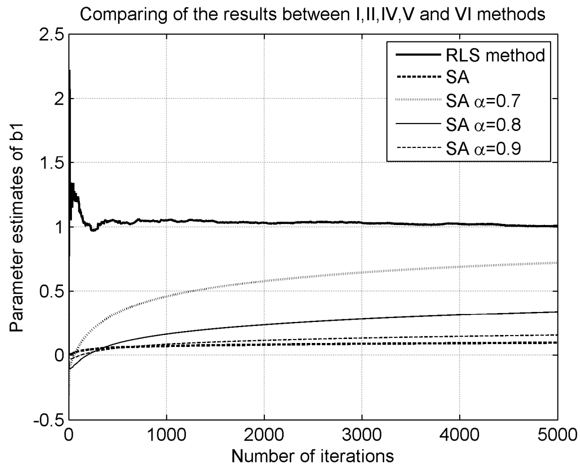

Figure 22: The values of parameter b_1 for the precisions algorithms

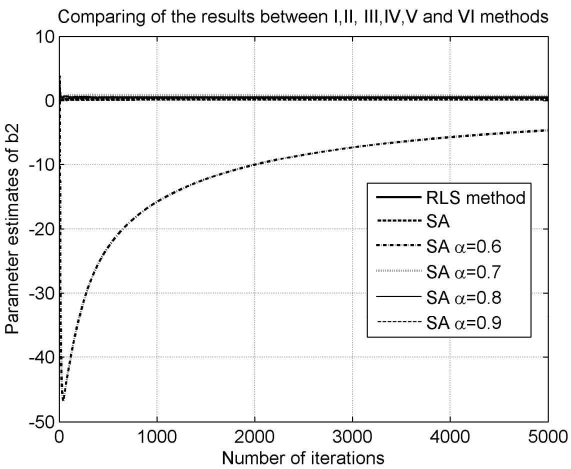

Figure 23: The values of parameter b_2 obtainig with simulations in all algorithms

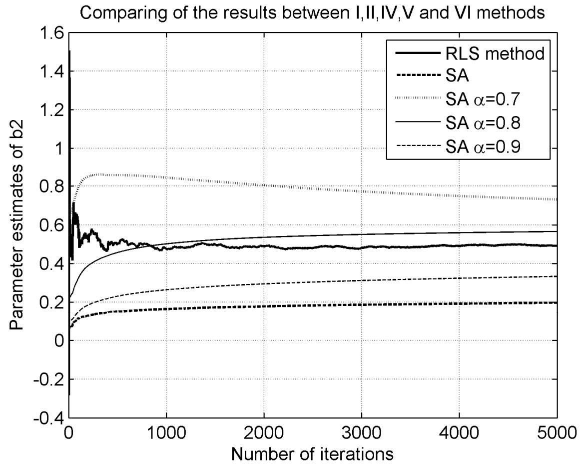

Figure 24: The values of parameter b_2 for the precisions algorithms

4. COMPARING THE SQUARE ERRORS

In order to find which algorithm can on the best way simulate the real values of parameters the smallest value of errors could also show us that result.

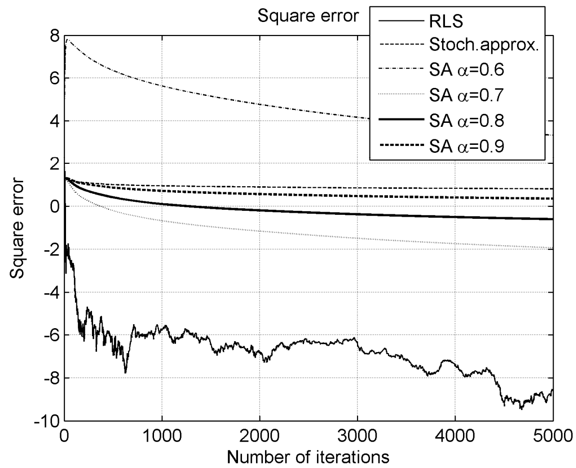

Figure 25: Square errors for all algorithms

5. COMPARING THE MEAN SQUARE ERRORS

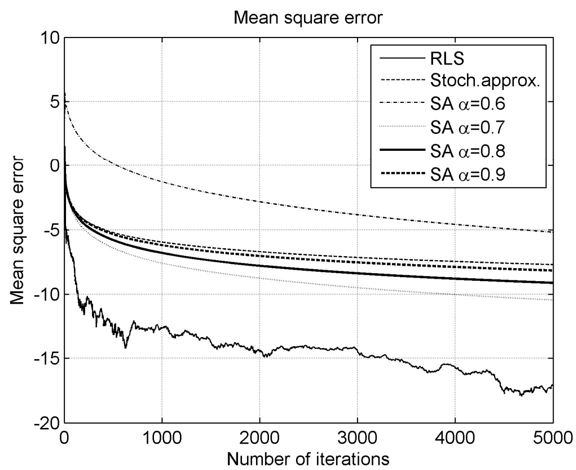

Figure 26: Mean square errors for all algorithms

Since expressions (7) – (10) could show the logarithm values of square errors and mean square errors, so the minimal values of errors of those logarithms will show which algorithm has the best simulation results.

6. GAUSSIAN NOISES E(K) AND U(K)

For the values of the signals u(k) and e(k) are taken the Gaussian noise (random variables with normal density spectar) in this simulations for this ARX model.

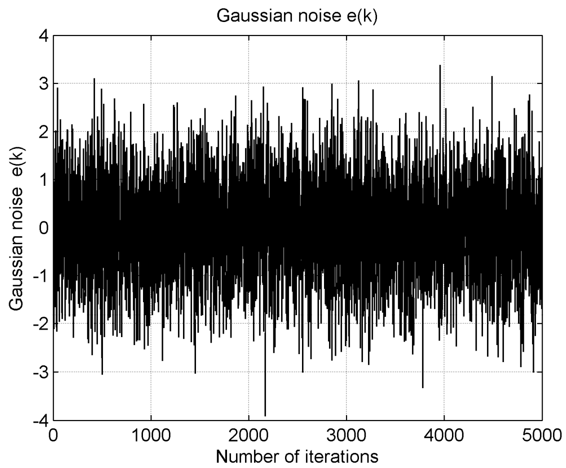

Figure 27: The disturbance value of e(k)

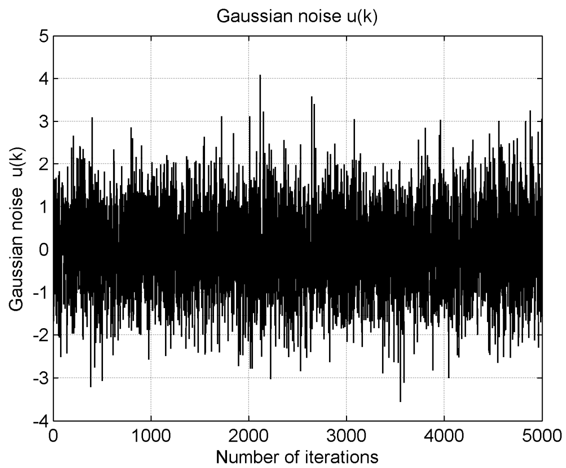

Figure 28: The input signal of u(k)

ACKNOWLEDGEMENTS

This article is written in scope of presentation the results and activities of the project „ Bridge technical differences and social suspicions contributing to transform the Adriatic area in a stable hub for a sustainable technological development" with acronym ADRIA – HUB from the IPA ADRIATIC CBC 2007 – 2013 programme.

CONCLUSION

Based on an algorithm simulation for each individual evaluation of parameters and comparison of the parameters with its correct values we conclude from Fig.18, Fig.20, Fig.22 and Fig.24 that recursive least square method and stochastic approximation with averaging where $\alpha = 0.8$ are the algorithm which fastest converge to the exact values of the parameters of this ARX model. The least square error and mean square error (Fig.25 and Fig.26) are also for this two algorithms, i.e. the method of least squares (RLS) – I algorithm and stochastic approximation with averaging of $\alpha = 0.8$ - V algorithm.

The best results for this type of ARX model shows the method of recursive least squares (RLS) because of its logarithmic value of errors which are minimal in negative values for all number of simulations and the second best algorithm is stochastic approximation with averaging for α=0.8. It is necessary to note that for the other random variables of e(k) and u(k) the best identification method remains recursive least square method, but the second best algorithm is one of the stochastic approximation with averaging. This becomes due to the fact that for the different value of inputs system will show its different characteristic described with system parameters, but the recursive least square method will at the best way do the system identification in all cases.

All simulations were done software package MATLAB [3], which code exceed the scope of this article.

REFERENCES:

[1] Sasa Lj. Prodanovic,Vesna S. Brasic „Simulation results of parameter estimation for a given ARX model-system identification", Proceedings of VIII International Conference "Heavy Machinery-HM 2014", Zlatibor, 25-28 June 2014

[2] Polyak, B.T. (1990), New method of stochastic approximation type. Automation and Remote Control, 51, pp. 937-946

[3] Comuter Software: Gemax Laboratory Solutions, (2009), MATLAB and Simulink, Version:7.8.0.347 (The Language of Technical Computing); Licence Number: 161051; produced by The MathWorks Inc.

[4] Ljung, L (1999), System Identification. Theory for the User.Prentice – Hall, New Jersey

Robust Recursive Identification of Multivariable Processes

Vladimir Đorđević[1*], Vojislav Filipović[1]
[1]Faculty of Mechanical and Civil Engineering, University of Kragujevac, Kraljevo (Serbia)

Many industrial processes have the multivariable nature (boiler plant, evaporators, distillation columns, etc.). One of the key requests of production is energy saving and product quality improvement (these two categories are tightly connected). In order to achieve this it is necessary to carefully design process control strategies. Therefore, the quality mathematical model of the process is needed. In this paper it is assumed that the process is described with multivariable ARX (AutoRegressive model with eXogenous input) model. The key assumption, justified with numerous studies of real processes, is that the stochastic disturbance has non-Gaussian distribution. That fact affects on form of recursive identification algorithm. The algorithm becomes nonlinear. Simulations are performed that demonstrate the superiority of the proposed algorithm over the standard algorithms.

Keywords: Multivariable systems, ARX model, Non-Gaussian distribution, Robust recursive identification

1. INTRODUCTION

The task of identification is estimation of unknown dynamics based on measurement data. This is a key ingredient for areas of adaptive control and adaptive signal processing. Theory of identification covers wide range of problems [1]-[5]. New impulse in the development of the theory is given by the area of statistical learning theory [6]-[9].

Multivariable systems represents very important class of systems in practice. Special attention is devoted to their identification [10]-[13]. In this area, the problem of identification is considered in the deterministic framework or with the assumption that the stochastic disturbance has a Gaussian distribution. Intense practical studies [14]-[15] have not shown justification of the assumption of normal distribution of disturbances. Namely, in population of observations there are rare large observations and the result is that stochastic disturbance has a non-Gaussian distribution. As a result, the efficiency of the identification algorithm based on the assumption of the Gaussian distribution of disturbances is reduced. Because of this, a great effort has been invested for the synthesis of robust identification algorithms that have low sensitivity to changes in the disturbance distribution. The fundamental contribution, in this sense, was given by Huber [16-17] who laid the foundations of an area known as robust statistics. This theory, rather than the assumption of exactly known distribution of the stochastic disturbance, introduces the assumption of a priori known distribution class to which the disturbance belongs. The application of these ideas in system identification is exposed in [18-20], and in adaptive control in [21-22].

A single-input single-output (SISO) system is considered in references [18-22]. In this paper, the robust recursive identification of multivariable ARX models is considered. It is assumed that the classes of probability distributions, to which stochastic disturbances and unknown parameters of the dynamic system belong, are known. A priori information on the disturbances introduces a nonlinear transformation of the prediction error, which makes the nonlinear recursive algorithm, and a priori information on the parameters defines the initial conditions of the algorithm for the parameter vector and the gain matrix.

At the end of the paper, simulations that illustrate the behaviour of the robust identification algorithm are presented.

2. MULTIVARIABLE ARX MODEL

Assume that the considered system is described with linear multivariable ARX model with r-dimensional input and p-dimensional output

$$A(q^{-1})y_k = B(q^{-1})u_k + w_k \tag{1}$$

where $A(q^{-1})$ and $B(q^{-1})$ are matrix polynomials in the shift-back operator $q^{-1}y_k = y_{k-1}$. Degrees of polynomials $A(q^{-1})$ and $B(q^{-1})$ are n and m, respectively

$$A(q^{-1}) = I + A_1 q^{-1} + \ldots + A_n q^{-n} \tag{2}$$

$$B(q^{-1}) = B_1 q^{-1} + \ldots + B_m q^{-m} \tag{3}$$

where $A_i\,(i = 1,2,\ldots,n)$ are $p \times p$ matrices, and $B_i\,(i = 1,2,\ldots,m)$ are $p \times r$ matrices.

The stochastic disturbance $\{w_k\}$ is a martingale-difference in relation to the nondecreasing family of σ-algebras $\{F_k\}$.

Unknown matrices' coefficients are

$$(\theta^M)^T = [A_1, A_2, \ldots, A_n, B_1, B_2, \ldots, B_m] \tag{4}$$

Now model can be written in following form

$$y_k = (\theta^M)^T X_k + w_k \tag{5}$$

where

$$X_k^T = [-y_{k-1}^T \ldots y_{k-n}^T u_{k-1}^T \ldots u_{k-m}^T], \qquad X_k \in \mathbb{R}^{(np+mr)\times 1} \tag{6}$$

Let us introduce the matrix

$$\varphi_k = \begin{bmatrix} X_k^T & & 0 \\ & \ddots & \\ 0 & & X_k^T \end{bmatrix} = I \otimes X_k^T \tag{7}$$

where $\otimes$ denotes Kronecker product.

*Corresponding author: Dositejeva 19, 36000 Kraljevo (Serbia) and djordjevic.v@mfkv.kg.ac.rs

A $p \times r$ matrix $U = \left[u_{ij} \right]$ is introduced. Let us define the operator "col" as the operator that generates a column vector by setting the columns of the matrix U one below the other.

$$\text{col } U = \begin{bmatrix} U^1 \\ U^2 \\ U^r \end{bmatrix}, \text{col } U \in \mathbb{R}^{pr \times 1} \tag{8}$$

Based on (8) following vector is introduced

$$\theta = \text{col } \theta^M \tag{9}$$

Using relation (5), (7) and (9) vector form of multivariable ARX model is obtained

$$y_k = \varphi_k \theta + w_k \tag{10}$$

where $\varphi_k \in \mathbb{R}^{p \times p(np+mr)}$ and $\theta \in \mathbb{R}^{p(np+mr) \times 1}$.

We will further consider the problem for a random vector:

$$w_k^T = \left[w_k^1 w_k^2 ....w_k^p \right] \tag{11}$$

Let us assume that components of the vector w_k are independent. Each component has the approximately normal distribution:

$$p_i\left(w_k^i\right) = (1-\varepsilon) N\left(0, \sigma_i^2\right) + \varepsilon G\left(w_k^1\right), \ i = 1,2,...,p \tag{12}$$

Applying Huber’s methodology, the least favourable probability density on a class of approximately normal distributions is obtained.

$$p_i^*\left(w_k^i\right) = \begin{cases} \dfrac{1-\varepsilon}{2\pi\sigma_i} \exp\left\{ -\dfrac{\left(w_k^i\right)^2}{2\sigma_i^2} \right\}, & \left|w_k^i\right| < k_\varepsilon \\ \dfrac{1-\varepsilon}{2\pi\sigma_i} \exp\left\{ -\dfrac{k_\varepsilon}{\sigma_i^2} \left(\left|w_k^i\right| - \dfrac{k_\varepsilon}{2} \right) \right\}, & \left|w_k^i\right| > k_\varepsilon \end{cases}$$

(13)

where the relationship between the contamination degree ε and the parameter k_ε of Huber’s function is given by the following relation:

$$\frac{2\Phi_N\left(k_\varepsilon\right)}{k_\varepsilon} - 2\Phi_N\left(-k_\varepsilon\right) = \frac{\varepsilon}{1-\varepsilon}, \quad \Phi_N(x) = \frac{1}{\sqrt{2\pi}} \int_{-\infty}^{x} e^{-\frac{y^2}{2}} dy$$

(14)

Due to the independence of the components of the vector w_k, the least favourable probability density of the vector w_k will be:

$$p^*\left(w_k\right) = \prod_{j=1}^{p} p_i^*\left(w_k^i\right) \tag{15}$$

On the basis of (15), based on the maximum likelihood methodology, it can be defined the loss function:

$$\Phi(x) = -\log p^*(x) \ , \ \Phi(\cdot): R^p \to R^1 \tag{16}$$

and based on it, the identification criterion can be defined:

$$J_1(\theta) = E\left\{ \Phi\left(e_k\right) \right\} \ , \tag{17}$$

$$e_k = y_k - \varphi_k \theta \tag{18}$$

where $E\{\cdot\}$ represents the mathematical expectation operator. The criterion (17) generates robust (optimal on the class) algorithms.

Now let us define, more closely, the system distribution G in the relation (16). We will assume that it has a normal distribution with a significantly greater variance than the first component N. The form of the probability density of the non-Gaussian distribution of the stochastic disturbance w_k for the i-th component is:

$$p_i\left(w_k^i\right) = \frac{1-\varepsilon}{\sigma_{1i}\sqrt{2\pi}} \exp\left\{ -\frac{\left(w_k^i\right)^2}{2\sigma_{1i}^2} \right\} + \frac{\varepsilon}{\sigma_{2i}\sqrt{2\pi}} \exp\left\{ -\frac{\left(w_k^i\right)^2}{2\sigma_{2i}^2} \right\}$$

$$, \ \sigma_{2i}^2 \gg \sigma_{1i}^2 \tag{19}$$

On the basis of Huber’s approach, it is obtained a criterion $J_1(\theta)$ that generates algorithms which are optimal on the class.

3. ROBUST RECURSIVE ALGORITM

For the synthesis of a robust recursive algorithm for identification of multivariable systems, the model (10) and the empirical functional will be used.

$$J_{rk}\left(\theta_k\right) = \frac{1}{k} \sum_{i=1}^{k} \Phi\left(e_j\right) + \frac{1}{k} L\left(\theta_a - \theta\right) \tag{20}$$

where $L\left(\theta_a - \theta\right)$ is the loss function, on the basis of fiducial probability.

The recursive minimization of the criterion (20) can be realized by applying the Newton-Raphson algorithm:

$$\theta_k = \theta_{k-1} - \left[k\nabla_\theta^2 J_{rk} \theta_{k-1} \right]^{-1} \left[k\nabla_\theta J_{rk}\left(\theta_{k-1}\right) \right] \ , \tag{21}$$

Based on the relation (20) it follows:

$$J_{rk}(\theta) = \frac{k-1}{k} \left\{ \frac{1}{k-1} \sum_{j=1}^{k-1} \Phi\left(e_j\right) + \frac{1}{k-1} \Phi\left(e_k\right) + \frac{1}{k-1} L\left(\theta_a - \theta\right) \right\} =$$

$$= \frac{k-1}{k} \left\{ J_{r(k-1)}(\theta) + \frac{1}{k-1} \Phi\left(e_k\right) \right\}$$

(22)

Using the relation (22) it is obtained:

$$k\nabla_\theta J_{rk}(\theta) = (k-1) \nabla_\theta J_{r(k-1)}(\theta) + \nabla_\theta \Phi\left(e_k\right) \tag{23}$$

We will now list an auxiliary result in a form of lemma.

Lemma 1 Let us define $x \in R^m$, the vector function $y(x) \in R^n$ and real function $f(y) \in R^1$. Then

$$\frac{\partial f(y(x))}{\partial x} = \frac{\partial y^T(x)}{\partial x} \frac{\partial f(y)}{\partial y} \ \blacksquare$$

In accordance with **Lemma 1** for the last member in relation (23), it is obtained:

$$\nabla_\theta \Phi\left(e_k\right) = \left(\frac{\partial\left(e_k\right)}{\partial\theta} \right)^T \frac{\partial\Phi\left(e_k\right)}{\partial\left(e_k\right)} = -\varphi_k^T \psi\left(e_k\right) \tag{24}$$

in which

$$\psi(x) = -\nabla_x \ln p(x) \ , \ \psi(x) \in R^{px1} \tag{25}$$

$$e_k = y_k - \varphi_k \theta \tag{26}$$

For large k, the following relation holds:

$$\nabla_\theta J_k(k-1)\left(\theta_{k-1}\right) \cong 0 \tag{27}$$

Based on relations (23), (24) and (27) finally, for the first derivative of the functional, it is obtained:

$$k\nabla_{\theta} J_{rk}\left(\theta_{k-1}\right) = -\varphi_k^T \psi\left(e_k\right) \tag{28}$$

Now we will observe the functional $J_1\left(\theta\right)$, defined by the relation (17). This gives:

$$\nabla_{\theta}^2 J_1\left(\theta\right) = \nabla_{\theta\theta^T} J_1\left(\theta\right) = E\left\{\varphi_k^T \psi'\left(e_k\right)\varphi_k\right\} \tag{29}$$

where $\psi'\left(\cdot\right) \in R^{pxp}$

For large k, at the point θ_{k-1} it holds that:

$$e_k \cong w_k \tag{30}$$

Let us note:

$$E\left\{\varphi_k^T \psi'\left(w_k\right)\varphi_k\right\} = Etr\left\{\varphi_k \varphi_k^T \psi'\left(w_k\right)\right\} = trE\left\{\varphi_k \varphi_k^T \psi'\left(w_k\right)\right\}$$
$$= trE\left\{\varphi_k \varphi_k^T\right\} E\left\{\psi'\left(w_k\right)\right\} = trE\left\{\varphi_k \varphi_k^T\right\} \cdot M =$$
$$trE\left\{\varphi_k \varphi_k^T M\right\} = E\left\{\varphi_k^T M \varphi_k\right\} \tag{31}$$

in which $M = E\left\{\psi'\left(w_k\right)\right\}$.

Based on (31) it follows:

$$\nabla_{\theta}^2 J_1\left(\theta_{k-1}\right) \cong E\left\{\varphi_k^T M \varphi_k\right\} \tag{32}$$

Approximating of the mathematical expectation operator, it follows from the last relation:

$$\nabla_{\theta}^2 J_1\left(\theta_{k-1}\right) = \frac{1}{k}\sum_{i=1}^{k} \varphi_j^T M \varphi_j \tag{33}$$

On the other side, for the second member of the empirical functional (20), it holds that:

$$L\left(\theta_a - \theta\right) = -\ln p_f^*\left(\theta_a - \theta\right) =$$
$$\ln\frac{1}{\left(2\pi\right)^{d/2}\left(\det S_a\right)^{1/2}} + \frac{1}{2}\left(\theta_a - \theta\right)^T S_a^{-1}\left(\theta - \theta_a\right) \tag{34}$$

The first and the second derivative of $L\left(\theta_a - \theta\right)$ have the following forms, respectively:

$$\nabla_{\theta} L\left(\theta_a - \theta\right) = S_a^{-1}\left(\theta_a - \theta\right) \tag{35}$$

$$\nabla_{\theta}^2 L\left(\theta_a - \theta\right) = S_a^{-1} \tag{36}$$

From relations (20), (33) and (36) it follows that:

$$k\nabla^2 J_{rk}\left(\theta_{k-1}\right) = \sum_{i=1}^{k} \varphi_j^T M \varphi_j + S_a^{-1} \tag{37}$$

We will now determine more precisely the size of M in the relation (37). From the relation (32), taking into account the independence of components w_{ki} $\left(i = 1, 2, ..., p\right)$, it follows that:

$$M = \begin{bmatrix} \dfrac{\partial \psi_1\left(w_{k1}\right)}{\partial w_{k1}} & & 0 \\ & \ddots & \\ 0 & & \dfrac{\partial \psi_p\left(w_{kp}\right)}{\partial w_{kp}} \end{bmatrix} \tag{38}$$

Based on the relation (15) it is obtained:

$$\psi_i\left(w_{ki}\right) = -\frac{\left(p^*\left(w_{ki}\right)\right)'}{p^*\left(w_{ki}\right)} \tag{39}$$

Also, it holds:

$$E\left\{\psi_i'\left(w_{ki}\right)\right\} = \int_{-\infty}^{\infty} \psi'\left(w_{ki}\right) p^*\left(w_{ki}\right) dw_{ki} \tag{40}$$

For symmetrical probability distributions it holds that:

$$\psi_i\left(w_{ki}\right) = -\psi_i\left(-w_{ki}\right) \tag{41}$$

Using relations (39) - (41) and applying a partial integration of the relation (40) it is obtained:

$$\int_{-\infty}^{\infty} \psi_i'\left(w_{ki}\right) p_i^*\left(w_{ki}\right) dw_{ki} = -\int_{-\infty}^{\infty} \psi_i\left(w_{ki}\right) \frac{p_i^*\left(w_{ki}\right)'}{p_i^*\left(w_{ki}\right)} p_i^*\left(w_{ki}\right) dw_{ki} =$$
$$= \int_{-\infty}^{\infty} \frac{\left(p_i^*\left(w_{ki}\right)'\right)^2}{\left(p_i^*\left(w_{ki}\right)\right)^2} p_i^*\left(w_{ki}\right) dw_{ki} = E\left\{\frac{\left(\left(p_i^*\left(w_{ki}\right)'\right)\right)^2}{\left(p_i^*\left(w_{ki}\right)\right)^2}\right\} = I_i\left(p_i^*\right) \tag{42}$$

where $I_i\left(p_i^*\right)$ is the Fisher information. The matrix M is, therefore, diagonal with diagonal elements $I_i\left(p_i^*\right)$ $\left(i = 1, 2, ..., p\right)$, i.e. $M = diag\left\{I_1\left(p_i^*\right), ..., I_p\left(p_i^*\right)\right\}$.

For the probability distribution (19), which is discussed in this paper, the Fisher information are:

$$I_i\left(p_i^*\right) = \frac{1}{\left(1-\varepsilon\right)\sigma_{1i}^2 + \varepsilon\sigma_{2i}^2} \quad , \quad \varepsilon \in \left[0, 1\right) \quad , \quad \sigma_{2i}^2 \gg \sigma_{1i}^2 \quad ,$$
$$\left(i = 1, 2, ..., p\right) \tag{43}$$

Based on relations (21), (29) and (37) it is obtained:

$$\theta_k = \theta_{k-1} + \left[\sum_{i=1}^{k} \varphi_j^T M \varphi_j + S_a^{-1}\right]^{-1} \varphi_k^T \psi\left(e_k\right) \tag{44}$$

Let us introduce the matrix P_k

$$P_k = \left[\sum_{i=1}^{k} \varphi_j^T M \varphi_j + S_a^{-1}\right]^{-1} \tag{45}$$

Let us note that for the class of probability distribution (19), a nonlinear transformation of the prediction error is Huber’s function:

$$\psi_i\left(e_{ki}\right) = \max\left\{-k_{\varepsilon} \quad , \quad \min\left(k_{\varepsilon}, e_{ki}\right)\right\} \tag{46}$$

and its derivative $e_k \cong w_k$

$$\psi_i'\left(w_{ki}\right) = \begin{cases} 1 & \left|w_{ki}\right| < k_{\varepsilon} \\ 0 \ , & otherwise \end{cases} \tag{47}$$

From relations (44) and (45), by applying the matrix inversion lemma to the relation (45), the recursive robust identification algorithm is obtained. The explicit form of the algorithm is given in the following table where the notation $N\left(\theta_N \, \Sigma_N\right)$ denotes a normal distribution with the mean θ_N and the covariance matrix Σ_N.

Robust recursive Algorithm

- A priori information of stochastic disturbance

$$P = (1-\varepsilon) N(0,\Sigma_1) + \varepsilon N(0,\Sigma_2), \quad \varepsilon = [0,1)$$

$$\Sigma_1 = \begin{bmatrix} \sigma_{11}^2 & & 0 \\ & \ddots & \\ 0 & & \sigma_{1p}^2 \end{bmatrix}, \qquad \Sigma_2 = \begin{bmatrix} \sigma_{21}^2 & & 0 \\ & \ddots & \\ 0 & & \sigma_{2p}^2 \end{bmatrix}$$

$$\sigma_{1i}^2 \ll \sigma_{2i}^2, \qquad (i = 1,2,\ldots,p)$$

- A priori information of parameters

$$P_f = N(\theta_a, S_a)$$

- Estimation of parameters

$$\theta_k = \theta_{k-1} + P_k \varphi_k^T \psi(e_k)$$

$$e_k = y_k - \varphi_k \theta_{k-1}$$

- Matrix gain

$$M = \begin{bmatrix} \dfrac{1}{(1-\varepsilon)\sigma_{11}^2 + \varepsilon\sigma_{21}^2} & & 0 \\ & \ddots & \\ 0 & & \dfrac{1}{(1-\varepsilon)\sigma_{1p}^2 + \varepsilon\sigma_{2p}^2} \end{bmatrix}$$

- Initial condition of the algorithm

$$\theta_0 = \theta_a$$

$$P_0 = S_a$$

- Nonlinear transformation of prediction error and its derivate

$$\psi_i(e_{ki}) = \max\{-k_\varepsilon, \min(k_\varepsilon, e_{ki})\}$$

$$\psi_i'(w_{ki}) = \begin{cases} 1 & |w_{ki}| < k_\varepsilon \\ 0 & otherwise \end{cases}$$

$$(i = 1,2,\ldots,p)$$

4. SIMULATION RESULTS

For the simulation purpose the ARX model with one input and two outputs has been used:

$$y_k + A_1 y_{k-1} + A_2 y_{k-2} = B_1 u_{k-1} + B u_{k-2} + w_k$$

where

$$A_1 = \begin{bmatrix} 0 & 0,5 \\ 1 & 0 \end{bmatrix}, \quad A_2 = \begin{bmatrix} 1,2 & 0 \\ 0 & 0,5 \end{bmatrix}$$

$$B_1 = \begin{bmatrix} 0 \\ 1 \end{bmatrix}, \qquad B_2 = \begin{bmatrix} 2 \\ 3 \end{bmatrix}$$

$u_k \sim N(0,1)$ and $w_k \sim (1-\varepsilon)N(0,1) + \varepsilon N(0,100)$ for different values of contamination ε .

Figures 1-4 show errors for different values of contamination.

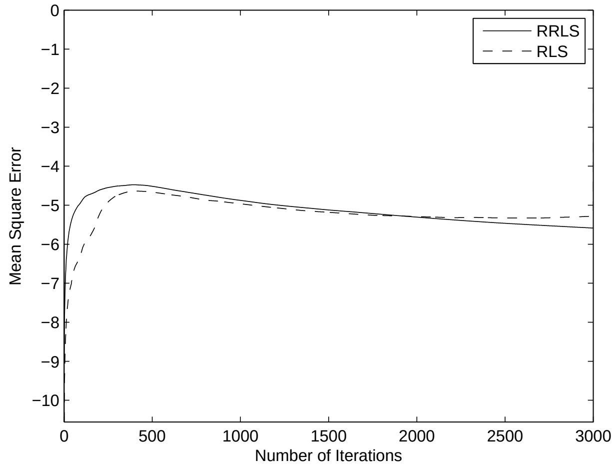

Figure 1: Errors of RRLS and RLS algorithm for $\varepsilon = 0,05$

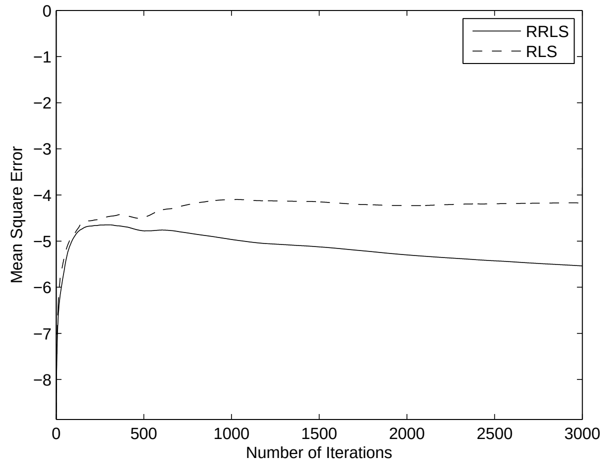

Figure 2: Errors of RRLS and RLS algorithm for $\varepsilon = 0,1$

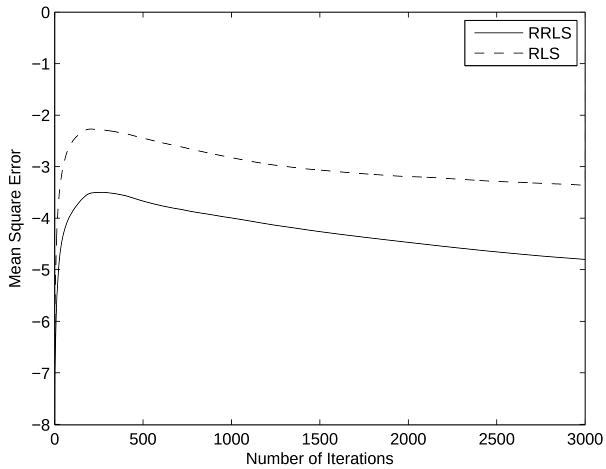

Figure 3: Errors of RRLS and RLS algorithm for $\varepsilon = 0,15$

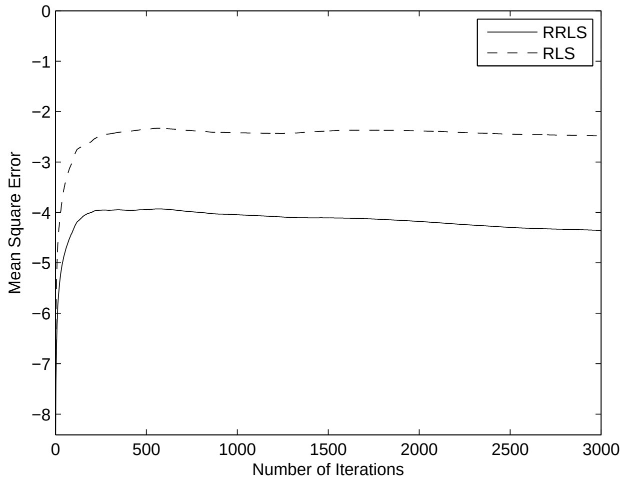

Figure 4: Errors of RRLS and RLS algorithm for $\varepsilon = 0,2$

Figures 5-7 show estimated parameters of matrices A_1, A_2, B_1 and B_2 for contamination $\varepsilon = 0.15$. Solid lines show parameters estimated with robust recursive algorithm, dashed lines show parameters estimated with recursive algorithm, and dotted lines show exact values.

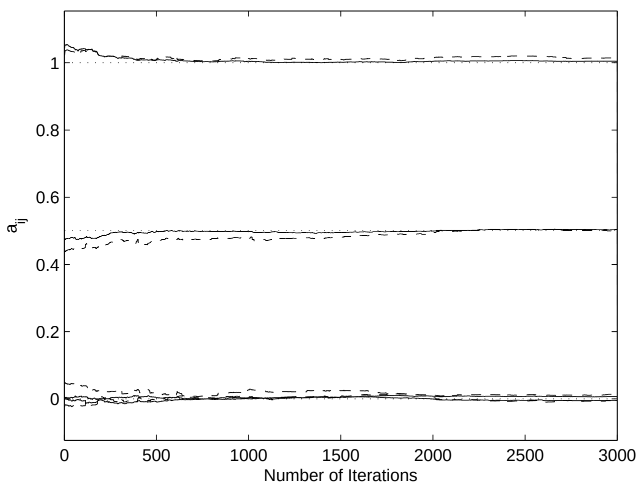

Figure 5: Estimated parameters of matrix A_1 *for* $\varepsilon = 0,15$

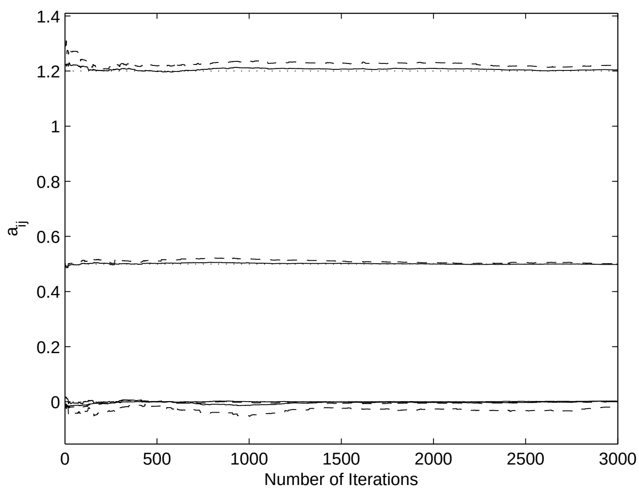

Figure 6: Estimated parameters of matrix A_2 *for* $\varepsilon = 0,15$

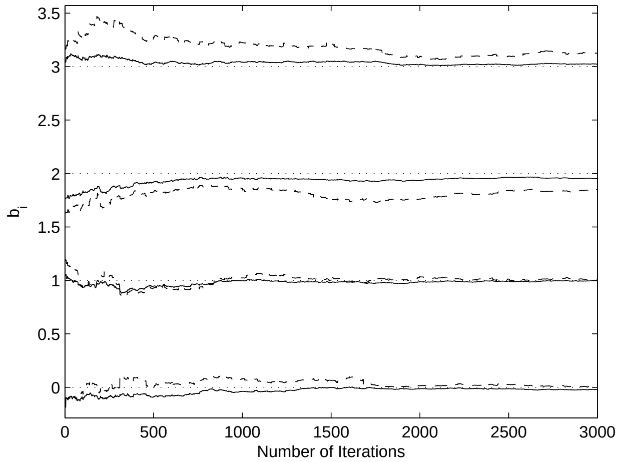

Figure 7: Estimated parameters of matrices B_1 *and* B_2 *for* $\varepsilon = 0,15$

5. CONCLSION

This paper considers the problem of parameter estimation of multivariable ARX models. It assumed that measurements are disturbed by Non-Gaussian noise.

Simulation results have demonstrated the efficiency of the proposed robust estimation method in the presence of outliers.

ACKNOWLEDGEMENTS

The authors wish to express their gratitude to the Ministry of Education, Science and Technological Development of the Republic of Serbia for supporting this paper through project TR33026 and project TR33027.

REFERENCES

[1] L. Ljung, "System Identification: Theory for the User," Prentice-Hall, New Jersey (USA), (1999)

[2] R. Isermann and M. Münchhof, "Identification of Dynamic System," Springer, Berlin (Germany), (2011)

[3] F. Giri and E. Bai (eds.), "Block-Oriented Nonlinear System Identification", Springer, Berlin (Germany), (2011)

[4] Tsybakov A. , "Introduction to Nonparametric Estimation", Springer, London (England), (2009)

[5] A. Djouambi, A. Voda and A. Charef, "Recursive Prediction Error Identification of Fractional Order Models", Communications in Nonlinear Science and Numerical Simulation, Vol. 17, pp. 2517-2524, (2012)

[6] T. Hastie, R. Tibshirani and J. Friedman, "The Elements of Statistical Learning", Springer, Berlin (Gremany), (2001)

[7] C. Rasmussen and C. Williams, "Gaussian Processes for Machine Learning", MIT Press, Massachusetts (USA), (2006)

[8] Y. Tang, Z. Li and N. Guan, "Identification of Nonlinear System Using Extreme Learning Machine Based Hammerstein Model", Communication in Nonlinear Science and Numerical Simulation, Vol. 19 ,pp. 3171-3183, (2014)

[9] L. Ljung and T. Chen, "Convexity Issue in System Identification", 10th IEEE International Conference on Control and Automation (ICCA), Hangzhou (China), 12-14 June 2013, pp. 1-9 (2013)

[10] Y. Zhu, "Multivariable System Identification for Process Control", Elsevier Science, London (England), (2000)

[11] K. Chan, J. Bao and W. Whten, "Identification of MIMO Hammerstein Systems Using Cardinal Spline Function", Journal of Process Control, Vol. 16, pp. 659-670, (2006)

[12] J. Liu and F. Ding, "Convergence Properties of the Least Squares Estimation Algorithm for Multivariable Systems", Applied Mathematical Modelling, Vol. 37, pp. 476-483, (2013)

[13] M. Darby and M. Nikolaou, "Identification Test Design for Multivariable Model-Based Control: An Industrial Perspective", Control Engineering Practice, Vol. 22, pp. 165-180, (2014)

[14] V. Barnett and T. Lewis, "Outliers in Statistical Data", Third Edition, Wiley, New Your (USA), (1994)

[15] R. Pearson, "Exploring Data in Engineering – The Sciences, and Medicine", Oxford University Press, Oxford (England), (2011)

[16] P. Huber, "Robust Estimation of a Location Parameter", Annals of Mathematical Statistics, Vol. 35, pp. 73-101, (1964)

[17] P. Huber and E. Ronchetti, "Robust Statistic", Wiley, London (England), (2009)

[18] Y. Tsypkin and B. Polyak, "Adaptive Estimation Algorithms: Convergence, Optimality, Stability", Automation and Remote Control, Vol. 43 pp. 71-81, (1979)

[19] Y. Tsypkin, "Foundations of Information and Identification Theory (in Russian)", Nauka, Moscow (Russia), (1984)

[20] V. Filipović and B. Kovacević, "On Robust AML Identification Algorithms", Automatica, Vol. 30, pp. 1775-1778, (1994)

[21] V. Filipović and B. Kovacević, "On Robustness of Adaptive Minimum Variance Controller", International Journal of Control, Vol. 65, pp. 117-129 (1996)

[22] V. Filipović, "Stochastic Multivariable Self-Tuning Tracker for Non-Gaussian Systems", International Journal of Applied Mathematics and Computer Science, Vol. 15, pp. 351-357 (2005)

SESSION E

MACHINE DESIGN AND MECHANICS

Gear Drive Unit with Continual Variation of Transmission Ratio

Sanja Vasin[1*], Milosav Ognjanović[1], Marko Miloš[1]
[1]Faculty of Mechanical Engineering/Machine Design Department, University of Belgrade, Belgrade (Serbia)

In wind power exploitation, electricity production depends of winds nature and availability in the year. For capturing the wind, it is possible to make an optimal layout of Wind Turbines (WT) in the field, but the main problem remains - existing WT's produce electricity with variable frequency due to wind speed variation. Therefore, to be synchronized with electric net, frequency must be rectified which causes significant power losses in the system. Subject of this work is a new type of WT gearbox, which can provide direct synchronization with electric net, based on its ability to continually vary the transmission ratio according to wind speed variation. It is a hybrid gearbox consisting of mechanical system which includes specific design of two stage planetary gearbox with total transmission ratio i=1/25, and one planetary gear set for continual variation of transmission ratio (CVT) together with electro-electronic system and control system based on corresponding software system. The objective of the paper is to present design structure of gear drive unit, operating process of the system and design procedure for this hybrid technical systems development.

Keywords: Planetary gear units, Wind turbines, CVT

1. INTRODUCTION

From the perspective of wind as renewable source of energy for exploitation and use in electricity production, potential is very high. Due to variation of wind speed and power, existing wind turbines produce electricity with variable frequency, which has to be synchronized with public electric net. Synchronization process demands continuous rectification of frequency, which leads to overall power losses. From perspective of engineering design development of wind power system was mainly focused on rotor and electric generator design and control system. Such approach resulted with no significant increase in of system efficiency. There is an on-going tendency to allocate development focus from rotor and generator to WT gear transmission design and operating principle. Present gear transmissions do not have capability to change transmission ratio. Design is oriented to gearbox mass and size reduction, good load distribution between planetary gears, reduction of bearing reaction forces, gain of maximal torque and transmission ratio and in combination with CVT hydraulic converter, with all designs having fixed transmission ratio. Principle of Hansen uses two normal gearboxes and one planetary gearbox connected to rotor to give transmission ratio i=100, for WT up to 5MW power. Winergy design has connected rotor to planetary gearbox carrier with ring gear fixed in housing and sun gear on exit, to gain maximal transmission ratio. Renk designed Multibird by putting double row of planets in mesh with ring gear, which is connected to rotor. This design solution is applicable for middle range speeds (200rpm). Maag gives another solution - DPPV design with load transfer from rotor to planet carrier of first transmission stage, and to ring gear of second transmission stage. Exit shaft is connected to sun gear of first stage. Bard VMW patent is similar to Maag with multiple planets for maximal increase of torque and reduction of bearing reaction forces. With GDC-s, patent Flex-pin good load distribution between planets is provided. Voith is proposing WinDrive, double planetary gear set with CVT hydraulic converter, connected to synchronous generator with constant speed and generated frequency of 50Hz. There is no need for frequency conversion but solution is applicable only for drivetrains with fixed transmission ratio, Höhn [1]. For achievement of more efficient, reliable and economical wind power systems, researches haw turned to implementation of CVT system between WT and generator. For behavior analysis, numerical simulations have been applied [2]. Experimental evaluation of in order to prove suitability of CVT in Wind power systems, has been performed for two operating scenarios, with CVT as ordinary gearbox with constant transmission ratio, and second with CVT as variable ratio gearbox. Comparing results with variable transmission ratio, increase of annual produced energy with high percentage can be achieved [3]. Hybrid machine is a machine where its drive system integrates two types of motors - the servo motor and the CV (constant velocity) motor. Due to lack of control system, CV motor introduces fluctuations to servomotor and system. Control strategy demands modeling of fluctuations and incorporation in controller of servomotor [4]. Intelligent WT control is based on data mining, model predictive control, and evolutionary computation, with multi-objective model, in response to variable wind conditions and operational requirements [5]. Integration of hardware and software system results in mechatronic structure, which can be achieved with simultaneous design. Aim is to find an optimal balance between mechanical and electro-electronic and software control, based on embedded control functions and system integrity [6]. Developed software tools for system identification are based on functional modes and requirements. Simulation mode allows user to evaluate main stages of identification from input design signal to model validation simultaneously and interactively on user specified dynamical system. Real data mode allows user to load experimental data's [7]. Researchers propose integration of V-model and modeling language for advanced mechatronic systems design, for good understanding between software and system design engineers; robust and adaptive control; support and quality

*Corresponding author: Kraljice Marije 16, 11120 Belgrade, e-mail: vasinsanja@gmail.com

assurance through whole design process; system overview at every stage, and compatibility with existing design techniques, [8].

The leading edge of this work is to develop a new type of WT gearbox with constant output rotation speed which will power the generator with ability of direct synchronization to electric net. For constant gearbox output speed, transmission ratio will continuously vary according to variation of wind power and speed. Design methodology of such system comprehends the synergy of mechanical, electro-electronic and software system, providing complete analysis, validation and verification of gearbox under wide range of operating conditions.

2. DESIGN OF GEAR TRAIN TRANSMISSION

2.1. Operating principle

In Figure 1 schematically is presented new wind turbine gearbox with marked positions of components vital for realization of gearbox operating principle. Depending on wind speed variation, gearbox has ability to vary the transmission ratio, providing all the time constant output rotation speed for generation of electricity with constant frequency of 50Hz, for the need of public electric net. Under wind influence, WT rotor is moving, giving the input speed to gearbox. Gearbox is connected to Wind rotor with elastic coupling (1), which is placed on the end of gearbox input shaft (2). By means of ring gear carrier (3), mechanical energy is being transferred from input shaft to the first planetary stage of gear unit. First stage consists of ring gear (4), which rotates together with its carrier (3) at speed of wind rotor. With its inner tooting, ring gear is in mesh with first set of five planet gears (5), which are supported with planet gears carrier (6). Planet gears are placed on axles (7) which are fixed with their position inside carrier. Second stage of planetary gear set consists of another ring gear (8), fixed without rotation in

the gear unit housing. With its inside tooting ring gear is in mesh with second set of five planet gears (9), which are the same as in the first set. Both planet gear sets are placed on the same axles. Two stage planetary gear unit has fixed transmission ratio, i=1/25 and is connected to another planetary gear unit with ability to vary the overall transmission ratio of gearbox. Through planet gears carrier (10) mechanical energy is transferred on set of three gear planets, which are on one side in mesh with ring gear (11) and on other side with sun gear (12). Ring gear (11) is toothed on both sides, inside and out and it is not fixed. Supported with its carrier (13), ring gear has freedom of rotation. With external tooting, ring gear is in mesh with gear (14) which is directly connected to motor-generator set (15). The output sung gear is directly connected to electric generator (16) with elastic coupling (17). Motor-generator set has an important role for variation of gearbox overall transmission ratio. When wind speed is low, motor-generator speeds up the ring gear (11), providing constant output speed of gear (12) and output shaft, which is coupled to input shaft of electric generator. When wind speed is high, motor-generator slows down ring gear (11) and provides constant output speed of gear transmission unit. Relation between electric generator (17) speed of rotation and motor generator (15) action is under control of electronic system and software, which together with mechanical gear transmission create hybrid technical system.

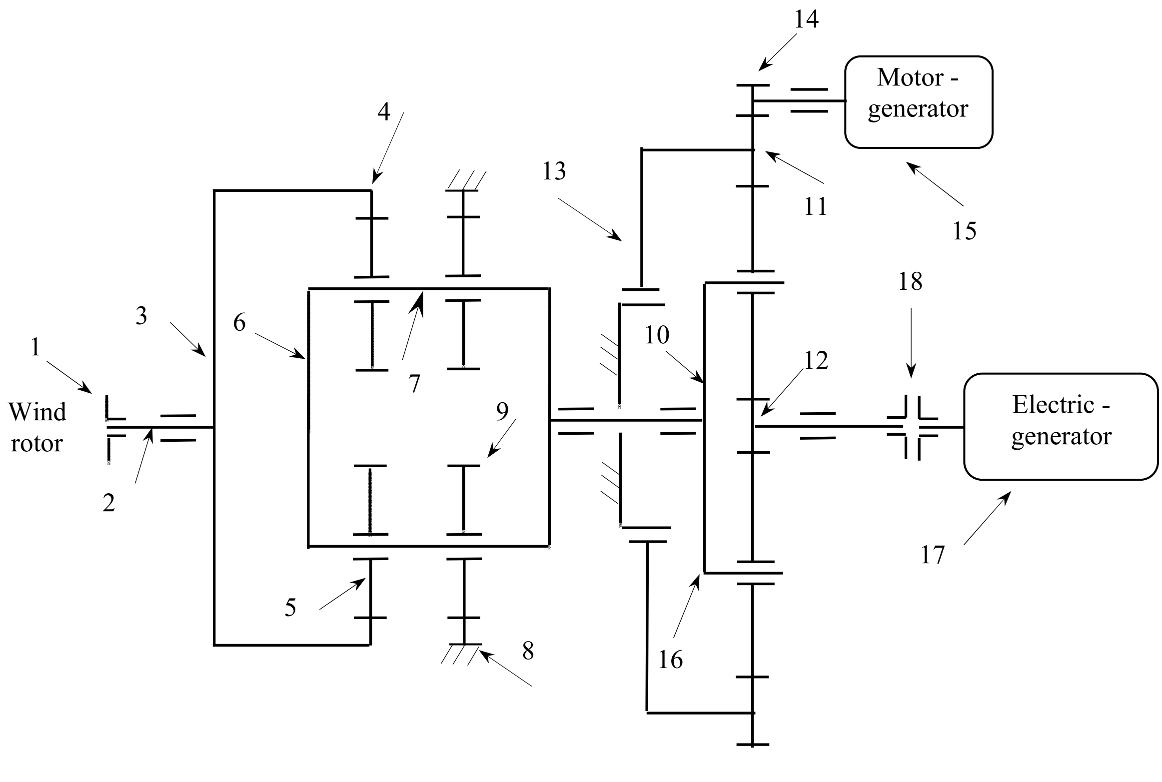

Figure 1: Schematic representation of WT gear transmission

2.2. Design of Planetary Gear Unit

Design of WT drive train is based on function requirements, material selection, robust design methodology and design constraints and parameters harmonization. Function requirements are input speed of gearbox 12rpm, which is equal to wind rotor operating speed, input torque of 1200kNm and output gearbox speed 1500rpm. These values correspond to transmission of 1.5MW mechanical power in the course of total operating life. Since wind and rotor speed vary, the operating power of gearbox also vary in the range of 0.4…2.5MW. To obtain the maximal load capacity with minimum of gearbox dimensions, material selection is made together with gear teeth thermal treatment (surface carbonized and grindeed teeth). Selection of design parameters is achieved by use of robust design methodology which includes possible stohastic operation conditions, and stohastic failure probability of gear teeth flanks. Main constraints in design parameters definition were desired gear drive reliability and duration of gear drive unit service life. In Figure 2 is presented a 3D model of new WT drive train design with emphasized design details. Gearbox design consists of two planetary gear stages. First planetary gear stage has fixed transmission ratio, *i*=1/25 while the other gear set has ability to vary the total transmission ratio of gearbox according to wind speed a

nd power variation. In Figure 2a, is presented 3D model of new WT drive train design with emphasized design details, Figure 2b and 2c.

Gear stage (i=1/25) includes shaft assembly, planet gears carrier, two sets of five planet gears, two ring gears and ring gear carriers. With elastic coupling, gearbox is connected to wind turbine rotor shaft. Rotor shaft has speed, which is also an input speed of gear unit. The planet gear and ring gear parameters are calculated and adopted. For calculated transmission ratio of planet gears and ring gear, i=4.89 and modulus, m_n=6 mm, planet gear has diameter, d_{pl1}=228 mm, and teeth number, z_{pl1}=38. For same modulus, ring gear has diameter, d_1=1116 mm, and teeth number, z_1=186. Gear width is same for planet gears and ring gear, b=153 mm. Housing of the unit and planetary gear carriers are welded design structures.

On entrance of gearbox housing, is placed a double-row cylindrical roller bearing (1) to support the gearbox input shaft (2) (Fig.2b). The input shaft has multiple roles in the system - to connect gearbox with rotor shaft, transfer the input load torque from rotor to ring gear, and to support the planet gears carrier (3).

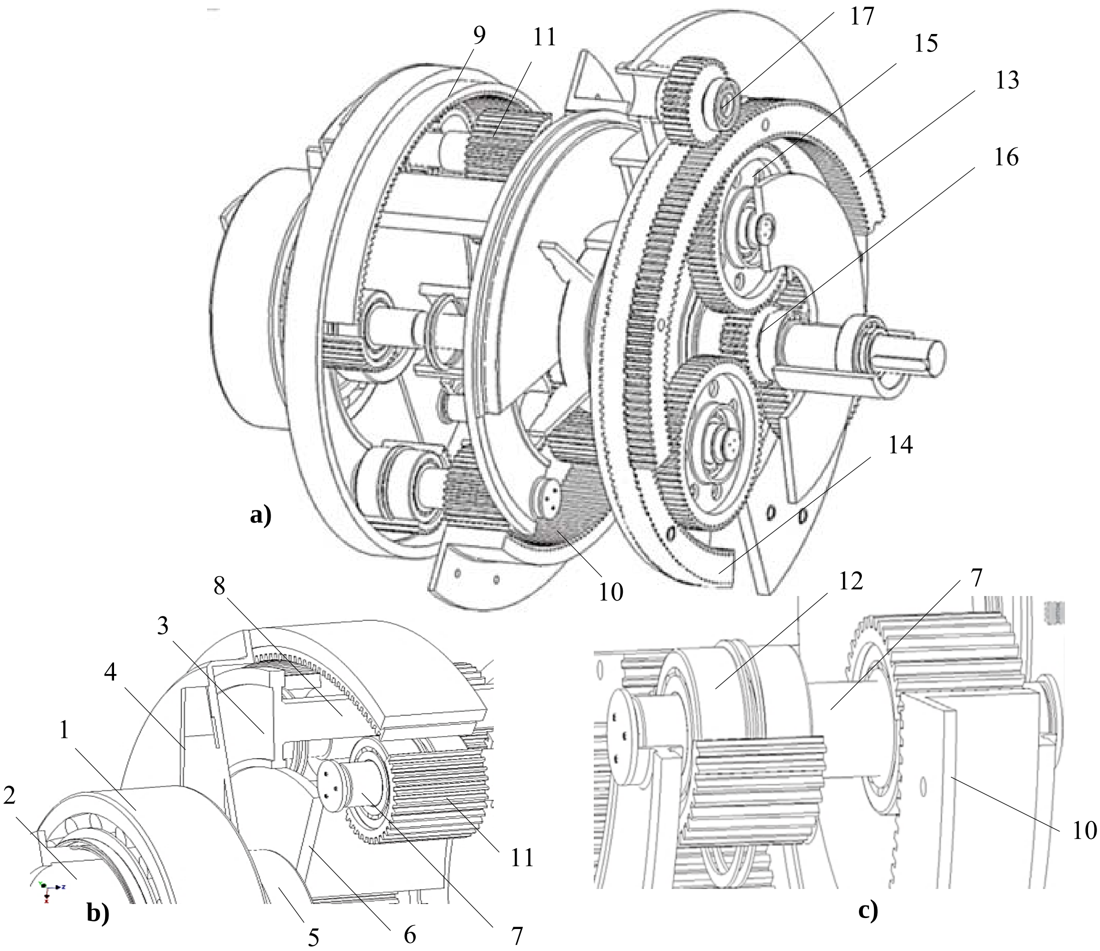

Figure 2: 3D model of gear unit a) Complete gear unit disposition b) Input side with first planetary gear set, c)Planet gears of gear unit past with fixed transmission ratio

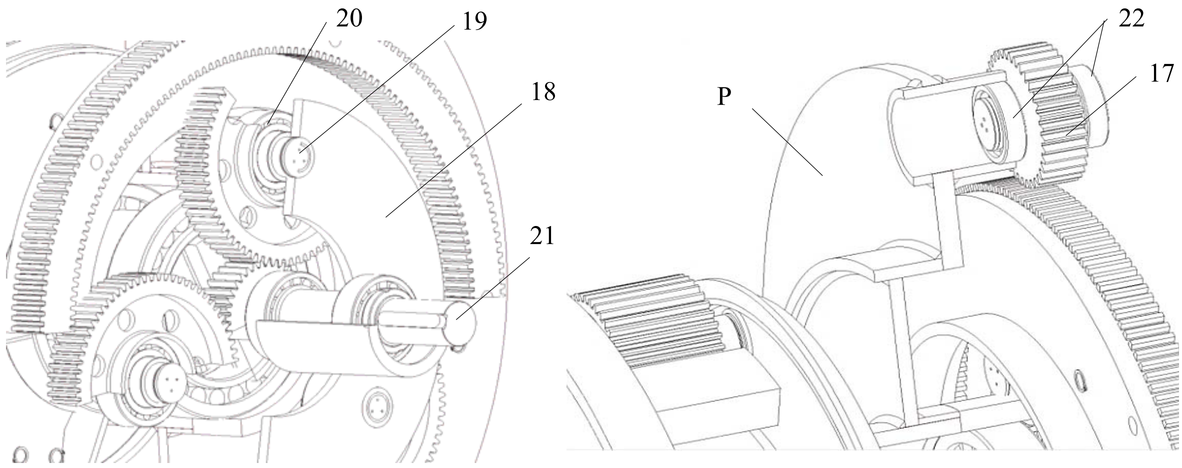

a) b)

Figure 3:Output planetary gear set for transmission ratio variation: a) Output shaft side, b) Motor-generator drive of both side toothed ring

This is provided with input shaft assembly design. The input shaft (2) is welded to ring gear carrier (4) on two places, first on left side of shaft and second on right end of shaft. Ring gear carrier (4) consists of one cylinder and three plates welded together and connected to the shaft supported with double-row cylindrical roller bearing (1). On inner ring, bearing is fastened with two fixing elements by means of screw joint. On outer ring, bearing is supported inside gearbox housing. Along cylinder, strengthening ribs' (4) are welded to provide the needed rigidity of ring gear carrier. The ribs are placed axisymmetric, with one end welded to cylinder and other end welded to carrier plate. Shaft assembly is connected to planet gears carrier *by* means of screw joint. To support the planet gears carrier (3), inside right end of shaft assembly, spherical roller bearing (5) is placed on console, which is welded to carriers plate. Carrier has two plates (6) with holes in which are placed axles (7) to support planets. Between plates are profiled ribs (8) to secure the rigidity of carrier.

First gear stage (i=1/25) contains two inside toothed ring gears, where one ring gear is input (drive) gear (9) and another one (10) is fixed, without rotation (Fig.2a). Both ring gears are in mesh, with two sets of five planet gears (11), giving the total transmission ratio, i=1/25 to the gear planets carrier (3). First set of planets is in mesh with input gear without a sun gear. Inside each planet is a pair of spherical roller bearings (12 – Fig.2c). Second set of planets is in mesh with ring gear, which is fixed inside gearbox housing. First set of planets is connected to other set with axles (7) which are fixed with their position inside planet gears carrier.

2.3. Design of Gear Set for Transmission Ratio Variation

Output planetary gear set provides continual variation of transmission ratio. This set consists of one ring gear toothed on both sides (13), inside and outside, ring gear carrier (14), set of three planets (15), sun gear (16) and additional gear (17), which is connected to motor-generator set (Fig.2a). In Fig. 3 is presented more design details of this assembly. The plate P in Fig. 3b is the part of gear unit housing and provides fix position of motor-generator pinion. In standing position of motor-generator, pinion is acting as the brake to both toothed ring. Standing position of planetary ring provides certain transmission ratio of planetary gear set. For increase of transmission ratio, motor-generator will operate as the motor and will rotate ring in one direction. For reducing of transmission ratio, direction of pinion and ring rotation has to be changed or to slow down. If motor-generator is acting as the brake of toothed ring, it is acting as electric generator. Control of direction and speed of motor-generator rotation provides electronic system together with software control.

This exit planetary set is separate assembly from planetary set with constant transmission ratio. These two assembles are connected through spline joint. The exit shaft of complete unit (Fig.2a and 3a) connects to coupling by the key, and the shaft is supported by the two bearings. The bearings are placed on shell, supporting the joint and ring gear carrier. The ring gear (13-Fig. 2a) has freedom of rotation, together with its carrier, around cylindrical roller bearing placed inside the central wall of gearbox housing. With its internal teeth system ring gear is in mesh with the three planet gears (15) supported with planet gears carrier (18-Fig.3). Planet gears carrier is directly connected to the first gear set. It consists of two plates welded together with strengthening ribs. Inside plates are holes in which are placed axles (19) to support the planet gears. Inside each planet is placed one cylindrical roller bearing (20), allowing the planet to rotate free around axle. Outside teeth system of the ring is in mesh with pinion (17) connected to motor-generator with reverse rotation which provides variation of transmission ratio according to wind speed in order to provides constant speed of output shaft (21). The pinion (17) is placed on the end of motor-generator shaft, which is supported with a pair of cylindrical roller bearings (22). With freedom of rotation, gear is fixed with its position inside gearbox housing. Output, sun gear is in mesh with three planet gears, rotating on the end of output shaft. Output gearbox shaft is supported with pair of cylindrical roller bearings, placed

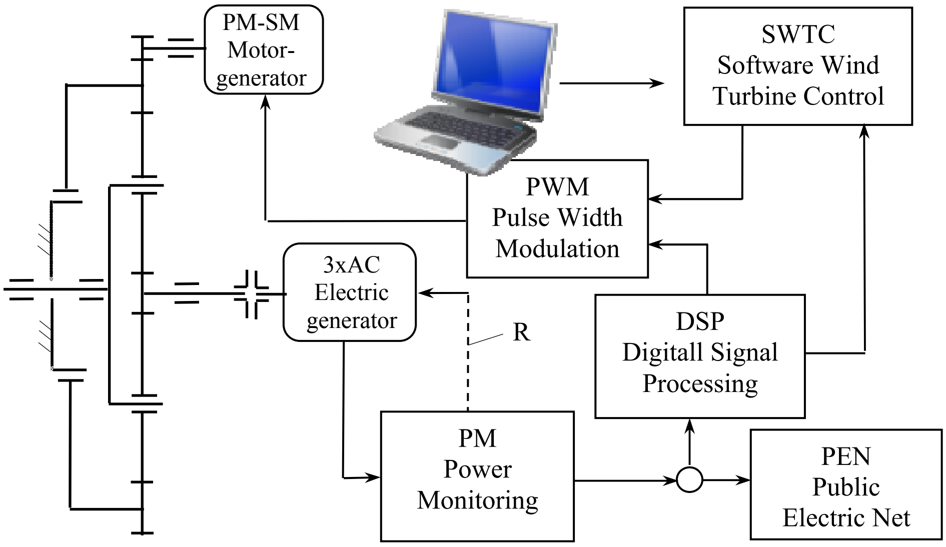

Figure 4: Concept of control system

on exit of gearbox housing. With elastic coupling, output shaft is directly connected to electric generator.

3. DESIGN OF ELECTRONIC AND SOFTWARE SYSTEM

The control system has an important role in providing transmission ratio continual variation. Control system generates wide set of commands, based on wind speed measurements, providing optimal system control.

When wind is low, control system speeds up the gearbox, when wind is high control system slows down the gearbox, giving permanently constant speed 1500rpm of gearbox output shaft and 3-phase AC generator. In Fig 4, is given a conceptual design of control system.

This function carry out pinion (14) connected to gear ring (11) – Fig. 1. The pinion (14) is driven by PM-SM servo motor-generator (Fig.4). Electric current produced by 3-phase AC generator is under monitoring of power monitoring system (PM). This is usual electronic system for monitoring of electric generator operation. Some of the main tasks are identification of the power level, frequency of electric current, vibration level, temperature etc. Of the 3-phase of electric current frequency synchronization with public electric net (PEN) is one of the main tasks. Phase differences between current in PEN and produced electricity provides reaction R of PM (Fig.4). In the cases when regulation effects R not enough, PM disconnect electric generator from PEN. Monitoring of voltage transformation before transfer in the PEN is also incorporated in PM.

Digital signal processor (DSP) is connected to PM and can use in the form of input data, all analogous values indicated in PM. For this purpose is especially important current frequency. Digital data are important for processing in the software system (SWTC) and for modulation in PWM in order to prepare control signals for PM-SM reaction. Motor-generator (PM-SM) has very important function, alternatively change of direction and speed of rotation, to consume and produce electricity. This reversible process can be separate from electric net.

Produced electricity can be accumulated and then consumed. On this way, efficiency of WT is additionally increased. The speeds of rotation of PM-SM are relative small and very often with speed equal to zero (standing position). These are very strong operating conditions for PM-SM system which has to be equipped by additional electronic for protection. In addition, control and reaction of PM-SM control system has to be very fast in order to kip current frequency in the process of random variation of the wind.

Software for wind turbine control (SWTC) adapts DSP and PWM functional characteristics. This process is in interaction with power monitoring system operation, using corresponding logarithmic procedure. These procedures are not the same in various operating conditions, such as low speeds of wind, middle speeds of wind and very strong (hurricane) wind speeds. Majority of existing wind turbines (WT) stop to operate when the wind speed is too low or too high. One of advantages of these design solutions is possibility to coordinate position of the blades of wind rotor, transmission ratio of gear transmission and current frequency control. SWTC makes decision about subroutine which will take frequency control i.e. control of speed and direction of PM-SM rotation, to consume electricity or produce electricity. Mentioned algorithms are the base for the SWTC development. Algorithms and software is in direct relation with electronic components input and outputs, operating conditions and other properties of control system, which will be identified by farther development and system testing.

Professional software system comprehends development of software, which adjusts interactions between models based on identification of system states and referent parameters and decision making on necessary actions. Software is connected to on board and remote computer system, allowing continuous system monitoring and prediction of future actions based on past and present system states (efficient system exploitation).

Basic structure of new hybrid WT drive train consist of mechanical and electro-electronic system which interactions during exploitation can be synchronized with development of software system which will provide continuous feedback for optimal drive train control. By use of mathematical models, which include real properties of whole system and its components, synchronization process can be achieved through integration of systems functions, behaviors and implementation of decision predictive control model. Mathematical model of mechanical system can be decomposed on functional requirements structure which level of realization can be evaluated based on predefined indicators. Electro-electronic system can be modeled based on static and dynamic characteristics of its components.

Input to the software system is set of predefined variables which measurement and acquisition is provided with electronic system. Sensors receive data which are then transferred through system and classified according to type and size, through appropriate channels in the course of processing time and energy saving. Processor extracts relevant parameters, forming a group of parameters within defined value range, marking the critical values. Next is data filtration and integration into executive functions for action performance, analysis of chosen actions and decision paths, distribution of commands to working organs. Filtration process is used for separation of basic signal from noise. As a feedback, process identification is performed by comparing the results of real actions with desired ones. Definition of generator and motor-generator set and mechanical system models for identification and system coordination could make control system very reliable and efficient.

4. CONCLUSION

Presented design of gear train transmission with variable transmission ratio, contains promotion of the new approach in the gear train transmission and in the wind turbines development and exploitation, which provides significant advantages in comparing to existing solutions. This is hybrid solution with maximal compatibility and robustness of design. Electronic system and software make control of planetary gear train transmission unit in the wide range of exploitation conditions. The main advantages of the new WT drive trains are (a) efficient energy transformation without transformation of electric current frequency in order to synchronize to public electric net (b) increase of the level of transformed energy by significant increase of the WT rotor speed range and without braking in order to keep rotor speed in the narrow range speeds of rotation and (c) more efficient software control of WT's system.

ACKNOWLEDGEMENTS

This work is a contribution to the Ministry of Education and Science of Serbia funded project TR 035006.

REFERENCES

[1] B.R. Höhn, "Future transmissions for wind turbines," Mechanism and Machine Science Vol.13, pp. 99-111, (2013)

[2] L. Mangialardi, G. Mantriota, "Automatically Regulated C.V.T. in Wind Power Systems," Renewable Energy Vol.4, No. 3, pp. 299-310, (1993)

[3] A. Mihailidis, K. Panagiotidis, G. Karaoglanidis, I. Nerantzis, I. Makropoulou, "Experimental Evaluation of the Efficiency of a CVT System for Wind Energy Converters," Proceedings of III International Conference "Power Transmissions 2009", Chalkidiki (Greece), 1-2 October 2009, pp. (2009)

[4] P.R.Quyang, Q. Li, W.J. Zhang, L.S. Guo, "Design, Modelling and Control of a Hybrid Machine System," Mechatronics Vol. 14, pp. 1197-1217, (2004)

[5] A. Kusiak, L. Wenyan, Z. Song, "Dynamic Control of wind turbines," Renewable Energy Vol.35, pp. 456-463, (2010)

[6] R. Isermann, "Mechatronic Systems - Innovative Products with Embedded Control," Control engineering Practice Vol.16, pp. 14-29, (2008)

[7] J.L. Guzmán, D.E. Rivera, S. Dormido, M. Berenguel, "An Interactive Software Tool for system Identification," Advances in Engineering Software Vol.45, pp. 115-123, (2012)

[8] R. Sell, M. Tamre, "Integration of V-model and SysML for Advanced Mechatronics system design," Proceedings of VI World Conference of Mechatronics "REM 2005", (France), 30 June - 1 July 2005, pp. (2005)

http://www.researchgate.net/publication/259513345_Integration_of_V-model_and_SysML_for_advanced_mechatronics_system_design

CAD Model of Disc Brake for Eliminating Noise Problems

Jasna Glišović[1*], Jovanka Lukić[1], Dobrivoje Ćatić[2], Vanja Šušteršič[3]
[1]Faculty of Engineering University of Kragujevac, Department for Motor Vehicles and Motors, Serbia
[2] Faculty of Engineering University of Kragujevac, Department for Mechanical Structures and Mechanization, Serbia
[3] Faculty of Engineering University of Kragujevac, Department of Energy and Process Engineering, Serbia

Highway safety and stopping power are always at the forefront of discussions within the commercial vehicle industry. Air disc brake (ADB) systems have been available for commercial vehicles since the 1970s. The technology initially suffered teething problems, but brake manufacturers say today's air disc brakes are highly dependable and reliable with superior stopping characteristics that make them an obvious candidate for fleets wanting to make certain they are in compliance with the new stricter regulations. One of vehicle components that occasionally generate unwanted vibration and unpleasant noise is the brake system. As a result, carmakers, brake and friction material suppliers face challenging tasks to reduce high warranty payouts.

This study takes into consideration three major aspects of modelling of a real disc brake so that the model can be built in a more realistic way. There are the structural model, the friction model and the contact model. A fully numerical method is used where all the disc brake components are modelled and analysed using finite element software packages. Having developed the disc brake components, modal analysis is carried out at the brake components and assembly levels. Friction and contact model are included when all the brake components are brought together.

Keywords: CAD, disc brakes, FEM, modeling, noise

1. INTRODUCTION

Highway safety and stopping power are always at the forefront of discussions within the commercial vehicle industry. Air disc brake (ADB) systems have been available for commercial vehicles since the 1970s. The technology initially suffered teething problems, but brake manufacturers say today's air disc brakes are highly dependable and reliable with superior stopping characteristics that make them an obvious candidate for fleets wanting to make certain they are in compliance with the new stricter regulations.

ADBs are now accepted as the primary foundation brake in Europe. Drum brakes are still used on off-road vehicles (mining, construction, military, etc.) and on vehicles for export to other continents - 18 percent of total European Union (EU) brake demand.

Among the reasons for introduction of ADBs in EU are:

− With ADBs, brake fade is virtually eliminated, proven from Alpine testing.

− Inherent high-efficiency (greater than 95 percent) and low hysteresis ensure a negligible pull (different brake performance left and right) to deliver controlled vehicle steering and braking stability

− This same high-efficiency and stability enable the highest-quality of control functions for electronic control systems like ABS, electronic braking systems (EBS) and electronic stability systems. (ADBs were introduced in parallel with EBS in the EU during 1996)

− ADBs support intelligent functions, such as continuous wear sensors, brake pad wear monitor and, in the future, electronic clearance control

− New ADBs designs reduced stopping distance up to 30 percent at the time of introduction in the EU, compared with then-current drum brakes

− ADBs enable simpler, quicker pad change vs. drum shoes and have an integrated automatic wear adjuster function.

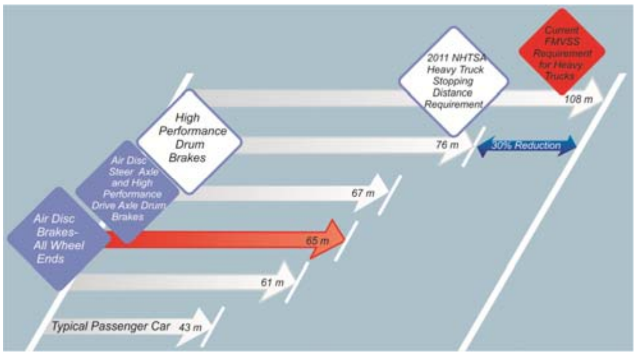

Figure 1: Comparsion of FMVSS Stopping Distance Requirements from 60 MPH

More than 90 percent of trucks in the United States still spec s-cam drum brakes. However, ADBs are widely used on refuse trucks and transit vehicles. There are several reasons contributing to the slow adoption of ADBs in North America (NA). Firstly, in Europe, the truck OEMs decide the vehicle specs, whereas NA is predominately a customer spec market. Next, there is a different service infrastructure. Trucks are serviced at OEM dealers in Europe by factory-trained and equipped technicians, so technology changes can be more easily managed and facilitated. In NA, vehicles are serviced at a wide variety of service locations, so conversion to new parts and training is more complex. Another factor is that trucks in North America are dynamically different so the impact of ADBs is less. Plus, the upfront costs for ADBs are more than drum brakes. Further, in general, technology application lags in North America compared to Europe.

Some of the brakes trends in the North American market are:

*Corresponding author: Sestre Janjić 6, 34000 Kragujevac, Serbia, e-mail: jaca@kg.ac.rs

− CSA (Compliance, Safety, Accountability) is putting more emphasis on brakes for service and reliability.

− Weight is becoming a factor as larger drum brakes, emissions equipment and pending GHG (Greenhouse Gas) regulations all shift the focus.

− Air disc brakes are widely available - a factor that influences choice.

− An array of safety innovations, such as collision mitigation and lane departure warning, compete for ADB dollars

− Data sophistication is growing with real-time telematics-based systems.

Among the major differentiators of ADB vs. drum brakes are feel and safety. As for feel, the ADB's linear output and stability drive the preference. With regard to safety, the difference is multi-faceted. With better brake feel there is less driver fatigue. Because there is less brake fade, less skill is required, making for safer drivers. In addition, stopping distance is slightly better. ADBs cost more than drum brakes but this has to be factored against future truck residual value, maintenance and service savings (pad changes are up to 75 percent faster than drum shoe changes and no periodic lubrication is required) and uptime improvement (adjuster mechanism and pistons are environmentally sealed for life and there are no current "out-of-adjustment" conditions). Greater adoption of ADBs in North America will continue to progress as vehicle owners and operators become more educated on their benefits and advantages compared to drum brakes [1].

In the testing sequence, two tractor-trailers were driven side-by-side on a closed test track with simultaneously applied full brake pressure to stop the vehicles at 75 mph. The stopping distance for air disc brake-equipped truck was within the range of 305 to 325 feet. The drum brake-equipped truck stopped in the range of 450 to 518 feet initially when cold, but as the drums heated up, the stopping distances became progressively longer. Stopping distance for the hot drum brake-equipped vehicle exceeded 750 feet, while the air disc brakes consistently stopped at around 320 feet.

The performance advantages for air disc brakes at higher speeds are particularly noteworthy when considering that during night-time driving, low-beam headlights only provide 350 feet of visibility. This is within the range of the air disc brakes' ability to stop a vehicle, but is not the case for drum brakes.

At 60 mph, the air disc brake-equipped truck stopped in the range of 185 to 210 feet in both the hot and cold brake temperature conditions. The drum brake-equipped truck stopped in the range of 255 to 292 feet with cold brakes and more than 425 feet with hot brakes [2].

The disadvantage of disc brakes is the high sensitivity (susceptibility) to self-excited vibrations. Most of the kinetic energy of a moving vehicle is converted into heat through friction. However, a small part of the kinetic energy is converted into acoustic energy and creates noise. The squealing brake is difficult and expensive to fix. It is better to solve the noise problem in the design phase [3]. Modern disc brakes with floating caliper are highly developed mechanical engineering device. They have to work reliably over a long lifetime, tolerating huge mechanical and thermal loads.

On the other hand, in recent decades, there has been a significant increase of engine power, but also the expectations in terms of comfort. This means that the noise levels, and especially brake noises, which are to be acceptable 20 or 30 years ago, are no longer tolerated by the modern user. Noise and vibration have become an important issue in the design of braking systems for motor vehicles. Efforts to improve today's braking systems must take into account the problems of noise and vibration. Good understanding of the generation mechanism of brake noise in this manner has become an important factor in the competition to design successful braking systems. It should be noted that, according to the manufacturers of brakes, brake noise is generally only a problem of comfort, and that according to them, does not affect the operation of the brakes. Although there are some new solutions in the field of braking systems ("brake by wire"), it did not affect the problem of brake noise until the brakes are working with the energy dissipation due to dry friction.

Vibrations in the braking process are a major problem of today's engineers, as can be seen by the existence of the NVH Department (Noise, Vibration and Harshness) in a number of companies. Frequently, these NVH teams focus on the problem of braking systems in terms of brake noise caused by high frequencies vibration with low amplitude. These oscillations are produced in the process of friction when the brake linings come into contact with the rotating elements. Created sound is much like that produced when writing or scraping on a chalkboard, an energy-dissipating frictional vibration occurs. Because frictional or self-excited vibrations are so different from resonant and forced vibrations, different methods of study need to be implemented when trying to understand, measure, and remedy these situations [3].

2. COMPUTER AIDED DESIGN (CAD) OF DISC BRAKE FOR ELIMINATING NOISE PROBLEMS

Computer aided design has evolved from the simple replacement of traditional drafting equipment to a very sophisticated, highly visual design tool. The earlier CAD programs used the computer to generate lines for 2D drawings. As the software and hardware advanced, these 2D drawings could be converted into 3D objects. Modern software used for solid modelling often functions in the reverse order; the three-dimensional object is drawn and then two-dimensional, orthographic drawings are generated from that model.

Modern software provides all the necessary tools for advanced designers and specialists involved in structural analysis. The processes covered include stress, frequency, thermo-mechanical, buckling and contact analysis with multiple load, restraint and mass complex configurations. Analysis can be performed on single parts as well as on hybrid models mixing solid, shell and beam elements. This allows for a wider number of mechanical behaviour and sizing assessments of parts and assemblies earlier in the product development process.

Analytical methods have proven to be inadequate to achieve complete understanding of squeal phenomena, as well as providing tools for the prediction and suppression of squeal. Besides, the analytical approaches are often limited to the study of a certain influential parameter. However, analytical methods are, despite its limitations, very useful for a concise explanation of the instability of the system. These disadvantages can be overcome by numerical methods, using the finite element method, which allows the development of models with a large number of degrees of freedom. Numerical methods take into account the deformability of elements during modelling, while the analytical approach is often treated them as rigid. Experimental methods are essential not only to quantify the nature of squeal noise and impact of different working conditions on this phenomenon, but also to ensure the validation of the results of the numerical approach and quality of brakes in terms of brake noise before going to market.

In recent years, the finite element method has become most commonly used tool for studying disc brakes squeal among researchers of this problem. The reason for this lies in the fact that this method offers a much faster and more economically cost effective solutions with regard to the experimental methods and can predict the performance of squealing noise in the early stage of the structural development of the product [4]. It also can achieve more realistic representation of disc brakes, including non-linearity and elasticity of disc brake's components. The previously listed great advantages suggest to the high promising future of finite element method with respect to the other methods. However, much research remains to be done to make the method reliable in predicting the occurrence of squeal. During development of the disc brake's model using the finite element method, it is important to validate it, in order to get the model that correctly represents the actual structure in terms of geometry and material characteristics. Validated model should be able to sufficiently accurately predict the occurrence of squeal [5, 6].

There are generally two major categories among simulation and analysis methods in the prediction of squealing brakes: the complex eigenvalues analysis in the frequency domain and the dynamic transient analysis in the time domain. Both analyzes have their advantages and disadvantages. The complex eigenvalue analysis can reveal which system modes of vibration are unstable but a shortcoming of this technique is that they do not allow time-dependent material properties and could not take into account full effect of nonlinearity away from steady sliding [7]. Meanwhile, divergence of a transient solution indicates that instability is present in the system and this technique could overcome the shortcomings in complex eigenvalue analysis. But the drawback of such technique is its long computing time and slow turnaround time for design iterations. A comparison between the two analyses is also made.

Dynamic analysis of transient processes (sometimes called the time-history analysis) is a technique used to determine the dynamic response of the structure under the effect of any time-dependent load. This type of analysis can be used to determine the time-varying displacements, deformations, stresses, and forces in the structure, because it is suitable for any combination of static, transient and harmonic loads. The load range during time is such that the effects of inertia and damping are considered important. If the effects of inertia and damping are not important, you may be able to use static analysis.

In recent years, the complex eigenvalue becomes the most preferred method in the brake research community to study brake squeal than the transient analysis. The positive real parts of the complex eigenvalue indicate the degree of instability of the linear model of a disc brake and are thought to show the likelihood of squeal occurrence or the noise intensity [8]. On the other hand, instability in the disc brake can be associated with an initially divergent vibration response using transient analysis. Liles [8] was the early researcher who incorporated complex eigenvalue analysis with the finite element method whilst Nagy et al. [9] pioneered dynamic transient analysis with the finite element method. Complex eigenvalue analysis allows all unstable frequencies to be found in one run for one set of operating conditions and hence is very efficient. However, not all unstable frequencies thus obtained can be observed in experiments. Transient analysis is able to predict true unstable frequencies (those found in experiments) in principle if the system model is correct. However it is very time-consuming. Moreover it does not provide any information on unstable modes.

It can be seen from the previous works [8,10] that the complex eigenvalue analysis required using a number of linear spring elements at the friction interface disc/pad in order to create the friction connected members (asymmetric stiffness matrix), which leads to complex eigenvalues, or unstable behavior where positive real parts indicate the likely occurrence of squeal. Fortunately, with the contribution of some researchers [11,12] and the initiative of a finite element software companies [13,9], linear spring elements are no longer required as friction coupling terms can now directly implemented into the stiffness matrix. As a result, the effect of non-uniform contact pressure and the influence of residual stresses can be included in the complex eigenvalue analysis [13]. Another advantage of this approach is that the surfaces in contact do not need to have the matching meshes, and in fact it can reduce data preparation time. Some former used approaches required nodes on two contacting surfaces to coincide and similar meshes. In some previous studies the authors have assumed full contact at the pads and disc interface [8, 7]. However, previous works related to the break contact pressure analysis [15, 16] has shown that the contact pressure distributions at the disc/pads interface are not uniform and that there exists partial contact over the disc surface.

In the past, simulation of disc brake squeal using the complex eigenvalue analysis, together with the finite element method was time consuming compared to the normal mode analysis. It is already known that the contact geometry between disc and friction material interface has a significant contribution to squeal generation [10, 17]. These researchers believed that squealing can generate at particular conditions of pads topography. This is true, because the material properties of friction materials are much lower compared to the disc as a result the friction materials are more prone to wear. Furthermore, the friction material has a much irregular/corrugated surface compare to disc. From the literature review, it was determined that none of the finite element models considered the friction material surface's topography. All the models assumed that the friction material had the smooth and flat interface, while, in reality, it is a rough surface. As previously mentioned, most of the FEM models are validated only at the component level or a combination of the components and assembly levels. In the literature, it was shown that the complex eigenvalue analysis was the most common method and most adopted by the industry to study their problems with squealing noise. This method depends largely on the results of contact analysis, which can determine the instability in the disc brake assembly. Determination of the dynamic contact pressure through the experimental methods still remains impossible. However, there are methods to obtain the static contact pressure, when the disc is stationary. The reference [14] shows that the static contact pressure distribution and its magnitude can be used as a validation tool where the correlation between the calculated and the measured results can be established. Therefore, this level of validation can enhance one's confidence in the developed model, as well as to provide better prediction of squeal.

It must be understood that the disc/pads contact is not complete. There are gaps in the contact interface, and the contact area varies during brake's vibration. There are several methods for modeling the contact in the literature, such as the gap element, the spring element, etc. The surface element for disc/pad interface was used for the contact model, while the spring element is used to represent the contact interaction between the other components of the disc brakes that are in contact. The real contact surface of the friction material can be used instead of the assumed ideal contact surface. This can lead to new insights how to get better predictable results. Due to wear, the contact between the disc and the pads can be changed over time. Perhaps this may explain the elusive nature of the squeal phenomena [14]. Another important aspect is the friction model. It is believed that the friction is the primary cause of squeal. The basic Coulomb friction model is used in this paper. It can be assumed that the friction coefficient is constant or depends on the speed. Previous studies of squeal occurrence were based on the hypothesis that the negative slope of μ-v function greatly contributes to the occurrence of squeal. However, this hypothesis was subsequently replaced by other mechanisms called sprag-slip and modal joining that did not require this friction characteristic. Instead, it is also shown that the constant coefficient of friction generates a squealing. The effects of both friction characteristics on the squeal occurrence are simulated in this study. In addition to these most important characteristics, the impact of heat on the contact pressure distribution and the occurrence of squeal can also be an important influential parameter [14, 18]. Research of the complex combined effects of thermal expansion and the contact loads between pads and disc at a moment when they are exposed to temperature changes during the braking process is presented in [18].

3. MODAL ANALYSIS OF FEM MODEL OF DISC BRAKES ASSEMBLY

A detailed three-dimensional finite element model (FEM) of disc brake assembly is developed. Figure 2a) and 2b) show a real disc brake assembly with floating caliper, and its FE model. The FE model consists of a disc, a piston, a caliper, a mounting bracket, interior and exterior pads, two bolts and two guide pins. The rubber seal (attached to the piston), and the two rubber washers (attached to the guide pins) are not included in the FE model. Damping shims are also not present in the model since they have been removed in the squeal experiments. The FE model uses 35169 solid finite elements and approximately 37,100 degrees of freedom (DOFs). This figure excludes the spring elements that have been used to connect the disc brake components.

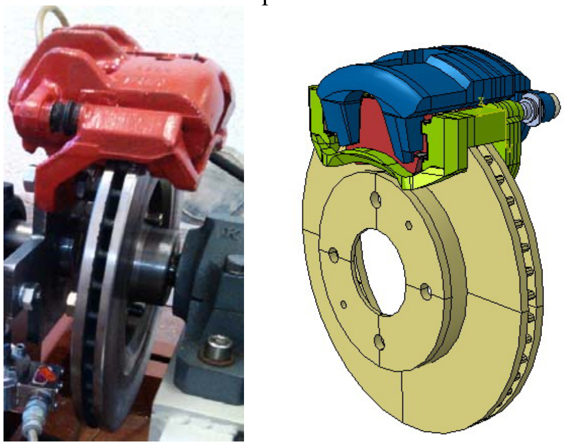

a) b)

Figure 2: Disc brake assembly a) the real disc brake b) FE model [19]

The disc, brake pads, piston, guide pins and bolts are developed using a combination of 8-node (C3D8) and 6-node (C3D6) linear solid elements, while the other components developed using a combination of 8-node (C3D8), 6-node (C3D6) and 4-node (C3D4) linear solid elements. Details for each of the components are given in Table 1. Since the contact between the disc and friction material surface is crucial, realistic representation of these interfaces should be made. Friction material has a rougher surface and is softer in terms of properties than the disc, which has quite smoother and flat surface, and is less prone to wear.

Table 1: Finite element models of disc brake's components

Disc brake's components		***Type of finite element***	***Number of elements***	***Number of nodes***
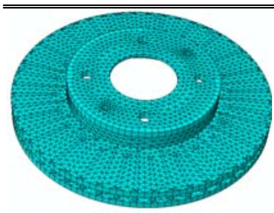	Disc	C3D8 C3D6	8177	7866
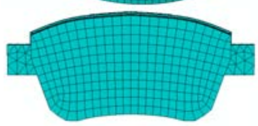	Friction Material	C3D8	2735	1804
	The back plate	C3D4		

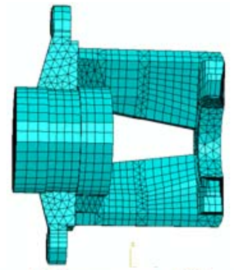	Caliper	C3D8 C3D6 C3D4	8138	5135
	Mounting Bracket	C3D8 C3D6 C3D4	7204	3803
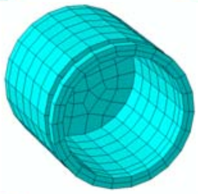	Piston	C3D8 C3D6	383	678
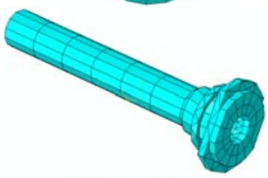	Guide Pin	C3D8 C3D4	802	662
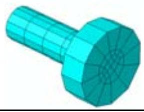	Bolt	C3D8	112	186

3.1. Components Interfaces

Many different methods can be used in the FEA modeling of a contact between the components. These methods are (in order of simplest to most complex):

- Merged nodes
- Multi-point constraints
- Linear spring elements
- Contact elements.

Merged nodes are shared between neighboring elements so that the components are effectively connected together. Although this is simple, it does not allow the application of any type of interfacial property such as contact stiffness or damping. Contact surfaces are by far the most advanced methods of coupling components together. There are sophisticated contact surface models that allow some level of motion between the components, which include the specifying normal and tangential contact stiffness. Here a more realistic representation of what is a highly non-linear feature can be applied. Unfortunately, it requires a considerable computational process compared to the other three methods.

Upon completion of the modeling, all the disc brake's components must be integrated into the assembly model. Contact interaction between the disc brake components is represented by the linear spring elements (SPRING 2 in *ABAQUS* nomenclature), with the exception of the disc/pad interface where surface-to-surface contact are introduced (see Table 2). This selection was made due to the fact that the contact pressure distributions at the disc/pads interface are more significant than other component contact interface. This type of spring element has three degrees of freedom in the translational direction and the relative displacement across the spring element is the difference of the *i*-th component at the spring's first node and *j*-th component of the spring's second node:

$$\Delta u = u_i^1 - u_j^2 , \tag{1}$$

where i and j are the degrees of freedom in the translational direction. This spring element allows the users to specify different spring stiffness for different directions.

Figure 3 shows a schematic diagram of the contact interaction that has been used in a model of the disc brake assembly. A rigid boundary condition is imposed at the bolt holes of the disc and of the mounting bracket, where all six degrees of freedom are rigidly constrained.

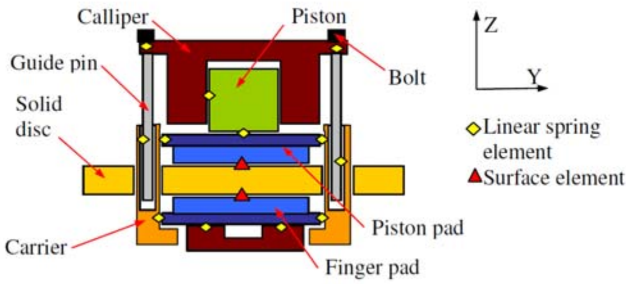

Figure 3: Schematic diagram of contact interaction in a disc brake assembly [14]

Some of the components need to be fixed-should be tied, for example, bolt and caliper.

Table 2: The contact interaction between components

Components	Interaction
Disc-Brake Pads	*Surface-to-surface*
Caliper- Brake pads	*Node-to-surface*
Piston-Brake pads	*Node-to-surface*
Clip-Brake pads	*Node-to-surface*
Guide Pin-Mounting Bracket	*Node-to-surface*
Piston- Caliper	*Node-to-surface*

The model used for analysis of this braking system has the three-dimensional elements that are used from the library of elements:

- C3D6 - first order 3D continuous wedge element with 6 nodes,
- C3D8 - first order 3D continuous hexahedral element with 8 nodes,
- C3D4 - first order 3D continuous tetrahedral elements with 4 nodes.

Contact surface elements are used in areas where the contact is occurred.

It is not necessary to apply the final sliding of contact pairs in any contact location within the model of the brake system. Most of these locations show negligible relative slip when the brake is loaded. The only exception is the disc/pads interface, where obviously the rotation of the disc leads to the high sliding speed in a physical brake system. However, in the contact analysis used in the *ABAQUS*, it is simply a case of defining the boundary conditions of the disc's speed. Table 3 shows an overview of the parameters used for each contact interface within the brake assembly.

Table 3: Contact interface in the ABAQUS model of disc brake assembly

Interface	Type	The initial clearance, mm	µ
Disc / Friction lining	Small sliding	.005	0.336
Inner plate/Piston	Small sliding	.005	0.12
The outer plate/Housing	Small sliding	.005	0.12
Plate/Mounting Bracket	Small sliding	.005	0.12
Piston/Caliper Housing	Small sliding	.001	0.05
Guide pin/Mounting Bracket	Small sliding	.001	0.05
Guide pin/Caliper Housing	Tied	.01	-

The chosen values of initial contact clearance are 0.005 mm for all the pad's surfaces, because they all should have surfaces that lie on each other at the beginning of the analysis, and 0.005 mm represents the geometric resolution of the geometry. Clearance between pad and caliper's surfaces is 0.001 mm because these surfaces are not designed to be in the initial contact and are modeled with a finite clearance. The value of 0.001 mm ensures there is no adjustment of nodes on these contact surfaces prior to analysis. The value of clearance between caliper housing and guide pin is 0.01 mm, and this ensures that all contact surfaces are completely adjusted and connected even if some nodes are separated even 0.005 mm for tolerance modeling.

Static analysis establishes the basic state of the system with typical load of the brake, then perform complex eigenvalue analysis to determine the stability of the system around this basic state:

1. Static preload, nonlinear static analysis. The pressure is applied to the back of the piston and inside the cylinder in the caliper housing. No rotation is applied to the rotor for this step and the system reflects a stationary brake with pressure applied. This allows non-linear solver to more easily determine the contact conditions at the disc/pad, guide pin and piston interfaces without the complication introduced by rotation. Stabilization of solutions, which involves applying artificial damping to control rigid body motions, is applied to the bodies that are not constrained prior to contact being established. The damping is small enough not to affect the final static solution when all the contact conditions have been properly established.
2. Adding rotation, non-linear static analysis. Velocity boundary condition was added to the disc from the static loaded state from step 1. The pads react to frictional forces at the disc/pad interface and begin to translate until they are fully captured by the pad abutment regions on the mounting bracket. The system converged into its basic state during a brake application. This provided the basic state for the analysis steps that followed.
3. Normal modes. The normal modes solution provides a subspace of modes to be used for complex eigenvalue solution in the step 4. Number of modes extracted was 107 and covers a frequency range from 1 to 10 kHz. The number of modes in this step needed to be greater than the number of complex modes requested for step 4 adequately to allow the complex modes to be represented.
4. Complex modes. Complex eigenvalue solution to provide the stability response of the base statically loaded state. Complex modes were extracted taking into account the effect of friction interface [5, 6].

4. RESULTS

The second phase of the methodology is to determine the dynamic characteristics of the disc brake assembly's model. The previous separated components of the disc brake must be now coupled together to form the assembly model. Modal analysis was carried out to obtain the natural frequency of the assembly (Table 4). The resulting out-of-plane modes of disc brake assembly are shown in Figure 4.

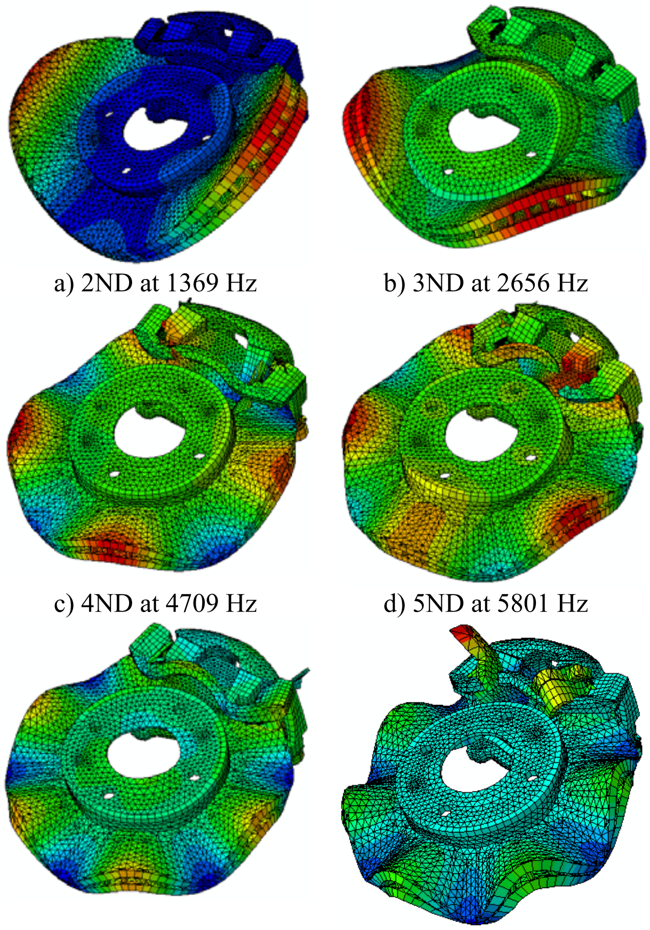

a) 2ND at 1369 Hz b) 3ND at 2656 Hz

c) 4ND at 4709 Hz d) 5ND at 5801 Hz

e) 6ND at 7782 Hz f) 7ND at 9055 Hz

Figure 4: Mods of disc brake assembly [19]

Table 4: Modes of disc brake assembly in a free-free boundary conditions

Mode Nº	Frequency, Hz	Mode Nº	Frequency, Hz
2ND	1369	5ND	5801
3ND	2656	6ND	7782
4ND	4709	7ND	9055

4.1. Nonlinear contact analysis

ABAQUS defines the contact pressure between the surfaces at a point, p, as a function of the over-closure, h, of the surfaces. A hard contact model is considered where the disc and pad surfaces will separate (or contact constraint is removed), when the contact pressure between them becomes zero or negative and on the other hand, the disc and pad surface will interact (or contact constraint is applied) when the contact pressure between them is larger than zero. Two regimes for *p=f(h)* are given in the formulations below [13]:

$$\begin{cases} p = 0 \text{ за } h < 0 \, (open) \\ h = 0 \text{ за } p > 0 (closed) \end{cases} \quad (2)$$

When surfaces are in contact, they usually generate shear (friction) and the normal forces across the sliding interface. A relation between these two components of force is described in terms of friction between the bodies in contact. Typically, when deriving friction in a theoretical context, the critical value of the tangential force is defined as:

$$F_{crit} = \mu \cdot F_N \,, \quad (3)$$

where F_{crit} is the critical shear force, μ is the friction coefficient, and F_N is the normal force. Due to the discretization process used by the finite element method, the critical value is not defined in terms of a critical load (F_{crit}), but as a critical shear stress (τ_{crit}) that is a function of the pressure (p), as given below:

$$\tau_{crit} = \mu \cdot p \,. \quad (4)$$

The value of the shear stress that compares with the critical value, defined above, is the magnitude of the resultant shear stress in the x and y-directions:

$$\tau_{eq} = \sqrt{\tau_x^2 + \tau_y^2} \,. \quad (5)$$

If the value of the equivalent shear stress is greater than value of the critical shear stress, sliding contact will be initiated, and the restoring shear stress will be equivalent to τ_{crit}. In the case of sticking condition, the shear stress will balance that applies to the contact interface.

ABAQUS provides various friction models to describe the relative tangential motion of the contact surfaces. A basic Coulomb friction model is used, where, by default, friction coefficient can be defined as a function of sliding speed, contact pressure and average temperature at the contact point. The users can also define different coefficients of friction, ie. static friction and kinetic friction coefficients (Figure 5). In this model, it is assumed that the friction coefficient exponentially decreasing from the static value to kinetic value based on the following equation:

$$\mu = \mu_k + (\mu_s - \mu_k) e^{-d_c v} \,, \quad (6)$$

where μ_k is the kinetic friction coefficient, μ_s is the static coefficient, d_c is a decay coefficient and v is the sliding speed. During the specifying static and kinetic friction coefficient, *ABAQUS* allows the users to change the friction coefficient during the analysis. This is adopted in the entire study where the static friction coefficient is used during the first step, and the kinetic friction coefficient in the following steps. *ABAQUS* also provides an anisotropic friction model that allows the users to specify different friction coefficients in the two orthogonal directions on the contact surface. The users can also develop their own friction model using user-defined subroutine [13].

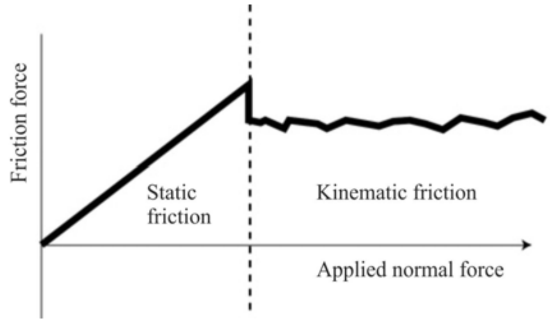

Figure 5: The relationship between static and kinetic friction coefficient

There are three types of contact schemes available in *ABAQUS* namely, small, finite and infinitesimal sliding. By default, *ABAQUS* treats finite sliding by which contact surfaces may allow for arbitrarily separation, sliding and rotation. Using finite sliding, the slave nodes may come in contact anywhere along the master surface and the load transfers are updated throughout the analysis. Whilst for small sliding the contact formulation assumes that the contact surfaces may undergo arbitrarily large rotations, but that a slave node will interact with the same local area of the master surface during analysis. Therefore the slave nodes are not monitored that in contact along the entire master surface. With the final and small sliding consider geometric nonlinearity, infinitesimal sliding ignores this effect and assume both relative motions and the absolute motions of the contacting bodies are small. Accordingly, infinitesimal sliding is unsuitable for the disc brake analysis.

Further, comparison between the two sliding schemes is made in terms of the contact pressure distribution, the contact area and simulation time. The previously developed model will be used in analysis. The experimental data were used for the maximum braking performance regime, and the corresponding maximum friction coefficient. The pressure in braking installation of 1.84 MPa and the rotation speed of 44.52 rad/s were introduced in the model. For the contact interface between the pads and the disc, the kinetic coefficient of friction of μ=0.336 is applied. A penalty friction constraint is chosen for comparison. The obtained results will suggest which sliding scheme should be adopted throughout this research.

From figures 6a) and 6b), it can be seen that contact pressure distributions are almost the same for both the piston and finger brake pads. Maximum contact pressures are also nearly identical for both sliding schemes.

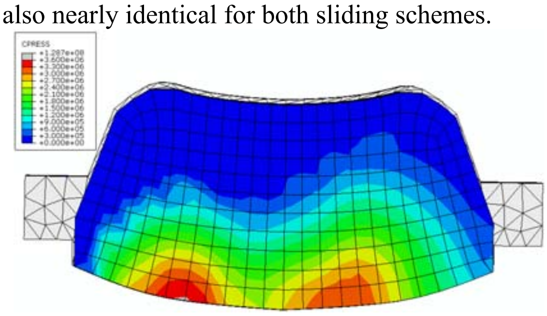

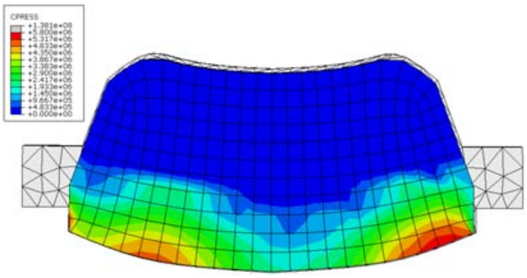

a) Small sliding

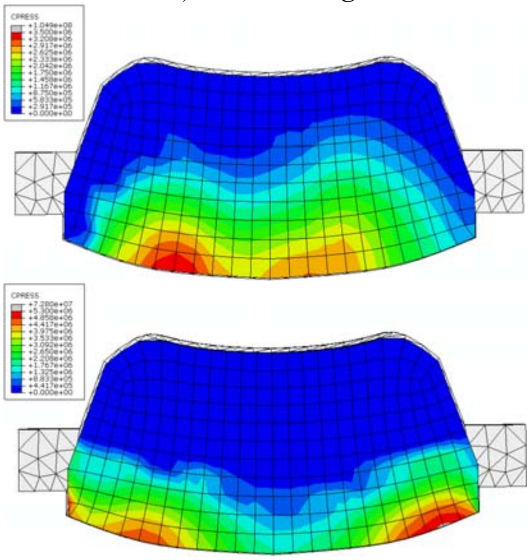

b) Final sliding

Figure 6: Contact pressure distribution between small (a)and the finite sliding (2)schemes at the piston (left) and finger (right) pads.Left of the diagrams is the leading edge

Comparisons between small and finite sliding in terms of the contact area, maximum pressure and simulation time are described in Table 5. As previously mentioned, the finite sliding scheme is more demanding in terms of computation time that the small sliding scheme. This is proved to be true as indicated in Table 5, in which the finite sliding takes about 2893 s to complete the simulation, while small sliding only takes about 2000 s, which is a reduction of 30.87%. It appears that the two schemes have little difference in the contact analysis in particular for the disc brake contact analysis. Based on the results, small sliding scheme will be adopted for subsequent analysis due to its computational advantages over the finite sliding, while a similar contact pressure distribution, contact area and maximum pressure can be obtained for both schemes. Furthermore, using finite sliding should be paid more attention in smoothing the master contact surfaces and nothing need to be done for a small sliding.

Table 5: Comparison between the small and finite sliding

Parameter	Small slip		Final slip	
	Piston	Finger	Piston	Finger
Contact area, m²	$2.209 \cdot 10^{-3}$	$1.475 \cdot 10^{-3}$	$2.565 \cdot 10^{-3}$	$1.459 \cdot 10^{-3}$
The highest contact pressure, MPa	3.6	5.8	3.5	5.3
Time simulation, s	2000		2893	

In this study, it is assumed that the pads will come in interaction with the same profile of the rotating disc surface. Therefore, small sliding scheme is chosen. The convergence could also be easily obtained, compared with the finite and infinitesimal sliding formulation. Furthermore, small sliding scheme provides considerably computation time savings in comparison with the finite sliding model.

There are two stiffness methods for friction constraints that are available in *ABAQUS*, namely, a penalty method and the Lagrange multipliers method. The penalty method (default by *ABAQUS*) permits some relative motion of the surfaces when the surfaces should be sticking whilst the Lagrange method should be used when no slip is allowed in sticking condition. Using the Lagrange method can increase the computational cost of the analysis because it adds more degrees of freedom to the model and quite often increases the number of iterations needed to obtain a converged solution. In addition, the Lagrange formulation may prevent convergence of a solution. In the case of the finite sliding, the considered model of disc brake, there was no convergence of solution. Therefore, in this study the penalty method is employed to ease convergence restriction, as well as to obtain minimum computational cost [13].

The results obtained using the method of Lagrange multipliers are presented in Table 6. The results obtained using the small sliding scheme are used. By looking at Table 5 and 6, particularly with respect to the contact area and the maximum pressure can be seen that there are no differences between the two schemes. Similarly, the contact pressure distributions as shown in Figures 7a) and 7b) in both schemes are identical. However, in terms of the computational cost, Lagrange multipliers scheme requires more time for completing the simulation compared to the penalty scheme. Lagrange multipliers scheme requires about 2819 s for a single analysis, whereas the penalty method only takes about 2000 s, which is an increase of 29% in the computational time. Results indicate that for disc brake squeal problem exact sticking condition is not necessary. It has been observed that one of the main characteristic of squeal is that no obvious sticking state is present at the disc/pad contact interface. Even though one can argues that this (no apparent sticking) may be applied at the macroscopic level, but not in the microscopic state. Since this paper only considers squeal occurrence at the macroscopic level, any conditions or behavior that is present at the microscopic level is not considered. Therefore, it is considered that the penalty scheme is most suitable for this study due to its advantages in terms of computational cost over Lagrange multipliers and will be used in subsequent analyses.

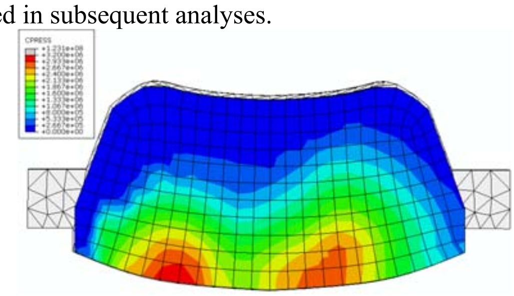

a)

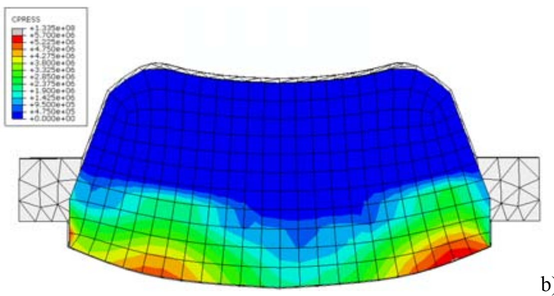

b)

Figure 7: Contact pressure distribution using Lagrange multipliers formulation at the piston (up) and finger (down) pads. The left side of the diagram is the leading edge [19]

Table 6: Simulation results of contact analysis

Parameter	Lagrange Multipliers	
	Piston	Finger
Contact area, m^2	$2.3 \cdot 10^{-3}$	$1.457 \cdot 10^{-3}$
The highest contact pressure, MPa	3.2	5.7
Time simulation, s	2819	

5. CONCLUSION

This paper describes the development and validation of the FE model of disc brake. The proposed methodology has two stages as follow:

- Validation of the disc brake mechanism's components using modal analysis,
- Validation of the disc brake assembly using modal analysis.

Using modal analysis has shown that a good agreement is reached at the component's level and brake disc assembly's level. This can only be achieved after the adjusting process or an update in which the material characteristics' values of the components and the spring stiffness is adjusted at each level. It was also established that there are a number of natural frequencies of the brake components are close to each other.

Previous studies using the FE method assume a perfectly flat surface on the disc/pad interface. Improved FE model should include the actual topography of a pad's friction material surface, which can be measured by using the linear micrometers. It is also shown that current mesh of individual FE model, particularly of the brake pads, are sufficiently dense to give a realistic prediction of the contact pressure distribution, and also to capture mode shapes of natural frequencies up to 9 kHz. However, the current predicted results can be improved by using a better mesh quality. Due to the accurate representation of components and brake assembly, the later simulation can achieve much better prediction.

Next part of paper was focused on the non-linear contact analysis of the disc brake model with the main objective of determining of contact pressure distribution, the contact area and maximum contact pressure. These three parameters are useful for subsequent work, especially in comparing predicted results from one model to another. Several potential contact interaction schemes that are available in *ABAQUS* were described. The first comparison is made between small sliding and finite sliding schemes. It was found that, although the small sliding scheme assumes the slave node could slide relatively a small amount at the master surface compared to the finite sliding scheme, predicted results between the two schemes are almost identical. The main advantage of the small sliding scheme over the finite sliding scheme is that it saves about 30.87% of computational time.

The second comparison is made to examine two friction stiffness constraints, namely the penalty method and Lagrange multipliers method. The penalty method allows some relative motion of the surfaces during sticking, while Lagrange multipliers do not allow at all the relative motion during sticking state. In addition, Lagrange multipliers can enforce more precisely the sticking and sliding constraints than the penalty method. However, computational cost is an issue as Lagrange method takes more time for a single analysis. This is proved to be true because Lagrange method requires 2819 s compared to 2000 s using the penalty method, which is an increase of 29% in computational time. On the other side, the predicted results for both methods are identical. By looking at those results, the penalty method is more suitable and will be used together with small sliding scheme for further research.

ACKNOWLEDGEMENTS

This paper was realized within the researching project "The research of vehicle safety as part of a cybernetic system: Driver-Vehicle-Environment" ref. no. 35041, funded by Ministry of Education, Science and Technological Development of the Republic of Serbia.

REFERENCES

[1] D. A. Kolman, "Air disc brakes for heavy trucks offer performance advantages to drum brakes", http://www.vehicleservicepros.com/news/10987170/air-disc-brakes-for-heavy-trucks-offer-performance-advantages-to-drum-brakes

[2] "Test results support advantages of air disc brakes over drum brakes", Trailer / Body Builders, Vol. 45 Issue 2, p11, (2003)

[3] Q. Cao, Friswell, M. I., Mottershead, J. E., James, S., "Car disc brake squeal: theoretical and experimental study", Materials Science Forum (Volumes 440 - 441), Volume: Modern Practice in Stress and Vibration Analysis, Glasgow, pp. 269-276., (2003)

[4] D. Stanef, A. Papinniemi, and J. Zhao, "From Prototype to Production - The Practical Nature of Brake Squeal Noise", 24th Annual Brake Colloquium and Exhibition, TX, USA, Session: NVH: Product and Anti-Noise Shim Design, Paper Number: 2006-01-3217, DOI: 10.4271/2006-01-3217, (2006)

[5] A. Papinniemi, J.C.S. Lai, and J. Zhao, "Vibro–Acoustic studies of brake squeal", Proceedings of ACOUSTICS, 3-5 November, Gold Coast, Australia, pp. 129-134, (2004)

[6] A. Papinniemi,"Vibro-acoustic Studies of Brake Squeal Noise", A thesis submitted for the Degree of Doctor of Philosophy, School of Aerospace, Civil and

Mechanical Engineering, The University of New South Wales, Australian Defence Force Academy, (2007)

[7] H. Ouyang, W.V. Nack, Y. Yuan, F. Chen, "Numerical analysis of automotive disc brake squeal: a review", International Journal Vehicle Noise and Vibrations, Vol. 1, No. 3-4, DOI: 10.1504/IJVNV.2005.007524, pp. 207-230, (2005)

[8] G.D. Liles, "Analysis of disc brake squeal using finite element methods", Technical Report 891150, SAE, Warrendale, PA, SAE, (1989)

[9] L.I. Nagy, J. Cheng, and Y. Hu, "A new method development to predict brake squeal occurrence", SAE Technical Paper 942258, (1994)

[10] Z.B.M. Ripin, "Analysis of disc brake squeal using the finite element method", PhD Thesis, Department of Mechanical Engineering, University of Leeds, UK, (1995)

[11] Y. Yuan, "An eigenvalue analysis approach to brake squeal problems", Proceedings of the 29th ISATA Conference Automotive Braking Systems, Florence, Italy, (1996)

[12] P. Blaschke, M. Tan, A. Wang, "On the analysis of brake squeal propensity using finite elements", Technical Report 2000-01-2765, SAE, Warrendale, PA, (2000)

[13] ABAQUS Manual Version 6.4, Hibbitt, Karlsson & Sorensen, Inc., (2003)

[14] A. R. Abu Bakar, "Modelling and Simulation of Disc Brake Contact Analysis and Squeal", Department of Mechanical Engineering, PhD Thesis, Faculty of Engineering, University of Liverpool, Liverpool, United Kingdom, (2005)

[15] F. Samie, D.C. Sheridan, "Contact analysis for a passenger car disc brake", SAE Technical Paper 900005, (1990)

[16] M. Tirovic, A. J. Day, "Disc brake interface pressure distributions", Proceedings of I.Mech.E., Vol. 205, pp. 137-146, (1991)

[17] H.A. Sherif, "Investigation on effect of surface topography of pad/disc assembly on squeal generation", Wear, Vol. 257, Nos. 7-8, pp. 687-695, (2004)

[18] M. Z. Hassan, "Thermal Deformation Analysis of Automotive Disc Brake Squeal", PhD Thessis, The University of Leeds, School of Mechanical Engineering, (2009).

[19] J. Glišović, "Theoretical and experimental research of high-frequency noise of disc brakes", PhD Thesis, Faculty of Engineers University of Kragujevac (2012)

Influence of Sub-structures' Shape on Vibration Behaviour of Sandwich Walls

Aleksandar Vranić[1*], Snežana Ćirić Kostić[1], Bojan Tatić[1]
[1]The Faculty of Mechanical and Civil Engineering in Kraljevo, University of Kragujevac, (Serbia)

Modal behaviour, as characteristic structure property, is determined by material and geometric properties (mass, stiffness and damping) and boundary conditions of the structure. Change of any of those characteristics leads to changes of modal behaviour. Increasing of stiffness is very important for good resistance to natural vibrations. On the other hand, lightweight design (weight reduction) is requirement that is met by modern designers with increased occurrence. The two requirements are contradictory to each other from the aspect of the modal behaviour of the structure. This paper presents an analysis of possibilities to resolve the contradiction by additive manufacturing technologies. The technologies enable manufacturing of complex lattice structures and design of optimal sandwich structures that satisfy both lightweight design and reduction of vibration and noise. Numerical methods were applied and their results allowed for analytical clarification of processes in elastic structure of system. A modal analysis of different shapes of the sandwich walls, designed for production by additive manufacturing, was performed using software package ANSYS.

Keywords: vibrations, modal analysis, light-weight design, sandwich walls, lattice structures

1. INTRODUCTION

The structure of the emitted noise of a mechanical system is in direct correlation with the modal behaviour of its housing. It is established fact that housings, designed to reduce the internal noise, generate additional noise due to excitation of their natural vibration modes by the internal disturbances. For example, in gearboxes, these disturbances are gear meshing, bearings, etc. Therefore, from the point of view of noise emission, housing walls act as insulator of primary sound waves, as transmitter of secondary sound waves and generator of tertiary (structural) sound waves [1]. Excitation of certain modal shapes (modes) is correlated with elastic deformations of the structure and the excitation frequencies. Modal damping of the vibrations, which are consequence of complex processes of wave motion through the walls, is also a key parameter of modal behaviour of a structure. In addition, vibration modes, as structure properties, are determined by the material properties (mass, stiffness and damping), and boundary conditions imposed by structures. Change of any of these characteristics leads to changes of vibration modes.

The idea of the paper is to consider use of AM technologies for manufacturing of complex lattice and cellular structures that would meet two requests: reduction of mass and reduction of vibrations and noise emission of housing walls. It presents initial results of research of modal behaviour of sandwich walls with various shapes of lattice structures, with the ultimate goal to determine the best sub-structure of the panel from aspect of reduction of vibrations and sound emission. For example, it has been shown [2] that it is possible to reduce noise emission of gearboxes by increasing the structural stiffness and reduction the vibration of walls with large and positive acoustic contribution coefficients.

Sandwich walls consist of two parallel thin plates and core between them. The parallel plates withstand normal forces which arise from bending, tension or pressure, and the core withstands shear forces, like in the case of I-beam geometry. The stiffness of the sandwich structure can be increased by appropriate selection of core height and the core structure. More than 700 honeycomb core structures for sandwich components were produced in the past 50 years only by one manufacturer [3,4,5]. However, sandwich walls with arbitrary core structure are almost impossible to be manufactured by means of traditional manufacturing technologies.

For the purpose of analysis of influence of shapes and dimensions of sub-structures (core structure) on vibration behaviour of sandwich walls are used the results of modal analysis by FEM analysis.

2. AM TECHNOLOGIES

Unlike traditional methods of manufacturing, where product is made by removing or deforming of material, additive manufacturing technologies make product by joining of successive layers of material. There are various types of additive manufacturing technologies, using different materials. While introduction of additive manufacturing technologies made immediate impact to numerous applications connected with manufacturing of prototypes [6, 7, 8], their application for manufacturing of end parts was limited by poor mechanical properties of used materials.

The AM technology that enables manufacturing of products with mechanical properties comparable to those made by traditional technologies is called Selective Laser Sintering (SLS). SLS offers freedom to quickly build complex and freeform parts that are more durable and provide better functionality over other AM technologies. SLS technology uses laser beam directed by optical system to melt plastic or metal powder. The melted powder is cooling and sintering after the illumination, thus forming a horizontal cross-section of a 3D object. After sintering, the layer is lowered and a new layer of powder is applied on

*Corresponding author: Dositejeva 19, 36000 Kraljevo, Serbia; vranic.a@mfv.kg.ac.rs

top of it. The new layer is then melted, thus forming the next section, but during the cooling phase it is simultaneously joining with the previous layer. Therefore, during the cooling phase the melted powder is joining in both horizontal and vertical direction. The process is repeated until the 3D object is made.

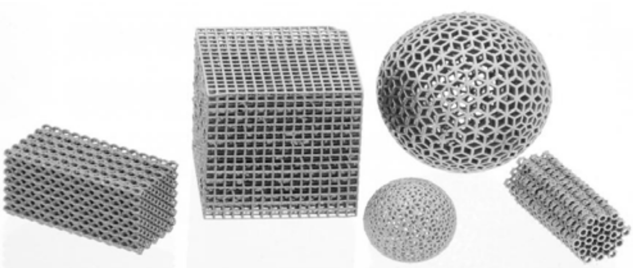

a)

b)

c)

Figure 1: Lightweight structures manufactured by SLS:
a) Cellular structures
b) Sandwich structure with low core density;
c) Titanium bracket with optimized topology

This new technology enables manufacturing of complex structures with low mass, high stiffness good stress resistance with cellular structure (Figure 1a). SLS machine manufacturer EOS also demonstrated ability to produce metal sandwich structures using this technology (Figure 1b). It means that it is possible to manufacture various types of sandwich structures of housing walls by SLS technology [9, 10].

SLS opens many possibilities for lightweight design as well. EADS has been testing wind brackets (Figure 1c) and hinges, for engine covers to evaluate technical and commercial feasibility of producing parts by SLS [11, 12]. Considerable savings and weight reduction is gained without endangering bracket functionality.

However, SLS technology has limitations as well. The main limitations are connected to limited minimal thickness of the parts, limited selection of materials and limited dimensions of the manufactured objects.

Test specimens for the research presented in this paper will be manufactured using SLS technology on machine EOS M280 (Figure 2).

Limitation parts manufactured by EOS M280 are threefold:

- Maximal dimensions have to be smaller than dimensions of building volume, 250 x 250 x 325 mm.
- Minimum wall thickness is 0.4 mm and minimum layer thickness is 0.020-0.040 mm.
- Available materials are 15-5 Stainless Steel, Maraging Steel, Cobalt Chrome, Titanium Ti64, Nickel Alloy N62 and Aluminium alloys.

Figure 2: Machine for SLS of metal parts EOS M280

With EOS M280, parts are being manufactured on building platform, which has role to remove heat and prevent motion and deformation of objects that may occur due to the residual stresses caused by thermal dilatation. The manufactured parts are connected to the platform by supports that are manufactured simultaneously with the object. The supports sometimes present an additional limitation in design for additive technologies.

3. MODELS DEVELOPMENT

For the purpose of analysis of the influence of substructure shape on natural vibrations of sandwich walls were developed twenty-three geometric models of sandwich wall structures with variable core structure. Thicknesses of sandwich walls were 15 mm and thickness of cover plates was 1 mm.

Models were made using Solid Works software. Three different methods for modelling of 3D models of substructures were used. The first method was extrusion of a 2D sketch to 3D solid model (Fig. 3a). The second method was application of Boolean operations to construct the model by adding or subtracting primitives (Fig. 3b). The third method was multiplication of 3D solid blocks obtained by extruding of a 2D sketch (Fig 3c).

All of the walls had the same dimensions 15x300x200 mm. The solid block with the same dimensions would be 7850 kg/m^3 and its weight would be 7.065 kg. Densities of the sandwich walls varied from 1823.33 kg/m^3 to 4338.88 kg/m^3, and weights varied from 1.641 kg to 3.905 kg.

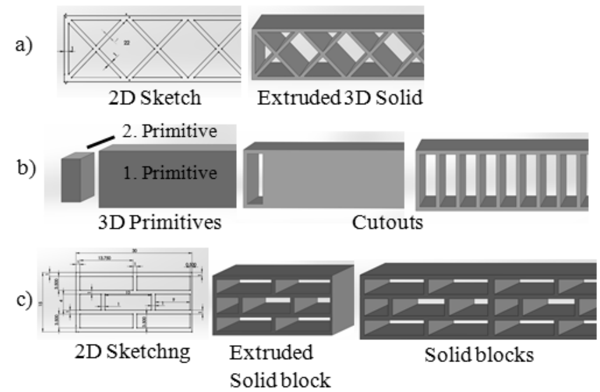

Figure 3: Illustration of different methods
for modelling of sandwich walls

The developed models of sandwich walls are presented in Table 1.

Table 1: Sandwich structures with various sub-structures' shapes

Ver.	Sandwich structure design	Mass kg	Density kg/m^3	No of modal shapes	Ver.	Sandwich structure design	Mass kg	Density kg/m^3	No of modal shapes
V1		1.88	2088.9	8	V14	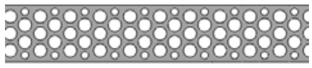	3.91	4333.3	7
V2		2.16	2400.0	7	V15	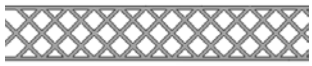	3,16	3511.1	7
V3		1.74	1944.4	9	V16		2.38	2644.4	9
V4		2.19	2433.3	10	V18		2.38	2644.4	11
V5	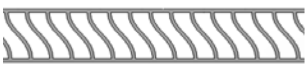	2.16	2400.0	11	V19	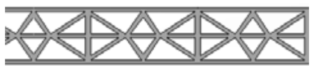	2.84	3155.5	7
V6	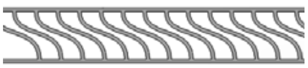	2.48	2755.5	12	V20	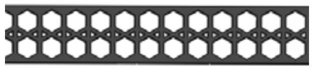	3.51	3888.8	7
V8	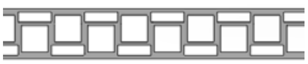	2.65	2944.4	9	V21	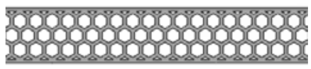	3.59	3988.8	7
V9		2.78	3088.8	10	V22		1.64	1822.2	9
V10	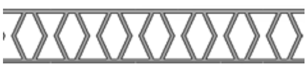	2.10	2333.3	11	V23		2.19	2433.3	10
V11	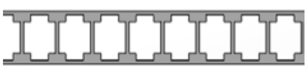	2.35	2611.1	9	V2.1	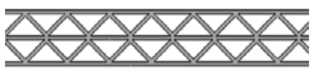	2.72	3022.2	7
V12	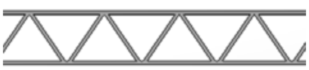	1.68	2866.6	7	V2.2	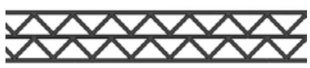	2.72	3022.2	7
V13		1.77	1966.6	10	Solid model		7.06	7850	6

4. MODAL ANALYSIS

Modal analysis represents the first step in research of vibrations of mechanical systems. Natural frequencies and modal shapes of the studied types of sandwich walls were determined using ANSYS.

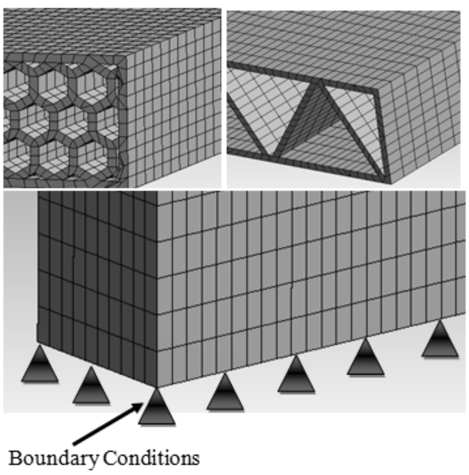

Fig.4 The discretized model of a sandwich wall

Modal analysis was performed by applying the finite elements method with the linear 3D-brick finite elements with 8 nodes. Each of the elements has 24 degrees of freedom (three translations per each node). Total number of the finite elements varied from minimal 33500 for the solid wall to maximal 157986 for model V21, depending on complexity of the core geometry. The discretized model of a sandwich wall is shown in Fig. 4. Boundary conditions are defined by fixing nodes at the bottom side of walls (Fig. 4).

Frequency range for modal analysis is from 0 to 3000 Hz. The assumed material of the models in the presented modal analysis was steel.

5. RESULTS AND DISCUSION

For solid model of wall, 6 natural frequencies and modal shapes of oscillations are determined within the studied frequency range. For the sandwich structure models, the number of determined vibration modes in the frequency range was between 7 and 12 (Table 1). Some of the modal shapes are presented in Fig 5.

Minimal number of 7 vibration modes was determined for nine of the sandwich walls: V2, V12, V14, V15, V19, V20, V21, V2.1, V2.2. Natural frequencies of these models of sandwich walls are presented in Table 2. A brief analysis of the obtained results shows that the solid model has the highest density and the lowest natural frequencies (Fig. 6) of all studied model.

Table 2: Mode frequencies for the selected types of sandwich walls

	Frequency, Hz									
Mode	Solid wall	V2	V12	V14	V15	V19	V20	V21	V2.1	V2.2
1	316.32	388.88	413.6	342.88	357.59	344.83	353.78	358.49	352.58	350.5
2	568.5	650.63	680.61	569.7	606.52	578.17	588.59	606.29	592.7	589.61
3	1277.5	1384.7	1464.2	1204.7	1279.1	1228.3	1254.9	1291.1	1255.9	1251.1
4	1937.8	2240.9	2319.4	2056.2	2120.3	2015.7	2109.3	2129.6	2050.3	2009.4
5	2257.6	2536.4	2600.5	2284.9	2398.4	2264.7	2325.6	2382	2317.8	2290.4
6	2754.1	2743.8	2726.6	2524.1	2661.7	2538.9	2568.1	2654.2	2597.7	2584.3
7	2754.1	2875.7	2974.4	2732.7	2718.9	2780	2717.7	2782.3	2835.1	2835

Table 3: Max displacements for the selected types of sandwich

	Displacement, mm									
Mode	Solid wall	V2	V12	V14	V15	V19	V20	V21	V2.1	V2.2
1	24.07	43.24	48.98	31.96	35.84	37.76	34.05	33.63	38.57	38.54
2	36.09	64.27	72.52	48.52	54.18	56.84	51.32	50.38	57.54	57.35
3	35.62	64.11	70.76	50.01	55.90	57.75	52.07	50.74	57.80	57.64
4	28.77	47.99	55.67	36.63	39.17	41.74	37.41	37.16	42.13	41.31
5	32.23	57.43	64.74	46.32	51.06	52.28	47.41	46.32	52.16	51.05
6	45.8	38.60	43.24	67.94	75.24	76.03	70.59	67.93	75.21	73.10
7	-	81.74	85.87	27.68	32.31	33.00	29.40	29.43	34.00	34.00

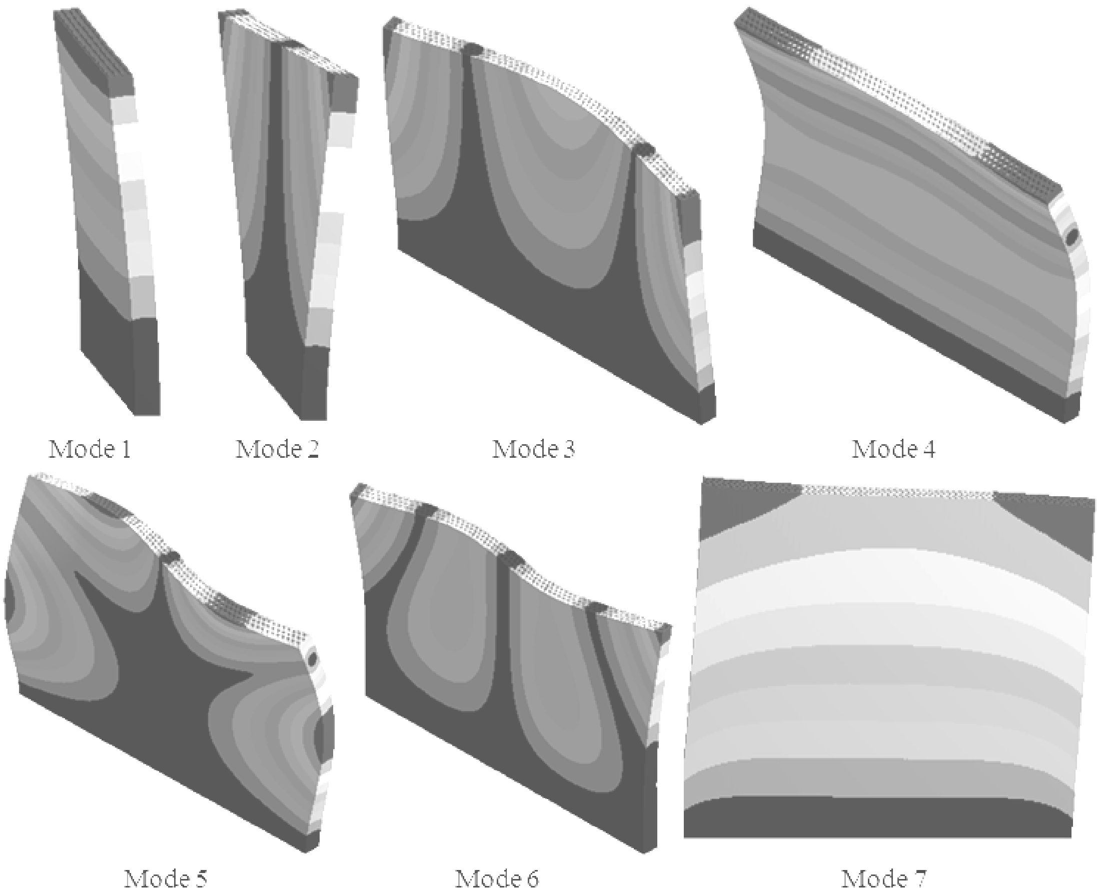

Fig.5. Modal shapes of a sandwich wall - model V21

It means that the sandwich structures have substantially lower weights and wider operational bandwidths than solid walls, which justifies the effort to replace solid walls by sandwich walls. Of course, the corresponding amplitudes of natural vibrations of solid walls are the smallest (Table 3, Fig.7), which means that all aspects of vibration behaviour of sandwich structures need careful consideration before a selection is made for a specific application.

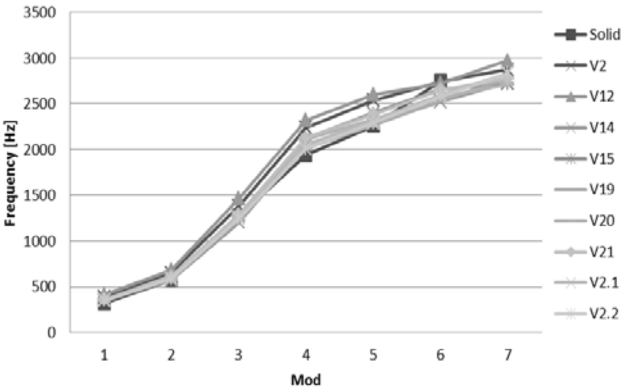

Fig. 6. Diagram of the natural frequencies

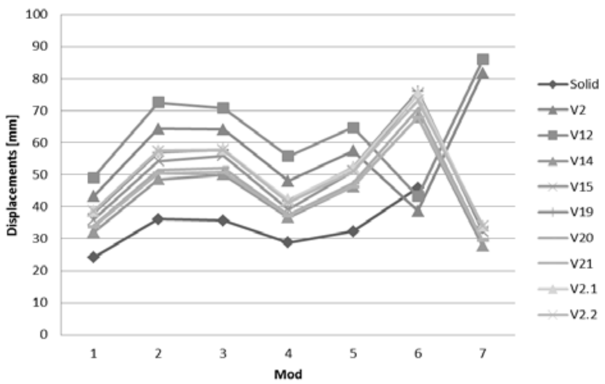

Fig. 7. Diagram of the maximal displacements

In general, the corresponding amplitudes decrease with increase of density, regardless of the shape of the sandwich core, which is presented in the Fig. 8, where these two quantities are shown in a log-log diagram.

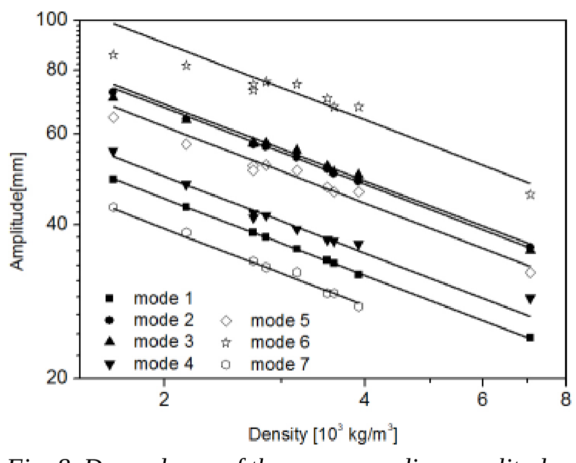

Fig. 8. Dependence of the corresponding amplitudes on the density of the sandwich walls

The solid lines have slope equal to -1/2, which corresponds to proportionality of the amplitudes to inverse square root of the density, as it is the case with solid walls. The figure shows that low-frequency modes obey the inverse-square-root dependence for all samples. On the other hand, high-frequency modes show significant deviations from the inverse-square-root dependence. It means that the shape of the substructure of the core influences the amplitudes of natural vibrations at high frequencies. Such behaviour may be explained by ratio between the wavelengths of vibrations and characteristic dimensions of the substructures. When the wavelengths of vibrations are large in comparison with characteristic dimensions of the substructure, then the whole volume of the substructure cells is subjected to approximately constant stress, as it is the case with solid walls. Therefore, the differences between shapes of the substructures have no influence on the amplitudes of low-frequency vibrations. On the other hand, when the wavelengths of vibrations are small, then various parts of the substructure cells are subjected to various stresses, and the shape of the substructure influences the amplitudes of the vibrations.

6. CONCLUSON

The presented research considered influence of core substructure on modal behaviour of twenty-three types of sandwich walls, with the idea to study possibilities of lightweight design opened by introduction of additive manufacturing technologies capable of manufacturing of end parts. To that purpose were calculated frequencies and corresponding amplitudes of natural vibrations of the sandwich walls in the frequency range between 0 Hz and 3000 Hz.

The results have shown that the amplitudes of the natural vibrations depend on the shape of substructure when the wavelength of the vibrations is comparable to characteristic dimensions of the substructure.

On the other hand, the frequencies of natural vibrations depend on the shape of the core substructure in a complex manner that cannot be easily explained. However, it appears safe to conclude that the natural frequencies of sandwich walls are always higher than the natural frequencies of the solid wall with the same thickness. This property makes vibration behaviour of sandwich wall structures worthy of further research, which will be oriented towards variations of parameters of core shape parameters.

7. ACKNOWLEDGEMENT

The authors wish to express their gratitude to Ministry for education, science and technology of Republic of Serbia for support through research grants TR35006.

8. REFERENCES

[1] S. Ćirić-Kostić, and M. Ognjanović. "The Noise Structure of Gear Transmission Units and the Role of Gearbox Walls." FME Transactions 35 (2), pp. 105-112 (2007)

[2] J. Zhou, W. Sun, Q. Tao, "Gearbox Low-Noise Design Method Based on Panel Acoustic Contribution", Mathematical Problems in Engineering, vol. 2014, Article ID 850549, 10 pages, (2014)

[3] G. Kopp, J. Kuppinger, H. E. Friedrich, F. Henenning, "Innovative Sandwich Structures for Functionally Integrated Lightweight Design", ATZ worldwide, Volume 111, Issue 4, pp. 44-49, (2009)

[4] E. Nilsson, A. C. Nilsson, "Prediction and measurement of Some Dynamic properties of Sandwich Structures with Honeycomb and Foam Cores", Journal of Sound and Vibration, 251(3), pp. 409-430, (2002)

[5] R. Harish, R. S. Sharma, "Vibration Response Analysis of Honeycomb Sandwich Panel with Varying Core Height", International Journal of Emerging Technologies in Computational and Applied Sciences (IJETCAS), 13-433, pp. 582-586, (2013)

[6] K. C. Cheung, N. Gershenfeld, " Supplementary Materials for Reversibly Assembled Cellular Composite Materials", DOI: 10.1126/science.1240889, (2013)

[7] C. Atwood, "Manufacturing Advances, Applications, and Challenges." Additive/Subtractive Manufacturing Research and Development IN Europe, Vol. 1001, pp.25-33, (2005)

[8] K. C. Cheung, N. Gershenfeld, "Reversibly Assembled Cellular Composite Materials", Science Vol.341, pp. 1219-1221, (2013)

[9] D. L. McCarthy, C. B. Williams, " Creating Complex Hollow Metal Geometries Using Additive Manufacturing and Electroforming ", International Solid Freeform Fabrication Symposium, pp. 108-120, (2012)

[10] D. Suman, et al. "Direct Laser |Freeform Fabrication of High Performance Metal Components." Rapid Prototyping Journal 4.3, pp.112-117, (1998)

[11] M.Tomlin, J.Meyer. "Topology Optimization of an Additive Layer Manufactured (ALM) Aerospace Part." The 7th Altair CAE Technology Conference, pp.1-9, (2011)

[12] Additive manufacturing " Strategic Research Agenda" (2014)

Numerical-Experimental Identification of a Working Unit Module Dynamic Characteristics

Aleksandar Košarac[1*], Milan Zeljković[2], Cvijetin Mlađenović[2], Aleksandar Živković[2]
[1]Faculty of mechanical engineering, University of East Sarajevo, East Sarajevo, BiH
[2]Faculty of Technical Sciences, University of Novi Sad, Novi Sad, Serbia

This paper shows identification of dynamic characteristics of working unit module, based on application of ANSYS Workbench software. Working unit module (quill unit) is in fact the main spindle fitted in a module quill attached to the drive-transmission structure for the main rotational and the auxiliary rectilinear movement. Natural frequencies along with the main modal shapes are determined for main spindle (with and without bearings), module quill and working unit module. Validation of gained results was obtained by experimental examination using impact testing.

Key words: Working unit module, module quill, main spindle, LabVIEW, ANSYS, natural frequencies

1. INTRODUCTION

In the course of massive production and manufacturing it is quite justified to use special systems for producing a range of similar products. However, taking into consideration the fact that even mass manufactured products relatively quickly become out-dated in modern society it is necessary to enable certain level of flexibility by using flexible manufacturing systems.

One of methods to increase flexibility of manufacturing systems is based on the modular principle of its design [1]. By applying modular principle of designing of production systems it is possible to change the purpose of manufacturing system by simple replacement of appropriate module and thereby to increase its flexibility, setting the conditions for re-configurability of manufacturing systems.

Within the project [2] flexible manufacturing systems for wide areas of parts have been developed in the field of high volume and mass production processed with rotational tools. These flexible manufacturing systems are designed based on the modular principle and one of the main modules of such designed manufacturing systems, apart from the module of the rotary table, is the working unit module. Behaviour of the working unit module, performing main and auxiliary movement with such systems, determines the behaviour of flexible manufacturing system as a whole.

The work piece and the carriage system of the working unit module remain stationary throughout process while the tool makes the main and auxiliary movements.

Working unit module, figure 1, is in fact the main spindle fitted in a mobile quill attached to the drive-transmission structure for the main rotational and the auxiliary rectilinear movement. Due to such constructional design these modules are called the quill units [3].

The working unit module is intended for processing the following surface shapes [3]:

- Outer and inner cylinder surfaces,
- Flat front surfaces achieving changes between rotational surfaces or interrupting them,
- Conical or arbitrary functional rotational surfaces,
- Inside or outside threading by appropriate tools.

As mentioned before, the behaviour of working unit module determines the behaviour of flexible manufacturing system as a whole and in the purpose of meeting harsher demands set before the manufacturing systems it is necessary to foresee, as reliably as possible, the dynamic behaviour of this module when being exploited.

This paper presents the manner to identify the basic dynamic characteristics of working unit module and containing elements based on ANSYS Workbench software. Experimental verification of numerically obtained results was done by impact testing. Within the frame of basic dynamic characteristics, natural frequencies, modal shapes and damping ratio are determined.

2. STRUCTURE OF THE WORKING UNIT MODULE

Working module unit is consisted of the main spindle, quill, housing, elements of carriage structure, drive engine and transmitter for main and auxiliary movement, figure 1.

Figure 1. Working unit module
1. main spindle, 2. quill, 3. housing. 4. carriage elements, 5. motor, 6. main movement system

Main spindle is supported by the two sets of angular contact ceramic ball bearings in front, SKF S7011

*Corresponding author: Vuka Karadžića 30, 71123 Istočno Sarajevo, akosarac@gmail.com

CD/HCP4A and two sets of angular contact ceramic ball bearings in rear SKF 7008 CD/HCP4A, installed back to back, figure 2. Layout of the main spindle assembly is provided in the figure 2. Values of bearing stiffness depending on the preload are provided in the table 1 [8]. Described module of the working unit, due to the need for axial movement of quill has specific constructional solution of the main spindle assembly, with free end of main spindle of relatively large length. Therefore it is quite interesting to observe dynamic behaviour of such an assembly.

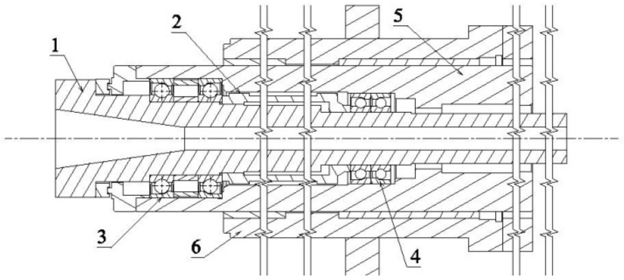

Figure 2. Main spindle assembly 1. shaft, 2. spacer, 3. front bearing set, 4. rear bearing set, 5. quill 6. housing

Table 1. Stiffness of bearing [8]

	Preload					
	Small		Middle		Big	
	Front brg set	Rear brg set	Front brg set	Rear brg set	Front brg set	Rear brg set
Radial stiffness N/µm	400	280	560	387	690	475
Axial stiffnes N/µm	69	48	115	82	170	120

3. NUMERICAL MODAL ANALYSIS OF COMPONENTS OF WORKING UNIT MODULE

When exploiting, the behaviour of main spindle assembly has the largest influence on dynamical behaviour of machine tool, as a whole. Modal analysis of the main spindle assembly presents the primary issue when analysing dynamical characteristics, taking into consideration the influence of vibrations over the quality of processing and influence on surface roughness, dimensional precision, etc), cutting tool-state (tool wear or tool breakage), or damage machine tool components, etc. As determined earlier, working unit module is consisted of the large number of different parts, sub-assemblies of different level of complexity. However, for simplified analysis the module of the main spindle can be observed, bedded in appropriate manner, figure 3 [10].

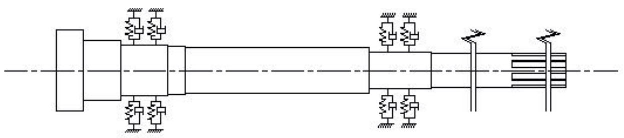

Figure 3. Equivalent dynamic model of a main spindle

When defining main spindle support models, spindle bearing could be modelled in two different ways. In the first case by modelling bear elements and applying the appropriate types of contacts between, figure 4 (by modelling bearing inner and outer race, balls...).

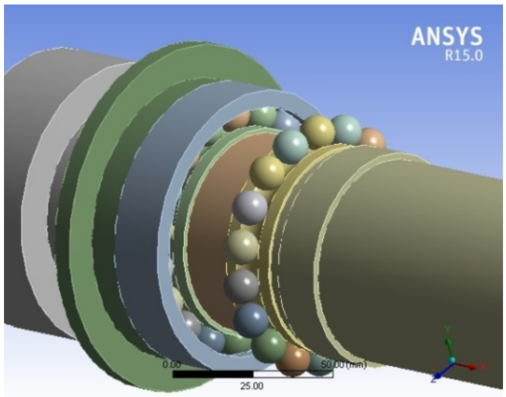

Figure 4. Main spindle modelled in ANSYS Workbench

In the second case, spindle is supported by linear spring-damper elements (COMBIN14) bedded around the main spindle, figure 5. Total stiffness of these elements, within each plane, corresponds to the stiffness of bearing provided in table 1. Even though both, stiffness and dumping, are imminent to COMBIN14 element, given the fact that damper has little influence on the natural frequencies of the transversal vibrations, the damper element can be ignored [5].

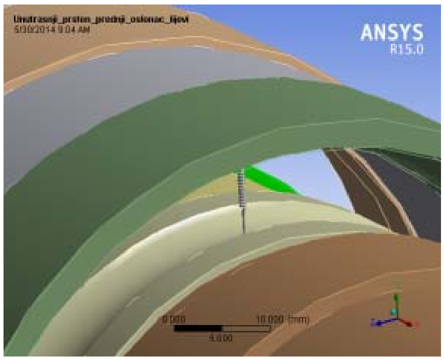

Figure 5. Model of bearing with COMBIN 14 linear spring - damper element

When modles are done, mesh is generated authomatically. The material is linear isotropic structure steel. Young's modulus is 2*10MPa, Poisson's ratio is 0.3. Contact Analysis Parameters are set as follows: Several types of behavior of contact are given in ANSYS Workbench, which are symmetric, asymmetric and auto symmetric.Here asymmetric contact is chosen between two contact surfaces of this model. For different interests and different kinds of problems, different contact algorithms can be chosen to solve the model. Here the Augmented Lagrange contact algorithms is chosen. Between the ball and the raceway frictional contacts are chosen and friction coefficient is µ=0.002

Considering that this is a modal analysis, no load was applied to the structure. Boundary condition is of great importance for the structure analysis because under different kind of boundary condition, the structure will respond differently.

The boundary conditions in ANSYS Workbench applied to the front bearing set was shown in figure 6. The outer ring is fixed (surface E, F) and there is no degree of freedom left (fix constraint). The inner ring cannot only move in the x direction, axialy (displacement costraint, surface A,B,C,D). Frictionless support (applied to outer ring cilindricay surface) means the body cannot move in the normal direction of the surface but can slide in the tangential direction (surface G).

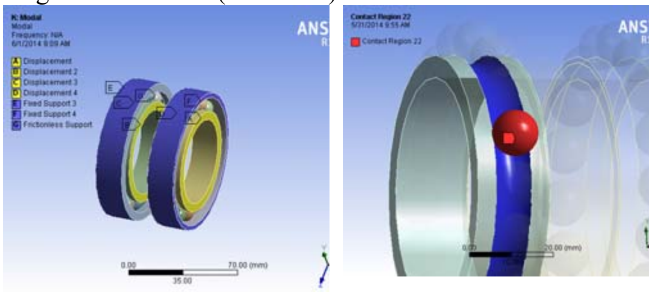

Figure 6. Boundary condition and contact surfaces

4. EXPERIMENTAL MODAL ANALYSIS

The excitation by impact hammer was given to mechanical structure and then the vibration response was obtained experimentally. Based on Fast Fourier Transform of time domain response data range of frequencies that includes the natural frequencies of the examined elements was determined.

Vibration measurement chain to identify the dynamic behaviour consists of excitation and response subsystems and subsystem for data acquisition and processing, figure 7 [10].

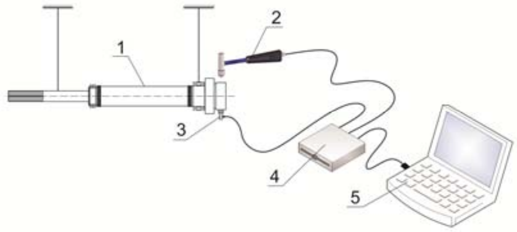

Figure 7. Experimental setup layout for determination of dynamic characteristic of mechanical systems by impact hammer excitation: 1. main spindle, 2. impact hammer, 3. accelerometer , 4. data acquisition module, PC - LabVIEW and Matlab (data processing)

The excitation subsystem provides excitation force. The excitation to the structure can be provided by an electromagnetic or hydraulic shaker where its tip is fastened to the point of interest. A more practical approach is to use the Fourier analysis where an impulsive force instead of a harmonic one can be used to excite a wide range of frequencies in one test. This approach has been commonly used in impact tests where a point on the structure is excited using an instrumented hammer and the response at the same or another point is measured by a sensor, usually an accelerometer.

For excitation main spindle (without bearing and with bearing and spacer between front and rear bearing sets), suspended for free-free measurement, impact hammer Brüel & Kjær 8206 was used. Image and dimensions of impulse hammers are given, figure 8. Impulse hammer has three replaceable tips, aluminium, plastics and rubber. Because it is not feasible to change the stiffness of the test object, therefore the frequency content is controlled by varying the stiffness of the hammer tip. For this test aluminium tip was used, allowing shorter pulse duration and thus the higher the frequency content.

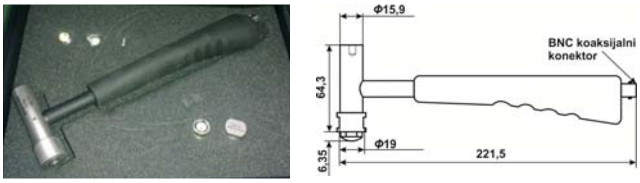

Figure 8. Impact hammer Brüel & Kjær 8206

For excitation of working units module and module quill (without main spindle), impact PCB Piezotronics Model 084A32 with the tip model 086D50 (hard tip) was used, figure 9.

The response subsystem consists of sensor of acceleration. Although the response can be measured by many different sensor types such as displacement or velocity transducers, the most common method is to use accelerometers. For this testing accelerometer METRIX Instruments SA6200A with piezo-ceramic was used. The accelerometer has the following characteristics: the sensitivity 100mV/g, possibility of measuring up to 10 kHz and 50 g. Accelerometer was mounted directly using a magnetic holder to module quill, figure 10, as well as to spindle free end, figure 11.

For data acquisition and processing National Instruments equipments consisting of National Instruments cDAQ chassis 9172, and the analogue card NI 9233 with four analog input voltage range of ± 5 V, and the maximum speed selection signal channel 50 kS / s (kilo samples per second) were used. For data acquisition LabVIEW softer was used, and Matlab software to get FFT. Detail from experimental testing of module quill is shown in figure 10, and testing of free-free suspended main spindle in figure 11.

Figure 9. Impact hammer PCB Piezotronics model 086D50

Figure 10. Experimental setup for module quill testing: 1. NI cDAQ 9172 with NI 9233 card, 2. piezoelectric accelerometer METRIX Instruments

Modal parameter identification procedure is as follows: accelerometer was attached to the tested structure. The impact hammer, containing the force transducer, was moved from point to point, and at each location the structure was impacted several times. In doing so, an aluminium top is used since it gives more energy for excitation. Accelerometer is mounted on the opposite side from the spot of hammer impact. Then, time domain response data (impulse versus time and response versus time) are recorded using NI equipment described above. During acquisition equipment and software needs to be set taking into account that the maximum useful frequency in digital Fourier results is half the sampling rate.

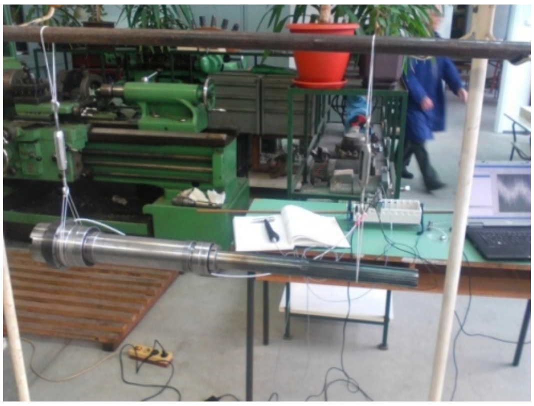

Figure 11. Overview of main spindle "free-free" supported experimental setup

Figure 12a i 12b shows time domain impulse data and response data. Using Matlab time domain response data are transformed to the frequency domain (using the Fast Fourier Transform (FFT)) and frequency response curves were determined. Frequency response curves containing first four natural frequencies is shown in figure 12c.

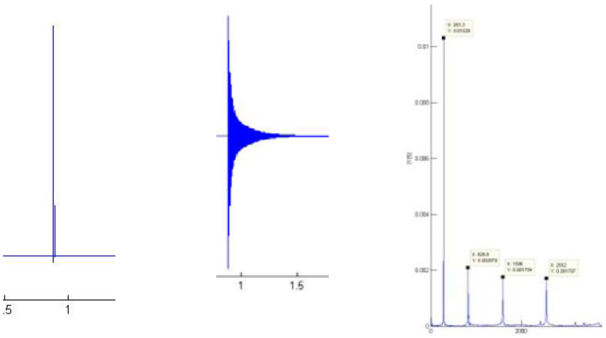

a. Time domain impulse data *b. Time domain response data.* *c. Frequency response curve.*

Figure 12. Modal parameter identification

Based on the determined FFT, it can be seen for most of conducted measurements that modal frequencies are separated by a sufficient frequency margin so that the spectral peaks are distinct (except in quill module mounted in housing) i.e. frequency response curve were not overlapped $\omega_{oi} - \omega_{oi-1} >> \Delta\ \omega_{oi} + \Delta\omega_{oi-1}$. Such vibration system can be consider as single degree of freedom systems on each natural frequency.

Bearing in mind the above mentioned to determine the damping ratio will be used well-known "half-power bandwidth" method. The half-power bandwidth method can be used to estimate the damping ratio and corresponding Q value from the frequency response function of a structure which has been excited by applied force. It is then assumed that half the total power dissipation in this mode occurs in the frequency band between ω_1 and ω_2, where ω_1 and ω_2 are the frequencies corresponding to an amplitude $\omega_n/\sqrt{2}$ (-3 dB points are also referred to as the half power points on the frequency response curve). Figure 13. illustrates procedure for finding damping ratio. Also it can be seen that damping ratio can be calculated as

$$2\zeta = \frac{1}{Q} = \frac{\omega_2 - \omega_1}{\omega_n} \qquad (1)$$

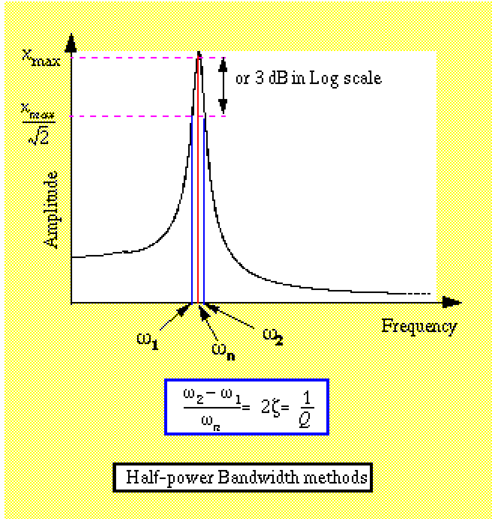

Figure 13. "Half-power bandwidth" method

Although the literature usually takes the width of the frequency response curves at the height of an amplitude $\omega_n \frac{\sqrt{2}}{2}$ (half-power bandwidth method), in this paper another method was used also for the same purpose. This method is very similar to previously shown, only difference is the frequency response curves width is taken on amplitude $\frac{\omega_n}{2}$. Using this damping ratio is calculated by equation:

$$2\zeta = \frac{1}{Q} = \frac{\omega_2 - \omega_1}{\sqrt{3}\omega_n \omega_n} \qquad (2)$$

Table 2 shows the values of damping ratio of main spindle without bearing and with bearing and spacer, both suspended for free-free measurement, as well as working unit module damping ratio. Damping values were obtained by the above mentioned methods. Comparing obtained values can be concluded that in the case modal frequencies curve peaks are distinct and there is no overlap between frequency curve (in this case, during testing main spindle without with and without bearing suspended for free-free measurement), using both method dumping ratio values are approximately equal. Specifically difference damping ratio for the first and second natural frequency ranged from 2.2% to 7.3% which can be considered very satisfactory.

Difference between obtained values for the third natural frequency is slightly bigger than 20%. In reaching conclusions, we must bear in mind the impossibility of accurate readings the values of the frequency points on the frequency response curve.

Table 2.Obtained values of damping ratio

	ω_i	$\omega_n \frac{\sqrt{2}}{2}$ meth.	$\frac{\omega_n}{2}$ meth.	Diff. [%]

Damping ratio free-free suspended main spindle without bearings	283,2	$2\zeta = \frac{283,5 - 283}{283,2} = 0,001765$	0,001835	3,97 %
	826,6	$2\zeta = \frac{827,6 - 825,1}{826,6} = 0,0030244$	0,002933	3%
	1596	$2\zeta = \frac{1598 - 1592}{1596} = 0,0037599$	0,002894	23%
Damping ratio free-free suspended main spindle with bearings	277,8	$2\zeta = \frac{279 \quad 276,4}{277,8} = 0,00935$	0,009560	2,2%
	915,5	$2\zeta = \frac{924 - 906,7}{915,5} = 0,018889$	0,01747	7,3%
Damping ratio working unit module	145	$2\zeta = \frac{152,9 - 136,1}{145} = 0,122$		

5. COMPARING THE RESULTS OF FEM ANALYSIS AND EXPERIMENTAL MODAL ANALYSIS

A number of numerical and experimental analysis of components, subassemblies and assembly of working unit module were done in way described in section 2 and 3. The following shows results of these analysis.

Tables 3-6. include the value of natural frequencies of free-free main spindle without bearing, free-free main spindle with bearing and spacer, module quill and working unit module, obtained using the ANSYS Workbench software and experimental testing. In the table below the results obtained by impulse excitation and by Gen Rad 2515 system are shown also [8]. If, with respect to all inaccuracy that goes along with experimental testing, adopt that experimental tests are more accurate than numerical, we can come to a conclusion about the validity of the numerical model. Comparing the results of numerical simulations and experimental tests, the deviation of the first, second and third natural frequencies of main spindle suspended for free-free measurement, without bearing, shown in table 3 are respectively -1.47%, -1.15% and -2.75%, while the deviations of the experimental results and results presented in [8] is less than 1%. Deviations results gained by numerical analysis of the experimental results for the first and second natural frequencies of main spindle suspended for free-free measurement, with bearing and spacer, shown in table 4 are respectively 1.5%, and 3.8%, while deviations experimental results of results presented in [8] are 1,98% and 2,7%. Deviations results gained by numerical simulations of module quill of experimental results for the first, second and third natural frequencies are respectively 0,95%, 1,15% and 0,4% , table 5. Deviations results gained by numerical analysis of the experimental results for the first natural frequency of working unit module, are 1.04% and 0.3% depending on the method for modelling main spindle support, table 6. In this case more accurate results were obtained by modelling ball bearing.

Figures 14-17 show first mod of vibration of tested element gained numerically by ANSYS, and FFT of time domain response data, indicating the values of natural frequencies. Based on the first mod of vibrations can be concluded that the largest are spindle end displacements, while the displacement of the top of the spindle are relatively small. From the standpoint of accuracy of the machine it is satisfactory, but a relatively large displacement of the spindle end make a dynamic excitation force of elements of the main movement system. As a result vibration and noise of main movement system increase. In this case main movement system is with toothed belt.

Table 3. Natural frequencies free-free suspended main spindle

	Spindle suspended for free-free measurement (without bearing) Hz		
	First natural frequency	Second natural frequency	Third natural frequency
Experimental results	283,2	826,6	1595
ANSYS	279.19	817.1	1551.2
According to [8]	285	832,9	-

Table 4. Natural frequencies free-free suspended main spindle

	Spindle suspended for free-free measurement (with bearing) Hz		
	First natural frequency	Second natural frequency	Third natural frequency
Experimental results	277,8	915,5	-
ANSYS	281,97	950,63	-
According to [8]	283,3	940,2	-

Table5. Natural frequency module quill

	Module quill Hz		
	First natural frequency	Second natural frequency	Third natural frequency
Experimental results	778,8	1047	2080
ANSYS	786,21	1059,1	2088,3

Table 6. Natural frequencies of working unit module

	Working unit module Hz (1^{st} natural frequency)	
	(supported by COMBIN 14 spring damper element)	(supported by bearing model with balls)
Experimental results	147,5	
ANSYS	149,03	147,93

Main spindle vibration

ANSYS FFT

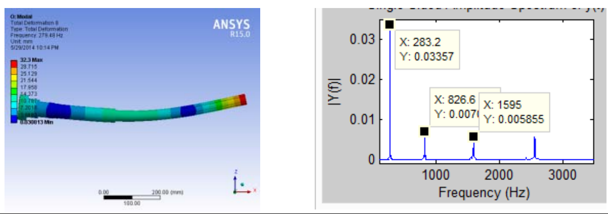

Figure 14. Free-free suspended main spindle

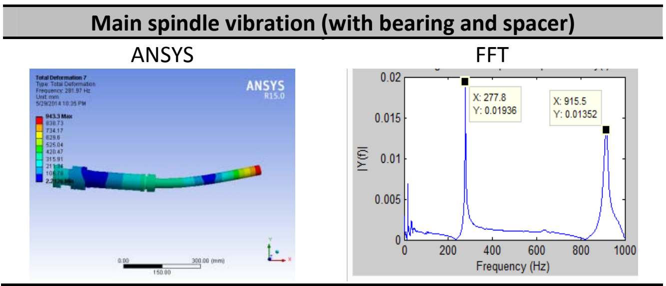

Figure 15. Main spindle with bearing (free - free state)

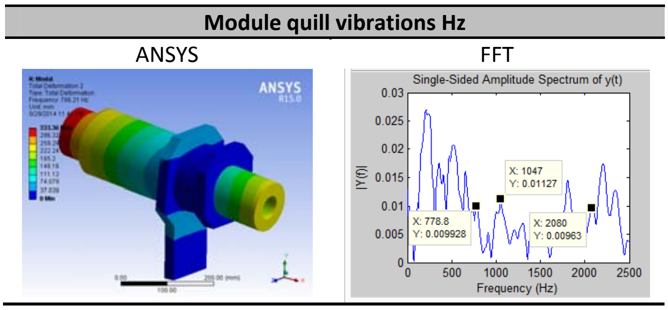

Figure 16. Module quill

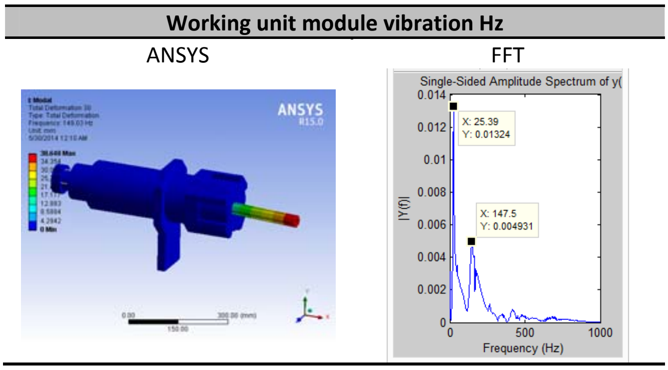

Figure 17. Working unit module

6. CONCLUSION

This paper describes the application of finite element method in the identification of modal parameters, natural frequencies and mode shapes of working unit module, and compare the obtained results with experimental results. Modeling geometry and modal analysis of working unit were done using ANSYS Workbench environment. Natural frequencies of main spindle with and without bearing (in free-free state), module quill and working unit module were determined. Comparing the modal parameters obtained using the finite element method and experimentally can be seen a little deviation of the results. Therefore numerical simulation obtained quite satisfactory results. Discussed ways of supporting the main spindle model at each end by set of bearing or linear spring - damper element COMBIN 14 indicates that the differences in the results is very small. Consequently simplified representation of the spindle system with spring - damper element can be found in literature more often.

Research may contribute to the detection and prevention of chatter vibration of working unit module, as the most sensitive element of the mechanical structure of the machine tool from the point of the dynamic behaviour.

ACKNOWLEDGMENT

In this paper some results of the project: *Contemporary approaches to the development of special solutions related to bearing supports in mechanical engineering and medical prosthetics* – TR 35025, carried out by the Faculty of Technical Sciences, University of Novi Sad, Serbia, are presented. The project is supported by Ministry of the science and technological development of the Republic of Serbia.

LITERATURA

[1] Rekecki, J., Zeljković, M., Novaković, D., Borojev, Lj.: Modularni koncept gradnje specijalnih mašina alatki za obradu rotacionim alatima, Deseto jubilarno savetovanje BIAM '90, Zbornik radova JUREMA 35, Svezak 4, str. 50-53, 11.-13. Jun 1990., Zagreb, ISBN: 86-81517-05-2.

[2] Rekecki, J., Zeljković, M., Borojev, Lj., Novaković, D.: Jedinica pinole sa hidrauličnim pomakom – PJH 55, Elaborat ispitivanja, Institut za proizvodno mašinstvo FTN, Novi Sad, 1989.

[3] Zeljković, M., Borojev, Lj., Rekecki, J., Novaković, D.: Eksperimentalna identifikacija ponašanja modula radne jedinice, IV naučno – stručni skup Fleksibilne tehnologije – MMA '90, Institut za proizvodno mašinstvo FTN, 25-27. Septembar, str. 899- 909, 1990, Novi Sad.

[4] Zeljković, M., Borojev, Lj., Rekecki, J., Novaković, D.: Experimental Identification of the Behaviour of A Working Unit Module, Publications of The School of Ebgineering Sciences, University of Novi Sad, Vol. 21&22, pp.115-125, Novi Sad, 1990&1991. ISSN: 0350-428X.

[5] Deping Liu, Hang Zhang, Zheng Tao, Yufeng Su: Finite Elemet Analysis of High - Speed Motorized Spindle Based on ANSYS, The Open Mechanical Engineering Journal, 2011, 5, 1-10

[6] S.Szath Abuthakeer, P.V.Mohanram, G Mohan Kumar: Dynamic Characteristics Analysis of High Speed Motorized Spindle, Annals of Faculty Engineering Hunedoara - International Journal of Engineering Tome IX (Year 2011). Fascicule 2. (ISSN 1584 - 2665)

[7] Anayet U. Patwari,1 Waleed F. Faris,2 A. K. M. Nurul Amin,1 and S. K. Loh3: DynamicModal Analysis of VerticalMachining Centre Components, Hindawi Publishing Corporation, Advances in Acoustics and Vibration, Volume 2009, Article ID 508076, doi:10.1155/2009/508076

[8] Zeljković, M.: Sistem za automatizovano projektovanje i predikciju ponašanja sklopa glavnog vretena mašina alatki, Doktorska disertacija, Fakultet tehničkih nauka, Novi Sad, 1996.

[9] Zeljković, M., Gatalo, R. (1999): *Experimental and computer aided analysis of high-speed spindle assembly behavior*, CIRP Annals - Manufacturing Technology, ISSN: 0007-8506 Vol. 48/1, Pages 325–328.

[10] Košarac A.: Razvoj mašina alatki primenom virtualnih modela sa posebnim osvrtom na dinamičko ponašanje skkopa glavanog vretena, Doktorska disertanija - radni materijal, Fakultet tehničkih nauka Novi Sad, 2013

The Use of Virtual Models in the Design of Mechanisms

Ivan Milićević[1*], Stojan Savković [1], Milosav Šekarić[1], Radomir Slavković [1], Nedeljko Dučić [1], Marko Popović [1]
[1]Faculty of technical science, Čačak, University of Kragujevac, Serbia

The subject of this work are research related to the development of the design of mechanisms using the virtual model obtained by integrating various modern software packages, specialized in certain areas of computer-aided design. For example coulisse mechanism, it's made the design, analysis and simulation of the considered mechanism. Virtual model control algorithm was implemented in Matlab SimMechanics, as an open kinematic's chain. The analysis requires the necessary movements to achieve the production cycle of the considered mechanism. The analysis of certain parameters of the system, most preferably features of the individual components are selected in order to obtain the required characteristics of the mechanism. To define the 3D model, SolidWorks software package was used.

Keywords: virtual model, analysis, simulation, Simulink, Matlab, SolidWorks

1. INTRODUCTION

The development of computer science in recent years has enabled the emergence of numerous software which can efficiently solve various engineering problems. However, the principle of so-called modern integrated design approach [1-5] (*Fig.1*), due to the need for a comprehensive analysis in order to obtain satisfactory results, it is often obtruded a necessity to make the integration of modern software packages, which are specialized for certain areas of the design to a program unit. Thus, for example, in the design of mechanisms [6-8] it is necessary to consolidate some of the CAD software which can be implemented geometric 3D models with software in which the next simulation of movement can make the analysis of kinematics and dynamics of the moving parts of the mechanism, as well as design management through appropriate control algorithms. [9], [10]

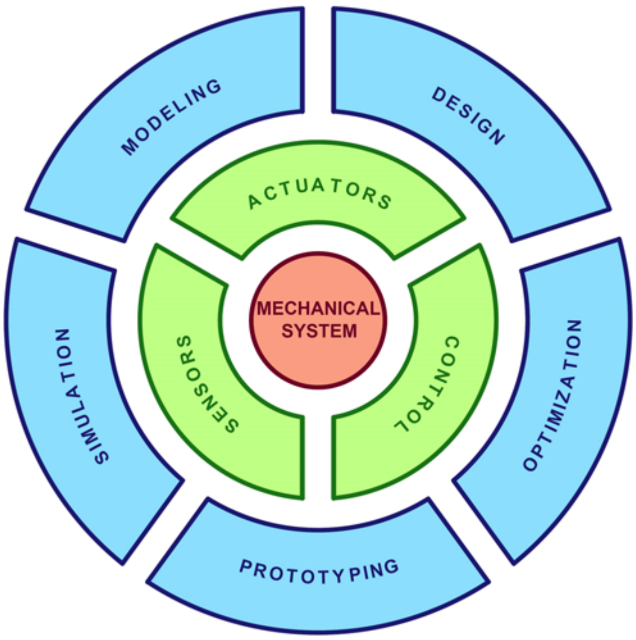

Figure 1: Integrated design approach

MATLAB is widely applicable multidisciplinary engineering software that allows mathematical calculations, developing algorithms, simulation and process analysis, data processing, visualization, and all this through interactive and programmatic work [11-13].

Simulink, as part of the software package Matlab is used for simulation of dynamic models (graphical environment). They can analyze linear, nonlinear, time-continuous and/or discrete time models with multiple inputs and outputs and with concentrated parameters. Simulink is used for the generation of the control algorithm, and the analysis of the simulation model [14].

To generate the model geometry it was used ***SolidWorks*** software package [15-20]. 3D models of individual components as .stl files (StereoLitography or Standard Tessellation Language - a standard format that is used to describe the geometry of three-dimensional object) imported into the Matlab environment.

2. MODELING OF PLANER MECHANISM

To generate the Simulink model of any mechanism, in Matlab is available library of standard components. For modeling coulisse mechanism of shaping tool, from Simulink/Simscape/SimMechanics libraries are used blocks:

- *Ground* - grounding one side of the joint (*Joint*) for a fixed point in the global coordinate system.
- *Body* - is a user defined rigid body defined by its mass, moments of inertia, dimensions, and its center of gravity in the home position.
- *Revolute* - a link that allows you to rotate around the pivot axis defined;
- *Gear Constraint* - block defining the coupling of normal cylindrical gear pair;
- *Prismatic* - a link that allows translational movement along a randomly chosen axis.

In the next step from the *Simulink* library were taken two blocks, „*Joint sensor"*, connected to the block „*Scope"* in which graphicly can be displayed the position, velocity and acceleration of the observed elements in the course of the cycle.

Block „*Joint actuator"* is used to set the initial conditions, apropos the generalized force/torque, and linear/angular position.

*Corresponding author: 65 St. Save street, e-mail: ivan.milicevic@ftn.kg.ac.rs

Gravitational center of the pinion gear is set at a distance of 2m from the center of the driven gear, which is the axial distance. The block „*Gear Constraint*“ has been selected to the radius of the pinion is 0.5m, and the driven 1.5m (*Fig.2*).

At a distance of 1m from the center of the driven gear in the y-axis direction (*Fig.3*), is defined the position of the cam, or item for which the associated slide (*Fig.6*), whose movement is defined by introducing block „*Prismatic*“

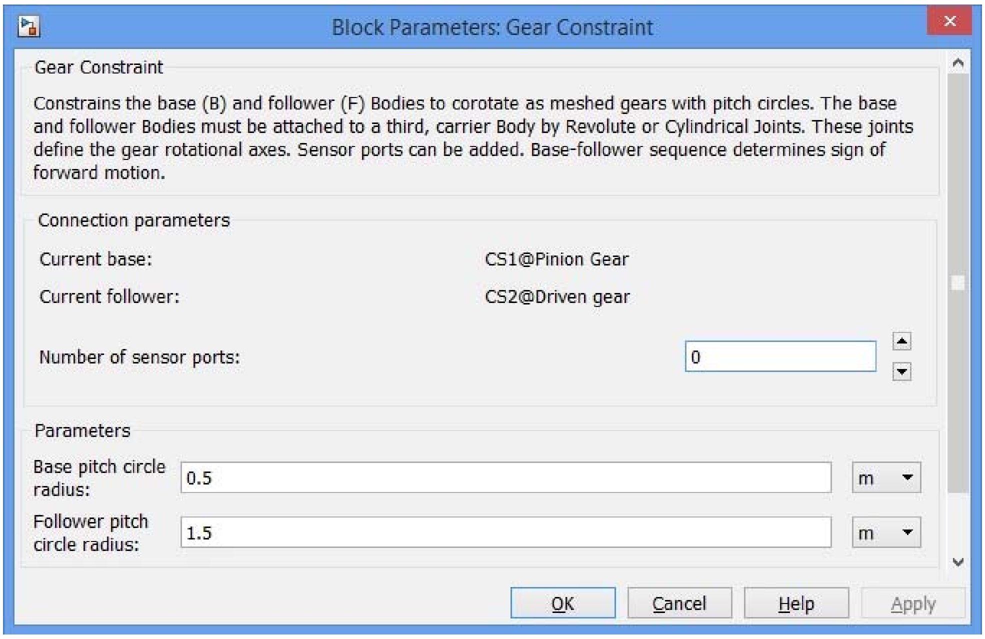

Figure 2: Defining the parameters of Gear Constraint

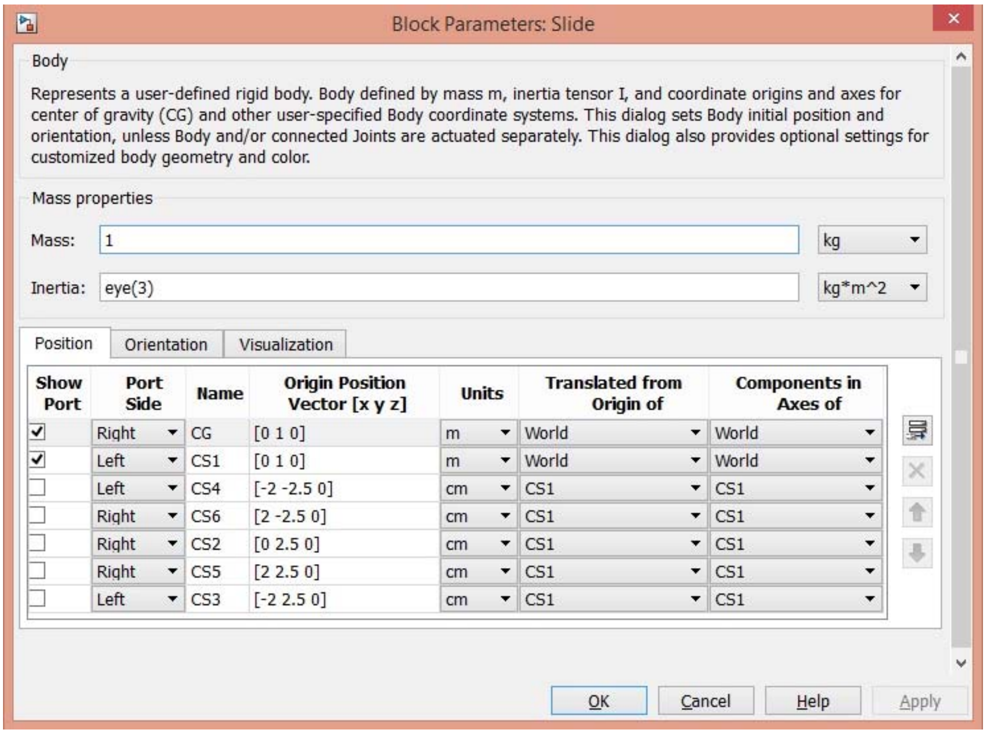

Figure 3: Defining the parameters slide of coulisse

The slider is connected by joint with a coulisse (rotation around the z-axis).

Coulisse has one end connected to a joint with the ground, and the other end is also a joint, making the straight movement and is achieved by the movement of the lever carrying the executive body (working tools).

On Fig.4 is shown the window that defines all the parameters scenery . The stroke was achieved by using the block „*Prismatic*“ link that represents the guideline for translational motion in the x-axis direction lever to the executive body.

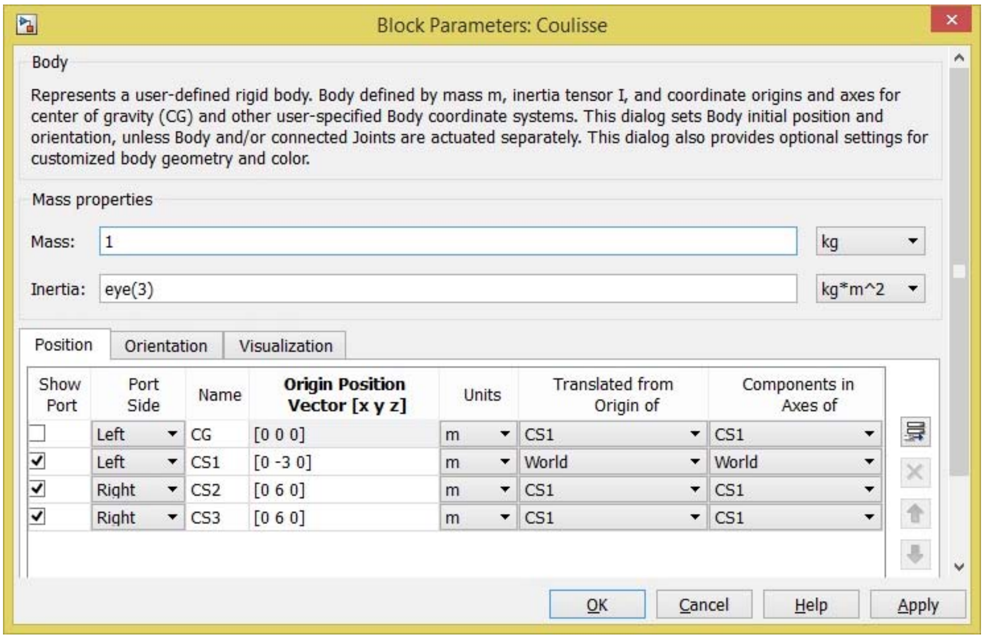

Figure 4: Defining the parameters of coulisse

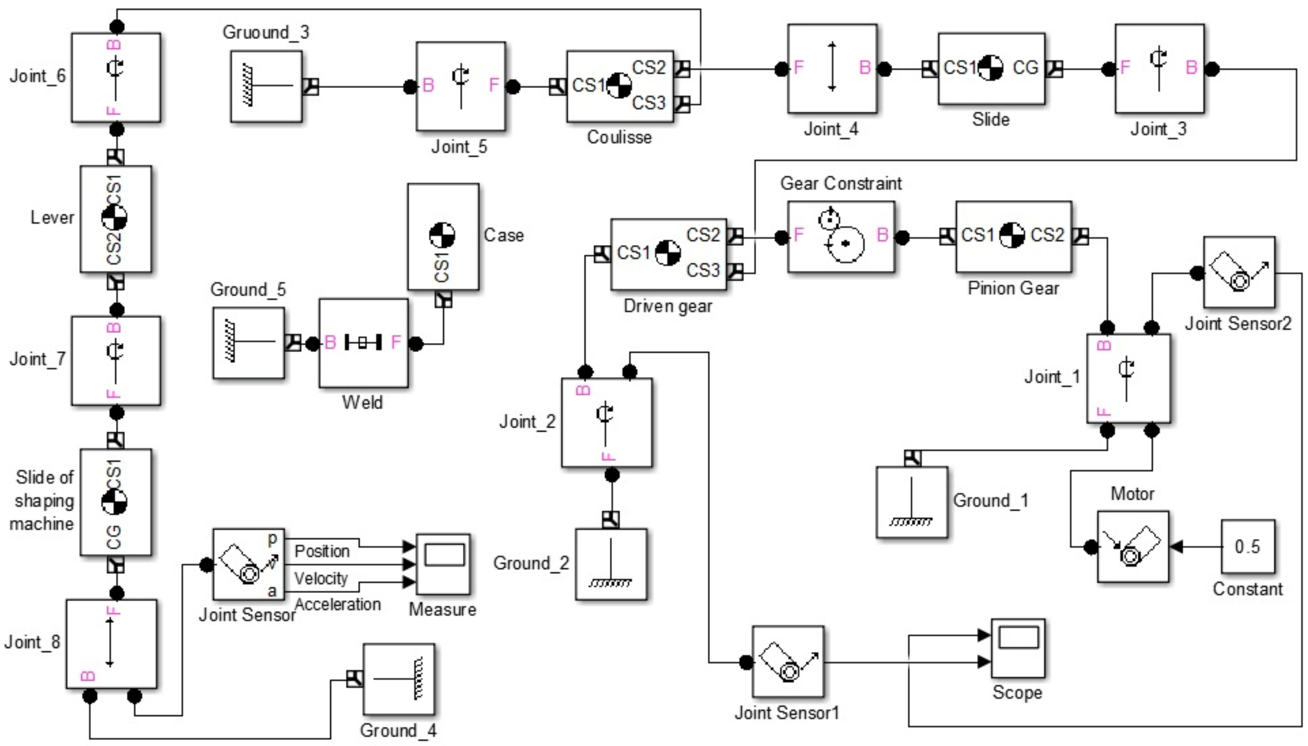

Figure 5: Block diagram of the mechanism SimMechanics

After connecting the individual blocks, we get a block diagram of the entire mechanism (*Fig.5*).

Importing 3D models from SolidWorks software package [3-6] as stl. file in *Matlab* environment and starting the program produces a graphical display of the entire mechanism (*Fig.6*).

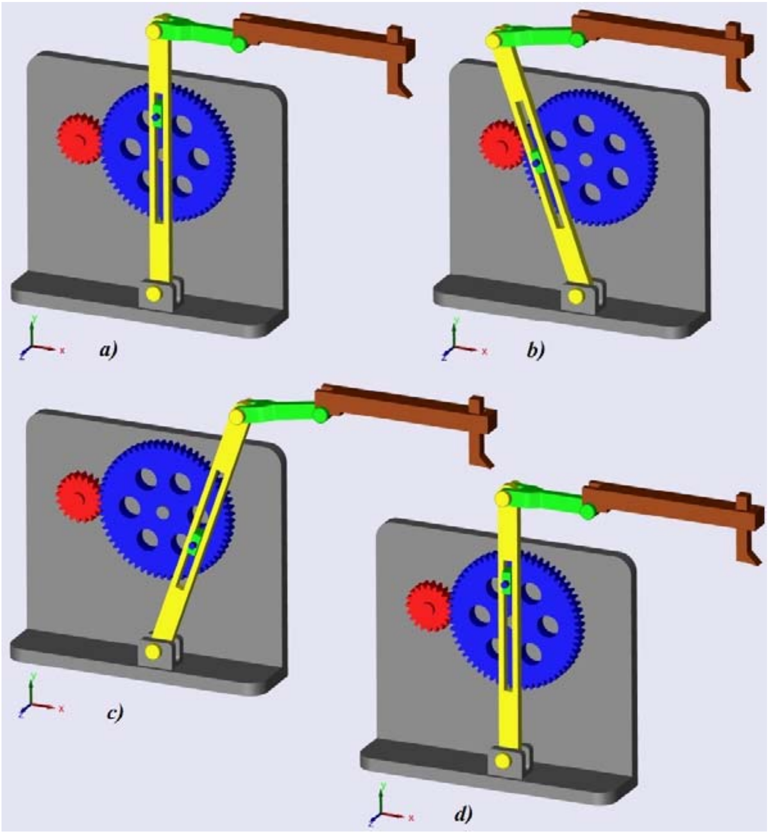

Figure 6: Model of coulisse mechanism: a) initial position, b) an arbitrary position 1, c) an arbitrary position 2, d) the final position

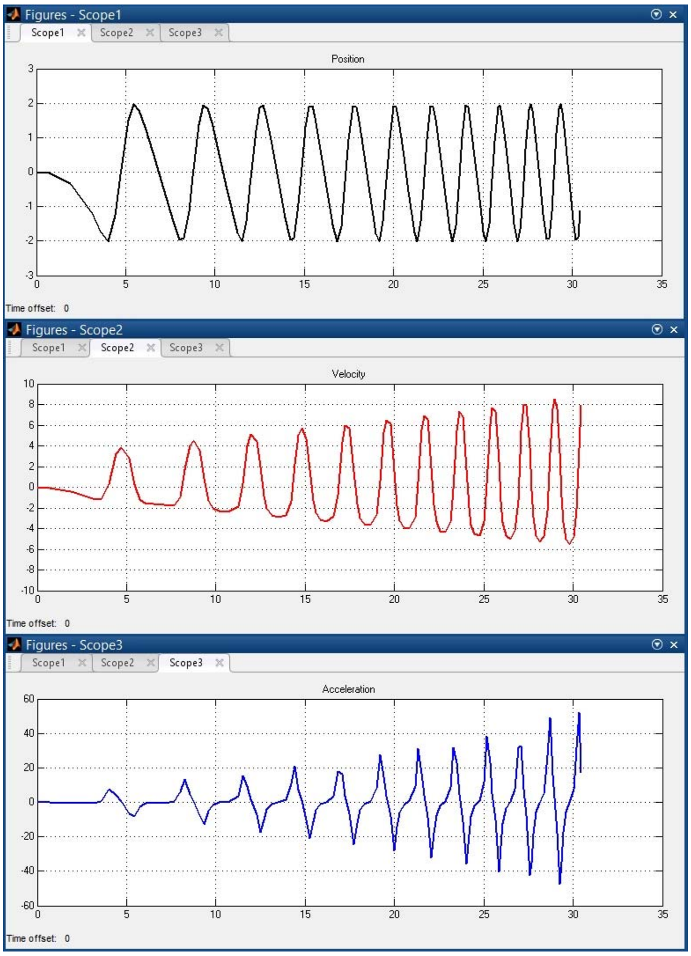

Figure 7: Diagrams of position , velocity and acceleration of the executive body, respectively

Starting Simulink program begins the process of simulating movement coulisse mechanism whereby it can monitor the desired process parameters for the duration of the simulation. On *Fig.7*, as an example, shows the graphic changes of position, velocity and acceleration of the executive body of the planer.

The effect of changing any parameter of any component on the specific characteristics of the system can be easily monitored with simulation of the system operation and monitoring of the desired parameters. The analysis of certain parameters of the system, can select the most advantageous characteristics of the individual components in order to obtain the required characteristics of the mechanism. Simulations can be performed for different parameters, in diferent time frames, cases of overloading, which can occur in the operating conditions, etc.

3. CONCLUSION

The integration of two differently oriented software tools in the design process mechanisms, allowed to analyze all the necessary elements in order to determine the optimal parameters of the system. The analysis requires the necessary movements to achieve the production cycle of the considered mechanism. The analysis of certain parameters of the system, most preferably features of the individual components are selected in order to obtain the required characteristics of the mechanism.

The basis of this approach is the application of virtual models [20-23], which in this case, not only have the task to construct a visual representation of certain segments of the mechanism, but also to describe and simulate its physical behavior, which is of great importance both to the proper sizing and defining individual segments system, and observing the functioning of the entire mechanism as a whole. Also, unlike physical models, virtual models can take advantage of modern computer technology, which allows the focus of the design process move from physical to virtual environment. The virtual models can be used for simulation and verification of the properties of the entire system before the implementation of a physical model, which achieves significant savings of time and resources required to create and modify physical models.

REFERENCES

[1] Arai, E., Arai, T.: Mechatronics for Safety, Security and Dependability in a New Era, ISBN 978-0-08044-963-0, Elsevier Ltd., Great Britain, 2007.

[2] Bishop, R.H.: Mechatronics: An Introduction, ISBN 0-8493-6358-6, CRC Press, Taylor & Francis Group, US, 2006.

[3] Onwubolu, G.C.: Mechatronics: Principles and Applications, ISBN 0-7506-6379-0, Elsevier Ltd., Great Britain, 2005.

[4] Craig, K.: Mechatronic System Design, ISBN 978-0-791-80049-2, American Society of Mechanical Engineers, US, 1997.

[5] Brezina, T., Jablonski, R.: Recent Advances in Mechatronics, ISBN 978-3-642-05021-3, Springer-Verlag Berlin Heidelberg, 2009.

[6] Rao, J. S, Dukkipati, R.V.: Mechanism and Machine Theory, ISBN 81-224-0426-X, New Age International, Ltd., Publishers, New Delhi, 2006.

[7] Zhonghe, Y., Zhaohui, L., Smith, M.R.: Mechanisms and Machine Theory, ISBN 7-04-009234-4, National Ministry of Education, Higher education press, China, 2001.

[8] Ефанов, А. М., Ковалевский В. П.: Теория механизмов и машин, ISBN 5-7410-0011-8, М-во образования Рос. Федерации, Оренбург, 2006.

[9] García-Prada, J.C, Castejón, C.: New Trends in Educational Activity in the Field of Mechanism and Machine Theory, ISBN 978-3-319-01835-5, Springer International Publishing, Switzerland, 2014.

[10] Viadero-Rueda, F., Ceccarelli, M.: New Trends in Mechanism and Machine Science: Theory and Applications in Engineering, ISBN 978-94-007-4901-6, Springer Dordrecht Heidelberg, New York, London, 2013.

[11] Gilat, A.: MATLAB An Introduction with Applications (4th edition), ISBN 978-0-470-76785-6, John Wiley & Sons, Inc., 111 River Street, Hoboken, 2011.

[12] Hasbun, J.E.: Classical Mechanics with MATLAB applications, ISBN 0763746363, Jones and Bartlett Publishers, Sudbury MA, 2009.

[13] Wilson, H.B., Turcotte, L.H., Halpern, D.: Advanced mathematics and mechanics applications using MATLAB, ISBN 1-58488-262-X, Chapman & Hall/CRC, A CRC Press Company, Boca Raton, Florida, 2003.

[14] SimMechanics™ Getting Started Guide, TheMathWorks, Inc., USA, 2012.

[15] Lombard, M., SolidWorks 2010 Bible, ISBN: 978-0-470-55481-4, Wiley Publishing, Inc., Indianapolis, Indiana, 2010.

[16] Lombard, M., SolidWorks Surfacing and Complex Shape Modeling Bible, ISBN: 978-0-470-25823-1, Wiley Publishing, Inc., Indianapolis, Indiana, 2008.

[17] Pancoast, D., Advanced Part Modeling, Dassault Systèmes SolidWokrs Corporation, Concord, Massachusetts, USA, 2009.

[18] Pancoast, D., Advanced Surface Modeling, Dassault Systèmes SolidWokrs Corporation, Concord, Massachusetts, USA, 2009.

[19] Pancoast, D., Mold Design Using SolidWorks, Dassault Systèmes SolidWokrs Corporation, Concord, Massachusetts, USA, 2009.

[20] Pancoast, D., SolidWorks Drawings, Dassault Systèmes SolidWokrs Corporation, Concord, Massachusetts, USA, 2009.

[21] Mandić, V., Virtuelni inženjering, Mašinski fakultet, Kragujevac, 2007.

[22] Mandić, V., FE simulacije procesa, Virtuelna proizvodnja – izazov za budućnost, Mašinski fakultet, Kragujevac, 2007.

[23] Mandić, V., Erić, D., Adamović, D., Janjić, M., Jurković, Z., Babić, Ž., Ćosić, P.: Concurrent engineering based on virtual manufacturing, Technical Gazette, ISSN 1330-3651, Vol.19, No4, pp.885-892, 2012.

[24] Milicevic, I., Slavkovic, R., Mandic, V., Jugovic, Z., Popovic, M., Virtual Models Application for the Analysis of Strain-Deformation States in the Process of Metals Processing by Plastic Deformation, IMK-14 – Research & Developement in Heavy Machinery 19(2013)3, EN 89-96.

Contribution to the Determination of the Load on Suspension Ring of the Underframe of the Hydraulic Excavator

Slaviša Šalinić [1*], Goran Bošković[1], Marko Nikolić [1]
[1] University of Kragujevac, Faculty of Mechanical and Civil Engineering Kraljevo, Dositejeva 19, 36000 Kraljevo (Serbia)

In this paper it is presented a method for determining the load on the suspension ring of underframe of hydraulic excavator which binds radial-axial bearing. The approach is based on the use of Kane's equations with undetermined multipliers of constraints. The expressions are derived in symbolic form for the forces which suspension ring is exposed during the operation of digging. In addition to the kinematic and inertial parameters of the excavator, in these expressions are included the forces in hydro cylinders as well as parameters that characterize the operation of digging. For specific numerical values of the system parameters, numerical analysis is carried out and the appropriate load graphics are presented.

Keywords: Hydraulic excavator, Suspension ring, Multibody, Dynamics

1. INTRODUCTION

Excavators are universal construction machines with cyclic work, which primary task is excavation of soil, and the secondary is transport of excavation to the place of disposal or loading in appropriate transportation means. Their working cycle consists of: digging of soil with the bucket filling, the bucket lifting, transfer of excavated material to the place of discharge, bucket discharge and taking up the original position.

Excavator (Fig. 1) consists of the basic machine and excavation device. The basic machine consists of running gear device and rotating part of machine, while the excavator device is composed of boom, bucket stick and bucket. Depending on type of the running gear device there are two types of excavators: wheel excavators and crawler excavators which are most common in the application.

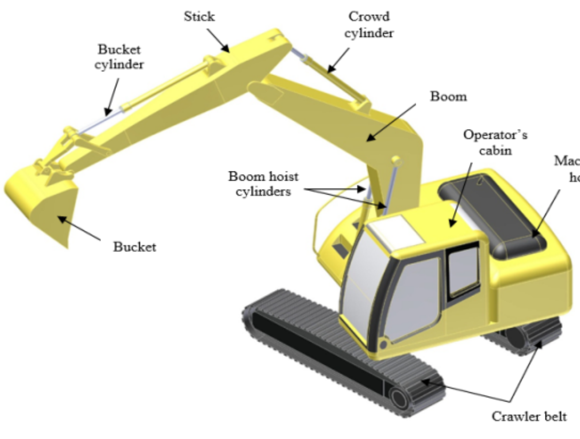

Fig.1. *The basic elements of a hydraulic excavator with caterpillar tracks*

Crawler excavators are self-propelled machines, whose running gear device allows moving the excavator from one to another place of excavation, while not performing transport of excavated material. The running gear device of excavator consists of frame, caterpillar running gear machine and mechanism for drive and braking. Caterpillar tracks have independent drive by individual hydraulic motors by a system mechanical transmission, thereby providing a synchronized or separated movement of the caterpillar tracks.

Rotating platform is the basic metal construction of the excavator, on which are mounted working device, hydraulic drive, cabin with driving system and rotating mechanism. The main objective of placement of devices on rotating platform is achievement of best static moment, by which it prevents the overturning of the excavator. For that reason, on rotary platform is placed the counterweight. Rotating platform with rotating-supporting ring is connected with running gear machine, and thus own and working loads that acting on working device during operation, are transferred to the ground.

The underframe is integral part of the running gear device of the excavator and it represents one of the most important parts of the supporting structure of the excavator. Its main task is to transfer the load from the upper frame, by slewing bearing on mechanism for movement. Support ring respresent a part of underframe which binds to slewing bearing. It is usually welded structure made from sheet metal, whose elements are made by cutting and folding.

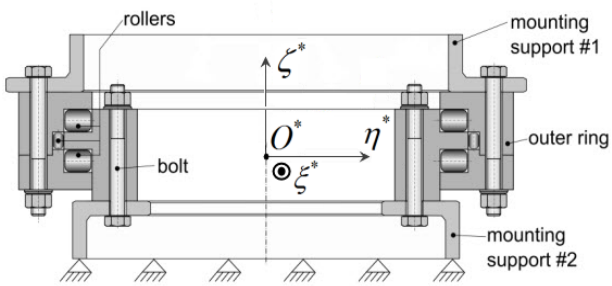

Fig. 2. Connection of slewing bearing, suspension ring and rotating platform

Besides transferring the load, slewing bearing have task to ensure the stability and to allow undisturbed functioning of the rotating part of excavator. This bearing is made in the form of one or more rows of balls or rollers, with gearing on the bearing ring which is connected to support ring by bolts (Fig.2). Bearing is usually composed of three rings, between which are mounted rolling elements (balls, rollers or combined).

*Corresponding author: salinic.s@mfkv.kg.ac.rs

Loads that will be defined and determined in this paper will have multiple functions in future research:

- More precise calculation of bearing loading and selecting it on the basis of calculations
- Calculation of bearing life in accordance with exploitation parameters
- Possibilities of further structural development of support ring and modification of underframe construction
- Possibilities of detailed calculations of the required lubrication parameters

2. HYDRAULIC EXCAVATOR KINEMATIC RELATIONS

In Fig. 3, the multibody meodel of a hydraulic excavator is showen [1]. The bodies (V_i) $(i=0,1,...,4)$ represents, respectively, chassis with caterpillars, roboting platform with driver's cab, boom, stick, and bucket. The considerations in the paper are based on the assumptions of rigid soil foundation and immovable caterpillars. The motion of the excavator with respect to the fixed inertial reference frame $Oxyz$ is described by the generalised coordinates q_i $(i=1,...,4)$. At that, the vertical z axis is directed upwards and the x axis represents the axis of material symmetry of body (V_0). The coordinate q_i represents the relative rotation of body (V_i) with respect to (V_{i-1}) carried out about the joint axis determined by the unit vector $\boldsymbol{e}_i$ fixed to the body (V_{i-1}). The local coordinate frames $C_0\xi_0\eta_0\zeta_0$ and $O_i\xi_i\eta_i\zeta_i$ $(i=1,...,4)$ are fixed to bodies (V_i) $(i=0,1,...,4)$, respectively, in a manner shown in Fig.3. For the purposes of the further considerations, let us introduce a coordinate frame $O^*\xi^*\eta^*\zeta^*$ fixed to body (V_0) at point O^* representing the center of the slewing bearing. The vectors $\boldsymbol{e}_{\lambda^*}, \boldsymbol{e}_{\mu^*}$, and $\boldsymbol{e}_{\nu^*}$ denote the unit vectors of the axes ξ^*, η^*, and ζ^*, respectively.

Without loss of generality, it is assumed that the configuration $q_1=0$, $q_2=0$, $q_3=0$, $q_4=0$ is a reference configuration of the excavator and that, in this configuration, the axes of all local coordinate frames are parallel to the corresponding axes of the inertial reference frame, that is, $\xi_i \parallel x$, $\eta_i \parallel y$, . $\zeta_i \parallel z$.

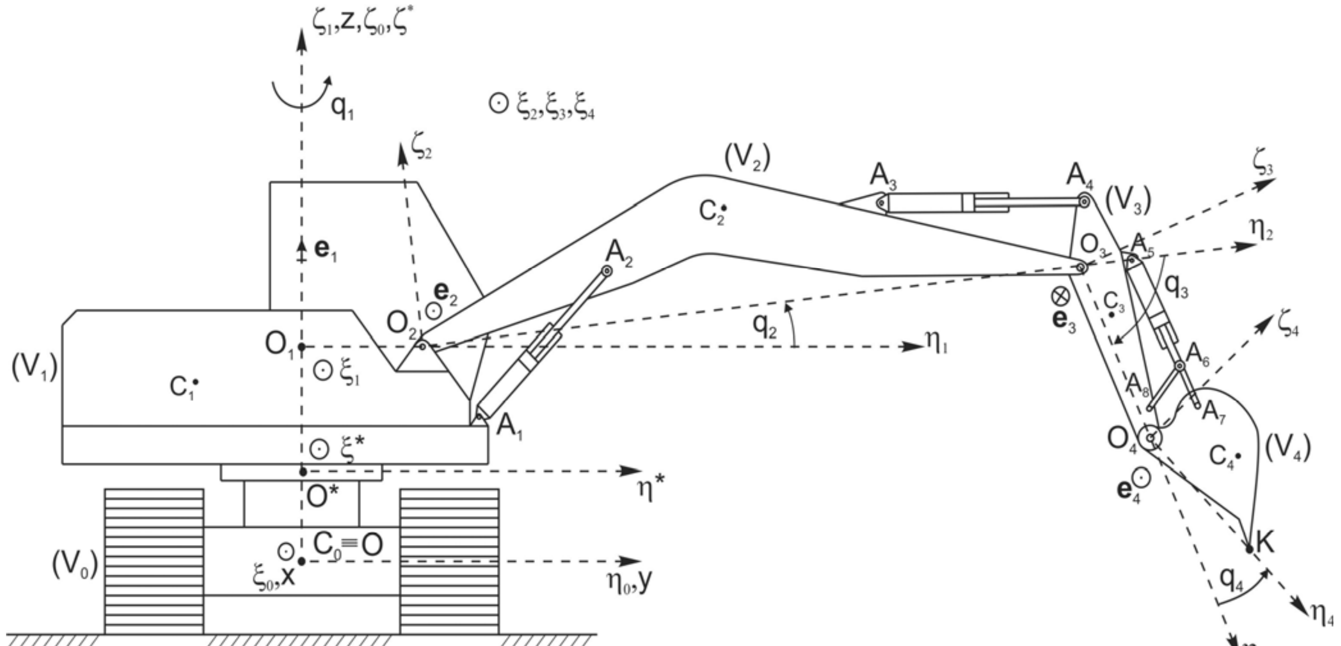

Fig. 3. *Multibody model of a hydraulic excavator*

The mass centres of bodies (V_i) $(i=0,1,...,4)$ are denoted by C_i $(i=0,1,...,4)$. According to [2,3], the transformation matrix $\boldsymbol{A}_{i,j}$ $(i=0,...,4;\ j=1,...,4)$ from $O_j\xi_j\eta_j\zeta_j$ to $O_i\xi_i\eta_i\zeta_i$ reference frames ($i=0$ corresponds to the frame $C_0\xi_0\eta_0\zeta_0$) has the form:

$$\boldsymbol{A}_{i.j} = \prod_{k=i+1}^{j} \boldsymbol{A}_k^r = \prod_{k=i+1}^{j} [\,\boldsymbol{I} + (1-\cos q_k)(\tilde{\boldsymbol{e}}_k^{(k)})^2 + +\tilde{\boldsymbol{e}}_k^{(k)} \sin q_k\,], i<j, \tag{1}$$

where $\boldsymbol{A}_k^r \in R^{3x3}$ is the Rodriguez matrix [2], $\boldsymbol{I} \in R^{3x3}$ is the identity matrix, and $\tilde{\boldsymbol{e}}_k^{(k)} \in R^{3x3}$ is the skew – symmetric matrix [2,4] associated with the vector $\boldsymbol{e}_k^{(k)}$. In further considerations the right superscript (k) indicates that components of the corresponding vectors and matrices are given in the $O_k\xi_k\eta_k\zeta_k$ local frame. In regard to [5,6], the following kinematic relations of the considering hydraulic excavator hold [1]:

$$\boldsymbol{\omega}_i^{(i)} = \boldsymbol{A}_{i-1,i}^T \boldsymbol{\omega}_{i-1}^{(i-1)} + \dot{q}_i \boldsymbol{e}_i^{(i)},\ i = 1,...,4 \tag{2}$$

$$\boldsymbol{\varepsilon}_i^{(i)} = \boldsymbol{A}_{i-1,i}^T \boldsymbol{\varepsilon}_{i-1}^{(i-1)} + \ddot{q}_i \boldsymbol{e}_i^{(i)} + \dot{q}_i \boldsymbol{A}_{i-1,i}^T \tilde{\boldsymbol{\omega}}_{i-1}^{(i-1)} \boldsymbol{e}_i^{(i-1)},\ i = 1,...,4 \tag{3}$$

$$\boldsymbol{V}_{C_i}^{(i)} = \boldsymbol{A}_{i-1,i}^T (\boldsymbol{V}_{C_{i-1}}^{(i-1)} + \tilde{\boldsymbol{\omega}}_{i-1}^{(i-1)} (\boldsymbol{l}_{i-1}^{(i-1)} - \boldsymbol{l}_{C_{i-1}}^{(i-1)})) + \tilde{\boldsymbol{\omega}}_i^{(i)} \boldsymbol{l}_{C_i}^{(i)},\ i = 1,...,4 \tag{4}$$

$$\boldsymbol{a}_{C_i}^{(i)} = \boldsymbol{A}_{i-1,i}^{T}(\boldsymbol{a}_{C_{i-1}}^{(i-1)} + \tilde{\boldsymbol{\varepsilon}}_{i-1}^{(i-1)}(\boldsymbol{l}_{i-1}^{(i-1)} - \boldsymbol{l}_{C_{i-1}}^{(i-1)})) + (\tilde{\boldsymbol{\omega}}_{i-1}^{(i-1)})^2(\boldsymbol{l}_{i-1}^{(i-1)} - \boldsymbol{l}_{C_{i-1}}^{(i-1)})) + \tilde{\boldsymbol{\varepsilon}}_{i}^{(i)}\boldsymbol{l}_{C_i}^{(i)} + (\tilde{\boldsymbol{\omega}}_{i}^{(i)})^2\boldsymbol{l}_{C_i}^{(i)}, \quad (5)$$

$i = 1,...,4$

where $\boldsymbol{\omega}_i, \boldsymbol{\varepsilon}_i, \boldsymbol{V}_{C_i}$ and $\boldsymbol{a}_{C_i}$ are, respectively, the angular velocity, the angular accelerations, the velocity of the mass centre C_i and the acceleration of the mass centre of body (V_i), and where $l_i = |\overrightarrow{O_iO_{i+1}}|$ $(i = 1,...,3)$, $l_0 = |\overrightarrow{C_0O_1}|$, $l_{C_i} = |\overrightarrow{O_iC_i}|$ $(i = 1,...,4)$, and $l_{C_0} = [0,0,0]^T$.

Since the body (V_0) is immovable, the following holds:

$$\boldsymbol{V}_{C_0}^{(0)} = [0,0,0]^T, \quad \boldsymbol{a}_{C_0}^{(0)} = [0,0,0]^T. \quad (6)$$

3. DETERMINATION OF THE LOAD ON SUSPENSION RING OF THE UNDERFRAME DURING THE DIGGING TRANSPORTATION TASK

The interaction between the bucket and the soil during the excavation phase is shown in Fig. 4. The digging force $\boldsymbol{F}_W$ acts on the centre K of the cutting edge of the bucket. The force $\boldsymbol{F}_W$ depends on various factors such as the depth of the bucket tip K, the width of the bucket, the terrain slope, and the soil physical characteristics. Different expressions for the magnitude F_W of the force $\boldsymbol{F}_W$ can be found in [7,8,9,10]. The digging angle is denoted by θ_{dg} and θ_b represents the angle between the bucket bottom and the η_4 - axis. In regard to [7,11], the angle δ varies in the interval $0,1 \leq \delta \leq 0,45$ and depends on the digging angle, digging condition, and the wear of the bucket cutting edge. As in [7,11,12], in this paper it is taken that this angle is constant and equal to $\delta = 0,1$.

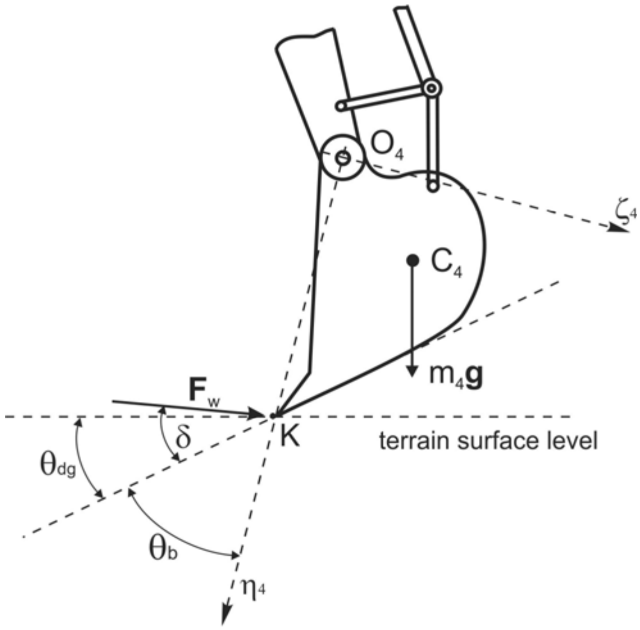

Fig.4. *Interaction between the bucket and the soil*

In accordance with Fig.4, the force $\boldsymbol{F}_W$ can be written as

$$\boldsymbol{F}_W^{(4)} = [0, -F_W\cos(\delta+\theta_b), F_W\sin(\delta+\theta_b)]^T. \quad (7)$$

The moment of the force $\boldsymbol{F}_W$ relative to point C_4 is determined by the following expression:

$$\boldsymbol{M}_4^{(4)} = -\tilde{\boldsymbol{F}}_W^{(4)}(\overrightarrow{O_4K}^{(4)} - \boldsymbol{l}_{C_4}^{(4)}). \quad (8)$$

Hence, the external force system exerted on bucket can be represented by a force system consisting of a force equal to $\boldsymbol{F}_W$ that passing through the mass centre C_4, the gravity force $m_4\boldsymbol{g}$ of the bucket, and a couple with torque $\boldsymbol{M}_4$.

Based on approach from [14], the load of the suspension ring can be represented by a force passing through the point O^*:

$$\boldsymbol{R}^* = [\lambda_1, \lambda_2, \lambda_3]^T \quad (9)$$

and a couple with torque

$$\boldsymbol{M}^* = [\lambda_4, \lambda_5, 0]^T \quad (10)$$

where λ_i $(i = 1,...,5)$ are the projections of the vectors $\boldsymbol{R}^*$ and $\boldsymbol{M}^*$ onto the corresponding axes of the frame $O^*\xi^*\eta^*\zeta^*$. Based on [14], these projections are determined by the following expressions:

$$\lambda_r = \sum_{p=1}^{4}[\boldsymbol{F}_p^{(p)T}\boldsymbol{b}_{p,r}^{V(p)} + (\boldsymbol{M}_p^{(p)})^T\boldsymbol{b}_{p,r}^{\omega(p)}] - \sum_{p=1}^{4}m_p(\boldsymbol{a}_{C_p}^{(p)})^T\boldsymbol{b}_{p,r}^{V(p)} - \sum_{p=1}^{4}(\boldsymbol{I}_{C_p}\boldsymbol{\varepsilon}_p^{(p)} + \tilde{\boldsymbol{\omega}}_p^{(p)}\boldsymbol{I}_{C_p}\boldsymbol{\omega}_p^{(p)})^T\boldsymbol{b}_{p,r}^{\omega(p)}, \; r = 1,...,5 \quad (11)$$

where it is taken that an external force system exerted on body (V_p) $(p = 1,...,3)$ is represented by an equivalent force system consisting of a force $\boldsymbol{F}_p$ passing through the mass centre C_p together with a couple with torque $\boldsymbol{M}_p$. In Eq. (11), $\boldsymbol{I}_{C_p}$ represents the centroidal inertia tensor of the body (V_p) expressed in the local frame $C_p\xi_p\eta_p\zeta_p$ whose axes are chosen so that $C_p\xi_p \parallel O_p\xi_p$, $C_p\eta_p \parallel O_p\eta_p$ and $C_p\zeta_p \parallel O_p\zeta_p$ hold.

Taking this into account, the projections of vectors in both coordinate frames $C_p\xi_p\eta_p\zeta_p$ and $O_p\xi_p\eta_p\zeta_p$ are the same.

Based on the considerations in [14], the vectors $\boldsymbol{b}_{p,r}^{\omega(p)}$ and $\boldsymbol{b}_{p,r}^{V(p)}$ are determinined by the following expressions:

$$\boldsymbol{b}_{p,r}^{\omega(p)} = \begin{cases} [0,0,0]^T, r = 1,2,3; \; p = 1,...,4 \\ \boldsymbol{A}_{0,p}^T[1,0,0]^T, r = 4; \; p = 1,...,4 \\ \boldsymbol{A}_{0,p}^T[0,1,0]^T, r = 5; \; p = 1,...,4 \end{cases} \quad (12)$$

$$\boldsymbol{b}_{p,r}^{V(p)} = \begin{cases} \boldsymbol{A}_{0,p}^T[1,0,0]^T, r=1; p=1,...,4 \\ \boldsymbol{A}_{0,p}^T[0,1,0]^T, r=2; p=1,...,4 \\ \boldsymbol{A}_{0,p}^T[0,0,1]^T, r=3; p=1,...,4 \\ \tilde{\boldsymbol{e}}_{\lambda^*}^{(1)}\left(\overrightarrow{O^*O_1}^{(1)} + \boldsymbol{l}_{c_1}^{(1)}\right), r=4; p=1 \\ \tilde{\boldsymbol{e}}_{\mu^*}^{(1)}\left(\overrightarrow{O^*O_1}^{(1)} + \boldsymbol{l}_{c_1}^{(1)}\right), r=5; p=1 \\ \tilde{\boldsymbol{e}}_{\lambda^*}^{(p)}\left(\boldsymbol{A}_{1,p}^T\overrightarrow{O^*O_1}^{(1)} + \boldsymbol{l}_{c_p}^{(p)} + \sum_{j=1}^{p-1}\boldsymbol{A}_{j,p}^T\boldsymbol{l}_j^{(j)}\right), r=4; p>1 \\ \tilde{\boldsymbol{e}}_{\mu^*}^{(p)}\left(\boldsymbol{A}_{1,p}^T\overrightarrow{O^*O_1}^{(1)} + \boldsymbol{l}_{c_p}^{(p)} + \sum_{j=1}^{p-1}\boldsymbol{A}_{j,p}^T\boldsymbol{l}_j^{(j)}\right), r=5; p>1 \end{cases} \quad (13)$$

where:

$$\left.\begin{array}{l} \boldsymbol{e}_{\lambda^*}^{(p)} = \boldsymbol{A}_{0,p}^T[1,0,0]^T \\ \boldsymbol{e}_{\mu^*}^{(p)} = \boldsymbol{A}_{0,p}^T[0,1,0]^T \\ \overrightarrow{O^*O_1}^{(1)} = [0,0,\overline{O^*O_1}]^T \end{array}\right\} . \quad (14)$$

4. NUMERICAL EXAMPLE

For purposes of determining the numerical values of projections $\lambda_i (i=1,...,5)$ the following values of the excavator parameters are used (see [7,11,12]): $m_1 = 6420\,\text{kg}$, $m_2 = 1566\,\text{kg}$, $m_3 = 735\,\text{kg}$, $m_4 = 432\,\text{kg}$, $I_{C_2\xi_2} = 14250.6\,\text{kg m}^2$, $I_{C_3\xi_3} = 727.7\,\text{kg m}^2$, $I_{C_4\xi_4} = 224.6\,\text{kg m}^2$, $l_1 = 0.05\,\text{m}$, $l_2 = 5.16\,\text{m}$, $l_3 = 2.59\,\text{m}$, $\overline{O_4K} = 1.33\,\text{m}$, $\overline{O^*O_1} = 0.76\,\text{m}$, $l_{C_1} = 0.61\,\text{m}$, $l_{C2} = 2.71\,\text{m}$, $l_{C3} = 0.64\,\text{m}$, $l_{C4} = 0.65\,\text{m}$, $\gamma_4 = 1.92$, $\angle(\boldsymbol{l}_{C_1},\eta_1) = 3.49305$, $\angle(\boldsymbol{l}_{C2},\eta_2) = 0.2566$, $\angle(\boldsymbol{l}_{C3},\eta_3) = 0.3316$, $\angle(\boldsymbol{l}_{C4},\eta_4) = 0.3944$, $\theta_b = 1.0472$. The quantities $I_{C_i\xi_i}\ (i=2,3,4)$ represent second-order inertial moments about the axes through the gravity centres $C_p\xi_p\ (p=2,3,4)$, respectively. At that, as in [13], it is taken that the time interval of the considered digging task reads $0 \le t \le 3\,s$ and that:

$$\left.\begin{array}{l} q_1(t) \equiv 0, \\ q_2(t) \equiv -0.1744, \\ q_3(t) \equiv 0.436, \\ q_4(t) = -0.1744t^3 - 0.7848\,t^2 \end{array}\right\} \quad (15)$$

and

$$F_w(t) = 2.1812t^3 - 18.097t^2 + 35.9936t\,[kN]. \quad (16)$$

The external force systems acting on the bodies (V_i) $(i=1,...,4)$ are defined as follows:

$$\boldsymbol{F}_i^{(i)} = \boldsymbol{A}_{0,i}^T[0,0,-m_i g]^T \ , \ i=1,2,3 \ , \quad (17)$$

$$\boldsymbol{F}_4^{(4)} = [0,-F_w\cos(\delta+\theta_b), F_w\sin(\delta+\theta_b)] + \\ +\boldsymbol{A}_{0,4}^T[0,0,-m_4 g]^T \quad (18)$$

$$\boldsymbol{M}_i^{(i)} = [0,0,0]^T \ , \ i=1,2,3 \ , \quad (19)$$

and $\boldsymbol{M}_4^{(4)}$ is defined by the relation (8).

The graphs of the magnitude of the force $\boldsymbol{F}_w$ and projections λ_2, λ_3 and λ_4 are shown in Figs. 5, 6, 7, 8.

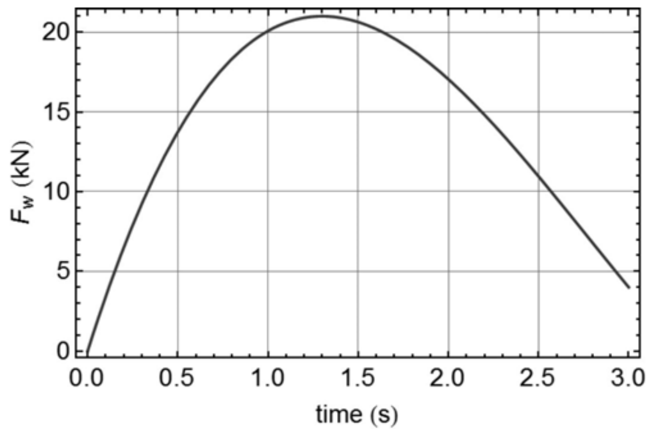

Fig.5. *Magnitude of resistance digging (cutting) force* $\boldsymbol{F}_w$ *versus time*

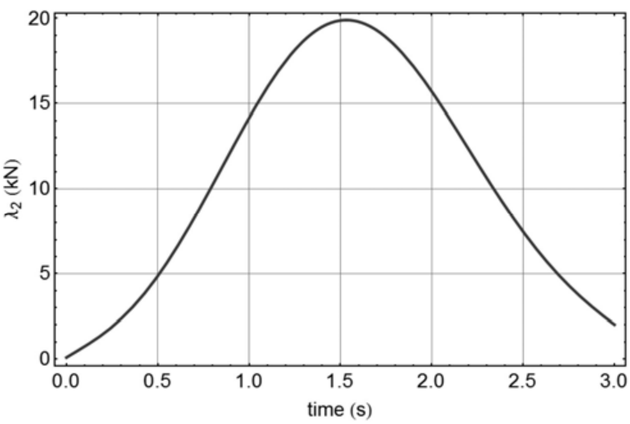

Fig.6. *The projection* λ_2 of the force $\boldsymbol{R}^*$ *onto the axis* $O^*\eta^*$

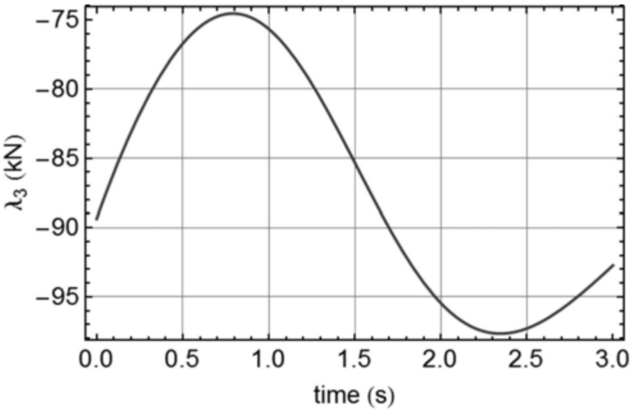

Fig.7. *The projection* λ_3 of the force $\boldsymbol{R}^*$ *onto the axis* $O^*\zeta^*$

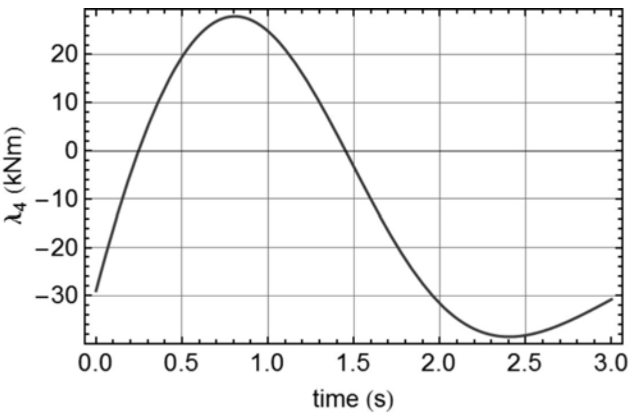

Fig.8. *The projection* λ_4 of the torque $\boldsymbol{M}^*$ *onto the axis* $O^*\xi^*$

For the considering digging transportation task, the following holds:

$$\lambda_1(t) \equiv 0\,, \tag{20}$$

$$\lambda_5(t) \equiv 0\,. \tag{21}$$

5. CONCLUSIONS

In this paper, expressions in symbolic form for projections of the force $\boldsymbol{R}^*$ and the torque $\boldsymbol{M}^*$, which is exposed to suspension ring of the underframe, are presented. These expressions allow us that, during the excavation phase, to examine the effect of various design parameters of excavator and the relevant factors in process of interaction between the bucket and the soil to the load of the suspension ring. The expressions (12) and (13) can be used also in the case of the lifting and returning transport operations. Approach from paper [14] allows the loading of the suspension ring be determined without the need for determining reaction forces in the joints O_2, O_3, and O_4, so that, in the meaning of computation, it is superior in regard to the Newton-Euler approch [15].

ACKNOWLEDGEMENTS

Support for this research was provided by the Ministry of Education, Science and Technological Development of the Republic of Serbia under Grants No. TR35006 and No. TR35038. This support is gratefully acknowledged.

REFERENCES

[1] S.Šalinić, G.Bošković, M.Nikolić, "Dynamic modelling of hydraulic excavator motion using Kane's equations," Automation in Construction, Vol. 44, pp. 56–62, (2014)

[2] A.A.Shabana, "Dynamics of Multibody systems, Validation," third ed. Cambridge University Press, New York, 2005.

[3] V. Čović, M. Lazarević, "Mechanics of Robots," Faculty of Mechanical Engineering of Belgrade, Belgrade, 2009. (in Serbian)

[4] P. Nikravesh, "Computer-aided Analysis of Mechanical Systems," Prentice Hall, Englewood Cliffs, New Jersey, 1988.

[5] J. Angeles, O. Ma, "An algorithm for the inverse dynamics of n-axis general manipulators using Kane's equations," Comput. Math. Appl. 17 (1989) 1545-1561.

[6] J. Angeles, "Faundamentals of Robotic Systems: Theory, Methods, and Algorithms," 3rd ed., Springer-Verlag, New York, 2007.

[7] A.J. Koivo, M. Thoma, E. Kocaoglan, J. Andrade-Cetto, "Modeling and control of excavator dynamics during digging operation," J. Aerosp. Eng.9 (1996) 10–18.

[8] T.V. Alekseeva, K.A. Artem'ev, A. Bromberg, "Machines for Earth Moving Work: Theory and Calculations," A. A. Balkema, Rotterdam, 1992.

[9] H. Cannon, S. Singh, "Models for automated earthmoving," Experimental Robotics VI, Lecture Notes in Control and Information Sciences, vol. 250, Springer Verlag, 2000, pp. 163–172.

[10] S.P. DiMaio, S.E. Salcudean, C. Reboulet, S. Tafazoli, K. Hashtrudi-Zaad, "A virtual excavator for controller development and evaluation," Proceedings of the 1998 IEEE International Conference on Robotics and Automation, Leuven, Belgium, vol. 1, 1998, pp. 52–58.

[11] P.K. Vähä, A.J. Koivo, M.J. Skibniewski, "Excavation dynamics and effects of soil in digging," Proceedings of the 8th International Symposium on Automation and Robotics in Constructions, ISARC-8, Stuttgart, Germany, 1991, pp. 297–306.

[12] P.K. Vähä, M.J. Skibniewski, "Dynamic model of excavator," J. Aerosp. Eng. 6 (1993) 148-158

[13] Z. Towarek, Dynamics of a single-bucket excavator on a deformable soil foundation during the digging of ground, Int. J. Mech. Sci. 45 (2003) 1053–1076.

[14] S. Šalinić, "Determination of joint reaction forces in a symbolic form in rigid multibody systems," Mech. Mach. Theory 46 (2011) 1796–1810

[15] J.Y.S. Luh, M.W. Walker, R.P.C. Paul, "On-line computational scheme for mechanical manipulators," Transactions of ASME, Journal of Dynamic Systems, Measurement, and Control 102 (1980) 69-76.

Influence of Plasticity Reduction on Integrity and Service Life of Turbine Runner Cover of the Hydroelectric Generating Set A4 at Hydro Power Plant „Đerdap“

Miodrag Arsić[1*], Srđan Bošnjak[2], Vencislav Grabulov[1], Brane Vistać[1], Zoran Savić[1]
[1]Institute for Materials Testing, Belgrade (Serbia)
[2]Faculty of Mechanical Engineering, Belgrade (Serbia)

Vertical Kaplan turbines, manufactured in Russia and with nominal output power of 200 MW, have been installed in 6 hydroelectric generating units at 'Djerdap 1'. This paper presents results of experimental tests performed on four specimens cut from runner cover which was made of cast steel 20 GSL. These results indicated that values of yield strength (YS), tensile strength (TS) and impact energy KCU for all specimens meet the demands of standard, and also that values which define plasticity of base material - elongation A5 and contraction Z have significant dispersion. Two of four specimens met the demands of standard (A5 = 23% and 27%), but two had significantly lower values of elongation (A5 = 8% and 9%). Taking into account that values A5 and Z are not universal and also that it is impossible to implement fracture mechanism for this material, analytical and numerical calculations of stress state and experimental tests performed in order to determine fracture mechanics parameters have been carried out. Results of tests performed in order to determine fatigue crack diving force da/dN indicated that internal deformations of circular or elliptical shape (imperfections detected through ultrasonic testing), with initial size of 6 mm, do not obstruct 29 years long reliable operation of runner cover.

Keywords: Hydro turbine, runner cover, plasticity, duration time

1. INTRODUCTION

Design, assembly and putting into operation of the hydro power plant comprise complex tasks. Due to limited possibilities of performing periodic inspections and state analyses, hydro turbines and their components are being projected for 40 years long service life. That's why extensive researches and state analyses have been done in order to determine the state of hydro power plant equipment. Tests performed in order to determine the state of domestic turbine and hydro mechanical equipment are very modest and of recent date. Vertical Kaplan turbines, manufactured in Russia and with nominal output power of 200 MW, have been installed in 6 hydroelectric generating units at 'Djerdap 1' [1]. In figure 1 the appearance of the turbine is shown, while in figure 2 the runner cover, made of cast steel 20 GSL, is shown, in accordance with the standard [2].

2. EXPERIMENTAL TESTS

Experimental tests have been performed in order to determine mechanical properties and fracture mechanics parameters of cast steel 20 GSL. For the fabrication of specimens the sample taken from the runner cover has been used.

2.1. Results of tests performed in order to determine chemical composition and mechanical properties of cast steel 20 GSL

Results of tests performed in order to determine chemical composition (quantitative spectrophotometric method) and mechanical properties of cast steel 20 GSL are presented in tables 1 and 2 [3].

2.2. Results of tests performed in order to determine fracture mechanics parameters of cast steel 20 GSL

Obtained values of fracture mechanics parameters (critical stress intensity factor - K_{IC}, critical fatigue crack length - a_c , fatigue threshold - ΔKth, constant in Paris equation - C, exponent in Paris equation - m_p, fatigue crack growth rate - da/dN) are presented in table 3 and figures 3 and 4 [4].

Table 1. Results of analysis of chemical composition, mass percentage

	C	Si	Mn	S	P	Ni	Cr	Mo	V	Al
Sample 1	0,213	0,747	1,349	0,014	0,028	0,221	0,296	0,041	0,009	0,058
Sample 2	0,217	0,758	1,380	0,017	0,030	0,214	0,291	0,046	0,009	0,063
GOST 977	0,22-0,28	0,60-0,80	1,00-1,30	max 0,30	max 0,30	max 0,30	max 0,30	-	-	-

*Corresponding author: Bulevar vojvode Mišića 43, miodrag.arsic@institutims.rs

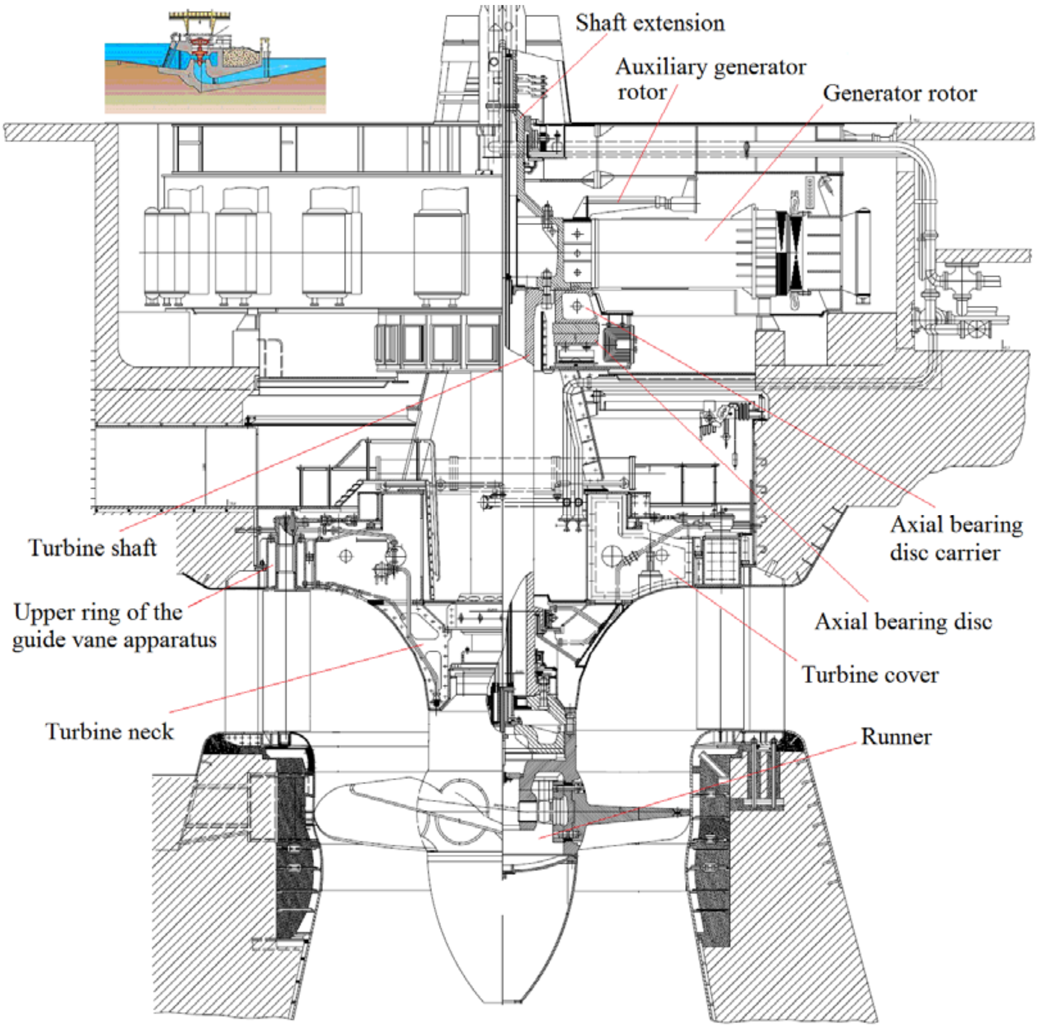

Figure 1: Appearance of the vertical Kaplan turbine, nominal power 200 MW

3. INFLUENCE OF PLASTICITY REDUCTION DURING RUNNER COVER CASTING ON FATIGUE STRENGTH

Influence of plasticity reduction and existence of internal defects on fatigue of cast steel 20 GSL is important concerning the establishment of technical conditions for casting, norms for allowable defects and quality inspection. For that purpose and with participation of representatives of LMZ factory and Mechanical Engineering Institute from Saint Petersburg, the mechanisms of microcrack initiation and conditions of propagation of microcracks to macrocracks have been established. Tests have been carried out on large specimens with dimensions from 100 to 300 mm. Analysis of test results helped the establishment of the empirical dependency which enabled the evaluation of resistance to fatigue of cast steel with internal defects, or in other words with reduced plasticity:

$$\sigma_{-1}^{*} = \frac{\sigma_{-1}}{(1+\beta \cdot d_{max})^{1/2}} \tag{1}$$

where: σ_{-1} - lower limit of fatigue strength dispersion; β - coefficient which depends on properties of the metal; d_{max} - maximum size of the defect in cast material.

As a result of testing of cast steels with reduced plasticity, the following dependency between stress amplitude σ_{-1} and maximum number of loading cycles N has been obtained [3]:

$$lg\,(\sigma_{-1}) = 2,69 - 0,155 \times lg\,(N) \tag{2}$$

It was determined that defect sizes from 0,2 to 0,5 mm in 20 GSL do not influence fatigue strength, as well as that maximum allowable defect size of d = 1.5 mm causes the reduction of fatigue strength from σ_{-1} = 118,5 MPa to σ_{-1} = 91,15 MPa, in which case the corrosion-fatigue strength reserve (safety factor) is still satisfactory, S_σ = 1,63.

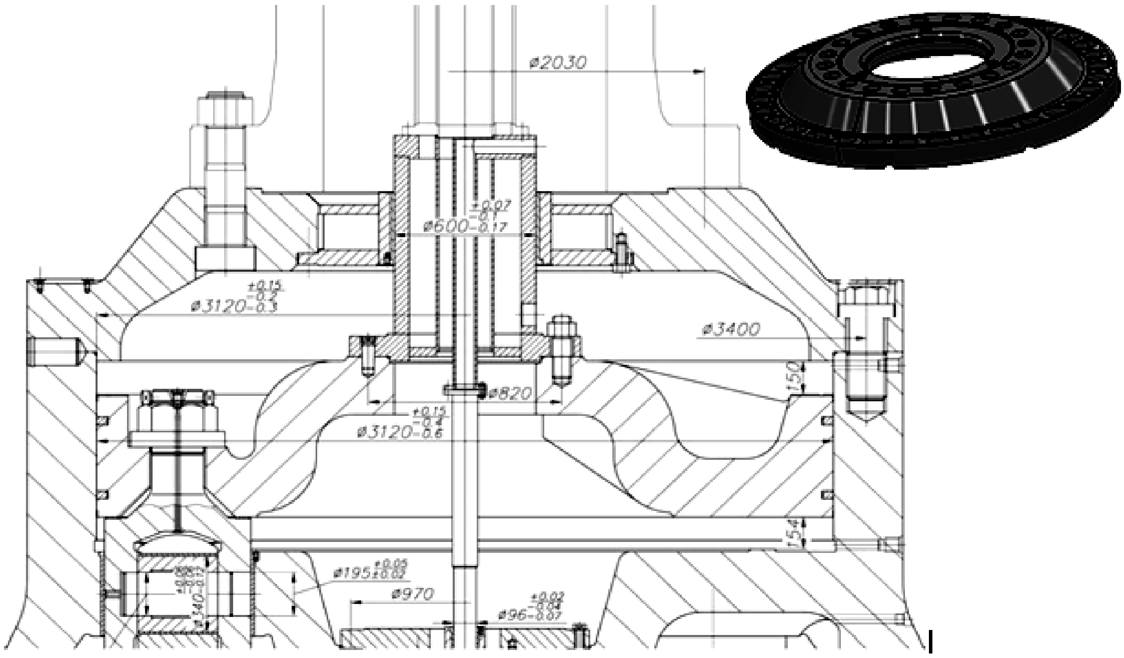

Figure 2: Turbine segment and runner cover model

Table 2. Mechanical properties, values for normalized and annealed state of material

Material	Yield strength YS [N/mm^2]	Tensile strength TS [N/mm^2]	Elongation A5 [%]	Impact energy KCU [J/cm^2]
Sample 1	426	612	23	81
Sample 2	387	568	8	68
Sample 3	412	582	27	76
Sample 4	396	573	9	72
GOST 977-88	min 350	min 540	min 19	min 65

Table 3. Fracture mechanics parameters at 23°C, for the stress intensity factor range ΔK = 10 Pa·m$^{1/2}$

Specimen	K_{IC} [MPa·m$^{1/2}$]	a_c [mm]	ΔKth [MPa·m$^{1/2}$]	C [(m/cycle)/ (MPa·m$^{1/2}$)^{mp}]	m_p	da/dN [m/cycle]
With reduced plasticity	46,3	9,3	7,4	5,7 · 10-11	3,15	6,36 · 10-08
With adequate plasticity	50,4	10,2	8,7	3,0 · 10-11	3,02	5,11 · 10-08
Minimum allowed value of KIc for 20 GSL at temperatures below 0° C is KIc = 41 - 44 [MPa·m$^{1/2}$]						

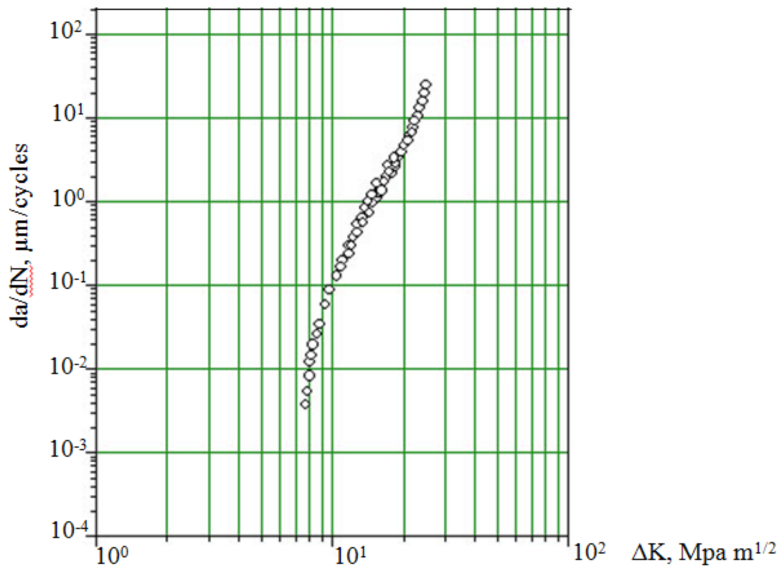

Figure 3: Diagram of dependence da/dN - ΔK with reduced plasticity

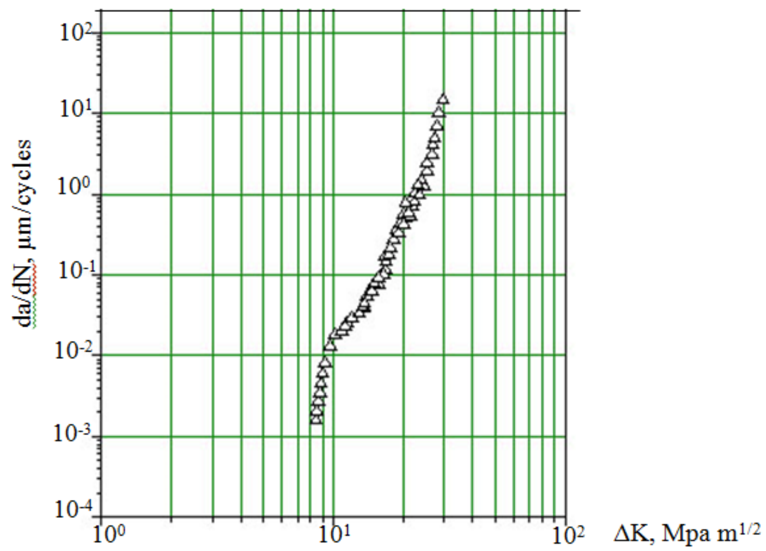

Figure 4: Diagram of dependence da/dN - ΔK with adequate plasticity

4. ESTIMATION OF SERVICE LIFE OF THE RUNNER COVER THROUGH THE USE OF FRACTURE MECHANICS

Estimation of runner cover service life through the use of fracture mechanics has been carried out according to methodology presented in paper [5]. In the area of stable crack growth, Paris' equation describes the behaviour of the material with sufficient accuracy:

$$\frac{da}{dN} = C \cdot (\Delta K)^{m_p} \tag{3}$$

where: ΔK - stress intensity factor range, which is being calculated using the following equation:

$$\Delta K = \Delta\sigma\sqrt{\frac{1.21\pi a}{Q}} \tag{4}$$

For the internal defect measuring 6 mm in diameter in the steel cast 20GSL, detected by ultrasonic testing, characteristic value is circle radius or half-length of the short axis of the ellipse, which value a_0 is being calculated using the following equation:

$$a_0 = \frac{\sqrt{3}}{2}d = \frac{\sqrt{3}}{2}6 = 5{,}2mm \tag{5}$$

Stress intensity factor K_I is being calculated using the following equation, in case of existence of an internal defect:

$$K_I = \sigma_{\max}\sqrt{Ma_0} = 98{,}5\sqrt{2.38\times 0.0052} = 11 \text{ MPa}\sqrt{\text{m}} \tag{6}$$

where: σ_{max} – maximum operational stress ; M – coefficient which depends on shape and dimensions of defects and structure, M = 1,25 π / Q; a_0 – characteristic size of the defect; Q – defect shape parameter; Δσ – stress range, which is being calculated using the following equation:

$$\Delta\sigma = \frac{\sigma_{\max} - \sigma_{\min}}{2} = \frac{98{,}5 - 93{,}6}{2} = 2{,}45mm \tag{7}$$

For the ratio of half-lengths of the short and long axis of the defect ellipse a/2c = 0.3, as well as for the ratio of the maximum projected stress on the turbine cover and yield strength for the specimen with the lowest plasticity σmax / R_{02} = 98,5/ 309 = 0,32, value of the defect shape parameter is Q = 1.65 [6].

Critical length of the internal crack in cast steel in which deformation weakening occurs, which can cause the fracture in the structure, can be calculated using the equation (6):

$$a_{cr} = \frac{1}{M}\left(\frac{K_{Ic}}{\sigma_{\max}}\right)^2 = \frac{1}{2{,}38}\left(\frac{46{,}3}{98{,}5}\right)^2 = 92{,}8mm \tag{8}$$

Number of cycles until reaching the critical size of the internal defect within the turbine runner cover, made of cast steel 20 GSL with reduced plasticity, is calculated through the integration of Paris' equation, as well as values from table 1 and other calculated values:

$$N = \frac{2}{(m_P - 2)\cdot C_P \cdot M^{\frac{m_P}{2}} \cdot \Delta\sigma^{m_P}}\left(\frac{1}{a_0^{\frac{m_P-2}{2}}} - \frac{1}{a_{cr}^{\frac{m_P-2}{2}}}\right) = 2{,}61\cdot 10^{10} \tag{9}$$

Number of load cycles during the one year period is:

$$N_u = n_h \cdot 60 \cdot 7000 \cdot 30 = 71{,}43 \cdot 60 \cdot 7000 \cdot 30 = 9 \cdot 10^8 \mathit{cycles} \tag{10}$$

where: n_h – number of revolutions of the hydroelectric generating set, n_h = 71.43 o/min; 60 – number of minutes per hour; 7000 – overall number of hours of operation of the hydroelectric generating set during a one year period; 30 – number of years of operation of the hydroelectric generating set.

Estimated service life of the turbine runner cover with reduced plasticity is:

$$n = \frac{N}{N_u} = \frac{2{,}61\cdot 10^{10}}{9\cdot 10^8} = 29 \quad \text{years} \tag{11}$$

5. CONCLUSION

Results of fatigue strength tests carried out on large specimens, as well as obtained values of fracture mechanics parameters, enabled the estimation of service life of turbine runner cover with reduced plasticity.

ACKNOWLEDGEMENTS

The authors acknowledge the support from the Serbian Ministry of Education and Science for projects TR 35002 and TR 35006.

REFERENCES

[1] Manufacturer's Documentation for the vertical Kaplan turbine, LMZ, Sankt Petersburg.

[2] Отливки стальные. Общие технические условия, 1988.

[3] Test carried out by LMZ factory and Institute for Mechanical Engineering AN, Saint Petersburg., 2005.

[4] Arsić M. and Vistać B. : Analysis of operational capability during the 40 years long service life, Institute for Materials Testing, Belgrade, 2005.

[5] Bošnjak S., Arsić M., Zrnić N., Rakin M., Pantelić M. (2011), Bucket wheel excavator: Integrity assessment of the bucket wheel boom tie – rod welded joint, Engineering Failure Analysis, Vol.18, pp. 212 – 222.

[6] Hertzberg R. Hertzberg R. (1995), Deformation and Fracture Mechanics of Engineering Materials, New York, John Wiley & Sons, Inc., 1995.

Coupling of Bending in Horizontal Plane and Twist of A Truss Beam with Triangular Cross-section

Milan Dedic [1*], Milica Todorovic [2]
[1] Faculty of Mechanical and Civil Engineering in Kraljevo, University of Kragujevac, Serbia
[2] High Technical Mechanical School, Trstenik, Serbia

Truss beams with repeated cells of triangular cross-section are among the most frequently used load carrying structures in mechanical and civil engineering because of their high load-to-weight ratio capacity and other advantages. In this paper an important feature of this type of truss is considered – if it is bent in horizontal plane, it twists about the longitudinal axis, and vice versa, if twisted it undergoes bending as well, so that these two modes of deformation are coupled. General formulas for the angles of bending and twist produced by the corresponding moments acting at the truss free end are derived. Also the influence of characteristic structural parameters to deformation angles is analysed. The expressions for the equivalent bending and torsion rigidities are also derived so that this type of truss can be calculated as a continuum beam. The rates of coupling these two modes are defined, and effects of coupling are analysed on a number of examples of practical importance.

Keywords: Bending, Torsion, Equivalent stiffness

1. INTRODUCTION

Truss beams repeated cells as in Fig.1 are widely used in mechanical and civil engineering as load carrying structures because of their high strength to weight ratio and other good properties. They are the most commonly calculated by means of finite element method (FEM).

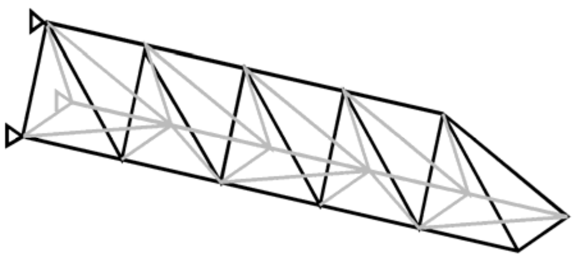

Figure 1 A truss with repeated cells

An alternative approach to calculate this type of truss beam is to consider them as a continuum body. The general idea of that method can be found in [1] and [2]. There are several different variants of that method, and the give formulas of comparable accuracy to FE method. An advantage of continuum modelling approach is that it enables easier analysis of influence of different structural parameters – filling angle, relative cell length to the overall length of a truss, etc. Also, continuum modelling approach makes easier optimization procedures, because we see more clearly how a single parameter affects the behaviour of the truss as a whole.

Using theory of continuum modelling (TCM) one can obtain the equivalent strength characteristic, for example, equivalent bending and shearing rigidity needed to calculate deflections and slopes. An useful feature of TCM is that it gives a possibility to simply and quickly analyse influence of different design quantities and parameters to the overall quality of the structure. One of the TCM methods is a direct energy approach, elaborated in Refs. [3] and [4].

Calculation procedure in this paper is based on the method developed by the same authors in the following references. In [5] and [6] a procedure for calculating the end deflection of planar truss similar to the one in Fig.1 was developed. The truss consisted of repeated cells with constant filling angle, and was loaded with a transverse force at its free end. It was shown in the paper that the end deflection consisted of two components that can be identified as structural bending and structural shearing. The concepts of the equivalent bending and the equivalent shearing rigidity were introduced based on an analogy to the corresponding quantities of a continuum beam with bulk cross-section. It was shown also how a number of cells affect the overall behaviour of the truss.

In paper [7] the procedure and concepts introduced in the previous two papers were extended to a planar truss of the same type loaded with distributed transverse load in the plane of the truss. The concepts of the equivalent bending and shearing rigidities (in the structural sense of these terms) proved effective again.

Paper [8] brought the extending of the theoretical approach presented above to a spatial truss with triangular cross-section, loaded with two transverse forces at its free end. This type of the cantilever truss beam is widely used in civil engineering cranes and many other structures demanded to have high load to self weight ratio.

The paper [9] dealt with the analysis of different types of filling bars patterns, namely how they influence the strength characteristics of a planar truss loaded with a transverse force at its free end. Values of the equivalent bending and shearing rigidities for some cases of a practical importance were calculated and discussed.

*Corresponding author: Dositejeva 19. Kraljevo, dedic.m@mfkv.kg.ac.rs

In paper [10] a truss similar to the one in [6] was analysed. Influence of cross-section areas to the free end deflection was considered in a number of numerical examples. It was shown how a theory developed in the above mentioned papers can be utilized to seek for an optimum structure.

Paper [11] brought an procedure of calculating the end slope of planar truss loaded with a transverse force at its free end. Concepts of the structural bending and shearing rigidity were extended to this type of deformation.

Finally the procedure of calculating various deformations of the planar and spatial trusses was extended in papers [12] to [15] to the trusses with cross-section areas that differ in two spans so that a lighter structure, with higher load to self weight ratio, can be achieved.

1. GEOMETRY AND MATERIAL DATA AND NOTATION

We consider in this paper a statically determinate cantilever truss made of pin jointed bars with constant cross-section, Fig.1. The bars are bound in n repeated cells except for the free end cell ($k = 1$) with unstressed "t" and "v" bars omitted. Ordinal number of a cell is denoted by k, Fig.2.

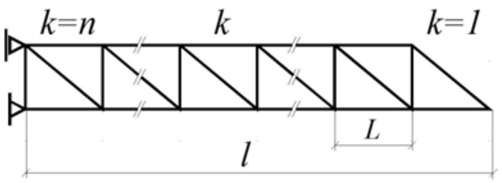

Figure 2 Numeration of cells

The cell length is L, and the overall length of the truss is $l = nL$. Coordinate system x, y, z is presented in Fig.3. Axes z and y lay in the plane of symmetry, although the truss is not symmetric in strict sense of meaning, which is discussed later.

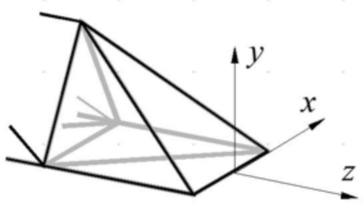

Figure 3 Coordinate system

Notation of bars in a cell is, see Fig.4: first indices "b" refer to bottom bars, "t" to top, "v" to 'vertical', "d" to diagonal and "p" to transverse bars. Second indices "l" and "r" refer to the left and right side bars, Fig.5, and the second index "b" to the bottom diagonal bars. We assume that "v" and "p" bars belong to the right hand cell in Fig.2, i.e. to the cell with smaller k. Consequently, for the rightmost "p" bar in Fig.2, the one to which the coordinate system is attached, $k = 0$.

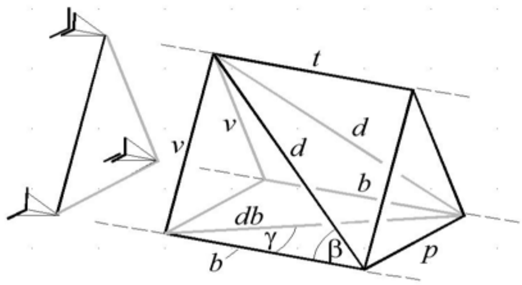

Figure 4 Notation of bars and angles

The truss has vertical plane of symmetry except for zigzagging "db" bars, Fig.4. Length of the bars are $l_{bl} = l_{br} = l_t = L$, $l_{vl} = l_{vr} = l_v$, $l_{dl} = l_{dr} = l_d$, $l_p = p$ *and* l_{db}. The hight of the truss cross-section is h, Fig.5. Angles of oblique bars are α, β and γ, and they are related via $\mathrm{tg}\gamma = 2\sin\alpha\,\mathrm{tg}\beta$. It is noteworthy that of these lengths and angles only three are independent quantities. Cross-section areas of bars are denoted $A_{bl} = A_{br} = A_b$, A_t, $A_{vl} = A_{vr} = A_v$, $A_{dl} = A_{dr} = A_d$, A_p and A_{db} .

Modulus of elasticity of all bars is E. However, the procedure developed in the further text can be applied to trusses with different moduli E. Since the bars are pin jointed, they are strained in pure extension or compression.

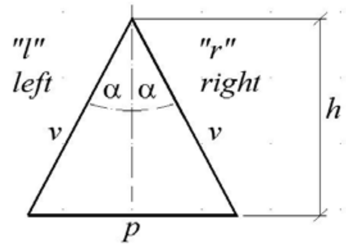

Figure 5 Notation of sides and the angle of sides

The truss is loaded by two couples of forces moments at its free end, see *Fig.6,* the first couple makes bending moment

$$M_{\mathrm{fy}} = F_{\mathrm{H}}\, p$$

in the horizontal plane, and the second couple makes twisting moment

$$M_{\mathrm{t}} = F_{\mathrm{V}} p$$

about the truss longitudinal axis z.

With the supports as in *Fig.3-top* the truss is statically determinate, and forces in the bars can be calculated from equilibrium conditions. For the left side, the one closer to a viewer in Fig.1, we get:

$$N_b(k)_l = \left(\frac{M_{fy}}{p} + \frac{M_t}{p\cos\alpha\,\mathrm{tg}\beta} \right), \left(\frac{M_{fy}}{p} \right) \qquad (1)$$

$$N_v(k)_l = \frac{M_t}{p\cos\alpha} \qquad (2)$$

$$N_d(k)_l = -\frac{M_t}{p\cos\alpha\sin\beta} \qquad (3)$$

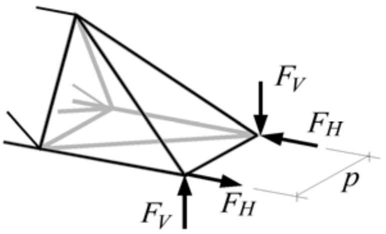

Figure 6 Couples of forces representing bending and twisting moment

The left brackets on the right hand side of (1) hold for odd *k* and the second brackets, after comma, for even *k* .

For the right side bars we get:

$$N_b(k)_r = \left(-\frac{M_{fy}}{p} \right), \left(-\frac{M_{fy}}{p} - \frac{M_t}{p\cos\alpha\,\mathrm{tg}\beta} \right) \qquad (4)$$

$$N_v(k)_r = -\frac{M_t}{p\cos\alpha} \qquad (5)$$

$$N_d(k)_r = \frac{M_t}{p\cos\alpha\sin\beta} \qquad (6)$$

Again, the left brackets on the right hand side of (4) hold for odd *k* and the second brackets, after comma, for even *k*.

All "t" bars are unstressed due to the fact that they lay in the plane of symmetry. Therefore the equilibrium conditions of forces lead to:

$$N_t(k) = 0 \qquad (7)$$

Finally for the bottom side, of bottom plane of the truss, we get from the equilibrium conditions:

$$N_p(0) = N_p(n) = \frac{M_t}{p}\mathrm{tg}\alpha \quad \text{... and} \qquad (8)$$

$$N_p(k) = 0 \quad \text{for} \quad k = 1, 2, 3 \ldots n-1 \qquad (9)$$

$$N_{db}(k) = \mp \frac{2\mathrm{tg}\alpha M_t}{p\sin\gamma} \qquad (10)$$

The upper signs in (10) holds for odd *k* and plus sign for even *k*.

2. DEFORMATIONS OF THE FREE END

We use the Castigliano's theorem to calculate the free end deformations – in this case the angular deformations. The deformation energy of the truss is sum of its components in all stressed bars:

$$A_d = \frac{1}{2}\sum_{k=1}^{n}\left[\frac{N_{bl}^2(k)L}{EA_b} + \frac{N_{br}^2(k)L}{EA_b} + \frac{N_{vl}^2(k)l_v}{EA_v} + \frac{N_{vr}^2(k)l_v}{EA_v} + \frac{N_{dl}^2(k)l_d}{EA_d} + \frac{N_{dr}^2(k)l_d}{EA_d} + \frac{N_{db}^2(k)l_{db}}{EA_{db}} \right] + \frac{N_p^2(0)p}{EA_p} + \frac{N_p^2(n)p}{EA_p} \qquad (11)$$

After changing forces (1) to (10) we get:

$$A_d = \frac{l}{2EA_b p^2}\left[M_{fy}^2 + \left(M_{fy} + \frac{L}{h}M_t \right)^2 \right] + \frac{l}{2Ep^2Lh^2}\left[\frac{2l_v^3}{A_v} + \frac{2l_d^3}{A_d} + \frac{p^3}{A_p n} + \frac{l_{db}^3}{A_{db}} \right] M_t^2 \qquad (12)$$

with trig functions of α, β and γ in (1) to (10) replaced by length ratios that can be easily established combining Figs.2, 4 and 5:

$$\cos\alpha = \frac{h}{l_v}$$

$$\mathrm{tg}\alpha = \frac{p/2}{h} = \frac{p}{2h}$$

$$\sin\beta = \frac{l_v}{l_d}$$

$$\mathrm{tg}\beta = \frac{l_v}{L}$$

$$\sin\gamma = \frac{p}{l_{db}}$$

to supply A_d for more condensed form.

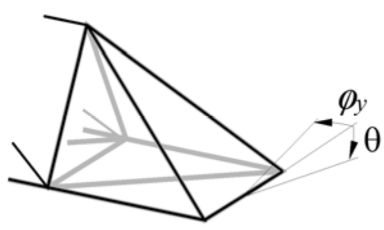

Figure 7 Angular deformations of the free end

Couples of forces F_H and F_V produce rotations (angular deformations) φ_y in the horizontal plane and θ in the vertical plane of the rightmost "*p*" bar, see Fig.7, and we want to calculate them. For that purpose we derive A_d , expression (12) by M_{fy} and M_t:

$$\varphi_y = \frac{\partial A_d}{\partial M_{fy}} = \alpha_{yy} M_{fy} + \alpha_{yz} M_t \tag{13}$$

$$\theta = \frac{\partial A_d}{\partial M_t} = \alpha_{zy} M_{fy} + \alpha_{zz} M_t \tag{14}$$

Quantities α_{yy}, α_{zz} and $\alpha_{yz} = \alpha_{zy}$ are influential coefficients and they read:

$$\alpha_{yy} = \frac{2l}{EA_b p^2} \tag{15}$$

$$\alpha_{yz} = \alpha_{zy} = \frac{lL}{EA_b p^2 h} \tag{16}$$

$$\alpha_{zz} = \frac{l}{Ep^2 Lh^2}\left[\frac{L^3}{A_b} + \frac{2l_v^3}{A_v} + \frac{2l_d^3}{A_d} + \frac{p^3}{A_p 2n} + \frac{l_{db}^3}{A_{db}}\right] \tag{17}$$

Values φ_y and θ obtained this way are exactly the same as those calculated by finite element method (FEM).

We see that the horizontal bending is carried solely by "*b*" or bottom longitudinal bars, while the twist is carried by all bars except for "*t*" or top longitudinal bars that remain unstressed in both modes of deformation.

In realty, however, "*t*" bars are stressed by the truss own weight that produces bending in the vertical plane, the effect not included in this analysis. An interested reader may find a solution for that in paper [7] in the manner similar to the one in this text. Also, since only 0-th and *n*-th "*p*" bars are stressed, their influence is small, and it rapidly decreases with *n* increasing, as can be seen in penultimate term in (17).

3. COUPLING OF DEFORMATIONS

We see that angles produced by M_{fy} and M_t are coupled, i.e. either one of them acting alone produces both φ_y and θ. It is because the truss does not have a horizontal plane of symmetry, and it behaves like a thin walled continuum beam with the same symmetry properties.

We introduce here a measure of coupling. First, if M_{fy} acts alone, i.e. $M_t = 0$, we have from (13) and (14):

$$\varphi_y = \alpha_{yy} M_{fy} \tag{18}$$

$$\theta = \alpha_{yz} M_{fy} \tag{19}$$

Eliminating M_{fy} from the two relations we can define a *torsion-bending rate of coupling* in the form:

$$K_{\theta/\varphi y} = \frac{\theta}{\varphi_y} = \frac{\alpha_{yz}}{\alpha_{yy}} \tag{20}$$

Secondly, if M_t acts alone, i.e. $M_{fy} = 0$, we have:

$$\varphi_y = \alpha_{yz} M_t \tag{21}$$

$$\theta = \alpha_{zz} M_t \tag{22}$$

and now eliminating M_t from the above relations we can similarly define a *bending-torsion rate of coupling*:

$$K_{\varphi y/\theta} = \frac{\varphi_y}{\theta} = \frac{\alpha_{yz}}{\alpha_{zz}} \tag{23}$$

Numerical values of these parameters for typical truss geometry data are discussed in the Chapter 5 .

Using expression (14) one can also get a twisting moment M_{t0} needed to annihilate twist produced by M_{fy}. After putting $\theta = 0$ we obtain the following expression:

$$M_{t0} = -\frac{\alpha_{yz}}{\alpha_{zz}} M_{fy} \tag{24}$$

We see that the multiplier in front of M_{fy} in the above expression is the negative of $K_{\varphi y/\theta}$ in (23).

4. EQUIVALENT RIGIDITIES

Formulas (13) and (14) enable to define equivalent rigidities of this type of structure in the same way as it has been done by these authors for the truss subject to bending in the vertical plane, papers [6] to [9]. In Strength of materials we have formula for the angle of flexion of the free end of a continuum cantilever beam produced by bending moment M_{fy}:

$$\varphi_y = \frac{M_{fy}\, l}{E\, I_y} = \frac{M_{fy}\, l}{B_{fy}} \tag{25}$$

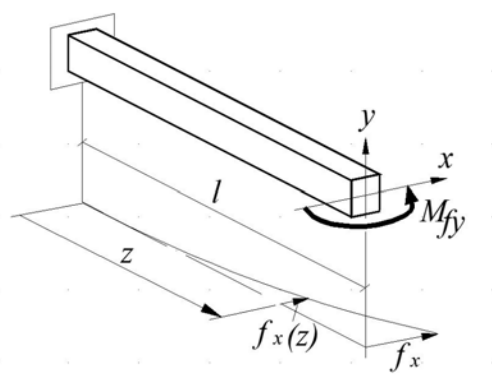

Figure 8 Deflections of a continuum beam

Letting $M_t = 0$ in (13) we have $\varphi_y = \alpha_{yy} M_{fy}$, and comparing these two relations we see that the equivalent bending rigidity of our truss would read:

$$B_{fye} = (EI_{ye}) = \frac{l}{\alpha_{yy}} \tag{26}$$

With this quantity we can make a formula for the free end deflection of an equivalent truss in Fig.8:

$$f_x = \frac{M_{fy} l^2}{2EI_{ye}} = \frac{M_{fy} l^2}{2B_{fye}} \tag{27}$$

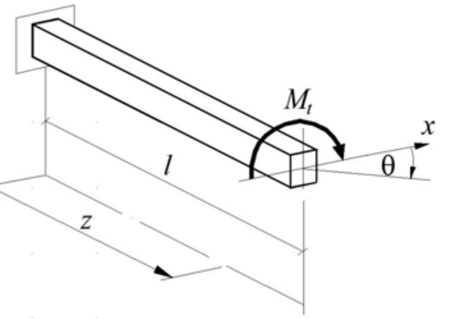

Figure 9 Torsion of a continuum beam

Similarly, formula for the twist of a continuum bar, Fig.9, reads:

$$\theta = \frac{M_t\, l}{G\, I_t} = \frac{M_t\, l}{B_t} \tag{28}$$

Letting $M_{fy} = 0$ in (14) we get: $\theta = \alpha_{zz} M_t$ and we can now define the equivalent torsion rigidity of the truss:

$$B_{te} = \frac{l}{\alpha_{zz}} \tag{29}$$

With equivalent bending rigidity B_{fye}, formula (24), we can write formulas for the slope and deflection of the truss in the horizontal plane produced by M_{fy} at a distance z from the supports:

$$\varphi_y(z) = \frac{M_{fy} z}{B_{fye}} \tag{30}$$

$$f_x(z) = \frac{M_{fy} z^2}{2B_{fye}} \tag{31}$$

Again the results obtained by (31) are the same as those obtained by FEM. Finally with equivalent torsion rigidity B_{te}, see.(29), we can write formula for the twist produced by M_t at a distance z from the supports:

$$\theta(z) = \frac{M_t z}{B_{te}} \tag{33}$$

5. NUMERICAL EXAMPLES

We shall consider here an example of a truss in Fig.1. It is circa 10 meters long and h = 100 cm high. In fact, it is designed to carry vertical load that produces 10000 kNcm moment at the supported end (which corresponds to the vertical load of a metric ton at an arm of 10 meters). The truss is made of steel tubes of different diameters but not smaller than 2,5cm. The compressed bars are designed to withstand the buckling force with the safety factor 2,6. The self-weight was also taken into account, save that only the weight of tubes was taken into account and not additional structural elements, like braces and other elements for strengthening of joints.

Table 1

$\beta = 30^o$			
α [°]	20	25	30
L [cm]	184	191	200
$\alpha_{yy}x10^6$ [kN^{-1}cm^{-1}]	2.58	1.56	1.01
$\alpha_{zz}x10^6$ [kN^{-1}cm^{-1}]	16.5	10.6	7.32
$\alpha_{yz}x10^6$ [kN^{-1}cm^{-1}]	2.38	1.51	1.01
$K_{\theta/\varphi y}$	0.922	0.956	1
$K_{\varphi y/\theta}$	0.144	0.141	0.138

Table 2

$\beta = 35^o$			
α [°]	20	25	30
L [cm]	152	158	165
$\alpha_{yy}x10^6$ [kN^{-1}cm^{-1}]	3.57	1.88	1.22
$\alpha_{zz}x10^6$ [kN^{-1}cm^{-1}]	19.7	10.5	7.36
$\alpha_{yz}x10^6$ [kN^{-1}cm^{-1}]	2.71	1.48	1.01
$K_{\theta/\varphi y}$	0.760	0.788	0.825
$K_{\varphi y/\theta}$	0.138	0.141	0.147

With these data on the lengths and cross-section areas Tables 1 and 2 in the further text were made. For different values of angles α and β cell length L, influential coefficients (15), (16) and (17) and coupling rates (20) and (23) have been calculated and tabulated in it. Here are some conclusions that we may draw out of them.

Values of influential coefficients clearly show that this form of structure is very sensitive to twisting, figures for α_{zz} are five or more times larger than for α_{yy}.

The above mentioned fact implies that the influence of bending moment to the coupled twist θ, see values of $K_{\theta/\varphi y}$, is greater than the influence of the twisting moment to the coupled angle φ_y of bending in the horizontal plane, see the values of $K_{\varphi y/\theta}$ for comparison.

What could be the purpose of this analysis? We know that this type of truss is designed primarily for carrying the load in the vertical plane. However, from the previous text we can see that it can be sensitive to the lateral load or bending in the horizontal plane. This is important not only in cases of horizontal forces acting upon it, but in cases where horizontal acceleration produces inertial forces. Importance of this lies in the fact that the truss will undergo a twist as well, and the designer should bear that in mind.

6. CONCLUSION

Analysis presented in this paper considers a truss with triangular cross-section having vertical plane of symmetry under the action of a bending moment in horizontal plane and twisting moment, both of them resulting from action of couples of forces at its free end. The analysis shows that deformations of these moments are coupled in the sense that these moments produce angular deformations in the planes of both couples of forces. The expressions for these angles through influential coefficients have been derived. The coupling coefficients have been defined. Numerical calculations in a number of typical geometry parameters have shown a great influence of horizontal bending to the twist. Also equivalent bending and twisting rigidities for this type of truss have been defined.

The formulas derived enable a designer to quickly calculate the main deformations of this type of truss and easily analyze influence of different geometry data to the overall behavior of the structure.

REFERENCES

[1] Noor, A. K., Mikulas, M. M. “Continuum Modeling of Large Lattice Structures”, Status and Projections, NASA Technical Paper 2767, (1988).

[2] Dow, J. O., Su, Z. W., Feng, C. C., Bodley, C. “Equivalent Continuum Representation of Structures Composed of Repeated Elements”, AIAA Journal, , Vol.23, No.10, pp.1564-1569, (1985).

[3] Burgardt, B., Cartraud, P. “Continuum Modelling of Beamlike Lattice Trusses”, Advances in Computational Techniques for Structural Engineering, Budapest, Hungary, pp.51-59, 21.-23. August (1996),.

[4] Teughels, A., De Roeck, G. “Continuum Models for Beam- and Platelike Lattice Structures”, IASS-IACM

2000 Fourth International Colloquium of Computations of Shell & Spatial Structures, pp.1-20, Channia Crete, Greece, 5.-7. June (2000),.

[5] Dedic M., Todorovic M., "An Analysis of The Equivalent Stiffnesses of Beam-like Trusses with Constant Cross-section", Proceedings of The 1st International Congress of Serbian Society of Mechanics, 10-13th April, 2007., Kopaonik, pp. 347-352, (2007).

[6] Todorovic M., Dedic M., "An Analysis of The Deformation of a Beam-like Truss Structure using Method of Equivalent Continuum Beam", 7th International Conference Research and Development in Mechanical Industry RaDMI 2007, 16th-20th September 2007., Belgrade, Serbia, Session C, pp.670-674, (2007).

[7] Dedic M., Todorovic M., "Calculation of the Free End Deflection and Slope of a Cantilever Truss in Distributed Load", Proceedings of the The Sixth International Conference ‘Heavy Machinery HM ‘08’, Kraljevo, Yugoslavia, June 24th – 29th. 2008., pp.E.1-E.4., (2008).

[8] Todorovic M., Dedic M., "A Deformation Analysis of A Spatial Truss Beam with Triangular Cross-section by Means of Continuum Modeling", Proceedings of the The Sixth International Conference ‘Heavy Machinery HM ‘08’, Kraljevo, Yugoslavia, June 24th – 29th. 2008., pp.E.67-E.70., (2008).

[9] Todorovic M., Dedic M., "A Deformation Analysis of Trusses with Different Types of Filling Bars", Proceedings of The 8th International Conference ″Research and Development in Mechanical Industry″ RaDMI 2008**,** 14 - 17. September 2008., Uzice, Serbia., pp.366-369,(2008).

[10] Todorovic, M., Dedic, M., Cajetinac, S., Jevremovic, V.: "Influence of Cross-section Areas of Bars to Deformations of a Truss Beam", 9th International Conference „Research and Development in Mechanical Industry″ RaDMI 2009, 16 - 19. September 2009, Vrnjacka Banja, Serbia, , pp. 395-400, (2009).

[11] Todorovic, M., Dedic, M.: "Calculation of Cantilever Truss Beam Deformations Using Continuum Modeling", Journal of Modelling and Optimization in the Machines Building Field (MOCM), MOCM -15, Vol. 2 (2009). pp 87-98, (2009).

[12] Todorovic, M., Dedic, M., Cajetinac S., Jevremovic V.: "Determination of Deflection and Slope of Spatial Truss Beams by Continuum Modelling", 10th International Conference „Research and Development in Mechanical Industry″ RaDMI 2010, 16 - 19. September 2010, Donji Milanovac, Serbia, pp. 442-447, (2010).

[13] Dedic M., Tododrovic M.: "Calculation of The Free End Deflection of A Truss Beam with Variable Cross-section", Proceedings of the The Seventh International Conference ‘Heavy Machinery - HM 2011, Kraljevo, Serbia, June 29th – July 2nd, Vrnjacka Banja, pp.G.13-G.16, (2011).

[14] Todorovic M., Dedic M.,: "An Analysis of Equivalent Rigidities of A Truss Beam", Proceedings of the The Seventh International Conference ‘Heavy Machinery - HM 2011, Kraljevo, Serbia, June 29th – July 2nd, Vrnjacka Banja, pp.G.33-G.38, (2011).

[15] Todorovic M., Dedic M., Jevremovic V., Mijatovic M.,: "A Deformation Analysis of A Truss Beam with Variable Cross-Sections in Distributed Load", Proceedings of the 13th International Conference „Research and Development in Mechanical Industry″ RaDMI 2013, Volume 1, 12 - 15 September., Kopaonik, Serbia, pp.A.277-A.282, (2013).

Freight Wagon Mass Reduction using Parametric Optimization

Marko Topalović[1*], Vladimir Milovanović, Milan Blagojević, Aleksandar Dišić, Dragan Rakić, Miroslav Živković[1]
[1]Laboratory for engineering software, Faculty of Engineering, University of Kragujevac, Serbia

Advancements in the railroad industry are driven by the need to have faster, lighter trains, while adhering to rigorous safety standards. Implementation of FEM analysis in wagon design enables engineers to examine every aspect of wagon construction in virtual space and to affirm that all safety requirements are satisfied before the first prototype is made. Using FEM, engineers can identify areas of stress concentration in wagon construction, and if those calculated stresses exceed maximum permissible stress, they need to modify the design of the wagon until safety factor is reached. Also, finite element results can be used to identify over dimensioned part of construction which unnecessarily increase the weight and cost of wagon. Every change in design requires entire wagon to be re-analyzed for every prescribed load condition, which can become a very tedious endeavour. Implementation of the parametric optimization in wagon design is an advanced approach which automates the process of changing numerous plate thicknesses simultaneously while keeping maximum stresses within safety limits. If the initial design satisfies all safety requirements this procedure helps engineers to further improve wagon design, while if the initial design is flawed, parametric optimization can be used to search for a solution that meets all safety conditions. This technique is used to enhance design of freight wagon which will be used for transportation of granular materials. Optimization results identified several plates which thickness can be reduced, while overall wagon design is proven to be very well dimensioned.

Keywords: Parametric Optimization, Design Improvement, Weight Reduction, FEM, Freight Wagon

1. INTRODUCTION

Since the invention of the locomotive in the late 18th century by James Watt, railroads have been driving force of modernization and industrialization enabling fast and cheap transportation of materials and goods [1]. Speed of freight trains is hampered by the great weight of wagons and cargo as well as a high centre of gravity, which increases chance of wagon leaving the track in railway curves with short radius [2]. Weight reduction is one of the main concerns in designing new wagons which also lowers wagon centre of gravity, material used, and unit production price [3].

Development of computer hardware and software lead to increasing use of computers for modelling and designing of wagons [4]. Finite Element Method (FEM) is used to simulate the wagon response to different loading condition, thus reducing design time and improving overall wagon characteristics [5]. FEM was successfully used to analyze welded joints of wagon constructions [6], creation and development of fractures in wagon construction [6],[7], heat conductivity of elements of wagon structure [8]. FEM is used for crash simulations [9], [10] and for determination of stress fields [11]. FEM analysis is the fastest way to determine if the proposed wagon design satisfies safety norms prescribed in numerous documents such are [12]-[15].

During wagon development process, based on FEM results, designers can see if there are areas in the wagon construction that have higher than prescribed stresses and to make design changes to reduce these high stress concentrations. FEM can also show if some parts of wagon construction have much lower stress than prescribed, and in that case, designers can choose to use plates with less thickness, to reduce weight and cost of wagon. For each change they make, designers must run a series of FEM analysis to check if the new design satisfies all loading conditions prescribed in standards [12]-[15]. If designers can vary the thickness of several parts of wagon structure, design process prolongs and becomes very tedious. This process of thickness variation and FEM verification can be automated using optimization [16].

Optimization techniques can be used to enhance production process [17]-[19] or to enhance design of the final product, which will be shown in this paper.

In railway industry optimization techniques are still insufficiently implemented, but in recent years several papers have been published introducing this advanced approach to railroad engineers. Example of good practice of optimization implementation is management of freight wagon distribution [20]. Selection process of material which will be used in wagon construction can also be optimized as shown in [21]. Finite elements results are used in optimization of composite material used for construction of light rail vehicle [22].

In this paper, we present an implementation of finite element analysis and structural optimization of freight wagon for transportation of granular material. Compared to the above mentioned related work, this paper demonstrates advantages of structural optimization methodology application in the railroad industry for the wagon weight reduction based on selection of an optimum combination of plate thicknesses.

In the next sections theoretical background is given, followed by a simple cantilever example, which is used to explain and highlight the advantages of the optimization procedure. This procedure is then applied on full model of freight wagon designed for transportation of granular materials, with all load conditions and all safety factors prescribed in regulating standards [12]-[15]. Results and discussion show that initial wagon design was very good, with only few plates that were initially over-dimensioned by engineers so this methodology can be successfully used to further improve wagon design.

*Corresponding author: Sestre Janjić 6 34000 Kragujevac, topalovic@kg.ac.rs

2. MATERIALS AND METHODS

2.1. Review of Optimization Theory

Structural optimization can be defined as the process of design improvement by finding best results under given conditions. There are two kinds of structural optimization: parametric and shape optimization (Fig. 1).

Shape optimization performs changes of part geometry until best combination of dimensions is reached [23],[24], while parametric optimization performs changes only to the properties of structures while geometry stays the same [25].

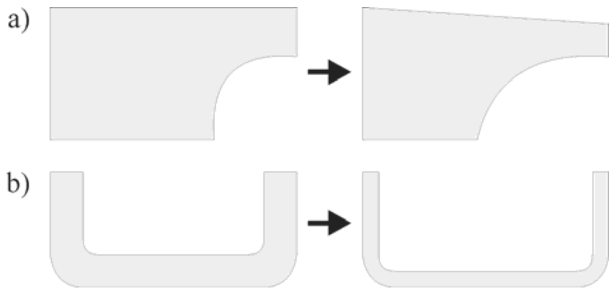

Figure 1: Types of optimization: a) shape optimization, and b) parametric optimization

Parameters are properties that describe the design of observed system (in case of the wagon, parameters are plate thicknesses). Parameters can be unchangeable (if certain plates of wagon construction must be made in specified thickness) or changeable (plate thickness can vary during the optimization procedure). Changeable parameters (also called design variables) $x_i \;\; i=1,2,...n$, form vector of design variables which describes current configuration of modelled wagon [26].

$$\mathbf{X} = \begin{Bmatrix} x_1 \\ x_2 \\ \cdots \\ x_n \end{Bmatrix} \qquad (1)$$

The goal of the optimization in engineering is often weight reduction and it is defined with objective function $f(\mathbf{X})$ which is a function of design variables vector i.e. function of combination of all shell thicknesses [27]. Design sensitivity coefficients (partial derivatives) describe the rate of change of objective function in relation to changes of design variable in particular shell thickness [28]. Restrictions that limit design variable values are called constraints [29]. Constraints can be a function of the design variables vector, or side constraints. Functional constraints can be inequality constraints $g_j(\mathbf{X}) \le g_{\max}$ or equality constraints $h_k(\mathbf{X}) = h_{def}$ [29].

Optimization can be viewed as:

minimize $f(\mathbf{X})$ (objective function)

subjected to:

$g_j(\mathbf{X}) \le g_{\max} \qquad j=1,...,n_g$ (inequality constraints)

$h_k(\mathbf{X}) = h_{def} \qquad k=1,...,n_h$ (equality constraints)

$x_i^l \le x_i \le x_i^u \quad i=1,...,n$ (side constraints)

where $\mathbf{X} = \{x_1, x_2, ..., x_n\}$ is a vector of the design variables, $g_{\max}$ is the maximum allowed value of structural response, n_g number of inequality constraints, h_{def} response value that must be achieved, n_h number of equality constraints, x_i^l lower side constraint for considered design variable, x_i^u upper side constraint for considered design variable.

Design variables $x_i \;\; i=1,2,...n$ form n-dimensioned space called design space [27]. Two dimension design space is shown in Figure 2, while multi dimension design space like the one we have in wagon optimization cannot be visualized, all the rules that govern two dimension design space apply to multi dimensioned space as well [29]. Constraints divide design space into the feasible region (wagon satisfies all requirements as all stresses are below prescribed maximum stress) $g_j(\mathbf{X}) < g_{\max}$ and infeasible region (stresses in some wagon plates exceed maximum prescribed stress) $g_j(\mathbf{X}) > g_{\max}$ [29]. Objective function of weight reduction defines surfaces in design space which are represented by contours of constant value objective function (same weight for different combination of plate thicknesses) $f(\mathbf{X}) = c = const$ [27]. Figure 2b shows that for every vector of design variables we can define usable-feasible region which contains lesser objective functions (less total wagon weight) than of the observed vector [29]. During the optimization process, optimizer searches usable-feasible region (Fig. 3) for the design variable vector which has the minimum objective function (minimum wagon weight that satisfy all safety requirements).

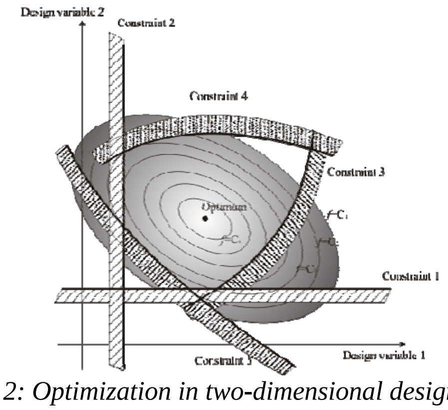

Figure 2: Optimization in two-dimensional design space: Design space with constraints

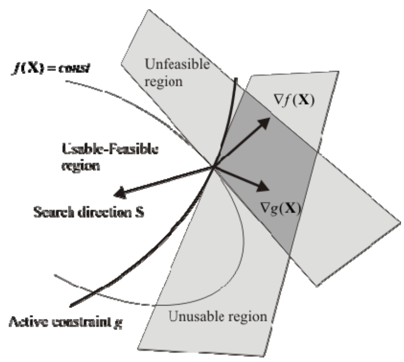

Figure 3: Active constraint with a usable-feasible region

Optimization is performed by following steps

1. Optimization starts with initial test design variable vector $\mathbf{X}_i$
2. Usable-feasible search direction $\mathbf{S}_i$ is determined
3. For search direction $\mathbf{S}_i$ corresponding scalar parameter λ_i^* is found
4. New design variable vector $\mathbf{X}_{i+1}$ is calculated using $\mathbf{X}_{i+1} = \mathbf{X}_i + \lambda_i^* \mathbf{S}_i$
5. New design variable vector $\mathbf{X}_{i+1}$ is checked for convergence to the optimum, and if optimum is achieved search for optimum is stopped, if optimum is not achieved increment is increased and procedure returns to step 2.

Based on position of initial test design variable vector $\mathbf{X}_i$ in regard to constraints, optimization can be with violated constraints, with active constraints or unconstrained [31],[32].

If some constraints are violated (stress in shell exceeds maximum prescribed stress), design variable vector is in infeasible region, and optimizer's first goal is to reach feasible region, even if it means increasing objective function $f(\mathbf{X})$. For violated constraint $g_j(\mathbf{X})$ search direction is opposite to $\nabla g_j(\mathbf{X})$. If the feasible region is not achieved in the first iteration, for the next iteration scalar move parameter λ_i^* is increased and also in every subsequent iteration as well. If feasible region is not reached in 20 iterations, the optimization process is stopped, as finding design variable vector $\mathbf{X}_i$ which would satisfy violated constraints is judged unlikely. In this case, an engineer needs to try with different initial design variable vector $\mathbf{X}_i$ or to change design of construction.

If a design variable vector is near a constraint (a region defined by +/- 3% of constraint value) constraint is considered active. In this case the search direction must reduce objective function while keeping design variable vector $\mathbf{X}_i$ within feasible region (Fig. 2). Mathematically usable search direction $\mathbf{S}$ must satisfy

$$\nabla f(\mathbf{X}) \cdot \mathbf{S} \le 0 \tag{2}$$

while feasible search direction $\mathbf{S}$ must satisfy

$$\nabla g(\mathbf{X}) \cdot \mathbf{S} \le 0 \tag{3}$$

Unconstrained optimization occurs when there are no active or violated constraints. In that case the goal is to reach optimum in as few as possible iterations. The Steepest Descent Method (Cauchy Method) is the simplest optimum search algorithm which defines the search direction as opposite of objective function gradient in that iteration [34].

$$\mathbf{S}_i = -\nabla f(\mathbf{X}_i) \tag{4}$$

When the value of objective function starts to increase, another search direction is defined (Fig. 4). This new direction is perpendicular to previous one. After each iteration, the objective function is closer to optimum. This "zigzag" path (shown in Figure 4) is inefficient and more advanced methods have been developed, such as Broyden-Fletcher-Goldfarb-Shanno method (BFGS), used in [31]. Optimization using BFGS algorithm is performed by following steps

1. Optimization starts with initial design variable vector $\mathbf{X}_1$ and with $n \times n$ positively defined symmetric matrix $[B_1]$ which approximate inverse Hessian of goal function f (usually for $[B_1]$ identity matrix $[I]$ is taken). Iteration counter is set to $i=1$.
2. Gradient of the objective function f is calculated for design variable vector $\mathbf{X}_i$ and search direction is determined $\mathbf{S}_i = -[B_i]\nabla f_i$
3. Optimal scalar move parameter λ_i^* is calculated and used to obtain new design variable vector $\mathbf{X}_{i+1} = \mathbf{X}_i + \lambda_i^* \mathbf{S}_i$
4. Convergence criteria are assessed and if convergence is achieved the optimization process is finished.
5. If convergence is not achieved optimization continues and matrix $[B_i]$ is updated using
$$[B_{i+1}] = [B_1] + \frac{\mathbf{d}_i \mathbf{d}_i^T}{\mathbf{d}_i^T \mathbf{g}_i}\left(1 + \frac{\mathbf{g}_i^T [B_1] \mathbf{g}_i}{\mathbf{d}_i^T \mathbf{g}_i}\right) - \frac{[B_1]\mathbf{g}_i \mathbf{d}_i^T}{\mathbf{d}_i^T \mathbf{g}_i} - \frac{\mathbf{d}_i \mathbf{g}_i^T [B_1]}{\mathbf{d}_i^T \mathbf{g}_i}$$
where
$$\mathbf{d}_i = \mathbf{X}_{i+1} - \mathbf{X}_i = \lambda_i^* \mathbf{S}_i$$
$$\mathbf{g}_i = \nabla f(\mathbf{X}_{i+1}) - \nabla f(\mathbf{X}_i)$$
6. Value of iteration counter is increased $i = i+1$ and optimization process returns to step 2

Advantages of the BFGS method in comparison to the Steepest Descent Method are illustrated in Figure 4.

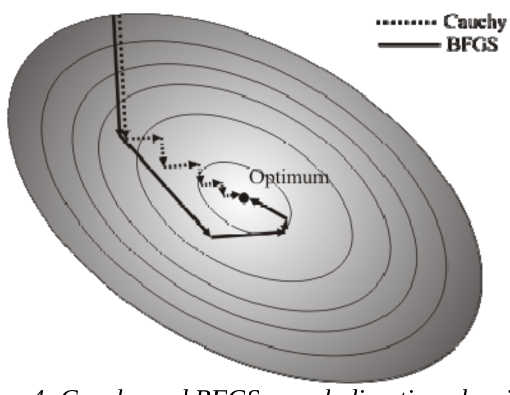

Figure 4: Cauchy and BFGS search direction algorithms

Optimum can lie on active constraint, it can be on constraint intersection or it can be unconstrained. To check if optimum is reached, unified criterion must be defined [33]. Kuhn-Tucker condition states that the vector sum of the objective and all active constraints must be equal to zero. For two active constraints with an optimum at their intersection Kuhn-Tucker condition is shown in Figure 5.

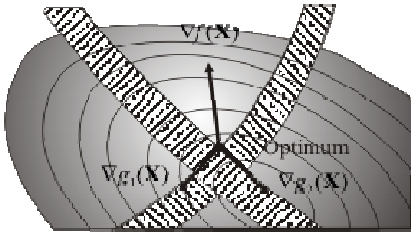

Figure 5: Kuhn-Thucker condition for constrained optimum

If there are no active constraints, objective is unconstrained and gradient of the objective function is equal to zero [31].

2.2. Parametric Optimization of Sheet Metal Constructions

In this section parametric optimization of sheet metal constructions is demonstrated on simple T-shaped cantilever. The initial cantilever design consists of two metal plates, 1 mm thick, made from the same material (Fig. 6)

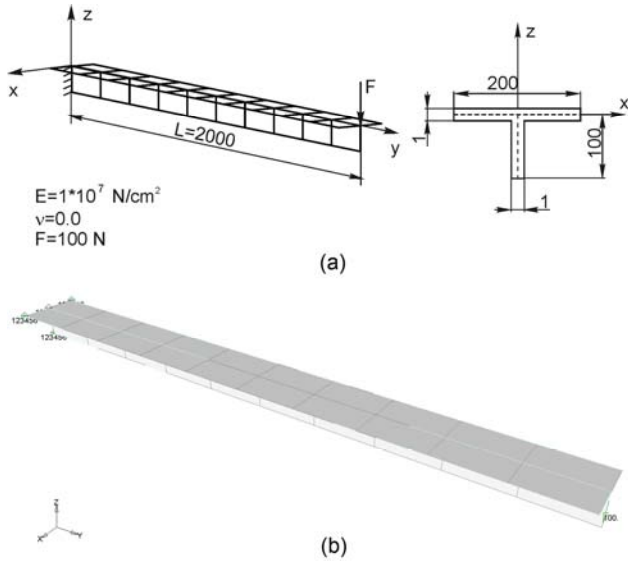

Figure 6: T-shaped cantilever: a) model, b) cross-section, c) finite element model, and d) material characteristics

To demonstrate optimization technique, we want to make cantilever of thinner plates. The goal is to determine the best combination of upper and lower plate thickness, which satisfies maximum stress criteria, while minimizing the total weight of the cantilever. Sheet metal constructions must withstand many different load conditions, and to optimize their design all load cases must be taken into consideration. We optimized cantilever subjected to two load cases, one is the vertical load at the free end of the cantilever modeled as a nodal force of 100 N, while the second load case is the horizontal load, also acting on the end of the cantilever, modeled as a nodal force of 150 N. These loads do not act at the same time; instead, only one load can be active at the time. Plate thickness of upper and lower part of cantilever profile must be chosen to withstand both loads, but not both at the same time.

Material characteristics and dimensions are shown in Figure 6. For each plate property is created defining the plate thickness. Model ready for analysis and optimization is shown in Figure 6b. The optimizer will increase thickness values in several iterations, until optimum combination is found. These thicknesses can change 5% per iteration. Optimization limits (constraints) are defined for both properties: Von Misses Stress must be between 0 and 30 MPa.

Optimum is found after 11 iterations (Table 1)

Table 1: optimization results for T-shaped cantilever

Iteration	Lower plate thickness	Upper plate thickness
0 initial	0.3 mm	0.3 mm
1	0.35 mm	0.35 mm
2	0.4 mm	0.4 mm
3	0.45 mm	0.45 mm
4	0.5 mm	0.48 mm
5	0.55 mm	0.51 mm
6	0.6 mm	0.54 mm
7	0.65 mm	0.58 mm
8	0.7 mm	0.61 mm
9	0.75 mm	0.65 mm
10	0.8 mm	0.7 mm
11 final	0.8 mm	0.7 mm

Overall weight reduction of the T shaped cantilever is 26%. Weight reduction of constructions varies depending on the quality of initial design which is based on engineer skill and experience.

2.3. Parametric Optimization of Freight Wagon

Analyzed wagon is 4-axle bogie wagon designed for the transport of sand (grain size 0–2mm), and gravel (grain size 8-32mm), with high resistance to atmospheric influence. Wagon loading is carried out through an opening at the top of the box, and unloading is done outside the rail, using two funnels (on each side of the car), as well as fixed and extra funnels mounted on the bottom of the box. Design, construction and equipment of the wagon is in accordance to the regulations prescribed in the standards [12]-[15]. Construction of wagon is shown in Figure 7.

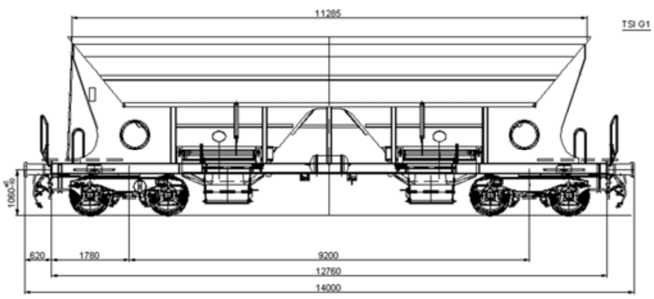

Figure 7: Drawing of 4–axle freight wagon

The wagon is modeled using the FEMAP software with NX Nastran solver. According to the construction type, shell elements of the appropriate thickness and 3D elements (for modeling of the support plate, compensating ring, traction stop) are used for creating the FEM mesh. The structure is modeled in details with 155045 elements and 156326 nodes and within the calculation there is a system of about nine hundred thousand equations being solved. General element side length is about 40 mm. This element size enables obtaining accurate analysis results within a reasonable amount of time. Figure 8 shows the FEM model of the whole wagon without bogies. Static linear analysis was performed with material with physical and mechanical characteristics given in Table 2

Table 2: physical and mechanical characteristics of material

Physical Characteristics			
Steel mark	E [N/mm^2]	ρ [kg/mm^3]	N
S355J2+N	2.1 10^5	7.85 10^{-6}	0.3
Mechanical Characteristics			
Steel mark	R_e [N/mm^2]	R_m [N/mm^2]	KV [J]
S355J2+N	355	470 – 630	27

The model consists of two subassemblies, underframe and wagon box, which are analyzed using FEM. Taking in consideration symmetry of the wagon, a quarter of the model is used in FEM simulation and optimization. FEM simulation is performed on all elements (3D and shell), while parametric optimization can be done only on shell elements. Some parts of a structure are already made of thinnest possible plates, some cannot be optimized due to the nature of the manufacturing process and some parts are too small and reduction of their mass would be insignificant in regards to mass of entire wagon.

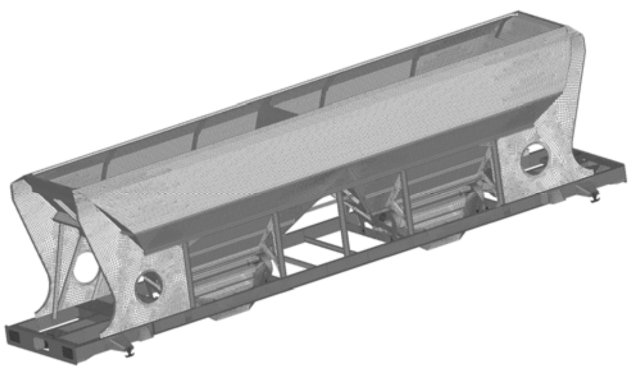

Figure 8: Finite element model of freight wagon

Plates that are taken into optimization process are shown in Figure 9 using dark gray color, while the light gray represents parts that cannot be optimized

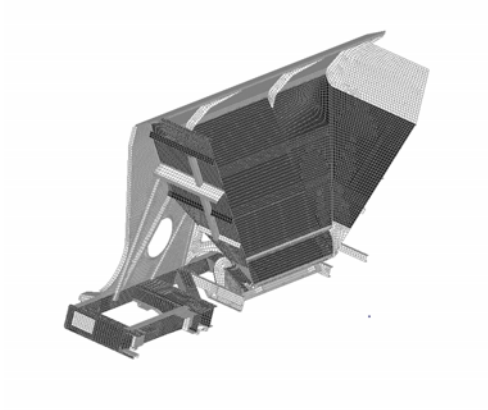

Figure 9: quarter of the model used for FEM analysis and parametric optimization

Wagon loaded with sand and grovel is shown on Fig. 10.

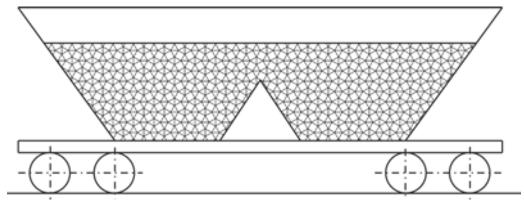

a)

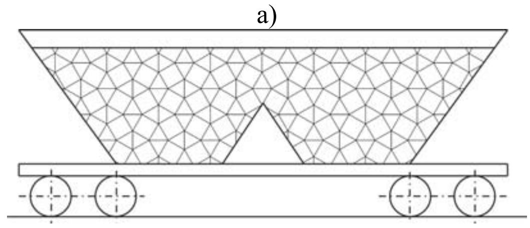

b)

Figure 10 Wagon loaded with a) sand b) gravel

3. RESULTS AND DISCUSSION

A Since FEM analysis showed that maximum calculated stresses are concentrated in certain areas, while the rest of the wagon is stressed well below permissible stress, we wanted to see if we could use thinner plates for wagon construction while keeping design within safety limits. Parametric optimization can vary plate thickness of numerous wagon elements within the constraints defined by maximum stress. Initial wagon design satisfies all constraints, and therefore it belongs to feasible region so we used it as starting point for our optimization procedure. For FEM analysis all plates with same thickness are given the same property. For optimization purposes, every plate that we want to optimize must have its own property. Plate thicknesses are design variables, and their combination is vector of design variables. Maximum stress in every plate must be under permissible stress defining inequality constraints while side constraints limit plate thickness between 4 and 10 mm. Optimization was performed for every load case. It showed us a great variation of minimum required plate thickness depending on load case. Overall, as expected, load combinations were most demanding in terms of minimum required plate thickness. Optimization showed that wagon underframe was initially very well dimensioned, only thickness of one plate can be reduced (Figure 11). On the other hand, wagon box is over dimensioned and could be made of thinner plates (Figure 12).

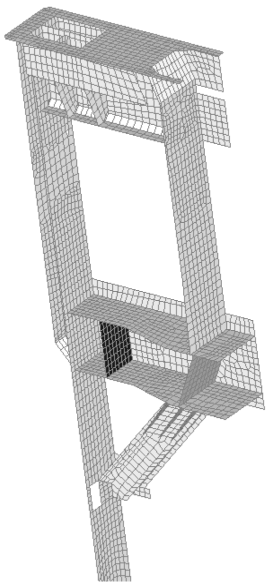

Figure 11: Dark gray represents optimized plates: view focused on the underframe,

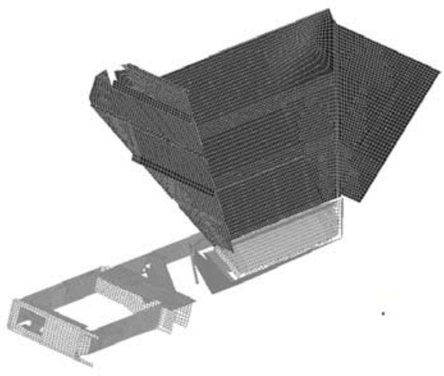

Figure 12: Dark gray represents optimized plates: view focused on wagon box

Optimization results, presented in Figures 11 and 12 show that initial wagon design had very well dimensioned elements and that there is little room for improvement. Out of 21 plates which we optimized, for 7 plates (1 in underframe and 6 in wagon box) weight reduction is achieved. The total weight reduction is 488.68 kg, which is 2.32% of empty wagon mass.

Numerical analysis of real life structures faces issues of results accuracy and reliability due to approximations and assumptions that engineers make during problem modeling. Since we obtained system response to various loading conditions prescribed in standards using FEM, and used those responses as input to parametric optimization, results that we get are also subjected to scrutiny, same as FEM. Parametric optimization itself is also influenced by choices engineers make when determining initial design and optimization parameters. Our assumption is that existing design (all plate thicknesses satisfy all safety criteria) of wagon which we optimized is the best starting point for optimization. We could also use minimum allowed plate thickness for all plates as starting point; or maximum plate thickness for that matter. Choosing existing design as a starting point ensures that initial design is in feasible region, and hopefully close to optimum. Another starting point might yield better results, or worse, or we might end up with the same plate thickness combination that we get using existing design as the starting point. Initial starting point for optimization process is one of the most important decisions that must be done by engineers, and optimization software cannot help them make the perfect choice, it's all up to the skill and experience of engineers.

Achieved weight reduction of 2.32% may bring into question if parametric optimization is really worth invested time and money. Compared to weight reduction of a cantilever beam, which we used to demonstrate techniques, one might expect the same results with wagon optimization, on the other hand, one should have in mind that initial cantilever design was over-dimensioned in order to demonstrate optimization process, while the initial design of the wagon was almost perfect. Nearly half a ton in saved material per unit, in large production series, can lead to great savings in material and money, justifying application of the optimization procedure in the final stages of designing a new wagon

4. CONCLUSION

Title This paper presents the implementation of parametric optimization in wagon design, which uses FEM results to determine the best combination of plate thickness in wagon design. FEM analysis has been used for years to simulate behavior of wagon under different loading conditions. These computer simulations reduced design time while ensuring safe behavior under operational load defined in regulations. Parametric optimization based on FEM analysis is the next logical step in computer aided design which has profound influence on ecological and economical aspects of wagon construction. It enables engineers to find the best combination of plate thicknesses, while adhering to safety regulations which are implemented through constrains into the optimization process. Implementation of parametric optimization during wagon designing results in reduced usage of material, production cost and energy consumption of locomotive during wagon operation lifetime. Improved characteristics of optimized wagons ensure their competitiveness and commercial success. In this paper state of the art theory is shown which is implemented in optimization software. Usability of the procedure is demonstrated on a simple cantilever problem, while the real life application is shown on the freight wagon. Achieved a weight reduction justified the implementation of parametric optimization in wagon design. Railroad engineers can greatly benefit from this technique by gathering experience on which parts they tend to over-dimension, which are crucial and which are non-essential parts of the construction. Parametric optimization can help young engineers develop skills more quickly and improve their experience all within the safety of virtual design space length.

ACKNOWLEDGEMENTS

This research is supported by Ministry of Education, Science and Tehnological Development, Republic of Serbia, Grant TR32036.

REFERENCES

[1] D.J. Forkenbrock, "Comparison of external costs of rail and truck freight transportation", Transport. Res. A-Pol., Vol. 35, pp. 321–337, (2001)

[2] A. Von Jena, B. Fischer, V. Mágori, "Intelligent sensor for monitoring freight-wagon working conditions", Sensor Actuat. A: Phys, Vol. 42, pp. 347–353, (1994)

[3] C.P. Barkan, "Improving the design of higher-capacity railway tank cars for hazardous materials transport: Optimizing the trade-off between weight and safety", J. Hazard. Mater, Vol. 160, pp. 122-134, (2008)

[4] R. Ferrara, G. Leonardi, F. Jourdan, "Numerical Modelling of Train Induced Vibrations", Procedia. Soc. Behav. Sci. Vol. 53 pp. 155–165, (2012)

[5] M. Dhanasekar, W.L. Bayissa, "Structural adequacy assessment of a disused flat bottom rail wagon as road bridge deck", Eng. Struct, Vol. 33, pp.1838–1849, (2011)

[6] V. Milovanović, V. Dunić, D. Rakić, M. Živković, "Identification causes of cracking on the underframe of wagon for containers transportation – Fatigue strength assessment of wagon welded joints", Eng. Fail. Anal, Vol. 31, pp.118–131, (2013)

[7] Z. Song, S. Fang, Y. Zhang, J. Xie, "Cracking analysis of bolster cover plate in C70 freight wagons", Eng. Fail. Anal, Vol. 30, pp. 43–60, (2013)

[8] L. Wu, Z. Wen, W. Li, X. Jin, "Thermo-elastic–plastic finite element analysis of wheel/rail sliding contact", Wear, Vol. 271, pp. 437–443, (2011)

[9] Y.A. Abdel-Nasser, "Frontal crash simulation of vehicles against lighting columns using FEM", Alexandria Eng J, (2013)

[10] X. Zhang, X. Jin, W. Qi, Y. Guo, "Vehicle crash accident reconstruction based on the analysis 3D deformation of the auto-body", Adv. Eng. Softw, Vol. 39, pp. 459–465, (2008)

[11] S.D. Akbarov, A. Yildizc, M. Eröz, "FEM modelling of the time-harmonic dynamical stress field problem for a pre-stressed plate-strip resting on a rigid foundation", Appl. Math. Model, Vol. 35, pp. 952–964, (2011)

[12] TSI Standard - Commission Decision of 28 July 2006 concerning the technical specification of interoperability relating to the subsystem rolling stock — freight wagons of the trans-European conventional rail system *(notified under document number C(2006) 3345)*

[13] EN 12663:2000 - Railway applications – Structural requirements of railway vehicle bodies, European Standard

[14] EN 10025 - European structural steel standard – Grade designations, properties and nearest equivalents.

[15] Eurocode 3: Design of steel structures - Part 1.9: Fatigue.

[16] R. Roy, S. Hinduja, Teti R, "Recent advances in engineering design optimization: Challenges and future trends", CIRP Ann Manuf Technol, Vol. 57, pp. 697–715, (2008)

[17] Z. Pahlavani, R. Ebrahimi, "Optimization of specific die profiles in thin walled tube extrusion", Iranian Journal of Science and Technology, Transactions of Mechanical Engineering, Vol. 37, No. M2, pp. 203-215, (2013)

[18] F. Ghaemi, R. Ebrahimi, R. Hosseinifar, "Optimization of die profile for cold forward extrsion using an improved slab method analysis", Iranian Journal of Science and Technology, Transactions of Mechanical Engineering, Vol. 37, No. M2, pp. 189-202, (2013)

[19] M. Savković, M. Gašić, D. Ćatić, R. Nikolić, G. Pavlović, "Optimization of the box section of the main girder of the bridge crane with the rail placed above the web plate", Struct Multidiscip O, Vol 47, pp. 273-288, (2013)

[20] A. Ballis, L. Dimitriou, "Issues on railway wagon asset management using advanced information systems", Transport Res C-Emer, Vol 18, pp.807–820, (2010)

[21] F. Findik, K. Turan, "Materials selection for lighter wagon design with a weighted property index method", Mater Design, Vol. 37, pp. 470–477, (2012)

[22] A. M. Harte, J. F. McNamara, Roddy ID, "A multilevel approach to the optimization of a composite light rail vehicle bodyshell", Comp Struct, Vol. 63, pp. 447–453, (2004)

[23] M. Firl, R. Wüchner, K. U. Bletzinger, "Regularization of shape optimization problems using FE-based parametrization", Struct Multidiscip O, Vol 47, pp. 507-521, (2013)

[24] B. Hassani, S. M. Tavakkoli, H. Ghasemnejad, "Simultaneous shape and topology optimization of shell structures", Struct Multidiscip O, (2013)

[25] S. Hertelé, W. De Waele, R. Denys, M. Verstraete, J. Van Wittenberghe, "Parametric finite element model for large scale tension tests on flawed pipeline girth welds", Adv Eng Softw Vol. 47, pp. 24–34, (2012)

[26] S. Kitayama, M. Arakawa, K. Yamazaki, "Sequential approximate optimization for discrete design variable problems using radial basis function network", Appl Math Comput, Vol. 219, pp. 4143–4156, (2012)

[27] D. Van Nguyen, "Global maximization of UTA functions in multi-objective optimization", Eur J Oper Res Vol. 228, pp. 397–404, (2013)

[28] M. Ohsaki, "Design sensitivity analysis and optimization for nonlinear buckling of finite-dimensional elastic conservative structures", Comput Method Appl M Vol. 194, pp. 3331–3358, (2005)

[29] J. París, F. Navarrina, I. Colominas, M. Casteleiro, "Stress constraints sensitivity analysis in structural topology optimization", Comput Method Appl M, Vol. 199, pp. 2110–2122, (2010)

[30] Y. Luo, M. Y. Wang, Z. Kang, "An enhanced aggregation method for topology optimization with local stress constraints", Comput Method Appl M Vol. 254, pp. 31–41, (2013)

[31] N. Andrei, "Accelerated scaled memoryless BFGS preconditioned conjugate gradient algorithm for

unconstrained optimization”, Eur J Oper Res Vol. 204, pp. 410–420, (2010)

[32] L. Woodward, M. Perrier, B. Srinivasan, “Real-time optimization using a jamming-free switching logic for gradient projection on active constraints”, Comput Chem Eng Vol. 34, pp.1863–1872, (2010)

[33] S. I. Birbil, J.B.G. Frenk, G. J. Still, “An elementary proof of the Fritz-John and Karush–Kuhn–Tucker conditions in nonlinear programming”, Eur J Oper Res Vol. 180, pp. 479–484, (2007)

[34] M.A. Hassan, W.J. Leong, M. Farid, “A new gradient method via quasi-Cauchy relation which guarantees descent”, J Comput Appl Math Vol. 230, pp. 300–305, (2009)

[35] Hassan MA, Leong WJ, Farid M, (2009) A new gradient method via quasi-Cauchy relation which guarantees descent, J Comput Appl Math 230:300–305.

Natural Frequencies of a Tapered Cantilever Beam of Constant Thickness and Linearly Tapered Width

Aleksandar Nikolić*[1], Slaviša Šalinić[1]
[1] Faculty of Mechanical and Civil Engineering
University of Kragujevac, 36000 Kraljevo, Dositejeva 19 (Serbia),

A method for determination of natural frequencies of a tapered cantilever beam in free bending vibration by a rigid multibody system is proposed. The considerations are performed in the frame of Euler-Bernoulli beam theory. The method consists of two steps. In the first step, the tapered cantilever beam is approximated by n flexible straight beam, and after that all of the n segments are divided into k segments. In the second step, all of the flexible straight beams are replaced by three rigid beams connected through revolute and prismatic joints with the corresponding springs in them. The results of the proposed method are compared with similar methods proposed in literature.

Keywords: Free bending vibration, tapered cantilever beam, rigid multibody system, natural frequencies

1. INTRODUCTION

Research on dynamic characteristics of flexible tapered cantilever beams is very important in different engineering fields. These types of beams appear most frequently as the result of a need for saving in material, reduction of weight, better utilization of material, increased rigidity, etc. A significant number of papers dedicated to the solution of this problem have been recently published.

This paper presents a new approach to approximative determination of natural frequencies of free vibration of this type of beams using the main ideas presented in [6] and [7]. A short analysis and adaptation of approaches from [1], [2], and [3] will be carried out for the purpose of comparing the obtained results with the results from similar approaches so that the procedure of analysis of this type of beams could be feasible. Comparison between the presented approach and the two mentioned approaches will be performed on the example from [4], where exact values of frequencies of the stepped cantilever beam are determined. Also, the results of the presented approach will be compared with the results from [5], where the tapered cantilever beam of a rectangular cross section, constant thickness and linearly tapered width is analysed.

2. A RIGID MULTIBODY MODEL OF A TAPERED CANTILEVER BEAM

Let us consider free vibration of the flexible tapered cantilever beam with the length L, where its end A is clamped, and the end B is free, as shown in Fig. 1. The beam thickness h is constant, whereas its width changes linearly along the beam, starting from b_A in the clamped end of the beam, up to b_B at the free end:

$$f_b(x) = \frac{b_B - b_A}{L} x + b_A,\ 0 \le x < L, \quad (1)$$

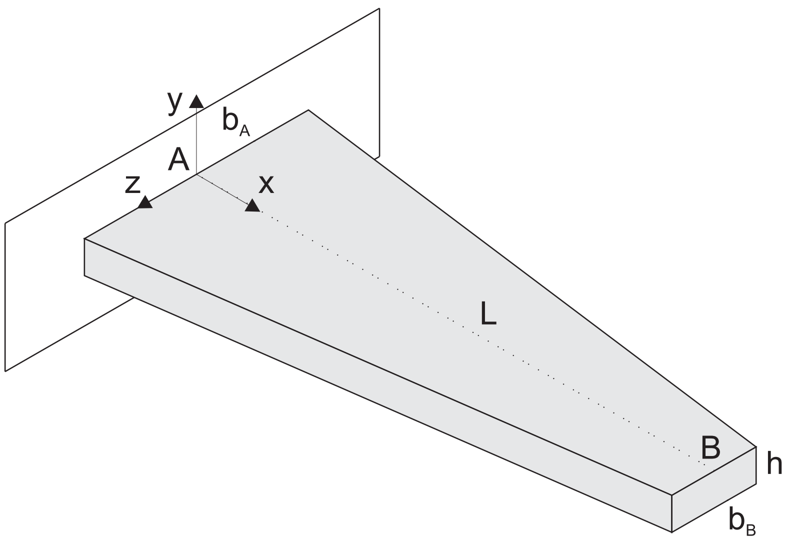

Figure 1: Tapered cantilever beam

*Corresponding author: Dositejeva 19 (Serbia), nikolic.a@mfkv.kg.ac.rs

A rigid multibody model of the tapered cantilever beam will be created in two steps. In the first step, the exact shape of the cantilever beam is approximated with *n* flexible segments of constant width. In the second step, each n flexible segment is divided into *k* equal flexible segments. In further text, the division in the first step will be called primary division, and the division in the second step will be called secondary division. Primary division should approximate the exact shape of the cantilever beam in the best way, and secondary division should additionally increase accuracy.

The parameters which define each of the obtained segments are:

-the modulus of elasticity of the material *E*,

-the shear modulus of the material:

$$G = \frac{E}{2(1+\mu)}, \tag{2}$$

-the Poisson coefficient μ,

-the density of the material ρ,

-the length of the segment after primary division:

$$L_i = \frac{L}{n}, i = 1,\dots,n, \tag{3}$$

-the width of the segment after primary division:

$$b_i = \begin{cases} f_b(\frac{L_1}{2}),\ i=1, \\ f_b(\sum_{k=1}^{i-1} L_k + \frac{L_i}{2}),\ 1 < i \le n, \end{cases} \tag{4}$$

-the area of the cross section of the segment after primary division A_i,

-the axial moment of inertia for the principal axis z of the cross section of the beam after primary division I_{zi},

The approximative shape of the tapered beam after primary and secondary divisions is shown in Fig. 2 by dashed lines.

2.1. Our approach

Each of $n{\cdot}k$ flexible segments is divided into three rigid segments, where the first and second rigid segments are interconnected through a prismatic joint, and the second and third segments through a revolute joint (see Fig. 3a).

The springs of corresponding stiffness are placed in the joints. The approximative model of the flexible tapered cantilever beam is thus obtained in the form of an opened kinematic chain without branching made of $2n{\cdot}k$ rigid segments connected through the corresponding joints and springs in them (see Fig. 4). Let us determine the parameters of the observed mechanical system which are necessary for further considerations.

The stiffness of springs in the joints of the *i*-th segment based on [7], for the case of bending of the beam in one plane, are:

$$c_r = k^3 \frac{12E \cdot I_{zi}}{L_i^3},\ c_s = k\frac{EI_{zi}}{L_i}, \tag{5}$$

where the indices *r* and *s* are:

$$\begin{aligned} r &= 2j - 1 + 2k(i-1), \\ s &= 2j + 2k(i-1),\ i = \overline{1,n},\ j = \overline{1,k}, \end{aligned} \tag{6}$$

The length of the rigid segments is:

$$l_r = \frac{l_i'}{2}, \tag{7}$$

$$l_s = \begin{cases} \frac{3}{2} l_i',\ j < k, \\ l_i' + l_i'',\ j = k \wedge i < n, \\ l_i',\ j = k \wedge i = n, \end{cases} \tag{8}$$

where

$$l_i' = \frac{L_i}{2k},\ l_i'' = \frac{L_{i+1}}{4k}, \tag{9}$$

The mass of the rigid segments is:

$$m_r = \rho A_i l_r,$$

$$m_s = \begin{cases} \rho\left(A_i l_i' + A_{i+1} l_i''\right),\ j = k \wedge i < n, \\ \rho A_i l_s, \end{cases} \tag{10}$$

The position of the centre of mass of each rigid segment is defined by the local position vector of the centre of mass in relation to the beginning of the segment:

$$\boldsymbol{\rho}_{c_u} = \begin{bmatrix} \xi_{c_u} & \eta_{c_u} & \zeta_{c_u} \end{bmatrix}^T, \tag{11}$$

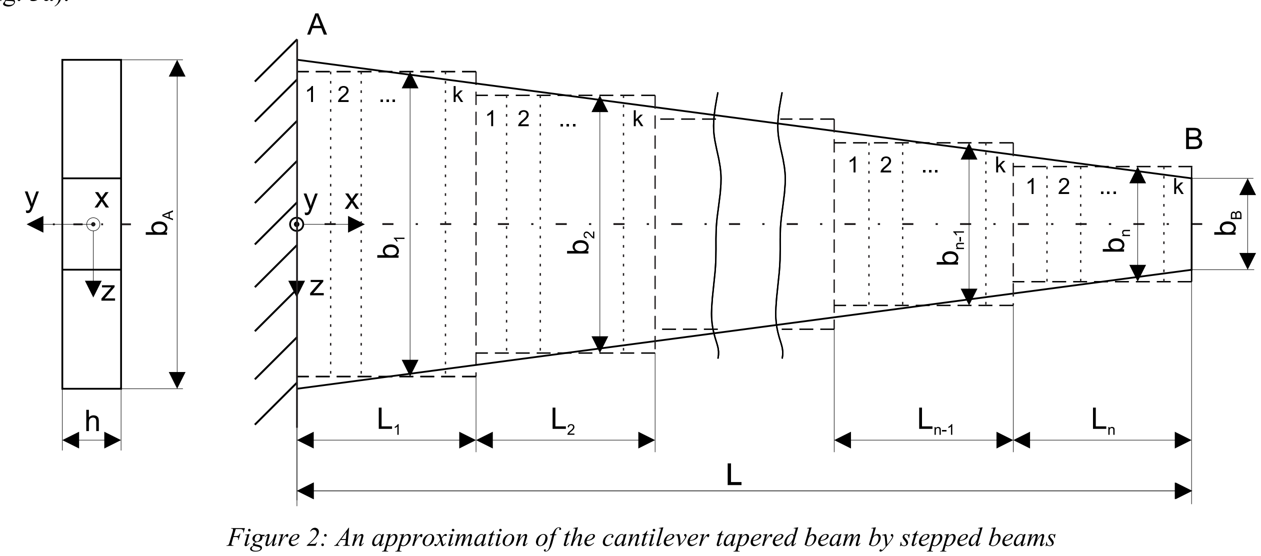

Figure 2: An approximation of the cantilever tapered beam by stepped beams

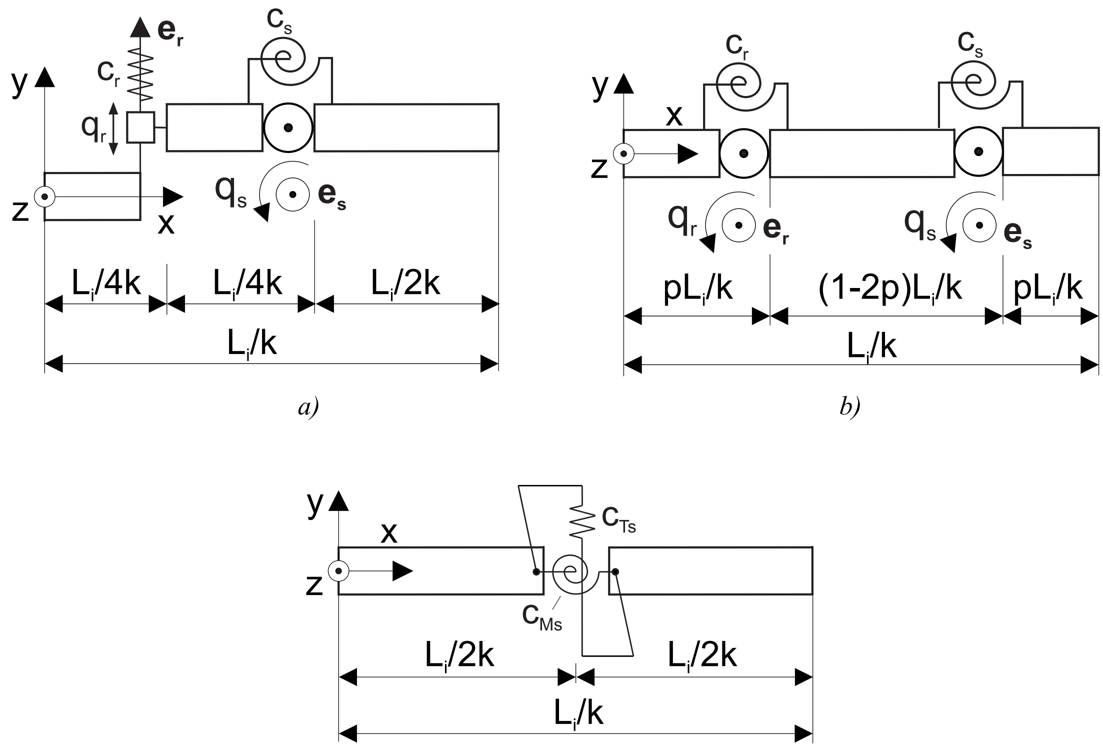

c)

Figure 3: The rigid multibody model of the i-th flexible beam segment: a) Presented approach, b) Ref. [1], c) Ref. [2], [3]

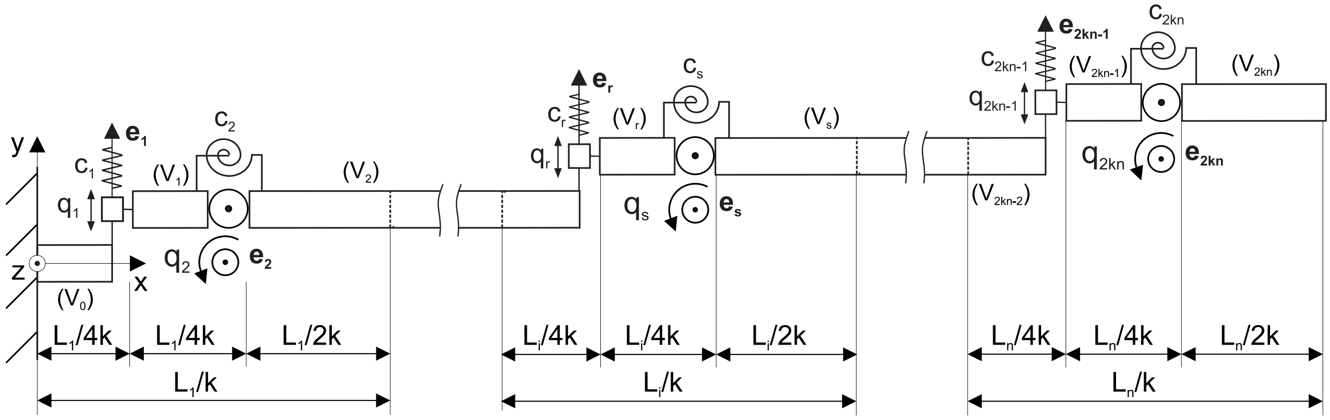

Figure 4: The rigid multibody model of the flexible beam

where

$$\xi_{c_r} = 0.5 \cdot l_r,$$

$$\xi_{c_s} = \begin{cases} \dfrac{0.5 A_i l_i'^2 + A_{i+1} l_i'' \left(l_i' + 0.5 \cdot l_i'' \right)}{A_i \cdot l_i' + A_{i+1} l_i''}, \; j = k \wedge i < n, \\ 0.5 \cdot l_s, \end{cases}$$

$$\eta_{c_u} = 0, \; \zeta_{c_u} = 0, \; u = \overline{1,2kn}, \tag{12}$$

The local vectors of the rigid segments are:

$$\boldsymbol{\rho}_u = \begin{bmatrix} l_u & 0 & 0 \end{bmatrix}^T, u = \overline{1,2kn}, \tag{13}$$

The moment of inertia of the rigid segment in relation to the axis ζ perpendicular to the plane of rotation is:

$$J_{c_r \zeta} = \frac{m_r}{12}\left(a_r^2 + l_r^2 \right),$$

$$J_{c_s \zeta} = \begin{cases} \rho A_i l_i' \left(\dfrac{1}{12}\left(a_i^2 + l_i'^2 \right) + \left(\xi_{c_s} - \dfrac{l_i'}{2} \right)^2 \right) \\ + \rho A_{i+1} l_i'' \left(\dfrac{1}{12}\left(a_{i+1}^2 + l_i''^2 \right) + \left(l_i' + \dfrac{l_i''}{2} - \xi_{c_s} \right)^2 \right), \\ j = k \wedge i < n, \\ \dfrac{m_s}{12}\left(a_i^2 + l_r^2 \right), \end{cases} \tag{14}$$

where:

$$\mathbf{a}_i = \begin{cases} h, \text{ if the cross section is rectangular ,} \\ \frac{\sqrt{3}}{2} d_i, \text{ if the cross section is circular ,} \end{cases} \quad (15)$$

The unit vectors of the axis of the u-th joint are:

$$\mathbf{e}_u = \begin{cases} \begin{bmatrix} 0 & 1 & 0 \end{bmatrix}^T, \text{ if the } u\text{-th joint is prizmatic,} \\ \begin{bmatrix} 0 & 0 & 1 \end{bmatrix}^T, \text{ if the } u\text{-th joint is revolute,} \end{cases} \quad (16)$$

where $u = \overline{1, 2kn}$.

The coefficients χ_u and $\bar{\chi}_u$ represent identifiers of the joint type, where it holds that:

$$\chi_u = \begin{cases} 1, \text{ if the } u\text{-th joint is prismatic,} \\ 0, \text{ if the } u\text{-th joint is revolute,} \end{cases} \quad (17)$$

as well as that $\bar{\chi}_u = 1 - \chi_u$

2.2. Approach from [1]

Each of $n{\cdot}k$ flexible segments is divided into three rigid segments, where the first and second rigid segments, as well as the third and fourth ones, are interconnected with a revolute joint (see Fig. 3b). The springs of the corresponding rigidity are placed in those joints. Similarly to our approach, the approximative model of the flexible tapered cantilever beam in the form of an open kinematic chain without branching made of $2n{\cdot}k$ rigid segments connected with the corresponding joints and springs in them is obtained. Let us determine the parameters of the observed mechanical system which are necessary for further considerations.

The stiffnesses of springs in the joints of the i-th segment based on [1] are:

$$c_r = c_s = 2k\frac{EI_{zi}}{L_i}, \; i = \overline{1,n}, \quad (18)$$

where the indices r and s are defined in the expression (6).
The length of the rigid segments is:

$$l_r = \frac{1-2p}{p} l_i', \quad (19)$$

$$l_s = \begin{cases} 2l_i', j < k, \\ l_i' + l_i'', j = k \wedge i < n, \\ l_i', \; j = k \wedge i = n, \end{cases} \quad (20)$$

where

$$l_i' = p\frac{L_i}{k}, \; l_i'' = p\frac{L_{i+1}}{k}, \quad (21)$$

and where $p = \frac{1}{2}\left(1 - \frac{1}{\sqrt{3}}\right)$ is the coefficient of division of the beam. Reference [1] shows that, especially for this value of the coefficient, the assumed model of the beam is reduced to a simpler shape which contains springs only in the joints (see Fig. 3b). In an opposite case, the model of the beam also contains a spring which connects the first and third rigid bodies, and then the process of modelling the flexible beam by this method becomes considerably complicated.

The local position vector of the centre of mass of rigid segments $\boldsymbol{\rho}_{c_u}$, the mass of the rigid segments m_u and the moment of inertia of the rigid segment in relation to the axis ζ $J_{c_u\zeta}$ $(u = \overline{1, 2k \cdot n})$ may be defined from the expressions (10)-(14), where l_i' i l_i'' are given in the expression (21).
The unit vectors of the axis of the u-th joint are:

$$\mathbf{e}_u = \begin{bmatrix} 0 & 0 & 1 \end{bmatrix}^T. \quad (22)$$

All joints in the kinematic chain are revolute, so that:

$$\bar{\chi}_u = 1, \; u = \overline{1, 2n \cdot k} \quad (23)$$

2.3. Approach from [2], [3]

References [2] and [3] propose discretization of each of $n{\cdot}k$ flexible segments so that they are divided into two equal rigid segments which are interconnected by one cylindrical spring and one revolute spring with the corresponding rigidity (see Fig. 3c). This division results in an open kinematic chain without branching made of $n{\cdot}k$ rigid segments connected by the corresponding springs.
The stiffnesses of springs in the joints of the u-th segment based on [2] and [3] are:

$$c_{T_s} = k\frac{GA_i}{L_i}, \; c_{M_s} = \frac{EI_{zi}}{L_i}, \quad (24)$$

where the index s is:

$$s = j + k(i-1), \; i = \overline{1,n}, \; j = \overline{1,k}, \quad (25)$$

The length of the rigid segments is:

$$l_s = \begin{cases} 2l_i', j < k, \\ l_i' + l_i'', j = k \wedge i < n, \\ l_i', \; j = k \wedge i = n, \end{cases} \quad (26)$$

where

$$l_i' = \frac{L_i}{2k}, \; l_i'' = \frac{L_{i+1}}{2k}, \quad (27)$$

The local position vector of the centre of mass of the rigid segments $\boldsymbol{\rho}_{c_u}$, the local vectors of the rigid segments $\boldsymbol{\rho}_u$, the mass of the rigid segments m_u and the moment of inertia of the rigid segment of constant width in relation to the axis ζ $J_{c_u\zeta}$ $(u = \overline{1, 2k \cdot n})$ may be determined from the expressions (10)-(14), where l_i', l_i'' i l_s are given in (26) and (27).

3. EIGENVALUE PROBLEM

Reference [1] and our approach use relative coordinates for description of the system, whereas [2] and [3] use absolute coordinates. That is the reason why the formation of differential equations of motion will be presented for the cases of using relative coordinates (for our approach and the approach in [1]) and absolute coordinates (for the approaches in [2] and [3]).

3.1. Relative coordinates

The potential energy of the system of springs in the joints reads:

$$\Pi_c = \frac{1}{2}\sum_{u=1}^{2kn} c_u q_u^2, \tag{28}$$

where q_u (u=1,…,2kn) are relative joint displacements.
The kinetic energy of the system is

$$T = \frac{1}{2}\sum_{\alpha=1}^{2kn}\sum_{\beta=1}^{2kn} m_{\alpha\beta}(\mathbf{q})\dot{q}_\alpha \dot{q}_\beta, \tag{29}$$

where an overdot denotes the derivative with respect to time, $\mathbf{q}=[q_1,q_2,\ldots,q_{2kn}]^T$ is the vector of generalized coordinates and

$$m_{\alpha\beta}(\mathbf{q}) = \sum_{u=\beta}^{2kn}\left(m_u \frac{\partial \mathbf{r}_{c_u}}{\partial q_\alpha}^T \frac{\partial \mathbf{r}_{c_u}}{\partial q_\beta} + \bar{\chi}_\alpha \bar{\chi}_\beta J_{C_u\zeta} \mathbf{e}_\alpha{}^T \mathbf{e}_\beta \right), \tag{30}$$

the metric tensor coefficient of the inertia matrix of the system. For more details see [9].

In Equation (30), m_u is the mass of the u-th rigid segment in the chain, $J_{C_u\zeta}$ is its axial moment of inertia relative to the principal axis which is perpendicular to the plane of beam bending, $\mathbf{r}_{cu}$ is the vector of position of the centre of masses of the rigid body (V_u) in relation to the inertial frame $Axyz$. The configuration $\mathbf{q}_0=[q_1=0,\ldots,q_{2kn}=0]^T$ in which $\dot{q}_u(t)\equiv 0,\ \ddot{q}_u(t)\equiv 0$ (u=1,...,2kn) corresponds to the equilibrium position of the flexible beam shown in Fig. 4 in the absence of gravity and force at the free end of the beam B. Linearized differential equations of motion of the considered system of rigid bodies in the surroundings of the equilibrium position read (see [8]):

$$\mathbf{M}\ddot{\mathbf{q}} + \mathbf{K}\mathbf{q} = \mathbf{0}_{2n\times 1}, \tag{31}$$

where $\mathbf{0}_{2n\ 1}\in \mathrm{R}^{2kn\times 1}$, $\mathbf{K} = diag(c_1,\ldots,c_{2kn})$ is the stiffness matrix, and $\mathbf{M}\in \mathrm{R}^{2kn\times 2kn}$ is the mass matrix, whose members are:

$$m_{\alpha\beta}(\mathbf{q}_0) = \sum_{u=\beta}^{2kn} m_i \left(\frac{\partial \mathbf{r}_{c_u}}{\partial q_\alpha}\right)_{\mathbf{q}_0}^T \left(\frac{\partial \mathbf{r}_{c_u}}{\partial q_\beta}\right)_{\mathbf{q}_0} + \sum_{u=\beta}^{2kn} \bar{\chi}_\alpha \bar{\chi}_\beta J_{C_u\zeta} \mathbf{e}_\alpha(\mathbf{q}_0)^T \mathbf{e}_\beta(\mathbf{q}_0),\ (\alpha,\beta=\overline{1,2kn}), \tag{32}$$

The partial derivative of the position vector $\mathbf{r}_{cu}$ relative to generalized coordinate q_α at the position $\mathbf{q}_0$ reads:

$$\left(\frac{\partial \mathbf{r}_{c_u}}{\partial q_\alpha}\right)_{\mathbf{q}_0} = \begin{cases} \bar{\chi}_\alpha \mathbf{e}_\alpha(\mathbf{q}_0)\times\left(\sum_{k=\alpha+1}^{u} \boldsymbol{\rho}_{k-1}(\mathbf{q}_0) + \boldsymbol{\rho}_{C_u}(\mathbf{q}_0)\right) \\ +\chi_\alpha \mathbf{e}_\alpha(\mathbf{q}_0), \quad \alpha<u, \\ \bar{\chi}_\alpha \mathbf{e}_\alpha(\mathbf{q}_0)\times \boldsymbol{\rho}_{C_u}(\mathbf{q}_0) + \chi_\alpha \mathbf{e}_\alpha(\mathbf{q}_0), \quad \alpha=u, \\ \mathbf{0}, \quad \alpha>u \end{cases} \tag{33}$$

3.2. Absolute coordinates

The potential energy of the system of springs in the joints reads:

$$\Pi_c = \frac{1}{2}\sum_{v=1}^{kn}\left(c_{M_v}\Delta\varphi_v^2 + c_{T_v}\Delta y_v^2\right), \tag{34}$$

where $\Delta\varphi_v$ and Δy_v are relative joint displacements which, expressed as a function of absolute coordinates, read:

$$\Delta\varphi_v = \varphi_v - \varphi_{v-1}, \tag{35}$$

$$\Delta y_v = y_v - zl_v\varphi_v - y_{v-1} - zr_{v-1}\varphi_{v-1},\ \varphi_0 = 0,\ y_0 = 0. \tag{36}$$

$$zl_v = \xi_{c_v},\ zr_v = l_v - \xi_{c_v}, \tag{37}$$

The absolute coordinates y_v and φ_v represent transverse displacements of the centres of masses and rotation about that centres of the v-th rigid segment in relation to the horizontal position, respectively. Axial displacements of the centres of masses of the v-th rigid segment are neglected because of the assumption of small deformations of the beam.
The kinetic energy of the system is

$$T = \frac{1}{2}\sum_{v=1}^{kn}\left(m_v \dot{y}_v{}^2 + J_{c_v\zeta}\dot{\varphi}_v{}^2\right), \tag{38}$$

where an overdot denotes the derivative with respect to time. By applying the Lagrange equations of the second kind for the case of conservative systems,

$$\frac{d}{dt}\left(\frac{\partial L}{\partial \dot{y}_v}\right) - \frac{\partial L}{\partial y_v} = 0,$$
$$\frac{d}{dt}\left(\frac{\partial L}{\partial \dot{\varphi}_v}\right) - \frac{\partial L}{\partial \varphi_v} = 0, \tag{39}$$

where $v=\overline{1,k\cdot n}$, and $L = T - \Pi$ is the Lagrange function, differential equations of motion of the mechanical system are obtained in the form:

$$\mathbf{M}\ddot{\mathbf{z}} + \mathbf{K}\mathbf{z} = \mathbf{0}_{2kn\times 1}, \tag{40}$$

where $\mathbf{0}_{2kn\ 1}\in \mathrm{R}^{2kn\times 1}$, $\mathbf{z}=[\mathbf{z}_1,\ \mathbf{z}_2,\ldots,\mathbf{z}_{kn}]^\mathrm{T}$ is the vector of absolute coordinates, and it holds that $\mathbf{z}_v=[y_v,\ \varphi_v]^\mathrm{T}$ (v=1,…,kn).
The mass matrix is:

$$\mathbf{M} = diag(\mathbf{M}_{1,1},\ \mathbf{M}_{2,2},\ldots,\mathbf{M}_{kn,kn}), \tag{41}$$

where:

$$\mathbf{M}_{v,v} = diag\left(m_v, J_{c_v\zeta}\right), \tag{42}$$

The stiffness matrix is:

$$\mathbf{K} = \begin{bmatrix} \mathbf{K}_{1,1} & .. & 0 & 0 & 0 & .. & 0 \\ .. & .. & \vdots & \vdots & \vdots & \vdots & \vdots \\ 0 & .. & \mathbf{K}_{v-1,v-1} & \mathbf{K}_{v-1,v} & 0 & .. & 0 \\ 0 & .. & \mathbf{K}_{v,v-1} & \mathbf{K}_{v,v} & \mathbf{K}_{v,v+1} & .. & 0 \\ 0 & .. & 0 & \mathbf{K}_{v+1,v} & \mathbf{K}_{v+1,v+1} & .. & 0 \\ \vdots & :: & \vdots & \vdots & \vdots & :: & \vdots \\ 0 & .. & 0 & 0 & 0 & .. & \mathbf{K}_{kn,kn} \end{bmatrix}, \tag{43}$$

where:

$$\mathbf{K}_{v,v-1} = \begin{bmatrix} -c_{T_{v-1}} & -c_{T_{v-1}} zr_{v-1} \\ c_{T_{v-1}} zl_{v-1} & -c_{M_v} + c_{T_{v-1}} zr_{v-1} zl_v \end{bmatrix}, \tag{44}$$

$$\mathbf{K}_{v,v} = \begin{bmatrix} c_{T_{v-1}} + c_{T_v} & c_{T_{v-1}} zl_v + c_{T_v} zr_v \\ -c_{T_{v-1}} zl_v + c_{T_v} zr_v & \begin{matrix} c_{M_{v-1}} + c_{M_v} \\ +c_{T_{v-1}} zl_v{}^2 + c_{T_v} zr_v{}^2 \end{matrix} \end{bmatrix}, \tag{45}$$

$$\mathbf{K}_{v,v+1} = \begin{bmatrix} -c_{T_v} & c_{T_v} zl_{v+1} \\ -c_{T_v} zr_v & -c_{M_v} + c_{T_v} zl_{v+1} zr_v \end{bmatrix}, \tag{46}$$

For more details, see [2] or [3].

Finally, the eigenvalue problem, formulated on the basis of (31) and (40), reads:

$$\left(\mathbf{K}-\omega^2\mathbf{M}\right)\mathbf{v}=\mathbf{0}_{2kn\times 1}, \tag{47}$$

where ω is the natural frequency of free vibration of the flexible tapered cantilever beam, and $\mathbf{v}\in R^{2kn\;1}$ represents the eigenvector which corresponds to the given frequency. Approximate values of natural frequencies of the considered cantilever beam are obtained by solving the eigenvalue problem (47).

4. NUMERICAL EXAMPLE AND VERIFICATION OF THE METHOD

Verification of the efficiency of the presented method will be performed through two examples. The first example will treat the problem of determination of natural frequencies of the flexible cantilever beam with three stepped changes of the circular cross section. Thus, primary division is carried out in advance, so that *n*=4, and the influence of secondary divisions of the beam on the accuracy of our method will be analyzed. Exact values of natural frequencies of such a beam are determined in [4], so it is a good example for comparing the accuracy of the proposed approach with the relevant approaches presented in [1] and [2]. The second example analyzes the tapered cantilever beam of a rectangular cross section, constant thickness and linearly variable width. The influence of primary division on the accuracy of our method will be analyzed in this example. The results achieved by using our approach will be compared with the results from [5].

4.1. Example 1

Let us observe the flexible cantilever beam with three stepped changes of the circular cross section with the following characteristics:

- Young’s modulus: $E=2.068\times10^{11}\ N/m^2$,
- mass density: $\rho=7850\ kg/m^3$,
- total length: $L=2.0\ m$,
- diameter: $d_1=0.03\,m$,
- diameters ratio: $d_2/d_1=0.8$ $d_3/d_1=0.65$, $d_4/d_1=0.25$,
- length of the segments: $L_1=0.25L$, $L_2=0.3L$, $L_3=0.25L$, $L_4=0.2L$,
- area of the cross section of the segment after primary division of the beam:
  $$A_u=\frac{\pi d_u^2}{4},$$
- axial moment of inertia for the principal axis z of the cross section of the beam:
  $$I_{zu}=\frac{\pi d_u^4}{64},$$

In further considerations, for convenience of comparisons with the results from paper [4], the non-dimensional frequency coefficients $\beta L=\sqrt[4]{\omega^2\rho A_1 L^4/(EI_{1z})}$ are used. Using the above theory, the approximative numerical values of the first three non-dimensional frequency coefficients are obtained. These frequency coefficients along with the corresponding relative errors are shown in Table 1. The errors are calculated as:

$$\frac{approximative\ \ value}{exact\ \ value}\cdot 100-100[\%].$$

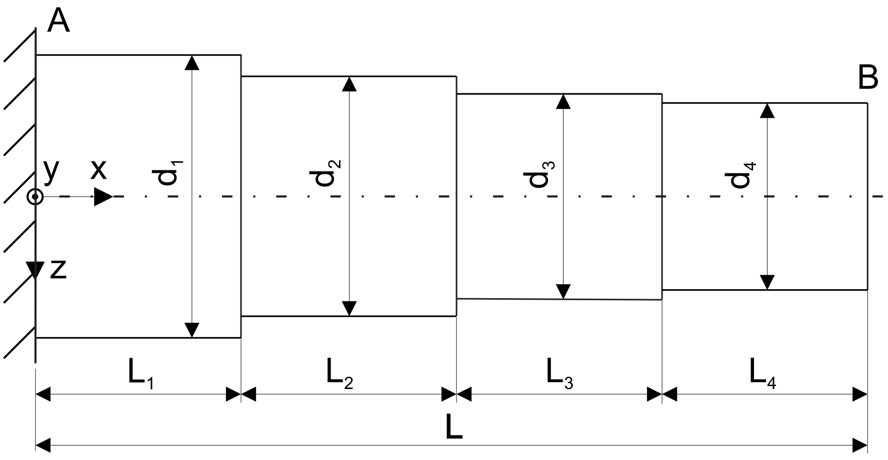

Figure 5: The three-stepped cantilever beam

Table 1 gives the comparative results obtained by using all three presented methods of discretization depending on the number of secondary divisions of each segment of the beam. It also shows relative errors of the obtained values of frequencies in relation to the exact values of frequencies from [4]. It can be noticed that the values of obtained frequencies, at the increased number of secondary divisions of beam segments, converge faster toward the exact values if our approach is used, exept for the third frequency where the approach from [2] is slightly better. Besides, the relative error in determination of the first frequency with one division of the beam segment is 0.059 %, i.e. the error is far smaller than 1%. This fact is particularly important if it is taken into account that the values of the first frequency are of most significance in studying dynamic characteristics of various technical objects.

4.2. Example 2

Let the tapered cantilever beam of constant thickness and linearly tapered width be given (see Fig. 1). The material of the beam is the same as in the previous example. The beam length is $L = 0.5\ m$, and the thickness is $h = 0.005\ m$.

The area of the cross section of the segment after primary division of the beam is:

$$A_u = b_u h,$$

The axial moment of inertia for the principal axis z of the cross section of the beam is:

$$I_{zu} = \frac{b_u h^3}{12},$$

The beam width at the beginning and the end of the beam will be varied in order to obtain necessary relations of these dimensions for the needs of comparison of results. That is why the parameter related to the degree of beam tapering is introduced:

$$c = 1 - \frac{b_B}{b_A}, \tag{48}$$

Let us also introduce the concept of the *i*-th non-dimensional frequency $\bar{\omega}_i$, which is connected with the *i*-th frequency $\omega_i\left(rad/s\right)$ in the following way:

$$\bar{\omega}_i = \sqrt{\frac{\rho A_1 L^4}{E \cdot I_{zi}}} \cdot \omega_i, \tag{49}$$

Table 2 gives the values of the first three non-dimensional frequencies, where the value of the parameter *c* changes from 0 to 1, with the step 0.1, and for *n*=10 and *n*=20, respectively. It can be noticed that there is very good agreement between our results and the results from [5]. It is obvious that the convergence of frequency toward the values from [5] is faster at smaller values of the parameter *c*, i.e. when the beam is less tapered (see Fig. 6 and Fig. 7). In that case it is enough for the number of segments of constant width (primary divisions) to be n=10, and to achieve the satisfactory accuracy.

Table 1: Natural frequencies of the cantilever beam – comparison of the present paper results and the results from [4]

Number of divisions	Non-dimensional frequency coefficients								
	$\beta_1 L$			$\beta_2 L$			$\beta_3 L$		
	Relative error [%]			Relative error [%]			Relative error [%]		
	Our appr.	Appr. from ref. [1]	Appr. from ref. [2]	Our appr.	Appr. from ref. [1]	Appr. from ref. [2]	Our appr.	Appr. from ref. [1]	Appr. from ref. [2]
1	2.51159	2.51000	2.56814	4.31315	4.43415	4.87846	5.47403	5.79999	6.10351
	0.059	-0.004	2.312	-2.975	-0.254	9.741	-5.938	-0.337	4.878
2	2.51200	2.49390	2.52396	4.43100	4.43826	4.53171	5.74267	5.77220	5.86927
	0.076	-0.645	0.552	-0.324	-0.161	1.941	-1.322	-0.815	0.853
3	2.51114	2.49524	2.51612	4.44160	4.43855	4.48271	5.78781	5.77304	5.84107
	0.042	-0.592	0.240	-0.086	-0.155	0.839	-0.546	-0.800	0.369
5	2.51051	2.49909	2.51213	4.44470	4.44009	4.45832	5.80856	5.78317	5.82606
	0.016	-0.439	0.081	-0.016	-0.120	0.290	-0.190	-0.626	0.111
7	2.51030	2.50156	2.51104	4.44514	4.44120	4.45167	5.81386	5.79064	5.82184
	0.008	-0.340	0.037	-0.006	-0.095	0.141	-0.099	-0.498	0.038
10	2.51018	2.50375	2.51046	4.44527	4.44222	4.44815	5.81658	5.79763	5.81958
	0.003	-0.253	0.014	-0.003	-0.072	0.061	-0.052	-0.378	-0.001
Exact solution [4]	2.5101			4.44542			5.81961		

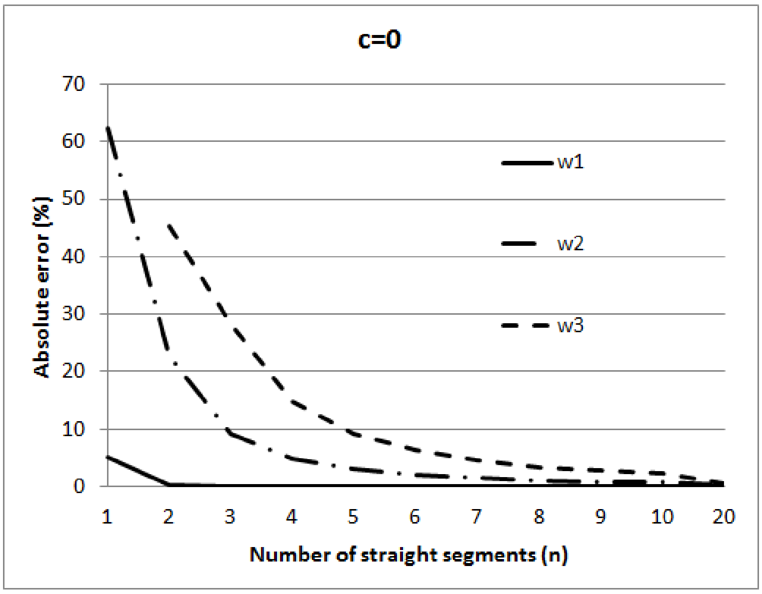

Figure 6. Absolute error of natural frequency of: straight beam (c=0) in comparison with [5]

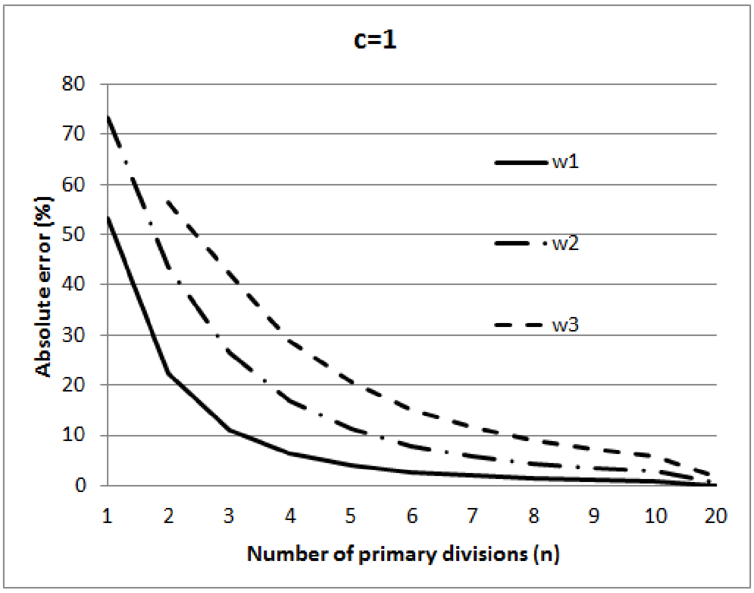

Figure 7. Absolute error of natural frequency of: maximum tapered beam (c=1), in comparison with [5]

Table 2: Natural frequencies of the cantilever beam – comparison of the present paper results and the results from [5]

c	Non-dimensional frequencies								
	$\bar{\omega}_1$			$\bar{\omega}_2$			$\bar{\omega}_3$		
	Our results		Ref. [5]	Our results		Ref. [5]	Our results		Ref. [5]
	n=10	n=20		n=10	n=20		n=10	n=20	
0	3.5169	3.5162	3.5160	21.8890	21.9984	22.035	60.3636	61.3642	61.6970
0.1	3.6307	3.6309	3.6310	22.0992	22.2156	22.254	60.5474	61.5696	61.9100
0.2	3.7612	3.7624	3.7629	22.3361	22.4607	22.502	60.7573	61.8044	62.1530
0.3	3.9125	3.9152	3.9160	22.6073	22.7417	22.786	61.0019	62.0784	62.436
0.4	4.0913	4.0956	4.0970	22.9240	23.0704	24.021	61.2942	62.4068	62.776
0.5	4.3067	4.3130	4.3152	23.3039	23.4659	23.519	61.6556	62.8145	63.199
0.6	4.5728	4.5822	4.5853	23.7773	23.9606	24.021	62.1238	63.3458	63.751
0.7	4.9134	4.9271	4.9317	24.4012	24.6162	24.687	62.7728	64.0892	64.527
0.8	5.3703	5.3907	5.3976	25.2983	25.5668	25.656	63.7744	65.2537	65.747
0.9	6.0272	6.0595	6.0704	26.7946	27.1727	27.299	65.6527	67.4945	68.115
1	7.0805	7.1374	7.1422	30.1108	30.8063	30.970	71.1455	74.3753	75.653

5. CONCLUSION

This paper presents a new method of approximative determination of frequency of the tapered cantilever beam which can serve as an alternative to relevant approaches from [1], [2] and [3]. In such discretization of the flexible tapered cantilever beam, a well-developed methodology for mechanics of a system of rigid bodies is used for the formation of the characteristic problem. It results in obtaining a computer-efficient algorithm for determination of approximate values of frequencies of the beam. Comparison of our method with the results from relevant approaches in [1], [2] and [3] was carried out on the example from paper [4]. It was shown that the relative errors of obtained frequencies in relation to the exact values given in paper [4] are smaller for first two frequencies if our approach is used than if the approaches from [1], [2] and [3] are used. For the third frequency approach from [2] give slightly better results. Then the results of our approach are compared with the results from [5]. In [5], the *Initial value method* was used for analysis of free vibration of the beam, where the *Runge-Kutta method* of numerical integration was used for determination of frequencies. That is why this algorithm is demanding in terms of computing. It was shown that the results obtained by using our approach agree to a considerable extent with the results from [5].

Based on everything previously stated, it is clear that the presented method is less demanding in terms of computing than the algorithm presented in [5], and it achieves better results than the relevant algorithms from [1], [2] and [3] for first two natural frequencies. The presented methodology can also be used for treating more complex models of flexible beams, frames, etc.

However, the question remains how the position of the prismatic joint in the rigid multibody model of the tapered cantilever beam affects the accuracy of the exposed algorithm. We assume that prismatic joint is placed in the middle of the first half of the beam. In [1] the authors have shown for which partition coefficient *p* algorithm achieved the best accuracy and simple approximate model of the beam. This analysis will be the subject of further research by authors.

ACKNOWLEDGEMENTS

This research was supported under grants no. ON174016 and no. TR35006 by the Ministry of Education, Science and Technological Development of the Republic of Serbia. This support is gratefully acknowledged.

REFERENCES

[1] Schiehlen WO, Rauh J, “Modeling of flexible multibeam systems by rigid-elastic superelements”, Rev Bras Cienc Mec 8(2):151–163, (1986)

[2] Z.A. Parszewski, J.M.Krodkiewski, J. Skoraczynski, “RIGID FEM INA CASE HISTORY OF BOILER FEED PUMP VIBRATION”, Computers&Structures, Vol. 31, No.1, pp.103-110, (1989)

[3] J.M.Krodkiewski, “MECHANICAL VIBRATION”, THE UNIVERSITY OF MELBOURNE, Department of Mechanical and Manufacturing Engineering, (2008)

[4] S. Naguleswaran, “Vibration of an Euler–Bernoulli Beam on Elastic End Supports and with up to Three Step Changes in Cross-Section”, *International Journal of Mechanical Sciences*, **44**, pp. 2541-2555, (2002)

[5] C.Y. Wang, “Vibration of a tapered cantilever of constant thickness and linearly tapered width”, Arch. Appl. Mech. Vol. 83, pp. 171-176, (2013)

[6] S. Šalinić, “Modeling of a light elastic beam by a system of rigid bodies”, Theoret. Appl. Mech., Vol. 31, No. 3-4, pp. 395-410, (2004)

[7] S. Šalinić, A. Nikolić, “On the determination of natural frequencies of a cantilever beam in free bending vibration: a rigid multibody approach”, Forsch Ingenieurwes, Vol.77: pp.95–104, (2013)

[8] L. Meirovitch, “Fundamentals of vibrations”, McGraw-Hill, New York (2001)

[9] V. Čović, M. Lazarević, “Mechanics of robots” Faculty of Mechanical Engineering, University of Belgrade (in Serbian) (2009)

An Analysis of The End Deflections of Spatial Trusses with Rigidity Variable in Intervals

Milica Todorovic [1*], Milan Dedic [2]
[1]School of Mechanical Engineering of Applied Study, Trstenik (Serbia)
[2]Faculty of Mechanical and Civil Engineering in Kraljevo, Kraljevo (Serbia)

Method of continuum modelling based on replacing a truss structure by corresponding bulk cross-section beam can be used in deformation analysis of truss structures. In this paper equivalent bending and equivalent shearing rigidities are calculated by means of geometry and material characteristics of a truss. Cantilever beam-like trusses with rectangular and triangular cross-sections are analysed by that method in order to calculate the equivalent rigidities and flexion displacement due to a concentrated force. The results obtained are analysed in numerical examples for different filling angles and overall truss length.

Keywords: spatial trusses, continuum modeling, variable cross-section, deflection

1. INTRODUCTION

Truss beams are widely used in civil engineering - bridges, roofing and in many transport machines and cranes. Truss structures are used in the mentioned cases due to their high specific load carrying capacity.

For the sake of using standardized structural elements trusses with paralel longitudinal bars, constant cross-section and repeating filling pattern are frequently used.

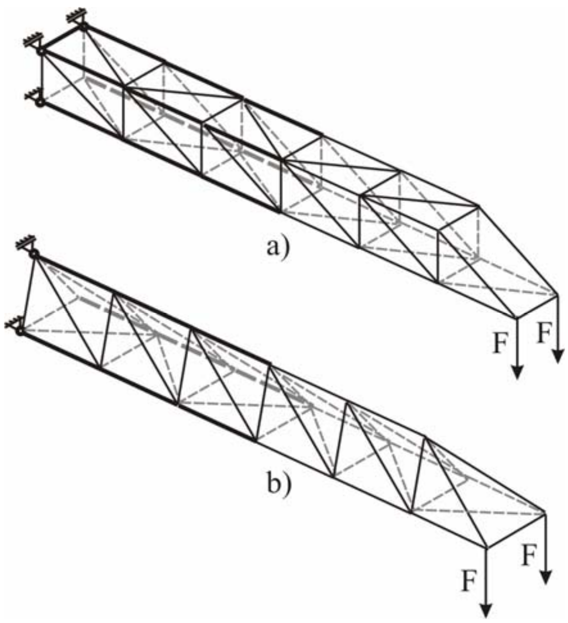

Figure 1: Truss beams with variable cross- section

Deformation and stress analysis of a truss with uniform filling bars can be performed by means of FE method software, but it can be also performed using continuum modelling in which a given truss is replaced by a beam with bulk cross-section. [1,2,3,4,5]. That way we can establish relations between geometry and material characteristics of the truss beam and its equivalent beam with bulk cross-section. Parameters of the equivalent continuum beam, ie. equivalent bending and equivalent shearing rigities, are calculated for every type of a given truss beam according to a given load, geometry data and type of filling [6,7,8, 9, 10].

Advantages of this method come to light during preparatory phase of design when defining of overall dimensions and design parameters are more important than dealing with specific design details. More over this approach, unlike purely numerical solution methods, brings a clear insight in influence of different structural parameters (number of cells, bar cross-section areas, slope of diagonal filling bars, etc.), [6,9].

This paper presents a procedure for calculating free end deflexions of cantilever beam trusses with rectangular and triangular cross-sectionx and with different bars in two spans along length loaded with concentrated forces at their free end (Fig. 1). A case of constant height of cells and constant filling angle is considered. The spans differ solely in cross-section areas of belonging bars.

Cost evaluation of trusses clearly shows that a gross component in the total is the material cost. This fact justifies effort to minimize the truss weight, and the truss with different rigidities in intervals is intended to achieve right that.

2. CALCULATION OF DEFLECTION OF A PLANSYMMETRIC TRUSS BEAMS

For the starting analysis a static determinate planar cantilever truss is taken into consideration. Geometry properties of the truss are shown in Fig.2. The bars are bound in repeated cells with constant length L, height h and filling angle β. Bottom longitudinal bars are denoted with subscript "*b*", top bars with "*t*", vertical bars with "*v*" and diagonal bars with "*d*". The truss is loaded by a transverse force F at the free end.

All the bars are of the same material and are pin jointed. The bars are solely extended or compressed, and the axial forces in them can be calculated from the equilibrium conditions.

This type of truss is the most commonly manufactured with the same cells throughout its length. However, for the sake of structural strength and making good use of material it is convenient to have the truss with two spans, so that the span near supports, the one in higher bending moment, is made of bars with greater cross-

*Corresponding author: Radoja Krstica 19, Trstenik, mtodorovic_vtms@yahoo.com

section areas. This can make the structure lighter and closer to an optimum design.

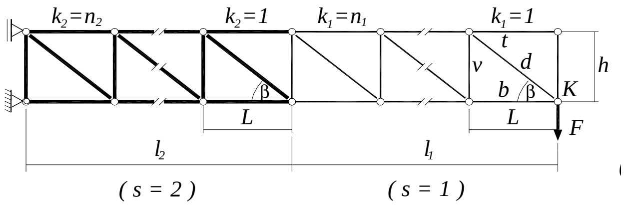

Figure 2: Geometry and load of a two span cantilever truss

We shall observe in this paper a truss that consists of two spans with the same L, h and β. The first span, span index s = 1, has length l_1 and number of cells n_1, so that $l_1 = n_1L$. Similarly in the second span, with index s = 2, we have l_2, n_2 so that $l_2 = n_2 L$. Cell ordinal numbers k_1 = 1, 2, 3 … n_1 and k_2 = 1, 2, 3 … n_2 are counted from right to left, Fig.2.

Vertical bars are assumed to belong to the *right hand* adjoining cell. Consequently the vertical bar connecting the two spans belongs to the first span. The rightmost top and vertical bars are unstrained, but they have been kept here for the purpose of structural continuity. Bars in the first span have the cross-section areas A_{b1}, A_{t1}, A_{v1} and A_{d1}, and bars in the second span A_{b2}, A_{t2}, A_{v2} and A_{d2}, and they all have the modulus of elasticity E.

In the case of a truss loaded with a force at its free end (Fig.2) we first calculate forces in the bars [8] and then deformation energy of the whole truss U_d. After that we apply Castigliano's theorem to obtain the transverse displacement f_K at the free end (ie. displacement in the direction of the force):

$$f_K = \left[\frac{F\,l_1^3}{3E\,I_{xe1}(n_1)} + \frac{F(l_1+l_2)^3}{3E\,I_{xe2}(n_1+n_2)} - \right.$$
$$\left. - \frac{F\,l_1^3}{3E\,I_{xe2}(n_1)} \right] + \left[\frac{F\,l_1}{S_{e1}} + \frac{F\,l_2}{S_{e2}} \right] \qquad (1)$$

In the above formula quantities $I_{xe(s)}(n)$ are functions of n and the span index s in the form:

$$I_{xe(s)}(n) = \left[\frac{1}{h^2 A_{b(s)}} \left(1 + \frac{3}{2n} + \frac{1}{2n^2} \right) + \right.$$
$$\left. + \frac{1}{h^2 A_{t(s)}} \left(1 - \frac{3}{2n} + \frac{1}{2n^2} \right) \right]^{-1} \qquad (2)$$

It is shown in the [7] that this quantity is a result of deformation in which the longitudinal bars "*b*" and "*t*" remain parallel, but compressed and elongated at the same time, so that this deformation mode can be ascribed to the bending mode of a truss as a whole. Since the bars are not bent, we call this the *structural bending* of a truss. We call $I_{xe(s)}(n)$ the equivalent moment of inertia of the truss cross-section, and consequently the product $EI_{xe(s)}(n)$ the equivalent bending stiffness. Thus the sum in the first square brackets in (1) represent the bending component of the total end deflection f_K.

The quantities $S_{e(s)}$ in (1) have the form:

$$S_{e(s)} = E \left[\frac{tg\beta}{A_{v(s)}} + \frac{1}{\sin^2\beta \cos\beta \, A_{d(s)}} \right]^{-1} \qquad (3)$$

and can be associated with deformations of solely "*v*" and "*d*" bars, while "*b*" and "*t*" bars remain parallel. This can be understood as the *structural shearing mode* of the truss. Consequently, fractions F/S_{e1} and F/S_{e2} in (1) represent the components of the first and second span slopes to the horizontal direction. Thus, the sum in the second square brackets in (1) is the shearing component of the total end deflection f_K.

Let us observe now a continuum cantilever beam loaded by a transverse force at its free end, Fig.3.

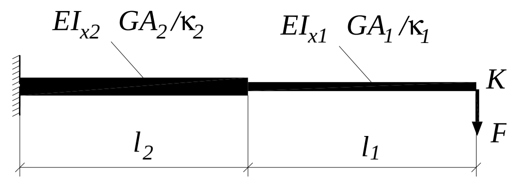

Figure 3: A continuum beam with two spans in bending by a transverse force

Let both spans have constant strength characteristics along their lengths, as indicated in the figure. $I_{x(s)}$, $A_{(s)}$, $\kappa_{(s)}$, E and G denote axial moment of inertia, area and shear number of the cross-section area and the moduli of elasticity and shearing respectively. Conventional method give for the free end deflection of a beam in Fig.3:

$$f_K = \left[\frac{Fl_1^3}{3EI_{x1}} + \frac{F(l_1+l_2)^3}{3EI_{x2}} + \right.$$
$$\left. - \frac{Fl_1^3}{3EI_{x2}} \right] + \left[k_1 \frac{Fl_1}{GA_1} + k_2 \frac{Fl_2}{GA_2} \right]$$

Comparing term by term the above expression with (1) we can see full analogy. There are, however, a couple of minor differences. One is in that the continuum beam employs G, since it undergoes shearing in material, while a truss does not undergo it, hence in both (2) and (3) modulus of elasticity is employed. We see that equivalent shearing rigidities S_{e1} and S_{e2} in the truss stand for GA_1/κ_1 and GA_2/κ_2 in a continuum beam. Second difference is in that the moments of inertia for the continuum beam depend only on the cross-section geometry. However, the equivalent moments of inertia introduced by the exp. (2) depend on the number of cells n (n_1 and n_2), and therefore on the relative length of the truss. A detailed analysis in [6] has shown that the influence of n decreases when n grows.

3. CALCULATION OF THE FREE END DEFLECTION OF SPATIAL TRUSSES

This paper considers statically determinate cantilever trusses with one direction slope of filling diagonal side bars in repeated cells with rectangular and triangular cross-sections. Geometry of the trusses is shown in Figs. 4 and 6. The cells have constant length L, height h and filling angle β.

3.1. The truss beam with rectangular cross-section

A spatial truss beam, Fig.4, consists of four planar trusses. The top and bottom side filling bars are low strained and we can neglect effects of their deformations. Therefore, in the further analysis we can observe a planar truss with rigidity varying in spans that is loaded with force F, and is one half of a spatial truss, Fig.5.

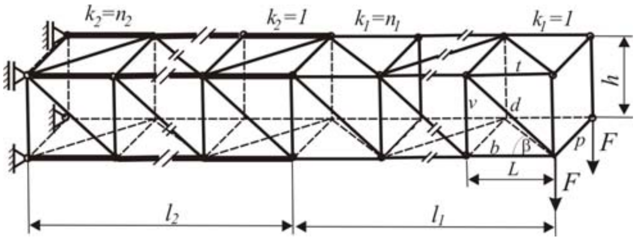

Figure 4: The truss with rectangular cross-section

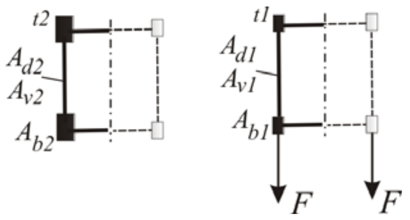

Figure 5: Rectangular cross-section

All the bars are either compressed or extended, and their axial forces in the first span, s = 1, can be calculated from the equilibrium conditions:

$$N_{b1}(k_1) = k_1 \frac{F}{tg\beta}$$

$$N_{t1}(k_1) = (k_1 - 1)\frac{F}{tg\beta}$$

$$N_{v1}(k_1) = F$$

$$N_{d1}(k_1) = \frac{F}{\sin\beta}$$

and in the secon span, for s = 2:

$$N_{b2}(k_2) = (n_1 + k_2)\frac{F}{tg\beta}$$

$$N_{t2}(k_2) = (n_1 + k_2 - 1)\frac{F}{tg\beta}$$

$$N_{v2}(k_2) = F$$

$$N_{d2}(k_2) = \frac{F}{\sin\beta}$$

The deformation energy of the whole truss can be obtained by summing up deformation energies of all the bars in the first span:

$$U_{d1} = \sum_{k_1=1}^{n_1} U_{db_1} + \sum_{k_1=1}^{n_1} U_{dt_1} + \sum_{k_1=1}^{n_1} U_{dv_1} + \sum_{k_1=1}^{n_1} U_{dd_1} =$$
$$= \frac{1}{2}\sum_{k1=1}^{n1}\left[\frac{N_{b1}^2(k_1)L}{EA_{b1}} + \frac{N_{t1}^2(k_1)L}{EA_{t1}} + \right.$$
$$\left. + \frac{N_{v1}^2(k_1)l_v}{EA_{v1}} + \frac{N_{d1}^2(k_1)l_d}{EA_{d1}}\right]$$

and bars in the second span:

$$U_{d2} = \sum_{k_2=1}^{n_2} U_{db_2} + \sum_{k_2=1}^{n_2} U_{dt_2} + \sum_{k_2=1}^{n_2} U_{dv_2} + \sum_{k_2=1}^{n_2} U_{dd_2} =$$
$$= \frac{1}{2}\sum_{k2=1}^{n2}\left[\frac{N_{b2}^2(k_2)L}{EA_{b2}} + \frac{N_{t2}^2(k_2)L}{EA_{t2}} + \right.$$
$$\left. + \frac{N_{v2}^2(k_1)l_v}{EA_{v2}} + \frac{N_{d2}^2(k_2)l_d}{EA_{d2}}\right]$$

The total deformation energy of both spans will thereby be:

$$U_d = U_{d1} + U_{d2}$$

Using Castigliano's theorem we get the expression for the end deflection in the same form as in Exp. (1). Also, the expressions for the equivalent moment of inertia $I_{xe(s)}(n)$ and the equivalent shearing rigidity $S_{e(s)}$ are identical to the Exp. (2) and (3) for a planar truss.

3.2. The truss beam with triangular cross-section

In case of spatial truss beam with triangular cross-section with the side slopes α, (Fig. 6), one can also consider one symmetric half of the truss.

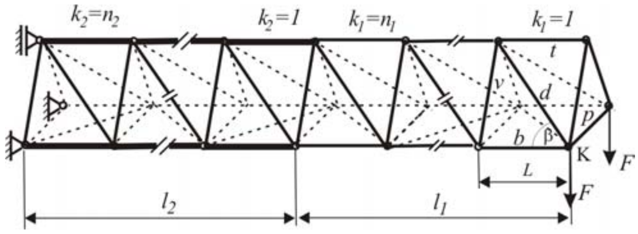

Figure 6: The truss with triangular cross-section

The top longitudinal bars are assumed to have cross-section area $2A_{t(s)}$ with internal force $2N_{t(s)}$, to supply the structure for symmetry. That way the upper half of the beam loaded with the force F comprises "t" bar with area A_{t1} in the first span, and area A_{t2} in the second span (Fig. 7).

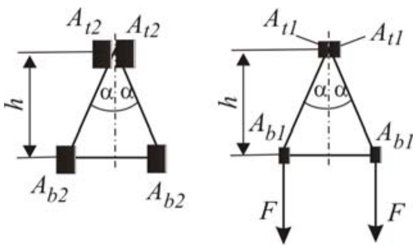

Figure 7: Triangular cross-section

The length of "v" bars differ to the height h, and we have the relation

$$h = l_v \cos\alpha$$

All the filling bars of the bottom (horizontal) side are unloaded except for the transverse bars at the truss ends. Decomposing F in Fig.8 in directions of the "v" and "p" bars we get the component in the side plane:

$$F' = F / \cos\alpha$$

The truss is effectively symmetric (except for the base plane diagonal bars which are zigzagging, but that does not affect the overall behavior of the structure).

The truss is symmetrically loaded so the forces in "b", "t" , "v" and "d" bars also exhibit symmetry.

Bars "*b*" i "*v*" are compressed and "*t*" and "*d*" bars are extended. The end transversal or „p" bars with cross-section A_p are compressed.

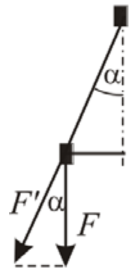

Figure 8: Compopent force F

Regarding all mentioned above we can obtain forces in the bars in the first span from equilibrium conditions:

$$N_{b1}(k_1) = \frac{k_1(F/\cos\alpha)}{tg\beta} = \frac{k_1 F'}{tg\beta}$$

$$N_{t1}(k_1) = \frac{(k_1-1)(F/\cos\alpha)}{tg\beta} = \frac{(k_1-1)F'}{tg\beta}$$

$$N_{v1}(k_1) = \frac{F}{\cos\alpha} = F'$$

$$N_{d1}(k_1) = \frac{(F/\cos\alpha)}{\sin\beta} = \frac{F'}{\sin\beta}$$

$$N_{p1}(0) = \frac{F}{\cos\alpha}\sin\alpha = F'\sin\alpha$$

$$N_{p1}(k_1) = 0, k_1 = 1,2,..n_1$$

and forces in the bars in the second span:

$$N_{b2}(k_2) = \frac{(n_1+k_2)F'}{tg\beta}$$

$$N_{t2}(k_2) = \frac{(n_1+k_2-1)F'}{tg\beta}$$

$$N_{v2}(k_2) = F'$$

$$N_{d2}(k_2) = \frac{F'}{\sin\beta}$$

$$N_{p2}(n_2) = F'\sin\alpha$$

$$N_{p2}(k_2) = 0,\ k_2 = 1,2,..,n_2-1$$

Summing deformation energies of all the bars in first and second span, and applying Castigliano's theorem to it we can obtain the end deflection in the form:

$$f = \left[\frac{F\,l_1^3}{3EI_{xe1}^{fF}(n_1)} + \frac{F(l_1+l_2)^3}{3EI_{xe2}^{fF}(n_1+n_2)} - \frac{F\,l_1^3}{3EI_{xe2}^{fF}(n_1)}\right] + \left[\frac{F\,l_1}{S_{etr1}} + \frac{F\,l_2}{S_{etr2}}\right] + \frac{Fl}{EA_p}\frac{\sin^3\alpha}{\cos^2\alpha}tg\beta\frac{2}{n_1+n_2} \tag{4}$$

Formula for the equivalent moments of inertia in (4) is the same as (2), but length *h* is now the vertical distance, see Fig.7. Instead of the equivalent shearing stiffness (3) we use here the modified form for triangular cross-section:

$$S_{etr(s)} = E\left[\frac{tg\beta}{A_{v(s)}} + \frac{1}{\sin^2\beta\cos\beta\cdot A_{d(s)}}\right]^{-1}\cos^2\alpha \tag{5}$$

The third term in (4) is an addititon due to N_p in the horizontal transverse bars. Its influence for n_1, $n_2 > 2$ is small and it may be omitted.

4. NUMERICAL RESULTS

The equivalent shearing rigidity and deflections of spatial truss beams with two equal length spans are analysed here. Material is steel with modulus of elasticity $E = 2{\cdot}10^5 \text{N/mm}^2$.

Since forces in „v" and „d" bars do not depend on number of cells in both spans, their cross-section areas can be taken equal: $A_{v1} = A_{d1} = A_{v2} = A_{d2} = A_p = A_v$. That way expressions (3) and (5) become simplified and uniform for the whole length of the truss:

$$S_e = EA_v\frac{\sin^2\beta\cos\beta}{1+\sin^3\beta}$$
$$S_{etr} = EA_v\frac{\sin^2\beta\cos\beta}{1+\sin^3\beta}\cos^2\alpha \tag{6}$$

Diagram in Fig.9 shows functions $S_e/A_v=f(\beta)$ and $S_{etr}/A_v=f(\beta)$, ie. how the equivalent shearing rigidites devided by A_v depend on filling angle β (in an interval between 30 and 60 degrees).

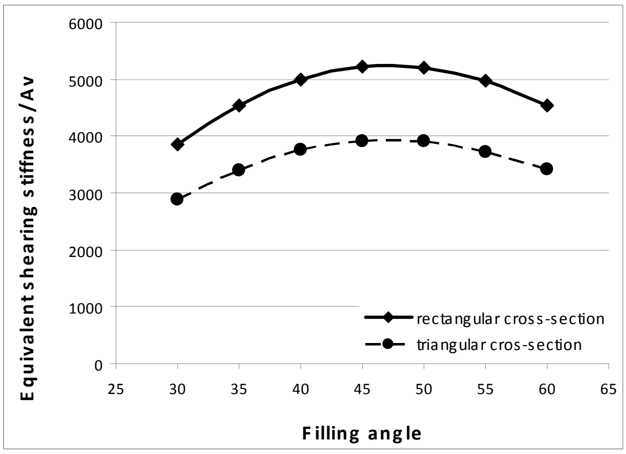

Figure 9: Variation of the equivalent shearing rigidity

The equivalent shearing rigidity of the triangular cross-section is smaller compared to the one of the rectangular cross-section for the same length *l* and the width of sides l_v. The diagram shows also that the maximum is reached for $\beta = 45^0$.

Forces in longitudinal bars of the truss with the rectangular cross-section depend on the load, filling bars slope β and on cell numbers n_1 *and* n_2. If $A_{b1} = 2A_{t1}$ in the first span and $A_{b2} = 2A_{t2}$ in the second span, expression (2) for the equivalent bending rigidity acquires the simpler form:

$$I_{xe(s)}(n) = A_{b(s)}\frac{l_v^2}{3\left(1-\frac{1}{2n}+\frac{1}{2n^2}\right)} \tag{7}$$

Now the equivalent bending rigidity of each span depends on the cross-section of longitudinal bars, on the span length (ie. cell number) and the hight $l_v = h$.

Expression for the equivalent bending rigidity with the triangular cross-section, with the same dimensions L and l_v of the sides, has a smaller value due to the side angle α:

$$I_{xe(s)}(n) = A_{b(s)} \frac{l_v^2}{3\left(1 - \frac{1}{2n} + \frac{1}{2n^2}\right)} \cos^2 \alpha$$

It should be noted here that $A_{b(s)}$ (which is proportional to force $N_{b(s)}$) also depends on the cell number, that is $A_b = A_b(n)$. Diagram in the Fig.10 shows equivalent bending rigidity to longitudinal bars cross-section ratio as function to cell number n: $I_{xe}(n)/A_b(n)=f(n)$ for the truss with triangular cross-section for the side angles $\alpha = 30^0$, 25^0 and 20^0.

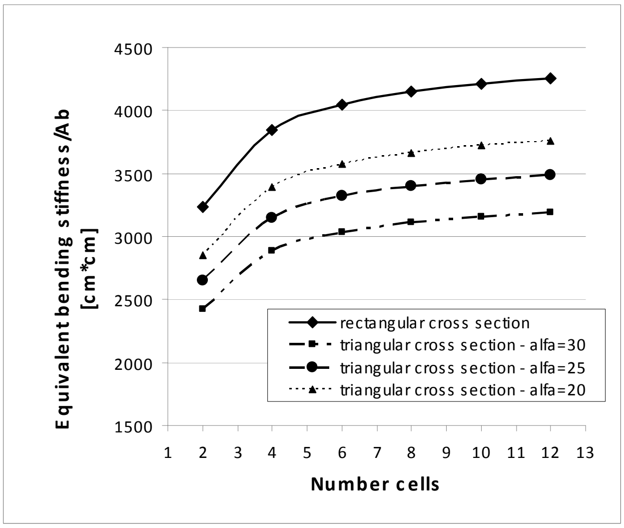

Figure 10: Promena ekvivalentne savojne krutosti

We can see in Diagram 10 that the equivalent bending rigidity from expression (7) reaches a constant value after $n = 6$. Values $I_{xe}(n)/A_b(n)$ for triangular trusses are smaller compared for trusses with rectangular cross-section depending on the side angle – about 11.7% for $\alpha = 20^0$ and 25% for $\alpha = 30^0$.

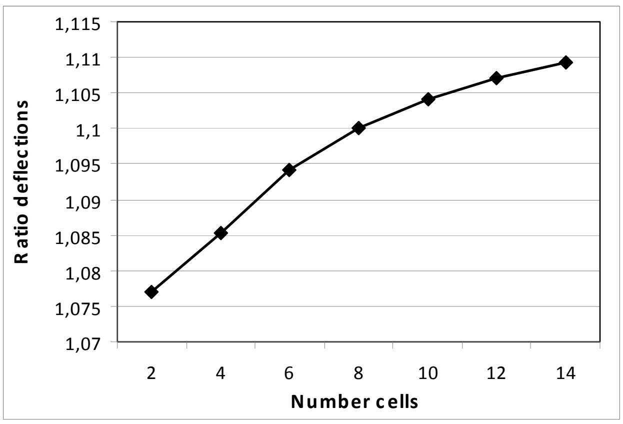

Figure 11: The ratio of the end deflections for the rectangular truss with variable and constant rigidity

Using (1) and (4) the end deflections of rectangular and triangular truss with $\alpha = 30^0$ were calculated. Cross-section areas of the extended bars were calculated for the same allowed stress, and of the compressed bars for the allowed stress regarding buckling. A ratio of the total end deflections of rectangular truss of the variable to the constant rigidity truss is shown in Fig.11.

The shearing components of the end deflection of constant and variable rigidity are equal, but their bending components differ, and their ratio is shown in Fig.12.

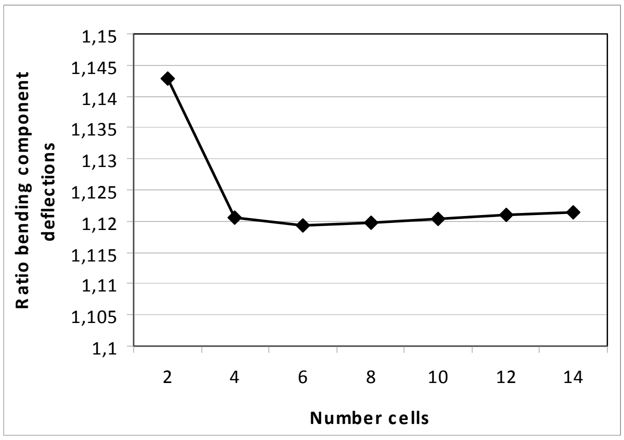

Figure 12: The ratio of the bending components of deflections for the rectangular truss with variable and constant rigidity

The diagram in Fig.12 shows that longer truss with variable rigidity (two spans) has the bending component 12% greater then the truss with constant rigidity. The ratio of the total deflection of the variable and constant rigidity encreases with their length, and regarding that the influence of the shearing component decreases, this ratio tends to the value 1.125 (ie. the end deflection of the variable rigidity truss is 12.5% higher).

Ratio of bending components of deflections of the variable and constant rigidity triangular trusses has the form shown in Fig.12 and the ratio of the total deflections is shown in Fig.13.

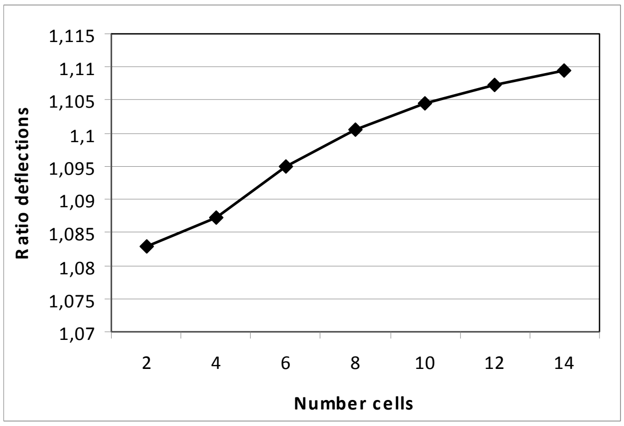

Figure 13: The end deflection ratio of a triangular truss with variable and constant rigidity

Diagrams in Figs. 11 and 13 have similar form and a difference occurs only in short trusses (n = 2) because triangular truss, accordingly to formula (4), includes the component induced by two horizontal transverse bars at its ends.

5. CONCLUSION

In this paper the equivalent bending and shearing rigidities of spatial trusses with rectangular and triangular cross-section and variable rigidities in intervals have been derived. Also formulas for the end deflections of these trusses have been derived.

The formulas obtained were used in order to analyze the influence of the length l and filling angle β to the equivalent rigidities. The figures of the end deflection and their components were compared for the figures of spatial trusses with constant rigidity.

The end deflections of a truss with variable rigidity along two spans are 12.5% higher compared to deflections of a truss with constant rigidity. However, a material and weight saving is not negligible.

REFERENCES

[1] A. K. Noor, M. M. Mikulas, "Continuum Modelling of Large Lattice Structures", Status and Projections, NASA Technical Paper 2767, (1988)

[2] W. S. Kenner, "Lattice Truss Structural Response Using Energy Methods", North Carolina A&T State University, A Thesis Submitted to the Faculty of Old Dominion University in Partial Fulfilment of the Requirement for the Degree of Master of Sciences, 129 pages, NASA-TM-112361, (1987)

[3] B. Burgardt, P. Cartraud, "Continuum Modelling of Beamlike Lattice Trusses", Advances in Computational Techniques for Structural Engineering, Budapest, Hungary, 21.-23. August 1996, pp 51-59, (1996)

[4] A. Teughels, G. De Roeck, "Continuum Models for Beam- and Plate like Lattice Structures", IASS-IACM 2000, Fourth International Colloquium of Computations of Shell & Spatial Structures, Channia Crete, Greece, June 5-7, pp.1-20, (2000)

[5] H. I. Park, C. G. Park, "An Approximate Method for Permuting Frame with Repeated Lattice Structure to Equivalent Beam", The Open Ocean Engineering Journal, Vol. 4, pp 55-59, (2011)

[6] M. Todorović, "Calculation of deformations in the plane of a load carrying truss beam with the constant cross-section by method of equivalent continuum beam", Ph.D. Thesis, Faculty of Mechanical Engineering in Kraljevo, University of Kragujevac, (2010)

[7] M. Todorović, M. Dedić, "Calculation of Cantilever Truss Beam Deformations Using Continuum Modelling", Journal of Modelling and Optimization in the Machines Building Field (MOCM), MOCM -15, Vol. 2, pp 87-98, (2009)

[8] M. Dedić, M. Todorović, "Calculation of The Free End Deflection Analysis of A Truss Beam with Variable Cross-section", The Seventh Triennial International Conference "Heavy Machinery HM 2011", Volume 7, No 7, G. 13-16, June 29th- July 2nd 2011, Vrnjacka Banja, ISBN 978-86-82631-58-3, (2011)

[9] M. Todorovic, M. Dedic, "An Analysis of Equivalent Rigidities of A Truss Beam", Proceedings of the The Seventh International Conference "Heavy Machinery HM 2011", Kraljevo, Serbia, June 29th – July 2nd, Vrnjacka Banja, pp.G.33-G.38, ISBN 978-86-82631-45-3, (2011)

[10] M. Todorovic, M. Dedic, V. Jevremovic, M. Mijatovic, "A Deformation Analysis of A Truss Beam with Variable Cross-Sections in Distributed Load", Proceedings of the 13th International Conference „Research and Development in Mechanical Industry RaDMI 2013", Volume 1, pp.A.277-A.282, 12 - 15 September 2013., Kopaonik, Serbia, ISBN 978-86-6075-042-8, (2013)

VIII International Conference "Heavy Machinery-HM 2014", Zlatibor, 25-28 June 2014, E.77-82

Shaping the Housing of Transmission Gear With High Specific Power

Vojkan Nojner[1*], Dragan Milčić[2]
[1] GOŠA FOM, Equipment and Machines Company, Industrijska 70, 11420 Smed. Palanka, Serbia
[2] Faculty of Mechanical Engineering Niš, Aleksandra Medvedeva 14, 18000 Niš, Serbia

The shape and size of the gearbox casing with enlarged power which works outdoors are conditioned from the basic requirements for bearings and gears which are dimensioned according to the load capacity, as well as significantly depend on the required factors of application, main requirements for binding to the stand, lifting, transport; filling, inspection and drain the oil; requirements for heating and additional monitoring.

The shape highly depends on the heat calculation, the nature of the cooling (use the fan) and requirements for the universality of the performance, and installation.

Keywords: High-power gearboxes, Forms of thermally stable housing, Geometric relationships in the housing

1. INTRODUCTION

The transmission gears are the most abundant group of mechanisms that are used in mechanical engineering. Therefore, their research, development, manufacturing, testing, inspection, conservation, packaging, transportation, storage, unpacking, deconservation, installation, commissioning and running-in, exploitation, monitoring, maintenance, repair and recycling of great attention. In fact, most of the world's leading manufacturer of universal gear reducer was able to, in the same frame size reducers, and at the same time increase the capacity and the highest transmission ratios, for approximately 100%, which was a very large, significant, and it is fair to say, surprising progress. This increase has occurred, with multistage gear, thanks to the abandonment of the previous concepts coaxial gearboxes (which allowed the reduction of the diameter of the first gear), increasing the gearboxes overall dimensions, mostly wide (enabling the increase in centre distance), changing the concept of first gear (instead of the previous setting the first gear on the motor shaft, at the largest transmission ratio, is carried out in a stamping them off, or a special nut, which allows reduction of the diameter of the first gear), a small reduction in the number of teeth of gears (which allowed an increase in the module and thus the capacity of the gears), opening the low speed and/or fast-running chamber housing gear (which enable the installation of large gears), offering two sets of gears in the same housing (higher gear ratios with less capacity and lower gear ratios with a higher capacity), etc.

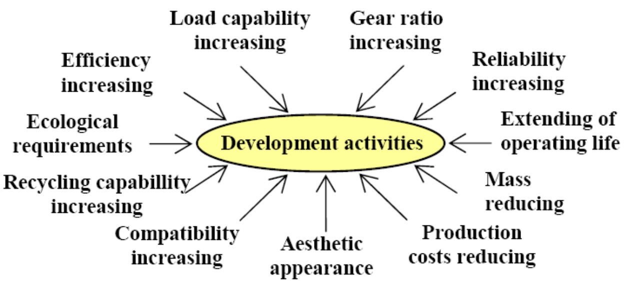

Figure 1: Schematic review of usual ways for gear units improving [1]

All of these, seemingly, small interventions have enabled a large increase in transmission capacity gear ratio and thus, of course, and gear in general. These practices are conditioned to take special care in gearboxes large specific power should be given to the construction of the gear unit housing. This paper presents a comparative view of considering the characteristics of the gear unit housing on belt conveyor drives with power P≥250 kW in mining machinery in open cast mines in Serbia (Kolubara, Kostolac).

For gear reducer seeks to increase effectiveness (among other things by reducing the number of gear pairs and bearings), quality improvement (by using quality materials and advanced technology development), improving the technical characteristics (applying rational structural solutions), design improvements (engagement renowned designer), reducing cost (by using cheaper materials and more modern production technology), decreased weight (applying rational structural solutions and lighter materials), reducing the overall dimensions (using the simple structural solutions and quality materials), reducing noise and vibration (applying quality work, greater accuracy and more rational structures), etc.

2. THE GEARBOXES OF BELT CONVEYOR DRIVE

High power gearboxes are designed for operation of belt conveyor drives on the mining machinery in open pit mines for the excavation of top soil and coal, as well as tailings - bucket wheel excavators, drive stations and spreaders. Two or three stages gearboxes are horizontal with bevel-helical gears and flanged output shaft. They continuously work throughout the year in all weather conditions.

For these conveyors transmission ratios are in the range of 8-16 for two-stage-, or 14-25 for three-stage-gearboxes. Nominal motor speed is 1000 rpm, frequently regulated in the range 600-1200 rpm. Output speed is in the range 60-125 rpm.

The relationship of centre distances in the gearbox housings was once clearly and certainly that could be determined from the catalogue and label of gearboxes, and is now kept as a trade secret.

*1 GOŠA FOM, Equipment and Machines Company, Industrijska 70, 11420 Smed. Palanka, Serbia, vojkan.nojner@gosafompr.com

3. OVERVIEW AND FEATURES OF THE GEARBOX HOUSING OF BELT CONVEYORS

Comparative overview and features of the gearbox housings of belt conveyors drives with power P≥250 kW on the mining machinery in open cast mines (Kolubara, Kostolac) are given in the following figures [2].

In Figure 2 is given housing of the gearbox type CKFY-400, with two feet, enlarged rear part and vertical ribs. Cooling is without a fan.

This casing provides the (possibility) ability to change gearbox execution without opening the housing halves and repackaging rotating parts. Halves are identical. It is designed for rated power 315 kW at 1450 rpm. Rated power of gearbox corresponds to the application factor Ka=1.4. The ribs are positioned vertically (laterally), relative to the main longitudinal axis of gearbox.

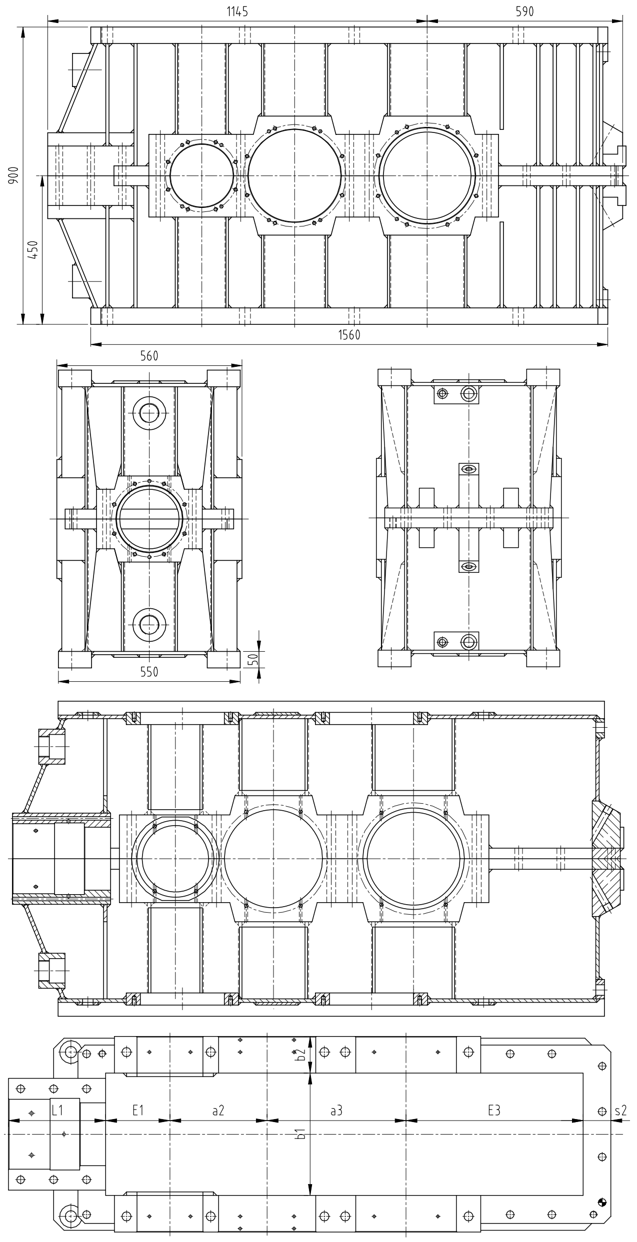

Figure 2: Housing CKFY-400

Display modified housing type CKFZ-400, with the usual feet for a connection to the drive unit base is shown in the following figure. Designed for rated power 315 kW too, but at 1000 rpm; factor Ka=1.4 also. It made the ribs necessary. New are attachment points for monitoring (Pt-100 resistance thermometers and the vibration diagnostics on all the bearing points).

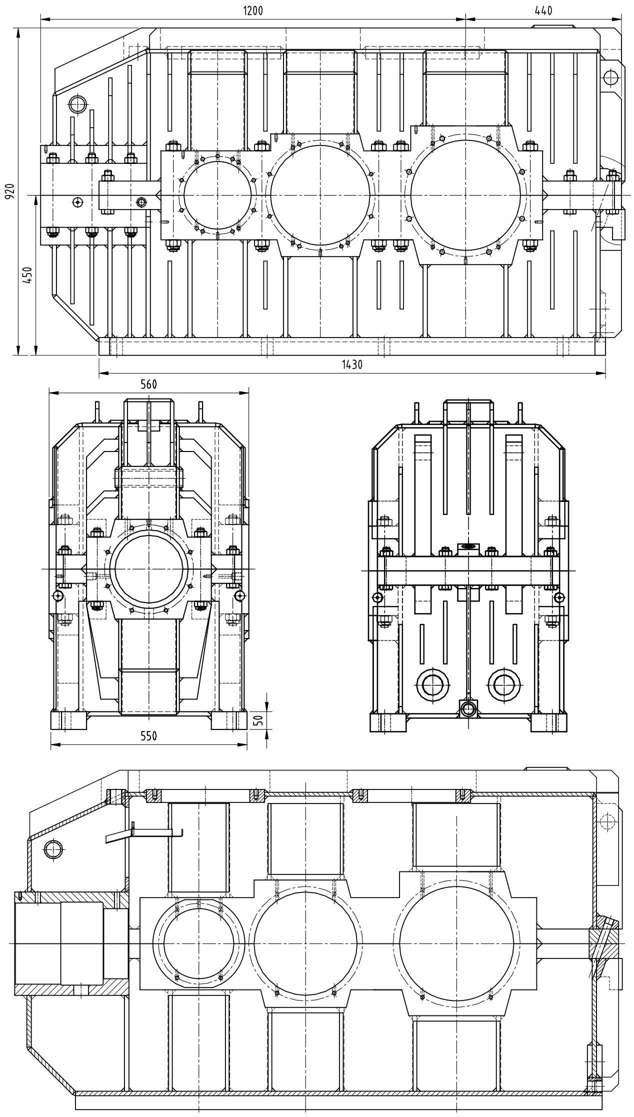

Figure 3: Housing CKFZ-400

Display of the gear unit housing with enlarged structure type BKFZ-360, -400 and -450, with a non-standard centre distances, the installed capacity 250, 315 and 450 kW of electric motors, with two feet (identical housing halves), without fan, with heater and thermostat (provided points for monitoring of bearings input shaft) is shown in Figure 4 and 5.

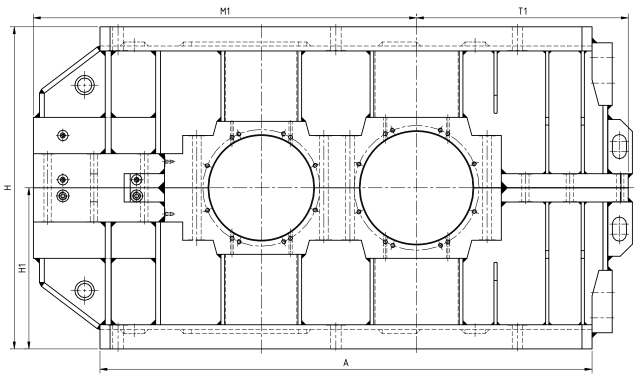

Figure 4: Housing types BKFZ-360, -400, -450

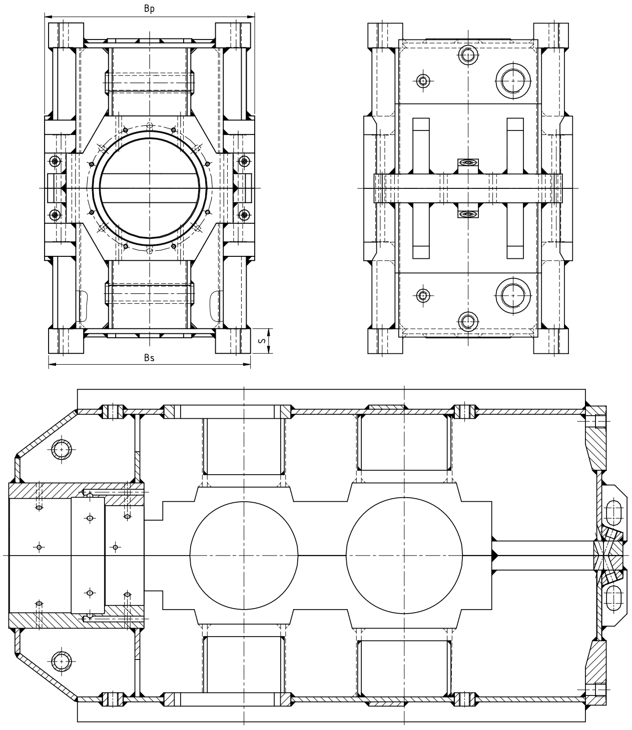

Figure 5: Housing types BKFZ-360, -400, -450

Table 1:. Characteristic measures on the housing

Type/Measure	A	H	H1	M1	T1	Bs	Bp	s
BKFZ-360	1220	800	400	950	525	490	510	60
BKFZ-400	1350	900	450	1050	590	560	550	65
BKFZ-450	1530	1000	500	1170	655	610	600	70

Display of the gear unit housing with enlarged structure type BKFZ-530 is shown in Figure 6 and 7; with a non-standard centre distance, the installed capacity 500 kW of electric motor, 2 feet (identical housing halves), with fan and focusing hood, heater and resistance thermometers for bearing input shaft and oil sump, as well as provided the vibration diagnostics on all bearing points.

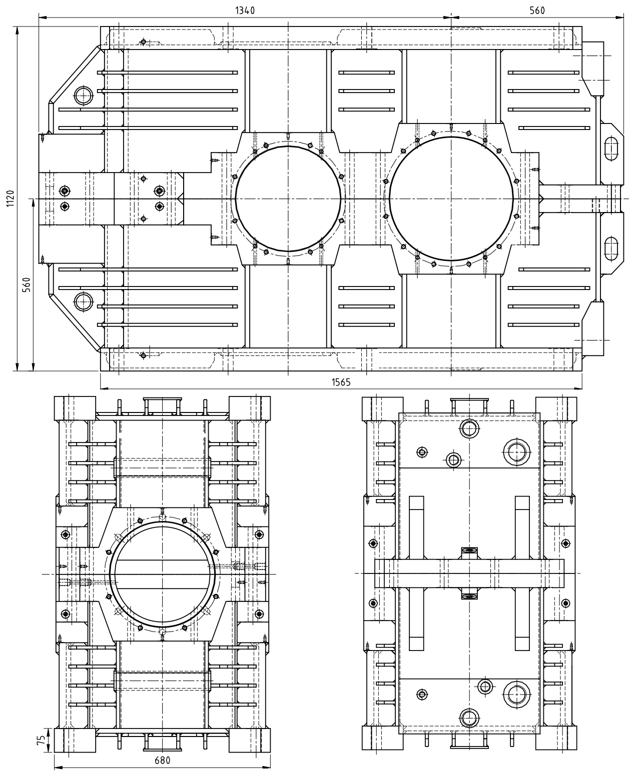

Figure 6: Housing BKFZ-530

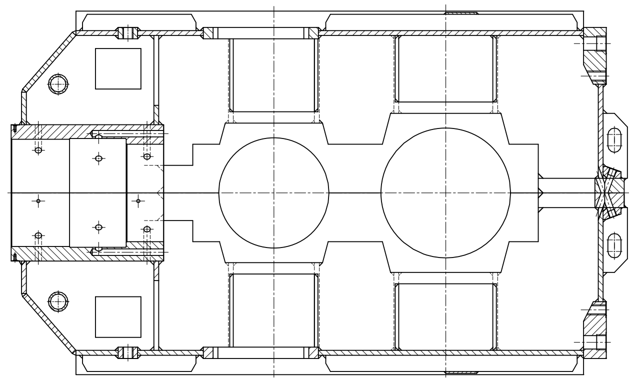

Figure 7: Housing BKFZ-530

Display of classic gear unit housing type CK-560, with a standard centre distances, with feet only on the lower half (different housing halves), no fan, with heater and thermostat (not provided monitoring) is shown in Fig.8.

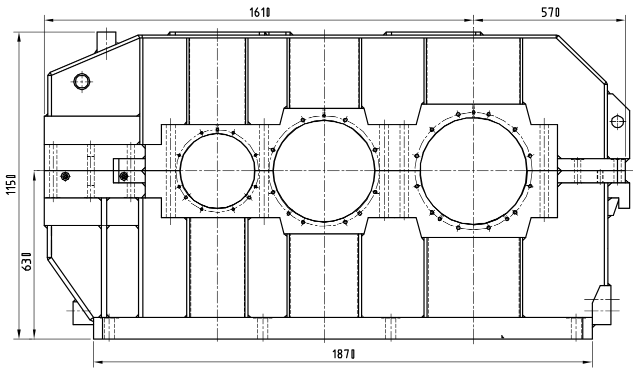

Figure 8: Regular type of housing CK-560

Display ribbed casing of gearbox enlarged structure type CKFZ-560, with a standard centre distances, the installed capacity 630 kW of electric motor, with 2 feet (identical halves of housing), with fan and focusing hood, heater and thermostat for oil sump, provided measuring for the bearing temperature of the input shaft (not provided the additional vibration diagnostics) is shown in Figure 9 and 10.

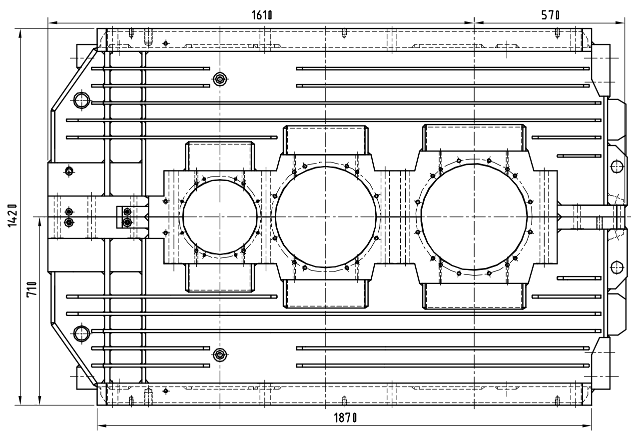

Figure 9: Ribbed modified housing CKFZ-560

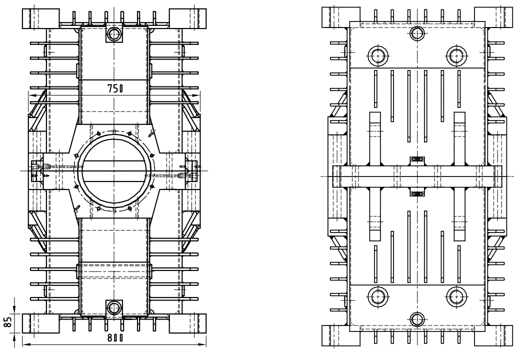

Figure 10: Ribbed modified housing CKFZ-560

Display of ribbed gearbox housing enlarged structure type CKFZ-580, with a non-standard centre distances, the installed capacity 1000 kW of electric motor, factor Ka=1.8, with the feet on the lower housing half, the fan with fixed wings, focusing hood and the roof (to reduce the influence of radiation of sunlight and protection from overheating the gearbox inner space in the summer) can be seen in Figure 11. It has been modified centre distances. There are mounted three heaters and resistance thermometers for bearing input shaft and oil sump, as well as provided additional monitoring - the vibration diagnostics on all bearing points.

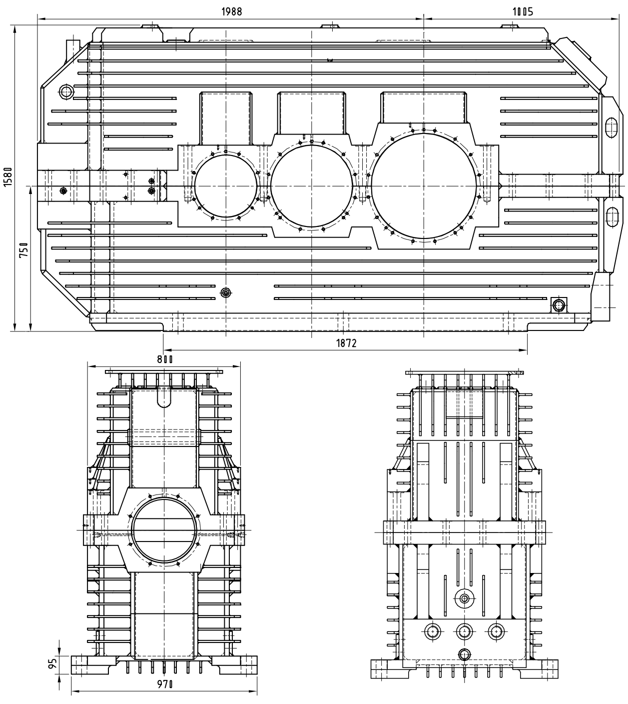

Figure 11: Housing CKFZ-580

4. HOUSING

The housings are welded from sheet metal thickness from 8 to 200 mm of high-quality steels S355J2+N for responsible sheets (hubs, flanges, feet, etc.), or S235J2+N for the rest of the casing. These materials have guaranteed mechanical properties (tensile strength and resilience) up to a temperature -20 °C. It is generally sufficient for the climate zone on open cast mine of the former Yugoslavia. However, manufactured housing with the possibility of additional heating in the winter. Depending on the gearbox size is usually placed per one hole for heater and thermostat to turn it on/off or resistant thermometer (Pt-100) to continuously monitor the oil temperature. They are usually provided on the backside of the housing lower part, for classic form of housing (different halves), or with plugs in the upper half.

Feet are especially designed and adapted to be transmitted load from the gearbox in the stand. Provides stability and support gearbox on a flat surface. Each foot has 3 or 4 holes, depending on the number of gears and casing size. Also, for two identical halves are designed threaded bores and holes for connecting bolts with 2D- or 3D-eyelet.

When using fan, the ribs on the housing are welded horizontally and longitudinally due to favourable flow air from the fan array of construction.

Space within the housing is partly ribbed for stability and increased internal surface area exposed to the heat created.

For gear units with two feet that has a universal mounting in a horizontal position, there are specific components that affect specific installation and further complicated the construction:
- cooling fan,
- backstop,
- gear pump.

At the customer's request of the possibility of turning the entire gearbox without opening and repacked inside the housing, in the case of mounting of gear pump to the housing must be a double installation for forced lubrication, i.e. equal internal pipe line in both halves.

5. THERMAL CALCULATION

When sizing gearbox for continuous mode (24h per day, 365 days per year) mainly critical is thermal analysis. It requires a specific housing surfaces has been developed, which is sufficient for transmitting (disclosure) of the external surroundings of temperature that is generated in gearbox due to friction - the resistance of the bearings, the teeth engagement, etc. This area is increased by elongation of the casing in the area behind the output shaft, additional ribbing of casing and covers. In this way the basic surface (gearbox "shadow") is increased 2-3 times.

Display of such gearbox is shown in Fig.3-5, 7, 8.

According to literature [3], the heat transfer (air flow) factor in the open without fan is ~22 (15-25) $W/(m^2 \cdot K)$ and with fan ~35 (30-40) $W/(m^2 \cdot K)$ (about 1.6 times higher).

Reducers work outdoor and natural flow of air (wind speed) is usually sufficient in most year period (autumn, winter and spring). The fan is necessary only for the summer period. Temperature on the outside surface of the housing in the sun during the hottest times of the day can reaches up to 65°C (e.g. measured in open cast mine Drmno). Having regard to the required maximal allowable temperature of 80°C inside the gearbox when working with mineral oil, it's clear that the heating is highly dependent on the thermal characteristics of the housing.

5.1. Efficiency

Losses per one stage are 1-1.5%, so for example, for the three-stage bevel-helical reducer is about 4%. At first glance it does not look much, but for EM rated power 1000 kW, the losses amount to about 40 kW. Then the thermal calculation becomes dominant and authoritative to gearbox parts shaping.

Additional reducing the amount of heat generated in the gearbox under the influence of the sun at the summer time is achieved by placing a protective roof over the gearbox. Reduction gear is protected against corrosion by protective paint systems that have a lifetime usually over 15 years. Lighter shade of topcoats may slightly reduce the heating within the housing. Also, can be used a special kind of paint that improves the rejection of the sun's rays.

6. GEOMETRIC RELATIONSHIPS IN HIGH POWER GEARBOX HOUSING

Main longitudinal (oversized) measures the casing are total length L, width B and height H.

In the main horizontal plane (fitting surface of the lower and upper halves) housing is always symmetrical regarding to the main longitudinal axis, so as to ensure the execution of the right-hand or left-hand performance.

The length of the housing impact the following measures (see, e.g. Fig.2):

- The length of the front of the casing for mounting of input shaft (bevel pinion) L1;
- The length of the interior space to accommodate bevel gear (built-in measure E1);
- Centre distance of the second stage a_2 (and, if exist, third stage a_3), obtained by toothing calculation of the helical gears;
- Length of the interior space in the rear of the casing (behind the large output gear) E3;
- Width of flange for bolts connection of the rear housing s2.

For similar types of housing can be reviewed and compared some of the following parameters - relations measures actual centre distance, i.e. space to accommodate the bevel gear (e.g. a3 / a2 / E1); relationship length E1 and space for mounting of input shaft L1; relationship last space E3 of enlarged and regular housing, etc.

Width of the housing B is dependent on the width of the inner space B1 and width hub B2. Width of the interior is primarily dependent on the width of driven gear second and third stage (if exist). They are sized according to the criteria K_A x P_M ("application factor" x "motor rated power"), for the tooth flank factor S_H=1.2 and tooth root factor S_F=1.4. Gears can be slightly displaced in width due to the favourable ratio s/L (ratio of "distance middle gearing to the main longitudinal axis of the housing" / "gap between the bearings axis") in calculating the load capacity teeth and proper distribution of transmission ratio. (Depending on the size of the three-stage reducer, the gaps between two gear wheel, and between the gear and the bearing can be made of a few and up to 30 mm (usually 15-25 mm)).

The height of the housing H (i.e. the height of the lower half H1 from foot to connecting surface) is designed so that it can accommodate a driven (output) gear (for the highest gear ratio in the family of the same type), and depends on the thickness of the foot for connection with gear unit base. Can be discussed and compared the measures on foot (thickness, width, distance between the feet). Height of the gearbox housing (height of the lower housing part) is larger than the radius of the drum brake coupling on the input shaft.

Can be considered some of the relations between the different types of housing:

- Relations between overall dimensions L / B / H -

a) For regular type of enclosures with one foot on the lower half (e.g., CK-560, Fig.6) are about 3: 1: 1.6.

b) For housing type CKFZ-560 with two feet and the casing type CKFZ-580 with one foot relations overall dimensions are very similar: L: B: H=~3.5: 1: ~1.9.

- The relation $h1/a_n$ of the lower half height H1 and the last centre distance a_n is usually greater than 1, because under or near to output gear should be installed additional electrical equipment.

- The ratio of width across the feet and the width of the housing. In classic housing approximately the same value; the difference is typically 10 to 20 mm.

Applicable to the analysis and comparison of the geometric relationships with respect to centre distance of the last stage a_n, such as the distance of space from the output shaft axis to the rear flange E3, height of the lower housing part h1, the height of the interior space h1*, width of the interior of the housing to accommodate the insides parts b1, width of the side hub b2.

The main measures in housing of different gearboxes belt conveyor large forces are given in Table 2.

Table 2. Characteristic geometric relations in the housing

Type / size	E3/an	h1/an	h1*/an	b1/an	b2/an
CK-560 (regular)	0,857	1,125	0,982	0,821	0,241
CKFZ-560	0,857	1,268	1,116	0,821	0,241
CKFZ-580	1,536	1,302	1,137	0,868	0,260
CKFY-400	1,275	1,125	1	0,875	0,263
CKFZ-400	0,878	1,098	0,976	0,854	0,256
BKFZ-530	0,868	1,057	0,915	0,792	0,236
BKFZ-360	1,182	1,039	0,883	0,831	0,247
BKFZ-400	1,244	1,098	0,939	0,854	0,256
BKFZ-450	1,253	1,099	0,945	0,835	0,253

From these table can be seen that the characteristic relationships E3/an is range from 0.85 to 0.9, which is typical for classic gearboxes, to the ratio 1.2-1.3, which value is required for the heat-stable housing. In extreme cases, this ratio goes up to 1.55.

The typical ratio of the width in the housing b1/an are usually around 0.85 with small deviations (range 0.8-0.9), and the ratio of the hub width around b2/an = 0.25.

With respect to the height, characteristic ratio of the free space height in the housing h1*/an is at least 0.9 for the regular casing, and for thermally stable housing relation is in the range from 1 to 1.15.

7. CONCLUSION

It can be concluded, that for the company GOŠA FOM almost every new type of gearbox is prototype, since there is no catalogue of high power gearboxes and still working on the specific requirements of customers.

The gearbox thermal calculation and its consequences (required increased casing surface) have a great influence on the shape, appearance and size of the high power gearbox housing. Consideration of the gearbox thermal calculation is extremely important, because the losses of a few percent for large installed capacity become significant (ca. 40-50 kW e.g. for three-stage gearboxes).

Depending on customer requirements have been developed gearbox housing construction with different or identical upper and lower halves. This will influence the shape and number of outlets for lifting and transport.

Lifting lugs and eyes (thimbles) can be realised on plates as round holes, slots or fully open (so-called "hook"), as eyebolts or tubes that are welded in construction.

Depending on whether the fan is required or not, additional ribs are placed horizontally along the structures housing or a vertical cross.

For gearbox with installed motor power of at least 630 kW and application factor Ka=1.8-2, the fan is absolutely necessary. For the power of the 250-400 kW (and factor Ka=1.4-1.8), the fan is typically not used. For the power of the 400-500 kW (and factor Ka=1.8-2), the fan is desirable, but it depends on the unification with other sites and customer requirements.

REFERENCES

[1] S. Kuzmanović, M. Vereš, “New Development Trends of Universal Gear Reducers” Journal of Mechanical Engineering Design, Vol. 9 No 1, pp. 6-15, (2006)

[2] GOŠA-FOM - Workshop documentation

[3] G. Niemann, H. Winter, “Machine Elements, Volume II - Gearboxes general, Spur gearbox”, Springer Verlag, (1985). (in german)

SESSION F

RAILWAY ENGINEERING

The Wave Distorortion Analysis of the Voltage for Contact Line System at Serbian Railways

Branislav Gavrilovic[1*], Zoran Bundalo[1], Milutin Djuricic[3], Savo Gavrilovic[1]
[1] Railway College of Vocational Studies, Belgrade (Serbia)
[3] Business College of Vocational Studies, Uzice (Serbia)

The paper deals with the wave distortion analysis of the contact system line voltage at the operation of electric motive power with diode traction converters. The ascertained harmonic values are important for the prepared european standards and guidelines about interoperability not only from the point of view of the energy measurements on board trains working conditions, but also from the point of view to insure the regenerative breaking safety of new AC motive power. The analysis respects the filter-compensation equipment installed in Serbian Railways traction substations.

Keywords: Wave distortion of the voltage, Contact line system, European standards

1. INTRODUCTION

In recent years, an ever increasing attention has been paid to harmonic distortion in railway traction systems. The analysis of harmonic distortion in railway systems is essential in assessing its effects on the adjacent distribution power network. The Serbian Railways (ŽS) have had in operation electric locomotives equipped with diode traction converters. The diode converter gives a locomotive character of significant non linear load manifestated as current generator with poor value of the power factor and with large content of odd harmonics. The harmonic contents of contact current system produce sine wave distortion of the contact line system of 25 kV, 50 Hz.

Specifying of distortion rate is very important from the viewpoint of description of work conditions for:

a) watt-hour and var-hour electricity meters applied on the board of electric locomotive,

b) traction converter of electric locomotive used in regenerative breaking regime.

2. HARMONIC DISTORTION

Harmonics are steady-state components of periodical alternating voltage or current. They should not be confused with inter-harmonics or transients. Magnitudes of the individual harmonics are often expressed as a percentage of the fundamental component, or of the Root Mean Squared (RMS) magnitude of the overall voltage or current. Due to its negative influence on electrical appliances, harmonic distortion in supply network has become of increasing concern. A non-sinusoidal waveform can always be represented as a sum of a certain number of sinusoidal components with multiple frequencies [1]. Harmonic frequencies are integral multiples of the fundamental supply frequency.

Any periodic signal (waveform) can be described by a series of sine and cosine functions, also called Fourier series.

$$u(t)=U_{dc}+\sum_{n=1}^{\infty}\left(U_{(n)s}\cdot\sin(n\cdot\omega\cdot t)+U_{(n)c}\cdot\cos(n\cdot\omega\cdot t)\right) \quad (1)$$

The coefficients are obtained as follows:

$$U_{(n)s}=\frac{1}{\pi}\int_0^{2\pi}u(t)\cdot\sin(n\cdot\omega\cdot t)dt \quad (2)$$

$$U_{(n)c}=\frac{1}{\pi}\int_0^{2\pi}u(t)\cdot\cos(n\cdot\omega\cdot t)dt \quad (3)$$

Where n - an integer, $\omega=\frac{2\pi}{T}$, T - the fundamental period time.

Total Harmonic Distortion (THD_U) is often used as an overall measure of harmonic distortion. THD_U calculation equation is presented below:

$$THD_U=\frac{\sqrt{\sum_{n=2}^{n=40}U_{(n)}^2}}{U_{(1)}} \quad (4)$$

Where $U_{(1)}/U_{(n)}$ - the RMS of the first harmonic or the n[th] harmonic component of voltage.

Effective value:

$$U_{RMS}=\sqrt{\frac{1}{T}\int_0^T u(t)^2\,dt}=U_{(1)}\sqrt{1+THD_U^2} \quad (5)$$

For low distortion levels, e.g. for voltage, $U_{RMS}\approx U_{(1)}$.

According to the EN 50160 standard, values of individual higher harmonics (n) at the location of transmission to the 25[th] higher harmonic with a percentage of the nominal voltage U= 25 kV showed in Table 1 [3].

Table 1: Values of individual higher harmonics (n) at the location of transmission to the 25[th] higher harmonic

Odd-numbered higher harmonics not divisible by 3		Odd-numbered higher harmonics divisible by 3		Even-numbered higher harmonics	
Harmonic	$U_{(n)}$ %	Harmonic	$U_{(n)}$ %	Harmonic	$U_{(n)}$ %
5	6.0	3	5.0		
7	5.0	9	1.5	2	2.0
11	3.5	15	0.5	4	1.0
13	3.0	21	0.5	6 to 24	0.5
17	2.0				
19	1.5				
23	1.5				
25	1.5				

*Corresponding author: Railway College of Vocational Studies, Zdravka Celara 14, 11000 Belgrade, gavrilovicbranislav5@gmail.com

According to the EN 50160 standard, during the each ten minute interval, the value of THD_U has to be less than 8% of the first harmonic value. On the other hand, the values of individual harmonics can have values (shown in Table 1) between 0.5% and 6% of the of the nominal voltage $U = 25$ kV.

Higher harmonics are most commonly produced by higher harmonics of nonlinearly loaded electro-traction vehicles, which are connected at difference distances from the electro-traction substation. These higher harmonics produce other higher harmonics inside the overhead line at the location of pantograph. On the other hand, an increasing use of frequency converters and similar devices on electro-traction vehicles causes an increase in the value of inter-harmonics, whose permitted values are still not defined within the EN 50160 standard. However, lower intensity inter-harmonics can also cause flickers and interference in signaling-safety devices with the three-phase control.

3. PRESUMPTIONS AND PHASES OF THE ANALYSIS

A) The so-called „amplitude law“ describes the percentage value of current harmonic components for the electric ŽS locomotives fitted with the diode traction converter:

$$I_{(n)} \cong \frac{100}{n}\% \,,\; n = \frac{f}{50} \quad \text{(harmonic number, order)} \qquad (6)$$

B) Input impedance of the railway feeding system from the viewpoint of ŽS locomotives includes following elements:

• the impedance of the contact line system between the locomotive and the traction substation,

• the input impedance of the contact line system between locomotive and open end of the contact line system

• the input impedance of the filter-compensation equipment (FCE) installed in the traction substation for reducing the harmonic components feed into 110 kV line and for improving the electric locomotive power factor of feeding 110 kV line,

• the substitute reactance of the substation traction transformer,

• the impedance of feeding line 110 kV is neglected.

C) The foresaw FCE equipment has two *LC* branches, one for the 3rd and the other for the 5th harmonic and decompensation branch [2]. Both *LC* branches are supposed to be tuned exactly on 150 Hz and 250 Hz. The decompensation branch is supposed to be disconnected, because inductive power of the locomotive is equal to capacitive power of both *LC* branches.

Under presumptions described above analysis could be divided into 3 phases, with different frequency ranges:

1. *For frequencies 150 Hz and 250 Hz* - the substitute reactance of the substation traction transformer could be neglected, because both *LC* branches create short circuits for these frequencies.

2. *For frequencies from the 7th up to the proximity of the first resonance frequency for whole traction feeding system* - the substitute reactance of the substation traction transformer is connected in parallel to the FCE. The traction substation has an inductive character composed with:

• the substitute inductive reactance of the substation traction transformer,

• the substitute inductive reactance of the *LC* branches, because the 7th harmonic and the next frequencies are higher then tuned frequencies of both *LC* branches.

3. *For frequencies near the first resonant frequency of whole traction feeding system* - the feeding system is composed of:

• contact line system considered as homogeneous electric line,

• the traction substation with both *LC* branches and the substitute reactance of the traction transformer,

• the electric locomotive similar to current generator of harmonic components.

3.1. Phase of analysis No. 1

The distortion of sine wave contact system voltage depends on:

• electrical parameters of contact line system.

• distance of electric locomotive from the traction substation,

• values of the 3rd and 5th locomotive current spectral components.

The analysis is based on the electrical parameters of the contact line system having following values per kilometer [2]:

• inductance $L \cong 1mH/km$,

• capacitance $C \cong 15nF/km$.

The characteristic (surge) impedance that is independent on length of contact line system is $Z_0 = 258{,}2\Omega$ and the phase-shift constant for the 50 Hz spectral component is $\alpha_1 = 1{,}217 \cdot 10^{-3} rad/km$. The absolute value of the input impedance of non dissipative contact line with length $l_{TV} km$ is:

$$|Z_{TV}| = Z_0 \cdot tg(\alpha_1 \cdot l_{TV} \cdot n) \qquad (7)$$

3.1.1. Example to the phase of analysis No. 1

Let the situation is described with these values:

• the distance of the electric locomotive from the traction substation $l_{TV} = 25km$

• the 50 Hz component of the locomotive primary current $I_{LOK,(1)} = 200A$,

• the percentage of the locomotive current harmonic components $I_{LOK,(n)} = \frac{100}{n}\%$.

According to the Ohm′s law:

• the 3rd component of the locomotive voltage is 1572 V (5,7 % of nominal voltage),

• the 5th component of the locomotive voltage has the same value.

The same values correspond for the feeding system of double track contact line system as well, because both FCE′s *LC* branches formed signified short circuits for the 3rd and 5 rd components.

3.2. Phase of analysis No. 2

This phase of analysis deals with current harmonics from the 7th (350 Hz) up to the proximity of the first resonant frequency of the whole traction feeding system.

Supplementary electric parameters should be newly defined:

• the substitute reactance of the traction transformer $L_{TT} = 23mH$,

• the capacitance of the capacitor group for the 3rd harmonic branch $C_3 = 6\mu F$,

• the inductance of the 3 rd harmonic branch coil $L_3 = 188mH$,

• the capacitance of the capacitor group for the 5th harmonic branch $C_5 = 2\mu F$,

• the inductance of the 5 th harmonic branch coil $L_5 = 203mH$.

The definition of the whole substation substitute impedance forms the first step of this analysis phase. This whole substation is composed of:

• substitute reactance of traction transformer,

• substitute inductance of the 3rd harmonic branch (350 Hz >150 Hz),

• substitute inductance of the 5th harmonic branch (350 Hz >250 Hz).

Common formula for the substitute inductance $\overline{L}(f)$ of the LC branch in case that the frequency f is higher then the resonant frequency $f_{LC,REZ}$ of the LC branch is:

$$\overline{L}(f) = L \cdot \left[1 - \left(\frac{f_{LC,REZ}}{f}\right)^2\right] \tag{8}$$

According to this formula, for example, the substitute inductances of the LC branches have following values on the 7th harmonic:

- the 3rd harmonic LC branch $\overline{L}_{3,7} = 153mH$,
- the 5th harmonic LC branch $\overline{L}_{5,7} = 99{,}4mH$.

These two substitute inductances and the substitute reactance of the traction transformer are connected in parallel. Thus the substitute inductance of the whole substation is $L_{TNS,7} = 16{,}65mH$ for the 7th harmonic.

Provided that ***the single track-rail*** contact line system has from the viewpoint of the locomotive following components on the 7th harmonic:

• the contact line system between the locomotive and the traction substation,

• the traction substation represented with its substiute inductance $L_{TNS,7}$ formed the shunt impedance of the homogeneous electric line.

The input impedance $Z_1(n)$ of the finite length of the homogeneous electric line with shunt impedance $Z_2(n)$ is commonly:

$$Z_1(n) = Z_0 \cdot \frac{Z_2(n) + j \cdot Z_0 \cdot tg(\alpha_1 \cdot n \cdot l)}{Z_0 + j \cdot Z_2(n) \cdot tg(\alpha_1 \cdot n \cdot l)} \tag{9}$$

This common formula could be written in analyze of situation:

$$Z_1(n) = j \cdot Z_0 \cdot \frac{100 \cdot \pi \cdot n \cdot \overline{L}_{TNS} + Z_0 \cdot tg(\alpha_1 \cdot n \cdot l_{TV})}{Z_0 - 100 \cdot \pi \cdot \overline{L}_{TNS} \cdot tg(\alpha_1 \cdot n \cdot l_{TV})} \tag{10}$$

The result is for example *on the 7th harmonic* $Z_1(7) = j \cdot 95{,}37\Omega$.

Three supplementary assumptions in the case of ***the double track-rail*** contact line system are:

• lengths of both contact lines are equal,

• the locomotive is situated at the end of the contact line system,

• the other contact line system is unloaded.

The input impedance of the unloaded contact line system $Z_{TV,2}(n) = -j \cdot Z_0 \cdot \cot g(\alpha_1 \cdot n \cdot l_{TV})$ have to be connected in parallel to the substitute impedance of the whole traction substation.

The formula for the input impedance $Z_2(n)$ of the whole feeding system with double track line is from the viewpoint of the locomotive:

$$Z_2(n) = j \cdot Z_0 \cdot \frac{100 \cdot \pi \cdot n \cdot \overline{L}_{TNS} \cdot [\cot g(\alpha_1 \cdot n \cdot l_{TV}) - tg(\alpha_1 \cdot n \cdot l_{TV})] + Z_0}{Z_0 \cdot \cot g(\alpha_1 \cdot n \cdot l_{TV}) - 200 \cdot \pi \cdot \overline{L}_{TNS}}$$

For example the result is ***on the 7th harmonic*** $Z_2(7) = j \cdot 96{,}66\Omega$.

The difference of both values $Z_1(7) = j \cdot 95{,}37\Omega$ and $Z_2(7) = j \cdot 96{,}66\Omega$ from the viewpoint of the locomotive could be explained as follows:

• the input impedance of the whole traction substation is $Z_{TNS}(7) = 100 \cdot \pi \cdot 7 \cdot L_{TNS,7} = 36{,}62\Omega$

• the input impedance of the unloaded contact line system is $Z_{TV}(7) = -j \cdot Z_0 \cdot \cot g(\alpha_1 \cdot 7 \cdot l_{TV}) = 1194{,}2\Omega$

The connection of the unloaded contact line system to the substation has ***for the 7th harmonic*** component no essential influence upon the input impedance from the viewpoint of the locomotive.

3.2.1 Example to the phase of analysis No. 2

In a similar way it is possible to calculate the 7th spectral component of the contact voltage line system on the locomotive pantograph. The value of the 7th locomotive spectral current component is $I_{LOK,7} = \frac{200}{7} = 28{,}57A$.

The input impedances from viewpoint of the locomotive have ***for the 7th harmonic*** component approximately equally values $Z_1(7) \cong Z_2(7) \cong 96\Omega$ .The voltage 7th component in the locomotive pantograph is therefore $2743V \Rightarrow cca10\%$ of the nominal traction voltage.

3.3 Phase of analysis No. 3

The input impedance of the whole traction feeding system (traction substation, both LC branches, contact line system of single or double track) could be derived on the condition, when the input impedance reaches theoretically unlimited value.

According to this theorem and all input of example's parameters we can make up three values of the resonant frequency:

• the **first** resonance frequency $f_{REZ,1} = 141{,}0Hz(n_{REZ,1} = 2{,}82)$ this frequency is practically independent on the length of contact system,

- the **second** resonance frequency $f_{REZ,2} = 238{,}5 Hz \left(n_{REZ,2} = 2{,}82\right)$ this frequency is practically independent on the length of contact system too,
- the **third** resonance frequency $f_{REZ,3}$ depends on the length of contact system and as follows in Table 2.

*Table 2: Dependence of the **third** resonance frequency $f_{REZ,3}$ on the length of contact system*

No. of tracks	Double track		Single track	
Lengt $l_{TV}\,[km]$	$f_{REZ,3}\,[Hz]$	n_{REZ}	$f_{REZ,3}\,[Hz]$	n_{REZ}
25	1215	24,3	1565	31,3
30	1085	21,7	1385	27,7
35	990	19,8	1240	24,8
40	910	18,2	1130	22,6
45	840	16,8	1035	20,7
50	785	15,7	955	19,1

Remarks to this table are:

- The 1st and the 2nd resonance frequencies are dependent first of all on parameters of both *LC* branches and that is why they are independent on the length of contact line system. This values are situated far a field from the odd harmonics (the 3rd and the 5th) produced by the locomotive.
- Further harmonics occur above the 3rd resonance harmonic, because the function „cotangent" is periodical. For example the 4th resonance harmonic component of double track 25 km is $f_{REZ,4} = 2580 Hz \left(n_{REZ,4} = 51{,}6\right)$.

4. FINAL COMPREHENSIVE RESULTS FROM ALL THREE PHASES OF THE ANALYSIS

A) The voltage distortion of the contact line system in the proximity of the electric locomotive going at the line end is under supposed traction feeding system configuration differ for the analysed frequency components.

B) The results of phase analysis No. 1 for the 3rd and 5th harmonic components are under supposed conditions lower than 7th, 9th etc. harmonic components discussed in the phase analysis No. 2.

C) Figure 1 describes the per cent voltage distortion of the harmonic components with harmonic order from 3 up to 15 for lengths of single track line 25 up to 50 km. Figure 2 describes the same for a double track line.

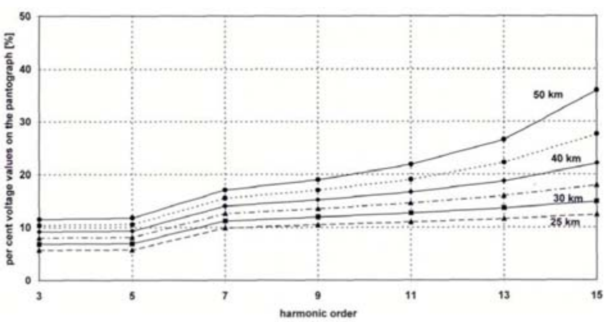

Figure 1: Per cent voltage values on the locomotive pantograph located at the end of the single track feeding line

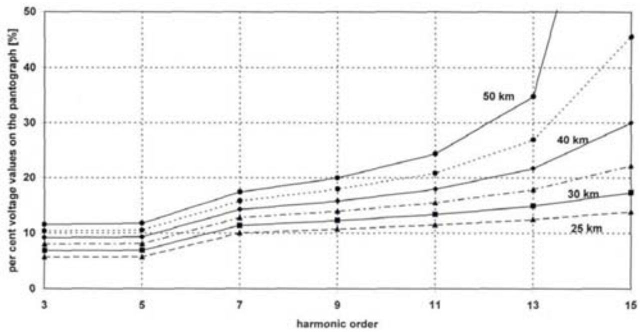

Figure 2: Per cent voltage values in the locomotive pantograph located at the end of the double track feeding line

D) The straight lines connecting the calculated points are valid only as visual aid, not for interpolation.

E) Figure 3 gives an answer to the analysed above point of view A) special for the 5th harmonic component percentage distortion for locomotive currents 50 Hz from 50 A up to 200 A.

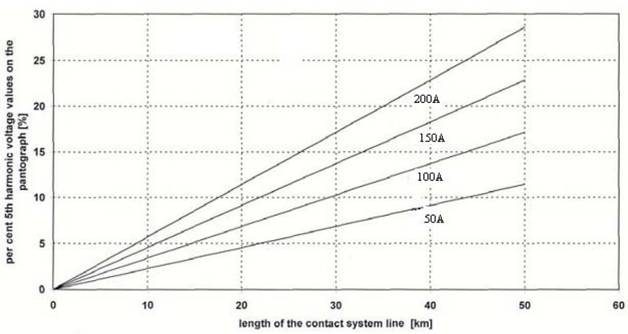

Figure 3: Per cent 5th harmonic values of the voltage on the pantograph going at the end of the feeding line

F) Figure 4 is based on the results of all three analysis phases for the traction substation output voltage with the utilization of contact line system electric simulation on the frequency from the 7th up to 15th and length of double track line from 25 km up to 50 km.

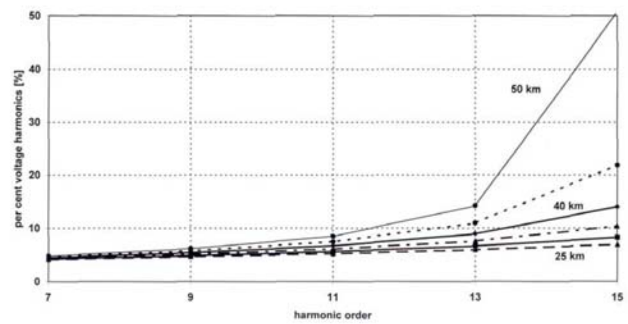

Figure 4: Harmonics of the traction substation output voltage for the double track line and for the locomotive going at his end

G) The traction substation output voltage 3rd and 5th spectral components are omitted, because they are under supposed conditions short cut with the both *LC* branches.

H) Figure 5 describes single and double track line resonance frequencies of the whole traction feeding system for the length from 25 km up to 50 km.

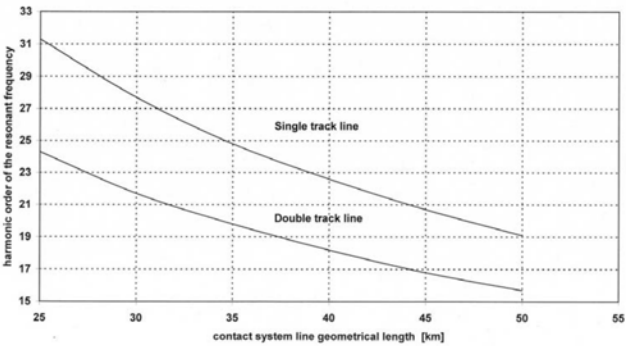

Figure 5: Dependence of the whole traction feeding system resonant frequency on the contact system line geometrical length

I) The voltage distortion of the contact line system for frequencies in proximity to the resonance frequency of the whole traction feeding system is essentially dependent on the rate of traction feeding system damping due to the traction real power consumption. None analysis has been given for these frequencies laying in working railway conditions above the 15th, because their influence on the locomotive traction converter in the mode of regenerative breaking and on the electricity meters is assumed to be negligible.

J) Figure 6 describes *THD* values of the contact voltage line system for the locomotive at the end of the single and double track feeding system, on frequencies from the 3th up to the 15th and length from 25 km up to 50 km.

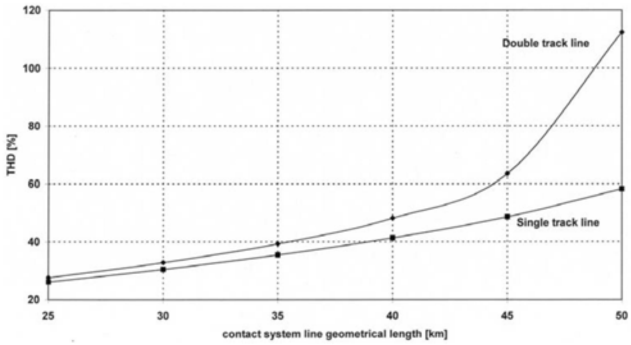

Figure 6: THD Voltage values on the pantograph going at the end of contact system line

K) Figure 7 describes THD values of the traction substation voltage output for the double track line.

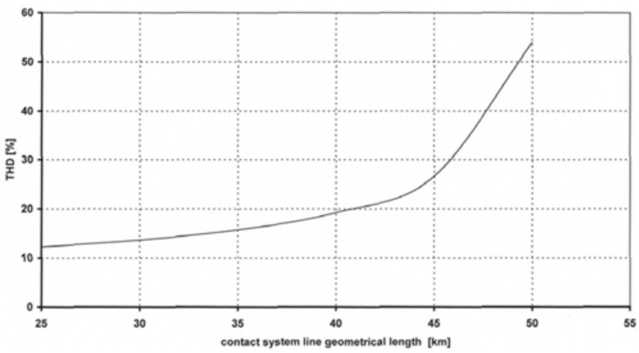

Figure 7: THD of traction substation output voltage

L) The voltage spectral components and *THD* values on the unloaded track line are in the whole length the same as the traction substation output voltage spectral components.

M) The voltage spectral components values for 4 points of the loaded line laying between the traction substation and the feeding line end are described on Figure 8 for the locomotive approaching the end of the track line and for the line length of 25 km.

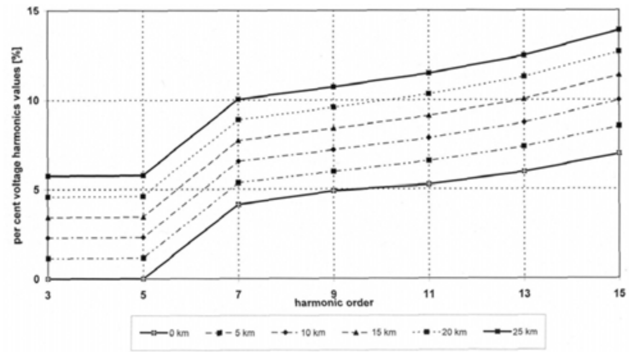

Figure 8: Contact system line voltage harmonics in individual points for system length 25 km and the locomotive at the end of this line

N) The *THD* values of contact voltage line system on various points of the contact line with the length 25 km and the locomotive at the end of the line comprises Fig. 9.

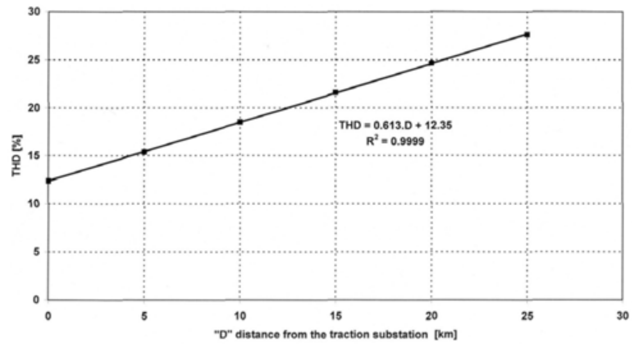

Figure 9: THD of the contact system line voltage for the system length 25 km and locomotive at the end of this line

O) Figure 10 describes the same case like Fig. 8, but for the line length 50 km.

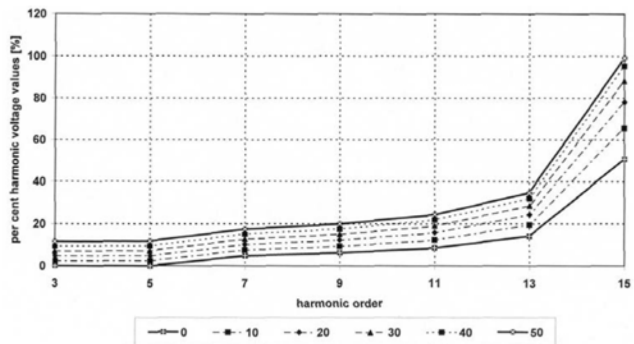

Figure 10: Contact system line voltage harmonics in individual points for the system length 50 km and locomotive at the end of this line

P) Figure 11 describes the same case like Figure 9, but for the line length 50 km.

Q) Figure 12 gives an comprehensive result of the contact voltage line system *THD* values on various points of contact line (expressed in %) for line length 25 km up to 50 km, the locomotive at the end of the line, with addition of regression curves.

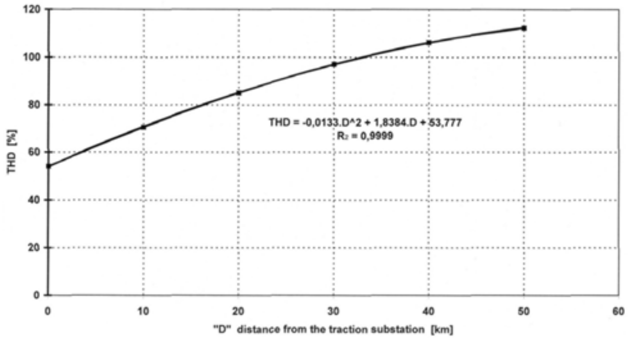

Figure 11: THD of contact system line voltage for the system length 50 km and locomotive at the end of this line

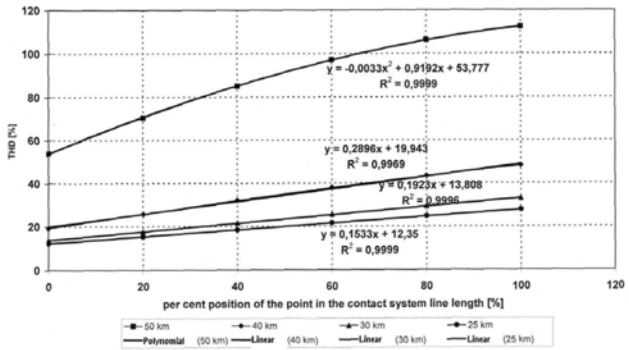

Figure 12: THD of the contact system line voltage in individual points of the contact system

5. MEASUREMENT RESULTS

For objective verification of descriptived results used the apparatus to measure instantaneous values of voltage and current was designed for long term monitoring. The whole equipment consisted of an industrial computer, data acquisition converter card, input transducers, cables, and special software.

Figure 13 shows a block diagram of the measuring process in the traction transformer substation.

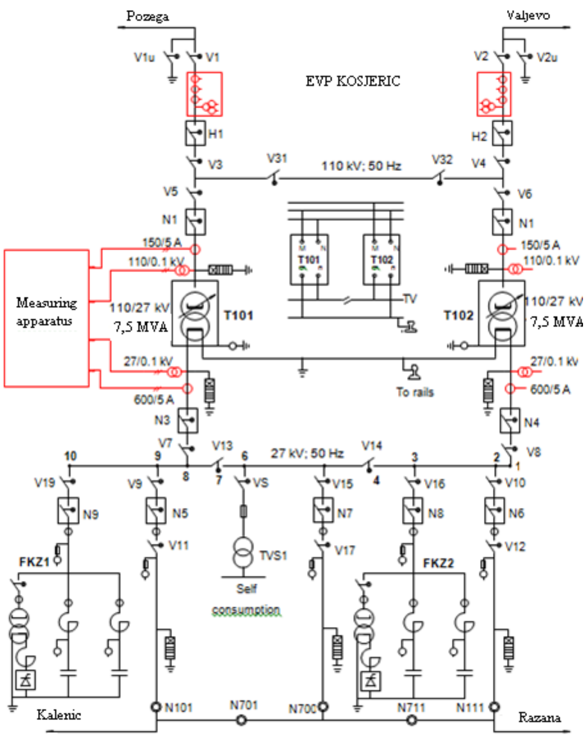

Figure 13: Simplified diagram of traction transformer substation with connected measuring equipment

Measurements were carried out at the traction transformer substation in Kosjeric, Serbian Railway, on July 11-17, 2013. Measurements of harmonics were carried out on 110kV high voltage network. Total harmonic distortion was calculated according to standards, as a 95% percentile.

Illustrations of total harmonic distortions of voltages in 110kV high voltage network at Kosjeric substation are presented in Figure 14.

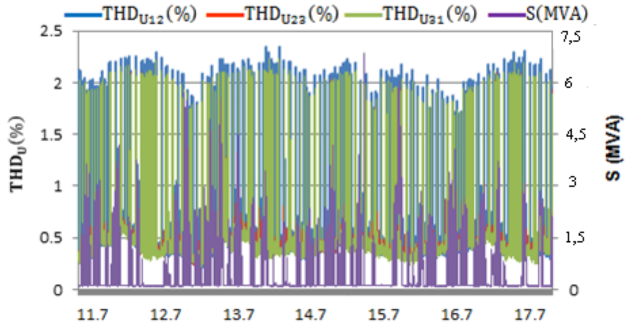

Figure14: THD_U at Kosjeric substation on 11-17.07.2013.

Simulation focused on line-to-line voltage harmonic distortion in a 3-phase 110 kV system which was influenced by single-phase traction load. Simulation was carried out with described above analysis. In the coupling point, a locomotive can be represented by several current harmonic generators, whose frequencies are multiples of the fundamental harmonic. Simulation was carried out for odd harmonics from 1st to 19th. Values of current harmonics were put in in accordance with measurement results.

Figure 15 shows the results of harmonic voltages simulation at Kosjeric substation.

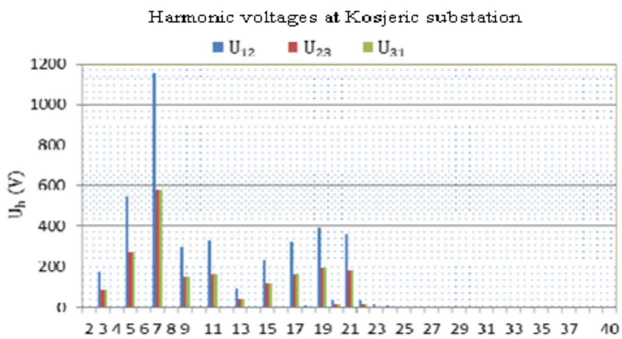

Figure 15: Voltage harmonics at Kosjeric substation: simulation results

Line-to-line voltage U_{12} harmonics are considerable, due to the single phase load connected to the system. This load also causes differences in voltage amplitudes in the threephase system, i.e. voltage unbalance. The highest values are typical of low orders odd harmonics, such as 3rd, 5th and 7th harmonic component. 7th harmonic has the highest value. From 21st harmonic on, values are very low for both substations. Generally speaking, single-phase nonlinear loads cause high 5th and 7th harmonics. The fact that 5th harmonic is lower than 7th can be attributed to negative sequence impedance of electrical machines, or to long line resonance.

3rd and 7th current harmonics are higher than the rest, 3rd and 9th voltage harmonics are lower than 5th and

7th harmonics, and they show a rather constant level with no obvious load variations. A comparison of current harmonics between measurements and simulation results, is shown in Figure 16.

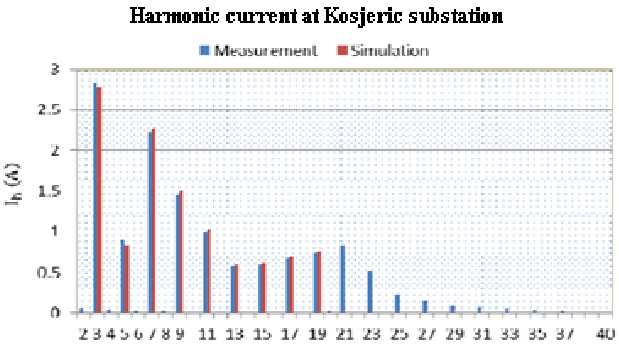

Figure16: Comparison of current harmonics for measurement and simulation at Kosjeric substation

Total harmonic distortion for Kosjeric substation was larger for simulation than for measurement. At substation, the highest simulated $THD_{U12}(\%) = 1.2787\%$, the highest harmonics being 5th and 7 th. The highest recorded $THD_{U12}(\%) = 0.9872\%$, where 5th and 7th harmonics were dominant again.

Considering the simulation process as opposed to reality, simulation could be more favorable than measurement. These differences can be caused by some error in measurement, the influence of thyristor regulation of current in the decompensating reactor or voltage distortions in the feeding distribution network.

Table 3 shows line-to-line voltage total harmonic distortions for Kosjeric substation.

Table 3: Total harmonic distortion of voltages (THD_U) for Kosjeric substation

	Content	Total harmonic distortion		
		THD_{U12} [%]	THD_{U23} [%]	THD_{U31} [%]
Kosjeric	Measurement	0,9872	0,7518	0,6088
	Simulation	1,2787	0,636	0,6372

6. CONCLUSION

An analysis of harmonic measurement results was carried out according to international standards and technical reports regarding power quality in distribution networks. Maximum measured values were compared with those given by the standard (maximum 95% weekly values were not reached). Maximum measured values were much lower than limits given in the IEEE Std. 519-1992 standard (2.5% on power supply 110kV) and EN 50160 (8%). Hence, evaluation of the measured data proved that harmonic distortion of the voltages at Kosjeric substations met conditions specified by standards for the operation of distribution systems.

Simulation results for all three substations were compared. Maximum *THDU* value was simulated for Kosjeric, for U_{12} line-to-line voltage, the highest harmonic being 5th and 7 th . That is caused by single-phase load connected to this phase. Simulation results were later compared with measurement results for all three measuring points, for all three line-to-line voltages. Both measurement and simulation results were within the limits stated by IEEE Std. 519-1992 and EN 50160. Differences were found between measurement and simulation results for line-to-line voltage U_{12}, while for the other two voltages the differences were insignificant.

Differences between measurement and simulation results may have been caused by a lack of data. Measurement results for even harmonics were higher than their simulated results, probably due to thyristor regulation of current in the decompensating reactor, or some measurement error.

ACKNOWLEDGEMENTS

This work was supported by the Serbian Railways . The authors would like to thank for this support.

REFERENCES

[1] T. T. Vo: "Effect on Power quality of the electric railway traction in distribution power network," Proceedings of the 13th International Scientific Conference Electric Power Engineering 2012, Brno (Czech Republic), November 2012, pp.13-16,(2012)

[2] B.Gavrilovic: "Modelling the Harmonic Components of Voltage and Current in Electric Traction Supply System of the "Serbian Railways,"" Journal of Electrical and Electronics Engineering (JEEE), Vol. 3(1), pp. 77-83, (2010)

[3] J.Altus, M. Novak, A. Otcenasova, M. Pokorny and, A. Szelag: "Quality parameters of electricity supplied to electric railways," Scientific Letters of the University of Żilina - Communications, Vol. 2-3, pp. 19-34, (2001)

[4] F. Foiadelli, P. Pinato and D. Zaninelli, "Statistical Model for Harmonic Propagation Studies in Electric Traction Supply Systems", Proceedings of 11th International Conference on Harmonics and Quality of Power, Lake Placid (USA), 12-15 September 2004, pp.157-164, (2004)

[5] R. Langella, A. Sollazzo and A. Testa, "Modeling Waveform Distortion Produced by DC Locomotive Conversion System," Part 1-2 in Proceedings of 11th International Conference on Harmonics and Quality of Power, Lake Placid (USA), 12-15 September 2004, pp.124-132, (2004)

[6] A. Dán, J. Kisvölcsey and Gy. Varjú: "Filtering of harmonics generated by thyristor controlled AC traction systems," Proceedings of 2nd International Conference on Harmonics in Power Systems, Winnipeg, 6-7 October , 1986, pp. 404-413, (1986)

[7] D.Kostic, N.Jevtic and P.Markovic: "Testing Methods and Analysis of the Main Electrical Properties of Modernized Locomotives," International Journal for Traffic and Transport Engineering (IJTTE), Vol. 1(2), pp. 108 – 114, (2011)

[8] J. Paleček, V. Kolář, V. Stýskala, P. Mičulka and T. Zaruskaia: "Analysis of the Impact electric chariots on the power system - measurement of asymmetry," Proceedings of the fifth international scientific symposium on Electric Power Engineering, Košice (Czech Republic), October 2009, pp. 2454-2458, (2009)

Development of Key Performance Indicators for Maintenance of the Railway Signalling System

Margarita Georgieva[1*], Nelly Stoytcheva[1]
[1] Department of Telecommunication and Signalling, Todor Kableshkov University of Transport, Sofia (Bulgaria)

The railway infrastructure asset needs an innovative and integrated solution for interoperability requirements for the improvements in safety and security, reliability and maintainability. Properly planned maintenance not only ensures the safety and performance, but also creates additional value in the business process. The purpose of maintenance management is to increase the safety of the system at minimal cost.

In this regard, the development of key indicators (MPI - Maintenance Performance Indicators) for maintenance management of rail safety equipment during the life cycle is particularly important.

An important issue for the maintenance management of rail safety equipment is to check whether activities undertaken maintenance provide the expected results linked to technical, economic and organizational issues. It is also necessary to classify the degree of effect for each MPI, i.e. create logical causal structure.

The main purpose of this paper is to identify and analyze indicators of the quality of maintenance of the Railway Signalling System, and their use in the planning, operation and maintenance of the railway infrastructure, find a structured, reliable and cost-effective method using these key indicators to facilitate the functioning of the maintenance process and the process of decision-making.

Keywords: Maintenance, Key Performance Indicators, Maintenance management

1. INTRODUCTION

In full compliance with the national vision and priorities, the mission of the transport sector has been formulated in *Strategy 2012-2021* of the National Railway Infrastructure Company (NRIC), as follows:

The main goal of the transport sector of the Republic of Bulgaria is to facilitate the economic and social development of the country by:

- Providing efficicient (with maximum benefit), effective (with minimum costs) and sustainable (with minimum external influences) transport

- Supporting a balanced regional development

- Assisting in the full integration of the Republic of Bulgaria in the European structures, taking into account its crossroad location and transit potential.

The following vision for the development of the transport sector has been derived on the basis of the principles mentioned above:

By 2020 Bulgaria should have a modern, safe and reliable transport system in order to satisfy the demand for high-quality transport services and to provide better opportunities for citizens and business.

Modernising the transport system is a prerequisite for its successful integration within the European transport system. It represents also an important prerequisite for improving the quality of life, for rapid economic growth and for improving the environment.

2. MAINTAINANCE RAIL POLICY

Infrastructure improvement is an important and crucial condition to increase both the country's attractiveness for foreign investors and the competitiveness of Bulgarian economics. This calls for complex and interrelated development of the various types of transport – railway, bus, water, air, and intermodal. The government for European development of Bulgaria formulates the major activity priorities in the field of transport:

- Ensuring easily accessible and safe transport in all regions of the country.
- Maintenance, modernization, and construction of transport infrastructure.
- Creating conditions to oppose effectively unloyal competition in the transport sector.
- Improvement of project management and implementation, EU funds including.

The successfully implemented transport policy contributes to improvement of human life quality.

Subject to Art. 25 (1) of the Railway Transport Act, the State participates in the financing of activities related with the construction, maintenance, development and operation of railway infrastructure. The funds provided by it on an annual basis through the State Budget Act, are targeted with priority to sites of close national interest for which no financing may be provided under international programmes and funds, which are provided through capital transfers.

To provide for unbiased planning of the required funds for repair and maintenance of railway infrastructure, the NRIC introduced annual and long-run planning mechanisms and planning system. The expiration of the contract between the State and the NRIC called for development and signing of a new 5-year contract valid until 2015. The indicators in the contract between the State

*Corresponding author: 158 Geo Milev Str. 1574 Sofia, Bulgaria and margarita_georgieva@abv.bg

and the NRIC can be measured objectively – rating grade for the condition of the railroad by a track measurement laboratory, implementation of the train-kilometre work, reduction of the number of accidents on the railroad and more. For better optimization of the Company's activity and for the purpose of evaluating the implementation rate of the objectives and tasks assigned to it, new indicators were introduced in the new contract. Through these new indicators the Manager undertakes:

• to not allow the amount of liabilities to providers and staff for the current year to exceed the amount of liabilities from the previous year, except where such increase is justified by objective reasons.

• to optimize its activity-related costs and to report the progress through the indicator „operational costs per one person occupied".

• to optimize the number of staff per one kilometer of railroad

As an inseparable part of the Contract, new methods were also developed to account for the above-mentioned indicators, which constitute a set of indicators whose values assess the successful or failed implementation of the indicators and in case of failed implementation, the Manager is imposed sanctions whose amount is determined after the methods.

As a result of the provision of funds out of the State budget, commensurate with the needs of railway infrastructure, during the recent years, high results were achieved with respect to the following indicators:

- increase of traffic speeds in the repaired sections of the railway network;
- increase of carriage safety by reduction of the number of accidents occurred through the fault of the NRIC;
- increase of railway infrastructure quality, as measured by the rating grade.

The development, modernization, maintenance, and repair of railway infrastructure is a complex and continuous process, which depends not only on work organization, but on the provided financing as well.

The reduction of operational costs for the maintenance of second-class and losing railway branches and the security of decommissioned railway lines, as well the lack of orders from carriers for the provision of freight or passenger carriage, called for termination of the operation and dismantling of 133 km of railroad, with subsequent complete or partial recultivation of the track at a later stage, after the relevant findings and decisions of the committees nominated for the purpose.

So far, a procedure has been carried out in keeping with the order and terms of the Ordinance on Assignment of Small Public Procurement and 6,550 km of the 86-th railway line (Bourgas–Pomorie deviation) have been dismantled. Work is underway to conduct a public procurement for the conclusion of framework agreement for mechanical lifting, carriage, storage, and dismantling (disassembly)of the upper construction of the remaining 126,450 km of railroad. The railroad thus dismantled will be assessed by experts from the *Railroad and Railway Equipment Department, whereas the railway material fit for further use* will be accounted for on the balance sheet and used for current maintenance and repair of the railroad, while the left-over metal scrap (rails, connecting and fixing material) will be sold under the terms established so far.

Dismantling of another 259,873 km of station tracks and 808 pcs. of railway switches is envisaged, as well as re-cultivation of the terrain cleared out after such dismantling.

The development objectives for Bulgarian railway infrastructure are determined based on the objectives of the European Transport Policy, the national transport policy, including economic agreements, plan criteria and the way in which the different operational activities and maintenance activities will be allocated among the individual territorial units and the way in which they will be implemented (Fig. 1).

The AMS (Asset Management System) of the NRIC should comprise and combine any types of dedicated systems for observation, data collection, and assistance of the decision-making process. This is valid not only for the railroad, but also for all other railway infrastructure components, such as bridges, switches, and junctions, contact networks, levels, tunnels, drains etc. AMS should also be furnished with certain aspects, such as management of environment and risks, as well as with emergency response systems.

Upon its integration, the AMS should service everybody who is related in some way or other to the railway system, such as the owner of the infrastructure, the contractors of various types of works, the railway operators, and everybody else. Each of these organizations should be able to use the AMS, to retrieve data for operational or long-term strategic objectives, as well as to feed relevant data into the system.

The final „design "of the system should provide for problem-free integration of geographic mapping, database management, and multimedia technologies for effective data use in modern railway environment. It should also comprise some technologies, such as Internet, so as to be able to provide global access to the whole railway information and to create conditions for quick and easily centralized data management. Moreover, it should perform some functions, such as information exchange between the different users and their departments, updating of the database, and integration of the digital information exchanged between the users.

3. KEY MAINTENANCE PERFORMANCE INDICATORS (MPIS)

The key maintenance performance indicators reflect the effectiveness of the performed maintenance works and compare infrastructure's actual condition with the specific established conditions (requirements/objectives). They are used to measure maintenance performance and should be associated with realistic objectives for taking the required decisions at the appropriate organizational level to provide for added value of the business processes. They are associated with reduction of idle time in case of failure, reduction of cost, and reduction of the wear-out of invested materials and equipment. On the other hand, their implementation is associated with increase of capacity, efficiency, quality safety, and working conditions

The key railroad maintenance performance indicators according to the Strategy for Development of the NRIC during 2012-2021 are shown on Table 1.

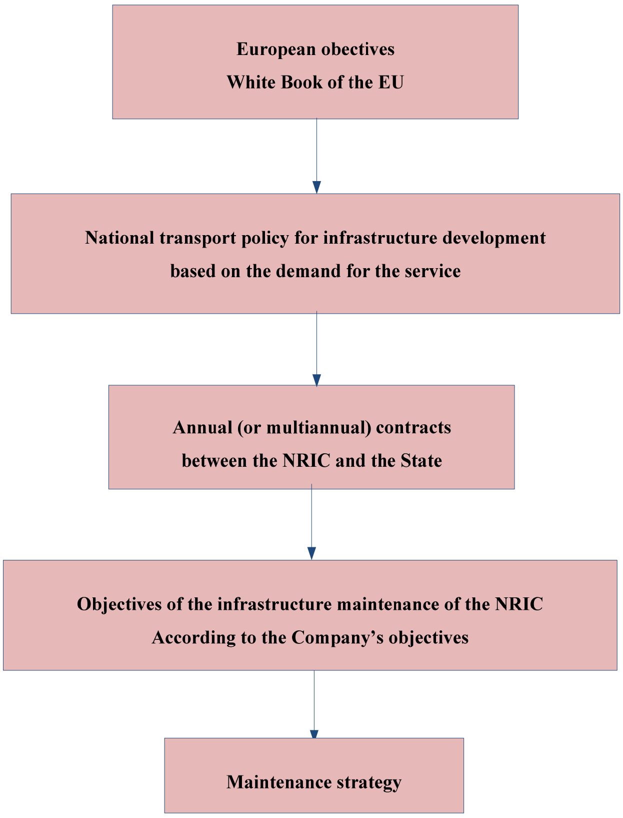

Fig. 1 Operational activities and maintenance activities allocated among the individual territorial units

Table 1: Key railroad maintenance performance indicators

Objectives of the NRIC	**Sub-objectives**	**Key railroad maintenance performance indicators**	**Relation with other stakeholders**
Provision of easily accessible and safe transport in all regions of the country.	Improvement of infrastructure use	Capacity use	Users
		Capacity restrictions	Users
	Reduction of death cases	Number of accidents with rolling stock	Users
		Number of accidents at levels	Users
Maintenance, modernization, and construction of transport infrastructure	Reduction of train delays	Railroad-caused train delays	Transport process
	Reduction of freight carriage interruptions	Railroad-caused freight train delays/ hours	Transport process
		Number of delayed freight trains because of the railroad	Transport process
	Enhancement of maintenance effectiveness	Number of train traffic interruptions because of the railroad	Transport process
		Railroad standardization rate	Transport process
		Standard allowance	Transport process
		Maintenance cost per km	Transport process
		Traffic amount	Financing
		Average speed km/h	Transport process
		Repaired railway lines – km	Transport process Financing
		Constructed railway lines – km	Transport process Financing
		Rehabilitated railway lines – km	Transport process Financing
		Use of recycled materials	Innovations
		Use of ecologically hazardous materials	Innovations

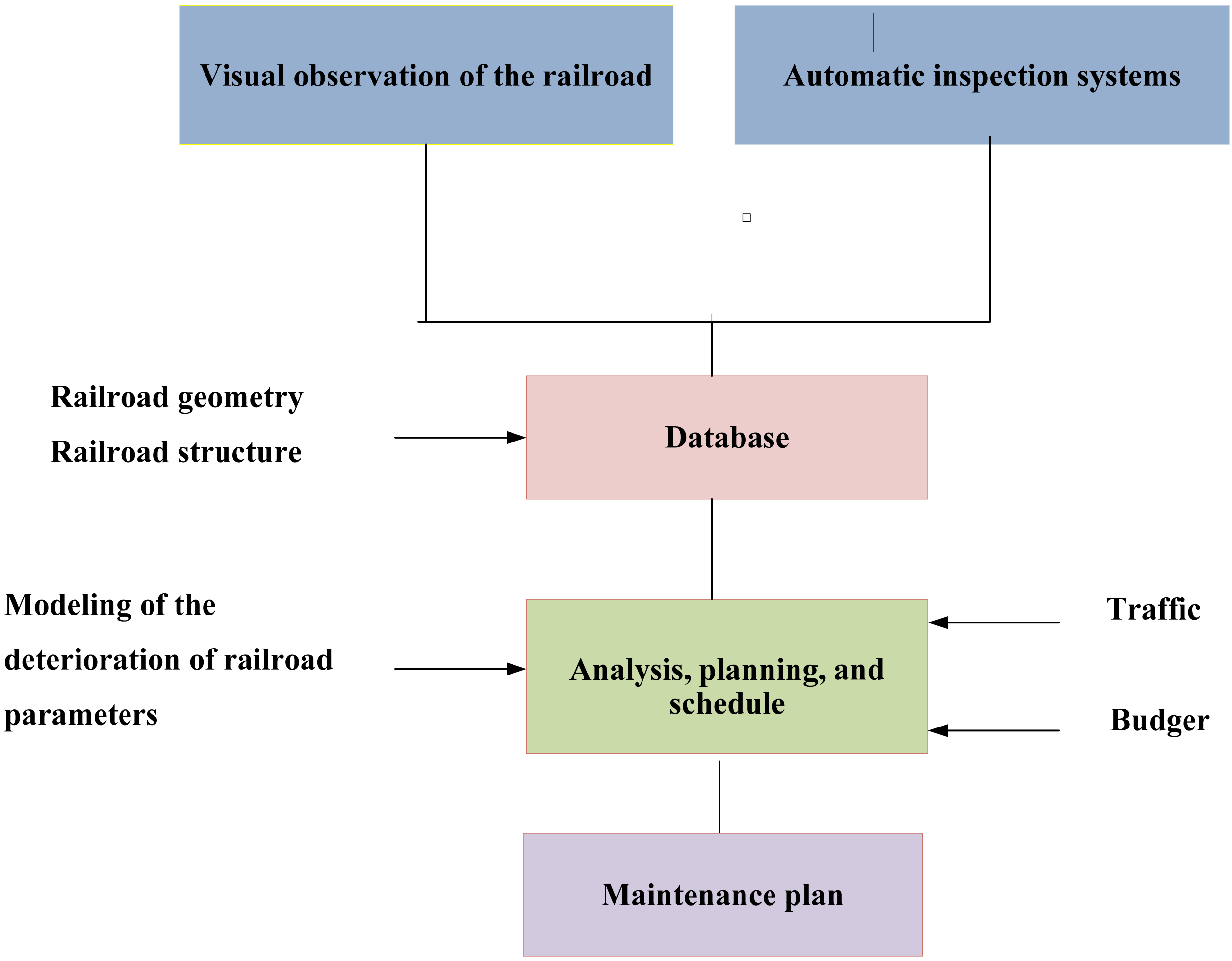

Fig. 2 Maintenance planning activities

4. MAINTENANCE PRESCRIPTIONS

To elaborate effective strategy and railway maintenance plan, the NRIC should observe the prescription provided in Figure 2.

5. CONCLUSIONS

Effective asset maintenance will result in increase of network capacity.

The effective planning of planned maintenance is based on the monitoring means for the railway network's condition, which results in reduction of maintenance time and improvement of maintenance logistics. The purchase of new mechanical equipment for monitoring and control of railway condition was considered in the previous points.

REFERENCES

[1] Strategy for the Development of the Transport System of the Republic of Bulgaria Until 2020

[2] Five year program for the development and using of railway infrastructure for the period 2011-2015

[3] Journal of Quality in Maintenance Engineering, 12, 2, 133-149.

[4] Espling, U. (2007) Maintenance strategy for a railway infrastructure in a regulated environment, Doctoral Thesis 2007:54, Luleå, Luleå University of Technology.

[5] Amaratunga, D. and Baldry, D. (2002) Moving from performance measurement to performance management. Facilities, 20, 5/6, 217-223.

[6] Andersen, B. and Fagerhaug, T. (2002) Eight steps to a new performance measurement system. Quality Progress, 35, 2, 112.

[7] http://www.communities.gov.uk/archived/publications/corporate/multicriteriaanalysis manual, (2007-11-07).

Effective Strategy for Maintenance of the Railway Assets

Nelly Stoytcheva[1], Margarita Georgieva[2*]
[1] Department of Telecommunication and Signalling, Todor Kableshkov University of Transport, Sofia (Bulgaria)

In accordance with the policy of the European Union increased the role of rail transport. To maintain the level of rail services in accordance with quality standards, all items in the rail system must function reliably in accordance with its intended purpose. This requirement is the basis of the management strategy for the maintenance of railway assets. Maintenance of all subsystems of the railway assets is a complex issue , making it difficult planning and execution of maintenance tasks . Maintenance is essential to ensure safety, strict observance of the schedule, the use of the full capacity and lower costs.

Major milestone in planning maintenance activities is detailed and comprehensive assessment of the technical condition of the assets. One important elements of the planning of maintenance is the cost analysis that includes a breakdown of the actions of unit operations and the necessary resources - material, human, time and administrative

The main objective of paper is based on the identification, analysis and comparison of existing strategies to form an effective strategy for comprehensive planning maintenance of railway assets by creating separate phases of decision models for optimization of the maintenance process.

Keywords: Strategy for Maintenance, Railway Assets, Assets management

1. INTRODUCTION

Bulgaria has vested interest in the development of international railway links. Building an appropriate transport infrastructure will create political and economic preconditions for commercial and industrial prosperity and democratic, market-oriented development of our country. Having regard to the fact that the European Commission will concentrate its funds on the development of the key transport nodes, Bulgaria should also focus its efforts on preparing and implementation of projects aimed at modernization of the railway transport sector.

According to the document *Programme for development and operation of the railway infrastructure 2012-2016*, most of the railway lines in Bulgaria (including those forming part of the trans-European transport axes) were built many years ago with geometries, formations and facilities designed for speeds not exceeding 100 km/h, the second tracks added during the last 20 to 30 years also have speed limitations due to their geometries, the condition of the formation and facilities, and the track systems within stations. The main railway line sections with breached maintenance cycles account for more than 30% of the total track length (TTL) and speed reductions apply to circa 5% of TTL.

The overall condition of the network infrastructure is such that it requires urgent measures for renewal, improvement and increasing the performance of tracks, catenary, communication and security equipment, with priority on the lines belonging to the trans-European technical corridors.

Despite the unsatisfactory condition of the railway infrastructure, it should still be the basis for determining the capacity of the transport network. This should be followed by designing measures for increasing the capacity and by economic assessment of the proposed enhancement of the transport network capacity.

2. MAINTENANCE AND OPERATION OF RAILWAY TRACKS

A certain set of track repair activities counteract the deterioration of track physical and geometrical condition during operation:

The scope, type and proportions of individual activities depend on many factors:

- Superstructure type;
- Load;
- Track and substructure specificities.

The type of repair has to ensure the required technical condition at optimum/minimum labour and equipment costs.

According to Article 3 of *INSTRUCTIONS ON THE REPAIRS OF LONG-TERM TANGIBLE ASSETS IN NRIC* the regular activities connected with the maintenance of long-term tangible assets are:

1. **Preventive maintenance** – all the planned preventive inspections, technical operations, routine and regular repairs aiming to reduce the probability of a failure or accident.

2. **Scheduled** preventive maintenance – periodic inspections of the condition of long-term tangible assets in accordance with regulations, aiming to reduce the probability of a failure or deterioration of the operation of a certain long-term tangible asset (unit, component).

*Corresponding author: 158 Geo Milev Str. 1574 Sofia, Bulgaria, margarita_georgieva@abv.bg

3. **Routine repairs** – maintenance as a combination of all technical and respective administrative actions, which aim to retain or restore a long-term tangible asset (unit, component) in or to a specified state in which it can perform its required functions.

4. **Overhaul** – complete or partial replacement or regeneration of major parts, structural elements and equipment representing long-term tangible assets as well as the works where existing but worn out materials, structural elements and structures are replaced, or new types of work are carried out to recover their serviceability, improve their efficiency, cut down production costs, improve the quality of offered product or service, and extend their service life.

Overhauls are of two types: planned and emergency.

Planned overhauls are carried out periodically based on evaluation of the technical condition of long-term tangible assets, in compliance with Article 12, paragraph 1. The need for such overhauls is substantiated before NRIC so that they can be included in short-term or annual investment plans. Depending on the approved financial resources under Article 6, NRIC management specifies the sites of priority to be funded in the year.

Emergency repairs are necessitated by unexpected unscheduled events like natural calamities (floods, storms, earthquakes, fire etc.), break-downs, accidents and others. Emergency repairs aim to recover an installation (unit) to the state in which it can perform its assigned functions.

2.1. Organisation

Overhauls in NRIC are carried out in the following ways:

1. By outsourcing the works to external contractors under the terms and conditions of the Public Procurement Act and the Regulation on awarding public contracts under the thresholds laid down in PPA Art. 70, paragraph 1;
2. Using its internal resources, namely by assigning the works to the various NRIC enterprises on the basis of assignment letters and memoranda of understanding.

If a project is implemented with the company's internal resources, but includes large volumes of works and related supplies of materials, which the responsible enterprise is unable to carry out itself because of not having the workforce or equipment to do so, such works and supplies are outsourced as minor services to external contractors. These services and supplies are always subject to terms and conditions of the PPA and the Regulation on awarding public contracts under the thresholds laid down in PPA Art. 70, paragraph 1.

The Investor in the overhaul projects is NRIC. The enterprises develop plans for funding the overhaul projects and submit them for approval to NRIC before the beginning of the financial year.

2.2. Funding of scheduled track maintenance activities

The scheduled track maintenance activities are funded from the following sources:

1. The state budget;
2. Infrastructure charges;
3. Own resources;
4. State-guaranteed loans;
5. EU funds;
6. Other operational revenues.

2.3. Structure of the Tracks and Facility chapter of the investment plan.

2.3.1. Guiding principles applied in planning the resources required for maintenance and repair of tracks and facilities:

- Prioritizing the required repairs;
- Maximum use of the company's own heavy machines for routine mechanized maintenance and repair activities;
- Installation of CWR (continuous welded rail) and neutralization of tensions;
- Provision of sustainable speed conditions for the Train Schedule;
- Stabilization of the rails-and-sleepers grid in the stretches where its condition is regarded as critical;
- Proactive endeavours for minimizing to the maximum possible extent the existing speed limitations, both temporary and permament;
- Reinstatement and reaching the design speeds.

2.3.2. Main items of the annual plan-programme

The itemized list of sites to be overhauled includes

- Percentage of the capital transfers in the overall budget;
- Percentage of the infrastructure charges in the overall budget;
- Works performed with own (internal) resources;

Works performed by external contractors („outsourcing").

2.3.3. Expected benefits

The realization of the planned repair works aims to achieve:

- Higher running speeds;
- Removal of permanent speed limitations;
- Stabilization of the subgrade;
- Sustainable Train Schedule;
- Continued efforts for improving the quality of surfacing at level crossings;
- Efficient use of the workforce directly involved in the maintenance operations;
- Improving the level of transport equipment/services available at railway sections;
- Reducing the proportion of manual and unattractive labour.

Account should be taken of the cumbersome and lengthy procedures for selection of contractors as per the

PPA. These can take up to 6 or 7 months and any appeal process thereafter can seriously disrupt the investment intentions (schedules). We believe that there is scope for improvement in this area and that the bureaucratic process can be simplified.

3. KEY ISSUES RELATED WITH THE TECHNICAL MAINTENANCE OF RAILWAY INFRASTRUCTURE

A high-quality approach to the planning of the technical maintenance of railway tracks and facilities requires understanding of the maintenance related problems.

The problems related with the maintenance of rail tracks in Bulgaria are clearly stated in NRIC's business plans and safety reports. For the most part they are financial ones. A systematic view of the problems looks like this:

• The railway tracks and related facilities continue to deteriorate in terms of technical condition. This is due to overdue maintenance cycles. The load bearing capacity and the reliability of the superstructure and the facilities are deteriorating. The process reaches a point where the condition of the tracks and facilities does not conform to the regulatory requirements.

• Insufficiency of technical specialists and operative staff

The insufficiency of heavyweight and lightweight specialised machinery and equipment means that labour in the railway sector is unattractive. Other problems stem from the never-ending reforms going on during the recent years. These factors also elicit, to a certain extent, a sense of uncertainty and many qualified staff members are leaving the company.

This issue should be addressed as a number of projects of national importance are starting or are about to start.

• Problems with the heavy track maintenance machines

The condition of the heavy track maintenance machines operated by the Track and Facilities division is very poor. The machines are heavily amortised as many of them were imported 25-30 years ago. There is direct correlation between the condition of the track maintenance machines and the condition of the tracks.

Another problem is the maintenance of the equipment and therefore the service guarantee. Where the equipment is maintained by the manufacturer there is a guarantee, but the maintenance costs are higher. Furthermore, each maintenance activity must be tendered under the PPA! Hence there is scope for improvement of the regulatory/legal base, i.e. there is a conflict between the legal framework and the requirements of the maintenance equipment manufacturers.

It should be borne in mind that the Bulgarian market for maintenance of specialised track maintenance equipment is limited, which translates in higher prices. The rail enterprises do not have the equipment required for purpose and as a result the repairs are of poor quality.

• Railway materials for proper maintenance

The financial gaps during the recent years have also resulted in undersupply of the required materials. In turn, this reflects on the quality of the repair works (i.e. the track parameters) and the maintenance cycles. As an illustrative example, the last major import of rails was in the year 1989.

In most tenders for materials, the only selection criterion is the price. However, there is a correlation between price and quality. It is advisable to require proof of quality, certificates, etc. This has direct bearing on the level of the repair works.

• Level and quality of control

With a system driven by condition-based maintenance of tracks and facilities, the guiding management principle is control.

The idea is to ensure that the control is a preventive one. It is about timely detection, evaluation and remediation of the problems in order to ensure the required level of safety.

There are two methods for exercising control – objective and subjective.

o Objective control by fault non-destructive testing of switches and rails.

This testing is carried out on annual and monthly basis in accordance with testing schedules. The main lines are tested two times per annum and secondary lines are tested once per annum.

The problems associated with this type of control stem from the outflow of specialists due to the unattractive working conditions and equipment. Teams of non-destructive testers and test equipment need to be setup in this area as a matter of urgency.

o Subjective control by periodic visual inspection of superstructure elements

Subjective controls are carried out by linesmen, stewards at weak points and technical personnel from the railway sections. This personnel exercises the routine daily controls.

In addition, visual inspections are carried out at certain intervals (one month) by heads of sections, technicians and team leaders.

By way of example, as a result of the never-ending structural changes at NRIC the number of railway sections (units) is down from 13 to 4 and as such the stretch to be monitored by each linesman has become much longer. According to statistical data, for an inspection to be efficient, the monitored stretch should be 4 kilometers long, and now it has reached 7 or 8 kilometers. This requires using more workforce or changing the technology. New sections may even require rosters of linemen.

The present tendency towards consolidation of the railway sections and reduction of the personnel directly involved in technical maintenance activities requires introduction of modern, highly productive equipment in order to ensure the quality of maintenance operations.

For example, acquisition of combined traction vehicles may significantly increase the length of the monitored stretch – a team of two linesmen can traverse 70 to 100 kilometers during natural windows.

3.1. Best European practices regarding railway infrastructure maintenance

3.1.1. Maintenance costs

Railway transport has risen up impulsed by the increase of demand in the last decade. Moreover, several

European States prioritize policies tending to transfer road transport (passengers and freight) to rail in order to reduce road congestion, and taking into account the inability to build new roads due to lack of land and space.

Longer operating time, higher number of services and trains increase the annual traffic load and accelerate the infrastructure deterioration; this results into an increase of the number, severity and frequency of renewal work and maintenance operations and, on the other hand, it has decreased the available time for maintenance as railway services posses the infrastructure and rolling stock most of the 24 hours of the day. The need for more maintenance and the increase of right-of-way, RoWtime to carry it out, is in conflict with the increment of the infrastructure use by train services to satisfy the demand.

In addition to the above issues, the European directive regarding infrastructure charges and capacity allocation (EU OJ, 2001) defines an organizational and regulatory framework tending to an optimization of the railway infrastructure.

All this factors have make maintenance costs scale severely and the infrastructure administrator and railway operator to balance these factors by management systems that provide a reasonable solution to users regarding many aspects of the service (quality, safety, cost).

The interest of all railway administrations and operators to keep costs bounded have fostered, in the last years, to invest efforts in R&D programmes to easy a practical solution to this problem

Orders of magnitude of maintenance costs in some sectors are presented in Cross (1988) as a percentage of the total operating costs.

These costs are affected by factors such as:

- ✓ increases of maintenance actions due to higher quality standards,
- ✓ increases of manpower costs of maintenance personnel,
- ✓ increases of management costs.

Preventing maintenance is an increasing area of importance due to the economic interest to reduce maintenance costs. Corrective maintenance tasks will be never avoided because of unexpected failures. These failures provoke disruption of the production/service and cause not only additional costs for production losses but additional malfunctions/damages to other related components and equipments.

Predictive maintenance is a step forward intended to minimize corrective maintenance. This is one of the most active area of research in maintenance, as it is most founded in inferring models that predicts the risk of failure and residual life of components, to integrate these single component models into the system model composed of its components, and finally to merge them into the equipment predictive model. The difficulties encountered in this bottom-up modelling process may end up with conservative prediction scheduling actions that might increase the maintenance actions subjected to the equipment over those strictly needed. This conservative behaviour gives lieu to an increment in the maintenance costs, due to earlier part replacement with still substantial residual life.

The four maintenance types can be coordinated under a scheduling scheme, by combining activities, in order to minimize the period of time the equipment is idle. This approach helps saving costs. This way of proceeding has also consequences. The replanning of the maintenance scheduling should be carefully optimized in order to avoid non-attention to previous maintenance scheduled tasks, which might additional increase costs.

4. STRATEGY FOR MAINTENANCE AND PRESERVATION OF RAILWAY ASSETS

4.1. Analysis

At national level, one of the major documents with reference to the future development of Bulgarian transport infrastructure and, railway infrastructure in particular, is the National Development Programme: Bulgaria 2020 whose development is currently underway. The major objective and one of the major priorities underpinning the working version of the document’ strategic framework is the construction of infrastructural networks providing optimal conditions for the development of economics and proper and healthy environment for the population. The major sub priorities related with the implementation of the major priority, Improvement of Transport Connectedness and Market Access are:

- Establishment of a sustainable railway transport system through sector reforming.
- Effective maintenance, modernization, and development of transport infrastructure.
- Integration of the Bulgarian transport system into the European one.
- Achievement of high degree of transport safety and security.
- Restriction of the negative transport impact on environment and human health.
- Sustainable development of mass public transport.

The analysis and the additional survey of the condition of railway infrastructure reveal that, as of now, in the technical aspect, the individual elements do not comply with the requirements of the Trans European Railway System. An entire set of factors is available impacting the poor technical condition of the railroad, power supply, contact network, signalling equipment (SE) and telecommunications (TC), which affect the quality of the railroad’s technical condition and equipment (artificial equipment, SE and TC), which results in reduction of the project speed along the major railway lines.

Figure 1 shows the ratio of traffic speed and project speed. With average project speed of 105, 2 km/h for the major railway lines, the allowed speed according to the schedule book is 83,7 km/h, i.e. a difference of 21,5 km/h is available which is quite appreciable.

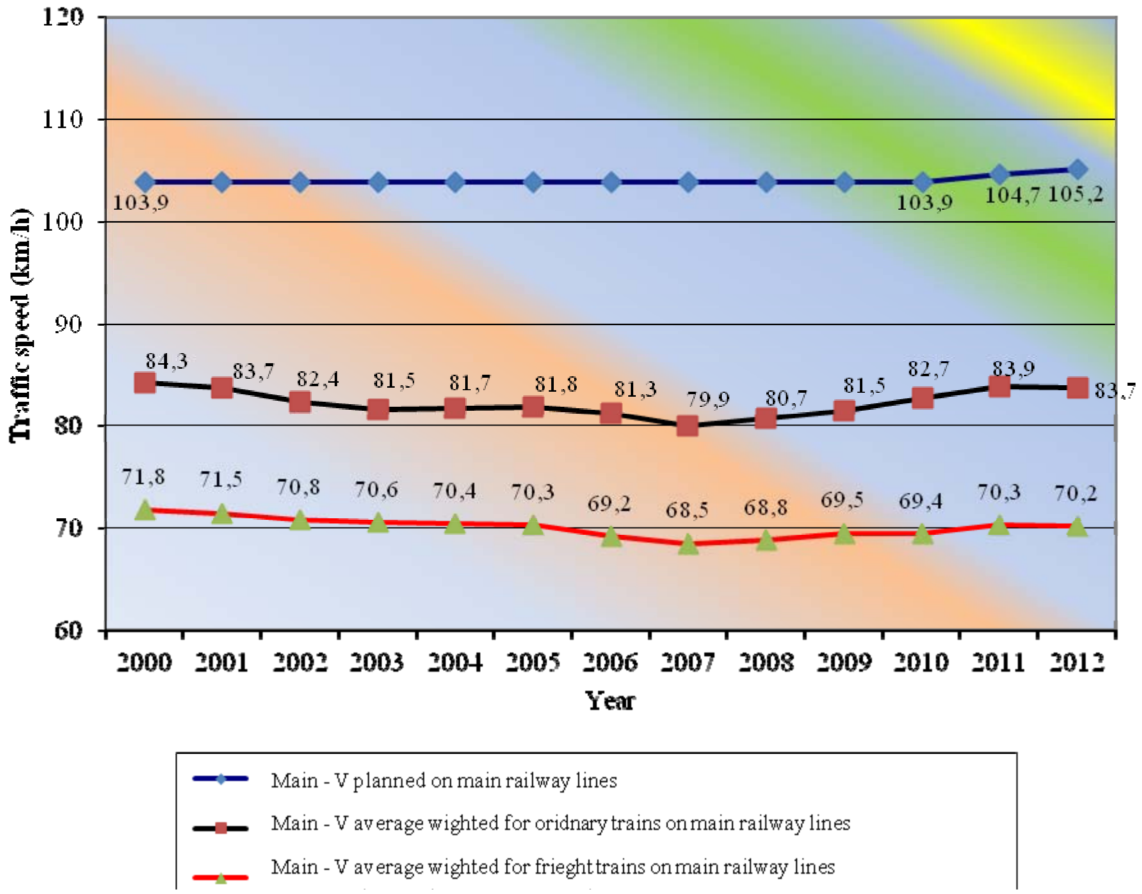

Fig.1 Average weighed trafficspeed depending on the railroad`s technical condition as of 31.03.2012

4.2. Maintenance strategy

The Maintenance Strategy has been formulated taking into account:

- the annual financing according to the Contract between the NRIC and the State;
- contracts with clients/contractors/organizations;
- contract duration, scope, payments to external contractors;
- contracts with operators and prepared train traffic schedule, while focusing on the effectiveness and ability to implement the schedule;
- normative regulations;
- safety requirements;
- pursuit for accurateness combined with competitiveness in traffic management and maintenance activities;
- available assets of various complexity, age, and standard;
- restricted access to the railroad during the implementation of maintenance activities;
- planning of the activities with time;
- life cycle cost (LCC) of the articles and total cost of asset management;
- Public Procurement Act.

Railways are facing the competition of the other types of transport, which calls to improve reliability, effectiveness and travelling time. The resulting requirements for increase of speed and axial loadings mean that the conditions under which railroad is operated are becoming increasingly hard. The establishment of a cost-effective railway network satisfying such need in future requires improving railroad monitoring methods and introducing reliable forecasting and planning methods.

The NRIC undertakes actions related with railway infrastructure monitoring (RIM), which is one of the most important components of the Asset Management System (AMS).

The overall managerial potential of the AMS depends very much on the quality of the available monitoring systems. Special attention should be paid to the monitoring techniques and assessment of railroad condition. The successful analysis of railroad condition and the subsequent management should be implemented in combination with other types of railway infrastructure. Other infrastructural sites and the means for their management should be considered. Special attention should be paid to the monitoring of lower construction, switches, and junctions, since their impact on railroad condition is significant.

The reason which requires monitoring is usually bilateral. Naturally, the first and immediate reason is the need to detect faults, which may jeopardize the safety and reliability of railway traffic. The monitoring technique should be continuous and sufficiently expedient to provide for the implementation of successive monitoring cycles at regular intervals. Thus, the exclusively important time aspect is observed, which is of primary significance to the application of a condition-dependant approach. Such monitoring technique provides detailed data about the behaviour of infrastructure components with time. And this, in its turn, provides to forecast the condition and accordingly, the planning of repair activities, which is the ultimate objective of any condition monitoring.

The maintenance and restoration of railway networks require large funds.

Only 11 % of these amounts have been spent on mechanized current maintenance of railroads, and 5 % – on manual current maintenance. This shows that the large costs are associated with restoration – capital repair works of railroads. To achieve an effective cost reduction, decision-takers should possess accurate information. Objective data of such type make the process more transparent and therefore, better controllable.

Computerized Track Maintenance Management Systems (TMMS) are a logical constituent of Asset Management Systems (AMS). As of this day, AMS are not sufficiently developed and completely adopted as a concept. TMMS exist to a greater degree as isolated systems. TMMS should be designed, which will furnish the NRIC with a valuable instrument for management of railroad and pertaining infrastructure.

Proper railroad maintenance management requires vast amount of data. Effective railroad analysis requires data to be divided into segments. Actually, the whole information is bound by the track segment it refers to.

4.2.1. System functions and processes

For the purpose of serving planning specialists and the management, the structure of TMMS has been divided into five basic applied functions – one for each level, each one providing an increasingly detailed view onto the functional model,

Level 1 – Initial diagnostics

Need of repair and restoration works by railroad components. For each railway segment, based on decision-taking rules, the system implements a fully automated diagnostic procedure and displays the major demands for additional data, required for more detailed diagnostics of the segments in need of repair and restoration works.

Level 2 – Detailed diagnostics

This level is based on additional data to be provided to the user and on additional decision-taking rules. In this part of its, the procedure is interactive. The result is a *Preliminary Repair and Restoration Works Plan*.

Level 3 – Coordination of the individual repair and restoration works

The works established as required at Level 2, are subject to fully automated consistence analysis based on decision-taking rules. The works are evaluated in a way providing to combine activities of the same type, if they are planned sufficiently close to one another in time and space. Also, the various types of restoration activities, planned for a given section of the railroad and close in time, are grouped, such as restoration of sleepers and fasteners and cleaning/restoration of ballast; restoration of sleepers and fasteners and restoration of rails, or restoration of rails and cleaning/restoration of ballast. The result is a final *Draft Repair and Restoration Works Plan*.

Level 4 – Optimization of resource allocation

This level is based on an interactive man–machine process. At this level, assessment of the expenditure plan is made and the long-term planning of repair and restoration works along the selected railroad is optimised. The expenditures for continuous and one-time repair and restoration works are included. The user chooses the best option according to the repair and restoration practice of the railway enterprise.

5. CONCLUSION

A major factor when planning maintenance activities is the detailed and complex assessment of railroad condition. The preparation of such an assessment requires, apart from the introduction of computerized Track Maintenance Management Systems (TMMS), to also develop more precise and more reliable models of railroad deterioration. The continuously increasing amount of high-quality data about railroad condition shows that railroad condition and the relevant maintenance and restoration activities should no longer be considered separately from the other railway infrastructure components. The major conclusion is that railroad management should be combined with management of lower construction, upper construction, contact network, telecommunication and signalling, and other systems.

The reasons for this are numerous. First, it has been known for a long time that other railway infrastructure elements, such as lower construction, have by far more material impact on the behaviour of upper construction. This is especially valid in places where persisting and recurring railroad-related problems are observed. The practice of other railway administrations has established that, without the use of TMMS of sufficiently high quality, this aspect could not be satisfactorily assessed, because only the use of such systems provides to simultaneously superimpose different types of data about the condition of the railroad, which allows for multi-aspect assessment of its condition.

The lack of reliable, effective, and economic methods for continuous and reproducible observation of lower construction aggravates further the problem. Second, the continuously increasing needs and strict norms regarding railroad operation absolutely necessitate complex management of the entire railway infrastructure.

These two factors, jointly with the constant strive for higher effectiveness and cost reduction call for the development of a new management concept by the NRIC based on Asset Management System (AMS).

REFERENCES

[1] Ling, D. (2005) Railway Renewal and Maintenance Cost Estimating. School of Applied Sciences, Cranfield University, PhD Thesis.

[2] Thomas Åhrén, (2008) Maintenance performance indicators (MPIs) for railway infrastructure: identification and analysis for improvement, PhD Thesis, Luleå University of Technology, Swedish.

[3] Strategy for the Development of the Transport System of the Republic of Bulgaria Until 2020

[4] Strategy for the Development of the Transport Infrastructure of the Republic of Bulgaria by 2015

[5] National Strategy for Environment 2009 – 2018

[6] White paper "European transport policy for 2010: time to decide"

[7] Five year program for the development and using of railway infrastructure for the period 2011-2015

[8] Zoeteman, A. (2004), State of the art in railway maintenance management: planning systems and their application in Europe. IEEE International Conference on Systems, Men and Cybernetics

Application of GPSS Queuing Network Model to Evaluate the Performance of the Transportation Technological System

Kiril Karagyozov
Technology, Organization and Management of Transport, Todor Kableshkov University of Transport, Sofia (Bulgaria)

This paper aims to show the possibilities of using GPSS queuing network simulation to model specific transport technology systems. Specific examples of structural technological schemes of individual railway station subsystems operating in certain rail yards are given to illustrate the general methodological approach for their description as a queuing networks, determining the arrival flow rates and service times in each technological subsystem.

Keywords: queuing network, GPSS simulation, rail yard operation

1. INTRODUCTION

The paper is aimed at presenting functionality of the model of an open queuing network (OQN) created by using simulation system GPSS World (tm). The simulation model developed is applied to determine the performance measures of QS open network with general probability distribution for characterizing service and inter-arrival times without limitations of queue sizes at the entrances to individual QSs. The complex nature of the simulation model is with independence of the main modelling segment of QS network structure: number of QS; routing matrix, which give a possibility to determine the arrival rates in each QS in the network; unique external arrival flow and QS service times with general probability distributions.

The number of systems, the matrix of routing probabilities, the parameters of service of individual QSs (the mean and coefficient of variation of service times) are performed in the segment of setting the input parameters of the simulation model. A separate procedure approximates the overall functions of probability distribution with a given mean and coefficient of variation by gamma, exponential and hyper-exponential distribution respectively. To model complex transport systems, it is appropriate to consider them as a network of linked and interacting technological systems. The processes in these systems can be modelled using the theory of queuing systems. For this purpose, they are presented as queuing systems (QS) where the impact of random factors on both on the time intervals between the arrival of customers at the QS entrance and the times to service customers in individual QS.

References contain a great number of studies using different approaches to determine the number of tracks required in a given yard at the station, such as modelling of yards as an open or closed queuing system [6], [4], models that take into account the impact of the limited dimensions of track yards on the service rate of technological queuing systems in the yard [4]; simulation [1], [8]; deterministic models, etc.

Aside from the number of tracks in a given yard, an approximate model of open queuing networks [6],[3],[4] can be used with l-class of customers (trains), with arrival rate and coefficient of variation of the arrival flow in the yard λ_0 and Ca_0 .

2. OPEN QS NETWORK WITH L CLASS CUSTOMERS, POISSON ARRIVAL FLOW FROM THE EXTERNAL ENVIRONMENT WITHOUT ROUTING BETWEEN CLASSES

2.1. Arrival flows in each QS of the open network

Let network consists of N queuing systems of type Gi/G/S. For each class *l* there is special arrival flow of the external environment λ_0^l, the matrix of routing probabilities with q_{ij}^l, for *i, j = {0, N}*, i.e. the probability customer of class *l* after service in QS *i* to enter for service in QS *j*. State *0* corresponds to the external environment. For each QS *I* the arrival rate of L class in the i-th QS - λ_i^l and as the visit ratio $e_i^l = \lambda_i^l / \lambda_0^l$ are obtained from the solution of system N linear equations describing the flow conservation in the network made separately for each class:

$$\begin{aligned} \lambda_i^{(l)} &= \lambda_0^{(l)} q_{0,i}^{(l)} + \sum_{j=1}^{N} \lambda_j^{(l)} q_{j,i}^{(l)} \quad & i = 1...N \\ e_i^{(l)} &= q_{0,i}^{(l)} + \sum_{j=1}^{N} e_j^{(l)} q_{j,i}^{(l)} \quad & i = 1..N \end{aligned} \qquad (1)$$

The total arrival flow from the external environment and for each QS *i* for all classes is:

$$\lambda_0 = \sum_{l=1}^{L} \lambda_0^{(l)} \; ; \quad \lambda_i = \sum_{l=1}^{L} \lambda_i^{(l)} \qquad (2)$$

2.2. Processes of service in QS

Each QS *i* has S servers , as for each class *l* the service times are random variables specified with the first two of central moments – mean $\bar{t}s_{il}$ and variation σ_{il}^2, or coefficient of variation Cs_{il}, which are determined:;

$$\begin{aligned} & E(ts_{il}) = \bar{t}s_{il} = 1/\mu_{il} \,; Var(ts_{il}) = \sigma_{il}^2 = E(ts_{il}^2) - E^2(ts_{il}) \\ & \therefore \cdots Cs_{il}^2 = \sigma_{il}^2 / \bar{t}s_{il} = \mu_{il}\, \sigma_{il}^2 \end{aligned} \qquad (3)$$

The mean of the service time, the service rate of the combined flow of all classes respectively is determined:

*Corresponding author: 158 Geo Milev Str. 1574 Sofia, Bulgaria, kskaragyozov@gmail.com

$$E(ts_i) = \bar{t}s_i = 1/\mu_i = \sum_{l=1}^{l} \frac{\lambda_i^{(l)}}{\lambda_I} \bar{t}s_{il}$$
$$E(ts_i^2) = \sum_{l=1}^{l} \frac{\lambda_i^{(l)}}{\lambda_I} E(ts_{il}^2) = \sum_{l=1}^{l} \frac{\lambda_i^{(l)}}{\lambda_I} \bar{t}s_{il}^2 \left(Cs_{il}^2 + 1\right) \tag{4}$$

After algebraic transformations, the coefficient of service time in QS *i* is obtained to be :

$$E(ts^2{}_i) = \bar{t}s_i^2\left(1 + Cs_i^2\right) = \sum_{l=1}^{l} \frac{\lambda_i^{(l)}}{\lambda_I} \bar{t}s_{il}^2 \left(Cs_{il}^2 + 1\right) \tag{5}$$

$$Cs_i^2 = \mu_i^2 \sum_{l=1}^{l} \frac{\lambda_i^{(l)}}{\lambda_I} \bar{t}s_{il}^2 \left(Cs_{il}^2 + 1\right) - 1 \tag{6}$$

Thus the problem is reduced to an open network with a single arrival flow.

2.3. GPSS model of a QS open network with limitation of the number of customers in the network

The suggested GPSS model is based on the transformation of the QS open network model developed in [1] as the following changes] are reflected: each QS is modelled as a multi-server QS (blocks ENTER-LEAVE), instead of a single-server QS , the queues of each QS are unlimited), while the total number of customers in the network -Nmax is limited. Thus when the customer from external flow enters in the model and finds that the network has Nmax customers, then it queues in front of the network. Fig. 1 is a block diagram of the main segment of GPSS model, which implements the model of the QS open network with limitation of the number of customers in the network and Fig. 2 shows the programming code.

In order to implement the model it is necessary to initialize input data, mean values and coefficients of variation of the arrival flow intervals and the times of service in the individual QSs, capacity of multi-server devices, values of the matrix of routing probabilities.

The paper presents an illustration of the possibility of using the QS open network model with limited maximum number of customers in the network in order to study performance of the receiving-departure area of a marshalling yard. Three types of flows of freight trains are examined: inbound trains to be classified, transit trains and outbound trains departing after being classified. The system of locomotive scheduling G3 and waiting for departure route G4 as type Gi/G/inf, i.e. infinite number of servers makes possible to consider the stochastic distribution of dwell times in these operations. In real systems these dwell times depend on the particular scheme of the station (number of rail sections served, the use of their capacity, the real scheme of locomotive scheduling, the number of locomotives, etc.), which are largely external factors not being dependent on the technology of the station. In our simple example, which is to show how to use the simulation model, the provision of departing trains with locomotives and expecting departure are aggregated in evaluation of the average time and its variation for such operations in the departure area. To assess the effect of performing other operations in system G2, a customer is generated in an additional segment with an interval of arrival flow by displaced exponential distribution with mean $\bar{I} = I_{\min} + I_2$ and standard deviation $\sigma_I = I_2$ ($I_{\min}$ - deterministic component and I_2 - exponentially distributed) that occupies G2 with the same time of service as in the main segment . In different scenarios, with different number of trains/day in the departure area, values $\bar{I} = I_{\min} + I_2 ; I_{\min} = I_2$ are set in a way to ensure further increase of G2 load by 25%. Fig. 3 and table 1 present technological operations in receiving-departure area as a QS network and Tab. 1 shows the structure of the train arrival flow in the main scenario.

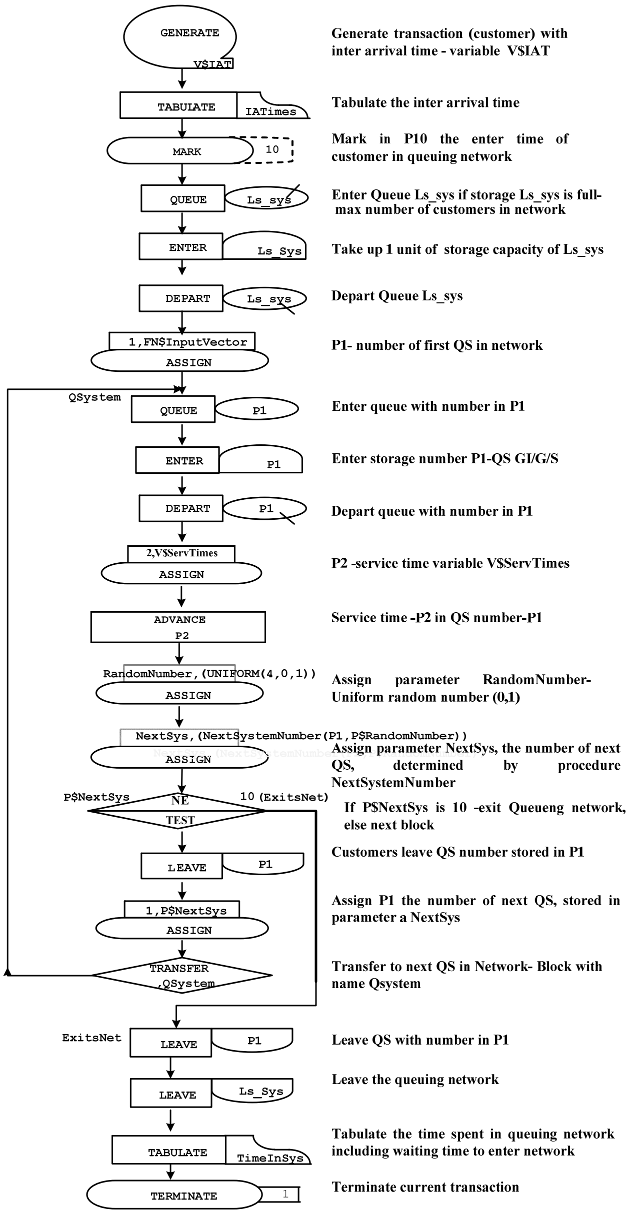

Fig.1 Block diagram of open queuing network with restricted max number of customers in network

tabl.1

Queuing System	Description	No of Servers	Inbound trains		Outbound trains		Transit trains	
			ST	CV	ST	CV	ST	CV
G1	Crew	S_{G1}=2	+	+	+	+	+	+
G2	Sorting	S_{G2}=1	+	+				
G3	Waiting locomotive	inf			+	+		
G4	Waiting available schedule	inf			+	+	+	+

GPSS programme statements

```
*Declarations
          RMULT 111,99,2147483536,55,101,46,56
*Variables
          *Variable  IAT-inter arrival time distribution - Input parameters
          *to procedure ProbDistr- (mean,CV)
IAT       FVARIABLE       (ProbDistr(1,(60/2),0.8))  ;Mean inter arrival time- 30min
ServTimes          FVARIABLE       (ProbDistr(3,FN$MeanServ,FN$CoefVarS))
*Tables
IATimes  TABLE   V$IAT,0.2,0.2,10              ;Tabulate inter arrival time
TimeInSys TABLEMP10,0,0.25,25                  ;Tabulate sojourn time in network
CurrLgSys          TABLE   (S$Ls_Sys+Q$Ls_Sys),0.99,1,20        ;Tabulate Number of Customers  in network
*QTables
          *Initializationof  queues (1-4) time frequency distribution tables.
QueueSys1          QTABLE          1,0.99,1,10
QueueSys2          QTABLE          2,0.99,1,10
*Matrix
          *Initialization of  routing matrix -ProbMatrix -( 5 x 5),
ProbMatrix MATRIX          ,5,5
*EQU
MatrixColumns EQU          5                              ;Assign value of max number of columns
*Matrix Elements
          *Initialization of routing probabilities-elements of  ProbMatrix
          INITIAL MX$ProbMatrix(1,2),0.25
          INITIAL MX$ProbMatrix(1,3),0.25
          INITIAL MX$ProbMatrix(1,4),0.5
          INITIAL MX$ProbMatrix(2,5),1.0
          INITIAL MX$ProbMatrix(3,4),1.0
          INITIAL MX$ProbMatrix(4,5),1.0
          INITIAL MX$ProbMatrix(5,1),1.0
*Storages
          *Definition of number of servers- Storage capacities QS (1-5) and numbers
Ls_1      EQU      1
Ls_1      STORAGE          2
Ls_2      EQU      2
Ls_2      STORAGE          1
Ls_3      EQU      3
Ls_3      STORAGE          1000       ;1000-as infinity
Ls_4      EQU      4
Ls_4      STORAGE          1000       ;100-as infinity
Ls_Sys    EQU      10
Ls_Sys    STORAGE          8          ;Maximal number of Customers in Network
          *                Service times and coefficients of variation   *
ServTimeSys1 EQU           45         ;Mean service time Queuing system 1
     Cs_1 EQU     0.4      ;Coefficient of variation QS -1
ServTimeSys2 EQU           50         ;Mean service time Queuing system 2
     Cs_2 EQU     0.4      ;Coefficient of variation QS -2
ServTimeSys3 EQU           60         ;Mean service time Queuing system 3
     Cs_3 EQU     0.5      ;Coefficient of variation QS -3
ServTimeSys4 EQU           60         ;Mean service time Queuing system 4
     Cs_4 EQU     0.5      ;Coefficient of variation QS -4
*Functions                                                          *
InputVector FUNCTION RN2,D3
          0.333333,1/0.666667,1/1.000000,1
          *FunctionMeanServ, return mean service time in QS (1-4)
MeanServ  FUNCTION P1,M4          ;mean service time QS with number stored in P1
          1,ServTimeSys1/2,ServTimeSys2/3,ServTimeSys3/4,ServTimeSys4
          *FunctionCoefVarS, return coef. of variation of service time QS (1-4)
CoefVarS  FUNCTION P1,M4
          1,Cs_1/2,Cs_2/3,Cs_3/4,Cs_4

*                    Modeling Segment          I                              *
*******************************************************************************
          GENERATE         V$IAT                  ;Generate transaction (customer) with inter-arrival time - variable  V$IAT
          TABULATE         IATimes                ;Tabulate the inter-arrival time
          MARK    10                       ;Mark in P10 the enter time of customer in queuing network
          Queue   Ls_Sys                   ;Enter Queue Ls_sys if storage Ls_sys is full- max number of customers in network
          ENTER   Ls_Sys                   ;Take up 1 unit of  storage capacity of Ls_sys
          Depart  Ls_Sys                   ;Depart Queue Ls_sys
```

```
        ASSIGN 1,FN$InputVector         ;In parameter P1- number of first QS in network, which the customer enter
QSystem Queue     P1                    ;Enter queue with number stored in P1
        Enter     P1                    ;Enter storage number P1-QS GI/G/S
        DEPARTP1                        ;Depart queue with number stored  in P1
        ASSIGN 2,V$ServTimes            ;Assign service time determined by variable V$ServTimes in P2
        ADVANCE        P2                         ;Service time -P2 in QS number-P1
        ASSIGN RandomNumber,(UNIFORM(4,0,1))  ;Assign parameter RandomNumber- Uniform random number (0,1)
        ASSIGN NextSys,(NextSystemNumber(P1,P$RandomNumber))  ;Assign parameter NextSys, the number of next QS,
                                                       determined by procedure NextSystemNumber
        TEST NE        P$NextSys,5,ExitsNet               ;If P$NextSys is 5 -exit Queueng network, else next block
        LEAVE  P1                       ;Customer leaves QS number stored in P1
        ASSIGN 1,P$NextSys              ;Assign P1 the number of next QS, stored in parameter  NextSys
        TRANSFER       ,QSystem                   ;Transfer to next QS in Network- Block with name Qsystem
ExitsNet LEAVE  P1                      ;Leave QS with number stored in P1
        LEAVE  Ls_Sys                   ;Leave the queuing network
        TABULATE       TimeInSys                  ;Tabulate the time spent in queuing network including waiting time
                                        to enter network
        TERMINATE 1                     ;Terminate current transaction (customer)
*Modeling Segment        II                       *
        GENERATE        10                        ;Generate 1 transaction every 10 time unit
        TABULATE        CurrLgSys                 ;Tabulate the current number in queuing network
        TERMINATE                       ;Terminate  transaction
*Modeling Segment        III                      *
        GENERATE       (EXPONENTIAL( 3, 150, 150))        ;Generate  other workload  in G2
        Assign    1,2                   ;Assign P1 the number of QS-2
        QUEUE  Form                     ; Enter queue Form
        ENTER  P1                       ;Enter QS-2
        Depart    Form                  ;Depart queue Form
        ASSIGN 2,V$ServTimes            ;Assign service time determined by variable V$ServTimes in QS-2
        ADVANCE        P2                         ;Service time -P2 in QS number-P1
        LEAVE  P1                       ;Leave QS-2
        TERMINATE                       ;Terminate transaction
*Realizations Count Modeling Segment            *
        START   1000,NP                 ;1000 transactions exit network
        RESET                           ;Keep current situation as initial conditions
        START   100000                  ;End of simulation after 100000 transactions exit model
*Procedures                                               *
        *Return the number of next QS after leaving current QS*
        PROCEDURE NextSystemNumber(MatrixRowNumber,RandomNumber)
        BEGIN
          TEMPORARY MatrixColNumber,AccumulProb;
        MatrixColNumber=1;AccumulProb=0;
          WHILE (MatrixColNumber<MatrixColumns+1) DO
          BEGIN
        AccumulProb=AccumulProb+ProbMatrix [MatrixRowNumber,MatrixColNumber];
           IF (RandomNumber<=AccumulProb) THEN BEGIN RETURN MatrixColNumber;END;
        MatrixColNumber=MatrixColNumber+1;
          END;
        END;
        *Return random variable from generalprobability distribution approximated on the base*
        *of input parameters mean-Ex and coefficient of variation-Cx              *
        PROCEDURE ProbDistr(RNG,Ex,Cx)
        BEGIN
          TEMPORARY Es,Alfa,Prob1,Prob2,ts1,ts2,URN;
          IF (Cx<1) THEN
        BEGIN
           IF (Cx=0) THEN BEGIN RETURN Ex; END;
           ELSE
           BEGINEs=(Ex#(Cx^2)); Alfa=(1/(Cx^2)); RETURN (GAMMA(RNG,0,Es,Alfa));  END;
          END;
          ELSE IF (Cx=1) THEN       BEGIN RETURN (EXPONENTIAL(RNG,0,Ex));  END;
          ELSE IF (Cx>1) THEN
        BEGIN
           Prob1=(0.5#(1+SQR((Cx^2-1)/(Cx^2+1))));Prob2=(1-Prob1);
           ts1=(Ex/(2#Prob1));ts2=(Ex/(2#Prob2));
           RETURN ((ts1+(RN5'LE'(Prob2#1000))#(ts2-ts1))#(Exponential(RNG,0,1)));
        END;
END;
```

Fig. 2. GPSS Programming code

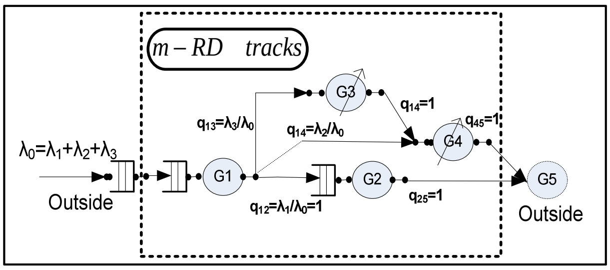

Fig.3 Structural scheme of receiving-departure area

tabl.2

Arrival flows				Basic Scenario 1	
Train/day			Ni/N	Train/h	
Total	N	48	1	λ0	2,00
Inbound	N1	12	0,25	λ1	0,50
Transit	N2	24	0,5	λ2	1,00
Outbound	N3	12	0,25	λ3	0,50

With the given times of service of each train category in QS-Gi, after using dependencies (1) - (6), the rates of arrival flows, the mean service time and their coefficients of variation for each QS are obtained. For all scenarios it is assumed that they are already defined by dependencies (1) - (6) - Table 4. The routing matrix for all scenarios is presented in Table. 3.

Routing matrix q_{ij} tabl.3

QSi\Qsj	1	2	3	4	5
1	0	0,25	0,25	0,5	0
2	0	0	0	0	1
3	0	0	0	1	0
4	0	0	0	0	1
5	0	0	0	0	0

tabl.4

Service proccess			
Queing System	Service time	Coefficient of Variation	Number of servers
Qsi	ts (min)	Cs	S
G1	45	0,4	2
G2	50	0,5	1
G3	60	0,8	inf
G4	60	0,8	inf

3. RESULTS OF SIMULATION MODEL

To illustrate the possibilities to use the simulation model, various scenarios related to changes of the total arrival flow N trains /day (24,48,60) and any changing the number of tracks in the station m-(6,7,8,9) are implemented.

Due to the extremely numerous outcomes concerning both QS and the entire network, connected average characteristics, their disperses, probability distributions of the number of customers, the probability of retention of trains due to busy track, etc. considering only some summarised results characterizing the work of the entire network.

For the basic scenario N = 48 trains/day, some of the overall results are given such as the average number of trains in the RD area- L_{sm}, mean queue to enter RD area- Lq_0, probability of arrival train from outside to find all tracks busy P (n> m) - Table 5, Fig. 5 and Fig. 6, state probabilities in queuing network Fig.3. Table 5 shows that after the comparison of parameters mean- L_{net} and standard deviation σ_{Lnet} the number of trains in the model of QN, these values correspond to a Poisson distribution with mean - L_{net}. For the case m = 9 and Lnet = 4.84 Fig. 4 shows the theoretical Poisson distribution with this average value. It is evident from the comparison with other distributions obtained by simulation that there is a confirmation that they can be approximated by Poisson distribution.

tabl.5

m	Lsm	Lq0	Lnet	σLnet	P(n>m)
6	4,53	0,65	5,17	2,52	0,36
7	4,65	0,29	4,94	2,32	0,19
8	4,65	0,15	4,86	2,27	0,10
9	4,78	0,06	4,84	2,22	0,05

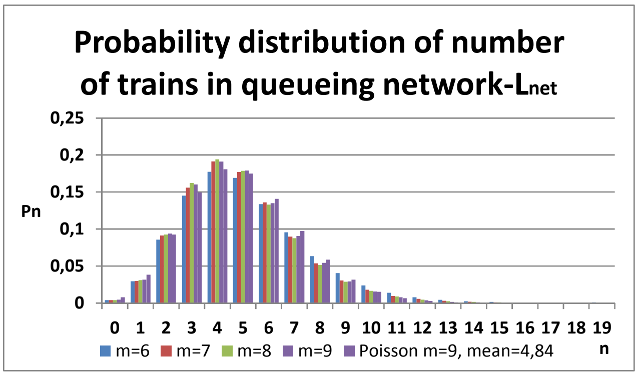

Fig.4 State probabilities in queuing network

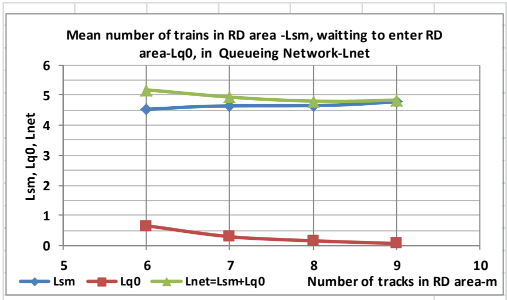

fig.5 Mean number of trains in RD area and in queuing network

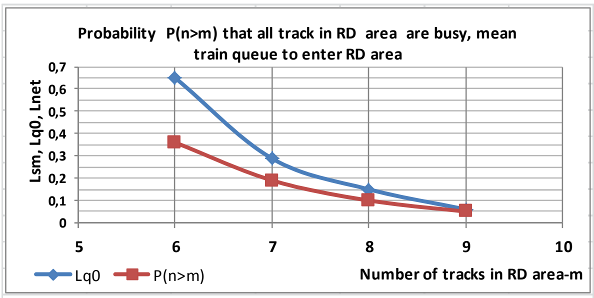

fig.6 Probability to find tracks busy and mean queue to enter RD area

To illustrate the possibilities of analysis with a volume different from the volume of the basic scenario N = 36 and N = 60, let assume for each volume that this number of tracks m * where the probability of train retention to the approach to RD area is less 0.05, i.e. P (n> m *) <0.05 - tabl.6.

tabl.6

N	m*	Lsm	Lq0	Lnet	σLnet	Tracks utilization	P(n>m*)
36	7	3,21	0,02	3,22	1,61	0,46	0,03
48	9	4,78	0,06	4,84	2,22	0,68	0,05
60	10	4,83	0,03	4,86	2,23	0,69	0,03

These results illustrate only part of possibilities to model the operation of technological processes distributed in different areas of marshalling yards.

A more detailed study on the parameters for service of different classes of trains, their distribution as random variables, the increase of the service capacity of technological systems by increasing the number of inspection crews, the number of persons in one team, the increase of the capacity of individual technological systems presented as separate QS type Gi/G/S on the network through modernization and automation of their technical equipment. Even for the limited number of scenarios considered above, the results obtained are partly discussed in this paper.

CONCLUSION

The purpose of this article is to present the possibilities to use the developed model of an open network of queuing systems. They are of type Gi/G/S with limitation of the total number of customers in the network of service systems and unlimited queue at the network entrance. The main advantages of the developed simulation model are:

- The main segment modeling the network is universal and each particular network is defined by the input parameters.
- It allows approximation of the distributions of intervals arrival flow from external environment and service times based on their parameters (mean and standard deviation).
- It allows to obtain empirical probability histograms of all random variables in the individual QSs and to explore their nature and character.

Trends for future research and development

Some of future investigations and improvement of GPSS simulation model are related with the next features:

- Possibility of modeling a network of several different classes of customers through input parameters.
- Opportunities to expand possibilities to define the service itself or only the queue outside the defined total network limited in the total number of customers.
- Time dependent arrival rate from outside and modelling the interruption in service processes due to failures and other planned times .

REFERENCES

[1] К. Карагьозов, С.Димитров:Комлексен имитационен модел на отворени мрежи от системи за масово обслужване с произволна структура, Годишник на ВТУ 5/2014 ISSN 1314-362X

[2] K. Karagiozov: On the approximation of the moments and operational characteristics of GI/G/S queuing System, International conference 'OPERATION RESEARCH 1990', Vienna , 1990

[3] K. Karagiozov: Approximate method for modelling of open queueing networks, International Conferance 'OPERATION RESEARCH 1990' , 'OPERATION RESEARCH 1990', Vienna , 1990

[4] K. Karagiozov, D.Kupenov: The Railyard Queuing Model, EURO XI 11th, European Congress on operations research. RWTH AACHEN, BRD, July 16-19, 1991.

[5] L. Kleinrock: Queuing System Volume II: Computer applications,, Willey&Sons,1976

[6] W.Whitt: “Performance of the queueing network analyzer”, The bell system technical journal, Vol. 62, No. 9, November 1983

[7] М. Тодорова: Оптимизиране на маневрената дейност в разпределителна гара ПДТ, XXI Научна конференция с международно участие- “ТРАНСПОРТ 2003”, ВТУ“Тодор Каблешков” 13-14 ноември, София

[8] Т.Размов: Анализ на транспортните системи, чрез дискретно-събитийно моделиране. Списание “Механика, транспорт, комуникации“, ISSN 1312-3823,бр.3,2013.

Web Based System for the Integration of the Overhaul Process for Railway Braking Devices

Zdravko Tešić[1], Branislav Stevanov[1*], Danijela Gračanin[1]
[1]Faculty of Technical Sciences/Department for Industrial Engineering and Management, University of Novi Sad, Novi Sad (Serbia)

The overhaul process of railway braking devices includes many subjects such as railway companies, overhaul companies, and business partners such as spare parts suppliers as the elements of supply chain. Relation and communication between the participants in the supply chain is of vital importance. This encompasses the need for the data management, covering every element of the business, including data about current jobs, railway braking devices information, the data needed for the documentation in the overhaul process, current job status and many more. This paper presents the overhaul process of railway braking devices, the model for integrating all participants of the supply chain, data management for the process support and the appropriate web software which is developed. The software provides functions for process planning, process execution and for the data administration.

Keywords: Overhaul process, Integration, Supply chain, Web software

1. INTRODUCTION

In competitive markets industrial companies struggle to achieve performance with the minimum of costs. In order to adapt to changing environment industrial companies must be aware of its business processes which connect them to all other subjects in the supply chain. In the case of the overhaul process for the railway braking devices the overhaul company is only a part of the supply chain. Other important elements of the supply chain are railway companies which are usually state held companies, the spare parts suppliers and the spare parts manufacturers. In this paper an overhaul process is presented on a concrete case study. The process participants are integrated by developed web software. The first part of the paper presents theoretical background in business process modeling and management and the second part presents the case study.

2. THEORETICAL BACKGROUND

2.1. Business process modelling

Business process can be defined as a set of internal activities performed to serve a customer [1]. Business processes represent key factor in integrating an enterprise [2]. For a successful industrial system management the understanding of basic processes which constitute the business is essential. Better process understanding is easy to achieve when process model exists. Business process modelling presents creation of model of business process by some formal technique. Business process model can include:

- process activities,
- process participants such as individuals and companies,
- process data – usually in a form of some documents generated during process execution,
- process constraints – such as procedures, contracts, laws etc.

There a numerous modelling techniques and methods developed. Many methods and techniques are unified, which means that they create the family of similar methods. Methods used in this paper belong to two method families, the IDEF family of methods and the UML family of methods.

The IDEF family consists of several methods which enable to look the process from different perspectives. IDEF is an acronym for Integrated Definition Methods. One of the most used methods from IDEF family is IDEF0. IDEF0 is set as a standard methodology for modeling by the National Institute of Standards and Technology, USA [3]. Given standard describes the IDEF0 methodology as a modeling language (syntax and semantics) and set of rules and techniques for development of structural systems views on industrial enterprises and other functional units. This methodology enabled development of the functions model in the system (processes, activities, operations and tasks) and setting the relationship between functions and data (information or objects) that support system integration. IDEF0 is independent of the CASE (Computer Aided Software Engineering) tools and methods, but can be used as a starting point. IDEF0 modeling is a combination of graphics and text that are presented in an organized and systematic manner, with the aim of understanding, supporting analysis, providing the logic for potential changes, definition of requirements and the process integration. The model consists of a hierarchical series of diagrams that gradually show more details about the functions and processes and their relationships with other parts of the system. Graphic language IDEF0 describes a method of functional analysis through sets of diagrams. Each diagram has a limited amount of detail defined by the appropriate syntax and semantics. Diagrams are interconnected through system of labeling, in order to show a hierarchical system, from top to bottom.

*Corresponding author: Faculty of Technical Sciences, Novi Sad, branisha@uns.ac.rs

Besides IDEF, another method family is the UML. UML is an acronym for Unified Modeling Language. The UML family of methods can be divided into two groups:

- Methods for describing the structure of the system,
- Methods for describing the behavior of the system.

Methods for describing the system behavior are used for business process modelling. To model a business process modeller can use different diagram types such as:

- Use-case diagrams,
- Activity diagrams,
- Sequence diagrams,
- Collaboration diagrams,
- Statechart diagrams.

For the purpose of this paper the activity diagram is used. Activity diagram is used for modelling the sequential (or parallel) steps of some process [4]. Activity diagrams are consisted of activities, participants, flows, conditions and forks. For distinction of the participants in the process the swim lanes are used. Forks are used for transitions from sequential to parallel activity execution and vice versa.

In order to successfully automate the business processes, the business process management systems are developed. Business process management presents the automation of business process in a whole or part during which documents, information or tasks are passed from one participant to another for action, according to a set of procedural rules [5]. Business process management is also viewed as supporting business processes using methods, techniques, and software to design, enact, control, and analyze operational processes involving humans, organizations, applications, documents and other sources of information [6].

Given the presented theoretical insight into business process models and management system definitions the research problem can be defined. The observed problem which is presented in this paper is how to integrate process activities, participants and different business rules which exist in the overhaul process of the railway braking devices. To enable successful business process management, the overhaul process is first modelled using the described methods and then the web software is developed to automate all the elements of business process. The research took study of the overhaul process in one railway overhaul company from Serbia.

3. CASE STUDY

3.1. Company description

The company has three plant locations deployed at a distance of 20 km. In Figure 1 they are labeled by letters *A*, *B* and *C*. In the factory plant *A* the railway coaches are overhauled. The testing, overhauling and repairing of railway braking devices are carried out in the factory plant *B*. The warehouse of spare parts of the overhauled and repaired brakes is situated there, too. Some spare parts are purchased from the company's suppliers, while the others can be made within the company in the factory plant *C*.

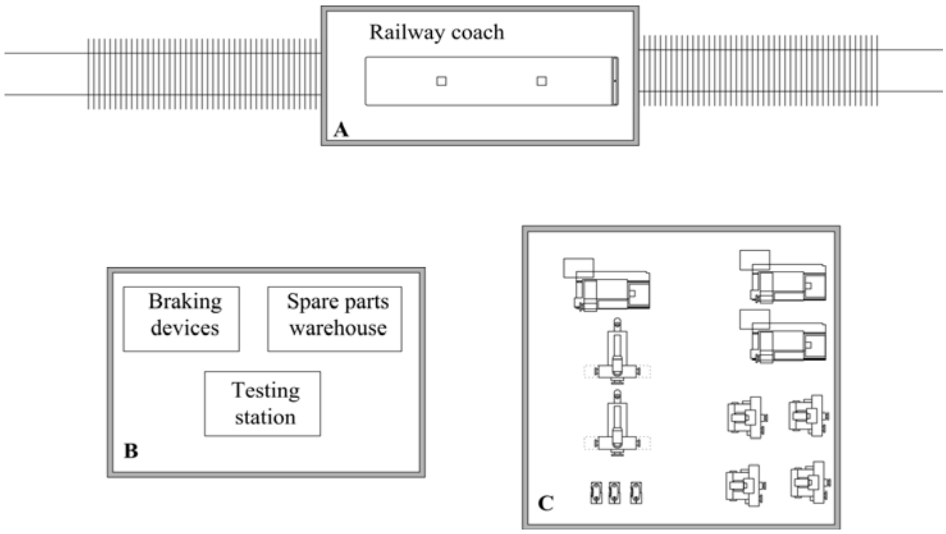

Figure 1. Three plant locations of the company[7]

The company provides different overhaul services for the railway. One of these services is the overhaul of railway braking devices.

3.2. Overhaul process modelling

In order to understand the integration software, first the overhaul process and the basic document types must be introduced. The overhaul process is shown on Figure 2. Figure 2 shows the IDEF0 model of the observed process. The overhaul process consists of four main activities:

- Reception and visual inspection of the braking device,
- Disassembly of the braking device and defect detection,
- Parts preparation and assembly,
- Braking device inspection and functional testing.

The process starts with reception and visual inspection of the braking device. The customer brings the braking device to the overhaul workshop and the braking technician specialist does the visual inspection. The document generated in this activity is the record of receipt and visual review.

The next activity is the disassembly of the braking device. Main input for this process activity besides the braking device is the technical documentation for the overhaul process. The technical documentation presents manual for the overhaul process of the braking device. For a railway braking device there are two types of parts which can be replaced:

- Type of parts which are replaced every time the braking devices goes to overhaul (rubber parts),
- Type of parts which are replaced only when needed that is only when they are damaged (metal parts).

After the cleaning and disassembly of the braking device the parts list is made also with the document of the noted defects. The work order for the overhaul of the braking device is issued.

For the parts preparation and assembly activity the spare parts are retrieved form the warehouse. The assembled braking device is sent to testing.

Braking device inspection and functional testing is done on the testing table by testing the braking device with different levels of working pressures in a controlled environment. Test results are printed in the form of functional testing diagram and in the form of the inspection protocol (serves like a table for inputting actual parameters).

The overhaul process includes different subjects such as railway companies, overhaul companies, and business partners such as spare parts suppliers as the elements of supply chain. For defining the interactions between the process participants an UML activity diagram is created, corresponding to the given process description. The activity diagram is shown on Figure 3.

4. WEB SOFTWARE FOR PROCESS INTEGRATION

In order to integrate all the process participants, the web software is developed. Web software provides the possibility to track the overhaul process execution and to have access to the documentation which is generated in the process. The web software consists of three parts:

- Jobs planning,
- Jobs execution,
- Administration.

Jobs planning part of the software provides the search of the existing overhaul jobs by identification number and adding the new overhaul jobs. Also the empty forms of the overhaul documentation can be downloaded. Every item from the jobs list contains:

- identification number,
- job description,
- the name of the business partner for which the overhaul job is done,
- the beginning and the ending date for the job,
- braking device data.

Jobs list is shown on Figure 4. Adding new jobs is shown on Figure 5. Every new job must be classified. Jobs can be classified as:

- Repair, overhaul, maintenance and modernization of railway vehicles,
- Repair, overhaul and maintenance of towed vehicles,
- Reconstruction of wagons,
- Repair, overhaul and maintenance of vehicles for railway purposes,
- Manufacture, repair and testing of railway braking devices, components and parts.

For every new there is also possibility to assign workers.

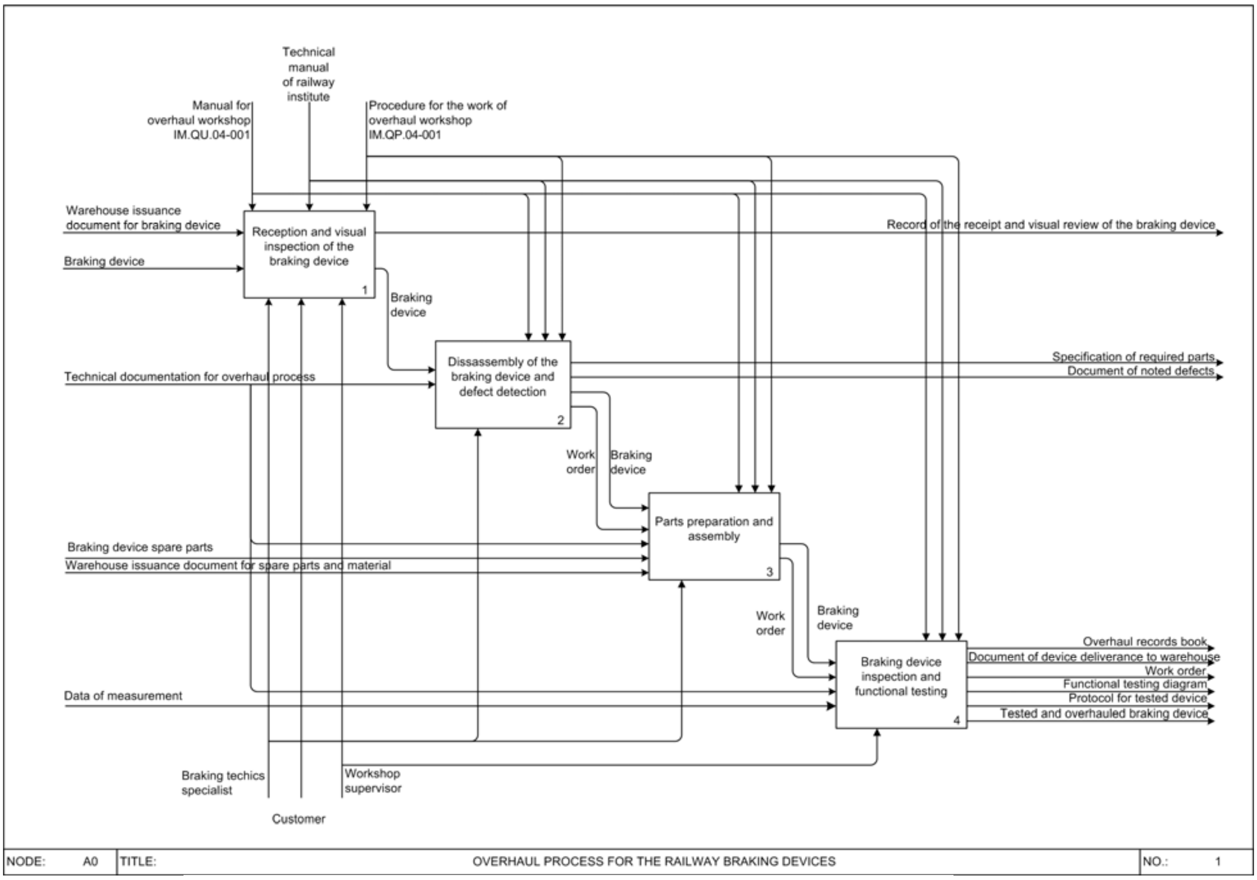

Figure 2. IDEF0 model of the overhaul process for the railway braking devices [8]

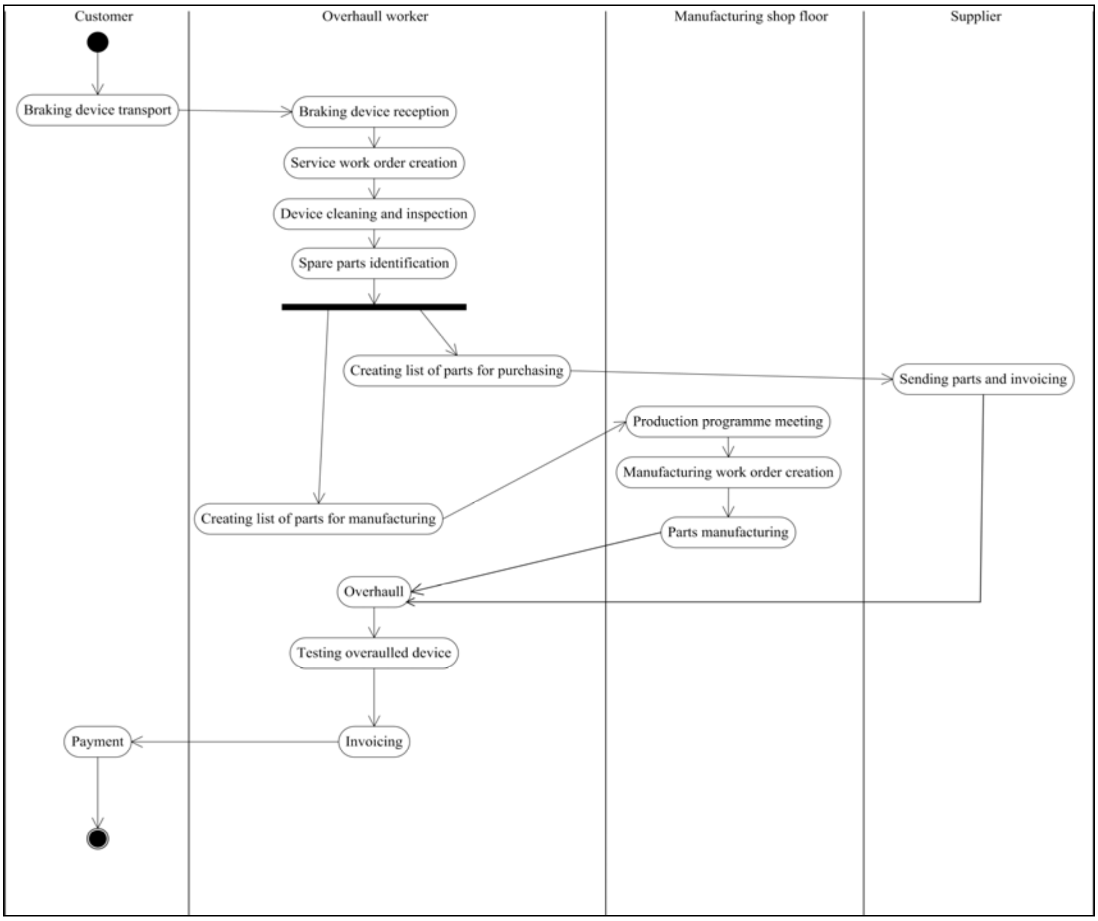

Figure 3. UML activity diagram of overhaul process[7]

Figure 4. Overhaul jobs list

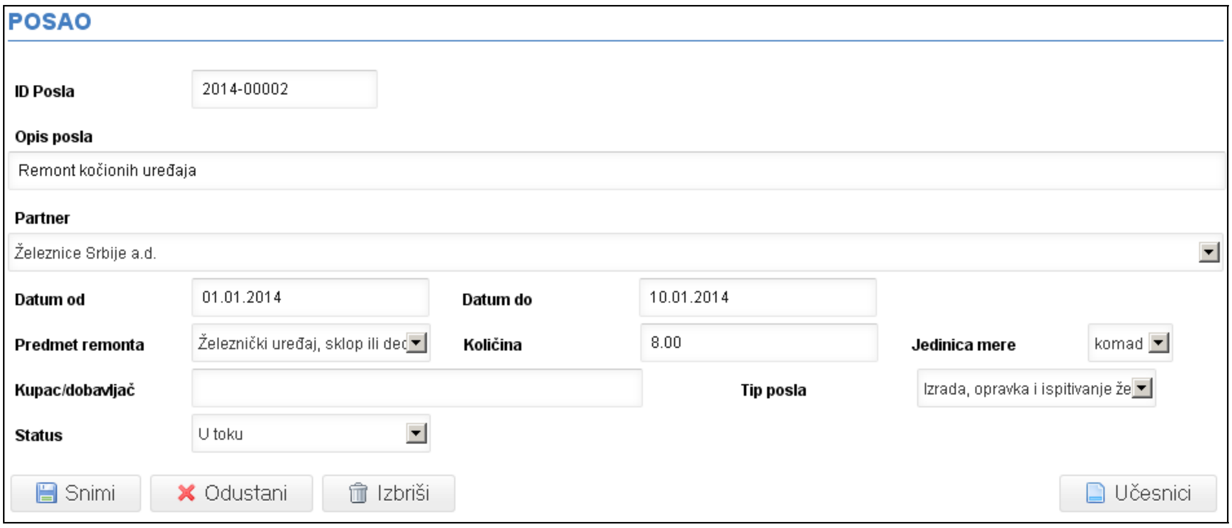

Figure 5. Adding new overhaul job

Jobs execution part of the web software provides the functionality to overview the overhaul jobs in a certain period (Figure 6) and to track a single overhaul job (Figure 7). The data for the job can also be seen from the single job tracking module (Figure 8).

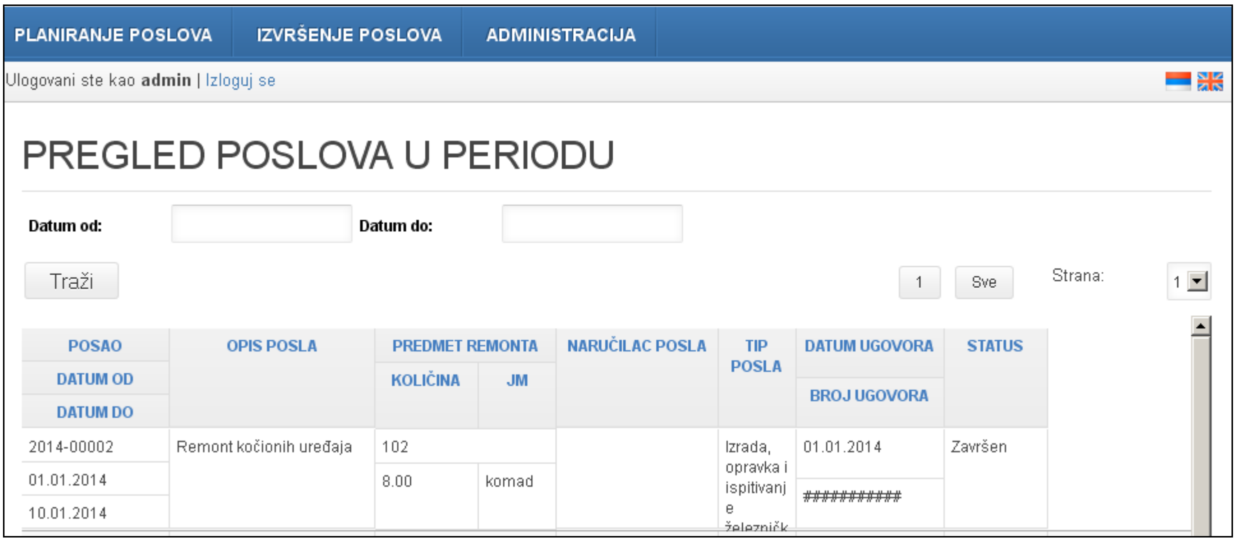

Figure 6. Overview of overhaul jobs in a given period

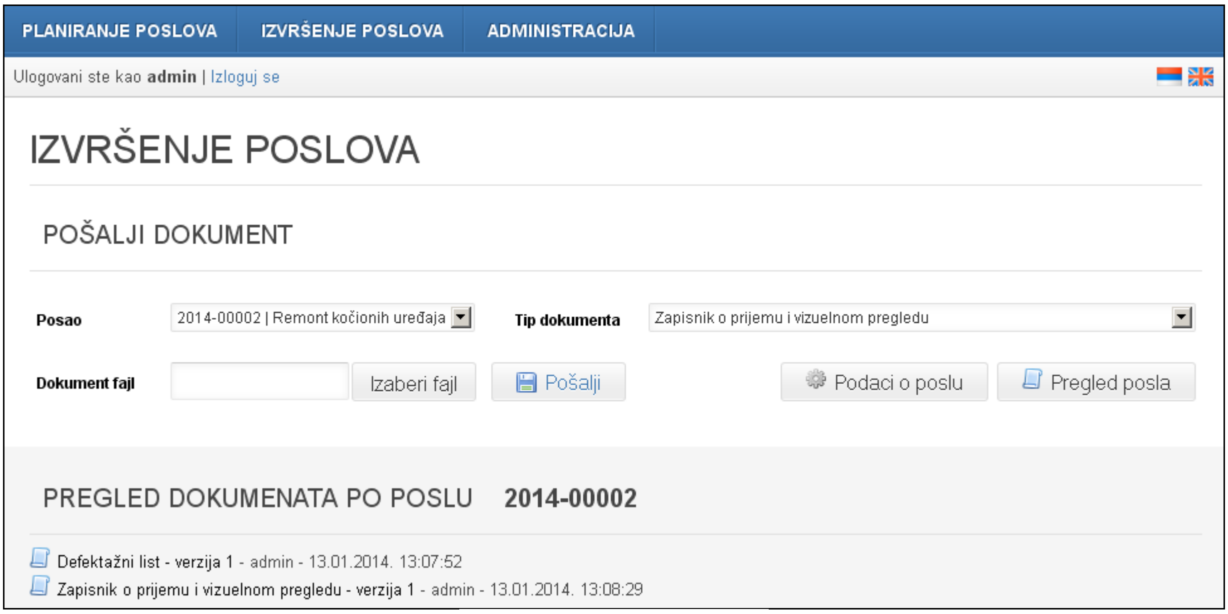

Figure 7. Single job tracking

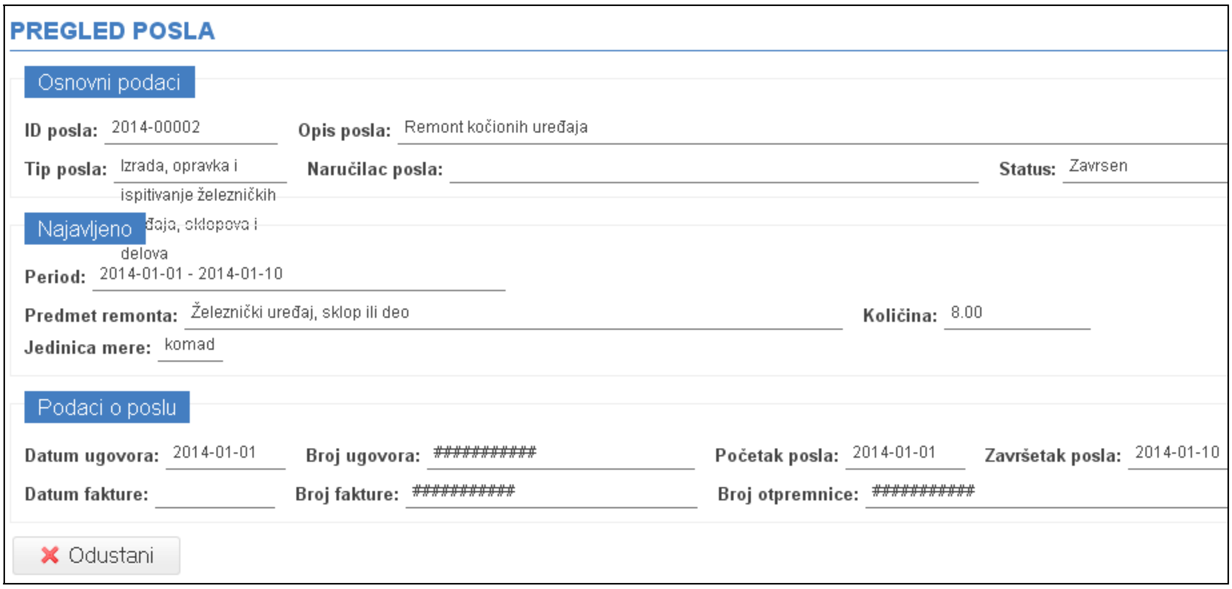

Figure 8. Single job data

The administration part of web software provides the administration of operators, business partners and process documents.

Overhaul process integration is achieved by covering main process areas which concern overhaul job planning, overhaul job execution, documents creation and documents flow management. Concerning the given IDEF0 and activity models, three parts of the web software can cover the whole overhaul process.

Not all information is stored in the web software database, because the company has its own enterprise resource planning system. The web software provides the functionality which is needed to support supply chain integration, without interfering into internal information system of the company.

CONCLUSION

Railway braking devices present devices which have overhaul process which is important for their everyday exploitation. The process involves many participants and documentation. The paper presents one approach to process integration. The process models were created and then the appropriate web software for integrating planning and execution of the overhaul process is developed. Further research issues will concern the development of the model for tracking of the railway braking device during its overhaul lifecycle phases.

ACKNOWLEDGEMENTS

Research for this article was conducted under the project — Development of software to manage repair and installation of brake systems for rail vehicles, Ministry of Science of Serbia, no.035050, for the period 2011.-2014.

REFERENCES

[1] I. Jacobson, "The Object Advantage," Addison-Wesley, ISBN: 0-201-42289-1, (1995)

[2] R. Aguilar-Saven, "Business Process Modelling Techniques and Tools," Department of Production Economics, WP291, Linkoping Sweden, (2001)

[3] Integration Definition for Function Modelling (IDEF0), Draft Federal Information Processing Standards Publication 183, National Institute of Standards and Technology, USA, (1993).

[4] G. Booch, J. Rumbaugh, I. Jacobson, "The Unified Modelling Language User Guide" Addison-Wesley Longman, Inc., (1999)

[5] P. Lawrence, "Workflow Handbook", Workflow Management Coalition, John Wiley and Sons, New York, (1997)

[6] W.M.P. Van Der Aalst, A.H.M. Ter Hofstede, M. Weske, "Business process management: A survey", Business process management, pp. 1-12. Springer Berlin Heidelberg, (2003).

[7] B. Stevanov, D. Gračanin, I. Kesić, S. Ristić, "An Application of Period Batch Control Principles and Computational Independent Models for Supporting the Overhaul Process of Railway Braking Devices, International Journal of Industrial Engineering and Management IJIEM, Vol. 4(2), pp. 95-101, (2013)

[8] D. Gračanin, B. Stevanov, N. Sremčev, Z. Tešić, " Manufacturing shop control integration: a concept and an example", 1. Regional Conference – Mechatronics in Practice and Education (MECHEDU), Subotica (Serbia), pp. 180-185, (2011)

Imitation Model of Dispatching System for Control on Processes in Metropolitan-Sofia

Emiliya Dimitrova[1], Vasil Dimitrov[2*]
[1]Faculty of Telecommunications and Electrical Equipment in Transport / Department of Telecommunications and Signalling, Todor Kableshkov University of Transport – Sofia (Bulgaria)
[2] Department of Power Engineering and Electrical Equipment in Transport, Todor Kableshkov University of Transport – Sofia (Bulgaria)

The paper presents the elaborated imitation model of systems DISIM-V for operational dispatching on the train traffic and DISIM-E for monitoring and control on electrical equipment and traction substations. Such advanced and efficient SCADA – systems are implemented in the Central Dispatcher Post (CDP) of Metropolitan – Sofia and cover all technological processes for monitoring and control on train traffic and power supply. The imitation model is based on the previously developed structural models of the object levels of systems. Other fundamental elements of SCADA-system are the standard module for automation, which includes the system maintaining the human-machine interface (HMI), the software on servers at the CDP, as well as the database of the state of all objects. The imitation model of the systems includes the described main blocks.

A simulator based on the synthesized imitation model has been elaborated. The presence of laboratory models of these SCADA – systems in the Todor Kableshkov University of Transport is extremely useful in the learning process. This simulation model is used for students and staff training as well as for increasing the qualification of operational staff in the underground, electricity distribution companies and railway infrastructure.

Keywords: SCADA (Supervisory Control and Data Acquisition systems); metropolitan, simulation model

1. INTRODUCTION

SCADA technologies are perceived as essential and increasingly promising method for automated control on complex dynamic processes in vital and critical areas in terms of safety and reliability. Many automated control systems in transport, energy, military, and others spheres are built on the basis of this method. Field of application of such systems is the automatic monitoring and control on non-concentrated objects in different sectors of the economy. The term "non-concentrated objects" means objects which are territorially separated each from other and from the Central Dispatcher Post (CDP), but they are united by a common process and interconnected by appropriate means of communication.

A contemporary and efficient SCADA-system is in operation in the metropolitan – Sofia and covers all the technological processes. It consists of several independent systems, the most important of which are DISIM-V for operational dispatching on the train traffic and DISIM-E for monitoring and control on electrical equipment and traction substations [1, 2, and 3].

The extensive study of the modern SCADA – systems DISIM-V and DISIM-E is not possible due to the special mode and permission of entrance. The access to the information about them is very difficult, simply because if such information is available, it is primarily commercial and advertising. This is why structural and mathematical models of these two systems have been made in advance [4]. The aim of this paper is to design an imitation model and a simulator based on these models. The purpose of elaboration of such a simulator is to learn the trainees in functions and operation of the dispatchers, as well as to penetrate into the structure and the principles of operation of a SCADA – system.

2. SCADA – SYSTEM FOR DISPATCHING CONTROL ON METROPOLITAN - SOFIA

The SCADA – system DISIM implemented in Metropolitan – Sofia performs many technological, systems and supplementary functions as follows:

- Technological functions of monitoring and dispatching control on the train traffic and electrical equipment in substations. *Monitoring functions* include continuous and automatic data collection about current status of train movements, track elements and electrical devices, as well as automatic continuous data transmission to the CDP. This information is processed and automatically displayed on video terminals and light panels. There is a possibility to print a part of this information on command from the operator. Automatic backup in chronological order of information for emergencies, dispatching commands and other events is provided. *Dispatching control functions* cover reliably sending the operator dispatch commands to the subjects and their implementation, reliable protection and prevention of illegal and wrong manipulation (password, incorrectly set or nonexistent command, unable to execute commands, etc.), automatic tracking of train number, automatic interlocking etc.

- System functions of control and internal diagnostics of the system at all its devices, including the software. These functions include an updated database maintenance for each object (underground stations, traction substations and electrical devices), as well as maintenance of a system time and date. Internal automatic control and diagnosis of the condition on all system devices is provided. Control of the condition of communication is also ensured. Locating the site and nature of any fault is possible. Monitoring and diagnostics

*Corresponding author: Todor Kableshkov University of Transport – Sofia, Faculty of Telecommunications and Electrical Equipment in Transport, 158 Geo Milev str., 1574 Sofia, Bulgaria, vdimitroff@abv.bg

of the software and formation of alarm messages for failures occurring in the system during operation are provided.

- Additional functions related to events data archiving, data analysis, preparation of various reports, printing etc. They include development of events protocol, alarms and non-alarm messages protocol, report of executed and outstanding commands, as well as testing of apparatus, software and communication channels.

All functions are fully described in [1].

The system DISIM as any other SCADA - system consists of three formal levels [1, 5, 6, and 7].

- Upper (Dispatching) level, which is situated in the CDP and include servers, video-walls, Dispatchers working places, personal computers, printers etc.;

- Communication level, which consists of Ethernet network in the CDP, optical transmission medium between the CDP and objects of control and Ethernet network in any object;

- Lower (Object) level – these are all underground stations and their interlocking, track circuits and signaling, as well as all traction substations and electrical equipment for power supply.

The structural scheme of the *system DISIM-E* is shown in Fig. 1. The object level covers all traction substations ensuring uninterruptible power supply of the underground railways. Dispatching and communication levels are independent of the number of stations on the object level. Only one substation is fully described in the Fig. 1, because all substations are constructed on the same principle.

The connection between the CDP and each substation is ensured by programmable logic controllers (PLC) Simatic S7-300 situated in the object level. They have modular structure that allows easy configuration and reconfiguration if necessary (e.g. when there are changes at the object). Electrical devices connected to input/output controller's modules are the following:

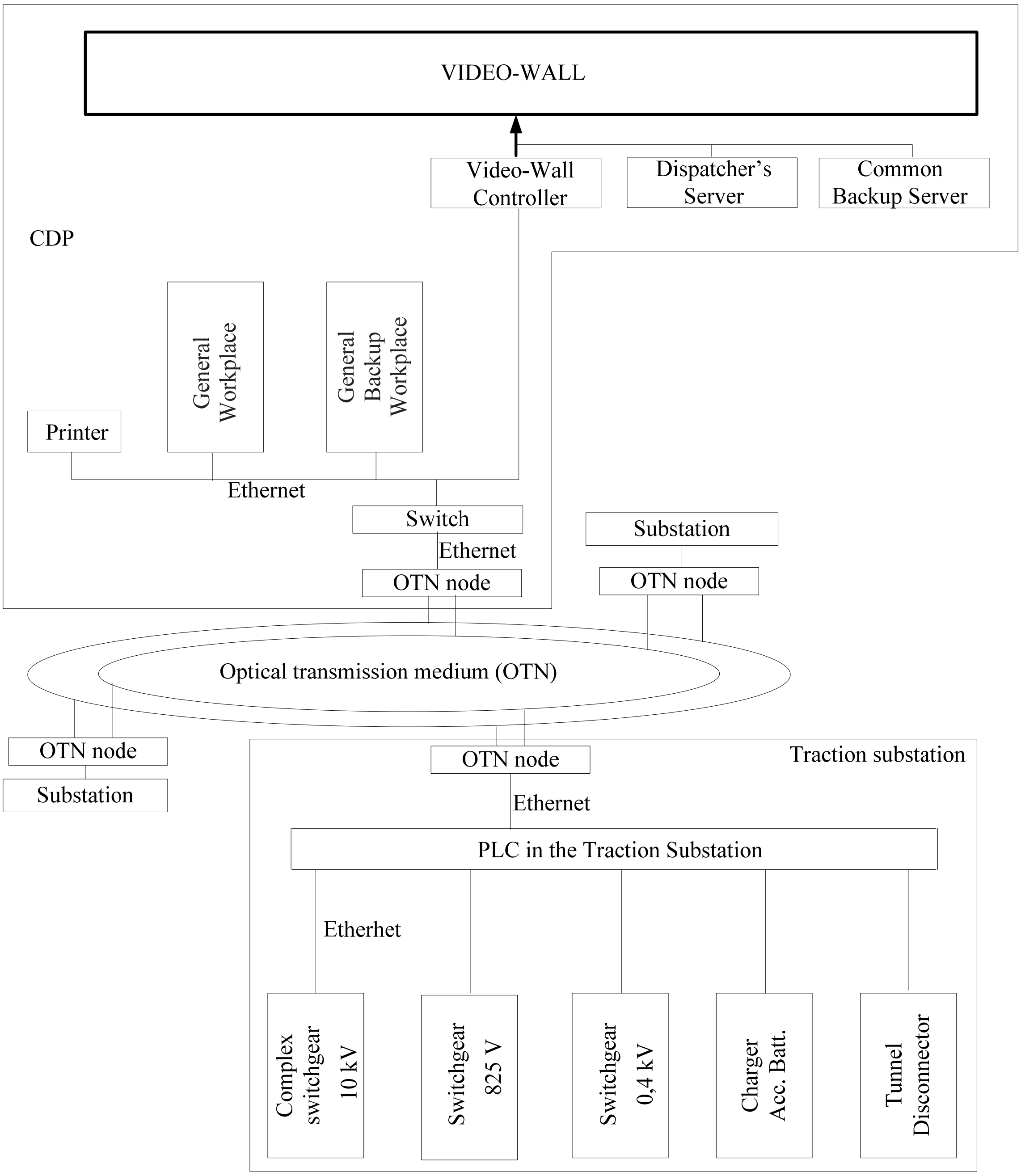

Figure 1: Structural scheme of SCADA-system DISIM-E

- Complex switchgear 10 kV, connected to the PLC (for example by Siprotec protection equipment and PROFIBUS DP). Siprotec is used for line protection of high voltage networks. The relay performs all functions of backup protection supplementary to transformer differential protection and provides control of the circuit-breaker, further switching devices and automation functions;

- Switchgear 825 V, connected to the PLC (for example by Sitras PRO and optical channel). Sitras PRO combines DC protective unit for DC railways and controller. It protects DC switchgear and contact line systems against critical operating conditions and detects short-circuits during the current rise even before the maximum short-circuit currents are reached;

- Switchgear 0,4 kV, connected to the PLC (for example by Simatic ET 200S and PROFIBUS DP). ET 200S is a multifunctional, highly modular I/O system. Fast I/O modules, isochronous mode and an extremely fast internal data transport increase the performance of the ET 200S. Interface modules with an integral CPU transfer the computing power of an S7-300 CPU directly into the I/O device and constitute a local controller. They offload the central PLC, and permit rapid responses to time-critical signals;

- Tunnel disconnectors, connected to the PLC (for example by Simatic ET 200S and optical channel);

- Chargers of the accumulator batteries.

Information about the state of the electrical equipment in the substations is transmitted to the CDP through the communication level by optical channels. Thus the connection between object level PLCs and computers situated in the CDP is ensured.

The object level in the *system DISIM-V* is based on the same principle. The PLC is connected to the electrical interlocking devices. The main controlled elements are points, traffic lights, track circuits and general alarm and signaling. Normally trains run on automatic locomotive signaling indications for automatic speed regulation (ALS-ASR) in the cab. In case of failure of one of the elements of ALS-ASR trains run on automatic block system signals.

The data about the track circuits state and the current status of the station are translated to the CDP by the PLC through the communication level.

The communication level in both systems is built on the principle of Optical Open Transport Network (OTN) [8, 9, and 10]. Its key features are absolute reliability, its openness, simplicity, the ability to cover very large distances (up to 2000 km), and future-proof design. It offers full connectivity with all current standards, which makes it very user friendly. Two optical rings are implemented to assure higher reliability.

Operating an OTN involves neither complex routines, nor extensive parameterizing to program a connection. Each node has several ports where the peripherals can be plugged in through interface cards. This fact eliminates the need for additional converters, codecs or multiplexers. A user-friendly OTN Management System (OMS) controls the network down to interface level. This reduces the need for training and the risk of errors.

The data received from the all objects enter in "Train Dispatcher Server" or "Power Supply Dispatcher Server" respectively. There their treatment is carried out according to the system algorithm.

The main components of these SCADA – systems are PCs and specialized and custom-developed software. IBM computers with high reliability and extended warranty are used. The system DISIM works in a Linux environment and provides a comfortable and simple dialogue and an opportunity for easy manipulation. Dialogue with the system is in Bulgarian and performed via keyboard and mouse – standard peripherals of computers. DISIM is running under control of a complex program structure, which consists of high standard software package and specialized applications. Different programming facilities at all of the system levels are involved [9, 11]. The software includes field controller program, database development and operator workstation application software. There is programming involved at the controller level, the communications level and the workstation level which integrates all elements of the system and ensures its functional work. Software has been developed on a modular basis and each module performs a technological or system function. The standard software used in the system is: OS LINUX; Graphics upgrade X-Window System; X.org server; Package management windows - Metacity; Software to work with a video wall controller; Software for use with a programmable controllers' object level; Standard Java Virtual Machine; Implementation of the CORBA specification TAO / ACE, omniORB; Management System database – PostgreSQL.

3. IMITATION MODEL OF SCADA – SYSTEMS DISIM-V AND DISIM-E

Based on the developed structural models of the object levels of systems for monitoring and control on train movement and traction substations and electrical equipment developed in [4], an imitation model of the system for monitoring and management of processes in the underground is synthesized (see Fig. 2). Besides the object levels, another fundamental elements of SCADA-system are the standard module for automation, which includes the system maintaining the man-machine interface, the software on servers at the CDP, as well as the database of the state of all objects.

The imitation model of the object levels of the systems is built up by the following main blocks:

Block 1 – models of functioning of the system for management of train movement and electrical equipment;

Block 2 – models of assessment and analysis of the state of train movement, electrical equipment and management system;

Block 3 – models of decision making in the system for management of train movements and electrical equipment.

The following subsystems are included in the structure of Block 1:

6 – Models of functioning of the train movement;

8 – Models of functioning of the substations and electrical equipment;

7 – Model of interaction of the components and subsystems;

9 – Model of the environmental impact (disturbances);

10 – Imitation model of the results of using the target management system.

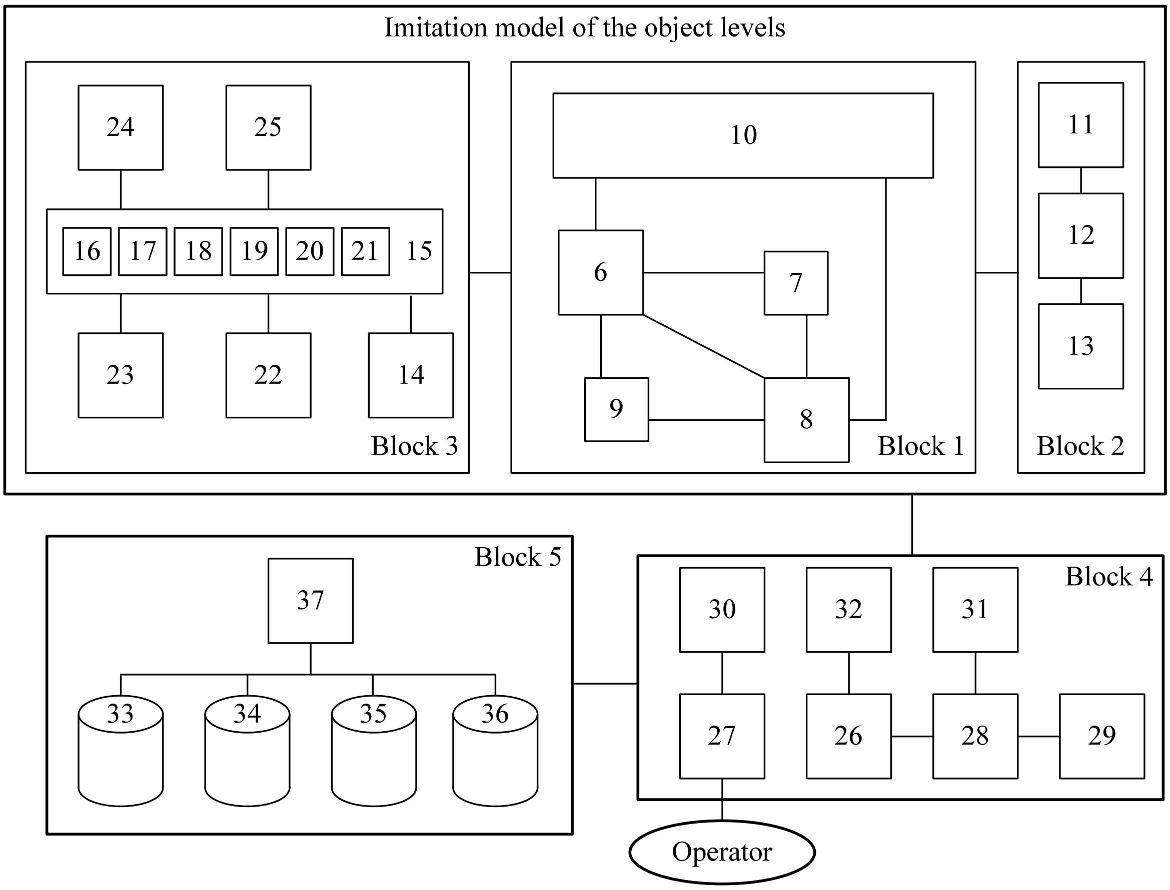

Figure 2: Aggregated structural scheme of the imitation model of the system for monitoring and control on the processes in metropolitan

Block 2 is built up of the following modules:
11 – Models and algorithms of assessment and analysis of the state of technical devices in the system for management and control of the train movement;
12 – Models and algorithms of assessment and analysis of the state of substations and electrical equipment;
13 - Models and algorithms of assessment and analysis of situations.

The following subsystems are included in the structure of Block 3:
14 – Models and algorithms of long-term and operational planning of interaction operations in the system for management of train movement, train schedules;
15 – Models and control algorithms of structures in the system for management of train movement and electrical equipment: topological models of stations (block 16), models of technical devices (block 17), technological models of substations and electrical equipment (block 18), a model of the organizational structure (block 19), a model of the structure of special software and mathematical base (block 20), a model of the information structure (block 21).
22 – Models and algorithms for solution of various possible situations;
23 – Algorithm of switching substations and electrical equipment after assessment of the situation;
24 – List of basic events;
25 – List of alarms and non-alarm messages.

An important element in the imitation model is Block 4 - system for control, joining and interpretation that connects the operator and the system. The following blocks are included in its structure:
27 – Common dialog system of control on the specialized software and mathematical base;
30 – Block for processing, analysis and interpretation of the results of operator's management (protocol of the submitted commands);
26 – Software for visualization of the state of objects of control;
28 – Software for initialization and visualization of alarms and non-alarm messages;
29 – Block for making recommendations and proposed solutions;
31 – Protocol of events (records);
32 – Train-graph.

The information base (Block 5) plays important role in the synthesis process. Its structure includes:
33 – Database of the state of train movement;
34 – Database of the state of substations and electrical equipment;
35 – Database of the state of control system;
36 – Database of the analytical and imitation models of functioning and decision making;
37 – System of control on databases.

4. SIMULATION MODEL OF SCADA – SYSTEMS DISIM-V AND DISIM-E

The simulator is installed on five computers – one server with two monitors and four stations. It represents a model of the SCADA–systems DISIM-V and DISIM-E. The imitation model (Fig. 2) is implemented by special software. The object levels of both systems (Blocks 1, 2, 3 and 5 in Fig. 2) are installed only on the server. The communication level consists of only Ethernet network between the five computers. The dispatcher level (Block 4 in Fig. 2) is installed on all computers, but the four stations use the server for the communications with the objects.

The lecturer has to select which system to be started: DISIM-V or DISIM-E. After the server is working properly in the selected mode the rest computers must be also started in the same mode.

Once the system DISIM-V is turned on and running, the image of the Main dispatcher panel appears at the bottom of the monitor. This is the status-bar including the following buttons representing several functions: *Stations*; *Schedule*; *Automatic tracking of the train number*; *Active events*; *Commands*; *Records* (Protocol of events); *Train-graph*; *Change of the Dispatcher*; *Instruments*.

Six subway stations are included in the simulation model of DISIM-V. Their track development and signalling represent following real metropolitan stations (MS) of first and second diameters: MS "Obelya" with two points, MS "Slivnitsa" (MS 01 with six points – see Fig. 3), MS "Lyulin" (MS 02 without points), MS "Lomsko shosse" (MS201 with two points), MS "Beli Dunav" (MS202 without points) and MS "Nadejda" (MS203 without points).

Besides the points, track circuits and traffic lights the following elements are displayed on the schemes: indicators and buttons for Dispatching or Backup Local Control ("ЦДУ" or "РМУ"), buttons to reverse points („ОСБ", „стр.1" ... „стр.6"), a main button for annulment („ГОБ"), performance indicators of the automatic block system („АБ"), interlocking („ЕЦМ"), charger („КТЗУ"), etc.

The PLC in the appropriate station is simulated by tables representing its inputs and outputs. The lecturer could select between two modes: Real Mode or Emulation Mode ("Emul Mode") using the button "*Instruments*". Real Mode is used for the simulation of the response of the controller to a command issued in system DISIM-V. The trainees could activate any command in the graphic station image and watch the appropriate change in the table representing PLC of the same station. In Emul Mode the trainees can simulate signals – they could activate any bit of the table representing station PLC and watch the appropriate change of the station state. There is a possibility of randomly generated bits giving the interval (in seconds) and the number of generated signals per 1 sec.

Registered events and submitted commands can be reviewed by button "*Records*". It is used to extract the reports to the operation of the system. Some filters could also be used.

A menu to select the list of active events for the station or for the whole system appears pressing the button "*Active Events*". Active events are arranged in a table, sorted by time of recording. Most previously registered events are at the top. In first column the different color squares define the event: emergency events are colored in purple, warning – in orange and informational – in gray. Each event must be confirmed.

The module "*Automatic tracking of the train number*" is particularly important module of the system DISIM as in normal operation dispatcher most often communicate with it. Functions of this module are as follows:

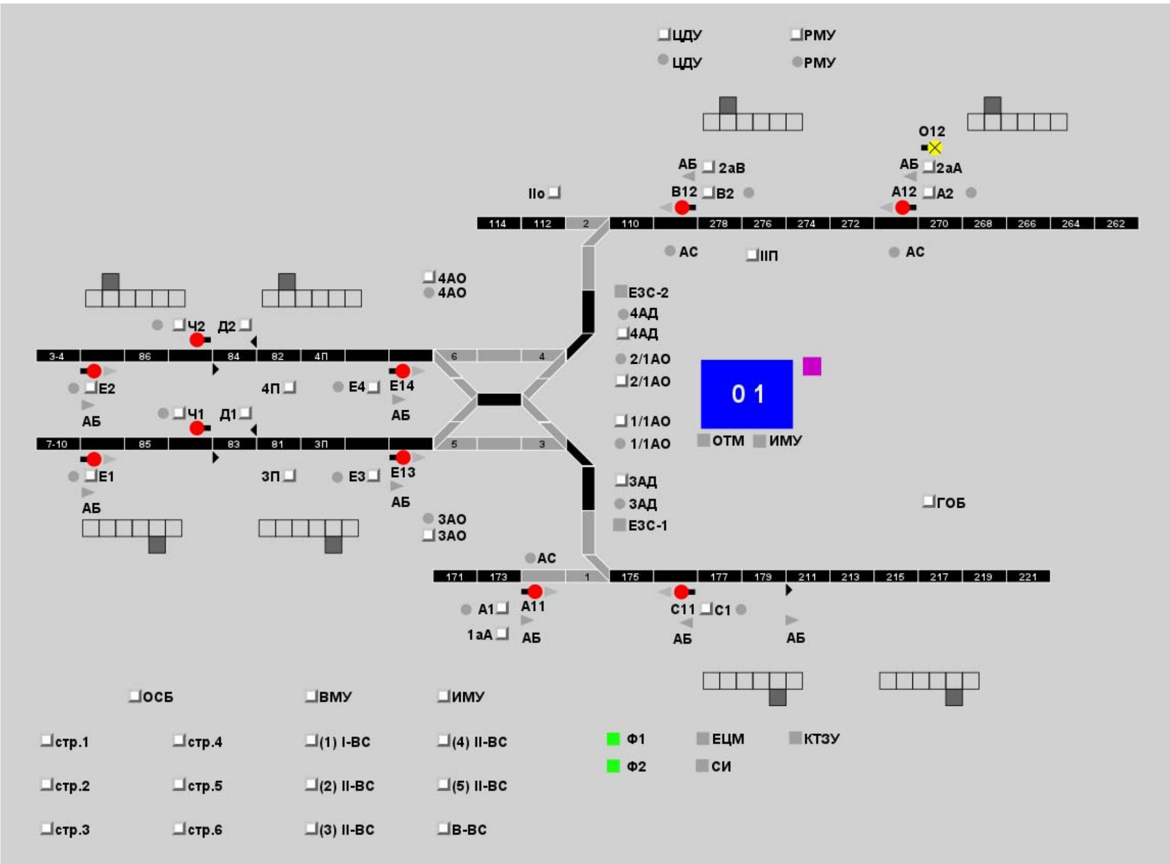

Figure 3: Simulation model of MS "Slivnitsa" (MS 01)

- Automatic and manual numbering of trains running on the route;
- Ensuring that the trains run on time and reporting the time delay of each train;
- Automatic transmission of the train number;
- Generate data for module "Train-graph".

The trains move at a different number each course, but it must retain its route. Therefore, at the beginning of the course the new train number is to be determined. Defining track circuits are the places where the module "*Automatic tracking of the train number*" defines the new train number and where the dispatcher could manually set the train number based on the active schedule.

Each occurrence of message "Time delay of a train" is emergency event and the dispatcher must immediately confirm it and call the train driver to understand causes.

Module "*View schedule*" allows the dispatcher to view schedules that were included in the simulation model. Window "View schedule" consists of the following parts: "List of schedules", which have been introduced into the system; "Buttons of choice of course" (next or preview); "Course number"; "Visualization of the time of arrival of the train in selected station" etc.

Dispatcher has to enter the information about damaged track circuits using the button "*Track circuits out of control*". These track circuits are colored in blue or purple. The track circuits that are properly working are colored in black ("free"), red ("occupied") or yellow ("locked in route").

A detailed description of the possibilities of examination of the simulator of the system DISIM-V has been done in [12, 13].

In the simulation model of the system DISIM-E, four stations representing the real models of traction substations (TSS) of the second diameter of the Metropolitan Sofia are included. The aggregated view of these stations is shown in Fig. 4: TSS-34 (ТПС-34), adjacent to the MS-205 (metropolitan station "Maria Louisa"); TSS-33 (ТПС-33), adjacent to the MS-206 (metropolitan station "Central railway station"); TS-32 (transmission substation ПС-32), adjacent to MS 207 (metropolitan station "Lions Bridge"); TSS-31 (ТПС-31), adjacent to MS 208 (metropolitan station „Serdica II").

The detailed view of the selected station can be shown by clicking on its number. The ability to monitor the state and management of the facilities in the area has been achieved. The topological description of the selected station is illustrated by following symbols used in schemes: squares (with numbers 81, 85, 87, 86, 88, 82 – Switchgears with remote control situated in Complex switchgears 10 kV; with numbers 71, 72 – remotely controlled Switchgears near to transformers; 61-65 – remotely controlled Fast Acting Switchgears 825 V); circles (with numbers 80, 171, 172 – remotely controlled disconnectors in circuits providing traction power supply; with numbers 31,32 – remotely controlled disconnectors in circuits providing power supply of the metropolitan station; with numbers 41-57 – tunnel disconnectors with remote control).

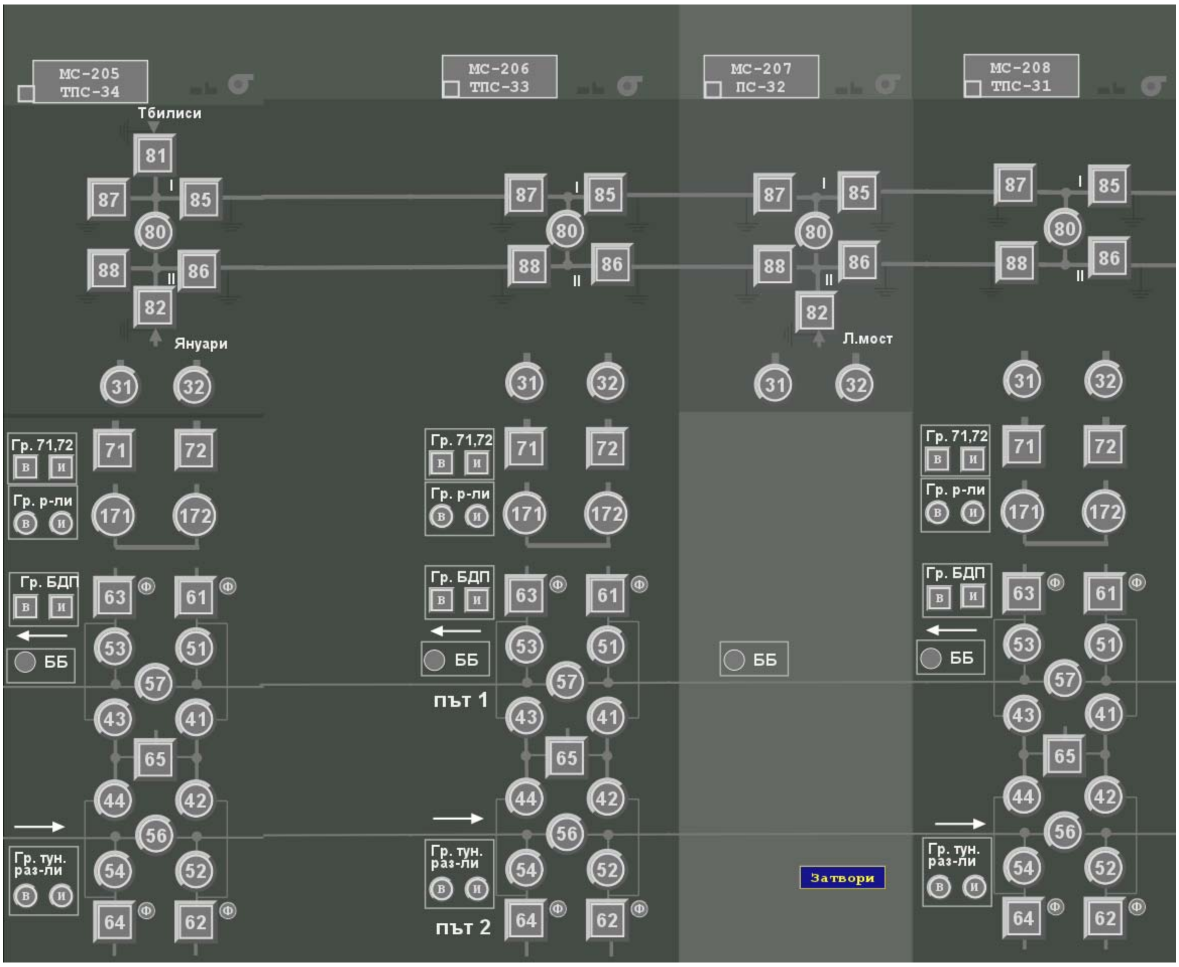

Figure 4: Aggregated view of the four substations (Level II))

Group buttons to turn On and Off are also provided (Гр.71,72; Гр.р-ли, Гр.БДП, Гр.тун.р-ли). There are alarm indicators near to each device. Each transmission substation providing 10 kV power supply has its own name (Тбилиси, Януари, Л.мост). An emergency button (ББ) is provided at each underground station.

The use of this simulation model is similar to the system DISIM-V. It should be noted that the states of the objects are much more and the necessary address space of the programmable logic controllers is greater. Using the button "Stations" in the Main dispatcher panel each station can be displayed on the monitor (Level III) and the state of its components can be watched (transformers, rectifiers, switchgears, disconnectors, circuit breakers, alarm indicators, fuses, buttons, groundings, batteries etc.)

The state of the electrical equipment can be changed by module "Instruments" in two modes – Real and Emulation, similar to the system DISIM-V. Each object on the screen at any time is colored according to its state at that time, namely: Green (the object is off); Red (the object is turned on); Yellow (the object is grounded); Orange (Active Event "Warning"); Purple (active event "Breakdown" or "Breakdown" and "Warning"); Gray (the object has not defined condition). A detailed description of the possibilities of examination of the simulator of the system DISIM-E has been done in [14].

5. CONCLUSION

The availability of contemporary simulation models of SCADA – systems DISIM-V and DISIM-E in the Todor Kableshkov University of Transport is extremely useful for students in the learning process. It simulates real monitoring and control on the processes in a complex system such as the underground. This simulator enables trainees to deepen their knowledge in the core of modern SCADA – technology and offers an opportunity for them to gain knowledge in the real application of a system managing highly complex industrial site, its structure and rich functionality. There is no other simulator with such features, functions and purpose in Bulgaria.

The simulator illustrates the implementation of all basic functions for dispatching control on train movement and electrical equipment. The capability to simulate a number of real modes is created by:

1) Monitoring of the objects of control: trainees can watch their state and proper operation, observing alarms and non-alarm messages waiting confirmation and adequate reaction from them (dispatcher).

2) Operational dispatching on train traffic: trainees have an opportunity to order route, to pull out and introduce track circuits under dispatcher control, to choose the operating schedule, to monitor on correct functioning of signalling. They are required to take adequate solutions for each situation such as a train dispatcher on duty.

3) Dispatcher monitoring and control on traction substations and electrical equipment: trainees have to perform switching to provide uninterrupted power supply with the necessary voltage, to turn off a substation or device at failure and ensure power supply from adjacent substation, to turn on the repaired devices if it is necessary. Thus trainees are required to take adequate solutions after assessment of the particular situation such as a power dispatcher on duty.

Therefore this simulation model is very useful for training students and staff working in the operation of underground, railway infrastructure and electricity distribution companies.

REFERENCES

[1] Е.Д. Горанов, Е. А. Димитрова, "Системи за дистанционен контрол и управление в транспорта", ВТУ, София, (E. D. Goranov, E. A. Dimitrova, "Systems for Remote Monitoring and Control in Transport", Manual, Todor Kableshkov University of transport, Sofia (Bulgaria), (2010)

[2] Technical documentation of SCADA – system DISIM-V, Sofia (Bulgaria), (2012)

[3] Technical documentation of SCADA – system DISIM-E, Sofia (Bulgaria), (2012)

[4] E. Dimitrova, "Models of objects of control in SCADA– System for Monitoring and Operational Dispatching on Metropolitan-Sofia", XLIX International Scientific Conference on Information, Communication and Energy Systems and Technologies "ICEST 2014", Nis (Serbia), (2014)

[5] K. Stouffer, J.Falco, K.Kent, „Guide to Supervisory Control and Data Acquisition (SCADA), and Industrial Control Systems Security", National Institute of Standards and Technology, Gaithersburg (USA), (2006)

[6] D. Bailey, E. Wright, "Practical SCADA for Industry", Newness, Elsevier Inc., Philadelphia (USA), (2003)

[7] "System automation in substation", available on: http://www.roconbg.com/en/engineering-services/system-automation-in-substation-12

[8] "Technical documentation of ETR-150 Network card", OTN Siemens, Brussels (Belgium), 2003

[9] G. Clarke, D. Reynders, E. Wright, "Practical Modern SCADA Protocols", Newness, , Elsevier Inc., Philadelphia (USA), (2004)

[10] "OTN Systems – Dedicated Networks for Critical Environments", available on: http://www.otn.be/

[11] S. G. McCrady, "Designing SCADA Application Software: A Practical Approach", Elsevier Inc., Philadelphia (USA), (2013)

[12] E. Dimitrova, "Laboratory SCADA – System for Control on Railway Traffic", Proceedings of XLVIII International Scientific Conference on Information, Communication and Energy Systems and Technologies "ICEST 2013", 26 – 29 June 2013, Ohrid, Macedonia, Vol. 2, pp. 479-482 (2013)

[13] E. Dimitrova, V.Dimitrov, " SCADA–system for control on train movement – laboratory simulator", University of Ruse "Angel Kanchev", Proceedings, Vol. 52 (3.2) "Electrical Engineering, Electronics, Automation", pp. 91-95, Ruse (Bulgaria), (2013)

[14] E. Dimitrova, " Simulator of SCADA – system for remote control on electrical equipment", Proceedings of Technical university of Sofia, Vol. 63 (5), pp. 313-320, Sofia (Bulgaria), (2013)

Optimization of Freight Wagons Fleet of Republic of Bulgaria

Valeri Nikolov[1], Boris Galev[1]
[1]Machinery and Construction Technologies in Transport/Transport equipment, Todor Kableshkov University of Transport, Sofia (Bulgaria)

As a result of the political changes and decreased volume of freight traffic an optimization of the freight rolling stock had to be performed.

A study has been conducted for this purpose, which included analysis of the volume of transported goods by type of cargo and type of traffic (domestic, I/E, transit) and analysis of the freight wagons fleet, including analysis of turnover and technical condition of wagons according to their classification.

Analysis of the maintenance conditions, construction, purchasing and renting as well as analysis of the operational processes were also performed.

Determination of the requested freight wagons fleet size, as a result of the optimization of the number of freight wagons for domestic and international traffic, has been accomplished after completion of the abovementioned studies and analyses. The annual rate of amortization charges, as well as values of the loss of revenues from not carried goods for one turn (wagon) and the number of unproved (rejected) wagons were taken into account for defining of the general cost for optimization of the number of freight wagons

Keywords: rolling stock, railway maintenance, innovation, vehicle dynamic, freight wagons

1. INTRODUCTION

The Republic of Bulgaria began the reconstruction program of entire economy from planned economy to a free market system since 2007. This restructuring program aims to direct economic activity towards the steady growth in the short and medium term. General economic situation in the country requires a thorough structural analysis of the freight wagon fleet of the country. Consequently, the large decline in economic activity and restructuring of production leads to a sharp reduction in the volume of freight carriages. This reflected on the maintenance of a large freight rolling stock fleet irrelevant to the current needs which caused its reduction. One part of the wagon were decommissioned under the general name "wagons in isolation". For these wagons were not applied amortizations as they didn't participate in the transport process and were not considered as impoverished?

On the other hand it is expected that freight volume will increase due to the economic growth, which requires commissioning of newly purchased or repaired wagons. However, the change in the structure of the services requires maintaining an appropriate fleet of freight wagons.

Determining the optimum number of freight cars in series is an important point to overcome the problem of inefficient use of resources, while satisfying the maximum request.

In recent years the European Union has a steady downward trend in the market share of rail transport and increase the growth of road transport. This trend is due to the fact that the growth rate of rail transport is less than the rate of growth of road transport.

The analysis of indicators - volume of cargo in mill. tons and performed work in million tonkm shows that the main competitor to rail transport in the distribution of the transport market is still road transport with a clear tendency that the last one will increase its market share.

In the context of growing competition and in order to work effectively railways should calculate actual savings through the establishment of appropriate objective functions of the transport models. However, the models should take into account how different options will affect the ability of the railway company to meet the requirements of their customers that will help to increase the revenue.

Management of the number and structure of the freight wagon fleet is important issues, that requires application of a model. Vehicles must be specifically examined by series as individual types of loads using appropriate types of wagons. To correct model is necessary to make a detailed analysis of the status and performance indicators for freight wagon fleet by type wagons.

2. EXAMINATION OF VOLUME OF CARRIAGES

2.1. General analysis of carriages

The table shows data about carried goods. The process of slow growth began in 2005, and continued in 2008.

The data shows increase in more than 1 million tons compared to 2005. Gradually overcome the sharp reduction in shipments in 2003 and 2004, but in 2009 there is a sharp decrease in shipments, which in 2010-2013 slightly increased [1, 2, 3].

Comparing the percentage of increase in tonnes transported in 2012 to 2011 (12.47 million tons in 2012 against 11.61 million tons in 2011, or 7.4%) in proportion to the work done for the same years shows that the reduction of PCD is not only due to new carriers, but also to change the nature of transport by increasing shipments on shorter distances.

*Corresponding author: 158 Geo Milev Str., Sofia, Bulgaria, val1953@abv.bg

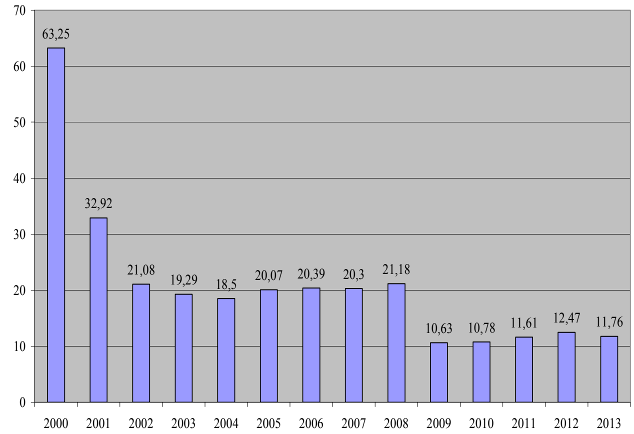

Fig.1. Carried mill. tones by years

2.1. Analysis by types of goods

Railway transport is preferred for transporting of so called bulk cargoes on medium and long-haul distances: coal and coke, which occupy over 22 % of all goods transported by rail transport. ores and concentrates - about 21% , oil - about 9% , metals - about 12% , fertilizers - just over 2%, cement - 2%, cereals - around 2%, chemicals and chemical products - 7-8%, etc...

Railways mainly transport solid mineral fuels (about 75%) , crude oil (100%) , iron ore and scrap (60%), ores of nonferrous metals (about 95%), metal products (about 75%) , natural and chemical fertilizer (60-65 %). Shares of rail and road transport in carriages of chemicals, pulp and paper waste and construction ceramics are approximately equal, and for all other groups of goods road transport is preferred.

The structure of the main bulk cargoes (coal, ores and concentrates, metals, oil and oil products, fertilizers, cement, etc.) remaines relatively constant over time.

Data from the first quarter of 2014 shows that there is an increase of shipments for: food and feed and solid mineral fuels (Table 1).

By type of cargo volumes are as follows**:** According to NHM in the first quarter of 2014 compared to the same period of 2013 is **an increase** of transported cargo volume in:

• Foods and feeds with 11 thousand tons;
• Solid mineral fuels with 453 thousand tons;
• Ores and metal scrap with 7 thousand tons;
• Processed and unprocessed mineral resources with 16 thousand tones;
• Chemical substances and products with one thousand tons.

Reduction of carried goods is reported for:

• Agricultural products and live animals 19 thousand tons;
• Products of ferrous and nonferrous metallurgy with 9 thousand tons;
• Fertilizers 38 thousand tons;
• Machinery, vehicles, manufactured goods 33 thousand tons.

Table 1

Goods	3Q 2014			3Q 2013			2014/2013	
	'ooo t	Share	Mln. tkm	'ooo t	Share	Mln. tkm	'ooo t	Mln. tkm
Agricultural products and live animals	30,6	1%	7,2	49,9	3%	11,6	-39%	-38%
Foods and feeds	61,1	3%	12,7	49,9	3%	10,9	22%	17%
Solid mineral fuels	1146,5	50%	148,4	711,3	37%	59,4	61%	150%
Oil and petroleum products	182,1	8%	44,3	182,4	10%	52,3	0%	-15%
Ores and metal scrap	208,4	9%	56,2	201,2	11%	54,4	4%	3%
Products of ferrous and nonferrous metallurgy	108,9	5%	32,0	117,6	6%	35,1	-7%	-9%
Processed and unprocessed mineral resources	180,2	8%	45,0	164,2	9%	40,5	10%	11%
Fertilizers	27,2	1%	7,2	65,2	3%	14,7	-58%	-51%
Chemical substances and products	85,1	4%	24,4	84,0	4%	23,5	1%	4%
Machinery	242,0	11%	67,3	275,1	14%	84,9	-12%	-21%
Total	**2 272,3**	**100%**	**444,9**	**1 900,7**	**100%**	**387,5**	**20%**	**15%**

2.2. Analysis by type of traffic

Goods carried by type of carriage for the three months of 2014 compared to the business plan and report for the same period in 2013 are shown in Table. 2.

Table 2

Indicators	Report 3Q 2014	Plan 3Q 2014	1/2 (%)	Report 3Q 2013	1/3 (%)
Handled goods ('000 tons)	**2 272,3**	**2 360,0**	**-3,7%**	**1 900,7**	**19,6%**
-carried goods ('000 t)	1 678,4	1 699,2	-1,2%	1 275,5	31,6%
-tonekm, mln.	291,6	293,3	-0,6%	211,2	38,1%
-carried goods ('000 t)	593,9	660,8	-10,1%	625,2	-5,0%
-tonekm, mln.	153,2	192,8	-20,5%	176,3	-13,1%

For the first quarter of 2014 railways transported 1 678,4 thousand tons of cargo in domestic traffic, which represents 74% of the total cargo transported during the reporting months. Amount of transported goods in domestic traffic is 402.9 thousand tons transported over the same period of the previous year and 20.8 thousand tons less than budgeted in the business plan. 291.6 million net tone kilometers were produced, with 80.4 million tones more than the previous year and 1.6 million net tones less than in the business plan.

In international traffic are transported 593.9 thousand tons of cargo, which represents 26% of the total cargo transported during the reporting period. Compared to the same period of the previous year, numbers had declined by 31.3 thousand tons, compared to the business plan were carried 66.9 thousand tons less. 153.2 million tkm were produced with 23.1 million tkm less than the corresponding period previous year and 39.5 million net tonnes less compared to the business plan.

For the first quarter of 2014 shipments of goods in international traffic decreased compared to the first quarter of 2013, the total fell by 31.3 thousand tons compared to the corresponding period of the previous year or with 5%.

Export and import, respectively, had an increase of 11.5% and 17.7% of the transported goods, but it can not compensated for the significant drop of 35.6% in transportation.

Table 3

International traffic	Carried goods ('000 t)				Difference +/-	%
	1Q. 2014	Share %	1Q 2013	Share %	2014 - 2013	2014 /2013
International - export	207,6	34,9%	186,2	30%	21,4	11,5%
International - import	228,7	38,5%	194,2	31%	34,4	17,7%
Transit	157,7	26,5%	244,8	39%	-87,1	-35,6%
Total	**593,9**	**100,0%**	**625,2**	**100%**	**-31,3**	**-5,0%**

Import represented *38.5%* of the total cargo transported in international traffic in the first quarter of 2014 by "BDZ - Cargo". Quantities of imported goods are *34.4* thousand tons more than the imported during the period of 2013.

Transit represents *26.5%* of the total cargo transported in international traffic in the first quarter of 2014 from "BDZ - Cargo". The decrease in transportation, compared to the corresponding period of 2013 was *87.1* thousand tons or *35.6%.*

The volume and techno-economic indicators characterizing the operational activity of "BDZ - Cargo" in the first quarter of 2014 are shown in the following table.

Improvement was observed in the following indicators:

• average daily wagon performance based on netto tkm produced has increased by *10.4%* compared to that recorded in the first quarter of 2013

Productivity of the freight wagon from operating fleet shows netto tkm work produced by one wagon from the operating fleet, i.e. quality and efficiency of managed assets. This leads to improved quality of service and helps to reduce the relative cost of transport per tone load.

• Turnover of the wagon for the first quarter of 2014 was 8.8 days and is reduced by *12.1%* from that reported in the corresponding period of the previous year, when it was 10 days. This indicator reflects the time from one to the next load the wagon. The turnover of the wagon depends on the time of loading and unloading. It can be influenced by the work in the intermediate stations where were processing with the wagons, as well as at the start and end stations. The lowest turnover had the specialized wagons (grain, saddle), as they allow faster processing (loading and unloading). Wagons for general cargo have a slower turnover. It is necessary to keep roadworthy the specialized wagons.

• The rate of empty mileage was reduced by *41%* in the first quarter of 2013 to *38.8 %* in the same period of the 2014. This is a good result and shows that freight wagons from operating fleet were used effectively. This indicator is directly dependent on the type and structure of freight and the use of specialized wagons.

• The average static load capacity shows the use of wagons. It depends on the type of load and the structure of the vehicle. The highest average static load is for bulk goods - corn, grain, sand, coal, cement and others. For the first three months of 2014 this indicator has improved by *1.1 %* compared to the same period in 2013 and is *46* tons.

• The average gross weight of the cargo trains increased by *11.6%* compared to the first quarter of 2013 and is *868* tons.

• Trainkm operation was reduced with only *1%,* i.e. with fewer trains were carried nearly *15%* more tonne-kilometers .

• Section and technical speeds are slightly lower compared to the first three months of 2013. This is due to repairs on the railway network and the speed limits on it.

3. ANALYSIS OF FREIGHT WAGONS FLEET

3.1. Dynamics of the freight wagons fleet

Freight wagon fleet consists of about H units that as type and number meets the transport needs at this stage. A special feature of the park is that *98 %* of cars are four-axel with boogie Y 25 CS, which is unified and operated in the majority of European railway undertakings. These bogies allow wagons to move at a maximum speed 120 km/h in an empty state and *100 km/h* in loaded with axle load *20 t/axle*. In a constructive attitude wagons meet the requirements for operation in international traffic. The main problems that exist are mainly related to the technical condition and above all, with the condition of the cargo spaces of open wagons.

Over the years under conditions of constant competition with road transport, much of the inventory fleet of wagons becomes redundant and logically decreases. This is dictated by the continuous decrease in the volume of shipments by rail.

In connection with the provisions of Art. 7 (1), item 5 and Art. 115a , # 6 of the Railway Transport Act and Article 14, #4 and 5 of Directive 96/48/EC and 2001/16/E, the need arose to build a number of registers in the railways.

One of the most important elements is the Information System "eRegister of rolling stock".

The main goal of building eRegister is to systematize data on existing rolling stock owned by public or private institutions to its adequate management and full integration of the Bulgarian railway system in the European Union.

Table 4 shows the decrease in rolling stock fleet in the last 5-6 years.

Table 4. Freight wagons fleet in operation by years

serie/year	2003	2005	2007	2009	2011	2013
Covered	1 159	1 156	1 054	1 059	945	910
Platform	2 163	2 175	1 518	1370	1261	1200
Opened	5 154	5 065	6 094	6017	5682	4890
For grains	994	1 126	817	834	811	702
For ores	664	664	728	726	682	548
Saddle	414	414	490	485	467	412
Hoppers	439	0	27	27	27	27
Tank	2 499	2 240	1 044	865	840	631
Isotermic	58	58	50	50	50	50
For cement	666	645	500	451	355	302
Total	14 210	13 543	12 322	11 901	11120	9 672

3.2. Age analysis of the fleet

"Aging" and looting the fleet had a significant impact on the technical condition of the wagons, a large part of which remain on station tracks inoperable [4, 5].

Table 5 shows that the main share of wagons is between 15 and 30 years and these are just open wagons, which carry the main quantities of bulk goods for the industry, metallurgy and energy.

Table 5. Condition of wagon feet by the age

Type of wagons	Total number	Under 15 y	15-20 y	20-25 y	25-30 y	Over 30 y
Covered	910		156	538	110	106
Platform	1 200	111		905	161	23
Opened	4 890	98	1506	1752	1455	79
For grains	702		391	176	135	
For ores	548		524	17	7	
Saddle	412		321	91		
Hoppers	27			4	20	3
Tank	631	114	184	191	82	60
Isotermic	50		0	50		
For cement	302		100	101	101	
TOTAL	9 672	323	3 182	3825	2 071	271
%		3,3	32,9	39,5	21,4	2,8

3.3. Analysis of freight rolling stock condition

If we look at the park of wagons over the last six years, will see that as it decreases. Reduction comes from the aging of the wagons - their subsequent repair is impractical, due to their technical condition these cars are scrapped.

In terms of volume of traffic over the years from mines, ports, bases for processing of metal waste and bulk requires removal of open wagons and saddle from isolation and introduction into service.

Open wagons are the most widely used wagons for the transport of goods. Relatively insufficient thickness of which are built side walls and floor of this wagon, the use of inappropriate material handling harms their technical condition.

The significant presence of corrosion and deformation components of the cargo space makes them unsuitable especially for the carriage of bulk cargoes. Open wagons are highly crumble when loaded with scrap metal, *5438* open wagons, of which *548* were for transport of ore. Serviceable are *3533* cars, but about *800* pieces are with strong corrosion of cargo space and unfit for the carriage of bulk cargoes.

Since the beginning of 2005 modernization of the park of open wagons was started by building a new cargo space with increased thickness of the walls, floor and extra ribs. This is a positive trend for rescuing the park with this type of wagons.

3.4. Analysis of options for repair, rental and purchase of wagons

Even before the actual separation of NC "BDZ" into two separate companies - "BDZ" and "Railway Infrastructure", the railway industry was privatized. All railway works for the construction of new wagons were privatized and separated as independent companies outside the structure of the railways – they worked on open market.

Wagon repare deport (VRD) for implementation of small repair are located in the key train stations and are directly subordinated to the Headquarter of “Cargo” unit in the structure of "BDZ". In VRD are ongoing the repairs and maintenance of freight rolling stock, and certain types of mid repairs.

"BDZ" lacks the capacity to carry out the plan (capital and mid) repairs for all wagons. Scheduled maintenance is performed 4 to 6 years depending on the type of wagons. For this purpose is announced tender for carrying out planned factory repair, with indicated type and number of wagons to be repaired. Depending on the capabilities of Wagon factories, that won tenders, periodically BDZ passes them for repair wagons. Average time for repair of a wagon is 15-20 days.

Planned repairs are carried out according to established regulations for carrying out the overhaul and repair of wagons. Mid repair consists of complete revision of the axle box, draw gear, automatic train brake, bogies and partial repair of the body and the floor of wagons, painting. Capital repair consists of all above operations together with replacement of the floor, the side and end walls of wagons.

When recycled from wagons are used only the frames, the cargo space is built entirely with new material.

Given that the wagons are aged more than 20 years, performance of planned factory repair and modernization of many of them is inappropriate.

Available freight rolling stock is sufficient, given the amount of inventory fleet and quantity of used cars. It is necessary to select the best technically freight wagons, which can be carried out relevant plans repair and modernization. This is mainly related to the bulk wagons.

It’s needed to purchase or lease some new types of wagons: wagons for *22.5 t* axle load; coaches with ladders walls (H and On) ; low-floor wagons for the transport of large containers and trailers, vehicles and other; wagons for Ro-La. The wagons for Ro-La are unfortunate to purchase and to hire due to the fact that their maintenance is very expensive. Their wheels have small diameter *360-480 mm*, which leads to rapid wear and their frequent repair.

Covered wagon type H and Ha with ladders walls are very effective and sought to carry shipments of white goods and cargo protected from the weather. In 2007, "BDZ" rented certain units from Hbbins type which are highly sought after and used, especially to transport appliances. BDZ undertakes a study of the possibility of hiring a 4 -axle wagons of the same type. Private carriers also resorted to hiring wagons.

3.5. Analysis of the use of wagons by series

Operational data for loaded wagons shows the following values for the index turnover of wagons and average static load:

From the indicated loads in the table makes sense to analyze only series wagons with significant loadings.

4. DETERMINATION OF THE REQUIRED WAGON FLEET

4.1. Methodology for determining the required wagon fleet

The methodology applied below is based on a study of transport costs and loss of earnings (loss of revenue)

BDZ related to freight rolling stock. [6]

In the process of implementation of transport services has the potential to deny your request due to lack of timely provision of wagons for loading. The loss of these unmet requests can form lost revenue and worsen the economic situation of the railways. If formed wagon fleet that satisfies all requests, this would lead to unreasonably high costs for initial investment for the purchase of cars and significant costs for its maintenance. So we need to optimize the number of wagons in different series.

When the task is made a target function, including both the costs of maintaining the park, and the possible loss of revenue from not transported queries is set.

In the process of using fixed assets, they are consumed with a certain lapse of time it takes to recover (to be replaced with new ones). This requires funds to be provided through depreciation.

Lost revenue from uninsured wagons request load can generally be defined as the product of the rate for one not transported (insecure) wagon for a turnover and the number of not transported (uninsured) wagons. This is accomplished according to the formula:

$$E_i^{nz} = C_i^{nz}.N_i^{nz} \text{ , BGN/year,} \quad (1)$$

where: C_i^{nz} - lost revenue from not transported request per turnover (wagon); N_i^{nz} – number of non-submitted (uninsured) wagons year.

The determination of the two components in this embodiment will be described in the following subsections.

The determination of income foregone, not transported from one query is dependent on revenue and expenditure for one revolution of the wagons in terms of its movement.

The function will have the form:

$$C_i^{nz} = P_i^{oborot} - R_i^{oborot} \text{ , BGN/year,} \quad (2)$$

where: P_i^{oborot} – income from a turnover BGN/wagon; R_i^{oborot} – cost per turnover BGN/wagon

For wagons from series the cost per turnover can be defined as part of the overall costs that will correspond to the carriage of a wagon by a series of one turnover. For this purpose, can be used total annual operating costs.

Total cost associated with the movement is the annual costs of implementing the transportation - freight at a certain distance in a year). These are operating costs that are directly related to the manufacturing process and cost of service, organization and management of rail transport (including infrastructure charges, fuel, electricity costs for locomotives) .

Cost of goods trains constitute 63.79% of total operating expenses (passenger and freight trains) .

Costs that we have to take into account are: materials; fuel for the traffic; electricity for traffic; infrastructure charges; costs for locomotives (in their part for movement of goods).

4.2. Summarized performance data for freight transport

__Income from a turnover.__

Revenues from one turnover are those revenues (transport fare prices ETPT) that we have taken from the transport of goods, in wagons that series in one turn.

Calculation of freight charges is performed according to:

- the type of shipment
- the type and ownership of the used car ;
- nature of the cargo - name, position, class load
- tariff weight categories and the weight of the consignment;
- distance traveled
- other conditions provided for in the Tariff

The fare for wagon loads are calculated according to the ownership of the car, the unit freight rate shown in the table for the total weight of the shipment but not less than the determined mass to charge.

Revenue from a turnover of weight depends on the tariff rate class load, the average distance traveled, average load and is given by:

$$P_i^{oborot} = \frac{C_i^{ton}.Z_i^{nat}}{N_i^{nat}} = C_i^{ton}.T_i^{st} \text{ , BGN/turnover,} \quad (3)$$

where: C_i^{ton} – unit cost of rail freight tariff ETPT (lev/ tone) for the average distance traveled; Z_i^{nat} - total weight of goods carried by wagons series i (t) for the year; N_i^{nat} - number of wagons shipped complete series (i) for the year; T_i^{st} - static load wagon series (i)

4.3. Determining the number of filed (uninsured canceled) wagons

Behavior of shippers depend on the specifics of the load, the price of the service and especially the ability of the carrier to file a timely fit to load rolling stock. Collective impact of these factors determines the number of dropout clients and consequent loss of the carrier.

For analytical determination of the probability of failure of clients in untimely filing of freight wagons used development "Approximation of the probability of failure to satisfy client requests wagons". Failure probabilities of customers obtained through pre-developed imitation model. Using regression analysis are approximated several predefined functions of probabilities depending on the rate of reserve fleet, the coefficients of variation of client requests and turnover of wagons.

__Time to repair wagons__

Given that the capital repairs of wagons are carried out on a relatively long period (4-6 years), it is essential to have a predominantly repair of wagons for each series. Accordingly, the time for the repair, there are two main components corresponding to the two types of repair.

The timing of each of the two repairs consists of waiting time at the time of repair and the repair itself. Expected the repair includes all time in recruiting the necessary staff shall send for repair, travel time to the place of repair to the entry in the landfill for repair. Usually running repairs can be more than one for a year and in this regard the formula involved and the average number of entries for repair during the year.

4.4. Determination of the required wagon fleet

Determination of the required freight rolling stock is carried out for each series wagons separately using the methodology. Estimates are prepared with estimates for the next calendar year.

CONCLUSION

As a result of research and analysis following conclusions could be made:

1. Reserve ratio depends on the type of wagons. Due to differences in the coefficient of variation, rates, the price of cars to get different optimal reserve ratios.

2. Optimal value for the number of wagons forecast is better to adopt a higher than specified, since some types of wagons left side of the graph of expenditure is steeper than the right, i.e. there is less risk in adopting a larger reserve.

3. Comparing the results of required number of wagons in H series and the number of cars in operation can be concluded that as the amount of the railroad has the necessary rolling stock to meet the needs of transport. The main problem is that the majority of wagons have expired revisions and the prompt execution of repair and reconstruction of a number of wagons depends on the needs. Since the main income is provided by open-top wagons it will be cost effective and appropriate to pay to these wagons more attention.

4. To improve efficiency and competitiveness of freight rolling stock fleet operator would deliver new wagons with axle loading of *22.5 tons/axle*, covered wagons with large side walls and other, for which there is market demand for transport services.

REFERENCES

1. http://abzp.eu – Hoding BDZ – Consolifated Report of economical results for 2010 – 2014г
2. BDZ-CARGO - Analysis of activity for 2010 – 2014
3. Stoilov V., Condition and problems of the railway transport, Railway and Intermodal Transport, Internet magazine, issue 3 /2013
4. Atmadzhova D., A Dzaleva-Chonkova, Condition and problems of the railway transport in Bulgaria: production, scientific and educational potential, XVI Science conference with international participance VTU T. Kableshkov, 2006
5. Atmadzhova D., I. Milenov Condition and problems of the railway transport in Bulgaria Sofia, XVI Science conference with international participation VTU T. Kableshkov, 2006
6. Nikolov V., Master diploma work, VTU T. Kableshkov, 2009

Influence of the Design of Brake Discs on the Thermal Efficiency

Vasko Nikolov[1*]
[1]Department Transport equipment, "Todor Kableshkov" University of Transport, Sofia (Bulgaria)

Abstract: *A method for evaluation of the heat efficiency using analytical approach is described. The brake disks are mounted on the wheels and on the axles and they can be solid and ventilated. The most brake disks are ventilated, thereby cooling. In this study efficiency of the ventilated disks by basic equations of thermal convection is investigated, as well as the volume of air flow through the ribs of the disk.*

Keywords: thermal convection, heat efficiency, railway brakes.

1. INTRODUCTION

In order to develop more resistant to high temperatures, brake disc for rolling stock is considered the accumulation of heat during braking. The purpose of this study is to improve the cooling efficiency of this important safety element of the design of the rolling stock.

Disc brakes appeared in the late 19 and early 20 century. [13] In the first half of the 20th century application of disc brakes in automobiles and railway transport [3]. Individual researchers [6,12,14] describe different constructions drives in their reports. Other calculated temperature in unventilated [1,2,4] and ventilated discs [10,11]. In [7], the parameters of which are summarized on the disc as follows: the thickness of the friction surfaces should be 20-30 mm as a compromise between the heat capacity and weight. The ribs should have as much as possible and a thickness of about 8-10 mm. Since the air velocity over the ribs is important for the effectiveness of cooling, the effects of the number of the ribs on the flow. [5] It was found that the thick bearing surfaces leads to a lower thermal resistance against cracks due to a reduction of the strength of the mold [8].

As mentioned above, there are few studies on the structure of the brake discs. Some of them give limited advice on how to improve their design in terms of efficiency of their cooling. Therefore, a process for the preparation of evaluating the effectiveness of the cooling, it is necessary analytical approach using the basic equation of convection, followed by experimental tests and braking measurements of air speed.

The basic equations give heat transfer coefficient of the cooling rate:

$$\alpha = \frac{hA}{mC} \tag{1}$$

where:
h – coefficient of convection;
A – area of convection;
C – specific heat capacity;
m – mass of the disk.

This parameter can be used for evaluation of the heat storage and its maximum value after a series of stops to separate the rolling stock unit. Methods for the construction, using this parameter, it may be a tool for the design of brake disks, which are suitable for specific conditions.

2. ANALYTICAL ANALYSIS

Newton's law of cooling with convection reads:

$$\frac{dQ_h}{dt} = hA(T - T_0) \tag{2}$$

where:
Q_h – convection heat flow;
T – temperature of the disk;
T_0 – ambient temperature.

On the other hand, the heat exchange in the heat transfer is:

$$\frac{dQ_c}{dt} = mC\frac{dT}{dt} = mC\frac{\Delta T}{\Delta t} \tag{3}$$

where:
$\Delta T/\Delta t$ – temperature change per unit time which can be achieved experimentally.

Heat balance requires condition $\frac{dQ_h}{dt} = \frac{dQ_c}{dt}$, where an expression is obtained:

$$mC\frac{\Delta T}{\Delta t} = hA(T - T_0) \tag{4}$$

As a substitute $(\Delta T/\Delta t)/(T - T_0)$ with α, we get:

$$\alpha = \frac{hA}{mC} \tag{5}$$

*Corresponding author: Bulgaria, Sofia, 158 Geo Milev Str., e-mail: va_r_nikolov@abv.bg

When the disc is rotated at a constant speed, the thermal convection is a constant, as it is in a static state, i.e., does not change with time, and therefore in the same condition is α. Hence, the value of $\Delta T/\Delta t$ и $T - T_0$ can be obtained by monitoring the change in temperature over time.

The parameter α includes thermal conductivity to the axis on which the discs are attached, and to the air convection. Therefore, the assessment of the parameter for the thermal conduction to the axis α_0 is needed to obtain the thermal convection of air on the disc. The basic equation for the thermal conductivity is:

$$\frac{dQ_c}{dt} = mC\frac{\Delta T}{\Delta t} = \frac{-hA(T-T_0)}{l} \tag{6}$$

Therefore:

$$\alpha_0 = \frac{\Delta T/\Delta t}{T-T_0} = \frac{-(hA/l)}{mC} \tag{7}$$

Heat transfer coefficient h may be obtained from the expression:

$$h = \frac{\alpha' mC}{A} \tag{8}$$

where:
α' – empirical value obtained from the cooling history.

If heat transfer to the axis is displayed on the total value of α', the coefficient of heat transfer to the air during the rotation will be:

$$h = \frac{(\alpha'-\alpha_0)mC}{A} \tag{10}$$

It is known that a dimensionless number of Nusselt (Nu) of the thermal convection is associated with the number of Reynolds (Re) in a turbulent flow through the relationship:

$$Nu = 0{,}037\ Pr^{0{,}35}Re^{0{,}8} \tag{11}$$

The number of Prandtl (Pr), the air density, viscosity and thermal conductivity are:

$$Pr=0{,}7 \tag{12}$$

$$\rho = 0{,}18177.\frac{273{,}16}{273{,}16.T}.\frac{P}{760}\ kg/m^3 \tag{13}$$

$$\mu = 1{,}5726.10^{-6}.\frac{393{,}16}{393{,}16+T}.\left(\frac{273{,}16+T}{273{,}16}\right)\ Pa\ s \tag{14}$$

$$\lambda = 6{,}14.10^{-6}\ W/m\ K \tag{15}$$

Let h_1 and h_2 are the coefficients of convection for the friction surfaces, and A_1 and A_2 are the respective surfaces of the one side surface of the rib. Then the full heat transfer coefficient h is given by the expression:

$$h = \frac{A_1}{A}h_1 + \frac{A_2}{A}h_2 \tag{16}$$

The flow on the friction surface is turbulent under the Reynolds number ($5{,}6.10^5$@35 m/s). The air flow through the ribs also moves turbulent. Therefore, h_1 and h_2 are equal to:

$$h_1 = \frac{0{,}037\ Pr^{0{,}35}\,(\lambda/\nu^{0{,}8})\,(r_2\tilde{\omega})^{0{,}8}}{r_2^{0{,}2}} \tag{17}$$

$$h_1 = 0{,}037\ Pr^{0{,}35}\frac{\lambda}{\nu^{0{,}8}}\frac{\nu_2^{0{,}8}}{(r_2-r_1)^{0{,}2}} \tag{18}$$

where:
$\nu = \mu/\rho$.
r_2 – length of the sliding surface;
$r_2 - r_1$ – length of the surface side of the ribs.

Here the Reynolds number is defined as a representative length multiplied by representative rate divided by dynamic viscosity.

When $\frac{\frac{\Delta T}{\Delta t}}{T-T_0} = \alpha = const.$ temperature profile in the cooling process after braking is given by the equation:

$$T(t) - T_0 = (T(0) - T_0)e^{-\alpha t} \tag{19}$$

where:
T_0 – temperature of the brake disc in the place of measurement when the braking is terminated and the cooling is turned off.

Using equation (17) the change in temperature from T_2 to T_1 for a time t_2 is:

$$T_1 - T_0 = (T_2 - T_0)e^{\alpha t_2} \tag{20}$$

$$T_2 - T_1 = (T_2 - T_0)(1 - e^{\alpha t_2}) \tag{21}$$

Therefore, the maximum temperature $T_{max} - T_0$ after several cycles of braking is obtained in a saturated state at the temperature as the temperature is increased in a braking cycle is equal to the reduction in temperature during the cooling process. Namely the reduction from T_{max} to T_1 is given by the expression $(T_{max} - T_0)(1 - e^{\alpha t_2})$ and $T_{max} - T_1$ is the increase in temperature at one braking cycle $[E/(mC)]$ when has reached the saturation temperature. T_{max} can be average temperature at the measuring point:

$$(T_{max} - T_0)(1 - e^{\alpha t_2}) = \frac{E}{mC} \tag{22}$$

Therefore:

$$T_{max} = \frac{E/C_dM}{1-e^{\alpha t_2}} + T_0 \tag{23}$$

Tests for braking to stop, simulation tests and measurements of the volume of the flow through the ribs of the brake disc were conducted.

3. TEST RESULTS

The simulation was planned so that the speed of rotation was as close as possible to the operational one. The last five braking have almost the same initial speed and braking intervals. The final temperature is close to the maximum. The maximum temperature of the disc 3 is 375°C and that of the disk 1 – 525°C, respectively, which are in the measurement points. Disc 1 is modified to provide the passage of air through the ribs over and to extend the inlet. However, in a further test for the modified disk 2 is obtained a maximum temperature of 460°C, which is still higher than that of the disk 3. Results prove the assertion that the higher value of α, so the lower the maximum temperature.

Experiments show that the inflow area has to be large at least as much as the minimum area between the ribs. The average air velocity is calculated from the velocity of air between the ribs in each position of the radius. The experimental results are similar to those calculated in equations (16, 17, 18).

Experimental results show that the larger values of α provide better cooling efficiency, and a lower maximum temperature. Therefore, when designing the discs, the ratio $hA/(mC)$ should be as widely as possible. Area A for solid discs is about half of the ventilated discs. Therefore, when designing a compact discs, which naturally have a low cooling efficiency, the cooling performance has to be taken into account in order to provide the required maximum temperature in operation.

The maximum temperature of the brake during braking cycles may be estimated by equation (23), wherein the braking cycles have almost same condition. Current simulation tests that led to this study also have maximum temperatures at the end of consecutive stops. Measured temperatures are compared to theoretical results. Clearly, equation (23) gives a good estimate of the maximum temperature in operation.

Particular attention should be paid to the maximum operating temperature for the case of short brake intervals Δt, if $\alpha\Delta t << 1$.

$$T_{max} - T_0 = \frac{E/mC}{1-e^{\alpha t_2}} \approx \frac{E/mC}{\alpha \Delta t} = \frac{E}{\alpha}\frac{1}{hA} \qquad (24)$$

It is clear from equation (24) that hA is to be as widely as possible. However, where there are limitations in the design, such as an outer diameter or a thickness of the disc, hA have to be designed so that it is suitable for the operating conditions.

4. CONCLUSION

This study evaluated the efficiency of cooling by convection in the brake discs using analytical and experimental approach. The results achieved are as follows:

- The parameter for the degree of cooling $\alpha=(\Delta T/\Delta t)/(T - T_0)$ gives us evaluate the efficiency of cooling and temperature in the braking cycles in operation;
- The parameter for the degree of cooling is also derived from the design parameters of the disc, namely the coefficient of convection h, the surface area for heat convection A, a specific heat capacity C and the mass of the disc m, so that $\alpha = hA/(mC)$. The coefficient of heat transfer can be evaluated by means of the air velocity between the ribs and by the dimensions of the disc;
- The maximum temperature was evaluated by the displayed equation and compared with the experimental results. Equation (23) gives an estimate of the maximum temperature and agreed well with the measured values. Here T_{max} is the maximum temperature, E is the energy absorbed by the disc, Δt is the time interval of the brake and T_0 is the room temperature.

REFERENCES

[1] Abbas, S. A., Bubitt, N. J. and Hook, C. F. Design and thermal analysis of no-coning brake discs. J. Mech. Engng. Sci., 1972.
[2] Abbas, S. A., Bubitt, N. J. and Hook, C. F. Temperature distribution in disc brakes. Proc. Rnstn Mech. Engrs. 1969.
[3] Bradbury, F. J. and Schmidt, E. Disc brakes for motor vehicles. Glasers Annln. 1959.
[4] Dike, G. O. Optimum design of disc brakes. ASME paper 73-WA/DE-5, 1973.
[5] Ehler, H. R. Uber ben Gegenwartigen der Froschung auf den Gebriet Scheiben bremsen fur Schienenfarzeuge. Jb. Eisenbahn Wesens, 1962.
[6] Laplaiche, M. The disc brake. French Railway Techq., 1973.
[7] Munkow, H. Die Schsbremsscheibe und Ihre Problems. OET-Eisenbahn Technik, 1976.
[8] Rainbolt, J. D. Effect of disc material selection on disc brake rotor configuration. SAE paper, 1976.
[9] Sakamoto, H. Heat convection and design of brake discs. Proc. Instn. Mech. Engrs. IMechE 2004.
[10] Schwartz, H. W. in Proceedings of the IMechE International Conference on Railway Braking, 1979.
[11] Schwartz, H. W., Hartter, L. L., Rhee, S. K. and Byers, J. E. Evaluation of gray iron brake discs for trucks by thermal modeling. SAE paper, 1970.
[12] Tickle, C. T. F. The rail vehicle disc brake principle and practice. In Proceedings of the IMechE Conference on Railway Braking, 1979.
[13] Tompkin, J. B. Development of the disc brakes with particular reference to British

railway application. K. Inst. Loco Engrs. 1969.

[14] von Wagner, O. H. Scheibenbremsen for Schienenfahrzeuge, Vereker Technik, 1963.

Influence of Track Subsidence on Rolling Stock Derailment Risk

Dobrinka Atmadzhova[1], Tsvyatko Penchev[1],
[1]Machinery and Construction Technologies in Transport/Transport equipment, Todor Kableshkov University of Transport, Sofia (Bulgaria)

The paper presents the analysis of the factors influencing on the process of derailment focusing on "track subsidence". The extreme case combining the place of subsidence with a broken rail connection and especially with significant differences of the levels of the two connecting rails is examined as well as with failure of the rolling stock wheeled part.

Keywords: railway vehicles, rolling stock, wheel-rail contact, derailment

1. INTRODUCTION

The presence of track subsidence and track unevenness in all cases negatively affects safety against derailment of railway rolling stock. Due to unevenness, based on a bogie and a vehicle, obliquely symmetrical forces arise that cause overload (extra load) on some wheel and unloading of other by vertical force. The wheels where the vertical force Q is reduced might be at risk of derailment due to the increase of the criterion Y/Q (the ratio between the horizontal to vertical forces) above the permissible value at the point of contact of the wheel with the attacking rail.

If there is a case of falling down (unevenness) of the track being "rail threshold", i.e. a sudden change in the level of the rail head at the place of connection as well as of broken rail", then to the factor mentioned above determined by the vertical load of attacking wheel, another factor as equally dangerous superimposes and it is the subject this paper. Its action is based on the change in the location of the "wheel - rail" contact point on the wheel tire operation area and in particular on its flange. Without dwelling on the issue of contact points (more exactly contact spots ellipses, etc.), we will only note that regardless of what type of contact between the attacking wheel and external rail in a curve, single or of two points, in all cases the displacement of the contact point on the surface of the flange from its base to the top (especially in the zone of the roundness R20 and after it) deteriorates safety against derailment and even leads to inevitable derailment. Due to the displacement of the contact in direction towards the top of the flange, the angle of inclination β to its horizontal and at the same time, due to the greater roughness of the surface in this area the friction angle ρ substantially increases, respectively the friction coefficient. The impression is that the derailment of this type described largely resembles what is caused by "sharp flange, i.e. a steep trimmed flange of a sharp edge.

It is interesting to note that the most significant cause to prepare this paper is the incident that has occurred recently in the railway network of Bulgaria: the derailment of a passenger car caused by rail threshold of height *h = 42 mm* in a curve of radius *R = 175 m* at a speed of *25 km/h.*

2. DANGER OF DERAILMENT WITH "TRACK THRESHOLD"

Let observe the rail crew movement in a curve when the attacking wheel passes through the so-called "track threshed", which is the difference of the levels between the two parts of the rail in the place of connection or breaking (Fig. 1). Then, abstracting from the complex geometry of the wheel tire profile, presenting it in a simple way as an ordinary cylindrical body, the point of "wheel-rail" contact (which will be shown as a point) immediately shifts to distance L from point A in point A' (Fig. 1).

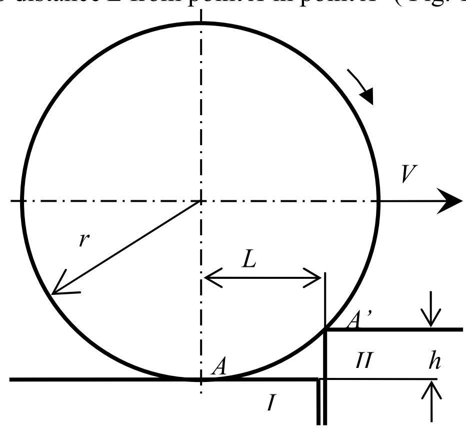

Fig.1. Increasing rail threshold.

2.1. In the case of the so-called "increasing threshold"

In the case of the so-called "increasing threshold", i.e. when the level of the receiving rail (rail head) is higher compared to the previous level (Fig. 1), threshold height h and radius r of the circumference of rolling, distance L called transmitting distance (because the contact point is transmitted instantaneously from A to A') is determined by the dependency

$$L = \sqrt{r^2 - (r-h)^2} \quad (1)$$

Considering the actual wheel tire profile and the angle of attack α of the attacking wheel relative to the rail (Fig. 2), it is seen that due to its rotation of the same angle α (viewed in plan), it will divert at distance Δy_A towards the receiving rail. This distance is approximately equivalent to

$$\Delta y_A = L.\alpha \quad (2)$$

*Corresponding author: 158 Geo Milev Str. 1574 Sofia, Bulgaria, atmadzhova@abv.bg

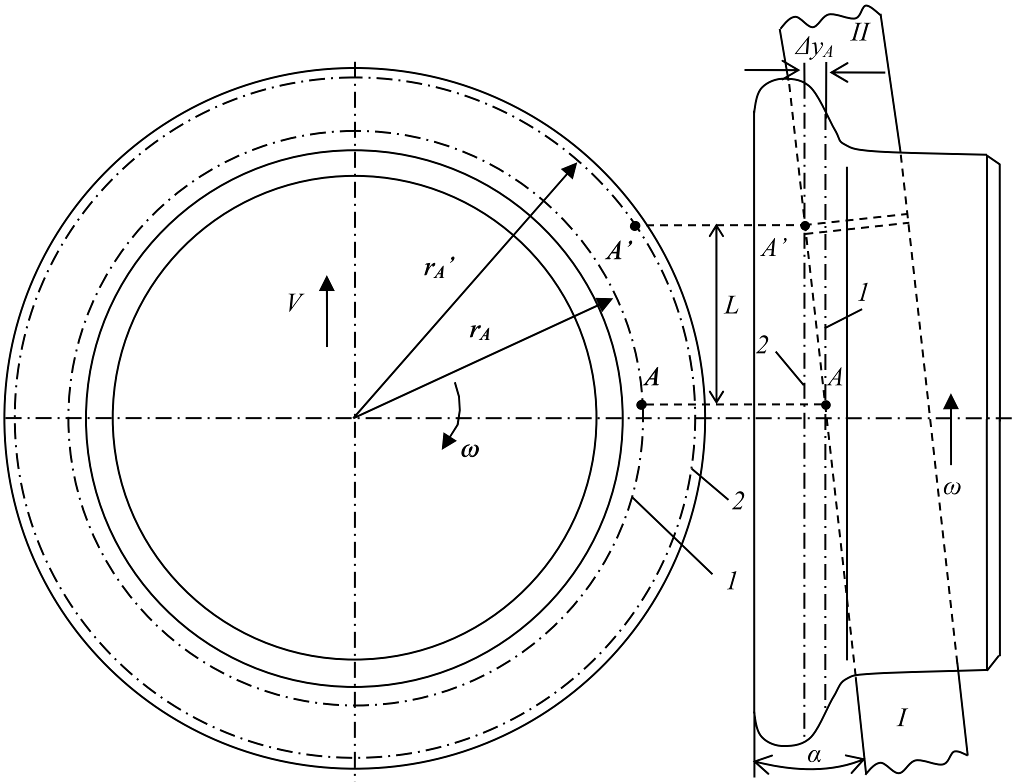

F*ig.2. Contact point of the attacking wheel at "increasing rail threshold".*

Assuming that the same value (Δy_A) is approximately the transverse horizontal displacement between the circumferences 1 and 2 of the wheel tire contact points just before and after the moments of transition between rails I and II, and introducing the coordinate system with axes Δy_A and Δr_A at start point A (Fig. 3), it will be necessary to work out the analytic functional dependence for the particular profile

$$\Delta y_A = \varphi(\Delta r_A) \tag{3}$$

Furthermore, taking into account that at the moment of transition in the threshold of height h that the wheel terminates rolling on track I with circumference 1 of radius r_A and begins rolling on rail II with circumference 2 of radius $r_A' = r_A + \Delta r_A$, the simplified scheme of Fig. 1 is transformed and takes the kind shown in Fig. 4. As it is seen in this figure, the sought transition distance L with the actual scheme described in this way can be defined with the help of substituting simpler scheme, which is reduced to circumference 2 of radius $r_A' = r_A + \Delta r_A$ and imaginary rail threshold of height $h' = h + \Delta h = h + \Delta r_A$ (Fig. 4). Based on that dependency (1) is modified as follows:

$$L = \sqrt{(r_A')^2 - (r_A' - h')^2} =$$
$$= \sqrt{(r_A + \Delta r_A)^2 - [r_A + \Delta r_A - (h + \Delta r_A)]^2} \ ,$$

or $$L = \sqrt{(r_A + \Delta r_A)^2 - (r_A - h)^2} \ , \tag{4}$$

where Δr_A – change of the rolling radius due to the transition in the rail threshold is still unknown.

After substitution of (4) in (2) it is obtained that the transverse displacement Δy_A between the wheel under examination and receiving rail II, i.e. between the circumferences of contact points (and wheel rolling) before and after the moment of transition, is, as follows:

$$\Delta y_A = \alpha . \sqrt{(r_A + \Delta r_A)^2 - (r_A - h)^2} \tag{5}$$

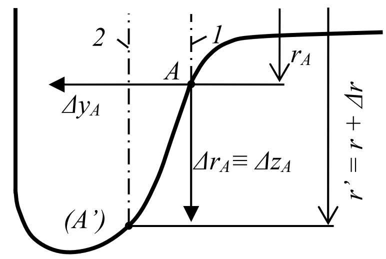

Fig. 3. Coordinate system Δy_A - Δr_A, defining the contact points on the surface of the wheel tire profile.

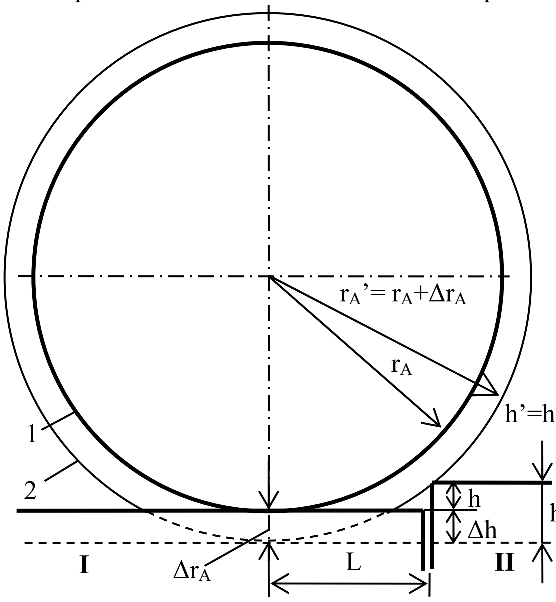

Fig. 4. Actual and substituting simple schemes of transition in the threshold of height h.

As it can be seen from the approach presented above for obtaining equation (5), it expresses the "wheel-rail" kinematics dependency in a curve with presence of increasing rail threshold and contains two unknown values: Δy_A and Δr_A. To determine them, one more equation is needed: this is equation (3), which expresses the dependency between Δy_A and Δr_A. This dependency derives from the shape of the wheel tire profile.

For the wheel tire profile in unworn condition used in TCDD (Turkish Railways), provided that the origin (point A) is at a distance of 10 mm below the average circumference of rolling, equation (3) can be approximated as follows:

- for the conical part of the flange, i.e. with $0 < \Delta r_A \leq 0{,}00684$ –

$$\Delta y_A = \Delta r_A / tg\beta_A \text{, in m,} \tag{6}$$

where: β_A is the angle of inclination in point A and the forming line in the cone;

- for the section of the roundness R20 in the profile, i.e. with $0{,}00684 \leq r_A \leq 0{,}01732,\ m$ –

$$\Delta y_A = 0{,}021283 - \sqrt{0{,}0004 - \Delta r_A^{\ 2}} \text{, in m,} \tag{7}$$

etc. .... – for the next sections.

The scheme of the approximated profile, which the formulas (6) and (7) are derived from, is given in Fig. 5.

Thus, solving the system of 2 equations – (5) and (6), (5) and (7) , etc. - for instance, by equating their right parts, taking into account the addition $y_{os,}$ we obtain the final determination of the unknown Δr_A.

- for the conical part of the flange

$$\frac{\Delta r_A}{tg\beta_A} = \alpha.\sqrt{(r_A + \Delta r_A)^2 - (r_A - h)^2} + y_{os} \text{, in m,} \tag{8}$$

- for the section of the roundness R20 in the profile

$$0{,}021283 - \sqrt{0{,}0004 - \Delta r_A^{\ 2}} = \\ = \alpha.\sqrt{(r_A + \Delta r_A)^2 - (r_A - h)^2} + y_{os} \text{, in m,} \tag{9}$$

where the addition y_{os} is a a relative transverse displacement between the rails at the location of the threshold; such one almost always exists with sign „+” and should not be neglected, especially in the case of a "broken rail" because the place of fracture (breaking) is generally in the area between the sleepers and there is always a significant elastic deformation of rail I in positive direction (i.e. outside of the curve) by the action of the steering effort Y.

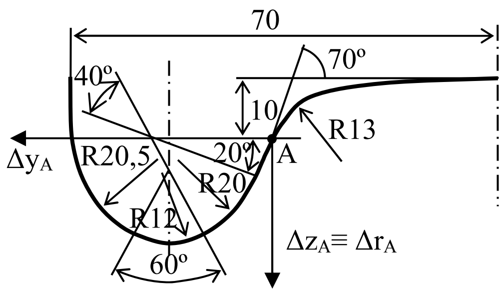

Fig. 5. Scheme of the approximated profile of the flange corresponding to formulas (6) and (7).

2.2. For the case of the so-called "lowering threshold",

For the case of the so-called "lowering threshold", i.e. when the head of the receiving rail is at a lower level than the previous one, there are many features that are in common with the examined case of increasing threshold but the same time there are radical differences from it in terms of the approach to solve it. First, the problem here is related to the ballistic task of mechanics, which in this case is specified to determine the distance of the attacking wheel bounce and the coordinates of its contact point with rail II.

Keeping the basic definitions, terminology and serigraphy as introduced above, we will use two coordinate systems (CS) - mobile $A\Delta x_A\Delta y_A\Delta z_A$ and immovable CS $A\Delta X_A\Delta Y_A\Delta Z_A$ with a common origin for contact point A on the wheel tire surface at the time of its separation from rail I (Fig. 6). The immovable CS remains at that point and the mobile one moves in a translational way (as a whole with the wheel) along trajectory k to contact A' with rail II retaining its original location against the wheel tire of the wheel, which is treated as a non-rotating .

Axes Δx_A, Δz_A and Δy_A of the mobile CS are directed as follows: Δx_A - horizontally in direction of movement of the attacking wheel; $\Delta z_A \equiv \Delta r_A$ - down the vertical or the radius (as the relative error of identification $\Delta z_A \equiv \Delta r_A$ under the most unfavorable conditions of normal railway lines – for the angle of attack $\alpha = 0{,}03\ rad$ and flange tilt $\beta_A = 78°$ it is under 1% (Fig. 7); Δy_A - horizontal cross to the middle part of the wheel axle (or to the left for the right attacking wheel Fig. 6)

It is only the displacement of contact point A on the wheel that is referred by the so-defined movable CS, being aside from the wheel rotation during the transition.

The axes $\Delta X_A\Delta Y_A\Delta Z_A$ on immovable CS are directed in the same way as the mobile one. The main purpose of immovable CS is to define the law of wheel motion with the transition (bounce) between contact points A and A', where we also aside from its rotation.

The design of rolling stock and its possible faults (especially in regards to the features of the "axlebox-frame" connection) defines the type of trajectory described by the attacking wheel with its transition in lowering rail threshold, e.g.:

a) completely free trajectory, i.e. "pure ballistics" – only under the action of gravity and air resistance, with an initial speed V_{X0} in horizontal longitudinal direction to the direction of movement and providing a non-existent (defective) longitudinal link "axlebox-frame";

b) limited ballistics at a constant speed in longitudinal direction to the direction of movement $V = V_{X0} = const$;

c) limited ballistics of additional vertical force.

The most common types of trajectory in real operation are those of limitations "b" and "c" acting jointly or separately, e.g. where:

- the "axlebox-frame" connection in longitudinal direction in order is in the attacking wheel under examination moves at the speed of the respective rolling stock (at limit "b");

- on the issue attacking wheel with mass m (more precisely the appropriate axlebox) acts not only force mg but also the reduced force of springs exempted from load completely or partially after separation of the wheel from the rail I (limitation "c").

A completely free trajectory of type "a" is possible only with structures of bogies of missing or very little static deformation f_{st} of springs in the first suspension, e.g. with empty wagons where the "axlebox - frame" connection in longitudinal direction is broken and also in case of a broken spring in the first spring degree on the

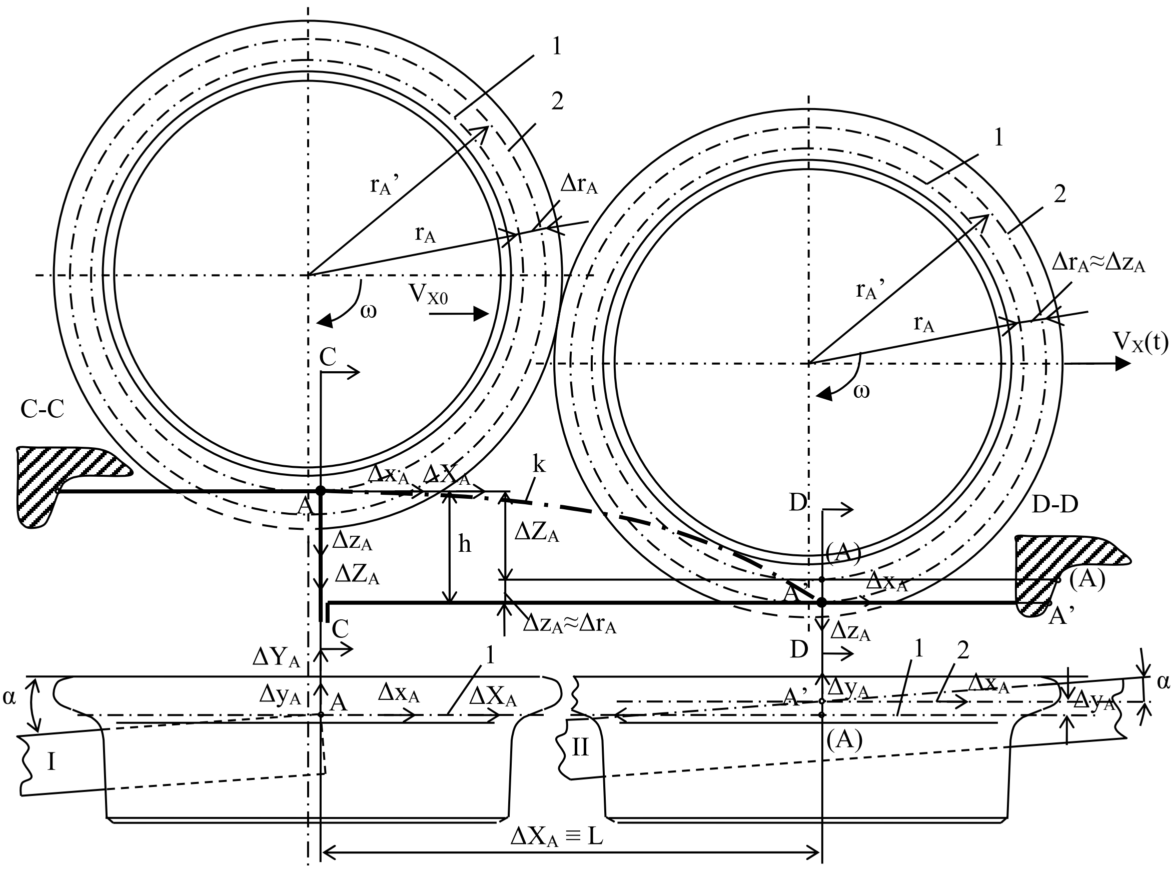

Fig.6. Contact points of the attacking wheel at lowering threshold.

side of the attacking wheel being an object of the treated accident.

To determine the trajectory of the transmission movement "in the air", i.e. when there is no contact between the rail and attacking wheel of mass *m* in lowering rail threshold in the general case, assuming that all possible forces in operation act on the wheel, a system of differential equations is created along the coordinate axes ΔX_A and ΔZ_A with argument time *t* as follows:

$$\left| \begin{aligned} & m.\frac{d^2(\Delta X_A)}{dt^2} + km\frac{d(\Delta X_A)}{dt} = 0 \\ & m.\frac{d^2(\Delta Z_A)}{dt^2} + km\frac{d(\Delta Z_A)}{dt} - c.(f_{st} - \Delta Z_A) - mg = 0 \end{aligned} \right. \qquad (10)$$

where: *c* – reduced coefficient of elasticity in [N/m] of springs to the respective wheel; *k* – coefficient of of air resistance; f_{st} – static deformation of springs adjacent to the attacking wheel; *g* – ground acceleration.

The solution of the system of differential equations (10) with initial conditions: at $t = 0$, $\Delta X_A = 0$; $\Delta \dot{X}_A = V_{X0}$; $\Delta Z_A = 0$; $\Delta \dot{Z}_A = 0$ is:

$$\left| \begin{aligned} & \Delta X_A = \frac{V_{X0}}{k}(1 - e^{-kt}) \\ & \Delta Z_A = -\frac{cf_{st} + mg}{c} e^{\alpha t}.\cos \beta t + \\ & \quad + \frac{\alpha}{\beta}.\frac{cf_{st} + mg}{c} e^{\alpha t}.\sin \beta t + \frac{cf_{st} + mg}{c} \end{aligned} \right. \qquad (11)$$

where: $\alpha = -k/2; \quad \beta = \sqrt{D}/2; \quad D = k^2 - 4c/m$.

This decision determines the law of transmitting motion of the wheel between contact points *A* and *A'*, as by argument *t* (time) the equation of the trajectory can be represented in a coordinate system $A\Delta Z_A \Delta Y_A$ (but is it not required with the approach adopted here).

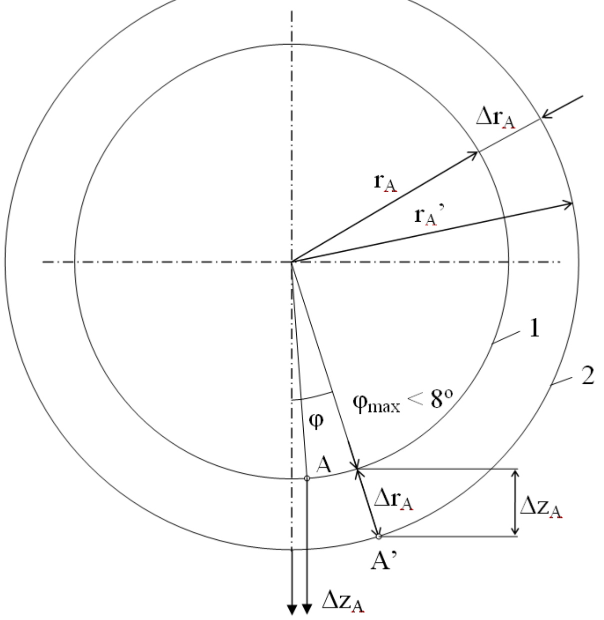

Relative error:

$$\delta\% = \frac{\Delta r_A - \Delta z_A}{\Delta r_A}.100 = (1 - \cos\varphi), \%$$

Fig. 7. Rationalization of identification $\Delta z_A \equiv \Delta r_A$.

In the first equation at system (11), which gives us the distance of rebound ΔX_A in the first for approximation[1], the horizontal transverse displacement Δy_A of the contact point A' in regard to A on the wheel tire surface is directly obtained multiplying by the angle of attack α, i.e.

$$\Delta y_A \approx \alpha.\Delta X_A, \qquad (12)$$

or $$\Delta y_A \approx \alpha \frac{V_{X0}}{k}(1-e^{-kt}), \qquad (12a)$$

and taking into account the consideration from the previous point that always there is a cross shift of rail I against rail II with sign "+ ", it has to add y_{os}, to the right side, i.e.

$$\Delta y_A \approx \alpha \frac{V_{X0}}{k}(1-e^{-kt}) + y_{os} \qquad (13)$$

In the second equation at system (11), it is necessary to put the condition of the difference between the elevation of contact points A and A', i.e. the height of rail threshold h, taking into account their relative displacement to each other Δz_A in the very wheel tire profile; therefore the substitution

$\Delta Z_A = h - \Delta z_A$ (see Fig. 6). (14)

When solving this problem, it is necessary to take into account the geometry of the wheel tire profile by dependencies (3), which citing (6) and (7) in p.p.2.1 can be specified in the same kind and further used in the paper and examples without additional explanations and preconditions. At that, it is dependency (7) that will be mainly used for the area of roundness R20 because it is most indicative.

In summary of the foregoing, it can be seen that the system of algebraic equations to solve this problem with the effect of all possible powers can be:

$$\left|\begin{aligned} &\Delta y_A = \alpha \frac{V_{X0}}{k}(1-e^{-kt}) + y_{os} \\ &h - \Delta z_A = -\frac{cf_{st}+mg}{c}e^{\alpha t}.\cos\beta t + \\ &\qquad + \frac{\alpha}{\beta}.\frac{cf_{st}+mg}{c}e^{\alpha t}.\sin\beta t + \frac{cf_{st}+mg}{c} \\ &\Delta y_A = \frac{\Delta z_A}{tg\beta_A} \quad or \quad = 0{,}021283 - \sqrt{0{,}0004 - \Delta z_A^{\,2}} \\ &\quad ets, \quad in\ [m], \end{aligned}\right. \qquad (15)$$

which contains three unknowns: the coordinates Δz_A and Δy_A and time t.

For the majority of cases with the actual operation of rolling stock it is appropriate to apply the relationships mentioned above in a simpler form, e.g.:

1) Member $km\dfrac{d(\Delta X)}{dt}$ in the first differential equation of the system (11) does not apply if the longitudinal link "axlebox - frame" exists and is in good condition; the same member can be ignored also with the non-existing "axlebox-frame" connection at relatively low speeds when the influence of air resistance is negligible. Therefore in case of "1" the movement of the wheel under examination in longitudinal direction is the speed of vehicle V, i.e. $\Delta \dot{X}_A = V$, $\Delta X_A = V.t$ with $V = V_{X0} = const$.
2) Based on the previous p.1 since $\Delta X_A = V.t$, the first equation of (15) can obtained a maximally simplified form, i.e.

$$\Delta y_A \approx \alpha.V.t + y_{os} \qquad (15a)$$

3) Member $km\dfrac{d(\Delta Z)}{dt}$ in the second differential equation considering air resistance in vertical direction can be ignored for the very small distance (actual or effective height ΔZ_A) and negligible speed that can be achieved. Therefore in case "3" if there is no additional vertical force on the wheel or this force can be ignored, the second equation of (15) can also obtain a maximally simplified form:

$$h - \Delta z_A \approx g.t^2/2. \qquad (15b)$$

4) Taking into account the difficulties in solving system (15) in the in the kind presented above, the second equation, with all possible forces, the solution was made with neglecting air resistance; besides that the effect of the additional vertical force on the wheel is recorded based on the ratio of torsion stiffness of the vehicle c_t and obliquely symmetrical wheel load $\pm Q_k = c_t.H$ (where H is the total single unevenness (twisting); with the classic type of rolling stock (bogie) of 4 wheels the theoretical coefficient c_t can be performed using expression $c_t = 0{,}25.c.\xi.(2b/2s)^2$, where c is the stiffness of the first spring rate for a axle box, ξ - a coefficient of reporting frame twisting (typically $\xi = 0{,}8 \div 0{,}9$), $2b/2s$ - the ratio of the cross distance between axlebox $2b$ to the distance between wheels $2s$.

Taking into account all considerations and dependencies given above, the differential equation in coordinate ΔZ_A gets the kind of:

$$\Delta \ddot{Z}_A + 0{,}4.\frac{c}{m}\Delta Z_A = \frac{c}{m}f_{st} + g \qquad (16)$$

where 0,4 is the approximate value of the coefficient to calculate obliquely symmetrical load on wheels with taking into account the characteristic "twisting stiffness of vehicle (wagon)" – under B55-ERRI.

The solution of differential equation (16) under initial conditions: t = 0, $\Delta Z_A = 0$, $\Delta \dot{Z}_A = 0$ is obtained:

$$\Delta Z_A = -\frac{cf_{st}+mg}{c}.\cos\left(\sqrt{0{,}4.\frac{c}{m}}.t\right) + \frac{cf_{st}+mg}{c} \qquad (17)$$

and the solution of the system of algebraic equations has to be sought under the same conditions for its left side, i.e. $\Delta Z_A = h - \Delta z_A$,

therefore the second equation in system (15) obtains the kind of:

$$h - \Delta z_A = -\frac{cf_{st}+mg}{c}.\cos\left(\sqrt{0{,}4.\frac{c}{m}}.t\right) + \frac{cf_{st}+mg}{c}, \qquad (18)$$

which is adapted for use in medium conditions for classic rail vehicle with 4 wheels taking into account the characteristic "twisting stiffness of vehicle (wagon)" in [1].

[1] Because ΔX_A is a component of the transfer movement of the wheel, any possible longitudinal relative displacement of contact point A' on the wheel tire itself Δx_A is not taken into account, i.e. it is assumed that the position of contact point A' towards the vertical geometrical axis of the wheel in plane $A'x_Az_A$ remains the same as that of contact point A.

For the general case (without a reverse relation with B55) it is preferable to use the final formula without coefficient *0,4* as parameters *c* and *m* must be reduced (i.e. aligned).

2.3. Numerical examples of the danger of derailment at presence of a "rail threshold"

2.3.1. To assess the growth of derailment risk due to an increasing "rail threshold" with the following data:
- height of the rail threshold $h = 42\ mm$;
- speed $V = 25\ km/h$ ($6,9444\ m/s$)
- curve radius $R = 175\ m$;
- angle of attack $\alpha = 0,0222\ rad$;
- transverse displacement between rails I and II $y_{os} = 3\ mm$;
- nominal radius of the wheel in rolling circle $r = 500\ mm$;
- radius of the contact point *A* of the wheel r_A before the accident $r_A = 510\ mm$.

The solution is made on the basis of (9) where with substitution of the above data, i.e.

$$0,021283-\sqrt{0,0004-\Delta r_A^{\ 2}}=$$
$$=0,0222.\sqrt{(0,5+\Delta r_A)^2-(0,5-0,042)^2}+0,003$$

it is obtained that

$\Delta r_A = 0,015206\ m$.

On the basis of the relationship:

$$\beta = 90° - arcsin\frac{\Delta r_A}{R20}$$

The value of angle β is obtained –

$\beta = 40,51°$

and criterion $tg(\beta - \rho)$ with the nominative value of angle ρ ($\rho = 19,8°$)

$tg(\beta - \rho) = tg(40,51 - 19,8) = 0,378$

This result shows that the admissible value of criterion $tg\ (\beta - \rho)$ is reduced 3,17 times compared with the value determined by UIC regulations *1,2* provided that the angle of friction ρ is with value $19,8\ ^o$ by UIC regulations typical of the flange "operation" area.

2.3.2. To assess derailment risk increasing due to lowering "rail threshold" with the same data of track and rolling stock as in 2.3.1 using different relationships:

a) at a maximally simplified setting – with no additional vertical force of the springs and neglected air resistance.

Under these conditions this system should be used:

$$\left|\begin{array}{l}\Delta y_A = \alpha.V_{X0}.t + y_{os}\\ h-\Delta z_A = \dfrac{g.t^2}{2}\\ \Delta y_A = 0,021283-\sqrt{0,0004-\Delta z_A^{\ 2}} \qquad (\mathit{for\ section\ R20})\end{array}\right.$$

or

$$\left|\begin{array}{l}\Delta y_A = 0,0222.6,9444.t+0,003\\ 0,042-\Delta z_A = \dfrac{9,81.t^2}{2}\\ \Delta y_A = 0,021283-\sqrt{0,0004-\Delta z_A^{\ 2}}\end{array}\right.$$

where the coordinates of new contact point *A'* (related to point *A*) of the wheel with rail II are obtained: $\Delta z_A = 0,018495m;\ \Delta y_A = 0,013672m;\ t = 0,069224s.$

where the unknowns are obtained: $\Delta z_A = 0,018495m;\ \Delta y_A = 0,013672m;\ t = 0,069224s.$

The angle of inclination β to the horizontal in contact point A', which is in the top area of the flange is (at ≈ 3 mm the top horizontal) and is

$\beta|\ \Delta r_A = 0,018495\ | \approx 15^o.$

The safety criterion against derailment $Y/Q \le tg(\beta-\rho)$ with the value regulated by the UIC for the angle of friction $\rho = 19,8°$ is obtained to be unreal (with a negative value), which means that it is absolutely inadmissible.

b) with more accurate setting - taking into account the additional vertical force of the springs for the general case and air resistance of horizontal ΔX_A -axis, provided that the "axlebox - frame" does not exist longitudinally – changing the following data: coefficient of air $k = 0,003\ ms^{-1}kg^{-1}$; speed $45\ km/h$ ($12,5\ m/s$); reduced mass of the wheel $m = 1000\ kg$; reduced modulus of elasticity to 1 wheel $c = 10^6 N/m$; static deformation of the first spring degree $f_{st} = 0,05m$.

Under those conditions the first equation of the system will contain ratio *c/m* under the square root with coefficient *1* and therefore the system will have the form:

$$\left|\begin{array}{l}\Delta y_A = \alpha\dfrac{V_{X0}}{k}(1-e^{-kt})+y_{os}\\ h-\Delta z_A = -\dfrac{cf_{st}+mg}{c}.cos(\sqrt{\dfrac{c}{m}}.t)+\dfrac{cf_{st}+mg}{c}\\ \Delta y_A = 0,021283-\sqrt{0,0004-\Delta z_A^{\ 2}}\end{array}\right.$$

or:

$$\left|\begin{array}{l}\Delta y_A = 0,0222.\dfrac{12,5}{0,003}(1-e^{-0,003.t})+0,003\\ 0,042-\Delta z_A = \dfrac{10^6.0,05+10^3.9,81}{10^6}cos(\sqrt{\dfrac{c}{m}}.t)+\\ \qquad +\dfrac{10^6.0,05+10^3.9,81}{10^6}\\ \Delta y_A = 0,021283-\sqrt{0,0004-\Delta z_A^{\ 2}}\end{array}\right.$$

where the following values of the coordinates of contact point *A'* of the wheel with rail II and time *t* are obtained:

$\Delta z_A = 0,017316m;\ \Delta y_A = 0,011275m;\ t = 0,029823s.$

The angle of inclination to the horizontal is determined by the dependency:

$$arcsin\frac{\Delta r_A}{R20} = 90° - \beta\ ;\ \beta = 90° - arcsin\frac{\Delta r_A}{R20}$$

$$\beta = 90° - arcsin\frac{0,017316}{0,020} = 90° - 59,974°$$

$$\beta = 30,026°$$

The safety criterion against derailment $Y/Q \le tg(\beta-\rho)$ with the value of $\rho \approx 20°$ by the UIC regulations is $Y/Q \le 0,177$.

Taking into account that the value by the UIC regulations is $Y/Q \le 1,2$ (with $\beta = 70^o$ and $\rho \approx 20^o$), it should be concluded that the admissible value of *Y/Q* is reduces nearly *7* times.

c) with more accurate setting – taking into account the additional vertical force of springs in the general case without considering air resistance along ΔZ_A and ΔX_A with existing longitudinal "axlebox-frame" connection – with all the rest data in 2.3.2.b.

Under the conditions given the 2nd and 3rd equations of the system will be one and the same with those in the previous example 2.3.2.b, and the 1st equation will have the kind of:

$\Delta y_A = \alpha.V.t + y_{os}$

The system of 3 equations in numerical kind is:

$$\begin{cases} \Delta y_A = 0{,}0222.12{,}5.t + 0{,}003 \\ 0{,}042 - \Delta z_A = \dfrac{10^6.0{,}05 + 10^3.9{,}81}{10^6} cos(\sqrt{\dfrac{10^6}{10^3}}.t) + \\ \qquad + \dfrac{10^6.0{,}05 + 10^3.9{,}81}{10^6} \\ \Delta y_A = 0{,}021283 - \sqrt{0{,}0004 - \Delta z_A^{\ 2}} \end{cases}$$

and has the following solution: $\Delta z_A = 0{,}017316m;$ $\Delta y_A = 0{,}011276m;$ $t = 0{,}029823s$, that is practically equal with the previous one from example 2.3.2.b. The conclusion is also same as the one in 2.3.2.b.

d) with taking into account the obliquely symmetrical wheel load according B55-ERRI and assuming all other data as identical to those in 2.3.2.b, we get the system:

$$\begin{cases} \Delta y_A = 0{,}0222.\dfrac{12{,}5}{0{,}003}.(1 - e^{-0{,}003.t}) + 0{,}003 \\ 0{,}042 - \Delta z_A = \dfrac{10^6.0{,}05 + 10^3.9{,}81}{10^6} cos(\sqrt{0{,}4.\dfrac{10^6}{10^3}}.t) + \\ \qquad + \dfrac{10^6.0{,}05 + 10^3.9{,}81}{10^6} \\ \Delta y_A = 0{,}021283 - \sqrt{0{,}0004 - \Delta z_A^{\ 2}} \end{cases}$$

and solution is:

$\Delta z_A = 0{,}01916m;$ $\Delta y_A = 0{,}015548m;$ $t = 0{,}045222s.$

Therefore, the value obtained for Δz_A ($\Delta z_A = 0{,}01916$) is higher than that for the top of the flange ($max\Delta z_A = 0{,}01893m$); that means that contact point A' will be behind the the flange top, i.e. its on the other (back) side, which is absolutely dangerous.

Under these conditions distance of bounce ΔX_A is obtained to be $\Delta X_A = \Delta y_A / \alpha = 0{,}01916/\alpha = 0{,}7\ m.$

e) taking into account the obliquely symmetrical wheel load according to B55-ERRI and accepting all other data as identical to those in 2.3.2.d, the solution obtained is with almost identical values to those in 2.3.2.d, i.e. $\Delta z_A = 0{,}01916m;$ $\Delta y_A = 0{,}015549m;$ $t = 0{,}045222s,$ hence the conclusion is the same as in 2.3.2.d.

f) at the speed of vehicle V = 25 km/h (6,944 m/s) and assuming all other data and conditions as identical to those in 2.3.2.e, the solution of the system is: $\Delta z_A = 0{,}016753m;$ $\Delta y_A = 0{,}010358m;$ $t = 0{,}047734s$ where $\beta = 33{,}107^o$, criterion $tg(\beta - \rho) = 0{,}236$ are obtained from, hence the admissible value of criterion $tg(\beta - \rho)$ is reduced 5,07 times compared to standard one 1,2.

Under these conditions distance of bounce ΔX_A is $\Delta X_A = \Delta y_A / \alpha = 0{,}010358/0{,}0222 = 0{,}466\ m.$

g) at the speed of vehicle $V = 25\ km/h$ ($6{,}944\ m/s$) and assuming all other data and conditions as identical to those in 2.3.2.e, we get the same solution as in the previous example; hence the same conclusion as that in 2.3.2.f.

2.4. Analysis of results

From the calculations made with different data of the track and vehicle and using different dependencies, it is reasonable to consider those that have faithfully taken into account as many factors as possible as most accurate. It must add to the overall assessment that in many cases (considering mainly p.2.2, especially related to air resistance) that is not of paramount importance, since the methods presented in the paper is approximate in nature. It is because first, it discusses the issue in quasi aspect without considering the dynamic and crash processes, thus being inappropriate and even inapplicable for normal and high speeds.

Furthermore, although the method is quasi-static in its nature, it uses some settings that determine not quite accurate results even in a quasi-static aspect. This refers mostly to the assumption that longitudinal coordinate Δx_A does not vary with transition through a "lowing threshold". This coordinate belongs to new contact point A' on the wheel surface, the bandage respectively, considered under the assumption that the wheel does not rotate, Based on the existing dependencies [2], to displace contact point Δx_A along its length and vertical $\Delta z_A \equiv \Delta r_A$, the dependency between them can be worked out:

$$\Delta x_A = 2\Delta z_A / \alpha.tg\beta \qquad (19)$$

and obtained Δx_A can be to adjust the length of the bounce ΔX_A, used for the first equation of system (15) where it can obtain the kind of:

$$\Delta y_A = \alpha\left[\frac{V_{X0}}{k}(1 - e^{-k.t}) + 2\Delta z_A / \alpha.tg\beta\right] + y_{os}, \qquad (20)$$

but this is hardly appropriate considering that the above-mentioned basic relations are derived with small displacements of the contact point and conical surfaces (or approximated to such ones) and in this case none of these conditions is fulfilled. At this stage iterative approach could be applied but in compliance to avoid superimposing of errors with the large number of steps.

Concerning the accuracy of the method, in conclusion it can be said that the relative error of the method exposed in this kind is estimated to be *3-5 %* for standard railways under normal conditions and up to *8-10%* under extreme conditions. Obviously, more accurate estimates and dependencies can be obtained after carrying out experimental tests.

The results obtained for criterion $tg(\beta - \rho)$ must be interpreted necessarily taking into account that, as above mentioned, with shifting the contact point towards the top of the flange the danger of derailment increases. It is not only due to the reduction of angle β, but also due to the action of increasing angle of friction ρ. If we take the numerical example 2.3.1 with the "least dangerous " value of $tg\ (\beta - \rho) = 0{,}378$, it should be noted that this value is calculated for the regulation value of the angle of friction ($\rho = 19{,}8\ ^o$, as it is in the flange "operation " area at the base; but since in this case contact point A' with coordinate $\Delta z_A \equiv \Delta r_A = 0{,}015206\ m$ is too aligned with the top (at *3,6 mm* from its radius, there is friction angle ρ and the friction coefficient μ respectively have obviously higher values and depending on their change, criterion *tg* $(\beta - \rho)$ and ratio $1{,}2/tg\,(\beta\text{-}\rho)$ will greatly alter in unfavorable direction as follows:

ρ	19,8º	25º	30º
μ	0,366	0,466	0,577
$tg(\beta - \rho)$	0,378	0,277	0,185
$1{,}2/tg(\beta - \rho)$	3,17	4,33	6,49

For more detailed and visual assessment of the influence of the contact point location and angle of friction (ratio respectively) with different values of Δz_A and β is given in Table 1.

Table 1

Values of criterion tg(β - ρ) with different values of $\Delta z_A \equiv \Delta r_A$, β, $\rho \rightarrow \mu$

$\Delta z_A \equiv \Delta r_A$, mm		6	12	14	16	17	17,32
β°		70	53,13	45,57	36,87	31,79	30
$tg(\beta\text{-}\rho)$	ρ/μ= 19,8/0,36	1,20	0,66	0,48	0,31	0,21	0,18
	ρ/μ= 25/0,47	1,00	0,53	0,37	0,21	0,12	0,09
	ρ/μ= 30/0,58	0,84	0,42	0,28	0,12	0,03	0

From the analysis of the results, it can conclude that their credibility does not arise any doubt about the existing real threat of derailment caused by "rail threshold".

CONCLUSION

Based on this theoretical studies accomplished in this paper, the resulting dependencies and solved examples it can be reasonably argued that track subsidence (roughness) of "rail threshold" type could pose a serious danger of derailment and cause inevitable derailment even with its independent action (without other factors) including at relatively low speeds.

REFERENCES

[1] ORE/ERRI B55: „Entgleisungssicherheit von Guterwagenin Ggleisverwindungen". Arbeitsergehnis NN 1-8, Utrecht, 1962-1982

[2] Heumann H., GRUNDZUGE DER FUHRUNG DER SCHIENEN-FAHRZEUGE-SONDERDRUCK AUS ELEKTRISCHE BAHNEN VERLAG R. OLDENBOURG MUNCHEN, 1954

A Crash Buffer For Railway Vehicles

Venelin Pavlov[1*], Dobrinka Atmadzhova[1]
[1]Machinery and Construction Technologies in Transport/Transport equipment,
Todor Kableshkov University of Transport,
Sofia (Bulgaria)

The subject of the paper is a crash buffer for railway vehicles (wagons or passenger coaches). The main requirements are: storing and usage of a massive amount of energy, simple constructive solution, low costs. The technical challenge solved by this design is a buffer with a simplified structure, allowing energy storage in two phases: elastic and plastic.

Keywords: railway vehicles, buffer, crash, wagons, passenger coaches

1. INTRODUCTION

Buffers are structural components of rail vehicles that first take shock loads between vehicles at collision each other. Many scientists are involved in designing and testing buffer structures and their features [1, 2, 3, 4, 5, 6, 7, 8, 9].

Crash technologies used in locomotives, freight and passenger cars are aimed at enhancing safety. The use of such technologies in certain types of rail vehicles is required by UIC fiches [10]. Buffer "crash" technology absorbs much of the impact energy in an irreversible process, thereby increasing the safety of people, cargo and the vehicle [11, 12].

According OTIF (former RID) regulations [13] and UIC fiche 573 of tank cars for transportation of hazardous materials (toxic materials and flammable gases), it is mandatory to mount 2T and 2F buffers by the end of 2012. For wagons manufactured later than 2007 each buffer must absorb energy of *400 kJ* and *250 kJ* for wagons, which are already in use.

The Bulgarian State Railways use buffers with rubber-metal elements (RME), rubber pads and elastomeric capsules.

Fig. 1 Photos of buffers and components.

Fig. 1 shows pictures of some buffers and components at the moment of inspection and testing at the National Research Institute for Transport Ltd. (NRIT) in Sofia.

The railway vehicles operated in the Republic of Bulgaria, are equipped with rubber-metal packages as energy absorbing element in draw gears.

The buffer with a rubber-metal package is subjected as a whole to appropriate tests in NRIT [14]: the first stage of the test is taking down static characteristics. The buffer was tested in a complete state as mounted on the wagon for operation. The ambient temperature is *15° C*.

The load on the buffer is done using a laboratory press at a rate no greater than *0.05 m/s*. The buffer is unloaded immediately after the load continuously registering the deformation obtained.

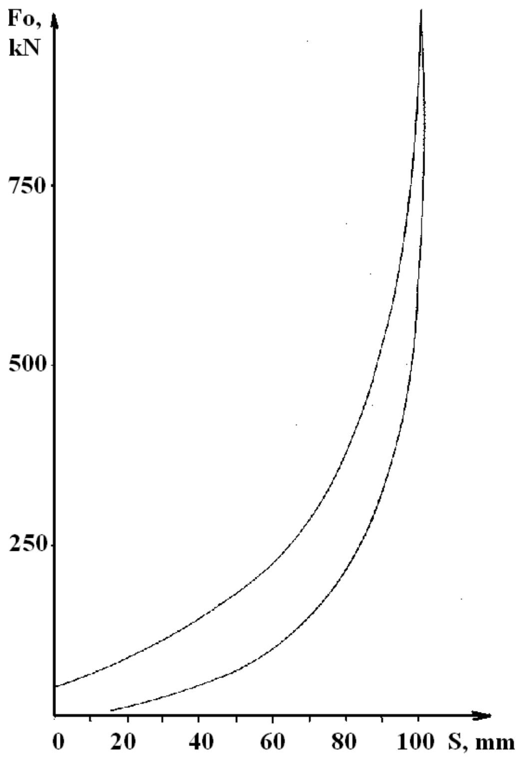

Fig. 2 Static characteristics

The static deformation characteristics obtained (Fig. 2) has a progressive character typical for rubber-metal packages. The maximal force of *1000 kN* is obtained at the maximal deformation stroke of *105 mm*. Preload is about *20 kN*.

*Corresponding author: 158 Geo Milev Str., Sofia, Bulgaria, atmadzhova@abv.bg

The total energy absorbing by buffer *We = 23.5 kJ*, which is significantly greater than the determined limit of *12.5 kJ*, irreversible energy absorbing *We = 12.5 kJ*, which is *53%*.

Buffers are also subjected to strength requirements, they are loaded along the axis with force *F> 2,500 kN* and shear $F_2 > 200$ *kN* (F_2 is applied to the buffer body).

It has been found that the buffer continues to function normally as there are no residual deformations. Also, after loading the bearing plate with a force of *2500 kN* no residual deformations have been established. It should be pointed out that regulations allow residual deformations commensurate with the variations in size with manufacturing, which should not be greater than *0.2%*.

The dynamic tests of buffers were conducted by a device for impact tests at various speeds. The maximum absorbing of *30 kJ* was obtained under the maximal force of *1000 kN*. The results are plotted on the dynamic feature (Fig. 3).

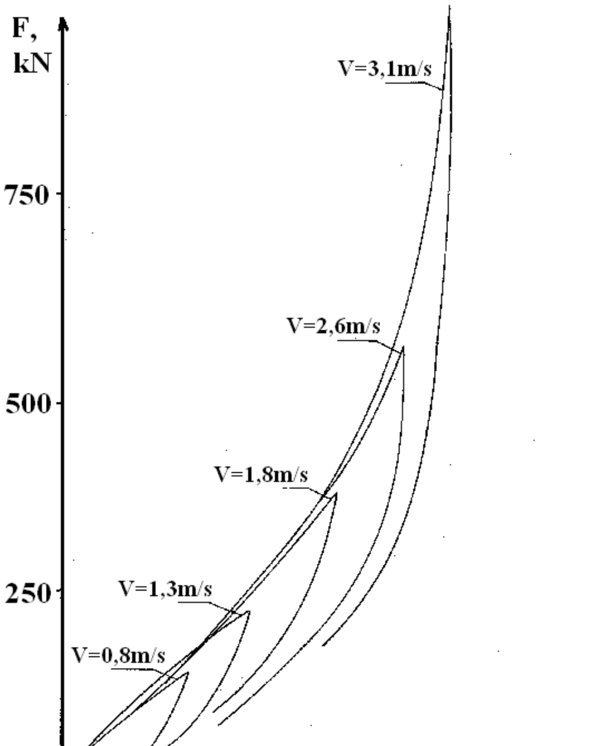

Fig. 3 Dynamic characteristics

With maximal use of the interior of the sleeve and a right choice of rubber mixture, it is possible to make a buffer that meets the requirements of fiches UIC 526-1 and 528 [10].

The main advantages are that they have a relatively low cost and satisfactory reliability. Along with that these buffers have a number of disadvantages, the most important of which are:

1. The accumulated and especially absorbed energy has small values. By these indicators they are at the boundary of admissible by the UIC, which makes their effectiveness and feasibility of domestic and especially international transport doubtful.

2. The qualities of rubber-metal package are extremely dependent on the composition of the rubber mixture and manufacturing technology. In this sense, even small deviations from the approved recipe or manufacturing technology, lead to significant differences in the power characteristics of the buffer and thus to failure to comply with the standards of UIC. This is the main reason why it can not be declared that the Bulgarian freight wagons are equipped with draw gears matching fiches 526-1 and 528.

3. The buffers with rubber-metal package have relatively low durability that is disproportionate to the durability of the wagon body. The main reason for this is aging of rubber as a result of oxidation and variable temperatures during operation. The observations in repairer shops show that for the period of wagon operation it is necessary to replace rubber-metal package completely 5-6 times, which significantly increases the repair costs.

4. This type of elastic elements has non-linear parabolic increasing characteristics. Therefore, at the end of running the force acting on the buffer is equal approximately to the maximally admissible one for both draw gear and the metal car body in wagon.

This leads to extremely unfavorable consequences related to strength of the front beam and other structural elements, keeping cargo or the passengers' comfort in carriages.

The studies made have shown that even with a significant increase in the size of rubber-metal package, the increased necessary absorption according to current requirements for wagon structure cannot be achieved.

The RME performed studies on energy absorbing elements for buffers of high absorbing class "C" by preliminarily developed methodology. Three types of such elements were tested, two types of hydro pneumatic capsules 4 EC-80 and 5SC produced by OLEO Company, England, and capsules with elastomeric of KZE-5 type manufactured in Poland. The material of the elastomeric capsule is "polastosil ABM": it is widely used in buffers for freight and passenger wagons and is also used to make buffers for locomotive.

It has become necessary to use a new type of energy absorbing element ensuring sufficient energy absorbing: 25% greater than the existing one structures implemented in the draw gears (DG) as at the same time durability is comparable to the lifetime of wagons and requires no maintenance during operation.

2. ABSORBING DEVICE FOR BUFFERS WITH INCREASED ENERGY ABSORPTION

2.1. Theoretical setting

The rubber deformation cycle has a pronounced specificity, which is determined by a number of peculiarities: relative extensions, sliding and rotation angles of the order of one. Also, the relationship between stress and the deformation components is not expressed by Hook's regulation. As a consequence of these features displacements appear as a nonlinear function of the forces acting on the rubber element. Nonlinearity is reflected in the analytical findings of the nonlinear theory of elasticity - formulas for deformation, equations for the equilibrium of the volume element and formulas giving the relationship between stress and deformation components.

What is characteristic of the rubber deformation cycle, it is also the underlined process irreversibility caused by the availability of dissipative forces. The proportion of these forces related to the conservative ones depends on the rate of deformation.

The characteristics mentioned above complicates the study on deformation of elastic elements to such a degree, which makes impossible to reach an exact solution. Even with adoption of simplifying assumptions of a physical nature such as linear independence of the relative energy of deformation from only invariants of the strain state and with implementing the method of Ritz, it turns that practically it is possible to treat a narrow circle of elastic elements and with such geometric shapes and acting forces, which have very essential significance to practice.

The statistical theory of molecular networks is of particular interest in studying the theoretical concept of elasticity of high-molecular compounds such as rubber. However today, with the help of that theory, the deformation of high-molecular compounds can be interpreted well only qualitatively. Modern statistical theory gives only a rough quantitative match with experience.

What has been said is a factor that requires finding another way to solve this question.

In the field of small deformations, the relationship between current force P acting on metal-rubber element (RME) and its deflection Δ is linear [15, 16], i.e.:

$$P = D\Delta(\chi\theta)^{-1}.h^{-1}, \tag{1}$$

where: D-coefficient determined by the mechanical properties of the rubber, which RMEs are made of; χ, θ - coefficients determined by the geometry of the RME and the manner of loading; h - thickness of gum of RMEs.

In presence of force characteristics $P_m(\Delta_m)$ of a given RME with known values of coefficients D_m, χ_m, θ_m, rubber layer thickness h_m and method of loading called "model", for the force characteristics of the designed RME of certain values of coefficients D, χ, θ, rubber layer thickness h and method of loading, according to equation (1) the following relationship can be written [17]

$$\frac{P.\chi h}{\Delta}.\frac{\Delta_m}{P_m.\chi_m h_m} = \frac{D}{D_m}\frac{\theta_m}{\theta}, \tag{2}$$

or after differentiation of expression (2) with respect to the relative deflection ξ

$$\frac{dP}{d\xi}:\frac{dP_m}{d\xi} = \frac{D}{D_m}\frac{\theta_m}{\theta} \tag{3}$$

where:

$$\xi = \Delta/(\chi h) = \Delta_m/(\chi_m h_m) \tag{4}$$

For equation (3), unlike to equation (2), there are no limitations for the values of deformation. If RMEs are geometrically similar, made of vulcanized rubber and loaded under the same scheme, then ratio D/D_m will be constant. In this case, after the integration of equation (3) and taking into account ratio (4), the following equations are obtained for determining the coordinates of a point of the designed RME power characteristics based on the coordinates of a point of the model RME power characteristics:

$$P = (\theta_m/\theta).P_m; \quad \Delta = (\chi/\chi_m).(h/h_m).\Delta_m \tag{5}$$

Equation (5) gives reason to speculate that it could be used also for RMEs that are not geometrically similar, are loaded in different ways and made of different rubbers. Practice shows that the accuracy in this case is completely satisfactory. That is due to the fact that rubbers, which springs are made of, do not have a wide range of mechanical properties. The ratios of their geometric parameters also vary in a large interval.

As the value of relationships θ_m/θ and χ/χ_m are not associated with the deformation values, the coefficients χ and θ are defined for different configurations and load on RME with "small" deformations at different points. The last one is a complex but solvable problem. The ratio D/D_m is determined experimentally taken out from power characteristic of RMEs of equal configuration and load, made of the rubber of model and designed RMEs.

As first approximation of the power characteristic of the model RME can be used also that obtained from equation (1) for the RME under design.

The determination of coefficients χ and θ made is made based on the theorem of minimum potential energy.

The relative energy W of RME deformation for small deformations considered with the properties of rubber of keeping its volume with deformation is a function of the second invariant of the deformed state J_2, i.e.:

$$W = DJ_2, \tag{6}$$

where:

$$J_2 = -\varepsilon_x.\varepsilon_y - \varepsilon_y.\varepsilon_z - \varepsilon_z.\varepsilon_x + (1/4).\left(\gamma_{xy}^{\ 2} + \gamma_{yz}^{\ 2} + \gamma_{zx}^{\ 2}\right)$$

ε, γ- linear and angular deformation respectively.

Determination of coefficients for χ and θ for a ring-like RMEs under pressure [17].

The geometrical parameters of the ring (Fig. 4) are: R_1 - internal radius, R_2 - external radius, h - the rubber layer thickness, r_0, - radius defining the layer, wherein the radial deformation ρ is equal to zero- ρ = 0.

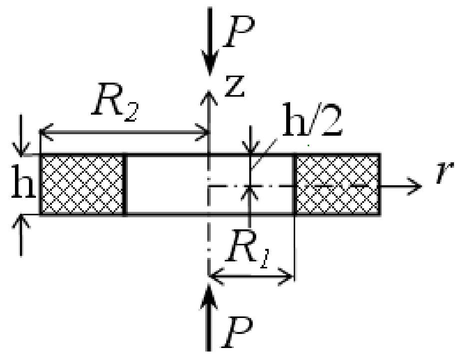

Fig. 4 Geometrical parameters of the ring.

Treating the problem, it is appropriate to deploy elements in a cylindrical coordinate system – z, r, ψ. The components of displacements can be expressed as follows: $w(z)$ - axis z; $\rho = \rho(r, z)$ – along axis r; ψ - angle.

The deformation components are:

$$\varepsilon_z = \frac{\partial w}{\partial z}; \ \varepsilon_r = \frac{\partial \rho}{\partial r}; \ \varepsilon_\psi = \frac{\rho}{r}.$$

From the condition for the non-changeability of rubber volume it follows that:

$$\frac{\partial w}{\partial z}+\frac{\partial \rho}{\partial r}+\frac{\rho}{r}=0\,, \qquad (7)$$

or $$-\frac{1}{r}\frac{\partial}{\partial r}(r\rho)=-\frac{\partial w}{\partial z}=-f(z)$$

After integrating equation (7) it is obtained that:

$$r\rho=-0{,}5.r^2 f(z)+c$$

Constant C is determined by the boundary condition - in $r = r_0$, $\rho = 0 - c = 0{,}5.\ r_0^2 f(z)$, or

$$\rho=-0{,}5.(r-r_0^2/r)f(z) \qquad (8)$$

In compliance with equation (8) the deformation components are:

$$\varepsilon_z=f(z)\,;\varepsilon_\rho=-(1/2).(1+r_0^2/r^2)f(z)\,;$$

$$\varepsilon_\psi=-(1/2).(1-r_0^2/r^2)f(z)\,;$$

$$\gamma_{zr}=-(1/2).(r-r_0^2/r)f'(z)\,;\ \gamma_{r\psi}=0\,;\ \gamma_{\psi z}=0\,.$$

The relative energy of deformation W of RME (6) is equal to:

$$W=D\left[(1/4)\left(3+r_0^4/r^4\right)f^2(z)+(1/16)\left(r+r_0^2/r\right)f'^2(z)\right].$$

Strain energy U is equal to:

$$U=\int_{-h/2}^{h/2}\int_{R_1}^{R_2}\int_0^{2\pi}W dr.rd\psi.dz$$

Having performed the indicated actions, the following expression for determining the value of strain energy U is obtained:

$$U=2\pi D\int_{-h/2}^{h/2}\left\{0{,}25\left[1{,}5\left(R_2^2-R_1^2\right)-\right.\right.$$
$$\left.-0{,}5r_0^4\left(R_2^{-2}-R_1^{-2}\right)\right]f^2(z)+(1/16)\left[0{,}25\left(R_2^4-\right.\right.$$
$$\left.\left.\left.-R_1^4\right)+r_0^4\ln(R_2/R_1)-r_0^2\left(R_2^2-R_1^2\right)\right]f'^2(z)\right\}$$

Since the potential V of the external force P is equal to $V=-P\Delta=-P\int_{-h/2}^{h/2}f(z)dz$, the total energy of the system Π ($\Pi = U - V$) is equal to:

$$\Pi=\int_{-h/2}^{h/2}\left\{\pi.D/2\left[1{,}5\left(R_2^2-R_1^2\right)0{,}5r_0^4\left(R_1^{-2}-\right.\right.\right.$$
$$\left.\left.-R_2^{-2}\right)\right]f^2(z)+(\pi.D/8)\left[0{,}25\left(R_2^4-R_1^4\right)+\right.$$
$$\left.+r_0^4\ln(R_2/R_1)-r_0^2\left(R_2^2-R_1^2\right)\right]f'^2(z)+$$
$$\left.+Pf(z)\right\}dz=\int_{-h/2}^{h/2}\phi dz \qquad (9)$$

To be the total energy of minimal value Π, function f (z) must satisfy the equation of Euler:

$$\frac{d}{dz}\frac{\partial\phi}{\partial f'}-\frac{\partial\phi}{\partial f}=0 \qquad (10)$$

Based on equation (9) and taking into account equation (10), for function $f''(z)$ it is obtained that:

$$f''(z)-\frac{\left(6+\dfrac{2r_0^4}{R_2^2R_1^2}\right)f(z)+\dfrac{4(\pi D)^{-1}.P}{\left(R_2^2-R_1^2\right)}}{\dfrac{R_2^2+R_1^2}{4}+\dfrac{r_0^4}{R_2^2-R_1^2}\ln\dfrac{R_2}{R_1}-r_0^2}=0 \qquad (11)$$

When performing the following applications to equation (11):

$$\left(6+\frac{2r_0^4}{R_2^2R_1^2}\right)\left(\frac{R_2^2+R_1^2}{4}+\frac{r_0^4}{R_2^2-R_1^2}\ln\frac{R_2}{R_1}-r_0^2\right)^{-1}=\psi^2$$

$$2P.\left[\pi D\left(3+\frac{r_0^4}{R_2^2R_1^2}\right)\left(R_2^2-R_1^2\right)\right]^{-1}=\varphi\,,$$

the following differential equation is obtained:

$$f''(z)-\psi^2\left[f(z)+\varphi\right]=0 \qquad (12)$$

When completing the application $f(z) + \varphi = F$, equation (12) obtains the kind of:

$$F''-\psi^2F=0 \qquad (13)$$

The solution of equation (13) is:

$$f(z)=A_1ch\psi z+A_2sh\psi z-\varphi \qquad (14)$$

To determine constants A_1 and A_2, the following boundary conditions are used:

1. $z = 0$ и $\rho(0) = \rho_{max}$;

therefore - $\dfrac{\partial\rho}{\partial z}=0$ and $f'(z) = 0$;

2. $z = h/2$ and $\rho(h/2) = 0$ (due to the effect of reinforcing plates, which can be considered as absolutely rigid) therefore - $f(h/2) = 0$.

Considering the values of $f'(0)$ and $f(h/2)$, determined by the boundary conditions, the constants have the following values: $A_2 = 0$ and $A_1 = \varphi/[ch\psi h/2]$.

With the so-defined values of constants, equation (14) takes the kind of:

$$f(z)=\varphi\left(\frac{ch\psi z}{ch\psi h/2}-1\right)$$

The total displacement Δ of RME is determined by the expression:

$$\Delta=-\int_{-h/2}^{h/2}f(z)dz=-\int_{-h/2}^{h/2}\varphi\left(\frac{ch\psi z}{ch\psi h/2}-1\right)dz=$$
$$=\varphi h\left(1-\frac{th\psi h/2}{\psi h/2}\right) \qquad (15)$$

Comparing the dependencies (1) and (15) it follows that:

$$\frac{2}{\pi\left(3+\dfrac{r_0^4}{R_2^2R_1^2}\right)\left(R_2^2-R_1^2\right)}=\theta\,;\qquad 1-\frac{th\psi h/2}{\psi h/2}=\chi$$

The value of the parameter r_0 corresponds to the maximum value of deformation Δ.

It is convenient to finf out the value of parameter r_0 once in tabular or graphical form function $\Delta = \Delta(r_0)$ is expressed and its minimum is determines.

The results of calculations with seven pieces RME are given in fig 5.

$\Delta_{min} = 0{,}630365\ m$; $\psi = 107{,}5083$;

The deformation of the package consisting of 7 elements with a given force of *1 MN* will be *105 mm*. From here, the values of coefficients χ and θ, namely: $\chi = 0.990698$ and $\theta = 45.9373$.

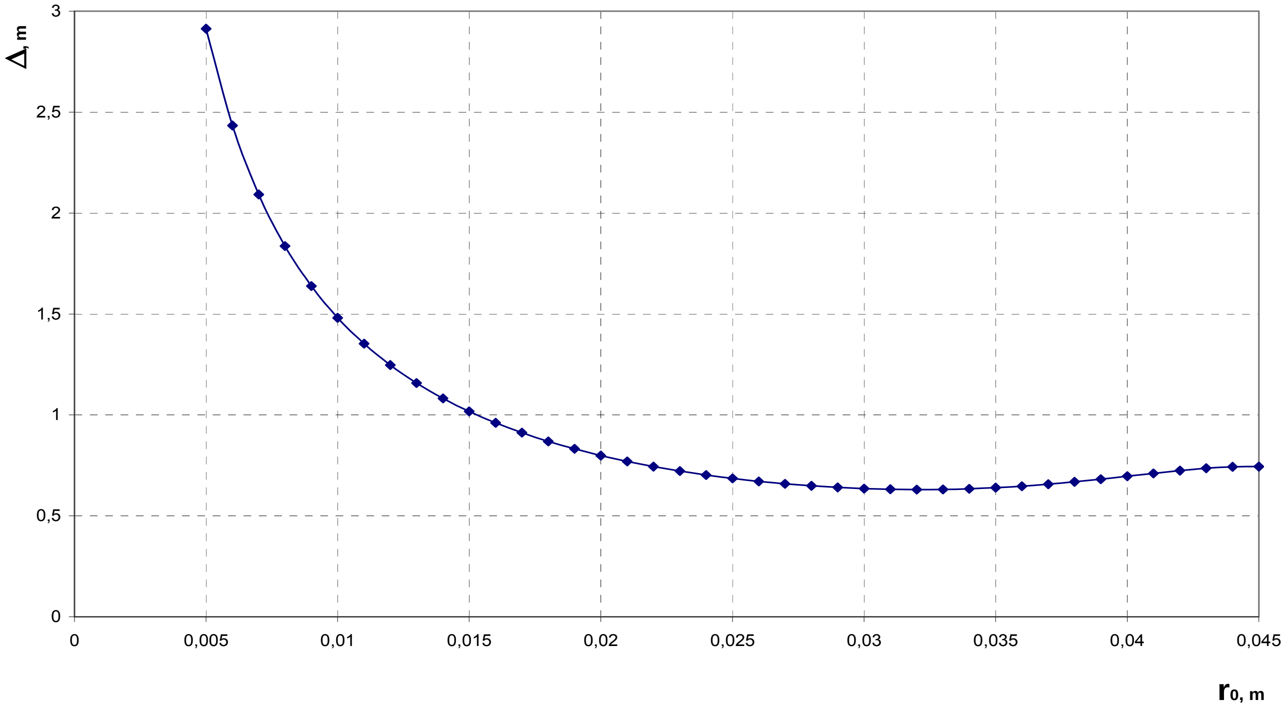

Fig. 5 The value of the parameter r_0 corresponds to the maximum value of deformationΔ.

2.2. DUREL - Polymer springs, sets for absorbing devices of buffers [18, 19]

DP 30 is a universal spring system that can be applied in all absorbing device of buffers with static characteristics shown in Fig. 6.

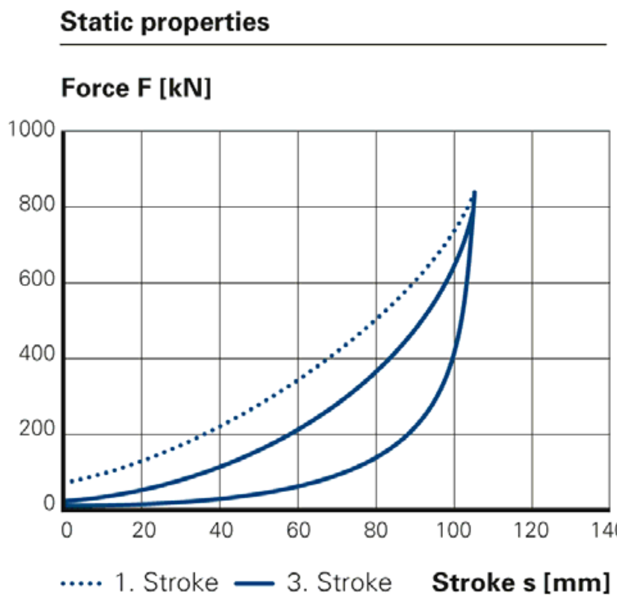

Fig. 6. Static characteristics

DP 30 belongs to buffers of A + / 40kJ (dynamic) category and it is in line with UIC specifications 526-1 and 827-1 and has certification EBA numbered 01J07A.

DUREL high-performance polymer springs are resistant to chemicals, fats, oils and solvents.

2.3. Calculation of strength deformation condition of the absorbing device

The absorbing device built of *7* DUREL elements and *5* metal plates is calculated using software SolidWorks 2010. The device is loaded with a compressive force (along its axis) with a value of *1000 kN.*

As a result of the calculations made, the maximal values of stress by Von Misis criterion is *298.604 MPa* (fig.7 and table 1) in the middle part and in the connection of DURAL elements with the metal plates.

Table 1. Results from the strength study of absorbing device

Name	Type	Max	Location
Stress1	VON: von Mises Stress	298.604 MPa Node: 14967	(21.01 mm, 220.74 mm, 37.80 mm)
Displa-cement1	URES: Resultant Displacement	0.53999 mm Node: 115	(8.92 mm, 27.56 mm, -23.34 mm)
Strain1	ESTRN: Equivalent Strain	0.00193 Element: 595	(21.04 mm, 47.96 mm, 16.59 mm)

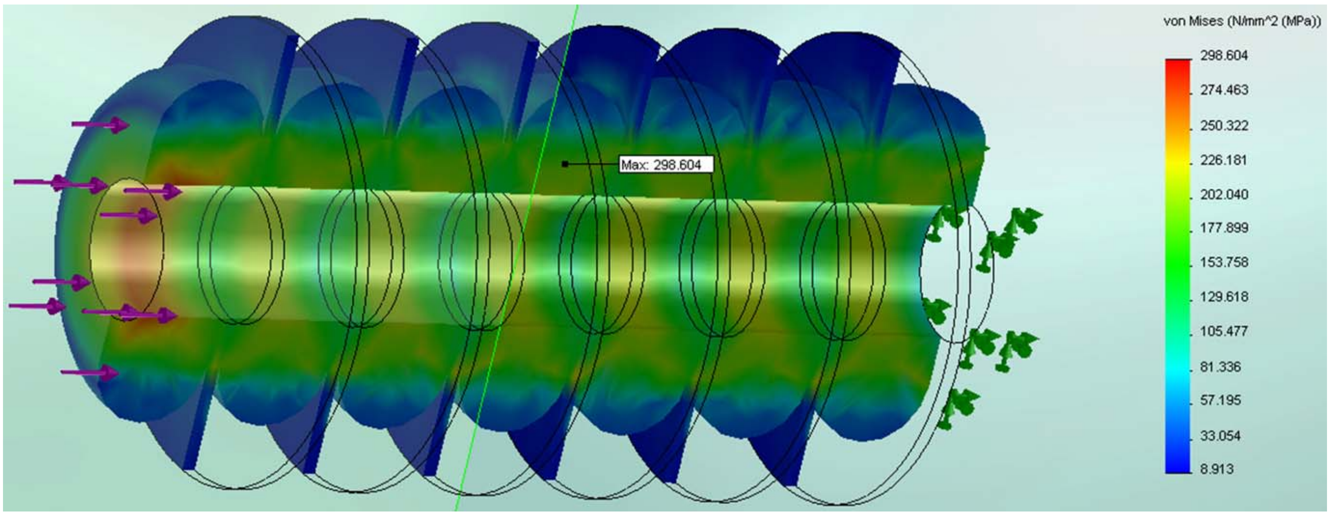

Fig. 7. Stressed state of the absorbing device at a stroke of 105 mm.

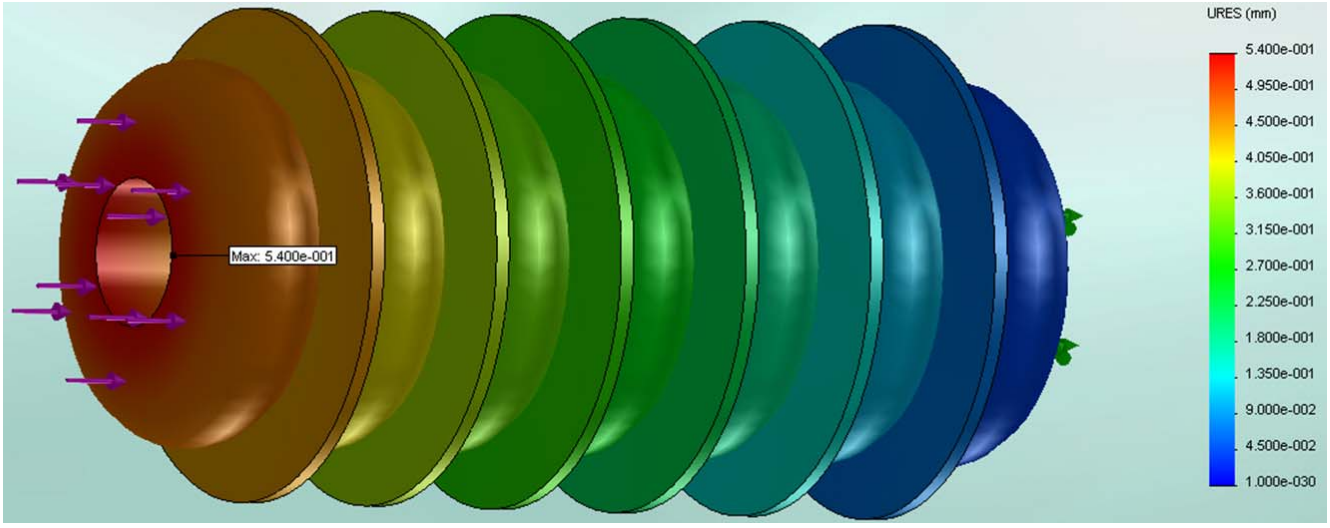

Fig. 8. Additional deformation of the absorbing device at a stroke of 105 mm.

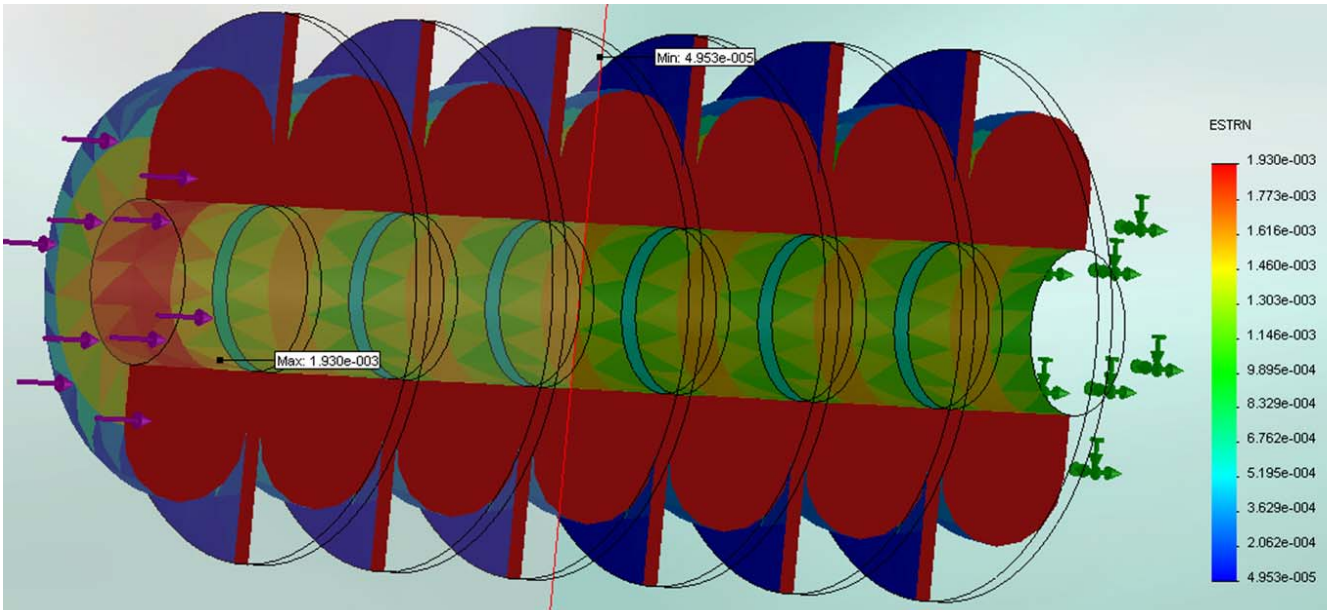

Fig. 9. Distribution of the coefficient of risk of absorbing device at a stroke of 105 mm.

The total deformation of the device is *105.54 mm* (fig.8). The risk coefficient is *0.0019* in the upper abutment surface and the inner diameter of the first elastic ring DURAL (fig.9).

3. REVIEW ON "CRASH" ELEMENTS OF BUFFER STRUCTURES

A lot of buffers equipped with "crash" modules have been developed. These modules use the effect of permanent plastic deformation [20, 21]:

- breaking elements of the buffer frame;
- expansion (plastic) or forcing pipes (pipe-in-pipe system);
- cutting pipes (peeling technology) and
- deformation of additional elements such as a box.

3.1. "Crash" elements - breaking elements of the buffer frame

This system is known in two variants - breaking one or two areas of the external sleeve of the buffer frame.

The crash EST buffer combines a standard buffer for railway vehicles and a "crash" element for energy absorption – an element for deformation in a single component. The element with the additional function of deformation is integrated into the buffer frame so that no additional space is required even after deformation. The overall dimensions and the dimensions of the support flanges are identical to those of a standard buffer according to UIC 526-1. With the planned deformation of the buffer frame the energy absorbed is *10* to *20 times* more than in the standard conventional buffer. This corresponds to the maximal speed of crash between vehicles at about 30 km/h. Under similar conditions, the maximal speed of crash with traditional, conventional buffers is about *10 km/h*.

3.2. "Crash" elements - extension (plastic) or forcing pipes (pipe in pipe system)

The principle of TSB technology uses the phenomenon of plastic expansion (or movable in some structures) of metal pipe with a special tool to expand.

The main elements of this type of buffers are TSB absorbing device and deformation area (area with plastic deformation). The effectiveness of this method of energy absorption gives a possibility to embed an additional module in the buffer, as the buffer total length does not significantly differ from the length of the standard buffer. Moreover, during the stroke it is possible for the stroke to reach *275 mm*.

The requirements of OTIF distinguish the level of absorbed energy for newly produced wagons (400 kJ) and the level for wagons currently in use (250 kJ).

3.3. "Crash" elements - system with pipe cutting (peeling technology)

The "Crash" module developed by AXTONE uses a unique technique for energy absorption based on metal cutting. This technology allows designing a buffer, wherein the degree of absorbed energy can be controlled in a wide range. The crash energy is absorbed by resilient elastic deformation of a steel strip cut from the buffer body changing mechanical energy into heat energy. The level of absorbed energy depends on the size of the final strip, a wide range of adjustment depending on the needs of specific application. The effectiveness of this innovative technology allows utilization of more than *1 MJ* of energy while keeping the gauge of typical buffers category C in accordance with UIC 526-1.

Generally this type of phenomenon is relatively well studied; however, in this particular application, because of the short time of event (less than *0.15 seconds*), and the subsequent cutting speed, it is necessary to perform additional analysis and experiments. These actions are designed to optimize the process in terms of the technology, used in the railway buffer.

3.4."Crash" elements – deformation of additional elements as a box

"Crash" elements based on deformation of the additional box-like elements are EST buffers with deformation system Duplex G1.A1.

3.5. Frame buffer "Crash" elements – in operation in Bulgarian State Railways

Buffers of "Crash" elements mounted on sleeping cars produced by TUVASAS, Turkey, TYPE R1-200 M/S/ST [22] have been in operation since April 2013 (Fig. 10).

Fig.10. Photos of buffer TYPE R1-200 M/S/ST.

Fig. 11 shows the static characteristics of the above-mentioned buffer, fig.12 show dynamic load during the conflict of EST shock buffer.

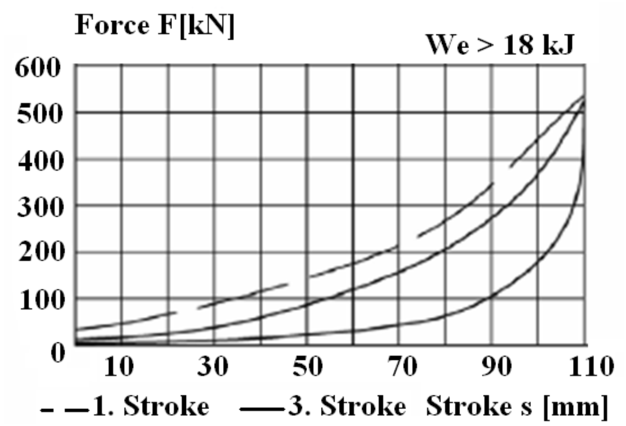

Fig.11 Static characteristics of EST crash buffer R1 in a normal mode (buffer function) [12]

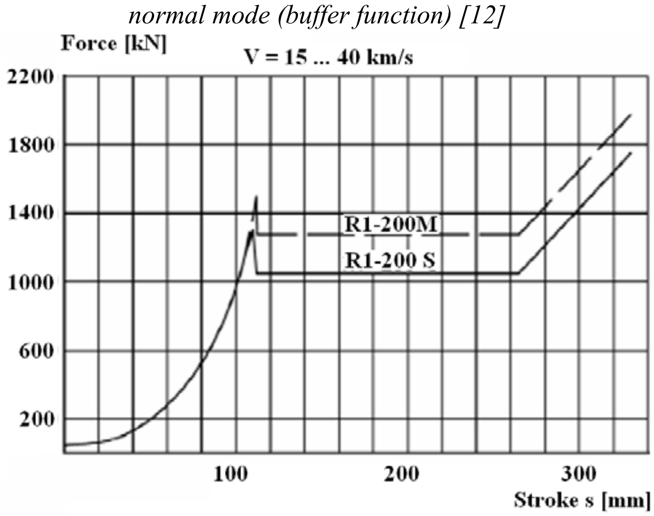

Fig. 12: Properties of force and track used by high dynamic load during the conflict of EST shock buffer.

On fig.13 and fig.14 are shown buffer functions.

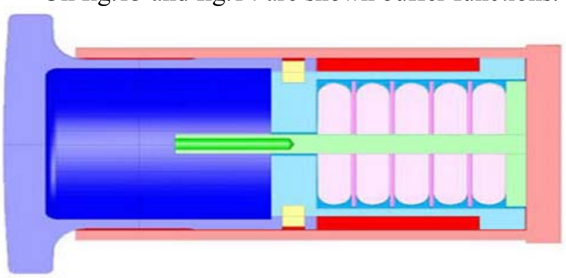

Fig.13 Condition of maximum springing (buffer function) or the state of separation (transition to conflict)

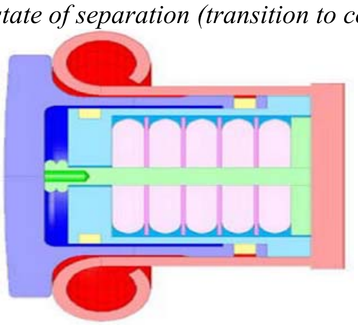

Fig.14 Condition after deformation, maximum deflection (buffer function)

EST Shock buffer R1 is characterized with:

- Progressing feature, low power, compatibility with other vehicles.
- The buffer head is made of highly wear- resistant sphere-granite cast iron of low wear-out and low coefficient of friction.
- Polymer spring does not need maintenance/service.
- Sliding surfaces inside are insensitive to pollution.
- Dynamic stabilization of the buffer spring has a high capacity of energy absorption with minimum *25 kJ* requirements by UIC.

Spring system DUREL ® DR 20 of company DUREL GmbH, İngelbach (Germany) is used.

The spring is of an elastic material based on polyethylene or polyester (TEEE) of the family of thermal plastic elastomeric. The benefits specified below make the spring comfortable to use as EST crash buffer R1:

- High energy density, compact installation dimensions;
- High energy reserve of absorption, minimum *18 kJ* against the UIC requirement (10kJ) or *25 kJ* (din.), which has been experimentally demonstrated;
- High load capacity;
- Long-term use (usually a period of typical use: 20 years);
- It does not require maintenance;
- -100% recyclable;
- Full compliance with the UIC 528.

Totally each crash buffer can consume about 300 kJ of energy (version R1-200 S), i.e. 30 times more than required for energy absorption of reverse energy by the conditions of UIC 528 and 10 times more than required by for coaches in terms of UIC 526-1.

If EST crash buffer has not reached the block condition, unless the changes in the stroke buffer there is no possibility of damages both in its own vehicle and in the opposite one.

In most cases at the crash speed (*15 ... 40 km/h*) the typical characteristics of strength and path of EST shock buffer remain unchanged without significant dependence on speed. EST shock buffer is designed for scenarios with higher speed collisions of multi-degree deformed systems, it is also suitable as preliminary and backup (e.g. the EST deformation system in the steering means is DUPLEX).

Structural characteristics according to UIC 528

- Buffer group passenger train and a buffer of integrated crash element (special buffer)
- Strength of start/setting in operation *1500 kN -0 / + 300 kN*
- Aaverage deformation force of plastic zone *1300kN* (typical)
- Energy intake of elastic zone W_c *(stat.)* $\geq$ *18kJ*
- Energy intake of elastic and plastic zones $\geq$ *350 kJ*
- Length of the structure *650 mm ± 4 mm*
- Buffer time (time of oscillation of the elastic system) *110 mm ± 5 mm*
- Deformation path (donuşumsuz alan) *220mm ± 10 mm*
- Diameter of the buffer plate *1500 mm ± 100 mm*
- Size of the buffer plate *660 x 360 mm*

4. DESIGN OF A "CRASH" ELEMENTS AS REQUIRED BY UIC

4.1. Description of the proposed buffer with increased energy absorption and a "crash" element

The subject of this paper is to describe the design of a buffer with increased energy absorption and a "crash" element that can be mounted on wagons.

The proposed structure of the hull consists of an external and internal sleeves, which are the "crash" element, absorbing device consisting of 7 packages DURAL, an axle and taller.

With crashing in the buffer, the elastic stroke occurs by shrinkage of the 7 packages DURAL as the stroke is *105 mm*. Proper treatments of the inner surfaces of the outer sleeve and the inner sleeve regulate the attenuation of the body section and occurrence of plastic deformation. Upon depletion of the elastic stroke of *105 mm* the weakened sections of the two bearings coincide.

4.2. Calculations of the "crash" element of the proposed buffer

The calculations of the "crash" element of the proposed buffer are implemented with software SolidWorks 2010 according to the final elements method of (FEM).

The buffer deformation comprises of two phases:

- Elastic deformation with a crash speed of *12 km/h* and forces not exceeding *1,5 MN*;

- Elastic + plastic deformation at speeds above *12 km/h* and forces over *1,5 MN*.

The elements constituting the "crash" element of the proposed buffer – internal sleeve and external sleeve are loaded with force of *1 MN*.

The maximal value of stresses is *316.104 MPa* in the weakened section. The admissible stress for the selected material is *351.57 MPa*, so with loading above *1112 kN* plastic deformation of the outer sleeve is expected.

The maximal value of the stresses is *316.836 MPa* in weakened part of the section. With loads above *1112 kN*, plastic deformation of the inner sleeve is expected.

4.3. Parameters of the proposed buffer

The buffer deformation is comprised of two phases:

- Elastic deformation at a speed of *12 km /h* and forces that do not exceed *1,5 MN*;

- Elastic +plastic deformations at speeds above 12 km/h and forces over *1,5 MN*.

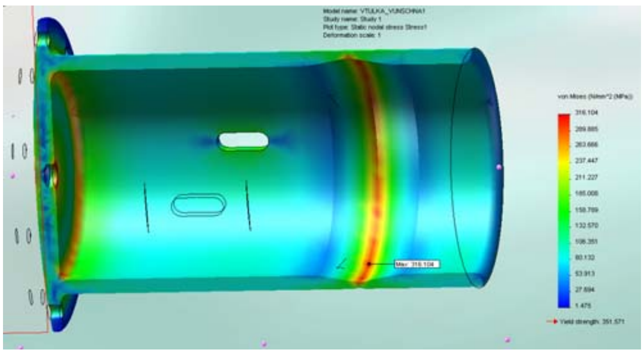

Study 1-Stress-Stress1
Fig. 15 Stress state.

Table 2. Results of the strength study on an external sleeve.

Name	Type	Max	Location
Stress1	VON: von Mises Stress	316.104 MPa Node: 8443	(122.7 mm, 584.7 mm, -51.3287 mm)
Displa-cement1	URES: Resultant Displacement	0.578 mm Node: 2206	(16.17 mm, 256.16 mm, 9.10e-005 mm)
Strain1	ESTRN: Equivalent Strain	0.00105 Element: 354	(-86.61 mm, 271.25 mm, -8.62 mm)

The maximal value of stresses is *316.104 MPa* (fig.15 and table 2) in the weakened section. The admissible stress for the selected material is *351.57 MPa*, so with loading above *1112 kN* plastic deformation of the outer sleeve is expected.

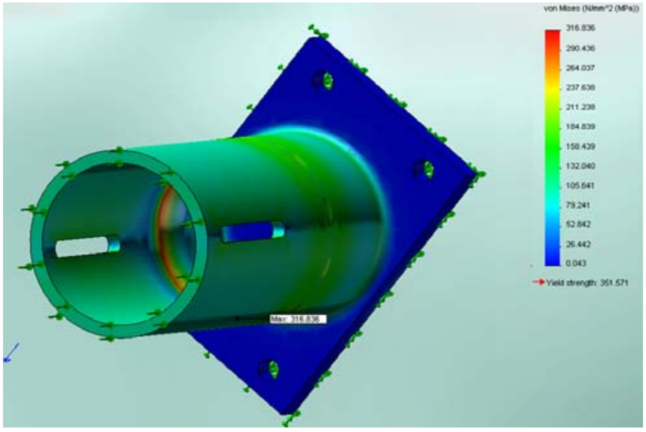

Study 1-Stress-Stress1
Fig. 16 Stress state.

Table 3. Results of the internal sleeve strength examination

Name	Type	Max	Location
Stress1	VON: von Mises Stress	125.796 MPa Node: 22239	(363.076 mm, 89.7476 mm, 59.1108 mm)
Displa-cement1	URES: Resultant Displacement	0.5391972 mm Node: 7710	(61.7214 mm, 251.946 mm, 77.7817 mm)
Strain1	ESTRN: Equivalent Strain	0.00039537 Element: 11949	(356.492 mm, 87.534 mm, 57.4527 mm)

The maximal value of the stresses is 125.796 MPa (fig.16 and table 3) in weakened part of the section. With loads above 1112 kN, plastic deformation of the inner sleeve is expected.

4.3. Technical specifications of "crash" buffer

Length: *620 mm* (UIC 526-1)

Base plate: *550 x 340 mm* (UIC 527-1 and ERRI B12 DT 84)

Category of buffer, UIC classification: Category 6 (UIC 526-1)

Stroke of the buffer: *105 mm* (0/-5mm, UIC 526-1)

Absorbed energy (dynamic): approx. *40 kJ*
Base plate with holes for threaded bolts: *280 x 160 mm*, M24
Striking force of the buffer: *1500 kN*
Average deformation force of the buffer: 1112 kN
Maximal axial deformation: approx. *200 mm*
Total absorbed energy of the vehicle (dynamic): approx. *600 kJ*
Weight of the buffer: *127 kg*

CONCLUSION

Based on the analysis of various structures of buffers, the results of tests and calculations of the proposed "crash" buffer structure, the following conclusions can be drawn:

1. Buffer rubber-metal packages – RMP are of widest application in BDZ. These elements are optimized and to increase their energy absorption and irreversibly absorbing is practically impossible. With heavier traffic and crashes at higher speeds, the dynamic characteristics do not meet the requirements.

2. Based on the analysis made above, taking into account the value of irreversible absorption coefficient and the low cost of buffer capsules of elastomeric type Tecs Pak or DUREL, the paper presents an attempt to embed elements of elastomeric type TecsPak or DUREL in a buffer and absorbing device of buffers.

4. For "crash" elements it is provided to construct buffer bushings that will be destroyed with crash between wagons at a crash speed of *12 km/h* and power > *1.5 MN.*

REFERENCES

1. Petrović D., Dynamic of impact of wagons, Zadu`bina Andrejević, Beograd, 2001
2. Petrović D, Rakanović R, Šoškić Z, Stress and strain waves at impacts of Waggons, XIII International Conference Transport, 13-14 novembar, Sofija, Bugarska, 2003, str. 143-148
3. Petrović D, Rakanović R, Šoškić Z, Waggon impact coefficient of restitution, XII International Conference Transport, 14-15 novembar, Sofija, Bugarska, 2002, str. 181-184
4. Petrović D., M. Biţić, M. Đelošević, R. Rakanović IDENTIFICATION OF WAVE PHENOMENA AT WAGONS IMPACT, HM 2011, Kraljevo, 2011
5. Vrangova V., Topalov S. Increasing the effectiveness of buffers for railway rolling stock, Rail Magazine, vol. 3, pp. 19-23, S. 1984
6. Karadjov T. Dimitrov G. Wagons Technique, 1988
7. Stoilov, V. M. Komitovski, I. Angelov. Buffer for railway wagons with high energy payment. Third International Conference on ICE, ATF and the rolling stock, MOTAUTO "96 Varna 26-28.09. 1996
8. Stoilov V., M. Komitovski, I. Angelov. Manufacturing capabilities of buffers for railway wagons highly absorbing. S., Rail, 3/1998
9. Stoilov V.M. Analysis of technical requirements and trends in buffers railway wagons. S., Rail 2/1998
10. UIC 526-1; 526-3; 528; 573
11. EN 15227:2008+A1:2010: Railway applications – Crashworthiness requirements for railway vehicle bodies [Required by Directive 2008/57/EC]
12. EN 15551:2009+A1:2010: Railway applications - Railway rolling stock-Buffers [Required by Directive 2008/57/EC]
13. Commission Decision 2006/861/EC of 28 July 2006
14. Static and dynamic (impact) test, "NRIT", 1990-1995
15. Ruzhekov TG Determination of deformation properties of rubber spring members, Yearbook of the Research Institute po ZHPT, pp. 34-49, S., 1964
16. Ruzhekov TG Use metalogumeni packages draw gear for rail vehicles Rail magazine, kn.4, pp. 17-19, S., 1967
17. Ruzhekov TG Penchev T. Dimitrov E. Theory and construction of railway equipment, S. 2010
18. http://www.railway-technology.com/contractors/brakes/durel/
19. http://www.durel.de/EN/Products-and-Services/buffer-springs/buffer-spring_DUREL_DP30.php
20. http://www.minerent.com/products
21. www.INNOVA-SysTech.com
22. Overall documentation TUVASAS

Validation of a Railway Vehicle Model Based on Cumulative Distribution Functions

Nebojša Bogojević [1*], Jelena Tomić[1], Slobodan Todosijević[1], Vojkan Lučanin[2]
[1] Faculty of Mechanical and Civil Engineering Kraljevo, University of Kragujevac, Kraljevo (Serbia)
[2] Faculty of Mechanical Engineering, University of Belgrade, Belgrade (Serbia)

Recent improvement of computers and numerical tools gave the engineers a possibility to develop and use very complex numerical models. One of the essential steps in the process of development of models is a process of verification and validation. The methodology for model validation based on the comparison of the cumulative distribution function is presented in this paper. Two well-known validation metrics – Area validation metric and Kolmogorov-Smirnov test were used for validation of a rail vehicle model. Results obtained from numerical simulation were compared to experimental data using denoted validation metrics. Applied validation metrics does not give clear answer for model "goodness". Therefore, a new validation metrics for validation of the models of the rail vehicles should be developed.

Keywords: Validation, Rail vehicle, Model, Simulation

1. INTRODUCTION

Experimental investigation of railway vehicles is the most reliable way to determine their properties and the crucial criterion for the approval of their exploitation. However, experimental investigations are extensive, time-consuming and expensive so alternative methods, used in the design of vehicles are of greatest interest. Numerical simulations of the railway vehicle running behaviour, which allows the calculation of dynamical quantities in the time and frequency domain based on the mathematical models of the vehicle and track, are developed in that purpose.

In the field of the railway vehicle dynamics the simulations of the vehicle behaviour are used for:

- Design and development of the vehicle in all stages,
- Predict vehicle behaviour in various exploitation conditions,
- To determine compliance with the requirements of running security and safety of the vehicle,
- Analyse how modification in vehicles will affect on the dynamic behaviour of the vehicle
- Analysis of the vehicle behaviour in the cases when it's not possible to perform experimental investigation.

Taking into account that numerical models are used in all stages of the vehicle design and development, it is necessary to develop a methodology to assess how much we may rely on the results obtained from simulations.

The process which determines or perform evaluation of agreement of the experimental results with the results obtained by numerical simulation is called the process of model validation and verification.

Verification and validation was developed 1979 by the Society for Computer Simulation and it may be presented in the form of "Sargent Circle" [1], as it is shown in Figure 1.

The model validation is the process where is possible to determine the degree that a model is an accurate representation of the real system [2], [3].

The verification process is focused on the identification and elimination of errors in the development of mathematical and computer models [1].

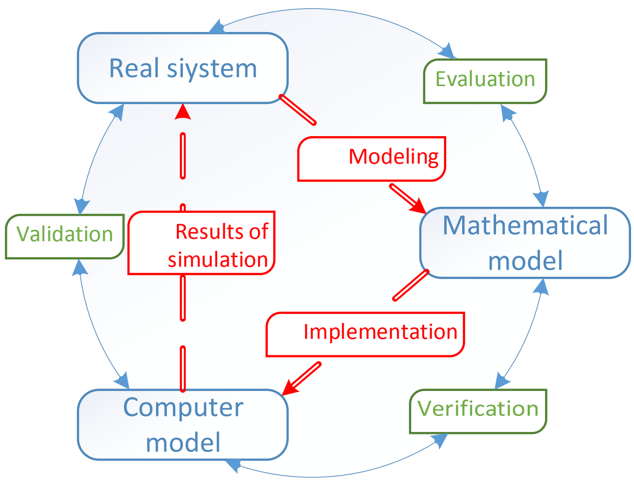

Figure 1. Graphical representation of the verification and validation process

The mathematical model comprises the conceptual model, mathematical equations, and modeling data needed to describe real system [1], [2], [3].

The computer model represents encapsulation of the mathematical model in the form suitable for execution on a computer [1].

The methodology for evaluation of the agreement between the results obtained by simulation and experimental investigation has not been defined in the field of the railway vehicle dynamics. The model validation, applied from different authors [4], [5], [6], [7], [8] was performed by comparing the characteristic parameters, such as accelerations in vertical and horizontal plane and forces in the wheel-rail contact, in time and/or frequency domain.

The model validation may be performed using five different approaches, as it is shown in Figure 2.

Graphical methods are based on the comparison of various graphs. The results of simulations are plotted

*Corresponding author: Dositejeva 19, 36000 Kraljevo, Serbia, e-mail: bogojevic.n@mfkv.kg.ac.rs

together with the results from experiments on the same graph. This method does not provide quantitative measure of matching between the results obtained by simulations and experiments. The model validation performed by this method is highly subjective and depends on the experience of the reviewer. In the field of railway vehicle dynamics, graphical comparison of different parameters is the most common method used for model validation.

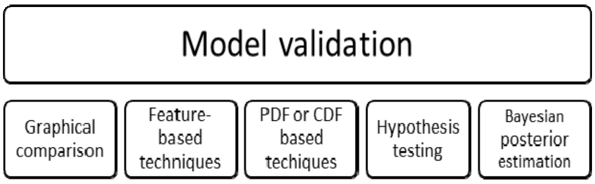

Figure 2. Model validation techniques

Feature-based techniques draw conclusions on the model validation based on the difference between characteristic features of the obtained results, such as magnitude, shape, phase, etc. Various metrics are used as a measure of the difference. One of the most known metrics is defined by Sprague and Geer [9], and it is based on the difference between magnitudes and phases of the results of simulations and experiments. The Russell metrics [10, 11] are very similar to the SG metric. EARTH metrics [12] take into account the shape of scalar series, which is not the case with SG and Russell metrics.

Model validation based on PDF (the probability density function) or CDF (the cumulative density function) techniques draw conclusions based on the difference between PDF or CDF functions of the obtained results. During the last fifty years, researchers have developed several validation metrics for comparison of PDF/CDF functions. The Kolmogorov-Smirnov metric [13] is one of the most used metrics for model validation. It measures the distance between two CDF functions along the ordinate axis. Anderson–Darling [14] validation metric is very similar to Kolmogorov-Smirnov metric. However, instead the distance along ordinate, Anderson–Darling metric has introduced the weighted quadratic CDF statistic to measure the distance between the two CDF functions. It was shown that the Anderson-Darling validation statistic had more power than the Kolmogorov-Smirnov metrics [13]. The third validation metrics – Area validation metrics is based on the calculation of the area between the two CDF functions [15]. The area metrics depend on the scale used to present the distributions, and any kind of normalization would destroy the meaning of the metrics [18].

This paper presents the model validation of the freight railway vehicle with three piece bogie "Motion Control M976 Truck System" of Amsted rail Co, by comparing CDF functions of the accelerations on the carbody floor, vertical and lateral forces in the wheel-rail contact.

2. THE MODEL OF THE VEHICLE WITH THREE PIECE BOGIE

Freight railway vehicle with three piece bogie consist of carbody for load transportation and two three piece bogies. Basic characteristics of the railway vehicle for iron ore transportation are given in Table 1.

Three piece bogie has relatively simple design. Basic parts of the bogie are two side frames (1) which are connected with bolster (2), as it is shown in Figure 2. The connection between carbody and bogie has been established over center plate. Side frames are connected to wheelset (7) over elastic adapters (6).

Table 1. Basic data for railway vehicle

Distance between center plates	6,744 m
Vehicle length	10,3 m
Vehicle height	3,64 m
Load	102 t
Weight of the empty vehicle	21,6 t
Weight of bogie	4650 kg
Distance between wheelset in the bogie	1,778 m
Wheel diameter	0,915 m
Maximal speed	70 km/h

The elastic connection between side frame and wheelset gives possibility of the wheelset to have a higher lateral movement's compared to conventional three piece bogie. This possibility for lateral motion of the wheelset gives better curving characteristics and possibility to increase the vehicle speed [8].

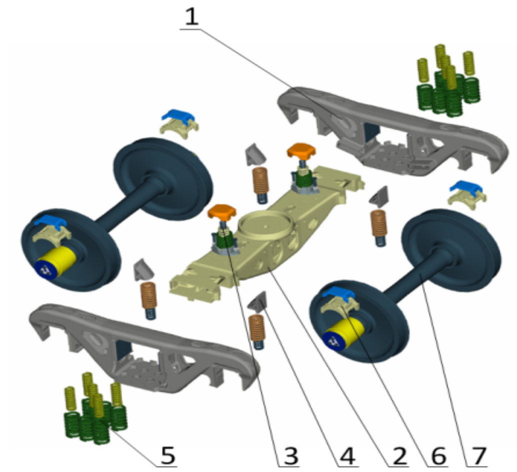

Figure 3. Three piece bogie "Motion control M975"- Amsted rail, 1 side frames, 2 bolster, 3 side bearers, 4-wedge, 5-suspension system, 6 elastic adapter, 7-wheelset

Despite the fact that the three-piece bogie is very simple, it is source of large number of the nonlinearity in the vehicle model. One of the main sources of the nonlinearity is suspension system which consists of the set of coil springs (5) that connect the side frames (1) and bolster (2) and second set of springs which connect the side frame (1) and wedge (4). The wedges in suspension system are sliding over bolster, from one side, and over side frame, from second side, as it is shown in Figure 3.

The connection between bolster and wedge has been described with one dimensional Saint Venant element, as it is shown in Figure 5 a), and connection between the wedge and the side frame has been described as two dimensional frictional Saint Venant element. The characteristics of Saint Venant element is possibility to introduce so called "stick-slip" movement into model.

The excitation in friction block, in Figure 4 marked as u, has harmonic characteristics, which arise from the model of the suspension system shown in Figure 3.Due to harmonic excitation, hysteresis loop has a characteristic shape, as it is shown in Figure 5 b [18].

Taking into account the mass of the side frame and bolster, the mass of the wedge in the model can be neglected.

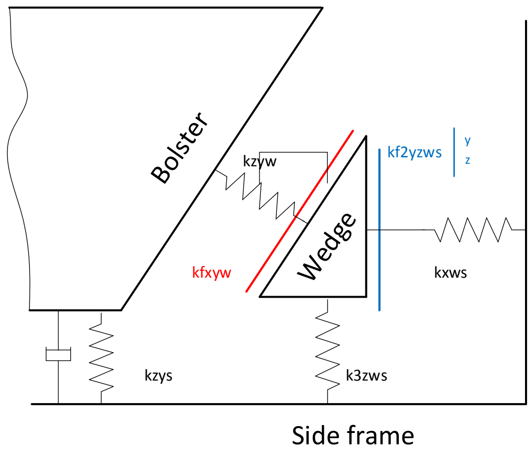

Figure 4. The suspension system model

The normal force which arises in the contact between bolster-wedge-side frames has been used for determination of the frictional force in Saint Venant element. The coefficient of friction, on the wedge sides cannot be exactly determined. Taking into account the excitation of the suspension system, the materials of the wedge, the bolster and the side frame, the value of the coefficient of friction has been estimated [7],[19].

The carbody has been connected to bogie over center plate and two side bearers, as it is shown in Figure 5.

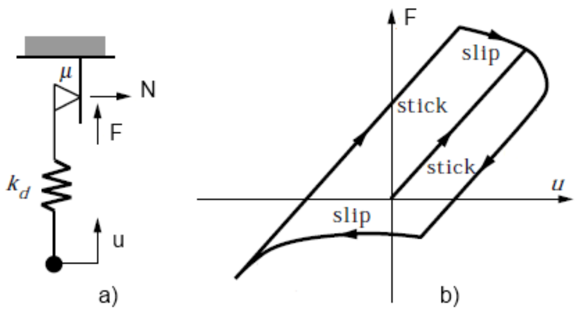

Figure 5. a) The model of the Saint Venant one dimensional friction block, b) Hysteresis loop

The side bearers are in constant contact with carbody, which continuously provide the friction force in longitudinal direction. The central plate provides the connection between the carbody and the bolster in vertical direction with possibility of rotation in yaw and sway direction. Due to carbody rotation around vertical axes, the frictional force arises in the side bearers, which is leading to better running stability of vehicle. In the case of the empty wagon, the side bearers are loaded with 80% of the carbody weight, and the rest of the weight is carried by the central plate. In the case of the loaded wagon, the central plate is loaded with 90% of the vertical load, while 10% is carried by the side bearers.

The model assumptions can be summarized as follows:

- Car body, bolster, side frames and wheels are modelled as rigid bodies,
- Side bearers have always contact with car body,
- Wedges are massless elements,
- Contact between the bolster and the wedge is a one dimensional friction block,
- Contact between wedge and side frame is a two dimensional friction block – in lateral and vertical direction,
- Adapter is modelled as rubber element with high stiffness in vertical direction,
- Clearances between elements are implemented in the model (bolster-side frame, axle-side frame, etc).

The model of the vehicle is developed in software package "Gensys".

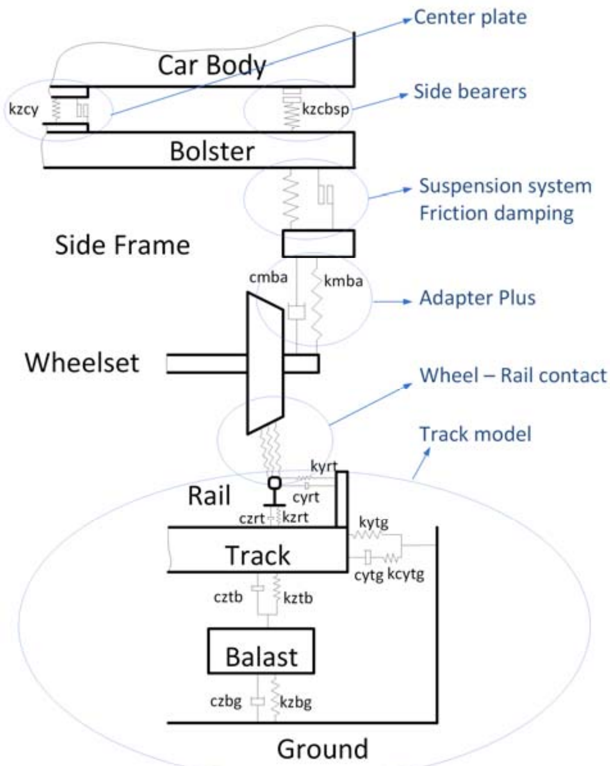

Figure 6. The model of the rail vehicle with three piece bogie

2.1. Railway track

The model shown in Figure 6 takes into account vertical and horizontal stiffness of the track. By variation of the characteristics of the springs and the dampers in the model, tracks with wooden and concrete sleepers may be modelled, as well as different track stiffness, for example track stiffness during summer and winter ambient conditions [8].

Since the wheelsets are exposed to increased load of 32t, wheel profiles WP4 especially optimized for high-load and reduced wear, were developed.

During the vehicle negotiating the curve, due to centrifugal forces on the outside wheel, increased vertical and lateral forces arise. For this purpose, in the curves with small radius, outside rails have the optimized MB1 profile. On inner rail in the curve and on tangent tract rails have BV50 profile with inclination 1:30.

The MB1 profile on outside rail leads to decreasing of the wheel sliding over rail head and decreasing of the forces on outside wheel, which leads to decreasing of the wear of the wheels and rails in the curves.

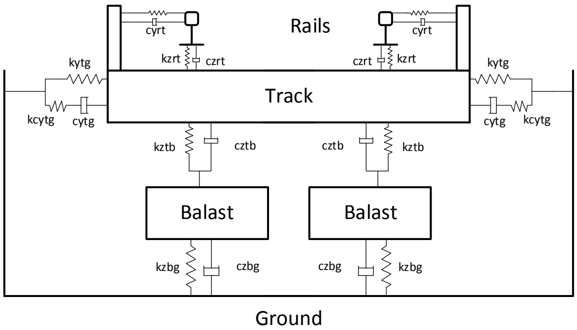

Figure 7. The model of the track

The wheel-rail contact has been described by Kalker nonlinear theory [20] using kpfr functions in the software package „Gensys". For measured profiles of the wheel and the rails, the equivalent conicity has been calculated.

Track geometry as well as track irregularities, such as longitudinal level, cant irregularity and gauge irregularity, have been recorded with measurement vehicle and introduced as excitation in vehicle dynamic simulations.

3. THE EXPERIMENTAL INVESTIGATION OF DYNAMIC BEHAVIOUR OF VEHICLE

Experimental investigations of the railway vehicle have been performed on commercial track, in north part of Sweden, between city Kiruna and port Luleå.

Experimental investigations have been performed during summer period with sunny days, on the dry track. On the basis of the weather conditions the value of 0,4 of the friction coefficient in the wheel-rail contact has been assumed. The coefficient of friction in the wheel-rail contact may have big influence in the calculation of the forces.

Measured gauge variations on the track parts chosen for model validation were ±3 mm. In simulations of empty and loaded vehicle the standard track gauge of 1435 mm has been assumed.

For simulation of the dynamic behaviour of the railway vehicle is assumed that vehicle is running with constant speed. The value of the vehicle speed has been calculated as the average value of real speed on each track part. The variations of the real speed was in the range of ± 0,4 km/h.

The accelerations in vertical and lateral directions have been measured with B12/200 inductive sensors. Measurement of the forces in wheel-rail contact has been performed with instrumented wheelset.

In the experimental investigation of the rail vehicle the following parameters have been measured:

- Accelerations above leading bogie, on the carbody floor, in vertical and horizontal plane,
- Accelerations in the middle of the carbody floor, in vertical and horizontal plane,
- Accelerations on side frame on leading bogie, in vertical direction,
- Vertical and lateral forces on wheels measured whit instrumented wheelset.

The instrumented wheelsets, produced by Interfleet, Stockholm, Sweden, have been installed on leading bogie.

In this paper, for model validation, the following parameters have been compared:

- Accelerations above leading bogie, on the carbody floor, in vertical and horizontal plane,
- The forces in the wheel-rail contact on leading wheelset in leading bogie, in horizontal and lateral directions.

4. VALIDATION METRICS

Model validation and verification are important steps in the process of the model developing. The selection of appropriate validation metrics is essential step in order to get an answer on the question "How good my model represent a real system?". The well-known Kolmogorov-Smirnov metric and Area validation metric were been used for validation of the model of rail vehicle. Both validation metrics are based on comparison of the cumulative distribution functions (in future text denoted with CDF).

4.1. Kolmogorov – Smirnov test

The two- dimensional Kolmogorov-Smirnov test is nonparametric test for equality of probability distribution functions. The maximal vertical distance between two CDF function is well known Kolmogorov-Smirnov metric. This metric mathematically may be expressed as following:

$$d_{ks} = sup\left|F_{1,n}(x) - F_{2,n'}(x)\right| \quad (1)$$

where $F_{1,n}$ and $F_{2,n}$ are two CDF from the signals obtained from simulation and from experiment which are compared.

Obtained K-S statistics is future is used for hypothesis testing where the null hypothesis is rejected at significance level α if a probability p has value which is greater than critical value.

The hypothesis are defined as following:

H_0: the data in vectors x1 and x2 are from the same continuous distribution

*H_1: the data in vectors x1 and x2 are **not** from the same continuous distribution*

The decision to reject the null hypothesis, in this paper, is based on comparing the p-value with the significance level α, not by comparing the test statistic with a critical value.

The statistics defined in this manner does not describe the common underling distribution. Statistic only tests does two data sample have same distribution.

The Kolmogorov–Smirnov test can be modified to serve as a goodness of fit test. In the special case of testing for normality of the distribution, samples are standardized and compared with a standard normal distribution [16].

4.2. Area validation metrics

Area validation metrics measure the difference between area of CDF of the simulation an experimental CDF. Mathematically, the area between two curves is the integral of the absolute value of the difference between CDF's:

$$d_{av} = \int_{-\infty}^{\infty} \left|F_{1,n}(x) - F_{2,n'}(x)\right| dx \quad (3)$$

or, in the case of the discrete functions area validation metrics may be expressed as:

$$d_{av} = \sum_{x=1}^{\infty} \left| F_{1,n}(x) - F_{2,n'}(x) \right| \quad (4)$$

Area validation metrics is a function of the shape of the distribution, but it is not readily interoperable as function of underlying random variable [15].

Figure 8 illustrates the area validation metrics as the mismatch between two CDF functions, where the difference has been denoted with gray colour. More about the area validation metrics may be found in literature [15].

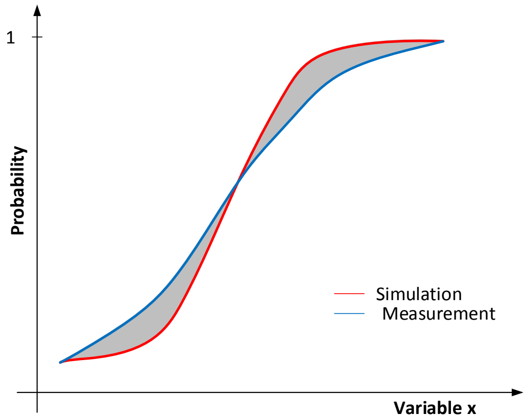

Figure 8. Example of the area validation metrics

5. RESULTS

The simulations of the vehicle behaviour have been performed for the vehicle running in the curves with radius from 670 m. The track profiles, curve radii, curve cant and track irregularities were measured and used as the input data for simulations. The length of the sections for estimation of the vehicle behaviour was chosen to be 250 m.

Described metrics was applied for comparison of following parameters:

- Acceleration of carbody in lateral direction
- Acceleration on carbody in vertical direction
- Vertical force on outer wheel on leading direction
- Lateral force on outer wheel on leading wheelset

All signals, from simulation and from measurement, are filtered according to UIC recommendations [17]. On the basis of the signals in time domain the corresponding CDF functions are calculated and described metrics was used for model validation.

5.1. Acceleration of carbody in lateral direction

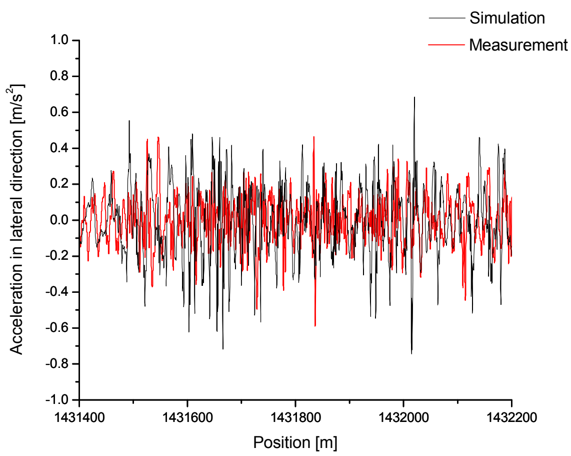

Figure 9. Acceleration of carbody in lateral direction – time domain

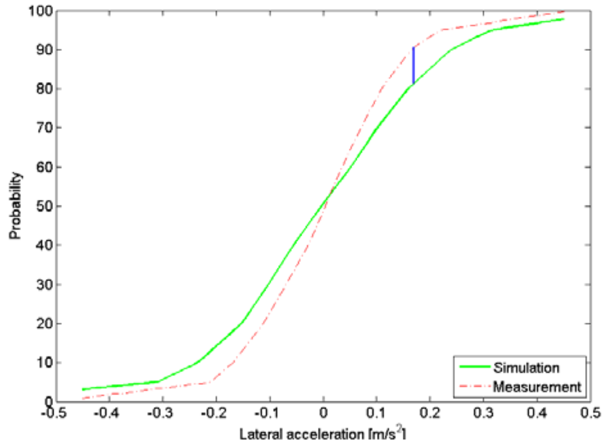

Figure 10. CDF function of simulation and measurement of lateral acceleration from simulation and experiment

The following results are achieved:

Metrics	Value
K-S metric	9.213
Area validation metrics	9.591

The CDF functions for lateral accelerations of the carbody obtained from simulation and experiment are described with 93 points (Figure 10). For two-tailed K-S hypothesis test, for significance level α=5% the probability value *p=0.2123* which leads that null hypothesis is accepted. This mean that results from simulation and results obtained from experiment has the same distribution.

5.2. Acceleration of carbody in vertical direction

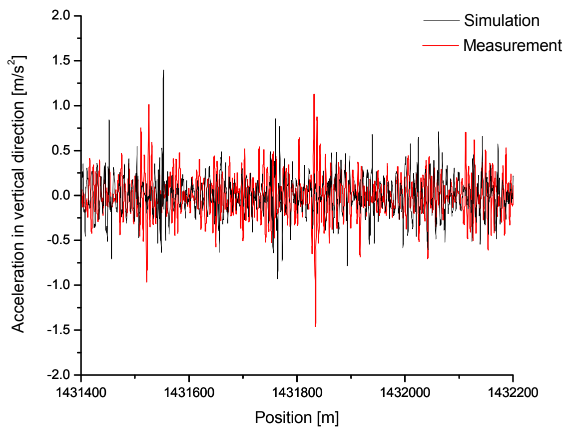

Figure 11. Acceleration of carbody in vertical direction – time domain

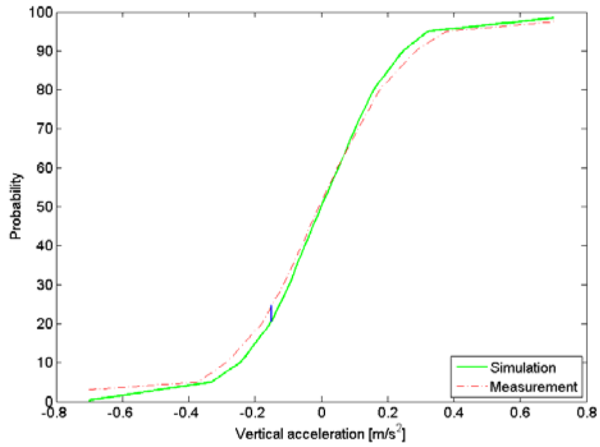

Figure 12. CDF function of simulation and measurement of vertical acceleration from simulation and experiment

Metrics	Value
K-S metric	3.9778
Area validation metrics	15.4271

The CDF functions for lateral accelerations of the carbody obtained from simulation and experiment are described with 141 points (Figure 12). For two-tailed K-S hypothesis test, for significance level α=5% the probability value *p=0.0579* which lead that null hypothesis is accepted. This mean that results from simulation and results obtained from experiment has the same distribution.

5.3. Lateral force on outer wheel

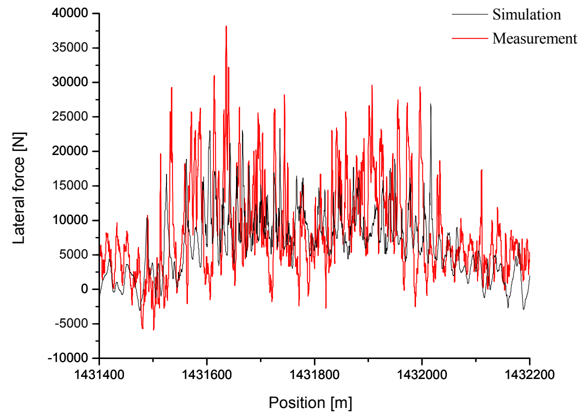

Figure 13. Lateral force on outer wheel – time domain

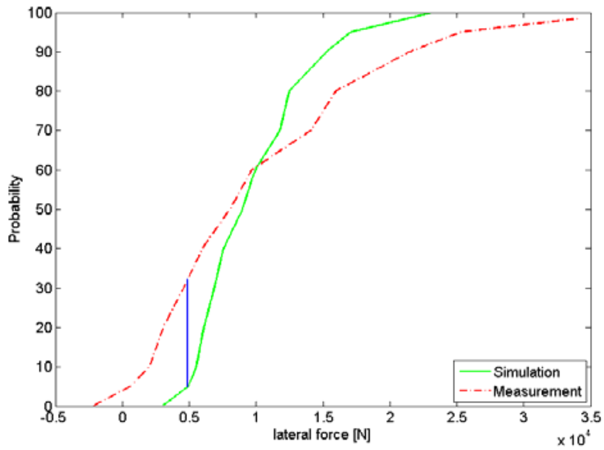

Figure 14. CDF function of simulation and measurement of lateral force on the outer wheel from simulation and experiment

Metrics	Value
K-S metric	27.3424
Area validation metrics	1.4188x10^6

The CDF functions for lateral accelerations of the carbody obtained from simulation and experiment are described with 391 points (Figure 14). For two-tailed K-S hypothesis test, for significance level α=5% the probability value *p=0.2361* which lead that null hypothesis is accepted. This mean that results from simulation and results obtained from experiment has the same distribution.

5.4. Vertical force on outer wheel

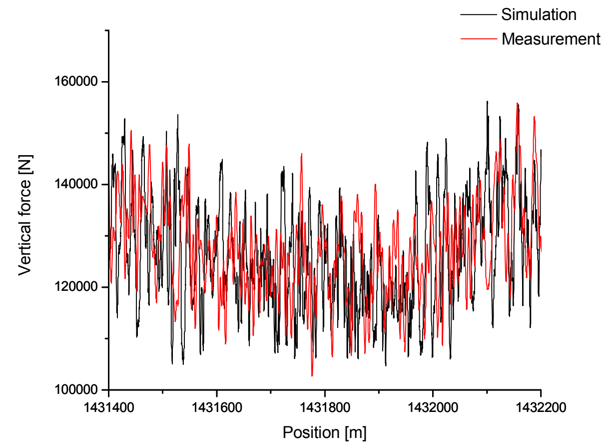

Figure 15. Vertical force on outer wheel – time domain

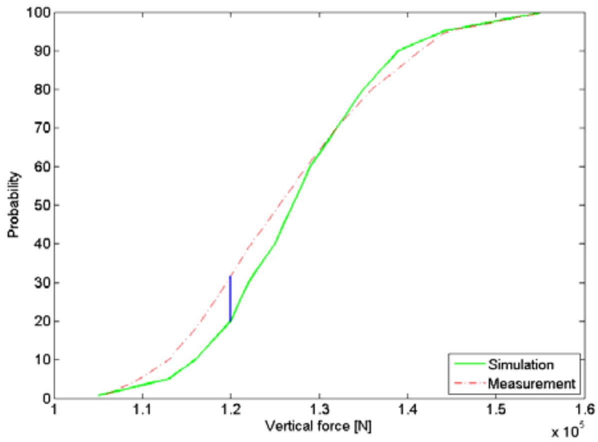

Figure 16. CDF function of simulation and measurement of vertical force on outer wheel from simulation and experiment

Metrics	Value
K-S metric	11.3501
Area validation metrics	1.37×10^5

The CDF functions for lateral accelerations of the carbody obtained from simulation and experiment are described with 56 points (Figure 10). For two-tailed K-S hypothesis test, for significance level α=5% the probability value *p=0.9649* which lead that null hypothesis is accepted. This mean that results from simulation and results obtained from experiment has the same distribution.

6. CONCLUSION

The model validation has very important part in the model building and prediction of the behaviour of the mechanical systems. The nonlinear model of the freight rail vehicle where the real track condition and vehicle speed that are used as inputs for simulation of the vehicle behaviour, has been presented in this paper.

The Kolmogorov-Smirnov metric, Area validation metric and Hypothesis testing based on Kolmogorov-Smirnov metric, has been chosen for model validation.

The Kolmogorov-Smirnov metric show the maximum distance in vertical direction between two CDF functions. The limits for acceptance of the model has not clear or does not exist. For each of the considered parameters the limit for acceptance should be separately defined, which will make the process of validation more complicated.

The area validation metric is based on the difference of the area between two CDF's. The same conclusion as for the KS metric may be applied in this case. The limits, which will clearly define the acceptable model, do not exist.

From three presented metrics, the clearest conclusion about model acceptance may be drawn from hypothesis testing based on Kolmogorov-Smirnov metric. However, hypothesis testing does not give the answer how similar are two CDF function – two compared signals.

Overall, all three presented metrics do not give clear answer for validation of the presented model. The probability values – *p values* from hypothesis testing looks promising and good starting point for development of new validation metrics for validation of the model of rail vehicles.

ACKNOWLEDGMENT

The authors wish to express their gratitude to Serbian Ministry of Education and Science for support through project TR37020 and TR37005.

REFERENCES

[1] Oberkampf, W. L., Trucano, T. G., and Hirsch, C. "Verification, Validation, and Predictive Capability in Computational Engineering and Physics," Appl. Mech. Rev., 57(3), pp. 345–384, (2004)

[2] Sornette, D., Davis, A. B., Ide, K., Vixie, K. R., Pisarenko, V., and Kamm, J. R., "Algorithm for Model Validation: Theory and Applications," Proc. Natl. Acad. Sci. U.S.A., 104(16), pp. 6562–6567, (2007)

[3] Ben H. Thacker, Scott W. Doebling, Francois M. Hemez, Mark C. Anderson, Jason E. Pepin, Edward A. Rodrigez, „Concepts of model verification and validation", Los Alamos National Laboratory, Los Alamos, (2004)

[4] S.D. Iwnicki, A.H. Wickens, Validation of a MATLAB Railway Vehicle Simulation Using a Scale Roller Rig, Vehicle System Dynamics, Volume: 30, Issue: 3, Publisher: Citeseer, Pages: 257–270, ISSN: 00423114, DOI:10.1080/00423119808969451, (1998)

[5] Pelle Carlbom, Carbody and Passengers in Rail Vehicle Dynamics, Doctoral Thesys, TRITA - FKT 2000:48, ISSN 1103 - 470X, ISRN KTH/FKT/D--00/48--SE

[6] J.R. Evans & P.J. Rogers "Validation of dynamic simulations of rail vehicles with friction damped y25 bogies", Vehicle System Dynamics: International Journal of Vehicle Mechanics and Mobility, 29:S1, 219-233, http://dx.doi.org/10.1080/00423119808969561, (1998)

[7] Jönsson P-A, Persson I and Stichel S: New Simulation Model for Freight Wagons with UIC Link Suspension. Vehicle System Dynamics, Volume 46, Supplement, pp 695- 704, (2008).

[8] N. Bogojević, P.A. Jonnson and S. Stichel, "Iron Ore Transportation Wagon with Three-Piece Bogies –

Simulation Model and Validation", Proceedings of VII International Conference "Heavy Machinery HM 2011", Vrnjačka Banja (Serbia), 29 June-2 July 2011, pp. 33-38, (2011)

[9] Sprague, M. A., and Geers, T. L., "A Spectral-Element Method for Modelling Cavitation in Transient Fluid-Structure Interaction," Int. J. Numer. Methods Eng., 15, pp. 2467–2499, (2004)

[10] Russell, D. M., "Error Measures for Comparing Transient Data: Part I, Development of a Comprehensive Error Measure," Proceedings of the 68th Shock and Vibration Symposium, Hunt Valley, MD, (1997)

[11] Russell, D. M., "Error Measures for Comparing Transient Data: Part II, Error Measures Case Study," Proceedings of the 68th Shock and Vibration Symposium, Hunt Valley, MD,(1997)

[12] H. Sarin, M. Kokkolaras, G. Hulbert, P. Papalambros, S. Barbat and R.J. Yang, "A comprehensive metric for comparing time histories in validation of simulation models on emphasis on vehicle safety applications", Proceedings of the ASME 2008 International Design Engineering Technical Conference and Computers and Information in Engineering Conference, (2009)

[13] A. Kolmogoroff, "Confindence limits for an unknown distribution function", Ann. Mathh. Statist. 12 461-463, (1941)

[14] Anderson, T. W.; Darling, D. A. "Asymptotic theory of certain "goodness-of-fit" criteria based on stochastic processes". Annals of Mathematical Statistics 23: 193–212. doi:10.1214/aoms/1177729437, (1952).

[15] Scott Ferson, William L. Oberkampf, Lev Ginzburg, "Model validation and predictive capability for the thermal challenge problem", Comput. Methods Appl. Mech. Engrg. 197 2408-2430, (2008)

[16] http://www.princeton.edu/~achaney/tmve/wiki100k/docs/Kolmogorov-Smirnov_test.html

[17] UIC testing and approval of railway vehicles from the point of view of their dynamic behaviour –safety- Track fatigue – Ride quality, Code 518 OR, 4th edition, Paris, (October 2009).

[18] B. D. Yang, M. L. Chu And C. H. Menq, Stick–slip–separation analysis and non-linear stiffness and damping characterization of friction contacts having variable normal load, Journal of Sound and Vibration 210 (4), 461-481, (1998).

[19] A. Orlova & Yu. Romen "Refining the wedge friction damper of threepiece freight bogies", Vehicle System Dynamics: International Journal of Vehicle Mechanics and Mobility, 46:S1, 445-455, (2008).

[20] J.J. Kalker, Wheel-rail rolling contact theory, Wear, Volume 144, Issues 1–2, Pages 243-261, ISSN 0043-1648, http://dx.doi.org/10.1016/0043-1648(91)90018-P, (1991)

Functions of Wheel-rail Contact Geometry

Milan Bižić[1*], Dragan Petrović[1], Isidora Pančić[2]
[1]Faculty of Mechanical and Civil Engineering in Kraljevo, University of Kragujevac, Kraljevo (Serbia)
[2]Faculty of Civil Engineering, University of Belgrade, Belgrade (Serbia)

The running of railway vehicles is based on the interaction of wheelset-track or wheel-rail with precisely defined nominal geometries. In this way, the geometric relationships which allowing smooth running in tangent and curved track are achieved. However, geometries in practice deviate from nominal to a greater or lesser extent. This cause the constant change of geometric relationships between wheels and rails and all dynamic parameters of railway vehicles during the running. For this reason, the modelling of wheel-rail contact geometry is very important task in rail vehicle dynamics. This paper gives a systematic approach to the analysis of wheelset-track and wheel-rail contact geometry. After introducing the parameters of wheelset and track geometry, the non-linear geometric relationships between wheel and rail profiles are analysed, and parameters of wheel-rail contact geometry are defined. In final stage, the functions which combines all analysed parameters are derived. A special discussion about the equivalent conicity as the most important function of wheel-rail contact geometry is given. The methods of its determination and influence on the dynamic behaviour of wheelset and vehicles are discussed. Considerations in the paper confirm the fact that wheel-rail contact geometry and equivalent conicty as function which representing it, play one of the most important role in dynamic behaviour of railway vehicles.

Keywords: Functions, Wheel-rail contact, Geometry, Equivalent conicity, Dynamic behaviour, Railway vehicles

1. INTRODUCTION

Analysis of dynamic behaviour of railway vehicles are primarily related to the wheelset-track and wheel-rail interaction. In that sense, one of the most important task is modelling the geometrical relations between wheelset and track, and wheel and rail [1–3]. Many studies have shown that the wheel-rail contact geometry has a great influence on the quality of dynamic behaviour of railway vehicles. In the first instance, the contact geometry has significant influence on the wheel-rail surface stress distribution [4]. In this way, it affects the most important dynamic parameters of vehicle-track interaction – wheel-rail contact forces [5]. Accordingly, the contact geometry has significant influence on the ride comfort and running stability of railway vehicles [6, 7]. Many researches have shown that wheel-rail contact geometry play an important role in wheel-rail wear [8]. It is very important to note that many of these studies take into account only nominal contact geometry which is considered as constant. Given in mind that the contact geometry in practice more or less deviates from the nominal one, its importance in dynamic analysis of railway vehicles is even more pronounced [9]. Based on this considerations it can be concluded that the analysis and modelling of geometry of wheel-rail contact has very large importance in rail vehicle dynamics. Since the geometries of wheel and rail profiles are non-linear, the problem is how to describe wheel-rail contact geometry during the running of railway vehicles [10]. In that sense, the task of this paper is systematic analysis of wheelset-track and wheel-rail contact geometry. This should result in obtaining of the parameters of wheel-rail contact geometry, and in final stage, to the functions which combines all analyzed parameters.

2. PARAMETERS OF TRACK GEOMETRY

It is very important to distinguish between nominal and real track geometry (track geometry in exploitation). Nominal track geometry is defined by the international standards or standards of individual Railways which must be strictly observed during the design and construction of tracks. Each newly built track meets the prescribed nominal geometry within a certain allowable tolerances. However, after a certain period of exploitation due to the different influences (primarily wheel-rail contact forces) the nominal geometry is degraded.

2.1. Nominal track geometry

The nominal track geometry is determined by the two groups of parameters – parameters of the cross-section and parameters of the line. The parameters of the cross-section are: track gauge, inclination, and cant.

The first and the most important parameter of the cross-section and the overall track geometry, is the track gauge G. It is measured 14 mm below the track plane, which is obtained by the connecting the upper points on the left and right rail (Fig. 1).

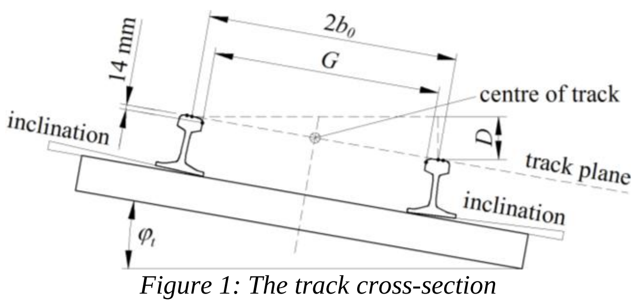

Figure 1: The track cross-section

Another very important parameter of the cross-section is rail inclination. As shown in Fig. 1, the rails are placed on the sleepers with a certain inclination towards the centre of the track. In combination with the wheel profile, this solution enables better transfer of load on the sleepers and ballast, as well as more uniform wear of wheel and rail contact surfaces. The third parameter of the cross-section is cant of outer rail in curve. If cant is marked with D, cant angle with φ_t, and distance between the nominal contact points with $2b_0$ (Fig. 1), they satisfy

*Corresponding author: Dositejeva 19, 36000 Kraljevo, Serbia, bizic.m@mfkv.kg.ac.rs; bizic.milan@gmail.com

the following relation:

$$\sin \varphi_t = D / 2b_0 \tag{1}$$

The parameters of the line are: radius of circular curve, length and shape of transition curve, longitudinal gradient, and radius of vertical curve. The line can be defined as three-dimensional longitudinal axis of track with characteristic changing of coordinates in space.

The first and the most important parameter of the line is radius of circular curve *R*. The main characteristic of horizontal circular curve is that its radius and cant have the constant values. The basic tendency in the track design is to avoid curves with small radius. It causes many harmful effects on wheel-rail contact forces, running safety, wear, energy consumption, cost-effectiveness, etc.

The second parameter of the line is length and shape of transition curve which may have linear or parabolic change of cant from zero to the value of cant in circular curve. The radius of the transition curve is changing continuously between the tangent track and circular curve. The changes of cant and radius in transition curve have the same start and end position.

The third parameter of the line is longitudinal gradient which is limited due to the characteristics of traction and braking. During the running on the uphill, there are increased wear of traction vehicles and energy consumption. On the other hand, during the running on the downhill, there are intensive wear of braking elements and thermal problems.

The last, fourth parameter of the line is radius of vertical curve which connects the ends of the track in transition from one longitudinal gradient to another. While vehicles passing across the connections there are intensive accelerations and wheel-rail contact forces, which is very unfavourable for ride comfort and running stability. The radius of vertical curve is limited in according to the maximal operating speed on given railway line and maximal vertical acceleration during the passing across connections.

2.2. Real track geometry

It is very important to note that the term "track geometry" always means the actual geometry or real track geometry in the exploitation. For proper evaluation of the track condition and analysis of dynamic behaviour of railway vehicles is very important to knowing the real track geometry. It is determined by measurement of deviations from the nominal geometry using specially equipped vehicles which is defined by the international standards EN13848. The parameters (deviations) which are measured are given in Table 1.

Table 1: The deviations from the nominal track geometry

Parameter	Remark
Deviations in longitudinal direction in vertical plane	Mean value of vertical deviations of left and right rails
Deviations in lateral direction in horizontal plane	Mean value of lateral deviations of left and right rails
Deviations of track gauge	Deviations from nominal track gauge
Deviations of cant	Deviations from nominal cant of outer rail in curve
Twist	Difference of cant between two cross section of track divided by certain distance

The track condition must be monitored in order to ensure timely response in case of exceeding the allowable values of deviations from the nominal geometry. The most of Railways classify their tracks just in accordance with these deviations. According to the international standards UIC 518 and EN14363, in terms of criteria of maintenance and eligibility for testing of railway vehicles, there are three classes of track quality [11, 12]:

- QN1: Require monitoring of condition of track or taking maintenance within regularly planned maintenance operations
- QN2: Require short term maintenance operations
- QN3: If it is exceeded, require exclusion of observed sections from acceptance analysis because track quality is not representative of usual quality standards

2.3. Rail profile

The rail profile has significant influence on the dynamic of railway vehicles. On the most European rail lines, the UIC 60 rail is used (Fig. 2).

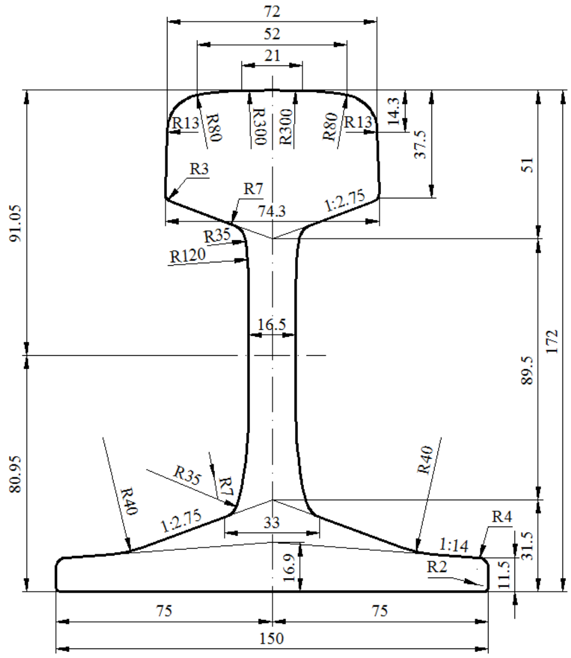

Figure 2: The cross-section of rail UIC 60

Depending on the permissible axle load and operating speed, the rails UIC 54, UIC 49, UIC 45, etc., are also used. During the exploitation, a very intense interaction with wheels leads to the wear of rail profile which can be uniform and non-uniform. The uniform wear implies that rail is worn over entire length, while non-uniform wear implies that rail has discrete damages at certain places. The most intensive uniform wear appears in curves where the highest values of wheel-rail contact forces is present. The typical worn profiles of outer and inner rail in curve is shown in Fig. 3.

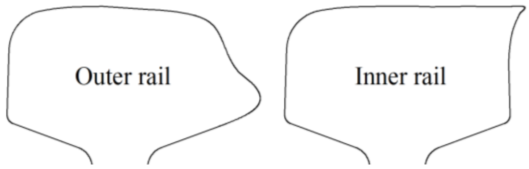

Figure 3: The typical worn profiles of rails in curve

For evaluation of track condition and precise dynamic analysis is very important to determine the real rail profile. This is usually done using the special measuring devices – profile-meters. It is important to note that wear of the rail head leads to the increasing of track gauge. Non-uniform wear is caused by different factors. It is characterized by small damages or corrugations of the rail head surface which cause very unfavourable oscillations and noise during the passing of vehicles.

3. PARAMETERS OF WHEELSET GEOMETRY

As in the case of the track, it is very important to make difference between the nominal and real wheelset geometry (geometry of wheelset in exploitation). The international standards define nominal wheelset geometry and allowable tolerances which must be respected from all manufacturers. After a certain period of exploitation, intensive wheel-rail contact forces cause deviation from the nominal geometry. The parameters of the typical wheelset geometry are (Fig. 4):

- wheel radius (nominal rolling radius) r_0 (at normal track gauge r_0=300÷600 mm),
- distance between nominal rolling radii $2b_0$ (at normal track gauge $2b_0$=1500 mm),
- inner distance between wheels $2b_a$ (at normal track gauge $2b_a$=1360 mm),
- outer distance between flanges of wheels $2b_f$,
- distance between axle-boxes $2b_l$ (at normal track gauge $2b_l$=2000 mm),
- flange height h_f (at unworn wheels h_f=28 mm),
- flange thickness t_f (at unworn wheels t_f=32,5 mm).

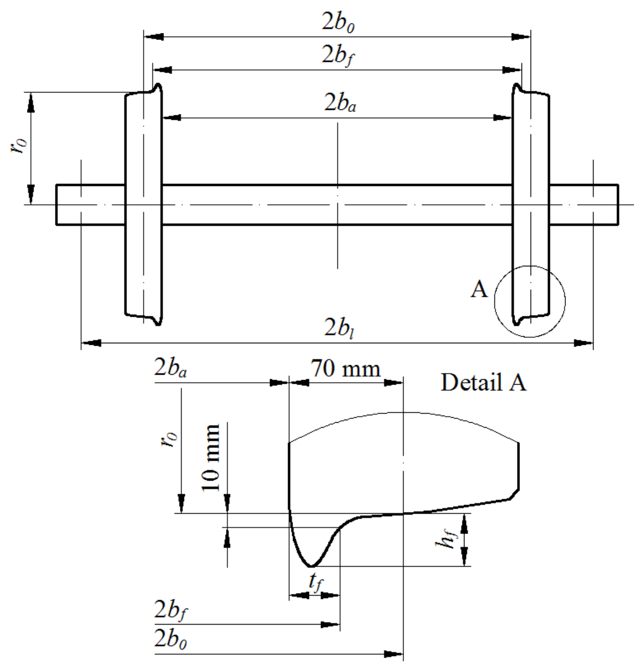

Figure 4: The parameters of wheelset geometry

During the running, the wheelset is exposed to a very intensive static, dynamic and thermal loads due to the interaction with the rail, braking, etc. This cause the wear whereby some of the mentioned parameters are changed. The most intensive wear is present on the wheel tread and flange, while the nominal wheel radius is decreased. The wheelset condition must be periodically observed during the exploitation with the aim to detect defects or exceeding the allowable values of deviations from the nominal geometry. Allowable values of wheelset and wheel wear are defined by the standard UIC510-2 [13].

3.1. Wheel profile

The wheel profile has a large influence on the ride comfort and running safety of railway vehicles. All wheel profiles have conical tread which provides steering of wheelset and passing through curves. One of the most used is profile S1002 which is shown in Fig. 5 [13].

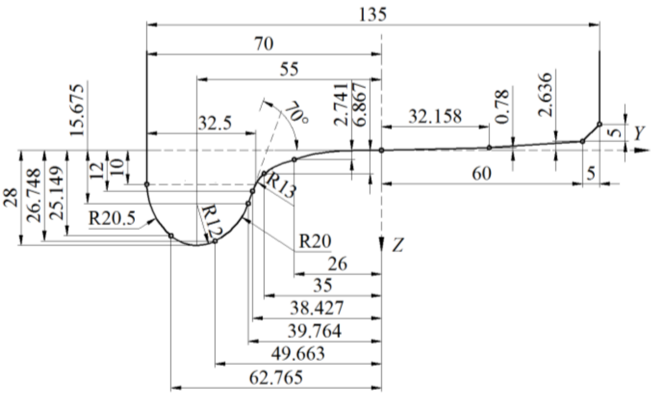

Figure 5: The nominal wheel profile S1002

It is very important to make difference between the new (unworn) and worn wheel profile. If the new wheel has a linear profile with straight cone, after certain period of exploitation it will be changed into the non-linear worn profile (uniform wear shown in Fig. 6.). After 100÷200 thousands of mileage each worn profile has typical shape independently from the type of starting new wheel profile [2]. Thus, in order to reduce wear and its influence on the dynamic behaviour of railway vehicles, new wheels have profiles that are adopted to wear (Fig. 6).

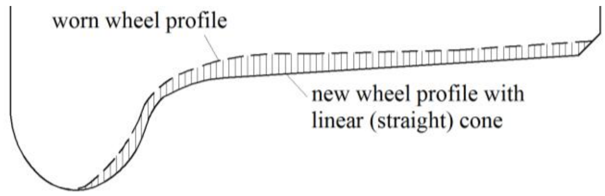

Figure 6: The uniform wear of wheel profile

In addition to the uniform, there is non-uniform wear which is consequence of different influences which cause the discrete damages (flats, dents, corrugations, peeling of material on the tread, damages of flange, eccentricity of wheel, etc). For precise dynamic analysis and evaluation of wheel condition is very important to determine the real wheel profile by special profile-meters.

4. PARAMETERS OF WHEEL-RAIL CONTACT GEOMETRY

The parameters of wheel-rail contact geometry are shape of the wheel profile, shape of the rail profile, and geometrical sizes which define their relative position (Fig. 7). Geometrical sizes that define relative position of wheel profile in relation to the rail profile are: track gauge G; rail inclination; inner distance between wheels $2b_a$; outer distance between flanges of wheels $2b_f$; and lateral clearance of wheelset on track Δb.

4.1. Track gauge

The track gauge has a large influence on the relative positions between wheel and rail profiles. Due to the wear, track gauge increases and in that way changing the boundaries of the possible lateral displacement of the wheelset on the track. It is important to note that track gauge changes along the line in an unpredictable and stochastic way. For more precise analysis of railway vehicles dynamic is very important to measure the real track gauge in function of longitudinal track position.

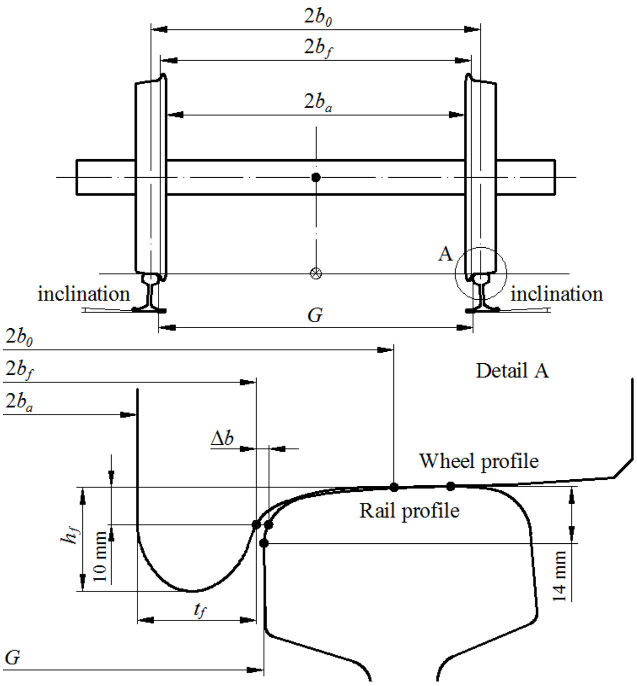

Figure 7: The parameters of wheel-rail contact geometry

4.2. Rail inclination

The rail inclination has an influence on the relative position between wheel and rail profiles only in the case of track with new rails which are placed exactly at certain transverse gradient (1:20, 1:40, etc.) relative to the reference horizontal plane, and which have new unworn profiles. If rails are in exploitation for a longer time, their nominal (initial) profile is degraded, so inclination has no influence on the relative position between wheel and rail profiles. For precise analysis is necessary to measure worn rail profile in relation to the some reference coordinate system. In this way the real inclination is taken into account via the rail profile and this parameter is redundant.

4.3. Inner distance between wheels

The inner distance between wheels directly affects the relative position of the wheel profile in relation to the rail profile. During the exploitation this parameter is less susceptible to changes due to the wear, but large deviations are possible due to the presence of eccentricity or similar damages of the wheel.

4.4. Outer distance between flanges of wheels

This parameter can be calculated based on the values of inner distance between wheels $2b_a$ and flange thickness of left and right wheel t_{fl} and t_{fr} as follows:

$$2b_f = 2b_a + t_{fl} + t_{fr} \tag{2}$$

Specially, if the flange thicknesses on the left and right wheel are identical then:

$$2b_f = 2b_a + 2t_f \tag{3}$$

Due to the wear, the flange thickness is decreased, so outer distance between flanges of wheels is also decreased. For a more precise dynamic analysis is very important to determine the real value of this parameter.

4.5. Lateral clearance of wheelset on track

When the wheelset is located in a central position on the track, between the wheel flange and rail head there is lateral clearance Δb which is measured 10 mm below the nominal rolling radius (Fig. 7). Within this clearance, wheelset can be moved from central position to the left and right side, until the wheel flanges come into contact with the rail heads. The value of Δb depends on the track gauge G and the outer distance between flanges of wheels $2b_f$. This value is in general case equal to the sum of lateral clearances of left and right wheel Δb_l and Δb_r:

$$\Delta b_l + \Delta b_r = G - 2b_f \tag{4}$$

Substitution the expression (2) in the previous expression (4) gives the value of total lateral clearance on the track in function of the flange thickness of left and right wheel, which generally do not have to be same:

$$\Delta b_l + \Delta b_r = G - 2b_a - t_{fl} - t_{fd} \tag{5}$$

At normal track gauge and unworn wheel and rail profiles, the total lateral clearance Δb=10 mm. Due to the wear, the lateral clearance is increased, so for exact dynamic analysis is very important to determine the real values of this parameter.

5. TYPES OF WHEEL-RAIL CONTACT

During the running, the constant change of parameters of geometry which define the relative position of wheel profile in relation to the rail profile causes that location of contact point between them is constantly changing. In reality, wheel-rail contact is realized over a certain area which usually has the shape of ellipse. So, in further considerations when is used the term "contact point", it refers to the contact area and point in its centre. The contact point position at any time during the running depends on the shapes of wheel and rail profiles, as well as their relative position. The two typical cases of wheel-rail contact are tread contact and flange contact (Fig. 8).

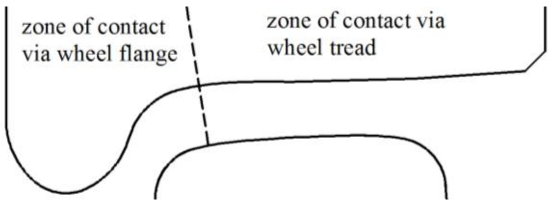

Figure 8: The typical zones of wheel-rail contact

5.1. Tread contact

The contact via the wheel tread is characteristic for running on tangent track or curves with higher radii. In this case, there is always one contact point, independently of the shapes of the wheel and rail profiles. If wheel and rail have worn profiles or profiles adopted to wear, contact point is continuously moving along the wheel and rail profiles, depending on the relative lateral displacement of wheel in relation to the rail. If the wheel and rail have other profiles (e.g. wheel profile with straight cone, etc.), contact point does not have to move continuously along the wheel and rail profiles, but can suddenly jump from one place to another. For wheel profiles S1002 and straight cone, in combination with the rail profile adopted to wear UIC60, the cases of tread contact are shown in Fig. 9.

It is very important to note that contact via the wheel tread belongs to the so-called non-conformal contacts. At these contacts, radii of curvature of wheel and rail profiles in contact points are more or less different, which cause that in very small contact areas there are very intensive loads. This is especially typical for the new profiles of the rails and wheels with straight cone.

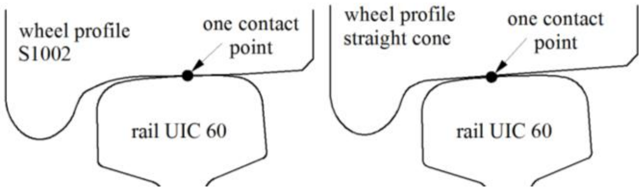

Figure 9: The tread contact in one point

5.2. Flange contact

Contact via the wheel flange is typical for running in sharp curves or in specific cases where there are larger deviations from the nominal track geometry. At contact via the wheel flange the following situations are possible: one contact point, two contact point, and conformal contact. If the wheel and rail have worn profiles or profiles adopted to wear, flange contact is realized via the one contact point, which is continuously moving along the wheel and rail profiles. On the other hand, if the wheel and rail have some other profiles (e.g. wheel profile with straight cone, etc.), flange contact can be realized via the one or two contact points, which can suddenly jump from one place to another. For wheel profiles S1002 and straight cone, in combination with the rail profile adopted to wear UIC60, the cases of flange contact are shown in Fig. 10.

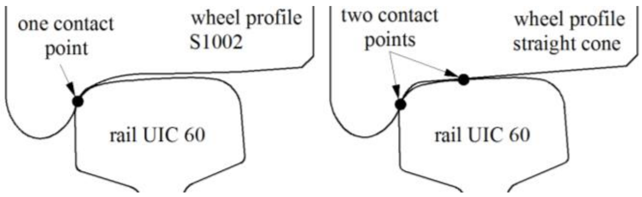

Figure 10: The flange contact in one and two points

The conformal contact exist when surfaces over which the wheel and rail are in touch are equal or very similar, or when the radii of curvature of wheel and rail profiles in contact point are equal or very similar. In such case the contact is realized via a larger contact area which is greater if the surfaces in touch are more conformal. The conformal contact is typical for transition between tread and flange, and worn wheel and rail profiles (Fig. 11).

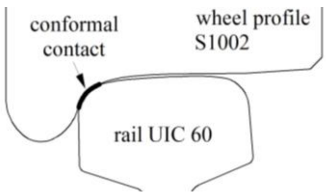

Figure 11: The conformal flange contact

6. FUNCTIONS OF WHEEL-RAIL CONTACT GEOMETRY

During the running, wheelset is moving in lateral direction in relation to the track centre line. The maximal lateral displacement Δy are limited by the wheel flanges contacts with rail heads. At a certain lateral displacement Δy, the mutual positions of wheels and rails profiles are changed, as well as the following geometric sizes in contact of left and right wheels and rails (Fig. 12): contact points positions; rolling radii in contact points on left and right wheel r_l and r_d; contact angles in contact points on left and right wheel γ_l and γ_d; and rotation angle of the wheelset around longitudinal axis of track (roll angle) φ.

In addition, the radii of touching surfaces are changed, which cause the changing the shape and size of contact areas. The changes of all mentioned geometric sizes are depend on the parameters of wheel-rail contact geometry and are expressed as a function of wheelset lateral displacement in relation to the track centre line Δy.

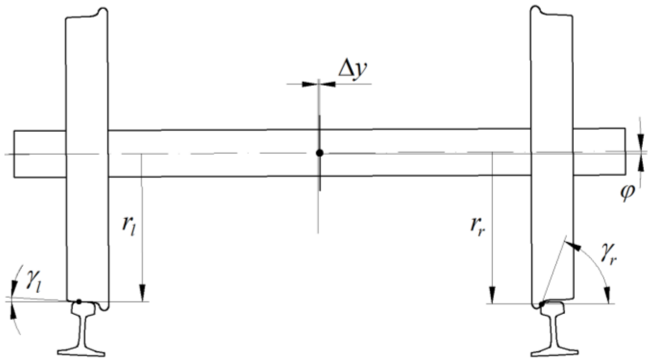

Figure 12: The geometric sizes in wheel-rail contact which are changed at lateral displacement of wheelset

Since in practice there are various combinations of parameters of wheel-rail contact geometry and profiles of wheels and rails, in order to easier characterization and analysis, the functions of wheel-rail contact geometry are introduced. Suppose that, in some point of time during the running, the wheel is moved laterally in relation to the rail for value Δy. At the same time, there is a raising of wheel for value Δz, increasing of rolling radius for value Δr, and changing of contact angle γ, as shown in Fig. 13. The changes of these three sizes in function of wheel lateral displacement are called wheel-rail contact geometry functions or contact functions [2]. The contact functions have strongly nonlinear character and are defined as:

$$\Delta r = f(\Delta y) \tag{6}$$

$$\Delta z = g(\Delta y) \tag{7}$$

$$\gamma = h(\Delta y) \tag{8}$$

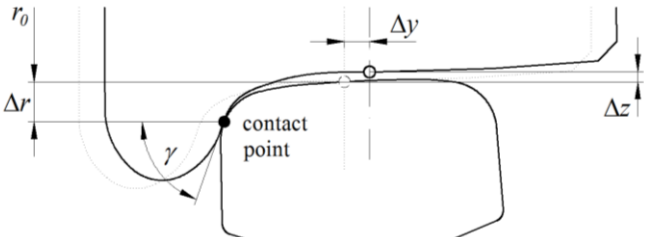

Figure 13: The wheel-rail contact geometry functions

In the expressions (6–8) f, g, and h are functions that depend on the parameters of wheel-rail contact geometry, especially the shapes of wheel and rail profiles. If contact point is continuously moving over the wheel profile, the contact functions are continuous. If contact point suddenly jumping from one place to another over the wheel profile, the contact functions have interruptions.

For practical characterization of wheel-rail contact geometry another function is used. It's about equivalent conicity which is determined for different combinations of wheel and rail profiles and different parameters of wheel-rail contact geometry.

6.1. Conicity

At the beginning of development of railways, the wheels had profiles with straight cone. The profile was linear, usually with cone 1:20, which was in correlation with the rail inclination, which was also 1:20. For modelling of such wheel-rail contact geometry, the simplified model shown in Fig. 14 is usually analysed. It is assumed that wheels have identical conical profiles which are rolling on the rails whose profiles are circular. Also it is assumed that there is no contact between the wheel flanges and rail heads. In this case, there is only one contact point between wheel and rail profiles.

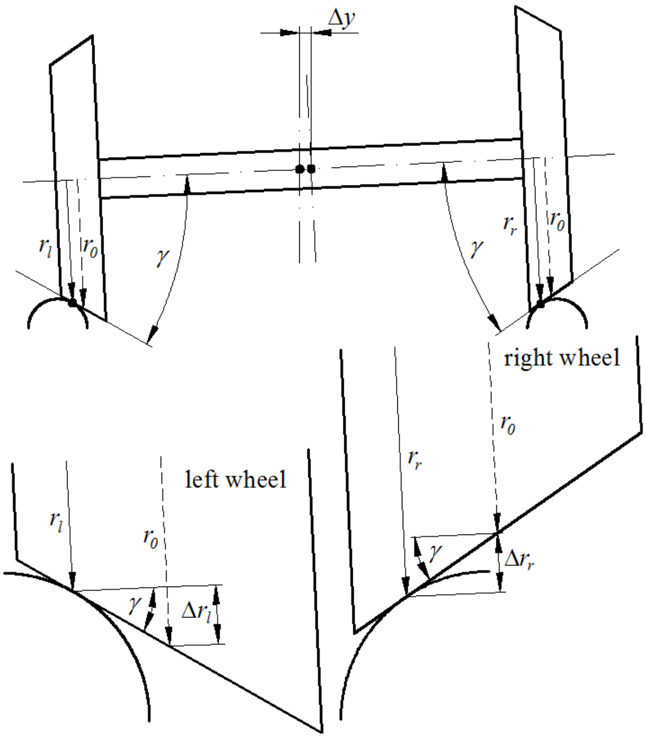

Figure 14: The wheel-rail contact geometry – wheel profile with straight cone and circular rail profile

When the wheelset is located in central position on the track, rolling radii of the left and right wheel are equal:

$$r_l = r_r = r \tag{9}$$

If the wheelset is moved laterally for value Δ*y*, the changes of rolling radii on the left and right wheel will be Δr_l and Δr_r, respectively. The total difference between rolling radii on the left and right wheel is:

$$\Delta r = \Delta r_l + \Delta r_r \tag{10}$$

Since the profiles of the wheels have linear shape and equal conicity, these two changes are equal:

$$\Delta r_l = \Delta r_r = \Delta r / 2 \tag{11}$$

The rolling radii of left and right wheel are:

$$r = r_0 - \Delta r_l \tag{12}$$

$$r = r_0 + \Delta r_r \tag{13}$$

Substituting the expression (11) in the previous expressions is obtained:

$$r_l = r_0 - \Delta r / 2 \tag{14}$$

$$r_r = r_0 + \Delta r / 2 \tag{15}$$

Therefore, the difference between the rolling radii of the left and the right wheel is:

$$\Delta r = r_r - r_l \tag{16}$$

Since at any given time the difference between the rolling radii depends on the lateral displacement of wheelset centre, it can be written:

$$\Delta r(y) = r_r(y) - r_l(y) \tag{17}$$

From Fig. 16 the following relation can be seen:

$$\tan\gamma = \frac{\Delta r_l}{y} = \frac{\Delta r_r}{\Delta y} \tag{18}$$

Substituting the expression (11) in the previous expression (18) is obtained:

$$\tan\gamma = \frac{\Delta r}{2}\frac{1}{\Delta y} \tag{19}$$

Based on that, function Δ*r* can be expressed as:

$$\Delta r = 2 \cdot \Delta y \cdot \tan\gamma \tag{20}$$

For small angles γ (as is the case with the wheel profile with straight cone 1:20) is $\tan\gamma \approx \gamma$, so the following relation is obtained:

$$\Delta r = 2 \cdot \Delta y \cdot \gamma(y) \tag{21}$$

In this way, the relation between lateral displacement of the wheelset Δ*y*, conicity γ, and rolling radii difference Δ*r*, is established through function (21). This function is, for wheelset with wheels profiles with straight cone, a linear function which describes wheel-rail contact geometry for any lateral position of wheelset on the track. The change of function (21) for bi-linear wheel profiles (two straight cones with different slopes, one in tread and one in flange zone) is shown in Fig. 15.

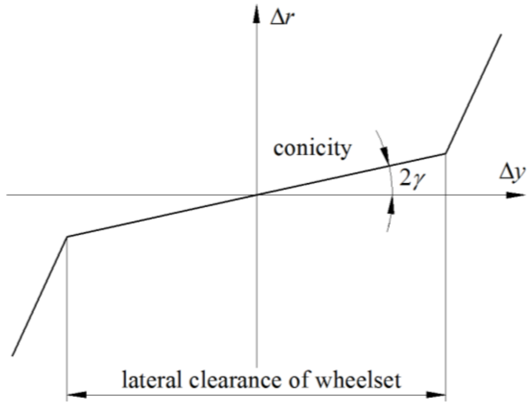

Figure 15: The change of rolling radius in function of wheelset lateral movement (wheels profiles with straight cone)

6.2. Equivalent conicity

In contrast to the wheels profiles with straight cone, in practice there are worn wheel profiles or profiles adopted to wear. These profiles are non-linear, so the previously exposed methodology based on constant conicity is not applicable for analysis and characterization of such wheel-rail contact geometry. In this case, the difference between rolling radii will not be the same as in the case of wheels with straight cone (Fig. 16).

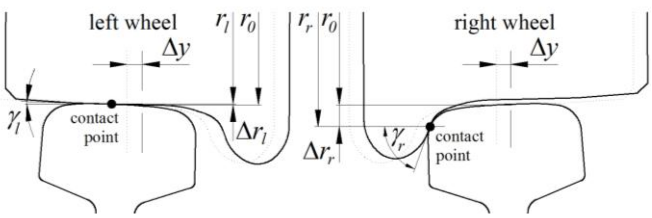

Figure 16: The wheel-rail contact geometry – worn wheel profile

For the case in Fig. 16, the difference between the rolling radii of the left and the right wheel is:

$$\Delta r = r_r - r_l \tag{22}$$

Wherein:

$$r_r = r_0 + \Delta r_r \tag{23}$$

$$r_l = r_0 - \Delta r_l \tag{24}$$

The difference between the rolling radii depends on the lateral displacement of wheelset, and based on that is:

$$\Delta r(y) = r_r(y) - r_l(y) \tag{25}$$

However, this function does not have a linear character, but is strictly a nonlinear function. In that sense, the key question is how to describe the geometry of the wheel-rail contact for non-linear worn wheel profiles. For this reason, and based on previous analysis of the conicity of wheels with straight cones expressed via the equation (21), the so-called equivalent conicity is introduced:

$$\lambda_e = \frac{\Delta r}{2 \cdot \Delta y} \tag{26}$$

Substituting the expression (22) in the previous expression is obtained:

$$\lambda_e = \frac{r_r - r_l}{2 \cdot \Delta y} \tag{27}$$

At the end, substituting the expression (23) and (24) in the previous expression (27) is obtained:

$$\lambda_e = \frac{\Delta r_r - \Delta r_l}{2 \cdot \Delta y} \tag{28}$$

The equivalent conicity λ_e for wheels with worn profiles has the same physical meaning as conicity γ for wheels with straight cones. Practically, it is linearization of nonlinear changes of rolling radii of wheels at a certain wheelset lateral displacement $\Delta y=\pm y'$ (Fig. 17).

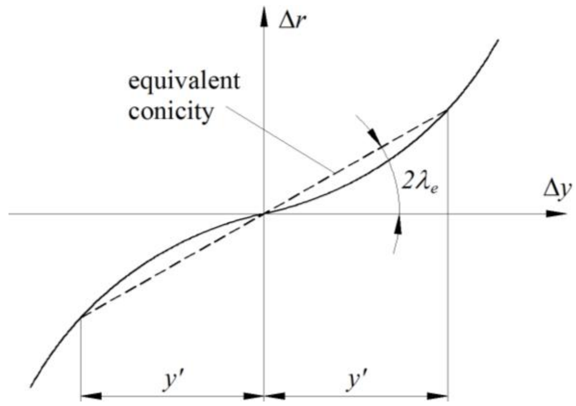

Figure 17: The change of rolling radius in function of wheelset lateral movement (worn wheel profile)

Equivalent conicity for the wheel profiles with straight cone is equal to the conicity $\lambda_e=\gamma$. It is very important to emphasize that due to the wear, all linear profiles with straight cone after a certain period of exploitation becomes worn and nonlinear. On the other hand, optimization from the aspects of wear and improving the dynamic behaviour of railway vehicles is leads to the optimal wheel profiles or profiles adopted to wear. Such profiles with nonlinear shape (Fig. 5) are today most used in production of new wheels and wheelsets. Based on this it can be concluded that for describing and analysing the wheel-rail contact geometry of most wheelsets and tracks in exploitation is necessary to use the equivalent conicity. The main parameters influencing the equivalent conicity are: wheel profile; rail profile; relative lateral displacement of wheelset Δy; track gauge G; inner distance between wheels $2b_a$; flange thickness t_f; and rail inclination.

The considered constant change and difference in rolling radii on the left and right wheel causes the sinusoidal motion of the wheelset (Fig. 18). The oscillations caused by sinusoidal motion are the most unfavourable effects in running of railway vehicles on the tangent track and curve with large radii. Besides very negative influence on ride comfort, they can cause vehicle instability at certain critical speeds and leads to the derailment with huge consequence. That is why the sinusoidal motion is key influential parameter on the lateral dynamic stability and its analysis is one of the most important task in rail vehicle dynamics.

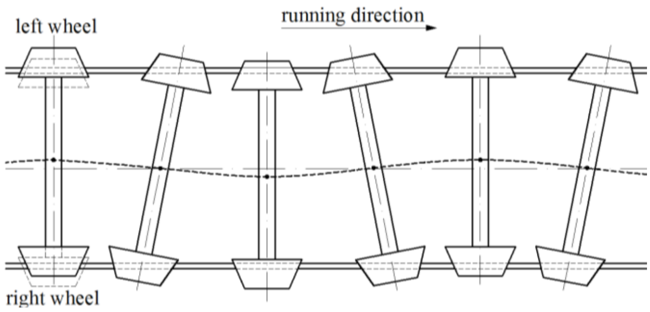

Figure 18: The sinusoidal motion of wheelset

The sinusoidal motion is described by Klingel equation which establishes relation between the wavelength of sinusoidal oscillation of wheelset centre L_w, half distance between nominal rolling radii b_0, nominal rolling radius r_0, and equivalent conicity λ_e (or conicity γ for wheels profiles with straight cones) [14]:

$$L_w = 2\pi \sqrt{\frac{b_0 \cdot r_0}{\lambda_e}} \tag{29}$$

As can be seen from Klingel's equation, the equivalent conicity is one of the dominant influential parameters on the frequency of sinusoidal oscillations. In that sense, the standard UIC 518 defines the limit values of equivalent conicity from the point of maximal operating speed and running safety [11].

Bearing in mind the non-linearity and stochasticity of a large number of influential parameters, accurately determining the equivalent conicity is a very complex task. Depending on the given wheelset lateral displacement, for determination of equivalent conicity three methods can be used [2].

The first and the most simplest method involves the determination of equivalent conicity using equations (26–28), whereby the difference between the rolling radii at only one amplitude of the lateral displacement is taken into account. This is usually the maximal amplitude $\Delta y=\pm 4$ mm. The method does not include the non-linearity in the range of changes in the amplitude of lateral displacement.

The second method involves the determination of equivalent conicity using equations (26–28), whereby a few amplitudes of lateral displacement are taken into account. For example, these amplitudes can be $\Delta y=\pm 1$, ± 2, ± 3, and ± 4 mm. It provides more accurate results and a much better picture about changes of equivalent conicity.

Third, the most complicated way involves the determination of equivalent conicity according to the method proposed in the standards UIC 519 and EN15302 [15, 16]. According to this method, the wavelength of oscillations of wheelset sinusoidal motion on given track is determined or measured, at amplitude of lateral displacement $\Delta y = \pm 3$ mm. After the determination of wavelength, the equivalent conicity is determined by Klingel equation (29). This practically means that the equivalent conicity of nonlinear worn profile is defined as a certain conicity of linear profile which, at a certain lateral displacement of wheelset, gives the equal wavelength of sinusoidal oscillations as nonlinear worn profile.In this way, the nonlinear change of rolling radii in range of changes of amplitude of lateral displacement is taken into account.

It is very important to emphasize that all three methods provide a single value of equivalent conicity for given or assumed value of wheelset lateral displacement in relation to the central position on the track. These methods are only attempts to describe a very complex geometrical relationships that exist in the wheel-rail contact. For a more accurate dynamic analysis is very important to analyse the influence of nonlinear geometrical relationships in the wheel-rail contact on the dynamic behaviour of railway vehicles. Consequently, it may be of large interest to improve the way of current description and characterization of wheel-rail contact geometry.

7. CONCLUSION

This paper gives a systematic approach to the analysis of wheelset-track and wheel-rail contact geometry. In first phase, the parameters of wheelset and track geometry are introduced, while particular attention is paid to the geometry of wheel and rail profiles. In the second phase, the interaction wheelset-track and wheel-rail is analysed. The special attention is paid to the nonlinear geometric relationships between wheel and rail profiles. This led to the defining the parameters of wheel-rail contact geometry. In the final, third stage, the functions which combines all analysed parameters are derived. The emphasis is placed on the deriving the expressions for conicity and equivalent conicity. The methods of determination of equivalent conicity and its influence on the dynamic behaviour of wheelset and railway vehicles are discussed. Its correlation with the most important phenomenon of running of railway vehicles on the tangent track – sinusoidal motion of wheelsets, is established and analysed. Considerations in the paper confirm the fact that wheel-rail contact geometry and equivalent conicty as function which representing its characterization, are one of the most important influential parameters on the dynamic behavior of railway vehicles.

ACKNOWLEDGEMENTS

The authors express their gratitude to Serbian Ministry of Education, Science and Technological Development for supporting this paper through project TR35038.

REFERENCES

[1] S.D. Iwnicki, “Handbook of Railway Vehicle Dynamics”, CRC Press, Taylor & Francis Group, Boca Raton (USA), (2006)

[2] E. Andersson, M. Berg, S. Stichel, “Rail Vehicle Dynamics”, Railway Group KTH, Stockholm (Sweden), (2007)

[3] I.Y. Shevtsov, “Wheel/Rail Interface Optimisation”, TU Delft, Delft (Holland), (2008)

[4] J. Gerlici, T. Lack, “Contact geometry influence on the rail/wheel surface stress distribution”, Procedia Engineering, 2, p. 2249–2257, (2010)

[5] S. Mace, R. Pena, N. Wilson, D. DiBrito, “Effects of wheel-rail contact geometry on wheel set steering forces”, Wear, 191, p. 204-209, (1996)

[6] O. Polach, “Influence of wheel/rail contact geometry on the behaviour of a railway vehicle at stability limit”, Proceedings of 5th EUROMECH Nonlinear Oscillations Conference – ENOC-5, Eindhoven (Netherlands), 7 August-12 August, p. 2203-2210, (2005)

[7] D. Baldovin, S. Baldovin, “The Influence of the Wheel Conicity and the Creep Force Coefficients to the Hunting Motion Stability of a Bogie with Independently Rotating Wheelsets”, Revue Roumaine des Sciences Techniques – Série de Mécanique Appliquée, 56, No. 1, p. 11-19, (2011)

[8] J. Sadeghi, B. Akbari, “Field investigation on effects of railway track geometric parameters on rail wear”, Journal of Zhejiang University SCIENCE A, 7(11), p. 1846-1855, (2006)

[9] R. Jandora, “Modelling of railway vehicle movement considering non-ideal geometry of wheels and rails”, Applied and Computational Mechanics, 1, p. 489-498, (2007)

[10] O. Polach, “Characteristic parameters of nonlinear wheel/rail contact geometry”, Vehicle System Dynamics: International Journal of Vehicle Mechanics and Mobility, Vol. 48, Suppl. 1, Special Issue: IAVSD Supplement, p. 19-36, (2010)

[11] UIC CODE 518 OR, “Testing and approval of Railway vehicles from the point of view of their dynamic behavior – Safety – Track fatigue – Running behavior”, 4th edition, International Union of Railways – UIC, (2009)

[12] EN 14363, “Railway applications – Testing for the acceptance of running characteristics of railway vehicles – Testing of running behavior and stationary tests”, European Committee for Standardization – CEN, (2005)

[13] UIC CODE 510-2 OR, “Trailing stock: wheels and wheelsets. Condition concerning the use of wheels of various diameters”, 4th edition, International Union of Railways – UIC, (2004)

[14] J. Klingel, “Uber den Lauf von Eisenbahnwagen auf gerader Bahn, Organ fur die Fortschritte des Eisenbahnwesens”, Neue Folge 20, 113–123, Tafel XXI, (1883)

[15] UIC CODE 519 OR, “Method for determining the equivalent conicity”, 1st edition, International Union of Railways – UIC, (2004)

[16] EN15302: “Railway applications – Method for determining the equivalent conicity”, European Committee for Standardization – CEN, (2011)

Numerical Simulation of Wagons Impact

Dragan Petrović[1*], Milan Bižić[1], Dragan Pančić[2], Dragić Mirković[2]
[1] – Faculty of Mechanical and Civil Engineering in Kraljevo, University of Kragujevac, Kraljevo (Serbia)
[2] – Wagon Factory, Kraljevo (Serbia)

Impact of wagons and change in moving tempo cause very intensive longitudinal forces and accelerations that affect the stress-strain state of the supporting structures of wagons. The magnitudes of impact loads can be such to constitute a risk to the support structure, and therefore for passengers and cargo. This paper is focused on an accurate analysis of the impact of two wagons. The analytical formulation of wagons impact is established and equations are solved numerically. The obtained results are compared with results of experimental testing of wagons impact. Comparative analysis of numerical and experimental results has shown satisfactory agreement. In that way, the formed analytical model can be used for determining the dynamic parameters of the impact in the design of new wagons.

Keywords: Numerical simulation, Impact, Railway vehicle, Wagon

1. INTRODUCTION

Generally, the construction of wagon consists of body, underframe, bogies, buffers, braking system, and various additional parts and equipment. Impact causes the dynamic parameters such as forces and accelerations, whose changes and maximum values depend on the speed of the impact and the characteristics of the mentioned sub-assemblies, as well as the type of cargo and its fixing for the supporting structure of wagon.

Such a complex system with many degrees of freedom is replaced with the simpler theoretical models with a limited number of degrees of freedom. In the formation of mathematical models the following restrictions are usually introduced: the construction of wagons and bogies, as well as cargo, are considered to be absolutely rigid bodies, the railway track is horizontal, centres of masses of cargo and wagons move in parallel, i.e. there is no relative movement between the cargo and wagons.

Experimental testing has shown that these simplifications lead to the insufficiently accurate results in analysis of wagons impact. The most frequently used models of wagons impact do not take into account the influence of cargo movement during the impact, gaps in assemblies of wagons, influence of the loss of energy during the impact, etc [1, 2].

In order to determine the above-mentioned influences on the values of forces on the buffers during the impact of two wagons, more accurately and somewhat more complex model has been formed [3].

2. THEORETICAL ANALYSIS OF IMPACT OF TWO WAGONS

Consider the case of two wagons impact with buffers stiffness c_1 and c_2, and stiffness of underframes c_{ns1} and c_{ns2}. Wagon whose mass is m_1 is moving with the speed $\vec{v}_1$ and collides with wagon of mass m_2 which moves with the speed $\vec{v}_2$. Wagons are loaded with cargoes whose masses are m_3 and m_4. This is resulted with the relative movement of masses over the wagons for values $\vec{x}_3$ and $\vec{x}_4$. In addition, between the wagons and cargoes there are elastic connections with stiffness c_3 and c_4.

Apart from that, the relative movements of cargoes with masses m_3 and m_4 are opposed by forces of dry friction and forces of viscous friction. These forces are proportional to the first degree of speeds of relative movements of cargoes $\dot{\vec{x}}_3$ and $\dot{\vec{x}}_4$. Also, the movements of the first and the second wagon are opposed by forces of rolling friction $\mu_1 \cdot g \cdot (m_1 + m_3)$ and $\mu_2 \cdot g \cdot (m_2 + m_4)$.

The process of impact is observed from the moment when buffers of two wagons touch each other. All buffers have the same elastic properties, so that the total buffers movement is $2\Delta\ell$.

Since the impact of wagons can be considered as event in an isolated system where the forces, speeds, accelerations or other dynamic sizes of the wagons and cargoes are in the same direction before and after the impact, they can be written without vector label.

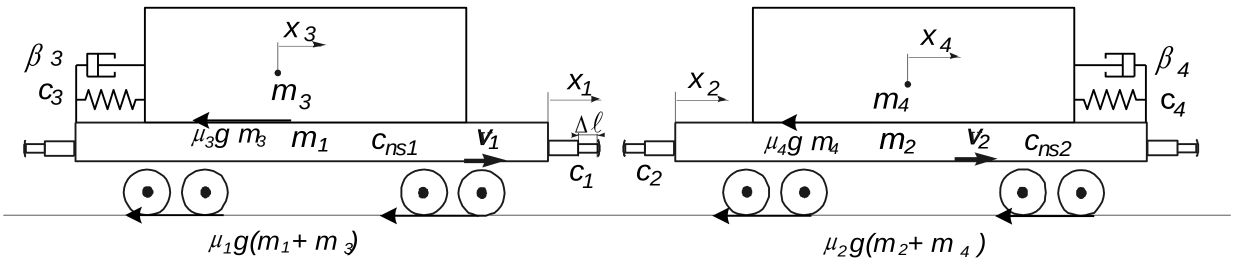

Figure 1: The impact of two wagons when the movement of cargo is present

*Corresponding author: Dositejeva 19, 36000 Kraljevo, Serbia, petrovic.d@mfkv.kg.ac.rs

Equations for kinetic energy E_k, potential energy E_p and dissipation function Φ_r of the system on Fig.1 are [4]:

$$
\begin{aligned}
&E_k=\frac{1}{2}m_1\dot{x}_1^2+\frac{1}{2}m_2\dot{x}_2^2+\frac{1}{2}m_3\left(\dot{x}_3+\dot{x}_1\right)^2+\frac{1}{2}m_4\left(\dot{x}_4+\dot{x}_2\right)^2\\
&E_p=\frac{1}{2}c_s\left(x_2-x_1\right)^2+\frac{1}{2}c_3x_3^2+\frac{1}{2}c_4x_4^2\\
&\Phi_r=\mu_1(m_1+m_3)g\left|\dot{x}_1\right|+\mu_2(m_2+m_4)g\left|\dot{x}_2\right|+\\
&\quad+\mu_3m_3g\left|\dot{x}_3\right|+\mu_4m_4g\left|\dot{x}_4\right|+\frac{1}{2}\beta_3\dot{x}_3^2+\frac{1}{2}\beta_4\dot{x}_4^2
\end{aligned}
\tag{1}
$$

where:

- c_s – equivalent stiffness of the system at the moment of impact,
- μ_1, μ_2, μ_3 and μ_4 – coefficients of dry friction,
- β_3 and β_4 – dynamic viscosities that define the environment resistance,
- g – acceleration due to gravity.

As the system is influenced by the conservative and dissipative forces, the Lagrange equations of second kind have the following form:

$$
\frac{d}{dt}\frac{\partial E_k}{\partial \dot{q}_i}+\frac{\partial \Phi_r}{\partial \dot{q}_i}+\frac{\partial E_p}{\partial q_i}=0 \tag{2}
$$

By changing the equations for kinetic and potential energy into the previous equations, as well as changing the equation for dissipation function, we get the following differential equations:

$$
\begin{aligned}
&\left(m_1+m_3\right)\ddot{x}_1+m_3\ddot{x}_3+c_sx_1-c_sx_2+\mu_1(m_1+m_3)g\cdot sign\dot{x}_1=0\\
&\left(m_2+m_4\right)\ddot{x}_2+m_4\ddot{x}_4+c_sx_2-c_sx_1+\mu_2(m_2+m_4)g\cdot sign\dot{x}_2=0\\
&m_3\ddot{x}_3+m_3\ddot{x}_1+\beta_3\dot{x}_3+c_3x_3+\mu_3m_3g\cdot sign\dot{x}_3=0\\
&m_4\ddot{x}_4+m_4\ddot{x}_2+\beta_4\dot{x}_4+c_4x_4+\mu_4m_4g\cdot sign\dot{x}_4=0
\end{aligned}
\tag{3}
$$

The system of differential equations (3) defined in this way takes into account both the movement of cargoes and the influence of friction that occurs between the individual sub-assemblies when two wagons collide, and it is suitable for numerical solution.

Also, the function signum (sign) allows the determination of the sign of friction forces that depends on the speeds of the movement of wagons and cargoes.

In order to preparation for numerical solution of system of differential equations (3), the changing of the third equation in the first one, and the fourth equation in the second one, is performed:

$$
\begin{aligned}
&\ddot{x}_1=a_1(x_2\quad x_1)+a_2x_3+a_9\dot{x}_3-a_{10}sign\dot{x}_1+a_{13}sign\dot{x}_3\\
&\ddot{x}_2=a_3(x_1-x_2)+a_4x_4+a_5\dot{x}_4-a_{11}sign\dot{x}_2+a_{14}sign\dot{x}_4
\end{aligned}
\tag{4}
$$

By changing the first equation (4) in the third equation (3) and second equation (4) in the fourth equation (3) we obtain the following equations:

$$
\begin{aligned}
&\ddot{x}_3=a_1(x_1-x_2)-(a_2+a_{12})x_3-(a_9+a_7)\dot{x}_3+\\
&\quad+a_{10}sign\dot{x}_1-(a_{13}+a_{15})sign\dot{x}_3\\
&\ddot{x}_4=a_3(x_2-x_1)-(a_4+a_8)x_4-(a_5+a_6)\dot{x}_4+\\
&\quad+a_{11}sign\dot{x}_2-(a_{14}+a_{16})sign\dot{x}_4
\end{aligned}
\tag{5}
$$

The constants $a_1 \div a_{16}$ are given in the following Table 1.

Table 1: The values of the constants $a_1 \div a_{16}$

a_1	a_2	a_3	a_4
c/m_1	c_3/m_1	c/m_2	c_4/m_2
a_5	a_6	a_7	a_8
β_4/m_2	β_4/m_4	β_3/m_3	c_4/m_4
a_9	a_{10}	a_{11}	a_{12}
β_3/m_1	$\mu_1\frac{m_1+m}{m_1}$	$\mu_2\frac{m_2+m_4}{m_2}g$	c_3/m_3
a_{13}	a_{14}	a_{15}	a_{16}
$\mu_3\frac{m_3}{m_1}g$	$\mu_4\frac{m_4}{m_2}g$	$\mu_3 g$	$\mu_4 g$

This system, however, does not take into account the reduction of impact forces due to the loss of energy in oscillating structures of wagons during the impact. This effect can be taken into account by using Newton's coefficient of restitution. However, when it comes to the railway vehicles, the coefficient of restitution at impact can be determined only by the experimental testing [3, 5].

By introducing the following sizes:

$$
\begin{aligned}
&y_1=x_1,\quad y_2=\dot{x}_1,\quad y_3=x_2,\quad y_4=\dot{x}_2,\\
&y_5=x_3,\quad y_6=\dot{x}_3,\quad y_7=x_4,\quad y_8=\dot{x}_4
\end{aligned}
\tag{6}
$$

the final form of differential equations of two wagons impact is obtained:

$$
\begin{aligned}
&\ddot{x}_1=a_1(y_3-y_1)+a_2y_5+a_9y_6-a_{10}signy_2+a_{13}signy_6\\
&\ddot{x}_2=a_3(y_1-y_3)+a_4y_7+a_5y_8\text{-}a_{11}signy_4+a_{14}signy_8\\
&\ddot{x}_3=a_1(y_1-y_3)-(a_2+a_{12})y_5-(a_7+a_9)y_6+\\
&\quad+a_{10}signy_2-(a_{13}+a_{15})signy_6\\
&\ddot{x}_4=a_3(y_3-y_1)-(a_4+a_8)y_7-(a_5+a_6)y_8+\\
&\quad a_{11}signy_4-(a_{14}+a_{16})signy_8
\end{aligned}
\tag{7}
$$

Such defined system of differential equations takes into account the movement of cargoes during the wagons impact, and is suitable for solution in numerical way.

3. NUMERICAL SIMULATION OF IMPACT OF TWO WAGONS

Based on the formed system of differential equations which describe the dynamic process of the impact of two wagons, a program for their solution is made. It is important to note that method of Runge-Kutta of IV level and programming language Fortran 77 were used [6, 7]. Based on the underlying methodology, the process of two wagons impact is simulated whereby model enables calculations with and without movement of cargo during the impact.

Dynamic parameters that were followed during the impact are:

- t – time,
- x_1 – movement of the wagon that hits into the other one,
- $\dot{x}_1$ – speed of the wagon that hits into the other one,
- $\ddot{x}_1$ – acceleration of the wagon that hits into the other one,
- x_2 – movement of the wagon that is being hit,
- $\dot{x}_2$ – speed of the wagon that is being hit,

$\ddot{x}_2$ – acceleration of the wagon that is being hit,

x_3 – movement of the cargo on the wagon that hits into the other one,

$\dot{x}_3$ – speed of the cargo on the wagon that hits into the other one,

$\ddot{x}_3$ – acceleration of the cargo on the wagon that hits into the other one,

x_4 – movement of the cargo of the wagon that is being hit,

$\dot{x}_4$ – speed of the cargo of the wagon that is being hit,

$\ddot{x}_4$ – acceleration of the cargo of the wagon that is being hit,

F_u – the total force on the buffers.

Total force on the buffers in period until the complete compaction of buffers is:

$$x_1(t)-x_2(t)\le 2\Delta\ell; \qquad F_u(t)=F^o \tag{8}$$

where F^o is the force which occurs when buffers are completely compacted.

Total force on the buffers in period of solid impact occurs when buffers are completely compacted:

$$x_1(t)-x_2(t) > 2\Delta\ell; \qquad F_u(t)=F_u \tag{9}$$

Consequently, the mathematical model of change of force during the impact is defined by the following equation:

$$F_u(t)=\begin{cases} c_I\left[x_1(t)-x_2(t)\right]^{n_1} & ;x_1(t)-x_2(t)\le 2\Delta l \\ c_I 2\Delta l^{n_1}+c_{II}\left\lfloor x_1(t)-x_2(t)-2\Delta l\right\rceil^{n_2} & ;x_1(t)-x_2(t)>2\Delta l \end{cases} \tag{10}$$

In the above expressions, non-linearity between the force and the displacement is taken into account with coefficients n_1 and n_2. In the case of linear dependence between the force and displacement, these coefficients are equal 1.

4. ANALYSIS OF RESULTS OF NUMERICAL SIMULATION

The numerical calculation of dynamic parameters of impact is carried out for three types of wagons: Tadnss-z (Fig. 2), Uacns-z (Fig. 3), and Hccrrss-z (Fig. 4). These wagons are previously experimentally tested.

Figure 2: The wagon Tadnss-z for transportation of grain materials

Figure 3: The wagon Uacns-z for transportation of powdered materials

Figure 4: The wagon Hccrrss-z for transportation of cars

During the first period of impact, the overall stiffness of the system is $c_s=c_I$, while in the second period of rigid impact, the stiffness of the system is $c_s=c_{II}$. Here, a certain approximation is introduced, namely, the characteristics of stiffness can be considered linear only in static and quasi-static loads. However, at the dynamic load, the parameters of stiffness are nonlinear.

The experimental determination of the dynamic stiffness c_I and c_{II} could contribute to obtaining more accurate values of the requested parameters of wagons impact. In this paper the results of quasi-static tests [8–11] are used and according to them specific stiffness of buffers c_I and supporting structures of wagon which participating in the impact c_{II}, are determined.

Although in the calculation we get change more dynamic parameters of wagons impact, in the following analysis comparison of numerical results of parameters obtained by the experimental tests (Fig. 5) is performed.

Figure 5: The experimental testing of wagons impact

Table 2: The results of impact for wagon Uacns-z

Size	Unit	Exp. results	Num. results
F^o	[kN]	1280	1240
v^o	[m/s]	-	2.1
F_u^{max}	[kN]	2980	3020
a_2^{max}	[m/s^2]	+56/-55	+66/-52
t	[ms]	245	225

Table 3: The results of impact for wagon Tadnss-z

Size	Unit	Exp. results	Num. results
F^o	[kN]	1502	1480
v^o	[m/s]	-	2,36
F_u^{max}	[kN]	3540	3220
a_2^{max}	[m/s^2]	+55/-45	+58/-43
t	[ms]	243	223

Table 4: The results of impact for wagon Hccrrss-z

Size	Unit	Exp. results		Num. results	
		Empty	Full	Empty	Full
F_u^{max}	[kN]	1142	748	1161	761
t	[ms]	279	298	271	294

In previous Tables 2–3 v^o is the speed which occurs when buffers are completely compacted. When wagon Uah/Ra hits into an empty wagon Hccrrss-z, it should be taken into account that there is a movement of the roof and platform of this wagon. This movement is measured during the testing (Fig. 6) and was 11.8 mm [9]. By numerical calculation this value is 10.9 mm (Fig. 7.).

Figure 6: The testing of roof movement (wagon Hccrrss-z)

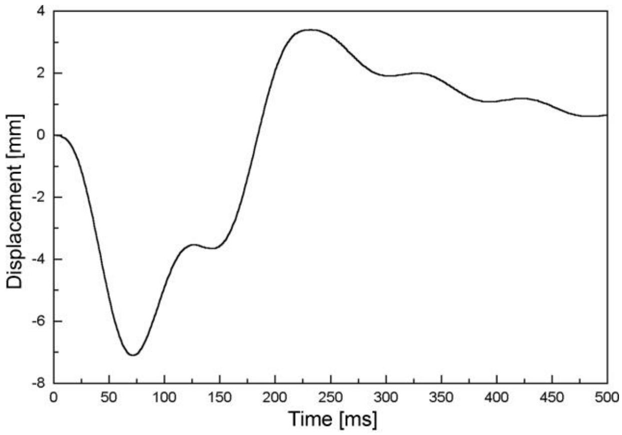

Figure 7: The diagram of roof movement obtained by the numerical simulation (wagon Hccrrss-z)

5. COMPARATIVE ANALYSIS OF EXPERIMENTAL AND NUMERICAL RESULTS

By summarizing the presented research and obtained results, it can be said that proposed methodology enables determination of behaviour and stability of the wagons supporting structure at the action of impulse loads. The way of determination of dynamic parameters (forces, displacements, accelerations, etc.) and the stress-strain state of main parts of the wagon supporting structure at impact is presented, by using the principles of non-linear dynamics and the theory of elasticity.

By analysing the duration time of impact at all three cases of tested wagons, the large similarity of the numerical and experimental results is noticed (Tables 2–4). The other dynamic parameters are also very similar. This is primarily related to the values of acceleration, maximal values of total forces, as well as values of forces at completely compacted buffers.

The diagrams obtained by numerical simulation are given in the following figures.

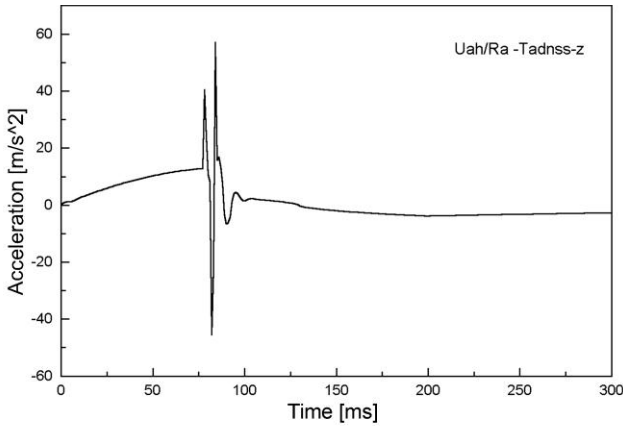

Figure 8: The diagram of acceleration change obtained by numerical simulation (wagon Tadnss-z)

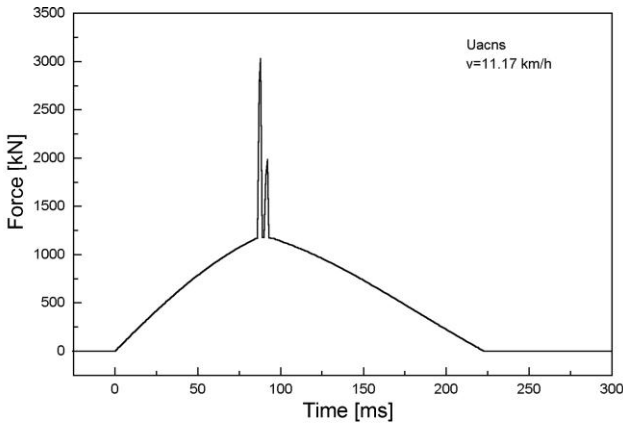

Figure 9: The diagram of total force on buffers of Uacns-z wagon obtained by numerical simulation

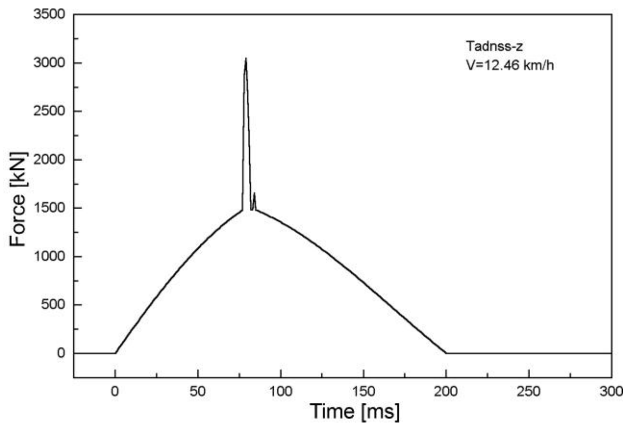

Figure 10: The diagram of total force on buffers of Tadnss-z wagon obtained by numerical simulation

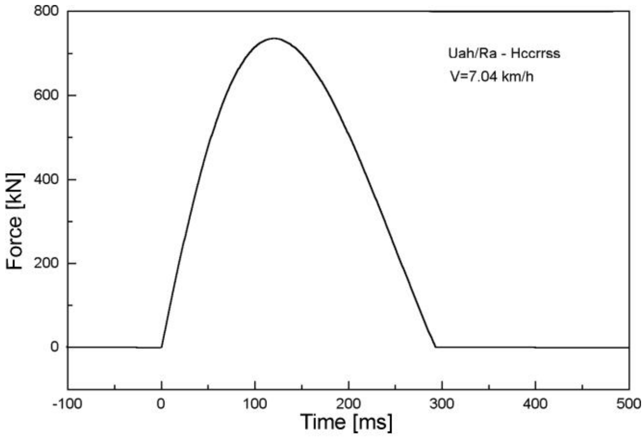

Figure 11: The diagram of total force on buffers of Hccrrss-z wagon obtained by numerical simulation (while there is cargo movement)

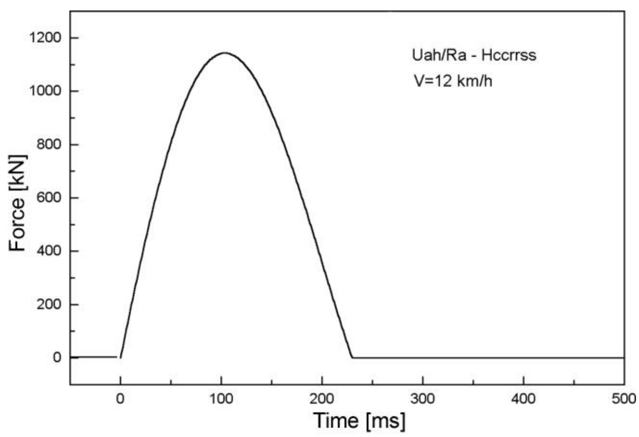

Figure 12: The diagram of total force on buffers of empty Hccrrss-z wagon obtained by numerical simulation

The diagrams of experimentally obtained results are given in the following figures.

The experimental tests are performed on the special polygon for testing the railway vehicles impact in Wagon Factory Kraljevo, Serbia (Fig. 5).

In contrast to the diagrams obtained by the numerical simulation which show total force on buffers, the diagrams obtained by the experimental tests show the individual force at each buffer.

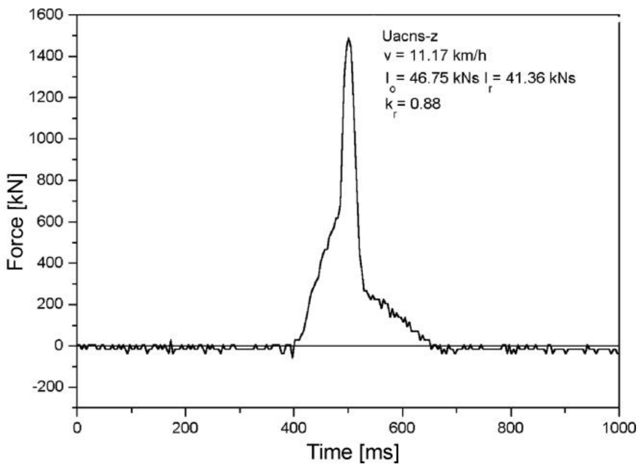

Figure 13: The diagram of force change on the first buffer of Uacns-z wagon obtained experimentally

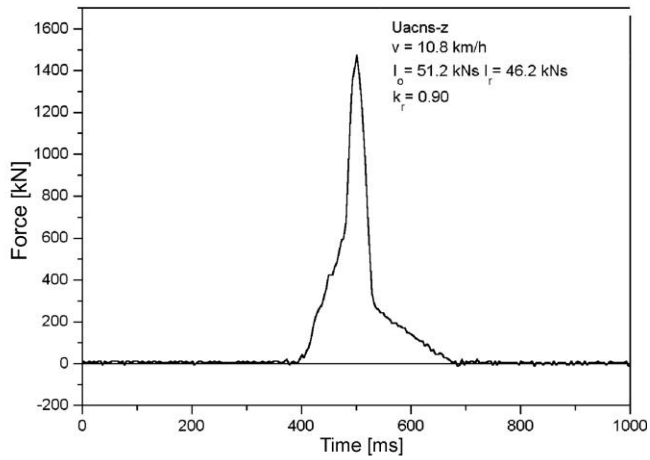

Figure 14: The diagram of force change on the second buffer of Uacns-z wagon obtained experimentally

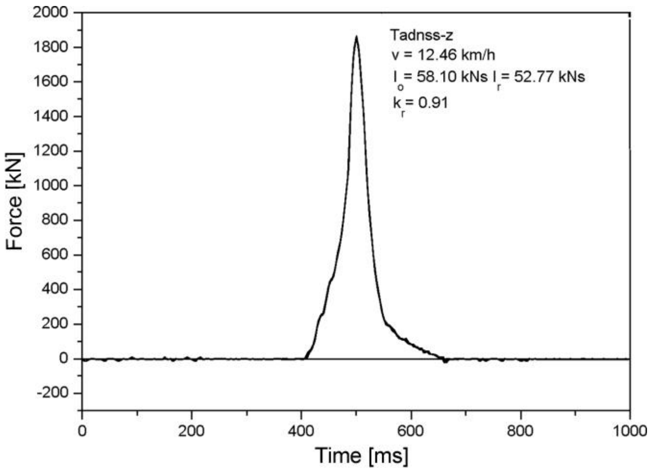

Figure 15: The diagram of force change on the first buffer of Tadnss-z wagon obtained experimentally

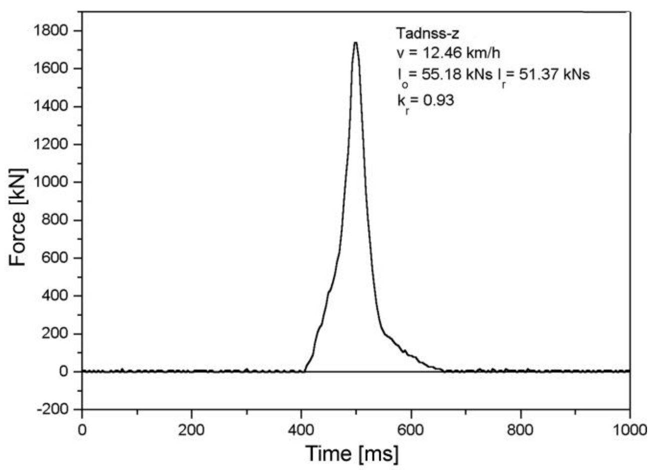

Figure 16: The diagram of force change on the second buffer of Tadnss-z wagon obtained experimentally

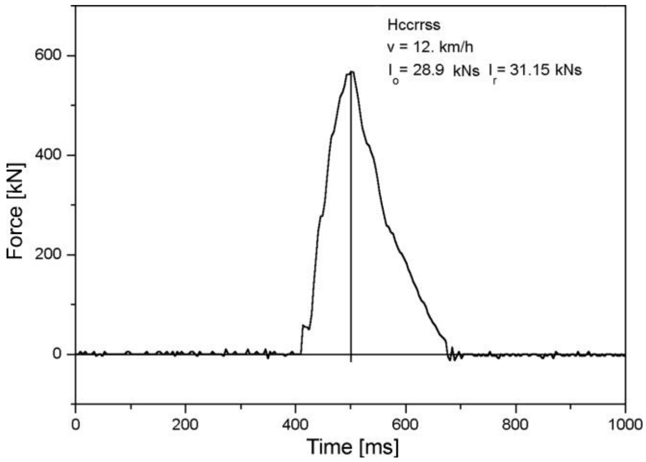

Figure 17: The diagram of force change on the buffer of empty Hccrrss-z wagon obtained experimentally

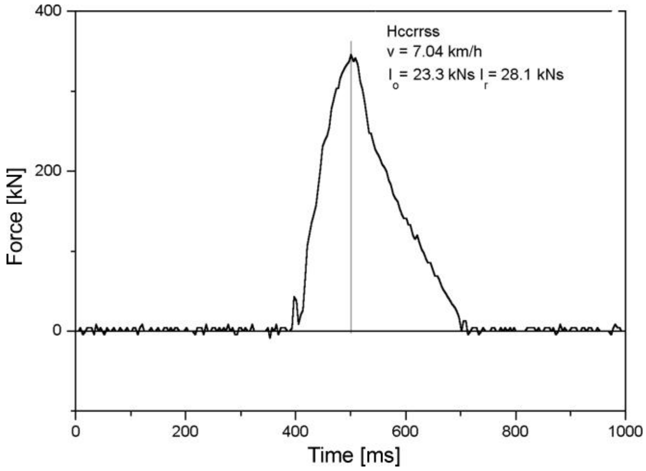

Figure 18: The diagram of force change on the buffer of laden Hccrrss-z wagon obtained experimentally (while there is cargo movement)

5.1. Results of numerical simulation which are not experimentally measured

In addition to the results obtained by numerical simulation which we could verify by experimental tests, the values of other dynamic parameters which are not experimentally measured (speeds of wagons during impact, movements and accelerations of cargoes and wagons, etc.) are obtained. These results of numerical simulation can be checked in future experimental tests. These results are given in the following figures.

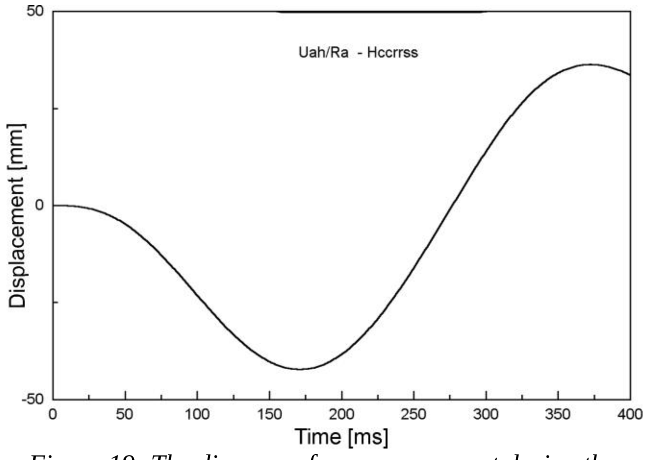

Figure 19: The diagram of cargo movement during the impact of Hccrrss-z wagon

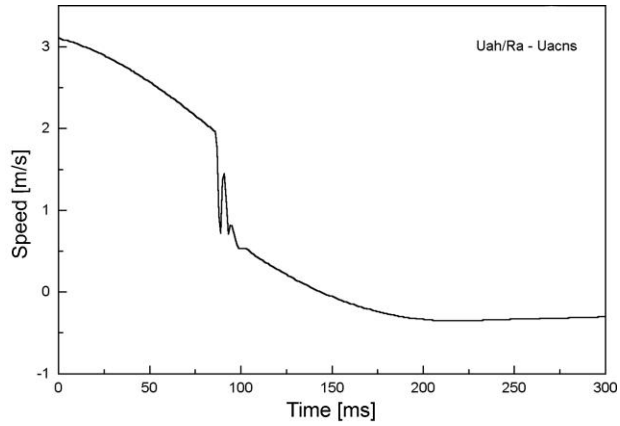

a)

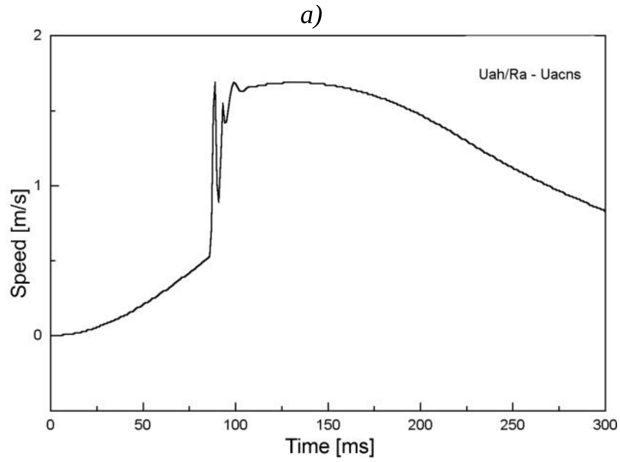

b)

Figure 20: The diagrams of speed change of first (a) and second (b) wagon Uacns-z during the impact

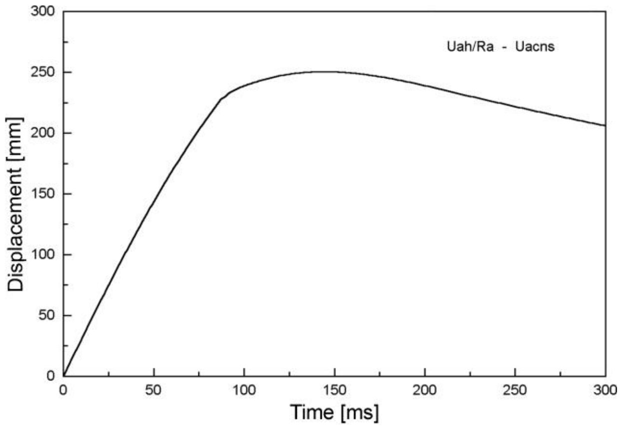

a)

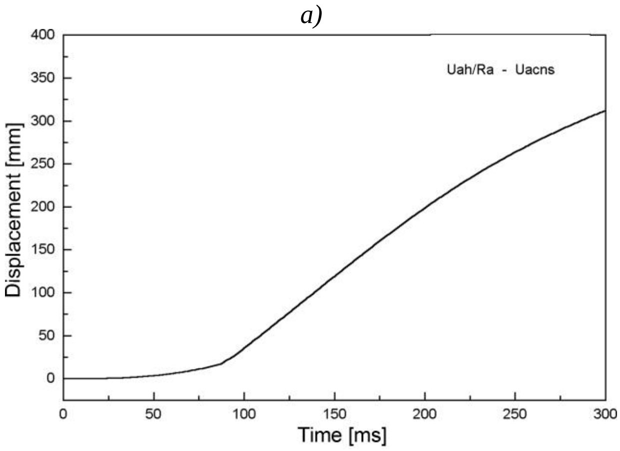

b)

Figure 21: The diagrams of movement change of first (a) and second (b) wagon Uacns-z during the impact

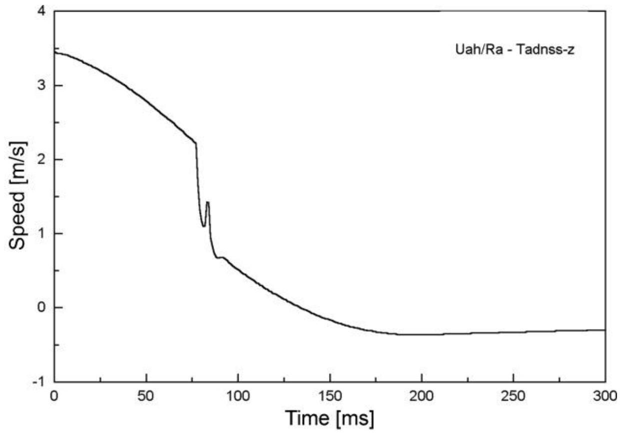

a)

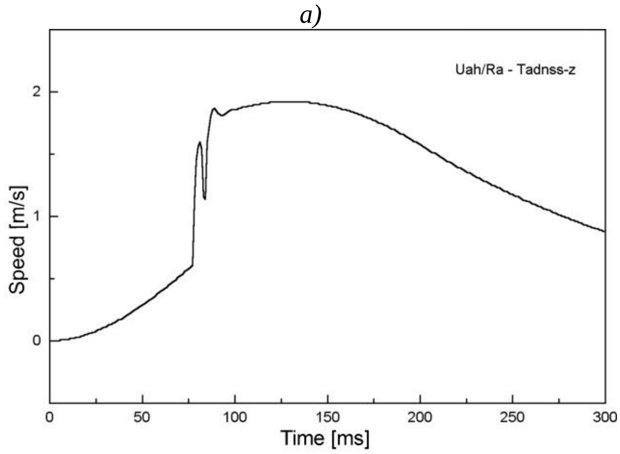

b)

Figure 22: The diagrams of speed change of first (a) and second (b) wagon Tadnss-z during the impact

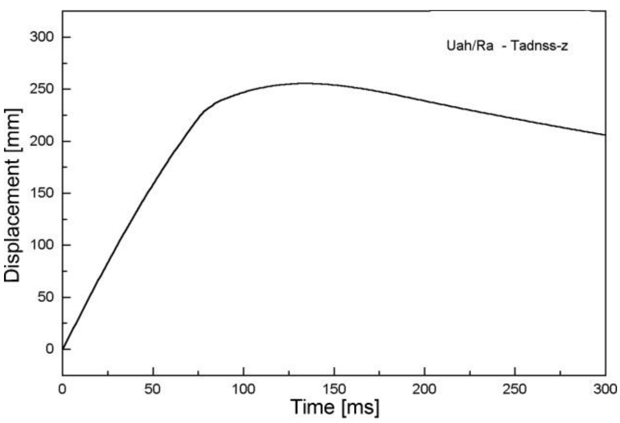

a)

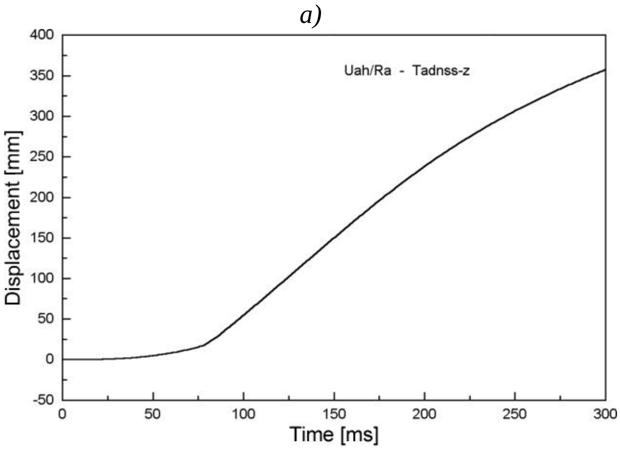

b)

Figure 23: The diagrams of movement change of first (a) and second (b) wagon Tadnss-z during the impact

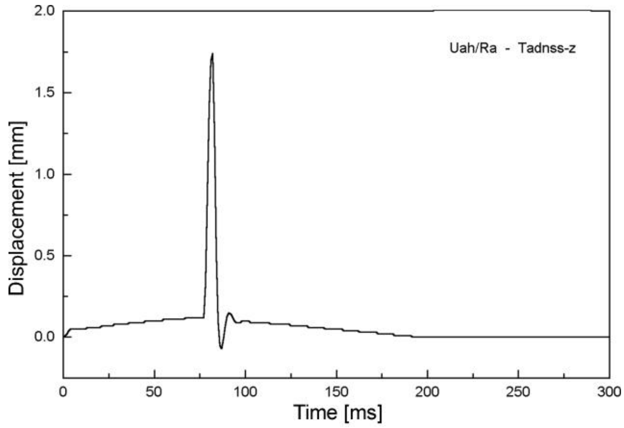

a)

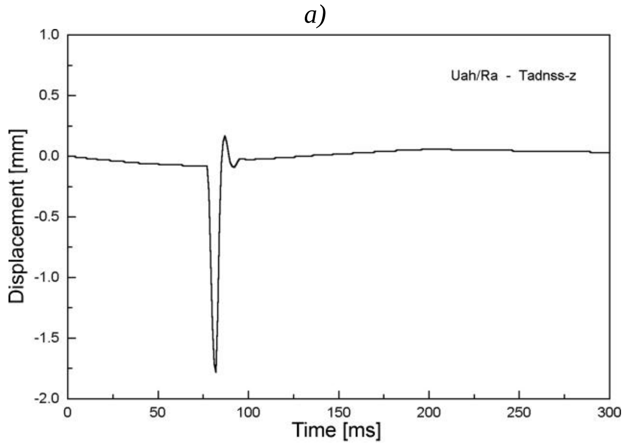

b)

Figure 24: The diagrams of cargo movement change of first (a) and second (b) wagon Tadnss-z during the impact

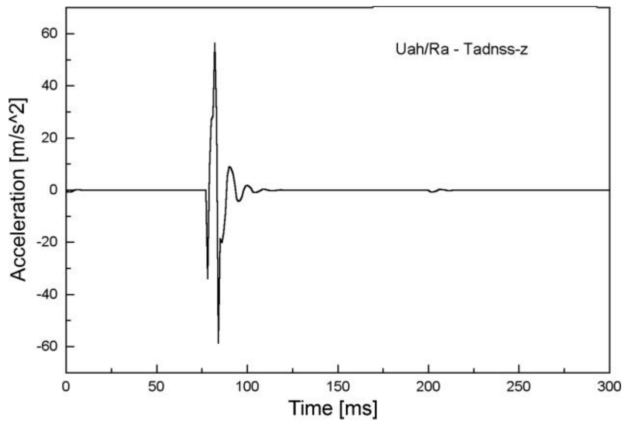

a)

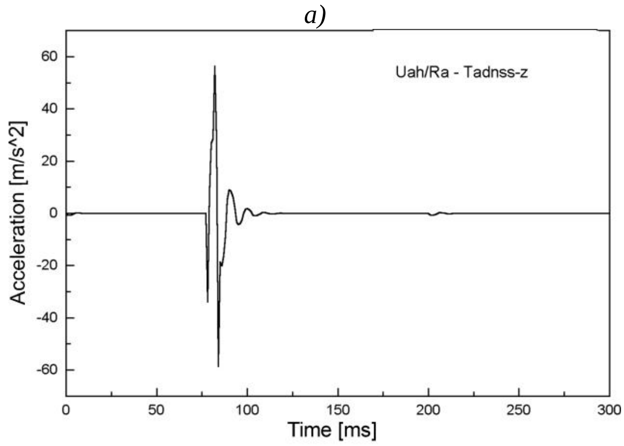

b)

Figure 25: The diagrams of cargo acceleration change of first (a) and second (b) wagon Tadnss-z during the impact

6. CONCLUSION

In the research of vehicle dynamics so far, significant results have been achieved, before all, by using experimental methods. Examinations of values of forces at the impact of wagons as well as those of the stress-strain state of the supporting structure have been carried out. In this paper, experimental research was done at three different wagons: the wagon for transportation of powdered materials Uacns-z, the wagon for transportation of grain material Tadnss-z, and the wagon Hccrrss-z which is used for transportation of cars.

Beside the results of experimental testing of mentioned wagons, the analytical model of impact of two wagons is developed. The model takes into account the movement of cargo during the impact. The established differential equations are solved by numerical way.

By analysing the obtained results of numerical simulation of impact of wagons presented in this paper, it can be concluded that they are consistent with the results obtained experimentally. In that way, the developed analytical model can be used for determination of the dynamic parameters of the impact in the design phases of new wagons.

The improvements of the proposed model can be achieved by further exploring of dynamic stiffness of the wagon supporting structure and its sub-assemblies, as well as determination of the energy that is lost on the oscillation of the wagon during the impact.

ACKNOWLEDGEMENTS

The authors wish to express their gratitude to Serbian Ministry of Education, Science and Technology for supporting this paper through project TR35038.

REFERENCES

[1] W. Goldsmith, “Impact, The theory and Physical behaviour of colliding solids”, Edward Arnold & Co, London, (1960)

[2] С.В. Вершинский, В.Н. Данилов, И.И. Челноков, “Динамика вагона”, Издательство: Транспорт, Москва, (1978)

[3] D. Petrovic, “Stability of waggon carrying structure at impact”, Ph. D. thesis, Faculty of Mechanical Engineering Kraljevo, Kraljevo, (2000)

[4] D. Petrovic, M. Bizic, M. Djelosevic, “Determination of dynamic sizes during the process of impact of railway wagons”, Archive of Applied Mechanics, Volume 82, Number 2, pp. 205-213, (2012)

[5] D. Petrovic, “Dynamic of impact of waggons”, Zaduzbina Andrejevic, Belgrade, (2001)

[6] B. Jovanović, D. Radunović, “Numerička analiza”, Naučna knjiga, Beograd, (1993)

[7] N. Parezanović, D. Kolar, “Fortran 77”, Naučna knjiga, Beograd, (1989)

[8] R. Rakanović, A. Babić, D. Petrović, i dr., “Elaborat 135/91: Statičko i dinamičko ispitivanje Tadnss-z kola”, Opitni centar FVK, Kraljevo, (1991)

[9] R. Rakanović, D. Petrović, A. Babić, i dr., “Elaborat 125/91: Proračun noseće strukture Tadnss-z kola”, Opitni centar FVK, Kraljevo, (1991)

[10] R. Rakanović, A. Babić, D. Petrović, i dr., “Elaborat 8/98, Ispitivanje kola za prevoz automobila Hccrrss”, Mašinski fakultet Kraljevo i Opitni centar FVK , Kraljevo, (1998)

[11] R. Rakanović, D. Petrović, A. Babić, i dr., “Elaborat 158/98: Ispitivanje Uacns kola za prevoz praškastih materijala”, Mašinski fakultet Kraljevo i Opitni centar FVK, Kraljevo, (1998)

[12] D. Petrović, M. Bižić, “Stability of reservoir of tank-wagon at longitudinal impact”, IMK-14 – Research and development, Volume 18, Number 1, pp. EN19-23, (2012)

Method of Control of the Train Movement Based on Natural Recuperation of Energy

V. A. Shevchenko[1*], V. Kh. Pshikhopov[1], M. Yu. Medvedev[1], A.R. Gaiduk[1], A. A. Zarifyan[1], Yu. P. Voloschenko[1]
[1] Southern Federal University, Taganrog, Russia

This paper proposes a method of energy saving planning movement of the train on the basis of natural recuperation which assumes the fullest use of the accumulated kinetic energy. The movement velocity of the train varies within acceptable values so as to maintain the required time of passage plot. We considered typical parts of the route on the basis of which, made a program that produces changes in the speed of the train depending on its position. This program can adjust itself in the process of movement of the train.

Research of the equations of motion of the train have been conducted. This research has shown that, from the energy standpoint, dispersal trains most advantageously carried out at the maximum possible traction force, which has an extreme character, depending on the speed of wheel slip. The proposed method of control maintains traction force trains with electric traction in extreme value.

Developed software package based on Matlab and "Universal Mechanism". Modeling of movement of freight train on a real track segment was produced. Effectiveness of the proposed method was demonstrated.

Keywords: Electric train, recuperation, method of planning, movement control, modeling of motion

1. INTRODUCTION

Control of the Train is planned in such a way that it passes stage at a constant speed. If the path on the stretch is not horizontal, then the average speed of the train is usually less than the maximum possible for a given weight.

Maintaining a constant speed leads to the fact that traction significantly increases when train movement up, but while going downhill is braked to avoid exceeding the setpoint.

Consequently, assuming reduction in speed when driving on the rise, then at the subsequent driving downhill, potential energy which been received on the rise naturally pass (recuperated) into kinetic energy and then the train will move at a given average speed.

2. METHOD OF THE MOTION PLANNING

Consider the quantitative relations, at which can occur the natural recuperation, and estimate potential energy effect of its application [1, 2].
Suppose profile path from point A to point B is known and has the form shown in Fig. 1. As seen in the path from A to B has an elevation, which leads to an increase in the path for h_1 , m, and decrease until h_2 , m, and increase less than decrease , i.e. $h_2 < h_1$. The rest of the path is horizontal. Assume also that is known the average speed V_0 , at where the train (locomotive + wagons) overcomes the path from A to B in a given time with the time on acceleration and stopping the train.

Need to find the speed V2, V3, distance Sy and the necessary in this section acceleration α. The solution of the problem is given by the following expressions:

$$V_2 = \sqrt{V_0^2 - 2gh_1},$$

$$0,5mV_0^2 - mgh_1 > 0 \qquad (1)$$

$$V_3 = \sqrt{V_0^2 - 2gh_2} \qquad (2)$$

$$S_y = \frac{1}{(V_0 - V_3)}(V_0(2S_3 - S_1 - S_2) - V_2(S_3 - S_1) - V_3(S_3 - S_2)) \qquad (3)$$

$$\alpha = \frac{1}{2S_y}[3V_0^2 - 4V_0V_3 + V_3^2], \qquad (4)$$

Similar expressions are obtained for the other profiles shown in Fig. 2.

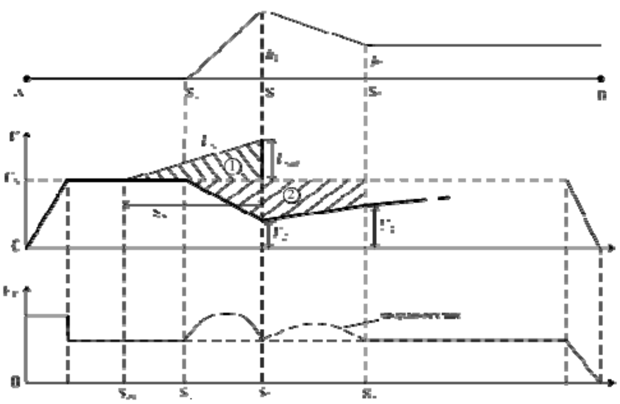

Figure 1: Graphs of profile of the track, speed and traction

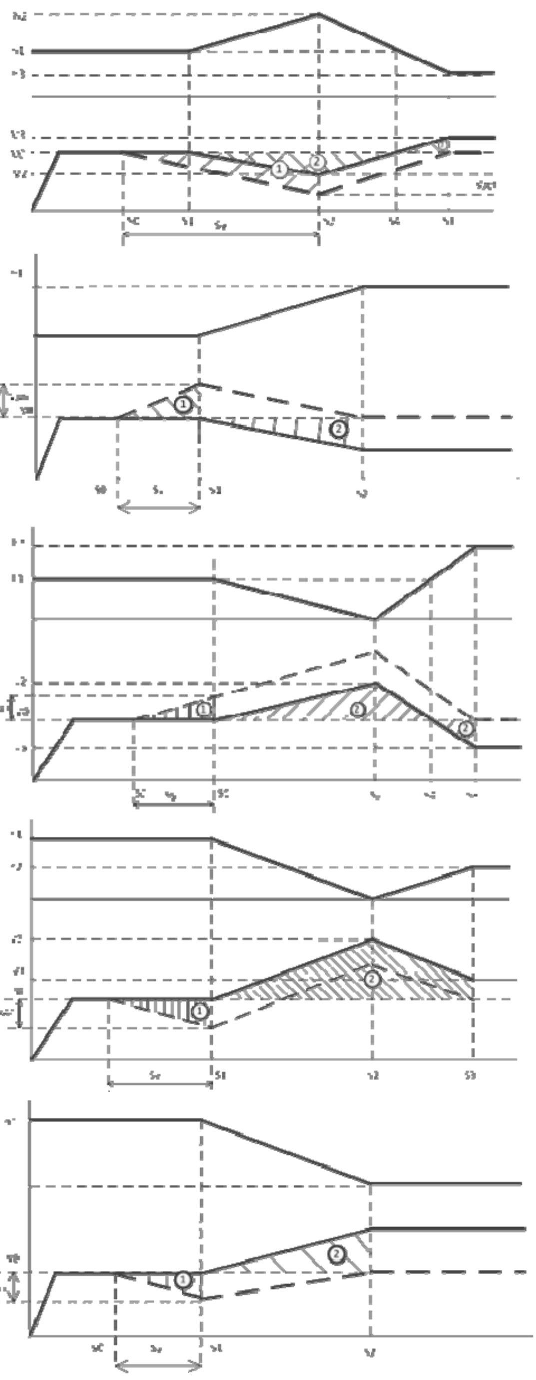

Figure 2: Graphs of various profiles path

Consider an example. Let the S1 = 2000m, S2 = 2300m, S3 = 2500m, h1 = 20 m, h2 = 12 m, V0 = 25 m / s, g = 10 m/s^2. Required to find the length of the acceleration section Sy and the acceleration at which the speed at the end of the descent and the average velocity of passing of the hill is V0.

1. Find the speed V2 and V3 at a constant trains traction: V2 = 15 m / s, V3 = 19,62 m / s, i.e. drop velocity is V0-V3 = 5,38 m / s.
2. Distance : Sy=1129 m.
3. Required acceleration: 0,131 m/s^2.
4. The start point of the acceleration: Soa=S2-Sy=2300-1129=1171.

Thus, to maintain the average speed during the passage of the hill in this case, it is necessary for the 1129 meters to the point of beginning of rise increase traction to give the train acceleration equal to 0.131 m/s^2 and keep it constant until arrival the train at the upper point of the hill. At this point the traction is lowered to a value corresponding to the movement of trains along a horizontal track section at a predetermined speed, in this case equal to 25 m/s.

We estimate the energy gain from the movement of trains with variable speed.

If the speed is kept constant during the passage of the hill, then at the passage of lifting 20 m with a constant speed of V0 m/s will be allocated an additional E12 = mgh1 = 200 Nm. When the train brakes at downhill, energy is equal to the change of potential energy in this sector, i.e. E23 = mg (h1-h2) = 80 Nm. Suppose half of this energy is provided by the work of the motion resistance forces, and the other half is provided by active inhibition. Then the full cost of energy to maintain a constant speed trains are 240 Nm.

When train moves on an elevated with variable speed on giving for train local accelerate will additionally expended in the amount of energy U = mgh2 = 120 Nm. Then the energy efficiency of the proposed method, path planning is

$$\eta_{эк} = \frac{240m-120m}{240m} = \frac{120}{240} = 0,5 \qquad (5)$$

3. METHOD OF EXTREME CONTROL OF THE MOVEMENT TRAIN

As a first approximation, the resistance force movement of the train is a quadratic function of the speed of the train and is described by [3]:

$$F_{дсп}(V_{лок}) = F_{дсп0} + F_{дсп1}V_{лок} + F_{дсп2}(V_{лок})^2 \qquad (6)$$

where $F_{дсп0}$, $F_{дсп1}$, $F_{дсп2}$ - constant coefficients depend primarily on the parameters of the train, the number and weight of railcars. At a constant, for example, the maximum possible traction force, steady speed trains on a horizontal, rectilinear path defined by the expression

$$V^*_{лок} = \frac{F_{дсп1}}{2F_{дсп2}}\left(-1+\sqrt{1+\frac{4F_{дсп2}}{F^2_{дсп1}}(F_{тг,max}-F_{дсп0})}\right)$$

It follows that the steady-speed trains is determined by the difference between the maximum possible traction force $F_{тг,max}$ and force of resistance at starting the train $F_{дсп0}$.

Consider the equation of motion of the train provided $F_{тг,с} = const$

$$\dot{V}_{лок} = \left(F_{тг,с} - F_{дсп0} - F_{дсп1}V_{лок} - F_{дсп2}V^2_{лок}\right)/m_п \qquad (7)$$

We rewrite (7) as a:

$$\dot{V}_{лок} = f(V_{лок})^2 + gV_{лок} + h \qquad (8)$$

where $f = -F_{дсп2}/m_п$, $g = -F_{дсп1}/m_п$, $h = (F_{тг,с} - F_{дсп0})/m_п$ – constant coefficients.

Equation (8) is a Riccati equation, as well as its coefficients - constants and $f \neq 0$, then the solution is equal to:

$$V_{лок}(t) = \frac{C[\exp(p_2 t) - \exp(-\bar{p}_1 t)]}{[C_1\exp(-\bar{p}_1 t) + C_2\exp(p_2 t)]} \qquad (9)$$

Where $C=\dfrac{F_{\text{дсп1}}}{4F_{\text{дсп2}}}\dfrac{a}{\sqrt{1+a}}$, $\overline{p}_1=F_{\text{дсп1}}(1+\sqrt{1+a})/2m_{\text{п}}$, $p_2=F_{\text{дсп1}}(-1+\sqrt{1+a})/2m_{\text{п}}$, $a=4F_{\text{дсп2}}(F_{\text{тг,с}}-F_{\text{дсп0}})/F_{\text{дсп1}}^2$.

Investigation of the solution (9) has shown that when accelerating trains constant traction force power consumption described by the expression:

$$Q_{\text{п}}(V_{\text{п,тр}})=\frac{F_{\text{тг,с}}m_{\text{п}}V_{\text{п,тр}}^2}{2(F_{\text{тг,с}}-F_{\text{дсп0}})}=\frac{m_{\text{п}}V_{\text{п,тр}}^2}{2}\left(1+\frac{F_{\text{дсп0}}}{F_{\text{тг,с}}-F_{\text{дсп0}}}\right) \quad (10)$$

Expression of (10) that is the most economical acceleration trains with maximum force of traction electric train. On the other hand, traction force of electric train equal force coupling, is proportional to the coefficient coupling $k_{\text{сц}}(V_{\text{ск}})$, whose dependence on the sliding velocity $V_{\text{ск}}$ has an extreme character. The maximum value of the force of adhesion is the optimal value of speed $V_{\text{ск}}^{\circ}$. Thus, the most efficient in terms of energy, is the acceleration train at a speed of $V_{\text{ск}}$ close to the optimal value $V_{\text{ск}}^{\circ}$.

Value $V_{\text{ск}}$, in which the equality $dF_{\text{сц}}/dV_{\text{ск}}=0$ corresponds extreme value adhesive force $F_{\text{сц,max}}$. This value can be calculated from the acceleration of train wheels, acceleration of locomotive and rate of change torque of traction motor. However, the study showed that the error in determining the acceleration $\ddot{\omega}_k$ and derivatives $\dot{M}_{\text{д}}$ and $\dot{V}_{\text{лок}}$ lead to unacceptably large errors in determining the derivative $\dot{V}_{\text{лок}}$. In fact, these errors do not allow to accurately determine the desired value of $V_{\text{ск}}^{\circ}$, at which the derivative $dF_{\text{сц}}/dV_{\text{ск}}$ becomes zero.

Therefore, to determine the extreme values of adhesive force $F_{\text{сц,max}}$ are encouraged to use a method based on the comparison of the differences of the extremal function and its argument.

In the developed system uses ascending of difference variables adhesive force and slip velocity, which are determined by the formulas

$$\Delta F_{\text{сц},k}=F_{\text{сц},k}-F_{\text{сц},k-1},\quad \Delta V_{\text{ск},k}=V_{\text{ск},k}-V_{\text{ск},k-1}, \quad (11)$$

k^* - marked the moments of time that correspond to the maximum values of adhesive force $F_{\text{сц,max}}$. Comparing the signs increments adhesive force $\Delta F_{\text{сц},k}$ and slip velocity $\Delta V_{\text{ск},k}$ is easy to see that an increase in the sliding velocity, for all $k\le k^*$ of signs of increments coincide, and when $k>k^*$ these signs are opposite. A similar situation occurs with decreasing sliding speed. In other words, value of the optimal slip velocity is consistent with the values of k, in which there is a change of sign of the multiplication of marks increments $\Delta F_{\text{сц},k}$ and $\Delta V_{\text{ск},k}$.

This allows us to offer the following method for determining and maintaining the extreme value of sliding speed locomotives. Suppose, under the influence of some initial voltage train with electric locomotive scored some minor speed. Control system of speed of the train identified a number of values of the slip velocity and adhesive force so that can calculate difference of $\Delta F_{\text{сц},k}$ and $\Delta V_{\text{ск},k}$. Suppose it happened at time $t_{k_{\text{и}}}=k_{\text{и}}T$. In the future, in order to ensure maximum traction, the motor voltage of electric train is changed of control system in accordance with the following expression:

$$u_{\text{д},k}=u_{\text{д},k-1}+u_{\Delta}\,\text{sign}(\Delta F_{\text{сц},k-1})\cdot\text{sign}(\Delta V_{\text{ск},k-1}),$$
$$k=k_{\text{и}},\ k_{\text{и}}+1,\ k_{\text{и}}+2,\ \dots, \quad (12)$$

where u_{Δ} – positive number (trial motion), the value of which determines the speed and magnitude of changes in the velocity slip. Typically, the value of u_{Δ} is determined experimentally.

Estimate of the effectiveness of this method was carried out by computer simulation equations of train in MATLAB. At the same time to reduce the effect of quantization by time, we used averaged over several periods of the variables.

Fig. 3,a is a graph of voltage change on engines of the test electric locomotive, and Fig. 3,b - corresponding graph of traction. Clearly visible trial movement - change the motor voltage and the corresponding changes in the slip velocity, due to these changes in the voltage. As can be seen, velocity of sliding a changes, first approaching the optimal value, and then oscillates in its vicinity.

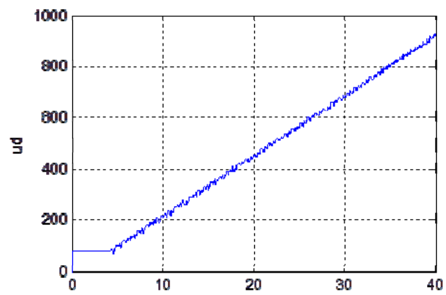

a)

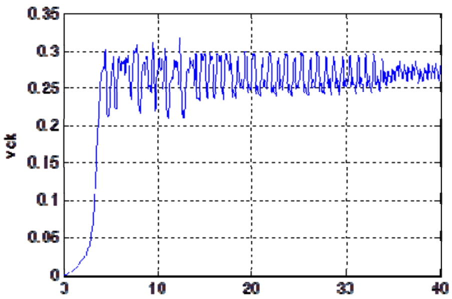

b)

Figure 3: Extreme motor control of electric locomotive

4. THE PROGRAM COMPLEX

For research, development and setting of the train control systems has been developed software based on the software package Matlab and "Universal Mechanism". Structure of the complex of simulation of train movement are shown in Figure 4.

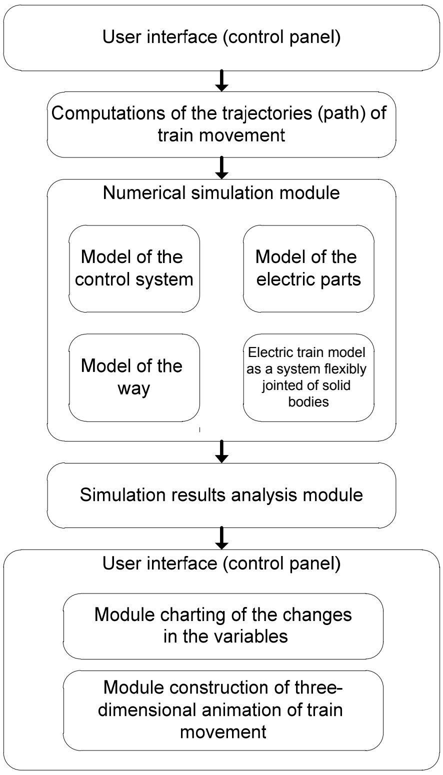

Figure 4: Structure of the software complex

Based on this software package implemented evaluation of energy efficiency of the proposed methods of train control. Was chosen track section 1785-1777 Km away from the station Tuapse to the station Armavir (Fig. 5). Length of section 8 km. Permissible speed of 46.7 Km/h.

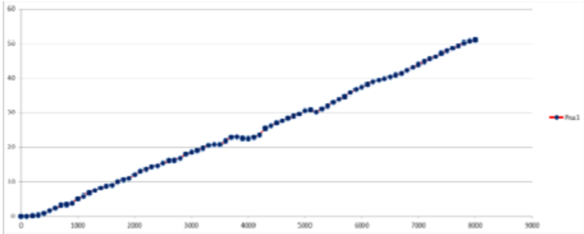

Figure 5: Plot of the path

Despite the fact that the section has been a steady increase proposed algorithms on small roughnesses give winnings of about 3% of the energy. This win will be more significant with the appropriate profile path.

5. REFERENCES

[1] Pshikhopov V.Kh., Gaiduk A.R., Medvedev M.Yu., Belyaev V.E., Poluyanovich N.K., Voloschenko Yu.P. Energy-saving control traction drive electric rolling / / Proceedings of the Southern Federal University. Technical sciences. - 2013. - № 2 (139). - S. 192 - 200. [Rus]

[2] Pshikhopov V.Kh., Medvedev M.Yu., Gaiduk A.R., Shevchenko V.A. Energy-saving control electric train under the profile irregularity the path / / Proceedings of the Southern Federal University. Technical sciences. - 2013. - № 3 (140). - S. 162 - 168. [Rus]

[3] Pshikhopov V.Kh., Medvedev M.Yu., Gaiduk A.R., Zarifyan A.A., Shevchenko V.A., Belyaev V.E. Energy-saving control trains with electric drive based on complex mathematical models. Collected materials of the Third International Scientific-Practical Conference "Intelligent Transport Systems". St. Petersburg, 3 - 5 April 2013. S. 238 - 245. [Rus]

SESSION G

URBAN ENGINEERING, THERMAL TECHNIQUE AND ENVIRONMENT PROTECTION

Environment Monitorization System in the Proximity of a Industrial Pollution Using a Raspberry Device

PhD Asist. Eng. Cristina Sescu Gal[1*], PhD, Lecturer. Eng. Mihail Savaniu[1]

[1]Faculty of Technological Equipment, Bucharest, Romania

The paper presents a control system of the main pollution emissions that are in the vecinity of industrial pollution. The device is based on a Raspberry platform connected to a group of sensors allowing for extended mobility. It offers the posibility of evaluation of the emissions by comparing measurements with the Limit Values issued by the Environment Regulator regarding industrial pollution. The system also allows for personal use.

Keywords: emissions, monitoring, Limit Values issued by the Environment, sensors.

1. INTRODUCTION

There has been an increase in the studies regarding the air quality in the surrounding environment. The future of the industries that have a pollution emissions in the EU depend on the politics and decision of the European Union, in the context of an ambitious plan to reduce the emissions in the atmosphere. According to EU legislation and directives, every industrial installation that generates emissions needs a „Environment Authorization" which proves that the ELV (emission limit values) are not exceeded. The limits are chosen so that they do not affect the population health, the environment and the local flora and fauna. Table 1 presents the types of emissions and VLE set to work burning clinker from the cement factory, reported a daily average of the installation.

Table1: ELV established for clinker burning process

Type activity	Pollutant emissions	V.L.E. as BAT/BREF mg/Nm^3
Clinker burning process	NO_X	200 - 3000
	SO_2	10 - 3500
	CO	5 - 2000
	Pulberi	5 - 200
	COT	5 - 500
	HCl	0,4 - 5
	HF	0,4 - 5
	Cd+Tl	0,01 – 0,3
	Sb+As+Pb+Cr+Co+ Cu+Mn+Ni+V	0,05 – 0,3
	Hg	0,01 – 0,3
	PCDD/PCDF	0,1 – 0,5 ng/Nm^3

[1] (Limit Values are reported for 10% oxigen in the gas).

The values presented above are refference values for choosing the appropiate evaluation device.

2. INDUSTRIAL MONITORIZATION SYSTEM FOR EMISSIONS FROM CIMENT MANUFACTURING

The monitorization of emission is done in accordance with the required specifications in the environment authorization: continously monitorization in-site or discontinously by taking samples to the laboratory. The sources of pollution of a cement plant are monitored depending on the type and content of the emissions, according to the scheme presented in figure 1.

The equipments and monitorization systems use analysis methods like : differential optical absorption spectrometry (DOAS), IR fotometry, UV fluorescence, chemiluminescence, photoluminiscence, NDIR–non dispersive infrared analysis, FTIR-Fourier Transform Infrared spectroscopy.

A complete system for emission monitorization in the industrial environment (figure 2) is composed of:

- gas analysis equipment for : CO, SO_X, NO_X, HCl, O_2;
- unit for concentration measurement of dust, particles and smoke density;
- unit for measurement and recording of evacuated gases .
- unit for emission evaluation , data acquisition for contiunous registration of values;
- unit for the formating of the data in the required form, has multiple interfaces and connection options.

*Corresponding author: Faculty of Technological Equipment, Calea Plevnei Nr.59, Bucharest, Romania, cristi.sescu@yahoo.com

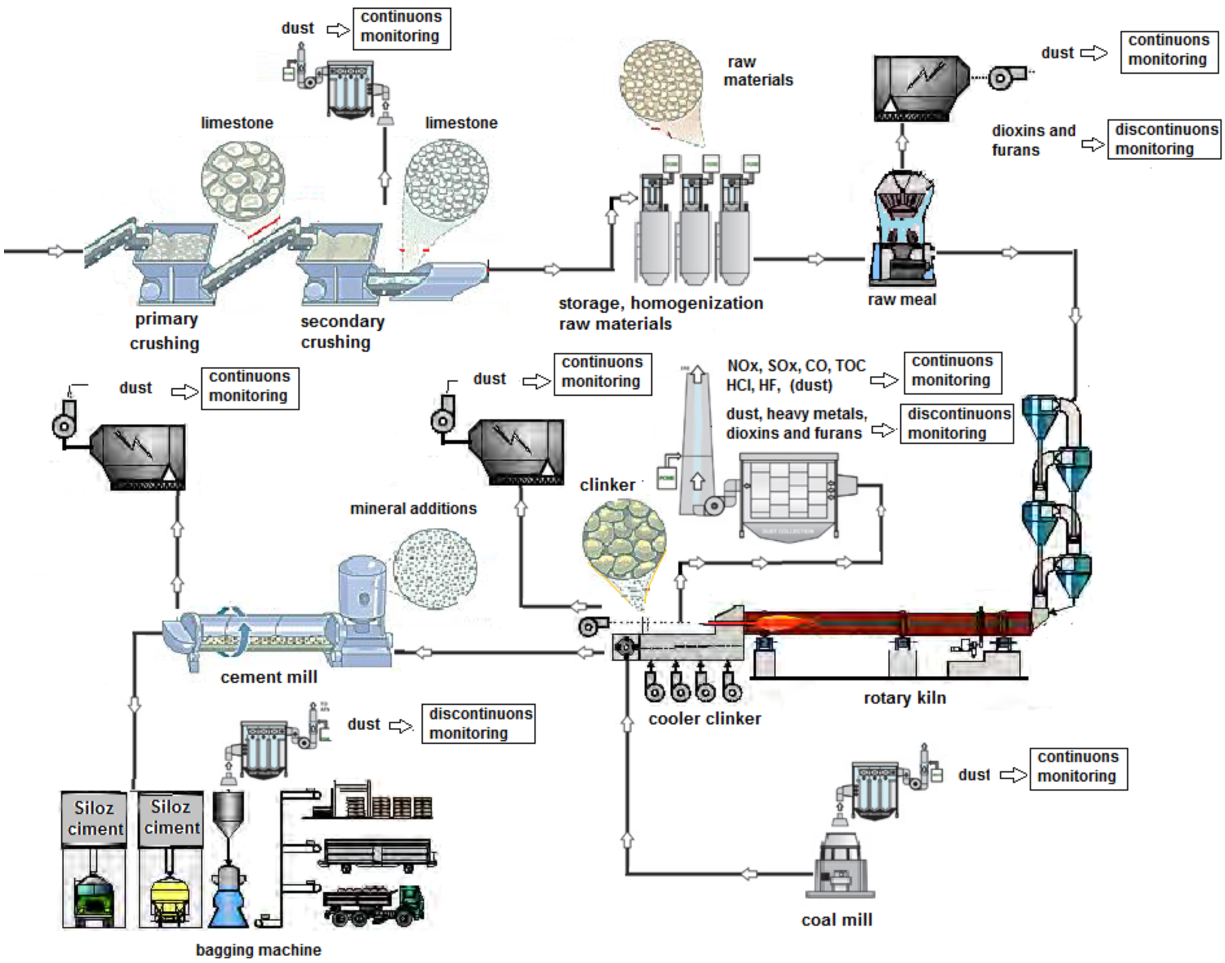

Figure 1: Points of monitoring emissions from a cement plant [2]

3. STRUCTURE METHODS FOR ESTABLISHING THE LEVEL OF EMISSIONS IN THE AIR

The determination of emissions in the air can be done by many methods, each of them with advantages, disadvantages and limits. The methods are: measurement of emissions, determination from a balance, corelations and determination on the base of characteristics emissions factors.

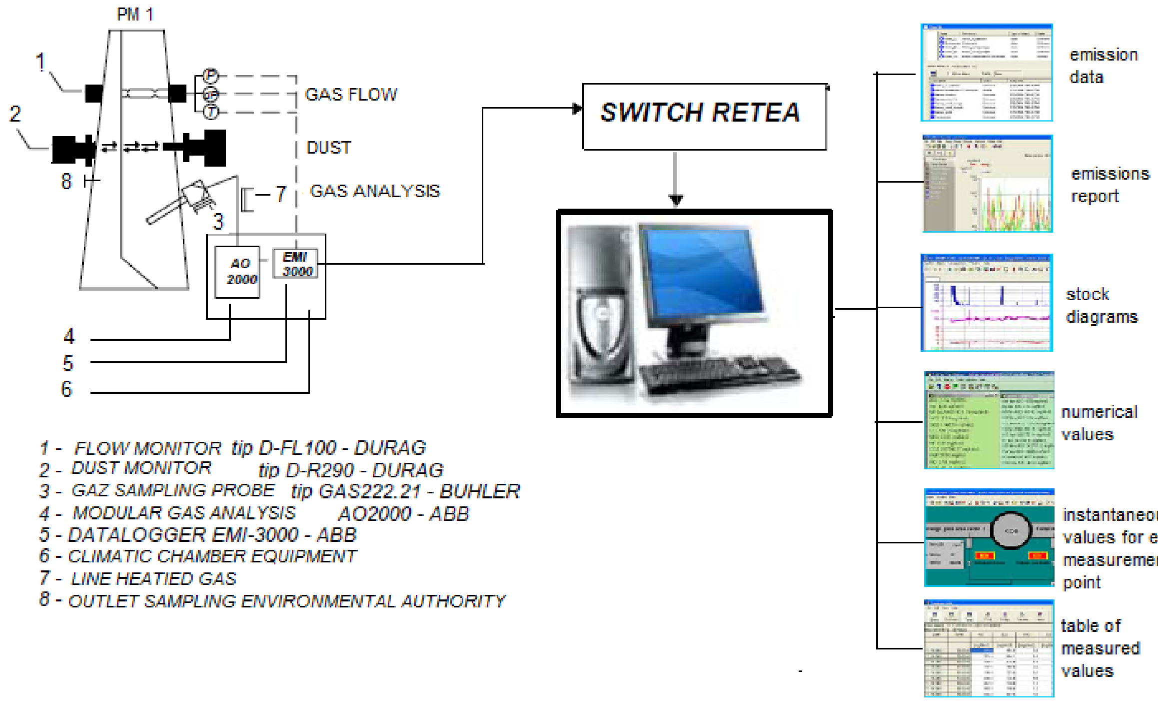

Figure 2: Complete system for emission measurement in a ciment factory[8]

3.1. Measurement of emissions

They are used in general at industrial sources that emit at a fixed point (evacuation chimney). Because they require complex equipment and it is expensive, they are only used in big industrial units.The measurements must be made using standards from the European Comittee for Standardization (CEN). If CEN standards are not available ISO, national or international standards can be applied.

Measuring points and/or gas sampling for testing should be established in areas where the speed exhaust chimney flue is large enough (recommended > 5 m /s). For circular section geometry standards recommend the following scheme of figures 3.1 and 3.2. And the geometry of the section of rectangular figure 3.3, the area is delimited in a number of areas equal to the dimensions of the chimney [3].

3.2. Determination of emissions through balance

It is based on the principle of matter conservation. The emissions of certain substances like Sulpher, Chlorine, heavy metals etc., can be determined by a balance [4] :

The equation for the balance is:

$$\sum A = \sum B + \sum C \tag{1}$$

where:

A - pollution entries as prime materials and fuel;

B - pollution as part of a finished product or waste;

C - pollution emission in the atmosphere and waste water.

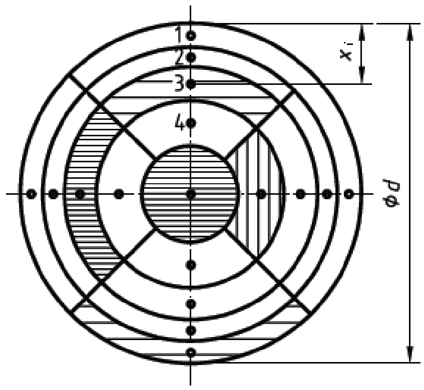

Figure 3.1. - Arrangement of measuring points, circular geometry, the general method

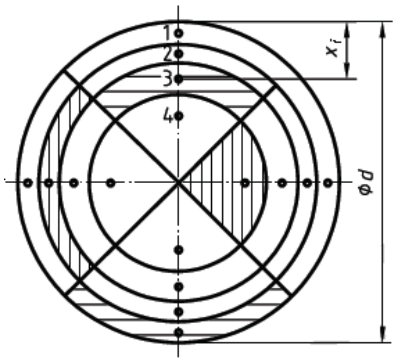

Figure 3.2. - Arrangement of measuring points, circular geometry, the tangential method

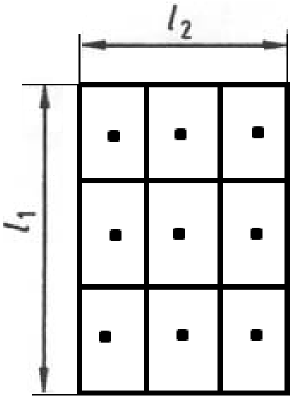

Figure 3.3. - Arrangement of measuring points, rectangular geometry

The determination of the mass of the studied element for different components of the balance is sometimes impeded by technical difficulties of analysis and sampling making applications limited. In practice it is only used for simple cases like emission from a oven or steam generator.

The general form of the relation that enables the calculation of emission:

$$E_{p,f} = Q_C \cdot T_{p,e} \cdot \left(1 - R_p\right) \cdot \frac{M_{p,f}}{M_{p,e}} \tag{2}$$

where:

$E_{p,f}$ [kg/s] – atmosphere emission of the pollution substance p in the f form;

Q_C [kg/s] – fuel flow;

$T_{p,e}$ – p substance share in the fuel p;

R_p - absorption in the installation of the p substance;

$M_{p,f}$ – molar mass of the p substance that enters the atmosphere in the p form;

$M_{p,e}$ – molar mass of the p substance.

The mass balances represents an alternative to direct measurement of air emissions, the method is expensive and difficult. It should be noted that some pollutants require further analysis to determine the portion emitted in the atmosphere as a part of this may be in various physical and chemical conditions (e.g., ash) are not released into the atmosphere.

The advantage of the method is based on mass balance, it is easy to realise, has low cost and doesn's need complex measurements. Most of the data required by the method is ready available from other processes that take place in every industrial unit on a daily basis. A major disadvantage of the mass balance is the low precision of the results because of the errors in measurement.

3.3. Emission determination through corelations

The method establishes a relation between the quantity of the emission in the atmosphere and the specific parameters of the analised procedure. The advantage of the method comes from the fact that these parameters are determined to lead the procedure and do not give birth to other supplementary costs.

To establish this relationship long and costly preliminary measurements are required for a viable statistically result.Periodical checks are required for the validation of the correlation. The method is limited by :

- initial investment , usually high;
- work conditions, frequently fluctuate and raise the cost of the solution;
- modelling of the emissions which is not possible.

3.4 Emission determination based on characteristic emission factors

The method utilises a preestablished function in accordance to the emission of a given substance and the variables descriptive of the source considered a given source. The method doesn’t differ much from the corellation method, the relationships are available only the data being necessary. The emission factors are used based on a hypotesis that all industrial units with the same production lines have the same emission structure. This method requires knowledge of the data on the activity in question, expressed in fuel consumption, production etc. It is widely used due to low cost, simplicity and in some cases lack of alternatives.

The emission factors are elaborated by organisations or government agencies (US EPA, EPA Australia, American Petroleum Institute – API etc.) or internaţional agencies (EMEP/EEA, OECD, CONCAWE, World Resources Institute – WRI etc.), and also by the equipment producers. The emission factors are presented as normalised values like: g/GJ, g/kg fuel, kg/t product, etc. according to *„Metodologiei de evaluare operativă a emisilor de SO_2, NO_X and CO_2 the thermal and thermoelectric central”* elaborated by the Strategic Division and Economical Development from CONEL , it presents the method calculation of the emission factor ,noted with e , and represents the efective quantity of pollution evacutated in the environment (atmosphere) , with respect to the heat and the relation [5]:

$$e = \frac{E}{B_{ef} \cdot Q_i^i} \cdot 10^3, \tag{3}$$

where:

E – mass flow of the pollutin entering the atmosphere (g/s);

B_{ef} – effective burned fuel flow;

Q_i^i - inferior heat of the fuel, with reference to the initial mass.

For SO_2 the emission factor is calculated with the relation:

$$e_{SO_2} = \frac{\frac{m_{SO_2}}{m_S} \cdot \frac{S}{100}}{Q_i^i} \cdot (1 - r), \tag{4}$$

where:

e_{SO_2} - emission factor for SO_2 (kg/kJ);

m_{SO_2} - SO_2 molecular mass;

m_S - S molecular mass ;

S – sulphur content of the fuel, determined as a average (%);

Q_i^i - inferior heat of the fuel, with reference to the initial mass.

r – sulphure retainment degree in ash and slag.

Similar to this algorithm the emission factors for the other pollution can be calculated.

The use of method emission characteristics is apparently easy to achieve, but it requires the intervention of experts who possess knowledge of the processes and phenomena studied.

As described above, the level values emission levels of polluting units are measured or estimated values directly into the output bin in the atmosphere. Air quality in the vicinity of these units is determined by the mode dispersion of emissions that can be determined or calculated by theoretical methods.

4. MOTIVATION FOR THE DEVICE

The motives that lead us to conceive the device was the fact that there is a possibility that in the natural environment surrounding the pollution entity the emission cloud to be concentrated in a limited area due to factors that influence the dispersion of the eliminated gases, factors that are variable in time and space.

In order to evaluate the pollution in the vecinity of a cement factory a specialized equipment can be used or a device can be built that is adapted to our needs. The specialized equipment is destined for the professionists in the industrial units but it is not available to residents that want to monitor the air components due to costs.

We have conceived a device that can continously measure the environment in the vecinity of the industrial pollution. It has a low cost making it affordable for residents, it can be mounted in different locations and allows the connection of other sensors for increased measuring capabilities.

The purpose is to realise these measurements for a long time interval and make comparison between the values reported by the entity that emits the pollution and the limits because in some situations (wear of the filtration installations, damage to the installation, start/stop fazes of the technological process) the limits can be exceeded affecting the environment. The continuous measurement methods used at the generation location of the emissions (imposed by the environment authorization) appreciates and registration the pollution quantities then expresses average values at certain time intervals. Besides the main objective of the device, measuring the air quality at certain points (next to industrial pollution) we want to identify the way it spreads geographically horizontally as well as vertical (in case a drone is used or a meteorological balloon). In order to achieve this we managed to create a mobile sistem that allows monitoring and recording continuously of the pollution emissions that exists in certain points in the analysed area.

We wished that the realised equipment is simple, executed with materials that are easy to procure but able to register de pollution emissions in the limits approximated by the authors (starting with the Limit Values, gas dispersion theories and influence factors that act upon the dispersion) to be at the recording place, taking into consideration the Limit Value levels for pollution entities that are in the area.

5. CONCEPT DESCRIPTION AND COMPONENTS

The concept is made from a Raspberry Pi and a Arduino platform capable. The Raspberry Pi platform was chosen due to it’s capabilities similar to a computer, featuring a mouse and keyboard connections, network connection for remote connection, HDMI and memory for a open source operating system (Linux) with the programming made in Python. To increase the sensors connection capabilities a Arduino board was added (figure 4). The Arduino platform collects the data from environment through the sensors and transmits the information to the Raspberry Pi which acts like a server.

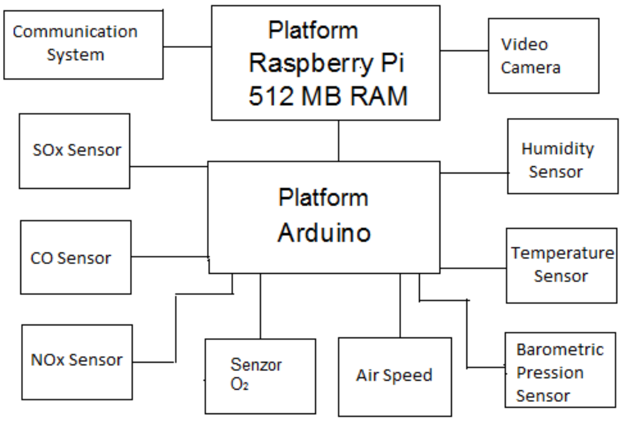

Figure 4: Main set-up for the monitorization system

Components in the main set-up:

- Raspberry Pi 512 Mb, Ethernet, HDMI, USB, ARM processor la 700 MHz for processes the information from the sensors, records and transmits the analysed information;

- Pitot tube for dynamic pressure, component for observation of the air speed, measures the air speed and has the possibility to determine the direction of air flow;

- Barometric pressure sensor MPL3115A2 range between 20 and 110 kPa. needed for the physical parameters of the air;

- Humidity sensor model HIH-4030 Breakout, range between 0 and 100%;

- Temperature sensor - TMP 102 with a range between +25°C and + 85°C;

- CO sensor, MQ -7 range between 20 and 2000 ppm.;

- Sensor Shield V2 for Raspberry Pi;
- NO sensor;
- SO sensor;
- O2 sensor;
- Video camera;
- Communication system – Wi-Fi , internet or 4G;

Starting from the base scheme we have created a beta version recording CO, temperature, humidity, barometric pressure and air speed. Another version will be created by adding the SO_2 and NO_2 sensors. Figure 5 presents the device with the programming tools and the elements of the device.

The next step is to write the code lines for each sensor, figure 6. For the temperature sensor the operation is possible directly on the Raspberry platform, for the other sensors Arduino was used.

Verification of the sensors was realised in a laboratory. For pollution a internal combustion engine was used and for the Pitot tube a fan.

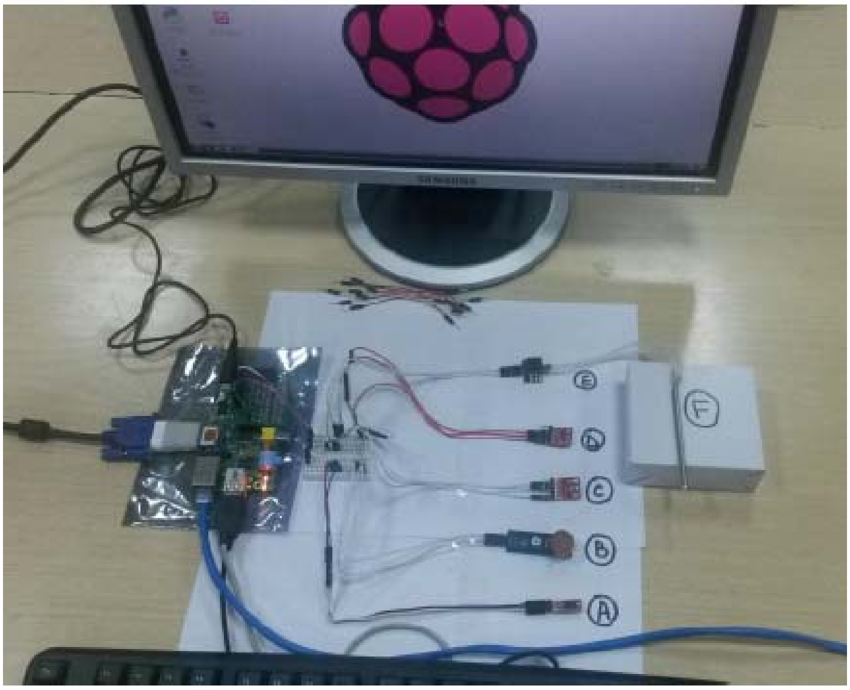

Figure 5: Device with programming components and elements of the device: A-humidity sensor, B-CO sensor, C-barometric pressure sensor; D – temperature sensor; E- pressure sensor; F- Pitot tube.

Figure 6: System programming

The next faze will be calibration with metrological equipment.

The results of the verification device obtained are shown in table 2 and the graph in figure 7. The components will be installed in a enclosure to protect the sensible parts from atmospheric conditions.

Table 2: Presents values registered after laboratory tests.

Time	Temperature	Barometric Pressure	Humidity	Air Speed	CO
minutes	Celsius	kPa	%	m/s	ppm
5	25.24	100.12	68	1.21	22
15	25.26	100.11	68	1.25	24
20	24.85	100.11	68	1.22	22
25	25.22	100.11	68	1.23	26
30	25.12	100.12	68	1.24	28
35	25.42	100.11	68	1.25	25

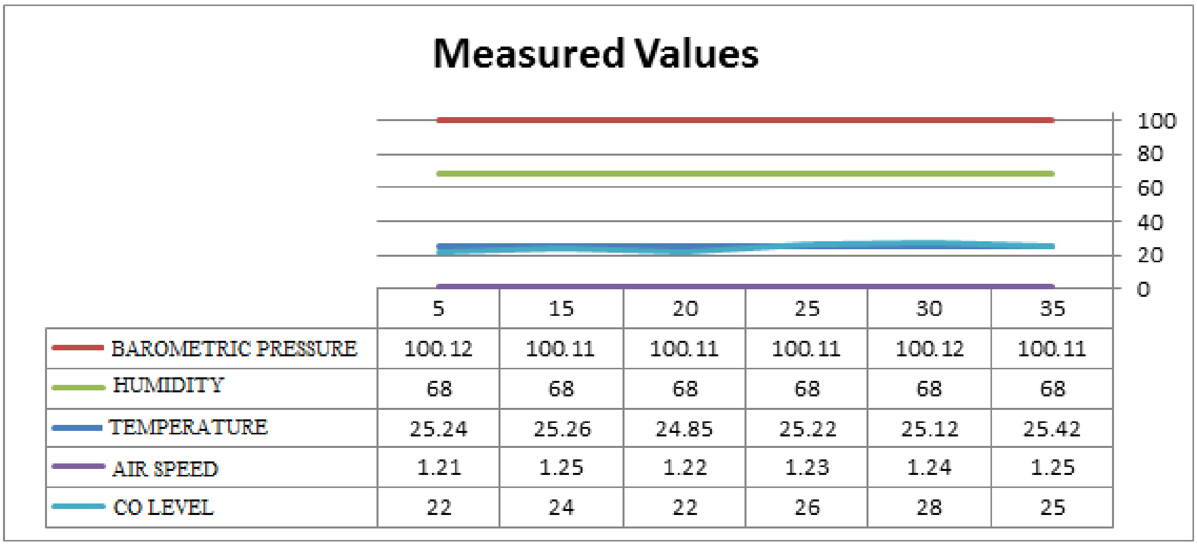

Figure 7: Graph records during laboratory tests

6. CONCLUSION

The device offers the possibility of observing and comparing the levels of pollution in different situations. The continuous monitorization enables the creation of a database with the recorded values which will determine if the Limit Values have been surpassed. The low cost makes it available for the average user and the extended connectivity allows for interconnections between different users so that a map can be created with the data from different devices in different locations.

7. BIBLIOGRAPHY

[1] BAT European Commission (2000) "Integrated Pollution Prevention and Control (IPPC) - Reference Document on Best Available Techniques in the Cement and Lime Manufacturing Industry " [http:// www. Scribed .com/ BAT-industry-the -Processing the cement-Si-Lime.], accessed March 2014

[2] C. Sescu Gal "Theoretical studies to improve monitoring emissions from cement plants" Research Report 2, Technical University for Constructions Bucharest, Faculty of Technological Equipment (Romania), 2014;

[3] "Guidelines for monitoring and self-monitoring of emissions of sulphur dioxide, nitrogen oxides and dust from large combustion plants "[http://mmediu.ro /legislatie/acte_ normative / control _poluarii / ima / Ghid_monitorizare.pdf], accessed April 2014;

[4] "Guidance on how to achieve local emission inventories and national inventory in line with the EMEP / EEA – 2009", Volume I, [http://arpmbuc.anpm.ro/upload/ 59236_Indrumar_VolI-CapI-III.pdf], accessed March 2014;

[5] E. F. Călugăru, "Possibilities for reduction of emissions resulting from combustion of liquid primary methods" PhD Thesis, Polytechnic University of Bucharest (Romania), 2011;

[6] "Guidelines for monitoring of emissions of volatile organic compounds due to the use of organic solvents in certain activities and installations" [www.anpm.ro /docfiles/view/13560], accessed April 2014;

[7] G. Lazaroiu "Modern solutions for air pollution" Agir Publishing, 2006, Bucharest (Romania), [http://www.agir. ro/carte /soluii-moderne-de-depoluare-a-aerului-110255. html], accessed May 2014;

[8] http://www.imatec.ro/uploades/files

[9] http://www.raspberrypi.org/;

[10] https://www.python.org;

[11] https://www.tindie.com/products/tmhrtly/airpi-kit/;

[12] http://www.uugear.com/portfolio/rasberrry-pi-reads-dht11-via-arduino

Effect of the Suspension on Whole Body Vibration: Comparison of High Power Agricultural Tractors

Boban Cvetanović[1*], Miljan Cvetković[1], Dragan Cvetković[2] Miloš Ristić[1]
[1]College of applied technical sciences Niš, Serbia
[2]Faculty of occupational safety, University of Niš, Serbia

The reduction of the whole body vibration (wbv) in agricultural tractor drivers should be done by the suspension of the driver's seat, of the tractor's cab or of the front and rear axles. The seat is a vital part of a tractor and is designed to provide comfort for driver and reduce high vibration levels that are harmful for the drivers. Regardless of the fact that the seat has active or passive suspension, it cannot fully protect the driver, so there should be an additional suspension system between the source of vibrations and the seat. Most of older tractor models, except in the seat and tires, don't have other efficiency suspension system, whereas the manufacturers of modern models constantly develop new solutions and suspension systems.

This paper gives comparative analysis of vibration levels in tractors of new generations, with different suspension systems: suspended front axle & suspended cabin tractor and fully suspended (front & rear axles) tractor. The measurement of vibrations was carried out in real "on-farm" conditions, during ploughing and cultivating.

On the basis of vibration levels at the driver's seat (for all three coordinates, x, y, z) and the period of exposure, the daily exposure of the driver will be calculated and whether the values are within the legal limits will be determined.

Keywords: High power, agriculture tractor, Whole body vibration

1. INTRODUCTION

During their everyday activities, agricultural tractor operators are exposed to many negative influences that have complex and harmful impact on the man. These influences come both from the tractor system (noise, vibrations, exhaust gases, bad ergonomy...) and from the working conditions (precipitation, high relative humidity, dust, agriculture chemicals, high or low temperatures etc.). One of the most important negative factors are vibrations [1]. Namely, during the operations, the entire tractor construction is subject to complex oscillatory processes induced by the combined influences of rough soil and a tractor aggregate and its implements. These high levels of vibrations that arise in such a complex system like the tractor are transferred from the cab floor to the seat and on to the whole body of the driver. Vibrations can have high values and unfavourable frequencies imposing great risk to the driver's health. Numerous scientific studies, bio-dynamic models and present knowledge of human body show that prolonged exposure to high-level vibrations can lead to low-back injuries, digestive system illnesses and cardio-vascular problems [2].

Some studies show that about 9% of all world's tractors, during 8-hour working time, are exposed to vibrations above exposure limit value (ELV), while in case of longer working time that percentage increases to 27%. As many as 95% of all tractor drivers during 8-hour working time are exposed to levels above exposure action value (EAV) [4].

In the reduction of the vibrations, the suspension of the tractor in the combination with the driver's seat plays the most important part. In older generations of tractors, the vibration reduction was done with the tires, the driver's seat and a simple suspension on the front axle, because the tractor manufacturers considered good quality suspension too difficult and too expensive.

Today, there are three types of tractor construction when it comes to suspensions [3]:

- suspended cabin tractor,
- suspended front axle & suspended cabin tractor
- fully suspended (front & rear axles) tractor.

During the 1970's many tractor manufacturer (Ford, John Deere, Massey Ferguson…) were developed tractor cab suspension system, but only Renault (now Claas) in 1987 developed and offered the Hydrostable cabin suspension system with four coil-over-damper suspensions at each cabin corner. There was the first, mass-produced tractor cab suspension system and is the most numerous in use. Today every tractor manufacturer either offers some form of cab suspension system, or is in the process of developing a system to meet perceived market demand. New Holland offers a Comfort Ride system where the front of the cab is on rubber-metal mounts and the rear cab corners are suspended on coil-over-damper suspensions over the rear axle [3,5].

During the 1980's many tractor manufacturer viewed tractor axle suspension as a complex design challenge of dubious economic benefit. The majority of system provided suspension of the tractor front axle only. Provision of rear axle suspension was considerably more complex tasks. Only JCB, towards the end of the 80's, launched the Fastrac, a front and rear axle suspended chassis. Over a two decade on, with an unchanged basic design and a range comprising six models, JCB can justly claim the Fastrac to be the most successful fully suspended agricultural tractor produced to date [6] (figure 1).

*Corresponding author: Nikole Uzunovića 55, Niš, boban.cvetanovic@vtsnis.edu.rs

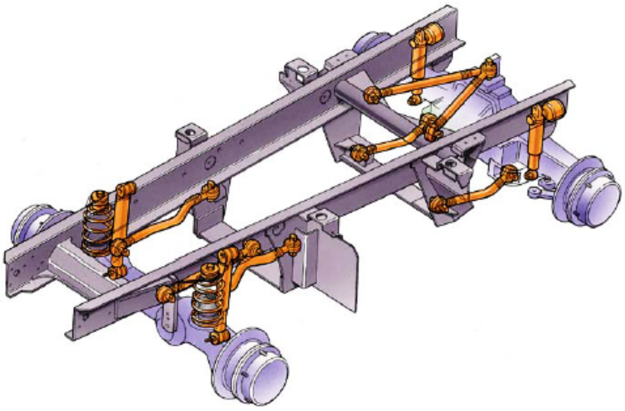

Figure 1: JCB Fastrac chassis and suspension system

Other tractor manufacturers (New Holland and John Deere) didn't develop fully suspended vehicle, but they developed optional front axle suspension and cab suspension systems which proved satisfactory on the market and can be considered a standard tractor suspension system in Europe today (figure 2)

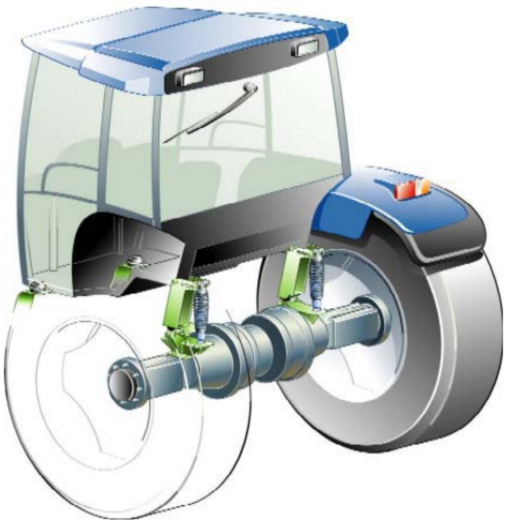

Figure 2. New Holland Series TM tractor 'Comfort Ride' cab suspension system

The system utilizes self-leveling air-over-oil (hydropneumatic) suspension elements, powered by the tractor hydraulic system and providing both springing and damping functions.

This paper will give the comparison of two suspension types of well-known manufacturers (*New Holland and JCB*) with respect to measured whole body vibration levels during various agricultural operations. An important aspect of measuring will be the estimation of driver's exposure to whole body vibration during referent eight-hour period, based on the previously measured values for shorter referent periods.

2. THE METHOD OF MEASUREMENT

The measurement of vibrations was carried out in real (on-farm) conditions, during several standard agricultural activities and two suspension types were compared:

(a) suspended front axle & cab suspended (at rear only) - New Holland TM 165 (figure 3)

Figure 3. New Holland TM 165

(b) suspended front & rear axles - JCB Fastract 3185 (figure 4)

Figure 4. JCB Fastract 3185

Some characteristics of the tractors are given in Table 1.

Table 1: Some characteristics of tractors

Tractor	Power	Engine type	Weight
New Holland TM 165	123kW (165hp)	New Holland turbocharged diesel liquid cooled	6556kg
JCB Fastract 3185	140kW (188hp)	Cummins 6BTA, intercooled turbodiesel 6-cylinder	6765kg

A summary of test tractor suspension seat specifications is given in Table 2

Table 2: Tractor suspension seat details

Tractor	Seat model	Suspension type		
		Z-axis	X-axis	Y-axis
New Holland TM 165	Sears SA 15748	Air spring (adj.) + damper (adj.)	Mech. spring (fixed) + damper (adj.)	None
JCB Fastract 3185	Grammer MSG95 A/721	Air spring (adj.) + damper (fixed)	Mech. spring (fixed) + damper (adj.)	None

"adj." = adjustable rate or pre-load: "fixed" = fixed rate: "Mech." = mechanical

The tractors performed their everyday regular agricultural activities (ploughing and cultivating) whose lengths were different, but the drivers' level of daily exposure to vibrations A(8) was measured for a referent 8-hour period.

Previous studies offer different indicators of the load upon the operator, and when the agricultural tractor operators are considered the most frequent standards are determined by ISO-2631 [7], depending on the level of vertical accelerations, their frequency and the period of exposure to those accelerations. In measuring and evaluating the impact of vibrations on operators, relevant standards define acceleration as a measurement and evaluation parameter corrected with frequency-weighting function.

Measuring of acceleration was carried out in such way that a tractor operator was sitting on his seat with an accelerometer, performing his everyday activities. The vibration measurement was carried out at the driver seat (figure 5).

Figure 5. Tractor wbv measurement instrumentation

As a measuring device a Brüel & Kjær type 4447 human vibration analyzer was used, with a type 4524-B acceleratometer built in a Seat Pad type 4515-B-002. The vibration levels were measured in three orthogonal measuring directions: z-direction (vertical), x-direction (afterward) and y-direction (sideward) (figure 6).

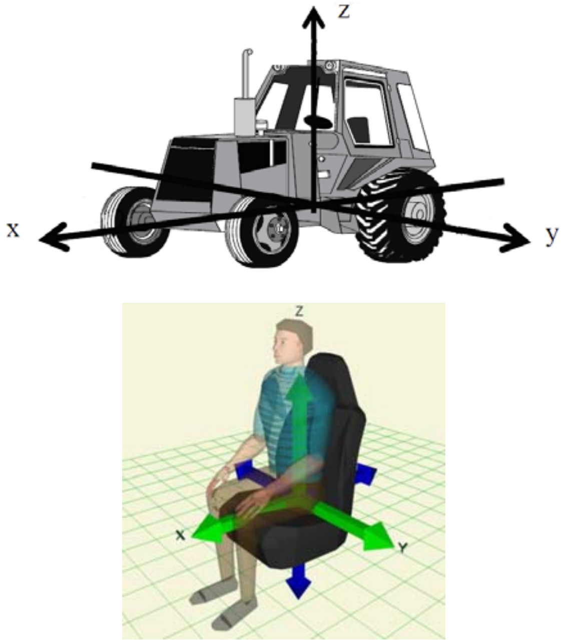

Figure 6. Defining of orthogonal measuring directions on the tractor and the operator

The level of vibrations expressed as RMS or effective value (root-mean-square) is equal to average acceleration, measured at the seat over the period of time during which the operator performing his task was sitting. Equivalent value of acceleration (Aeq) is a constant value of acceleration that has the energy value over some period of time T equal to the effective value of acceleration.

The obtained values were compared to maximal permitted values that are, in EU, regulated with the Directive 2002/44/EC [8]. Republic of Serbia incorporated the Directive 2002/44/EC into its legal framework. In case of daily exposure to whole body vibrations it specifies exposure limit value (ELV) of 1,15 m/s^2 which must not be exceeded in professional working conditions and exposure action value (EAV) of 0,5m/s^2, in case of which employers must control the risks coming from vibrations.

3. RESULTS

During the measurements, the RMS (root mean square) acceleration values for all three axes for New Holland were (table 3):

Table 3. RMS values for New Holland

Task	Duration [hr:min]	Average RMS (Aeq) acceleration [m/s^2]			
		X	Y	Z	Aeq
Ploughing	3.25	0.58	0.86	0.47	**0.86**
Cultivating	4.45	0.45	0.67	0.31	**0.67**

k- factor included in input values

Time history of weighted RMS seat accelerations (Y-axis) and running average of RMS acceleration (Aeq) (Y-axis) for tractor New Holland and cultivating are shown on figure 7.

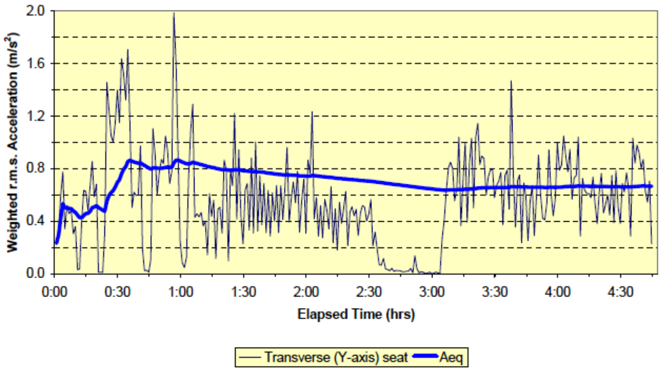

Figure 7. RMS seat accelerations (Y-axis) and Aeq (Y-axis) - New Holland (cultivating)

The RMS acceleration values for all three axes for JCB were (table 4):

Table 4. RMS values for JCB

Task	Duration [hr:min]	Average RMS (Aeq) acceleration [m/s²]			
		X	Y	Z	Aeq
Ploughing	4.00	0.54	0.93	0.33	**0.93**
Cultivating	4.00	0.89	1.39	0.63	**1.39**

k- factor included in input values

Time history of weighted RMS seat accelerations (Y-axis) and running average of RMS acceleration (Aeq) (Y-axis) for tractor JCB and ploughing are shown on figure 8.

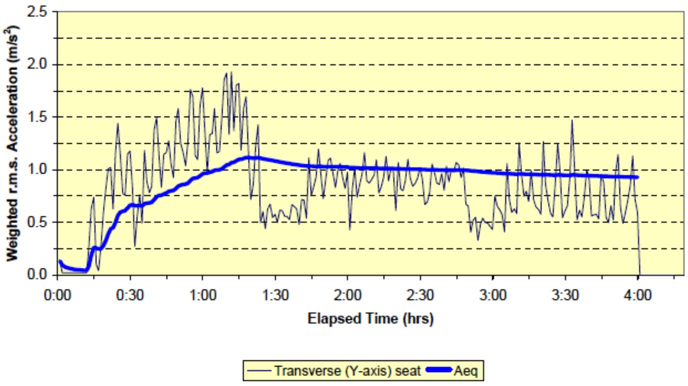

Figure 8. RMS seat accelerations (Y-axis) and Aeq (Y-axis) - JCB (ploughing)

Considering the durations of measurements it was necessary to establish daily values of exposure of the driver for 8-hour reference time A(8), which is usually the duration of one shift, in order to make comparison to legally permitted values.

The values of Aeq in Table 3. and Table 4. (bold) show what the daily value of exposure of the driver would have been, if he had spent 8 hours of his shift, operating with the tractor, without any interruptions, with the values of acceleration obtained during measuring.

The values of daily exposure A(8) in Table 5. and Table 6. (bold) show what the daily value of exposure of the driver would have been, if he had spent less time than eight hours operating with the tractor (eg 3:25hr, 4:45hr or 4hr) and the rest of the time performing some other activities not related to driving or having breaks during the shift.

Table 5. Daily exposure levels - New Holland

Task	*A(8) [m/s²]*	*Time to EAV [hr]*	*Time to ELV [hr]*
Ploughing	**0.55**	2.7	14.3
Cultivating	**0.52**	4.45	23.5

Table 6. Daily exposure levels – JCB

Task	*A(8) [m/s²]*	*Time to EAV [hr]*	*Time to ELV [hr]*
Ploughing	**0.66**	2.3	12.22
Cultivating	**0.98**	1.04	5.46

In order to calculate daily values of exposure for different periods of exposure, appropriate free software for calculating daily values of exposure A(8) for given periods is available (figure 9).

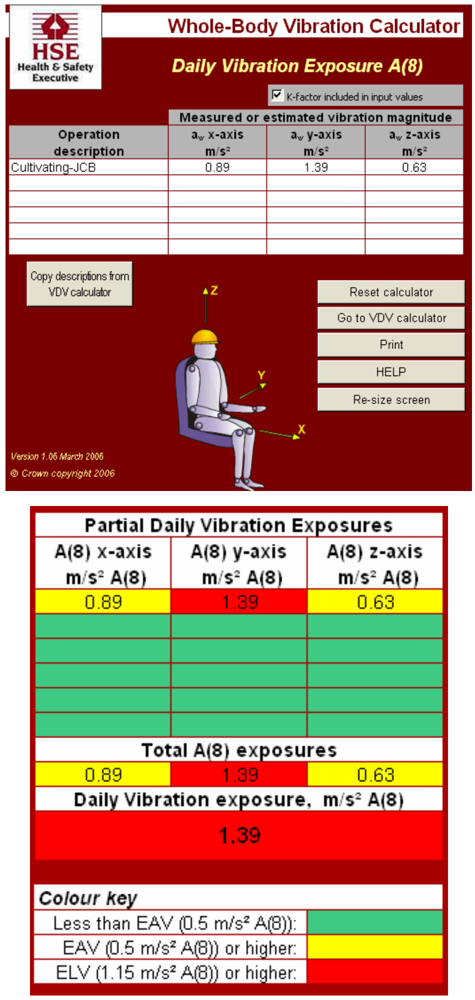

Figure 9.Wholy body vibration calculator

4. DISCUSSION

Both tractors (both suspension types) had highest vibration levels along Y axe (transverse). The reason for that is in the tractor suspension seat. Both tractors were fitted with scissor linkage – type suspension seats embodying air spring / hydraulic damper vertical (Z) suspension system and also all seats embodied limited longitudinal (X) axis mechanical spring and hydraulic damper suspension. In (Y) axis they didn't have any suspension type.

The comparison of calculated values to permitted exposure values regulated in Directive EC 2002/44 (action value EAV=0.5m/s^2 and limit value ELV=1.15m/s^2) shows that in case of New Holland EAV was exceeded in ploughing operation while in the case of cultivation operation daily exposure is near EAV. In case of JCB tractor, EAV was exceeded for both agriculture operation.

In these measurements the type of agricultural activity didn't have too much affect on the values of vibrations at the driver seat. However, time to EAV, in all operations, is below eight hours, which means that the drivers, in case of full working day (8 hours min.), will certainly be exposed to negative impact of whole body vibration.

5. CONCLUSION

According to calculated daily exposure levels to whole body vibration, for both tractors and for two different operations, it can be concluded that with respect to vibration reduction front axle & cab suspension system is more efficient than front & rear axles suspension system. However, it must be mentioned that vehicle whole body vibration emission levels are dependent not only upon vehicle design and the presence of vibration reduction features (e.g. suspended seats, cabs & axles), but also upon operating surface, forward speed and personal driving technique. Therefore, it cannot be simply concluded that fully suspended tractor always has higher vibration levels. To draw this conclusion, larger number of vehicles should be tested, with identical organizational and technical conditions, which is difficult to do in practice.

Also, we should know that vehicle whole body vibration emission levels are dependent not only upon vehicle design and the presence of vibration reduction features (e.g. suspended seats, cabs & axles), but also upon operating surface, forward speed and personal driving technique.

In tractors of older generations without suspension system or with primitive system, the situation with respect to driver's exposure to whole body vibration is worrying. Even in modern tractors with developed suspension systems, the vibration levels during work are relatively high. It seems that tractor manufacturers still don't consider protecting drivers from whole body vibration, having in mind the improvements achieved in other aspects (power, torque, transmission, electronic devices, etc.).

REFERENCES

[1] P. Servadio, A. Marsili, N. P. Belfiore, "Analysis of driving seat vibrations in high forward speed tractors", Biosystems Engineering 97 (2007) 171-180.

[2] R.M. Stayner, "Whole-body vibration and shock: A literature review" RMS Vibration Test Laboratory for the Health and Safety Executive, Ludlow (England), (2001)

[3] A.J. Scarlett, J.S. Price, D.A. Semple, R.M. Stayner, "Whole-body vibration on agricultural vehicles: evaluation of emission and estimated exposure levels", Silsoe Research Institute and RMS Vibration Test Laboratory for the Health and Safety Executive, (England) (2005)

[4] A.J. Scarlett, J.S. Price, R.M. Stayner, "Whole – body vibration: Evaluation of emission and exposure levels arising from agricultural tractors", Journal of Terramechanics. 44 (2007) 65-73.

[5] A.J. Scarlett, J.S. Price, R.M. Stayner, "Whole-body vibration: Initial evaluation of emissions originating from modern agricultural tractors", Silsoe Research Institute and RMS Vibration Test Laboratory for the Health and Safety Executive, (England) (2002)

[6] A. Marsili, L. Ragni, G. Santor, P. Servadio, G. Vassalini, "Innovative System to reduce Vibrations on Agriculture Tractors: Comparative Analysis of Acceleration transmitted through the Driving Seat", Biosystems Engineering. 81 (1) (2002) 35-47.

[7] ISO standard 2631 – 1 (1997) "Mechanical vibration and shock – Evaluation of human exposure to whole body vibration. Part 1: General Requirements".

[8] European Parliament and the Council of the European Union: Directive 2002/44/EC on the minimum health and safety requirements regarding the exposure of workers to the risks arising from physical agents (vibration), 2002., Official Journal of the European Communities, OJ l 177,13.

Investigation and Reduction of Noise Generated by Heavy Traffic in Urban Environment

Vasile Bacria[1], Nicolae Herisanu[1]
[1]Faculty of Mechanical Engineering, "Politehnica" University of Timisoara, Timisoara (Romania)

An important contribution to the noise from urban environment has the road traffic, which could include heavy traffic, especially if the ring road is not available. The noise generated by heavy road traffic is unfortunately present in the city of Timisoara and affects the life, comfort and healthy of citizens. Taking account of these unpleasant effects, we have investigated the noise generated by heavy traffic identifying the main characteristics, propagation ways, noxious effects and some means to mitigation. The paper presents the results of these investigations performed in Timisoara city.

Keywords: Noise investigation, Heavy road traffic

1. INTRODUCTION

Urban roads are permanently used by an important number of vehicles which generate noise and vibrations that affect the life, comfort and health of citizens. Among these vehicles, we often find heavy vehicles passing through the city, especially when there are not available facilities and alternatives to avoid urban roads. In these circumstances, heavy vehicles have an important contribution to generating noise and vibration pollution.

Taking into account the unpleasant effects of this pollution, there exist major concerns in developing comprehensive investigations aiming at diminishing noise and vibration levels which habitants are exposed to. In this line, Romania, which is a member of EU, should satisfy the requirements of European regulations in this matter and this is the starting point of our investigations. We have developed an investigation of the noise generated by heavy vehicles passing through the city of Timisoara identifying main factors which influence the noise level, propagation of the noise and its noxious effects.

In this paper we present the results of measurements performed and a corresponding analysis. In order to reduce the noise generated by heavy vehicles in the city of Timisoara, some mitigation methods were established and implemented, followed by an assessment of the obtained effects.

2. DECISIVE FACTORS IN NOISE GENERATION

The noise generated by heavy vehicles in urban environment is characterized by specific levels of acoustic pressure, frequency spectra and their variation in time.

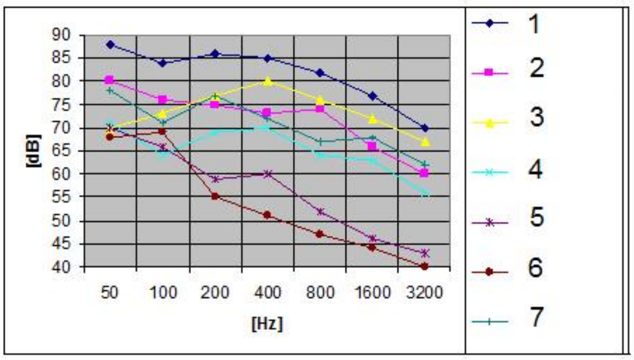

Figure 1: Characteristic spectra of different vehicles

Generally, it is known that the sources of noise from heavy vehicles (trucks, buses, trolleybuses, tractors) have a low and partly middle-frequency character, as it can be seen in fig.1 [3], where 1 – denotes the spectra of trucks with Diesel engine, 2 – trucks with gasoline engine, 4 – buses, 6 - trolleybuses.

The noise generated by heavy vehicles participating in urban road traffic is originated in the working of the engine, transmission system, brake system, air resistance or rolling. The noise sources depend on the type of heavy vehicle. More specific, in the case of buses, the most important sources are the engine, transmission elements, gases exhausting and even the passengers' discussions. In the case of trucks important noise sources are the engine, the transmission system, gases exhausting, the cooling fan and rolling on road.

The global noise generated by the vehicles in the urban environment depends on the intensity and composition of traffic, on the presence of heavy vehicles and on the speed of displacement, as well.

An increasing of the noise generated by heavy vehicles is due to unconformity generated by improper maintenance, nonstandard gases exhaust system or bad bake systems.

An important contribution to the noise generated by heavy vehicles has the nature and condition of the superstructure of the road. Emission of noise due to heavy vehicles in urban road is residential areas depends on their position beside the roads as well as on the nature of the propagation environment.

3. PROPAGATION WAYS AND NOXIOUS EFFECTS

The noise generated by heavy vehicles participating to the road traffic propagates in the environment as spherical and cylindrical waves, and at long distance, the propagation is realised as plane waves. In the case of the propagation of perturbations as spherical waves in an elastic homogeneous and isotropic environment, the acoustic pressure in a point from the acoustic field has the expression [4]

$$p = \rho_0 \omega \frac{A}{r} sin(\omega t - kr + \alpha) \qquad (1)$$

where r is the radial coordinate, A is the spherical wave's amplitude having the frequency f=ω/2π, which propagates

*Corresponding author: Bd.Mihai Viteazu,1, 300222 Timisoara, Romania, nicolae.herisanu@upt.ro

from the source with the speed c and k= ω/c is the wave number.

In case of perturbations which are transmitted as cylindrical waves which propagates uniformly, the acoustic pressure can be written as [4]

$$p = A[J_0(kr) + iY_0(kr)]e^{-i\omega t} \quad (2)$$

where r is the cylindrical coordinate, A is a constant, J_0 is the Bessel function of the first grade and zero order and Y_0 is Bessel-Newman function of second grade and zero order.

Taking into account the variation of functions J_0 and Y_0 in terms of the distance from the perturbation source, in the proximity of the source the expression (2) becomes

$$p = i\left(\frac{2A}{\pi}\right)ln(kr)e^{-i\omega t} \quad (3)$$

and at long distance from the source

$$p = A\sqrt{\frac{2}{\pi kr}}e^{i[k(r-ct)-\pi/4]} \quad (3')$$

In the same way, considering that the perturbation propagates as plane waves and taking into account only the case of divergent waves, the acoustic pressure in a point of the acoustic field has the expression [4]

$$p = \rho_0 \omega A \sin(\omega t - kr + \varphi) \quad (4)$$

Propagation of spherical, cylindrical and plane waves is characterised by the variation of the acoustic pressure in a point of the acoustic field. The acoustic pressure in a point of the field is obtained by addition of the acoustic pressures corresponding to each type of wave.

In a point of the acoustic field, the level of acoustic pressure is given by

$$L = 20\,lg\frac{p}{p_0} \quad (5)$$

where p is the acoustic pressure in a point of the acoustic field and $p_0=2\bullet10^{-5}$ [N/m^2] is the reference acoustic pressure.

Using the acoustic pressure one can compute the level of acoustic pressure defined by Eq. (5) and the equivalent noise level corresponding to an equivalent intensity which would be constant during a period of time T, defined by the expression

$$L_{Aeq,T} = 10lg\left[\frac{1}{t_2 - t_1}\int_{t_1}^{t_2}\frac{p_A^2}{p_0^2}dt\right] \quad (6)$$

where L_{Aeq} is the A-weighted continuous equivalent noise level, measured in dB, determined in a time interval which starts at t_1 and ends at t_2, p_0 is the reference acoustic pressure and $p_A(t)$ is the A-weighted instantaneous acoustic pressure.

The equivalent noise level can be obtained by computations based on Eq. (6) or, directly by measurements using an integrating sound level meter such as the Bruel & Kjaer 2250, which allows measuring and recording of the most important characteristic parameters of the noise, as well as a spectral analysis in 1/1 or 1/3 octave bands and a statistical distribution of the noise level.

The noise generated by heavy vehicles participating to the road traffic in urban environment is very detrimental for human's nervous system, generating psycho-physiological problems, blood circulation modifications and sleep disturbances. Moreover, noise exposure could affect the visual function, endocrine gland, lowers the auditory performances, generating sonorous trauma.

In order to reduce the noxious effects of the noise on human being, there are established limit values, which cannot be exceeded. These limits are characterised by the equivalent noise level defined by Eq. (6) and the noise-rating curves (C_z), which define the relation between the characteristic frequency of the noise and the level of acoustic pressure corresponding to an equivalent subjective sensitivity.

In this subject, the Romanian standard STAS 10009-88 "Urban acoustics" states the admissible limits of the urban noise level for different categories of streets, zones and functional facilities.

In case of the noise levels generated by vehicles on urban roads, to which also heavy vehicles have an important contribution, the admissible limits are presented in Table 1. Moreover, the placement of buildings on streets which belong to different technical categories and also the organization of road traffic should be done so that to assure the admissible limit of the exterior noise level on streets, which is established to 50 dB (measured at 2 meters distance from the building) and the noise curve C_z45, respectively.

Table 1: Admissible noise levels

Type of streets (STAS 10144-80)	L_{eq} [dB]	C_z [dB]	L_{10} [dB]
I-magisterial	75-85	70-80	85-95
II-linking	70	65	80
III-collecting	65	60	75
IV-local serve	60	55	70

4. REDUCING THE NOISE GENERATED BY HEAVY VEHICLES

Often it is found that the equivalent noise level and the noise curves admissible in urban environment are exceeded due to road traffic which involves the presence of heavy vehicles, so that the admissible values presented in Table 1 are exceeded. In this case, specific measures intended to noise decreasing should be established and implemented.

Noise mitigation measures should take into account that the noise can be reduced through active measures applied directly on the source or through passive methods applied on the propagation way. Moreover, the disposition of roads should be considered. In this respect, traffic restrictions could be adopted concerning traffic composition and speed of displacement.

The way in which we can achieve a mitigation of the noise levels by reducing the number of trucks in terms of traffic intensity can be observed in fig.2 [5].

The corrections which can be achieved to the noise levels in terms of truck concentration for different speeds of displacement can be estimated using the diagrams presented in fig.3 [5].

The way in which the reduction of the speed of displacement for cars and heavy vehicles leads to a reduction of the noise level by 4-5 dB can be observed in fig.4 [5].

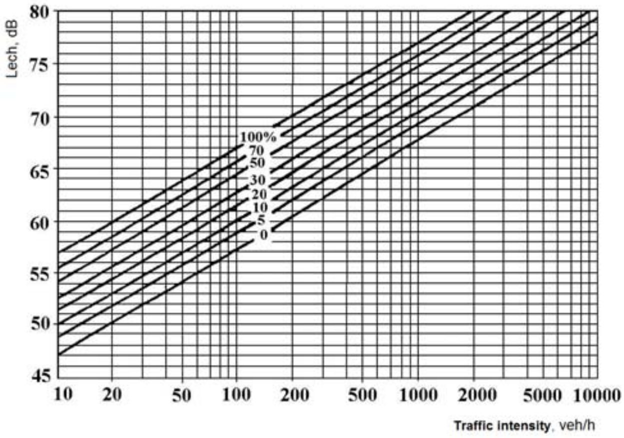

Figure 2: Noise levels generated by trucks [5]

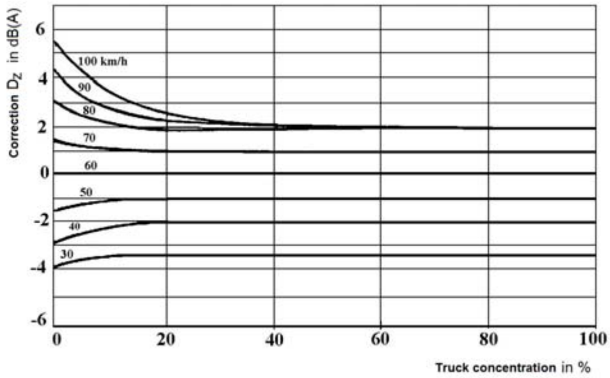

Figure 3: Corrections to the noise levels in terms of trucks concentration [5]

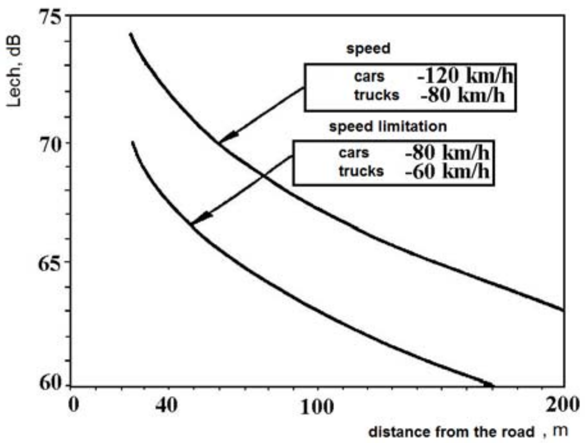

Figure 4: Reducing the noise levels by reducing the speed of displacement [5]

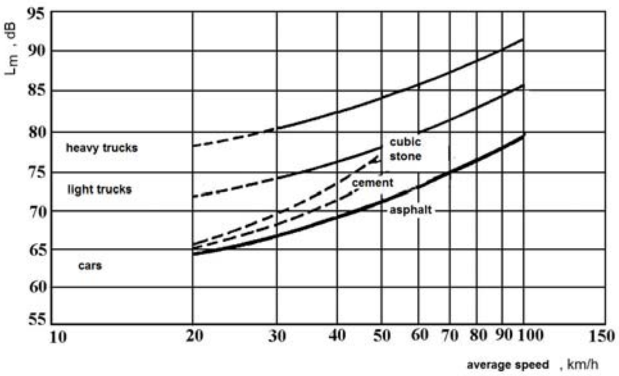

Figure 5: The influence of the nature of road superstructure on the noise levels generated by trucks [5]

It is known that the noise levels generated by heavy vehicles greatly depend on the rotational speed of their engine. This dependence is deeply analysed in [5].

An important reduction of the noise could be achieved by improving the quality of the road superstructure. In fig. 5 [5] can be observed the variation of the noise generated by trucks in terms of the speed and nature of the road superstructure.

As it is known, more than 70% of the traffic noise is originated at the contact between the tire and the road surface. In the actual stage of development of more silent vehicles, the tire/road interaction is the main source of noise to vehicles in normal driving conditions. Mitigation of noise level generated by the tire/road contact can be achieved by replacing regular asphalt with rubberized asphalt having better sound absorption properties. This kind of road superstructure ensures an attenuation of the noise level from 1 dB up to 6 dB, depending on the speed of displacement, the most significant attenuation arising in the frequency bands having the central frequency 1 kHz and 2 kHz. It was proved that sound absorption properties of rubberized asphalt are increasing at high speeds of displacements [9].

In order to protect residential areas against noise generated by heavy vehicles passing through urban roads one can employ natural sound barriers or artificial screens and sound barriers placed on the propagation way of acoustic waves. To obtain efficient attenuation values it is necessary that the dimension of these obstacles be a multiple of wavelength, even for low perturbing frequencies. The attenuation realised by a noise barrier depends on the height H, the wavelength λ of the perturbing noise, the distance R between barrier and the source S and the distance D between the barrier and the recipient O of the noise, as well as the distances above the ground for the source S and receiver O (fig.6).

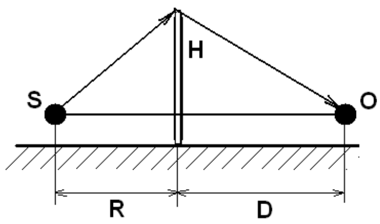

Figure 6: Noise barrier scheme

Considering the hypothesis that the source S and the recipient O are found at the same height above the ground, the attenuation ΔL realised by a noise barrier having the length very large comparing to the wavelength of the sound has the expression [1]:

$$\Delta L = 10 lg\, 20 \frac{2\left\{R\sqrt{1+\left(\frac{H}{R}\right)^2}-1\right\}+D\left\{\sqrt{1+\left(\frac{H}{D}\right)^2}-1\right\}}{\lambda\left[1+\left(\frac{H}{2}\right)^2\right]} \tag{7}$$

It was found that in general, a noise barrier having a high of 1.5-3 m above the source of noise and receiver, which is placed at 3-6 m from the source and receiver lead to achieving an attenuation of 5-10 dB in the case of low frequencies and 15-25 dB in case of high ones.

The efficiency of the barriers increases along with increasing their height and reducing the distance between the screen and the source or receiver. In case of less height screens, the obtained attenuation decreases along with increasing these distances. The attenuation of the noise obtained by using protection screens depends in general also on the heights from the ground of the noise source and receiver. In practical applications it is indicated to mention as exactly as possible the height of the noise source and when choosing the height H of the screen, the position of the perturbing source should be taken into account. Consequently, in the case of the noise due to heavy machinery participating in the road traffic, it will be taken into account that the noise generated by the tire/road contact is born at the level of the road, the noise due to the engine arises at 0.9-1.5 m height from the ground and the noise generated by the exhausting system of a truck at 2.1-2.4 m height.

Noise barriers design will be made avoiding the presence of other reflecting surfaces which could reflect the noise above or around the barrier reducing in this way its efficiency. It is recommended to be made of materials which are penetrable by sound with specific mass not less than 50 km/m^2.

Green zones consisting of trees, bushes, other vegetation with leaves, as well as the areas covered by grass contributes to an attenuation of the noise which depends on the dimensions of these zones [1].

The propagation of the noise through green zones is determined with the following expressions [3]:

- for a single-point source

$$L_n = L_7 - 20lg\frac{r_n}{r_7} - 1.5Z - \beta\sum_{i=1}^{Z} B_m \tag{8}$$

- for an array of sources in case $r_n \le s/2$

$$L_n = L_7 - 10lg\frac{r_n}{r_7} - 1.5Z - \beta\sum_{i=1}^{Z} B_m \tag{9}$$

- for an array of sources in case $r_n > s/2$

$$L_n = L_7 - 20\left(k\,lg\frac{0.55}{r_7} + lg\sqrt{\frac{r_n}{0.5s}} - \right. \\ \left. - 1.5Z - \beta\sum_{i=1}^{Z} B_m \right. \tag{10}$$

where L_n is the level of noise near a building located at distance r_n from the road for array sources having the distance s between them, L_7 is the level of noise measured at the distance r_7=7.5 m from the axis of the road, k is a coefficient whose value is known, β is the specific absorption of the acoustic energy realised by vegetation, B_m is the length of the green zone and Z is the number of elements compounding the green zone. The distance s for the traffic fluxes is given by the expression [3]

$$s = 1000\frac{v_{tr}}{N} \tag{11}$$

where v_{tr} is the speed of displacement and N is the traffic intensity.

However, it should be taken into account that attenuations due to green zones are not equally available in all four seasons.

Taking into account the effects of artificial screens and green zones on the noise attenuation, these facilities can be used for acoustical arrangement of urban environment in Timisoara city, especially on the penetration roads where the traffic intensity is high and many heavy vehicles are present in traffic composition. It is known that 20.000 vehicles are traversing each day Timisoara city and 6.000 of them are heavy trucks.

In many places, where the architecture permits, solid walls can be mounted in order to create a noise barrier which attenuates the noise. Having in view the desired attenuation, one can compute the necessary height of the wall and the optimal material to be used.

However, the acoustic field generated by transportation means is very complex and hence it is recommended to be experimentally assessed.

5. ACOUSTIC MEASUREMENTS AND ANALYSIS OF RESULTS

Measurements of the main characteristic parameters of the noise have been performed in 62 points located near some of the most important crossings from Timisoara city where a large number of heavy vehicles was involved [8], [10].

Measurements have been conducted using noise analysers which allowed recording of the main parameters of the noise: the equivalent noise level L_{eq}, exposure level L_{AE}, maximum noise level L_{max}, minimum noise level L_{min}, percent noise levels $L_{0.1}$, L_5, L_{10}, L_{50}, L_{90}, L_{95}, which were continuously recorded during a 8-hours period of time (7.30-15.30). During measurements, the microphone was mounted at the border of the road, at 7.5 m from the axis of the first runway, at 1.3 m height from the ground. Simultaneously, the composition and intensity of the road traffic were determined, as well as the speed of displacement.

The results of noise measurements as well as the intensity and composition of the urban traffic were used to develop a data base concerned with the study of phonic pollution generated by transportation means in Timisoara city.

The participation of heavy vehicles to the urban traffic recorded in the considered 62 points of measurement is illustrated in Table 2. Besides heavy vehicles, in the urban traffic participated cars, microbuses and motorcycles, and the intensity of the traffic raised up to 2681 vehicles per hour.

Table 2: Participation of heavy vehicles to road traffic

Transportation means	Minimum %	Maximum %
Autobuses	0.03	3.78
Trolleybuses	0.1	7.8
Trucks	0.3	17.9
Tractors	0.01	1.3

The distribution of noise and percentage of disturbed people in the considered 62 measurement points can be observed in Table 3.

Analysing the obtained results one can conclude that in 46 for the 62 points, which means 74.19% of them, the noise level exceeds the limits established by the Romanian standard STAS 10009-88 concerning "Urban acoustics".

Table 3: Distribution of noise and percentage of disturbing people

L_{eq} [dB]	Number of points	% of disturbed people
{53.4}	1	8
[55;60]	0	0
[60.3;64.6]	6	[25;41]
[65.2;70]	20	[42;60]
[70.1;74.9]	24	[60.1;79.9]
[75.1;79.5]	8	[80.1;97.9]
{81.8}	1	100
[85.5;85.9]	2	100

The limits were exceeded with an amount ranging from 0.1 up to 16.1 dB. Moreover, in the measured points, the equivalent noise level measures at 2 meters distance from the buildings, which should be maximum 50 dB, was generally exceeded with 1.3-32.9 dB. In was proved that heavy vehicles have an important contribution to these high noise levels.

6. MEASURES FOR NOISE MITIGATION

In order to reduce the noise generated by heavy machines on the urban roads from Timisoara city, there were established and implemented some decreasing measures, such as building up a ring road for the North-Est part of the town, restricting the access of some vehicles in some urban zones, improving the state and nature of the superstructure of the most part of the roads, improving the organization of crossings and introducing the “one way” traffic on many streets, introducing limitations of the speed of displacement, improving the infrastructure and superstructure of tramway, improving the traffic flows, introducing more silent buses and trolleybuses by replacing the old ones, using green noise barriers between the roads and residential areas.

In order to evaluate the effect of implementation of these noise decreasing measures, new measurements were performed in 9 points chosen near some of the most important crossings where heavy vehicles were significantly involved.

From the obtained data, we can conclude that in these 9 points, the equivalent noise level was reduced with 0.1-9.4 dB and in 5 points, which means 55.5% of them the noise level is below the admitted limit. The average noise level for the considered 9 points was 72.02 dB(A) for an average traffic intensity of 1595.6 veh/h before the implementation of noise decreasing measures while it decreases to 67.84 dB(A) for an average traffic intensity of 1712,8 veh/h after the implementation of established measures.

In what concerns the average noise level at 2 meters distance from the buildings, this was 65.6 dB(A) before and 62.7 after the implementation of noise decreasing measures. The percentage of the heavy vehicles present in the road traffic in the considered 9 points changed from 17.9 % to 11.7%.

Analysing the obtained results it is observed that in the actual stage of implementation of noise decreasing measures regarding heavy vehicles, it was obtained a reduction of the noise, but the limits mentioned in STAS 10009-88 are still exceeded. In this situation, supplementary methods intended to decrease the noise generated by heavy traffic should be designed and implemented. Therefore, new efforts should be directed to finalizing a ring road around the town (not only on the Nord-Est part), building up improved traffic nodes, applying a layer of rubberized asphalt on the most important penetration roads, extending the presence of acoustic screens between the roads and residential areas, and especially near hospitals, schools and universities, extending the rehabilitation of urban roads, designing new roads, conservation and expansion of green areas with noise attenuation effects, encouraging and sustaining thermo-acoustical rehabilitation of old buildings, rehabilitation of Bega naval channel in order to ensure a better valorisation of navy traffic and transportation, replacing the old public transportation means with a newer, more silent generation, building up some modern parking places, development of new runways for bikes, etc.

Therefore, finalizing the complete ring road will lead to diminishing the traffic intensity in urban area, excluding in this way from the urban traffic composition the most of heavy vehicles, characterized by a high level of phonic pollution. This will lead to a reduction of the noise level up to 3-4 dB in the urban area.

Replacing the regular asphalt with rubberized asphalt on the main routes will contribute to the reduction of noise level generated by vehicles participating in the urban traffic with 1-6 dB, depending on the speed of displacement [9].

In what concerns mounting acoustic screens between the urban roads and residential areas, the design and placement of screens will be made depending on the attenuation which is desired. From functional and aesthetical reasons, it would be recommendable to cover these screens with noise-absorbing materials and climbing plants whose leafs have attenuating and reflecting properties. These screens would be more efficient for high frequency domain producing a reduction of 15-18 dB to the noise level.

Developing a green zone between urban roads and buildings will contribute to a supplementary reduction of 2-3 dB at the receiver place, simultaneously improving aesthetical and ecological conditions.

For the areas where the emissions of the noise sources cannot be satisfactorily controlled and acoustic protections cannot be applied between roads and buildings (situation which is often encountered in Timisoara city), the thermo-acoustical rehabilitation of buildings should be resorted to, which would be recommendable to improve acoustical comfort of habitants. This treatment should produce an attenuation of minimum 38 dB for L_{Aeq}<60-70 dB, or 44 dB for L_{Aeq}>60-70.

In the same way, the others mentioned measures will significantly contribute to reducing the noise in the urban area, depending on its characteristics.

7. CONCLUSIONS

Identification of noise sources characteristic for heavy vehicle and measuring its noise level generated in road traffic besides the noise generated by other categories of vehicles allowed characterization of the level of noise pollution produced by transportation means in Timisoara city.

In order to reduce the phonic pollution and to diminish the percentage of disturbing people in Timisoara city there were established and implemented some adequate methods to reduce the noise.

The efficiency of implemented measures was proved by measurements. These decreasing methods can be applied in any practical situation concerning the noise generated by traffic or industrial noise.

Aligning to European regulations implies the implementation of the Directive 2002/49/EC concerning the management of the noise in the environment, which implies the realization of noise mapping and a permanent motorization of the noise in real conditions by real measurements.

REFERENCES

[1] M. Grumazescu, A. Stan, N. Wegener, V. Marinescu, "Combaterea zgomotului si vibratiilor", Ed. Tehnica, Bucuresti (Romania), (1964)

[2] A. Stan, et al. "Consideratii asupra nivelului intensitatii zgomotului in exteriorul cladirilor din zona central si semicentrala a municipiului Bucuresti", Constructii, Vol.10, (1973)

[3] E.Ia. Iudin, "Izolarea impotriva zgomotului", Ed. Tehnica, Bucuresti (Romania), (1968)

[4] N. Enescu, I. Magheti, M.A. Sarbu, "Acustica tehnica", Ed. ICPE, Bucuresti (Romania), (1988)

[5] *** Stadtbauliche Larmfibel. Hinweise fur die Bauleitplanung, Baden Wurtemberg, Innenministerium, (Germany), (1991)

[6] *** Larmbekamfung in Wien, Enwicklung Stand Tendenzen, Magistratsabteilung 22, Umweltschutz, (Austria), (1991)

[7] Directive 2002/49/EC, European Parliament and European Council, (2002)

[8] N. Herişanu, V. Bacria, M. Toader, S. Popa Radovan, „Investigation of noise pollution in an urban area", WSEAS Trans. on Syst, Vol. 7, p.1648, (2006)

[9] N. Herişanu, V. Bacria, „The effects of rubberized asphalt on decreasing the phonic pollution", Appl. Mech. Mater, Vol.430, p.257, (2013)

[10] V.Bacria, M.Toader, N.Herişanu, C.Oprişescu, V.Ciupa, C.Fiat, „Consideration concerning noise attenuation in urban environment", Proceedings of the IX-th Symposium „Acoustics and Vibration of Mechanical Structures-AVMS 2007", Timişoara (Romania), 24-25 May 2007, pp.7-12 (2007)

[11] V.Bacria, N.Herisanu, "Acoustical arrangement of the road superstructure", Proceedings of VII International Conference "Heavy Machinery HM 2011", Vrnjačka Banja (Serbia), 29 June-2 July 2011, pp. 1-6, (2011)

Reconstruction of Warehouse System in Pharmaceutical Industry

Dusan Petrovic[1], Ugljesa Bugaric[1*], Zoran Petrovic[2]
[1]Faculty of Mechanical Engineering Belgrade, Industrial Engineering Department, University of Belgrade, Belgrade (Serbia)
[2]Tecon sistem d.o.o., Belgrade (Serbia)

The paper presents the way how reconstruction of existing warehouse system in pharmaceutical industry was done. The main goal of reconstruction was increasing of storage capacity and design of new material handling system. New designed warehouse system introduces rack pallet system and adequate material handling devices. In this way technological function parameters of warehouse system are improved.

Keywords: Warehouse, Material handling, Reconstruction

1. INTRODUCTION

Whole area of the factory for drug production is located near town Kovin in lowland part of Serbia. Factory area is surrounded by agricultural land. Within factory area, shown on Figure 1, warehouse is situated in the south part near by access roads and gates. This factory warehouse will be analysed in this paper. [1]

Physically factory warehouse system is situated in two separate buildings mutually connected with corridor (objects 1 and 2 on Figure 1). Warehouse buildings are the same with dimensions 48×13×6.35 m (L×W×H). The existing warehouse is connected with production facilities by internal roads.

The main focus of the study presented in this paper is reconstruction of existing warehouse system and design of new material flow in warehouse system. Main goals of reconstruction were to: enlarge storage capacity by introducing rack pallet system and to select appropriate material handling and storage devices.

Side goal of warehouse reconstruction was to design system for monitoring, gathering, processing and archiving temperature and humidity of data. Due to geographical position of warehouse, region meteorological characteristic, construction and technical characteristic of objects as well as specific properties of stored goods, continuous monitoring and observance of temperature and humidity (microclimate) in required limits within whole warehouse system is necessary during the whole year. For optimal observance of microclimate parameters in warehouse system, it is necessary to install sensors for temperature and humidity monitoring on several places within warehouse system - characteristic spots. [2]

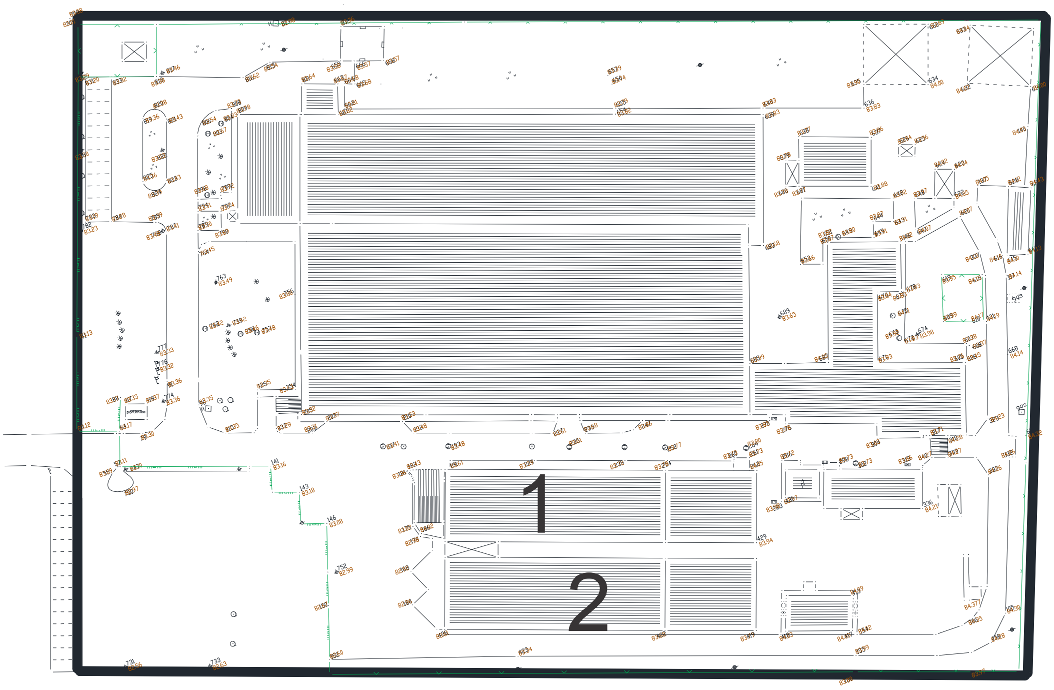

Figure 1: Factory layout

*Corresponding author: Faculty of Mechanical Engineering Belgrade, Kraljice Marije 16, 11120 Belgrade 35, Serbia; ubugaric@mas.bg.ac.rs

2. EXISTING SITUATION

Goods that are stored in factory warehouse system are: raw materials, final goods, packaging, auxiliary material characteristic for pharmaceutical industry.

Raw materials, auxiliary material and packaging are transported to warehouse system (factory), using means of road transport (trucks, lorry). Dimensions and types of packaging of those goods are different (standard and non-standard) and they are stored in original delivery packaging (packed by producer). Delivery of goods is in one shift.

Production in the pharmaceutical factory is performed in the production facilities situated next to warehouse system. The production is organised in two shifts, when needed even on Saturdays and Sundays). Production outcome of final goods per months is not uniform.

Delivery of final goods to warehouse system is done from daily production buffers by forklift trucks in one shift.

Raw material and existing assortment of final goods requires storage temperature in interval of 10°C÷20°C and humidity in interval of 0÷50% during the whole year.

2.1. Size and Orientation

Pages should have A4 (210x297 mm) format and portrait orientation. Top and bottom margins of the page should be 2 cm, while inside and outside borders should be 1.5 cm.

3. NEW WAREHOUSE TECHNOLOGY DESIGN

On the basis of: available storage space, optimal number of pallet places, analysis of goods which are to be stored and goods technological properties warehouse system is organized as: [1]

Part 1 (object 1) – raw material warehouse, which is designed for keeping bulk raw materials and auxiliary materials. Also in this object, quarantine for raw material as well as private custom warehouse is situated. Goods in this part of warehouse system are stored in racks.

Part 1 (object 1) consists of three technological parts. The capacities of technological parts are:

- 480 pallet places – for powder raw materials and auxiliary materials,
- 24 pallet places – raw materials quarantine,
- 72 pallet places – private custom storage, and
- 110 shelf places – separate part with extra entrance used mainly for spare parts.

Part 2 (object 2) - final goods warehouse, is designed for keeping final goods and packaging in racks. Some of goods in this part of warehouse system are packed in metal containers and crates and are stored on the floor - block system.

Capacity of the factory warehouse system is 1312 pallet places in racks and 56 places in block system.

Part 2 (object 2) also consists of three technological parts. The capacities of technological parts are:

- 512 pallet places – for final goods storage,
- 104 pallet places – for sample storage,
- 120 pallet places – for elastomer storage in racks, and
- 56 block places – for elastomer storage in block.

Receiving - shipping area (object 1) is equipped with twin I/O roll doors and inclining ramp as a connection with outdoor transport roads. This part is designed as I/O for people and transport devices. Beside this area there is a passage - connection between object 1 and 2 used by people and transport devices.

All technological parts in the warehouse system are connected with adequate transport paths which fulfils technical requests of chosen transport devices.

Acceptance, manipulation, storage of pallets in the warehouse together with order picking and distribution of final goods pallets is done by electric fork lift trucks and hand pallet trucks.

Racks in the whole warehouse system (object 1 and 2) consist of modules which can accept two or three euro pallets (1200×800×145 mm) per module, with four levels in height. Maximal load of one pallet place is 1000 kg. Layout and look of racks in warehouse are shown on Figures 2a, 2b and 2c. Technical dimensions of racks and rack modules are shown on Figure 3. Basic rack module of length 2700 mm, can accept three standard pallets (1200× 800 mm) or two non-standard pallets, while basic rack module of length 1800 mm, can accept two standard pallets (1200×800 mm) or one non-standard pallet. [3]

All double racks are equipped with protection poles and protection metal plate between them. Single racks are protected only with angular metal poles. Protection is placed in front of all racks towards the main transport path.

All double racks are equipped, up to the third level, with metal stops which prevent pallet shearing from horizontal beam. Fourth level on all racks is equipped with metal mesh deck which prevent possible drop of pallets, pallets shearing and pallet break. All metal mesh decks on fourth level have the same load capacity as horizontal beams i.e. 1000 kg per pallet place.

The rack which is designed for raw materials quarantine is equipped with metal wired doors. Purpose of those doors is to enable access to raw materials in quarantine only to authorised persons.

According to new designed solution Part 1 (object 1) of warehouse system is equipped with six four level height double racks with capacity of 20 pallet places per level. Racks consist of four modules with three pallet places and four modules with two pallet places. These racks are used for storage of powder raw materials, auxiliary and packaging materials. For raw materials quarantine one four level height single rack with eight pallet places per level is designed. Rack consists of two modules with three pallet places and one module with two pallet places. This rack is equipped with metal wired door, painted in red colour, which can be locked.

Private custom storage, situated in Object 1, is equipped with two single four level height racks with capacity of 9 pallet places per level. Racks consist of three modules with three pallets. Private custom storage is placed in separate in room with two passing through doors.

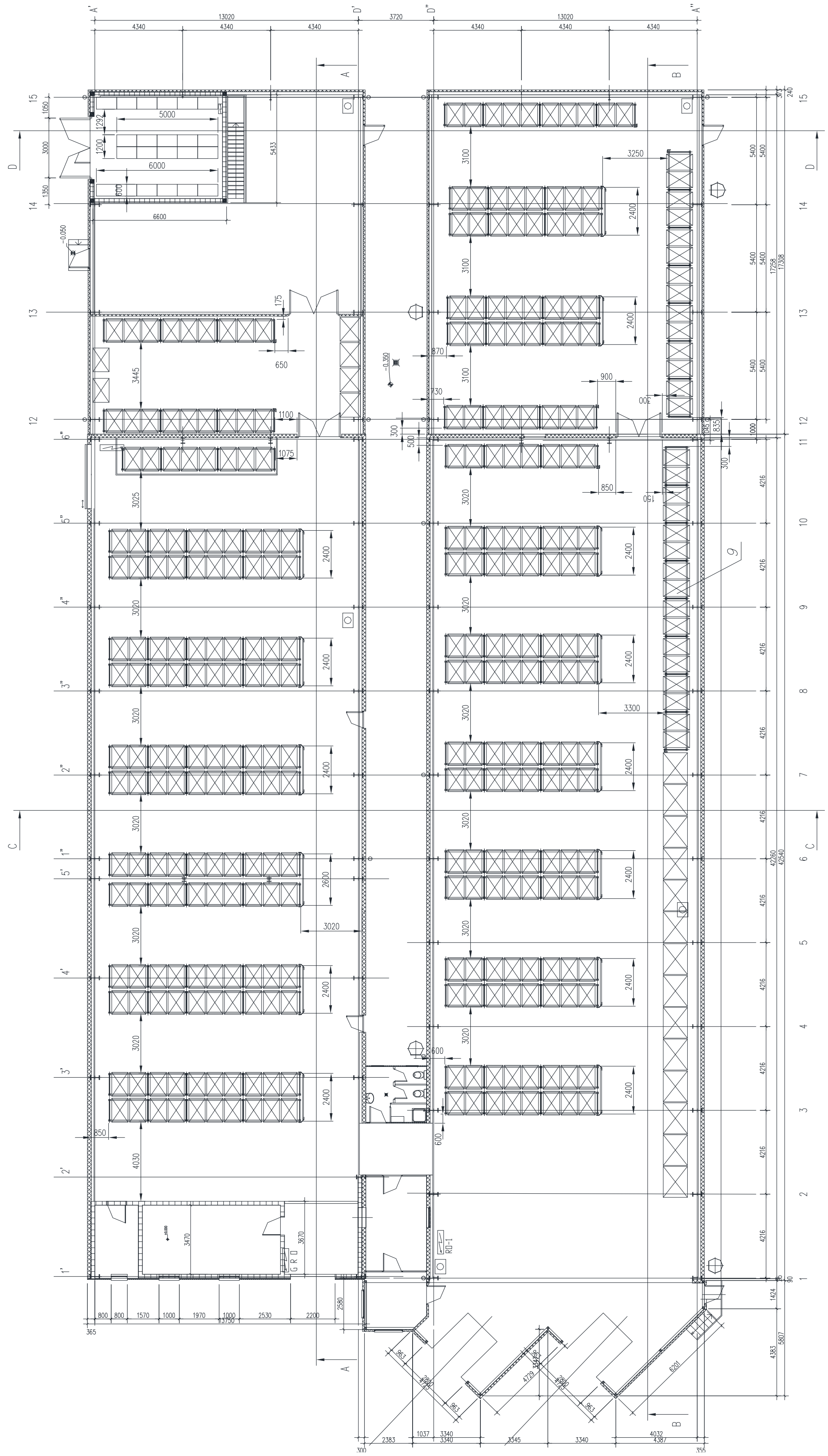

Figure 2a: Warehouse layout

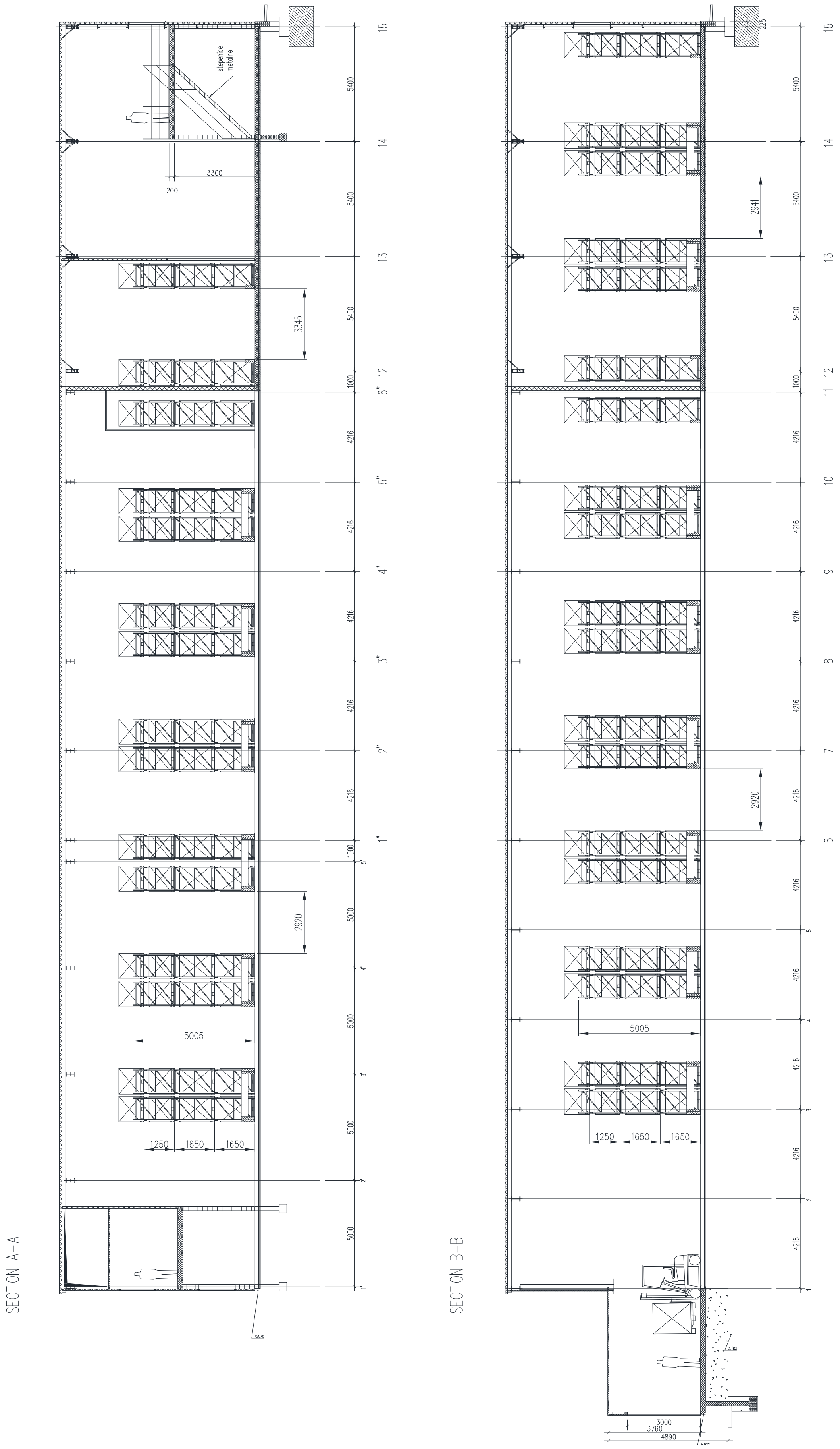

Figure 2b: Warehouse layout - Sections A-A & B-B

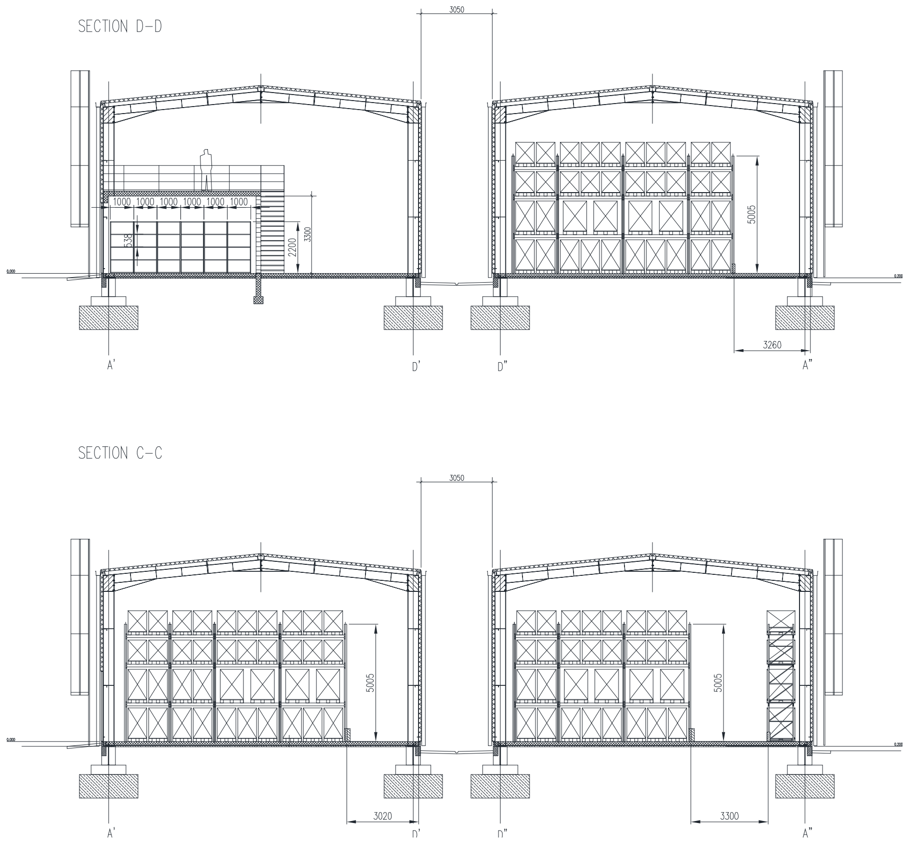

Figure 2c: Warehouse layout - Sections C-C & D-D

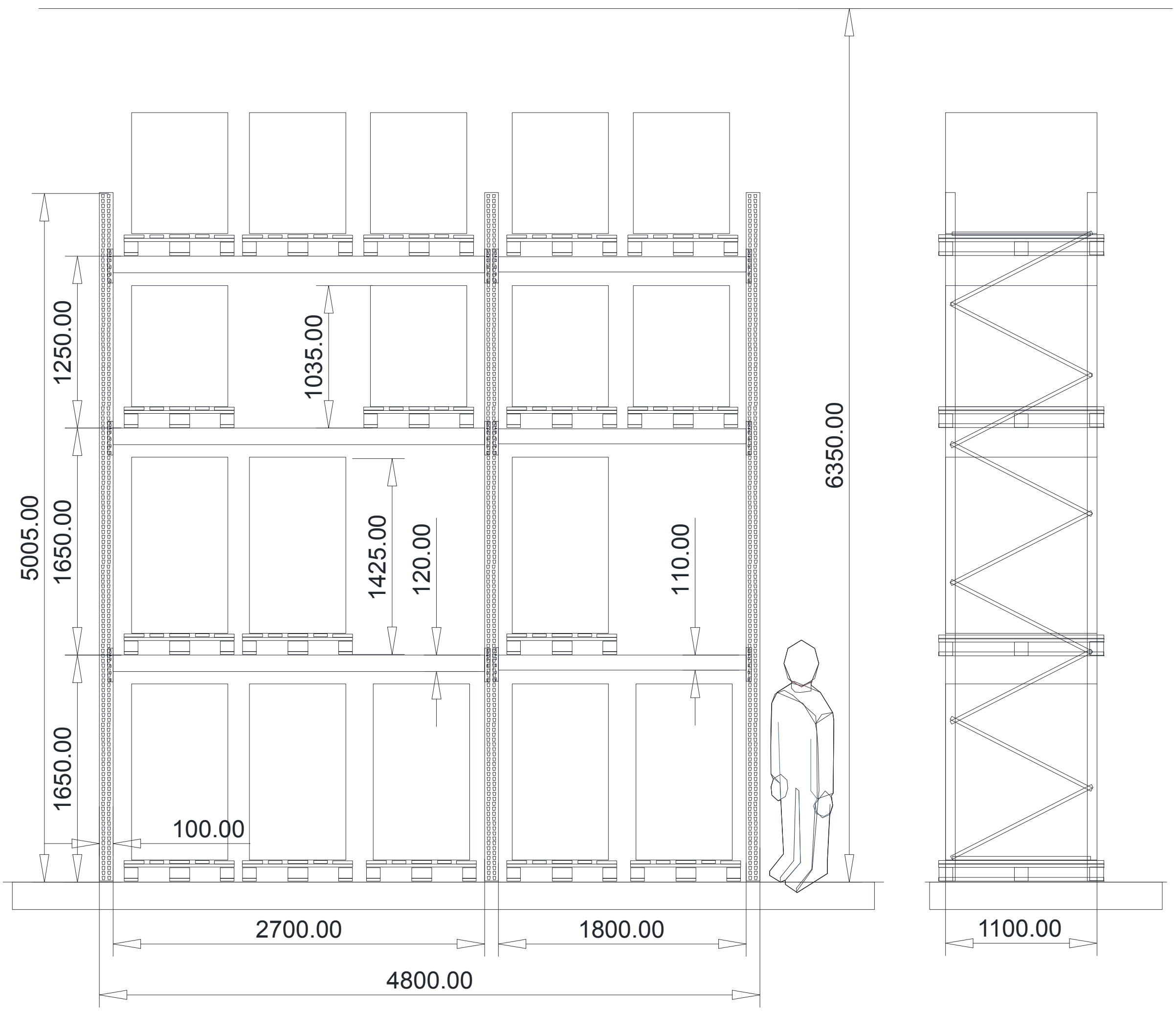

Figure 3: Dimensions of racks and modules

Separate part of the warehouse which has extra outside entrance is located at the corner of Object 1. It is equipped with shelf racks. In this separate part there are two single shelf racks with six modules which dimensions are 1000×600 mm (L×W) and load capacity 100 kg per module, with total shelf rack height of 2200 mm. In this part of warehouse there is also one double shelf rack with ten modules which dimensions are 1000×600 mm (L×W) and load capacity 100 kg per module, with total shelf rack height of 2200 mm. Shelf racks are used for storage of spare parts and small consumable material.

According to new designed solution in Part 2 (object 2) of warehouse system two loading bays with industrial doors, dock levellers and dock shelters are predicted. Lading bays are used for acceptance of raw materials and shipment of final goods.

In Part 2 (Object 2) of warehouse system on the right side near to passage - connection between object 1 and 2 there is area for fork lift battery charger, while on the left side towards the loading bays there is a stretch wrap packing machine installed.

Technological equipment in Part 2 (Object 2) of warehouse system consists of eight four level height double racks with capacity of 16 pallet places per level. Racks consist of four modules with three pallet places and two modules with two pallet places. These racks are used for storage of final goods and production samples.

This part also contains five single racks. Two four level height single rack with two modules with three pallet places and one module with two pallet places are used for storage of final goods. One four level height single rack with two modules with three pallet places and two modules with two pallet places is used for sample storage.

One four level height single rack with seven modules with two pallet places and one four level height single rack with eight modules with two pallet places are used for storage of elastomer packed on non-standard pallets.

4. CONCLUSION

The reconstruction of existing warehouse system and design of new material flow system in the warehouse was accomplished by introducing rack pallet system with appropriate material handling and storage devices. New designed rack pallet system, increased storage capacity i.e. number of pallets that can be stored in the warehouse system. Introduced new material handling devices (side fork lift trucks, loading bays etc.) enabled quicker and safer pallet manipulation in the warehouse system. Applied design solutions leads to better technological function parameters of warehouse system such as: simplest and shortest transport paths in warehouse, shorter fork lift truck cycle time, faster loading/unloading of pallets etc.

Also, original solution for observance of microclimate parameters (temperature and humidity) is developed and implemented in the warehouse system.

REFERENCES

[1] U. Bugaric, Z. Petrovic and D. Petrovic, "Main technological project - warehouse for raw materials and final goods", Tecon sistem d.o.o., Belgrade (Serbia), (2012)

[2] Z. Petrovic, U. Bugaric and D. Petrovic, "System for automatic gathering of temperature and humidity data in warehouse systems", Proceedings of V International Conference "The International Conference on Manufacturing Engineering - ICMEN 2014", Thessaloniki (Greece), 01 - 03 October 2014, (2014)

[3] U. Bugaric and D. Petrovic, "Modelling of servicing systems", Faculty of Mechanical Engineering Belgrade, Belgrade (Serbia), (2011)

Perspective or Airline Development, the Case of "Konstantin Veliki" Airport Niš

Vojislav Tomić [1*], Goran Petrović [1], Danijel Marković[1], Miloš Madić[1], Goran Marković[2]
[1]Faculty of Mechanical Engineering, University of Nis, Nis (Serbia)
[2]Faculty of Mechanical Engineering, University of Kragujevac, Kraljevo (Serbia)

Development of a new airline companies within the airport, represents a paper that examines possibilities for launching a regional airline in the southern part of Serbia. Selecting the optimal location for a new regional airline companies is one of the most important decisions of a company's management. In order to simplify the decision making process, in the first part of the paper a detailed analysis of airline market is given within Serbia and the Balkan Peninsula. In order to objectively analyze the level of locations' competence, in the second part of the paper the mathematical method of multi-criteria evauluation, Analytical Hierarchical Processes (AHP method), is used. Using AHP method has helped to evaluate and correlate potential locations based on many relevant criteria. The results obtained by mult-criteria evaluation clearly show that this method of location selection for new airline companies within airports is successful and applicable.

Keywords: Airline companies, location selection, multi-criteria decisions

1. INTRODUCTION

Air industry has had an impressive increment in recent years and this trend is still present in the distribution of people and goods. The distribution is supported by a significantly sustainable presence of global integrated logistic networks [1] and rapid progress of e-trade [2], while Air Company's (airlines) represent a link in the distribution process between macro and micro distribution. The development of the first flying objects, dirigibles, zeppelins, planes, and later jets, will result in changing traveling habits in the whole world who daily continues to change, and final results and possibilities are not discernible [3], [4].

In the past 40 years the volume of air travel has expanded tenfold and air freight has grown by a factor of fourteen. The world's economies have grown three to four times over the same period. Air transport has been one of the world's fastest growing economic sectors. Today, air centers for transporting goods and people represent one of the most important elements of the logistic system. Without these centers realization of the goods-flow in the urban national and international environments would be impossible to imagine. Among the different modes of transport, air transport has experienced the fastest growth. However, it must overcome the problem of its infrastructures becoming saturated. The European Union is therefore committed to modernising and adapting the infrastructure to increasing passenger flows, whilst also improving their rights and safety. In order to do this, the Union is working to implement the Single European Sky. Aviation provides the only rapid worldwide transportation network in Europe, which makes it essential for global business and tourism. Air transport is fundamental to European mobility, prosperity and political cohesion and essential to our daily life. Each year, million of passengers use the services of European airlines. Air transport plays a crucial role in the integration of an enlarged Europe, supplying essential links between Europe's regions and with the rest of the world.

On the territory of the Republic of Serbia there are about thirty airlines which through operating meet specific needs of the market, and make profit in the area of goods and people transport. Most famous airlines are stationary mostly by Nikola Tesla airport in Belgrade. Nikola Tesla plays vital role in facilitating economic growth of the Republic of Serbia. Among airlines on the territory of the Republic of Serbia there are some of the largest world airlines, such as "Turkish Airlines", "Air France", "Lufthansa", etc. Among airlines operating on the territory of the Republic of Serbia there is "JAT Airways", recently changed to "Air Serbia", as the only domestic airline beside "Aviogeneks" which deals with seasonal charter flights. Number of airlines in the Republic of Serbia is enough to understand the potentials and needs of the market which has ideal geographic position for development, not only air traffic, but all kinds of traffic which will be discussed further in this paper. In this paper, the idea of establishing new airlines on the territory of the Republic of Serbia has stemmed from the fact that Serbia, as a country that stands for the gateway that connects eastern and western trade, does not have a world-class airport. The aim of this paper is to do analysis of the air traffic market on the territory in the Republic of Serbia, and based on this analysis to search for the optimal location where a new airline would be stationed. The fact that a new airline must be stationed only in the framework of the existing airports, the number of potential locations is reducing. In order to simplify the decision-making process and to objectively analyze the level of competency of the locations, in this paper there are specified criteria used to facilitate fair selection of locations. For this purpose, mathematical method of multi-criteria evaluation has been used in this paper, Analytical Hierarchical Processes (AHP method). With the AHP method we evaluated and mutually compared more locations based on relevant criteria. As the final result of the research, in this paper optimal location for the development of a new airline has been suggested.

*Corresponding author: Faculty of Mechanical Engineering, University of Nis

2. AIR TRAFFIC ANALYSIS

As the aim of this paper is to find the most suitable locations for new airlines, it is necessary to analyze air traffic market first. This paper specifically refers to the number of passengers who use air traffic during one year, or the number of working positions that come from activities in air traffic.

Specifically, the research showed the following data [5], [6], [7]:

- 3.000.000.000 passengers use air traffic for business or leisure purposes every year;
- 57.000.000 people are employed in the field of air traffic around the world;
- 6.4000.000.000.000 dollars of goods are annually transported by airplane, figure 1;
- 3.5 % of world economy is based on aviation.

According to the data presented, the global economic downturn, rising fuel prices, and improving surface transport mode options not have dampened air transport and air cargo growth. It is clear that air traffic in the world is huge business, it includes the world’s largest companies that make profit in the field of air traffic.

According to the U.S. Central Intelligence Agency (CIA), on the territory of the European Union there are 3.102 airports, i.e. 4.958 on the territory of the entire European continent. Those airports make 98% of total passenger air transport in Europe. Namely, the most active airports in Europe transported in 2012 total of 1.353.981.493 passengers out of 1.369.214.863 passengers on the European continent. How big is this number illustrates Figure 2 which shows the usual sky over Europe on Sunday.

If we consider commercial airports only in Europe, it will be notice that 100 airports in Europe have a number of passengers per year in excess of 3 million.

The difference of 15.233.370 passengers in Europe is less than 2% of passengers, and it is achieved on all remaining airports in Europe, specially intended for commercial purposes. Based on these data, we can be aware of the fact that air traffic in Europe successfully takes place within the closed group of airports.

A viable aviation sector is essential to the sustainable growth of the European economy. As a pioneer in single-market liberalization, a global competitor and a key driver in innovation, it is key to the achievement of the Lisbon agenda. Aviation creates more than 5.1 million jobs in Europe, a number that should double by 2030, and contributes more than EUR 380 billion to European GDP.

The 30 European established service and scheduled network carriers represented by the AEA collectively carry 400 million passengers and 5.5 million tons of cargo each year, operating 2,550 aircraft serving 600 destinations in 160 countries with 10,000 flights a day. They provide around 370,000 jobs directly, and generate a total turnover of EUR 100 billion.

According to the words of Ken Dunlap, general director of IATA safety, current situation in the area of air traffic is not ready to whitstand twice the increase in passengers by 2030. Based on this words we can make two obvious conclusions:

- the number of passengers in air traffic will be doubled by 2030;
- because of inability of current resources to meet the needs of the air market by 2030, new airports will be constructed or the existing ones will be exploited;
- new airplanes and new airlines will be formed.

On the basis of this hypothesis, in this paper, the locations of existing airports have been taken as potential locations for new airlines development. Potential locations are necessary to be ranged on the basis of relevant criteria which will serve as a basis for optimal solution selection.

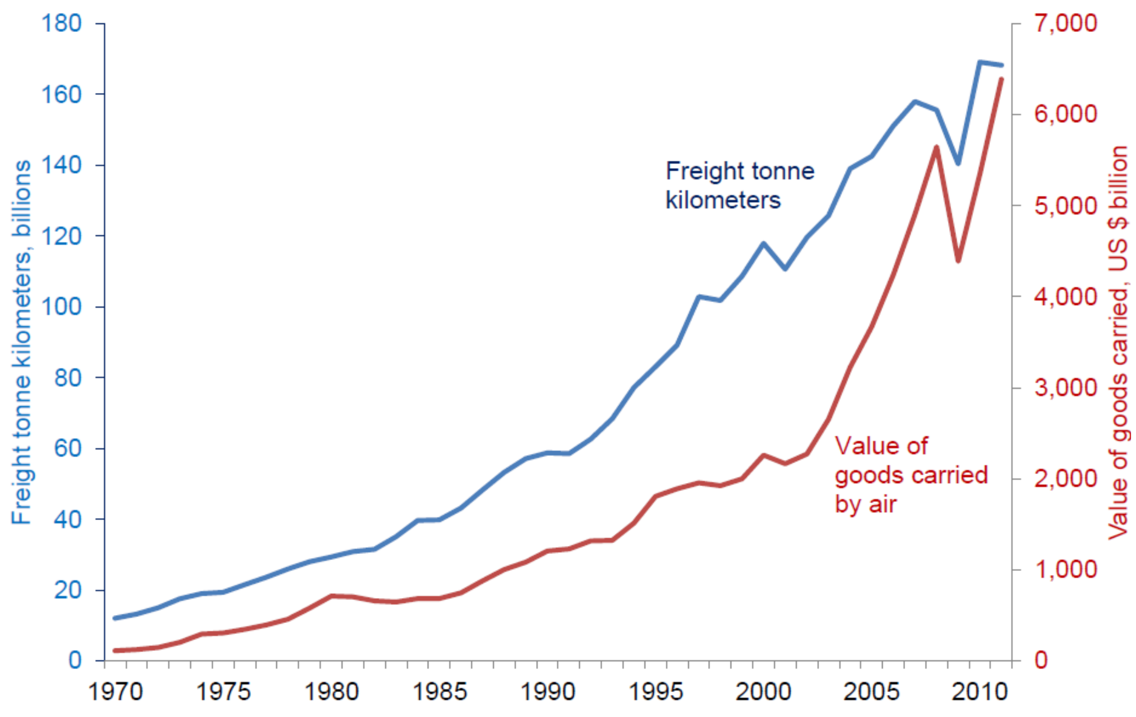

Figure 1: Air freight tonne kilometers flown and the value of goods carried

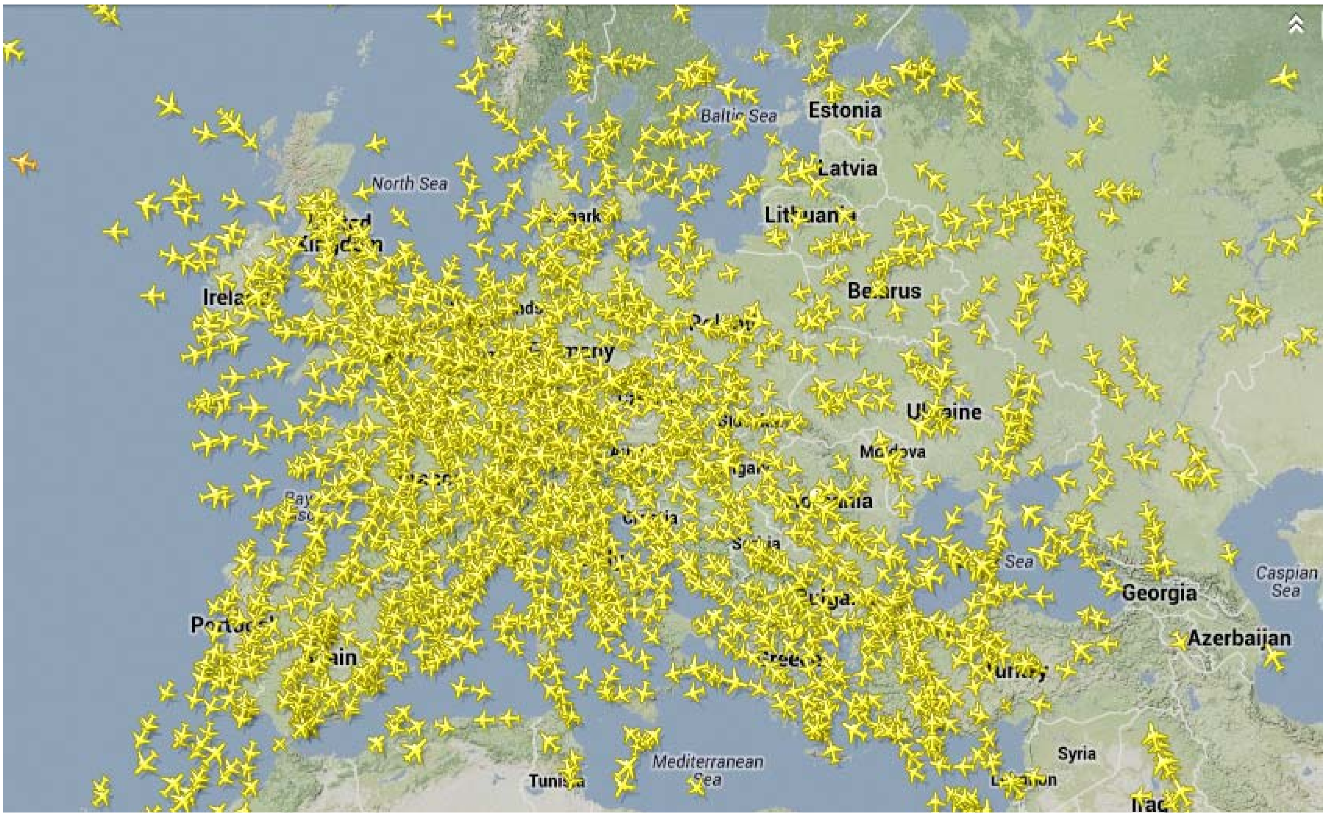

Figure 2: The usual sky over Europe on Sunday 13.10.2013. at 10:35

3. MATHEMATICAL PROBLEM DESCRIPTION

According to previous analysis of the air market, potential locations for new airlines have been presented. For all potential locations, the existing airports, located in the environment, have been selected. In order for all potential locations to be adequately ranged, special mathematical tools have been used in the form of methods of multi-criteria decisions.

Decision-making problems usually imply the selection of the best compromise solution. Besides the real criteria values by which a decision is made, the selection of the best solution also depends on the decision maker, that is, on his individual preferences. In order to simplify the decision-making process, many mathematical methods have been suggested. The Method of Analytical Hierarchical Processes (AHP) [8] represents one of the most frequently used methods of multi-criteria decisions. Besides this method, other ones are also available. The Preference Ranking Organization Method for Enrichment Evaluation (PROMETHEE) and the ELECTRE method have a significant place in the mathematical description of complex processes arising in the decision-making. All these methods have one basic task: to help the process of alternative evaluation [9].

AHP is a decision-making tool that can help describe the general decision operation by decomposing acomplex problem into a multi-level hierarchical structure of objectives, criteria, sub-criteria, and alternatives. AHP can be used in making decisions that are complex, unstructured, and contain multiple attributes [10]. The decisions that are described by these criteria do not fit in a linear framework; they contain both physical and psychological elements [11]. AHP provides a method to connect that can quantify the subjective judgment of the decision maker in a way that can be measured. In applying AHP to benchmarking, Partovi [9] describes the process in three broad steps: the description of a complex decision problem as a hierarchy, the prioritization procedure, and the calculation of results. AHP is a method of breaking down a complex, unstructured situation into its components parts, arranging these parts or judgments on the relative importance of each variable, and synthesizing the judgments to determine which variables have the highest priority and should be acted upon to influence the outcome of the situation. A problem is put into a hierarchical structure with level-I reflecting the overall goal or focus of the decision. Level-II contains factors or criteria for the decision, level-III contains sub-factors, and level-IV contains the decision options.

Methodologically speaking, AHP is a multi-criteria technique which is based on decomposition of a complex problem into hierarchy. The goal is at the top of the hierarchy, while the criteria (C_i), sub-criteria (C_{i-j}) and alternatives are on the lower level. Later, these criteria (C_{i-j}) are mutually compared in order to get the priority of each criterion in hierarchy (figure 2). Finally, all alternatives are compared in relation to the set of criteria (C_{i-j}) and in this way the comparison of alternatives is obtained.

Each comparison of two elements of the hierarchy is done by using Sati's scale (1) for the wide mathematical formula is given as follows:

$$s = \left\{ \frac{1}{9}, \frac{1}{8}, \frac{1}{7}, \frac{1}{6}, \frac{1}{5}, \frac{1}{4}, \frac{1}{3}, \frac{1}{2}, \frac{1}{1}, 1, 2, 3, 4, 5, 6, 7, 8, 9 \right\} \quad (1)$$

In order to get the final result, first it is necessary to compare sub-criteria mutually for each sub-criterion as recommended by Farkas [12]. The comparison of any two criteria C_i and C_j with respect to the goal is made using the questions of the type: of the two criteria C_i and C_j which is more important and how much, table 1. Saaty [8], suggests the use of a nine-point scale to transform the verbal judgments into numerical quantities representing the values of a_{ij}. During comparison of sub-criteria C_i with sub-criteria C_j by Saaty's scale, numerical coefficient a_i is determined and set on position a_{ij} (2), (3) in matrix A. Matrix A (4) is called a symmetrically reciprocal (SR) matrix and can be defined as:

$$A=[a_{ij}], \quad i,j=1,2,3...n. \tag{2}$$

$$a_{i,j}>0, \quad a_{ji}=\frac{1}{a_{ij}}, \qquad a_{ij}a_{ji}=1 \quad \text{for} \quad i\neq j \;\; \text{and} \quad a_{ii}=1, \quad i=1,2,3,...,n \tag{3}$$

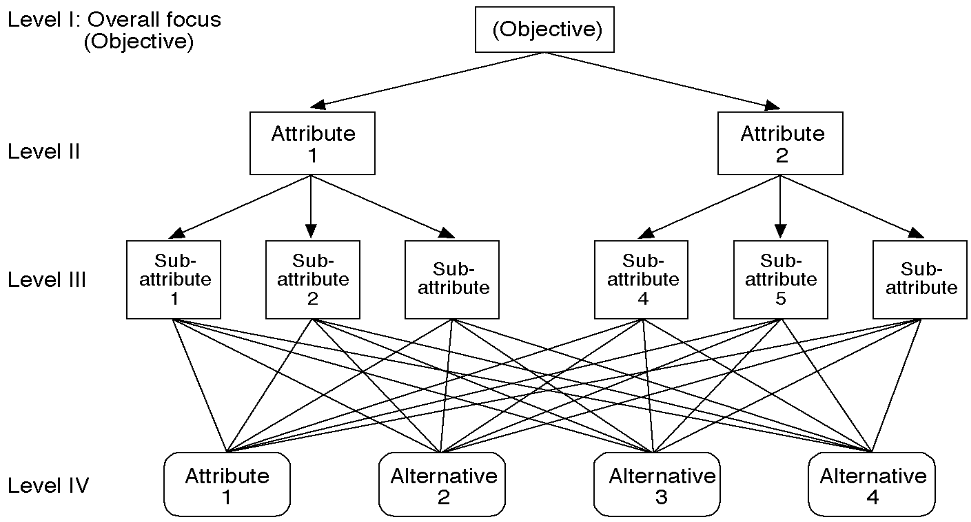

Figure 2: AHP methodology

Table 1: Pair-wise comparsion scale [8]

Intensity of importance	Definition
1	Equal importance of both elements
3	Weak importance one element over another
5	Essential or strong importance one element over another
7	Demonstrated importance one element over another
9	Absolute importance one element over another
2,4,6,8	Intermediate valued between two adjacent judgments

The intuition behind the AHP is that the pairwise comparison matrix A would be identical to the following matrix:

$$A=\begin{bmatrix} a_{11} & a_{12} & \cdots & a_{1n} \\ a_{21} & a_{22} & \cdots & a_{2n} \\ \vdots & & & \vdots \\ a_{n1} & a_{n2} & \cdots & a_{nn} \end{bmatrix} \cong \begin{bmatrix} \frac{W_1}{W_1} & \frac{W_1}{W_2} & \cdots & \frac{W_1}{W_n} \\ \frac{W_2}{W_1} & \frac{W_2}{W_2} & \cdots & \frac{W_2}{W_n} \\ \vdots & & & \vdots \\ \frac{W_n}{W_1} & \frac{W_n}{W_2} & \cdots & \frac{W_n}{W_n} \end{bmatrix} \tag{4}$$

where W_i is the relative weight of element i.

Here an entry a_{ij} from R_n represents a ratio, i.e, a_{ij} indicates the strength with which alternative A_i dominates alternative A_j with respect to a given sub-criterion $C_{i\text{-}j}$, $i,j=1,2,...,m$. Such a matrix is called a pairwise comparison matrix (PCM) and is usually constructed by eliciting experts' judgments. The basic objective is to derive implicit weights (priority scores), $W_1, W_2, ..., W_m$, with respect to each criterion $C_{i\text{-}j}$.

A vector of the weights, $W=[W_i]$, $W_i>0$, $i=1,...,n$, may be determined by using the eigenvalue formulation $AW=\lambda_{max}W$, λ_{max} is the principal eigenvalue of the matrix A.

In the transitive case the eigenvector method provides the true relative dominance of the alternatives. In reality, however, an individual cannot give his/her estimates such that they would conform to perfect consistency. Recognizing this fact, Saaty [8] proposed a measure for the inconsistency of a PCM: $\mu=(\lambda_{max}-n)/(n-1)$, where n is the matrix size. Results might be accepted if $\mu \leq 0.08$. Otherwise the problem should be reconsidered and the associated PCM must be revised. For all details of mathematical concept, see [8] or [9].

4. MATHEMATICAL MODEL IMPLEMENTATION

Fact that the number of passengers in international traffic will be doubled by 2030, leads to the conclusion that because of the position of the Balkan Peninsula that lies on the crossroads of airline routes, some of the airports in the region will inevitably develop as a significant international air port.

In this paper, as the initial alternatives airports with the current low capacity have been taken. The airports will be chosen from the territory of the former Yugoslavia countries for the simple reason that all these countries are in a similar economical, social, cultural and any other situation with similar affinities and perspectives.

The criterion for airport selection was that airports annually transported less than 100.000 passengers and not less than 100.000. There are five such airports in total on the territory of the former Yugoslavia countries (A_i=5, $i \in 1 \div 5$): "Rijeka" airport (A_1), "Osijek" airport (A_2), "Ohrid" airport (A_3), "Mostar" airport (A_4), and "Konstantin Veliki" airport (A_5). At the same time, these are locations (alternatives) taken for further research in this paper.

Further, based on the previous analysis of the air traffic shown in the second chapter, there will be defined exactly six criteria according to which each location will be mutually compared and evaluated. The following six criteria have been selected C_i=6, table 1:

- number of passengers transported (C_1);
- number of passengers who gravitate the airport (C_2);
- infrastructure availability (C_3);
- distance from the highway (km) (C_4);
- tourism potentials of environment (C_5),
- and weather conditions (C_6).

The values of criteria in relation to alternatives are shown in Table 1. After making the data matrix (Table 1), it is also necessary to define quantitative decision-making matrix (Table 2). After quantitative decision matrix, it is also necessary to define evaluation matrix.

Evaluation matrix is a matrix in which values of all the criteria are evaluated in relation to other criteria. So in this table for example, criterion C_2 compared to criterion C_1 is twice more important, which in this case means that the value of criterion C_2 compared to C_1 must be nine points according to Sati's scale (11). Units are on all diagonals, because each criterion is in relation to itself.

Final result applied by decision-making AHP method is shown in Table 3. On the basis of applied analytical hierarchical process, i.e. AHP method, we concluded that the airport with the highest perspective in the region is "Konstantin Veliki" airport, located in Nis, location number 5.

Table. 1: The values of criteria in relation to alternatives

Criteria discription		Location				
		A_1	A_2	A_3	A_4	A_5
C_1	number of passengers transported	61.833	20.827	45.000	36.875	25.112
C_2	number of passengers who gravitate the airport	0,8 mil.	0,7 mil.	0,5 mil.	1 mil.	3 mil.
C_3	infrastructure availability	good	very good	good	good	excellent
C_4-	distance from the highway	8	5	100	80	3
C_5	tourism potentials of environment	excellent	good	very good	good	very good
C_6	weather conditions	good	very good	very good	excellent	excellent

Table. 2: Quantitative decision-making matrix

	C_1	C_2	C_3	C_4	C_5	C_6
C_1	1	0,5	3	2	0,5	4
C_2	2	1	2	3	2	4
C_3	0,33	0,5	1	0,5	0,25	2
C_4	0,5	0,33	2	1	0,5	2
C_5	2	0,5	4	2	1	4
C_6	0,25	0,25	0,5	0,5	0,25	1
Σ	6,08	3,08	12,5	9	4,5	17

Table. 3: Final results, AHP method

A_1	0,216823	II
A_2	0,154248	V
A_3	0,194013	IV
A_4	0,198201	III
A_5	0,236715	I

5. RESULTS ANALYSIS AND CONCLUSION

In this paper, we have shown that the current situation in the area of air traffic is not able to withstand a doubling of the number of passengers in the world by 2030. For these reasons, in that period the sky above the Eastern Europe will become increasingly burdened and passengers' requirements for travel to Asia and Middle East and Africa will be continuously increasing. These facts are clear indicators that the number of airlines will increase as well as the number of airports.

Air transport markets and the airline industry have been transformed over the last 40 years. The number of passengers has risen tenfold and cargo volumes have grown fourteenfold, despite repeated shocks from recessions, terrorism and disease. Demand is volatile but consistently returns to a rapidly growing trend.

The development of new commercial airlines within smaller airports on the Balkan Peninsula is the investment that could certainly affect the development of this region in the next period.

The aim of the research in this paper is to obtain most suitable location solutions for new airlines on the Balkan Pension countries by using multi-criteria analysis. In this paper, the AHP method is used, as well as a mathematical tool in order to obtain best location solutions. The AHP method is ranked as one of the most famous and most frequently used methods of multi-criteria decisions. Theoretic basis of this method has been presented, and its application has been demonstrated by finding best location solutions for the Balkan Pension countries. By applying AHP method, we came to the conclusion that the most sutable solutions for new airlines is "Konstantin Veliki" airport in Nis. In addition to this location, there is also location of "Rjeka" airport which is also a good potential location for further investments of smaller commercial airlines.

Finally, using this method the aim is reached, a comparison of the Balkan Pension airports is done, and the most suitable airlines location is recommended.

REFERENCES

[1] A. Zhang, "Analysis of an international air cargo hub: the case of Hong Kong", Journal of Air Transport Management, Vol 9 (2), pp. 123–138, (2003).

[2] A. Zhang, Y. Zhang, "Issue on liberation of air cargo services in international aviation", Journal of Air Transport Management, Vol 8 (5), pp. 275–287, (2002).

[3] R. Aiying, G. Martin, "Shift designs for freight handling personnel at air cargo terminals", Journal of transportation research, pp. 725–739, (2009).

[4] Y. Nobert, J. Roy, "Freight handling personnel scheduling at air cargo terminals". Transportation Science 32, pp. 295–301, (1998).

[5] B. Pearce, "Airlines worlwide: The value they create and the challebges they face", International Air Transport Association, July, (2013).

[6] B. Pearce, "Profitability and the air trasnport value chain" IATA Economics Briefing, June, (2013).

[7] T. Tyler, "IATA Annual Review 2013", International Air Transport Association, June, (2013).

[8] T.L. Saaty, "Analytic Hierarchy Process, Planning, Priority Setting, Resource Allocation", McGraw Hill Inc., New York, (1980).

[9] V. Tomić, Z. Marinković, D. Janošević: "Promethee method implementation with multi-criteria decisions", The Scentific journal FACTA UNIVERZITATIS, Series Mechanical Engineering, Vol. 9 (2), pp. 193 – 202, (2011).

[10] F.Y. Partovi, Determining what to benchmark: an analytic hierarchy process approach, Int. J. Oper. Proj. Manage. 14 (1994).

[11] S.A. Mian, C.X. Dai, Decision making over the project life cycle: an analytical hierarchy approach, J. Proj. Manage. 30 (1) (1999).

[12] A. Farkas: Multi-Criteria Comparison of Bridge Designs, Acta Polytechnica Hungarica, Vol. 8,(1), pp. 173-191 (2011).

Application of Correlation Test to Criteria Selection for Multi Criteria Decision Making Problems in Domain of Logistics Systems

Goran Marković[1*], Zoran Bogićević[1], Mile Savković[1], Zoran Marinković[2], Vojislav Tomić[2]
[1]Faculty of Mechanical and Civil Engineering in Kraljevo, University of Kragujevac, Kraljevo (Serbia)
[2] Faculty of Mechanical Engineering in Niš, University of Niš, Niš (Serbia)

Generally, at considering any selection problem in domain of logistics and logistics systems there is a great number of technically feasible alternatives, and the task of designer is to choose from the set of possible solutions the one that best meets the technical and economic conditions defined by the terms of reference. Multi criteria decision making (MCDM) models are widely used in selection problems in the literature. Starting base at criteria defining is the fact that at solving each problem we can adopt various number and kind of criteria depending on corresponding decisions and information available. Also, an unique set of criteria of considered problem usually is not available to a decision maker. In this work the correlation test was used for getting the set of independent criteria and reducing their number to operating and acceptable level. It has been shown in the paper that the obtained set of independent criteria still fully represents the characteristics of the considered selection problem.

Keywords: criterion, rank, correlation test, Spearman’s correlation test, multi criteria decision making

1. INTRODUCTION

Key part of every logistics strategy or part of a supply chain that connects the manufacturers, deliverers and customers represents the transport – storage system. Modern transport engineering is characterized by constant development of devices for transport and manipulation and MCDM methods are the most common approach type applied for selection of material handling equipment. MCMD models try to answer the question of "what is the best alternative?" given a set of selection criteria and a set of alternatives. A model ranks the alternatives and the highest ranked one is recommended as the best alternative to the decision maker. At solving any problem we can adopt different number and kinds of criteria depending on corresponding decisions and information available. So, within the application of MCDM model, mostly the carrying out of the following steps is required [12]:

- defining relevant criteria and alternatives,
- giving numerical values for relative importance (weights), as well as alternatives influence on these criteria,
- getting numerical values that determine final result of alternatives ranking.

Decision maker, in great number of such real problems/situations, must meet one or more goals as well as the numerous conflict criteria. Final order of a problem's alternatives thus depends on applied technique of multicriteria decision-making, and especially on the procedure of defining the evaluation criteria, transformation (normalization) of criteria and determination of their relative importance. In application of multicriteria decision-making approaches, the selection criteria are directly taken without specific tests of checking their independency or other characteristics [12]. Because of the independent nature of criteria it is very important to limit their number to have a model which is sensitive to to changes in criteria weights, as well as the easier determination of their relative importance. From survey of literature [8,9], notable is the fact that generally the selection of criteria requires application of formal procedures to obtain an set of approximately seven plus or minus two independent criteria.

The research in this study is directed to the possibility of correlation test application for comparing the independent criteria and reduction of their number to operational and acceptable level. Correlation analysis are used to measure reletionship between two variables. Based on outcome of the correlation test, are analized the statistically significant differences between the initial and the reduced set of criteria to final ranking and it has been shown that the obtained set of independent criteria still fully represents the characteristics of the selection problem. Application of correlational test is illustrated on multicriteria decision-making problem of material handling equipment selection (forklift).

2. STATISTICAL HYPOTHESIS TESTING – MATHEMATICAL BACKGROUND

A statistical hypothesis test is a method of statistical inference using data from a scientific study. In statistics, a result is called statistically significant if it has been predicted as unlikely to have occurred by chance alone, according to a pre-determined threshold probability, the significance level.

These tests are used in determining what outcomes of a study would lead to a rejection of the null hypothesis for a pre-specified level of significance; this can help to decide whether results contain enough information to cast doubt on conventional wisdom, given that conventional wisdom has been used to establish the null hypothesis. The task of hypothesis testing in statistics theory is to quantify the degree of doubt in some hypothesis.

The critical region of a hypothesis test is the set of all outcomes which cause the null hypothesis to be rejected in favor of the alternative hypothesis (Figure 1).

*Corresponding author: Dositejeva 19, Kraljevo, Serbia; markovic.g@mfkv.kg.ac.rs

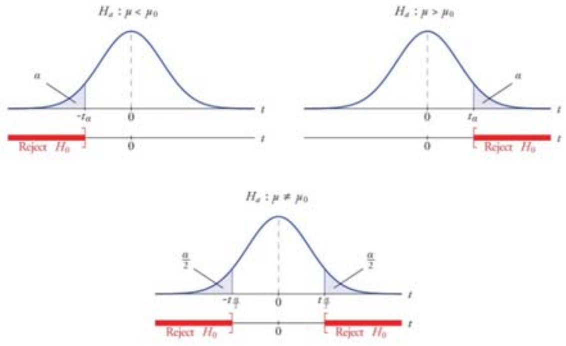

Figure 1: Rules of accepting the hypothesis [6]

In statistics, dependence is any statistical relationship between two random variables or two sets of data. Correlations are useful because they can indicate a predictive relationship that can be exploited in practice. The first step of testing is to state the relevant null and alternative hypotheses. The two hypotheses, namely H_0: there is no linear correlation between two variables and H_1: there is linear correlation between two variables are tested with correlation test. In the correlation test, correlation coefficient is used to test the hypothesis. There are several correlation coefficients, often denoted ρ or r, measuring the degree of correlation. The most common of these is the Pearson correlation coefficient, which is sensitive only to a linear relationship between two variables (which may exist even if one is a nonlinear function of the other). Simple linear correrlation coefficient can take values only in the interval -1 and 1, ie. $-1 \leq r \leq 1$. The correlation coefficient never has the values 1 or -1, because it would mean that between the phenomena there is a mathematical, not statistical connection.

Let (X,Y) be a random vector. From two-dimensional distribution of vectors (X,Y) we take a circumference sample n: (X_1,Y_1), (X_2,Y_2),…, (X_n,Y_n). Here the pairs (X_i,Y_i) are independent, while the random values from the same pair have specified common distribution and can be dependent, with correlation coefficient *r*:

$$r = \frac{\sum_{i=1}^{n}\left(X_i - \bar{X}\right)\cdot\left(Y_i - \bar{Y}\right)}{\sqrt{\left(\sum_{i=1}^{n}\left(X_i - \bar{X}\right)^2\right)\cdot\left(\sum_{i=1}^{n}\left(Y_i - \bar{Y}\right)^2\right)}} \tag{1}$$

For hypotheses testing, as for finding the confidence interval, of use is the following theoreme:

Theoreme 1: If random vector (X,Y) has two-dimensional normal distribution with ρ=0, then the statistics

$$t = r\sqrt{\frac{n-2}{1-r^2}} \tag{2}$$

has t (n-2) distribution.

Testing of hypothesis about simple linear equation coefficient on the basic set ρ, on the ground of its estimate from random sample r is based on the assumption about normality of common distribution for variables X and Y. Most commonly used parametric test of significance for testing the zero hypothesis is the Student's t-test. It is used for testing the significance of differences between two arithmetic means.

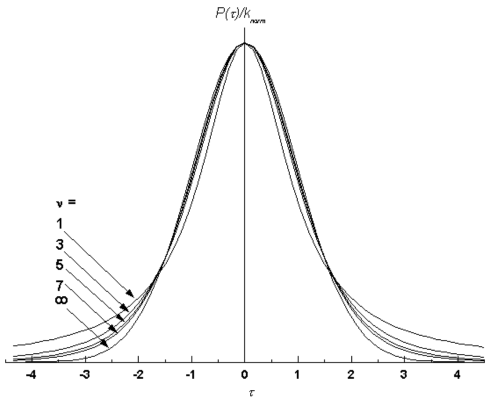

Figure 2: Student's t – distribution with ν degrees of freedom [6]

If the observed t-value is less than border table value for appropriate number ν and threshold (level) of significance, zero hypothesis is accepted as correct, and the alternative hypothesis is rejected. Reversely, if the observed t-value is equal or greater than the border table value, for corresponding number ν and threshold of significance, zero hypothesis is rejected as incorrect, and the alternative hypothesis is accepted. An alternative process is commonly used:

1. Compute from the observations the observed value *t* obs of the test statistic *t*.
2. Calculate the p-value. This is the probability, under the null hypothesis, of sampling a test statistic at least as extreme as that which was observed.
3. Reject the null hypothesis, in favor of the alternative hypothesis, if and only if the p-value is less than the significance level (the selected probability) threshold. Common values are 5% and 1%.

To analize the statistically significant differences between the original and the reduced set of criteria to final ranking Spearman's rank-correlation test is used. Spearman's rank correlation test, which is a special form of correlation test, is used when the actual values of paried data are substituted with the ranks which the values occupy in the respective samples [12]. In this study, Spearman's rank correlation test evaluates the similarity of the outcomes (rankings a set of forklift alternatives). To test the null hypothesis in Spearman's correlation test, test statistic Z is calculated using eqs. (3) and (4) and compared with a pre-determined level of significance α value. In eqs. (3) and (4), d_j represents the ranking difference between *j* results, *K* is the number of alternatives to be compared and r_s represents the Spearman's rank correlation coefficient.

$$r_s = 1 - \left[\frac{6\cdot\sum_{j=1}^{K}(d_j)^2}{K(K^2-1)}\right] \tag{3}$$

$$Z = r_s\sqrt{(K-1)} \tag{4}$$

3. ILLUSTRATION OF THE CORRELATION TEST

Generally, for the needs of multicriteria problems in selection of material handling equipment, different approaches have been developed [2,3,4,5,7,11]. Namely, at solving the multicriteria decision-making problem, and especially when it comes to the selection of material handling equipment, there is a variant when the criteria for choice of the most acceptable alternative are taken directly from manufacturers'catalogues. In that case, by applying the correlational test we expect to get the reduced and independent a set of criteria. The reason for test application lies in the already mentioned fact that in literature there is no clearly defined procedure of criteria selection.

For numerical illustration of correlational test in further works there will be considered a selection of three wheel electro forklift unit for warehouse operation [6]. It is a MCDM problem and for ranking a set of alternatives of forklifts that satisfy in advance required parameters, the initial set of 20 characteristics was observed (Table 1) as a initial set of selection criteria. Starting sample that is considered consists of 25 forklifts of different manufacturers. Their initial values are collected from appropriate catalogs. The task is to, from sample of 25 different values that takes 20 variables, using the correlational test, determine the intensity of connection between two variables and in this way reduce the initial number of independent criteria for evaluation of alternative solutions.

Table 1: Forklifts characteristical values for 20 criteria

Model	*Capacity (kg)*	*Max. lift height (mm)*	*Travel speed with the load (km/h)*	*Travel speed without the load (km/h)*	*Lift speed with the load (m/s)*	*Lift speed without the load (m/s)*	*Turning radius (mm)*	*Length to fork face (mm)*	*Engine power (kW)*	*Wheelbase (mm)*
7FBEST10	1000	3310	12	12.5	0.32	0.52	1230	1565	7.5	985
7FBEST13	1250	3310	12	12.5	0.31	0.52	1400	1725	7.5	1145
7FBEST15	1500	3310	12	12.5	0.3	0.52	1450	1780	7.5	1200
2ET2500	1300	3000	16	16	0.48	0.6	1440	1774	11.5	1249
2ETC3000	1600	3000	16	16	0.49	0.6	1548	1887	11.5	1357
2ETC3500	1800	3000	16	16	0.44	0.55	1548	1887	11.5	1357
2ETC4000	2000	3000	16	16	0.4	0.55	1655	1995	11.5	1465
J30XNT	1361	3032	15.7	15.7	0.39	0.65	1481	1808	4.8	1290
J35XNT	1588	3032	15.7	15.7	0.36	0.65	1577	1903	4.8	1386
J40XNT	1814	3032	15.7	15.7	0.34	0.65	1577	1903	4.8	1386
TX30N	1350	3300	14.5	14.5	0.34	0.515	1525	1895	10.7	1300
TX35N	1600	3300	14.5	14.5	0.31	0.515	1525	1895	10.7	1300
TX40N	1800	3300	16	16	0.32	0.6	1635	2005	14.6	1410
ERP13VC	1250	3320	12	12.5	0.3	0.51	1398	1724	6	1168
ERP15VC	1500	3320	12	12.5	0.3	0.51	1452	1778	6	1222
ERP15VT	1500	3320	16	16	0.43	0.59	1476	1805	12	1290
ERP16VT	1600	3320	16	16	0.43	0.59	1476	1805	12	1290
ERP18VT	1800	3390	16	16	0.41	0.58	1676	1896	12	1494
ERP20VT	2000	3390	16	16	0.4	0.58	1676	1999	12	1494
EFG110	1000	3000	12	12.5	0.29	0.5	1293	1623	6	1038
EFG113	1250	300	12	12.5	0.25	0.5	1401	1731	6	1146
EFG115	1500	3000	12	12.5	0.24	0.5	1455	1785	6	1200
EFG213	1300	3000	10	16	0.48	0.6	1440	1774	11.5	1249
EFG218	1800	3000	10	16	0.44	0.55	1655	1995	11.5	1465
EFG220	2000	3000	10	16	0.4	0.55	1655	1995	11.5	1465

Model	*Total width (mm)*	*Level of noise (dB)*	*Voltage (V)*	*Battery capacity (Ah)*	*Tilt (°)*	*Forklift mass (kg)*	*Forks length (mm)*	*Installation pressure (bar)*	*Battery weight (kg)*	*Total height to top of overhead guard (mm)*
7FBEST10	990	62.4	24	400	5	2550	800	140	372	2055
7FBEST13	990	62.4	24	700	5	2820	800	140	600	2055
7FBEST15	990	62.4	24	800	5	2930	800	140	676	2055
2ET2500	1060	66	24	400	7	2698	1150	200	679	2040
2ETC3000	1060	66	24	500	7	2957	1150	200	812	2040
2ETC3500	1120	66	24	500	7	3213	1150	200	812	2040
2ETC4000	1120	66	24	600	7	3331	1150	200	974	2040
J30XNT	1050	69	36	750	5	2313	1067	155	670	2070
J35XNT	1050	69	36	800	5	2372	1067	155	670	2070
J40XNT	1116	69	36	1000	5	2390	1067	155	700	2070
TX30N	1105	61	36	680	4	2955	1070	140	700	2110
TX35N	1105	61	36	680	4	3155	1070	140	700	2110
TX40N	1105	61	48	750	4	3365	1070	140	1050	2110
ERP13VC	996	59	24	735	5	2700	1000	155	570	1980
ERP15VC	996	59	24	840	5	2905	1000	155	642	1980
ERP15VT	1050	65	48	500	5	2990	1000	180	673	2070
ERP16VT	1050	65	48	500	5	2990	1000	180	673	2070
ERP18VT	1116	65	48	750	5	3280	1000	180	962	2070
ERP20VT	1116	65	48	750	5	3290	1000	180	962	2070
EFG110	990	63	24	625	5	2570	1150	160	481	2090
EFG113	990	63	24	875	5	2760	1150	185	648	2090
EFG115	990	63	24	1000	5	2870	1150	210	730	2090
EFG213	1060	66	24	400	7	2698	1100	200	679	2040
EFG218	1120	66	24	600	7	3156	1100	200	974	2040
EFG220	1120	66	24	600	7	3331	1100	200	974	2040

In the use of equation (1), n corresponds to the sample value of 25 forklifts, (X_i ,Y_i) represent the criteria pairs for which we calculate the correlation coefficient, and $\overline{X}$ and $\overline{Y}$ their average values.

$$r=\frac{\sum_{i=1}^{25}\left(X_i-\overline{X}\right)\cdot\left(Y_i-\overline{Y}\right)}{\sqrt{\left(\sum_{i=1}^{25}\left(X_i-\overline{X}\right)^2\right)\cdot\left(\sum_{i=1}^{25}\left(Y_i-\overline{Y}\right)^2\right)}} \tag{5}$$

After the calculated value of correlation coefficient for every pair of criteria, further testing of linear correlation coefficient is based on already mentioned Student's distribution with n-2 degrees of freedom. Statistic test p-value is compared to predefined significance level α which is a proof of positive relation between two criteria. In this research α=0.01 was chosen as critical value. In case that p-value is less than 0.01, we conclude that there is a proof of positive relation between two criteria and one of them can be eliminated.

For the needs of this work, because of easier carrying out the extensive calculations when getting the values of correlation coefficient and statistic test p-value, the shown procedure is automatized by development of program tools in the environment of Microsoft Excel. Given program tools have restrictions regarding the number of criteria (maximum 25). For arbitrary criteria pair (eg. Criterion A: Capacity and G: Turning radius) the program tool calculates the value of t-statistic of the two-tailed t-distribution with 23 (n-2) degrees of freedom, by using the eqs. (2). For this arbitrary criteria par, corresponding valies as t=12,263 and r=0.935. The program then determines, one-tailed and two-tailed p – value in t – distribution (Table 2).

Table 2: Correlation coefficient and p-values for criteria pairs: A – to G; B – to G, C – to G D – to G; E – to G, F – to G

r	0.179	0.345	0.657	0.344	0.339	0.935
t_p	0.871	1.763	4.176	1.759	1.729	12.683
p	0.804	0.954	1.000	0.954	0.951	1.000
p-1	0.196	0.046	0.000	0.046	0.049	0.000
p-2	0.393	0.091	0.000	0.092	0.097	0.000

r	0.196	0.203	0.242	0.172	0.157
t_p	0.956	0.995	1.194	0.838	0.763
p	0.826	0.835	0.878	0.795	0.773
p-1	0.174	0.165	0.122	0.205	0.227
p-2	0.349	0.330	0.245	0.411	0.453

When p-value for every criteria pair is calculated, two-tailed p-value is entered into the matrix under the main diagonal (Table 3), whereby the pairs, whose p-values are less than previously defined value 0.01, are marked above the main diagonal by the sign "X".

The elimination procedure itself, or reduction of criteria number (variables) that are in mutual correlation, from the shown table, could be presented through the following steps:

1. check if there are criteria which are not correlated to any other criteria (both by rows and columns of given table), and if this is the case, they should be chosen for independent criteria;
2. check the correlation of every criteria (by rows) with other members, and if there is such criterion, choose it as independent one, other criteria in corelation discard;
3. If there are undeleted criteria left, go back to step 1, otherwise the process of correlation analysis is finished.

Table 3: Criteria pairs correlation(pairs in correlation marked with "X")

	A	B	C	D	E	F	G	H	I	J	K	L	M	N	O	P	Q	R	S	T
A				X			X	X		X	X					X			X	
B	0.393																			
C	0.091	0.349		X		X							X							
D	0.000	0.330	0.005		X	X	X	X	X	X	X	X							X	
E	0.092	0.245	0.108	0.000		X			X	X	X	X		X	X			X		
F	0.097	0.411	0.003	0.000	0.002					X		X								
G	0.000	0.453	0.068	0.000	0.049	0.037		X	X	X	X					X			X	
H	0.000	0.479	0.088	0.000	0.068	0.057	0.000		X	X	X					X			X	
I	0.013	0.219	0.184	0.001	0.001	0.543	0.009	0.005		X	X			X		X			X	
J	0.000	0.377	0.038	0.000	0.009	0.009	0.000	0.000	0.006		X					X			X	
K	0.000	0.299	0.035	0.000	0.004	0.028	0.000	0.000	0.001	0.000						X			X	
L	0.081	0.716	0.094	0.000	0.002	0.000	0.060	0.105	0.970	0.018	0.033									
M	0.079	0.162	0.001	0.014	0.465	0.016	0.034	0.064	0.066	0.025	0.042	0.533			X					
N	0.408	0.317	0.910	0.079	0.000	0.682	0.383	0.482	0.003	0.685	0.496	0.555	0.601		X					
O	0.200	0.640	0.437	0.035	0.000	0.417	0.301	0.320	0.137	0.173	0.185	0.015	0.008	0.006				X		X
P	0.000	0.443	0.643	0.113	0.314	0.230	0.001	0.001	0.000	0.003	0.005	0.241	0.256	0.499	0.414				X	
Q	0.217	0.064	0.405	0.039	0.205	0.400	0.109	0.067	0.434	0.089	0.051	0.113	0.629	0.969	0.049	0.625		X		
R	0.079	0.203	0.862	0.031	0.004	0.602	0.128	0.188	0.083	0.075	0.190	0.029	0.286	0.172	0.000	0.139	0.001			
S	0.000	0.713	0.229	0.000	0.065	0.197	0.000	0.000	0.000	0.000	0.000	0.234	0.119	0.667	0.142	0.000	0.075	0.034		
T	0.993	0.442	0.158	0.625	0.248	0.736	0.669	0.520	0.518	0.836	0.354	0.682	0.015	0.347	0.009	0.808	0.536	0.276	0.676	

By using the listed rules of elimination procedure, the number of rules in this particular case is reduced from the initial 20 to the following six independent criteria: A-Capacity (kg), B-Maximum lift height (mm), C- Travel speed with the load (km/h), E-Lift speed with the load (m/s), Q-Forks length (mm) and T-Total height to top of overhead guard (mm).Thus obtained, the set of independent criteria satisfies the suggested number (seven plus or minus two) and it is possible to use it further in the following stage of solving the multicriteria decision-making problems, i.e. in the procedure of determining their relative weights and later also in the final ranking of suggested alternatives of the considered multicriteria problem [6].

3.1 Spearman's rank correlation test

In order to analyze statistical significances of the differences between the initial and the reduced number of criteria are developed the program tools in the environment of Microsoft Excel, that uses a special type of correlation test - Spearman's rank correlation test (Figure 3). Developed tool, it's possible for a given level of significance to compare the results of ranking the reduced and the initial set of criteria, and also compare outputs the ranking obtained using a different multiple criteria analysis approach. Testing the null hypothesis Ho, i.e. the Spearman's test statistic Z value is determined by using the expression (3) and (4) and compares it with a value that corresponds to a given significance level α. In this study, Z = 1.645 is selected as the critical value at the level of significance α = 0.05. If the calculated value of Z obtained by test exceeds the critical value the null hypothesis is rejected and it is concluded that there is evidence of a positive relationship - agreement between the two sets of rankings.

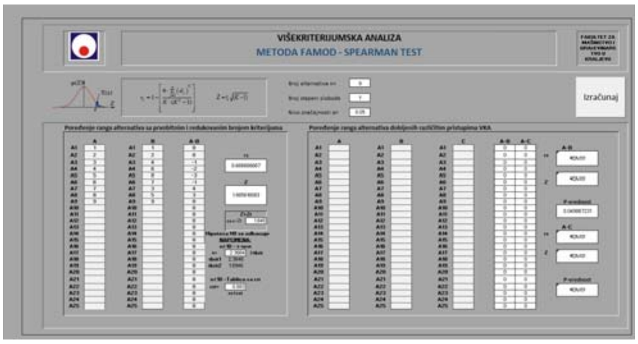

Figure 3: Spearman's rank correlation test program tool

A different MCDM approaches, FAMOD (Fuzzy Analytic Hierarchical process + MODification Promethee Methods), TOPSIS and Promethee methods, are used to obtain ranking scores and rank the forklift alternatives accordingly. Steps and application details of the methods are provided in literature [7,11,14].

Table 4: Two different weight sets used for MCDM approaches

Weight sets of initial 20 criteria			Weight sets of 6 independent criteria		
Criteria	W1	W2	Criteria	W1	W2
A	0.15	0.05	A	0.2	0.16666
B	0.15	0.05	B	0.2	0.16666
C	0.15	0.05	C	0.2	0.16666
D	0.02	0.05	E	0.15	0.16666
E	0.12	0.05	Q	0.15	0.16666
F	0.02	0.05	T	0.1	0.16666
G	0.02	0.05			
H	0.02	0.05			
I	0.02	0.05			
J	0.02	0.05			
K	0.02	0.05			
L	0.02	0.05			
M	0.02	0.05			
N	0.02	0.05			
O	0.02	0.05			
P	0.02	0.05			
Q	0.02	0.05			
R	0.02	0.05			
S	0.08	0.05			
T	0.05	0.05			

In order to compare the results of ranking with the initial set of criteria and a reduced number of criteria (in the present case the number was reduced from 20 to a set of 6 independent criteria), it is necessary for further calculations to determine a decision matrix and weights of criteria as inputs (Table 4).

Forklift alternatives
ERP15VT
ERP16VT
ERP18VT
7FBEST15
TX35N
TX40N
ERP15VC

Figure 4: Output screen of FAMOD elimination module for case study

Results of the final ranking of the seven alternatives (Figure 4.) considered problem obtained by FAMOD are shown in Table 5. The alternative with the highest rank is indicated by 1, while the alternative with the lowest rank indicated by 7. The MCDM methods calculations are performed with two different weight sets (W1 and W2) for the two separate criteria (20 initial criteria and 6 independent criteria). Firstly, in the analysis of results, the statistical signifance of the difference between the 20 and the 6 criteria for different weight sets (set W1 and W2) is tested. The Spearman's correlation test results indicate that the differences between rankings are not statistically significant (Z values respectively 2.362 and 2,187 are above the critical value of 1.645).

Table 5: Analysis of differences using Spearman's rank correlationn test

Alternatives	Ranking score				Analysis of differences using Spearmann's rank correlation test			
	(A) Initial set of 20 criteria		(B) Reduce set of 6 criteria		A-B		A	B
	W1	W2	W1	W2	W1	W2	W1-W2	W1-W2
ERP15VT	3	2	4	3	-1	-1	1	1
ERP16VT	2	1	2	2	0	-1	1	0
ERP18VT	1	3	1	1	0	2	-2	0
7FBEST15	7	7	7	7	0	0	0	0
TX35N	5	5	5	5	0	0	0	0
TX40N	4	4	3	4	1	0	0	-1
ERP15VC	6	6	6	6	0	0	0	0
Spearman's correlation coefficient r_s					0,96428	0,8928	0,8928	0,9642
Statistical signifance value Z					2,362	2,187	2,1870	2,362

A further analysis of the differeces among the rankings within each criteria set is needed to determine whether or not the sensitivity of the rankings to the changes in the criteria weights depends on the number of criteria.

Results for the values of correlation coefficient in this case for a set of seven alternatives are greater in the case of the six criteria than the 20, and shows on one side a great similarity ranking, but does not indicate a change in the sensitivity of the model to the change of criteria. It is expected that the increasing number of considered alternatives i.e. differences in the ranking are such that the value of the correlation coefficient in the case of the reduced number of criteria of lower value than the value of the original dataset, which would indicate less similarity ranking, and hence the conclusion that the reduces the number of criteria increases the sensitivity of a given multi-criteria model. Also, in this study to test the validity of outcomes obtained with different MCDM approaches, the ranking results are compared and presented in Table 6.

Table 6: Comparasion of forklift ranking approaches

Alternatives	Ranking score			Analysis of differences using Spearmann's rank correlation test	
	(A) FAMOD	(B) TOPSIS	(C) PROMETHEE	A-B	A-C
ERP15VT	3	3	4	0	-1
ERP16VT	2	2	2	0	0
ERP18VT	1	1	1	0	0
7FBEST15	7	7	7	0	0
TX35N	5	5	5	0	0
TX40N	4	4	3	0	1
ERP15VC	6	6	6	0	0
Spearman’s correlation coefficient r_s				1	0.9642
Statistical signifance value Z				2.449	2.362

As the outcome of the test, the statistical signifance rates of the differences in the rankings (Z) are illustrated in the last row of Table 6. It is evident that in all cases the value of Z exceeds the critical significance level of 0.05, and it can be concluded that the results of the ranking obtained with new approach FAMOD are statistically similar to the results obtained by other traditional approaches.

4. CONCLUSION

In this study, the fact was pointed out that solving the problem of decision-making requires firstly defining the criteria system, and then determining their relative significance before final ranking of the considered multicriteria problem alternatives. Also, the fact was pointed out that a unique set of criteria of considered problem most often is not available to decision-maker. Correlation test was used for getting a set of independent criteria, more precisely reduction of their number to operative and acceptable level for determining the relative weights and later on the procedure of ranking the alternatives. A key results in this analysis, are that when the number of criteria is reduced, the model clearly becomes more sensitive to the changes in criteria weights But, correlation test determines only the level of correlation for every criteria pair, and as it is determined there is not a unique way of obtaining the set of independent criteria (seven plus or minus two). Set of independent criteria can be different for the same value of correlation coefficient, but also by changing the values of significance level, the number of pairs in correlation changes. In this way the pairs in correlation become the pairs without correlation and vice resa. It becomes clear that defining the set of independent criteria requires, in that case, repetition and check of procedure for choosing the set of seven plus or minus two independent criteria. However, the result of such approach can lead to a situation where the available criteria, i.e. the most commonly used ones in previous researches, can become preferential to the less significant criteria, and as such be used for solving the equipment choice problem.

REFERENCES

[1] Chen, S-J, Hwang, C-L.: “Lecture notes in economics and mathematical systems”, Springer, Berlin, Germany, 1992.

[2] Chu, H. K., Egbelu, P. J.,Wu, C. T.:“ADVISIOR: A computer-aided material handling equipment selection system“, Int. J. Prod. Res., 33 (12):3311-3329,1995

[3] Dagdeviren, M.: “Decision Making in equipment selection: an integrated approach with AHP and PROMETHEE“, Journal of Intelligent Manufacturing,19,397-406, 2008

[4] Fisher, E.L., Farber, J. B., Kay, M. G.: “MATEHS: An expert system for material handling equipment selection”, Engineering Costs and Production Economics,14,297-310,1998

[5] Kim, K. S., Eom, J. K.: “An expert system for selection of material handling and storage systems”, Int. J. Ind. Eng., 4(2),1997,81-89

[6] Marković,G., Gašić, M., Savković, M., Marinković, Z., Tomić, V.:’’ Criteria system defining in multicriteria decision making problem at transport-storage system elements choice, 5th International conference – Transport and logistics, page.177-184, Niš, 2014.

[7] Marković, G., Gašić, M., Kolarević, M., Savković, M., Marinković., Z.: Application of the MODIPROM method to the final solution of logistics centre location, Transport 28(4), pp. 341-351, 2013.

[8] Miller, G.A.:”The magic number seven plus or minus two”, Psychol rev 63:81-97, 1965

[9] Park. Y.:ICMESE: “Intelligent consultant system for material handling equipment selection and evaluation“, Journal of Manufacturing Systems, 15(5),325-333, 1996

[10] Tabucanon, M. T., Batanov, D. N.,Verma, D.K.: “Intelligent decision support system (DSS) for the selection process of alternative machines for flexible manufacturing systems (FMS)”, Comuters in Industry, 25, 131-143, 1994

[11] Taha, Z., Rostam, S.: “A hybrid AHP-PROMETHEE decision support system for machine tool selection in flexible manufacturing cell”, J. Intell. Manuf. (2012) 23:2137-2149, 2012

[12] Yurdakul, M., Tansel, IC. Y.: “Application of correlation test to criteria selection for multi criteria decision making (MCDM) models”, International Advanced Manufacturing Technology (2009) 40:403-412, 2009

[13] Yurdakul, M., Tansel, I. Y.: Analysis of the benefit generated by using fuzzy numbers in a TOPSIS model developed for machine tool selection problems, Journal of Material Processing Technology, 209, 310-317,2009

Development of Micro Cogeneration Plants in Individual Houses

Jelica Dimitrijević[1 *], Stefan Pantović[2]
[1] Faculty of Engineering, University of Kragujevac, Serbia
[2] Faculty of mechanical and civil engineering Kraljevo, University of Kragujevac, Serbia

Micro Cogeneration CHP combined heat and power production is process in which the products are electric and thermal energy (for heating and/or cooling) with high efficiency of the process. Process includes three basic elements: simultaneous production of electricity and heat, criteria of high efficiency process and a criterion which takes into consideration the distance to the energy conversion unit and the consumer. Micro Cogeneration CHP is defined as a process of simultaneous production of electricity and heat to individual buildings, based on a relatively low conversion units. The Republic of Serbia hasn't special rules concerning microcogeneration. This paper presents the possibility for cogeneration in individual houses and its environmental aspects.

Keywords: Micro cogeneration, Heat, Electricity.

1. INTRODUCTION

The electricity systems of many countries are currently undergoing a process of transformation. Market liberalization has induced major mergers and acquisitions in the electricity sector, but has also forced companies to seek out new business areas. Environmental regulations, like the Kyoto process and the European Emissions Trading Scheme, are exposing the sector to external pressure [2]. New technologies – such as renewable energy, combined heat and power (CHP), or "clean coal" technologies – are emerging. Recent worldwide experiences with blackouts have once more put security of supply on the agenda. In Germany, the nuclear phase-out and decommissioning of outdated coal plants will lead to a need for replacement of more than one third of the current generation capacity by 2020 [1].

2. DEFINING MICRO COGENERATION

The principle of cogeneration has long been known. As early as the first decade of the 20th century, a number of cogeneration units were already supplying heat and electricity to houses and companies. Cogeneration, or combined heat and power production (CHP), is "the process of producing both electricity and usable thermal energy (heat and/or cooling) at high efficiency and near the point of use". It thus incorporates three defining elements: 1) the simultaneous production of electricity and heat; 2) a performance criterion of high total efficiency; and 3) a locationa criterion concerning the proximity of the energy conversion unit to a customer [3].

While the discussion on micro cogeneration, or micro CHP, has only recently gained momentum, the technological roots of micro cogeneration go back to the early development of steam and Stirling engines in the 18th and 19th century, respectively. Today, several technologies exist that are capable of providing cogeneration services, such as reciprocating engines, gas turbines, Stirling engines, and fuel cells. But, in principle, the exhaust heat from any thermal power plant, such as gas combined-cycle power plants or coal power plants, can be used for cogeneration applications [4].

Advances in the technology, as well as a general trend towards smaller unit sizes of power plants, have led to an increased interest in small CHP units, with the hope of ultimately developing units that can provide electricity and heat for individual buildings. This is what we call micro cogeneration which we define as: *the simultaneous generation of heat, or cooling, energy and power in an individual building, based on small energy conversion units below 15 kWel*. Whereas the heat produced is used for space and water heating inside the building, electricity produced is used within the building or fed into the public grid. Opposed to, for example, the EU cogeneration directive, according to which micro cogeneration is defined as "a cogeneration unit with a maximum capacity below 50 kWel" (EU 2004), we restrict the definition of micro cogeneration to systems below 15 kWel for the following reasons. Firstly, these systems are clearly systems for use in single-family dwellings, apartment houses, small business enterprises, hotels, etc., which can be distinguished from systems supplying heat to a district or neighborhood (i.e. district heating systems). Secondly, systems in this small power regime substantially differ from larger ones with respect to electricity distribution, ownership models, restructuring of supply relationships, and consumer behavior. Also, compared to conventional CHP, based on district heating, no additional heat distribution grid is required. Systems below 15 kWel can be directly connected to the threephase grid. Moreover, the barriers all CHP systems have to face are more pronounced in the case of such small systems [7].

The technological core of micro cogeneration is an energy conversion unit that allows the simultaneous production of electricity and heat in very small units. In addition to this core, further technology components are involved in a micro cogeneration system (*Figure 1*), such as well-developed grid access, including possible metering and control devices. In the remainder of this chapter, the various technological components of such a system will be described in detail [5].

*Corresponding author: Faculty of Mechanical and Civil Engineering in Kraljevo, Dositejeva 19, Kraljevo, Serbia, pantovic.s@mfkv.kg.ac.rs

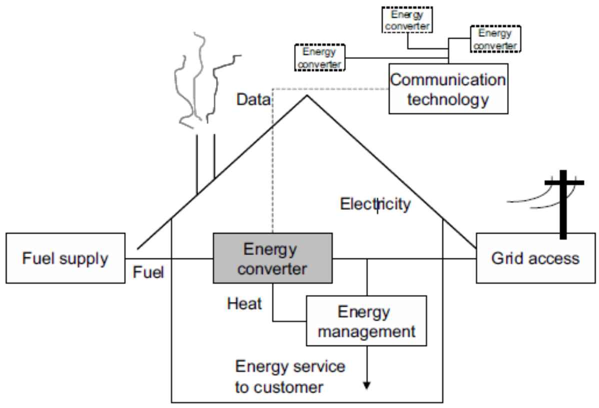

Figure 1: Technological components of a micro cogeneration system

2.1. Reciprocating Engines

Reciprocating engines are based on conventional piston-driven internal combustion engines. For micro cogeneration applications, typically, spark ignition (Otto-cycle) engines are used, comparable to those used in automobiles. In an Otto engine, a fuel, for instance natural gas, is mixed with air and compressed in a cylinder. This mixture is than ignited by an externally supplied spark. The now hot, expanding gas moves a piston, thereby causing the crankshaft to rotate. The mechanical energy produced by this combustion is then used to drive a generator. The exhaust heat as well as the heat from the lubricating air cooler and the jacket water cooler of the engine are recovered using heat exchangers, and then supplied to the heating system [4].

Reciprocating engines operate with less excess air compared to gas turbines. This leads to higher combustion temperatures, causing thermal NO_x production, due to the oxidation of the nitrogen contained in the air. There are two possibilities to reduce the amount of NO_x released. The engine can be operated in a lean mode, i. e. with excess air, so that reaction temperatures of the reaction are lowered. The second option is to operate the system almost stochiometrically (i. e. with an air/fuel ratio l=1) and to use a three-way catalyst.

The electrical efficiency of reciprocating engines, defined as net electrical energy output divided by natural gas input, depends strongly on the electrical capacity of the system *(Figure 2).* At sizes below 15 kWel, efficiency generally does not exceed 26 % [4].

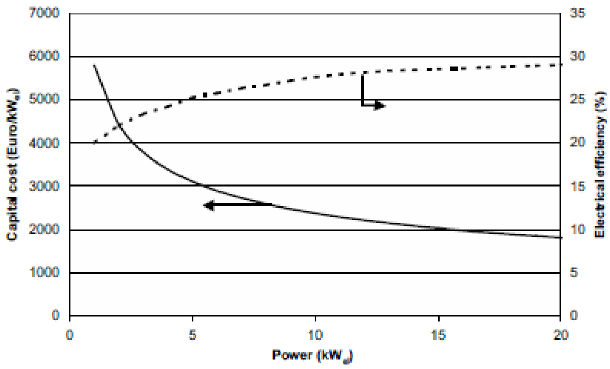

Figure 2: Capital cost and electrical efficiency of reciprocating engines as a function of the size of the system [4]

Thermal efficiency depends on the system and its level of heat integration (e.g., whether condensing heat is used). Combined electrical and thermal efficiency (total efficiency) varies between 80 and well above 90 %. Similar to electrical efficiency, capital costs per kW_{el} depend on the electrical capacity of the system. A significant decline of capital costs (scale effect) can be observed particularly as systems reach the 10 kW_{el} range (*Figure 3*).

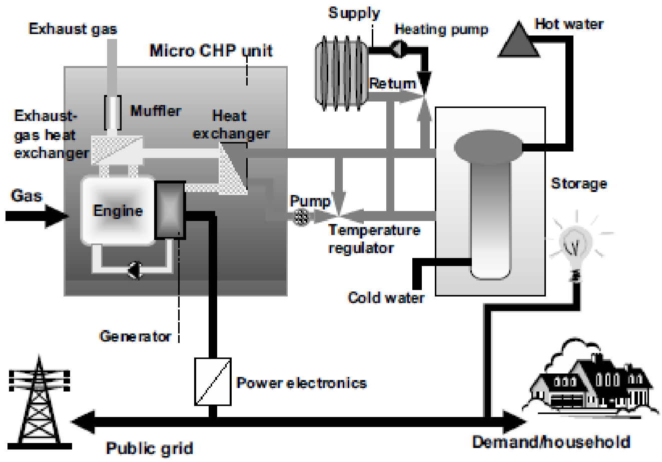

Figure 3: Principle components of a reciprocating engine system (adapted from Ecopower)

Reciprocating engines are commercially available and produced in large numbers by a variety of companies worldwide. The market leader is the Germany-based company Senertec. The Senertec model – called Dachs ("badger") – generates 5.5 kWel and a thermal power of 14 kW (Figure 4). It achieves 25 % seasonal electrical efficiency and thermal efficiencies above 80 % (depending on the building, over 90 % when using a condensor). As of fall 2004, Senertec had sold 10,000 of these models.

Other companies providing micro cogeneration units include Power Plus (recently purchased by the boiler company Vaillant) [13], with its 4.7 kW_{el} Ecopower module, capable of modulating its capacity, and the US-based Vector CoGen (5 and 15 kW_{el}), using a Kawasaki combustion engine. The latter is currently optimized for series production. According to the product specifications, Vector CoGen units achieve electrical efficiencies of around 28 to 34 % and total efficiencies between 70 and 79 %. In Japan, the companies YANMAR, Sanyo and AISIN also develop reciprocating engine based power stations.

Figure 4: Senertec Dachs (left) and PowerPlus Ecopower (right): examples of reciprocating engine micro cogeneration for apartment houses and small commercial enterprises (Sources: Senertec and Ecopower)

2.2. Stirling Engines

Unlike spark-ignition engines, for which combustion takes place inside the engine, Stirling engines generate heat externally, in a separate combustion chamber. In the Stirling engine, developed in 1816 by Robert Stirling, a working gas (for instance helium or nitrogen) is, by means of a displacer piston, moved between a chamber with high temperature and a cooling chamber with very low temperature. On the way from the hot to the cold chamber, the gas moves through a regenerator, consisting of wire, ceramic mesh or porous metal, which captures the heat of the hot gas and returns it to the gas as the cold gas moves back to the hot chamber.

Stirling engines can be designed in different configurations, distinguished by the position and number of pistons and cylinders and by the drive methods (cinematic and free-piston) [15]. The mechanical energy of the Stirling engine is used to drive a generator.

Due to the fact that fuel combustion is carried out in a separate burner, Stirling engines offer high fuel flexibility, in particular with respect to biofuels,
and, because of the continuous combustion, lower emissions. In principle, other heat sources, such as concentrated solar irradiation, can be used. Companies such as Solo and Sunmachine have developed parabolic mirrors for that purpose.

Stirling engines have the potential to reach high total (electrical plus thermal) efficiencies. Their electrical efficiencies, however, are only moderate. So far, 20 % seasonal average efficiency has been achieved in larger systems, with a predicted > 24 % for future models. Small Stirling engines are designed for low cost; consequently, they achieve lower electrical efficiencies than larger units, typically around 10 to 12 %.

Stirling engines are in between the pilot and demonstration phases and marketing. There are still field trials being carried out; but initial commercial products are already defined and on the verge of series production. The New Zealand-based company WhisperTech is developing a Stirling engine called WhisperGen, with a capacity of up to 1.2 kWel and 8 kW of heat (*Figure 5*). In the WhisperGen, four sets of piston cylinders are put in an axial arrangement. The British utility Powergen, part of Germany's E.ON, has ordered 80,000 WhisperGen power stations, due to be delivered by mid 2005. A prerequisite for this is the establishment of series production facilities. As Stirling engines require very precisely produced components, the scale-up from small-scale to series production presents a considerable challenge.

Figure 5: Example of small (≈ 1 kWel) Stirling engine micro cogeneration: WhispherTech

2.3. Fuel Cells

A fuel cell converts the chemical energy of a fuel and oxygen continuously into electrical energy. Typically, the fuel is hydrogen. The energy incorporated in the reaction of hydrogen and oxygen to water will be partially transformed into electrical energy [14].

The "secret" of fuel cells is the electrolyte, which separates the two reactants, H_2 and O_2, in order to avoid an uncontrolled, explosive reaction. Basically, the fuel cell consists of a sandwich of layers that are placed around a central electrolyte: an anode at which the fuel is oxidized; a cathode, at which the oxygen is reduced; and bipolar plates, which feed the gases, collect the electrons, and conduct the reaction heat (*Figure 6*). To achieve higher capacities, a number of single fuel cells can be connected in series. This is called a fuel cell stack.

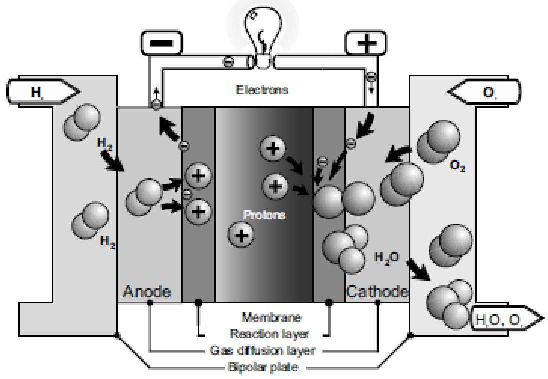

Figure 6: Basic construction of a fuel cell-example Polymer Electrolyte Fuel Cell

Fuel cell micro cogeneration units are either based on Polymer Electrolyte Fuel Cells (PEFC; also Proton Exchange Membrane Fuel Cell, PEMFC), using a thin membrane as an electrolyte and operating at about 80° C, or Solid Oxide Fuel Cells (SOFC), which are high-temperature fuel cells working at 800° C. Recent efforts have been working toward the development of high-temperature molten carbonate fuel cells for this lowpower segment.

Typically, natural gas is the available fuel for micro cogeneration applications. It mainly consists of the hydrogen-containing methane (CH_4), which is converted into hydrogen in a so-called reforming reaction. This takes place either in a separate device, the reformer, or, as in the case of high-temperature fuel cells, inside the stack (internal reforming).

Taking natural gas as the dominant fuel for fuel cells: In the short- and medium-term perspective, low temperature fuel cells (Proton Exchange Membrane Fuel Cells, PEMFC) in the low-power range may reach seasonal electrical efficiencies on the order of 28 to 33 %; in the long-term it is possible to achieve up to 36 % for domestic systems. However, it is so far unclear whether fuel cell systems can achieve the same thermal efficiencies as promised by the competing technologies. This is due to the fact that the heat cannot be extracted at well-defined points in the system, but rather at many dispersed heat sources, leading to greater measures being required for insulation and heat exchange.

2.4. Summary of technologies

In (*Table 1)* different conversion technologies are compared on the basis of selected criteria. In addition,

Table 1: Characteristics of micro cogeneration technologies

Conversion technology	h_{el}	h_{th}	Noise level	Pollutant emissions	Fuel flexibility	Market availability	Economic viability
Reciprocating engine	20-25	>85	Medium	Rather high, depending on catalyst/engine technology and maintenance	Medium	Commercially available	Given for certain applications
Stirling engine	10-24 (depending on the Stirling concept)	>85	Low	Very low to medium (depending on the burner type)	High	Near to market	Cost reduction necessary
Fuel cell	28-35	80-85	Low	Zero (H_2) to almost zero (hydrocarbons)	Medium	Pilot plants, R&D	High cost reduction necessary
h-efficiency; el-electric; th-thermal							

(*Figure 7)* depicts the status of market development of the various technologies.

Whereas *reciprocating engines* are commercially available, produced in large numbers and achieving high electrical and total efficiencies, they suffer from higher exhaust emissions compared to the competing micro cogeneration systems [6].

Because fuel combustion is carried out in a separate burner, *Stirling engines* offer lower emissions as well as high fuel flexibility, allowing, in particular, for the use of bio-fuels and solar irradiation. Stirling engines have the potential to achieve high total efficiency, though with only moderate electrical efficiency. Smaller Stirling engines have an even lower electrical efficiency and are primarily designed to be low cost. *Fuel cells* are still in the R & D phase, with a number of pilot plants currently being tested. They offer the potential benefit of the highest electrical efficiency and almost zero local emissions. Additionally, the high ratio of electrical to thermal efficiency (power to heat ratio) might increase the CHP electricity generation potential, because with given (and limiting) heat demand, more electricity can be produced. In the last decade, considerable efforts have been made to further develop this technology. However, it remains unclear whether fuel cell systems can ever achieve a total efficiency equaling those promised by competing technologies. Also, the high capital cost of early product generations remains a major challenge [16].

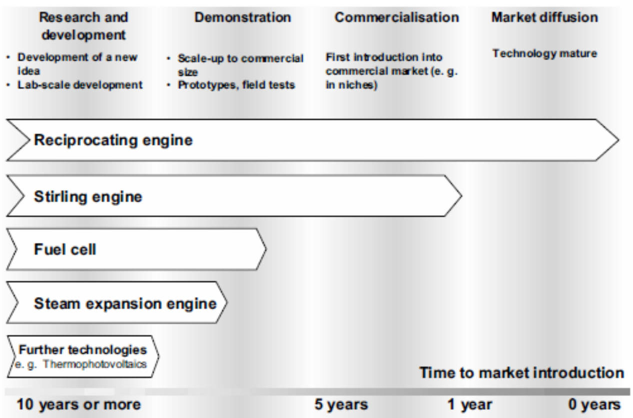

Figure 7: Status of market development of micro cogeneration technologies

3. CONVERSION TECHNOLOGIES

A conversion technology serves to convert chemical energy that is stored within a fuel into “useful” forms of energy, i.e. electricity and heat. A number of different conversion technologies have been developed which have domestic CHP applications *(Figure 8).* The conversion process can be based on combustion and subsequent conversion of heat into mechanical energy, which then drives a generator for electricity production (e.g. reciprocating engines, Stirling engines, gas turbines, steam engines). Alternatively,it can be based on direct electrochemical conversion from chemical energy to electrical energy (i.e. fuel cell). Other processes include photovoltaic conversion of radiation (e.g. thermo photovoltaic devices) or thermoelectric systems [8].

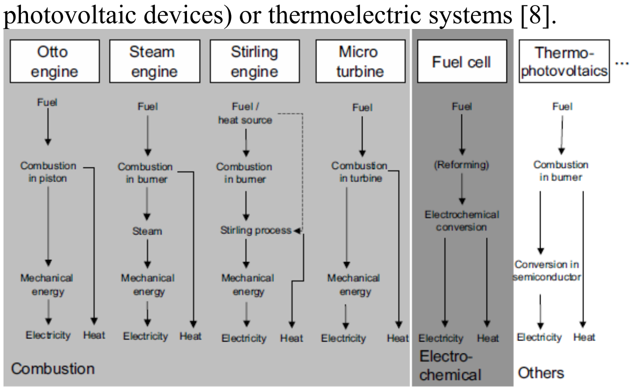

Figure 8: Cogeneration technologies and conversion steps

In principle, most conventional cogeneration systems can be downscaled for micro cogeneration applications. However, some of them have yet to be successfully implemented for very small applications. Micro gas turbines, for instances, have only been developed with capacities above 25 kWel and are thus not categorized as micro cogeneration technologies according to our definition.

4. ECONOMICS OF MICRO COGENERATION

The prospects of a broad diffusion of innovative micro cogeneration technologies depend significantly on their economic performance. In this chapter, the economic viability of micro cogeneration will be assessed from three different perspectives: that of two potential micro cogeneration operators, property owners and vertically integrated utilities, as well as that of society in general.

4.1. Micro Cogeneration Technologies

The economic performance of micro cogeneration plants is assessed with regard to a number of representative micro cogeneration technologies which are also used for the ecological assessment, allowing a direct comparison of the economic and ecological performance of these technologies [11].

The selected technologies represent micro cogeneration plants which are either already available on the market or are at an advanced stage of development and are expected to be brought onto the market round about by 2005. Due to the high capital costs of fuel cells and the considerable uncertainty surrounding their achievable target costs [17], we do not include fuel cells in the comparison of economic performance.

Reciprocating engines with an electrical capacity of about 5 kW and upwards have been available for many years. The Dachs by Senertec is the market leader in micro cogeneration plants in Germany with 10,000 engines having been produced by October 2004. Technologies 3, 4, and 5 in Table 1 correspond to different versions of the Dachs. The Ecopower by Power Plus Technologies is also a reciprocating engine and corresponds to technology 2 in Table 1. Some companies are currently developing smaller reciprocating engines. Since 2003, Osaka Gas in Japan has been marketing a reciprocating engine from Honda with an electrical capacity of 1 kW. The engine is sold together with a boiler and a heat storage tank for about € 5,500 in Japan but is not yet available in Europe. The package costs in Japan are used as the basis for the 1 kWel reciprocating engine, technology 1, in (*Table 2)*.

Stirling engines are being developed by a number of companies. Several companies (e.g. Enatec, Powerbloc, WhisperTech, MicroGen) are focused on developing engines with a capacity of about 1 kWel, since this size is well-suited to single-family houses. The Whispergen, developed by WhisperTech, is likely to be the first plant of this size to be brought onto the market in 2005. After the completion of field tests in the UK, the British E.ON company Powergen ordered 80,000 WhisperGen units which will be sold for about £ 3,000 in the UK.2 The WhisperGen is used for specifying reference technology 6. Reference technology 7 corresponds to a somewhat larger Stirling engine of 3 kWel, which is currently being developed by Mayer & Cie. Purchase costs for 2004 are quoted at € 13,000 [18]. Reference technology 8 refers to a Stirling engine of 9 kWel that has been developed by the company Solo.

About 40 plants have been sold so far. Purchase costs for 2003 are quoted at € 24,900 [19].3 Since the size and performance of these technologies vary, it should be noted that they are not directly comparable. In addition, some cost estimates or parameters are still associated with uncertainty. The results of the analysis can therefore only be indicative; but they do provide an initial assessment of the economic performance of different micro cogeneration technologies. *Table 1* summarizes the economic parameters for the reference technologies. The price basis of cost estimates is 2005.

4.2. Reference Buildings

Micro cogeneration technologies can be installed in different residential or commercial properties. The economic performance of the plants not only depends on investment, operation and fuel costs but also on the heat and electricity demand characteristics of the buildings. To reflect differences in heating and electricity demand, the economic performance of the eight reference technologies is assessed in five different buildings which represent typical potential applications in Germany.

We consider two single-family houses, two apartment buildings, and a hotel. The heat demand characteristics of these buildings are taken from a CHP simulation tool [20]. The electricity demand is based on a representative survey of households in Germany [21]. Key parameters of the five buildings are illustrated in (*Table 3*).

In Germany, the conditions for electricity supply from micro cogeneration plants have changed considerably with the liberalization of the electricity market. All electricity consumers, including buildings which are supplied with micro cogeneration plants, may choose their electricity supplier. In the case of single-family houses, micro cogeneration plants usually supply electricity and heat to the property owners who have chosen to install them. However, in apartment buildings an operator of a micro cogeneration plant cannot force the tenants to purchase electricity from the micro cogeneration plant. If a tenant prefers to be supplied with electricity from another

Table 2: Technical parameters and estimated costs of selected micro cogeneration technologies

	Reciprocating engines					Stirling engines		
	1	2	3	4	5	6	7	8
Capacity								
Electric [kW]	1	4.7	5.5	5.5	5	0.8	3	9.5
Thermal [kW]	3.3	12.5	13.9	14.9	12.6	8	15	26
Efficiency								
Electric [-]	20%	25%	25%	25%	25%	10%	15%	24%
Total [-]	85%	88%	88%	93%	88%	85%	90%	96%
Investment costs								
CHP module [€]	5,700	13,200	13,300	14,500	14,400	4,300	13,300	25,900
Other [€]	1,000	3,700	3,700	3,700	3,700	1,200	3,400	5,300
Maintenance costs [€/MWh$_{el}$]	50	36	26	26	26	20	15	10
Economic lifetime [h]	20,000	80,000	80,000	80,000	80,000	80,000	80,000	80,000

Table 3: Characteristics of reference buildings for the economic assessment of micro cogeneration plants

	Single-family houses		Apartment houses		Hotel
Heat demand	Low	Average	Low	Average	
Heating surface [m²]	131	112	457	913	1,263
Heating load [kW]	7	11	23	67	75
Heating demand [MWh/a]	9	16	29	109	84
Hot water demand [MWh/a]	2	3	12	19	38
Elecrticity demand [MWh/a]	4	3	13	27	49

supply company, the micro cogeneration plant operator is forced either to produce less electricity or to feed additional electricity into the grid. Feeding electricity into the grid or selling electricity to consumers elsewhere are both less attractive in economic terms. For micro cogeneration operators in properties with several parties, therefore, it is a key prerequisite that a large amount of the generated electricity be sold to consumers directly at the production site. Some operators of micro cogeneration plants offer a discount of 5 to 10 % in relation to the electricity price of the local utility to their consumers in apartment buildings. In practice, this incentive has proven to be sufficient for operators under Third Party Financing arrangements to be able to supply about 80 to 90 % of electricity consumers in apartment buildings. Where several parties are supplied by one operator, we calculate the economic performance on the assumption that only 80 % of the parties are supplied with electricity from a micro cogeneration plant.

In the absence of CHP, heat is usually provided by gas- or oil-fired boilers. In the case of apartment buildings, heat may be generated by a central boiler, which distributes heat to all apartments, or by small boilers for each apartment. In Germany, most apartment buildings are equipped with a central boiler. In this case, the boiler could be replaced or supplemented by a micro cogeneration plant operated by the owner of the building or a third party.

Supplying single apartments in apartment buildings with micro cogeneration is more difficult. In principle, Stirling engines of about 1 kWel could be used in individual apartments instead of boilers since they run rather noiselessly and are not expected to require frequent maintenance. However, in practice, the deployment of micro cogeneration in individual apartments would be difficult for two main reasons: Firstly, connecting a micro cogeneration plant would require modification of the electricity connection. Secondly, most apartments in Germany are rented and property owners do not have economic incentives to invest in micro cogeneration since they do not profit from saved energy costs and can only recoup investment costs to a limited extent via increased rents. In the context of energy-saving measures for buildings, this problem is broadly known and also referred to as the user-investor dilemma. As a result, we only consider centralized heat supply by a single boiler in the case of apartment buildings.

5. MICRO COGENERATION IN SERBIA

In order to encourage the introduction of cogeneration in Serbia, the Serbian government during 2009 issued a special decree on incentive measures for the production of electricity using renewable energy sources and cogeneration of electricity and heat energy. This regulation is supposed to be the trigger for the rapid development of cogeneration and our some sort of pairing with the European Union in this regard. From the contents of this Decree, Article 4, paragraph 2, it is seen that the reduced price of electricity at the power grid to be in the range of 7.6 to 10.4 s € / 1kWh. There are no special rules regarding microcogeneration.

5.1. General information about the object

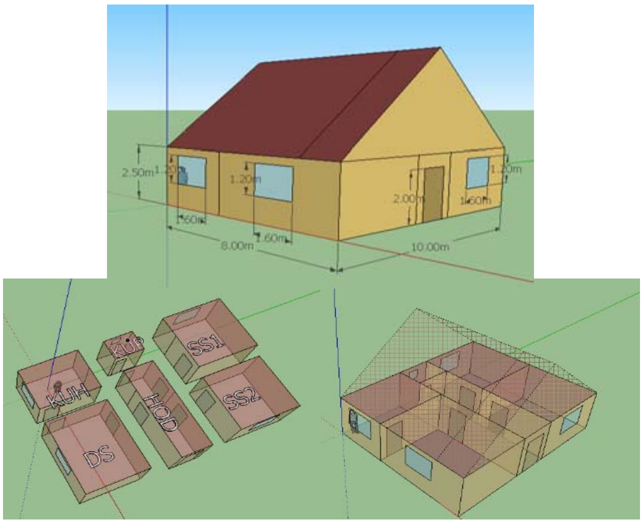

Figure 9: Appearance of the building

Table 4: General information

General information	
Year of construction	1991.
Total area	80 m²
Heating surface	80 m²
Heating volume	200 m³
Ceiling height	2,5 m
Floors	one floor

Energy demand facility, heat and electricity, is calculated as the average annual (six-month) compared to the previous combined consumption. For heating space heating facility used stove combustion efficiency of 80% ($\varepsilon = 0.8$) incorporating a central heating system. As fuel is used beech wood, the average consumption of 15 cubic meters during the heating season. Fifteen cubic meters of wood can be interchangeable volume of $V = 12\ m^3$. The density of beech wood in an absolutely dry state is $\rho = 680\ kg/m^3$, in dryish $720\ kg/m^3$ and $1070\ kg/m^3$ in raw [9]. For heating are used dripped wood. Lower heating value of wood with 15% of $CP = 15.4\ MJ/kg$ [10]. When this information is added and combustion efficiency of 80%, a simple way to calculate the heat may request object for one heating season *Qo [kWh]*.

$$Q_o = V \cdot \rho \cdot c_p \cdot \varepsilon$$

$$Q_o = 12 \cdot 720 \cdot 15{,}4 \cdot 10^6 \cdot 0.8$$

$$Q_o = 106444.8\ MJ = 29568\ kWh$$

Buffer tank for hot water storage that is part of microcogeneration plant for the storage of hot water which is heated object and provides domestic hot water. Heat therefore request should include the necessary heat for domestic hot water. Boiler *80 l*, contains the heater power of *2 kW*. The average daily consumption of this water heater is therefore approximately *4 kWh*, ie. consumed for domestic hot water during the heating season is:

$$Q_b = 720\ kWh$$

So the total heat requirement is:

$$Q = Q_o + Q_b = 29568 + 720 = 30288\ kWh$$

Required power (heat) SNR units is:

$$P_t = 8{,}42\ kW$$

As far as the average power consumption during the heating season it is done analyzing the current calculation for heating the season *2012 / 2013*. The analysis of the electricity bill gets to the average monthly consumption for the facility that calculates *485 kWh*, ie. that the average power consumption during the heating season:

$$E_o = 2914\ kWh$$

Since the power consumption required for heating domestic hot water, in case the installation mikrokogeneracionog plants compensated thermal energy from the water buffer is necessary to make a correction donijene average power consumption.

$$E_b = Q_b = 720\ kWh$$

Eb is the amount of electricity needed to heat the hot water during the heating season. So the corrected average electricity consumption for heating season *2012/2013*, in case the installed mikrokogeneracionog plants observed object is:

$$E = E_o - E_b = 2914 - 720 = 2194\ kWh$$

Required power facility (electricity) is:

$$P_e = 0{,}6\ kW$$

Microcogeneration units are selected based on the heat requirements of the building that are built. Based on thermal requirements of $Q = 30288\ kWh$ ie. $P_t = 8.42\ kW$ was chosen microcogeneration unit EcoPower 4.7. Vaillant Company [12, 13].

5.2. Environmental aspect, CO_2

On up the basis of date of monthly spending and given relations (burning 1 kg of coal is obtained about *2KWh* electricity, and without having emitted *2.93kg* CO_2), calculated as carbon dioxide emissions and saving coal for electricity production within microcogeneration by unit. In sum microcogeneration installing this unit during the period of the heating season, save to *1457kg* of coal and reduce greenhouse gas emissions (CO_2) to *3388kg* (*GHG* is *881.11kg* as CO_2, in the case of coal combustion was *4269.1kg*).

Table 5: Emissions from consumption

Months	Consumption *KWh*	Equivalent amount of coal *[kg]*	CO_2 emissions due to coal *[kg]*
October	326	163	477.6
November	501	250.5	734
December	511	255.5	748.6
Januar	565	282.5	827.7
February	445	222.5	652
March	566	283	829.2

Also analogous previous discussion, is equivalently calculated gas consumption required to drive microcogeneration community as well as the emissions created at the given ratio to that to generate *1kWh* of electricity requires about *0144m3,* and that *1m3* of natural gas is emitted about *2.1kg CO2*.

Table 6: Emissions from consumption

Months	Consumption *KWh*	Equivalent amount of gas *[kg]*	CO_2 emissions due to gas *[kg]*
October	326	46.9	98.49
November	501	72.1	151.41
December	511	73.6	154.56
Januar	565	81.36	170.9
February	445	64.1	134.6
March	566	81.5	171.15

6. CONCLUSION

This paper has dealt with micro cogeneration, the combined production of heat and power in small units for individual single family house. Its main characteristic is that power and heat generation takes place immediately at the consumer's site.

Micro cogeneration represents a socio-technical configuration that differs from the dominant architecture of contemporary electricity systems based on large-scale power generation with longdistance transmission to end-users. With micro cogeneration, consumers could potentially become operators of power plants. This would affect the roles and interests of a number of players in electricity markets to a more than marginal extent. For instance, electricity distribution and retail structures would be affected if micro cogeneration was broadly diffused.

With respect to ecological performance, we conducted an environmental analysis of micro cogeneration units. Compared to separate production, generating electricity and heat in micro cogeneration units leads to primary energy savings and greenhouse gas (GHG) benefits. Based on natural gas as a fuel, GHG emissions per kWh electricity and heat produced are typically 20 % – and under certain circumstances up to 45% – lower in comparison to condensing boilers and combined cycle power plants. In some cases, for example of technologies with low electrical and total efficiency, however, only little – if any – GHG mitigation can be achieved, compared to separate heat and power production with state-of-the-art technologies.

REFERENCES

[1]Rifkin J (2002) Wasser marsch. Frankfurter Allgemeine Zeitung, Frankfurt, Sept 24, 2002.
[2]Enquete-Kommission (2002) Nachhaltige Energieversorgung unter den Bedingungen der Globalisierung und der Liberalisierung. Deutscher Bundestag,Berlin.www.bundestag.de/parlament/kommissionen/ archiv/ener/index.html. Last accessed: Mar 15, 2005.
[3]Arndt U, Wagner U (2003) Energiewirtschaftliche Auswirkungen eines Virtuellen Brennstoffzellen-Kraftwerks. VDI-Berichte 1752:165-179.
[4]ASUE (2001) BHKW-Kenndaten 2001. Module, Anbieter, Kosten. Energiereferat der Stadt Frankfurt, Arbeitsgemeinschaft für sparsamen und umweltfreundlichen Energieverbrauch, Frankfurt Köln.
[5]Feldmann W (2002) Dezentrale Energieversorgung - zukünftige Entwicklungen, technische Anforderungen. Conference: Energie Innovativ 2002. VDI Verlag, Düsseldorf.
[6]Roon S (2003) Betriebskonzepte und Produkte virtueller Kraftwerke im liberalisierten Energiemarkt. Supervised by Pehnt M and Moers A. Thesis (Diplomarbeit) at the Technische Universität Berlin.
[7]WADE (2003) Guide to Decentralized Energy Technologies. World Alliance for Decentralized Energy, Edinburgh.
[8] Martin Pehnt, Martin Cames, Corinna Fischer, Barbara Praetorius , Lambert Schneider, Katja Schumacher , Jan-Peter Voß:" *Mikro Cogenertion"* Berlin 2002.g.
[9] http://sr.wikipedia.org/sr//Разговор:Буква .
[10] http://peletiranje.co.rs/pdf/Energija_u_preradi_drveta-1.pdf.
[11]Bernard R Kolanowski: "*SMALL-SCALE COGENERATION",* 700 Indian Trail, Lilburn, Georgia 2003.g.
[12]Planungsinformation ecoPOWER - Technische und inhaltliche Änderungen vorbehalten - Angaben ohne Gewähr, Vaillant, Deutshhland.
[13] http://www.vaillant.de/.
[14]Pehnt M (2002) Energierevolution Brennstoffzelle? Perspektiven, Fakten, Anwendungen. Wiley VCH, Weinheim.
[15]Educogen (2001) Educogen. The European Educational Tool on Cogeneration. Co-financed under the SAVE programme, Cogen Europe. www.cogen.org/projects/educogen.htm. Last accessed: Mar 9, 2005.
[16]Stephanblome T, Bühner V (2002) Virtuelles Kraftwerk: Energiewirtschaftliche Voraussetzungen & Leittechnik-Software. Conference: Energie Innovativ 2002. VDI Verlag, Düsseldorf.
[17] Krewitt W, Pehnt M, Temming H, Fischedick M (eds) (2004) Stationäre Brennstoffzellen Umweltauswirkungen, Rahmenbedingungen und Marktpotenziale. Study for the Ministerium für Umwelt, Naturschutz und Reaktorsicherheit (BMU). Erich Schmidt Verlag, Berlin.
[18]ASUE (2004) Infodienst neue Produkte. August 2004. Transferstelle für neue Produkte der Arbeitsgemeinschaft für sparsamen und umweltfreundlichen Energieverbrauch, Essen. www.transferstelle.info. Last accessed: March 15, 2005.
[19]ASUE (2003) Infodienst neue Produkte. August 2003. Transferstelle für neue Produkte der Arbeitsgemeinschaft für sparsamen und umweltfreundlichen Energieverbrauch, Essen. www.transferstelle.info. Last accessed: March 15, 2005.
[20]ZSW (2000) BHKW-Plan. Version 1.05.00. Excel Based Design Software for Small CHP Plants. Zentrum für Sonnenenergie- und Wasserstoff-Forschung, Stuttgart.
[21]FHG-ISI, DIW, GfK, IEU, TUM (2004) Energieverbrauch der privaten Haushalte und des Sektors Gewerbe, Handel, Dienstleistungen (GHD). Fraunhofer Institut für Systemtechnik und Innovationsforschung Deutsches Institut für Wirtschaftsforschung, GfK Marketing Services, GfK Panel Services Consumer Research, Institut für Energetik und Umwelt, Technische Universität München, Karlsruhe Berlin Nürnberg Leipzig München.

Developing Model of a Photoacoustic Measurement System

Slobodan Todosijević[1,2*], Slobodanka Galović[3,4], Jelena Tomić[1,2] and Zlatan Šoškić[2]
[1]Faculty of Electrical Engineering, University of Belgrade, Bulevar kralja Aleksandra 73 Belgrade (Serbia)
[2]Faculty of Mechanical and Civil Engineering, University of Kragujevac, Dositejeva 19 Kraljevo (Serbia)
[3]Vinča Institute of Nuclear Sciences, University of Belgrade, P. O. Box 522, 11001 Belgrade (Serbia)
[4]Joint Institute for Nuclear Research, Bogoliubov Laboratory for Theoretical Physics,
Dubna, Russia

This paper presents a complete view of instrumentation for photoacoustic measurements. The instrumentation consists of four substantial blocks: light source, lock-in amplifier, sound transducer and photoacoustic cell. The usual approach considers just the photoacoustic cell and physical processes that take part in it. The aim of the paper is to analyse the complete system and to develop a model capable of determining the transfer function of the system as a whole. Such a model would enable extension of the measurement range of photoacoustic instrumentation to higher and lower frequency regions.

Keywords: Experimental techniques, scientific instrumentation, photoacoustic effect

1. INTRODUCTION

For many years, the photoacoustic (PA) techniques have been used to determine thermal properties of semiconductors [1,2], metals [3,4], polymers [5], biopolymers [6], and composite materials such as silicon-epoxy systems [7] and two layered systems [8]. These studies have been done mostly using the open photoacoustic cell (OPC) configuration. The PA effect has also been used to study spectroscopic phenomena, such as the absorption coefficient as a function of wavelength, and to study electronic transitions. Photoacoustic (PA) cells, used to study solid samples, are usually constructed as open-ended [9-12], which implies that the PA chamber is at one end sealed by the sample itself.

An often employed variation of the design described above is referred to as open photoacoustic cell [13-15]. In this technique the air chamber is omitted and the sample is directly placed on an electret microphone. Only the small air volume within the microphone then serves as a transducer medium [31].

Another commonly used PA cell design encloses the sample inside the PA chamber [16-18]. This technique suffers from the same problems as the open-ended PA cell. In addition, it is unpractical because the PA cell has to be dismantled each time prior to replacement of the sample, which makes it unsuitable for *in situ* applications.

In the PA technique, two kinds of signals are obtained simultaneously as output data, and these are amplitude and phase of the PA response. By fitting these signals, it is possible to calculate thermal properties of the studied material [19-22]. In order to obtain those signals, using any kind of configuration, it is necessary to calibrate the microphone in dependence function of the frequency or the wavelength of the sound and, in some cases, in dependence of temperature.

The microphone response or instrumental function includes fluctuations of the light source, as well as electronic and environmental noises. After obtaining the instrumental function (IF), a two channel (amplitude and phase) fitting process is carried out to calculate the physical parameters (thermal diffusivity and absorption spectrum) of the sample under study.

Usually, instrumentation of open-ended PA cell consists of light source, microphone, lock-in amplifier and the PA cell itself. The contemporary trend in improvement of PA measurements is to reduce use of hardware devices by replacing hardware functions by software functions as much as it is possible. That way, the noise generated by instrumentation is reduced, and measurement error is decreased. With this idea are already implemented software solutions for frequency modulation of light beam (instead using a chopper) and lock-in amplifier, as it will be explained in more details later. An appropriate software interface that communicates with instrumentation through a PC is also developed.

As far as hardware components are concerned, the substantial part is the photoacoustic cell. A light source, powered by a signal generator, represents excitation of the system and a microphone is detector. Signals from the light source and the microphone are brought to the amplifier, which also represents a hardware device, and finally the amplified signals are led into the sound card of a PC.

This paper presents a detailed description of the existing instrumentation that is used for PA measurements in Serbia and proposes the following steps in its improvement.

2. THE THEORY OF PHOTOACOUSTIC EFFECT

The photoacoustic effect was first discovered by Alexander Graham Bell in his search for means of wireless communication. Bell succeeded in transmitting sound with an invention he called the “photophone,” which transmitted sound signals by a beam of sunlight that was reflected by a vocally modulated mirror. This effect essentially was forgotten until researchers at Bell (coincidence!) Labs, led by Allen Rosencwaig, rediscovered the effect and provided a theoretical basis for its explanation [23].

The basic principle of photothermal (PT) techniques is the absorption of light by a sample that, as a

*Corresponding author: Dositejeva 19, Kraljevo, todosijevic.s@mfkv.kg.ac.rs

consequence, changes its thermal state. The change may be either a change of temperature or other thermodynamic parameter of the sample related to the temperature. Measurements of temperature, density, or pressure change that occur due to optical absorption are substantially the basis for all PT spectroscopic methods. PT analysis can be considered as an indirect absorption measurement, as the measured quantity is not an optical signal. It should be noted that the classical absorption measurements are not direct measurements either [24]. However, the measured quantity in the presented case is an optical one, the transmitted light intensity, while the absorbed light intensity is calculated as the difference between the intensities of the incident and transmitted light. PT signal, which occurs due the sample heating, is directly proportional to the absorbed electromagnetic energy. Neither scattered nor reflected light contributes to the signal, which is in contrast to the conventional transmission spectroscopy. This is the reason why PT spectroscopy is particularly attractive for absorption measurements in different media (gaseous, liquid and solid) containing scattered particles, and on the boundaries of solids.

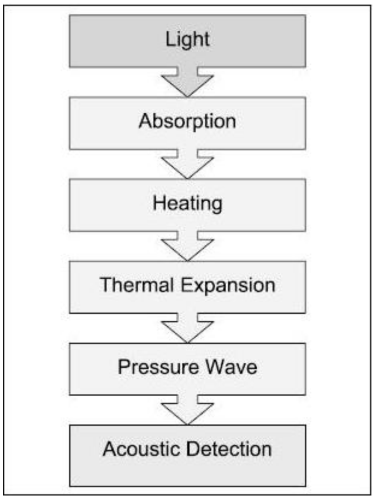

Figure 1: Principle of photoacoustic experiment

The most straightforward detection scheme for photoacoustic signal is the observation of the temperature change at the illuminated sample surface. The technique is called thermometric detection if this observation is carried out on the sample surface by temperature transducers. The detection of the thermal radiation emitted from the sample surface is more common technique, and it represents the temperature distribution within the sample. Photoacoustic (PA) techniques are PT absorption measurements that are based on detection of this sound wave. Pressure variation wave arises as a consequence of two mechanisms: thermal deformations of the sample (direct effect) and thermal expansion of the adjacent air adiabatically heated by the sample (indirect effect). This pressure variation wave in air represents a sound wave (sound signal).

The means for the detection of a PA signal are various: if the sample is in gaseous environment a microphone may be employed, whereas pressure fluctuations in a solid or liquid environment can be probed by pressure sensitive elements like piezoelectric transducers. Alternatively, the pressure fluctuations can be observed by optical methods. Although a PT effect can be induced by any light source, lasers are the preferred excitation source nowadays for two reasons: 1) the PT signal, to a first approximation, is proportional to the temperature rise in the sample and thus proportional to the absorbed energy, i.e. pulse energy, 2) the selectivity of a PT analysis in many applications, as it is the case with other absorption techniques, depends on the bandwidth of spectrum the excitation light beam.

The theory describes PA as a sequence of processes presented in Figure 1. At low frequencies, the theory shows that the PA response is dominated by the indirect PA effect [29], while at high frequencies the contribution of the direct PA effect becomes important [25]. Besides, the theory also shows [30] that at low frequencies heat transfer through the PA sample may be treated as a diffusion process, while at high frequencies the wave nature of heat propagation has to be considered.

The most important theoretical model, the one that is mostly used for construction of PA measurement equipment and in interpretation of PA measurement results, is "thermal piston model" developed by Rosencwaig and Gersho [30]. Thermal piston model considers thermal expansion of the adjacent air, i.e. indirect PA effect, as the dominant mechanism that generated PA response, and treats heat transfer as a diffusion process. Therefore, the "thermal piston" model is applicable for low modulation frequencies, and development of advanced PA measurements must be based on more general theoretical models.

3. EXPERIMENTAL SETUP

In this paper we analyse photoacoustic measurement system in Laboratory for atomic, molecular and laser spectroscopy of Institute of Physics in Zemun, near Belgrade (Serbia). The Figure 2 shows a diagram of the complete setup for PA measurements. The measurement system consists of four substantial parts: a light source, a sound transducer, a lock-in amplifier and a PA cell itself. The heating of the sample is achieved by the light source and the detection is performed by the sound transducer, a microphone in this case. The PA cell is designed in such way that it occupies small volume. Sample is not directly placed at the surface of a microphone, but on a rubber ring that is placed at the edge of the microphone. The rubber ring is sealed by vacuum grease to the surface of the microphone, and the sample is sealed by vacuum grease to the rubber ring. The reason for use of vacuum grease is insulation from the environment. In that way is created a very small sealed volume between the sample and the microphone, and that is PA cell. Therefore, the volume of a PA cell consists of the hole in the microphone and the part of volume obtained by lifting the sample for the thickness of the rubber ring. Figure 3 shows elements of assembly of a PA cell: a rubber ring, a microphone and a light source (laser diode) mounted on a photocell.

Samples that are used in PA measurements are in solid state. However, if a sample is not opaque, then it is necessary to put an absorption layer at the illuminated side of the sample to avoid direct illumination of microphone. The thickness of the absorption layer has to be much smaller than the thickness of the sample, so that the influence of the absorption layer on the mass and mechanical properties of the sample could be neglected. Because of high absorptivity, good thermal conductivity and small density aluminium foils are often used as absorption layers.

Photocell detects amplitude of the light after exiting from laser diode, but before it passes through the sample. Microphone detects amplitude of the sound. The electric signal from microphone and the electric signal from the photocell are led by separate cables to an amplifier, and the amplified signals are further led by a single cable to the sound card of a PC. Modulation of the excitation in wide spectrum of frequencies is achieved by a modulator which is put between the PC and the light source.

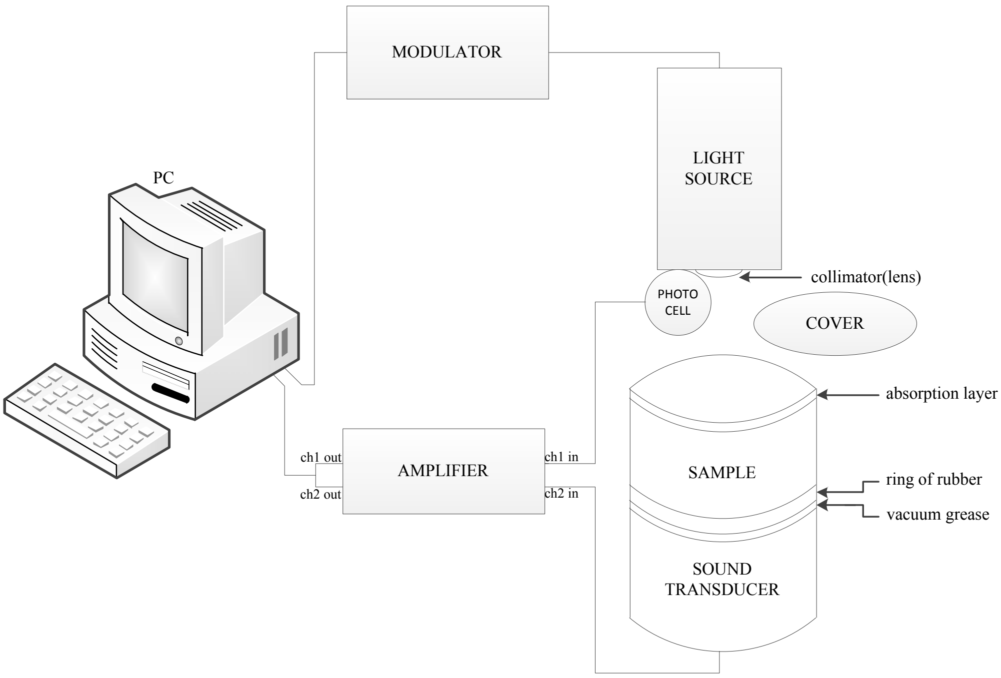

Figure 2: Schematic diagram of the photoacoustic cell coupled to the data acquisition system as well as the optical train of the heating source

The light source and the microphone with the sample, which make the PA cell, are fixed on a stand, as presented in the Figure 4.

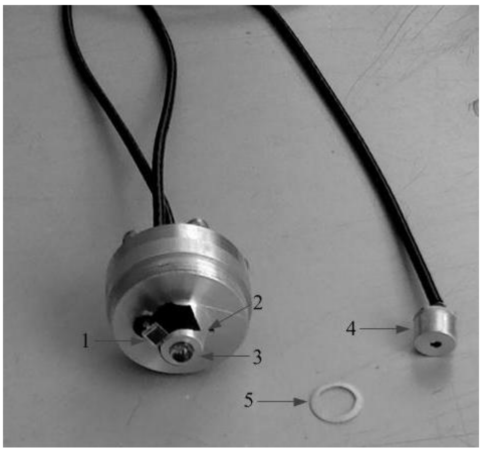

Figure 3: 1) photocell; 2) light source (laser diode); 3) lens (collimator); 4) microphone with preamplifier (sound transducer); 5) ring of rubber

Any signal may be represented by two derived signals, amplitude signal and phase signal; the PA signal can be described according to Equations. (1) - (3),

$$PA = r_A\left(\cos\theta_A + i\sin\theta_A\right), \tag{1}$$

$$r_A = \sqrt{x_A^2 + y_A^2} \;, \tag{2}$$

$$\theta_A = \arcsin\frac{y_A}{x_A} \;, \tag{3}$$

where r_A represents the amplitude signal and θ_A represents the phase signal. During the photoacoustic experiments, the detected signal (PA) consists of the direct ac signal from the sample (S_{ac}) and by the modulated dc noise, which is modulated by the ac source [26],

$$PA = S_{ac} + S_{dc} \tag{4}$$

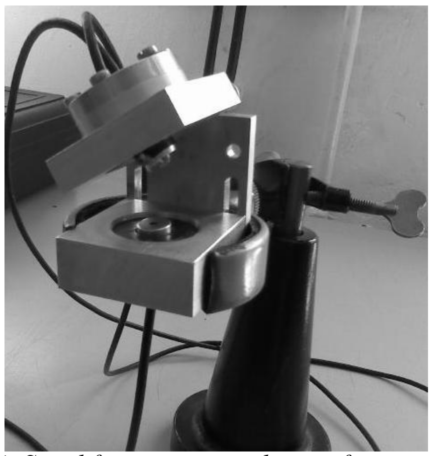

Figure 4: Stand for positioning devices for measurement

In order to derive the signal from the sample, it is necessary to subtract the modulated noise signal from the measured signal. In the Figure 2, between the light source and microphone, is shown a device called "the cover", which has a purpose to eliminate the illumination from the light source which causes signal from the sample, enabling separate measurement of the modulated noise signal. The cover has to be completely opaque. During the measurements of the noise signal, it is necessary to provide the identical conditions as during measurements with illuminated sample. Those conditions include humidity, temperature in the room, ambient noise and everything else that can affect the transfer characteristic of the system.

3.1. The light source

Light source is used to illuminate the sample. Two kinds of sources may be used: a laser diode and a LED. Laser diode has the wavelength of light 660 nm, average power of 15 mW (the range of power is 0 mW - 30 mW) and a lens which covers the diode. Lens is used to collimate the light and direct it to the sample. LED has a wide spectrum of wavelengths of emitted light, shown in the Figure 5, with the peak at 460 nm. The average power of LED is 8 mW and the light diverges to the sample. Light source is mounted on the stand (Figure 3) and its one end is connected with the modulator. The cover is mounted on the opposite end of the light source. The cable of the photocell passes through the frame of the light source.

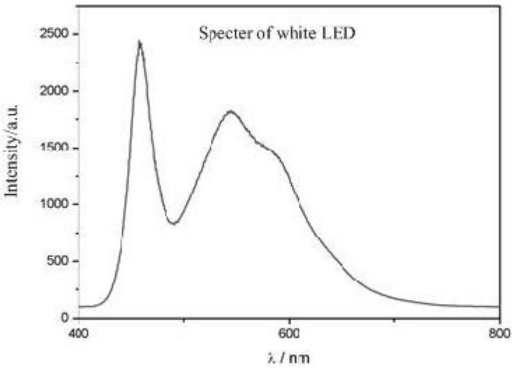

Figure 5: Spectrum of light source (LED)

3.2. Sound transducer

As it is shown in the Figure 3 and Figure 4, the sound transducer is an omnidirectional microphone. It is a part of "JININ electret condenser microphone units" set, model ECM-30. The sensitivity of microphone under conditions: 0 dB = 1 V/μbar, f = 1 kHz, VCC = 4.5 V, RL = 1 kΩ is within ±3 dB. Other characteristics are shown in the Table 1.

Table 1: Characteristics of the microphone

Characteristic	Data
Impedance	Low
Standard voltage	4.5 V
Operating voltage range	1.5 V to 10 V
Current drain	0.3 mA MAX
S/N ratio	40 dB or more
Maximum input sound pressure	120 dB SPL

The frequency response curve is presented in the Figure 6. The operating range of the microphone is from 30 Hz to 20 kHz with the largest deviation of 6 dB at 5 kHz. Besides, there is a significant deviation of 4 dB at 30 Hz. Frequency response curve is flat in the range 50 Hz-3 kHz, and it is used as the measurement range in PA measurements.

3.3. Lock-in amplifier

This part of experimental setup is usually implemented as hardware but the setup described in this paper uses lock-in amplifier implemented as software. The software code is written in C++ language. In the code, the signals from A/D converter are multiplied with sine and cosine functions and then signals are reconstructed saving information of amplitude and phase, because the signal from the A/D converter of sound card has information on both the amplitude and phase of the PA response. Two signals from A/D converter, signal from photocell and signal from the microphone, are the inputs of the lock-in amplifier. Both signals are influenced by electronic noise, and the lock-in successfully separates signals from noise.

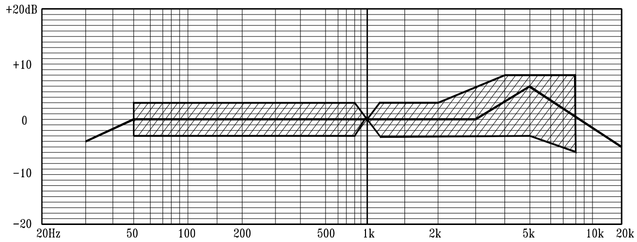

Figure 6: Microphone frequency response

The development of the software lock-in amplifier is the first advantage of the PA measurement setup, because any hardware device represents a new source of the unknown noise.

3.4. The modulator

The Figure 7 shows the front and the rear side of both the modulator and the amplifier.

The modulator is connected with BNC connectors on both ends - with PC at input and with light source at output. The third connector is for power supply, and the modulator may use a battery supply (lead accumulator, 12 V) or external power supply, which is shown in Figure 7 at front side. The coaxial cable which connects the modulator and PC has BNC connector at one end, but at the other end (the end which is connected with sound card of PC) has TRS connector (audio jack 3.5 mm connector). The cable which connects the modulator and the light source is also coaxial and has BNC connectors at both ends.

Figure 7: Front (on left) and rear (on right) side of the amplifier (black casing) and the modulator (white casing)

The modulator is the driver for the light source, and it is controlled by PC. In this way, the frequency of the light emission is determined by PC software and there is no need for hardware device for interruption of the light beam – chopper, where the speed of rotation of chopper then determines frequency of the excitation of the sample. However, the instability of rotation speed and inaccuracy in construction of the chopper make modulation not harmonic, thus introducing a new source of noise. The software control of modulation is the second advantage of the PA measurement setup.

3.5. The amplifier

This device shown in the Figure 7 has two input and two output channels, both with BNC connectors. The output signal of the microphone is significantly weaker than the signal from photocell and their amplifications are 100 and 10, respectively. The same switch is used for amplification of signals from photocell and microphone. There are two coaxial cables for input channels and two coaxial cables for output channels which become one coaxial cable with TRS connector (audio jack 3.5 mm stereo connector) at the end. The amplifier uses two NiMH (nickel-metal hydride) batteries for supplying by voltage of 8.4V.

3.6. PC Interface

The interface is GUI (Graphical user interface) implemented as in C++ program language. It has possibilities to set modulation frequency in pre-determined steps, initial and final frequencies, signal power and sampling rate.

The signal power is limited by the input range of the A/D convertor of the sound card. The amplitude of signal is highest at low frequencies, and with increasing of frequency the amplitude of the signal decreases. Therefore, if the input signal power overcomes input range of the sound card at the initial frequency, the measurement has to be stopped and repeated with decreased signal power.

The sampling rate is determined by characteristics of the sound card. Usually, the sampling rate is 8 kHz until the modulation frequency of 2 kHz and at modulation frequencies between 2 kHz and 20 kHz the sampling rate is 44.1 kHz.

The software has text file as output. The file contains the output data in five columns. The first column represents frequency, the second column represents amplitude of signal from the microphone, the third column represents signal from photocell, the fourth column represents ratio of amplitudes from the second and the third columns (normalisation) and the fifth column represents difference in phase between signals from photocell and the microphone. Besides, the software shows graph of amplitude of the response at a particular frequency.

3.7. Example

Measurement of PA response of a polypropylene sample with thickness of 666 μm will be presented as an example of PA measurements with the described measurement setup. Modulation frequencies were varied between 10 Hz and 3670 Hz in 10% steps. The amplification was 10 for modulation frequencies below 113 Hz, and 100 for higher frequencies. Power level was set at 40% of maximum for below 17 Hz, and at 100% for higher frequencies.

Data processing is performed by Matlab software package. The results are presented in Figures 8 and 9. The Figure 8 presents the ratio between the amplitudes, while the Figure 9 presents difference between the phases, of signals detected by microphone and photocell.

4. DISCUSSION AND CONCLUSION

This paper represents and initial step in an effort to further improve the described PA measurement system. The intended direction of the improvement is definition of an instrumental transfer function which would enable construction of instrument for material characterisation based on PA effect. Automation of the measurement process, which is impossible without knowledge of the instrumental transfer function, would substantially facilitate application of PA methods for general public.

The basic problem that makes experimental measurement of the instrumental transfer function difficult is that measurement cannot be performed without a sample, which means that it is not possible to experimentally separate instrumental transfer function and the transfer function of the sample.

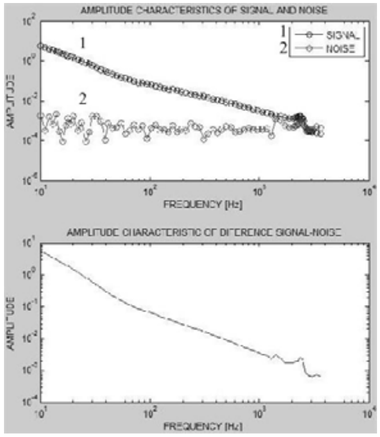

Figure 8: Ratio of amplitudes of signals detected by microphone and photocell

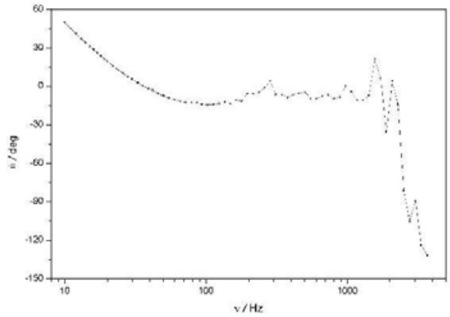

Figure 9: Phase difference between signals detected by microphone and photocell

Two concepts may be employed with the aim to experimentally measure instrumental transfer function of PA measurement system. The first procedure consists in application of reference samples, while the second consists in determining of separate transfer functions for each of the elements of the measurement chain, using appropriate calibration and characterization procedures.

Reference samples were already used for various purposes in PA measurements. Thin layers of gold or aluminium directly mounted onto the electret microphone were used to obtain the microphone response (constant time) [1,3,27]. In the case of PA spectroscopy, graphite was also used as the reference sample [28]. However, the use of reference samples for PA measurement has intrinsic conceptual drawback that it is not free of “Circulus vitiosus” remark, because the PA response of a sample may not be determined by other means.

On the other hand, measurement of the separate transfer functions of elements of the measurement chain has no conceptual deficiencies, but meets serious practical difficulties. The basic cause of the difficulties is that the absorption of the light beam, reflection of the light beam and sound propagation within a PA cell are spatial process that fundamentally depend on boundary conditions, meaning the exact shape and dimensions of the PA cell and PA sample. Therefore, even the processes of propagation of light and sound within a PA cell depend on the PA sample. For that reason, the characterization of measurement chain components should be performed without disassembling the PA measurement system, which represents a serious technical request.

Further improvements of the system are based on improvement of data acquisition process which should be performed by data acquisition board with 24-bits resolution. The application of the board will enable decrease of amplification of signals and application of digital filters, both leading to further electronic noise reduction.

ACKNOWLEDGEMENTS

Authors would like to express their gratitude to Laboratory for atomic, molecular and laser spectroscopy of Institute of Physics in Zemun for granting access to their research equipment and to Ministry of Education, Science and Technological Development of Republic of Serbia for financial support to this work through grant *TR37020*.

REFERENCES

[1] M. E. Rodriguez, J. J. Alvarado, I. Delgadillo, O. Zelaya, H. Vargas, F. Sánchez Sinencio, M. Tifito, and L. Baños, Phys. Status Solidi A **158**, 67 (1996).

[2] A. Pinto, H. Vargas, N. F. Leite, and L. C. Miranda, Phys. Rev. B **40**, 3924 (1989).

[3] C. Vazquez-Lopez, A. Calderon, M. E. Rodríguez, R. Colas, and S. Valtierra, J. Mater. Res. **15**, 85 (2000).

[4] P. Charpentier and F. Lepoutre, J. Appl. Phys. **53**, 608 (1982).

[5] J. A. Balderas-López and A. Mandelis, J. Appl. Phys. **90**, 2273 (2001).

[6] M. Yáñez-Limón *et al.*, Analyst (Cambridge, U.K.) **120**, 1953 (1995).

[7] M. E. Rodríguez, P. J. Mendoza, A. Mandelis, and L. Nicolaides, Nucl. Instrum. Methods Phys. Res. B **184**, 421 (2001).

[8] A. M. Mansanares, A. C. Bento, and H. Vargas, Phys. Rev. B **42**, 4477 (1990).

[9] K. Uchiyama, K. Yoshida X.-Z., Wu, and T. Hobo, Anal. Chem. **70**, 651 (1998).

[10] R. Takamoto, S. Yamamoto, R. Namba, M. Matsuoka, and T. Sawada, Anal. Chem. **299**, 387 (1995).

[11] K. Giese, A. Nicolaus, B. Sennhenn, and K. Kölmel, Can. J. Phys. **64**, 1139 (1986).

[12] V. A. Fishman and A. J. Bard, Anal. Chem. **53**, 102 (1981).

[13] M. V. Marquezini, N. Cella, A. M. Mansanares, H. Vargas, and L. C. M. Miranda, Meas. Sci. Technol. **2**, 396 (1991).

[14] L. F. Perondi and L. C. M. Miranda, J. Appl. Phys. **62**, 1 (1987).

[15] L. Mota, R. Toledo, F. A. L. Machado, J. N. F. Holanda, H. Vargas, and R. T. Faria, Jr., Appl. Clay Sci. **42**, 168 (2008).

[16] A. Rosencwaig, Rev. Sci. Instrum. **48**, 1133 (1977).

[17] M. Ohmukai, H. Mukai, and Y. Tsutsumi, Physica B **394**, 132 (2007).

[18] M. Silva, I. N. Bandeira, and L. C. M. Miranda, J. Phys. E: Sci. Instrum. **20**, 1476 (1987).

[19] S. Thomas, J. Isaac, and J. Philip, Rev. Sci. Instrum. **66**, 3907 (1995).

[20] O. Jr. Pessoa, C. L. Cesar, N. A. Pabel, H. Vargas, C. C. Ghizori, and L. C. Miranda, J. Appl. Phys. **59**, 1316 (1986).

[21] A. Cruz-Orea, I. Delgadillo, H. Vargas, A. Gudiño-Marinez, C. Vazquez- Lopez, A. Calderon, and J. J. Alvarado-Gil, J. Appl. Phys. **79**, 8951 (1996).

[22] B. Merté, P. Korpiun, E. Lüsher, and R. Tilgner, J. Phys. Colloq. **44**, 463 (1983).

[23] A. Rosencwaig, *Photoacoustics and Photoacoustic Spectroscopy* (R.E. Krieger Publishing Company, Malabar, Florida, (1980).

[24] C. Haisch and R. Niessner, Light and sound-photoacoustic spectroscopy, Spectroscopy Europe (2002).

[25] G. Rousset, F. Lepoutre, and L. Bertrand, J. Appl. Phys. **54**, 2383 (1983).

[26] Mario E. Rodríguez-García, Rubén Velásquez-Hernández, and María L. Mendoza-López, *Differential photoacoustic cell for electrochemical and dynamic process with temperature control*, REVIEW OF SCIENTIFIC INSTRUMENTS **78**, 034904 (2007).

[27] J. A. Balderas-Lopez, D. Acosta-Avalos, J. J. Alvarado, O. Zelaya-Angel, F. Sanchez-Sinecio, C. Falcony, A. Cruz-Orea, and H. Vargas, Meas. Sci. Technol. 6, 1163 (1995).

[28] O. Zelaya-Angel, J. J. Alvarado-Gil, R. Lozada-Morales, H. Vargas, and A. Ferreria da Silva, Appl. Phys. Lett. 61, 1 (1994).

[29] A. Rosencweig, A. Gersho, J. Appl. Phys. 47, 64 (1976).

[30] S. Galovic, D. Kostoski, J. Appl. Phys. 95, 2063 (2003).

[31] J. Kottmann, J. M. Rey, and M. W. Sigrist, New photoacoustic cell design for studying aqueous solutions and gels, REVIEW OF SCIENTIFIC INSTRUMENTS 82, 084903 (2011).

Developing Methodology for the Selection of Priority Local Infrastructure Projects to be Implemented in Specific Planned Period

Jovan Nešović[1,*] – Mirko Đapić[2]
[1]Public Energy Company "Toplana" Kraljevo
[2]Faculty for Mechanical and Civil Engineering Kraljevo

Selection of local infrastructure projects to be funded within one budget year is an important job for the management of local governments. On the one hand, the needs are very large (insufficient development of local infrastructure), and on the other hand, limited financial resources (especially in today's economic crisis). This paper defines a methodology how to determine priorities out of a large number of potential projects with use of two parameters (importance for the local community and cost of implementation). In this way we try to achieve the biggest effect for the community and assist local authorities in improving the quality of life within the limits of available funds.

Key words: project, criteria, ponder

0. INTRODUCTION

Implementation of local infrastructural projects is important for local governments from two aspects as follows:

- More quality infrastructure, satisfied citizens, creating better business environment to attract investments, which is of crucial importance for the economic development of local government,
- Employing local construction operative (which is particularly significant at times of economic crisis) therewith protecting workplaces in the local construction operative.

Public revenues of local governments in Serbia are nowadays limited and usually not nearly sufficient to fund all planned infrastructure projects in a one budget year. A list of proposed infrastructure projects (which may be called a "wish list") must comply with financial capabilities of local government. This is especially true for large infrastructure projects (often referred to as capital projects due to financial resources necessary for their implementation), whose implementation is a serious challenge for local governments. Therefore it is very important to make a good selection of projects for their implementation to provide most benefits to the community (social, environmental, utility, economic, etc.) at minimum cost. This paper presents a model of selection of infrastructure projects through a ranking process based on two parameters - importance for the community and costs of project implementation.

Project selection shall be done on the basis of analysis of multiple criteria with predefined number of criteria. All proposed projects shall be evaluated on the basis of same criteria, and projects to be financed, i.e. projects providing maximum benefit for the funds spent, shall be selected from the importance for the community and implementation cost diagram.

1. CRITERIA FOR THE EVALUATION OF LOCAL INFRASTRUCTURE PROJECTS

To select from among a series of infrastructure projects proposed for implementation the ones to be actually implemented in a specific planned period (allocate funds for implementation thereof) we shall use two parameters – importance of a given project for the local community and the amount of implementation cost.

Valuation of each projects shall be done on the basis of a point scale (specific weight of criteria for a given parameter) and by assigning ponder (significance of the parameter). To evaluate infrastructure projects, as proposed herein, there are eight criteria defined for the parameter of project importance for the community, with a scale from 1 to 10 points (according to general importance for the local community), and ponders (significance of project for the realization of a defined criterion), with a scale from 1 to 5 points. This number of criteria may even be larger. It is very important when these criteria are defined to include as much stakeholders and receive as much proposals and suggestions. Choose by selection the criteria and their numerical values whose application provides as true picture of local needs as possible, and beyond that also quality ranking and selection of projects for implementation. For the cost parameter, three criteria with a points scale 1 to 10, and pondering 1 to 5.

The overall procedure of preparation and implementation of MCA (Multi-Criteria Analysis) is shown in Fig. 1.

Project significance criteria defined herein are:

- Secured project documentation and required implementation permits,
- Contributing to the improvement of life quality,
- Impact on community economic growth,
- Completion/commencement level,
- Construction of a new object or reconstruction of an existing one,

*Corresponding author: PEC „Toplana“ Kraljevo, Cara Lazara 54, javor@ptt.rs

- Environmental impact,
- Increasing safety and
- Object exploitation cost.

Project financial aspect criteria are:

- Amount of funds required for project implementation,
- Possibility of construction in several phases,
- Securing part of funds from other sources.

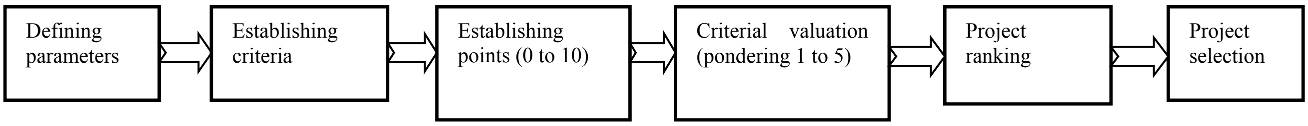

Figure 1. Schematic diagram of Multi-Criteria Analysis application

2. EXPLANATION OF CERTAIN CRITERIA

Secured project documentation and required implementation permits – this is very important criterion, and every implemented project must fully meet it. This criterion carries maximum points on the significance scale.

Contributing to the improvement of citizens' life quality – this criterion is important for a number of citizens of the community that will benefit from the implementation of the infrastructure project. If the number of citizens is larger, such will be the number of pondering point for this criterion and vice versa.

Impact to encourage economic development of the community – this criterion refers to easier functioning of businesses operating or planning to operate in that area. If this facilitates the operation, this criterion will be awarded more pondering points and vice versa.

Completion/commencement level – this criterion refers to the possibility of producing the infrastructure project in several phases. If some phases have already been completed, more pondering points shall be awarded at evaluation, but if object construction is to be commenced, it will be awarded less pondering points.

Construction of a new object or reconstruction of an existing one – if it is required to build a new object, more pondering points shall be awarded under this criterion in comparison to the number of points awarded when the object is to reconstructed. Reason for this is that if the object exists, citizens already have certain services (that we want to improve), but if a new object is constructed, citizens had not had any services (e.g. water supply).

Environmental impact – if a project affects the environment positively (pollution reduction, safety improvement), the criterion is awarded more pondering points and vice versa.

Increasing safety – if a project provides better safety (security) for the citizens, it is awarded more pondering points and vice versa.

Object exploitation cost – if maintenance cost during exploitation of the built object is large, this criterion is awarded less pondering points and vice versa.

Amount of funds required for project implementation – if less funds are required for project implementation, more pondering points are awarded for this criterion and vice versa.

Possibility of construction in several phases – if it is possible to implement the project in several phases, this criterion is awarded less pondering points and vice versa.

Securing part of funds from other sources – possibility to implement the project from a part of funds secured from other sources (donations, national level, etc.) provides this criterion with less pondering points. In reality we save local funds, i.e. if a project is financed with local funds only, this criterion is awarded maximum pondering points.

3. PROJECT POSITIONING

Konačnu ocenu o kvalitetu projekta donećemo na osnovu njegovog pozicioniranja u koordinatnom sistemu značaja za lokalnu zajednicu i visine troškova realizacije (Fig. 2.)

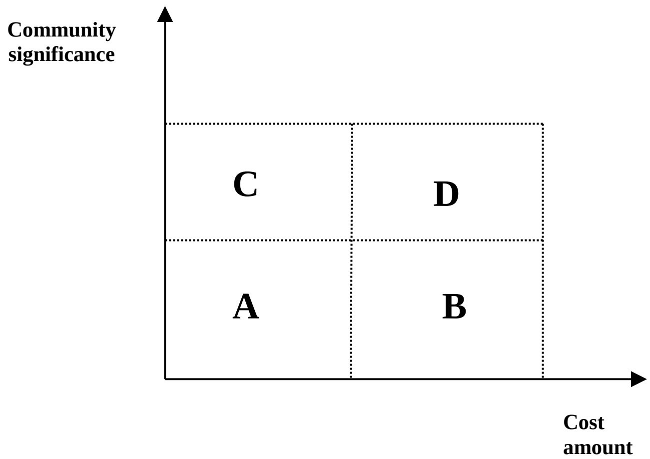

Figure 2. Project positioning diagram

As far as positioning projects in the diagram, we can conclude as follows:

- Project is quite low-cost and has small impact to life quality in the community (A field projects),
- Project is quite costly and has small impact to life quality in the community (B field projects)
- Project is quite costly and has significant impact to life quality in the community (D field projects)

- Project is quite low-cost and its implementation achieves significant improvement of life quality in the community (C field projects).

When choosing projects to be implemented, projects in the B field should be avoided, and the ones in the C field must be selected. Projects in the fields A and D are the matter of assessment of the decision makers (local political management). An attempt to move projects from the D field into the C field should certainly be made, and that is most often achieved by providing funds from additional sources or by implementing several phases.

4. EXAMPLE

The overall methodology for the selection of quality local projects to be financed in a planned period is implemented on three selected projects, as follows: road construction in a village, sewage network reconstruction in a suburb, and road construction in an industrial zone. Provided that the value of all projects is approximately the same, they are done in one phase and a part of funds for the road in the industrial zone is secured from a national source of financing.

Table 1. Example of quality evaluation of three local infrastructure projects

Project significance for the local community								
r. b.	Criterion	Significance	Construction of a local rural road		Reconstruction of sewage network in a suburb		Road construction in an industrial zone	
			Ponder	Total	Ponder	Total	Ponder	Total
1.	Secured project documentation and required implementation permits	10	5	50	5	50	5	50
2.	Contributing to the improvement of citizens’ life quality	6	4	18	4	24	2	12
3.	Impact to encourage economic development of the community	8	2	16	2	16	4	32
4.	Completion/commencement level	7	1	7	1	7	2	14
5.	Construction of a new object or reconstruction of an existing one	5	2	10	2	10	2	10
6.	Environmental impact	6	1	6	4	24	2	12
7.	Increasing safety	3	4	12	3	9	3	9
8.	Object exploitation cost	4	2	8	2	8	2	8
Total points				**127**		**148**		**147**
Project cost amount								
r. b.	Criterion	Significance	Construction of a local rural road		Reconstruction of sewage network in a suburb		Road construction in an industrial zone	
			Ponder	Total	Ponder	Total	Ponder	Total
1.	Amount of funds required for project implementation	6	4	24	4	24	4	24
2.	Possibility of construction in several phases	5	3	15	3	15	3	15
3.	Securing part of funds from other sources	7	5	35	5	35	2	14
Total points				74		74		53

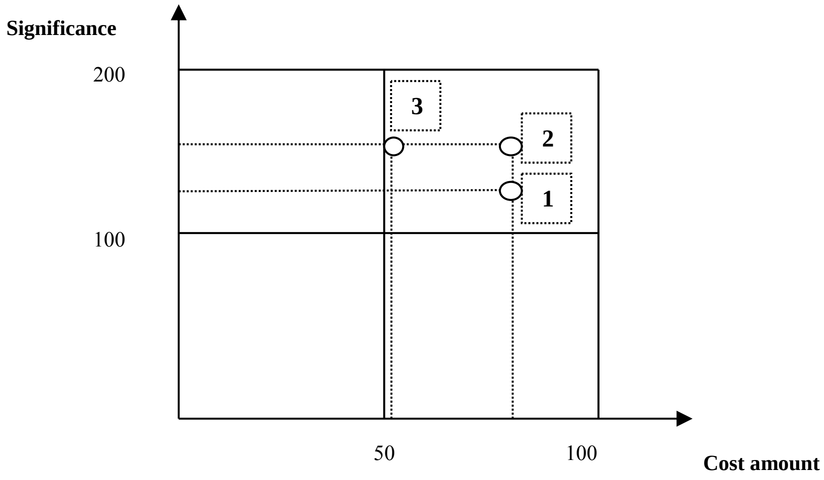

Figure 2. Position of analyzed local infrastructure projects

From this analysis, according to pre-defined criteria, we can conclude (diagram 2) that the first priority for implementation is the project No. 3 (road construction in the industrial zone), second priority is project No. 2 (reconstruction of sewage network in a suburb) and third priority is project No. 1 (construction of a local rural road). Probable inclusion of other criteria in the model, which may be related to demographic trends, agricultural development, may position differently these projects in the diagram.
What is very important is this whole process of project evaluation may be automated with the creation of a simple software. In this way, we may relatively quickly evaluate a large number of projects, make the rankings, and help decision-makers to choose projects within the range of available resources that will bring the most benefit to the local community. In addition, to ensure that criteria are as objective as possible, we may ask for an opinion of all relevant stakeholders from local governments who deal with the problems of planning and construction of local infrastructure, as well as stakeholders involved in local finances.

6. CONCLUSION

The presented methodology of ranking local infrastructure projects planned for implementation is under development. Ranking shall be done on the basis of two parameters – importance for the local community and project cost. Based on the project position, we can make a list of priorities and therewith choose the ones to be implemented that will bring the biggest effects to the local community against the funds invested. With a wide public debate with all interested stakeholders in the local government (public companies, public utility companies, public institutions, private sector, local communities, NGOs and others) we can define larger number of criteria than proposed herein. In the next phase, software may be developed on the basis of defined methodology, enabling the analysis of a large number of projects in a short period of time, thus improving the enactment of more quality decisions in local governments.

REFERENCES

[1] „Priručnik za planiranje kapitalnih investicija“ Program podrške opštinama IPA 2007., Beograd 2012.
[2] Ljiljana Brdarević „Razvoj lokalne infrastrukture kroz javno-privatna partnerstva“, Beograd 2012.
[3] Vanesa Belkić, Milica Hrnjaz „Lokalni ekonomski razvoj-evropski putokaz ka modernoj lokalnoj samoupravi“, Beograd 2010.
[4] Zakon o lokalnoj samoupravi, Službeni glasnik RS 129/2007.
[5] Jelena Bojović „Lokalni ekonomski razvoj – priručnik za praktičare“, THE URBAN INSTITUTE, Beograd 2010.

A Simplified Method for Data Processing of Discrete Time Signals with Heavy Data Transmission Losses

Jelena Tomić, Zlatan Šoškić, Nebojša Bogojević and Slobodan Todosijević
Faculty of Mechanical and Civil Engineering in Kraljevo, University of Kragujevac
Dositejeva 19, 36000 Kraljevo, Serbia

Measurements of machine vibrations are often influenced by heavy data losses during wireless transmission of signals, which is very sensitive to electromagnetic induction caused by electric motors. Since the data processing of the measured data is performed by computers, contemporary measurement processes are performed in discrete time moments. In this paper is analyzed the influence of phase and duration of transmission losses to simple harmonic signal spectra, as well as the influence of arbitrary pattern of data samples losses to spectra that consist of small number of spectral components. Also, the analytic expressions for corrupted signal spectra are determined according to known pattern of losses. The obtained results represent good basis for error reduction in the spectral analysis of signals with heavy data losses.

Keywords: Digital signal processing, Spectral analysis, Non-uniform sampling, Data transmission losses

1. INTRODUCTION

Contemporary development of measurement instrumentation is characterized by increased application of wireless transmission of signals. In mechanical engineering, the wireless data transmission is particularly suitable for diagnostics of machinery with rotating parts, because electric contact with sensors on rotating parts, which is necessary for data transmission by wire, is possible only by application of commutation. Due to the relative motion of rotating and stationary part of commutator, they are subjected to intensive wear. Besides, due to the sparks that appear between moving and stationary parts of commutators, they represent source of significant electric noise.

Wireless transmission is, on the other hand, sensitive to electromagnetic induction. In the considered application of wireless transmission for measurements in diagnostics of machinery with rotating parts, the electromagnetic induction is caused by work of electric motors used for machine drive. The electromagnetic induction influences voltage levels of transmitted signals, corrupting the transmitted data. In order to prevent further usage of the corrupted data, wireless data transmission is performed using sets of rules that are called transfer protocols. Wireless transfer protocols are developed in such a manner to detect and eliminate the data that were corrupted during data transmission processes.

Data processing of the measured data is performed by computers, which are essentially digital data processing devices. Due to the discrete nature of digital data, contemporary measurement processes are not performed continuously, but in discrete time moments. If all the intervals between the time moments have equal duration, than the acquired data are uniform (or regular) in time. Data processing of uniform data is significantly easier and faster than data processing of non-uniform data because equal duration of time intervals between moments of measurements enables simplification of calculations performed during the data processing procedures. Uniform discretization of the measured data is provided by proper programming of data acquisition equipment, which is programmed to acquire and send the data after expiration of selected time interval. Unfortunately, although the emitted data are uniform in time, the previously described elimination of data corrupted during wireless transfer makes the received data non-uniform in time. If data transmission losses are seldom and individual events, than the received data are made uniform by interpolation or even by zero-padding (arbitrary setting the missing values to be equal to zero). However, when strong electromagnetic induction is present, long series of consecutive data are corrupted and lost during the data transmission process, and such data transmission losses are called heavy data transmission losses. The received data in cases of heavy data transmission losses cannot be made uniform in a meaningful way. Instead, special data processing procedures are being developed for the analysis of the non-uniform data.

Frequency analysis represents one of the most important tools for data processing. On one side, frequency analysis provides insight into physical causes of behavior of the studied systems. On the other side, frequency analysis enables decomposition of arbitrary signals into harmonic signals, which further simplifies data processing because the results of data processing of harmonic signals are well known. The standard method for frequency analysis of continuous data is called Fourier analysis, as it was initially proposed by Jean Baptiste Fourier in the beginning of 19th century. The method for spectral analysis of discrete data, used for computer-based numerical calculations, is developed during the last quarter of 20th century and is known as “Discrete Fourier Transformation” (DFT). A whole family of fast methods for frequency analysis of uniform discrete data, known as "Fast Fourier Transformation" (FFT), is available in form of public domain code. The efficiency of FFT made it a fundamental part of all data processing software packages and that is why the majority of available software packages are mainly applicable for uniform data processing. For this reason, methods of spectral analysis of

*Corresponding author: Dositejeva 19, 36000 Kraljevo, Serbia, tomic.j@mfkv.rs

non-uniformly-discretized data, when FFT is not applicable, are recently regaining interest of researchers from various fields.

The approaches taken in spectral analysis of non-uniformly-discretized data are different. The initial researches on non-uniform data processing were made in astronomy 0. The initial method was straightforward application of DFT to non-uniformly-discretized data, equivalent to implicit zero-padding of a non-uniform signal. The obtained spectrum is known as Lomb–Scargle periodogram [2][3]. The second approach is deconvolution of the non-uniformly-discretized data by different methods that are taking into account information that some data are missing. One example is CLEAN algorithm [4] that estimates a spectrum by deconvolving the DFT spectrum of corrupted data into the true signal spectrum using the Fourier transform of the windowing function in an iterative process. The third approach is estimation of a spectrum by assuming certain quadratic functions of the available data, and such algorithms are known as multi-taper methods [5][6]. Both deconvolution methods and multi-taper methods are not useful when spectral lines are close. The third approach is application of parametric algorithms based on an autoregressive (AR) or autoregressive moving-average (ARMA) models, and they were used for spectral analysis of non-uniformly-discretized data in various occasions when high resolutions were necessary [7]-[10]. The parametric methods resulted in improved spectral estimations, but they turned out to be highly sensitive to errors in used AR or ARMA models. The fourth approach is application of various nonparametric adaptive filtering based techniques, as it is the case with GAPES algorithm [11][12], which iteratively interpolates the missing data to provide estimation of the spectrum, or PG-APES and PG-CAPON algorithms that deal with periodically gapped data [13]. However, these adaptive filtering based methods can only deal with missing data occurring in gaps. For the more general problem of missing data samples occurring in arbitrary patterns are developed MAPES algorithms that use “maximum likelihood” fitting criterion and “maximization of expectation” method to provide estimations of spectra [14]. An extensive overview of methods for spectral analysis of non-uniformly-sampled data is provided in [15].

This paper analyzes the influence of duration and phase of transmission losses to signal spectrum. To that purpose, the analytic expressions for spectrum of a harmonic signal were determined. Besides, the relationship between the spectra of the received and sent signal is expressed by analytic expressions derived according to known pattern of losses. In our previous papers [16], we analyzed continuous signals, and this paper, we present analysis of discrete signals.

2. INFLUENCE OF DATA TRANSMISSION LOSSES TO SPECTRA OF HARMONIC SIGNALS

Data losses cause reduction of signal power and hence the reduction of spectral power, but even basic considerations show that the distribution of power losses depends on the signal spectra and duration and distribution in time of loss events. For example, if a certain signal loses half of the data during transmission process, two extreme cases, with opposite effects to the spectra of the signal, are possible: the first case is that *all* transmission losses occur at consecutive moments of time, and the second case is that *no* transmission losses occur in consecutive moments of time. In the first case, the signal duration is effectively reduced to half of the transmission time, with the consequence that the separation between frequencies in the spectrum is doubled, which affects the whole spectrum, but essentially means that the low-frequency part of the spectrum is corrupted and lost. In the second case, the time interval between the moments of data acquisition is doubled, with the consequence that Nyquist frequency of the measurement process is reduced twice, which means that the high-frequency part of the spectrum is lost due to the aliasing. The influence of the aliasing effect is shown in Fig. 1, which demonstrates that a spectrum of signal with bandwidth B cannot be reproduced by measurement with sampling intervals longer than π/B.

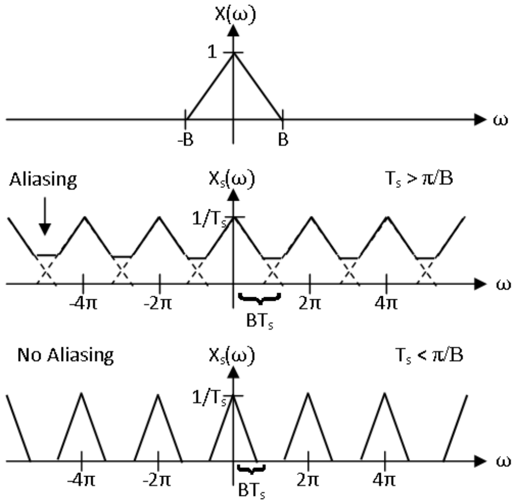

Figure 1: The aliasing effect

In practical cases of analysis of mechanical vibrations of machines, the spectra usually consist of small number of spectral components. Therefore, the influence of transmission losses to the spectrum of simple harmonic signal $x[n]$ with amplitude X_0, digital angular frequency $\omega_0 = 2\pi f_0/f_s$ (f_0-signal frequency and f_s-sampling rate) and phase θ_0, given by

$$x[n] = X_0 \cos(\omega_0 n + \theta_0) \qquad (1)$$

may serve as starting point for studies of influence of transmission losses to spectra of signals. Discrete-Time Fourier Transform (in following text denoted as DTFT) of the received signal is equal to the DTFT of signal $z[n]$, given by the expression

$$z[n] = x[n] \cdot g[n], \qquad (2)$$

where $g[n]$ represents transmission function, defined by

$$g[n] = \begin{cases} 1, \text{ sample received} \\ 0, \text{ sample lost} \end{cases}. \qquad (3)$$

In order to study the influence of position (phase) and duration of transmission losses on signal spectrum, the influence of the loss of N_L consecutive data samples will be analyzed. Transmission function may be expressed by the following equation

$$g[n] = 1 - \Pi(n - n_0), \qquad (4)$$

where $\Pi[n]$ represents a rectangular pulse given by

$$\Pi[n] = \sum_{i=-[N/2]}^{[N/2]} \delta[n-i], \tag{5}$$

where Kronecker delta function is denoted by δ[n].

As received signal $z[n]$ may be expressed by

$$z[n] = X_0 \cdot \frac{\exp(j\omega_0 n + j\theta) + \exp(-j\omega_0 n - j\theta)}{2} \cdot g[n] \tag{6}$$

DTFT of the received signal may be given by the following equation

$$\begin{aligned} Z(\omega) &= \frac{X_0 \exp(j\theta_0)}{2} G(\omega - \omega_0) \\ &+ \frac{X_0 \exp(-j\theta_0)}{2} G(\omega + \omega_0), \end{aligned} \tag{7}$$

where $G(\omega)$ denotes the Fourier transform of the transmission function $g[n]$ given by the expression

$$G(\omega) = \delta(\omega) - \exp(-j\omega n_0)\frac{\sin(\omega N_L/2)}{\sin(\omega/2)}. \tag{8}$$

As the Fourier transform of the signal $x[n]$ is given by

$$\begin{aligned} X(\omega) &= \frac{X_0}{2}\exp(j\theta_0)\delta(\omega - \omega_0) \\ &+ \frac{X_0}{2}\exp(-j\theta_0)\delta(\omega + \omega_0), \end{aligned} \tag{9}$$

it can be shown that the spectral difference $D(\omega) = X(\omega) - Z(\omega)$ may be expressed by the equation

$$\begin{aligned} D(\omega) &= \frac{X_0}{2}\exp(-j\omega n_0) \cdot \\ &\left(\frac{\sin((\omega-\omega_0)N_L/2)}{\sin((\omega-\omega_0)/2)} \exp(j(\omega_0 n_0 + \theta_0)) \right. \\ &\left. + \frac{\sin((\omega+\omega_0)N_L/2)}{\sin((\omega+\omega_0)/2)} \exp(-j(\omega_0 n_0 + \theta_0)) \right). \end{aligned} \tag{10}$$

The minimum spectral difference

$$\begin{aligned} |D_{\min}(\omega)| = \frac{X_0}{2} \Bigg| & \frac{\sin((\omega-\omega_0)N_L/2)}{\sin((\omega-\omega_0)/2)} \\ & - \frac{\sin((\omega+\omega_0)N_L/2)}{\sin((\omega+\omega_0)/2)} \Bigg|. \end{aligned} \tag{11}$$

is obtained when $\omega_0 n_0 + \theta_0 = (2k+1)\pi/2$, i.e. when the signal losses are centered at the zero of the signal x[n] (Fig. 2), while the maximum differences between the spectra of the original signal and corrupted signal

$$\begin{aligned} |D_{\min}(\omega)| = \frac{X_0}{2} \Bigg| & \frac{\sin((\omega-\omega_0)N_L/2)}{\sin((\omega-\omega_0)/2)} \\ & + \frac{\sin((\omega+\omega_0)N_L/2)}{\sin((\omega+\omega_0)/2)} \Bigg|. \end{aligned} \tag{12}$$

are obtained when $\omega_0 n_0 + \theta_0 = k\pi$, i.e. when the signal losses are centered at the signal’s maxima/minima (Fig. 3). The minimal and the maximal differences between the spectrum of the simple harmonic signal with frequency f_0=1 Hz and the spectrum corrupted by transmission losses which occurred at consecutive moments of time are shown in Fig. 4.

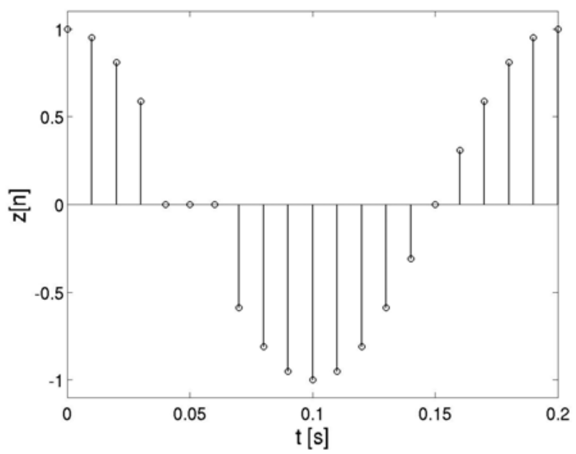

Figure 2: Transmission losses centered at signal minimum

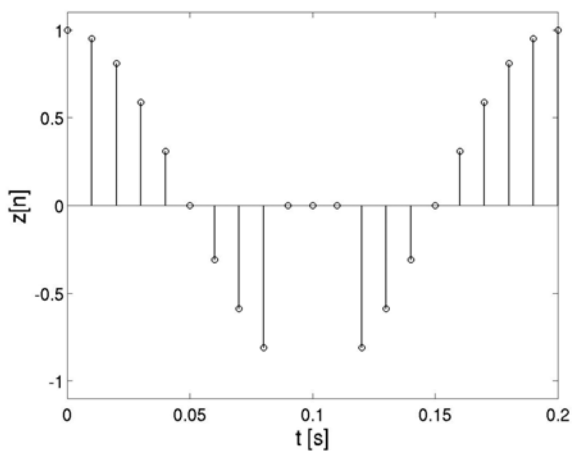

Figure 3: Transmission losses centered at signal maximum

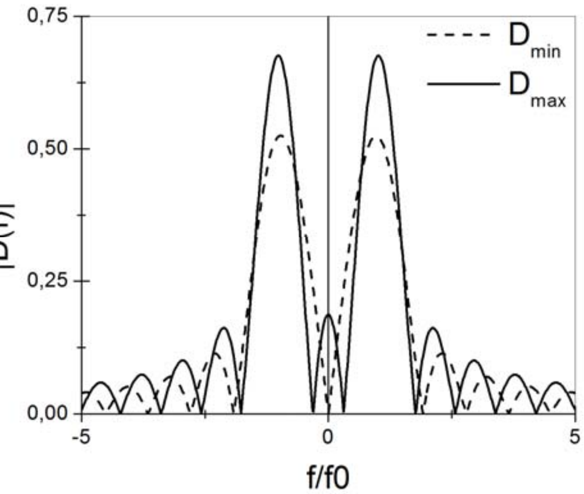

Figure 4: Minimum and maximum spectral differences

Transmission losses are affecting the spectra of harmonic signals in a manner that is similar to the effect of finite duration of recording of harmonic signals, which is in signal processing known as “windowing”. The finite duration of acquisition of infinite signals leads to “spectral leakage”, which means reduction of intensity of spectral lines of the original signal and appearance of sidelobes of spectral lines that do not exist in the spectra of original signal. Transmission losses also cause reduction of spectral power and introduction of new lines in spectra.

The intensity of the spectral line at original signal frequency decreases with increasing transmission loss duration, while the intensity of the spectral lines introduced by transmission losses depends on their frequency and has value |D(ω)|. Sidelobe width is inversely proportional to transmission loss duration and does not depend on original signal frequency. The influence of the loss duration $\tau = N_L/f_s$, where f_s represents sampling rate on spectral difference between the spectrum of harmonic signal with frequency f_0=1 Hz and signal corrupted by transmission losses which occurred at consecutive moments of time is shown in Fig. 5.

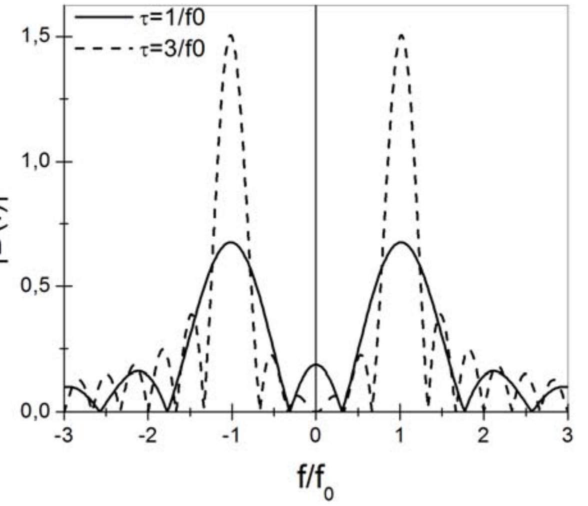

Figure 5: The influence of the loss duration on spectral difference

The analyzed dependence of the influence of position (phase) and duration of transmission losses on spectrum of the transmitted signal shows that the exact pattern of losses is important for analysis of the spectra of transmitted signals. An arbitrary pattern of losses may be represented by transmission function of the form

$$g[n] = \sum_{i=1}^{N_g} \delta[n - n_i], \qquad (13)$$

where n_i represents the ordinal number of the i^{th} successfully received sample, while N_g is the number of successfully received samples. DTFT of the received signal may be given by the equation (7) where $G(\omega)$ denotes the Fourier transform of the transmission function $g[n]$ given by the expression

$$G(\omega) = \sum_{i=1}^{N_g} \exp(-j\omega n_i). \qquad (14)$$

According to derived equations, it can be concluded that transmission losses influence the entire spectral range, which may be described by factors $r(\omega,\omega_0)$ that describe the relative influence of harmonic signal with angular frequency ω_0 to spectral line at frequency ω due to the transmission losses,

$$Z(\omega) = r(\omega,\omega_0) \cdot X_0. \qquad (15)$$

When the spectra consist of small number of spectral components and the signal has approximate form

$$x(t) = \sum_{n=1}^{N_x} X_n \cos(\omega_n n + \theta_n) \qquad (16)$$

with N_x being the number of spectral components, X_n the amplitude, ω_n the digital angular frequency and θ_n the phase of the n^{th} spectral component, the spectrum of the received signal $z[n]$ may be described by the expression:

$$Z(\omega) = \sum_{n=1}^{N_x} r(\omega,\omega_n) \cdot X_n \qquad (17)$$

where influence factors $r(\omega,\omega_n)$ are given by the following equation

$$r(\omega,\omega_n) = \frac{1}{2}\left[\exp(j\theta_n) G(\omega - \omega_n) + \exp(-j\theta_n) G(\omega + \omega_n)\right]$$
$$= \sum_{i=1}^{N_g} \exp(-j\omega n_i) \cos(\omega_n n_i + \theta_n)$$
(18)

3. EXAMPLE

The described procedure for analysis of the spectra corrupted by transmission losses is illustrated on example of the signal

$$x[n] = 3 \cdot \cos(2\pi(4/25)n) + \cos(2\pi(8/25)n), \quad (19)$$

which is regularly sampled at 25 Hz sampling rate in the interval [0,8). The defined signal is subjected to removal of 30% of points that are randomly selected. Amplitude spectrum, estimated using equations (17) and (18), is shown in Fig. 7. Instead of spectral components at 4 Hz and 8 Hz, as it is shown in Fig. 6, new spectral components that do not exist in the spectra of original signal appeared because the energy has leaked out into other frequencies, so the intensity of the spectral components of the original signal decreased. Intensity of the new spectral components depends on loss distribution and spectrum of the original, uncorrupted signal, i.e. on intensity and phase of the uncorrupted signal components, as it is defined by the equations (17) and (18).

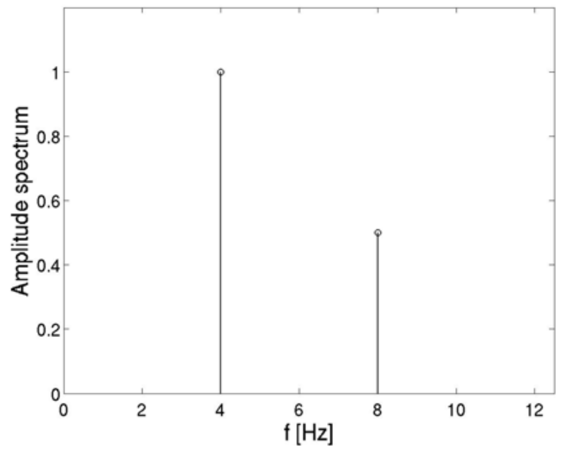

Figure 6: Amplitude spectrum of the uncorrupted signal

The peaks that can be noticed in Fig. 7 correspond to the spectral components of the original, uncorrupted signal, but as the number of the lost samples grows, new peaks can appear and/or the spectral components of the original signal can be masked because of higher spectral leakage. The masking of spectral lines by leaked energy is shown in Fig. 8, which represents the spectrum of the signal $x[n]$ subjected to removal of 60% randomly selected samples.

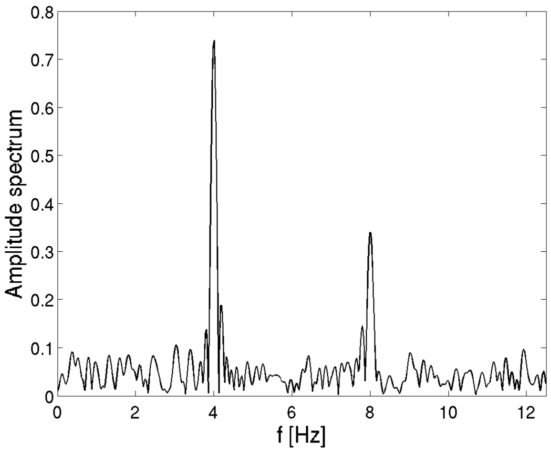

Figure 7: Estimated amplitude spectrum of the corrupted signal (30% of samples lost)

4. CONCLUSION

The paper presents an analysis of the influence of transmission losses to signal spectrum. In order to study the influence of duration and phase of transmission losses, analytic expressions for spectrum of a harmonic signal were determined. It was shown that transmission losses cause reduction of the spectral power and the extent of spectral leakage. The spectral difference between original and corrupted signal depends not only on transmission losses duration, but also on phase of transmission losses, so the exact pattern of losses is important for analysis of the spectra of transmitted signals.

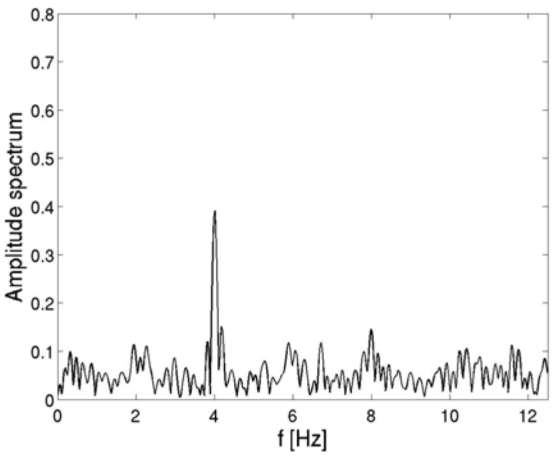

Figure 8: Estimated amplitude spectrum of the corrupted signal (60% of samples lost)

Further studies will enable estimation of spectra of signals affected by transmission losses by using simple method of data processing of discrete data with non-uniform distribution in time. The algorithm will be applicable to arbitrary patterns of missing data, which would be applied in the spectral analysis of signals with heavy data transmission losses. The algorithm is going to be particularly useful for spectra with small number of peaks, as it is often the case in diagnostics of machines with rotating parts, when the rotations represent the source of forced vibrations and oscillations.

ACKNOWLEDGEMENTS

The authors wish to express their gratitude to Ministry for education, science and technology of Republic of Serbia for support through research grants TR37020 and TR35006.

REFERENCES

[1] F.J.M. Barning, The numerical analysis of the light-curve of 12 Lacertae, Bulletin of the Astronomical Institutes of the Netherlands 17 (1962) 22-28

[2] N.R. Lomb, Least Squares Analysis of Unequally Spaced Data, Astrophysics and Space Science 39 (1976) 447-462

[3] J.D. Scargle, Studies in Astronomical Time Series Analysis, The Astrophysical Journal 263 (1982) 835-853

[4] J.A. Högbom, Aperture Synthesis with a Non-Regular Distribution of Interferometer Baselines, Astronomy and Astrophysics Supplement 15 (1974) 417-426

[5] T.P. Bronez, Spectral estimation of irregularly sampled multidimensional processes by generalized prolate spheroidal sequences, IEEE Transactions on Acoustics and Speech Signal Processing 36 (1988) 1862 -1873

[6] I. Fodor and P. Stark, Multi-taper spectrum estimation for time series with gaps, IEEE Transactions on Signal Processing 48 (2000) 3472 -3483

[7] R.H. Jones, Maximum likelihood fitting of ARMA models to time series with missing observations, Technometrics 22 (1980) 389–395

[8] B. Porat, B. Friedlander, ARMA spectral estimation of time series with missing observations, IEEE Transactions on Information Theory 30 (1986) 601–602

[9] Y. Rosen, B. Porat, Optimal ARMA parameter estimation based on the sample covariances for data with missing observations, IEEE Transactions on Information Theory 35 (1989) 342–349

[10] P. Broersen, S. de Waele, R. Bos, Estimation of autoregressive spectra with randomly missing data, in: Proceedings of the 20th IEEE Instrumentation and Measurement Technology Conference, Vail, CO, vol. 2, May 2003, 1154–1159

[11] P. Stoica, E.G. Larsson, J. Li, Adaptive filter-bank approach to restoration and spectral analysis of gapped data, The Astronomical Journal 120 (2000) 2163–2173

[12] E. Larsson, G. Liu, P. Stoica, J. Li, High-resolution SAR imaging with angular diversity, IEEE Transactions on Aerospace Electronics Systems 37 (2001) 1359–1372

[13] E. Larsson, J. Li, Spectral analysis of periodically gapped data, IEEE Transactions on Aerospace Electronics Systems 39 (2003) 1089–1097

[14] Y. Wang , P. Stoica , J. Li and T. L. Marzetta , Nonparametric spectral analysis with missing data via the EM algorithm, Digital Signal Processing 15 (2005) 191 - 206

[15] P. Babu, P. Stoica, Spectral analysis of non-uniformly sampled data - a review, Digital Signal Processing 20 (2010) 359-378

[16] Zlatan Šoškić, Jelena Tomić, Nebojša Bogojević and Snežana Ćirić Kostić, „Influence of Heavy Data Transmission Losses on Spectra of Signals", Applied Mechanics and Materials, 430, 125-134 (2013)

Simplified Modeling of Electrical Cabinets

Rade Karamarković[1*], Vladan Karamarković[1], Miljan Marašević[1], Anđela Lazarević[2]
[1]Faculty of Mechanical and Civil Engineering in Kraljevo, University of Kragujevac, Kraljevo (Serbia)
[2]Faculty of Mechanical Engineering, University of Niš, Niš (Serbia)

Calculating temperature inside an electrical cabinet by the use of e.g. VDI or ASHREA standards for sizing HVAC systems is not adequate because they are intended for: (i) sizing economically optimal HVAC systems, (ii) specific climate, (iii) average environment wind conditions, and (iv) typical building constructions. Electrical cabinets should secure functioning of electrical equipment in extreme weather conditions with as economical design as possible. This paper aims to present a relatively simple procedure to model temperature inside electrical cabinets and to analyze different cabinet constructions depending on the weather conditions. The model principle is based on seven dependent energy balances: on each side of a cabinet and of the airflow through it. Two different wall constructions as well as forced and natural ventilation of a cabinet were analyzed. The goal is to avoid using air conditioning systems in electrical cabinets and to use only if necessary fans or electrical heaters. Insulation of walls is suitable for colder continental climates whereas the use of walls consisting of two metal sheets, with air circulating freely between them, is suitable for hotter continental climates for the equipment with heat dissipation inside cabinets of up to 120 W/m³.

Keywords: electrical cabinets, heat transfer, natural convection, forced convection, wall construction

1. INTRODUCTION

An electrical enclosure is a cabinet for electrical or electronic equipment to mount switches, knobs, and displays and to prevent electrical shock to equipment users and protect the contents from the environment [1]. For the proper functioning and duration of electrical and electronic equipment inside an outdoor electrical cabinet, it is very important to keep the inside temperature in a required temperature range. This range is limited by minimal and maximal (peak) operating temperatures specified by the producer. For the majority of electrical equipment, these temperatures lies in the range from -10 to 50 °C. Exposing the equipment to higher and lower temperatures than these affects their functioning and lifetime. Depending on the environment conditions and heat dissipation inside an electrical cabinet, the manufacturers require precise answers what kind of wall construction to use, whether to use fans and/or electrical heaters or even air conditioners to maintain the inside temperature in a required temperature range. For these reasons, it is very important to predict the temperature inside an electrical cabinet in a simple and reliable manner. Calculating temperature inside an electrical cabinet by the use of e.g. VDI or ASHREA standards for sizing HVAC systems is not adequate because they are intended for: (i) sizing economically optimal HVAC systems, (ii) specific climate and (iii) average environment wind conditions, and (iv) typical building constructions.

This paper aims to present a relatively simple procedure to model temperature inside electrical cabinets and to analyze different cabinet constructions in summer and winter weather conditions. The intention was to develop as simple as possible model that can be implemented to different constructions of electrical cabinets.

Fig. 1 shows the modeled electrical cabinet, which is intended to store electrical appliances in open space. The cabinet is 1.2 x 1.4 x 0.7 m and has a steady heat gain from electrical appliances of 140 W. The cabinet stands on metal support, with the height 100 mm above the ground. For air intake, this metal support has in total 60 openings, 30 on the front and 30 on the back side, each opening with the dimensions 60 x 3 mm (see Fig. 1 and 2). After passing through these openings, the air enters into the cabinet from the bottom (see Fig. 1 and 2). At the top, there is double metal sheet that forms an "attic" with the variable height from 50 to 70 mm (see Fig. 2).

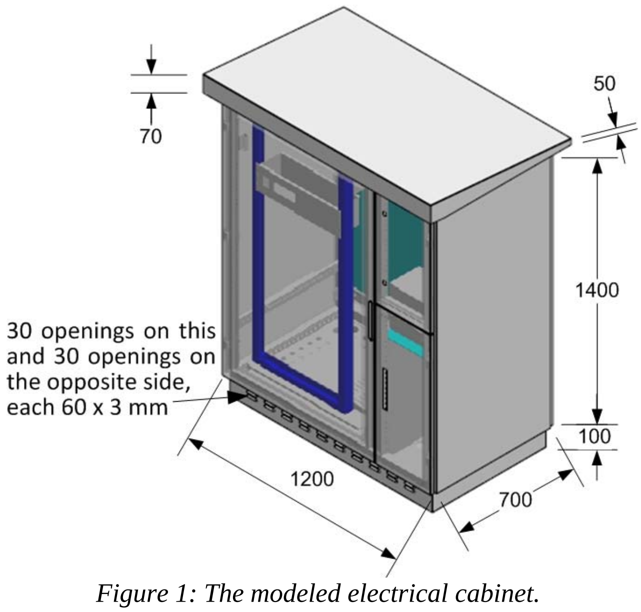

Figure 1: The modeled electrical cabinet.

Two different wall constructions are analyzed. The first one is composed of an outer metal sheet 1.55 mm thick, 20 mm K-FLEX ST insulation, and an inner metal sheet 0.55 mm thick. The proposed insulation has thermal conductivity 0.034 W/mK at -20°C, 0.036 W/mK at 0°C, and 0.040 at 40°C [2], see Fig. 2. The other common insulating materials that could be implemented have the thermal conductivity in the same range, see e.g. [3,4]. The

*Corresponding author: Dositejeva 19, 36000 Kraljevo, Serbia, karamarkovic.r@mfkv.kg.ac.rs

second analyzed wall construction is composed of two metal sheets, both 1.55 mm thick, at the distance 20 mm between them, see Fig. 2. In this space air flow is created by natural draft. To construct this kind of wall with forced convection is also possible but the manufacturing of the cabinet would be more difficult and expensive comparing with the analyzed case.

In the paper, the natural and forced draft through the cabinet are analyzed. In addition, submodels for heat transfer modelling of different parts of the cabinet are presented for the summer and the winter weather conditions.

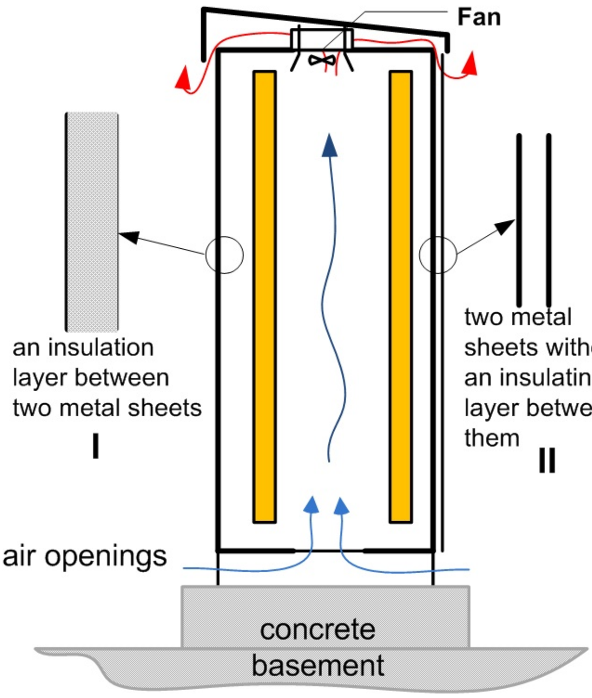

Figure 2: Cross section of the modeled cabinet. Two types of outer walls are examined. The first type of the wall I consists of two metal sheets with a 20 mm insulating layer between them. The second type II consists of two metal sheets that form 20 mm thick air passage between them.

2. MODELLING

Heat flow rate through the cabinet enclosure equals heat transfer rate of the air flowing through the cabinet:

$$\sum_{i=1}^{4}\dot{Q}_{wall,i}+\dot{Q}_{top}+\dot{Q}_{bottom}=\dot{m}_{air}c_{p,air}(t_{out}-t_o),\quad(1)$$

where $\dot{Q}$ in W are heat flow rates through the different parts of the enclosure, $\dot{m}_{air}$ is the mass flow rate of air in kg/s, $c_{p,air}$ is the specific heat capacity of air at constant pressure in kJ/kgK [5], t_o, t_{out} are in °C the temperatures of air at the inlet (environment temperature) and outlet of the cabinet respectively. As can be seen in (1) there is no accumulation of heat in the cabinet. This assumption is made because the mass of an electrical cabinet is relatively small and the majority of parts are made from metals, which have low heat capacity.

2.1. Heat transfer through the side walls

The heat gain or loss through the insulated wall, see Fig. 3 (a), is calculated by

$$\dot{Q}_{wall,i}=kA_i\Delta t_i \qquad (2)$$

where k is the overall heat transfer coefficient W/m^{2}K, A is the area of the wall m^2, and Δt_i is the temperature difference. The overall heat transfer coefficient is

$$k=\frac{1}{\frac{1}{\alpha_{in}}+\sum_i\frac{\delta_i}{\lambda_i}+\frac{1}{\alpha_{out}}}. \qquad (3)$$

In (3) α is the heat transfer coefficient in W/m^{2}K, subscripts in and out denote inner and outer side of the wall, respectively. λ is the thermal conductivity in W/mK, and δ is the thickness of a wall layer in m. The heat transfer coefficient for the average wind conditions at the outer side of the wall α_{out} are recommended to be 25 W/m^{2}K [3] and 17 W/m^{2}K [6] during the winter and summer period, respectively. The value for the winter period is used here whereas for the summer period, still weather is assumed and the heat transfer coefficient is calculated according to the model [7] for free convection near a vertical surface. These assumptions are on the safe side because wintry conditions accompanied with very cold weather lead to a very low temperature inside an electric cabinet. Oppositely, hot and still weather could cause overheating of a cabinet.

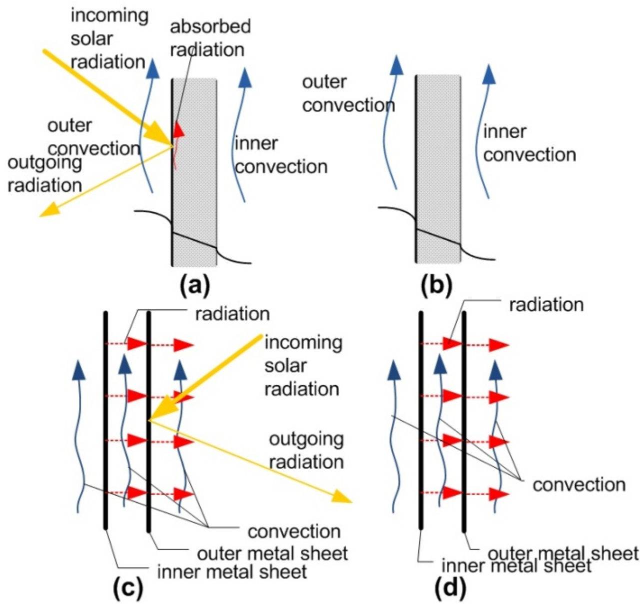

Figure 3: Heat transfer through the analyzed cabinet wall constructions: (a) insulated wall exposed to the Sun light, (b) insulated wall in the shade, (c) non-insulated wall with an air layer exposed to the Sun light, (d) non-insulated wall with an air layer in the shade.

To calculate natural convection at the outer wall surface, the average dimensionless heat transfer coefficient ([8] as cited in [7]) for laminar and turbulent flows near a vertical surface in the range from Ra = 10^{-1} to Ra = 10^{12} is defined by ([9] as cited in [7])

$$Nu=\left\{0.825+0.387\left[Raf_1(Pr)\right]^{1/6}\right\}^2 \qquad (4)$$

The function f1(Pr) allows for the effect of the Prandtl number in the range 0.001 < Pr < ∞ ([10] as cited in [7]):

$$f_1(Pr)=\left[1+\left(\frac{0.492}{Pr}\right)^{9/16}\right]^{-16/9} \qquad (5)$$

In (4) and (5), Pr, Nu, Ra, Gr are the Prandtl, Nusselt, Rayleigh Ra=GrPr, and Grashof number, respectively. The equations to calculate these numbers can be found e.g. in [11,12]. The characteristic length to calculate Nu, Ra, and Gr number is the height of the surface. The physical properties of air necessary to calculate these dimensionless numbers are taken at the average temperature $\frac{1}{2}(t_{wall} + t_0)$, which means that the iterations are needed to solve the system of equations. Two important assumptions regarding the temperatures are:

▶ an outer wall has a constant surface temperature. As the outer walls are made of metal sheet this assumption is in accord with reality, and

▶ the inner enclosure of a cabinet is at a constant temperature equal to the temperature of electrical equipment inside it. This temperature is the temperature of the cabinet. This assumption is made because the electrical equipment, which is mostly made of metal, is in a physical contact with the inner metal sheet of a metal cabinet.

To calculate heat gain or loss from the walls in the shade, for each wall (2)-(5) are used. The radiant heat gain or loss from these walls is neglected.

For the walls exposed to the Sun light, a sol-air temperature is calculated and then the same procedure using (2)-(5) implemented (see Fig. 3 (a) and 3 (b)). Sol-air t_{sa} temperature is a variable used to calculate cooling load of a building and determine the total heat gain through exterior surfaces [13]. It is the temperature, which under conditions of no direct solar radiation and no air motion, would cause the same heat transfer into a house as that caused by the interplay of all existing atmospheric conditions [14]. This temperature takes into account solar radiative flux and infrared exchanges from the sky and is calculated by [6]

$$t_{sa} = t_o + \frac{aI}{\alpha_s} - \frac{\varepsilon \Delta R}{\alpha_s}. \tag{6}$$

In (6) a is the degree of absorption, which is according to the Kirchhoff's law equal to the degree of emission. For a shiny iron sheet with zinc surface the degree of emission is 0.228 [15].

In (6) I is the global solar irradiance in W/m^2. The data on solar irradiance depending on local time, latitude, and longitude can be found in [6,16]. For the 20th of July, 15^{00} local time, the global solar irradiance on the horizontal surface is 634.3 W/m^2 and on the vertical surface is 595.1 W. α_s is the heat transfer coefficient calculated by (4) and (5).

In the last term on the right side of (6), ε is the degree of emissivity and ΔR in W/m^2 accounts for the infrared radiation due to difference between the external air temperature and the apparent sky temperature and radiation that the surface emits as a black body at the environment temperature [6]. In this paper this term is neglected as it is usually neglected for vertical surfaces in determining cooling load [6].

Heat transfer for the wall made of double metal sheet (see Fig. 3 (c) and (d)) with an air layer is composed of radiant and convective heat gain or loss and is determined by the use of a system of equations. For this kind of wall exposed to the Sun light two energy balance equations (7) and (13) and the equation for the natural draft through the space between metal sheets (14) are used. The energy balances are for the outer surface (8) and airflow through the space between these surfaces (14). Solar irradiance to the outer surface (see Fig. 3 (c)) is used to heat air on both sides of the wall and by radiation transferred to the inner surface:

$$\varepsilon I A = \alpha_{out} A(t_{wall} - t_o) + \alpha_{in} A(t_{wall} - t_a) + \frac{\sigma}{\frac{1}{\varepsilon_1} + \frac{1}{\varepsilon_2} - 1} A(T_{wall} - T) \tag{7}$$

t_o, t_{wall}, t_a in °C are the temperatures of the environment, the wall and the air flowing through the layer between two metal sheets, respectively. T_{wall}, T are absolute temperatures in K of the wall and inner metal sheet, respectively, and A is the surface area of the wall in m^2. As it is already mentioned and explained, the temperature of the inner metal sheet is equal to the cabinet temperature. α_{out} in W/m^{2}K is the heat transfer coefficient at the outer side of the wall determined by (4) and (5), which means that the subsystems (7)-(9) should be solved by iteration too. Still weather during the summer period is also assumed here. The third term on the right-hand side of (7) is the expression for the net thermal energy transferred by thermal radiation from the hotter to the colder surface for parallel plates of equal size. In this term $\varepsilon_1 = \varepsilon_2 = 0.228$ and $\sigma = 5.6704 \cdot 10^{-8}$ W/m^{2}K^4 is Stefan-Boltzmann constant.

α_{in} in W/m^{2}K is the heat transfer coefficient at the inner side of the wall. As heated vertical channels act as chimneys, the model for free convection in internal flows [17] is used to described this kind of convection for vertical channels:

$$Nu_s = Nu_s(Gr_s \cdot Pr) \tag{8}$$

$$Nu_s = \frac{\alpha s}{\lambda} \tag{9}$$

$$Gr_s^* = \frac{g\beta(T_w - T_A)s^3}{\upsilon^2} \cdot \frac{s}{h} \tag{10}$$

$$Pr = \frac{\nu}{a} \tag{11}$$

In the above equations, T_w and T_A are the wall and the air temperatures in K, respectively. β is the coefficient of volume expansion. The characteristic length s from which Nu and Gr are calculated is the width of the channel s=d in m. The reference temperature for the properties is the average between the wall and the air temperature. The Nusselt number, which is used to calculate the heat transfer coefficient in the duct, is calculated by:

$$Nu_s = 0.69(Gr_s^* Pr)^{1/4}. \tag{12}$$

The energy balance for the air flow through the space between two metal sheets (see Fig. 3 (c) and (d)) is

$$\alpha_{in} A(t_{wall} - t_a) + \alpha_{in,2} A(t - t_a) = \dot{m}_{air,c} c_{p,air}(t_{out,c} - t_o) \tag{13}$$

In (13) subscript c means channel, o at the environment temperature and *out* at the exit of the channel. The channel is open towards atmosphere at the top and at the bottom. t in °C is the temperature of the inner metal sheet, which is assumed to be equal to the temperature of the cabinet. $\alpha_{in,2}$ is obtained in the same manner as α_{in} but has a different value due to different temperature difference at the inner side of the wall.

Mass flow rate of air in the channel must be equal to the mass flow rate of air cause by natural draft in the channel

$$\dot{m}_{air,c} = \rho_o \frac{\pi d_h^2}{4}\left[\frac{2g(\rho_o-\rho_{out})h}{\frac{\lambda l \rho_{out}}{d_h}+\sum\zeta\rho_{out}}\right]^{1/2}, \qquad (14)$$

where ρ in kg/m^3 is the air density at the entrance *o*, and at the exit *out* of the channel, λ is the friction coefficient, *l* in m is the length of the channel (height in this case), d_h in m is the hydraulic diameter, $\sum\zeta$ is the summarized minor loss coefficient. Finally the heat loss or gain from this wall is

$$\dot{Q}_{wall} = \alpha_{in}A(t-t_a) + \frac{\sigma}{\frac{1}{\varepsilon_1}+\frac{1}{\varepsilon_2}-1}A(T_{wall}-T) \qquad (15)$$

(15) is also applied to calculate heat transfer from the non-insulated wall that stands in the shade, which is shown in Fig. 3 (d). The global solar irradiance in this case is zero, and two assumptions are made: (i) the outer metal sheet is at the ambient temperature $t_{wall} = t_o$, and (ii) the inner metal sheet is at the cabinet temperature. The characteristic length s from which Nu and Gr are calculated is the half of the channel width s=d/2 in (8)-(11) and instead (12), the following equation is used to calculate the Nusselt number

$$Nu_s = 0.61(Gr_s^* Pr)^{1/4}. \qquad (16)$$

For this wall, the same procedure with the same assumptions, which is used for the wall in the shade is used to calculate the heat loss from the cabinet during the winter period, because in the winter critical weather conditions for the equipment operation are during the night.

2.2. Heat transfer at the bottom of the cabinet

A mechanism of the heat transfer at the bottom of the cabinet in the summer period is shown in Fig. 4. The critical period is when the front or backside of the cabinet is exposed to the solar irradiance, see Fig. 1. In that case, a part of solar irradiance $\varepsilon I A_b$, where A_b is the net area of the bottom exposed to the Sun light, hits the metal part. All the absorbed heat is transferred to the circulating air:

$$\varepsilon I A_b = \dot{m}_{air} c_{p,air}\left(t_{in,c} - t_o\right) \textit{ where}, \qquad (17)$$

$t_{in,c}$ in °C is the temperature of air entering into the cabinet from below.

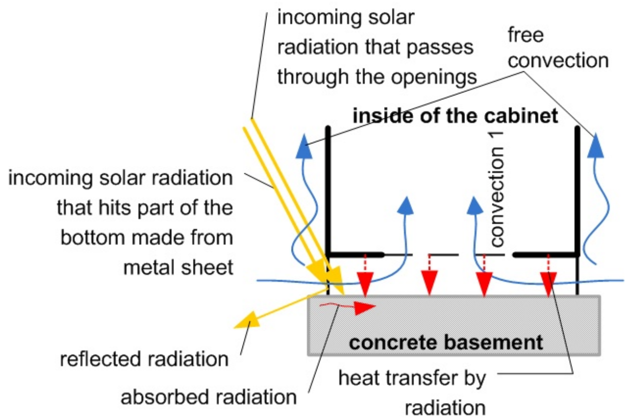

Figure 4: Heat transfer at the bottom of the cabinet. Convection 1 is forced convection when a fan is used to circulate air through the cabinet, otherwise it is free convection. Equal airflows from both sides are assumed.

This assumption (17) is made because there are 30 openings in the bottom part of the cabinet, so there is a relatively large area for the heat transfer between metal sheet and the incoming air. The solar irradiance that passes through the openings $A_{openings}$, which are modeled as black bodies, heats the concrete basement beneath the cabinet. This thermal radiation heats the concrete beneath the cabinet, which is assumed to be at 40°C. This is on the safe side because in practice this temperature is during summer lower than the ambient temperature. The heat transfer by radiation from the metal sheet to the concrete beneath the cabinet is

$$\dot{Q}_{bottom} = \frac{\sigma}{\frac{1}{\varepsilon_1}+\frac{1}{\varepsilon_2}-1}A_{bottom}(T - T_{concrete}), \qquad (18)$$

where ε_1 and $\varepsilon_2$are the degrees of emissivity for the shiny iron sheet with zinc surface and concrete, respectively.

During the winter weather there is no need for forced circulation of air through the cabinet. In that case As there is no need for forced circulation of air through the cabinet during winter, the heat transfer at the bottom of the cabinet is composed of the radiation and convection

$$\dot{Q}_{bottom} = \dot{Q}_{bottom,convection} + \dot{Q}_{bottom,radiation}. \qquad (19)$$

Heat transfer rate by radiation is calculated by (18) assuming that the temperature of the concrete beneath the cabinet is -3°C. This assumption is made according to the recommendations in [3].

Convective heat transfer is due to natural convection in the bottom space

$$\dot{Q}_{bottom,convection} = \alpha_b A_b (t - t_o). \qquad (20)$$

The temperature of air in that space is assumed to be equal to the environment temperature t_o, and the temperature of bottom part of the cabinet is assumed to be equal to the cabinet temperature. To calculate heat transfer coefficient, the model for free convection over horizontal surface [7] is used. For turbulent flow i.e. $Raf_2(Pr) > 7\cdot 10^4$ the Nusselet number, which is used to calculate heat transfer coefficient is calculated by [7]

$$Nu = 0.15[Raf_2(Pr)]^{1/3}. \qquad (21)$$

The function $f_2(Pr)$ defines the effect of the Prandtl number over the entire range 0<Pr<∞ and is given by [7]

$$f_2(Pr) = \left[1 + \left(\frac{0.322}{Pr}\right)^{11/20}\right]^{-20/11}. \qquad (22)$$

The characteristic length for calculating Ra and Nu numbers is l=ab/2(a+b) for rectangular surfaces. The physical properties of air are taken at the average temperature.

2.3. Heat transfer at the top of the cabinet

Heat transfer at the top of the cabinet is composed of radiation and convection

$$\dot{Q}_{top} = \dot{Q}_{top,convection} + \dot{Q}_{top,radiation}. \qquad (23)$$

The model of the heat transfer at the top of the cabinet is shown in Fig. 5. Absorbed solar irradiance is transferred from the top metal sheet by natural convection to the outside air, by forced convection to the inside air and by radiative heat transfer to the lower metal sheet:

$$\varepsilon I_t A_t = \alpha_{t,o}A_t\left(t_{sa,t} - t_o\right) + \alpha_{t,iu}A_t\left(t_{sa,t} - \frac{t_{a,in}+t_{out}}{2}\right) + \frac{\sigma}{\frac{1}{\varepsilon_1}+\frac{1}{\varepsilon_2}-1}A_t(T_{sa,t} - T). \qquad (24)$$

Air that flows in the attic above the cabinet exchanges heat by forced convection with the upper and the lower metal sheet

$$\dot{m}_{air}c_{p,air}\left(t_{out}-t_{a,in}\right)=\alpha_{t,iu}A_t\left(t_{sa,t}-\frac{t_{a,in}+t_{out}}{2}\right)+\alpha_{t,il}A_t\left(t-\frac{t_{a,in}+t_{out}}{2}\right) \quad (25)$$

The subscripts *t*, *o*, *i*, *sa*, *u*, *l* in (24) and (25) mean top, outside, inside, sol-air, upper, and lower, respectively. $t_{a,in}$ and t_{out} in °C are the inlet and the outlet air temperature in the space at the top of the cabinet, respectively. In other words, $t_{a,in}$ is the temperature at the exit of the fan (see Fig. 5). It was assumed that the lower metal sheet is at the temperature *T* of the cabinet, because air flows through openings in that surface. It is also assumed that the airflow is divided into two equal streams.

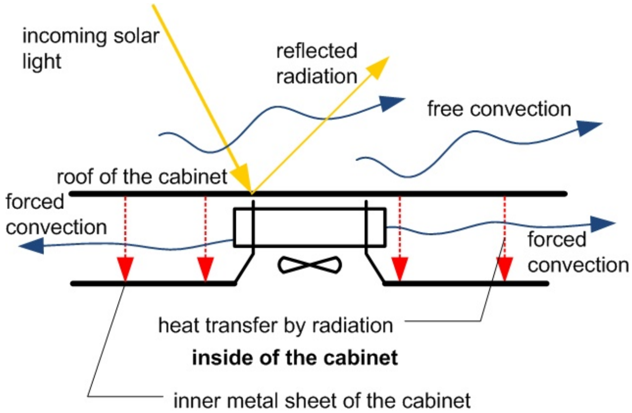

Figure 5: Heat transfer at the top of the cabinet.

$T_{sa,t}$ in K and $t_{sa,t}$ in °C is the sol-air temperature at the upper metal sheet. This temperature is calculated neglecting infrared exchanges from the sky by

$$t_{sa_t}=t_o+\frac{aI_t}{\alpha_{t,o}}. \quad (26)$$

The heat transfer coefficient above the top cover of the cabinet $\alpha_{t,o}$ in W/m²K is calculated by the model for free convection over horizontal surface [7] given by (21) and (22).

The heat transfer coefficients in W/m²K inside the attic, at the upper metal sheet $\alpha_{t,iu}$, and at the lower metal sheet $\alpha_{t,il}$, are both calculated by the model for forced convection presented in [18]. The procedure consists of calculating the Reynolds number first

$$Re=\frac{wd_e}{\nu}, \quad (27)$$

where w is the velocity of air, ν kinematic viscosity, and $d_e=4A/O$ equivalent diameter. As all the flows that are analyzed in this paper cause forced convection in the the transition region 2300 ≤ Re ≤10^4, the model of Gnielinski [18] is used. The model interpolates the regime between permanent laminar and turbulent flow. The equation is as follows

$$Nu=(1-\gamma)Nu_{lam,2300}+\gamma Nu_{tub,10^4} \quad (28)$$

where γ is given by

$$\gamma=\frac{Re-2300}{10^4-2300}, \text{ and } 0\leq\gamma\leq 1. \quad (29)$$

In (26) $Nu_{lam,2300}$ is the Nusselt number at Re=2300 obtained by (30)-(32), whereas $Nu_{tub,10^4}$ is the Nusselt number at Re=10^4 obtained by (33).

For constant wall temperature and laminar flow

$$Nu_{m,T,2300}=\left\{49.371+(Nu_{m,T,2,2300}-0.7)^3+Nu^3_{m,T,3,2300}\right\}^{1/3} \text{ where} \quad (30)$$

$$Nu_{m,T,2,2300}=1.615(2300Pr\frac{d_i}{l})^{1/3} \text{ and} \quad (31)$$

$$Nu_{m,T,3,2300}=\left(\frac{2}{1+22Pr}\right)^{1/6}(2300Pr\frac{d_i}{l})^{1/2}. \quad (32)$$

For constant wall temperature or constant heat flux and turbulent flow

$$Nu_{m,10^4}=\frac{(\frac{0.0308}{8})\cdot 10^4 Pr}{1+12.7\sqrt{\frac{0.0308}{8}}(Pr^{\frac{2}{3}}-1)}\left[1+(\frac{d_i}{l})^{2/3}\right]. \quad (33)$$

The range of validity for this model is 2300 ≤ Re ≤ 10^4, 0.6 ≤ Pr ≤1000 and d_i/l ≤ 1.

The Prandtl number of gases depends very little on temperature [18]. The effect on heat transfer exerted by variation of air properties is taken into account by [18]

$$Nu=Nu_m(\frac{T_{air}}{T_W})^{0.45}. \quad (34)$$

T_{air} and T_W are the average air and wall temperatures, respectively.

The model used to calculate heat loss at the top during the winter period is similar to the one used at the bottom of the cabinet and is composed of convective and radiative heat losses:

$$\dot{Q}_{bottom}=\dot{Q}_{bottom,convection}+\dot{Q}_{bottom,radiation}. \quad (35)$$

Three main assumptions are: (i) there is no airflow in the attic, (ii) the temperature of the lower metal sheet is equal to the cabinet temperature, and (iii) the temperature of the upper metal sheet is equal to the environment temperature. These assumptions allow the radiative heat loss to be calculated by the equations for radiative heat transfer between parallel plates of equal size (see the third term on the right-hand side of (24)). The convective heat loss is calculated by the model used to described natural convection over horizontal plates given by (21) and (22) [7].

2.4. Heat transfer inside the cabinet

During the winter period only the cabinet enclosure transfers heat with the surroundings whereas during summer there is airflow through the cabinet. The flow causes forced or natural convection inside the cabinet depending whether natural or forced circulation of air is created. If there is the forced circulation of air through the cabinet, the air receives heat by forced convection

$$\dot{m}_{air}c_{p,air}\left(t_{a,in}-t_{in,c}\right)=\alpha_{in}A_{in}\left(t-\left(\frac{t_{a,in}+t_{in,c}}{2}\right)\right), \quad (36)$$

where α_{in} in W/m²K is the heat transfer coefficient inside the cabinet, A_{in} in m² is the area for heat transfer inside the cabinet, and all other properties are explained in (1), (17), and (25). α_{in} is in this paper calculated by the use of the model for forced convection [18], which is explained in (27)-(34).

If air flow due to natural draft is used in the cabinet, it complicates its construction, because the air flow should be prevented during the winter. (1) and an additional equation for the air flow by natural draft should be solved. This equation is identical with (14), and should be solved overall and for all three sections of the cabinet through witch air flows. In addition, to calculate α_{in} in (36), the model used for natural convection, which is presented in (8)-(12), should be used.

3. RESULTS

For both analyzed cabinet construction it is taken: a constant internal heat dissipation of 140 W, the forced ventilation through the cabinet with the air exchange rate of 120 h^{-1} or 141.12 m^3/h, the area of $A_{in} = 10.08\,m^2$ for the internal heat transfer between the air and the interior of the vertical surface perpendicular to the sunlight, respectively.

The winter weather conditions are defined by: night time, average windy conditions at -20 °C.

the cabinet, and 50% of the cabinet cross section, i.e. 0.5(1.2x0.7) m^2 is free for airflow.

The summer weather conditions are defined by: the date is the 20th of July, daytime at 3 p.m., still weather with the temperature of 40°C. 634.3 W/m^2 and 595.1 W/m^2 are the global solar irradiance on the horizontal and

Results of the analysis for the summer weather conditions and the insulated cabinet are shown in Table 1 and in Fig. 6.

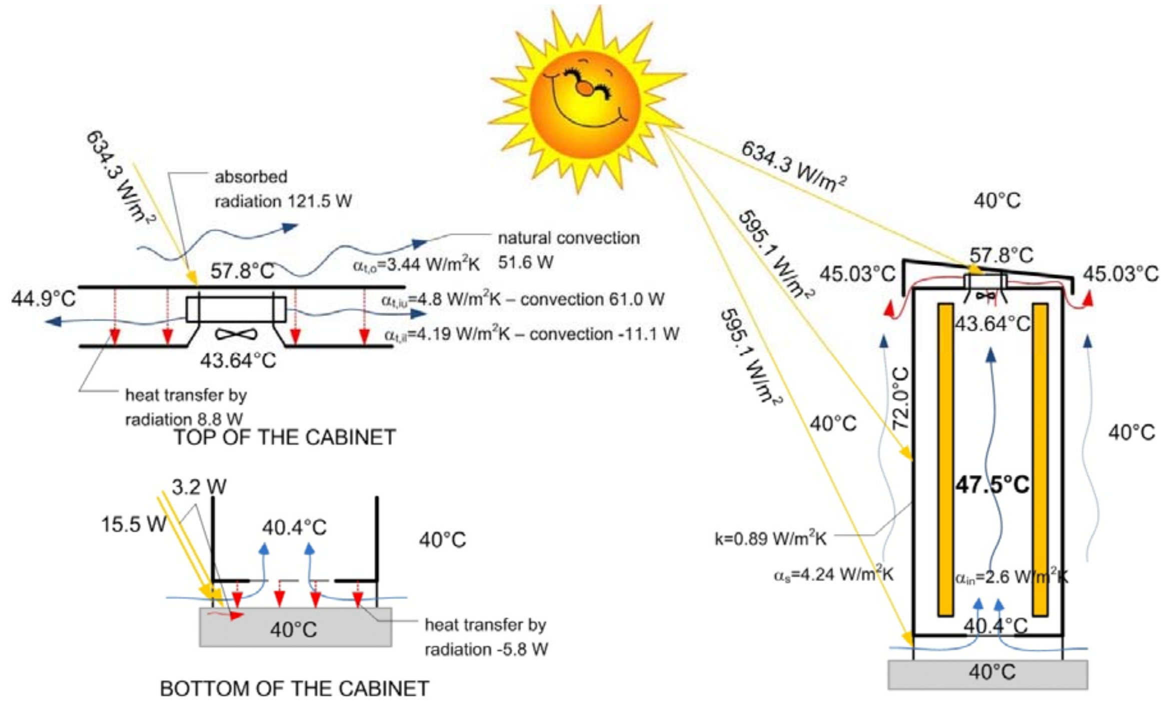

Figure 6: The characteristics of the heat transfer for the insulated cabinet and the summer weather conditions.

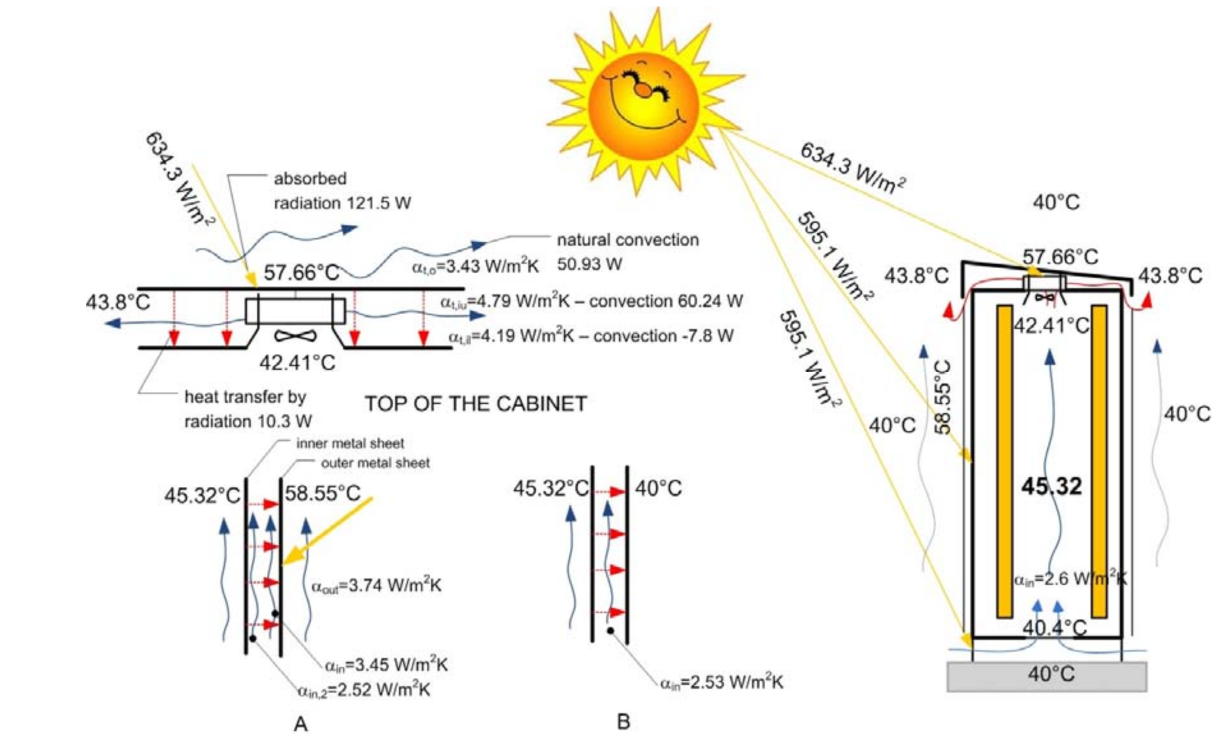

Figure 7: The characteristics of heat transfer for the non- insulated cabinet and the summer weather conditions. A- wall exposed to the Sun light, B – wall in the shade

Table 1: The energy balance for the insulated cabinet for the summer weather conditions. + is for heat gains, - for heat losses of the cabinet

Side of the cabinet	Area m^2	Radiation W	Convection W	Total W
Top	0.84	8.8	-11.1	-2.4
Side exposed to the Sun light	1.68	-	36.7	36.7
Rear side	1.68	-	-11.2	-11.2
Lateral side 1	0.98	-	-6.6	-6.6
Lateral side 2	0.98	-	-6.6	-6.6
Bottom	0.84	-5.8	0	-5.8
Heat gains of air inside the cabinet (W)				-144.1
Heat gains from thermal appliences				140,0

Applying the described procedure for the winter weather conditions and the insulated cabinet gives the temperature in the cabinet -2.8°C.

For the non-insulated cabinet the results for the summer weather conditions are shown in Table 2. and Fig. 7. Results shown in Fig. 6 for the bottom part of the insulated cabinet are identical for the non-insolated cabinet because the constructions of these parts of the cabinets are identical.

Table 2: The energy balance for the non-insulated cabinet for the summer weather conditions.

Side of the cabinet	Area m^2	Radiation W	Convection W	Total W
Top	0.84	10.3	-7.8	2.5
Side exposed to the Sun light	1.68	22.3	-3.8	18.5
Rear side	1.68	-8.2	-22.6	-30.8
Lateral side 1	0.98	-4.8	-13.2	-18
Lateral side 2	0.98	-4.8	-13.2	-18
Bottom	0.84	-4.1	0	-4.1
Heat gains of air inside the cabinet (W)				-90.2
Heat gains from thermal appliences				140,0

Applying the described procedure for the winter weather conditions and the non-insulated cabinet gives the temperature inside the cabinet -13.8°C.

4. CONCLUSIONS

This analysis is carried out for the specific heat gain inside the cabinet of 119 W/m^3, which means that the following conclusions apply for the cabinets with similar specific heat gains. Generally, to avoid using an air conditioning system in an electrical cabinet in the continental climate, air circulation should be promoted during the summer period, but during the winter period it should be prevented. In addition, to prevent absorption of solar radiation, the outer surface of an electrical cabinet should have as low as possible the degree of absorption.

Electrical cabinets with insulated walls are suitable for cold weather. The insulation prevents giving off heat during hot weather. Depending on the heat dissipation of the containing electrical equipment, this kind of cabinets are more likely to require forced ventilation during summer periods whereas during winter period they should need only proper air tightness. Insulated walls should be used when the containing electrical equipment has lower levels of heat dissipation, less than 120 W/m^3.

On the other hand, the cabinets, which have walls consisting of two metal sheets with ambient air freely circulating between them would for the heat dissipation level of 120 W/m^3, inside the cabinet require only natural ventilation during summer period, whereas during winter, except air tightness, they would require additional electrical heaters. This wall construction is suitable for hot conditions and higher levels of heat dissipation inside the cabinets, larger than 120 W/m^3. To release heat more easily, this construction could be improved with forced air circulation between two metal sheets, which would require a bit complicated manufacturing of the cabinets.

The weak point of this paper is the lack of experimental verification. The reason is that the company for which we developed this modeling procedure has not yet produced the designed electrical cabinet. Nevertheless, the modeling procedure uses verified heat transfer models as well as all the assumptions were made on the safe side.

ACKNOWLEDGEMENTS

This work was conducted within the project EE 33027 supported by the Ministry of Education, Science and Technological development of the Republic of Serbia.

REFERENCES

[1] http://en.wikipedia.org/wiki/Enclosure_%28electrical%29, (accessed May, 20, 2014)

[2] http://www.k-flex.ro/stduct.pdf, (accessed May, 7, 2014)

[3] B. Todorović, "Designing central heating installations (Projektovanje postrojenja centralnog grejanja)", sixth ed., Faculty of Mechanical Engineering, Belgrade (Serbia), (2009) (in Serbian)

[4] http://www.procena-rizika.com/zakoni-zze/Pravilnik-o-energetskoj-efikasnosti-zgrade.pdf, (accessed April, 8, 2014)

[5] R. Span, "Properties of Dry Air, in: VDI Gesellschaft, VDI Heat Atlas, second ed.", Springer, Heidelberg,pp. 172-191, (Germany), (2010)

[6] B. Todorović, "Air conditioning (Klimatizacija)", SMEITS, Belgrade, Belgrade (Serbia), (2009) (in Serbian)

[7] W. Kast, H. Klan," Heat Transfer by Free Convection: External Flows, in: VDI Gesellschaft, VDI Heat Atlas, second ed.", Springer, Heidelberg, pp. 667-671, (Germany), (2010)

[8] F.P Incropera, D.P. DeWitt, "Fundamentals of heat and mass transfer", Wiley & Sons, New York, (USA), (1966)

[9] W. Churchill, HHS Chu, "Correlating equations for laminar and turbulent free convection from a vertical plate,." Int. J. Heat Mass Tran., Vol. 18, pp:1323–1329, (1975)

[10] W. Churchill, R. Usagi,"A general expression for the correlation of rates of transfer and other phenomena", AIChE J, Vol. 18, pp: 1121–1128, (1972)

[11] Dj. Kozić, B. Vasiljević, B. Bekavac, "Handbook for Thermodynamics (Priručnik za termodinamiku)", Faculty

of Mechanical Engineering, Belgrade, (Serbia), (1995) (in Serbian).

[12] H. Martin, “Dimensionless Numbers, in: VDI Gesellschaft, VDI Heat Atlas, second ed.”, Springer, Heidelberg, pp. 11-14, (Germany), (2010)

[13] http://en.wikipedia.org/wiki/Sol-air_temperature, (accessed May, 10, 2014)

[14] http://encyclopedia2.thefreedictionary.com/sol-air+temperature, (accessed May, 10, 2014)

[15] S. Kabelac, P. Vortmeyer, “Radiation of Surfaces, in: VDI Gesellschaft, VDI Heat Atlas, second ed.”, Springer, Heidelberg, pp. 947-959, (Germany), (2010)

[16] http://www.pveducation.org/pvcdrom/properties-of-sunlight/arbitrary-orientation-and-tilt,(accessed April, 8, 2014)

[17] W. Kast, H. Klan, “Heat Transfer by Free Convection: Special Cases, in in: VDI Gesellschaft, VDI Heat Atlas, second ed.”, Springer, Heidelberg, pp. 681-684, (Germamy), (2010)

[18] V. Gnielinski,”Heat Transfer in Pipe Flow, in: VDI Gesellschaft, VDI Heat Atlas, second ed.”, Springer, Heidelberg, pp. 693-699, (Germany), (2010)

Energetic and Exergetic Evaluation of 4 Systems for a Rotary Kiln Improvement

Miljan Marašević[1*], Vladan Karamarković[1], Rade Karamarković[1], Nenad Stojić[1]
Faculty of Mechanical and Civil Engineeringin Kraljevo, University of Kragujevac, Kraljevo, Serbia

The energy balance of a rotary kiln used for calcination of 4400 kg/h of dolomite in a magnesium production company identified the kiln shell (26.35% of the input energy) and exhaust gases (18.95%) as the major sources of heat losses. To increase the efficiency of the kiln, the following systems are analyzed by the use of energy and exergy analysis: (i) system for preheating of the combustion air by heat exchange with the exhaust gas; (ii) system for space and DHW heating in the company by water heating with the exhaust gas sensible heat; (iii) system that consists of a recuperator that use sheat loss from the kiln shell to preheat the combustion air (designatedas iii-a) and the system given in (ii); and (iv) system that consists of (iii-a) and an cogeneration system that uses organic Rankine cycles upplied with heat by heat exchange with the exhaust gas. The system (ii) is the optimal solution by economic criteria because the company uses relatively expensive heavy fuel oil for space heating, where as exergetically, the most efficientis the the system (iv), which enables the kiln to have the exergetic efficiency of 36.02%.

Keywords: electrical cabinets, heat transfer, natural convection, forced convection, wall construction.

1. INTRODUCTION

This paper considers four systems for heat recovery. In each of the cases of the waste heat is used for the products of combustion rotary kiln. The waste heat is meant the losses contained in the natural heat of the combustion products and those who surrender to the surroundings through the mantle rotary kiln. Were considered forth the following systems for the utilization of waste heat rotary kiln:

- System for heating the combustion air, the heat contained in the flue gases (i).
- System for heating water (the water in the winter used to heat the hall, and in the summer for domestic hot water) heat contained in the flue gases (ii).
- The system for heating the water by heat contained in the exhaust gas in combination with a heat exchanger which uses the waste heat from the rotary kiln sheath (iii).
- System for the use of heat in the flue gases to produce electricity by Rankin - Klauzijus circular process with an organic working fluid in combination with a heat exchanger that uses waste heat from the mantle rotary kiln (iv).

RC process is historically the longest used to produce electricity. Today is to increase the degree of usefulness RC process when using a lower temperature heat source is often used instead of water vapour, organic working fluids in the ORC. Until the election of this process there is also the basis of the recommendations that can be found in the relevant literature. To approximately 1 MW of heat contained in the products from the rotary kiln on the basis of the diagram given in Figure 1 is the most optimal for the production of electrical energy using ORC.

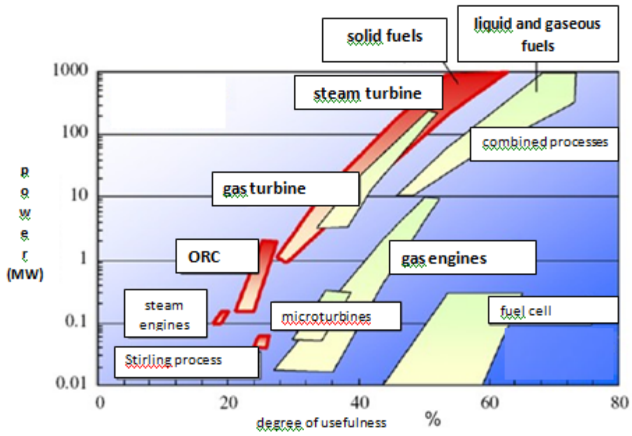

Figure 1: Degrees of usefulness and power ranges that use different systems for the production of electrical energy. ORC - Organic Rankine Cycle. (diagram originates from (Karl, 2004), and retrieved from (Karellas, et al, 2008))

2. POSSIBILITY USE OF WASTE HEAT FROM THE ROTARY KILN

Based on the previously approved system for the use of waste heat rotary kiln below to be shown the material and heat balances of each system.

2.1. System for heating the combustion air, the heat contained in the flue gases

The heat contained in the exhaust gas is used to heat air that is then used to fuel combustion in rotary kiln. Products of combustion at the entrance to the heat exchanger have a temperature of 343°C. In the heat exchanger products are cooled to a temperature of 150°C, wherein the combustion air is heated from 20°C to 312°C.

*Corresponding author: Kraljevo, Dositejeva 19., 36000 Kraljevo, Srbija, marasevic.m@mfkv.kg.ac.rs

Material and heat balance of the system is given in Table 1.

In order not to jeopardize the operation of the filter, the products must be neither too high nor too low temperature (condensation). To solve the problem of high temperatures in the existing structure products to mix with the surrounding air so that the temperature of the products is not higher than 130°C. A schematic representation of this system is shown in Figure 2. In Table 2, the calculation of fuel savings that can be achieved by using this solution.

Table 1: Material and heat balance system for heating degree air

The available heat which can be used for heating the air	1006,27	kJ/s
Mass flow rate of combustion air	3,379	kg/s
Inlet air temperature	20	°C
Assumed output air temperature	312,08	°C
Mean temperature of the heated air	166,04	°C
Specific heat capacity of air (for high temperature)	1,0197	kJ/kg K

Table 2: Calculation of fuel savings

		kJ/kgcal	%
Input energy	Combustion of fuels (Q_1) - LHV	7435,44	98,96
	Natural heat of fuel (Q_2)	41,07	0,55
	Natural heat of air (Q_3)	22,25	0,30
	Natural heat of the raw material (dolomite) (Q_4)	14,82	0,20
	Total:	7513,58	100,00
The input data			
Mass flow rate of fuel		0,184	kg/kgcal
Lower heating value of fuel - LHV		40410	kJ/kg
Specific heat capacity of the fuel		1,717	kJ/kg
The fuel temperature		130	C
Specific heat capacity of air		1,006	kJ/kgK
Specific heat capacity of the raw material (dolomite)		0,92	kJ/kgK
Production calcine		4399	kgcal/h
Calculation of fuel savings	Temperature of combustion air	312,08	°C
	Specific heat capacity of the heated air	1,01967	kJ/kgK
	Natural heat of air (Q_3)	879,89	kJ/kgcal
	The fuel consumption, the use of heated air	0,1629	kg/kgcal
	The difference in fuel consumption (savings)	0,0211	kg/kgcal
	The percentage of fuel savings	11,47	%
	The amount of fuel saved	2228,36	kg/ day

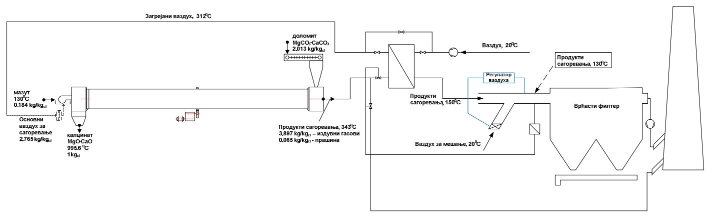

Figure 2: System for heating vazduka using the waste heat of the combustion products

2.2. The system for heating the water by heat contained in the exhaust gas

System for water heating is designed so that the water in the winter used to heat the hall, and in the summer for domestic hot water in a large central tank. Operating pressure in the system is 6 bars. The water is heated in the exchanger where the combustion products are cooled to 343°C to 150°C where in the water is heated from 50°C to 149,3°C. Material and heat balance of the system is shown in Table 3.

Table 3: Material and heat balance system for heating water

The available heat which can be used to heat the water	1006,27	kJ/s
The mass flow of water	2,40	kg/s
Water inlet temperature	50	°C
Assumed water outlet temperature	149,3	°C
Medium temperature water	99,65	°C
Specific heat capacity of water (for high temperature)	4,22	kJ/kg K

The system for heating the water is shown in Figure 3 wherein they are shown in the same figure, and the other components of the system. As has already been said bag filter must be provided as in the previous case.

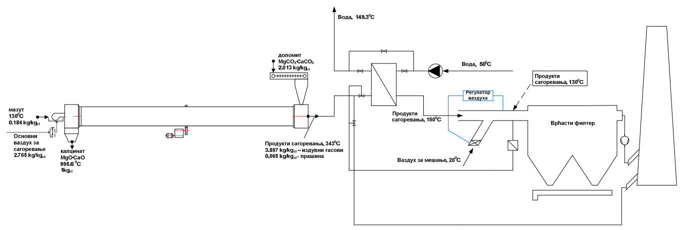

Figure 3: The system for heating the water by heat contained in the exhaust gas

2.3. The system for heating the water by heat contained in the exhaust gas in combination with a system for recovery of heat from the rotary kiln sheath.

This system relies on the previous with the existing components of the system adds heat exchanger where it heats the combustion air. Model exchanger with material and heat balance is given in the paper entitled „Recuperator for waste heat recovery from rotary kilns",Vladan Karamarković, Miljan Marašević, Rade Karamarković, Miodrag Karamarković, Applied Thermal

Engineering, Volume 54, Issue 2, 30 May 2013, Pages 470–480,DOI: 10.1016/j.applthermaleng.2013.02.027. Material and heat balance exchanger which heats water is the same as in the previous section. With this system, water is heated in the exchanger from 50°C to 149,3°C whereby the recuperator heats the combustion air to a temperature of 299,6°C. In Table 4, the calculation of fuel savings that can be achieved by using this solution. Figure 4 is a schematic showing alternative solution with components.

Table 4: Fuel savings using the heat exchanger

The total energy input	7513,58	kJ/kgcal
The temperature of the heated air	299,60	C
Specific heat capacity of the heated air	1,0454	kJ/kgK
The heat of the hot air	866,00	kJ/kgcal
Fuel consumption by using heat exchangers	0,1632	kg/kgcal
The amount of fuel saved per pound of product	0,0208	kg/kgcal

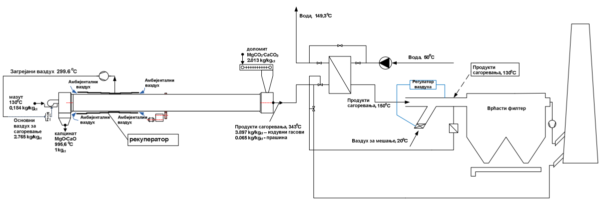

Figure 4: System for heating air and water using waste heat rotary kiln

2.4. System for the use of heat in the flue gases to produce electricity

With this system it is important to note that the analysis is carried out when the electricity generation using ORC cycle in combination with energy recovery that uses waste heat from the mantle rotary kiln (as in the previous case). Below is given a brief introduction of ORC systems with a choice of working medium.

2.4.1. ORC cycle theoretical basis

ORC is a thermodynamic process, which takes its name from the fact that it uses an organic fluid, high molecular weight, in which the phase change liquid-vapor takes place at lower temperatures than the saturation phase changes in water vapor in the case of Rankin's process.

Such cycles available thermal energy is converted into useful mechanical work, and continue this work can be converted into electricity. The first prototype was developed and introduced in 1961., Israeli engineers for solar energy Harry Zvi Tabor and Lucien Bronicki [16].

The principle of operation of ORC is similar to that of Rankine's process: the working fluid increases the pressure in the pump to the working pressure increased by the pressure drop in the heat exchangers and pipelines. The working fluid in the heat heat is applied, wherein the working fluid further heated by the supply of heat and evaporates. Then, the working fluid is expanded in a turbine and then is condensed in condenser. So chilled working fluid is returning to the beginning of the process, i.e. the pump.

2.4.2. ORC cycle for electricity production

This paper analyzes the possibilities of ORC processes as working medium using isopentane. Isopentane was selected on the basis of practical examples where in similar product temperature at the exit of the rotary kiln cement recommended this working fluid. Operating pressures of the process are 30 bar and 1.4 bar. The mass flow of the working fluid (isopentane) is 1.5 kg / s. The adopted parameters of the system are presented in Table 5 and the values of the thermodynamic properties characteristic points given in Figure 5.

Table 5: Parameters ORC system

Degree of goodness expansion turbine (%)	85
Mechanical efficiency level of the turbine (%)	99
Efficiency pumps (%)	98
Mechanical efficiency level generator (%)	98
Electrical efficiency level generator (%)	98

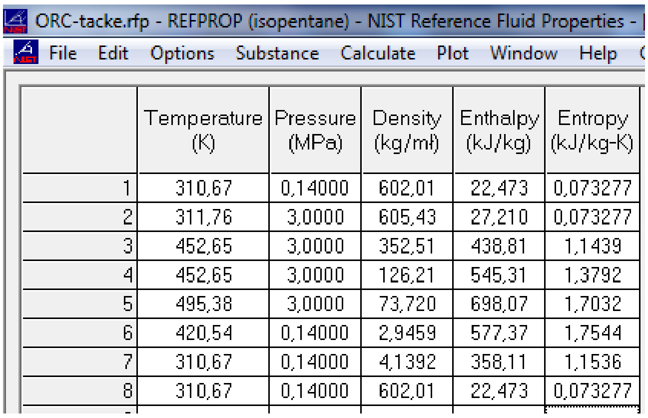

ORC-tacke.rfp - REFPROP (isopentane) - NIST Reference Fluid Properties -

File Edit Options Substance Calculate Plot Window Help

	Temperature (K)	Pressure (MPa)	Density (kg/m³)	Enthalpy (kJ/kg)	Entropy (kJ/kg-K)
1	310,67	0,14000	602,01	22,473	0,073277
2	311,76	3,0000	605,43	27,210	0,073277
3	452,65	3,0000	352,51	438,81	1,1439
4	452,65	3,0000	126,21	545,31	1,3792
5	495,38	3,0000	73,720	698,07	1,7032
6	420,54	0,14000	2,9459	577,37	1,7544
7	310,67	0,14000	4,1392	358,11	1,1536
8	310,67	0,14000	602,01	22,473	0,073277

Figure 5: Values characteristic points ORC process

With this system, the generator may get 172,18 kW of electric power, wherein in the condenser water is heated from 20°C to 103°C. In addition to the recuperator is heated combustion air to a temperature of 299,6°C. Figure 6 schematically shows alternative solution with components.

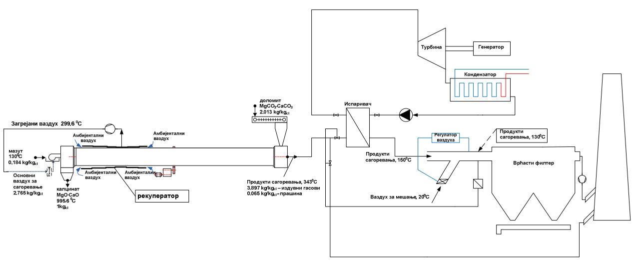

Figure 6: System for the use of heat in the flue gases through the ORC process

3. EXERGY ANALYSIS

On the basis of calculations in the previous section for each of the systems further in this paper was carried out Exergy calculation of selected solutions.

3.1.1. Technical Working power or exergy

The second law of thermodynamics indicates irreversible processes as the primary causes of energy loss. Their consequence is an increase in entropy ΔS which leads to energy losses. Loss of work and the amount of heat [2]:

$\Delta L = T_0\,\Delta S$ (3.1)

$\Delta Q = T_0\,\Delta S\,T/(T-T_0)$, (3.2)

Although previous formulas allow to calculate the loss of work (3.1) and the amount of heat (3.2), they do not provide a measure of the energy loss of the total energy that is participating in a process. This measure provides technical working power (Bošnjaković, 1978). For a substance that steady stream, it is a work that would theoretically could get if these substances on the reversible manner, brought into balance with its surroundings and pushed out into the environment. For technical working power Zoran Rant proposed name of Exergy (Bošnjaković, 1978). For that matter, current technical working power or exergy is:

$E = H - H_0 - T_0\,(S - S_0)$, (3.3)

where:

H and S refer to the state of matter which is not in equilibrium with the environment

H_0 and S_0- the state of matter in equilibrium with the environment (p_0,T_0)

Exergy E_Q some amount of heat Q, which is subtracted the heat source temperature T is:

$E_Q = Q\,(T-T_0)/T$. (3.5)

From equation (3.5) we see that the heat can be converted into work at temperatures higher than the ambient temperature T_0. Heat to the ambient temperature of the Exergy worthless because there is the potential to turn into a paper [2].

3.1.2. Exergy analysis of systems using waste heat rotary kiln

Exergy is the maximum work that can be produced by a system, the flow of fluid or energy in its bringing into balance with the reference environment [7] (taken from [8]). This thermodynamic condition takes into account the increase in entropy due to irreversibility, i.e. the second law of thermodynamics, and is a suitable tool for analyzing the process of energy transformation. Exergy balance of the test furnace, or of any other process of energy transformation can be represented in the following form, taking into account all energy flows entering and leaving the system:

$$\sum_{in} Ex_j = \sum_{out} Ex_k + I \quad (3.6)$$

where:

$\sum_{in} Ex_j$- the sum of all exergy input current.

$\sum_{out} Ex_k$- the sum of all exergy output current.

The difference between the sum of all input and output flows eksergijskih called irreversibility I. Irreversibility is the internal loss of exergy in the process of [9]. This loss is due to an increase in entropy caused by the irreversibility that occur due to: chemical reactions, heat and mass transfer and fluid flow [9].

Exergy amount of heat that the mantle rotary kiln is lost to the surroundings is:

$$Ex_Q = \sum_{i=1}^{24} Ex_{Q_{s,i}} = \sum_{i=1}^{24}\left(1 - \frac{T_0}{T_{s,i}}\right)\frac{Q_{s,i}}{m_{cl}}, \quad (3.7)$$

Analyzed a rotary kiln with appropriate exchangers has several inputs (fuel, air, dolomite, water) and output (calciner, combustion products, dust, water, electricity) material flows. For each of them, the exergy E_{xi} , is dependent on the composition (chemical exergy $Ex_{ch,i}$), and the temperature and pressure (the physical exergy $Ex_{ph,i}$):

$$Ex_i = Ex_{ch,i} + Ex_{ph,i} = m_i\left(e_{ph,i} + e_{ch,i}\right) \quad (3.8)$$

The physical exergy of a compound and is:

$$e_{ph,i} = (h - h_0)_i - T_0(s - s_0)_i \quad (3.9)$$

where:

h and s - the enthalpy and entropy of a given flow at a temperature and pressure

h_0 and s_0 - the enthalpy and entropy of a given flow at ambient temperature and pressure

Physical exergy of the combustion products is equal to the sum of the physical exergy of gaseous components contained in the exhaust gas.

Standard chemical exergy of a pure chemical compound (which is not a mixture) e^0_{ch} is equal to the maximum work obtained when this compound with pressure (po) and temperature (To) environment lead to the so-called. Dead state, determined that the same pressure (po) and temperature (To) temperature and concentration of the reference substance in a standard atmosphere

Standard reference condition defined by the temperature 298.15K and pressure of 101,325 kPa. Table 6 shows the standard chemical exergy of all the components shown in the material balance.

Table 6: Standard chemical exergy e^0_{ch}, [10], [11].

Gas	Standard chemical exergy e^0_{ch}(kJ/mol)	Solids	Standard chemical exergy e^0_{ch}(kJ/mol)
CO_2	19.48	Dolomite $CaCO_3{\cdot}MgCO_3$	32.2
SO_2	313.4		
H_2O	9.5	CaO	127.3
N_2	0.72		
O_2	3.97	MgO	59.1

The chemical exergy of the mixture, such as products of combustion, is dependent on the composition of the mixture and is defined by the formula:

$$e_{ch,mix} = \sum_i y_i e^0_{ch,i} + RT_0 \sum_i y_i \ln y_i \qquad (3.10)$$

Chemical exergy of the mixture is always lower than the sum of the individual components of exergy. The second member of the above equation is the so-called. Exergy of mixing and is always negative [9].

Chemical Exergy calciner depends on the mass fraction of CaO and MgO in it:

$$e^0_{ch} - \sum_i x_i \left(\frac{e^0_{ch,i}}{M_i}\right) - x_{CaO}\left(\frac{e^0_{ch,CaO}}{M_{CaO}}\right) + x_{MgO}\left(\frac{e^0_{ch,MgO}}{M_{MgO}}\right) \qquad (3.10)$$

Exergy efficiency level is the ratio of exergy that comes out of the system and the exergy entering the system [21]:

$$\psi = \frac{\sum_{out} Ex_k}{\sum_{in} Ex_j} \qquad (3.11)$$

Degree Exergy efficiency is defined as the ratio of useful exergy obtained and entered total exergy:

$$\psi_k = \frac{Ex_{product}}{\sum_{in} Ex_j} \qquad (3.12)$$

3.1.3. Exergy efficiency of the proposed solutions for the use of waste heat rotary kiln

In this part of the paper presents the exergy calculations of the proposed solutions and the values of exergy input and output streams [3].

Exergy analysis results performed for the case of heating of combustion air, the heat contained in the exhaust gas (Figure 2) are presented in Table 7.

Table 7: Exergy calculation of using the waste heat of the combustion products for heating the air

Output flows	I.1	Exergy combustion products	797,117	kJ/kgcal
	I.2	Exergy loss of heat from the mantle rotary kiln	815,25	kJ/kgcal
	I.3	Exergy calcine	2426,21	kJ/kgcal
	I.4	Exergy dust	25,26	kJ/kgcal
Input flows	U.1	Exergy dolomite	352,424	kJ/kgcal
	U.2	Exergy of air	1,404	kJ/kgcal
	U.3	Exergy fuel	7917,481	kJ/kgcal
Useful exergy efficiency ψ_k			29,33	%

Exergy analysis results performed for the case of hot water (water in the winter used to heat the hall, and in the summer for domestic hot water) heat contained in the flue gases. (Figure 3) are presented in Table 8. In this case, a useful exergy efficiency is defined:

$$\psi_k = \frac{\text{useful exergy}}{\text{total input exergy}} = \frac{E_{x\ calcine} + E_{x\ water}}{\sum_{in} E_{xj}} \qquad (3.13)$$

Table 8: Exergy calculation of using the waste heat of the combustion products for heating water

Output flows	I.1	Exergy combustion products	797,117	kJ/kgcal
	I.2	Exergy loss of heat from the mantle rotary kiln	815,25	kJ/kgcal
	I.3	Exergy calcine	2426,21	kJ/kgcal
	I.4	Exergy dust	25,26	kJ/kgcal
	I.5	Exergy heated water	172,899	kJ/kgcal
Input flows	U.1	Exergy dolomite	352,424	kJ/kgcal
	U.2	Exergy of air	1,404	kJ/kgcal
	U.3	Exergy fuel	7917,481	kJ/kgcal
	U.4	Exergy water	8,145	kJ/kgcal
Useful exergy efficiency ψ_k			31,39	%

Table 9 shows the results eksergijskog calculations for the case when the water is heated by the waste heat of the combustion products in combination with energy recovery that uses waste heat to pay rotary kiln (Figure 4).

Table 9: Exergy calculation of using the waste heat of the combustion products for heating water in combination with energy recovery

Output flows	I.1	Exergy combustion products	705,047	kJ/kgcal
	I.2	Exergy loss of heat from the mantle rotary kiln	404,75	kJ/kgcal
	I.3	Exergy calcine	2426,21	kJ/kgcal
	I.4	Exergy dust	25,26	kJ/kgcal
	I.5	Exergy heated water	172,899	kJ/kgcal
Input flows	U.1	Exergy dolomite	352,424	kJ/kgcal
	U.2	Exergy of air	1,404	kJ/kgcal
	U.3	Exergy fuel	6967,224	kJ/kgcal
	U.4	Exergy water	8,145	kJ/kgcal
Useful exergy efficiency ψ_k			35,46	%

In systems for the use of heat in the flue gases to produce electricity by Rankin-Klauzijusovog circular process with an organic working fluid (Figure 5) results eksergijskog calculations are shown in Table 10 should be noted that in this case the useful exergy efficiency is determined:

$$\psi_k = \frac{E_{x\ calcine} + E_{x\ electricity} + E_{x\ water}}{\sum_{in} E_{xj}} \qquad (3.14)$$

Table 10: Exergy calculation system for waste heat recovery products of combustion to produce electricity ORC cycle in combination with energy recovery

Output flows	I.1	Exergy combustion products	705,047	kJ/kgcal
	I.2	Exergy loss of heat from the mantle rotary kiln	404,75	kJ/kgcal
	I.3	Exergy calcine	2426,21	kJ/kgcal
	I.4	Exergy dust	25,26	kJ/kgcal
	I.5	Exergy heated water	72,244	kJ/kgcal

	I.6	Exergy derived electricity	140,907	kJ/kgcal
Input flows	U.1	Exergy dolomite	352,424	kJ/kgcal
	U.2	Exergy of air	1,404	kJ/kgcal
	U.3	Exergy fuel	6967,224	kJ/kgcal
	U.4	Exergy water	0,349	kJ/kgcal
	U.5	Exergy of electricity needed to operate the pump	5,933	kJ/kgcal
Useful exergy efficiency ψ_k			36,02	%

4. COMPARATIVE ANALYSIS SYSTEM OF THE USE OF WASTE HEAT COMBUSTION PRODUCTS

Based on the conducted energy and exergy analysis can be carried out comparison of the proposed solutions. Values useful exergy efficiency degree of usefulness and analyzed solutions are presented in Table 11.

Table 11: Useful exergy efficiency for the proposed system

	The proposed alternative solution for the use of waste heat	Useful exergy efficiency (%)
(i)	System with heated air	29,33
(ii)	System to heat water without the use of a recuperator	31,39
(iii)	System for heating water using a recuperator	35,46
(iv)	System for the production of electricity ORC process with recuperator	36,02

The analysis of the results shown in the table above it can be seen, as expected, that the use of heat from the mantle furnace and waste heat from flue gases more efficiently than using only waste heat from flue gases. Of all the systems the most efficient system in which the waste heat is used in the cogeneration process for the production of electricity. The reason lies in the fact that this process of most exergy of flue gases usefully spent. In the process of cogeneration least the irreversibility because the minimum temperature difference in the exchanger where the flue gas takes heat. Environmentally speaking, the process of cogeneration is the best because it reduces the emissions of pollutants from the power system of the Republic of Serbia. In fact, almost 70% of electricity in our country is produced in power plants. The system (ii) is the optimal solution by economic criteria because the company uses relatively expensive heavy fuel oil for space heating, where as exergetically, the most efficientis the the system (iv), which enables the kiln to have the exergetic efficiency of 36.02%.

REFERENCES

[1] V. Karamarković, M. Marašević, R. Karamarković, M. Karamarković, „Recuperator for waste heat recovery from rotary kilns“, Applied Thermal Engineering, Volume 54, Issue 2, 30 May 2013, Pages 470–480, DOI: 10.1016/j.applthermaleng.2013.02.027.

[2] R. Karamarković, „Exergy analysis auto term systems for biomass gasification, PhD thesis Rade Karamarković of Mechanical Engineering Kraljevo, 2011.

[3] M. Marašević, „Exergy optimization of rotary kiln for calcination of dolomite, PhD thesis Miljan Maraševića, Faculty of Mechanical and Civil Engineeringin Kraljevo, 2013.

[4] A.C. Caputo, Antonio, P.M. Pelagagge, P. Salini, Performance modeling of radiant heat recovery exchangers for rotary kilns, Appl. Therm. Eng. 31 (2011) 2578-2589.

[5] B.K.Chakrabati, Investigations on heat loss through the kiln shell in magnesite dead burning process: a case study, Appl. Therm. Eng. 22 (2002) 1339-1345.

[6] Z. Söğüt, Z. Oktay, H. Karakoç, Mathematical modeling of heat recovery from a rotary kiln, Appl. Therm. Eng. 30 (2010) 817-825.

[7] Z. Rant, Exergy a new word for technical available work, Forschungenim Ingenieurwesen, 22 (1956) 36-37 (in German).

[8] E. Coatanéa, M. Kuuva, H. Nordlund, P.E. Makkonen, T. Saarelainen, Int. J. of Eviron. Conscious Des. & Manuf. 13 (2007) 1-23.

[9] M.J. Prins, K.J. Ptasinski, F.J.J.G. Janssen, Energy and exergy analysis of the oxidation and gasification of carbon, Energy 30 (2005) 981-1002.

[10] J. Szargut, J., Appendix 1. Standard chemical exergy, MIT University, <web.mit.edu/2.813/www/readings/APPENDIX.pdf> (accessed 02.07.12).

[11] J. Szargut, Exergy. Guidance for calculating and applying (Egzergia. Poradnik obliczania i stosowania),Widawnictwo Politechniki Shlaskej, Gliwice, 2007 (in Polish).

[12] G. Kabir, A.I. Abubakar, U.A.El-Nafaty, Energy audit and conservation opportunities for pyroprocessing unit of a typical dry process cement plant, Energy 35 (2010) 1237-1243.

[13] Karellas S, Panopoulos KD, Panousis G, Kakaras E, Boukis I. Energetic andexergetic investigation of integrated RDF gasification energy systems, ECOS2010. In: Proccedings the 18th international conference on efficiency, costs,optimization. Lausanne, Switzerland: Simulation and Environmental Impactof Energy Systems; 2010 Jun 14e17.

[14] Bombarda P., Invernizzi M.C., Pietra C., Heat recovery from Diesel engines: Athermodynamic comparison between Kalina and ORC cycles, Applied ThermalEngineering 30 (2010), 212–219

[15] Papadopoulos I.A., Stijepovic M., Linke P., On the systematic design andselection of optimal working fluids for Organic Rankine Cycles, AppliedThermal Engineering 30 (2010), 760–769

[16] Yamamoto T., Furuhata T., Arai N., Mori K., Design and testing of the OrganicRankine Cycle, Energy 26 (2001), 239–251.

[17] Lucien Y. Bronicki, Organic Rankine cycle power plant for waste heatrecovery, (2007.)

[18] Fluid Thermodynamic and Transport Properties, NIST Standard Database 23, Version 8.0, (2007)

CIP - Каталогизација у публикацији
Народна библиотека Србије, Београд

621(082)
621.86/.87(082)
629.3/.4(082)
622.6(082)
INTERNATIONAL Triennial Conference Heavy
Machinery (8 ; 2014 ; Zlatibor)
Proceedings / The Eighth lnternational
Triennial Conference Heavy Machinery - HM
2014, Zlatibor, June 25 - June 28 2014. ;
[editor Milomir Gašić]. - Kraljevo: Faculty
of Mechanical and Civil Engineering, 2014
(Kraljevo : Satcip). - 1 knj. (razl. pag.) :
ilustr.; 3O cm

Na vrhu nasl. str.: University of Kragujevac.
- Tekst štampan dvostubačno. - Tiraž 120. -
Napomene uz tekst. - Bibliografija uz svaki
rad.
ISBN 978-86-82631-74-3
1. Fakultet za mašinstvo i građevinarstvo
(Kraljevo)
a) Машиноградња - Зборници b) Производно
машинство - Зборници c) Транспортна
средства - Зборници d) Шинска возила -
Зборници
COBISS.SR-ID 209599500

The Faculty of Mechanical
and Civil Engineering in Kraljevo
The University of Kragujevac
Serbia, 36000 Kraljevo, Dositejeva 19
Phone/fax +381 36 383 269, 383 377

E-mail: office@mfkv.kg.ac.rs
www.mfkv.kg.ac.rs